SANDIA REPORT

SAND91-0893/3 • UC-721
Unlimited Release
Printed December 1991

Preliminary Comparison with 40 CFR Part 191, Subpart B for the Waste Isolation Pilot Plant, December 1991

Volume 3: Reference Data

WIPP Performance Assessment Division

Prepared by
Sandia National Laboratories
Albuquerque, New Mexico 87185 and Livermore, California 94550
for the United States Department of Energy
under Contract DE-AC04-76DP00789

Issued by Sandia National Laboratories, operated for the United States Department of Energy by Sandia Corporation.

Available to DOE and DOE contractors from
Office of Scientific and Technical Information
PO Box 62
Oak Ridge, TN 37831

Prices available from (615) 576-8401, FTS 626-8401

Available to the public from
National Technical Information Service
US Department of Commerce
5285 Port Royal Rd
Springfield, VA 22161

NTIS price codes
Printed copy: A99
Microfiche copy: A01

SAND91-0893/3
Unlimited Release
Printed December 1991

Distribution
Category UC-721

PRELIMINARY COMPARISON WITH 40 CFR PART 191, SUBPART B FOR THE WASTE ISOLATION PILOT PLANT, DECEMBER 1991

VOLUME 3: REFERENCE DATA

WIPP Performance Assessment Division
Editors: Rob P. Rechard, Andrew C. Peterson, James D. Schreiber,[1]
Harold J. Iuzzolino[2], Martin S. Tierney, Jim S. Sandha[1]
Sandia National Laboratories
Albuquerque, New Mexico 87185

ABSTRACT

This volume documents the data available as of August 1991, which were used by the Performance Assessment Division of Sandia National Laboratories in its 1991 preliminary performance assessment of the Waste Isolation Pilot Plant (WIPP). Ranges and distributions for about 300 modeling parameters, several of which are spatially varying parameters with between 15 and 80 point values, and about 500 well locations and corresponding stratigraphic elevations are presented in both tables and graphics for the geologic and engineered barriers, global materials (e.g., fluid properties), and agents that act upon the WIPP disposal system such as climate variability and human-intrusion boreholes. Sources for the data and a brief discussion of each parameter are also provided.

[1] Science Applications International, Albuquerque, NM 87106
[2] Geo-Centers, Inc., Albuquerque, NM 87106

ACKNOWLEDGMENTS

The WIPP Performance Assessment Division is comprised of both Sandia and contractor employees working as a team to produce these annual preliminary comparisons with EPA regulations, assessments of overall long-term safety of the repository, and interim technical guidance to the program. The on-site team, affiliations, and contributions to the 1991 performance assessment are listed in alphabetical order:

Performance Assessment Division

Name	Affil.	Primary Author of Doc: Sect.	Major Code	Area of Responsibility
R. Anderson	SNL			Division Manager
B. Baker	TEC	V.2:§6.4		SEC02D, Hydrology, Office Manager
J. Bean	UNM	V.2:§4.2.1		BRAGFLO & BOASTII, 2-Phase Flow
J. Berglund	UNM	V.2:Ch.7 Editor V.2	CUTTINGS	Task Ldr., Undisturbed Repository, Cuttings/Cavings/ Engr. Mech.
W. Beyeler	SAI	V.2:§5.3; 6.1;6.3	PANEL GARFIELD	Geostatistics, Analytical Models, CAMCON Systems Codes
K. Brinster	SAI			Geohydrology, Conceptual Models
R. Blaine	ECO			SEC02D & CAMCON Systems Codes
T. Blaine	EPE			Drilling Technology, Exposure Pathways Data
J. Garner	API	V.2:§5.3	PANEL	Source Term, Sens. Anal.
A. Gilkey	UNM			CAMCON Systems Codes
L. Gomez	SNL			Task Ldr., Safety Assessments
M. Gruebel	TRI	V.1:Ch.1,2, 8,9,10		EPA Regulations
R. Guzowski	SAI	V.1:Ch.4		Geology, Scenario Construction
J. Helton	ASU	V.1:Ch.3,4 V.2:Ch.2,3	CCDFPERM	Task Ldr., Uncert./Sens. Anal., Probability Models
H. Iuzzolino	GC	Editor V.3	CCDFPERM	LHS & CAMCON System Codes
R. Klett	SNL			EPA Regulations
P. Knupp	ECO			STAFF2D & SECOTR, Comp. Fluid Dyn.
C. Leigh	SNL		GENII-S	Exposure Pathways
M. Marietta	SNL	Editor (Set)		Dep. Div. Manager, Tech. Coord.
G. de Marsily	UP	V.2:§6.2		Task Ldr., Geostatistics
R. McCurley	UNM	V.2:§4.2.3		SUTRA & CAMCON System Codes
A. Peterson	SNL	Editor V.3		Task Ldr., Inventory
J. Rath	UNM	V.2:§4.2.3		SUTRA, Engr. Mech.
R. Rechard	SNL	Editor V.2 & V.3		Task Ldr., CAMCON, QA, Ref. Data
P. Roache	ECO	V.2:§6.4	SECO	Task Ldr., Comp. Fluid Dyn.
D. Rudeen	UNM	V.2:§4.2.2; 6.5		STAFF2D, Transport
J. Sandha	SAI	Editor V.3		INGRES, PA Data Base
J. Schreiber	SAI	V.2:§4.2.1; 5.2.5 Editor V.3		BRAGFLO & BOASTII, 2-Phase Flow
P. Swift	TRI	V.1:Ch.5,11		Task Ldr., Geology, Climate Var.

M. Tierney	SNL	Editor V.3			Task Ldr., CDF Constr., Probability Models
K. Trauth	SNL				Task Ldr., Expert Panels
P. Vaughn	API	V.2:§5.1; 5.2;5.2.5; App.A	BRAGFLO		Task Ldr., 2-Phase Flow & Waste Panel Chemistry
J. Wormeck	ECO				Comp. Fluid Dyn. & Thermodyn.

The foundation of the annual WIPP performance assessment is the underlying data set and understanding of the important processes in the engineered and natural barrier systems. The SNL Nuclear Waste Technology Department is the primary source of these data and understanding. Assistance with the waste inventory comes from WEC and its contractors. We gratefully acknowledge the support of our departmental and project colleagues. Some individuals have worked closely with the performance assessment team, and we wish to acknowledge their contributions individually:

J. Ball	ReS	Computer System Manager
H. Batchelder	WEC	CH & RH Inventories
R. Beauheim	SNL	Natural Barrier System, Hydrologic Parameters
B. Butcher	SNL	Engineered Barrier System, Unmodified Waste-Form Parameters, Disposal Room Systems Parameters
L. Brush	SNL	Engineered Barrier System, Source Term (Solubility) and Gas Generation Parameters
L. Clements	ReS	Computer System Support
T. Corbet	SNL	Natural Barrier System, Geologic & Hydrologic Parameters, Conceptual Models
P. Davies	SNL	Natural Barrier System, Hydrologic & Transport Parameters, & 2-Phase Flow Mechanistic Modeling
P. Drez	IT	CH & RH Inventories
E. Gorham	SNL	Natural Barrier System, Fluid Flow & Transport Parameters
S. Howarth	SNL	Natural Barrier System, Hydrologic Parameters
R. Kehrman	WEC	CH & RH Waste Characterization
R. Lincoln	SNL	Project Integration
F. Mendenhall	SNL	Engineered Barrier System, Unmodified Waste Form Parameters, Waste Panel Closure (Expansion)
D. Munson	SNL	Reference Stratigraphy, Constitutive Models, Physical & Mechanical Parameters
E. Nowak	SNL	Shaft/Panel Seal Design, Seal Material Properties, Reliability
J. Orona	ReS	Computer System Support
J. Tillerson	SNL	Repository Isolation Systems Parameters
S. Webb	SNL	2-Phase Flow Sensitivity Analysis & Benchmarking

API = Applied Physics Incorporated
ASU = Arizona State University
ECO = Ecodynamics Research Associates
EPE = Epoch Engineering
GC = Geo-Centers Incorporated
IT = International Technology
ReS = ReSpec
SAI = Scientific Applications International Corporation
SNL = Sandia National Laboratories
TEC = Technadyne Engineering Consultants
TRI = Tech Reps, Inc.
UNM = Univ. of New Mexico/New Mexico Engineering Research Institute
UP = University of Paris
WEC = Westinghouse Electric Corporation

Peer Review

Internal/Sandia

T. Corbet
D. Gallegos
M. LaVenue
S. Hora

Management/Sandia

W. Weart
T. Hunter

PA Peer Review Panel

R. Heath, Chairman	University of Washington
R. Budnitz	Future Resources Associates, Inc.
T. Cotton	JK Research Associates, Inc.
J. Mann	University of Illinois
T. Pigford	University of California, Berkeley
F. Schwartz	Ohio State University

Department of Energy

R. Becker
J. Rhoderick

Expert Panels

Futures

M. Baram	Boston University
W. Bell	Yale University
G. Benford	University of California, Irvine
D. Chapman	The World Bank, Cornell University
B. Cohen	University of Pittsburgh
V. Ferkiss	Georgetown University
T. Glickman	Resources for the Future
T. Gordon	Futures Group
C. Kirkwood	Arizona State University
H. Otway	Joint Research Center (Ispra), Los Alamos National Laboratory
M. Pasqualetti	Arizona State University
D. Reicher	Natural Resources Defense Council
N. Rosenberg	Resources for the Future
M. Singer	The Potomac Organization
T. Taylor	Consultant
M. Vinovski	University of Michigan

Source Term

C. Bruton	Lawrence Livermore National Laboratory
I-Ming Chou	U.S. Geological Survey
D. Hobart	Los Alamos National Laboratory
F. Millero	University of Miami

Retardation

R. Dosch	Sandia National Laboratories
C. Novak	Sandia National Laboratories
M. Siegel	Sandia National Laboratories

Geostatistics Expert Group

G. de Marsily, Chairman	U. of Paris
R. Bras	Massachusetts Inst. of Tech.
J. Carrera	U. Politechnica de Cataluña
G. Dagan	Tel Aviv U.
A. Galli	Ecole des Mines de Paris
A. Gutjahr	New Mexico Tech.
D. McLaughlin	Massachusetts Inst. of Tech.
S. Neuman	U. of Arizona
Y. Rubin	U. of California, Berkeley

Report Preparation (TRI)

Editors:

Volume 1: M. Gruebel (text); S. Laundre-Woerner (illustrations)
Volume 2: D. Scott (text); D. Marchand (illustrations)
Volume 3: J. Chapman (text); D. Pulliam (illustrations)

D. Rivard, D. Miera, T. Allen, and the Word Processing Department
R. Rohac, R. Andree, and the Illustration and Computer Graphics Departments
S. Tullar and the Production Department

J. Stikar (compilation of PA Peer Review Panel comments)

PREFACE

This volume documents the data and other pertinent information used by the Performance Assessment (PA) Division of Sandia National Laboratories in its 1991 preliminary comparison of the Waste Isolation Pilot Plant (WIPP) with the Environmental Protection Agency's (EPA's) *Environmental Standards for the Management and Disposal of Spent Nuclear Fuel, High-Level, and Transuranic Radioactive Wastes (40 CFR 191).*

Besides the DOE project office in Carlsbad, New Mexico, which oversees the project, the WIPP currently has two major participants: Sandia National Laboratories in Albuquerque, New Mexico, which functions as scientific investigator; and Westinghouse Electric Company, which is responsible for the management of WIPP operations. The specific tasks of Sandia are (1) characterizing the disposal system and surrounding region and responding to specific concerns of the State of New Mexico, (2) assessing the performance of the WIPP (i.e., assessing regulatory compliance with *40 CFR 191*, except the Assurance Requirements), (3) performing analytic, laboratory, field experiments, and applied research to nuclear waste disposal in salt, relevant to support tasks 1 and 2 (disposal system characterization and performance assessment), and (4) providing ad hoc scientific and engineering support (e.g., supporting environmental assessments such as Resource, Conservation, and Reentry Act (1976) and the National Environmental Policy Act (1969). This volume helps fulfill the performance assessment task.

For the performance assessment, the PA Division at Sandia maintains a data base, the secondary data base, which contains interpreted data from many primary sources. The data are used to form a conceptual model of the WIPP disposal system. The secondary data base provides a set of parameter values (median, range, and distribution type where appropriate) and the source of these values. As better information becomes available, the parameter values reported herein will be updated. Thus, this volume is only a snapshot of the data in the secondary data base compiled as of August 1991. At a minimum, updated data reports will be issued annually as a separate volume of the *Preliminary Comparison with 40 CFR Part 191, Subpart B for the Waste Isolation Pilot Plant.* A previous data report was published in December 1990 (Rechard et al., 1990a).

The 1991 comparison and background information on the comparison are reported in Volumes 1, 2, and 4 of this report:

> SNL (Sandia National Laboratories) WIPP Performance Assessment Division. 1991. *Preliminary Comparison with 40 CFR Part 191, Subpart B for the Waste Isolation Pilot Plant, December 1991—Volume 1: Methodology and Results.* SAND91-0893/1. Albuquerque, NM: Sandia National Laboratories.
>
> SNL (Sandia National Laboratories) WIPP Performance Assessment Division. 1991. *Preliminary Comparison with 40 CFR Part 191, Subpart B for the Waste Isolation Pilot Plant, December 1991—Volume 2: Probability and Consequence Modeling.* SAND91-0893/2. Albuquerque, NM: Sandia National Laboratories.

SNL (Sandia National Laboratories) WIPP Performance Assessment Division. 1991. *Preliminary Comparison with 40 CFR Part 191, Subpart B for the Waste Isolation Pilot Plant, December 1991—Volume 4: Sensitivity Analyses.* SAND91-0893/4. Albuquerque, NM: Sandia National Laboratories. (In preparation)

Other compilations of data used by the WIPP Project are reported in:

Bayley, S. G., M. D. Siegel, M. Moore, and S. Faith. 1990. *Sandia Sorption Data Management System Version 2 (SSDMSII).* SAND89-0371. Albuquerque, NM: Sandia National Laboratories.

Krieg, R. D. 1984. *Reference Stratigraphy and Rock Properties for the Waste Isolation Pilot Plant (WIPP) Project.* SAND83-1908. Albuquerque, NM: Sandia National Laboratories.

Munson, D. E., J. R. Ball, and R. L. Jones. 1990a. "Data Quality Assurance Controls through the WIPP In Situ Data Acquisition, Analysis, and Management System" in *Proceedings of the International High-Level Radioactive Waste Management Conference, Las Vegas, NV, April 8-12.* Sponsored by American Nuclear Society and ASCE, New York, p. 1337-1350.

Providing the data as ranges and distributions to the PA Division is a major task. Although the PA Division is responsible for comparing the WIPP with *40 CFR 191, Subpart B*, the majority of data used for these comparisons is supplied by experimenters and analysts characterizing the disposal system and surrounding regional geology as noted in the acknowledgments.

In addition to individual contributors who established current data (and are listed in Appendix A of this volume), earlier contributors are also acknowledged. Much of the data provided prior to 1991 is summarized in *Systems Analysis Long-Term Radionuclide Transport, and Dose Assessments, Waste Isolation Pilot Plant (WIPP), Southeastern New Mexico; March 1989*, edited by Lappin et al. (1989). Because of this report's wide circulation, we found it convenient to refer to this report as a data source, although in many cases it only summarizes others' work. Its selection as a source is not meant to diminish the contributions of the original authors. However, Lappin et al. (1989) is the first report in which ranges were assigned for many parameters, so it does provide a primary reference for these ranges. Furthermore, some of the data has not yet been published and thus Lappin et al. (1989) may be the only source until the reports are complete.

We appreciate the time and suggestions supplied by the final peer reviewers: T. F. Corbet (6344) and A. M. LaVenue (INTERA, Inc.). Furthermore, K. Byle's and J. C. Logothetis' (New Mexico Engineering Research Institute) efforts in producing the tables and distribution figures, respectively, from the PA secondary data base for this report are greatly appreciated. In addition, the editorial help on the text and over 140 illustrations provided respectively by J. Chapman and D. Pulliam of Tech Reps, Inc., Albuquerque, New Mexico, greatly improved the report.

CONTENTS

FIGURES

TABLES

1. INTRODUCTION

1.1 Purpose and Organization of Report

The purpose of this volume is to present data and information compiled and available in August 1991 for use by the Performance Assessment (PA) Division of Sandia National Laboratories in its 1991 evaluation of the long-term performance ("performance assessment") of the Waste Isolation Pilot Plant (WIPP). The data are critical for generating a well-founded and defensible analysis. In this volume, performance assessment refers to the prediction of all long-term performance. For example, the data compiled can be used to compare WIPP performance with the requirements of the Environmental Protection Agency's (EPA's) *Environmental Standards for the Management and Disposal of Spent Nuclear Fuel, High-Level, and Transuranic Radioactive Wastes (40 CFR 191)*, with long-term safety goals for individual exposure (doses) which may be necessary for environmental impact statements (National Environmental Policy Act [NEPA, 1969]), and with hazardous waste regulations (Resource, Conservation, Recovery Act of 1976 [RCRA, 1976]).

About 300 distinct parameters are listed in this report for use in the consequence and probability models used in simulations of the WIPP. Most of these parameters specify the physical, chemical, or hydrologic properties of the rock formations (geologic barriers) in which the WIPP is placed; a substantial number of the parameters specify physical, chemical, or hydrologic properties of the seals, backfill, and waste form (engineered barriers); and some pertain to future climatic variability or future episodes of exploratory drilling at the WIPP. Dimensions of selected engineered features of the WIPP underground facility are also listed, although these dimensions are not counted as part of the 300 parameters.

The EPA Standard, *40 CFR 191*, explicitly acknowledges the uncertainties associated with scientific predictions, especially when predictions cover thousands of years, and mandates that this uncertainty be reported when making comparisons with *40 CFR 191*. One of several sources of uncertainty in scientific predictions is uncertainty in the data; consequently, this report not only tabulates median values and sources for these values but also lists estimates of the range and distribution (uncertainty) of the parameters. A brief discussion accompanies each parameter description.

The organization of this volume is as follows:

- The remainder of Chapter 1 presents conventions used in the data tables, and background information on the selection of distributions, performance assessments, and the WIPP. Chapter 1 is arranged so that information specific to the data is presented first, followed by more general information (e.g., background on the WIPP)

- Chapter 2 provides consequence-model parameters for geologic barriers

- Chapter 3 provides consequence-model parameters for the engineered barriers
- Chapter 4 provides consequence-model parameters for global materials such as fluid properties (e.g., Salado Formation brine compressibility) and properties of agents that act upon the WIPP disposal system such as climate variability and human-intrusion boreholes
- Chapter 5 provides probability model parameters for scenario-probability estimation
- Chapter 6 lists the specific parameters that were varied for the December 1991 preliminary comparison of the WIPP with *40 CFR 191*
- Appendices A and B provide endorsements of the data currently in use and tabulated data from numerous wells near the disposal system
- Following the cited references is a table of conversion factors between SI and common English units; a glossary of terms; and a list of variables, acronyms, and initialisms.

1.2 Conventions

Chapters 2 through 5 provide the data that make up the 1991 conceptual model of the WIPP. The tables in these chapters list modeling parameters by their median (x_{50}), range (a,b), units, distribution type, and data source. Plots of both probability and cumulative distribution functions (pdfs and cdfs) of these parameters depict the mean ($\bar{x}$) and median (x_{50}). These terms are defined below.

1.2.1 Median

The median (x_{50}), a measure of the central tendency of the distribution, represents the value in the cumulative distribution function (cdf) of the parameter that occupies the position at which 50% of the data lie above and below it (i.e., 0.5 quantile).

1.2.2 Mean

The mean ($\bar{x}$), another measure of the central tendency of the distribution, is the expected value (E) (first moment about the origin) of the x-variable with respect to a continuous or discrete probability distribution function (pdf).

$$\bar{x} = \int_{-\infty}^{\infty} f(x)dx \sim \sum_{\text{all } x} x_i f(x)_i = E(x) \qquad (1.2\text{-}1)$$

Because the mean is strongly influenced by the tails of the distribution, it is not tabulated; however, it is shown on plots of cdfs.

The sample mean, also denoted by $\bar{x}$, is the arithmetic average of sample data pertaining to a modeling parameter.

1.2.3 Range

The range of a distribution, (a,b), is the pair of numbers in which a and b are respectively the minimum and the maximum values that are taken by the random variable x.

Continuous Distribution

For PA work, continuous distributions with range $(-\infty,+\infty)$(e.g., the normal distribution) are truncated at the 0.01 and 0.99 quantiles.

Constructed Distribution (Empirical)

Empirical distributions, cdfs and pdfs, are constructed from sets of measurements of a variable. Empirical cdfs are represented by histograms, which are piecewise constant functions based on the empirical percentiles derived from a set of measurements; an empirical cdf constructed in this way is an unbiased estimator of the unknown cdf associated with the variable (Blom, 1989, p. 216). The PA Division may modify empirical distributions in one or more of the four ways described below.

(1) Since the range of measurements in a data set may not reflect the true range of the random variable underlying the measurements, the PA Division may estimate the range by $\bar{x} + 2.33s$, where $\bar{x}$ is the *sample* mean and s is the *sample* standard deviation. (The lower limit of this estimate is not allowed to be less than zero for an intrinsically positive variable: both the upper and lower limit are not allowed to exceed physical limits.) This estimate of range is justified by the fact that the indicated end-points are estimates of the 0.01 and 0.99 quantiles if the variable is normally distributed. If the variable is not normally distributed, the quantiles will differ in inessential ways (Table 1.2-1). For any distribution with finite mean and variance, Chebyshev's inequality states that the probability that the random variable x lies outside the interval $(\bar{x} - hs, \bar{x} + hs)$, $h > 0$, is a quantity less than $1/h^2$ (Blom, 1989, p. 121); i.e.,

$$P(|x - \bar{x}| \geq hs) \leq \frac{1}{h^2} \qquad (1.2\text{-}2)$$

If the pdf of the unknown distribution is known to be unimodal and symmetric about the mean value, then the right-hand side of Eq. 1.2-2 can be replaced with $4/(9h^2)$ (Gauss' inequality); i.e.,

$$P(|x - \bar{x}| \geq hs) \leq \frac{4}{9h^2} \qquad (1.2\text{-}3)$$

(2) If only two data points are available, the PA Division may estimate the range by $(\bar{x} \pm \sqrt{3}s)$ (see uniform distribution, Table 1.2-2).

Table 1.2-1. Probability of Parameters Lying within Range Defined by $\bar{x} \pm hs$ (after Harr, 1987, Table 1.8.2)

h	Chebyshev's Inequality	Gauss' Inequality	Exponential pdf	Normal pdf	Uniform pdf
1	0	0.56	0.86	0.68	0.58
2	0.75	0.89	0.95	0.96	1.00
2.33	0.82	0.92	0.964	0.9901	1.00
3	0.89	0.95	0.982	0.9973	1.00
4	0.94	0.97	0.993	0.99993	1.00

(3) Empirical cdfs for intrinsically continuous variables are always converted to piecewise linear cdfs by joining the empirical percentile points (including extrapolated end points) with straight lines in linear space (Tierney, 1990a, p. II-5). (Cumulative distribution functions in log space will be piecewise exponential.)

Constructed Distribution (Subjective)

Subjective distributions are histograms constructed from subjective estimates of range (the 0 and 1.0 quartiles) and at least one interior quartile (usually the 0.5 quartile) provided by experts in the subject matter of the variable of concern. The subjective cdf of an intrinsically continuous variable is always converted to a piecewise linear cdf by joining the subjective quartile points with straight lines in linear space (not log space). (Cumulative distribution functions in log space will be piecewise exponential.)

Variance and Coefficient of Variation

The variance, s^2, a measure of the width of a distribution, is the expected value of the square of the difference of the variable and its mean value (i.e., the second moment about the mean):

$$s^2 = \int_{-\infty}^{\infty} (x - \bar{x})^2 f(x)dx, \text{ or } s^2 = \sum_i (x_i - \bar{x})^2 f(x_i) \qquad (1.2\text{-}4)$$

The standard deviation, s, is the positive square root of the variance. The coefficient of variation, $s/\bar{x}$, is the ratio of the standard deviation to the mean value. The sample variance of a set of measurements of the x-variable, say x_1, x_2, x_3, ..., x_n, is the sum

$$\frac{1}{(N-1)} \sum_{n=1}^{N} (x_n - [\text{sample mean}])^2$$

The sample variance is an unbiased estimator of the variance (Blom, 1989, p. 197).

Table 1.2-2 Description of Several Probability Distributions

Probability Density Function f(x)	Cumulative Distribution Function F(x)	Expected Value μ	Variance σ^2
1. Beta $\frac{1}{B(\alpha,\lambda)} \frac{(x-a)^{\alpha-1} (b-x)^{\lambda-1}}{(b-a)^{\alpha+\lambda-2}}$ $a < x < b,\ \alpha > 0,\ \lambda > 0$ where $B(\alpha,\lambda) = \frac{\Gamma(\alpha)\,\Gamma(\lambda)}{\Gamma(\alpha+\lambda)}$ and $\Gamma(\gamma) = \int_0^\infty x^{\gamma-1} e^{-x} dx$ $= \frac{\alpha!\,\lambda!}{(\alpha+\lambda-1)!}$ if α and λ are integers	$\int_a^x f(\chi)\, d\chi$	$a = \frac{\alpha}{\alpha+\lambda}$	$\frac{(b-a)^2\,\alpha\lambda}{(\alpha+\lambda)^2(\alpha+\lambda+1)}$
2. Gamma $\frac{\lambda^\alpha x^{\alpha-1} e^{-\lambda x}}{\Gamma(\alpha)}$	$\int_0^x f(\chi) d\chi$	$\frac{\alpha}{\lambda}$	$\frac{\alpha}{\lambda^2}$
3. Exponential $\lambda e^{-\lambda x}$ $x \geq 0$	$1-e^{-\lambda x}$	$\frac{1}{\lambda}$	$\frac{1}{\lambda^2}$

Table 1.2-2 Description of Several Probability Distributions (Continued)

Probability Density Function f(x)	Cumulative Distribution Function F(x)	Expected Value μ	Variance σ^2
4. Normal $N(\mu, \sigma^2)$			
$\frac{1}{\sigma\sqrt{2\pi}} \exp\left[-\frac{(x-\mu)^2}{2\sigma^2}\right]$	$\int_{-\infty}^{x} f(\chi)d\chi$	μ	σ^2
$-\infty \le x \le \infty$			
but for WIPP PA			
$a \le x \le b$ where $P(x>a) = 0.99$ and $P(x>b) = 0.01$		$\mu = \frac{a+b}{2}$	$\left(\frac{b-a}{4.66}\right)^2$
5. Lognormal		$\exp\left[\mu(y) + \frac{\sigma^2(y)}{2}\right]$	
$\frac{1}{\sigma x\sqrt{2\pi}} \exp\left[-\frac{1}{2\sigma^2}(\ln x-\mu)^2\right]$	$\int_{o}^{x} f(\chi)d\chi$	Median $= e^{\mu(y)}$	$e^{2\mu(y)+\sigma^2(y)}\left(e^{\sigma^2(y)} - 1\right)$
$x \ge 0$			
$x = e^{y}$ where $y = N(\mu, \sigma^2)$			
but for WIPP PA			
$P(y>a) = 0.99$ and			
$P(y>b) = 0.01$		$\mu(y) = \frac{a+b}{2}$	$\sigma^2(y) = \left(\frac{b-a}{4.66}\right)^2$

Table 1.2-2 Description of Several Probability Distributions (Concluded)

	Probability Density Function f(x)	Cumulative Distribution Function F(x)	Expected Value μ	Variance σ^2
6.	Uniform		$\frac{a+b}{2} = \mu$	$\frac{(b-a)^2}{12}$
	$\frac{1}{b-a}$ $a \le x \le b$	$\frac{x-a}{b-a}$	$a = \mu - \sqrt{3\sigma}$	
			$b = \mu + \sqrt{3\sigma}$	
7.	Loguniform			
	$\frac{1}{x(\ln b - \ln a)}$	$\frac{\ln x - \ln a}{\ln b - \ln a}$	$\frac{b-a}{\ln b - \ln a}$	$(b-a)\left[\frac{(\ln b - \ln a)(b+a) - 2(b-a)}{2(\ln b - \ln a)^2}\right]$
	$a < x < b$		Median $= \sqrt{ab}$	
8.	Binomial (discrete)			
	$\frac{n!}{x!(n-x)!} \rho^x \left(1-\rho\right)^{n-x}$	$\sum_{\chi=0}^{x} f(\chi)$	np	np(1-p)
	$x = 0,1,2,\ldots,N;$			
9.	Poisson (discrete)			
	$\frac{u^x e^{-\mu}}{x!}$ $x = 0,1,2,\ldots,n$	$\sum_{\chi=0}^{x} f(\chi)$	μ	μ

1.2.4 Units

The units indicate how the parameter is expressed quantitatively. Only SI units are used in the tables and the PA secondary data base (except for radionuclide inventory activity, which is expressed in curies since EPA release limits for *40 CFR 191* are expressed in curies). However equivalent values in English units are given in the text. In addition, conversion factors for SI and English units are listed at the end of the report.

1.2.5 Distribution Type

The distribution types listed in the tables are grouped into four major categories (Table 1.2-2):

1. Continuous pdf: beta, normal, lognormal, uniform, or loguniform (Figure 1.2-1a)

2. Discrete pdf: Poisson (Figure 1.2-1b)

3. Constructed distributions: a piecewise linear cdf designated as "cumulative" (subjective); a piecewise uniform pdf designated as "data" or a piecewise uniform cdf designated as "delta" (Figure 1.2-1b)

4. Miscellaneous categories (null distributions): constant, spatial, and table.

The figures in the text emphasize the cdf of the distribution--the form of the distribution from which samples are taken; however, the pdf of the distribution is also shown.

Continuous Probability Density Functions

Five continuous pdfs are described below:

Beta. Beta designates the beta pdf, which is a versatile density function specified by two parameters (α, λ) that can assume numerous shapes in a specified range (a,b) (Harr, 1987, p. 79; Johnson and Kotz, 1970b, p. 37; Miller and Freund, 1977, p. 119).

Normal. Normal designates the normal pdf, a good approximation of many physical parameters. Most arguments for the use of the normal distribution are based on the central limit theorem (Miller and Freund, 1977, p. 104; Johnson and Kotz, 1970a, p. 40). The distribution is truncated at the 0.01 and 0.99 quantiles (i.e., the probability that the parameter will be smaller or larger is 1%), which corresponds to $\bar{x} \pm 2.33s$.

Lognormal. Lognormal designates a lognormal pdf, a distribution of a variable whose logarithm follows a normal distribution. The distribution is truncated at the 0.01 and 0.99 quantiles.

Uniform. Uniform designates a pdf that is constant in the interval (a,b) and zero outside of that interval.

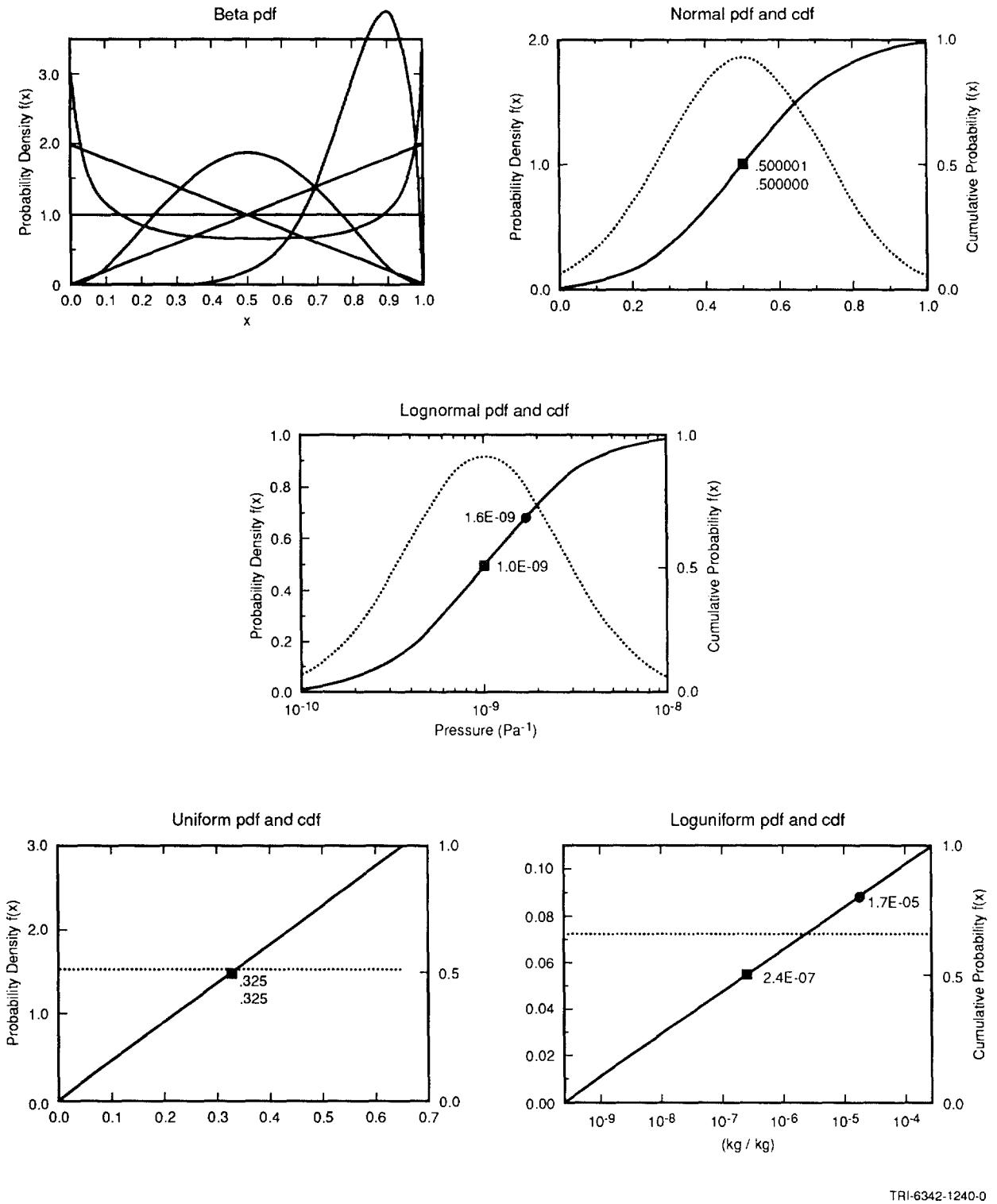

(a) Continuous Distribution Plots

Figure 1.2-1. Examples of Distribution Plots

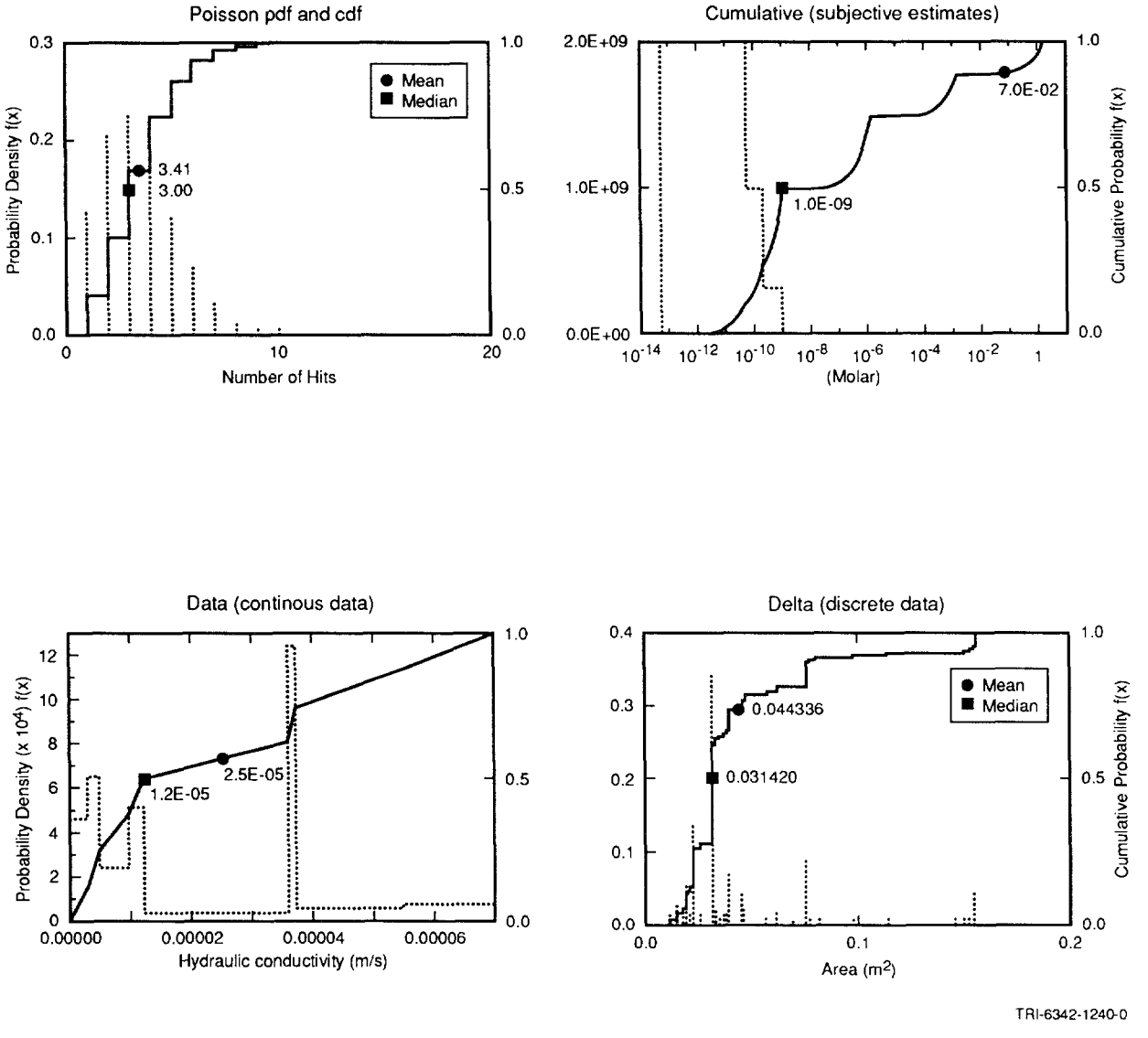

(b) Discrete and Constructed Distribution Plots

Figure 1.2-1. Examples of Distribution Plots (Concluded)

Loguniform. Loguniform designates a loguniform pdf, a distribution of a variable whose logarithm follows a uniform distribution.

Discrete Probability Density Function

One discrete probability density function, the Poisson, was used.

Poisson. Poisson designates a discrete Poisson pdf. The Poisson pdf is often used to model processes taking place over continuous intervals of time such as the arrival of telephone calls at a switch station (queuing problem) or the number of imperfections continuously produced in a bolt of cloth. The Poisson pdf is used in the probability model for human intrusion by exploratory drilling.

Constructed Distributions

The cumulative, data, and delta distributions are described below:

Cumulative. The cumulative distribution type refers to the piecewise linear cdf constructed by linearly connecting subjective point estimates of the distribution percentiles supplied by experts (Tierney, 1990a, Section 3.1). Distributions are stored in the secondary data base as a cdf when the distribution is subjectively estimated from sparse or no data. Plots of the subjectively estimated distributions show a corresponding piecewise uniform pdf, but the pdf is not used for calculations.

Data. The data distribution type indicates an empirical distribution (i.e., measured data points are stored in the data base and used to form the distribution). The pdf is piecewise uniform; the cdf, which is constructed from this data for purposes of Monte Carlo sampling, is piecewise linear (see Cumulative). However, the name indicates that the distribution is based on empirical information rather than subjective estimates.

Delta. The delta distribution type refers to a pdf where parameters must be assigned discrete values (i.e., the pdf is a series of dirac delta functions ($\Sigma\ \delta(x_i-x)$); the cdf is a series of step functions). As an example, in the 1990 preliminary comparison (Bertram-Howery et al., 1990) the drill-bit diameters used for the human-intrusion borehole were not assumed to vary continuously between the minimum and maximum drill bit sizes, but were fixed at diameters of bits that are actually available.

Miscellaneous Categories

The constant, spatial, and table distributions are described below:

Constant. When a distribution type is listed as constant, a distribution has not been assigned and a constant value is used in all PA calculations.

Spatial. The spatial category of data indicates that the parameter varies spatially. This spatial variation is shown on an accompanying figure. The median value recorded is a typical value for simulations that use the parameter as a lumped parameter in a model; however, the value varies depending upon the scale of the model. The range of a spatially varying parameter is also scale dependent.

Table. The table category of data indicates that the parameter varies with another property and the result is a tabulated value. For example, relative permeability varies with saturation; its distribution type is listed as table (also, the median value is not meaningful and is therefore omitted in the table).

Note on Correlations. Most of the uncertain variables studied during the 1991 PA calculations were assumed to be independent random variables, although it was known some were interdependent, i.e., correlated in some way. Correlations of the model variables may arise from the fact that there are natural correlations between the local quantities used to determine the form of the model variable (e.g., local porosity could be strongly correlated with local permeability); or correlations of model variables may be implicit in the form of the mathematical model in which they are used.

1.2.6 Sources

The source indicates the document in which the parameter value is cited. Several sources are cited when one source cannot supply all the data or information (e.g., median, range, distribution type, or explanatory information).

1.2.7 Note on Unnecessary Conservatism of Material-Property Parameters

The following arguments attempt to show why some of the current assignments of probability distributions to material-property parameters of WIPP performance models are unnecessarily conservative, given the present level of detail and spatial resolution of the models. Current methods of assigning uncertainty to some of the material-property parameters (e.g., including small-scale spatial variability as a source of uncertainty) may distort results of sensitivity analyses performed to identify those important model variables that are material-property parameters and result in unnecessary expense, but will probably not affect validity of results of the uncertainty analyses that are used to make preliminary comparisons with EPA standards.

WIPP performance models described in Volume 2 of this report are based on the numerical solution of one or more of three types of equations:

(a) Partial differential equations - which are reduced to a set of algebraic equations or ordinary differential equations in order to effect a solution by finite-difference or finite-element methods. Examples: the equations of groundwater and brine flow, solute transport, gas flow, and salt creep.

(b) Ordinary differential equations - which may be the result of a reduction of a partial differential equation or may directly model the dynamics of a lumped-parameter system, e.g., punctured brine reservoirs, leaching and decay of radioactive waste stored in a panel.

(c) Algebraic equations of the form

$$F(x_1, x_2, x_3, ..., x_n; y) = 0$$

which may arise indirectly from equilibrium solutions of ordinary differential equations (i.e., solutions for time $\rightarrow \infty$) or may directly express a model of some physical relationship between WIPP performance-model variables (x_1, x_2, x_3, ..., x_n) and y.

In addition to dependent variables and independent variables of position and time, certain constants, or free parameters, will appear in each of the three types of equations. In most cases, these free parameters are intended to represent physical and chemical properties of real materials of the WIPP system: e.g., the hydraulic conductivity, porosity, and specific storage in models of fluid flow in the Salado Fm.; the fracture spacing, dispersivity, diffusivity, and chemical distribution coefficients in models of solute transport in the Culebra Fm.; the porosity, permeability and solubility of waste forms emplaced in a typical WIPP panel. This kind of free parameter will be called a material-property parameter in the remainder of this note.

Many of the material-property parameters of WIPP performance models were included in the set of uncertain variables that was sampled in a recent study of variable sensitivity of performance models (Helton et al., 1991) and in a recent preliminary assessment of WIPP system performance (Rechard et al., 1990a). (Note: In these two reports, all uncertain model parameters were usually called "variables" or "independent variables.") In these studies, uncertainty associated with a sampled variable was quantified by assigning an empirical or subjective probability distribution to the values taken on by that variable within a predetermined range of values. Current procedures for the assignment of probability distributions are described in Section 3.1 of Tierney (1990a); these procedures include construction of empirical cumulative distribution functions (cdfs) from data sets or, if there is little or no data, construction of cdfs from subjective quantiles obtained by elicitation of expert opinion. Tierney (1990a; Chapter III) also briefly noted the problems involved in scaling uncertainty from measured data to model parameters and he suggested some rules for estimating the mean and variance of a material-property parameter using the sample mean and variance of a set of measurements of the material property.

The distribution of a material-property parameter needs to reflect spatial variability of the material property and also the scale of the model. The zones or cells of numerical models (finite-element, finite-difference, or lumped-parameter models) must be few in number in order to minimize computational time and expense; in a typical problem involving geologic media, these cells will have dimensions of tens of meters or more and volumes of thousands

of cubic meters. Material-property parameters must therefore represent the effects of a physical or chemical property of matter in these relatively large, arbitrarily defined volumes of space. It follows that material-property parameters are model dependent and usually not observable quantities, i.e., quantities that can be measured in the field or in the laboratory. On the other hand, with few exceptions (e.g., formation transmissivity measured by pumping tests) most physical and chemical properties of geologic or anthropogenic materials are actually measured on spatial scales typical of the laboratory or an exploratory borehole, a matter of at most a few tens of centimeters. In addition, natural materials and many man-made materials (e.g., defense waste) tend to be inhomogeneous on spatial scales characteristic of model cell sizes; accordingly, a set of measurements of a material property taken randomly from large volumes of real material may show wide variability. The question is: How to assign values to material-property parameters in a way that correctly reflects both cell size and the small-scale variability that may appear in measurements of the corresponding material property?

To begin to answer this question, assume that the material property can be represented as a scalar field in space, say $\phi(\mathbf{x})$, where $\mathbf{x} = (x,y,z)$ denotes position in space. (The assumptions of a scalar quantity in three dimensions are for the sake of simplicity of argument and involve no loss of generality; the property could be a vector or tensor.) It is argued in some modern textbooks that the material-property parameter, say Φ, to be used in type (a) equations (above) should be taken as a spatial average of ϕ over the cell or zone; for instance, in a cell or zone of volume V,

$$\Phi(V) = \frac{1}{V} \int_V \phi\ (\mathbf{x})\ d\mathbf{x} \qquad (1.2\text{-}5)$$

where dx is the volume element dxdydz. (Again, no loss of generality is involved; a line or surface average could replace the volume average.) The arguments for this choice of material-property parameter are highly technical and limitations of time and space preclude their inclusion in this note; however, see the discussion in de Marsily (1986, Chapter 3 and Section 4.4).

To account for spatial variability of $\phi(\mathbf{x})$, it can be assumed that ϕ is a *stationary, random scalar field* within a cell volume V, with realizations $\phi(\mathbf{x},\mu)$ and the following statistical properties:

$$\text{Expectation of } \phi(\mathbf{x},\mu) = E[\phi(\mathbf{x})] = \bar{\phi}, \text{ a constant,} \qquad (1.2\text{-}6)$$

and

$$\begin{aligned}\text{Covariance of } \phi(\mathbf{x},\mu) &= E\{[\phi(\mathbf{x}) - \bar{\phi}][\phi(\mathbf{y}) - \bar{\phi}]\} \\ &= \sigma^2 \rho(|\mathbf{x} - \mathbf{y}|),\end{aligned} \qquad (1.2\text{-}7)$$

where σ^2 is a constant (called the variance of ϕ), and $\rho(\bullet)$ is a function of $r = |x - y|$ with the properties

$$\begin{aligned} &\rho(r) \geq 0 \text{ for } r \in (0,\infty), \\ &\rho(r) \to 1 \text{ as } r \to 0 \\ &\rho(r) \to 0 \text{ as } r \to \infty. \end{aligned} \tag{1.2-8}$$

The function $\rho(\bullet)$ is called the autocorrelation function (Yaglom, 1962); it is a measure of the statistical dependence of the values of ϕ measured at two different points x and y. The assumptions of constant mean value $\bar{\phi}$ and variance σ^2 can be slightly weakened by allowing these quantities to depend on the coordinates of the center of the volume V; i.e., $\bar{\phi}$ and σ^2 may vary from cell to cell.

Treating $\phi(x)$ as a stationary random field with statistical properties 1.2-6 through 1.2-8 allows estimates of the mean value and variance of the volume average of ϕ, $\Phi(V)$, to be made. It is shown in many textbooks (see for instance Yaglom, 1962, pgs. 23-24) that

$$\text{Expectation of } \Phi(V) = E[\Phi(V)] = \bar{\phi}, \tag{1.2-9}$$

and

$$\text{Variance of } \Phi(V) = \frac{\sigma^2}{V^2} \int_V \int_V \rho(|x - y|)\, dx\, dy. \tag{1.2-10}$$

If $\bar{\phi}$, σ^2 and $\rho(r)$ were known, the problem would be essentially solved in that the distribution of the material-property parameter, $\Phi(V)$, could be approximated by a normal distribution with mean and variance given respectively by Eqs. 1.2-9 and 1.2-10. In general, $\bar{\phi}$, σ^2 and the function $\rho(r)$ must be estimated using sets of measurements of the material property ϕ, say $(\phi_1, \phi_2, \ldots, \phi_N)$. The estimators of $\bar{\phi}$ and σ^2 are the usual unbiased estimators of mean and variance (see Tierney, 1990a, pp. II-4,5) and, given a sufficiently large set of spatially coordinated measurements of ϕ, approximations to the autocorrelation function could be constructed and used in the numerical evaluation of the volume integrals in Eq. 1.2-10. This ideal solution to the problem cannot be implemented, however, since there are few measurements of the material properties appearing in WIPP performance models (and most are not spatially indexed; measured transmissivity, grain density, porosity, and tortuosity of the Culebra Formation are exceptions). Thus, one must try to use available measurements and insight to infer the statistical properties, given by Eqs. 1.2-9 and 1.2-10, of material-property parameters $\Phi(V)$. The following observations may be useful in inferring statistical properties of material-property parameters.

(1) The variance of a material-property parameter is less than or equal to the apparent variance of the material property. Note that because of the properties of $\rho(r)$ (Eq. 1.2-8), the integrand in the double volume integral of Eq. 1.2-10 is always less than one so that

$$\text{Variance of } \Phi(V) \leq \sigma^2.$$

In particular, if we take the special form of autocorrelation function ("cookie cutter"),

$$\rho(|\mathbf{x} - \mathbf{y}|) = 1 \text{ if } |\mathbf{x} - \mathbf{y}| \leq a,$$
$$= 0 \text{ otherwise,} \qquad (1.2\text{-}11)$$

then

$$\text{Variance of } \Phi(V) \approx \frac{v}{V}\,\sigma^2 \qquad (1.2\text{-}12)$$

where $v = \frac{4\pi}{3}\,a^3$ can be called the *volume of correlation*. Equation 1.2-12 suggests that if the volume of correlation is <<V, then the distribution of $\Phi(V)$ is peaked about the mean value of the material property, $\overline{\phi}$. If the coefficient of variation of the material property, $\sigma/\overline{\phi}$, is not large (say, of the order of one), the distribution of $\Phi(V)$ is more sharply peaked about the mean value, $\overline{\phi}$, than is the distribution of the material property, $\phi(\mathbf{x})$. If this tendency is strong enough, then $\Phi(V)$ can simply be assigned the mean value,

$$\Phi(V) \approx \overline{\phi}$$

This is what is usually done in studies with numerical models that are not probabilistic; that is, not directed explicitly towards sensitivity and uncertainty analyses.

(2) If, as suggested above, $\Phi(V) \approx \overline{\phi}$, then one must consider the uncertainty inherent in estimating the mean value $\overline{\phi}$ that arises from (a) a limited number of measurements of the material property, and (b) relationships between $\overline{\phi}$ and other uncertain problem parameters. Uncertainty of type (a) can be handled by fitting available data to a "t-distribution" (Blom, 1989) which, in a Bayesian approach, gives the distribution of the true mean of the material property about the sample mean of measurements. However, this was not done in assigning ranges to parameters and thus introduces conservatism. Uncertainty of type (b) is model dependent and must be handled on a case-by-case basis.

The standard techniques of statistical estimation cannot be directly applied when the distribution of the material property, $\phi(\mathbf{x})$, must be gained by subjective means, i.e., the elicitation of expert judgment. In such cases, the PA Division must make the unnecessarily conservative assumption that the distribution of the material property, $\phi(\mathbf{x})$, is also the distribution of the material-property parameter, $\Phi(V)$.

1.3 Background on Selecting Parameter Distribution

1.3.1 Requests for Data from Sandia Investigators and Analysts

When evaluating long-term performance, the PA Division follows a fairly well-defined procedure for acquiring and controlling the data used in consequence and probability models. A data base, called the secondary data base, contains the interpreted data and in essence embodies the conceptual model(s) of the disposal system. The data provided in this report are from the secondary data base as of July 1991 and are used in the 1991 preliminary performance assessment of the WIPP (Volume 1 of this report).

The major sources of the data are the task leaders and investigators at Sandia and from Westinghouse.

Identify Necessary Data

Each year, the PA Division identifies data that are necessary to perform the calculations for the preliminary performance assessment. Members of the PA Division informally compile data from published reports, personal communications with investigators, and other sources.

Request Median Value and Distribution

The PA Division then requests that the investigators provide a median value and distribution for each parameter in a large subset of the parameters. Some model parameters are specific to the PA calculations and so individuals in the PA Division are considered the experts for these parameters (e.g., probability model parameters).

Initially, the investigator is responsible for providing the median value and distribution for all parameters. As this procedure for acquiring data is repeated, a few parameters are evaluated through formal elicitation.

Update Secondary Data Base

The PA Division enters the endorsed or elicited data into the secondary data base. The PA Division then selects a subset of the data to sample, keeping all other values constant at the median or mean value, unless specifically noted.

Perform Consequence Simulations and Sensitivity Analyses

The PA Division runs consequence simulations and sensitivity analyses with the selected subsets of data from the updated secondary data base. The sensitivity analysis may evaluate either or both the sensitivity and the importance of a parameter in determining variation of the result (i.e., CCDF). During this time, the PA Division prepares a report that lists the data in the secondary data base at the time of these calculations (i.e., this data report).

Determine Whether Parameter Is Important in Analysis

By means of the sensitivity analyses, the PA Division can determine whether the parameter is significant in the calculations. If the parameter does not appear to be significant in the sensitivity analyses, and the review process of the Data Report does not question the parameter value, then the parameter is flagged as not likely to change or be sampled.

1.3.2 Construction of Distributions

The steps below describe the procedure developed by the PA Division to construct probability distributions (cdfs or pdfs) for the uncertain independent variables in consequence and probability models (Figure 1.3-1) (modified from Tierney, 1990a).

Step 1

Determine whether site-specific data for the variable in question exists, i.e., find a set of site-specific sample values of the variable. Data are usually either documented in a formal report or are described in an internal memorandum (see Appendix A). If data sets exist, go to Step 3; if no data sets are found, go to Step 2.

Step 2

Request that the investigator supply a specific shape (e.g., normal, lognormal) and associated numerical parameters for the distribution of the variable. If the investigator assigns a specific shape and numerical parameters, go to Step 5; if the investigator cannot assign a specific shape and appropriate parameters, go to Step 4. In responding to this request, the investigator may use his or her knowledge of global data to form an answer.

Step 3

Determine the size of the combined data sets. If the number of values in the combined data set is >3, use the combined data to evaluate the data range as $\bar{x} \pm 2.33s$ and construct a piecewise-linear cumulative distribution function or, alternatively, a discrete cumulative distribution function, and then go to Step 5. If the number of variables in the combined data set is ≤ 3, evaluate the data range as $\bar{x} \pm \sqrt{3}s$ and go to Step 4.

Step 4

Request that the investigator provide subjective estimates of (a) the range of the variable (i.e., the minimum and maximum values taken by the variable with at least 99% confidence and preferably 100% confidence) and (b) if possible, one of the following (in decreasing order of preference): (1) percentile points for the distribution of the variable (e.g., the 25th, 50th [median], and 75th percentiles), (2) the mean value and standard deviation of the distribution, or (3) the mean value. Again, in responding to this request, the investigator may use his or her knowledge of global data to form an answer. Then, using the maximum entropy formalism (MEF), construct one of the following distributions depending upon the kind of subjective estimate that has been provided (Tierney, 1990a; Harr, 1987):

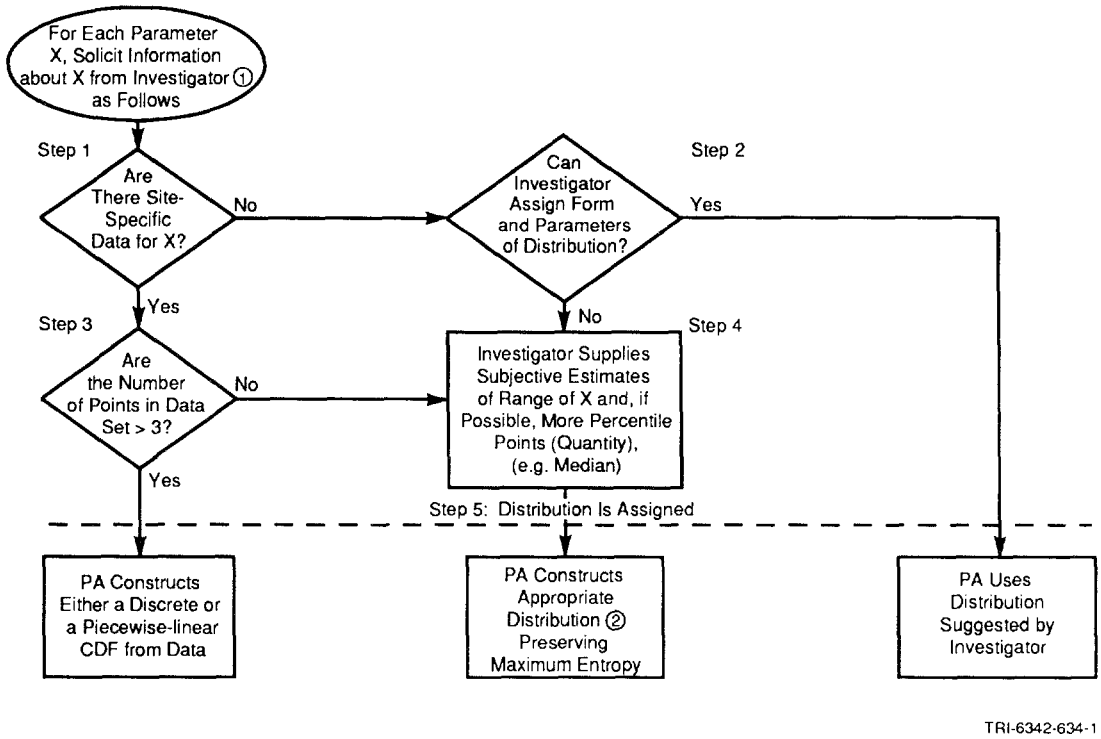

Figure 1.3-1. Five-Step Procedure Used to Construct Cumulative Distribution Functions (cdf) for the 1991 Performance Simulations. Investigator refers to expert in subject matter; MEF refers to maximum entropy formalism (after Tierney, 1990a).

- Uniform pdf over the range of the variable
- Piecewise-linear cdf based on the subjective percentiles
- Exponential pdf (truncated) based on the subjective range and mean value
- Normal pdf based on subjective mean value and standard deviation
- Beta pdf based on the subjective range, mean value, and standard deviation. (The beta distribution is not a maximum-entropy distribution under these constraints.)

Then go to Step 5.

Step 5

End of procedure; distribution is assigned. Computational restrictions may require later modification to some distributions and are discussed with each parameter.

1.3.3 Selection of Parameters for Sampling

For the 1991 preliminary performance assessment of the WIPP, the 45 parameters that were selected for variation (sampling) together with a brief description of why they were selected are discussed in Chapter 6. Other studies on subsystems of the WIPP disposal system (e.g., sensitivity of the repository to gas generation) may use different subsets of the approximately 300 parameters for which distributions are reported herein.

1.3.4 Elicitation of Distributions from Experts

This section discusses formal elicitation of probability distributions for model parameters that are uncertain and are considered significant in the performance assessment (e.g., estimate of radionuclide concentration in the disposal region [Trauth et al., 1991]). Formal elicitation is also being used in the performance assessment of the WIPP to hypothesize about possible futures of society and the effects of appropriate markers to warn future societies about the WIPP; these elicitation efforts are discussed elsewhere (Hora et al., 1991).

In all aspects of data gathering, professional judgment (i.e., opinion) must bridge the gaps in knowledge that invariably exist in scientific explanations. For example, the selection of methods to collect data (characterizing a site), interpretation of data, development of conceptual models, and selection of model parameters all require professional judgment by the investigator. This volume summarizes these judgments.

When data are lacking, either because of the complexity of processes or the time and resources it would take to collect data or when data have a major impact on the performance assessment, a formal elicitation of expert judgment is pursued. The procedure has the following advantages. First, formal elicitation offers a structured procedure for gathering opinions. Second, it encourages diversity in opinions and thus guards against understating the uncertainty. Finally, it promotes clear and thorough documentation of how the results were achieved (Hora and Iman, 1989).

The judgments that result from formal elicitation are a snapshot of the current state of knowledge. As new observations are made, the state of knowledge is refined. Even though the compilation of information through formal elicitation is often enlightening and helps to prevent bias, it does not create information. An important aspect of the elicitation, which occurs either during or following the procedure, is to examine how new data collected may improve understanding.

A successful formal elicitation of expert opinion includes the following five components (Hora and Iman, 1989):

Selection of Issue and Issue Statement

The first component of the formal elicitation process is a clear statement of the issue that cannot be practically resolved by other means. For example, the issue may not be resolved

For example, the issue may not be resolved either because of time (the judgment may be a temporary solution until laboratory or field data become available) or because the complexity of the issue prevents a resolution regardless of the resources applied.

Selection of Experts

The second component is the selection of experts with the recognized training and experience to address the issue. The experts should be free from motivational biases and represent a diversity of opinions. (Experts in a subject who may be motivationally biased can give testimony to the selected expert(s) as part of the training described below.) For controversial issues, the selection may require that an external committee select individuals from a list of nominees provided by diverse groups such as universities, the government, consulting firms, and intervenor groups.

Once selected, the experts may be asked to respond to a single question individually, respond to similar questions as a group, or become part of a team of experts who are expected to fully analyze a complex problem. The strategy selected is based on the importance of the issue and the time and resources available.

Elicitation Sessions

The third component consists of the elicitation sessions. Elicitation training includes informing the experts about the methods that will be used to process and propagate their subjective beliefs, introducing the assessment tools and practicing with these tools, providing calibration training using almanac questions, and introducing the psychological aspects of probability elicitation.

At the session (or a subsequent session), the issues are presented to the analysts. Included in each presentation is a proposed decomposition of the problem. Problem decomposition improves the quality of assessments by structuring the analysis so that the expert is required to make a series of simpler assessments rather than one complex assessment. Decomposition also provides a form of self-documentation since the expert's thought process is made explicit. The elicitation sessions are led by a normative analyst (i.e., an expert trained in decision analysis). The session may include a substantive analyst, who is an expert in the subject matter under discussion.

Recomposition and Aggregation

The fourth component is the recomposition of an expert's opinions and the aggregation of the diverse opinions from several experts. The tools employed in recomposing the assessments vary from issue to issue. In most issues, however, three levels of action are required. The first level is the modification of the assessed values to obtain cumulative distribution functions for any continuous quantities. The second level of action is the recomposition of

each expert's individual assessments to obtain a recomposed distribution for the specific issue in question. The final level is the aggregation of the experts' judgments to obtain the aggregated distribution.

Documentation

The final component is documentation of the elicitation process. Documentation usually includes a record of problem decomposition, the diversity of opinion, and the recomposition and aggregation performed.

1.4 Performance-Assessment Methodology

The Containment Requirements of the Standard state that:

> Disposal systems for spent nuclear fuel or high-level or transuranic radioactive wastes shall be designed to provide a reasonable expectation, based upon performance assessments, that the cumulative releases of radionuclides to the accessible environment for 10,000 years after disposal from all significant processes and events that may affect the disposal system shall:
>
> (1) Have a likelihood of less than one chance in 10 of exceeding the quantities calculated according to Table 1 (Appendix A); and
>
> (2) Have a likelihood of less than one chance in 1,000 of exceeding ten times the quantities calculated according to Table 1 (Appendix A). (§ 191.13(a))

As defined by the Standard, the term accessible environment means "(1) the atmosphere; (2) land surfaces; (3) surface waters; (4) oceans; and (5) all of the lithosphere that is beyond the controlled area" (191.12(k)). Controlled area is defined to be "(1) a surface location, to be identified by passive institutional controls, that encompasses no more than 100 square kilometers and extends horizontally no more than 5 kilometers in any direction from the outer boundary of the original location of the radioactive wastes in a disposal system; and (2) the subsurface underlying such a surface location" (191.12(g)). Table 1 of Appendix A of the Standard, which is referred to in the preceding Containment Requirements, is reproduced here as Table 1.4-1. The complete text of the Standard is reproduced as Appendix A of Volume 1 of this report.

For releases to the accessible environment that involve a mix of radionuclides, the limits in Table 1.4-1 are used to define normalized releases for comparison with the release limits. Specifically, the normalized release for transuranic waste is defined by

$$R = \sum_{i=1}^{nR} \left[\frac{Q_i}{L_i} \right] \cdot (1 \times 10^6 \text{ Ci/C}) \qquad (1.4\text{-}1)$$

where

Table 1.4-1. Release Limits for Containment Requirements (40 CFR 191, Appendix A, Table 1)

	Release limits (L_i) per 1000 MTHM* or Other Unit of Waste (Ci)
Americium (Am) -241 or -243	100
Carbon (C) -14	100
Cesium (Cs) -135 or -137	1000
Iodine (I) -129	100
Neptunium (Np) -237	100
Plutonium (Pu) -238, -239, -240, or -242	100
Radium (Ra) -226	100
Strontium (Sr) -90	1000
Technetium (Tc) -99	10000
Thorium (Th) -230 or -232	10
Tin (Sn) -126	1000
Uranium (U) -233, -234, -235, -236, or -238	100
Any other α-emitting radionuclide with $t_{1/2}$ > 20 yr	100
Any other non α-emitting radionuclide with $t_{1/2}$ > 20 yr	1000

* Metric tons of heavy metal exposed to a burnup between 25,000 megawatt-days per metric ton of heavy metal (MWd/MTHM) and 40,000 MWd/MTHM.

nR = number of radionuclides included in the analysis,

C = amount of TRU waste with half-lives greater than 20 years (1 x 10^6 Ci/C is the reciprocal of the waste unit factor f_w used in Chapter 3) (Ci) emplaced in the repository,

Q_i = cumulative release (Ci) of radionuclide i to the accessible environment during the 10,000-yr period following closure of the repository,

and

L_i = the release limit (Ci) for radionuclide i given in Table 1.4-1.

In addition, the EPA suggests that the results of a performance assessment intended to show compliance with the release limits in § 191.13 can be assembled into a single complementary cumulative distribution function (CCDF). Specifically, the nonbinding guidance contained in Appendix B of the Standard indicates that

> ... whenever practicable, the implementing agency will assemble all of the results of the performance assessments to determine compliance with § 191.13 into a "complementary cumulative distribution function" that indicates the probability of exceeding various levels of cumulative release. When the uncertainties in parameters are considered in a performance assessment, the effects of the

uncertainties considered can be incorporated into a single such distribution function for each disposal system considered. The Agency assumes that a disposal system can be considered to be in compliance with § 191.13 if this single distribution function meets the requirements of § 191.13(a). (U.S. EPA, 1985, p. 38088).

1.4.1 Conceptual Model for WIPP Performance Assessment

Construction of a CCDF for comparison to the Standard requires a clear conceptual representation for a performance assessment. A representation based on a set of ordered triples provides a suitable way to organize a performance assessment and leads naturally to the presentation of the outcome of a performance assessment as a CCDF (Kaplan and Garrick, 1981; Helton et al., 1991; Volume 1, Chapter 3). Specifically, the outcome of a performance assessment can be represented by a set R of ordered triples of the form

$$R = \{(S_i, pS_i, \mathbf{cS}_i), i = 1, ..., nS\}, \quad (1.4\text{-}2)$$

where

S_i = a set of similar occurrences,
pS_i = probability that an occurrence in set S_i will take place,
$\mathbf{cS}_i$ = a vector of consequences associated with S_i,

and

nS = number of sets selected for consideration.

In terms of performance assessment, the S_i are scenarios, the pS_i are scenario probabilities, and the $\mathbf{cS}_i$ are vectors containing results or consequences associated with scenarios.

The information contained in the pS_i and $\mathbf{cS}_i$ shown in Eq. 1.4-2 can be summarized in CCDFs. With the assumptions that a particular consequence result **cS** (e.g., normalized release to the accessible environment) is under consideration and that the values for this result have been ordered so that $\mathbf{cS}_i$ is less than or equal to $\mathbf{cS}_{i+1}$ for i = 1,2,...,nS-1, the resultant CCDF is shown in Figure 1.4-1. As illustrated in Figure 1.4-2, the EPA containment requirement in 191.13 specifies that the CCDF for normalized release to the accessible environment should fall below a CCDF defined by the points (1, 0.1) and (10, 0.001). The vertical lines in Figure 1.4-2 have been added for visual appeal but are not really part of the CCDF. A waste disposal site can be considered to be in compliance with the EPA release limits if the CCDF for normalized release to the accessible environment falls below the bounding curve shown in Figure 1.4-2.

Since the representation for a performance assessment in Eq. 1.4-2 and the resultant CCDFs in Figures 1.4-1 and 1.4-2 involve probabilities, there must be an underlying sample space. For performance assessments conducted to provide comparisons with the EPA release limits, the sample space is the set $\mathcal{S}$ defined by

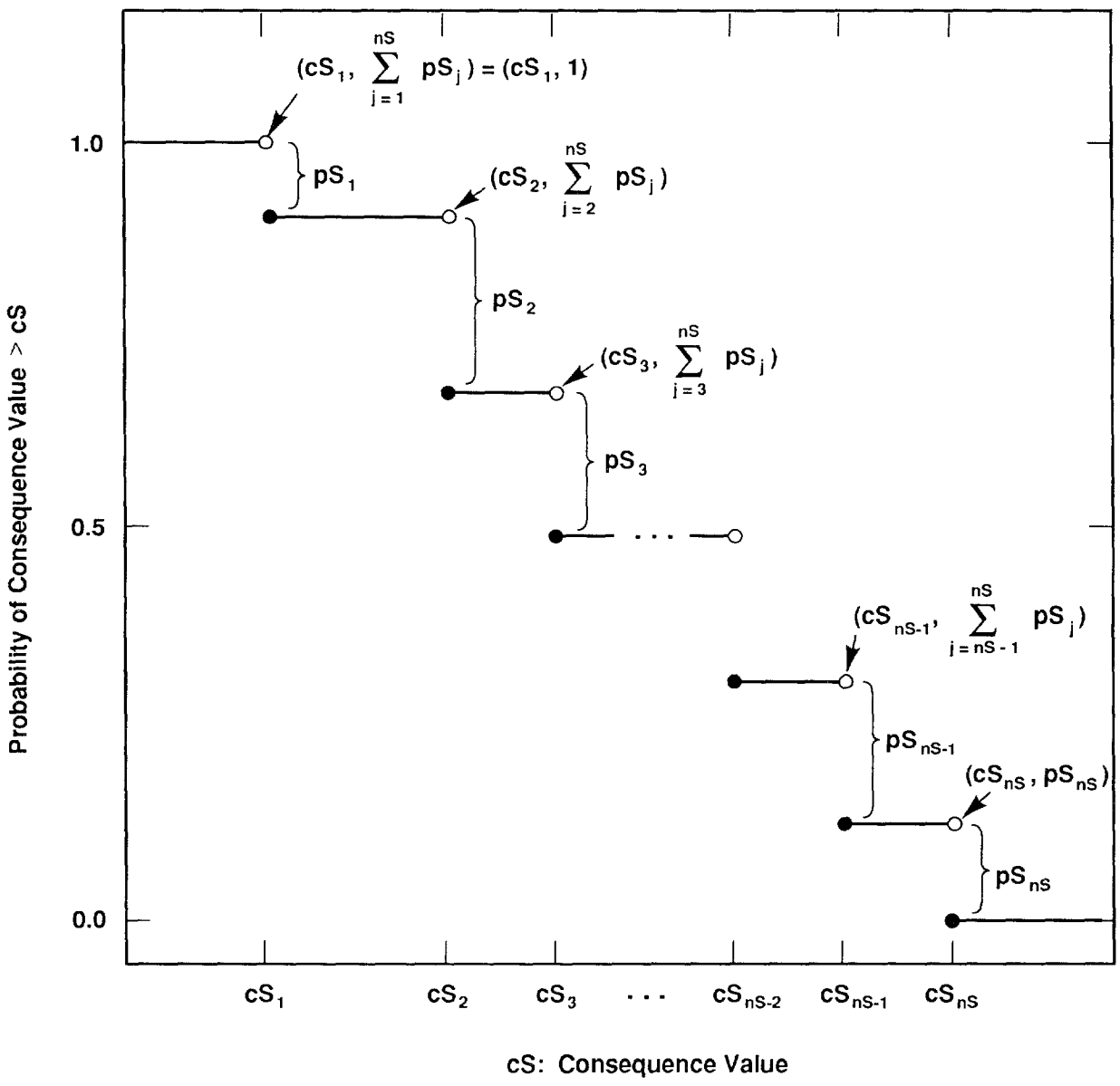

TRI-6342-730-5

Figure 1.4-1. Estimated Complementary Cumulative Distribution Function (CCDF) for Consequence Result **cS**. (Helton et al., 1991, Figure VI-1).

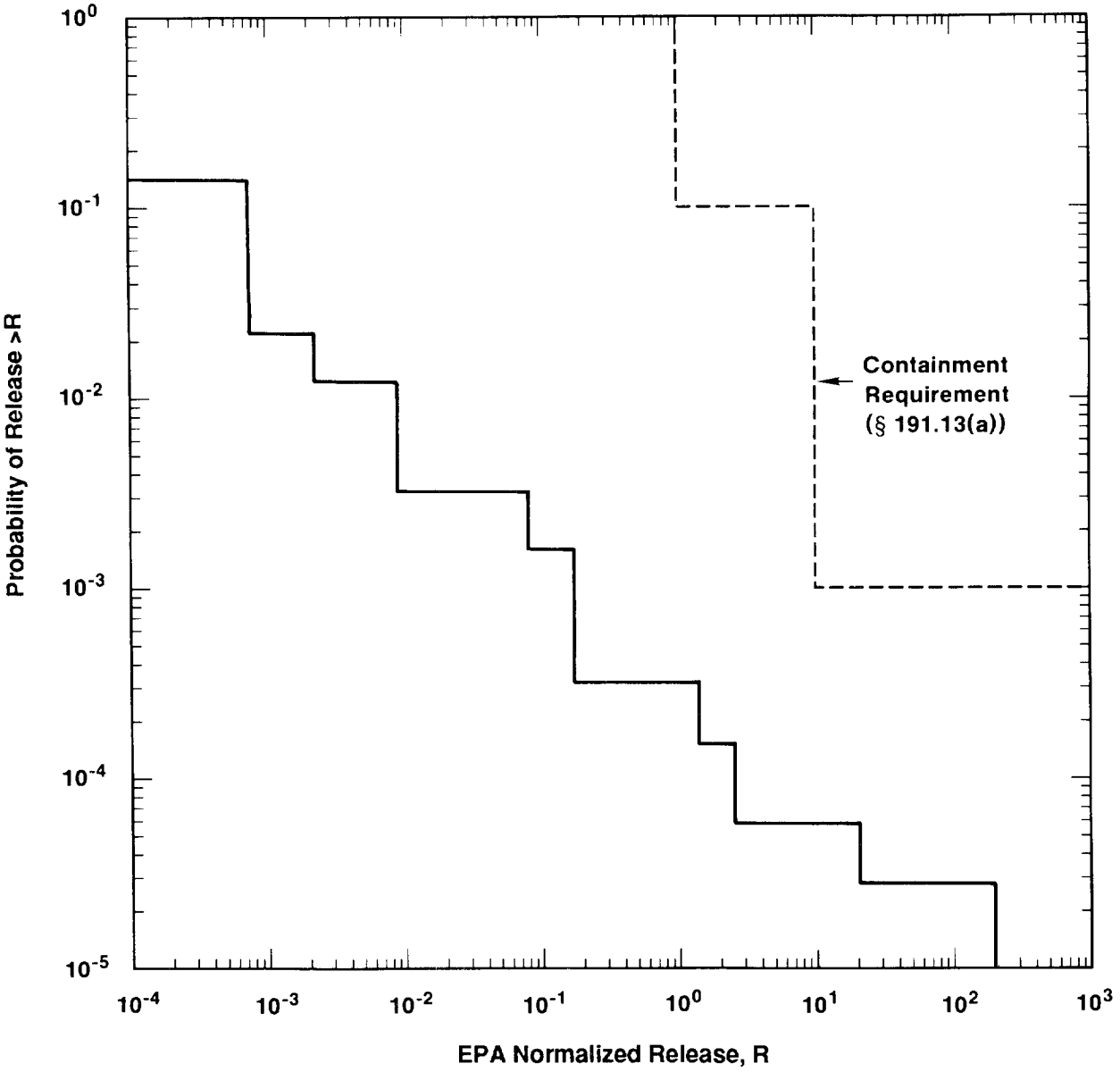

Figure 1.4-2. Comparison of a CCDF for Normalized Release to the Accessible Environment with the EPA Release Limits.

$$\mathcal{S} = \{x : x \text{ a single 10,000-yr time history beginning at decommissioning of the facility under consideration}\}. \quad (1.4\text{-}3)$$

Each 10,000-yr history is complete in the sense that it provides a full specification, including time of occurrence, for everything of importance to performance assessment that happens in this time interval. The S_i appearing in Eq. 1.4-2 are disjoint subsets of $\mathcal{S}$ for which

$$\mathcal{S} = \bigcup_{i=1}^{nS} S_i. \quad (1.4\text{-}4)$$

In the terminology of probability theory, the S_i are events and the pS_i are the probabilities for these events. It is the discretization of into the sets S_i that leads to the steps in the estimated CCDFs in Figures 1.4-1 and 1.4-2. The use of more sets will reduce the step sizes but will not alter the fact that CCDFs are the basic outcome of a performance assessment (Helton et al., 1991, Chapter VI).

Important parts of any performance assessment are the discretization of S into the sets S_i, commonly referred to as scenario development (Hunter, 1989; Ross, 1989; Cranwell et al., 1990; Guzowski, 1990), and the subsequent determination of probabilities for these sets (Mann and Hunter, 1988; Hunter and Mann, 1989; Guzowski, 1991). For radioactive waste disposal in sedimentary basins, many S_i result from unintended intrusions due to exploratory drilling for natural resources, particularly oil and gas. To construct CCDFs of the form shown in Figures 1.4-1 and 1.4-2, the time histories associated with these drilling intrusions must be sorted into disjoint sets such that (1) each S_i is sufficiently homogeneous that it is reasonable to use the same consequence result $\mathbf{cS}_i$ for all elements of S_i, (2) a probability can be determined for each S_i, and (3) estimation of pS_i and $\mathbf{cS}_i$ is computationally feasible.

Chapter 2, Volume 2 of this report describes a decomposition of drilling intrusions into computational scenarios on the basis of number of intrusions and their times of occurrence, and derives the necessary formulas to convert from drilling rates to scenario probabilities. Chapter 3, Volume 2 describes a computational procedure that can be used to determine CCDFs for intrusions due to drilling.

1.4.2 Uncertainty in Risk

A number of factors affect uncertainty in risk results, including completeness, aggregation, model selection, imprecisely known variables, and stochastic variation. The risk representation in Eq. 1.4-2 provides a convenient structure in which to discuss these uncertainties.

Completeness refers to the extent that a performance assessment includes all possible occurrences for the system under consideration. In terms of the risk representation in Eq. 1.4-2, completeness deals with whether or not all possible occurrences are included in the union of the sets S_i (i.e., in $U_i S_i$). Aggregation refers to the division of the possible occurrences into the sets S_i, and thus relates to the logic used in the construction of the sets S_i. Resolution is lost if the S_i are defined too coarsely (e.g., nS is too small) or in some other

inappropriate manner. Model selection refers to the actual choice of the models for use in a risk assessment. Appropriate model choice is sometimes unclear and can affect both pS_i and $\mathbf{cS}_i$. Similarly, once the models for use have been selected, imprecisely known variables required by these models can affect both pS_i and $\mathbf{cS}_i$. Due to the complex nature of risk assessment, model selection and imprecisely known variables can also affect the definition of the S_i. Stochastic variation is represented by the probabilities pS_i, which are functions of the many factors that affect the occurrence of the individual sets S_i. The CCDFs in Figures 1.4-1 and 1.4-2 display the effects of stochastic uncertainty. Even if the probabilities for the individual S_i were known with complete certainty, the ultimate result of a risk assessment would still be CCDFs of the form shown in Figures 1.4-1 and 1.4-2.

The calculation of risk is driven by the determination of the sets S_i. Once these sets are determined, their probabilities of pS_i and associated consequences $\mathbf{cS}_i$ must be determined. In practice, development of the S_i is a complex and iterative process that must take into account the procedures required to determine the probabilities pS_i and the consequences $\mathbf{cS}_i$. Typically, the overall process is organized so that pS_i and $\mathbf{cS}_i$ will be calculated by various models whose exact configuration will depend on the individual S_i. These models will also require a number of imprecisely known variables. It is also possible that imprecisely known variables could affect the definition of the S_i.

These imprecisely known variables can be represented by a vector

$$\mathbf{x} = [x_1, x_2, \ldots, x_{nV}], \tag{1.4-5}$$

where each x_j is an imprecisely known input required in the analysis and nV is the total number of such inputs. In concept, the individual x_j could be almost anything, including vectors or functions required by an analysis. However, an overall analysis, including uncertainty and sensitivity studies, is more likely to be successful if the risk representation in Eq. 1.4-2 has been developed so that each x_j is a real-valued quantity for which the overall analysis requires a single value, but it is not known with preciseness what this value should be. With the preceding ideas in mind, the representation for risk in Eq. 1.4-2 can be restated as a function of $\mathbf{x}$:

$$R(\mathbf{x}) = \{(S_i(\mathbf{x}), pS_i(\mathbf{x}), \mathbf{cS}_i(\mathbf{x})), \quad i=1, \ldots, nS(\mathbf{x})\} \tag{1.4-6}$$

As $\mathbf{x}$ changes, so will $R(\mathbf{x})$ and all summary measures that can be derived from $R(\mathbf{x})$. Thus, rather than a single CCDF for each consequence value contained in $\mathbf{cS}$, a distribution of CCDFs results from the possible values that $\mathbf{x}$ can take on.

The individual variables x_j in $\mathbf{x}$ can relate to different types of uncertainty. Individual variables might relate to completeness uncertainty (e.g., the value for a cutoff used to drop low-probability occurrences from the analysis), aggregation uncertainty (e.g., a bound on the

value for nS), model uncertainty (e.g., a 0-1 variable that indicates which of two alternative models should be used), stochastic uncertainty (e.g., a variable that helps define the probabilities for the individual S_i), or variable uncertainty (e.g., a solubility limit or a retardation for a specific element). Variable uncertainty may include uncertainty resulting from the incompleteness of data and measurement uncertainty resulting from systematic or random errors that may occur in the data. Measurement uncertainty has, in general, received little attention in this report because, as discussed in the following section, values for most variable parameters used in the performance assessment are assessed subjectively, not empirically. Even for those parameters for which values are derived empirically, the conservative use of total variability rather than variability about the mean discussed in Section 1.2 limits the potential to expand parameter uncertainty.

1.4.3 Characterization of Uncertainty in Risk

If the inputs to a performance assessment as represented by the vector **x** in Eq. 1.4-5 are uncertain, then so are the results of the assessment. Characterization of the uncertainty in the results of a performance assessment requires characterization of the uncertainty in **x**. Once the uncertainty in **x** has been characterized, then Monte Carlo techniques can be used to characterize the uncertainty in the risk results.

The outcome of characterizing the uncertainty in **x** is a sequence of probability distributions

$$D_1, D_2, \ldots, D_{nV}, \tag{1.4-7}$$

where D_j is the distribution developed for the variable x_j, $_j$=1, 2, ..., nV, contained in **x**. (Elsewhere in this volume these distributions are indicated by $F(x_j)$.) The definition of these distributions may also be accompanied by the specification of correlations and various restrictions that further define the possible relations among the x_j. These distributions and other restrictions probabilistically characterize where the appropriate input to use in the performance assessment might fall given that the analysis is structured so that only one value can be used for each variable under consideration. In most cases, each D_j will be a subjective distribution that is developed from available information through a suitable review process and serves to assemble information from many sources into a form appropriate for use in an integrated analysis. However, it is possible that the D_j may be obtained by classical statistical techniques for some variables. Details related to the probability distributions D_j used by WIPP PA are provided in the previous section.

Once the distributions in Eq. 1.4-7 have been developed, Monte Carlo techniques can be used to determine the uncertainty in $R(\mathbf{x})$ from the uncertainty in **x**. First, a sample

$$\mathbf{x}_k = [x_{k1}, x_{k2}, \ldots, x_{k,nV}], \; k=1, \ldots, nK \tag{1.4-8}$$

is generated according to the specified distributions and restrictions, where nK is the size of the sample. The performance assessment is then performed for each sample element $\mathbf{x}_k$, which yields a sequence of risk results of the form

$$R(\mathbf{x}_k) = \{(S_i(\mathbf{x}_k), pS_i(\mathbf{x}_k), \mathbf{cS}_i(\mathbf{x}_k)), i=1, ..., nS(\mathbf{x}_k)\} \quad (1.4\text{-}9)$$

for k=1, ..., nK. Each set $R(\mathbf{x}_k)$ is the result of one complete performance assessment performed with a set of inputs (i.e., $\mathbf{x}_k$) that the review process producing the distributions in Eq. 1.4-7 concluded was possible. Further, associated with each risk result $R(\mathbf{x}_k)$ in Eq. 1.4-9 is a probability or weight* that can be used in making probabilistic statements about the distribution of $R(\mathbf{x})$.

In most performance assessments, CCDFs are the results of greatest interest. For a particular consequence result, a CCDF will be produced for each set $R(\mathbf{x}_k)$ of results shown in Eq. 1.4-9. This yields a distribution of CCDFs of the form shown in Figure 1.4-3.

Although Figure 1.4-3 provides a complete summary of the distribution of CCDFs obtained for a particular consequence result by propagating the sample shown in Eq. 1.4-8 through a performance assessment, the figure is hard to read. A less crowded summary can be obtained by plotting the mean value and selected percentile values for each consequence value on the abscissa. For example, the mean plus the 5th, 50th (i.e., median) and 95th percentile values might be used. The mean and percentile values can be obtained from the exceedance probabilities associated with the individual consequence values and the weights or "probabilities" associated with the individual sample elements. If the mean and percentile values associated with individual consequence values are connected, a summary plot of the form shown in Figure 1.4-4 is obtained.

A point of possible confusion involving the risk representation in Eq. 1.4-2 is the distinction between the uncertainty that gives rise to a single CCDF and the uncertainty that gives rise to a distribution of CCDFs. A single CCDF arises from the fact that a number of different occurrences have a real possibility of taking place. This type of uncertainty is referred to as stochastic variation in this report. A distribution of CCDFs arises from the fact that fixed, but unknown, quantities are needed in the estimation of a CCDF. The development of distributions that characterize what the values for these fixed quantities might be leads to a distribution of CCDFs. In essence, a performance assessment can be viewed as a very complex function that estimates a CCDF. Since there is uncertainty in the values of some of the independent variables operated on by this function, there will also be uncertainty in the dependent variable produced by this function, where this dependent variable is a CCDF.

Both Kaplan and Garrick (1981) and a recent report by the International Atomic Energy Agency (IAEA, 1989) distinguish between these two types of uncertainty. Specifically, Kaplan and Garrick distinguish between probabilities derived from frequencies and probabilities that

---

* In random or Latin hypercube sampling, this weight is the reciprocal of the sample size (i.e, 1/nK) and can be used in estimating means, cumulative distribution functions, and other statistical properties. This weight is often referred to as the probability for each observation (i.e., each sample element x_k). However, this is not technically correct. If continuous distributions are involved, the actual probability of each observation is zero.

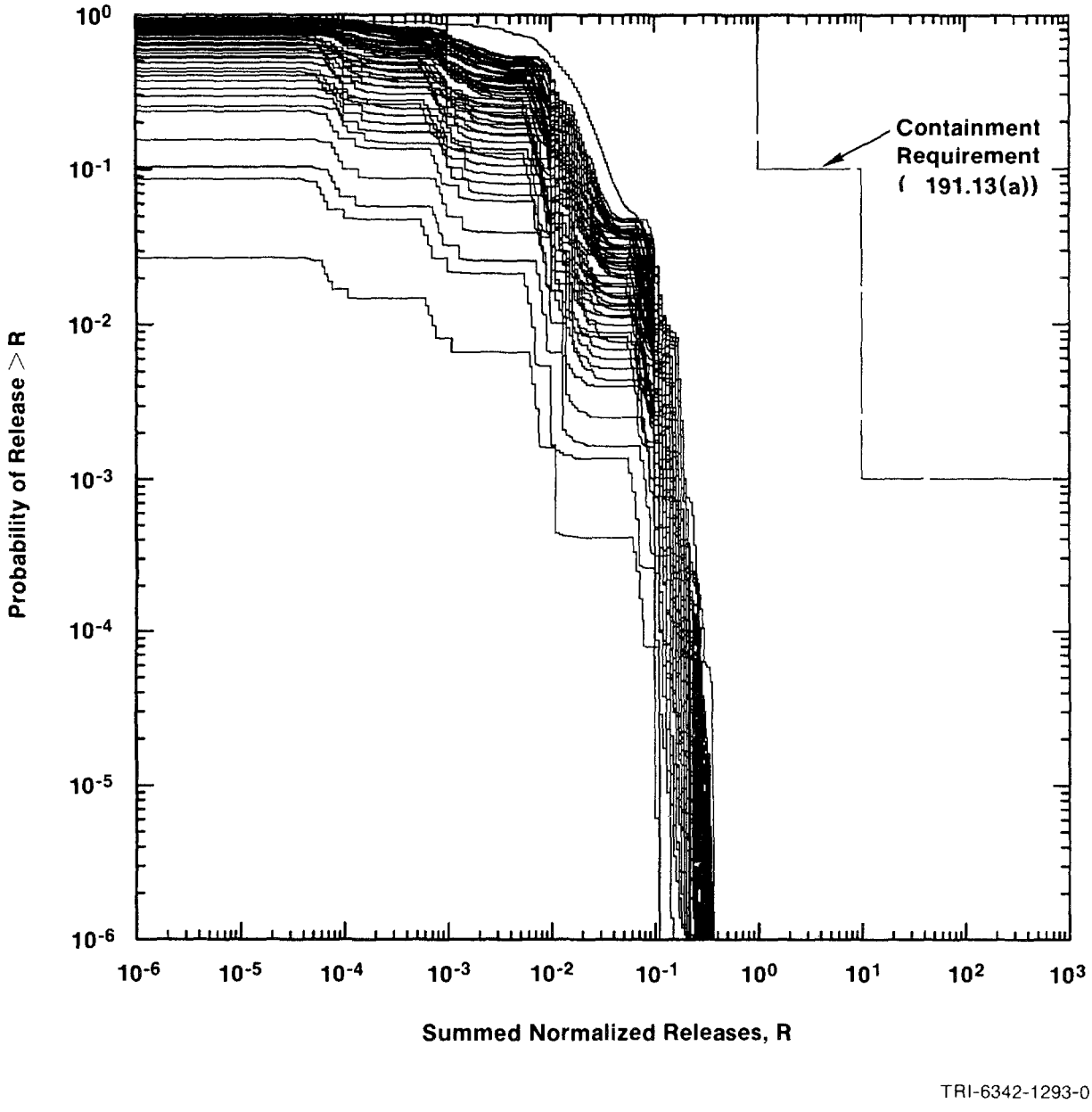

Figure 1.4-3. Example of CCDF Distribution Produced for Results Shown in Eq. 1.4-9.

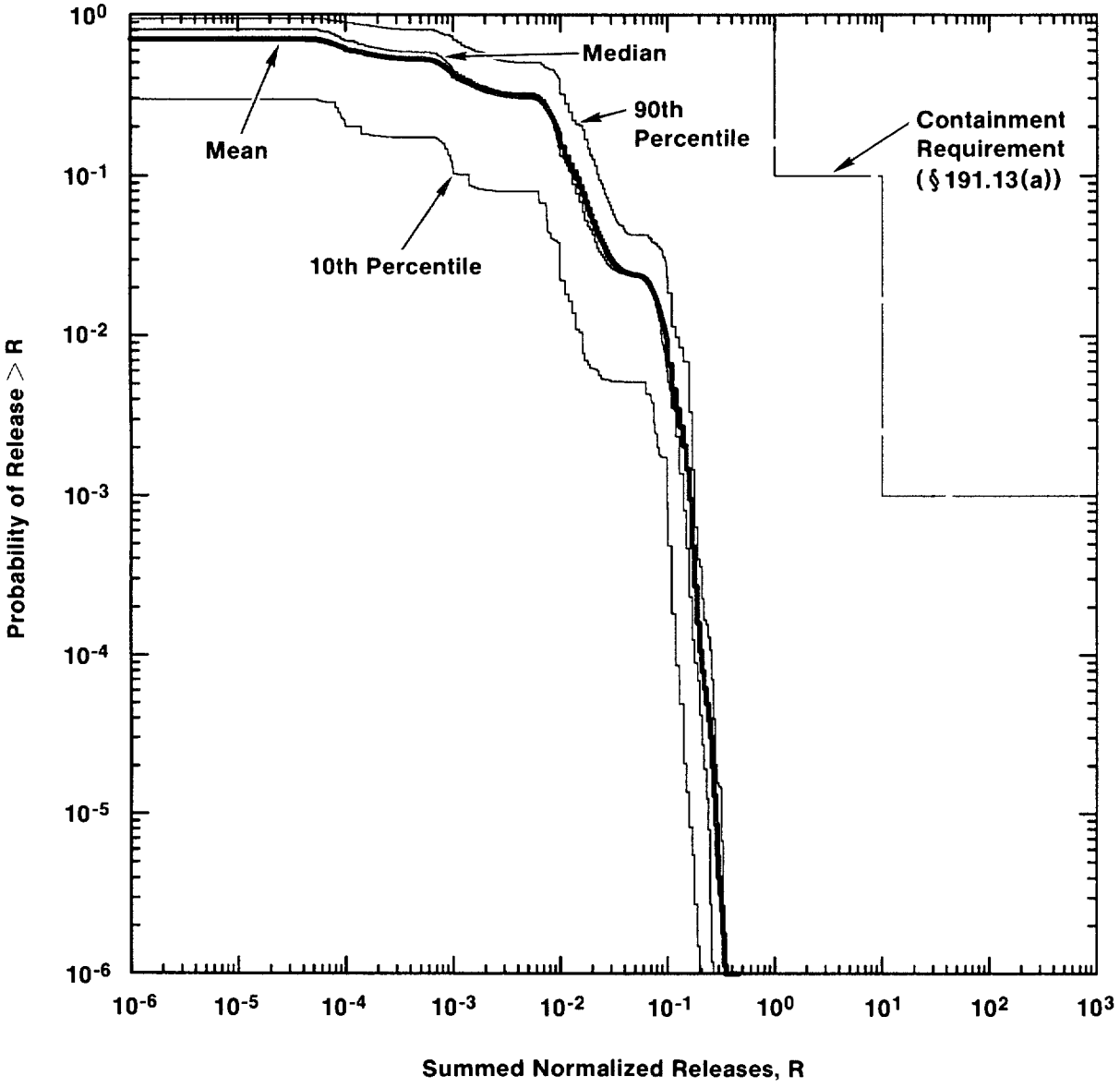

TRI-6342-1294-0

Figure 1.4-4. CCDF Summary Plot.

characterize degrees of belief. Probabilities derived from frequencies correspond to the probabilities pS_i in Eq. 1.4-2 while probabilities that characterize degrees of belief (i.e., subjective probabilities) correspond to the distributions indicated in Eq. 1.4-7. The IAEA report distinguished between what it calls Type A uncertainty and Type B uncertainty. The IAEA report defines Type A uncertainty to be stochastic variation; as such, this uncertainty corresponds to the frequency-based probability of Kaplan and Garrick and the pS_i of Eq. 1.4-7. Type B uncertainty is defined to be uncertainty that is due to lack of knowledge about fixed quantities; thus, this uncertainty corresponds to the subjective probability of Kaplan and Garrick and the distributions indicated in Eq. 1.4-7. This distinction has also been made by other authors including Vesely and Rasmuson (1984), Paté-Cornell (1986), and Parry (1988).

1.4.4 Calculation of Scenario Consequences

The $\mathbf{cS}_i$ in Eq. 1.4-2 are estimated for each sample element $\mathbf{x}_k$ using computer codes that comprise the consequence model. This model is deterministic and predicts an EPA normalized release to the accessible environment for each scenario S_i. The consequence model is actually composed of many individual models C_ℓ, ℓ = 1, ..., nM. The collective operation of these models can be represented by the relationship

$$\mathbf{cS}_i = C_{nM}\{...;C_2[\mathbf{x}_k;C_1(\mathbf{x}_k, S_i)]\} \qquad (1.4\text{-}10)$$

where

C_ℓ = consequence model ℓ,

$C_\ell(\mathbf{x}_k,S_i)$ = vector containing consequence results predicted by model ℓ for sample element $\mathbf{x}_k$ and scenario S_i,

and

nM = number of consequence models.

As indicated in the preceding relationship, the individual models predict results that depend on the $\mathbf{x}_k$ and S_i and also generate input to the next model in the computational sequence.

The consequence models C_ℓ are separate computational models (usually computer models) that are selected from several categories that represent physical processes and phenomena such as groundwater flow, dissolution of radionuclides in repository brine, and groundwater transport. As part of the 1991 WIPP performance assessment system, about 75 FORTRAN codes are grouped into 10 model categories, which are called modules. CAMCON is the software package designed and used by the PA Division to assemble the computational models from the various modules into the structure indicated in Eq. 1.4-10 (Rechard, 1989; Rechard et al., 1989). Chapter 4 (Volume 2) describes the C_ℓ and their application to undisturbed conditions. Chapters 5, 6, and 7 (Volume 2) describe the application of the C_ℓ to disturbed conditions for the S_i defined in Chapter 2 (Volume 2).

1.4.5 Uncertainty and Sensitivity Analyses

In the context of this report, uncertainty analysis involves determining the uncertainty in model predictions that results from imprecisely known input variables, and sensitivity analysis involves determining the contribution of individual input variables to the uncertainty in model predictions. Specifically, uncertainty and sensitivity analyses involve the study of the effects of subjective, or type B, uncertainty. As previously discussed, the effects of stochastic, or type A, uncertainty is incorporated into the WIPP performance assessment through the scenario probabilities pS_i appearing in Eq. 1.4-2. Sensitivity and uncertainty analyses for the results from the 1991 preliminary performance assessment are reported in Volume 4.

1.5 Background on WIPP

1.5.1 Purpose

The DOE was authorized by Congress in 1979 to build the WIPP as a research and development facility to demonstrate the safe management, storage, and eventual disposal of transuranic (TRU) waste generated by DOE defense programs (WIPP Act, 1979). Only after demonstrating compliance with *40 CFR 191* and other laws and regulations (e.g., RCRA [1976] and NEPA [1969]) will the DOE permanently dispose of TRU waste at the WIPP repository.

1.5.2 Location

The WIPP is located within a large sedimentary basin, the Delaware Basin, in southeastern New Mexico, an area of low population density approximately 38 km (24 mi) east of Carlsbad (Figure 1.5-1). Topographically, the WIPP is between the high plains of West Texas and the Guadalupe and Sacramento Mountains of southeastern New Mexico.

Four prominent surface features are found in the area--Los Medanos ("The Dunes"), Nash Draw, Laguna Grande de la Sal, and the Pecos River. Los Medanos is a region of gently rolling hills that slopes upward to the northeast from the eastern boundary of Nash Draw to a low ridge called "The Divide." The WIPP is in Los Medanos. Nash Draw, 8 km (5 mi) west of the WIPP, is a broad shallow topographic depression with no external surface drainage. Laguna Grande de la Sal, about 9.5 km (6 mi) west-southwest of the WIPP, is a large playa about 3.2 km (2 mi) wide and 4.8 km (3 mi) long formed by coalesced collapse sinks that were created by dissolution of evaporate deposits. The Pecos River, the principal surface-water feature in southeastern New Mexico, flows southeastward, draining into the Rio Grande in western Texas.

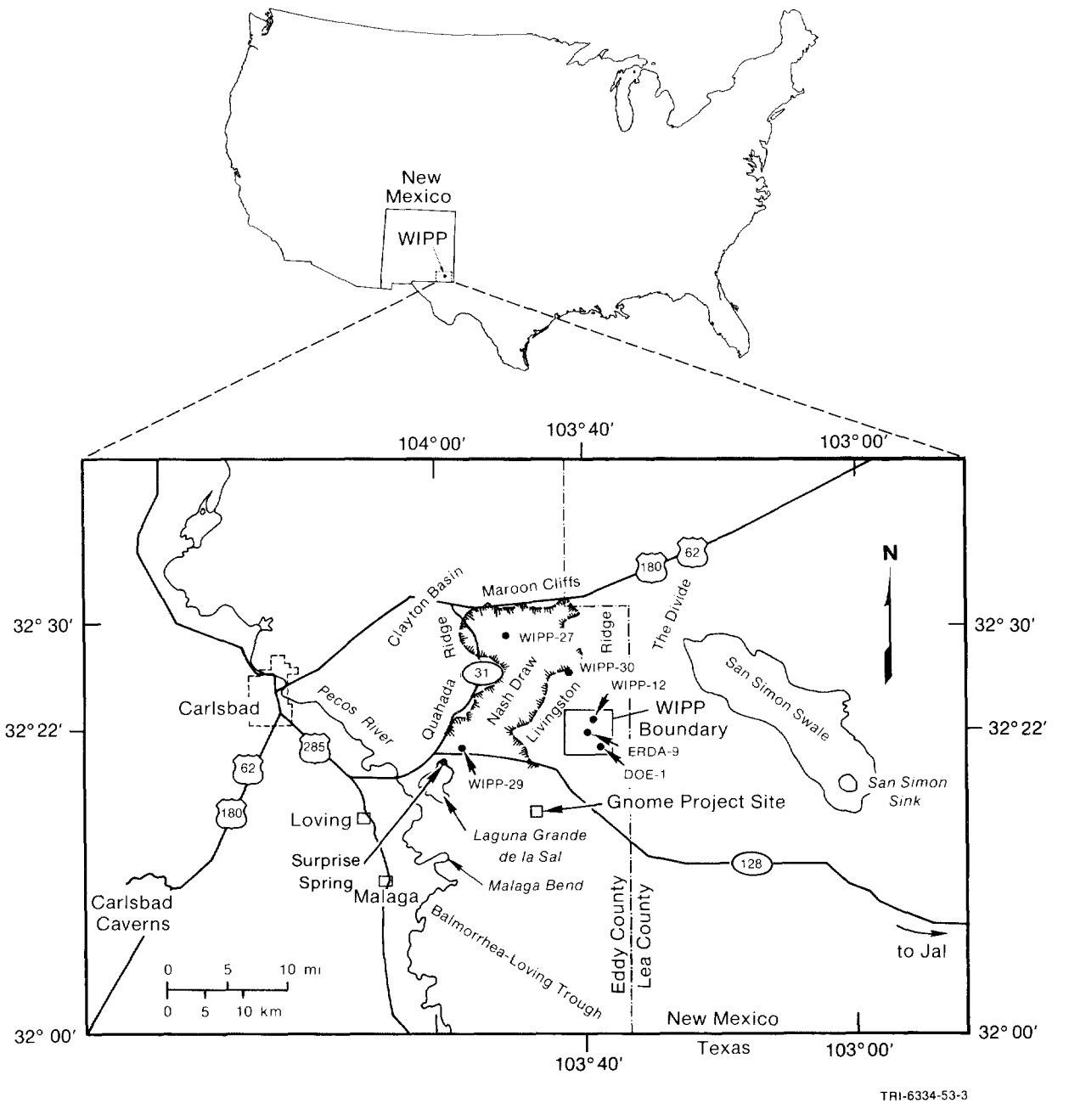

Figure 1.5-1. WIPP Location in Southeastern New Mexico (after Rechard, 1989, Figure 1.2).

1.5.3 Geologic History of the Delaware Basin

The Delaware Basin, an elongated, geologically confined depression, extends from just north of Carlsbad, New Mexico, into Texas west of Fort Stockton (Figure 1.5-2). The basin covers 33,000 km^2 (12,750 mi^2) and is filled with sedimentary rocks to depths as great as 7,300 m (24,000 ft) (Hills, 1984). Geologic history of the Delaware Basin began about 450 to 500 million years ago when a broad, low depression formed during the Ordovician Period as transgressing seas deposited clastic and carbonate sediments (Powers et al., 1978; Cheeseman, 1978; Williamson, 1978; Hiss, 1975; Hills, 1984; Harms and Williamson, 1988; Ward et al., 1986). After a long period of accumulation and subsidence, the depression separated into the Delaware and Midland Basins when the area now called the Central Basin Platform uplifted during the Pennsylvanian Period, about 300 million years ago.

During the Early and Middle Permian Period, the Delaware Basin subsided rapidly, resulting in a sequence of clastic rocks rimmed by reef limestone. The thickest of the reef deposits, the Capitan Limestone, is buried north and east of the WIPP but is exposed at the surface in the Guadalupe Mountains to the west (Figure 1.5-2). Evaporite deposits (marine bedded salts) of the Castile Formation and the Salado Formation, which hosts the WIPP, filled the basin during the late Permian Period and extended over the reef margins. Evaporites, carbonates, and clastic rocks of the Rustler Formation and the Dewey Lake Red Beds were deposited above the Salado Formation before the end of the Permian Period.

1.5.4 Repository

The repository is located in the Delaware Basin because the 600-m (2,000-ft)-thick Salado Formation of marine bedded salts (Late Permian Period) eventually encapsulates the nuclear waste through salt creep. The bedded salts, consisting of thick halite and interbeds of minerals such as clay and anhydrites, do not contain flowing water.

The repository level is located within these bedded salts 655 m (2,150 ft) below the surface and 384 m (1,260 ft) above sea level. The WIPP repository is composed of a single underground disposal level connected to the surface by four shafts (Figure 1.5-3). The repository level consists of an experimental area at the north end and a disposal area at the south end.

1.5.5 WIPP Waste Disposal System

The WIPP relies on three approaches to contain waste: geologic barriers, engineered barriers, and institutional controls. The third approach, institutional controls, consists of many parts, e.g., the legal ownership and regulations of the land and resources by the U.S. Government, the fencing and signs around the property, permanent markers, public records and archives, and other methods of preserving knowledge about the disposal system.

The WIPP disposal system, as defined by *40 CFR 191*, includes the geologic and engineered barriers. The physical features of the repository (e.g., stratigraphy, design of repository, waste form) are components of these barriers.

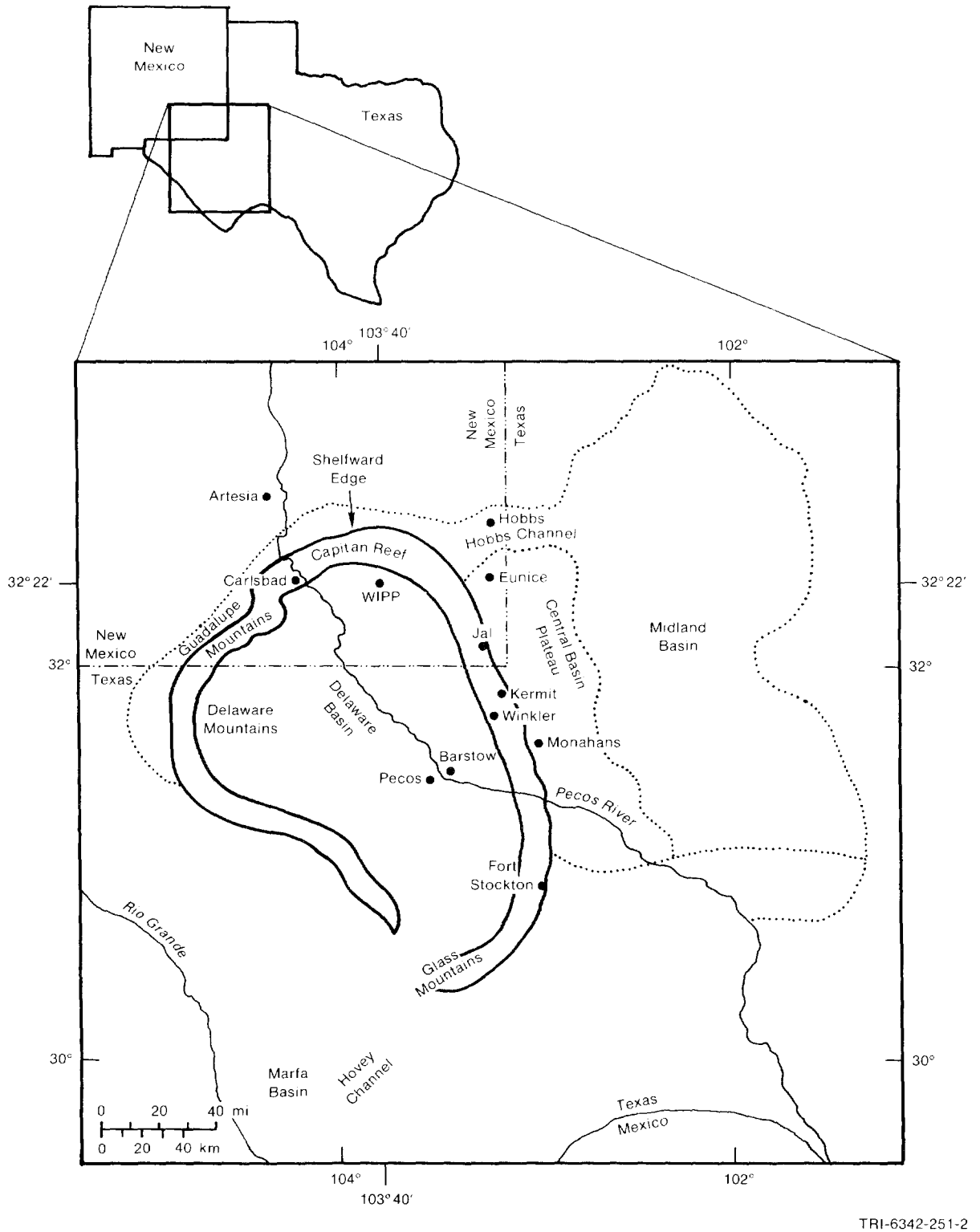

Figure 1.5-2. Location of the WIPP in the Delaware Basin (modified from Richey et al., 1985 and Lappin, 1988, Figure 1.4).

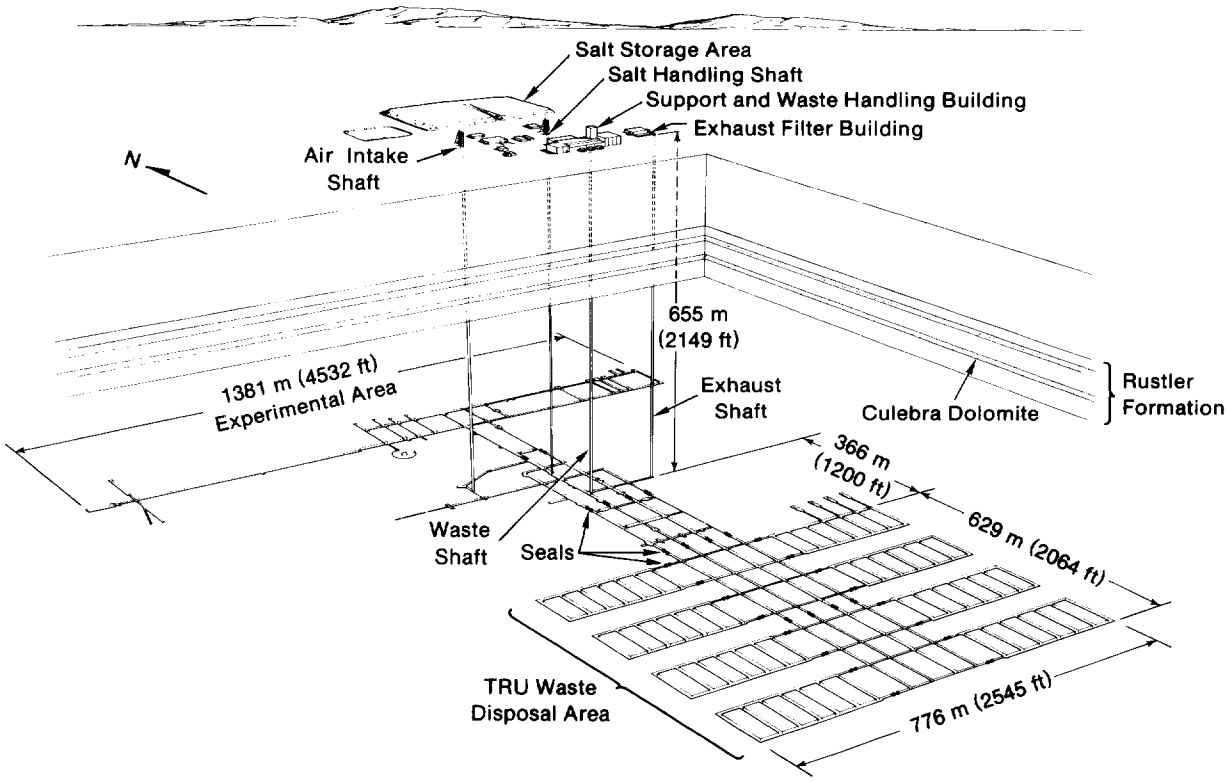

Figure 1.5-3. WIPP Repository, Showing Surface Facilities, Proposed TRU Disposal Areas, and Experimental Areas (after Nowak et al., 1990, Figure 2).

The geologic barriers are limited to the lithosphere up to the surface and no more than 5 km (3 mi) from the outer boundary of the WIPP waste-emplacement panels (Figure 1.5-4). The boundary of this maximum-allowable geologic subsystem is greater than the currently proposed boundary of the WIPP land withdrawal. The extent of the WIPP controlled area will be defined during performance assessment but will not be less than the area withdrawn, which will be under U.S. DOE administrative control (Bertram-Howery and Hunter, 1989).

Data for components of the geologic and engineered barriers are the subject of this volume. No data on institutional controls are contained in this volume.

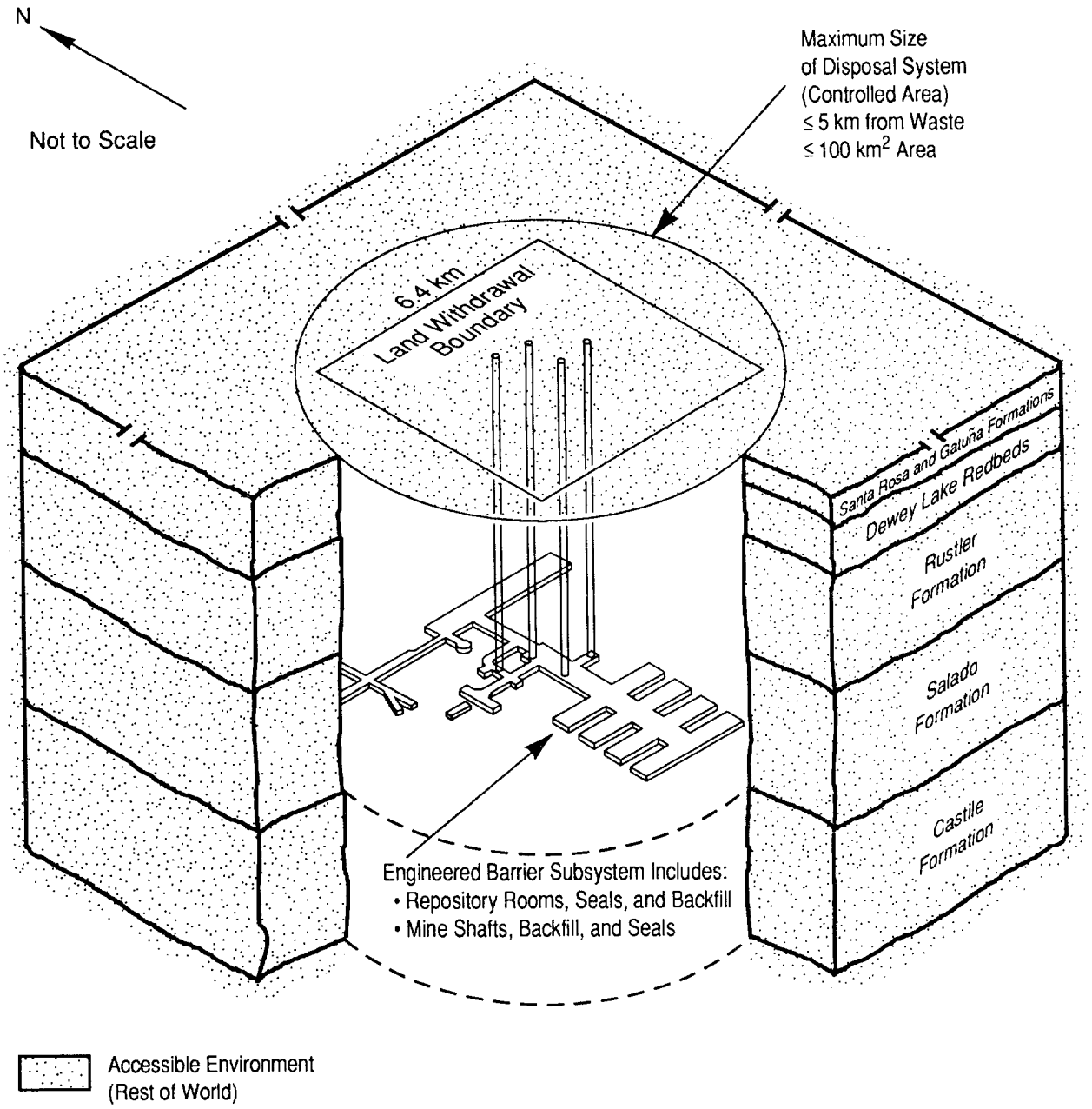

Figure 1.5-4 Geologic and Engineered Barriers of the WIPP Disposal System.

2. GEOLOGIC BARRIERS

The geologic barriers consist of the physical features of the repository, such as stratigraphy and geologic components.

2.1 Areal Extent of Geologic Barriers

Figure 2.1-1 shows the maximum areal extent of the geologic barriers. Figure 2.1-2 shows the UTM coordinates of the modeling domains. The UTM coordinates for the northeast and southeast corners of the land-withdrawal boundary were derived from values reported in Gonzales (1989). Because the township ranges shift at the land-withdrawal border, the UTM coordinates for the northwest and southwest corners were derived from information on the wells nearest the corners (i.e., Well H-6A for the northwest corner and Well D-15 for the southwest corner).

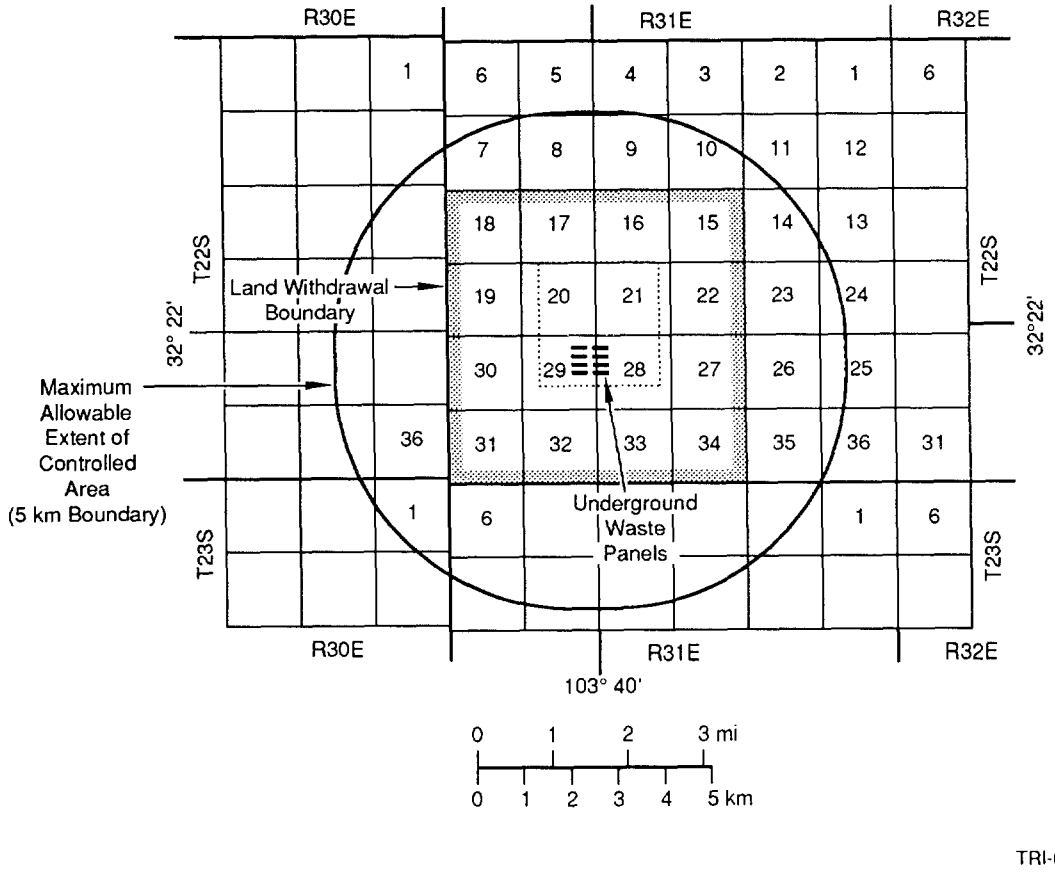

Figure 2.1-1. Position of the WIPP Waste Panels Relative to Land Withdrawal Boundary (16 Contiguous Sections), 5-km Boundary (40 CFR 191.12y), and Surveyed Section Lines (after U.S. DOE, 1989a, Figure 2.2).

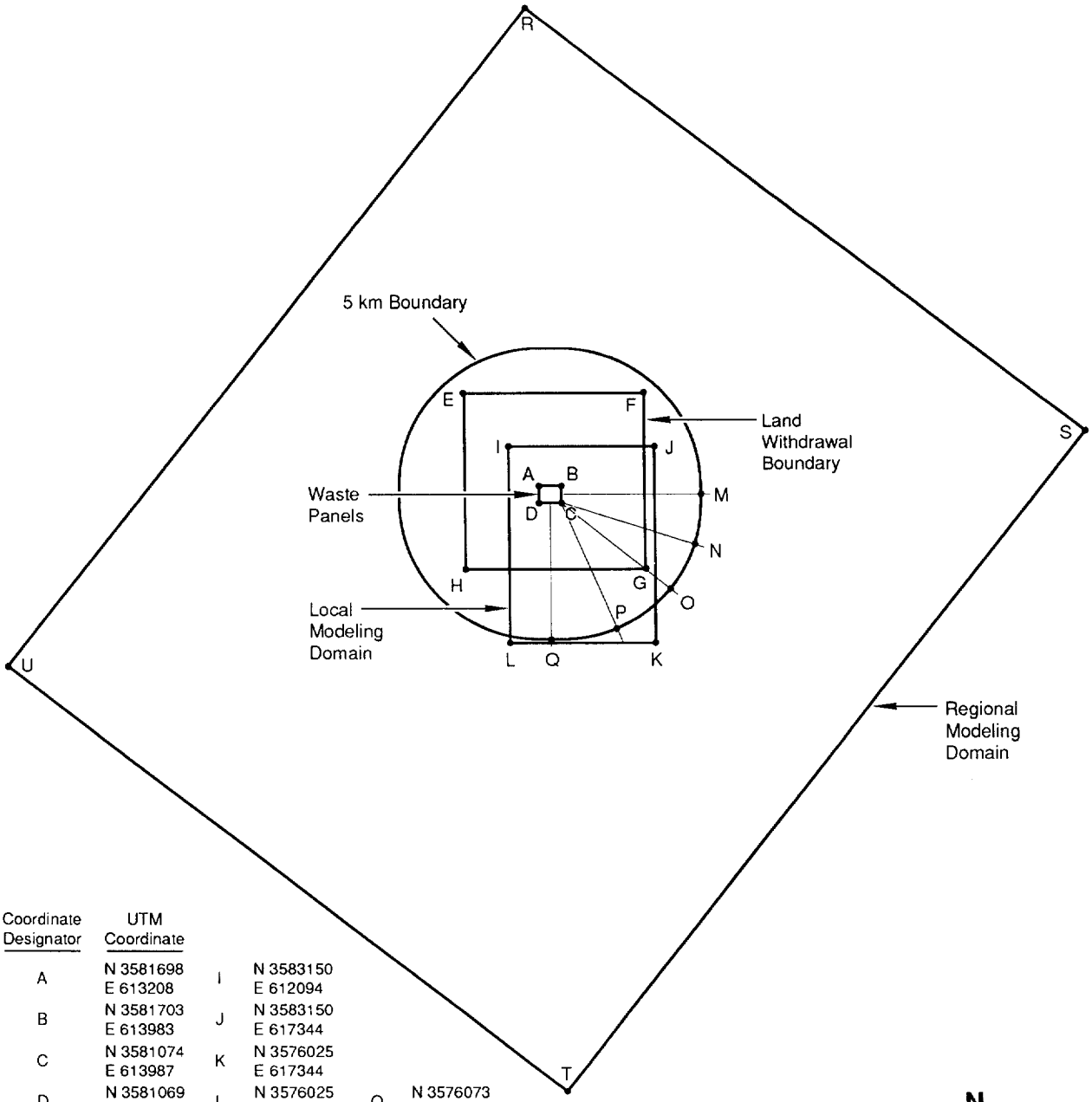

Coordinate Designator	UTM Coordinate				
A	N 3581698 E 613208	I	N 3583150 E 612094		
B	N 3581703 E 613983	J	N 3583150 E 617344		
C	N 3581074 E 613987	K	N 3576025 E 617344		
D	N 3581069 E 613212	L	N 3576025 E 612094	Q	N 3576073 E 613631
E	N 3585057 E 610496	M	N 3581420 E 618984	R	N 3598943 E 612819
F	N 3585109 E 616941	N	N 3579579 E 618791	S	N 3583551 E 632519
G	N 3578681 E 617015	O	N 3577945 E 617856	T	N 3559911 E 614049
H	N 3578612 E 610566	P	N 3576436 E 615991	U	N 3575303 E 594349

TRI-6342-1406-0

Figure 2.1-2. UTM Coordinates of the Modeling Domains.

Figure 2.1-3 shows the topography, the locations of wells used for defining the general stratigraphy, and the modeling domains near the WIPP typically plotted in the report. The well locations by universal transverse mercator (UTM), state plan coordinates, and survey sections are provided in Table B.1 (Appendix B). The elevations of the stratigraphic layers in each of the wells are tabulated in Table B.2 (Appendix B).

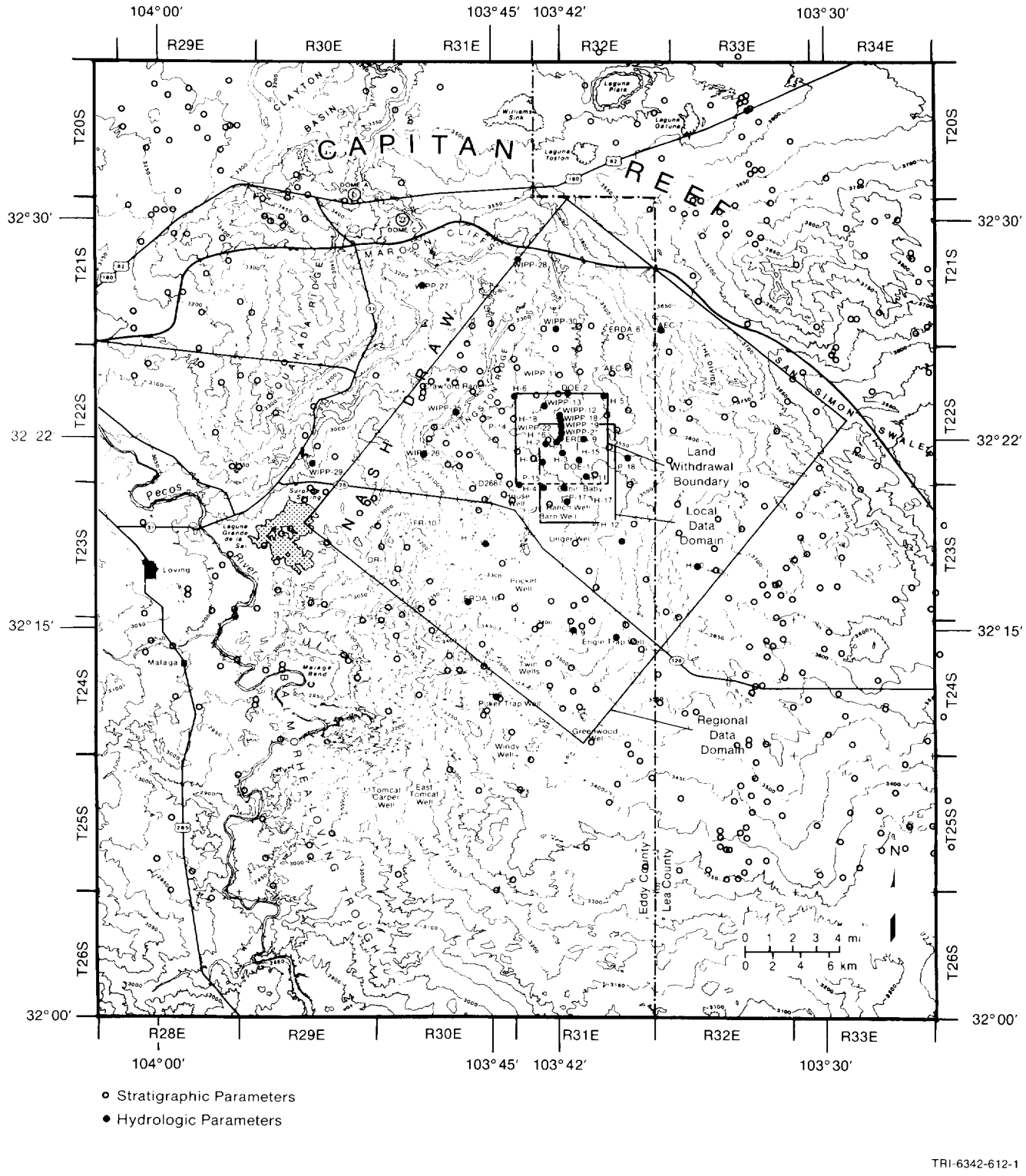

Figure 2.1-3. Locations of Wells for Defining General Stratigraphy and Regional and Local Data Domains Typically Plotted in Report.

2.2 Stratigraphy at the WIPP

The level of the WIPP repository is located within bedded salts 655 m (2,150 ft) below the surface and 384 m (1,260 ft) above sea level (Figures 2.2-1 and 2.2.2). The bedded salts consist of thick halite and interbeds of minerals such as clay and anhydrites of the late Permian period (Ochoan series) (approximately 255 million yr old)* (Figure 2.2-3). An interbed that forms a potential transport pathway, Marker Bed 139 (MB139), located about 1 m (3 ft) below the repository interval (Figure 2.2-3), is about 1 m (3 ft) thick, and is one of about 45 siliceous or sulfatic units within the Salado Formation consisting of polyhalitic anhydrite (Figure 2.2-4) (Lappin, 1988; Tyler et al., 1988). Figure 2.2-5 shows the lithostatic and hydrostatic pressure with depth.

Parameter:	**Anhydrite III elevation @ ERDA-9**
Median:	105
Range:	70
	140
Units:	m
Distribution:	Uniform
Source(s):	See text.

Parameter:	**Bell Canyon elevation @ ERDA-9**
Median:	-200
Range:	-170
	-230
Units:	m
Distribution:	Uniform
Source(s):	See text.

For most strata above the repository, the elevations (though varying) are well known because of numerous wells; however, the elevations of the Anhydrite III in the Castile Formation and the Bell Canyon directly below the repository can only be inferred from a geologic cross section (Figure 2.2-1). The geologic structure is uncomplicated, thus the uncertainty is likely small on the regional geologic scale. Yet the information is important to evaluating the potential and the corresponding size of any brine reservoirs under the repository. Hence, uncertainty bounds have been placed on these two elevations inferred from the geologic cross section. For the 1991 PA calculations, a uniform distributon with a mean of the elevation of the strata was inferred from using WIPP-12, and Cabin Baby-1, ERDA-10, or DOE-1 for the Anhydrite III strata and DOE, and Cabin Baby-1 or ERDA-10 for the Bell Canyon. The endpoints were estimated at $\overline{x} \pm \sqrt{3}s$.

* This age reflects the revised 1983 geologic timetable (Palmer, 1983).

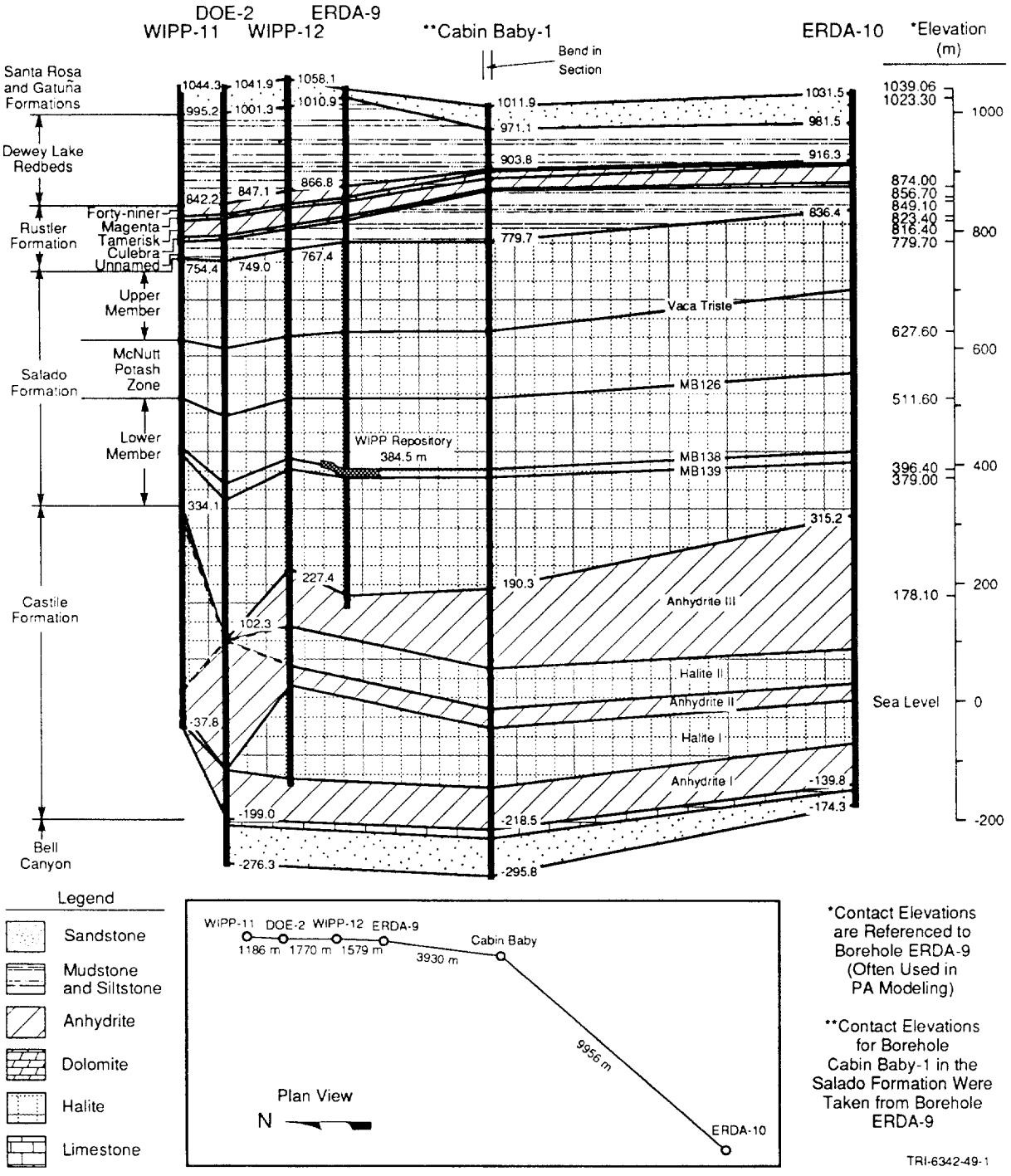

Figure 2.2-1. Level of WIPP Repository, Located in the Salado Formation. The Salado Formation is composed of thick halite with thin interbeds of clay and anhydrite deposited as marine evaporites about 255 million years ago (Permian period) (after Lappin, 1988, Figure 3.1).

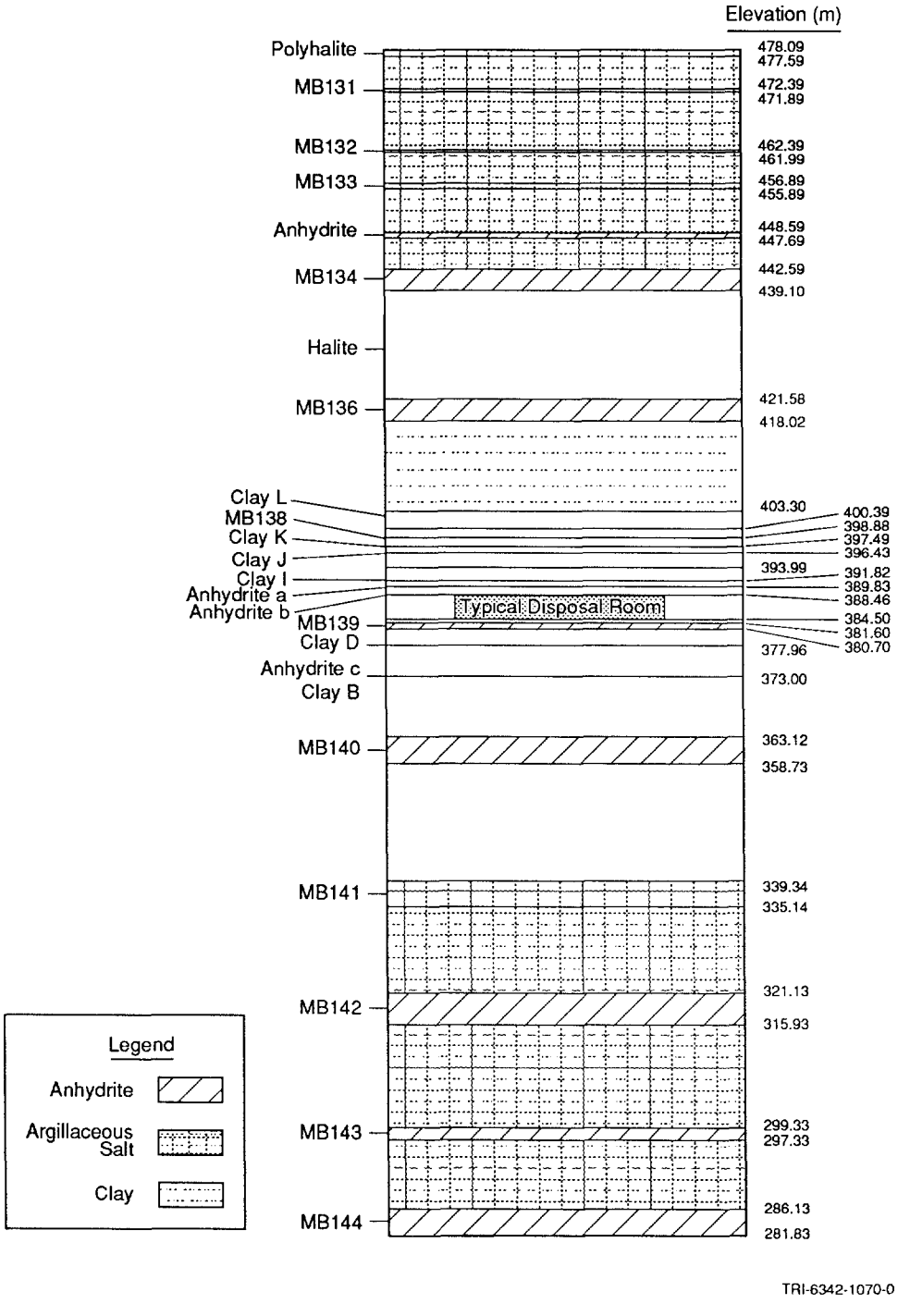

Figure 2.2-2. Reference Local Stratigraphy near Repository (after Munson et al., 1989, Figure 3-3).

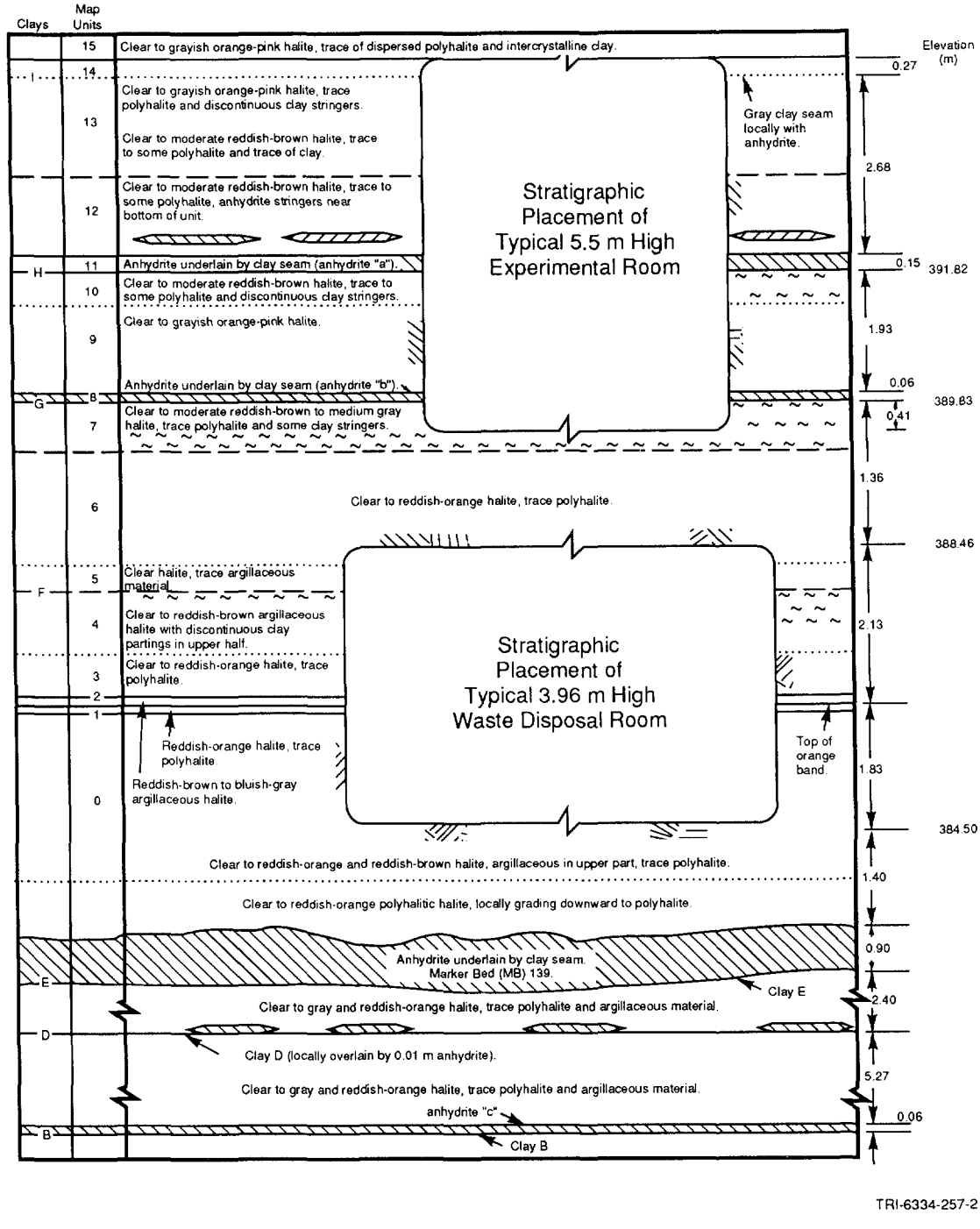

Figure 2.2-3. Stratigraphy at the Repository Horizon (after Bechtel, 1986, Figures 6-2, 6-3 and Lappin et al., 1989, Figure 4-12). Units in the disposal area dip slightly to the south, but disposal excavations are always centered about the orange marked band (reddish-orange halite).

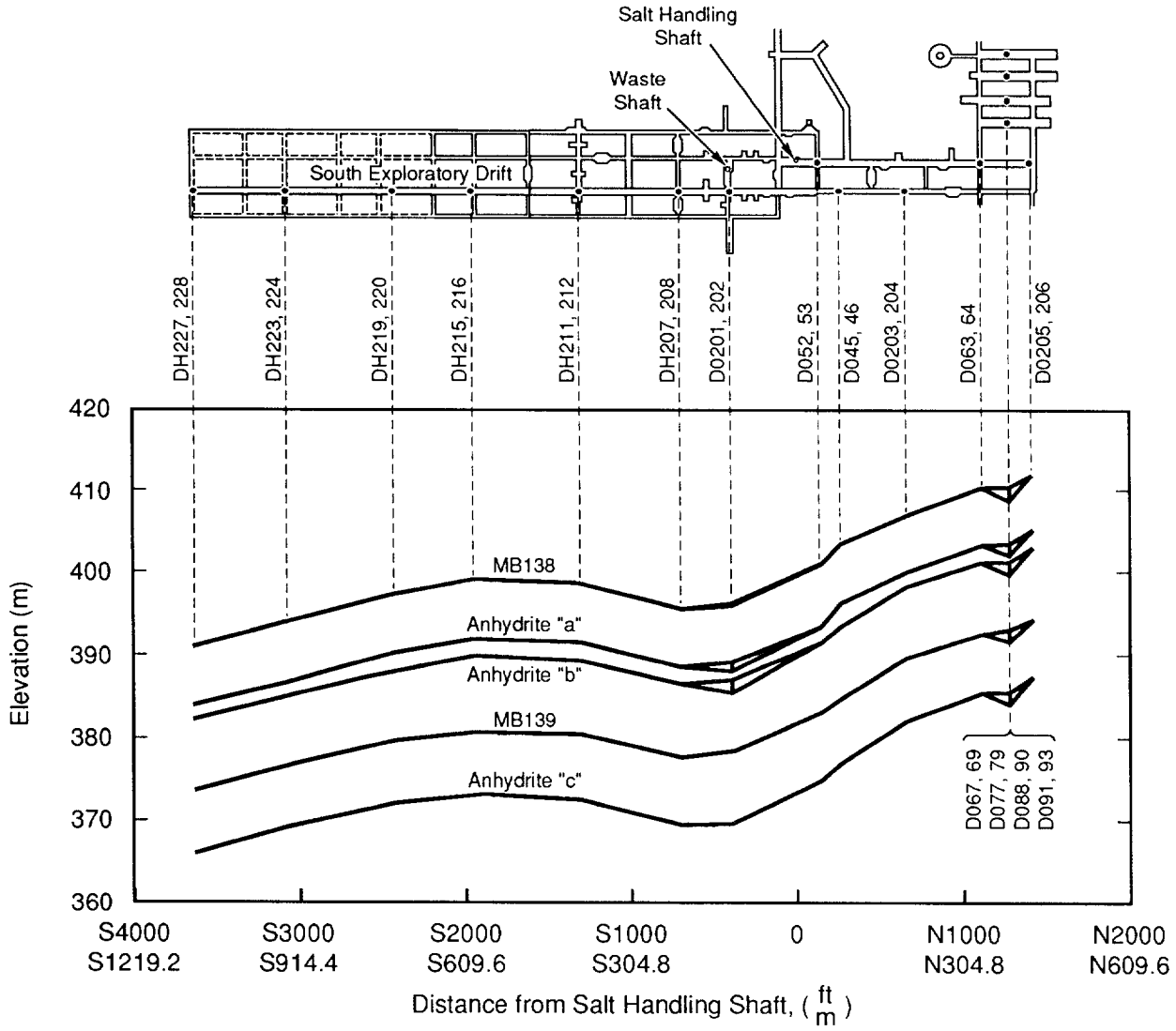

Figure 2.2-4. Marker Bed 139, One of Many Anhydrite Interbeds near the WIPP Repository Horizon (after Krieg, 1984, Figure 2).

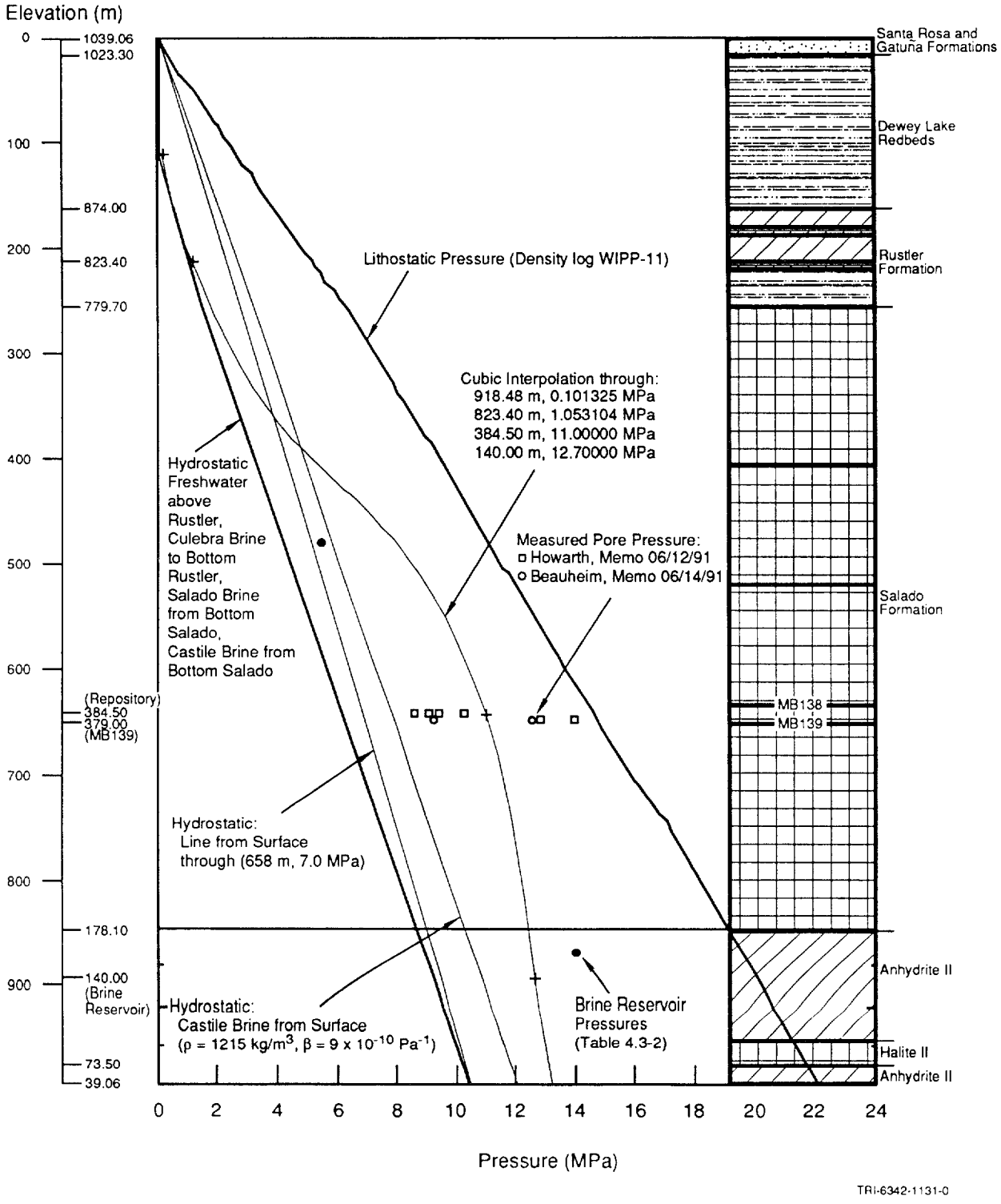

Figure 2.2-5. Lithostatic and Hydrostatic Pressure with Depth.

2.3 Hydrologic Parameters for Halite and Polyhalite within Salado Formation

The WIPP repository is located in the Salado Formation. The Salado Formation is composed of thick halite with thin interbeds of clay and anhydrite deposited as marine evaporites about 255 million years ago (Permian period). The parameters for the Salado Formation near the repository are given in Table 2.3-1.

Table 2.3-1. Parameter Values for Halite and Polyhalite within Salado Formation Near Repository

Parameter	Median	Range		Units	Distribution Type	Source
Capillary pressure (p_c) and relative permeability (k_{rw})						
Threshold displacement pressure (p_t)	2.3×10^{7}	2.3×10^{5}	2.3×10^{9}	Pa	Lognormal	Davies, June 2, 1991, Memo (see Appendix A); Brooks and Corey, 1964
Residual Saturations						
Wetting phase ($S_{\ell r}$)	2×10^{-1}	1×10^{-1}	4×10^{-1}	none	Cumulative	Davies and LaVenue, 1990b
Gas phase (S_{gr})	2×10^{-1}	1×10^{-1}	4×10^{-1}	none	Cumulative	Davies and LaVenue, 1990b
Brooks-Corey Exponent (η)	7×10^{-1}	3.5×10^{-1}	1.4	none	Cumulative	Davies and LaVenue, 1990b
Density						
Grain (ρ_g) Halite	2.163×10^{3}			kg/m^3	Constant	Carmichael, 1984, Table 2; Krieg, 1984, p. 14; Clark, 1966, p. 44
Grain (ρ_g) Polyhalite	2.78×10^{3}			kg/m^3	Constant	Shakoor and Hume, 1981 (p. 103-203)
Bulk (ρ_{bulk})	2.14×10^{3}			kg/m^3	Constant	Holcomb and Shields, 1987, p.17
Average (ρ_{ave})	2.3×10^{3}			kg/m^3	Constant	Krieg, 1984, Table 4
Dispersivity						
Longitudinal (α_L)	1.5×10^{1}	1	4×10^{1}	m	Cumulative	Pickens and Grisak, 1981; Lappin et al., 1989, Table D-2
Transverse (α_T)	1.5	1×10^{-1}	4	m	Cumulative	Pickens and Grisak, 1981; Freeze and Cherry, 1979, Figure 9.6
Partition Coefficient						
All species	0			m^3/kg	Constant	Lappin et al., 1989, p. D-17
Permeability (k)						
Undisturbed	5.7×10^{-21}	8.6×10^{-22}	5.4×10^{-20}	m^2	Data	Beauheim, June 14, 1991, Memo (see Appendix A)
Disturbed	1×10^{-19}	1×10^{-20}	1×10^{-18}	m^2	Lognormal	Beauheim, 1990
Pore pressure (p)	1.28×10^{7}	9.3×10^{6}	1.39×10^{7}	Pa	Data	Beauheim, June 14, 1991, Memo (see Appendix A); Howarth, June 12, 1991, Memo (see Appendix A)
Porosity (ϕ)						
Undisturbed	1×10^{-2}	1×10^{-3}	3×10^{-2}	none	Cumulative	Skokan et al.,1988; Powers et al.,1978; Black et al., 1983
Disturbed	6×10^{-2}			none	Constant	See text.
Specific storage	9.5×10^{-8}	2.8×10^{-8}	1.4×10^{-6}	m^{-1}	Cumulative	Beauheim, June 14, 1991, Memo (Appendix A)
Tortuosity	1.4×10^{-1}	1×10^{-2}	6.67×10^{-1}	none	Cumulative	See Culebra, text; Freeze and Cherry, 1979, p. 104

2.3.1 Capillary Pressure and Relative Permeability

Threshold Displacement Pressure, p_t

Parameter:	**Threshold displacement pressure (p_t)**
Median:	2.3×10^7
Range:	2.3×10^5
	2.3×10^9
Units:	Pa
Distribution:	Lognormal
Source(s):	Davies, P. B. 1991. *Evaluation of the Role of Threshold Pressure in Controlling Flow of Waste-Generated Gas into Bedded Salt at the Waste Isolation Pilot Plant.* SAND90-3246. Albuquerque, NM: Sandia National Laboratories.
	Davies, P. B. 1991. "Uncertainty Estimates for Threshold Pressure for 1991 Performance Assessment Calculations Involving Waste-Generated Gas." Internal memo to D. R. Anderson (6342), June 2, 1991. Albuquerque, NM: Sandia National Laboratories. (In Appendix A of this volume)

Discussion:

Threshold pressure plays an important role in controlling which Salado lithologies are accessible to gas and at what pressure gas will flow. The Salado Formation's thick halite beds with anhydrite and clay interbeds are similar in many respects to the consolidated lithologies presented in Figure 2.3-1. Similarities in pore structure exist between halite, anhydrite, and low-permeability carbonates; low-permeability sandstones and crystalline cements; and clay interbeds and shales. Given the general similarities, a best-fit power curve through the combined data set for consolidated lithologies was judged to provide the best available correlation for estimates of threshold pressure for the Salado Formation (Figure 2.3-1). Threshold pressure is also a key parameter in the Brooks and Corey (1964) model used to characterize the 2-phase properties of analogue materials for preliminary gas calculations (Davies and LaVenue, 1990). Because threshold pressure is strongly related to intrinsic permeability, an empirical estimate is used as follows:

$$p_t \text{ (MPa)} = 5.6 \times 10^{-7} [k \text{ (m}^2\text{)}]^{-0.346}$$

p_t is commonly referred to as the threshold displacement pressure. Hence, the capillary pressure can be evaluated given p_t, λ, $s_{\ell r}$, and s_{gr}. Some investigators define threshold pressure as the capillary pressure associated with first penetration of a nonwetting phase into the largest pores near the surface of the medium, which means that threshold pressure is equal to the capillary pressure at a water saturation of 1.0 (Davies, 1991, p. 9). Others define threshold pressure as the capillary pressure associated with the incipient development of a

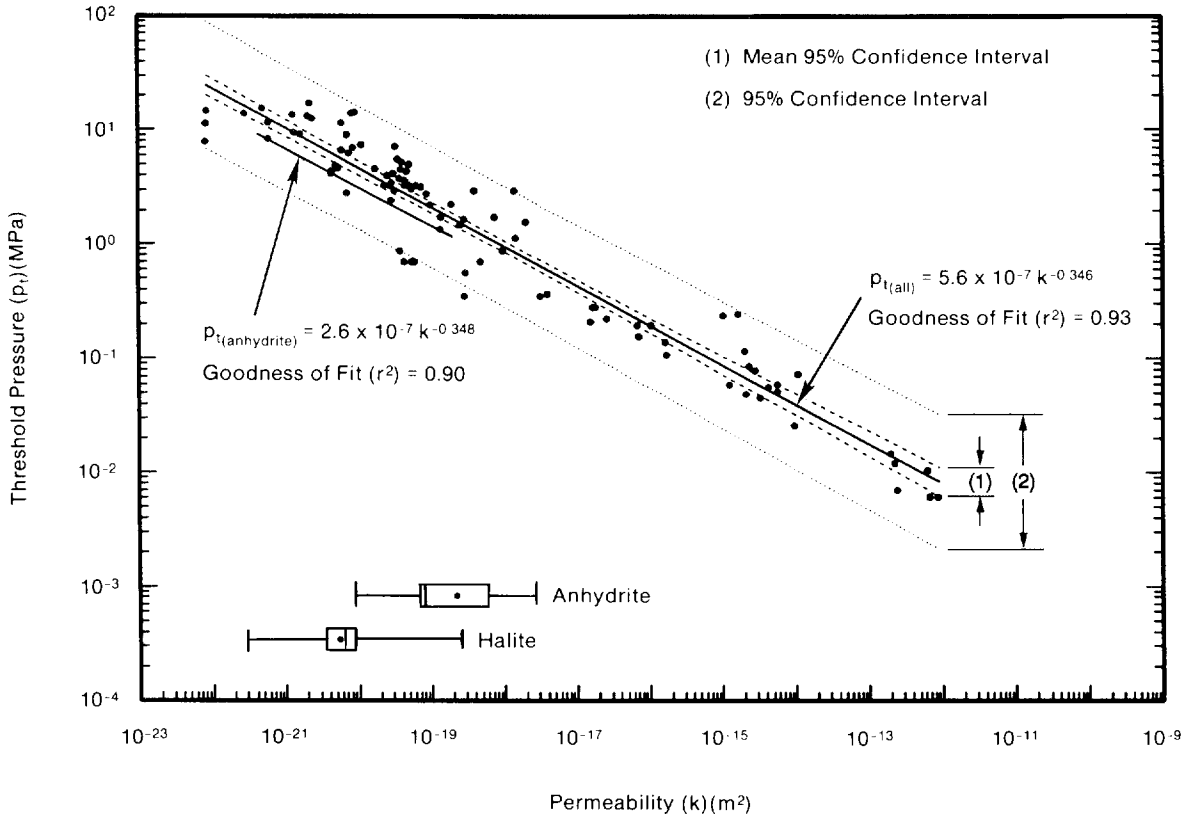

TRI-6344-730-1

Figure 2.3-1. Correlation of Threshold Pressure with Permeability for a Composite of Data from All Consolidated Rock Lithologies. Data from Ibrahim et al., 1970; Rose and Bruce, 1949; Thomas et al., 1968; and Wyllie and Rose, 1950. (after Davies, 1991, Figures 5 and 8)

continuum of the nonwetting phase through a pore network, providing gas pathways not only through relatively large pores, but also through necks between pores. This latter definition means that threshold pressure is equal to the capillary pressure at a saturation equal to the residual gas saturation (dashed lines in Figure 2.3-2).

Because flow of waste-generated gas outward from the WIPP repository will require that outward flowing gas penetrate and establish a gas-filled network of flow paths in the surrounding bedded salt, the latter definition has been adopted here.

Capillary Pressure and Relative Permeability

Figure 2.3-2a shows the values estimated for relative permeability for Salado salt. Figure 2.3-2b shows the estimated capillary pressure curve for Salado salt. Figure 2.3-3 is an example of variation in relative permeability and capillary pressure when Brooks and Corey parameters are varied.

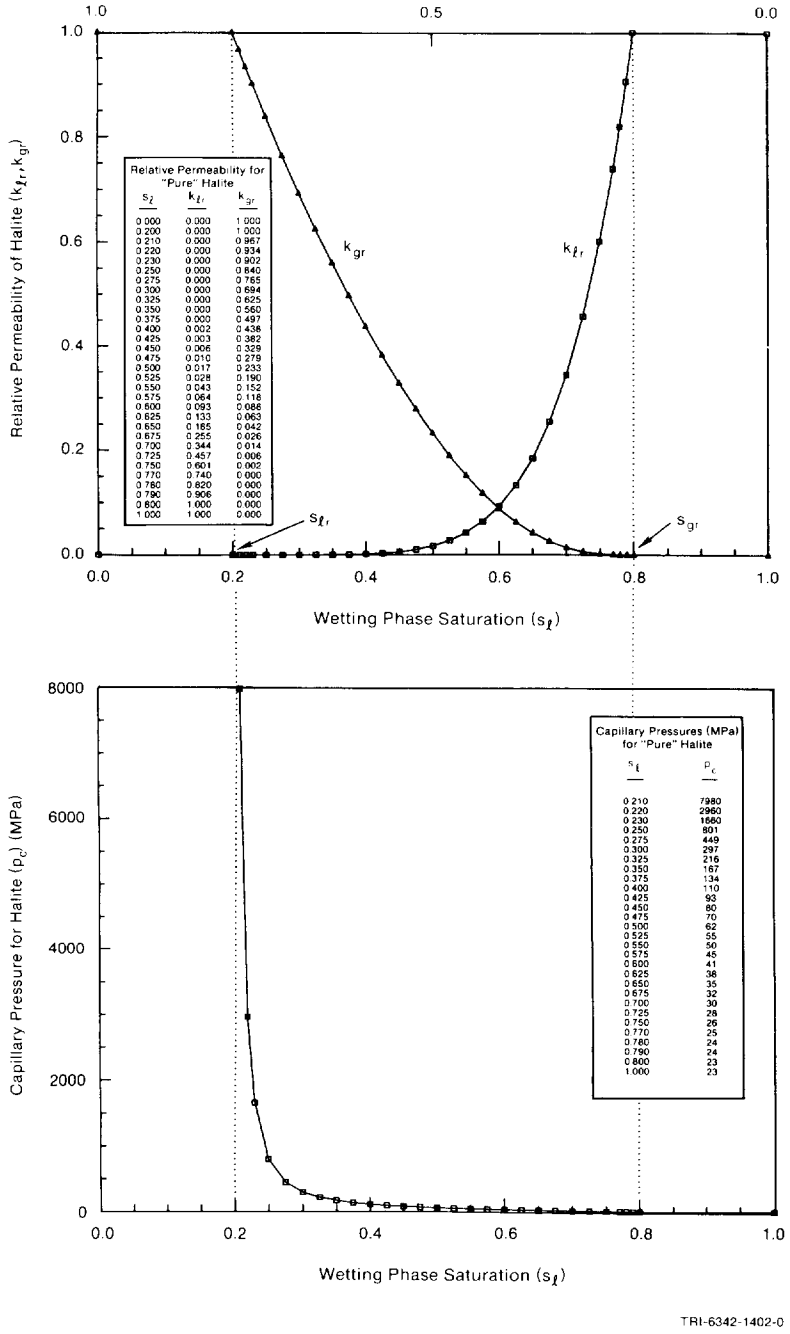

Figure 2.3-2. Estimated Capillary Pressure and Relative Permeability Curves.

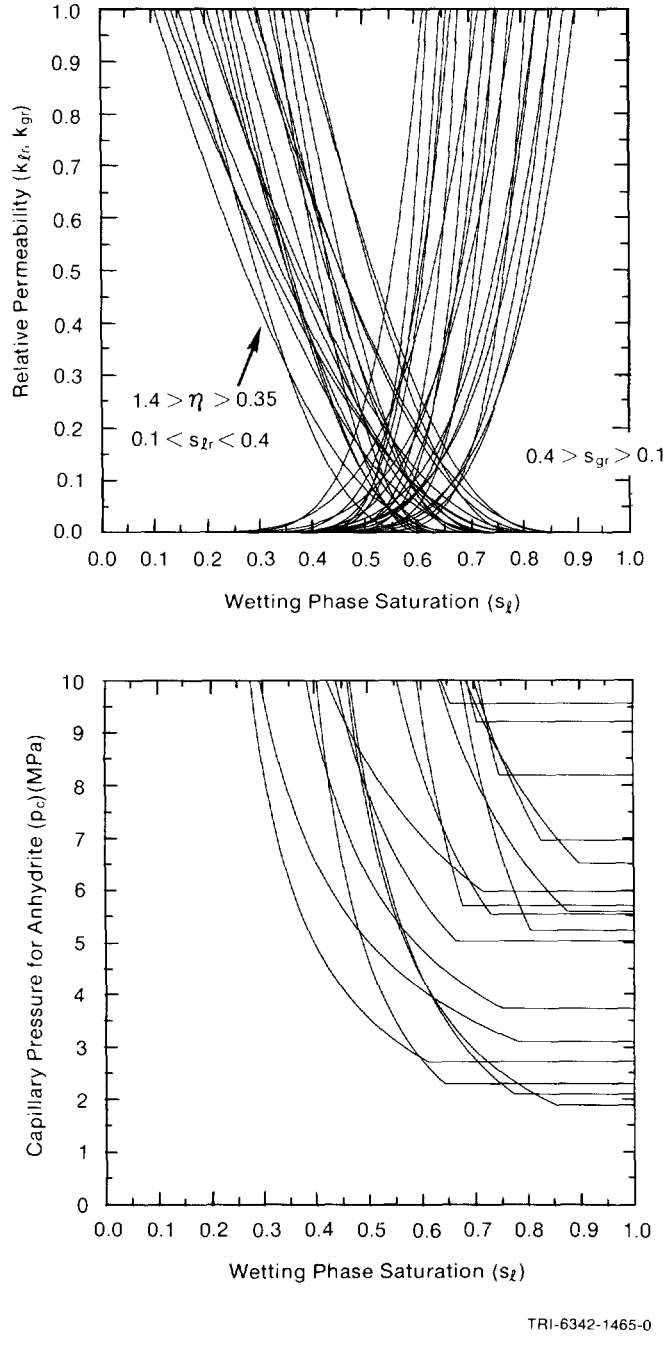

Figure 2.3-3. Example of Variation in Relative Permeability and Capillary Pressure When Brooks and Corey Parameters are Varied.

Residual Saturations

Parameter:	**Residual wetting phase (liquid) saturation ($S_{\ell r}$)**
Median:	2×10^{-1}
Range:	1×10^{-1}
	4×10^{-1}
Units:	Dimensionless
Distribution:	Cumulative
Source(s):	Davies, P. B. and A. M. LaVenue. 1990b. "Additional Data for Characterizing 2-Phase Flow Behavior in Waste-Generated Gas Simulations and Pilot Point Information for Final Culebra 2-D Model." Memo 11 in Appendix A of Rechard et al. 1990. *Data Used in Preliminary Performance Assessment of the Waste Isolation Pilot Plant.* SAND89-2408. Albuquerque, NM: Sandia National Laboratories.

Parameter:	**Residual gas saturation (S_{gr})**
Median:	2×10^{-1}
Range:	1×10^{-1}
	4×10^{-1}
Units:	Dimensionless
Distribution:	Cumulative
Source(s):	Davies, P. B. and A. M. LaVenue. 1990b. "Additional Data for Characterizing 2-Phase Flow Behavior in Waste-Generated Gas Simulations and Pilot Point Information for Final Culebra 2-D Model." Memo 11 in Appendix A of Rechard et al. 1990. *Data Used in Preliminary Performance Assessment of the Waste Isolation Pilot Plant.* SAND89-2408. Albuquerque, NM: Sandia National Laboratories.

Brooks and Corey Exponent

Parameter:	**Brooks and Corey exponent (η)**
Median:	7×10^{-1}
Range:	3.5×10^{-1}
	1.4
Units:	Dimensionless
Distribution:	Cumulative
Source(s):	Davies, P. B. and A. M. LaVenue. 1990b. "Additional Data for Characterizing 2-Phase Flow Behavior in Waste-Generated Gas Simulations and Pilot Point Information for Final Culebra 2-D Model." Memo 11 in Appendix A of Rechard et al. 1990. *Data Used in Preliminary Performance Assessment of the Waste Isolation Pilot Plant.* SAND89-2408. Albuquerque, NM: Sandia National Laboratories.

Discussion:

Capillary pressures and relative permeabilities for the Salado halite, the anhydrite layers, and waste have not been measured. As presented and discussed in Davies (1991), natural analogs were used to provide capillary pressure and relative permeability curves for these lithologies as follows:

Brooks and Corey defined s_e as

$$s_e = \frac{s_\ell - s_{\ell r}}{1 - s_{\ell r}} \qquad (2.3\text{-}1)$$

where s_ℓ is the wetting phase saturation (brine) and s_{ℓ_r} is the residual wetting phase saturation, below which the wetting phase no longer forms a continuous network through the pore network and therefore does not flow, regardless of the pressure gradient. This has been modified to account for residual (or critical) gas saturation, s_{gr}:

$$s_e = \frac{s_\ell - s_{\ell r}}{1 - s_{gr} - s_{\ell r}} \qquad (2.3\text{-}2)$$

Brooks and Corey observed that the effective saturation of a porous material, s_e, can be related to the capillary pressure, p_c, by

$$s_e = \left[\frac{p_t}{p_c}\right]^\lambda \quad \text{or} \quad p_c = \frac{p_t}{s_e^{1/\lambda}} \qquad (2.3\text{-}3)$$

where

λ and p_t = characteristic constants of the material.

p_c = $p_g - p_\ell$

p_g = pressure of the gas

p_ℓ = pressure of the wetting phase

In addition, after obtaining the effective saturation from Eq. 2.3-1 the relative permeability of the wetting phase ($k_{r\ell}$) is obtained from

$$k_{r\ell} = s_e^{\frac{2 + 3\lambda}{\lambda}} \qquad (2.3\text{-}4)$$

For the gas phase, the relative permeability (k_{rg}) is

$$k_{rg} = \left(1 - s_e\right)^2 \left[1 - s_e^{\frac{2 + \lambda}{\lambda}}\right] \qquad (2.3\text{-}5)$$

Although none of the four parameters that are used in Eqs. 2.3-2, 2.3-3, 2.3-4 and 2.3-5 has been measured for either the Salado halite, anhdyrites, or waste room, they were estimated from values that were obtained from the natural analogs (Davies, 1991; Davies and LaVenue, 1990b). The natural analogs consist of alternate materials that possess some of the same characteristics (i.e., permeability and porosity) as the anhydrite, halite, and waste room. The natural analogs applicable to the very low permeability of the halite and anhydrite were sands that were investigated during the Multiwell Tight Gas Sands Project (Ward and Morrow, 1985). The permeability for these sands typically ranges from 1 x 10^{-16} to 1 x 10^{-19} m^2 (1 x 10^{-1} to 1 x 10^{-4} mD). Although these permeabilities are higher than those of the anhdyrites and halites, no other material was found with a lower permeability for which capillary pressure and relative permeability curves had been measured. The following values have been selected for Salado halite: $\lambda = 0.7$, $s_{\ell r} = 0.2$, $s_{gr} = 0.2$. The values selected for the anhydrites and waste room are discussed in later sections.

The resulting curves for capillary pressure and relative permeability were shown in Figure 2.3-2.

The uncertainty surrounding these parameters is unknown. An initial range was selected for the purpose of being able to run sensitivity parameter studies. The ranges shown for the parameters are arbitrary, corresponding to a simple doubling and halving of the median values. The range of curves produced by sampling 20 times from the assigned distribution using LHS (Volume 2) is shown in Figure 2.3-3.

2.3.2 Density

Grain Density of Halite in Salado Formation

Parameter:	**Density, grain (ρ_g)**
Median:	2.163×10^3
Range:	None
Units:	kg/m^3
Distribution:	Constant
Source(s):	Carmichael, R. S., ed. 1984. *CRC Handbook of Physical Properties of Rocks*, Vol III. Boca Raton, FL: CRC Press, Inc. (Table 2) Krieg, R. D. 1984. *Reference Stratigraphy and Rock Properties for the Waste Isolation Pilot Plant (WIPP) Project.* SAND83-1908. Albuquerque, NM: Sandia National Laboratories. (p. 14) Clark, S. P. 1966. *Handbook of Physical Constants.* New York, NY: The Geological Society of America, Inc. (p. 44)

Discussion:

The published grain density of halite (NaCl) is 2,163 kg/m^3 (135 lb/ft^3) (Carmichael, 1984, Table 2; Krieg, 1984, p. 14; Clark, 1966, p. 44).

Grain Density of Polyhalite in Salado Formation

Parameter:	**Density, grain (ρ_g)**
Median:	2.78×10^3
Range:	None
Units:	kg/m^3
Distribution:	Constant
Source(s):	Shakoor, A. and H. R. Hume. 1981. "Chapter 3: Mechanical Properties," in *Physical Properties Data for Rock Salt.* NBS Monograph 167. Washington, DC: National Bureau of Standards. (p. 103-203)

Discussion:

The published grain density of polyhalite is 2,780 kg/m^3 (173.6 lb/ft^3) (Shakoor and Hume, 1981).

Bulk Density of Halite in Salado (Halite)

Parameter:	**Density, bulk** (ρ_{bulk})
Median:	2.14×10^3
Range:	None
Units:	kg/m^3
Distribution:	Constant
Source(s):	Holcomb, D. J. and M. Shields. 1987. *Hydrostatic Creep Consolidation of Crushed Salt with Added Water.* SAND87-1990. Albuquerque, NM: Sandia National Laboratories. (p. 17)

Discussion:

The PA Division uses a bulk density of halite near the repository of 2,140 kg/m^3 (133.6 lb/ft^3) as reported by Holcomb and Shields (1987, p. 17). This value corresponds to a porosity of 0.01 ($\phi = 1 - (\rho_b/\rho_g)$).

Average Density near Repository

Parameter:	**Density, average (ρ_{ave})**
Median:	2.3×10^3
Range:	None
Units:	kg/m^3
Distribution:	Constant
Source(s):	Krieg, R. D. 1984. *Reference Stratigraphy and Rock Properties for the Waste Isolation Pilot Plant (WIPP) Project.* SAND83-1908. Albuquerque, NM: Sandia National Laboratories. (Table 4)

Discussion:

The average density of the Salado Formation in a 107.06-m (351.25-ft) interval straddling the repository is 2,300 kg/m^3 (143.6 lb/ft^3). The interval includes anhydrite marker beds 134, 136, and 138 (above the repository) and anhydrite marker beds 139, 140, and polyhalite marker bed 141 (below the repository) (see Figure 2.2-4). (Marker beds 135 and 137 are very thin and not found in every borehole; therefore these marker beds are not included.) The sum of the thicknesses of all layers of halite and argillaceous halite is 90.92 m (298.29 ft). Assuming that 83.5% of this thickness is pure halite (89.12 m [292.39 ft]) with a grain density of 2,163 kg/m^3 (135 lb/ft^3) (see Table 2.4-1) and that the remaining thickness (17.94 m [58.86 ft]) (16.5% of total thickness) is anhydrite with a density of 2,963 kg/m^3 (185 lb/ft^3) (see Table 2.4-1) yields a weighted average density of 2,300 kg/m^3 (144 lb/ft^3) (Krieg, 1984, p. 14).

2.3.3 Dispersivity

Parameter:	**Dispersivity, longitudinal (α_L)**
Median:	1.5×10^1
Range:	1
	4×10^1
Units:	m
Distribution:	Cumulative
Source(s):	Pickens, J. F., and G. E. Grisak. 1981. Modeling of Scale-Dependent Dispersion in Hydrogeologic Systems. *Water Resources Research*, vol. 17, no. 6, pp. 1701-11.
	Lappin, A. R., R. L. Hunter, D. P. Garber, and P. B. Davies, eds. 1989. *Systems Analysis Long-Term Radionuclide Transport, and Dose Assessments, Waste Isolation Pilot Plant (WIPP), Southeastern New Mexico; March 1989.* SAND 89-0462. Albuquerque, NM: Sandia National Laboratories. (Table D-2)

Parameter:	**Dispersivity, transverse (α_T)**
Median:	1.5
Range:	1×10^{-1}
	4
Units:	m
Distribution:	Cumulative
Source(s):	Pickens, J. F., and G. E. Grisak. 1981. Modeling of Scale-Dependent Dispersion in Hydrogeologic Systems. *Water Resources Research*, vol. 17, no. 6, pp. 1701-11.
	Freeze, R. A. and J. C. Cherry. 1979. *Groundwater.* Englewood Cliffs, NJ: Prentice-Hall, Inc.

Discussion:

No solute transport tests have been run in the Salado Formation, and no relevant solute transport data exist for very low permeability media from which to estimate dispersivity (α). However, current models show limited fluid movement away from the disposal area (Rechard et al., 1989); hence, the rule of thumb applied in standard porous media (Pickens and Grisak, 1981) is assumed to apply, that is, the longitudinal dispersivity $\alpha_L \simeq 0.1 d_s$ where d_s is the distance traveled by the solute. For typical distances traveled, α_L is between 1 and 40 m (3 and 130 ft). The distribution for α_L is shown in Figure 2.3-4.

Transverse dispersivity (α_T) is usually linearly related to α_L. The ratio of α_L to α_T typically varies between 5 and 20 (see, for example, Bear and Verruijt, 1987; Freeze and Cherry, 1979, Figure 9.6; Dullien, Figure 7.13). However, at very low velocities the ratio can approach 1, while in some strata the ratio has been reported to approach 100 (de Marsily, 1986). Transverse dispersivity was assumed to be ten times smaller than α_L ($\alpha_T \sim 0.1\alpha_L$) for PA transport calculations. The current range for sensitivity studies is 1 to 25 (Figure 2.3-5).

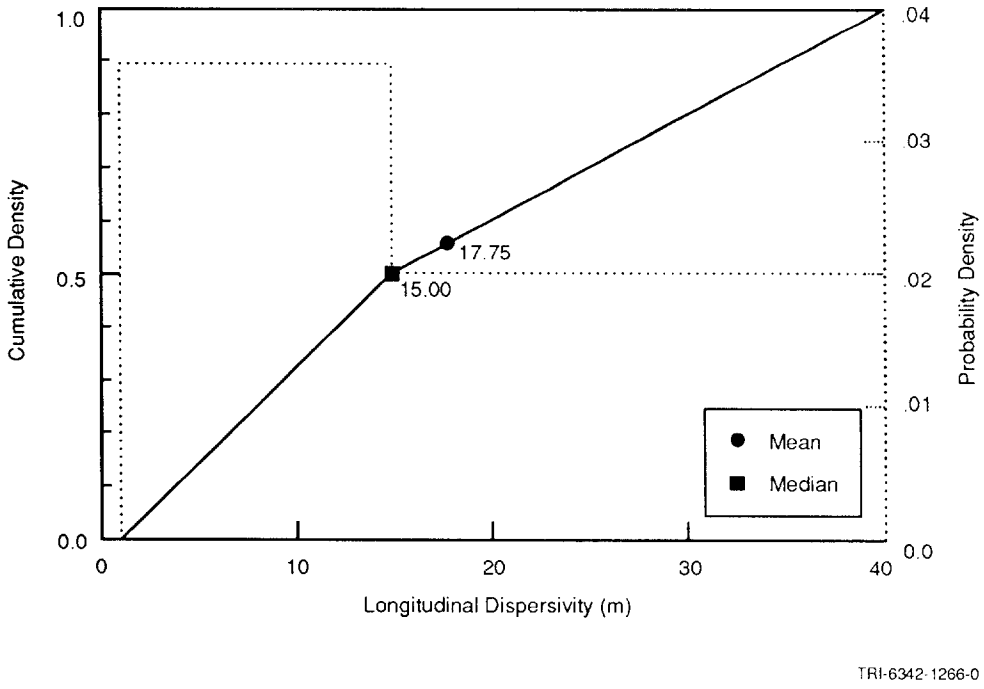

Figure 2.3-4. Estimated Distribution (pdf and cdf) for Longitudinal Dispersivity in Halite, Salado Formation.

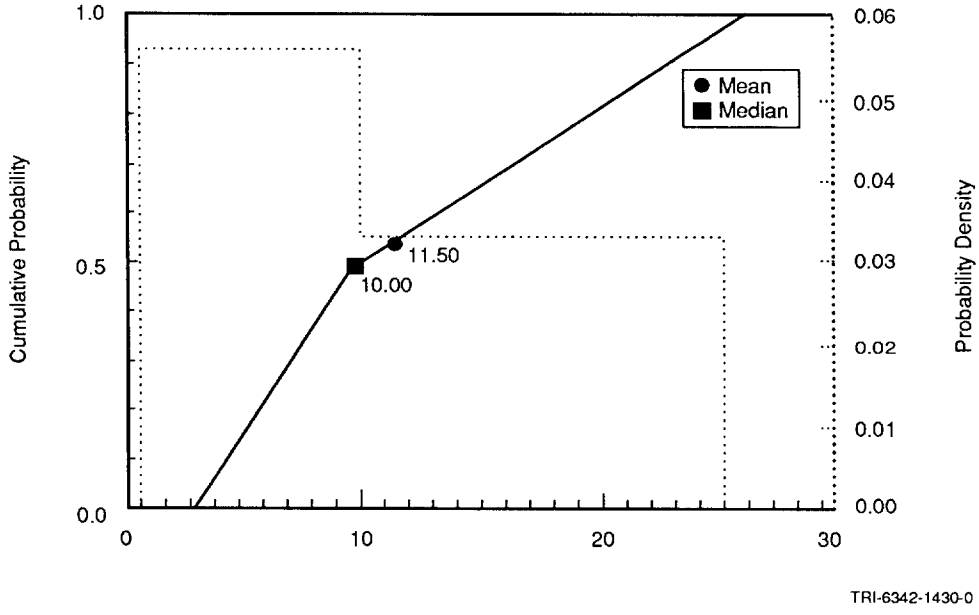

Figure 2.3-5. Estimated Distribution (pdf and cdf) for Transverse Dispersivity in Halite, Salado Formation.

2.3.4 Partition Coefficients and Retardation

Parameter:	**Partition coefficient for halite and polyhalite**
Median:	0
Range:	None
Units:	m^3/kg
Distribution:	Constant
Source(s):	Lappin, A. R., R. L. Hunter, D. P. Garber, and P. B. Davies, eds. 1989. *Systems Analysis Long-Term Radionuclide Transport, and Dose Assessments, Waste Isolation Pilot Plant (WIPP), Southeastern New Mexico; March 1989.* SAND89-0462. Albuquerque, NM: Sandia National Laboratories. (p. D-17)

Discussion:

The halite and polyhalite in the Salado Formation are assumed to not adsorb any contaminants; only clay layers in the Salado Formation are assumed to have this capability (see Sections 2.4.4 and 3.2.4).

2.3.5 Permeability

Undisturbed Permeability

Parameter:	**Permeability, undisturbed** (k)
Median:	5.7×10^{-21}
Range:	8.6×10^{-22}
	5.4×10^{-20}
Units:	m^2
Distribution:	Data
Source(s):	Beauheim, R. 1991. "Review of Salado Parameter Values To Be Used in 1991 Performance Assessment Calculations," Internal memo to Rob Rechard (6342), June 14, 1991. Albuquerque, NM: Sandia National Laboratories. (In Appendix A of this volume)

Figure 2.3-6 shows the values for permeability assuming no correlation with distance from excavation. Figure 2.3-7 shows a non-linear fit of halite permeability with distance from the excavation.

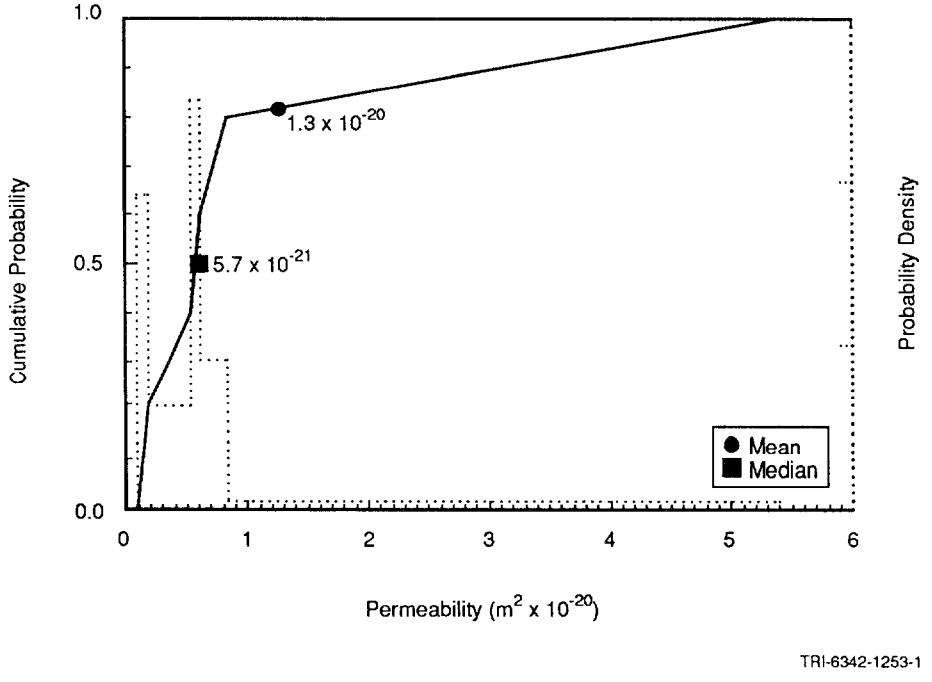

Figure 2.3-6. Estimated Distribution (pdf and cdf) for Salado Undisturbed Permeability.

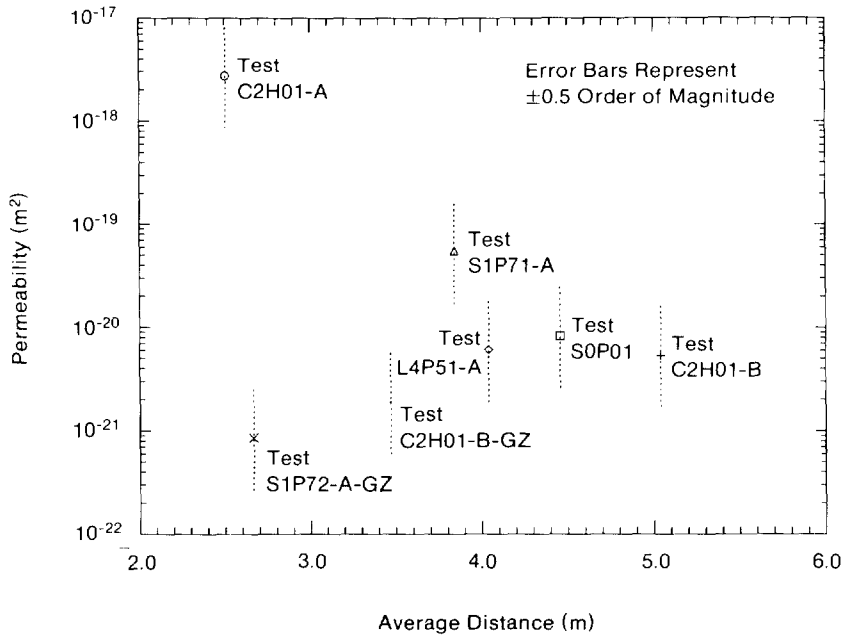

Figure 2.3-7. Logarithm of Halite Permeability Fitted to Distance from the Excavation.

Discussion:

Three experimental programs (Room Q, Small-Scale Brine Inflow, and Permeability Tests, described in the draft of the "Sandia National Laboratories Waste Isolation Pilot Plant Program Plan for Fiscal Year 1992") are evaluating permeability (and storativity and pore pressure) in the halite and anhydrite layers of the Salado Formation. In both 1990 and 1991 PA calculations (Rechard et al., 1990a, p II-13), we used values from the Permeability Test program (Beauheim et al., 1990; Beauheim, June 14, 1991, Memo [Appendix A]) until the Fluid Flow and Transport Division standardizes the interpretation of permeability tests.

Interestingly, over the past several years, the distribution of permeability in the halite has remained generally similar to a lognormal distribution with a range between 10^{-23} and 10^{-18} and a median of 3×10^{-21} m^2 (e.g., McTigue, 1988 in Lappin et al., 1989, p. A-97).

A fit of Beauheim's data to distance from excavation (Figure 2.3-6) shows that the $\log_{10}$ of the asymptotic value of undisturbed halite permeability is -20.83 ± 1.64. The probable error in this estimate can be construed as a one-sigma confidence limit on the asymptotic value.

Rank Correlation Between Halite and Anhydrite Permeability in Salado Formation. Available data are recorded in Table 2.3-2 (from Gorham, July 2, 1991, Memo, and Beauheim, June 14, 1991, Memo [Appendix A]):

Table 2.3-2. Data for Calculating a Rank Correlation between Halite and Anhydrite Permeability In Salado Formation.

Test[a]	Interval[a] (m)	Lithology[a]	Permeability (m^2)[b] Halite	Permeability (m^2)[b] Anhydrite
C2H01-A	2.09 - 2.92	halite	2.7×10^{-18}	
C2H01-A-GZ	0.50 - 1.64	halite		
C2H01-B	4.50 - 5.58	halite	5.3×10^{-21}	
C2H01-B-GZ	2.92 - 4.02	halite	1.9×10^{-21}	
C2H01-C	6.80 - 7.76	MB139		9.5×10^{-19}
C2H02	9.47 - 10.86	MB139		7.8×10^{-20}
L4P51-A	3.33 - 4.75	halite	6.1×10^{-21}	
L4P51-A-GZ	1.50 - 2.36	MB139		
S0P01	3.74 - 5.17	halite	8.3×10^{-21}	
S0P01-GZ	1.80 - 2.76	MB139		$<5.7 \times 10^{-18}$
S1P71-A	3.12 - 4.56	halite	5.4×10^{-20}	
S1P71-A-GZ	1.40 - 2.25	MB139		
S1P71-B	9.48 - 9.80	Anhydrite "c"		
S1P72	4.40 - 6.00	MB139		6.8×10^{-20}
S1P72-GZ	2.15 - 3.18	halite	8.6×10^{-22}	
SCP01	10.50 - 14.78	MB139		
L4P51-B	9.62 - 9.72	Anhydrite "c"		6.8×10^{-20}
S1P73-B	10.86 - 11.03	MB138		

[a] Gorham, July 2, 1991, Memo, Appendix A
[b] Beauheim June 14, 1991, Memo, Appendix A

Note that there are only *two* (halite, anhydrite) pairs of measurements from comparable intervals:

halite, 2.7×10^{-18} m^2 (2.09-2.92 m) + anhydrite, $<5.7 \times 10^{-18}$ m^2 (1.80-2.76 m)

and

halite, 5.3×10^{-21} m^2 (4.50-5.58 m) + anhydrite, 6.8×10^{-20} m^2 (4.40-6.00 m)

To compute a rank correlation with these data, we first make the following table (Table 2.3-3):

Table 2.3-3. Ranks Halite and Anhydrite Data

	(Halite)		Anhydrite	
i	x_i	$R(x_i)$	y_i	$R(y_i)$
1	2.7×10^{-18}	2	5.7×10^{-18}	2
2	5.3×10^{-21}	1	6.8×10^{-20}	1

where

$R(x_i)$ is the rank of x_i in the data set $x_1, x_2, ..., x_n$, and

$R(y_i)$ is the rank of y_i in the data set $y_1, y_2, ..., y_n$.

Conover (1980, p. 252, Eq. 6) suggests using the following formula for computing rank correlation (r_{rank}) when there are many "ties" in the paired data:

$$r_{rank} = \frac{\sum_{i=1}^{n} R(x_i)\, R(y_i) - n\left(\frac{n+1}{2}\right)^2}{\left[\sum_{i=1}^{n} R(x_i)^2 - n\left(\frac{n+1}{2}\right)^2\right]^{1/2} \cdot \left[\sum_{i=1}^{n} R(y_i)^2 - n\left(\frac{n+1}{2}\right)^2\right]^{1/2}}$$

Using the data for $R(x_i)$, $R(y_i)$ given in the table above, it can be seen that $r_{rank}=1$. (This result is expected since limited data are all tied.)

The most important information from the above result is that the correlation coefficient is positive. The actual value is most likely less than one. For current PA calculations, the rank correlation coefficient is assumed to be 0.80 (Figure 2.3-6). This value is high enough to greatly limit the probability that the anhydrite will have a lower permeability than the halite and thereby change the current conceptual model of brine flow within the Salado Formation.

Disturbed Permeability

Parameter:	**Permeability, disturbed** (k)
Median:	1×10^{-19}
Range:	1×10^{-20}
	1×10^{-18}
Units:	m^2
Distribution:	Lognormal
Source(s):	Beauheim, R. L. 1990. "Review of Parameter Values to be Used in Performance Assessment," Memo 3c in Appendix A of Rechard et al. 1990. *Data Used in Preliminary Performance Assessment of the Waste Isolation Pilot Plant (1990).* SAND89-2408. Albuquerque, NM: Sandia National Laboratories.

Discussion:

The disturbed permeability and porosity of the Salado Formation and interbeds vary from the intact properties to large, open fractures. These two disturbed properties also change as the stress field around the excavations change with time. Furthermore, the halite will likely heal to intact conditions over time (Lappin et al., 1989, p. 4-45; Sutherland and Cave, 1978). Often the PA Division does not model the disturbed zone when it is conservative to do so; however, when necessary the following values are typically used.

The disturbed permeability after consolidation and healing is assumed to vary between 1×10^{-20} m^2 (1×10^{-5} mD) (permeability at 0.95 of intact density [see Figure 3.2-3]) and the highest value measured. Beauheim et al. (1990, Table 7-1) reports one measurement from the disturbed rock zone in the Salado Formation of about 1×10^{-18} m^2 (1×10^{-3} mD). The median value was set about one and one-half orders of magnitude higher than the corresponding median value for the intact Salado Formation.

Figure 2.3-8 shows the estimated distribution for the disturbed permeability of the Salado.

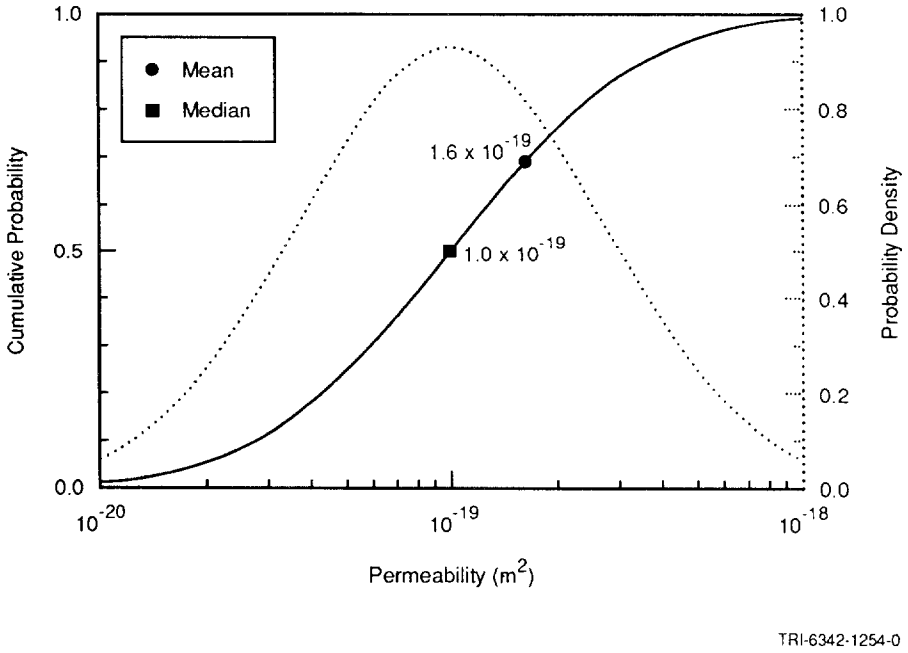

Figure 2.3-8. Estimated Distribution (pdf and cdf) for Disturbed Permeability in Halite, Salado Formation.

2.3.6 Pore Pressure at Repository Level in Halite

Parameter:	**Pore pressure** (p)
Median:	1.28×10^7
Range:	9.3×10^6
	1.39×10^7
Units:	Pa
Distribution:	Data
Source(s):	Beauheim, R. L. 1991. "Review of Salado Parameter Values to be Used in 1991 Performance Assessment Calculations," Internal memo to Rob Rechard (6342), June 14, 1991. Albuquerque, NM: Sandia National Laboratories. (In Appendix A of this volume)
	Howarth, S. 1991. "Pore Pressure Distributions for 1991 Performance Assessment Calculations," Internal memo to Elaine Gorham (6344), June 12, 1991. Albuquerque, NM: Sandia National Laboratories. (In Appendix A of this volume).

Figure 2.3-9 shows the estimated distribution for brine pore pressure in halite. Figure 2.3-10 shows two non-linear fits of brine pore pressure to distance from the excavation.

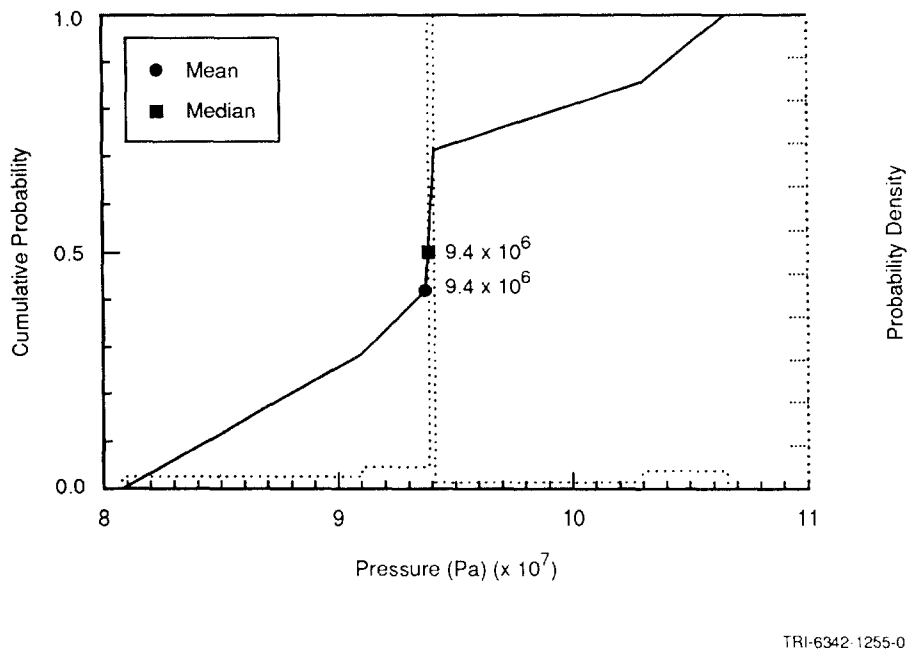

Figure 2.3-9. Estimated Distribution (pdf and cdf) for Brine Pore Pressure at Repository Level in Halite, Salado Formation.

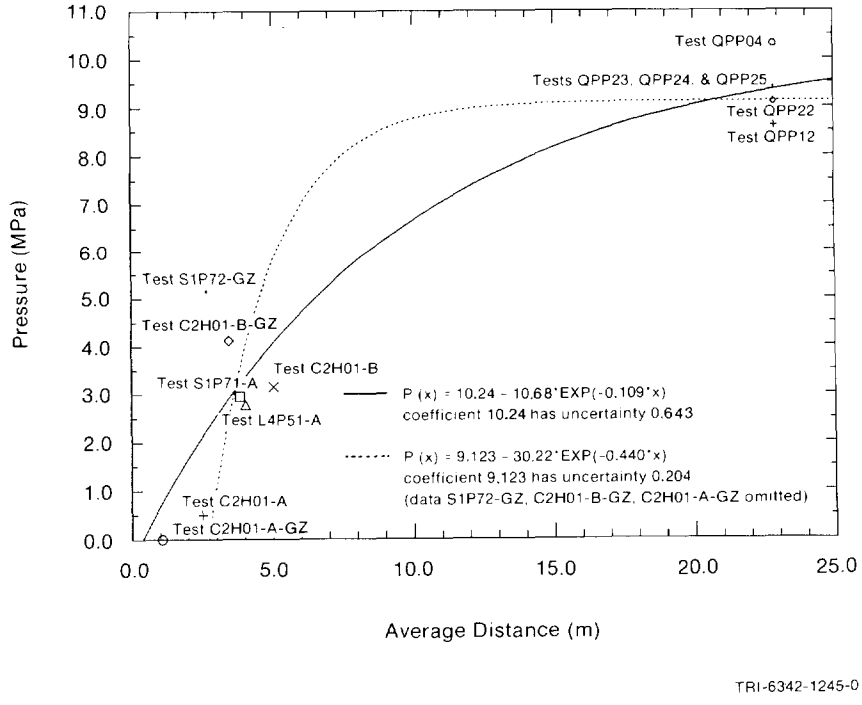

Figure 2.3-10. Non-Linear Fit of Halite Pore Pressure to Distance from Excavation.

Discussion:

In 1991, seven pore pressure measurements from borehole tests taken prior to excavation and located 22.9 m (75 ft) from any existing excavation were available from Room Q (Howarth, June 12, 1991, Memo [Appendix A]). (Beauheim [June 14, 1991, Memo, Appendix A] suggested that none of his pore pressure measurements in the halite be considered to represent far-field conditions.) One Room Q measurement (1 MPa) clearly showed the effects of depressurization. Although all remaining Room Q values are at or above hydrostatic pressure (~6 MPa [$z \cdot \rho_{brine} \cdot g$ $\rho_{Culebra}$] pore pressures, assuming 1 MPa at the Culebra), they are distinctly lower than measurements taken at the same time in the anhydrite layer, suggesting some depressurization. Consequently, the 1991 PA calculations use the pore pressure measured in the anhydrite where data suggest less depressurization.

Non-linear fits of pore pressure to distance (Figure 2.3-10) show that the asymptotic value of pore pressure is about 10 MPa with a probable error of about 0.6 MPa. The probable error can be construed as a one-sigma confidence limit.

2.3.7 Porosity

Undisturbed Porosity

Parameter:	**Porosity, undisturbed (ϕ)**
Median:	1×10^{-2}
Range:	1×10^{-3}
	3×10^{-2}
Units:	Dimensionless
Distribution:	Cumulative
Source(s):	Skokan, C., J. Starrett, and H. T. Andersen. 1988. *Final Report: Feasibility Study of Seismic Tomography to Monitor Underground Pillar Integrity at the WIPP Site.* SAND88-7096. Albuquerque, NM: Sandia National Laboratories.
	Powers, D. W., S. J. Lambert, S. E. Shaffer, L. R. Hill, and W. D. Weart, ed. 1978. *Geological Characterization Report, Waste Isolation Pilot Plant (WIPP) Site, Southeastern New Mexico.* SAND78-1596, vol. 1 and 2. Albuquerque, NM: Sandia National Laboratories.
	Black, S. R., R. S. Newton, and D. K. Shukla, eds. 1983. "Brine Content of the Facility Interval Strata" in *Results of the Site Validation Experiments,* Vol. II, Supporting Document 10. Waste Isolation Pilot Plant, U.S. Department of Energy.

Discussion:

The median porosity is assumed to be 0.01 based on electromagnetic and DC resistivity measurements (Skokan et al., 1989). This median value is identical to that calculated from a grain density of 2,163 kg/m^3 (135 lb/ft^3) for halite (see Table 2.7-1) and a bulk density of 2,140 kg/m^3 (133.6 lb/ft^3) ($\rho_b = (1-\phi)\rho_g$) (see Table 2.2-1). Although not varied in current PA calculations, the low of 0.001 is based on drying experiments (Powers et al., 1978), while the high of 0.03 is based on the low end of the DC resistivity measurements (Skokan et al., 1988).

Figure 2.3-11 shows the estimated distribution for the undisturbed porosity.

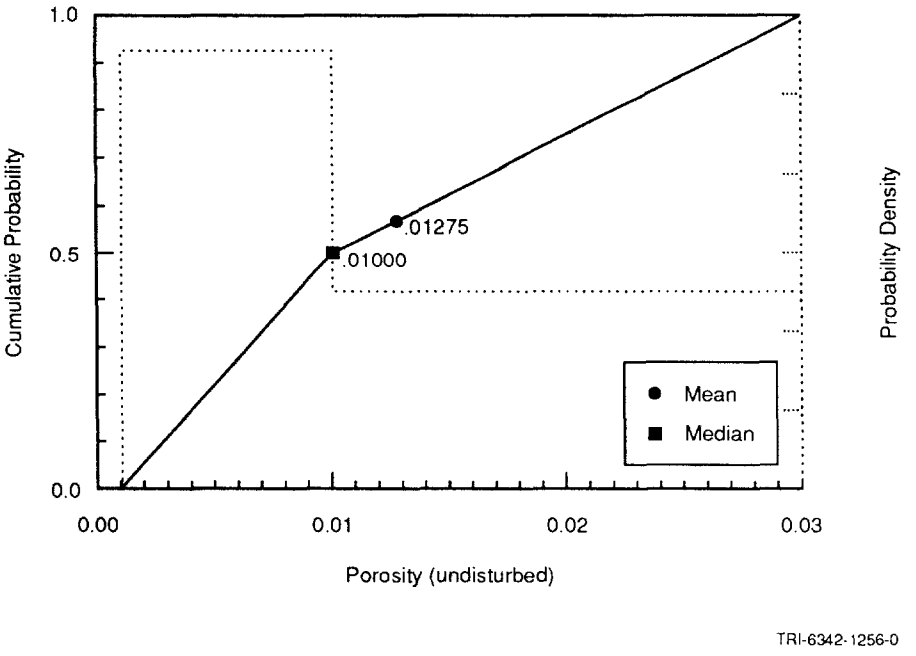

Figure 2.3-11. Estimated Distribution (pdf and cdf) for Undisturbed Porosity in Halite, Salado Formation.

Disturbed Porosity

Parameter:	**Porosity, disturbed (ϕ)**
Median:	6×10^{-2}
Range:	None
Units:	Dimensionless
Distribution:	Constant
Source(s):	See text below.

Discussion:

The disturbed porosity of 0.06 (after consolidation and healing [Lappin et al., 1989, p. 4-45; Sutherland and Cave, 1978]) is calculated assuming that the final density is 0.95 of the intact density ($0.95\rho_b = (1-\phi)\rho_g$) (refer to Figure 3.2-3).

2.3.8 Specific Storage

Parameter:	**Specific storage**
Median:	9.5×10^{-8}
Range:	2.8×10^{-8}
	1.4×10^{-6}
Units:	m^{-1}
Distribution:	Cumulative
Source(s):	Beauheim, R. 1991. "Review of Salado Parameter Values To Be Used in 1991 Performance Assessment Calculations," Internal memo to Rob Rechard (6342), June 14, 1991. Albuquerque, NM: Sandia National Laboratories. (In Appendix A of this volume).

Figure 2.3-12 shows the estimated distribution for specific storage.

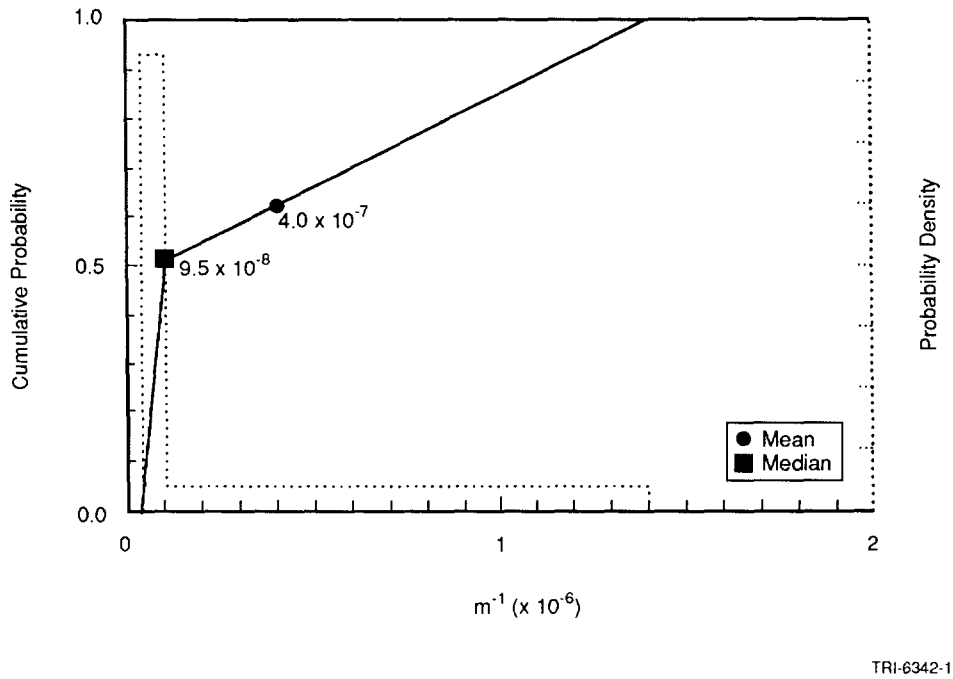

Figure 2.3-12. Estimated Distribution (pdf and cdf) for Specific Storage of Halite, Salado Formation.

The median and range on specific storage are based on laboratory measurements of rock and fluid properties (ϕ, ρ_f, β_f reported herein) and the theoretical definition of specific storage, which is the current procedure for interpreting permeability tests (Beauheim et al., 1991, p. 38).

Beauheim has combined constant-pressure flow tests with pulse tests. This combination allows him to identify the particular values of specific storage that best fit our data. As yet, however, he does not have many of these combined interpretations. Significantly, all of our preliminary values fall within the range established from laboratory experiments, though at the high end. Next year, Beauheim may be able to refine the range somewhat. For the 1991 PA calculations, we used the high end of the laboratory range.

The PA modeling codes all use a slightly different definition of specific storage. To clarify these differences, a detailed discussion of the specific storage term follows.

Derivation of Specific Storage Including Effects of Fluid, Matrix, and Solid Compressibility. Biot (1941) presented a theory for the combined effects of matrix deformation and fluid movement in a porous medium. Rice and Cleary (1976) reformulated Biot's equations in terms of physically identifiable parameters. In this section, we use the notation of Rice and Cleary to derive a general expression for specific storage allowing for fluid, matrix, and solid compressibilities. Direct notation is used with a single underline to identify vectors and double underline to identify 2nd order tensors. Assuming isotropic, linear elastic behavior, Biot's equations for strain, $\underline{\underline{E}}$, written in terms of total stress, $\underline{\underline{\sigma}}$ and fluid pressure p were given in Rice and Cleary as

$$2G\underline{\underline{E}} = \underline{\underline{\sigma}} + P\underline{\underline{I}} - \frac{\nu}{1+\upsilon}\,(\mathrm{tr}\,(\underline{\underline{\sigma}}) + 3p)\,\underline{\underline{I}} - \frac{2G}{3K_s}\,p\underline{\underline{I}} \qquad (2.3\text{-}6)$$

where

- G = drained shear modulus of elasticity
- ν = drained Poisson's ratio
- K_s = bulk modulus of elasticity of solid particles
- $\underline{\underline{I}}$ = identity tensor with components δij
  where $\delta ij = 1$ if $i = j$
  $= 0$ if $i \neq j$
- tr( ) = trace operator such that $\mathrm{tr}\,(\underline{\underline{\sigma}}) = \sigma_{11} + \sigma_{22} + \sigma_{33}$

Equation (2.3-6) can be rewritten using the drained bulk modulus of elasticity, K, for the porous matrix as

$$2G\underline{\underline{E}} = \underline{\underline{\sigma}} - \frac{1}{3}\left(1 - \frac{2G}{3K}\right)\mathrm{tr}\left(\underline{\underline{\sigma}}\right)\underline{\underline{I}} + \frac{2G}{3}\left(\frac{1}{K} - \frac{1}{K_s}\right)p\underline{\underline{I}} \qquad (2.3\text{-}7)$$

This expression can be further simplified by defining the "effective stress" tensor $\bar{\underline{\underline{\sigma}}}$

$$2G\underline{\underline{E}} = \bar{\underline{\underline{\sigma}}} - \frac{1}{3}\left(1 - \frac{2G}{3K}\right)\mathrm{tr}\left(\bar{\underline{\underline{\sigma}}}\right)\underline{\underline{I}} \qquad (2.3\text{-}8)$$

where

$$\bar{\underline{\underline{\sigma}}} = \underline{\underline{\sigma}} + \alpha \, p\underline{\underline{I}} \qquad (2.3\text{-}9)$$

$$\alpha = 1 - K/K_s \qquad (2.3\text{-}10)$$

This illustrates the fact that the deformation of the porous material is governed by the "effective stresses." It should be noted that $\underline{\underline{\sigma}}$ and p are increments of stress and fluid pressure from an unstressed state and it has also been assumed in Eqs. 2.3-7 and 2.3-8 that fluid pressure affects only the normal strain components and not the shear strain components.

Introducing the porosity, ϕ of a porous material where

ϕ = volume of voids in a unit volume of porous material

Rice and Cleary give an expression for porosity change in terms of total stress and fluid pressure

$$\phi - \phi_o = \frac{1}{3}\left(\frac{1}{K} - \frac{1}{K_s}\right)\left(\mathrm{tr}\,(\underline{\underline{\sigma}}) + 3p\right) - \frac{\phi_o}{K_s}\,p \qquad (2.3\text{-}11)$$

where, in this work, it is assumed that the compressibility of the solids making up the matrix can be described by a single bulk elastic modulus K_s. Biot however did not make this assumption. ϕ_o is the porosity in the unstressed state.

The mass of fluid, m_f, in a unit volume of the porous medium is given by

$$m_f = \rho_f \, \phi \qquad (2.3\text{-}12)$$

where

ρ_f = mass density of the fluid.

The continuity equation for fluid mass balance can be expressed by

$$\nabla \cdot \left(\rho_f \, \underline{q}\right) + \frac{\partial m_f}{\partial t} = 0 \qquad (2.3\text{-}13)$$

where

$\underline{q}$ = specific discharge

t = time

$\nabla\bullet$ = divergence operator

The specific discharge $\underline{q}$ is defined in terms of the average velocity of the fluid

$$\underline{q} = \phi \, \underline{v}_f \tag{2.3-14}$$

Darcy's law may be stated as follows

$$\underline{v}_f - \underline{v}_s = - \frac{\underline{\underline{K}}}{\phi \mu_f} \cdot \left(\nabla p + \rho_f g \, \nabla z \right) \tag{2.3-15}$$

where

$\underline{v}_s$ = the average solid phase velocity
$\underline{\underline{K}}$ = permeability tensor
∇ = gradient operator
g = gravitation constant
z = elevation

The specific discharge *relative* to the deforming solid is given by

$$\underline{q}_r = \underline{q} - \phi \, \underline{v}_s$$
$$\underline{q}_r = -\frac{\underline{\underline{K}}}{\mu_f} \cdot (\nabla p + \rho g \nabla z) \tag{2.3-16}$$

Specific storage is defined as the volume of fluid released from storage in a unit volume due to expansion of the fluid and compression of the porous matrix due to a decrease in hydraulic head.

In a non-deforming porous medium $\underline{V}_s = 0$ and $\underline{q}_r = \underline{q}$. This assumption is made in all PA code, however the effects of matrix compressibility are accounted for in the definition of specific storage. This assumption greatly simplifies the problem. Thus with $\underline{V}_s \approx \underline{0}$ the continuity equation becomes

$$- \nabla \cdot \left[\frac{\rho_f \underline{\underline{K}}}{\mu_f} (\nabla p + pg \, \nabla z) \right] + \frac{\partial m_f}{\partial t} = 0 \tag{2.3-17}$$

Since $m_f = \rho_f \phi$, we may express the second term in 2.3-17

$$\frac{\partial m_f}{\partial t} = \rho_f \frac{\partial \phi}{\partial t} + \phi_o \frac{\partial \rho_f}{\partial t} \tag{2.3-18}$$

Introducing the fluid bulk modulus K_f which is the inverse of fluid compressibility β_f where

$$K_f = \rho_f \frac{\partial P}{\partial \rho_f} = \frac{1}{\beta} \qquad (2.3\text{-}19)$$

$$\frac{\partial \rho_f}{\partial t} = \frac{\partial \rho_f}{\partial p} \frac{\partial p}{\partial t} = \frac{\rho_f}{K_f} \frac{\partial p}{\partial t}$$

$$\text{or } \frac{\partial m_f}{\partial t} = \rho_f \frac{\partial \phi}{\partial t} + \rho_f \frac{\phi_o}{K_f} \frac{\partial p}{\partial t} \qquad (2.3\text{-}20)$$

From Eq. 2.3-11 get an expression for $\partial\phi/\partial t$ such that

$$\frac{\partial m_f}{\partial t} = \rho_f \left[\frac{1}{3} \left(\frac{1}{K} - \frac{1}{K_s} \right) \left[tr \left(\frac{\partial \underline{\underline{\sigma}}}{\partial t} \right) + 3 \frac{\partial p}{\partial t} \right] - \frac{\phi_o}{K_s} \frac{\partial p}{\partial t} + \frac{\phi}{K_f} \frac{\partial p}{\partial t} \right] \qquad (2.3\text{-}21)$$

From this expression, it can be concluded that in general fluid mass changes are influenced by the stress changes as well as the fluid pressure changes.

If only vertical deformation is allowed, ($E_{11} = E_{22} = 0$), along with constant vertical total stress, $\sigma_{33} = 0$ with $\sigma_{11} = \sigma_{22}$, using Eq. 2.3-7, it is possible to derive an expression relating the horizontal σ_{11} (or σ_{22}) components of total stress with the fluid pressure. This relationship is given by

$$\sigma_{11} = \sigma_{22} = \frac{-2G \left(\frac{1}{K} - \frac{1}{Ks} \right)}{1 + (4G/3K)}$$

Also we may now compute $tr \left(\frac{\partial \underline{\underline{\sigma}}}{\partial t} \right)$

$$tr \left(\frac{\partial \underline{\underline{\sigma}}}{\partial t} \right) = 2 \frac{\partial \sigma_{11}}{\partial t} = \frac{-4G \left(\frac{1}{K} - \frac{1}{K_s} \right)}{1 + (4G/3K)} \frac{\partial p}{\partial t}$$

Substitution of this result into Eq. 2.3-21 gives

$$\frac{\partial m_f}{\partial t} = \rho_f \left[\left(\frac{1}{K} - \frac{1}{K_s} \right) \left(1 - \frac{4G}{3} \left(\frac{1 - \left(K / K_s \right)}{K + (4G/3K)} \right) \right) + \phi \left(\frac{1}{K_f} - \frac{1}{K_s} \right) \right] \frac{\partial p}{\partial t} \qquad (2.3\text{-}22)$$

or

$$\frac{\partial m_f}{\partial t} = \rho_f c \frac{\partial p}{\partial t}$$

where c is the capacitance (specific pressure storativity).

Under the conditions specified above, the specific storage (S_s) is defined as

$$\frac{\partial m_f}{\partial t} = \rho_f S_s \frac{\partial h}{\partial t} \qquad (2.3\text{-}23)$$

where

h = hydraulic head.

Our result is written in terms of fluid pressure, p, instead of hydraulic head; however, the two are related by

$$\frac{\partial h}{\partial t} = \frac{1}{\rho_f g} \frac{\partial p}{\partial t}$$

$$\frac{\partial m_f}{\partial t} = \frac{1}{g} S_s \frac{\partial p}{\partial t} \text{ and } S_s = \rho_f g c$$

$$\therefore S_s = \rho_f g \left[\left(\frac{1}{K} - \frac{1}{K_s} \right) \left(\frac{1 - \frac{4G}{3}(1-K/Ks)}{K + (4G/3)} \right) + \phi \left(\frac{1}{K_f} - \frac{1}{K_s} \right) \right] \qquad (2.3\text{-}24)$$

This is the equation for specific storage including the effects of pore fluid compressibility ($1/K_f$), matrix compressibility ($1/K$), and solid compressibility ($1/K_s$).

Typically, $K_s >> K$ and $K_s >> K_f$ and Eq. 2.3-24 may be simplified to

$$S_s = \rho_f g \left(\frac{1}{K + (4G/3)} + \frac{\phi}{K_f} \right) \qquad (2.3\text{-}25)$$

The term $\frac{1}{K + (4G/3)}$ is the inverse of the drained constrained modulus of elasticity porous media and is often denoted by β_s, the vertical compressibility. Letting $1/K_f = \beta_f$ gives the familiar result for specific storage.

$$S_s = \rho_f g (\beta_s + \phi \beta_f).$$

Some confusion may result because groundwater models often employ different definitions for the matrix compressibility β_s. For example SUTRA (Voss, 1984) defines β_s

$$\beta_s = \frac{1}{1 - \phi} \frac{\partial \phi}{\partial p}$$

but defines capacitance (specific pressure storativity) as

$$c = (1 - \phi)\beta_s + \phi\beta_f$$

thus

$$c = \frac{\partial \phi}{\partial p} + \phi\beta$$

STAFF 2D (Huyakorn et al., 1989) and HST3D (Kipp, 1987) defines β_s as

$$\beta_s = \frac{\partial \phi}{\partial p}$$

while BOAST II (Fanchi et al., 1987) and BRAGFLO (Volume 2 of this report) use

$$\beta_s = \frac{1}{\phi} \frac{\partial \phi}{\partial p}$$

It is important to recognize that each code uses a different definition of matrix compressibility and all ignore solid compressibility. Beauheim et al. (1991) note that the assumption that $K_s >> K$ may not be valid for halite (due to low porosity and compressibility).

2.3.9 Tortuosity

Parameter:	**Tortuosity** (τ)
Median:	1.4×10^{-1}
Range:	1×10^{-2}
	6.67×10^{-1}
Units:	Dimensionless
Distribution:	Cumulative
Source(s):	See text (Culebra, Section 2.6.7)
	Freeze, R. A. and J. C. Cherry. 1979. *Groundwater.* Englewood Cliffs, NJ: Prentice-Hall, Inc.

Discussion:

No direct measurements of tortuosity are available in the anhydrite (or halite) layers of the Salado Formation. The range reported is the maximum typical theoretical value of 0.667 for uniform-sized grains at low Peclet numbers (N_p) (Dullien, 1979, Figure 7.12) down to 0.01 observed in laboratory experiments of nonadsorbing solutes in porous materials (Freeze and Cherry, 1979, p. 104). The PA Division selected a median value equal to that of the Culebra Dolomite Member. This parameter primarily influences diffusion-dominated transport, a condition occurring only when the repository is undisturbed. The influence of the tortuosity on results was explored in a few 1991 PA calculations of the undisturbed summary scenario class (Volume 2 of this report).

2.4 Hydrologic Parameters for Anhydrite Layers within Salado Formation

Table 2.4-1 provides the parameter values for anhydrite layers near the repository within the Salado Formation. Marker Bed 139 (MB139), a potential transport pathway, is an interbed located about 1 m (3.3 ft) below the repository interval and thus is an anhydrite layer of particular interest. Figure 2.4-1 shows a cross section of MB139.

Table 2.4-1. Hydrologic Parameter Values for Anhydrite Layers within Salado Formation

Parameter	Median	Range		Units	Distribution Type	Source
Capillary pressure (p_c) and relative permeability (k_{rw})						
Threshold displacement pressure (p_t)	3×10^5	3×10^3	3×10^7	Pa	Lognormal	Davies, 1991; Davies, June 2, 1991, Memo (see Appendix A)
Residual Saturations						
Wetting phase ($S_{\ell r}$)	2×10^{-1}	1×10^{-1}	4×10^{-1}	none	Cumulative	Davies and LaVenue, 1990b
Gas phase (S_{gr})	2×10^{-1}	1×10^{-1}	4×10^{-1}	none	Cumulative	Davies and LaVenue, 1990b
Brooks-Corey Exponent (η)	7×10^{-1}	3.5×10^{-1}	1.4	none	Cumulative	Davies and LaVenue, 1990b
Density, grain (ρ_g)	2.963×10^3			kg/m^3	Constant	See text (anhydrite).
Dispersivity						
Longitudinal (αL)	1.5×10^1	1	4×10^1	m	Cumulative	Pickens and Grisak, 1981; Lappin et al., 1989, Table D-2
Transverse (α_T)	1.5	1×10^{-1}	4	m	Cumulative	Pickens and Grisak, 1981
Partition coefficient						
Am	2.5×10^{-2}			m3/kg	Constant	Lappin et al., 1989, Table D-4
Np	1×10^{-3}			m3/kg	Constant	Lappin et al., 1989, Table D-4
Pb	1×10^{-3}			m3/kg	Constant	Lappin et al., 1989, Table D-4
Pu	1×10^{-1}			m3/kg	Constant	Lappin et al., 1989, Table D-4
Ra	1×10^{-3}			m3/kg	Constant	Lappin et al., 1989, Table D-4
Th	1×10^{-1}			m3/kg	Constant	Lappin et al., 1989, Table D-4
U	1×10^{-3}			m3/kg	Constant	Lappin et al., 1989, Table D-4
Permeability (k)						
Undisturbed	7.8×10^{-20}	6.8×10^{-20}	9.5×10^{-19}	m^2	Cumulative	Beauheim, June 14, 1991, Memo (see Appendix A)
Disturbed	1×10^{-17}	1×10^{-19}	1×10^{-13}	m^2	Cumulative	Beauheim, 1990
Pore pressure	1.28×10^7	9.3×10^6	1.39×10^7	Pa	Data	Beauheim, June 14, 1991, Memo; Howarth, June 12, 1991, Memo (see Appendix A)
Porosity (ϕ)						
Undisturbed	1×10^{-2}	1×10^{-3}	3×10^{-2}	none	Cumulative	See text.
Disturbed	5.5×10^{-2}	1×10^{-2}	1×10^{-1}	none	Normal	See text.
Specific storage	1.4×10^{-7}	9.7×10^{-8}	1×10^{-6}	m^{-1}	Cumulative	Beauheim, June 14, 1991, Memo (see Appendix A)
Thickness (Δz)	9×10^{-1}	4×10^{-1}	1.25	m	Cumulative	Borns, 1985, Figure 3; WEC, 1989b; Krieg, 1984, Table I
Tortuosity	1.4×10^{-1}	1×10^{-2}	6.67×10^{-1}	none	Cumulative	See text (Culebra); Freeze and Cherry, 1979, p. 104

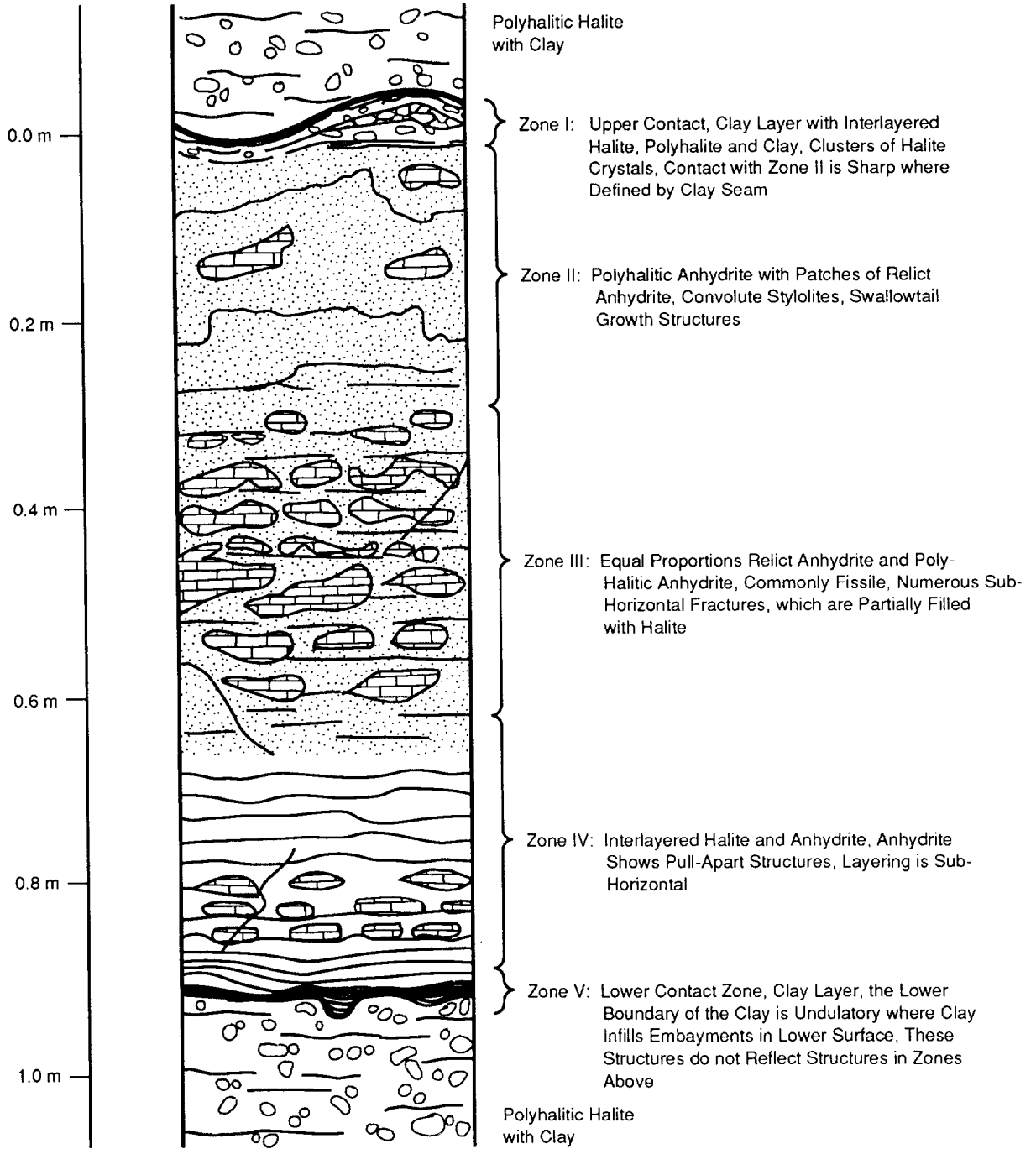

Figure 2.4-1. Generalized Cross Section of Marker Bed 139. The figure shows the internal variability of the unit and the character of both the upper and lower contacts (after Borns, 1985). The thickness varies spatially between 0.4 and 1.25 m with a reference thickness of 0.99 (WEC, 1989b; Krieg, 1984, Table I).

2.4.1 Capillary Pressure and Relative Permeability

Threshold Displacement Pressure, p_t

Parameter:	**Threshold displacement pressure (p_t)**
Median:	3×10^5
Range:	3×10^3
	3×10^7
Units:	Pa
Distribution:	Lognormal
Source(s):	Davies, P. B. 1991. *Evaluation of the Role of Threshold Pressure in Controlling Flow of Waste-Generated Gas into Bedded Salt at the Waste Isolation Pilot Plant.* SAND90-3246. Albuquerque, NM: Sandia National Laboratories.
	Davies, P. B. 1991. "Uncertainty Estimates for Threshold Pressure for 1991 Performance Assessment Calculations Involving Waste-Generated Gas." Internal memo to D. R. Anderson (6342), June 2, 1991. Albuquerque, NM: Sandia National Laboratories. (In Appendix A of this volume)

Residual Saturations

Parameter:	**Residual wetting phase (liquid) saturation ($S_{\ell r}$)**
Median:	2×10^{-1}
Range:	1×10^{-1}
	4×10^{-1}
Units:	Dimensionless
Distribution:	Cumulative
Source(s):	Davies, P. B. and A. M. LaVenue. 1990b. "Additional Data for Characterizing 2-Phase Flow Behavior in Waste-Generated Gas Simulations and Pilot Point Information for Final Culebra 2-D Model." Memo 11 in Appendix A of Rechard et al. 1990. *Data Used in Preliminary Performance Assessment of the Waste Isolation Pilot Plant.* SAND89-2408. Albuquerque, NM: Sandia National Laboratories.

Parameter:	**Residual gas saturation (S_{gr})**
Median:	2×10^{-1}
Range:	1×10^{-1}
	4×10^{-1}
Units:	Dimensionless
Distribution:	Cumulative
Source(s):	Davies, P. B. and A. M. LaVenue. 1990b. "Additional Data for Characterizing 2-Phase Flow Behavior in Waste-Generated Gas Simulations and Pilot Point Information for Final Culebra 2-D Model." Memo 11 in Appendix A of Rechard et al. 1990. *Data Used in Preliminary Performance Assessment of the Waste Isolation Pilot Plant.* SAND89-2408. Albuquerque, NM: Sandia National Laboratories.

Brooks and Corey Exponent

Parameter:	**Brooks and Corey exponent (η)**
Median:	7×10^{-1}
Range:	3.5×10^{-1}
	1.4
Units:	Dimensionless
Distribution:	Cumulative
Source(s):	Davies, P. B. and A. M. LaVenue. 1990b. "Additional Data for Characterizing 2-Phase Flow Behavior in Waste-Generated Gas Simulations and Pilot Point Information for Final Culebra 2-D Model." Memo 11 in Appendix A of Rechard et al. 1990. *Data Used in Preliminary Performance Assessment of the Waste Isolation Pilot Plant.* SAND89-2408. Albuquerque, NM: Sandia National Laboratories.

Capillary Pressure and Relative Permeability

Figure 2.4-2a shows the estimated relative permeability for anhydrite layers. Figure 2.4-2b shows the estimated capillary pressure for anhydrite layers. Figure 2.4-3 is an example of variation of relative permeability and capillary pressure when Brooks and Corey parameters are varied.

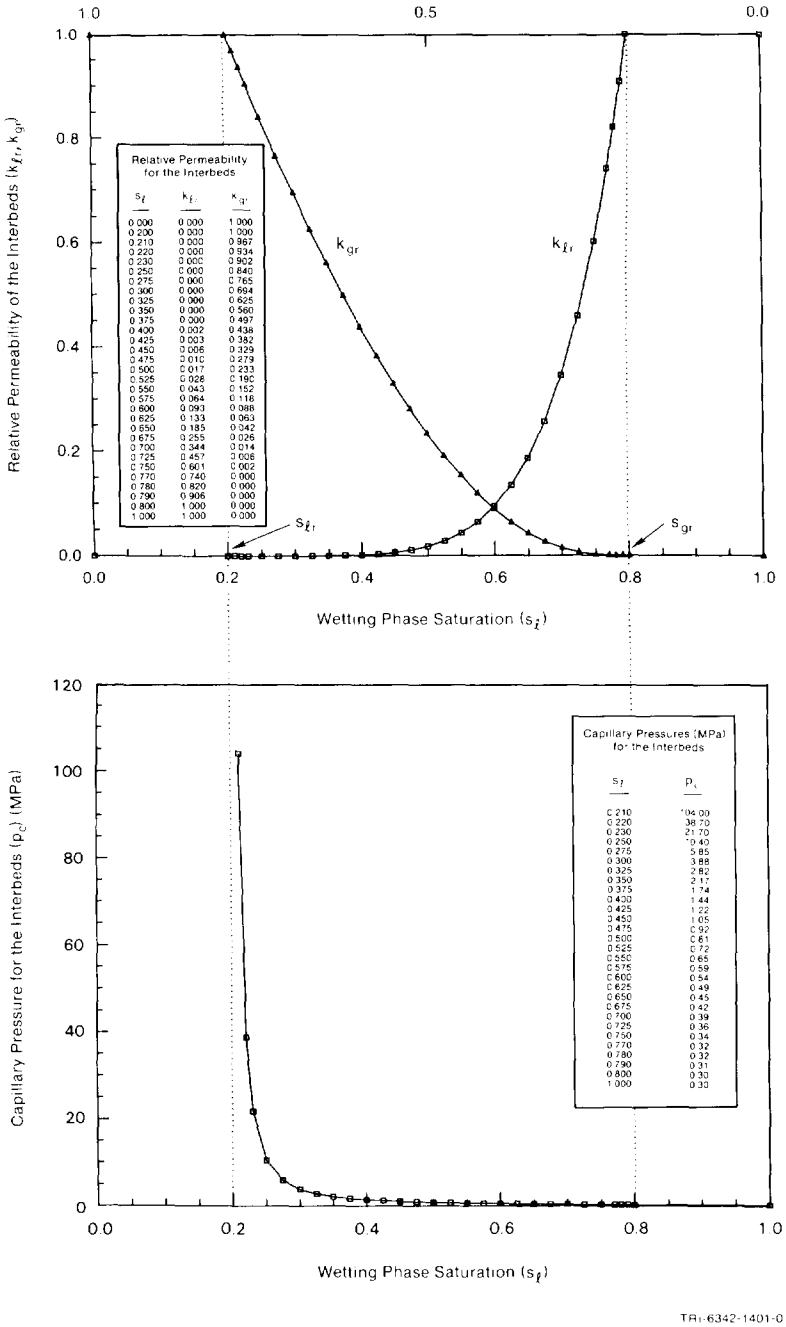

Figure 2.4-2. Estimated Capillary Pressure and Relative Permeability Curves for Anhydrite Layers.

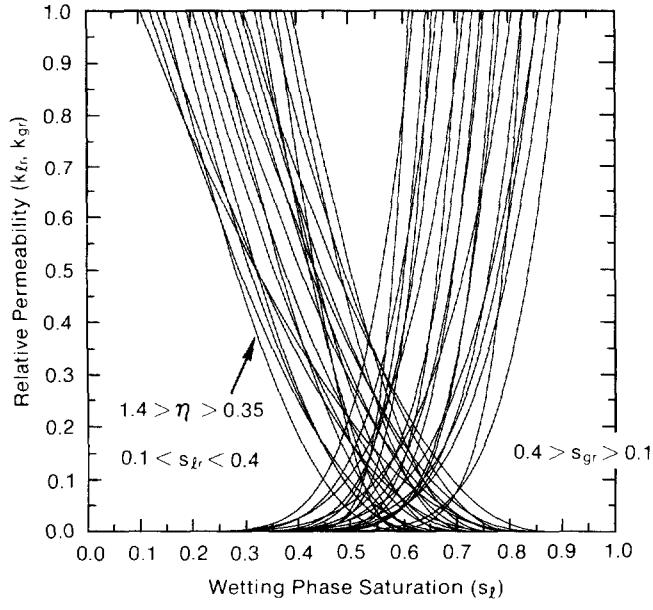

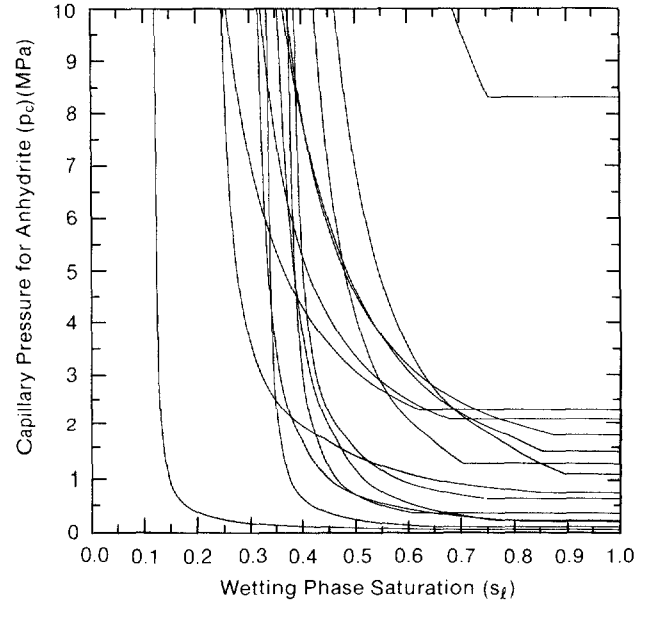

TRI-6342-1466-0

Figure 2.4-3. Example of Variation of Relative Permeability and Capillary Pressure for Anhydrite Layers in Salado Formation When Brooks and Corey Parameters Are Varied.

Discussion:

The correlations for these values were developed as discussed in the section, "Hydrologic Parameters for Halite and Polyhalite within the Salado Formation." Preliminary parameter values selected for MB139 and other anhydrite beds are the same as for Salado halite, except for a lower threshold displacement pressure (p_t), and were taken from experimental data measured for the tight gas sands (Davies and LaVenue, 1990; Ward and Morrow, 1985).

An initial range was selected for the purpose of being able to run sensitivity parameter studies. The ranges shown for the parameters are quite arbitrary, corresponding to a simple doubling and halving of the median values as discussed in Section 2.3.1, "Hydrologic Parameters for Halite in the Salado Formation." The relative permeability curves are identical to those of halite. Only the capillary curves differ because of the different range assumed for the threshold displacement pressure (Figure 2.4-3).

2.4.2 Anhydrite Density

Parameter:	**Density, grain (ρ_g)**
Median:	2.963×10^3
Range:	None
Units:	kg/m^3
Distribution:	Constant
Source(s):	Clark, S. P. 1966. *Handbook of Physical Constants.* New York, NY: The Geological Society of America, Inc. (p. 46)
	Krieg, R. D. 1987. *Reference Stratigraphy and Rock Properties for the Waste Isolation Pilot Plant (WIPP) Project.* SAND83-1908. Albuquerque, NM: Sandia National Laboratories. (p. 14)

Discussion:

The published grain density of anhydrite ($CaSO_4$) is 2,963 kg/m^3 (185 lb/ft^3) (Clark, 1966, p.46; Krieg, 1987, p. 14).

2.4.3 Dispersivity

Parameter:	**Dispersivity, longitudinal (α_L)**
Median:	1.5×10^1
Range:	1
	4×10^1
Units:	m
Distribution:	Cumulative
Source(s):	Pickens, J. F., and G. E. Grisak. 1981. Modeling of Scale-Dependent Dispersion in Hydrogeologic Systems. *Water Resources Research*, vol. 17, no. 6, pp. 1701-11.
	Lappin, A. R., R. L. Hunter, D. P. Garber, and P. B. Davies, eds. 1989. *Systems Analysis Long-Term Radionuclide Transport, and Dose Assessments, Waste Isolation Pilot Plant (WIPP), Southeastern New Mexico; March 1989*. SAND 89-0462. Albuquerque, NM: Sandia National Laboratories. (Table D-2)

Parameter:	**Dispersivity, transverse (α_T)**
Median:	1.5
Range:	1×10^{-1}
	4
Units:	m
Distribution:	Cumulative
Source(s):	Pickens, J. F., and G. E. Grisak. 1981. Modeling of Scale-Dependent Dispersion in Hydrogeologic Systems. *Water Resources Research*, vol. 17, no. 6, pp. 1701-11.

Discussion:

The dispersivity values are discussed in Section 2.3.3.

2.4.4 Partition Coefficients and Retardations

Table 2.4-2 provides the partition coefficients for anhydrite layers.

Table 2.4-2. Partition Coefficients for Anhydrite Layers (after Lappin et al., 1989, Table D-4)

Radionuclide	Partition coefficient* (m^3/kg)
Am	2.5×10^{-2}
Np	1×10^{-3}
Pb	1×10^{-3}
Pu	1×10^{-1}
Ra	1×10^{-3}
Th	1×10^{-1}
U	1×10^{-3}

* Assumed constant

Discussion:

The sorption of trace radionuclides onto salt-like minerals such as anhydrite is poorly understood; thus, current PA calculations assume partition coefficients of zero (the lower limit). However, because sensitivity studies require ranges of values, the upper limit was arbitrarily chosen to keep the calculated retardation below 10. The rough estimates on median values are those reported by Lappin et al. (1989). Generally, the reported experimental K_d data was reduced by several orders of magnitude as explained below.

Americium. K_d values for americium are decreased by factors of 3 to 1000 from values in Paine (1977), Dosch (1979), and Tien et al. (1983), because of the potential effects of organic complexation. (As a conservative measure, the likely degradation of the organic compounds was neglected.) For example, Swanson (1986) found that moderate concentrations (4×10^{-6} to 10^{-4} M) of EDTA significantly decreased americium sorption onto kaolinite and montmorillonite. The magnitude of this effect was a function of the pH and concentration of EDTA, calcium, magnesium, and iron in solution.

Uranium and Neptunium. In general, low K_ds for uranium and thorium have been measured in waters relevant to the WIPP repository. The K_d of uranium depends strongly on the pH, concentration of competing ions, and the extent of complexation by carbonate and organic ligands (Lappin et al., 1989). A low value (K_d = 1) has been assumed to account for these effects. Theoretical calculations (Leckie, 1989) and arguments based on similarities in speciation, ionic radii, and valence (Chapman and Smellie, 1986) suggest that the behavior of neptunium will be similar to that of uranium.

Plutonium. K_d values for plutonium are decreased by two to three orders of magnitude from the values in Paine (1977), Dosch (1979), and Tien et al. (1983), because of the potential effect of carbonate complexation.

Thorium. There are very few data for thorium under conditions relevant to the WIPP. Thorium K_d values were estimated from data for plutonium, a reasonable homolog element (Krauskopf, 1986). Data describing sorption of thorium onto kaolinite (Riese, 1982) suggest that high concentrations of calcium and magnesium will prevent significant amounts of sorption onto clays in the repository. Stability constants for organo-thorium complexes suggest that organic complexation could be important in the repository and may inhibit sorption (Langmuir and Herman, 1980).

Radium and Lead. There are very few sorption data for radium and lead under conditions relevant to the WIPP. K_d values were estimated by assuming homologous radium-palladium behavior (cf. Tien et al., 1983). Data from Riese (1982) suggest that radium will sorb onto clays but that high concentrations of calcium and magnesium will inhibit sorption. Langmuir and Riese (1985) presented theoretical and empirical arguments that suggest that radium will be coprecipitated in calcite, gypsum, and anhydrite in solutions close to saturation with respect to these minerals.

Retardation. See Section 2.6.10 for the discussion of retardation.

2.4.5 Permeability

Undisturbed Permeability

Parameter:	**Permeability, undisturbed** (k)
Median:	7.8×10^{-20}
Range:	6.8×10^{-20}
	9.5×10^{-19}
Units:	m^2
Distribution:	Data
Source(s):	Beauheim, R. 1991. "Review of Salado Parameter Values To Be Used in 1991 Performance Assessment Calculations," Internal memo to Rob Rechard (6342), June 14, 1991. Albuquerque, NM: Sandia National Laboratories. (In Appendix A of this volume)

Discussion:

The distribution of anhydrite permeability in the far field is based on five measurements from the Permeability Testing Program (Beauheim, June 14, 1991, Memo [Appendix A]). In the past, the general consensus for the permeability of anhydrite layers in general, and MB139 in particular, has been a median value of 1×10^{-19} (Rechard et al., 1990, p. II-16). The current data show an insignificant but somewhat smaller median value of 7.8×10^{-20}.

Figure 2.4-4 shows the distribution for undisturbed permeability in the anhydrite assuming no correlation with distance from excavation. However, a non-linear fit of permeability to distance shows an asymtoptic value near 8×10^{-20} m^2 (Figure 2.4-5). More specifically, the asymptotic value of $\log_{10}$ of anhydrite permeability is about -19, with a probable error of ± 0.6. The probable error can be interpreted as a one-sigma confidence interval.

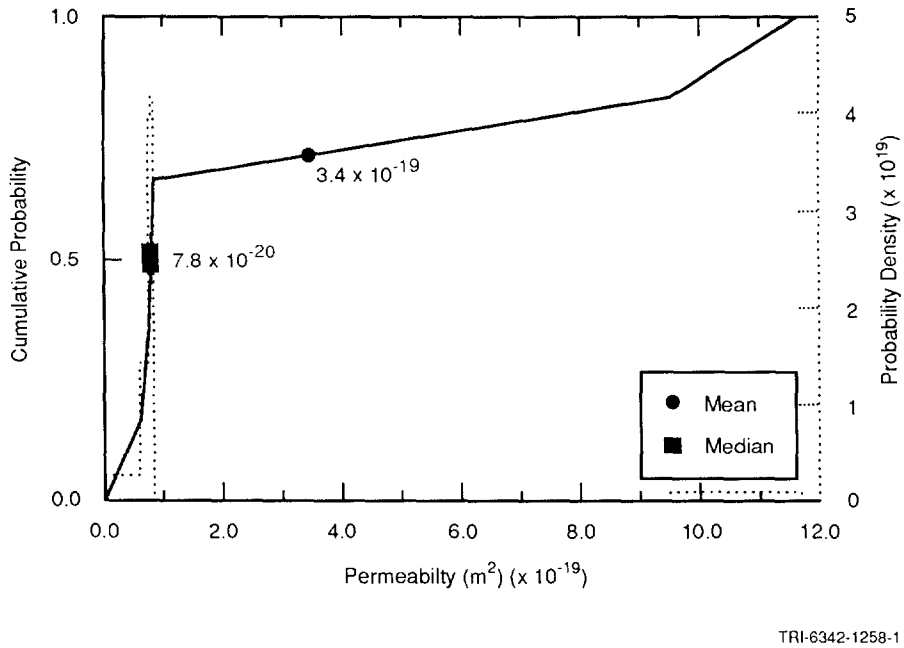

Figure 2.4-4. Estimated Distribution (pdf and cdf) for Undisturbed Permeability, Anhydrite Layers in Salado Formation.

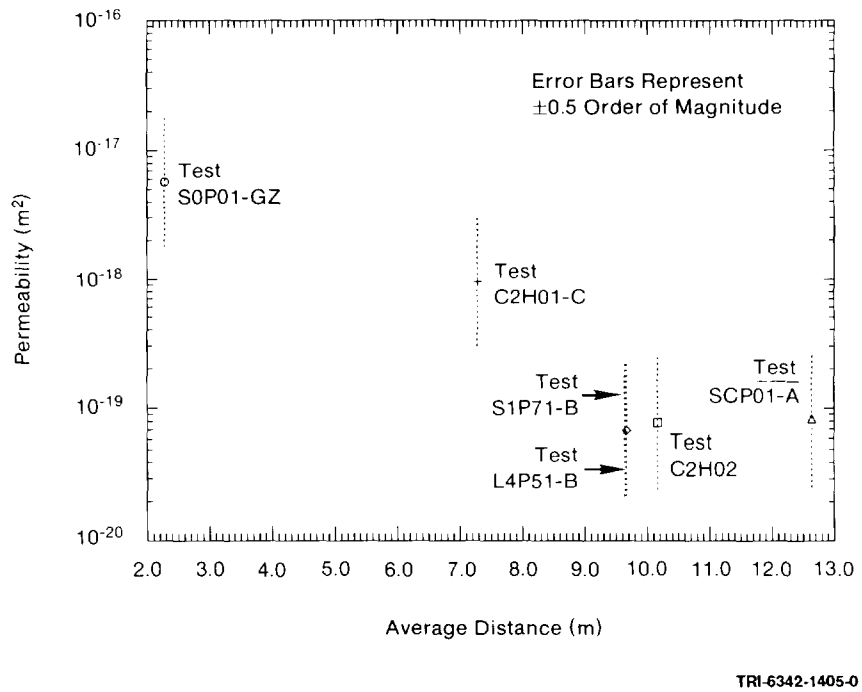

Figure 2.4-5. Non-Linear Fit of Anhydrite Permeability to Distance from Excavation.

Disturbed Permeability

Parameter:	**Permeability, disturbed** (k)
Median:	1×10^{-17}
Range:	1×10^{-19}
	1×10^{-13}
Units:	m^2
Distribution:	Cumulative
Source(s):	Beauheim, R. L. 1990. "Review of Parameter Values to be Used in Performance Assessment," Memo 3c in Appendix A of Rechard et al. 1990. *Data Used in Preliminary Performance Assessment of the Waste Isolation Pilot Plant (1990).* SAND89-2408. Albuquerque, NM: Sandia National Laboratories.

Discussion:

Following the logic described for permeability for the Salado halite, the disturbed permeability is assumed to vary between the median intact value and the highest measured value; the median value is set about two orders of magnitude below the undisturbed median value. The highest permeability measured to date in MB139 is 3.2×10^{-13} m^2 (3.2×10^2 mD) (from draft report by M. E. Crawley, "Hydraulic Testing of Marker Bed 139 at the Waste Isolation Pilot Plant, Southeastern New Mexico," Westinghouse Electric Co., Carlsbad, NM), but was rounded down to 1×10^{-13} m^2 (1×10^2 mD), the value used for unmodified TRU waste.

Figure 2.4-6 shows the estimated distribution for disturbed permeability for the anhydrite layers.

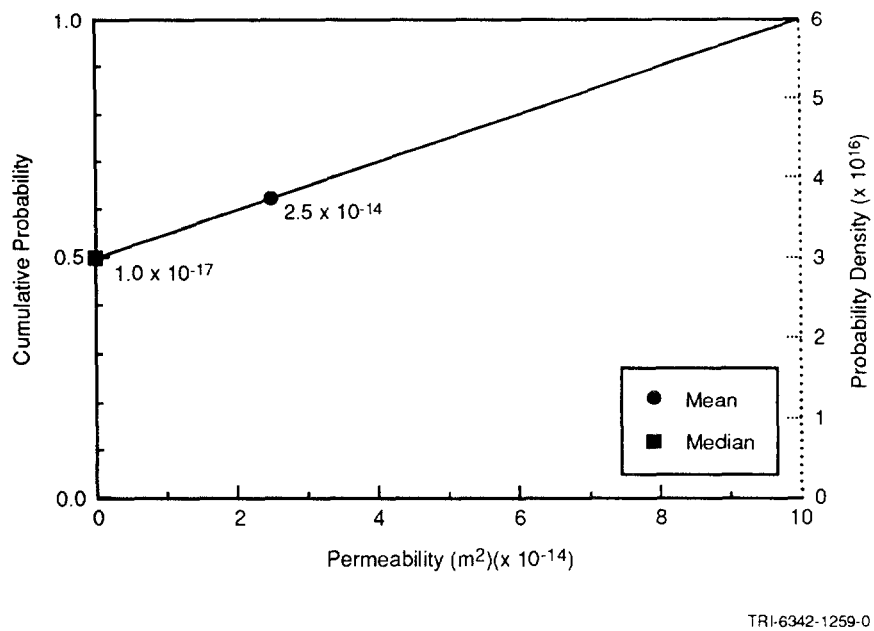

Figure 2.4-6. Estimated Distribution (pdf and cdf) for Disturbed Permeability, Anhydrite Layers in Salado Formation.

2.4.6 Pore Pressure at Repository Level in Anhydrite

Parameter:	**Pore pressure at repository level** (p)
Median:	1.28×10^7
Range:	9.3×10^6
	1.39×10^7
Units:	Pa
Distribution:	Data
Source(s):	Beauheim, R. L. 1991. "Review of Parameter Values to be Used in 1991 Performance Assessment." Internal memo to R. Rechard, June 14, 1991. Albuquerque, NM: Sandia National Laboratories. (In Appendix A of this volume)
	Howarth, S. 1991. "Pore Pressure Distributions for 1991 Performance Assessment Calculations," Internal memo to Elaine Gorham (6344), June 12, 1991. Albuquerque, NM: Sandia National Laboratories. (In Appendix A of this volume).

Figure 2.4-7 shows the distribution for brine pore pressure. Figure 2.4-8 shows the variation of pore pressure with distance from the excavation.

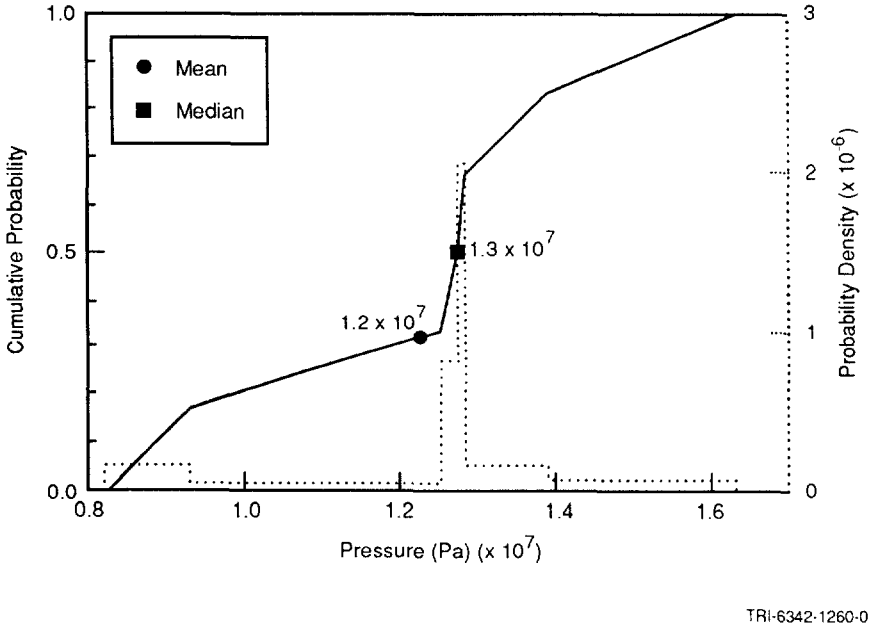

Figure 2.4-7. Estimated Distribution (pdf and cdf) for Brine Pore Pressure in Anhydrite MB139 at Repository Level.

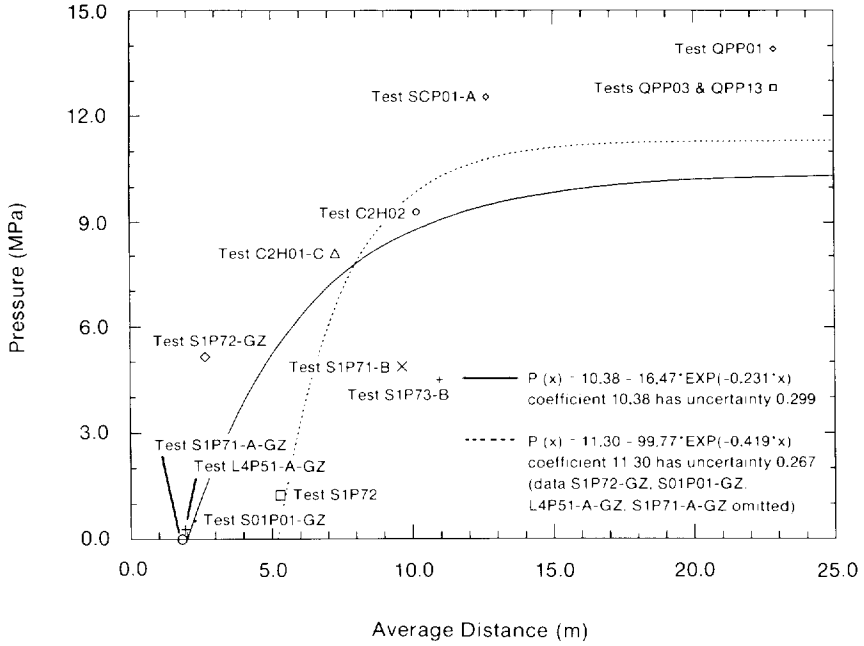

Figure 2.4-8. Non-Linear Fits of Pore Pressure in Anhydrite to Distance from Excavation. (Data from Beauheim, June 14, 1991, Memo and Howarth, June 12, 1991, Memo [Appendix A]).

Discussion:

For the 1991 PA calculations, the pore pressure measurements of investigator Beauheim (June 14, 1991, Memo [Appendix A]) and Howarth (June 12, 1991, Memo [Appendix A]) were combined to form a data distribution with a median of 12.8 MPa (128 atm) and a data range of 9.3 and 13.9 MPa (93 and 139 atm). (The sample range was 8.21 to 15 MPa [Figure 2.4-7].)

In comparison, for the 1990 PA calculations, two pore pressure measurements were reported for Anhydrite MB139: 9.3 MPa (93 atm) (Beauheim et al., 1990) and 12.6 MPa (126 atm). Assuming a uniform distribution, the mean and median were 11.0 MPa, and the range was $\bar{x} + \sqrt{3}s$ or 7 MPa (70 atm) and 15 MPa (150 atm) (Figure 2.4-6). The maximum corresponded to lithostatic pressure based on hydraulic fracturing experiments (Wawersik and Stone, 1985) and density log for WIPP-11 (Figure 2.2-5). The minimum of 7.0 MPa was the average of a pure water hydrostatic of 6.4 MPa and a Salado brine hydrostatic of 7.9 (Figure 2.2-5) or equivalently, the hydrostatic pressure of a column of fluid that linearly varied between pure water at the surface and Salado brine at 655 m (2,142 ft).

The non-linear fits of pore pressure (in anhydrite) to distance (Figure 2.4-8) indicate an asymptotic value of about 10 MPa with probable error of the order of 0.3 MPa. The probable error can be construed as a one-sigma confidence level.

2.4.7 Porosity

Undisturbed Porosity

Parameter:	**Porosity, undisturbed (ϕ)**
Median:	1×10^{-2}
Range:	1×10^{-3}
	3×10^{-2}
Units:	Dimensionless
Distribution:	Cumulative
Source(s):	See text.

Discussion:

PA calculations have assumed an undisturbed porosity similar to the undisturbed porosity of the Salado Formation as a whole.

Figure 2.4-9 shows the estimated distribution for undisturbed porosity for the anhydrite layers.

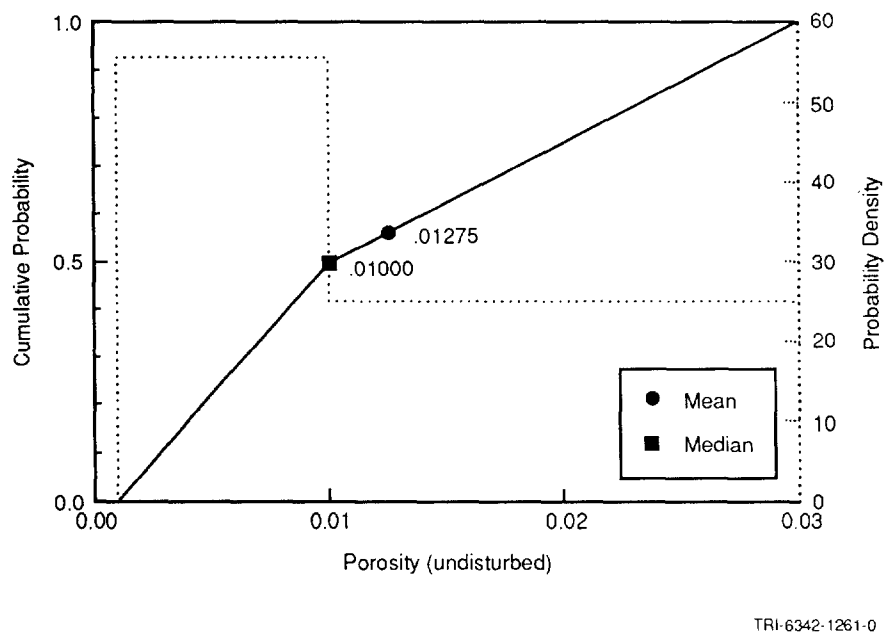

Figure 2.4-9. Estimated Distribution (pdf and cdf) for Undisturbed Porosity for Anhydrite Layers in Salado Formation.

Disturbed Porosity

Parameter:	**Porosity, disturbed (ϕ)**
Median:	5.5×10^{-2}
Range:	1×10^{-2}
	1×10^{-1}
Units:	Dimensionless
Distribution:	Normal
Source(s):	See text.

Discussion:

The lower range for disturbed porosity of the anhydrite layers after reconsolidation was set at 0.1. This value is an order of magnitude increase above the undisturbed porosity lower range and equal to the undisturbed median value. The reason for the increase is that the fractures that form within the brittle anhydrite beds during excavations will not heal completely. Shear displacement will likely cause abutment of asperities in the fractures which, in turn, will prop them open (Lappin et al., 1989, p. 4-62). The upper value of the range was set an order of magnitude above the lower value. Finally, the porosity was assumed to be normally distributed as in many materials (Harr, 1987, Table 1.8.1).

Figure 2.4-10 shows the distribution for the disturbed porosity for the anhydrite layers.

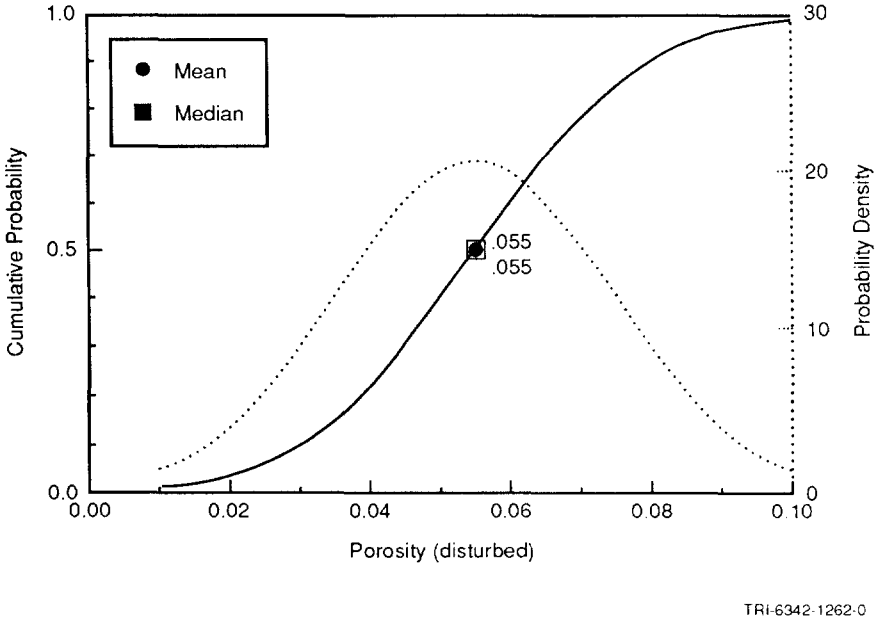

Figure 2.4-10. Estimated Distribution (pdf and cdf) for Disturbed Porosity for Anhydrite Layers in Salado Formation.

2.4.8 Specific Storage

Parameter:	**Specific storage**
Median:	1.4×10^{-7}
Range:	9.7×10^{-8}
	1×10^{-6}
Units:	m^{-1}
Distribution:	Cumulative
Source(s):	Beauheim, R. 1991. "Review of Salado Parameter Values To Be Used in 1991 Performance Assessment Calculations," Internal memo to Rob Rechard (6342), June 14, 1991. Albuquerque, NM: Sandia National Laboratories. (In Appendix A of this volume).

Figure 2.4-11 shows the estimated distribution for specific storage.

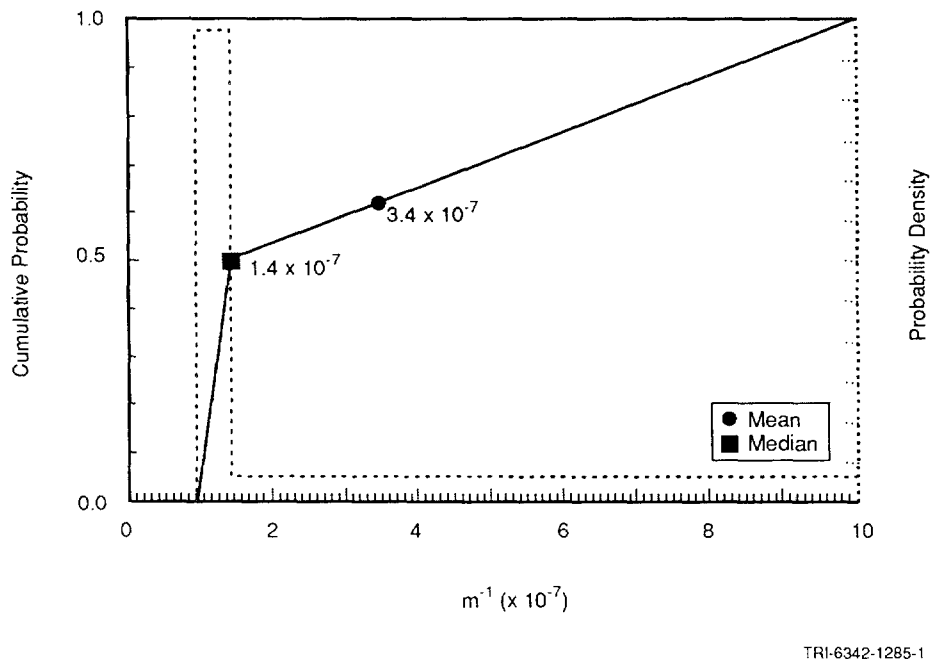

Figure 2.4-11. Estimated Distribution (pdf and cdf) for Anhydrite Specific Storage.

Discussion:

See Section 2.3.8 for complete discussion of specific storage.

2.4.9 Thickness of MB139 Interbed

Parameter:	**MB139 thickness** (Δz)
Median:	9×10^{-1}
Range:	4×10^{-1}
	1.25
Units:	m
Distribution:	Cumulative
Source(s):	Borns, D. J. 1985. *Marker Bed 139: A Study of Drillcore From a Systematic Array.* SAND85-0023. Albuquerque, NM: Sandia National Laboratories. (Figure 3)
	WEC (Westinghouse Electric Corporation). 1989b. *Geotechnical Field Data and Analysis Report, July 1987 through June 1988*, vols. 1 and 2. DOE/WIPP-89-009. Prepared for U.S. Department of Energy. Carlsbad, NM: Westinghouse Electric Corporation.
	Krieg, R. D. 1984. *Reference Stratigraphy and Rock Properties for the Waste Isolation Pilot Plant (WIPP) Project.* SAND83-1908. Albuquerque, NM: Sandia National Laboratories.

Discussion:

The thickness for MB139 in the generalized stratigraphy of the site is about 0.9 m (3 ft) (WEC, 1989b) and is used as the median value. Because the upper contact is irregular and undulates (caused from reworking of the interbed prior to further halite deposition), the thickness varies between 0.40 and 1.25 m (1.3 and 4.1 ft) (Borns, 1985, Figure 3; Krieg, 1984, Table I). Figure 2.4-12 shows the distribution for the thickness of the anhydrite layers in the Salado.

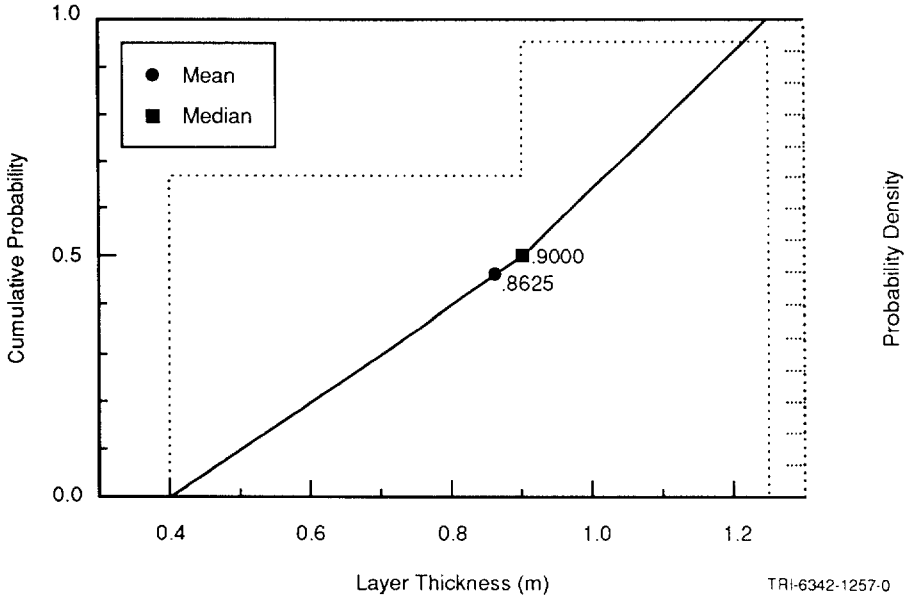

Figure 2.4-12. Estimated Distribution (pdf and cdf) for Thickness of Interbed.

2.4.10 Tortuosity

Parameter:	**Tortuosity** (τ)
Median:	1.4×10^{-1}
Range:	1×10^{-2}
	6.67×10^{-1}
Units:	Dimensionless
Distribution:	Cumulative
Source(s):	See text (Culebra, Section 2.6.7)
	Freeze, R. A. and J. C. Cherry. 1979. *Groundwater*. Englewood Cliffs, NJ: Prentice-Hall, Inc.

Discussion:

No direct measurements of tortuosity are available in the anhydrite (or halite) layers of the Salado Formation. The range reported is the maximum typical theoretical value of 0.667 for uniform-sized grains at low Peclet numbers (N_p) (Dullien, 1979, Figure 7.12) down to 0.01 observed in laboratory experiments of nonadsorbing solutes in porous materials (Freeze and Cherry, 1979, p. 104). The PA Division selected a median value equal to that of the Culebra Dolomite Member. This parameter primarily influences diffusion-dominated transport, a condition occurring only when the repository is undisturbed. The influence of the tortuosity on results was explored in a few 1991 PA calculations of the undisturbed summary scenario class (Volume 2 of this report).

2.5 Mechanical Parameters for Materials in Salado Formation

2.5.1 Halite and Argillaceous Halite

Elastic Constants

Salt Creep Constitutive Model Constants

Polyhalite Elastic Constants

Anhydrite Elastic Constants

2.6 Parameters for Culebra Dolomite Member of Rustler Formation

The Culebra Dolomite Member of the Rustler Formation is a finely crystalline, locally argillaceous (containing clay) and arenaceous (containing sand), vuggy dolomite ranging in thickness near the WIPP from about 7 m (23 ft) (at DOE-1 and other locations) to 14 m (46 ft) (at H-7). Figure 2.6-1 shows a detailed lithology of the Rustler Formation. Figure 2.6-2 is a cross-section across the WIPP disposal system. The Culebra Dolomite is generally considered to provide the most important potential groundwater-transport pathway for radionuclides that may be released to the accessible environment provided human intrusion occurs. Accordingly, the WIPP Project has devoted much attention to understanding the hydrogeology and hydraulic properties of the Culebra. Figure 2.6-3 shows the locations of wells used to define the hydrologic parameters for the Culebra Dolomite. Detailed hydrogeologic information is available in reports by Brinster (1991) and Holt and Powers (1988). The Culebra Dolomite has been tested at 41 locations in the vicinity of the WIPP. Results of these tests and interpretations have been reported by Beauheim (1987a,b,c; 1989), Saulnier (1987), and Avis and Saulnier (1990).

One early observation (Mercer and Orr, 1979) was that the transmissivity of the Culebra Dolomite varies by six orders of magnitude in the vicinity of the WIPP. This variation in transmissivity appears to be the result of differing degrees of fracturing within the Culebra Dolomite. The cause of the fracturing, however, is unresolved. Culebra transmissivities of about 1×10^{-6} m^2/s (0.93 ft^2/d) or greater appear to be related to fracturing. Where the transmissivity of the Culebra Dolomite is less than 1×10^{-6} m^2/s (0.93 ft^2/d), few or no open fractures have been observed in core, and the Culebra's hydraulic behavior during pumping or slug tests is that of a single-porosity medium. Where transmissivities are between 1×10^{-6} m^2/s (0.93 ft^2/d) and at least 1×10^{-4} m^2/s (93 ft^2/d), open fractures are observed in core, and the hydraulic behavior of the Culebra Dolomite during pumping tests is that of a dual-porosity medium (Beauheim, 1987a, b, c; Saulnier, 1987).

Parameter values for the Culebra Dolomite Member are given in Table 2.6-1.

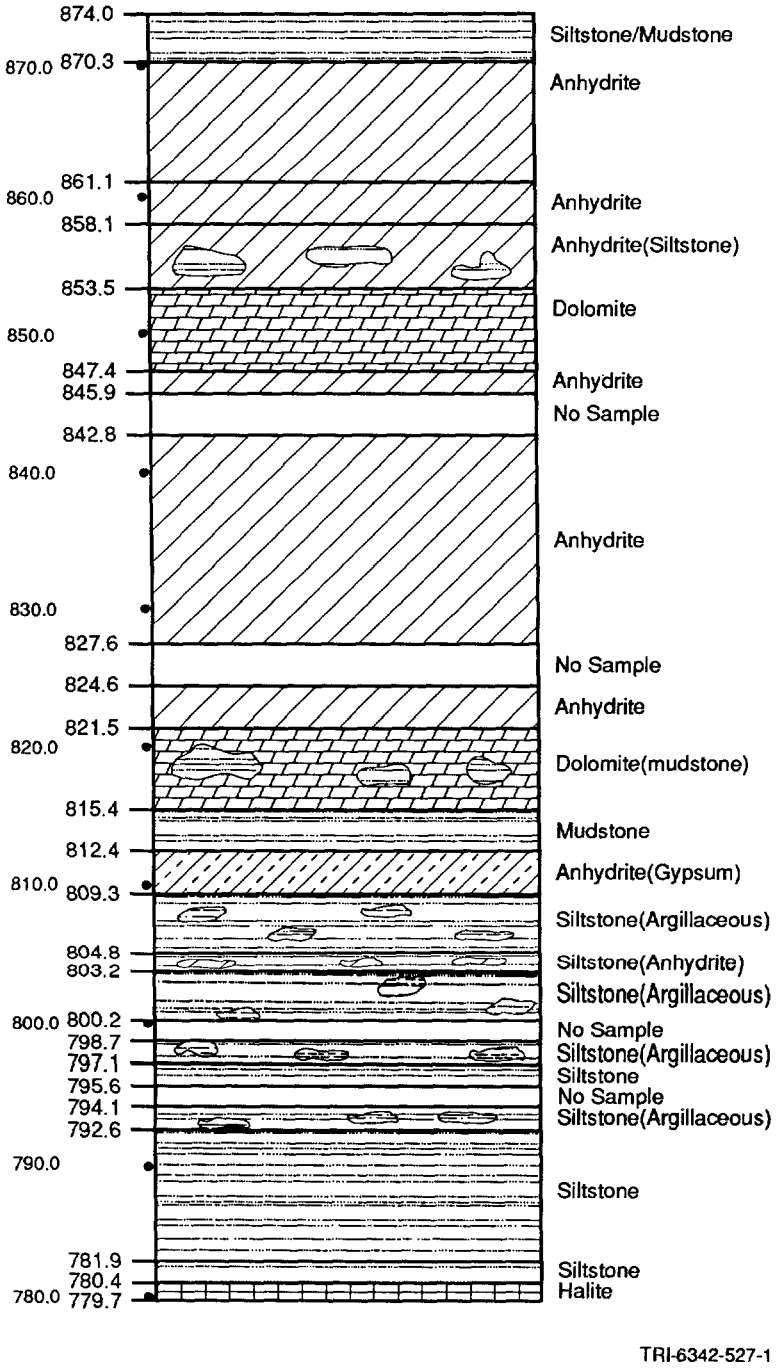

Figure 2.6-1. Detailed Lithology of Rustler Formation at ERDA-9 (after SNL and USGS, 1982b).

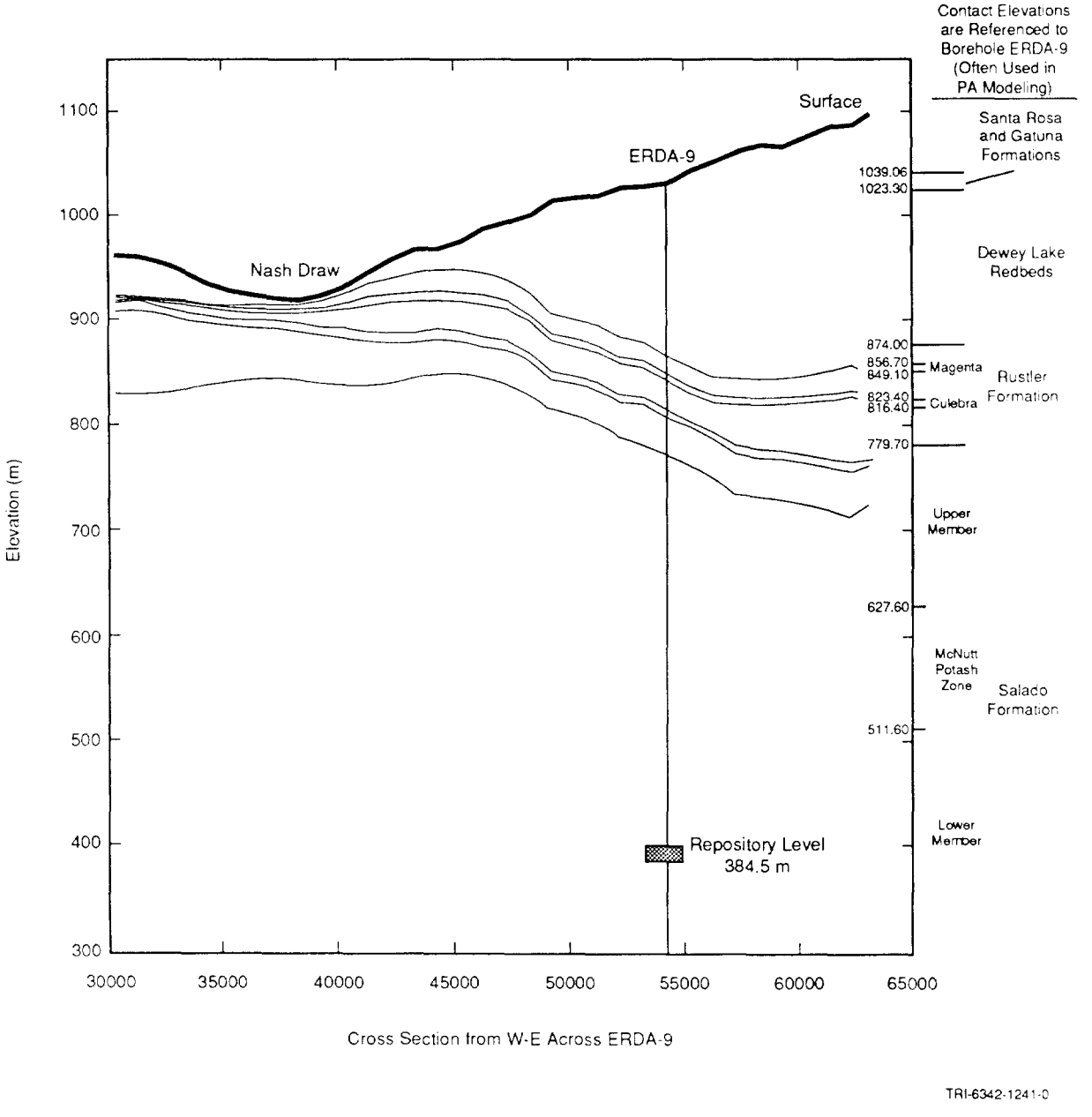

Figure 2.6-2. Interpolated Geologic West-East Cross Section across the WIPP Disposal System (after Mercer, 1983; Davies, 1989, Figure 53).

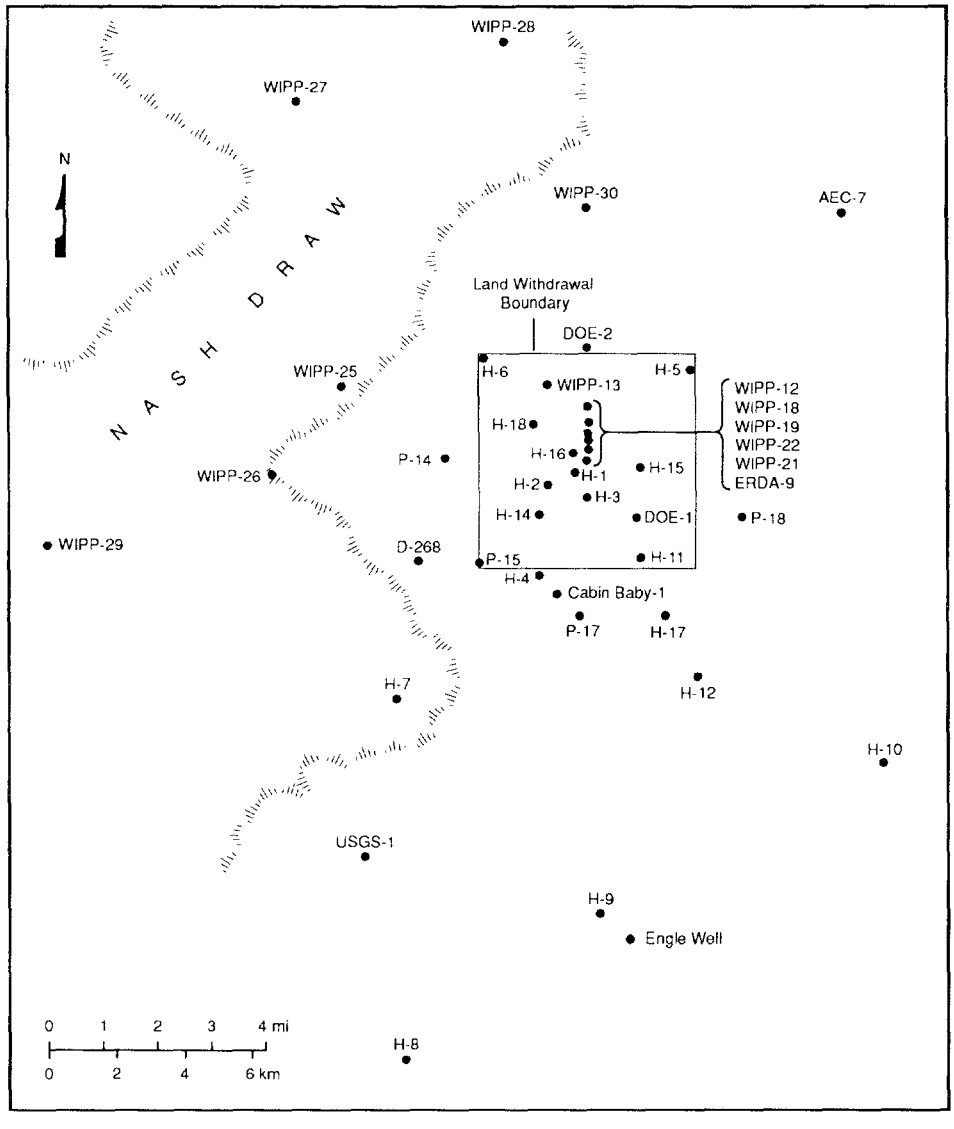

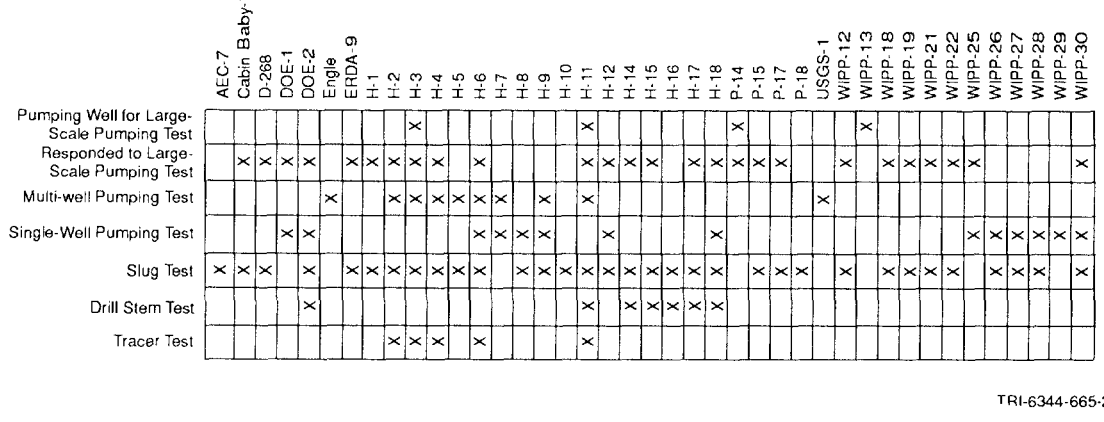

TRI-6344-665-2

Figure 2.6-3. Location of Wells Used to Define Hydrologic Parameters for Culebra Dolomite.

Table 2.6-1. Parameter Values for Culebra Dolomite Member of Rustler Formation

Parameter	Median	Range		Units	Distribution Type	Source
Density						
Dolomite, grain (ρ_g)	2.82×10^3	2.78×10^3	2.86×10^3	kg/m^3	Normal	Kelley and Saulnier, 1990, Tables 4.1, 4.2, 4.3
Clay, bulk (ρ_b)	2.5×10^3			kg/m^3	Constant	Siegel, 1990
Dispersivity,						
longitudinal (α_L)	1×10^2	5×10^1	3×10^2	m	Cumulative	Lappin et al.,1989, Table E-6
transverse (α_T)	1×10^1	5	3×10^1	m	Cumulative	Lappin et al., 1989, Table E-6
Fracture spacing (2B)	4×10^{-1}	6×10^{-2}	8	m	Cumulative	Beauheim et al., June 10, 1991, Memo (see Appendix A)
Clay filling fraction (b_c/b)	0.5	0.1	0.9	none	Normal	Siegel, 1990
Heads	9.32×10^2	9×10^2	9.4×10^2	m	Spatial	See text.
Hydraulic Conductivity						
Avg. pathway - 5 k	1.4574×10^{-6}	1.77×10^{-7}	1.2×10^{-5}	m/s	Lognormal	
Partition Coefficients						
Matrix						
Am	1.86×10^{-1}	0.0	1×10^2	m^3/kg	Cumulative	See text.
Cm	1.86×10^{-1}	0.0	1×10^2	m^3/kg	Cumulative	See text.
Np	4.8×10^{-2}	0.0	1×10^2	m^3/kg	Cumulative	See text.
Pb	1×10^{-2}	0.0	1×10^1	m^3/kg	Cumulative	See text.
Pu	2.61×10^{-1}	0.0	1×10^2	m^3/kg	Cumulative	See text.
Ra	1×10^{-2}	0.0	1×10^1	m^3/kg	Cumulative	See text.
Th	1×10^{-2}	0.0	1	m^3/kg	Cumulative	See text.
U	2.58×10^{-2}	0.0	1	m^3/kg	Cumulative	See text.
Fracture						
Am	9.26×10^1	0.0	1×10^3	m^3/kg	Cumulative	See text.
Cm	9.26×10^1	0.0	1×10^3	m^3/kg	Cumulative	See text.
Np	1	0.0	1×10^3	m^3/kg	Cumulative	See text.
Pb	1×10^{-1}	0.0	1×10^2	m^3/kg	Cumulative	See text.
Pu	2.02×10^2	0.0	1×10^3	m^3/kg	Cumulative	See text.
Ra	3.41×10^{-2}	0.0	1×10^2	m^3/kg	Cumulative	See text.
Th	1×10^{-1}	0.0	1×10^1	m^3/kg	Cumulative	See text.
U	7.5×10^{-3}	0.0	1	m^3/kg	Cumulative	See text.
Porosity						
Fracture (ϕ_f)	1×10^{-3}	1×10^{-4}	1×10^{-2}	none	Lognormal	Lappin et al.,1989, Table 1-2, Table E-6
Matrix (ϕ_m)	1.39×10^{-1}	9.6×10^{-2}	2.08×10^{-1}	none	Data	Kelley and Saulnier, 1990, Table 4.4
Storage coefficient (S)	2×10^{-5}	5×10^{-6}	5×10^{-4}	none	Cumulative	LaVenue et al.,1990, p. 2-18; Haug et al.,1987
Thickness (Δz)	7.7	5.5	1.13×10^1	m	Spatial	LaVenue et al.,1988, Table B-1
Tortuosity (τ)						
Dolomite	1.2×10^{-1}	3×10^{-2}	3.3×10^{-1}	none	Data	Kelley and Saulnier, 1990, Table 4.6; Lappin et al.,1989, Table E-9
Clay	1.2×10^{-2}	3×10^{-3}	3.3×10^{-2}	none	Cumulative	Kelley and Saulnier, 1990, Table 4.6; Lappin et al., 1989, Table E-9
Transmissivity	-4.9	-3.5	-8.9	log (m^2/s)	Spatial	See text.

2.6.1 Density

Parameter:	**Density, grain (ρ_g): Dolomite**
Median:	2.82×10^3
Range:	2.78×10^3
	2.86×10^3
Units:	kg/m^3
Distribution:	Normal
Source(s):	Kelley, V. A., and G. J. Saulnier, Jr. 1990. *Core Analysis for Selected Samples from the Culebra Dolomite at the Waste Isolation Pilot Plant Site.* SAND90-7011. Albuquerque, NM: Sandia National Laboratories. (Tables 4.1, 4.2, and 4.3)

Parameter:	**Density, bulk (ρ_b): Clay**
Median:	2.5×10^3
Range:	None
Units:	kg/m^3
Distribution:	Constant
Source(s):	Siegel, M. D. 1990. "Representation of Radionuclide Retardation in the Culebra Dolomite in Performance Assessment Calculations," Memo 3a in Appendix A of Rechard et al. 1990. *Data Used in Preliminary Performance Assessment of the Waste Isolation Pilot Plant (1990).* SAND89-2408. Albuquerque, NM: Sandia National Laboratories.

Discussion:

The grain density (ρ_g) of the Culebra Dolomite Member was evaluated for 73 core samples from 20 boreholes. For the 20 boreholes, the average and median are 2,815 kg/m^3 (175.7 lb/ft^3) with a range between 2,792 and 2,835 kg/m^3 (174.3 and 177.0 lb/ft^3). The 73 values varied between 2,780 and 2,840 kg/m^3 (173.5 and 177.3 lb/ft^3) with an average of 2,810 kg/m^3 (173.4 lb/ft^3) and a median of 2,830 kg/m^3 (176.7 lb/ft^3) (Kelley and Saulnier, 1990, Tables 4.1, 4.2, and 4.3).

The bulk density (ρ_b) of the minerals (gypsum and corrensite) lining the fractures of the Culebra Dolomite is 2500 kg/m^3 (156 lb/ft^3) (Siegel, 1990).

Figure 2.6-4 shows the spatial variation of density in Culebra based on averages from 20 boreholes.

Table 2.6-2 provides the average grain density of intact dolomite at 20 wells in the Culebra Dolomite Member.

Table 2.6-2. Average Grain Density of Intact Dolomite at 20 Wells in Culebra Member (Kelly and Saulnier, 1990, Tables 4.1 and 4.3)

Well ID	Average Grain Density* (kg/m^3)
H3B3	2.728×10^3
H2B	2.7925×10^3
H10B	2.7933×10^3
H11	2.795×10^3
WIPP30	2.8067×10^3
H2A	2.81×10^3
WIPP12	2.81×10^3
H2B1	2.8125×10^3
H3B2	2.815×10^3
H5B	2.815×10^3
WIPP26	2.8167×10^3
AEC8	2.8233×10^3
H7B2	2.83×10^3
H7C	2.83×10^3
WIPP28	2.83×10^3
H11B3	2.835×10^3
WIPP13	2.835×10^3
H6B	2.8375×10^3
H7B1	2.84×10^3
H4B	2.845×10^3

*Average of measurements from indicated well

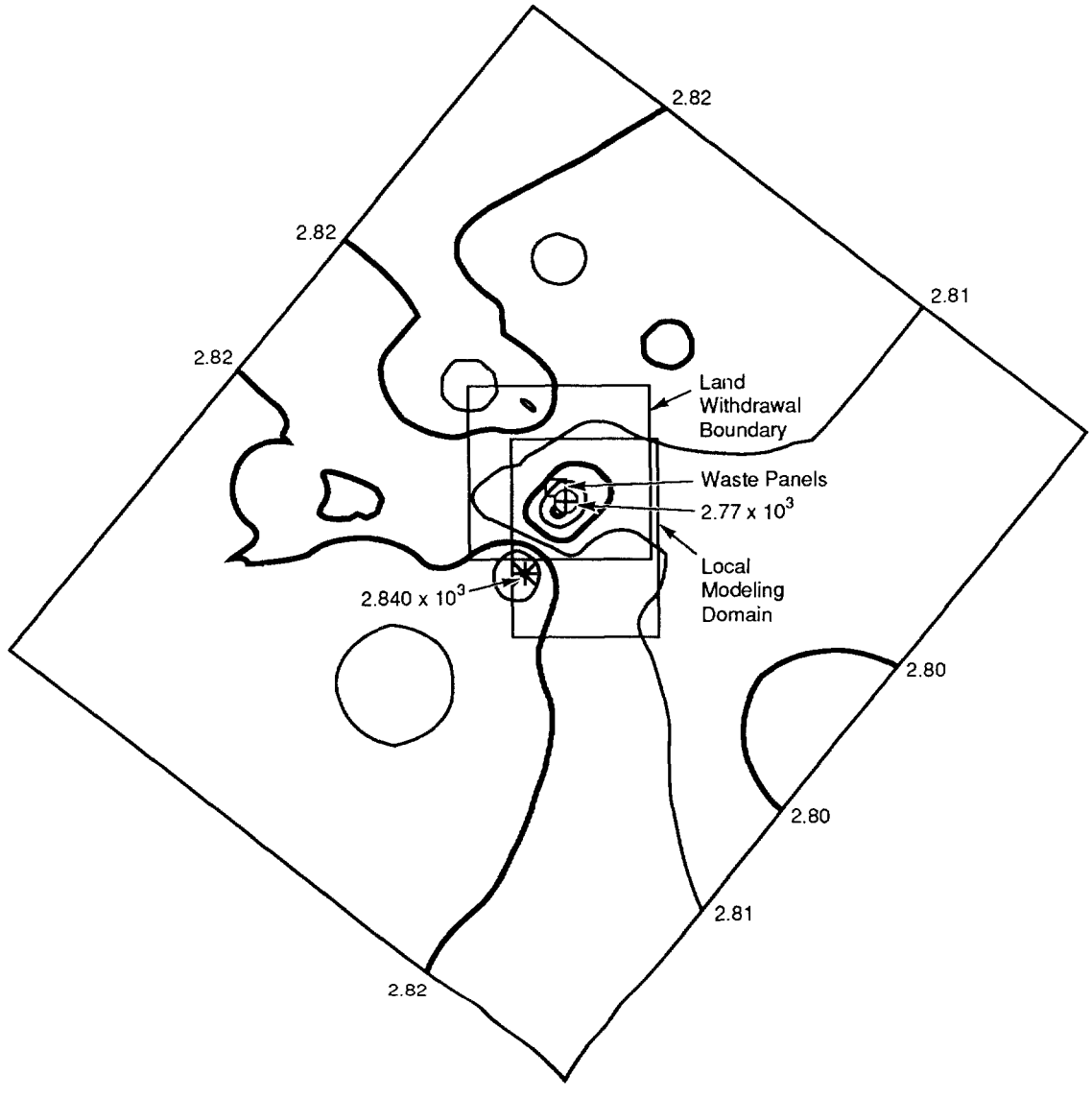

Figure 2.6-4. Spatial Variation of Grain Density in Culebra Based on Averages from 20 Boreholes.

2.6.2 Dispersivity

Parameter:	**Dispersivity, longitudinal (α_L)**
Median:	1×10^2
Range:	5×10^1
	3×10^2
Units:	m
Distribution:	Cumulative
Source(s):	Lappin, A. R., R. L. Hunter, D. P. Garber, and P. B. Davies, eds. 1989. *Systems Analysis Long-Term Radionuclide Transport, and Dose Assessments, Waste Isolation Pilot Plant (WIPP), Southeastern New Mexico; March 1989.* SAND89-0462. Albuquerque, NM: Sandia National Laboratories. (Table E-6)

Parameter:	**Dispersivity, transverse (α_T)**
Median:	1×10^1
Range:	5
	3×10^1
Units:	m
Distribution:	Cumulative
Source(s):	Lappin, A. R., R. L. Hunter, D. P. Garber, and P. B. Davies, eds. 1989. *Systems Analysis Long-Term Radionuclide Transport, and Dose Assessments, Waste Isolation Pilot Plant (WIPP), Southeastern New Mexico; March 1989.* SAND89-0462. Albuquerque, NM: Sandia National Laboratories. (Table E-6)

Discussion:

For moderate travel distances (on the order of kilometers), longitudinal dispersivity (α_L) roughly varies between 0.01 and 0.1 of the mean travel distance of the solute (Lallemand-Barres and Peaudecerf, 1978; Pickens and Grisak, 1981). As first adopted by Lappin et al. (1989), the PA Division has assumed α_L can vary between 50 and 300 m (164 and 984 ft) with a median value of 100 m (328 ft). The distribution for α_L is shown in Figure 2.6-5.

Transverse dispersivity (α_T) is usually linearly related to α_L. The ratio of α_L to α_T typically varies between 5 and 20 (see, for example, Bear and Verruijt, 1987; Freeze and Cherry, 1979, Figure 9.6; Dullien, Figure 7.13). However, at very low velocities the ratio can approach 1, while in some strata the ratio has been reported to approach 100 (de Marsily, 1986). Transverse dispersivity was assumed to be ten times smaller than α_L ($\alpha_T \sim 0.1\alpha_L$) for PA transport calculations. The current range for sensitivity studies is 1 to 25 (Figure 2.6-6).

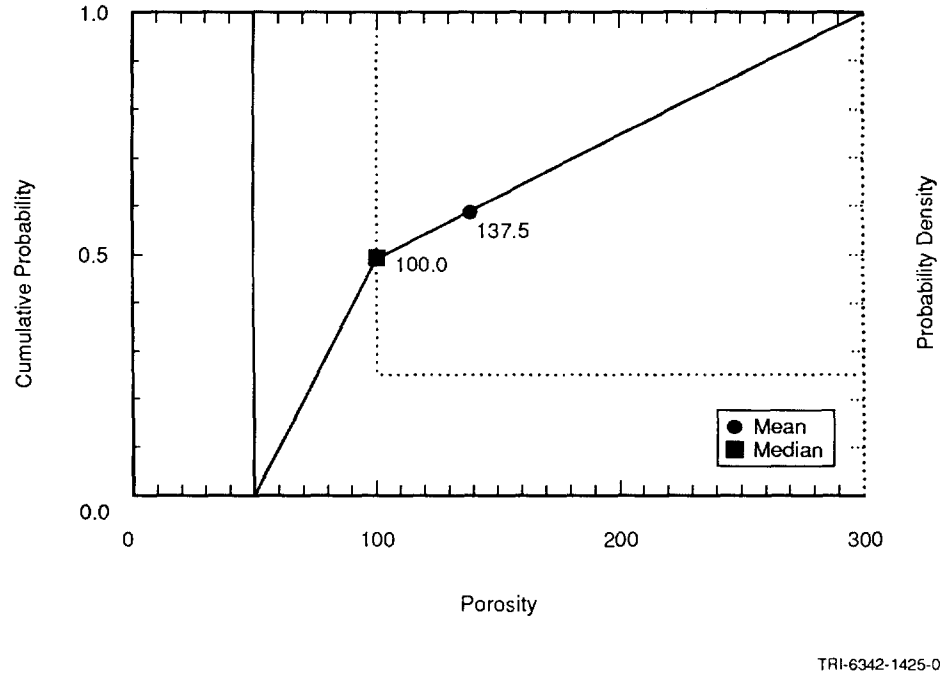

Figure 2.6-5. Estimated Distribution (pdf and cdf) for Longitudinal Dispersivity, Culebra Dolomite Member.

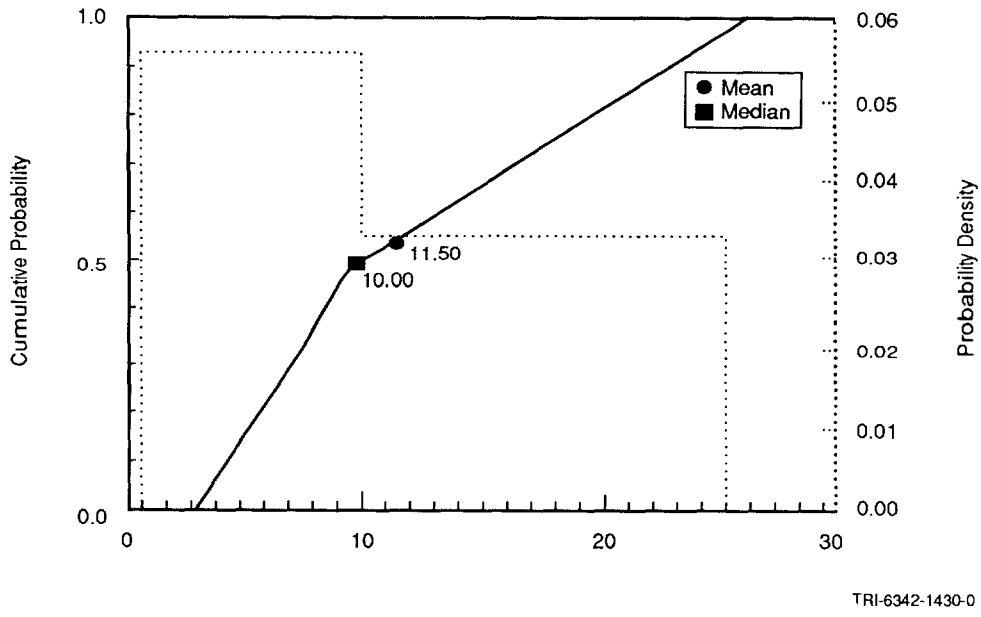

Figure 2.6-6. Estimated Distribution (pdf and cdf) for Transverse Dispersivity, Culebra Dolomite Member.

2.6.3 Fraction of Clay Filling in Fractures

Parameter:	**Clay filling fraction** (b_c/b)
Median:	0.5
Range:	0.1
	0.9
Units:	Dimensionless
Distribution:	Normal
Source(s):	Siegel, M. D. 1990. "Representation of Radionuclide Retardation in the Culebra Dolomite in Performance Assessment Calculations," Memo 3a in Appendix A of Rechard et al. 1990. *Data Used in Preliminary Performance Assessment of the Waste Isolation Pilot Plant (1990).* SAND89-2408. Albuquerque, NM: Sandia National Laboratories.

Discussion:

Within fractures of the Culebra Dolomite Member, gypsum and corrensite (alternating layers of chlorite and smectite) are observed. To evaluate the retardation of radionuclides within the fractures (caused by interaction with this material lining the fractures), the fraction of lining material (b_c/b) is needed, where b_c is the total thickness of clays and b is fracture aperture. At present, data are not available to estimate the true range or distribution of b_c/b in the Culebra. Siegel (1990) recommended a normal distribution with a maximum of 0.9 and a minimum of 0.1. Current PA calculations used a median of 0.5 to estimate the fracture retardation.

Figure 2.6-7 shows the estimated distribution for the fraction of clay filling.

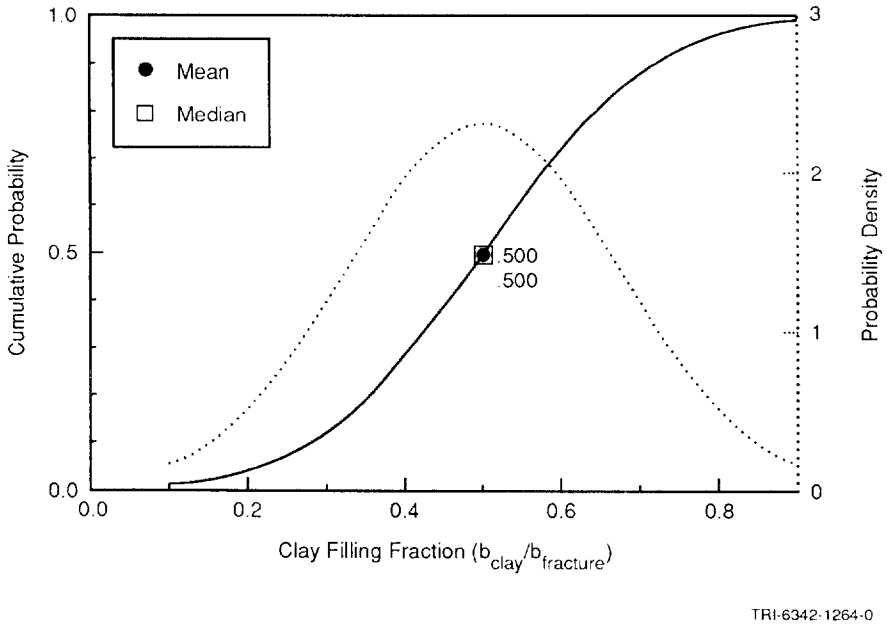

Figure 2.6-7. Estimated Distribution (pdf and cdf) for Clay Filling Fraction, Culebra Dolomite Member.

2.6.4 Porosity

Fracture Porosity

Parameter:	**Fracture porosity (ϕ_f)**
Median:	1×10^{-3}
Range:	1×10^{-4}
	1×10^{-2}
Units:	Dimensionless
Distribution:	Lognormal
Source(s):	Lappin, A. R., R. L. Hunter, D. P. Garber, and P. B. Davies, eds. 1989. *Systems Analysis Long-Term Radionuclide Transport, and Dose Assessments, Waste Isolation Pilot Plant (WIPP), Southeastern New Mexico; March 1989.* SAND89-0462. Albuquerque, NM: Sandia National Laboratories. (Table 1-2; Table E-6)

Discussion:

The fracture porosities interpreted from the tracer tests at the H-3 and H-11 hydropads are 2×10^{-3} (Kelley and Pickens, 1986) and 1×10^{-3}, respectively.

Both H-3 and H-11 lie near the expected transport pathway. The average value rounded to one significant figure was selected as the median and used for PA calculations. Similar to Lappin et al. (1989), the PA Division set the minimum and maximum one order of magnitude to either side of this median.

Figure 2.6-8 shows the estimated distribution for the fracture porosity.

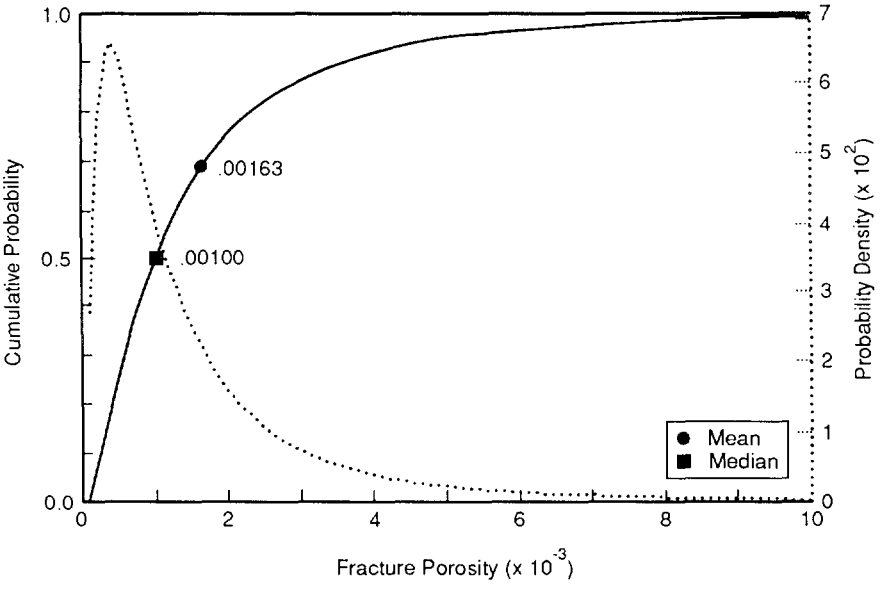

Figure 2.6-8. Estimated Distribution (pdf and cdf) for Fracture Porosity, Culebra Dolomite Member.

Matrix Porosity

Parameter:	**Matrix porosity (ϕ_m)**
Median:	1.39×10^{-1}
Range:	9.6×10^{-2}
	2.08×10^{-1}
Units:	Dimensionless
Distribution:	Data
Source(s):	Kelley, V. A., and G. J. Saulnier, Jr. 1990. *Core Analysis for Selected Samples from the Culebra Dolomite at the Waste Isolation Pilot Plant Site.* SAND90-7011. Albuquerque, NM: Sandia National Laboratories. (Table 4.4)
	Lappin, A. R., R. L. Hunter, D. P. Garber, and P. B. Davies, eds. 1989. *Systems Analysis Long-Term Radionuclide Transport, and Dose Assessments, Waste Isolation Pilot Plant (WIPP), Southeastern New Mexico; March 1989.* SAND89-0462. Albuquerque, NM: Sandia National Laboratories. (Table E-8)

Discussion:

Matrix porosity has been evaluated by the Boyles' law technique using helium or air on 79 samples taken from the *intact* portion of core from 20 borehole or hydropad locations near the WIPP and also by water-resaturation for 30 of the samples. The agreement between the two techniques was excellent with an r^2 of 0.99 (Kelley and Saulnier, 1990, p. 4-7). From the Boyles' law technique, an average porosity for the 20 wells of 0.139 was obtained, with a range of 0.096 to 0.208 (Kelley and Saulnier, 1990, Table 4.4). (Lappin et al., [1989, Table E-8] report an average of 0.153 with a range of 0.028 and 0.303 assuming each of the 79 measurements is independent.) For many of the wells, a large amount of core was lost in highly porous (vuggy) and/or fractured portions of the Culebra Dolomite Member. Thus only intact matrix porosity, the porosity not contributing to fluid flow in dual porosity computational models (e.g., STAFF2D or SWIFT [Rechard et al., 1989]) is reported here.

Table 2.6-3 provides a summary of porosity measurements of intact Culebra Dolomite at selected wells. Figure 2.6-9 shows the assumed density function for porosity of the Culebra Dolomite member. Figure 2.6-10 shows the spatial variation of the intact matrix porosity.

Table 2.6-3. Average of Porosity Measurements of Intact Culebra Dolomite at Selected Wells (after Kelley and Saulnier, 1990, Table 4.4)

Well ID	Median (m)	Low Range (m)	High Range (m)
AEC8	0.10333	0.05195	0.15471
H10B	0.0955	0.04228	0.14872
H11B	0.1618	0.00506	0.31854
H2A	0.1235	0.10512	0.14188
H2B	0.129	0.07576	0.18224
H2B1	0.1205	0.04391	0.19709
H3B2	0.178	0.15351	0.20249
H3B3	0.20775	0.14575	0.26975
H4B	0.2525	0.1435	0.3615
H5B	0.1784	0.04839	0.30841
H6B	0.11033	0.09884	0.12182
H7B1	0.2025	0.0733	0.3317
H7B2	0.1385	0.08829	0.18871
H7C	0.14433	0.1016	0.18706
WIPP12	0.1074	0.00213	0.21267
WIPP13	0.1796	0.03141	0.32779
WIPP25	0.115	0.115	0.115
WIPP26	0.12225	0.10606	0.13844
WIPP28	0.1616	0.10451	0.21869
WIPP30	0.16517	0.07372	0.25662

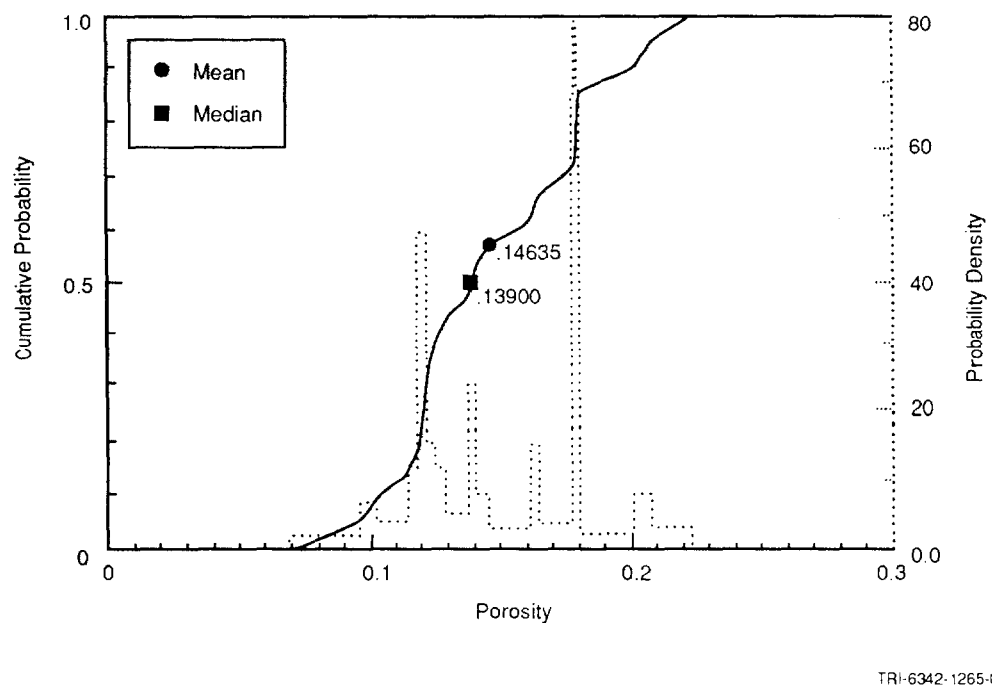

Figure 2.6-9. Assumed Distribution (pdf and cdf) for Intact Matrix Porosity of Culebra Dolomite Member Assuming No Spatial Correlation.

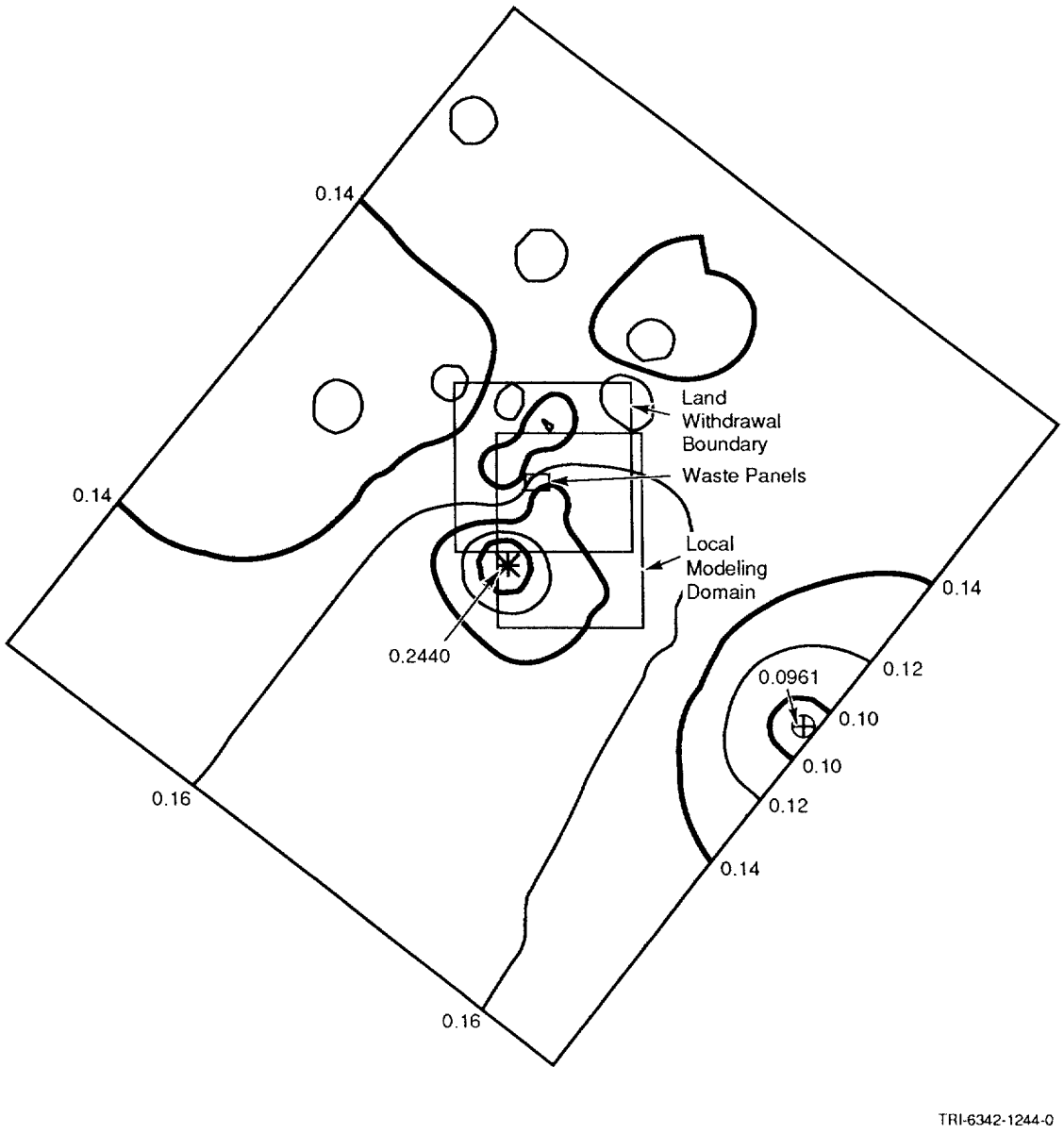

Figure 2.6-10. Variation of Intact Matrix Porosity of Culebra Dolomite Member as Estimated by 10 Nearest Neighbors Using Inverse-Distance-Squared Weighting.

Fracture Spacing

Parameter:	**Fracture spacing** (2B)
Median:	4×10^{-1}
Range:	6×10^{-2}
	8
Units:	m
Distribution:	Cumulative
Source(s):	Beauheim, R. L., T. F. Corbet, P. B. Davies, and J. F. Pickens. 1991. "Recommendations for the 1991 Performance Assessment Calculations on Parameter Uncertainty and Model Implementation for Culebra Transport Under Undisturbed and Brine-Reservoir-Breach Conditions." Internal memo to D. R. Anderson, June 10, 1991. Albuquerque, NM: Sandia National Laboratories. (In Appendix A of this volume).

Figure 2.6-11 shows the estimated distribution for fracture spacing.

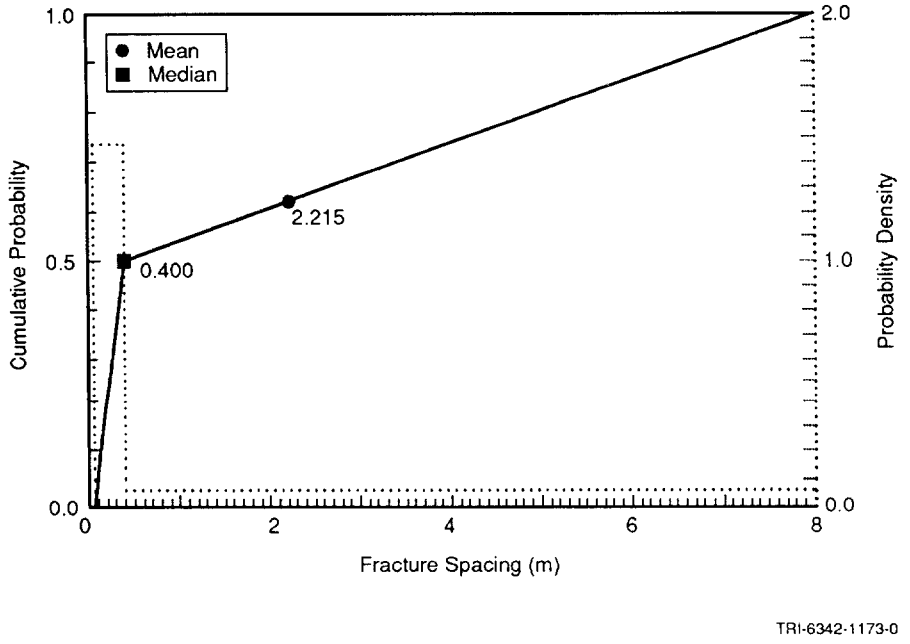

Figure 2.6-11. Estimated Distribution (pdf and cdf) for Culebra Fracture Spacing.

Discussion:

Both horizontal and vertical fracture sets have been observed in core samples, shaft excavations, and outcrops. A fracture spacing varying between 0.23 and 1.2 m (0.75 and 3.9 ft) has been interpreted for two travel paths at the H-3 borehole (Kelley and Pickens, 1986). Preliminary evaluation of the breakthrough curves for the H-6 borehole tracer test suggests a fracture spacing between 0.056 and 0.44 m (0.18 and 1.44 ft), and the H-11 borehole tracer test suggests a fracture spacing between 0.11 and 0.32 m (0.36 and 1.05 ft) (Beauheim et al., June 10, 1991 Memo [Appendix A]). From these data, Beauheim et al. (June 10, 1991, Memo [Appendix A]) suggested a minimum of 0.06 m (0.2 ft) and a maximum equivalent to the assumed uniform thickness of the Culebra (8 m [26.2 ft]). Finally, the average fracture spacing at the three wells (H-3, H-6, and H-11) is 0.4 m (1.3 ft).

2.6.5 Storage Coefficient

Parameter:	**Storage coefficient** (S)
Median:	2×10^{-5}
Range:	5×10^{-6}
	5×10^{-4}
Units:	Dimensionless
Distribution:	Cumulative
Source(s):	LaVenue, A. M., T. L. Cauffman, and J. F. Pickens. 1990. *Groundwater Flow Modeling of the Culebra Dolomite, Volume I: Model Calibration.* SAND89-7068/1. Albuquerque, NM: Sandia National Laboratories. (p. 2-18)
	Haug, A., V. A. Kelley, A. M. LaVenue, and J. F. Pickens. 1987. *Modeling of Groundwater Flow in the Culebra Dolomite at the Waste Isolation Pilot Plant (WIPP) Site: Interim Report.* Contractor Report SAND86-7167. Albuquerque, NM: Sandia National Laboratories.

Discussion:

Model studies of the Culebra (LaVenue et al., 1990, 1988; Haug et al., 1987) have used a storage coefficient (S) of 2×10^{-5}. The storage coefficient near the WIPP ranges over two orders of magnitude (5×10^{-6} to 5×10^{-4}) and is the basis for the range in Table 2.6-1. However, based on sparse well test data from 13 wells, the storage coefficient can range over four orders of magnitude (1×10^{-6} to 1×10^{-2}) in the Culebra (LaVenue et al., 1990, p. 2-18). Table 2.6-4 provides the storage coefficients at wells within the Culebra Dolomite Member. Figure 2.6-12 gives the estimated distribution for the storage coefficient. Figure 2.6-13 shows the spatial variation of the storage coefficient.

Table 2.6-4. Storage Coefficients at Wells within Culebra Dolomite Member (Cauffman et al., 1990, Table D.1)

Well ID	Storage Coefficients
H2	1.28×10^{-5}
H4	4.62×10^{-6}
H5	2.79×10^{-5}
H6	2.35×10^{-4}
H9	3.82×10^{-4}
H11	1.58×10^{-4}
H16	1×10^{-5}
P14	2×10^{-5}
USGS1	2×10^{-5}
WIPP25	1×10^{-2}
WIPP26	4.8×10^{-3}
WIPP27	1×10^{-6}
WIPP28	5×10^{-2}

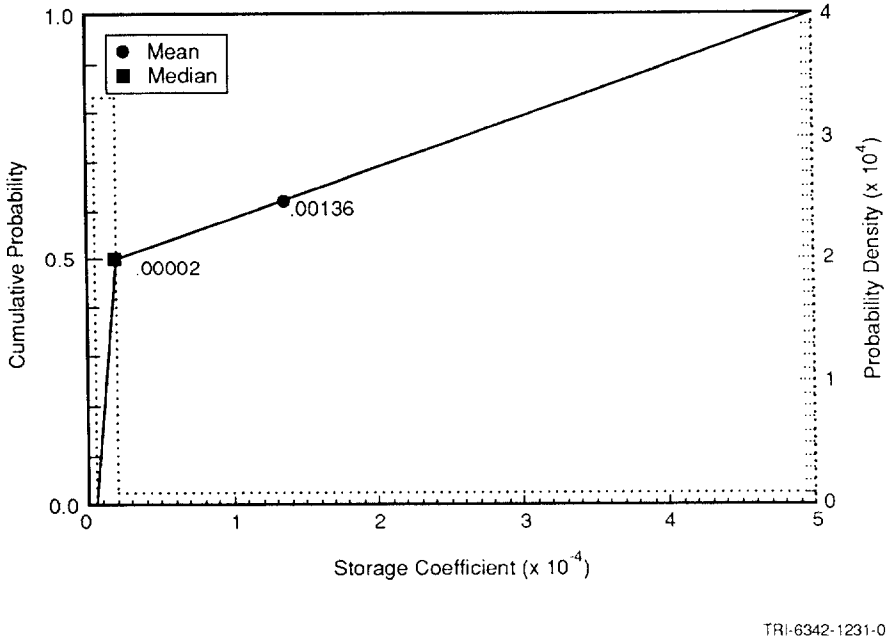

Figure 2.6-12. Estimated Distribution (pdf and cdf) for Storage Coefficient.

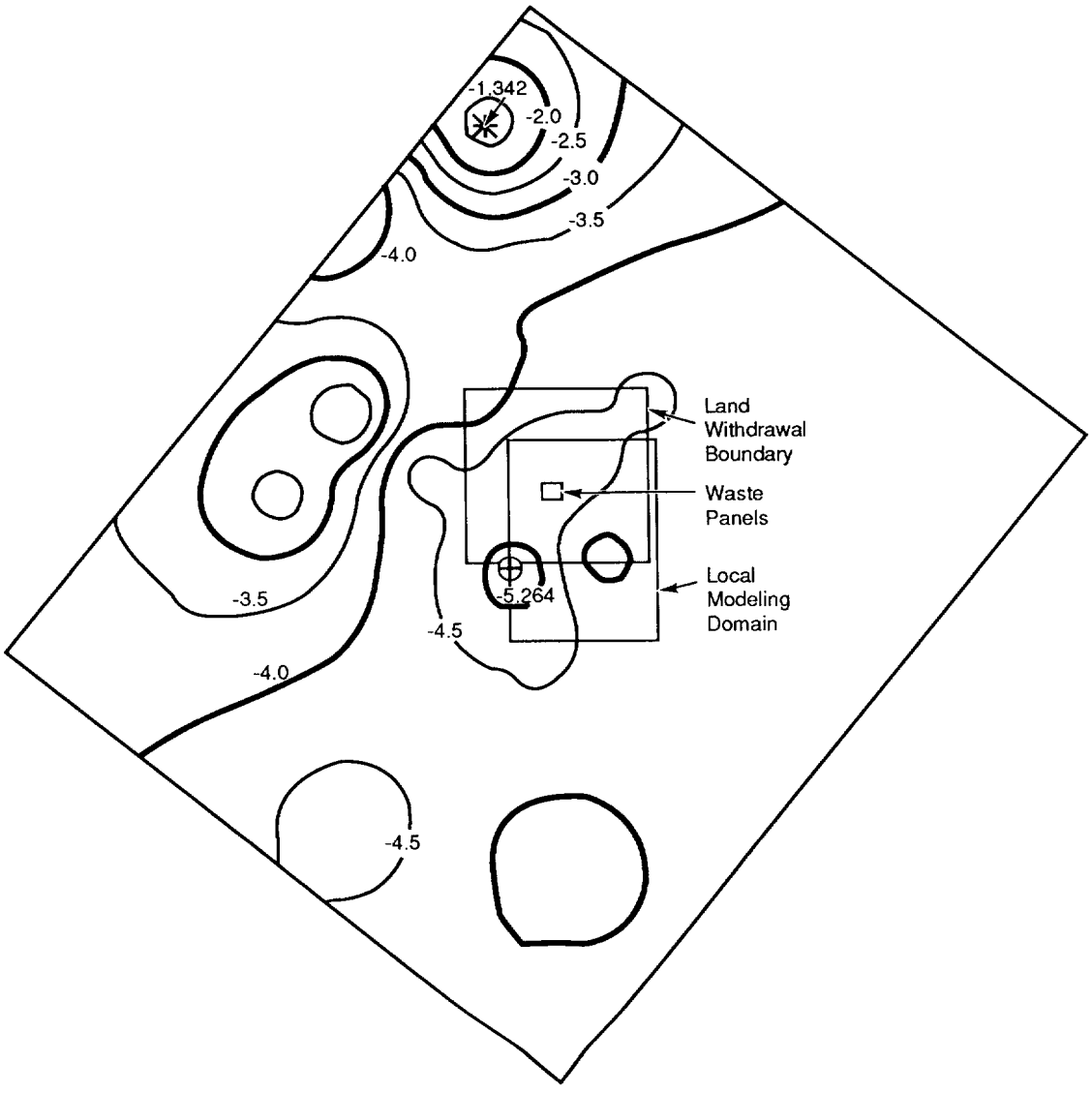

Figure 2.6-13. Spatial Variation of Logarithm of Storage Coefficients within Culebra.

2.6.6 Thickness

Parameter:	**Thickness** (Δz)
Median:	7.7
Range:	5.5
	11.3
Units:	m
Distribution:	Spatial
Source(s):	LaVenue, A. M., A. Haug, and V. A. Kelley. 1988. *Numerical Simulation of Ground-Water Flow in the Culebra Dolomite at the Waste Isolation Pilot Plant (WIPP) Site: Second Interim Report.* SAND88-7002. Albuquerque, NM: Sandia National Laboratories. (Table B-1)

Discussion:

The Culebra thickness reported in Table 2.6-1 is the constant thickness used in modeling studies reported by LaVenue et al. (1988, 1990) and used in PA calculations. Figure 2.6-14 shows the spatial variation of thickness (Δz) in the Culebra Dolomite Member estimated by kriging followed by two passes of a moving average of 15 nearest neighbors with a center weight of zero on a 500-m (1,635-ft) grid.

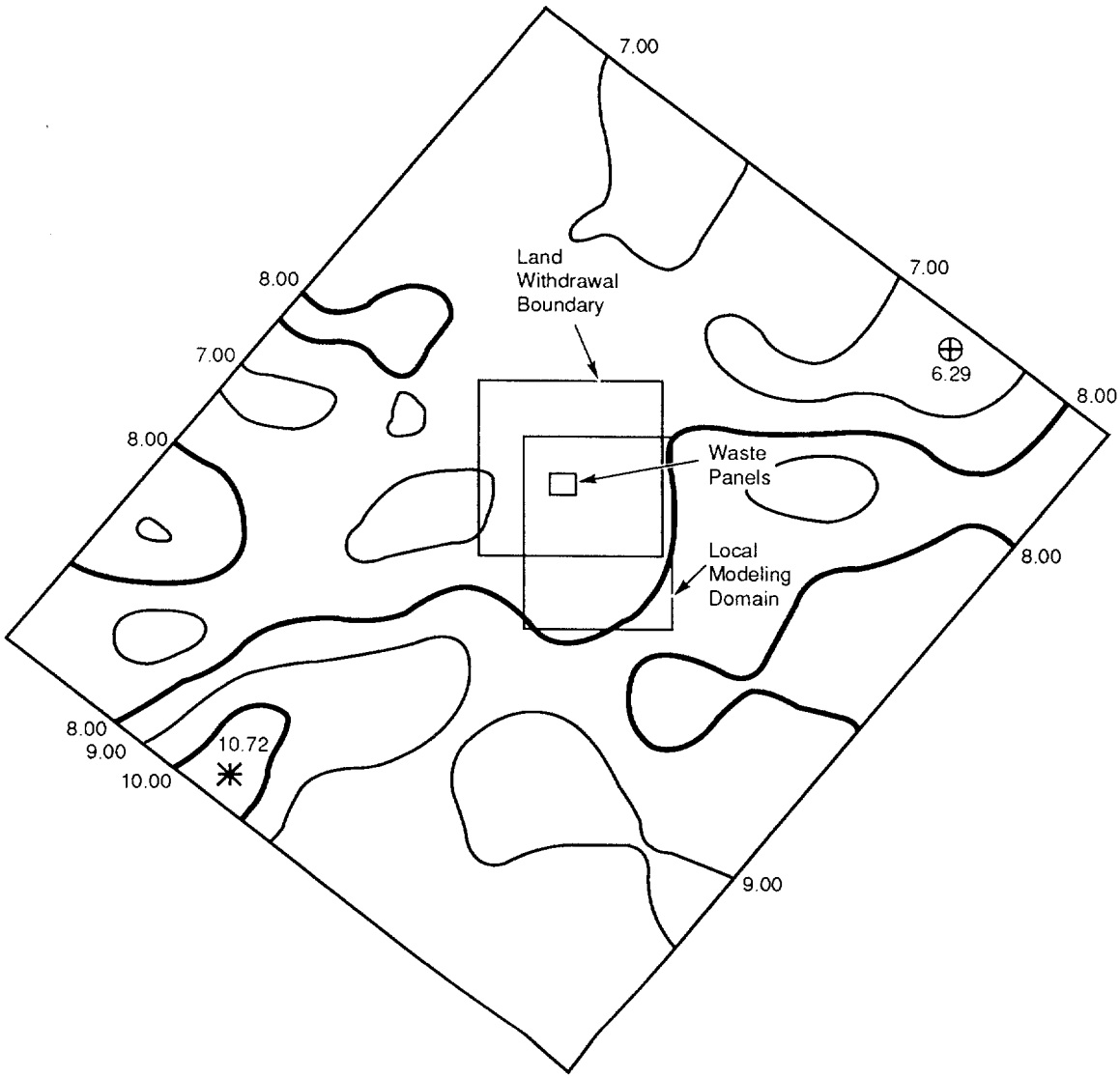

Figure 2.6-14. Variation of Culebra Member Thickness in Regional Modeling Domain. Estimate used kriging followed by two passes of a moving average of 15 nearest neighbors with a center weight of zero on a 500-m grid.

2.6.7 Tortuosity

Parameter:	**Matrix tortuosity (τ), Dolomite**
Median:	1.2×10^{-1}
Range:	3×10^{-2}
	3.3×10^{-1}
Units:	Dimensionless
Distribution:	Data
Source(s):	Kelley, V. A., and G. J. Saulnier, Jr. 1990. *Core Analysis for Selected Samples from the Culebra Dolomite at the Waste Isolation Pilot Plant Site.* SAND90-7011. Albuquerque, NM: Sandia National Laboratories. (Table 4.6)
	Lappin, A. R., R. L. Hunter, D. P. Garber, and P. B. Davies, eds. 1989. *Systems Analysis Long-Term Radionuclide Transport, and Dose Assessments, Waste Isolation Pilot Plant (WIPP), Southeastern New Mexico; March 1989.* SAND89-0462 Albuquerque, NM: Sandia National Laboratories. (Table E-9)

Parameter:	**Tortuosity in clay lining (τ_{clay})**
Median:	1.2×10^{-2}
Range:	3×10^{-3}
	3.3×10^{-2}
Units:	Dimensionless
Distribution:	Cumulative
Source(s):	See text.

Figure 2.6-15 shows the measured distribution for Culebra Dolomite Member tortuosity. Figures 2.6-16 gives the variation of matrix tortuosity measured from intact core samples of the Culebra Dolomite Member.

Discussion:

Intact Matrix Tortuosity. Intact matrix tortuosity is used to evaluate the effective molecular diffusion coefficient (D_m) from the coefficient of molecular diffusion ($D^{\square}$) in the pure saturating fluid ($D_m = \tau D^{\square}$), where τ equals $(\ell/\ell_{path})^2$, ℓ is the linear length, and ℓ_{path} is the length of the [tortuous] path that a fluid particle would take (Bear, 1972, p. 111).

Intact matrix tortuosity for the Culebra Dolomite Member was calculated from 15 core samples from 15 borehole locations using the helium porosity (ϕ_m) and a formation factor (R_ℓ/R_m) determined from electrical-resistivity measurements as follows: $\tau_m^2 = [(1/\phi_m)(R_\ell/R_m)]$, where R_m is the intact porous media saturated with a fluid of resistivity, R_ℓ. (For the Culebra core samples, a 100-g NaCl solution was used with an ambient pressure of 1.4 MPa.) Kelley and Saulnier (1990) state that "... the formation factor (R_ℓ/R_m)

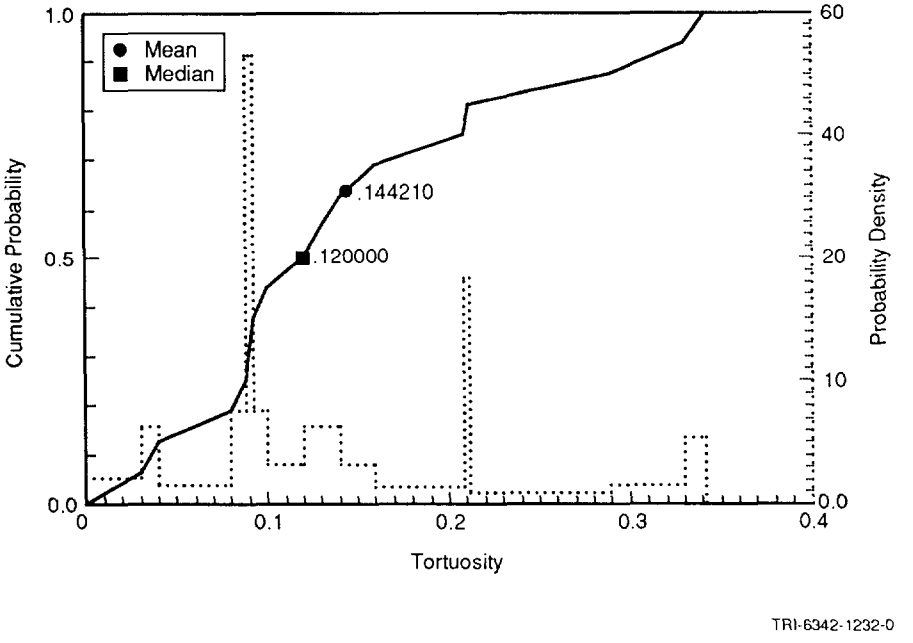

Figure 2.6-15. Measured Distribution (pdf and cdf) for Tortuosity of Culebra Matrix.

determined from electrical-resistivity measurements is usually smaller than that determined by diffusion studies." The values range from 0.03 to 0.33 with a median of 0.12 and an average of 0.14 (Kelley and Saulnier, 1990, Table 4.6; Lappin et al., 1989, Table E-9) (Figure 2.6-9). The spatial variation of tortuosity is shown in Figure 2.6-16. Within the local transport modeling domain, the tortuosity is near the median, 0.12.

Matrix Skin Resistance and Clay Tortuosity. In the dual porosity mathematical model implemented by STAFF2D (Rechard et al., 1989), the boundary condition for the matrix at the fracture matrix interface (Figure 2.6-17) is given by

$$C_i'(B,T) = C_i - \zeta D_n^* \frac{\partial C'}{\partial x}$$

where

C_i', C_i = concentrations of the ith nuclide in the matrix and fracture, respectively
$2B$ = the fracture spacing
D_n^* = diffusion coefficient in matrix
ζ = a parameter characterizing the resistance of a thin skin (e.g., clay lining adjacent to the fracture).

ζ is defined by

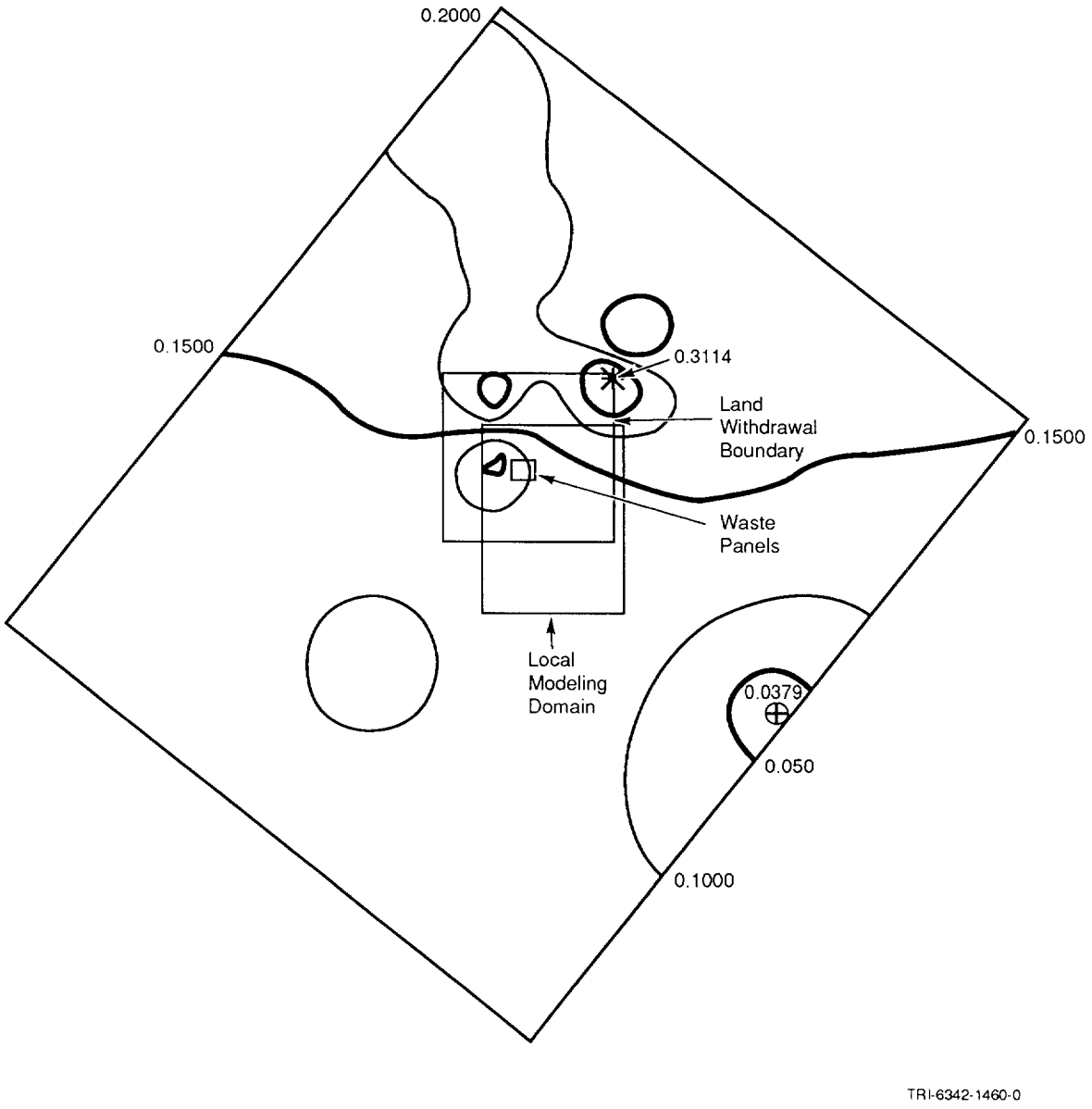

Figure 2.6-16. Variation of Matrix Tortuosity Measured from Intact Core Samples of Culebra Dolomite Member by 10 Nearest Neighbors Using Inverse-Distance-Squared Weighting.

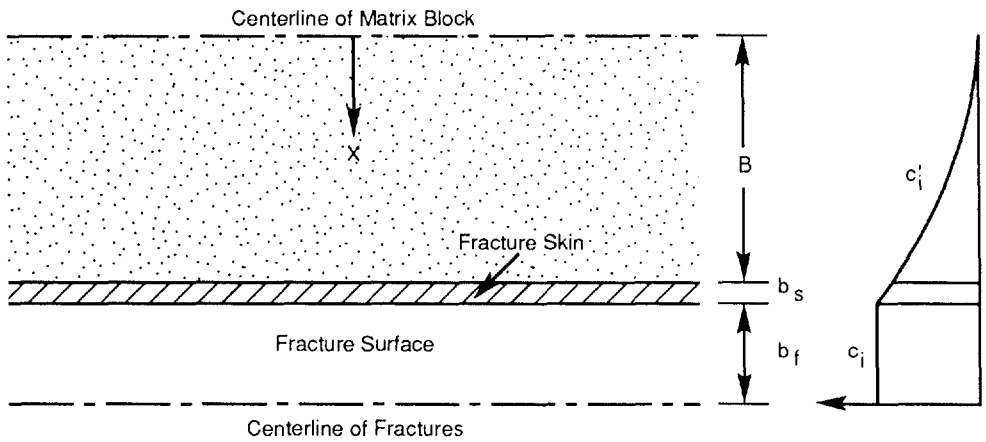

Figure 2.6-17. Boundary Condition for the Matrix at the Fracture Matrix Interface.

$$\zeta = \frac{b_s}{D_s}$$

where

b_s = the skin thickness
D_s = skin diffusion coefficient

For the current PA calculations, the following estimate of the skin resistance is used because of the clay lining in the fractures:

$$\zeta = \frac{f\phi_f(B + b_f)}{\tau_{clay} D^{\alpha}}$$

where

f = clay lining, fracture aperature ratio (b_s/b_f)
ϕ_f = fracture or secondary porosity ($b_f/[B + b_f]$) ~ b_f/B, $B >> b_f$

and as defined above, the diffusion coefficient D_s is skin (e.g., clay),

$$D_s = \tau_{clay} D^{\alpha}$$

where

τ_{clay} = tortuosity of clay lining
D^{α} = full molecular diffusion coefficient in the pure saturating fluid.

For 1991 PA calculations, the clay tortuosity is assumed to be one order of magnitude smaller than the Culebra Dolomite Member matrix tortuosity consistent with the generally observed apparent diffusion coefficients in clayey materials (i.e., 0.012). This conservative assumption reduces the amount of contaminants moving through the clay lining and ultimately being absorbed onto the matrix. Furthermore, only the median value of the molecular diffusion coefficient for the actinides was used (Section 3.3.6), rather than a value for each separate contaminant.

2.6.8 Freshwater Heads at Wells

Table 2.6-5 provides the freshwater head measurements in the Culebra Dolomite Member.

Table 2.6-5. Summary of Selected Steady-State Freshwater Head Measurements in Culebra Dolomite Member (after Cauffman et al., 1990, Table 6.2)

Well ID	Median (m)	Low Range (m)	High Range (m)
AEC7	9.3200×10^2	9.3014×10^2	9.3386×10^2
CABIN1	9.1120×10^2	9.0980×10^2	9.1260×10^2
D268	9.1520×10^2	9.1462×10^2	9.1578×10^2
DOE1	9.1390×10^2	9.0831×10^2	9.1949×10^2
DOE2	9.3530×10^2	9.3181×10^2	9.3880×10^2
H1	9.2330×10^2	9.1860×10^2	9.2796×10^2
H10B	9.2140×10^2	9.1627×10^2	9.2653×10^2
H11B1	9.1280×10^2	9.1000×10^2	9.1560×10^2
H12	9.1360×10^2	9.1080×10^2	9.1640×10^2
H14	9.1550×10^2	9.1457×10^2	9.1643×10^2
H15	9.1560×10^2	9.1234×10^2	9.1886×10^2
H17	9.1100×10^2	9.0890×10^2	9.1310×10^2
H18	9.3190×10^2	9.2887×10^2	9.3493×10^2
H2C	9.2400×10^2	9.2167×10^2	9.2633×10^2
H3B1	9.1710×10^2	9.1267×10^2	9.2153×10^2
H4B	9.1280×10^2	9.1140×10^2	9.1420×10^2
H5B	9.3400×10^2	9.3074×10^2	9.3726×10^2
H6B	9.3260×10^2	9.3027×10^2	9.3493×10^2
H7B1	9.1270×10^2	9.1200×10^2	9.1340×10^2
H8B	9.1240×10^2	9.1147×10^2	9.1333×10^2
H9B	9.0820×10^2	9.0680×10^2	9.0960×10^2
P14	9.2690×10^2	9.2480×10^2	9.2900×10^2
P15	9.1680×10^2	9.1494×10^2	9.1866×10^2
P17	9.1160×10^2	9.0997×10^2	9.1323×10^2
USGS1	9.0980×10^2	9.0922×10^2	9.1038×10^2
USGS4	9.0970×10^2	9.0947×10^2	9.0993×10^2
USGS8	9.1110×10^2	9.1087×10^2	9.1133×10^2
WIPP12	9.3310×10^2	9.3147×10^2	9.3473×10^2
WIPP13	9.3400×10^2	9.3120×10^2	9.3680×10^2
WIPP18	9.3000×10^2	9.2720×10^2	9.3280×10^2
WIPP25	9.2870×10^2	9.2637×10^2	9.3103×10^2
WIPP26	9.1940×10^2	9.1882×10^2	9.1998×10^2
WIPP27	9.3810×10^2	9.3647×10^2	9.3973×10^2
WIPP28	9.3700×10^2	9.3467×10^2	9.3933×10^2
WIPP29	9.0540×10^2	9.0482×10^2	9.0598×10^2
WIPP30	9.3510×10^2	9.3254×10^2	9.3766×10^2

2.6.9 Transmissivities for Wells

Table 2.6-6 provides the logarithms of selected transmissivity measurements in the Culebra Dolomite Member (Cauffman et al., 1990, Table C.1). Table 2.6-7 provides the logarithms of the calibrating points.

Table 2.6-6. Logarithms of Selected Transmissivity Measurements in Culebra Dolomite Member (after Cauffman et al., 1990, Table C.1)

Well ID	Median	Low Range	High Range
AEC7	-6.5535	-7.7185	-5.3885
CABIN1	-6.5213	-7.6863	-5.3563
D268	-5.6897	-6.8547	-4.5247
DOE1	-4.4271	-5.0096	-3.8466
DOE2	-4.0191	-4.6016	-3.4366
ENGLE	-4.3350	-4.9175	-3.7525
ERDA9	-6.2964	-7.4614	-5.1314
H1	-6.0290	-7.1940	-4.8640
H10B	-7.1234	-8.2884	-5.9584
H11B1	-4.5057	-5.0882	-3.9232
H12	-6.7132	-7.8782	-5.5482
H14	-6.4842	-7.6492	-5.3192
H15	-6.3804	-7.5454	-5.2154
H16	-6.1149	-7.2799	-4.9499
H17	-6.6361	-7.8011	-5.4471
H18	-5.7775	-6.3600	-5.1950
H2B1	-6.2005	-6.7830	-5.6180
H3	-5.6089	-6.1914	-5.0264
H4B	-5.9960	-6.5785	-5.4135
H5B	-7.0115	-7.5940	-6.4290
H6B	-4.4500	-5.0325	-3.8675
H7B1	-2.8125	-3.3950	-2.2300
H8B	-5.0547	-5.6372	-4.4722
H9B	-3.9019	-4.4844	-3.3194
USGS1	-3.2584	-3.8409	-2.6759
WIPP12	-6.9685	-8.1355	-5.8035
WIPP13	-4.1296	-5.2946	-2.9646
WIPP18	-6.4913	-7.6563	-5.3263
WIPP19	-6.1903	-7.3553	-5.0253
WIPP21	-6.5705	-7.7355	-5.4055
WIPP22	-6.4003	-7.5653	-5.2353
WIPP25	-3.5412	-4.1237	-2.9587
WIPP26	-2.9136	-3.4961	-2.3311

Table 2.6-6. Logarithms of Selected Transmissivity Measurements in Culebra Dolomite Member (after Cauffman et al., 1990, Table C.1) (Concluded)

Well ID	Median	Low Range	High Range
WIPP27	-3.3692	-3.9517	-2.7867
WIPP28	-4.6839	-5.2664	-4.1014
WIPP29	-2.9685	-3.5510	-2.3860
WIPP30	-6.6023	-7.7673	-5.4373
P14	-3.5571	-4.5124	-2.6018
P15	-7.0354	-8.2004	-5.8704
P17	-5.9685	-7.1335	-4.8035
P18	-1.0123×10^{1}	-1.1288×10^{1}	-8.9584

Table 2.6-7. Logarithms of Transmissivity of Calibrating Points (Pilot Points) for Culebra Dolomite Member (after Davies and LaVenue, 1990)

Well ID	Median	Low Range	High Range
PP1	-2.0700	-4.4233	2.833×10^{-1}
PP2	-2.2500	-4.5334	3.340×10^{-2}
PP3	-2.3200	-4.6267	-1.330×10^{-2}
PP4	-3.6200	-5.3442	-1.8958
PP5	-3.5800	-5.2576	-1.9024
PP6	-6.0200	-7.7675	-4.2725
PP7	-6.4200	-8.0044	-4.5656
PP8	-3.4100	-4.8779	-1.9421
PP9	-2.7100	-3.8913	-1.5217
PP11	-7.7200	-9.1413	-6.2987
PP12	-8.0800	-9.0353	-7.1247
PP13	-5.6400	-6.5953	-4.6847
PP14	-8.3400	-9.7846	-6.8954
PP15	-6.4900	-7.7482	-5.2318
PP16	-5.1300	-6.5280	-3.7320
PP17	-6.6000	-8.1378	-5.0622
PP18	-2.6300	-4.5173	-7.427×10^{-1}
PP19	-2.8600	-4.7939	-9.261×10^{-1}
PP20a	-2.9400	-4.8972	-9.828×10^{-1}
PP21a	-3.0000	-4.8407	-1.1593
PP23	-3.8500	-5.1548	-2.5452
PP24	-3.5000	-4.2689	-2.7311
PP25	-6.0000	-7.0718	-4.9282
PP26	-5.5000	-6.3388	-4.6612
PP27	-4.2500	-5.3684	-3.1316
PP28	-3.5000	-4.7582	-2.2418
PP29	-3.2500	-4.3451	-2.1549
PP30	-6.1600	-7.3250	-4.9950
PP31	-5.8700	-7.0350	-4.7050
PP32	-5.0000	-5.7223	-4.2777
PP34	-3.5900	-4.5453	-2.6347
PP35	-2.6700	-3.6253	-1.7147
PP36	-5.1700	-6.0787	-4.2613
PP37	-4.3100	-6.0342	-2.5858
PP38	-3.9000	-5.3446	-2.4554
PP39	-3.9000	-5.3446	-2.4554
PP40	-5.9300	-6.8853	-4.9747
PP41	-4.0000	-4.9553	-3.0447
PP42	-3.5000	-4.5951	-2.4049
PP43	-5.0000	-5.9553	-4.0447
PP44	-5.0000	-5.9553	-4.0447

2.6.10 Partition Coefficients and Retardations

A partitioning or distribution coefficient (K_d), which describes the intensity of sorption, is used to calculate the partitioning of species such as radionuclides between the groundwater and rock and, thereby, calculate the sorption capacity or retardation (R). A K_d value cannot be extrapolated with confidence to physiochemical conditions that differ from those under which the experimental data were obtained.

The recommended K_d cumulative distributions reported in Tables 2.6-8 and 2.6-9 are considered to be realistic in light of available data, but require a number of subjective assumptions that ongoing experiments may invalidate. The distributions were derived from an internal expert-judgment process regarding radionuclide retardation in the Culebra, which convened in April and May, 1991. The three Sandia experts involved were Robert G. Dosch (6212), Craig F. Novak (6344), and Malcolm D. Siegel (6315). The three experts participated in individual elicitation sessions for the purpose of developing probability distributions for the distribution coefficients for americium, curium, lead, neptunium, plutonium, radium, thorium, and uranium, for two sets of conditions. The first is the nature of the transport fluid: essentially Culebra or Salado brine. The second is whether the retardation takes place in the dolomite matrix or in the clay lining the fractures.

The K_d cumulative distributions that resulted from this panel are provided in Tables 2.6-8 and 2.6-9. The distributions are derived from a combination of values from two of the participants; a decision was made to not use Siegel's values in the 1991 PA calculations, as explained in the discussion that follows the tables. The rationales behind Dosch' and Novak's values are briefly described below; a more thorough description of Novak's values is provided in Appendix A of this report (Novak, September 4, 1991, Memo).

Dosch reviewed data from several experiments on distribution coefficients for various actinides in a variety of mediums. His own work (Lynch and Dosch, 1980) was included in his data set. He believed that even though some experiments were conducted using mediums different from the Culebra matrix and the Culebra clay, most of the data could not be discounted (personal communication from S. Hora, September 1991 regarding expert panel elicitation on May 1991). His justification for this was that experimental data directly applicable to the issue at hand was so scarce that no relevant data should be disregarded. In general, Dosch remarked that most of the experimental data deserved equal weight in any judgments about the behavior of actinides in the Culebra matrix and clay. Dosch declined to give any probability distributions for thorium and lead because he did not believe himself qualified to make enlightened assessments for those elements (personal communication from S. Hora, September 1991, regarding expert panel elicitation on May 1991).

Novak examined available research that detailed the experimental measurement of K_ds using substrates and water compositions pertinent to transport in the WIPP system (Novak, 1991). He showed that (1) data are not available for all elements of interest, (2) almost no data exist for clay substrates in the Culebra, and (3) existing data may not be applicable to current human-intrusion scenarios. In this study (Novak, 1991), Novak also questioned the use of the K_d model for estimating radionuclide retardation in the Culebra. Despite the limitations in existing data, Novak attempted to provide K_d values for use in the 1991 PA calculations.

Novak believes that the water composition called "Culebra H_2O" is the most representative among available data for Case One, which assumed that water reaching the Culebra would not change the composition of Culebra water significantly, except for the presence of radionuclides. Brine A best represented Case Two, which assumed that water reaching the Culebra would not be diluted and a concentrated brine contaminated with radionuclides would flow through the Culebra. Within each case, K_d estimates were needed for radionuclide sorption on the matrix (i.e., the dolomitic Culebra substrates), and in the fractures (i.e., on clay materials lining fractures). Each type of water was used for both matrix and fractures. Thus, for Case One, data from "Culebra H_2O" studies were used to estimate K_d values where actual data were not available. Similarly, Brine A data were used to estimate K_ds for Case Two.

Novak offered K_ds of 0 m^3/kg for all cdfs because he thought it possible that any of the elements could be transported with the fluid velocity. Upper bounds represent Novak's opinions on maximum values for K_ds observable under human-intrusion scenarios (Novak, September 4, 1991, Memo [see Appendix A]). Novak chose different sets of fractiles for different radionuclides. These represent his best estimates resulting from his studies of existing data and literature.

Novak further states that values obtained through the expert elicitation process are subjective estimates only because of large uncertainties in water composition, mixing within the Culebra, and the questionable utility of the K_d model. Finally, Novak argues that these cdfs for K_ds do not substitute for actual data, and believes that additional study is needed to quantify the potential for radionuclide retardation in the Culebra (Novak, September 4, 1991, Memo [Appendix A]).

Table 2.6-8. Cumulative Density Function for Partition Coefficients for Culebra Dolomite Member within Matrix Dominated by Culebra Brine (average of Dosch and Novak estimates)

Element	Median	Range		Partition Coefficient	Probability	Units	Source
Am	1.86×10^{-1}	0.0	1×10^{2}	0.0	0.0	m^3/kg	See text.
				1×10^{-2}	0.0139		
				9×10^{-2}	0.236		
				1×10^{-1}	0.271		
				1.5×10^{-1}	0.437		
				2×10^{-1}	0.525		
				4×10^{-1}	0.627		
				1	0.71		
				1×10^{1}	0.829		
				1×10^{2}	1		
Cm	1.86×10^{-1}	0.0	1×10^{2}	0.0	0.0	m^3/kg	See text.
				1×10^{-2}	0.0139		
				9×10^{-2}	0.236		
				1×10^{-1}	0.271		
				1.5×10^{-1}	0.437		
				2×10^{-1}	0.525		
				4×10^{-1}	0.627		
				1	0.71		
				1×10^{1}	0.829		
				1×10^{2}	1		
Np	4.8×10^{-2}	0.0	1×10^{2}	0.0	0.0	m^3/kg	See text.
				2.5×10^{-4}	0.1		
				7.5×10^{-4}	0.25		
				1.5×10^{-3}	0.4		
				1×10^{-2}	0.409		
				1×10^{-1}	0.625		
				2×10^{-1}	0.75		
				1×10^{1}	0.875		
				1×10^{2}	1		
Pb	1×10^{-2}	0.0	1×10^{1}	0.0	0.0	m^3/kg	See text.
				1×10^{-3}	0.25		
				1×10^{-2}	0.5		
				1×10^{-1}	0.75		
				1	0.99		
				1×10^{1}	1		
Pu	2.61×10^{-1}	0.0	1×10^{2}	0.0	0.0	m^3/kg	See text.
				1×10^{-4}	0.001		
				5×10^{-3}	0.112		
				1×10^{-2}	0.18		
				8×10^{-2}	0.347		
				1×10^{-1}	0.386		
				3×10^{-1}	0.528		
				1	0.75		
				1×10^{2}	1		

Table 2.6-8. Cumulative Density Function for Partition Coefficients for Culebra Dolomite Member within Matrix Dominated by Culebra Brine (average of Dosch and Novak estimates) (Concluded)

Element	Median	Range		Partition Coefficient	Probability	Units	Source
Ra	1×10^{-2}	0.0	1×10^{1}	0.0	0.0	m^3/kg	See text.
				1×10^{-3}	0.25		
				1×10^{-2}	0.5		
				2×10^{-2}	0.639		
				1×10^{-1}	0.85		
				1	0.972		
				1×10^{1}	1		
Th	1×10^{-2}	0.0	1	0.0	0.0	m^3/kg	See text.
				5×10^{-3}	0.25		
				1×10^{-2}	0.5		
				1×10^{-1}	0.75		
				1	1		
U	2.58×10^{-2}	0.0	1	0.0	0.0	m^3/kg	See text.
				2.5×10^{-4}	0.101		
				7.5×10^{-4}	0.252		
				1.5×10^{-3}	0.404		
				5×10^{-2}	0.574		
				1×10^{-1}	0.75		
				2×10^{-1}	0.875		
				1	1		

Table 2.6-9. Cumulative Density Function for Partition Coefficients for Culebra Dolomite Member within Fracture Dominated by Culebra Brine (average of Dosch and Novak estimates)

Element	Median	Range		Partition Coefficient	Probability	Units	Source
Am	9.26×10^{1}	0.0	1×10^{3}	0.0	0.0	m^3/kg	See text.
				9×10^{-1}	0.125		
				1	0.146		
				1.5	0.250		
				4	0.376		
				1×10^{1}	0.454		
				1×10^{3}	1		
Cm	9.26×10^{1}	0.0	1×10^{3}	0.0	0.0	m^3/kg	See text.
				9×10^{-1}	0.125		
				1	0.146		
				1.5	0.250		
				4	0.376		
				1×10^{1}	0.454		
				1×10^{3}	1		
Np	1	0.0	1×10^{3}	0.0	0.0	m^3/kg	See text.
				2.5×10^{-3}	0.1		
				7.5×10^{-3}	0.25		
				1.5×10^{-2}	0.4		
				1	0.5		
				1×10^{3}	1		
Pb	1×10^{-1}	0.0	1×10^{2}	0.0	0.0	m^3/kg	See text.
				1×10^{-2}	0.25		
				1×10^{-1}	0.5		
				1	0.75		
				1×10^{1}	0.99		
				1×10^{2}	1		
Pu	2.02×10^{2}	0.0	1×10^{3}	0.0	0.0	m^3/kg	See text.
				5×10^{-2}	0.05		
				8×10^{-1}	0.125		
				1	0.136		
				3	0.251		
				1×10^{1}	0.379		
				1×10^{3}	1		
Ra	3.41×10^{-2}	0.0	1×10^{2}	0.0	0.0	m^3/kg	See text.
				1×10^{-2}	0.225		
				5×10^{-2}	0.680		
				1×10^{-1}	0.75		
				1	0.875		
				1×10^{1}	0.995		
				1×10^{2}	1		

Table 2.6-9. Cumulative Density Function for Partition Coefficients for Culebra Dolomite Member within Fracture Dominated by Culebra Brine (average of Dosch and Novak estimates) (Concluded)

Element	Median	Range		Partition Coefficient	Probability	Units	Source
Th	1×10^{-1}	0.0	1×10^{1}	0.0	0.0	m^3/kg	See text.
				5×10^{-2}	0.25		
				1×10^{-1}	0.5		
				1	0.75		
				1×10^{1}	1		
U	7.5×10^{-3}	0.0	1	0.0	0.0	m^3/kg	See text.
				2.5×10^{-3}	0.2		
				7.5×10^{-3}	0.5		
				1.5×10^{-2}	0.8		
				1	1		

Discussion (Siegel, 1991):

The estimates provided by Siegel are similar to those he provided for the 1990 PA calculations and are shown in Tables 2.6-10 and 2.6-11. The decision to not incorporate these numbers into the 1991 panel's distributions was based on discussions with Steve Hora (University of Hawaii at Hilo) who conducted Siegel's elicitation session and who has worked extensively in the area of expert-judgment elicitation (e.g., U.S. NRC, 1990). The decision to not combine Siegel's values with the other two participants' responses was based on Siegel's values being fundamentally different from those provided by the other experts.

For example, two of the experts, Dosch and Novak, provided points on probability distributions that reflected their best judgments about the possible levels of retardation. Siegel chose, instead, to provide upper bounds on the fractiles of a probability distribution. Thus, the information obtained from Siegel is inherently different than the information obtained from the other two experts. The strategy that Siegel employed was to examine experimental evidence, determine a range of values for a specific quantile such as the median of the uncertainty distribution, and select the most conservative value from this range. Because experimental evidence is meager, Siegel did not believe that a sufficient scientific basis was available to justify forming a complete uncertainty distribution. He thus chose to bound the distribution.

Because the responses are fundamentally different, any attempt to aggregate Siegel's responses with the other participants would have led to an end product with no interpretable meaning. For this reason, Siegel's responses were not combined with those of the other experts and are not used in the 1991 performance assessment. The assessments provided by Siegel, however, are similar to those provided in 1990, which were used in the 1990 performance assessment.

Table 2.6-10. Cumulative Density Function for Partition Coefficients for Culebra Dolomite Member within Matrix Dominated by Culebra Brine (estimated by Siegel, 1991, 1990)

Element	Median		Range	Partition Coefficient[a] 1991	(1990)	Probability	Units	Source[b]
Am	1.2×10^{-1}	0.0	3.8×10^{-1}	0.0		0.0	m^3/kg	Anderson et al., 1991;
				1×10^{-1}		0.25		Siegel, 1990; Lappin
				1.2×10^{-1}	(1.1×10^{-1})	0.50		et al., 1989, Table
				2×10^{-1}		0.75		3-14, E-10, E-11, E-12
				3.80×10^{-1}		1.0		
Cm	8×10^{-1}	0.0	1.6	0.0			m^3/kg	Anderson et al., 1991;
				4×10^{-1}	(1×10^{-1})	0.25		Siegel, 1990; Lappin
				8×10^{-1}	ng	0.50		et al., 1989, Table
				1.2	(2×10^{-1})	0.75		3-14, E-10, E-11, E-12
				1.6	(1.2×10^{1})	1.0		
Np	6×10^{-4}	0.0	7.4×10^{-3}	0.0			m^3/kg	Anderson et al., 1991;
				3×10^{-4}	(5×10^{-5})	0.25		Siegel, 1990; Lappin
				6×10^{-4}	(1×10^{-4})	0.50		et al., 1989, Table
				1.5×10^{-3}	ng	0.75		3-14, E-10, E-11, E-12
				7.4×10^{-3}	(1×10^{-2})	1.0		
Pu = Th	8×10^{-2}	0.0	1	0.0			m^3/kg	Anderson et al., 1991;
				2.5×10^{-2}		0.25		Siegel, 1990; Lappin
				8×10^{-2}		0.50		et al., 1989, Table
				2×10^{1}	(1×10^{-1})	0.75		3-14, E-10, E-11, E-12
				1	(1.05)	1.0		
Ra = Pb	5×10^{-4}	0.0	1×10^{-3}	0.0			m^3/kg	Siegel, July 14, 1989 and
				2.5×10^{-4}	ng	0.25		June 25, 1991, Memos
				5×10^{-4}	(6×10^{-4})	0.50		(see Appendix A);
				7.5×10^{-4}	(1×10^{-3})	0.75		Siegel, 1990; Lappin
				1×10^{-3}	(7.5×10^{-3})	1.0		et al., 1989, Table 3-15
U	6×10^{-4}	0.0	7.4×10^{-3}	0.0			m^3/kg	Anderson et al., 1991;
				3×10^{-4}	ng	0.25		Siegel, 1990; Lappin
				6×10^{-4}		0.5		et al., 1989, Table
				1.5×10^{-3}	(1×10^{-3})	0.75		3-14, E-10, E-11, E-12
				7.4×10^{-3}	(7.5×10^{-3})	1.0		

[a] The parenthesis indicates the 1990 value; a blank indicates no change; and "ng" indicates that a value was not given in 1990.

[b] Anderson et al., 1991 is the source for the 1991 data; Siegel, 1990 and Lappin et al., 1989, are sources for the 1990 data.

Table 2.6-11. Cumulative Density Function for Partition Coefficients for Culebra Dolomite Member within Fracture Dominated by Culebra Brine (estimated by Siegel, 1991, 1990)

Element	Median	Range		Partition Coefficient[a] 1991	(1990)	Probability	Units	Source[b]
Am	2.3	0.0	4.1	0.0			m^3/kg	Anderson et al., 1991;
				5×10^{-1}	(2×10^{-1})	0.25		Siegel, 1990; Lappin
				2.3	(3×10^{-1})	0.5		et al., 1989, Table
				3	(5×10^{-1})	0.75		3-14, E-10, E-11, E-12
				4.1		1.0		
Cm	2.7	0.0	1.6×10^2	0.0			m^3/kg	Anderson et al., 1991;
				1.35	(2×10^{-1})	0.25		Siegel, 1990; Lappin
				2.7	(5×10^{-1})	0.5		et al., 1989, Table
				1.9×10^1	(2.7)	0.75		3-14, E-10, E-11, E-12
				1.6×10^2		1.0		
Np	5×10^{-2}	0.0	1.25	0.0			m^3/kg	Anderson et al., 1991;
				2×10^{-2}	(1×10^{-3})	0.25		Siegel, 1990; Lappin
				5×10^{-2}	(1×10^{-2})	0.5		et al., 1989, Table
				6.5×10^{-1}	(2×10^{-2})	0.75		3-14, E-10, E-11, E-12
				1.25	(5×10^{-2})	1.0		
Pu=Th	3×10^{-1}	0.0	4×10^1	0.0			m^3/kg	Anderson et al., 1991;
				1.5×10^{-1}	(1×10^{-1})	0.25		Siegel, 1990; Lappin
				3×10^{-1}		0.5		et al., 1989, Table
				2.3		0.75		3-14, E-10, E-11, E-12
				4×10^1		1 x 10		
Ra=Pb	5×10^{-2}	0.0	1×10^{-1}	0.0			m^3/kg	Seigel, July 14, 1989,
				2.5×10^{-2}	(1×10^{-3})	0.25		and June 25, 1991,
				5×10^{-2}	(1×10^{-2})	0.50		Memos (see Appendix
				7.5×10^{-2}	(2×10^{-2})	0.75		A); Siegel, 1990; Lappin
				1×10^{-1}	(5×10^{-2})	1.0		et al., 1989, Table 3-15
U	5×10^{-2}	0.0	1.25	0.0			m^3/kg	Anderson et al., 1991;
				2×10^{-2}	(1×10^{-3})	0.25		Siegel, 1990; Lappin
				5×10^{-2}	(1×10^{-2})	0.5		et al., 1989, Table
				6.5×10^{-1}	(2×10^{-2})	0.75		3-14, E-10, E-11, E-12
				1.25	(5×10^{-2})	1.0		

a The parenthesis indicates the 1990 value; a blank indicates no change; and "ng" indicates that a value was not given in 1990.

b Anderson et al., 1991 is the source for the 1991 data; Siegel, 1990 and Lappin et al., 1989, are sources for the 1990 data.

General Rationale for Values Recommended by Siegel (1990)

The general rationale for selecting the K_d value in each percentile of the cdf follows (Tables 2.6-10 and 2.6-11). Separate K_d distributions are given for the dolomite matrix and the clays lining the fractures in the Culebra Dolomite Member. In general, the recommended K_d values were reduced by several orders of magnitude from experimental K_d data. Many of the K_ds reported for the actinides are in the range of 10,000 to 100,000 mL/g (Lappin et al., 1989, Table 3-14). The following summarizes the discussion presented in Lappin et al. (1989).

The uncertainties in the composition of water in the Culebra Dolomite that will be produced by mixing fluids from the repository and aquifer require that large ranges of pH, Eh, organic content, and carbonate content of the groundwaters be considered in choosing K_d values. These possible variations in solution chemistry could result in order-of-magnitude changes of the K_ds from the values obtained in the experimental studies. The K_d values chosen for each element are explained further below.

Culebra brine is assumed to dominate the groundwater chemistry. The Culebra brine is represented by the average composition of a brine sample from well H-2b and H-2c.

Plutonium, Americium, and Curium. K_d values for plutonium are decreased from the values in Paine (1977), Dosch (1979), and Tien et al. (1983), because of the potential effect of carbonate complexation and competition for sorption sites by competing cations. K_d values for americium are decreased from cited values because of the potential effects of organic complexation and competition. K_d values for curium were decreased from the values listed in Tien et al. (1983) based on the assumption of behavior similar to americium and europium.

Uranium and Neptunium. In general, low K_ds for uranium and thorium have been measured in waters relevant to the WIPP repository. Low values (K_d = 1 or 10) have been assumed here to account for the possible effects of complexation and competition.

Thorium. There are very few data for thorium under conditions relevant to the WIPP. Thorium K_d values were estimated from data for plutonium, a reasonable homolog element for thorium (Krauskopf, 1986).

Radium and Lead. Siegel assumed that sorption of lead and radium will be controlled by the amount of clay in the matrix (1%) and fracture-filling clay (100%). (Note the fractures are assumed to be 50% filled by clays in the calculation of the retardation factor.) The matrix K_ds are obtained from the clay K_ds by multiplying by a utilization factor of 0.01 as discussed in Lappin et al. (1989). The maximum values are based on Tien et al. (1983) as cited in Lappin et al., (1989, Table 3-15).

Available data suggest that radium will sorb onto clays that are similar to those identified within the matrix and lining fractures in the Culebra Dolomite. The same data indicate that the degree of sorption is dependent upon the solution composition. Based on this information, values of 100 and 5 ml/g were chosen to represent the sorption of radium and lead onto clays in the Culebra. These K_d values correspond to sorption in dilute to moderately saline Culebra groundwaters (Case 1) and solutions with high contents of salt and organic ligands (Case 2), respectively. Retardation factors for the bulk matrix were calculated using the K_d values and a utilization factor of 0.01 to account for the occurrence of the clay as a trace constituent in the dolomite matrix.

General Rationale for Constructing Cumulative Distributions

The general rationale for selecting the K_d value in each percentile of the cumulative distribution follows (Tables 2.6-9 and 2.6-10).

Dolomite Matrix. A description of distributions for dolomite matrix is given below.

100th percentile: The highest K_d value for each radionuclide for the Culebra brine was used for the 100th percentile. If data for this brine were not available, the highest minimum value of the ranges from experiments carried out in WIPP Solutions A, B, and C (see Table 3-16 in Lappin et al., 1989) was used. The use of the minimum values introduces a degree of conservatism in the distributions. Data from experiments that include organic ligands were not considered.

75th percentile: The K_d values for the 75th percentile represent a compromise between the empirical data that show that sorption will occur under WIPP-specific conditions and theoretical calculations that suggest that many factors can decrease the extent of sorption significantly under other conditions that are possible in the Culebra. The values are identical to those used in Case I of Lappin et al. (1989, Table E-10).

50th percentile: The lowest reported K_d value for Culebra brine was used for the 50th percentile. If no data for Culebra brine were available, the lowest of the values reported for organic-free WIPP Solutions A, B, and C was used.

25th percentile: The 25th percentile represents conditions under which the solution chemistry is dominated by the influx of inorganic salts from the Salado and Castile Formations and includes the additional effects of organic ligands. The K_d values are identical to those of Case IIB of Lappin et al. (1989, Table E-10).

0th percentile: The use of a K_d value of zero increases the conservatism of the distribution because there is evidence some sorption will occur (Lappin et al., 1989, Table 3-14).

Clay in Fractures. A description of distributions for clay in fractures is given below. For the 1990 calculations, the fracture K_d values used were 3 orders of magnitude lower than the estimates provided.

75th and 50th percentiles: The values in Table E-11 in Lappin et al. (1989) and the lowest value for Culebra brine were compared; the larger of the two values was used for the 75th percentile. The smaller value was used for the 50th percentile. If no data for Culebra brine were available, the lowest value reported for WIPP Solutions A, B, and C (organic-free) was compared to the value in Table E-11, and the smaller value was used for the 50th percentile.

25th percentile: The 25th percentile represents conditions under which the solution chemistry is dominated by the influx of inorganic salts from the Salado and Castile Formations and includes the additional effects of organic ligands. The K_d values are identical to those of Case IIB of Lappin et al. (1989, Table E-11).

0th percentile: The use of a K_d value of zero increases the conservatism of the distribution because there is evidence some sorption will occur (Lappin et al., 1989, Table 3-14).

Retardation

For codes requiring retardation, the retardation for the matrix was calculated using the standard expression for retardation in a porous matrix (Freeze and Cherry, 1979, p. 404):

$$R_m = 1 + \rho_b K_d / \phi_m \qquad (2.6\text{-}1)$$

The retardation factor for the fractures was calculated from (Neretnieks and Rasmusson, 1984):

$$R_f = 1 + \rho_b K_d b_c / b \qquad (2.6\text{-}2)$$

where

- b_c = thickness of the minerals (e.g., clay) lining both sides of the fracture ($b_c/b = 0.5$, Table 2.6-1)
- b = fracture aperature
- K_d = partition coefficient (Tables 2.6-8 and 2.6-9)
- ϕ_m = matrix porosity (Table 2.6-1)
- ρ_b = bulk density of material (Table 2.6-1) = $(1 - \phi)\rho_g$

3. ENGINEERED BARRIERS AND SOURCE TERM

The engineered barriers consist of the repository design, waste form, seals, and backfill. Also discussed in this chapter are characteristics of the waste such as inventory of radionuclides and hazardous chemicals, solubility, and gas production potential.

3.1 Dimensions of Underground Facility

The WIPP repository is composed of a single 15-ha (38-acre) underground disposal level constructed in one stratigraphic interval, which dips slightly to the south. The repository level consists of an experimental region at the north end, the operations region in the center for waste-handling and repository equipment maintenance, and a disposal region at the south end. Figures 3.1-1 and 3.1-2 show the excavated and enclosed areas in the WIPP repository, and the planned dimensions of the WIPP disposal region and access drifts. The UTM coordinates shown in Figure 3.1-2 are derived from the state plane coordinates reported in Gonzales, 1989. To maintain consistency with coordinate values reported elsewhere in this volume, the UTM coordinates were computed by the Technology Application Center, University of New Mexico, Albuquerque, New Mexico 87106. Table 3.1-1 provides a summary of the excavated and enclosed areas and initial volumes of excavated regions (not considering disturbed rock zone [DRZ] or closure). At present, only the first panel has been excavated.

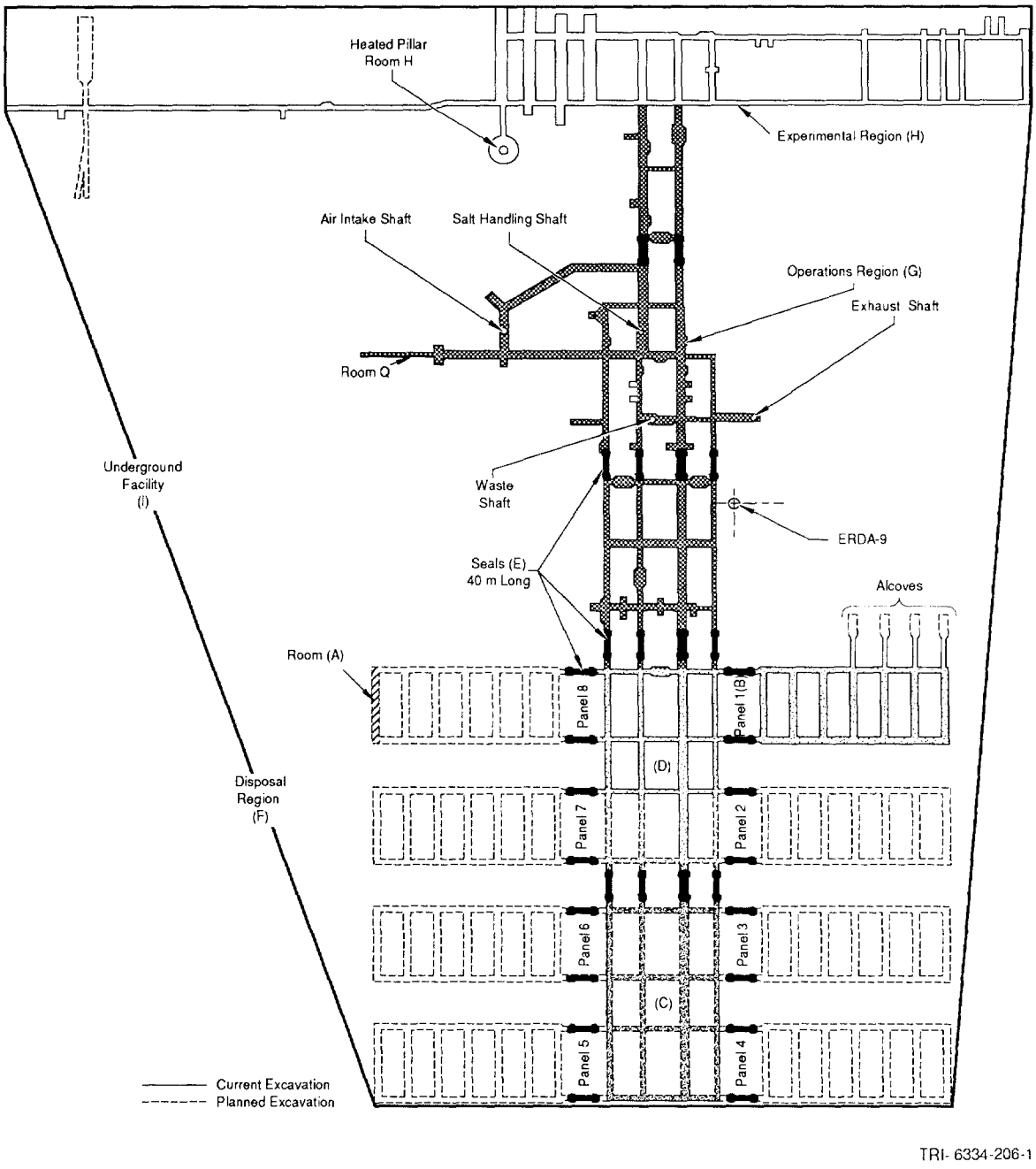

Figure 3.1-1. Excavated and Enclosed Areas in the WIPP Repository.

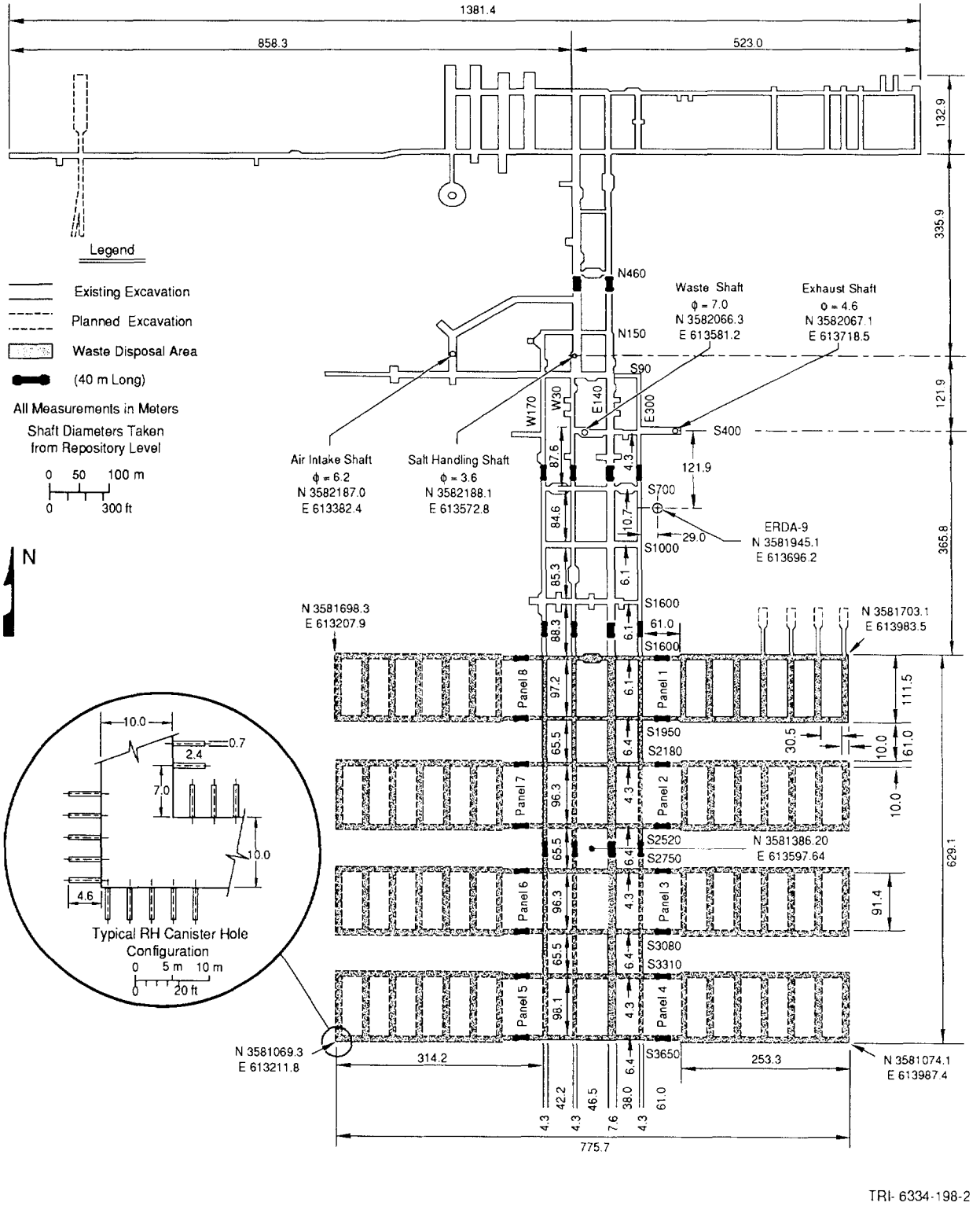

Figure 3.1-2. Planned Dimensions of WIPP Disposal Region and Access Drifts. (Dimensions originally specified in units of feet.) (after Bechtel, 1986)

Table 3.1-1. Summary of Excavated and Enclosed Areas and Initial Volumes of Excavated Regions within the WIPP Repository, Not Considering the DRZ or Closure (Rechard et al., 1990b, Table A-12)

Region*	Areas		Volume	
	Excavated (10^3 m^2)	Enclosed (10^3 m^2)	Excavated (10^3 m^3)	Enclosed (10^3 m^3)
Room (A)	0.9197	0.9197	3.644	3.644
One panel excluding seals (B)	11.64	29.42	46.10	116.59
Southern equivalent panel excluding seals (C)	8.820	49.46	32.26	180.90
Northern equivalent panel excluding seals (D)	9.564	53.68	34.98	196.34
Panel seals (20) (E)	4.133		15.119	
Total disposal region (F)	111.52	506.8	436.0	2008.0
Operations region (G)	21.84	283.6	78.07	1037.2
Four shafts (only) to base of Rustler Fm.	0.08691	0.08691	34.76	34.76
Experimental region (H)	21.61	298.1	71.90	1090
Total facility (I)	152.83	1748	583.4	6926

*Regions shown in Figure 3.1-1; detailed dimensions shown in Figure 3.1-2.

3.1.1 Disposal Region

All of the underground openings are rectangular in cross section. The disposal area drifts are generally 3.96 m (13 ft) high by 4.3 m (14 ft) wide; the disposal rooms are 4 m (13 ft) high, 10 m (33 ft) wide, and 91.4 m (300 ft) long. The width of the pillars between rooms is 30.5 m (100 ft). The total excavated volume in the disposal region is 4.334×10^5 m^3 (1.53×10^7 ft^3). The reported design disposal volume is 1.756×10^5 m^3 (6.2×10^6 ft^3) or about 36% of the excavated volume (Bechtel, 1986). The disposal volume, however, for waste changes depending on the type of containers, waste form, and volume of panel seals. Hence, the design volume is discussed in the description of the containers (Section 3.1.5).

3.1.2 Experimental Region

The experimental region (Figure 3.1-2) is located in the northern portion of the underground facility and consists of over ten rooms, which are used for in situ testing of salt creep and brine inflow (Matalucci, 1987, pp. 3,15). The sizes of the rooms vary, depending on the experiment. The excavated area of the experimental region is about 21.61 x 10^3 m^2 (23.2 x 10^4 ft^2), and its volume is about 71.90 x 10^3 m^3 (25.3 x 10^5 ft^3) (Table 3.1-1).

3.1.3 Operations Region

The operations region (Figure 3.1-2) consists of the access drifts located in the center of the underground facility. The drifts are used for transport of equipment and personnel to the experimental area and disposal region. All four shafts are connected to the operations region. The excavated area of the operations region is 21.84 x 10^3 m^2 (23.4 x 10^4 ft^2), and its volume is 78.07 x 10^3 m^3 (27.6 x 10^5 ft^3) (Table 3.1-1).

3.1.4 Shafts

The four shafts connecting the underground facility to the surface are (1) the Air Intake Shaft, 6.2 m (20 ft) in diameter; (2) the Exhaust Shaft, 4.6 m (15 ft) in diameter, (3) the Salt Handling (C&SH) Shaft, 3.6 m (12 ft) in diameter, and (4) the Waste Shaft, 7 m (23 ft) in diameter (Figure 3.1-2).

During operations, the Salt-Handling Shaft will transport personnel, equipment, and salt. The Waste Shaft will transport the waste, and the Air Intake and Exhaust Shafts will provide air flow. The Air Intake Shaft will also serve as a backup for transporting personnel and equipment.

At present, the shaft functions are the same as those described above, except that the Waste Shaft is not currently used to transport waste. It serves as a backup for transport of personnel and materials.

The Air Intake Shaft, the most recently constructed shaft (1988), provides fresh air to the underground. It also serves as a backup for transporting personnel and materials. In addition, in situ testing is being performed to investigate the disturbed rock zone (DRZ) surrounding the shaft and hydrologic properties of the Rustler Formation (Nowak et al., 1990).

The Exhaust Shaft, drilled in 1983-84, serves as the primary air exhaust for the underground facility (Bechtel, 1985).

The Salt-Handling Shaft (formerly called the Construction and Salt-Handling [C&SH] Shaft and the Exploratory Shaft [Bechtel, 1985]) was drilled in 1981. It was used during construction of the WIPP repository to remove salt and serve as the primary transport for personnel and equipment. The Salt-Handling Shaft continues to serve as the primary transport for personnel and equipment and as a secondary air supply to the underground facility.

The Waste Shaft (initially called the Ventilation Shaft) is designed to move radioactive waste between the surface waste-handling facilities and the underground facility. The Ventilation Shaft was enlarged from 2 m (6 ft) diameter to 6 m (20 ft) diameter in 1983-84, when it was renamed the Waste Shaft (Bechtel, 1985). Until waste transport begins, the Waste Shaft serves as a secondary means to transport personnel, materials, large, equipment, and diesel fuel. The Waste Shaft can continue to serve as backup for transporting personnel and materials whenever waste is not being transported.

All four shafts will be backfilled upon decommissioning of the WIPP (Nowak et al., 1990).

3.1.5 Waste Containers

Contact-handled (CH) transuranic (TRU) waste to be shipped to the WIPP is currently stored in 55-gal. drums, metal boxes, and fiberglass-reinforced plywood (FRP) boxes of various sizes (Table 3.1-2). The WIPP *Waste Acceptance Criteria* (see Section 3.4, Table 3.4-2) requires a metal overpack for all combustible boxes as a fire prevention measure, so FRP boxes and any other non-metal boxes will be overpacked and subsequently handled and disposed of in these overpacks. Furthermore, TRUPACT II, the transportation container for trucking TRU waste to the WIPP has space only for 7-pack drums and SWBs; hence, large boxes will have to be repacked unless a new transportation container is built in later years. CH-TRU waste in drums will be stacked three high in the waste-storage rooms.

The reference canister for the remotely handled (RH) TRU waste is a 0.65-m (26-in.) O.D. (outside diameter) right-circular cylinder made of 1/4-in. carbon steel plate. Caps are welded at both ends. The canister is 3 m (10 ft) in length, including the handling pintle. Inside, the waste occupies about 0.89 m^3 (30 ft^3) (U.S. DOE, 1990d).

Table 3.1-2. CH-TRU Waste Containers (U.S. DOE, 1990a, Dwg 165-F-001-W)

Container Description	Approximate Dimensions (h x w x l) m	Volume		
		Internal m^3	External m^3	Packing m^3
Approved for transportation:				
DOT 17C (metal) 55-gal steel drums	0.9 x 0.1 dia.	0.208	0.21	
7-Pack of 55-gal steel drums		1.451	1.47	2.2
Standard waste box (Dwg 165-F-001-W)	0.94 x 1.8 x 1.3	1.90	1.95	2.34
Other storage containers:				
Steel box	1.2 x 1.2 x 1.2		2.3	
Steel box	2.0 x 1.7 x 2.8		9.5	
Steel box (FRP box overpacked)	1.4 x 1.4 x 2.2		4.1	
Plywood Box	1.2 x 1.2 x 1.7		3.17	

3.1.6 Waste Placement and Backfill in Rooms

Figure 3.1-3 shows the ideal packing configuration of drums in the rooms and drifts. At the waste storage room, the waste packages (7-packs) will be removed from the transporter and stacked 3 high and 6 wide across the room. In the ideal packing configuration, a total of 6,804 drums (972 7-pack units) can be placed in one room. A 0.711-m air gap exists above the drums; also a thin plastic pallet is set between layers. For the 1991 calculations, the plastic sheet was assumed to be 0.30-m thick, consistent with the Bechtel initial reference design report (1986). Recently developed final plans (U.S. DOE, 1990d) for the plastic sheet call for 0.004-m-thick plastic on the top and bottom; hence, slightly more salt backfill will be used.

The standard waste box stacking (SWB) configuration depends upon the box size (Figure 3.1-4). Seven-packs and SWBs may be intermixed, as practical. To reach the original design capacity of 175,600 m^3 (6.2 x 10^6 ft^3), the SWBs were also assumed to be stacked three high. However, current plans call for stacking the SWBs only two high, which substantially reduces the disposal capacity of the WIPP.

The current placement technique for RH TRU waste in the WIPP is to emplace one canister horizontally every 2.4 m (8 ft) into the drift and room walls. Based on this technique, the capacity in each panel for RH-TRU canisters along drifts and rooms 10-m wide is 874 canisters or about 6,000 m^3. The intended capacity for RH-TRU waste is 7,080 m^3 (250,000 ft^3); hence, additional methods will be explored. Current PA calculations assume a capacity of 7,080 m^3.

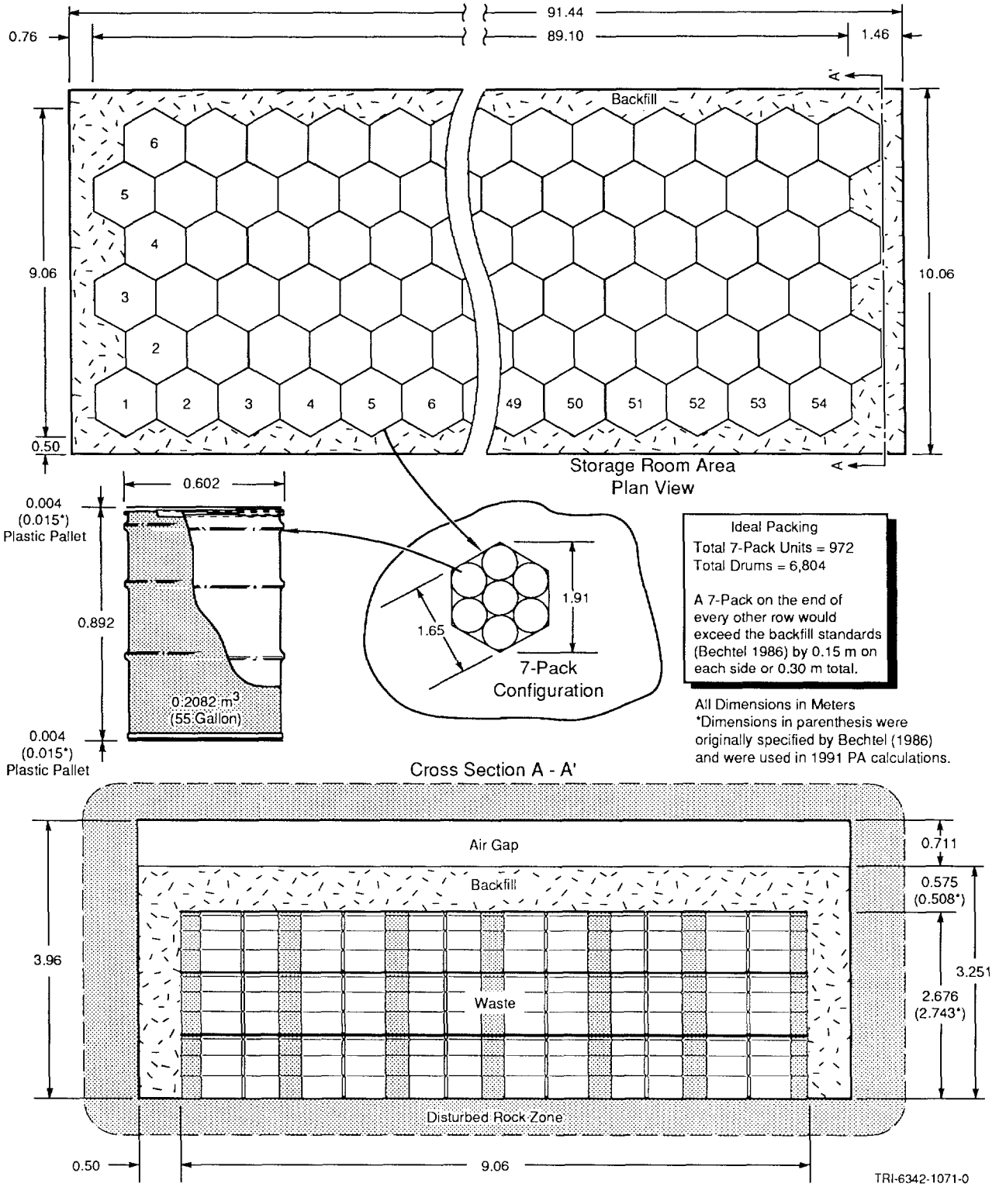

Figure 3.1-3. Ideal Packing of Drums in Rooms and 10-m-wide Drifts.

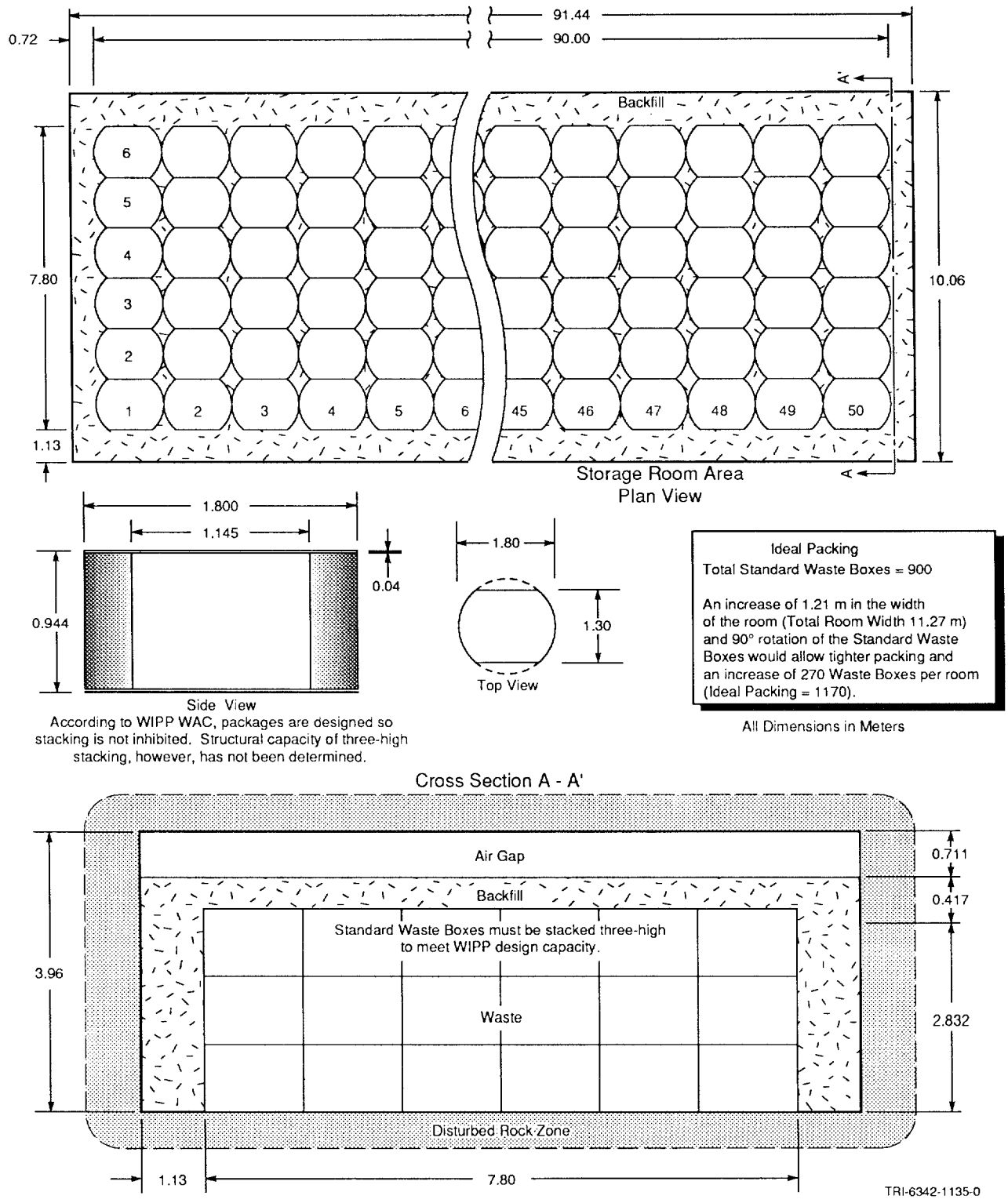

Figure 3.1-4. Ideal Packing of Standard Waste Boxes in Rooms and Drifts.

3.2 Parameters for Backfill Outside Disposal Region

This section presents parameters (such as permeability and porosity) for backfill placed in the shafts and access drifts when WIPP is decommissioned (Table 3.2-1).

Table 3.2-1. Parameter Values for Backfill Outside Disposal Region

Parameter	Median	Range		Units	Distribution Type	Source
Preconsolidated Salt (Lower shaft, drifts, panels)						
Density (ρ)						
Initial	1.71×10^3 (0.8ρSalado)			kg/m^3	Constant	Nowak et al., 1990, Figure 11
Final	2.03×10^3 (0.95ρSalado)			kg/m^3	Constant	Sjaardema and Krieg, 1987; Arguello, 1988
Height (Lower shaft)	2×10^2	1×10^2	3×10^2	m	Uniform	Nowak et al., 1990, p. 14.
Permeability (k)						
Initial	1×10^{-14}			m^2	Constant	Holcomb and Shields, 1987, Figure 4
Final	1×10^{-20}	3.3×10^{-21}	3.3×10^{-20}	m^2	Lognormal	Holcomb and Shields, 1987 Figure 4; Nowak et al., 1990, Figure 11, p. 14.
Salt Backfill in Drifts						
Density (ρ)						
Initial	1.28×10^3 (0.6ρSalado)			kg/m^3	Constant	Nowak et al., 1990, Figure 11
Final	2.03×10^3 (0.95ρSalado)			kg/m^3	Constant	Sjaardema and Krieg, 1987; Arguello, 1988
Permeability (k)						
Initial	1×10^{-11}			m^2	Constant	Holcomb and Shields, 1987, Figure 4
Final	1×10^{-20}	3.3×10^{-21}	3.3×10^{-20}	m^2	Lognormal	Holcomb and Shields, 1987, Figure 4; Nowak et al., 1990, Figure 11, p. 14.
Partition Coefficients for Salt Backfill						
Am	1×10^{-4}			m^3/kg	Constant	Lappin et al., 1989, Table D-5 ($K_{dclay}/1000$)
Np	1×10^{-5}			m^3/kg	Constant	Lappin et al., 1989, Table D-5 ($K_{dclay}/1000$)
Pb	1×10^{-6}			m^3/kg	Constant	Lappin et al., 1989, Table D-5 ($K_{dclay}/1000$)
Pu	1×10^{-4}			m^3/kg	Constant	Lappin et al., 1989, Table D-5 ($K_{dclay}/1000$)
Ra	1×10^{-6}			m^3/kg	Constant	Lappin et al., 1989, Table D-5 ($K_{dclay}/1000$)
Th	1×10^{-4}			m^3/kg	Constant	Lappin et al., 1989, Table D-5 ($K_{dclay}/1000$)
U	1×10^{-6}			m^3/kg	Constant	Lappin et al., 1989, Table D-5 ($K_{dclay}/1000$)
Concrete and Bentonite						
Permeability (k)						
Concrete	2.7×10^{-19}			m^2	Constant	Nowak et al., 1990, Figure 11, p. 13
Bentonite	1.4×10^{-19}			m^2	Constant	Nowak et al., 1990, Figure 11, p. 13

3.2.1 Description of the Reference Design for Backfill

The purpose of the reference backfill design, which Sandia has developed for backfilling the WIPP repository, is to provide a common basis for calculations performed in modeling tasks such as performance assessment and sensitivity analysis (Nowak et al., 1990; Nowak and Tyler, 1989). The reference design is a starting point for developing experiments and analysis from which a detailed design will evolve.

General Backfill Strategy

In general, the entire underground facility and shafts will be backfilled. As part of the reference design, portions of the backfill emplaced at several locations within the shafts and various drifts, which are specially prepared (i.e., preconsolidated salt with concrete plugs), are often termed "seals." However, the purpose of these prepared portions is not to act as the sole seal for the shaft or drift (in general, all the backfill fulfills this function), but instead to protect sections of the backfill from fluids (gases or liquids). Inhibiting fluids hastens backfill consolidation and thus greatly increases the probability that the salt backfill will rapidly (< 200 yr) assume properties similar to the surrounding host rock. Consequently, the term seal is misleading; however, since it has been used throughout the WIPP Project, it is also used here.

The strategy for backfilling specially prepared portions of the drift and shaft combines short- and long-term seal components; preconsolidated crushed salt is the principal long-term component in the Salado Formation salt. Clay -- a swelling clay material shown to be stable and to have low permeability to brines -- is the principal long-term component in the Rustler Formation. Concrete is the principal short-term component in both locations.

The combination of short- and long-term seals (backfill) is used so that short-term seals provide the initial sealing functions necessary until the long-term seal components become adequately reconsolidated (Nowak et al., 1990). Preconsolidated crushed-salt and clay components are expected to become fully functional for sealing within 100 yr after emplacement (Nowak and Stormont, 1987; Arguello, 1988). Then the long-term seals take over all sealing functions.

Short-term seal components consist of concretes developed specifically for the WIPP. The concrete components provide flow resistance to control the effects of possible gas generation in the waste disposal area and limit water inflow from above to protect the crushed salt from saturation with brine; they also provide physical containment for the swelling clay and consolidating crushed-salt materials (Nowak et al., 1990).

The long-term seals in the Salado consist of preconsolidated WIPP crushed salt in the shafts, drifts, and panel entries. The emplaced crushed-salt material is intended to have an initial density equal to 80% of the density of the intact WIPP host rock salt (80% relative density) (Nowak et al., 1990). Within 100 yr of emplacement, the preconsolidated salt backfill will be fully consolidated by creep closure of the host-rock salt to a state of low permeability, approximately 1 x 10^{-20} m^2 (Nowak and Stormont, 1987; Arguello, 1988; Lappin et al., 1989). This permeability value is in the expected permeability range for the host-rock salt (1 x 10^{-21} to 1 x 10^{-20}) (Nowak et al., 1988; Lappin et al., 1989). There is very little compositional difference between the reconsolidated WIPP crushed-salt material and the surrounding host rock from which it was mined. The crushed-salt seals, therefore, are expected to be mechanically and chemically stable in the WIPP environment (Nowak et al., 1990).

Seal Locations

In the reference design, multicomponent seals between 30 and 40 m (100 and 130 ft) long will be located in each of the four shafts, the entrances to the waste disposal panels, and selected access drifts (Nowak et al., 1990). (See Figures 3.1-1 and 3.1-2 for seal locations.) Seals near the Rustler Formation (upper shaft and water-bearing zone seals) serve to limit brine flow from water-bearing zones down into the crushed-salt backfill. Seals in the drifts serve to reduce fluid flow (gas and brine) from the repository area and thus limit the creation of a preferred pathway for contaminant migration. The drift entries to each filled disposal panel will be sealed during operations. The disturbed rock zone (DRZ), which occurs in the host-rock salt at the excavated openings, is expected to heal by creep closure (Nowak et al., 1990). The extent of a DRZ in the drift entries may be reduced by the use of concrete liners during operations. If necessary, however, the conceptual design for sealing the DRZ (both in drifts and shafts) and anhydrite interbeds (e.g., MB139 directly underneath the disposal area) envisions a salt-based grout (Nowak and Tyler, 1989) using grouting techniques that are currently under development (Figure 3.2-3). When all disposal panels are filled, the drift entries to the entire disposal area will be sealed. The shafts will be backfilled upon decommissioning of the WIPP (Figures 3.2-1 and 3.2-2) (Nowak et al., 1990).

Backfill in Upper Shaft, Water-Bearing Zone, and Dewey Lake Red Beds

According to current calculations, movement of radionuclides does not reach the upper shaft in 10,000 yr. Therefore, the actual properties of the backfill in the upper shaft and above have not been used in the 1991 PA calculations and properties are not given. Instead the initial placement properties of the lower shaft have been used.

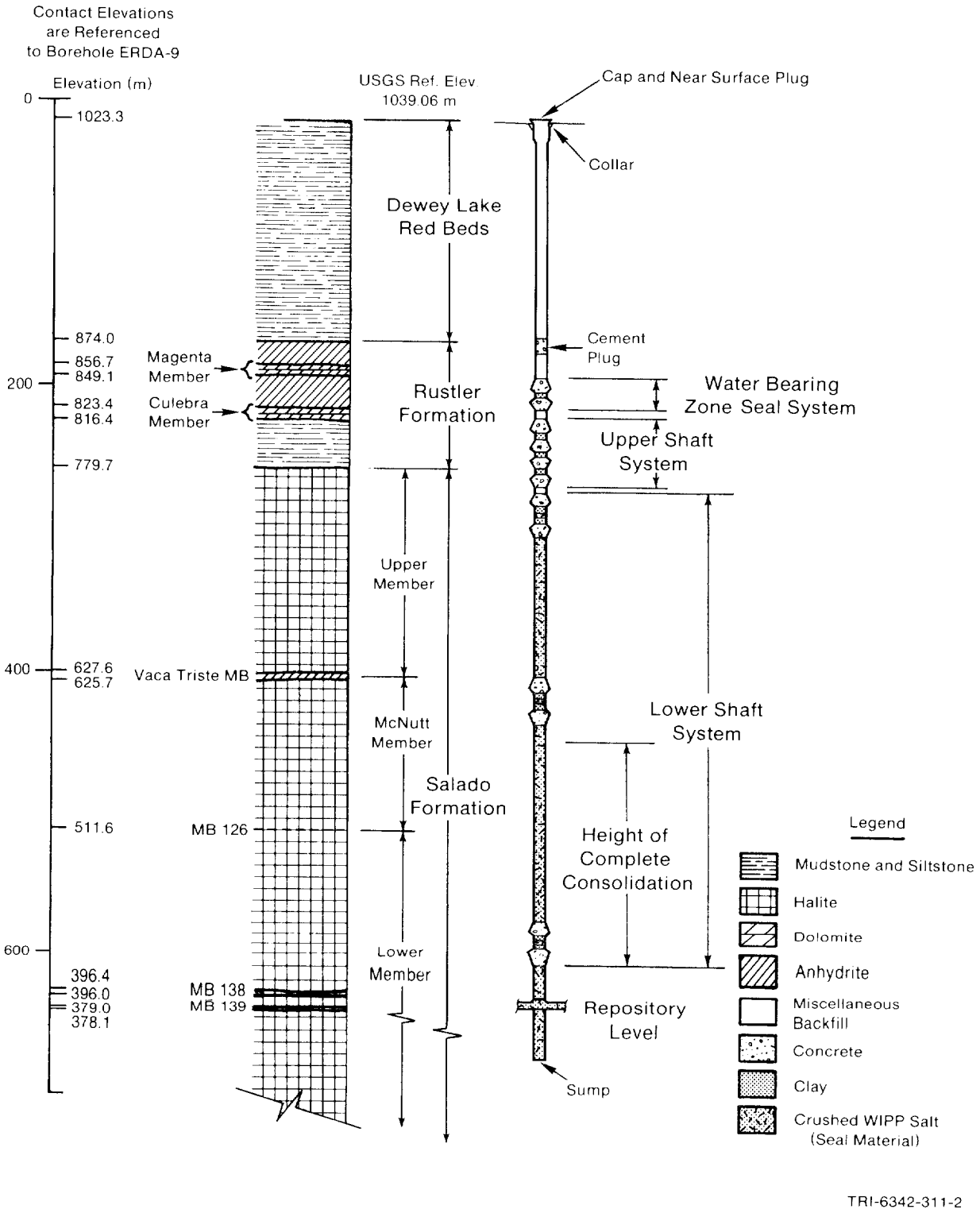

Figure 3.2-1. Diagram of Typical Backfilled Access Shaft (after Nowak et al., 1990).

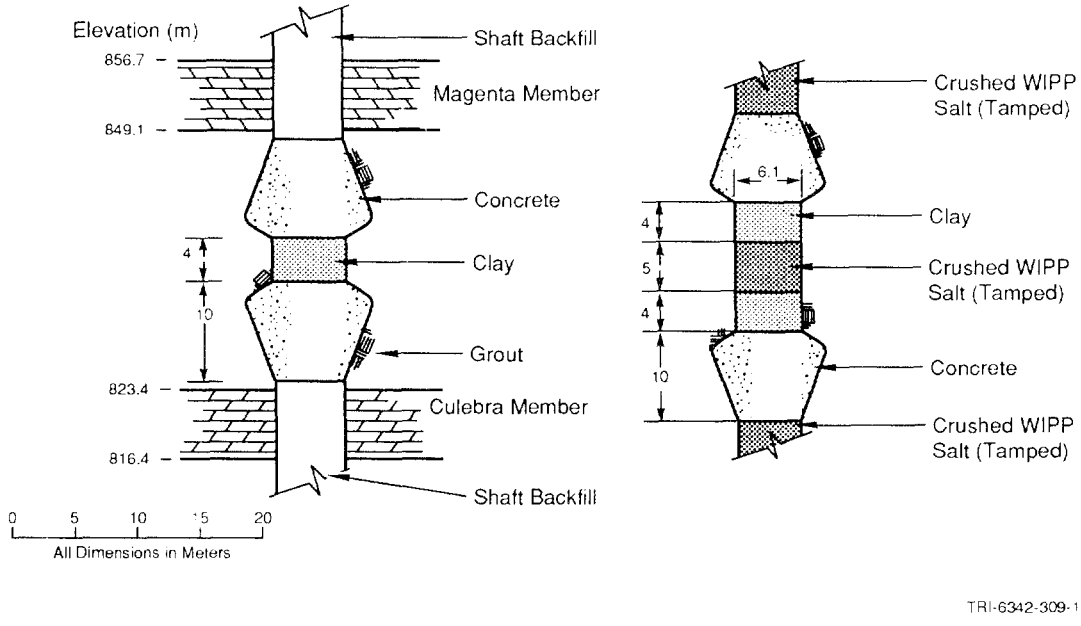

Figure 3.2-2. Diagram of Typical Concrete Plugs in Backfilled Shafts. The drawing shows concrete plugs between water-bearing units (e.g., Culebra Dolomite) (left) and for the Lower Shaft Backfill (e.g., at Vaca Triste) for Waste Shaft (right) (after Nowak et al., 1990).

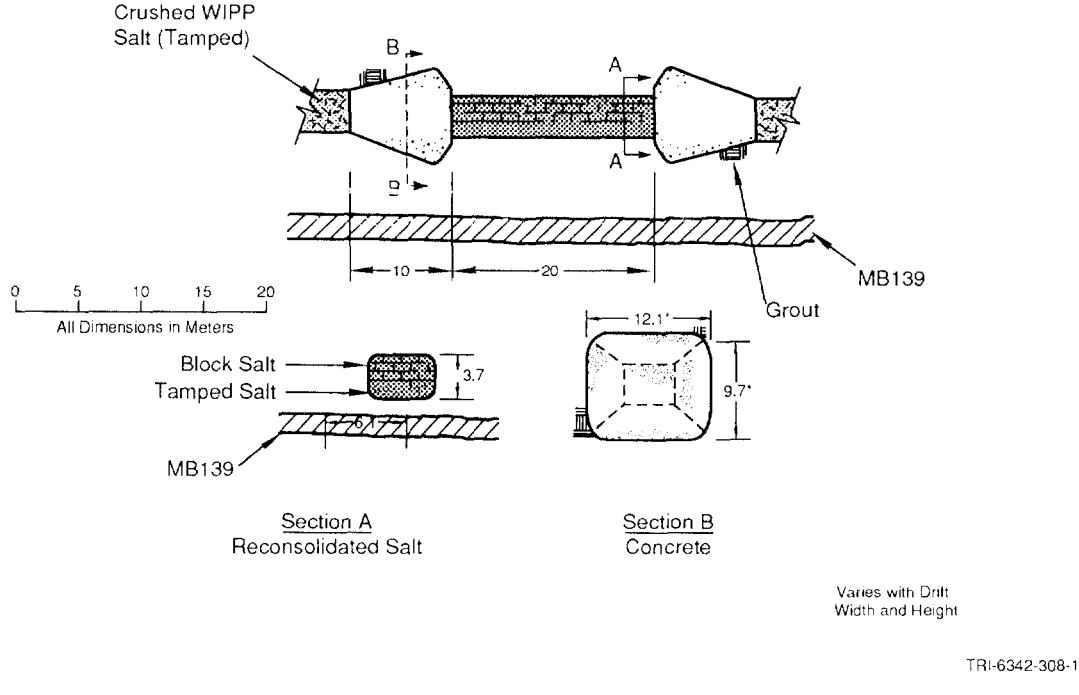

Figure 3.2-3. Diagram of Typical Concrete and Preconsolidated Salt Backfill for Drifts and Panels (after Nowak et al., 1990).

3.2.2 Preconsolidated Salt Backfill in Lower Shaft, Drifts, and Panels

The reference seal uses preconsolidated (tamped) crushed WIPP salt as the primary long-term seal material. For redundancy, concrete plugs and clay (Figure 3.2-2) are emplaced at three locations in the shaft: (1) near the bottom of the shaft, (3) at an intermediate position in the shaft just below the Vaca Triste Marker Bed, and (3) near the top of the Salado Formation.

The emplaced WIPP crushed salt is intended to have an initial density equal to 80% of the density of the intact WIPP host rock salt (80% relative density). Salt with 80% relative density will be created either by pouring and tamping crushed salt or by laying preconsolidated salt blocks. Creep closure of the lower part of the shaft will continue to consolidate this crushed salt.

Density for Preconsolidated Backfill ("Seals")

Parameter:	**Density, initial** (ρ)
Median:	1.71×10^3 ($0.8\rho_{Salado}$)
Range:	None
Units:	kg/m^3
Distribution:	Constant
Source(s):	Nowak, E. J., J. R. Tillerson, and T. M. Torres. 1990. *Initial Reference Seal System Design: Waste Isolation Pilot Plant.* SAND90-0355. Albuquerque, NM: Sandia National Laboratories. (Figure 11)

Parameter:	**Density, final** (ρ)
Median:	2.03×10^3 ($0.95\rho_{Salado}$)
Range:	None
Units:	kg/m^3
Distribution:	Constant
Source(s):	Sjaardema, G. D. and R. D. Krieg. 1987. *A Constitutive Model for the Consolidation of WIPP Crushed Salt and Its Use in Analysis of Backfilled Shaft and Drift Configurations.* SAND87-1977. Albuquerque, NM: Sandia National Laboratories. Arguello, J. G. 1988. *WIPP Panel Entryway Seal - Numerical Simulation of Seal Composite Interaction for Preliminary Seal Design Evaluation.* SAND87-2804. Albuquerque, NM: Sandia National Laboratories.

Discussion:

The initial placement density for the crushed-salt backfill is specified in the reference design as 0.8 of the intact Salado density ($0.8\rho_{Salado}$) (Nowak et al., 1990). A higher initial compaction than in the drift and panel backfill is specified to ensure faster consolidation. The estimated final density of 0.95 of the intact Salado density ($0.95\rho_{Salado}$) comes from salt creep modeling (Sjaardema and Krieg, 1987; Arguello, 1988). The initial and final porosity can be calculated directly from the densities. Assuming that the intact Salado density is 2.14×10^3 kg/m^3 with a porosity of 0.01 (see Table 2.3-1), the resulting initial and final porosities are 0.21 and 0.069, respectively.

Height of Complete Consolidation in Lower Shaft

Parameter:	**Height of complete consolidation in lower shaft**
Median:	2×10^2
Range:	1×10^2
	3×10^2
Units:	m
Distribution:	Uniform
Source(s):	Nowak, E. J., J. R. Tillerson, and T. M. Torres. 1990. *Initial Reference Seal System Design: Waste Isolation Pilot Plant.* SAND90-0355. Albuquerque, NM: Sandia National Laboratories. (p. 14)

Discussion:

The estimated range for the height of the final column of consolidated salt with 1×10^{-20} m^2 permeability is between 100 and 300 m, with an expected height of 200 m in each shaft (Nowak and Stormont, 1987; Lappin et al., 1989, p. 4-57). Figure 3.2-4 gives the distribution for height.

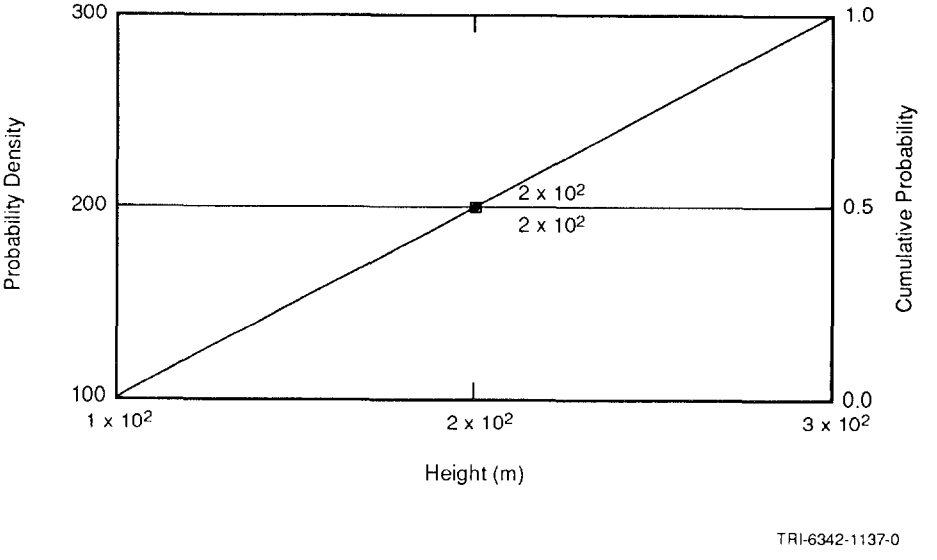

Figure 3.2-4. Estimated Distribution (pdf and cdf) for Height of Complete Consolidation in Lower Shaft.

Permeability for Preconsolidated Backfill ("Seals")

The initial and final permeability, porosity, and density of the salt component in the shaft, drift, and panel seals are as follows:

Parameter:	**Permeability, initial** (k)
Median:	1×10^{-14}
Range:	None
Units:	m^2
Distribution:	Constant
Source(s):	Holcomb, D. J. and M. Shields. 1987. *Hydrostatic Creep Consolidation of Crushed Salt with Added Water.* SAND87-1990. Albuquerque, NM: Sandia National Laboratories. (Figure 4)

Parameter:	**Permeability, final** (k)
Median:	1×10^{-20}
Range:	3.3×10^{-21} 3.3×10^{-20}
Units:	m^2
Distribution:	Lognormal
Source(s):	Holcomb, D. J. and M. Shields. 1987. *Hydrostatic Creep Consolidation of Crushed Salt with Added Water.* SAND87-1990. Albuquerque, NM: Sandia National Laboratories. (Figure 4) Nowak, E. J., J. R. Tillerson, and T. M. Torres. 1990. *Initial Reference Seal System Design: Waste Isolation Pilot Plant.* SAND90-0355. Albuquerque, NM: Sandia National Laboratories. (Figure 11, p. 14)

Discussion:

Knowing the initial and final salt density, the final permeability was estimated from laboratory experiments (Holcomb and Shields, 1987, Figure 4) (Figure 3.2-5). The resulting initial and final permeabilities were 1×10^{-14} and 1×10^{-20} m^2. Nowak et al. (1990, p. 14) places a range of 3×10^{-21} to 3×10^{-20} m^2 on the final permeability. The lower limit is equivalent to that found by extrapolating the data in Figure 3.2-5 to a relative density of 0.95. Figure 3.2-6 illustrates the assumed time-dependent permeability relationship of the preconsolidated and normal backfill.

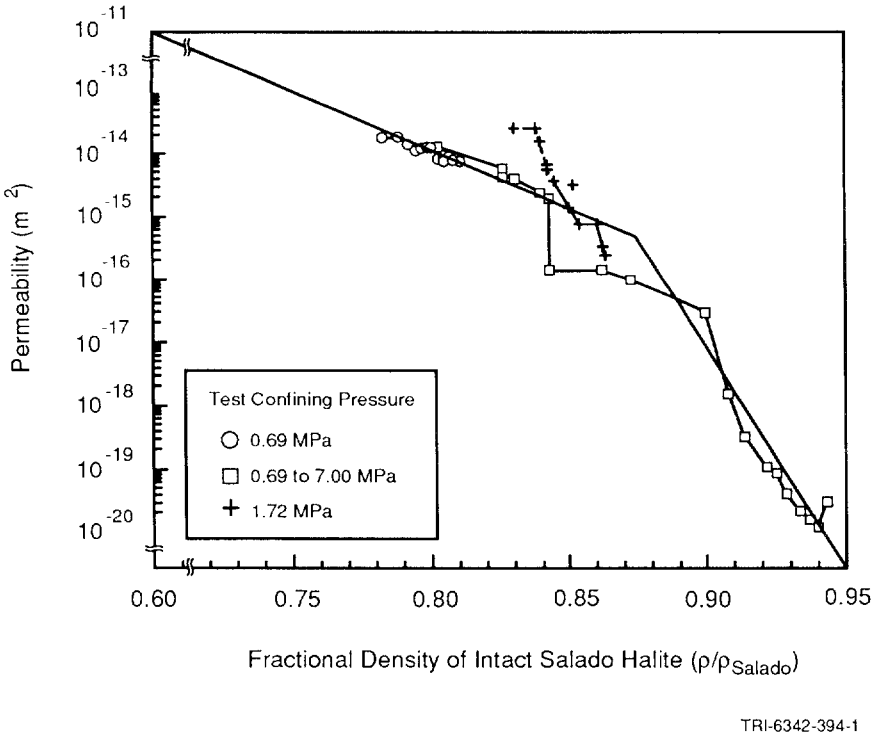

Figure 3.2-5. Permeability as a Function of Relative Halite Density (after Holcomb and Shields, 1987, Figure 4).

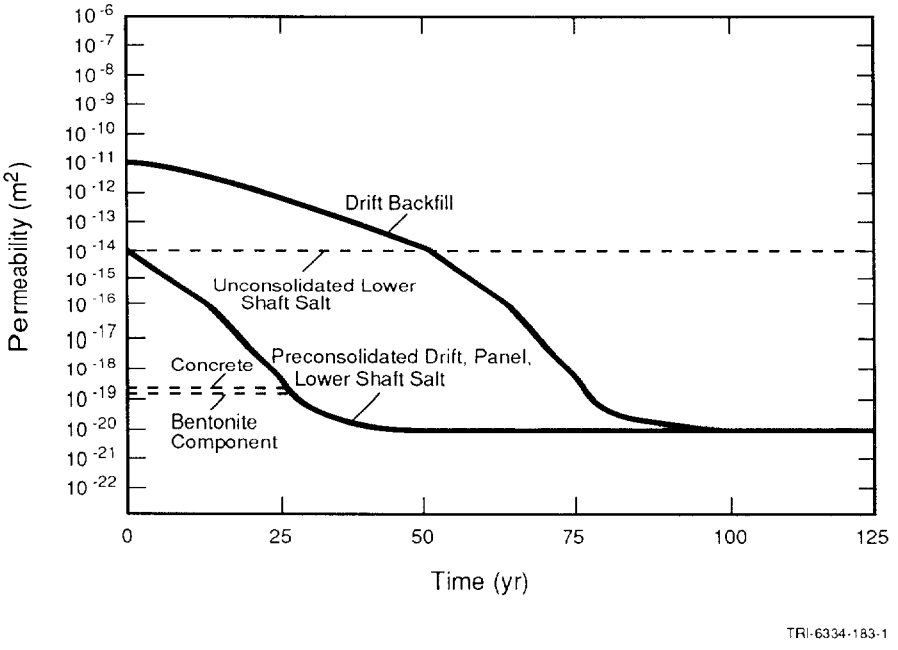

Figure 3.2-6. Time Variation of Permeability Decrease from Consolidation for Disposal Area, Drift, and Seal. Dashed line indicates seal permeability including the concrete/bentonite component (after Rechard et al., 1990b, Figure 3-30).

3.2.3 Salt Backfill in Drifts

Density for Backfill

Parameter:	**Density, initial (ρ)**
Median:	1.28×10^3 ($0.6\rho_{Salado}$)
Range:	None
Units:	kg/m^3
Distribution:	Constant
Source(s):	Nowak, E. J., J. R. Tillerson, and T. M. Torres. 1990. *Initial Reference Seal System Design: Waste Isolation Pilot Plant.* SAND90-0355. Albuquerque, NM: Sandia National Laboratories. (Figure 11)

Parameter:	**Density, final (ρ)**
Median:	2.03×10^3 ($0.95\rho_{Salado}$)
Range:	None
Units:	kg/m^3
Distribution:	Constant
Source(s):	Sjaardema, G. D. and R. D. Krieg. 1987. *A Constitutive Model for the Consolidation of WIPP Crushed Salt and Its Use in Analysis of Backfilled Shaft and Drift Configurations.* SAND87-1977. Albuquerque, NM: Sandia National Laboratories. Arguello, J.G. 1988. *WIPP Panel Entryway Seal - Numerical Simulation of Seal Composite Interaction for Preliminary Seal Design Evaluation.* SAND87-2804. Albuquerque, NM: Sandia National Laboratories.

Discussion:

The initial placement density for the crushed salt backfill is specified in the reference design as 0.6 of the intact Salado density ($0.6\rho_{Salado}$) (Nowak et al., 1990). The estimated final density of 0.95 of the intact Salado density ($0.95\rho_{Salado}$) comes from modeling (Sjaardema and Krieg, 1987; Arguello, 1988). The initial and final porosity can be calculated directly from the densities, assuming that the intact Salado density of 2.14×10^3 kg/m^3 with a porosity of 0.01 (see Table 2.3-1). The resulting initial and final porosities are 0.38 and 0.069, respectively.

Permeability

Parameter:	**Permeability, initial** (k)
Median:	1×10^{-11}
Range:	None
Units:	m^2
Distribution:	Constant
Source(s):	Holcomb, D. J. and M. Shields. 1987. *Hydrostatic Creep Consolidation of Crushed Salt with Added Water.* SAND87-1990. Albuquerque, NM: Sandia National Laboratories. (Figure 4)

Parameter:	**Permeability, final** (k)
Median:	1×10^{-20}
Range:	3.3×10^{-21} 3.3×10^{-20}
Units:	m^2
Distribution:	Lognormal
Source(s):	Holcomb, D. J. and M. Shields. 1987. *Hydrostatic Creep Consolidation of Crushed Salt with Added Water.* SAND87-1990. Albuquerque, NM: Sandia National Laboratories. (Figure 4) Nowak, E. J., J. R. Tillerson, and T. M. Torres. 1990. *Initial Reference Seal System Design: Waste Isolation Pilot Plant.* SAND90-0355. Albuquerque, NM: Sandia National Laboratories. (Figure 11, p. 14)

Discussion:

Knowing the initial and final salt density, the final permeability was estimated from laboratory experiments (Holcomb and Shields, 1987, Figure 4) (Figure 3.2-5); the initial permeability was found by extrapolating this data to the initial placement density of $0.6\rho_{Salado}$. The resulting initial and final permeabilities were 1×10^{-11} and 1×10^{-20} m^2. Nowak et al. (1990, p. 14) places a range of 3×10^{-21} to 3×10^{-20} m^2 on the final permeability. The lower limit can be found by extrapolating to a density of $0.95\rho_{Salado}$.

Figure 3.2-6 shows the assumed time variation of the decrease in permeability as the result of consolidation used in many current PA calculations. A linear permeability decrease over 50 yr was assumed until the drift backfill reached a density (and permeability) equal to the initial preconsolidated ("seal") permeability (1×10^{-14} m^2). Afterwards, the backfill permeability was assumed to decrease similar to the "seals."

3.2.4 Partition Coefficients for Salt Backfill

Table 3.2-2 provides the partition coefficients for salt backfill.

Table 3.2-2. Partition Coefficients for Salt Backfill Containing Trace (0.1%) Amounts of Clay (after Lappin et al., 1989, Table D-5)

Radionuclide	Partition Coefficient* (m^3/kg)
Am	1×10^{-4}
Np	1×10^{-5}
Pb	1×10^{-6}
Pu	1×10^{-4}
Ra	1×10^{-6}
Th	1×10^{-4}
U	1×10^{-6}

* Assumed constant

Discussion:

As mentioned for halite, none of the radionuclides is assumed to sorb onto halite ($K_d = 0$), but the crushed salt from the excavation will have small amounts of clay, which does sorb radionuclides. For those studies exploring the influence of retardation near the repository, partition coefficients similar to those for anhydrite (Section 2.4) are used, with the following exceptions: (1) americium and neptunium had larger values by a factor of 10 and (2) the values for anhydrite with clay were reduced by 1000 to account for only 0.1% clay volume in the backfill.

As a conservative assumption, the 1991 PA calculations do not consider adsorption of radionuclides in the salt backfill (similar to halite and anhydrite interbeds, Section 2.4).

3.2.5 Concrete and Bentonite

Parameter:	**Concrete permeability** (k)
Median:	2.7×10^{-19}
Range:	None
Units:	m^2
Distribution:	Constant
Source(s):	Nowak, E. J., J. R. Tillerson, and T. M. Torres. 1990. *Initial Reference Seal System Design: Waste Isolation Pilot Plant.* SAND90-0355. Albuquerque, NM: Sandia National Laboratories. (Figure 11, p. 13)

Parameter:	**Bentonite permeability** (k)
Median:	1.4×10^{-19}
Range:	None
Units:	m^2
Distribution:	Constant
Source(s):	Nowak, E. J., J. R. Tillerson, and T. M. Torres. 1990. *Initial Reference Seal System Design: Waste Isolation Pilot Plant.* SAND90-0355. Albuquerque, NM: Sandia National Laboratories. (Figure 11, p. 13)

Discussion:

Nowak et al. (1990, Figure 11) has specified maximum permissible permeabilities (as well as strength and expansion characteristics) for the concrete and bentonite (saturated in brine) components of the seals. The maximum permeabilities are 2.7×10^{-19} and 1.4×10^{-19} m^2 for the concrete and bentonite, respectively. Because all PA calculations have considered only the long-term salt components in the lower and upper shaft system and not examined the water-bearing zone shaft seal, these values have not been used to date.

3.3 Parameters for Contaminants Independent of Waste Form

The TRU waste for which the WIPP is designed is defense-program waste that has been generated at ten facilities since 1970. The waste consists of laboratory and production trash such as glassware, metal pipes, solvents, disposable laboratory clothing, cleaning rags, and solidified sludges. Current plans specify that most of the TRU waste generated since 1970 will be placed in the WIPP repository, with the remainder to be disposed of at other DOE facilities.

The ten defense facilities ("generators") that eventually will ship TRU waste to the WIPP are (1) Argonne National Laboratory-East (ANL-E), Illinois; (2) Hanford Reservation (HANF), Washington; (3) Idaho National Engineering Laboratory (INEL), Idaho; (4) Los Alamos National Laboratory (LANL), New Mexico; (5) Lawrence Livermore National Laboratory (LLNL), California; (6) Mound Laboratory, Ohio; (7) Nevada Test Site (NTS), Nevada; (8) Oak Ridge National Laboratory (ORNL), Tennessee; (9) Rocky Flats Plant (RFP), Colorado; and (10) Savannah River Site (SRS), South Carolina (U.S. DOE, 1990c).

The trash is contaminated by alpha-emitting transuranic elements, defined as having atomic numbers greater than uranium-92, half-lives greater than 20 yr, and curie contents greater than 100 nCi/g. Other contaminants include uranium and several radionuclides with half-lives less than 20 yr. Approximately 60% of the waste may be co-contaminated with waste considered hazardous under the RCRA, e.g., lead (WEC, 1989a).

Radioactive waste that emits alpha radiation, although dangerous if inhaled or ingested, is not hazardous externally. Most of the waste, therefore, can be contact handled (CH) because the external dose rate (5.6×10^{-7} Sv/s [200 mrem/h] or less) permits people to handle properly sealed drums and boxes without any special shielding.

A small portion of the TRU waste must be transported and handled in shielded casks (remotely handled [RH]), i.e., the surface dose rate exceeds 5.6×10^{-7} Sv/s (200 mrem/h). The surface dose rate of RH-TRU canisters cannot exceed 2.8×10^{-3} Sv/s (1000 rem/h); however, no more than 5% of the canisters can exceed 2.8×10^{-4} Sv/s (100 rem/h) (U.S. DOE, 1990d). The total curie content is being determined but the volume must be less than 250,000 m^3 and the curie content must be less than 5.1×10^6 Ci (1.89×10^{17} Bq) according to the agreement between DOE and the State of New Mexico (U.S. DOE/NM, 1984).

Subpart B of the Standard sets release limits in curies for isotopes of americium, carbon, cesium, iodine, neptunium, plutonium, radium, strontium, technetium, thorium, tin, and uranium, as well as for certain other radionuclides (Section 3.3.4 of this volume). Although the initial WIPP inventory contains little or none of some of the listed nuclides, they may be produced as a result of radioactive decay and must be accounted for in the compliance evaluation; moreover, any radionuclides not listed in Subpart B must be accounted for if those radionuclides would contribute to doses used in NEPA calculations (e.g., Pb-210).

Figure 3.3-1 shows the total activity for all stored, projected, and scaled CH waste. Figure 3.3-2 gives the same information for RH waste. Table 3.3-1 provides the parameters for TRU radionuclides. Table 3.3-2 provides the parameter values for TRU waste.

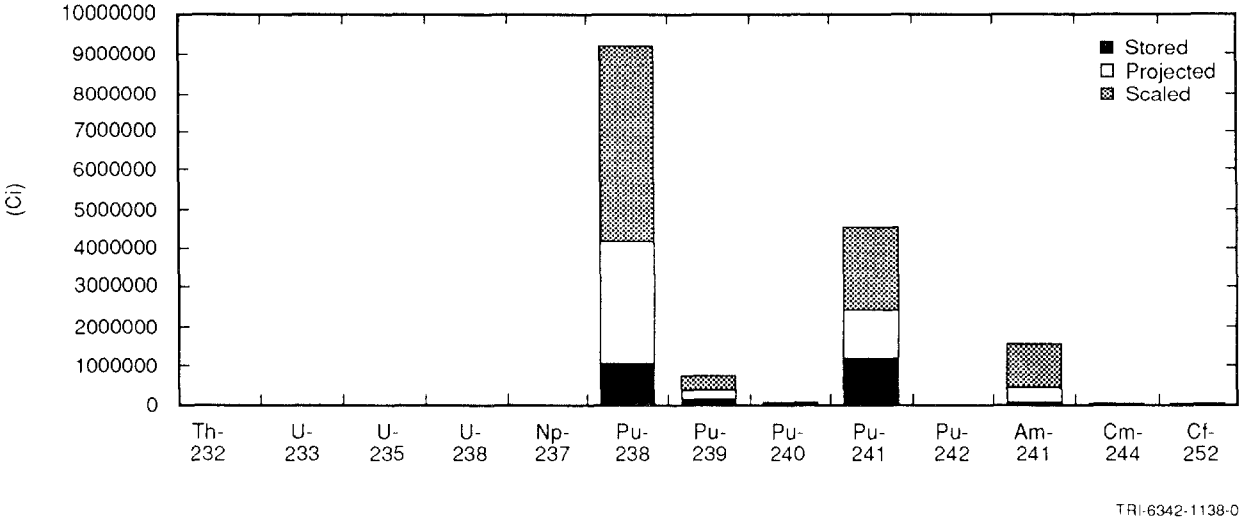

Figure 3.3-1. Total Activity for Stored, Projected, and Scaled CH Waste Activities.

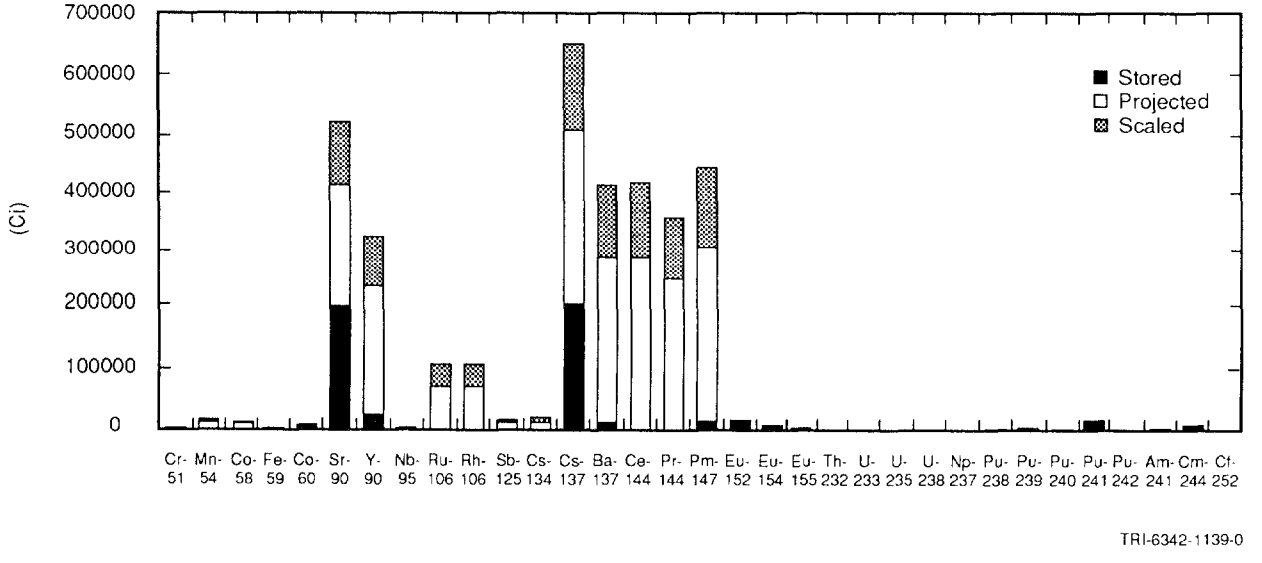

Figure 3.3-2. Total Activity for Stored, Projected, and Scaled RH Waste Activities.

Table 3.3-1. Inventory and Parameter Values for TRU Radioisotopes

Parameter	Median	Units	Source
Ac225			
Half-life	8.640×10^{5}	s	ICRP, Pub 38, 1983
Ac227			
Half-life	6.871×10^{8}	s	ICRP, Pub 38, 1983
Ac228			
Half-life	2.207×10^{4}	s	ICRP, Pub 38, 1983
Am241			
Activity conversion	3.43×10^{3}	Ci/kg	1.1281×10^{16}/(half-life(s)xAt.Wt.)
Half-life	1.364×10^{10}	s	ICRP, Pub 38, 1983
Inventory, Anticipated (1990)			
CH	6.65×10^{6}	Ci	See text.
RH	1.29×10^{3}	Ci	IDB, 1990; Peterson, 1990
Inventory, Design (1990)			
CH	1.65×10^{6}	Ci	See text.
RH	1.46×10^{3}	Ci	IDB, 1990; Peterson, 1990
Am243			
Half-life	5.822×10^{11}	s	ICRP, Pub 38, 1983
At217			
Half-life	3.230×10^{-2}	s	ICRP, Pub 38, 1983
Bi210			
Half-life	4.330×10^{5}	s	ICRP, Pub 38, 1983
Bi211			
Half-life	1.284×10^{2}	s	ICRP, Pub 38, 1983
Bi212			
Half-life	3.633×10^{3}	s	ICRP, Pub 38, 1983
Bi213			
Half-life	2.739×10^{3}	s	ICRP, Pub 38, 1983
Bi214			
Half-life	1.194×10^{3}	s	ICRP, Pub 38, 1983

Table 3.3-1. Inventory and Parameter Values for TRU Radioisotopes (Continued)

Parameter	Median	Units	Source
Cf252			
Activity conversion	5.38×10^{5}	Ci/kg	1.1281×10^{16}/(half-life(s)xAt.Wt.)
Half-life	8.325×10^{7}	s	ICRP, Pub 38, 1983
Inventory, Anticipated (1990)			
CH	1.27×10^{4}	Ci	See text.
RH	2.39×10^{3}	Ci	IDB, 1990; Peterson, 1990
Inventory, Design (1990)			
CH	1.84×10^{4}	Ci	See text.
RH	1.25×10^{2}	Ci	IDB, 1990; Peterson, 1990
Cm244			
Activity conversion	8.09×10^{4}	Ci/kg	1.1281×10^{16}/(half-life(s)xAt.Wt.)
Half-life	5.715×10^{8}	s	ICRP, Pub 38, 1983
Inventory, Anticipated (1990)			
CH	1.23×10^{4}	Ci	See text.
RH	8.75×10^{3}	Ci	IDB, 1990; Peterson, 1990
Inventory, Design (1990)			
CH	1.78×10^{4}	Ci	See text.
RH	4.63×10^{3}	Ci	IDB, 1990; Peterson, 1990
Cs137			
Activity conversion	8.70×10^{4}	Ci/kg	1.1281×10^{16}/(half-life(s)xAt.Wt.)
Half-life	9.467×10^{8}	s	ICRP, Pub 38, 1983
Inventory, Anticipated (1990)			
RH	3.33×10^{5}	Ci	IDB, 1990; Peterson, 1990
Inventory, Design (1990)			
RH	6.54×10^{5}	Ci	IDB, 1990; Peterson, 1990
Fr221			
Half-life	2.880×10^{2}	s	ICRP, Pub 38, 1983

Table 3.3-1. Inventory and Parameter Values for TRU Radioisotopes (Continued)

Parameter	Median	Units	Source
Np237			
Activity conversion	7.05×10^{-1}	Ci/kg	1.1281×10^{16}/(half-life(s)xAt.Wt.)
Half-life	6.753×10^{13}	s	ICRP, Pub 38, 1983
Inventory, Anticipated (1990)			
CH	1.47	Ci	See text.
RH	8.87×10^{-1}	Ci	IDB, 1990; Peterson, 1990
Inventory, Design (1990)			
CH	2.14	Ci	See text.
RH	1.29	Ci	IDB, 1990; Peterson, 1990
Np239			
Half-life	2.035×10^{5}	s	ICRP, Pub 38, 1983
Pa231			
Half-life	1.034×10^{12}	s	ICRP, Pub 38, 1983
Pa233			
Half-life	2.333×10^{6}	s	ICRP, Pub 38, 1983
Pb209			
Half-life	1.171×10^{4}	s	ICRP, Pub 38, 1983
Pb210			
Activity conversion	7.63×10^{4}	Ci/kg	1.1281×10^{16}/(half-life(s)xAt.Wt.)
Half-life	7.037×10^{8}	s	ICRP, Pub 38, 1983
Pb211			
Half-life	2.166×10^{3}	s	ICRP, Pub 38, 1983
Pb212			
Half-life	3.830×10^{4}	s	ICRP, Pub 38, 1983
Pb214			
Half-life	1.608×10^{3}	s	ICRP, Pub 38, 1983
Pm147			
Activity conversion	9.27×10^{5}	Ci/kg	1.1281×10^{16}/(half-life(s)xAt.Wt.)
Half-life	8.279×10^{7}	s	ICRP, Pub 38, 1983
Inventory, Anticipated (1990)			
RH	3.15×10^{5}	Ci	IDB, 1990; Peterson, 1990

Table 3.3-1. Inventory and Parameter Values for TRU Radioisotopes (Continued)

Parameter	Median	Units	Source
Inventory, Design (1990)			
RH	4.49×10^{5}	Ci	IDB, 1990; Peterson, 1990
Po210			
Half-life	1.196×10^{7}	s	ICRP, Pub 38, 1983
Po212			
Half-life	3.050×10^{-7}	s	ICRP, Pub 38, 1983
Po213			
Half-life	4.200×10^{-6}	s	ICRP, Pub 38, 1983
Po214			
Half-life	1.643×10^{-4}	s	ICRP, Pub 38, 1983
Po215			
Half-life	1.780×10^{-3}	s	ICRP, Pub 38, 1983
Po216			
Half-life	1.500×10^{-1}	s	ICRP, Pub 38, 1983
Po218			
Half-life	1.830×10^{2}	s	ICRP, Pub 38, 1983
Pu238			
Activity conversion	1.71×10^{4}	Ci/kg	1.1281×10^{16}/(half-life(s)xAt.Wt.)
Half-life	2.769×10^{9}	s	ICRP, Pub 38, 1983
Inventory, Anticipated (1990)			
CH	4.26×10^{6}	Ci	See text.
RH	5.14×10^{2}	Ci	IDB, 1990; Peterson, 1990
Inventory, Design (1990)			
CH	9.26×10^{6}	Ci	See text.
RH	1.33×10^{3}	Ci	IDB, 1990; Peterson, 1990
Pu239			
Activity conversion	6.22×10^{1}	Ci/kg	1.1281×10^{16}/(half-life(s)xAt.Wt.)
Half-life	7.594×10^{11}	s	ICRP, Pub 38, 1983

Table 3.3-1. Inventory and Parameter Values for TRU Radioisotopes (Continued)

Parameter	Median	Units	Source
Inventory, Anticipated (1990)			
CH	4.37×10^{5}	Ci	See text.
RH	1.45×10^{3}	Ci	IDB, 1990; Peterson, 1990
Inventory, Design (1990)			
CH	8.45×10^{5}	Ci	See text.
RH	1.31×10^{3}	Ci	IDB, 1990; Peterson, 1990
Pu240			
Activity conversion	2.28×10^{2}	Ci/kg	1.1281×10^{16}(half-life(s)xAt.Wt.)
Half-life	2.063×10^{11}	s	ICRP, Pub 38, 1983
Inventory, Anticipated (1990)			
CH	5.91×10^{4}	Ci	See text.
RH	2.89×10^{2}	Ci	IDB, 1990; Peterson, 1990
Inventory, Design (1990)			
CH	1.07×10^{5}	Ci	See text.
RH	2.98×10^{2}	Ci	IDB, 1990; Peterson, 1990
Pu241			
Activity conversion	1.03×10^{5}	Ci/kg	1.1281×10^{16}/half-life(s)xAt.Wt.)
Half-life	4.544×10^{8}	s	ICRP, Pub 38, 1983
Inventory, Anticipated (1990)			
CH	2.54×10^{6}	Ci	See text.
RH	1.32×10^{4}	Ci	IDB, 1990; Peterson, 1990
Inventory, Design (1990)			
CH	4.60×10^{6}	Ci	See text.
RH	1.35×10^{4}	Ci	IDB, 1990; Peterson, 1990
Pu242			
Activity conversion	3.93	Ci/kg	1.1281×10^{16}/(half-life(s)xAt.Wt.)
Half-life	1.187×10^{13}	s	ICRP, Pub 38, 1983
Inventory, Anticipated (1990)			
CH	1.84	Ci	See text.
RH	3.31×10^{-3}	Ci	IDB, 1990; Peterson, 1990
Inventory, Design (1990)			
CH	2.16	Ci	See text.
RH	4.07×10^{-3}	Ci	IDB, 1990; Peterson, 1990

Table 3.3-1. Inventory and Parameter Values for TRU Radioisotopes (Continued)

Parameter	Median	Units	Source
Ra223			
Half-life	9.879×10^{5}	s	ICRP, Pub 38, 1983
Ra224			
Half-life	3.162×10^{5}	s	ICRP, Pub 38, 1983
Ra225			
Half-life	1.279×10^{6}	s	ICRP, Pub 38, 1983
Ra226			
Activity conversion	9.89×10^{2}	Ci/kg	1.1281×10^{16}/(half-life(s)xAt.Wt.)
Half-life	5.049×10^{10}	s	ICRP, Pub 38, 1983
Ra228			
Half-life	1.815×10^{8}	s	ICRP, Pub 38, 1983
Rn219			
Half-life	3.960	s	ICRP, Pub 38, 1983
Rn220			
Half-life	5.560×10^{1}	s	ICRP, Pub 38, 1983
Rn222			
Half-life	3.304×10^{5}	s	ICRP, Pub 38, 1983
Sr90			
Activity conversion	1.36×10^{5}	Ci/kg	1.1281×10^{16}/(half-life(s)xAt.Wt.)
Half-life	9.189×10^{8}	s	ICRP, Pub 38, 1983
Inventory, Anticipated (1990)			
RH	2.80×10^{5}	Ci	IDB, 1990; Peterson, 1990
Inventory, Design (1990)			
RH	5.21×10^{5}	Ci	IDB, 1990; Peterson, 1990
Th227			
Half-life	1.617×10^{6}	s	ICRP, Pub 38, 1983
Th228			
Half-life	6.037×10^{7}	s	ICRP, Pub 38, 1983

Table 3.3-1. Inventory and Parameter Values for TRU Radioisotopes (Continued)

Parameter	Median	Units	Source
Th229			
Activity conversion	2.13×10^{2}	Ci/kg	1.1281×10^{16}/(half-life(s)xAt.Wt.)
Half-life	2.316×10^{11}	s	ICRP, Pub 38, 1983
Th230			
Activity conversion	2.02×10^{1}	Ci/kg	1.1281×10^{16}/(half-life(s)xAt.Wt.)
Half-life	2.430×10^{12}	s	ICRP, Pub 38, 1983
Th231			
Half-life	9.187×10^{4}	s	ICRP, Pub 38, 1983
Th232			
Activity conversion	1.10×10^{-4}	Ci/kg	1.1281×10^{16}/(half-life(s)xAt.Wt.)
Half-life	4.434×10^{17}	s	ICRP, Pub 38, 1983
Inventory, Anticipated (1990)			
CH	0.0	Ci	See text.
RH	0.0	Ci	IDB, 1990; Peterson, 1990
Inventory, Design (1990)			
CH	0.0	Ci	See text.
RH	0.0	Ci	IDB, 1990; Peterson, 1990
Th234			
Half-life	2.082×10^{6}	s	ICRP, Pub 38, 1983
Tl207			
Half-life	2.862×10^{2}	s	ICRP, Pub 38, 1983
U233			
Activity conversion	9.68	Ci/kg	1.1281×10^{16}/(half-life(s)xAt.Wt.)
Half-life	5.002×10^{12}	s	ICRP, Pub 38, 1983
Inventory, Anticipated (1990)			
CH	7.18×10^{1}	Ci	See text.
RH	2.86×10^{1}	Ci	IDB, 1990; Peterson, 1990
Inventory, Design (1990)			
CH	1.04×10^{2}	Ci	See text.
RH	2.02×10^{2}	Ci	IDB, 1990; Peterson, 1990
U234			
Activity conversion	6.25	Ci/kg	1.1281×10^{16}/(half-life(s)xAt.Wt.)
Half-life	7.716×10^{12}	s	ICRP, Pub 38, 1983

Table 3.3-1. Inventory and Parameter Values for TRU Radioisotopes (Concluded)

Parameter	Median	Units	Source
U235			
Activity conversion	2.16×10^{-3}	Ci/kg	1.1281×10^{16}/(half-life(s)xAt.Wt.)
Half-life	2.221×10^{16}	s	ICRP, Pub 38, 1983
Inventory, Anticipated (1990)			
CH	5.54×10^{-2}	Ci	See text.
RH	1.23×10^{-2}	Ci	IDB, 1990; Peterson, 1990
Inventory, Design (1990)			
CH	1.43×10^{-1}	Ci	See text.
RH	1.39×10^{-2}	Ci	IDB, 1990; Peterson, 1990
U236			
Half-life	7.389×10^{14}	s	ICRP, Pub 38, 1983
U238			
Activity conversion	3.36×10^{-4}	Ci/kg	1.1281×10^{16}/(half-life(s)xAt.Wt.)
Half-life	1.410×10^{17}	s	ICRP, Pub 38, 1983
Inventory, Anticipated (1990)			
CH	0.0	Ci	See text.
RH	7.83×10^{-2}	Ci	IDB, 1990; Peterson, 1990
Inventory, Design (1990)			
CH	0.0	Ci	See text.
RH	8.71×10^{-2}	Ci	IDB, 1990; Peterson, 1990

Table 3.3-2. Parameter Values for TRU Waste Radioelements

Parameter	Median	Range		Units	Distribution Type	Source
Gas generation						
Corrosion						
Inundated rate	6.3×10^{-9}	0	1.3×10^{-8}	$mol/m^2/s$*	Cumulative	Brush, July 8, 1991, Memo (Appendix A)
Relative humid rate	1×10^{-1}	0	5×10^{-1}	none	Cumulative	Brush, July 8, 1991, Memo (Appendix A)
Microbiological						
Inundated rate	3.2×10^{-9}	0	1.6×10^{-8}	mol/kg/s**	Cumulative	Brush, July 8, 1991, Memo (Appendix A)
Relative humid rate	1×10^{-1}	0	2×10^{-1}	none	Uniform	Brush, July 8, 1991, Memo (Appendix A)
Radiolysis	1×10^{-4}	1×10^{-7}	1×10^{-1}	mol/drum/yr	Constant	Brush, July 8, 1991, Memo (Appendix A)
Gas generation stoichiometry factor						
Corrosion	5×10^{-1}	0	1	none	Uniform	Brush and Anderson in Lappin et al., 1989, p. A-6
Microbiological	8.35×10^{-1}	0	1.67	none	Uniform	Brush and Anderson in Lappin et al., 1989, p. A-10
Am						
Diffusion coefficient***	1.76×10^{-10}	5.3×10^{-11}	3×10^{-10}	m^2/s	Uniform	Lappin et al.,1989, Table E-7
Am^{3+}						
Solubility	1×10^{-9}	5×10^{-14}	1.4	Molar	Cumulative	Trauth et al., 1991
Cm						
Diffusion coefficient	1.76×10^{-10}	5.3×10^{-11}	3×10^{-10}	m^2/s	Uniform	Lappin et al.,1989, Table E-7
Cm^{3+}						
Solubility	1×10^{-9}	5×10^{-14}	1.4	Molar	Cumulative	Trauth et al., 1991
Np						
Diffusion coefficient	1.76×10^{-10}	5.2×10^{-11}	3×10^{-10}	m^2/s	Uniform	Lappin et al.,1989, Table E-7
Np^{4+}						
Solubility	6×10^{-9}	3×10^{-16}	2×10^{-5}	Molar	Cumulative	Trauth et al., 1991
Np^{5+}						
Solubility	6×10^{-7}	3×10^{-11}	1.2×10^{-2}	Molar	Cumulative	Trauth et al., 1991
Pb						
Diffusion coefficient	4×10^{-10}	2×10^{-10}	8×10^{-10}	m^2/s	Cumulative	Lappin et al.,1989, Table E-7

* mole/m^2 surface area steel/s
** mole/kg cellulosics/s
*** Free liquid diffusion coefficient of the indicated species

Table 3.3-2. Parameter Values for TRU Waste Radioelements (Concluded)

Parameter	Median	Range		Units	Distribution Type	Source
Pb^{2+}						
Solubility						
Absence of CO^3	1.64	$1x10^{-2}$	$1x10^{1}$	Molar	Cumulative	Trauth et al., 1991
Presence of CO^3	$8x10^{-3}$	$1x10^{-9}$	$8x10^{-2}$	Molar	Cumulative	Trauth et al., 1991
Pu						
Diffusion coefficient	$1.74x10^{-10}$	$4.8x10^{-11}$	$3x10^{-10}$	m^2/s	Uniform	Lappin et al.,1989, Table E-7
Pu^{4+}						
Solubility	$6x10^{-10}$	$2.0x10^{-16}$	$4x10^{-6}$	molar	Cumulative	Trauth et al., 1991
Pu^{5+}						
Solubility	$6x10^{-10}$	$2.5x10^{-17}$	$5.5x10^{-4}$	Molar	Cumulative	Trauth et al., 1991
Ra						
Diffusion coefficient	$3.75x10^{-10}$	$1.88x10^{-10}$	$7.5x10^{-10}$	m^2/s	Cumulative	Lappin et al.,1989, Table E-7
Ra^{2+}						
Solubility						
Absence of CO^3 and SO^4	$1.1x10^{1}$	2	$1.8x10^{1}$	Molar	Cumulative	Trauth et al., 1991
Presence of CO^3	$1.6x10^{-6}$	$1.6x10^{-9}$	1	Molar	Cumulative	Trauth et al., 1991
Presence of SO^4	$1x10^{-8}$	$1x10^{-11}$	$1x10^{-6}$	Molar	Cumulative	Trauth et al., 1991
Th						
Diffusion coefficient	$1x10^{-10}$	$5x10^{-11}$	$1.5x10^{-10}$	m^2/s	Uniform	Lappin et al.,1989, Table E-7
Th^{4+}						
Solubility	$1x10^{-10}$	$5.5x10^{-16}$	$2.2x10^{-6}$	Molar	Cumulative	Trauth et al., 1991
U						
Diffusion coefficient	$2.7x10^{-10}$	$1.1x10^{-10}$	$4.3x10^{-10}$	m^2/s	Uniform	Lappin et al.,1989, Table E-7
U^{4+}						
Solubility	$1x10^{-4}$	$1x10^{-15}$	$5x10^{-2}$	Molar	Cumulative	Trauth et al., 1991
U^{6+}						
Solubility	$2x10^{-3}$	$1x10^{-7}$	1	Molar	Cumulative	Trauth et al., 1991

3.3.1 Inventory of Radionuclides in Contact-Handled Waste

The inventory (curie content) of radionuclides in the contact-handled (CH) waste was estimated from input submitted to the 1990 Integrated Date Base (IDB) (IDB, 1990). The information submitted to the IDB is separated into retrievably stored and newly generated (future generation), referred to herein as projected inventory. The anticipated total volume (stored plus projected) of CH waste submitted to the 1990 IDB was 1.06 x 10^5 m^3 (3.76 x 10^6 ft^3), which is less than the current design volume for the WIPP of about 1.8 x 10^5 m^3 (6.2 x 10^6 ft^3). To estimate the total curie content in the WIPP, if it contained a design volume of CH waste, the future-generated radionuclide inventories of the five largest future generators listed in the 1990 IDB were volume scaled to reach a design volume of waste. (Details of this volume scaling are discussed in Section 3.4.) This inventory per generator site is only a projected estimate and should not be considered a statement of what they will generate.

The weight fractions reported in the 1990 IDB were used to calculate the major radionuclides of the mixes reported. The IDB did not report the inventory of each radionuclide. Rather the inventory of each radionuclide at each site was based on the mix of waste streams reported. The Hanford submittal to the 1990 IDB indicated that the activity of some of the CH waste was currently unknown. Rather than underestimate the potential inventory, the Hanford input to the 1987 IDB was used. These inventories have not been independently checked and should be considered preliminary estimates.

The estimate of the radionuclide inventory for the retrievably stored waste at the 10 generator/storage sites is listed in Table 3.3-3. The estimated total curie content of the retrievably stored waste was 2.6 x 10^6 Ci (9.7 x 10^{16} Bq). The projected radionuclide inventory is also listed in Table 3.3-4. The estimated total curie content of the projected waste is 5.4 x 10^6 Ci (1.99 x 10^{17} Bq).

The estimated inventory of radionuclides, based on volume scaling, that could be emplaced in the WIPP if the total design volume were used is shown in Table 3.3-5; the total is about 1.65 x 10^7 Ci (6.1 x 10^{17} Bq). This inventory is different from that reported in Lappin et al. (1989, 1990). The input for this estimate was based on input to the 1990 IDB, whereas the earlier estimate was based on input to the 1987 IDB. Note that the estimate for Hanford was based on the 1987 input since the 1990 IDB input indicated that the total was unknown.

The estimated radionuclide inventory of CH waste by site and isotope is illustrated in Figure 3.3-3.

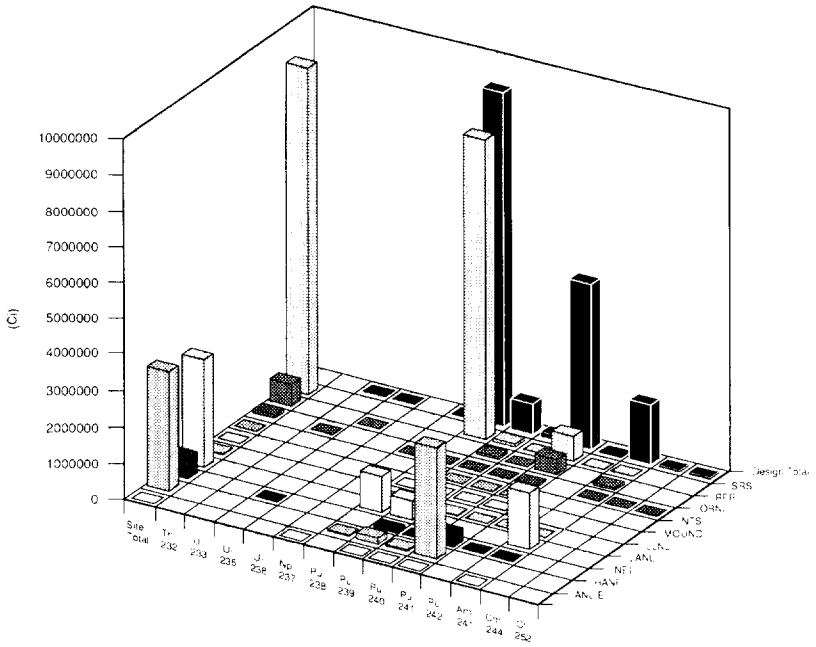

(a)

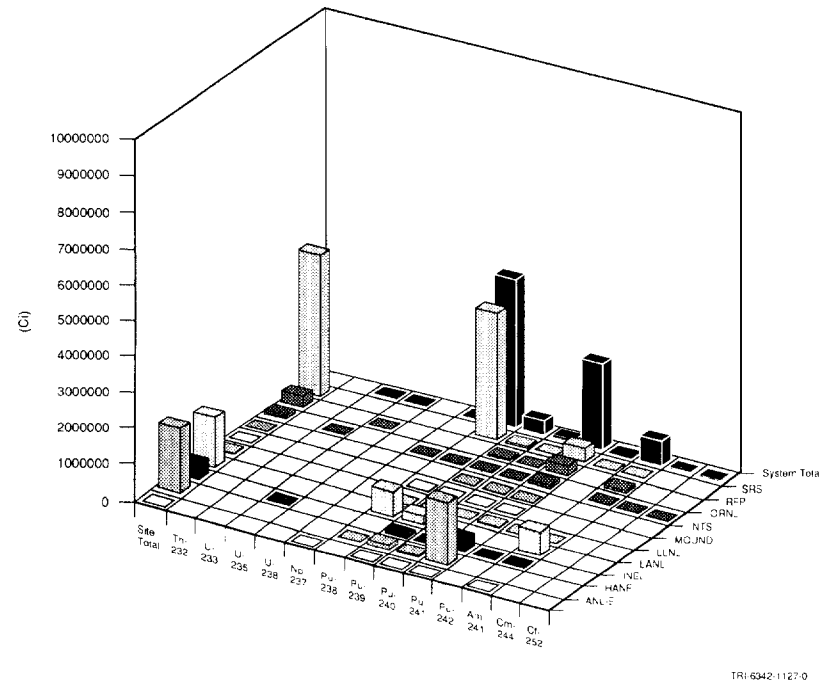

(b)

Figure 3.3-3. Estimate of Radionuclide Inventory of CH Waste by Site and Isotope for (a) Design Total, (b) Anticipated System Total, (c) Projected Total, and (d) Stored Total.

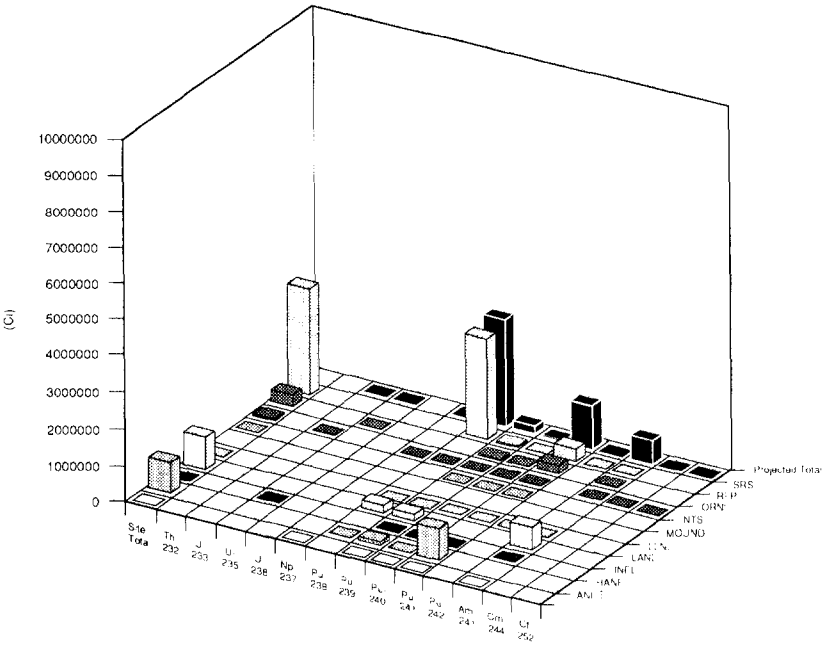

(c)

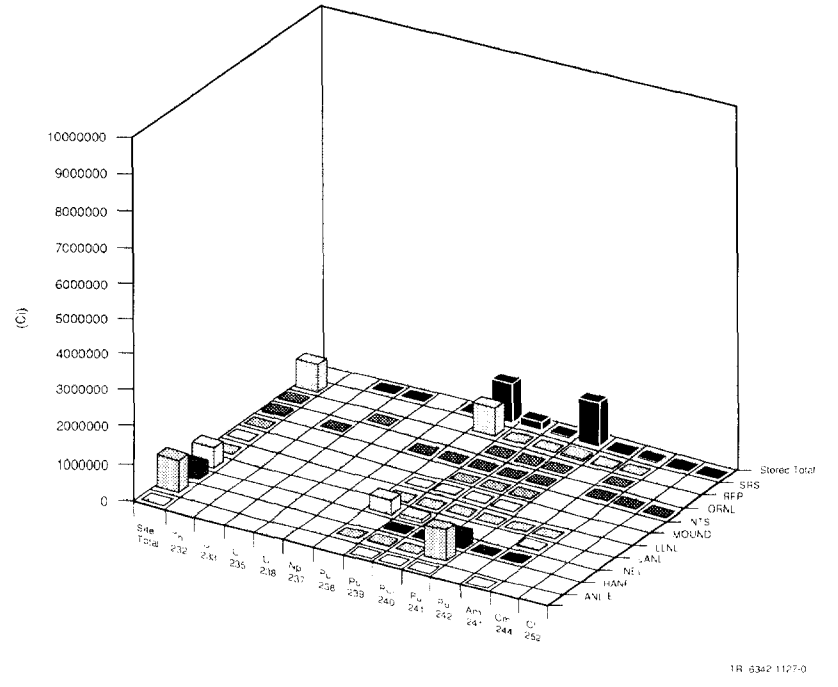

(d)

Figure 3.3-3. Estimate of Radionuclide Inventory of CH Waste by Site and Isotope for (a) Design Total, (b) Anticipated System Total, (c) Projected Total, and (d) Stored Total. (Concluded)

Table 3.3-3. Retrievably Stored[a] Design Radionuclide Inventory by Waste Generator for Contact-Handled Waste

Radionuclide	Half-Life (s)	ANL-E (Ci)	HANF[b] (Ci)	INEL (Ci)	LANL (Ci)	LLNL (Ci)	MOUND (Ci)	NTS (Ci)	ORNL (Ci)	RFP (Ci)	SRS (Ci)	Stored Total (Ci)
Th-232	4.4337×10^{17}	--	--	--	--	--	--	--	--	--	--	0.0
U-233	5.0018×10^{12}	--	--	--	--	--	--	--	4.0×10^{1}	--	--	4.0×10^{1}
U-235	2.221×10^{16}	--	--	--	--	--	--	--	--	4.69×10^{-4}	--	4.69×10^{-4}
U-238	1.41×10^{17}	--	--	--	--	--	--	--	--	--	--	0.0
Np-237	6.753×10^{13}	--	--	--	--	--	--	--	8.0×10^{-1}	--	--	8.0×10^{-1}
Pu-238	2.7688×10^{9}	--	3.819×10^{3}	--	3.558×10^{5}	9.377×10^{1}	2.312×10^{3}	--	6.86×10^{3}	--	7.460×10^{5}	1.115×10^{6}
Pu-239	7.5492×10^{11}	1.0	4.242×10^{4}	5.012×10^{4}	7.886×10^{4}	1.673×10^{3}	1.79	6.586×10^{1}	6.23×10^{2}	2.045×10^{3}	3.677×10^{3}	1.795×10^{5}
Pu-240	2.0629×10^{11}	4.3×10^{-1}	1.511×10^{4}	1.146×10^{4}	--	5.431×10^{2}	1.15	1.517×10^{1}	3.062×10^{2}	4.686×10^{2}	1.015×10^{3}	2.892×10^{4}
Pu-241	4.5422×10^{8}	1.922×10^{1}	7.687×10^{5}	3.571×10^{5}	--	1.308×10^{4}	1.04	6.31×10^{2}	3.405×10^{4}	1.119×10^{4}	5.283×10^{4}	1.238×10^{6}
Pu-242	1.1875×10^{13}		--	1.02	--	4.3×10^{-1}	--	--	--	--	1.7×10^{-1}	1.62
Am-241	1.3639×10^{10}	6.4×10^{-1}	--	2.722×10^{3}	4.022×10^{4}	1.371×10^{3}	--	--	5.045×10^{2}	2.113×10^{3}	5.687×10^{2}	4.75×10^{4}
Cm-244	5.715×10^{8}	--	--	--	--	--	--	--	6.796×10^{3}	--	--	6.796×10^{3}
Cf-252	8.3247×10^{7}	--	--	--	--	--	--	--	7.055×10^{3}	--	--	7.055×10^{3}
TOTALS		2.129×10^{1}	8.301×10^{5}	4.214×10^{5}	4.749×10^{5}	1.676×10^{4}	2.316×10^{3}	7.12×10^{2}	5.624×10^{4}	1.581×10^{4}	8.041×10^{5}	2.622×10^{6}

[a] Stored as of December 31, 1989 such that containers can be retrieved and shipped to the WIPP.

[b] Based on 1987 input since 1990 total was unknown.

Table 3.3-4. Projected[a] Radionuclide Inventory by Waste Generator for Contact-Handled Waste (Curies)

Radionuclide	ANL-E	HANF[b,c]	INEL[c]	LANL[c]	LLNL	MOUND	NTS	ORNL	RFP[c]	SRS[c]	Projected Total	(Projected + Stored) System Total 1990	(Projected + Stored) System Total 1987
Th-232	--	--	--	--	--	--	--	--	--	--	--	0.0	$2.74x10^{-1}$
U-233	--	--	--	--	--	--	--	$3.185x10^{1}$	--	--	$3.185x10^{1}$	$7.185x10^{1}$	$7.7x10^{3}$
U-235	--	--	$4.8x10^{-2}$	--	--	--	--	--	$6.924x10^{-3}$	--	$5.492x10^{-2}$	$5.539x10^{-2}$	$3.73x10^{-1}$
U-238	--	--	--	--	--	--	--	--	--	--	0.0	0.0	1.49
Np-237	$2.0x10^{-2}$	--	--	--	--	--	--	$6.5x10^{-1}$	--	--	$6.7x10^{-1}$	1.47	8.01
Pu-238	--	$4.362x10^{3}$	--	$2.231x10^{5}$	9.15	--	--	$5.529x10^{3}$	--	$2.913x10^{6}$	$3.146x10^{6}$	$4.261x10^{6}$	$3.91x10^{6}$
Pu-239	$3.212x10^{1}$	$4.742x10^{4}$	$4.415x10^{2}$	$1.554x10^{5}$	$1.876x10^{2}$	--	--	$5.053x10^{2}$	$3.016x10^{4}$	$2.288x10^{4}$	$2.571x10^{5}$	$4.366x10^{5}$	$4.24x10^{5}$
Pu-240	$1.148x10^{1}$	$1.689x10^{4}$	$1.824x10^{2}$	--	$4.574x10^{1}$	--	--	$2.468x10^{2}$	$6.912x10^{3}$	$5.897x10^{3}$	$3.02x10^{4}$	$5.912x10^{4}$	$1 x 10^{5}$
Pu-241	$6.255x10^{2}$	$8.593x10^{5}$	$6.409x10^{2}$	--	$1.302x10^{3}$	--	--	$2.744x10^{4}$	$1.65x10^{5}$	$2.509x10^{5}$	$1.306x10^{6}$	$2.54x10^{6}$	$4.1 x 10^{6}$
Pu-242	--	--	--	--	$5.0x10^{2}$	--	--	--	--	$1.7x10^{-1}$	$2.2x10^{-1}$	1.84	$1.83x10^{1}$
Am-241	$2.085x10^{1}$	--	$1.211x10^{2}$	$5.815x10^{5}$	$2.534x10^{1}$	--	--	$4.066x10^{2}$	$3.118x10^{4}$	$3.76x10^{3}$	$6.17x10^{5}$	$6.645x10^{5}$	$6.34x10^{5}$
Cm-244	--	--	--	--	--	--	--	$5.477x10^{3}$	--	--	$5.477x10^{3}$	$1.227x10^{4}$	$1.27x10^{4}$
Cf-252	--	--	--	--	--	--	--	$5.685x10^{3}$	--	--	$5.685x10^{3}$	$1.274x10^{4}$	$2.02x10^{3}$
Projected Totals	$6.9x10^{2}$	$9.28x10^{5}$	$1.386x10^{3}$	$9.6x10^{5}$	$1.57x10^{3}$	0.0	0.0	$4.532x10^{4}$	$2.333x10^{5}$	$3.196x10^{6}$	$5.367x10^{6}$	$7.99 x 10^{6}$	$9.19 x 10^{6}$
Percent of Design Total	0.0	5.63	0.01	5.82	0.01	0.0	0.0	0.27	1.41	19.38	32.54		
System Total		$1.401x10^{3}$	$3.233x10^{6}$	$4.25x10^{5}$	$2.961x10^{6}$	$1.99x10^{4}$	$7.12x10^{2}$	$2.139x10^{-3}$	$1.469x10^{5}$	$6.2x10^{5}$	$9.082x10^{6}$		

[a] Generated between 1990 and 2013

[b] Based on 1987 input since 1990 total was unknown.

[c] One of five DOE defense facilities, which produce the largest volume of waste and are used to scale the inventory.

Table 3.3-5. Design Radionuclide Inventory by Waste Generator for Contact-Handled Waste (Curies)

Radionuclide	ANL-E	HANF	INEL	LANL	LLNL	MOUND	NTS	ORNL	RFP	SRS	PA Calculations Design 1990	Waste Unit Factor
Th-232	--	--	--	--	--	--	--	--	--	--	0.0	0.0
U-233	--	--	--	--	--	--	--	1.037×10^{2}	--	--	1.037×1^{2}	--
U-235	--	--	1.243×10^{-1}	--	--	--	--	--	1.84×10^{-2}	--	1.427×10^{-1}	--
U-238	--	--	--	--	--	--	--	--	--	--	0.0	--
Np-237	4.0×10^{-2}	--	--	--	--	--	--	2.1	--	--	2.14	2.14
Pu-238	--	1.512×10^{4}	--	9.336×10^{5}	1.121×10^{2}	2.312×10^{3}	--	1.792×10^{4}	--	8.29×10^{6}	9.259×10^{6}	9.259×10^{6}
Pu-239	6.524×10^{1}	1.652×10^{5}	5.126×10^{4}	4.813×10^{5}	2.048×10^{3}	1.79	2.003×10^{2}	1.634×10^{3}	8.016×10^{4}	6.293×10^{4}	8.448×10^{5}	8.448×10^{5}
Pu-240	2.339×10^{1}	5.885×10^{4}	1.193×10^{4}	--	6.346×10^{2}	1.15	4.551×10^{1}	7.998×10^{2}	1.837×10^{4}	1.629×10^{4}	1.069×10^{5}	1.069×10^{5}
Pu-241	1.27×10^{3}	2.994×10^{6}	3.588×10^{5}	--	1.568×10^{4}	1.04	1.893×10^{3}	8.893×10^{4}	4.386×10^{5}	7.026×10^{5}	4.602×10^{6}	--
Pu-242	--	--	1.02	--	5.3×10^{-1}	--	--	--	--	6.103×10^{-1}	2.16	2.16
Am-241	4.234×10^{1}	--	3.036×10^{3}	1.546×10^{6}	1.422×10^{3}	--	--	1.318×10^{3}	8.285×10^{4}	1.031×10^{4}	1.645×10^{6}	1.645×10^{6}
Cm-244	--	--	--	--	--	--	--	1.775×10^{4}	--	--	1.775×10^{4}	1.775×10^{4}
Cf-252	--	--	--	--	--	--	--	1.843×10^{4}	--	--	1.843×10^{4}	--
TOTALS	1.401×10^{3}	3.233×10^{6}	4.25×10^{5}	2.961×10^{6}	1.99×10^{4}	2.316×10^{3}	2.139×10^{3}	1.469×10^{5}	6.2×10^{5}	9.082×10^{6}	1.649×10^{7}	1.187×10^{7}

3.3.2 Inventory of Remotely Handled Waste

The inventory of TRU waste that must be transported and handled in shielded casks because of dose rates at the surface above 200 mrem/hr (remotely handled [RH]) was estimated from the input submitted to the 1990 IDB (IDB, 1990). Estimates were made using a similar method to that used for the CH waste (discussed in Section 3.3.1).* Some differences between the methods for estimating CH and RH were in the estimation of the activity for RH waste reported as mixed fission products and the "unknown" distribution from Hanford. For the mixed fission products, a mixture of 10-yr-old fission products was assumed as the source term. For the Hanford "unknown," a slurry mixture from the Hanford high level waste tanks provided the isotopic distribution; it was estimated that a 2.15 x 10^{-6} C/(kg•s) canister will contain about 450 Ci of gamma emitters. For other mixtures reported in the 1990 IDB, the weight fractions reported were used to calculate the major radionuclides. A volume scaling method similar to that used for CH waste was used to increase the volume from about 5,300 m^3 (estimated from the 1990 IDB) to the maximum volume of 7,079 m^3.

The estimates of the radionuclide inventory for stored waste at the five generator sites are tabulated in Table 3.3-6. The estimated inventory of the stored RH waste was about 5.3 x 10^5 Ci (2.0 x 10^{16} Bq). The projected generated inventory is listed in Table 3.3-7 and the design radionuclide inventory is listed in Table 3.3-8. The estimated total curies content of the projected RH waste was 2.1 x 10^6 Ci (7.0 x 10^{16} Bq).

To estimate the inventory for the maximum volume of RH waste, the projected volumes at each site were volume scaled to provide the additional volume. The projected radionuclide inventory was also volume scaled to estimate the total inventory. The total additional scaled inventory was about 9.4 x 10^5 Ci (3.5 x 10^{17} Bq). Not including the radionuclides with short half-lives, the estimated inventory was 1.6 x 10^6 Ci (3.6 x 10^{16} Bq). By agreement with the State of New Mexico, the DOE will not emplace more than 5.2 x 10^6 Ci (1.9 x 10^{17} Bq) (U.S. DOE and NM, 1989). The current estimate was less than the allowed curie content.

Figure 3.3-4 provides a summary of the estimated activity of the stored, projected, and design radionuclide inventory. These are estimates for PA analyses and should not be considered as a statement of what each site will generate.

For the 1991 PA calculations, the RH-TRU waste was included in the cuttings releases. The RH-TRU waste has not been included in the long-term performance assessment inventory for most previous calculations (Marietta et al., 1989; Lappin et al., 1989; U.S. DOE, 1990b), because RH-TRU waste constituted less than 2% of the activity. Furthermore, as discussed in Section 3.5, the current procedure for emplacing RH waste in the pillar walls will minimize the interaction of the RH waste canisters and the CH waste rooms. Also a large amount of the activity in RH waste is from radionuclides with relatively short half-lives, which have a small consequence over the long term.

---

* An alternate method would be to scale the radionuclides so that the activity limit agreed upon by the State of New Mexico and the DOE--5.2 x 10^6 Ci--would be emplaced instead of the agreed upon volume limit.

Table 3.3-6. Retrievably Stored* Design Radionuclide Inventory by Waste Generator for Remotely Handled Waste

Radionuclide	Half-Life (s)	ANL-E (Ci)	HANF (Ci)	INEL (Ci)	LANL (Ci)	ORNL (Ci)	Stored Total (Ci)
Cr-51	2.3936×10^{6}	--	--	--	--	--	0.0
Mn-54	2.7×10^{7}	--	--	1.703×10^{2}	--	--	1.703×10^{2}
Co-58	6.1171×10^{6}	--	--	5.288×10^{1}	--	--	5.288×10^{1}
Fe-59	3.8473×10^{6}	--	--	--	--	--	0.0
Co-60	1.6634×10^{8}	--	1.667×10^{3}	--	--	4.794×10^{3}	6.461×10^{3}
Sr-90	9.1894×10^{8}	3.582×10^{1}	2.466×10^{4}	--	5.408×10^{2}	1.728×10^{5}	1.98×10^{5}
Y-90	2.304×10^{5}	3.582×10^{1}	2.466×10^{4}	--	5.408×10^{2}	--	2.523×10^{4}
Nb-95	3.037×10^{6}	--	--	8.963×10^{-1}	--	--	8.963×10^{-1}
Ru-106	3.1812×10^{7}	--	1.468	--	--	--	1.468
Rh-106	2.99×10^{1}	--	1.468	--	--	--	1.468
Sb-125	8.7413×10^{7}	--	--	--	--	--	0.0
Cs-134	6.507×10^{7}	--	--	--	--	--	0.0
Cs-137	9.4671×10^{8}	2.687×10^{1}	1.851×10^{4}	2.996×10^{3}	4.056×10^{2}	1.825×10^{5}	2.044×10^{5}
Ba-137m	1.5312×10^{2}	2.388×10^{1}	1.645×10^{4}	--	3.605×10^{2}	--	1.683×10^{4}
Ce-144	2.4564×10^{7}	--	1.468×10^{2}	1.603×10^{3}	--	--	1.75×10^{3}
Pr-144	1.0368×10^{3}	--	1.468×10^{2}	--	--	--	1.468×10^{2}
Pm-147	8.2786×10^{7}	2.687×10^{1}	1.868×10^{4}	--	4.056×10^{2}	--	1.911×10^{4}
Eu-152	4.2065×10^{8}	--	--	--	--	2.397×10^{4}	2.397×10^{4}
Eu-154	2.777×10^{8}	--	--	--	--	1.438×10^{4}	1.438×10^{4}
Eu-155	1.5652×10^{8}	--	--	--	--	--	0.0
Th-232	4.4337×10^{17}	--	--	--	--	--	--
U-233	5.0018×10^{12}	--	--	--	--	1.918×10^{2}	1.918×10^{2}
U-235	2.221×10^{16}	7.351×10^{-5}	5.429×10^{-3}	1.769×10^{-3}	2.916×10^{-3}	--	1.019×10^{-2}
U-238	1.41×10^{17}	--	6.145×10^{-2}	2.386×10^{-4}	2.723×10^{-4}	--	6.196×10^{-2}
Np-237	6.7532×10^{13}	--	--	--	--	--	0.0
Pu-238	2.7688×10^{9}	--	5.066×10^{2}	--	2.334	8.137×10^{2}	1.323×10^{3}
Pu-239	7.5942×10^{11}	1.508	4.801×10^{2}	4.306×10^{1}	2.57×10^{1}	2.876×10^{2}	8.38×10^{2}
Pu-240	2.0629×10^{11}	2.356×10^{-1}	2.589×10^{2}	1.667	8.608	--	2.694×10^{2}
Pu-241	4.5442×10^{8}	--	1.21×10^{4}	--	3.611×10^{2}	--	1.246×10^{4}
Pu-242	1.1875×10^{13}	--	--	--	1.609×10^{-3}	--	1.609×10^{-3}
Am-241	1.3639×10^{10}	--	--	--	--	--	0.0
Cm-244	5.7515×10^{8}	--	--	--	--	3.452×10^{3}	3.452×10^{3}
Cf-252	8.3247×10^{7}	--	--	--	--	--	0.0
TOTALS		1.51×10^{2}	1.183×10^{5}	4.868×10^{3}	2.651×10^{3}	4.032×10^{5}	5.291×10^{5}

* Stored as of December 31, 1989; these estimates were based on 1990 IDB input and were made by H. Batchelder (Westinghouse, WIPP) and transmitted by personal communication.

Table 3.3-7. Projected* Radionuclide Inventory by Waste Generator for Remotely Handled Waste (Curies)

Radiounculide	ANL-E	HANF	INEL	LANL	ORNL	Projected Total	(Stored + Projected) Anticipated System Total
Cr-51	--	--	$1.976x10^{2}$	--	--	$1.976x10^{2}$	$1.976x10^{2}$
Mn-54	--	--	$1.196x10^{4}$	--	--	$1.196x10^{4}$	$1.213x10^{-4}$
Co-58	--	--	$7.707x10^{3}$	--	--	$7.707x10^{3}$	$7.759x10^{3}$
Fe-59	--	--	$1.976x10^{2}$	--	--	$1.976x10^{2}$	$1.976x10^{2}$
Co-60	--	$1.889x10^{2}$	$1.559x10^{3}$	--	--	$1.748x10^{3}$	$8.209x10^{3}$
Sr-90	$4.403x10^{2}$	$2.067x10^{5}$	$1.558x10^{4}$	$5.519x10^{1}$	$2.088x10^{1}$	$2.228x10^{5}$	$4.209x10^{5}$
Y-90	$4.403x10^{2}$	$2.067x10^{5}$	--	$5.519x10^{1}$	--	$2.072x10^{5}$	$2.325x10^{5}$
Nb-95	--	$1.629x10^{3}$	--	--	--	$1.629x10^{3}$	$1.63x10^{3}$
Ru-106	--	$7.573x10^{4}$	--	--	--	$7.573x10^{4}$	$7.573x10^{4}$
Rh-106	--	$7.573x10^{4}$	--	--	--	$7.573x10^{4}$	$7.573x10^{4}$
Sb-125	--	$1.369x10^{4}$	--	--	--	$1.369x10^{4}$	$1.369x10^{4}$
Cs-134	--	$8.91x10^{3}$	$7.68x10^{3}$	--	--	$1.659x10^{4}$	$1.659x10^{4}$
Cs-137	$3.302x10^{2}$	$2.939x10^{5}$	$1.548x10^{4}$	$4.139x10^{1}$	$1.623x10^{2}$	$3.099x10^{5}$	$5.144x10^{5}$
Ba-137m	$2.935x10^{2}$	$2.779x10^{5}$	--	$3.679x10^{1}$	--	$2.782x10^{5}$	$2.95x10^{5}$
Ce-144	--	$2.53x10^{5}$	$3.825x10^{4}$	--	--	$2.913x10^{5}$	$2.93x10^{5}$
Pr-144	--	$2.53x10^{5}$	--	--	--	$2.53x10^{5}$	$2.531x10^{5}$
Pm-147	$3.302x10^{2}$	$2.957x10^{5}$	--	$4.139x10^{1}$	--	$2.961x10^{5}$	$3.152x10^{5}$
Eu-152	--	$1.149x10^{1}$	--	--	--	$1.149x10^{1}$	$2.398x10^{4}$
Eu-154	--	$1.607x10^{3}$	--	--	--	$1.607x10^{3}$	$1.599x10^{4}$
Eu-155	--	$2.939x10^{3}$	--	--	--	$2.939x10^{3}$	$2.939x10^{3}$
Th-232	--	--	--	--	--	--	--
U-233	--	--	--	--	6.696	6.696	$1.985x10^{2}$
U-235	$9.036x10^{-4}$	$8.782x10^{-4}$	--	$2.663x10^{-4}$	$5.079x10^{-4}$	$2.556x10^{-3}$	$1.276x10^{-2}$
U-238	--	$1.627x10^{-2}$	--	$2.486x10^{-5}$	$1.035x10^{-3}$	$1.733x10^{-2}$	$7.929x10^{-2}$
Np-237	--	$6.986x10^{-1}$	--	--	$1.881x10^{-1}$	$8.867x10^{-1}$	$8.867x10^{-1}$
Pu-238	--	5.275	--	$7.105x10^{-2}$	$3.305x10^{-2}$	5.379	$1.328x10^{3}$
Pu-239	$1.853x10^{1}$	$5.898x10^{1}$	$1.975x10^{2}$	$7.826x10^{-1}$	$5.14x10^{1}$	$3.272x10^{2}$	$1.165x10^{3}$
Pu-240	2.896	$1.6x10^{1}$	--	$2.001x10^{-1}$	$4.496x10^{-1}$	$1.955x10^{1}$	$2.89x10^{2}$
Pu-241	--	$7.075x10^{2}$	--	$1.099x10^{1}$	$1.053x10^{-2}$	$7.185x10^{2}$	$1.318x10^{4}$
Pu-242	--	$1.648x10^{-3}$	--	$4.899x10^{-5}$	--	$1.697x10^{-3}$	$3.306x10^{-3}$
Am-241	--	$9.409x10^{2}$	--	--	$6.481x10^{1}$	$1.006x10^{3}$	$1.006x10^{3}$
Cm-244	--	2.209	--	--	$8.073x10^{2}$	$8.095x10^{2}$	$4.262x10^{3}$
Cf-252	--	--	--	--	$8.629x10^{1}$	$8.629x10^{1}$	$8.629x10^{1}$
TOTALS	$1.856x10^{3}$	$1.969x10^{6}$	$9.88x10^{4}$	$2.42x10^{2}$	$1.20x10^{3}$	$2.071x10^{6}$	$2.6x10^{6}$

* Generated between 1990 and 2013; these estimates were based on 1990 IDB input and were made by H. Batchelder (Westinghouse, WIPP) and transmitted by personal communication.

Table 3.3-8. Design Radionuclide Inventory by Waste Generator for Remotely Handled Waste (Curies)

Radionuclide	ANL-E	HANF	INEL	LANL	ORNL	PA Calculations Design 1990	Waste Unit Factor
Cr-51	--	--	2.869×10^{2}	--	--	--	
Mn-54	--	--	1.753×10^{4}	--	--	--	
Co-58	--	--	1.124×10^{4}	--	--	--	
Fe-59	--	--	2.869×10^{2}	--	--	--	
Co-60	--	1.941×10^{3}	2.263×10^{3}	--	4.794×10^{3}	--	
Sr-90	6.747×10^{2}	3.247×10^{5}	2.262×10^{4}	6.213×10^{2}	1.728×10^{5}	5.214×10^{5}	
Y-90	6.747×10^{2}	3.247×10^{5}	--	6.213×10^{2}	--	--	
Nb-95	--	2.364×10^{3}	8.963×10^{-1}	--	--	--	
Ru-106	--	1.099×10^{5}	--	--	--	--	
Rh-106	--	1.099×10^{5}	--	--	--	--	
Sb-125	--	1.987×10^{4}	--	--	--	--	
Cs-134	--	1.293×10^{4}	1.115×10^{4}	--	--	--	
Cs-137	5.06×10^{2}	4.451×10^{5}	2.547×10^{4}	4.66×10^{2}	1.827×10^{5}	6.543×10^{5}	
Ba-137m	4.498×10^{2}	4.199×10^{5}	--	4.142×10^{2}	--	--	
Ce-144	--	3.673×10^{5}	5.713×10^{4}	--	--	--	
Pr-144	--	3.673×10^{5}	--	--	--	--	
Pm-147	5.06×10^{2}	4.479×10^{5}	--	4.66×10^{2}	--	4.489×10^{5}	
Eu-152	--	1.668×10^{1}	--	--	2.397×10^{4}	--	
Eu-154	--	2.333×10^{3}	--	--	1.438×10^{4}	--	
Eu-155	--	4.266×10^{3}	--	--	--	--	
Th-232	--	--	--	--	--	--	
U-233	--	--	--	--	2.015×10^{2}	2.015×10^{2}	
U-235	1.385×10^{-3}	6.704×10^{-3}	1.769×10^{-3}	3.298×10^{-3}	7.372×10^{-4}	1.389×10^{-2}	
U-238	--	8.507×10^{-2}	2.386×10^{-4}	3.086×10^{-4}	1.502×10^{-3}	8.712×10^{-2}	
Np-237	--	1.014	--	--	2.73×10^{-1}	1.287	1.287
Pu-238	--	5.143×10^{2}	--	2.438	8.137×10^{2}	1.33×10^{3}	1.33×10^{3}
Pu-239	2.84×10^{1}	5.657×10^{2}	3.298×10^{2}	2.684×10^{1}	3.622×10^{2}	1.313×10^{3}	1.313×10^{3}
Pu-240	4.438	2.821×10^{2}	1.667	8.9	6.525×10^{-1}	2.978×10^{2}	2.978×10^{2}
Pu-241	--	1.313×10^{4}	--	3.771×10^{2}	1.101×10^{-1}	1.350×10^{4}	
Pu-242	--	2.392×10^{-3}	--	1.68×10^{-3}	--	4.072×10^{-3}	4.072×10^{-3}
Am-241	--	1.366×10^{3}	--	--	9.406×10^{1}	1.46×10^{3}	1.46×10^{3}
Cm-244	--	3.206	--	--	4.624×10^{3}	4.627×10^{3}	
Cf-252	--	--	--	--	1.252×10^{2}	1.252×10^{2}	
TOTALS	2.844×10^{3}	2.976×10^{6}	1.483×10^{5}	3.004×10^{3}	4.049×10^{5}	1.697×10^{6}	4.410×10^{3}

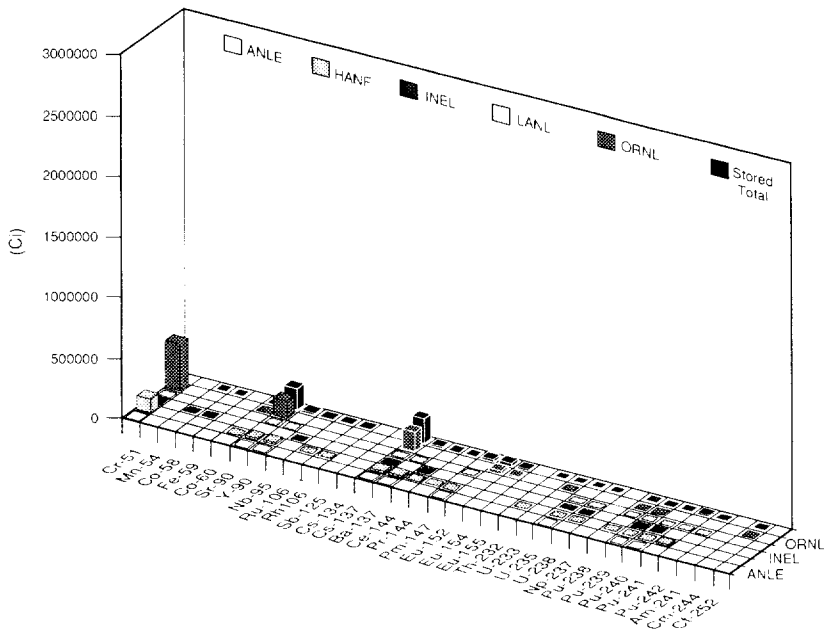

(a)

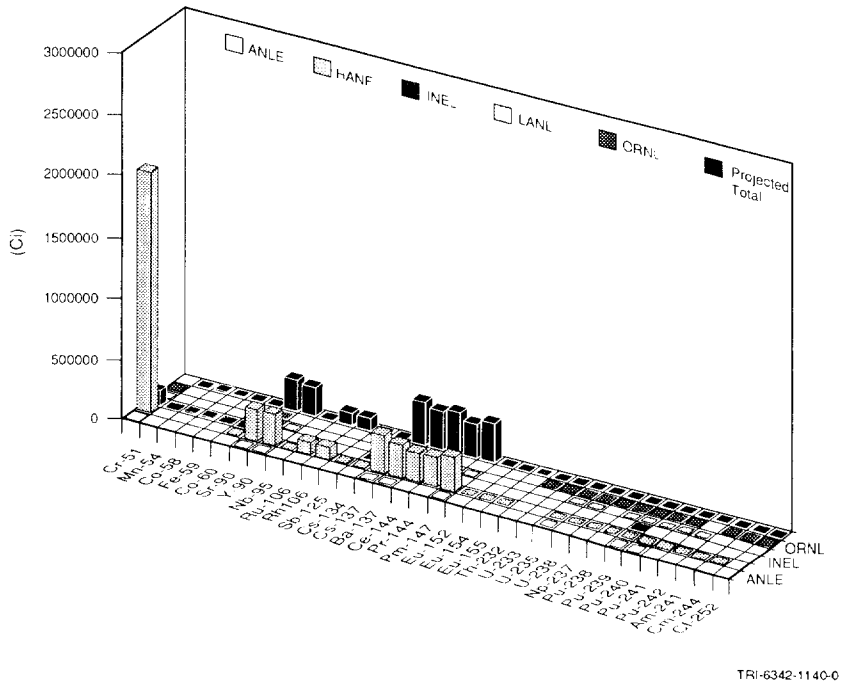

(b)

Figure 3.3-4. Activity of (a) Stored, (b) Projected, (c) Anticipated Actual System Total, and (d) Design Radionuclide Inventory of RH Waste.

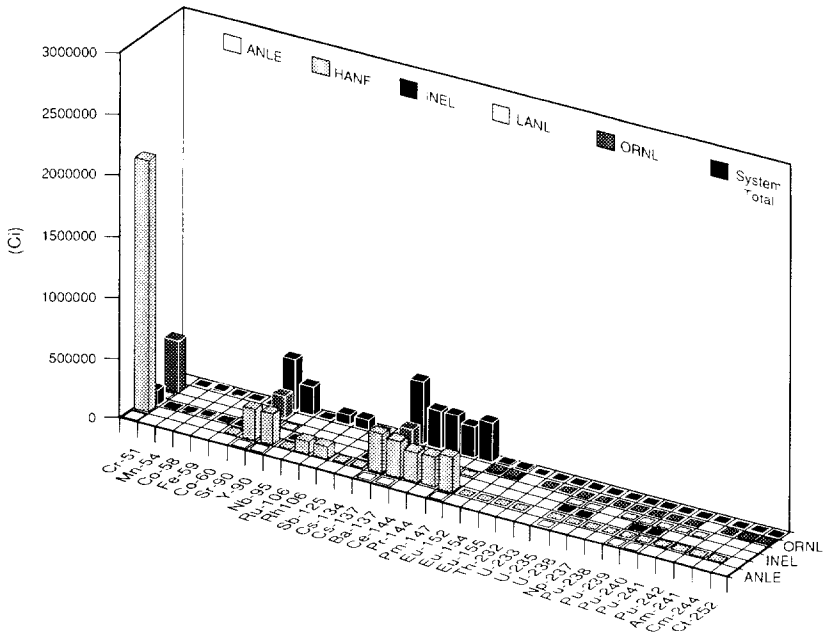

(c)

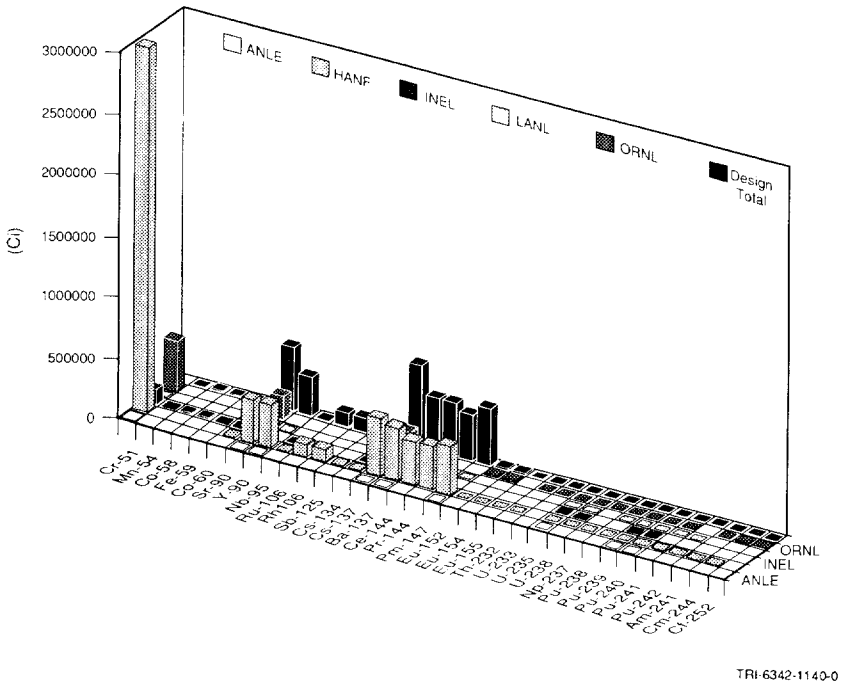

(d)

Figure 3.3-4. Activity of (a) Stored, (b) Projected, (c) Anticipated Actual System Total, and (d) Design Radionuclide Inventory of RH Waste (Concluded).

3.3.3 Radionuclide Chains and Half-Lives

The decay chains for the initial radionuclides in the CH and RH inventory are shown in Figures 3.3-5 and 3.3-6, respectively. The half-lives for each radionuclide as listed in the literature by ICRP Publication 38 (ICRP, Pub 38, 1983) and the mass of the initial inventory are also on Figure 3.3-5. For reference, the half-lives of the radionuclides in the initial WIPP inventory and decay products are tabulated in Table 3.3-9.

Many of the daughter radionuclides have extremely short half-lives, low activities, and make a small contribution to the curie inventory. Shortened chains are used when modeling as follows.

Radionuclides for Cuttings and Repository Modeling

From the 70 radionuclides shown in Figure 3.3-5, 23 are considered major contributors to the inventory and are used in calculating the radionuclide releases from drilling into the repository and bringing cuttings to the surface and when calculating concentrations within the repository prior to transport to the Culebra. In general, most radionuclides of plutonium, thorium, americium, curium, neptunium, californium, radon, and uranium are considered.

The RH inventory decay chains include the chains in the CH inventory shown in Figure 3.3-5 plus the three chains shown in Figure 3.3-6. The radionuclides in the RH cuttings releases included cesium-137, promethium-147, and strontium-90 in addition to all of the radionuclides in the CH releases.

Radionuclides for Transport Modeling

Seven radionuclides are considered in PA transport calculations for CH waste and are highlighted on Figure 3.3-5.

Figure 3.3-7 shows the change with time in radionuclide activity in one panel normalized to the EPA release limits for 11 of the 23 radionuclides not included in the transport calculations. The curies of each radionuclide may be calculated by multiplying the normalized activity by the EPA release limit and the total curies in the initial inventory (11.87×10^6 Ci). Figure 3.3-7 indicates that the total activity at 10,000 yr in a panel for all radionuclides omitted, except for radium-226, is less than 1% of the EPA limit. The normalized activity including radium-226 is less than 2% of the EPA limit.

Five additional radionuclides were not included. Californium-252, curium-244, and plutonium-241 were not included for transport because of their small initial quantities and relatively short half-lives, all less than 20 yr. Curium-248, a daughter of californium-252, was not included because of the small quantity and low radiological toxicity. Plutonium-244 was not included because of its small quantity also.

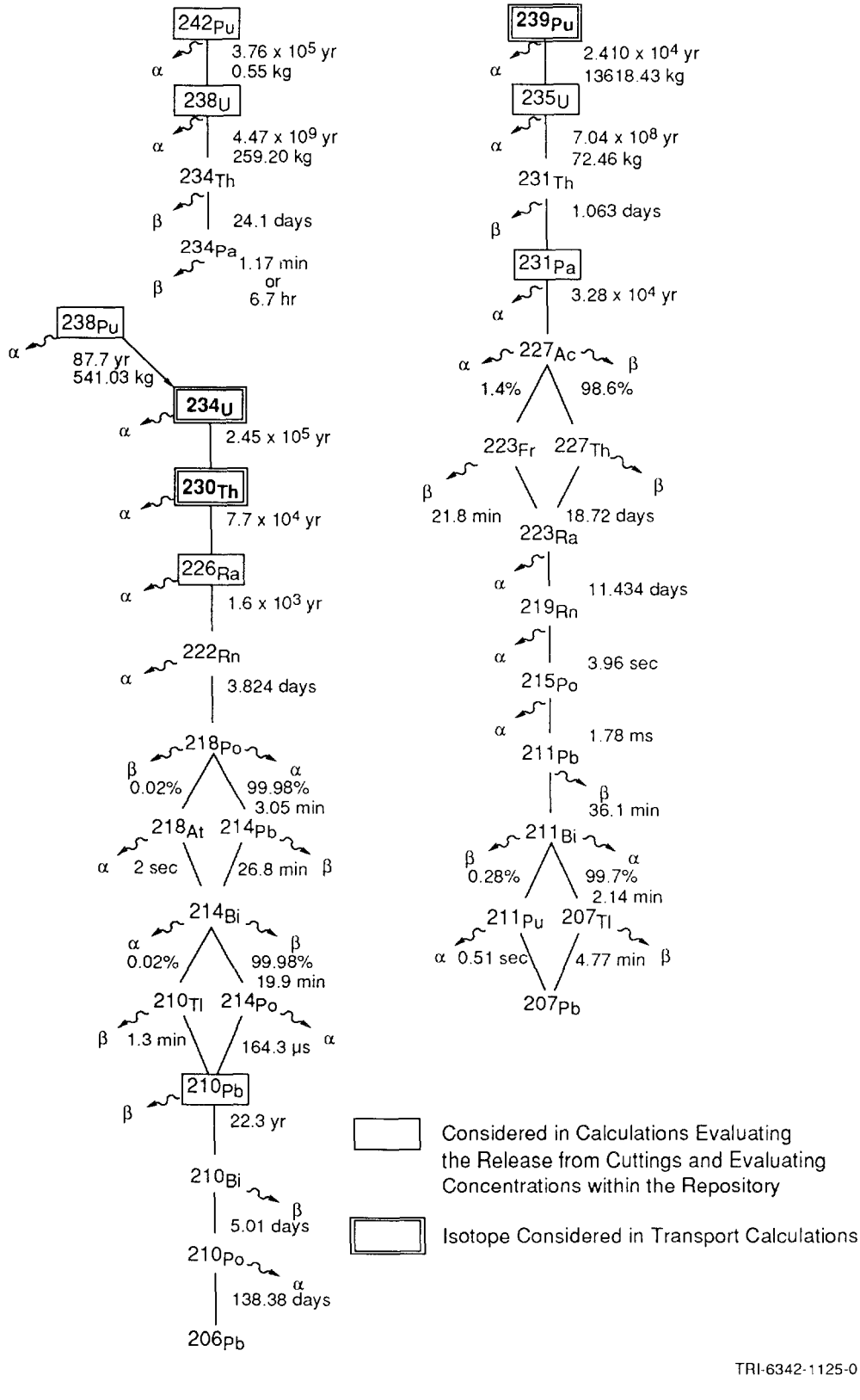

Figure 3.3-5. Decay of CH Radionuclide Chain in TRU-Contaminated Waste.

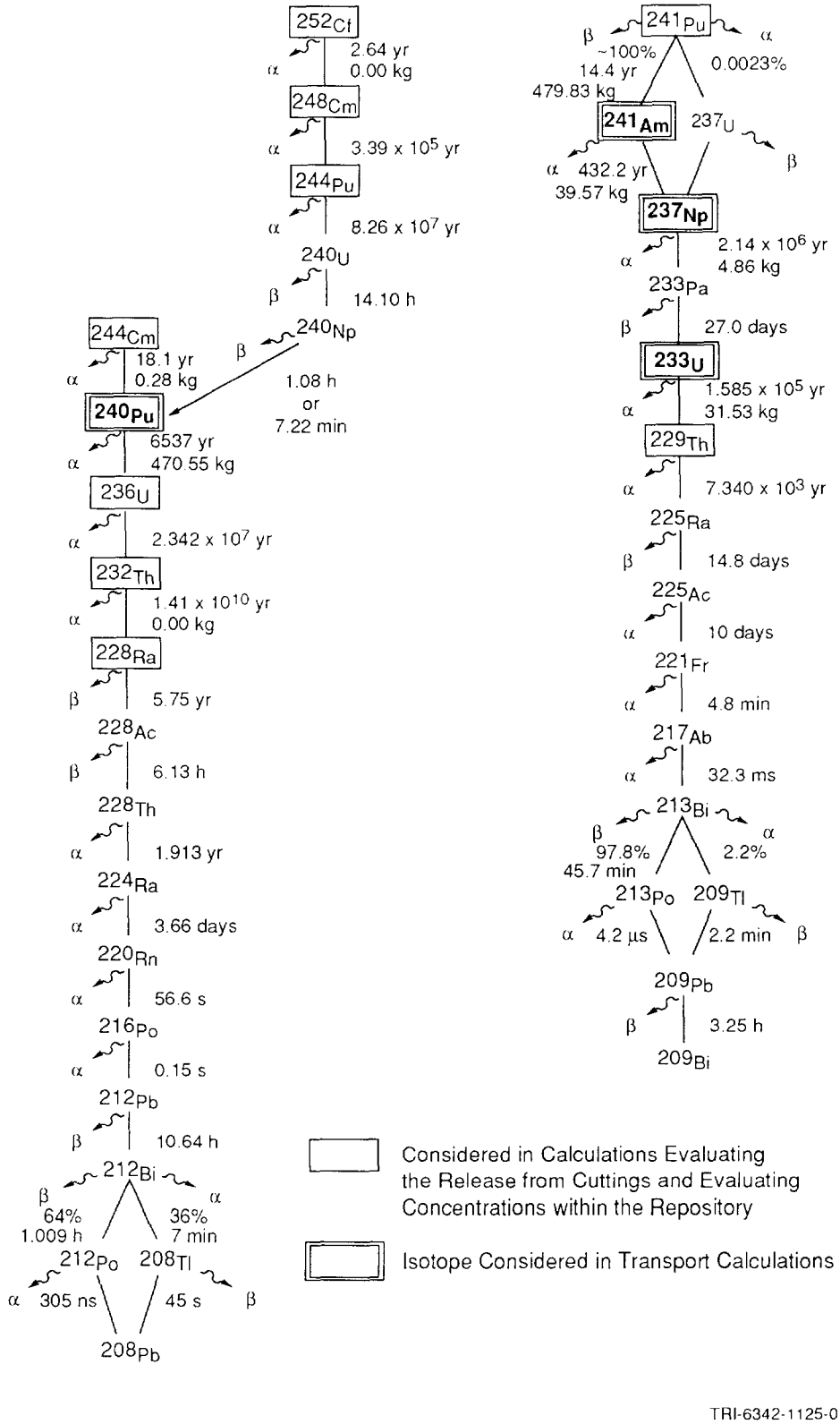

Figure 3.3-5. Decay of CH Radionuclide Chain in TRU-Contaminated Waste (Concluded).

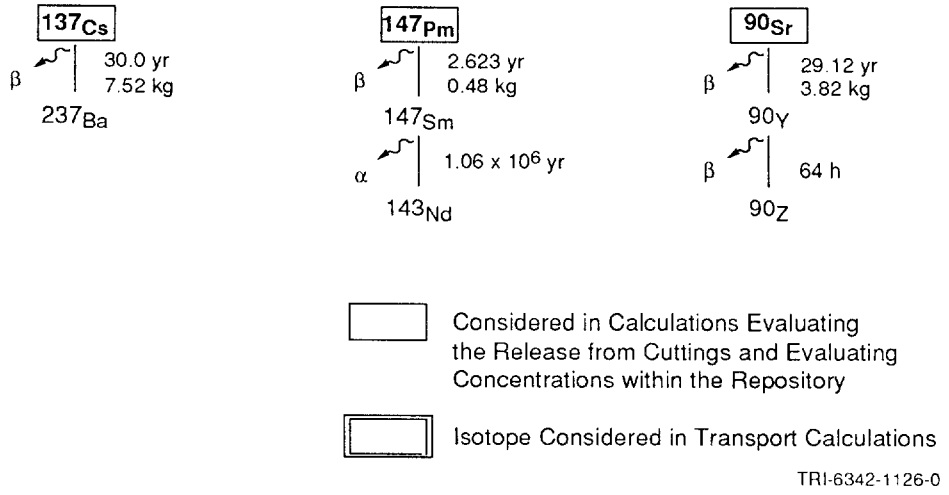

Figure 3.3-6. Decay of RH Radionuclide Chain in TRU-Contaminated Waste.

Table 3.3-9. Half-Lives of Isotopes Disposed or Created in WIPP (ICRP, 1983)

Radioisotope		Half-life ($t_{1/2}$) (s)	Reported
Actinium	^{228}Ac	2.207×10^{4}	6.13 h
	^{227}Ac	6.871×10^{8}	2.177×10^{1} yr
	^{225}Ac	8.64×10^{5}	10 day
Americium	^{243}Am	5.822×10^{11}	7.38×10^{3} yr
	^{241}Am	**1.364×10^{10}**	4.322×10^{2} yr
Antimony	^{125}Sb	8.741×10^{7}	2.77 yr
Astatine	^{217}At	3.23×10^{-2}	3.23×10^{-2} s
Barium	^{137m}Ba	1.531×10^{2}	2.552 min
Bismuth	^{214}Bi	1.194×10^{3}	19.9 min
	^{213}Bi	2.739×10^{3}	45.65 min
	^{212}Bi	3.633×10^{3}	60.55 min
	^{211}Bi	1.284×10^{2}	2.14 min
	^{210}Bi	4.33×10^{5}	5.012 day
Californium	**^{252}Cf**	**8.325×10^{7}**	2.638 yr
Cerium	^{144}Ce	2.456×10^{7}	284.3 day
Cesium	**^{137}Cs**	**9.467×10^{8}**	30.0 yr
	^{134}Cs	6.507×10^{7}	2.062 yr
Chromium	^{51}Cr	2.394×10^{6}	27.7 day
Cobalt	^{60}Co	1.663×10^{8}	5.221 yr
	^{58}Co	6.117×10^{6}	70.8 day
Curium	^{248}Cm	1.070×10^{13}	3.39×10^{5} yr
	^{244}Cm	**5.715×10^{8}**	18.11 yr
Europium	^{155}Eu	1.565×10^{8}	4.96 yr
	^{154}Eu	2.777×10^{8}	8.80 yr
	^{152}Eu	4.207×10^{8}	13.53 yr
Francium	^{221}Fr	2.88×10^{2}	4.8 min
Iron	^{59}Fe	3.847×10^{6}	44.53 day
Lead	^{214}Pb	1.608×10^{3}	26.8 min
	^{212}Pb	3.83×10^{4}	10.64 h
	^{211}Pb	2.166×10^{3}	3.61 min
	^{210}Pb	7.037×10^{8}	22.3 yr
	^{209}Pb	1.171×10^{4}	3.253 h
Manganese	^{54}Mn	2.7×10^{7}	312.5 day
Neptunium	^{239}Np	2.035×10^{5}	2.355 day
	^{237}Np	**6.753×10^{13}**	2.14×10^{6} yr
Niobium	^{95}Nb	3.037×10^{6}	35.15 day
Plutonium	^{244}Pu	2.607×10^{15}	8.76×10^{7} yr
	^{242}Pu	**1.187×10^{13}**	3.763×10^{5} yr
	^{241}Pu	**4.544×10^{8}**	14.4 yr
	^{240}Pu	**2.063×10^{11}**	6.537×10^{3} yr
	^{239}Pu	**7.594×10^{11}**	2.407×10^{4} yr
	^{238}Pu	**2.769×10^{9}**	87.74 yr
Polonium	^{218}Po	1.83×10^{2}	3.05 min
	^{216}Po	1.5×10^{-1}	1.5×10^{-1} s
	^{215}Po	1.78×10^{-3}	1.78×10^{-3} s
	^{214}Po	1.643×10^{-4}	1.643×10^{-4} s
	^{213}Po	4.2×10^{-6}	4.2×10^{-6} s
	^{212}Po	3.05×10^{-7}	3.05×10^{-7} s
	^{210}Po	1.196×10^{7}	138.4 day
Praseodymium	^{144}Pr	1.037×10^{3}	17.28 min
Promethium	**^{147}Pm**	**8.279×10^{7}**	2.623 yr

* Bolding indicates isotopes assumed in inital inventory for PA calculations

Table 3.3-9. Half-Lives of Isotopes Disposed or Created in WIPP (ICRP, 1983) (Concluded)

Radioisotope		Half-life ($t_{1/2}$) (s)	Half-life ($t_{1/2}$) Reported
Protactinium	^{233}Pa	2.333×10^{6}	27 day
	^{231}Pa	1.034×10^{12}	3.276×10^{4} yr
Radium	^{228}Ra	1.815×10^{8}	5.75 yr
	^{226}Ra	5.049×10^{10}	1.6×10^{3} yr
	^{225}Ra	1.279×10^{6}	14.8 day
	^{224}Ra	3.162×10^{5}	3.66 day
	^{223}Ra	9.879×10^{5}	11.43 day
Radon	^{222}Rn	3.304×10^{5}	3.824 day
	^{220}Rn	5.56×10^{1}	5.56×10^{1} s
	^{219}Rn	3.96	3.96 s
Rhodium	^{106}Rh	2.99×10^{1}	2.99×10^{1} s
Ruthenium	^{106}Ru	3.181×10^{7}	3.682×10^{2} day
Strontium	**^{90}Sr***	**9.189×10^{8}**	29.12 yr
Thallium	^{207}Tl	2.862×10^{2}	4.77 min
Thorium	^{234}Th	2.082×10^{6}	24.1 day
	^{232}Th	**4.434×10^{17}**	1.405×10^{10} yr
	^{231}Th	9.187×10^{4}	25.52 h
	^{230}Th	2.43×10^{12}	7.7×10^{4} yr
	^{229}Th	2.316×10^{11}	7.34×10^{3} yr
	^{228}Th	6.037×10^{7}	1.913 yr
	^{227}Th	1.617×10^{6}	18.72 day
Uranium	^{240}U	5.076×10^{4}	1.41×10^{1} hr
	^{238}U	**1.41×10^{17}**	4.468×10^{9} yr
	^{236}U	7.389×10^{14}	2.342×10^{7} yr
	^{235}U	**2.221×10^{16}**	7.038×10^{8} yr
	^{234}U	7.716×10^{12}	2.445×10^{5} yr
	^{233}U	**5.002×10^{12}**	1.585×10^{5} yr
Yttrium	^{90}Y	2.304×10^{5}	64.0 h

* Bolding indicates isotopes assumed in inital inventory for PA calculations

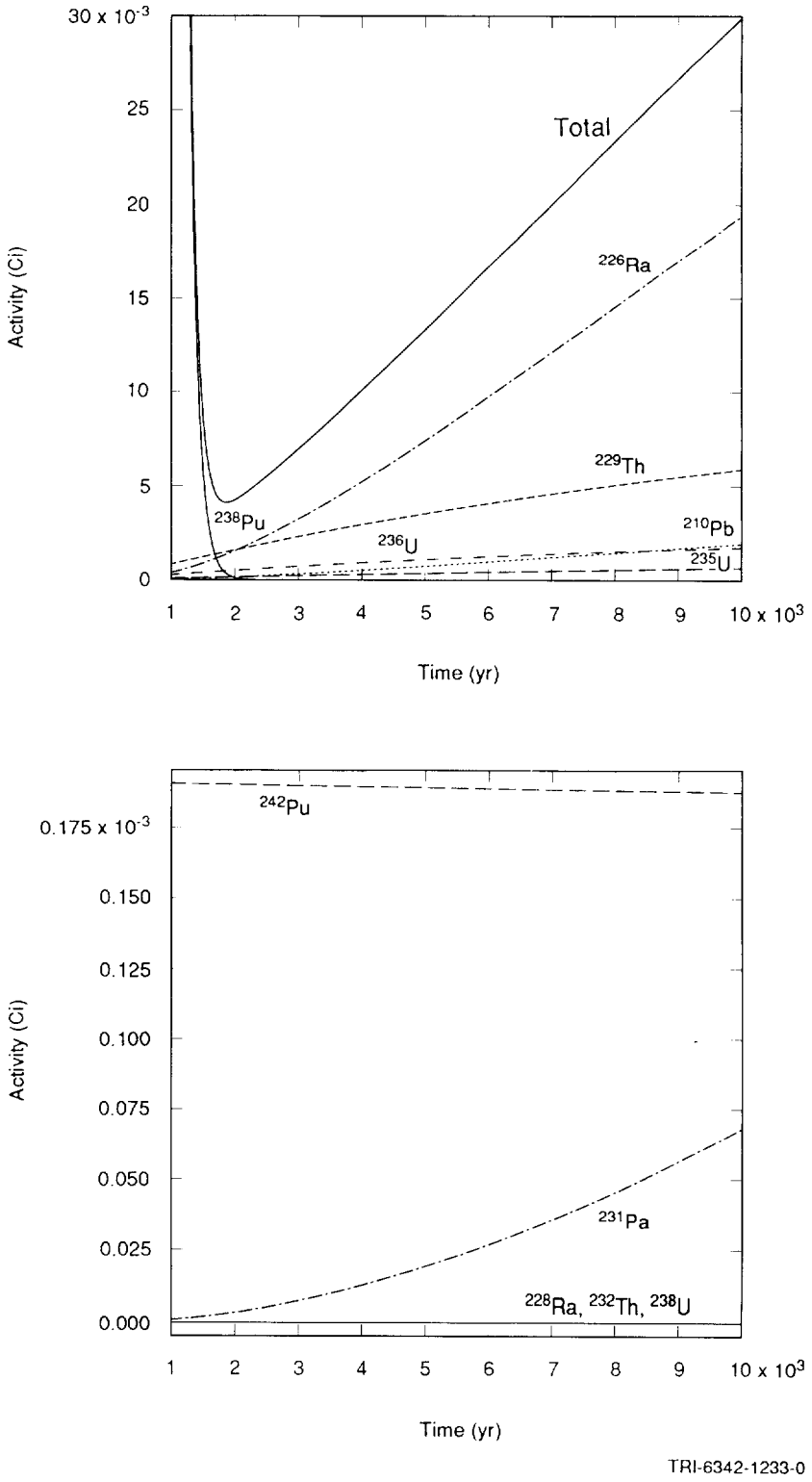

Figure 3.3-7. Radionuclides in One Panel Normalized by EPA Release Limits, Which Were Eliminated from Transport Calculations.

3.3.4 40 CFR 191 Release Limits and Waste Unit Factor

40 CFR 191 Release Limits

The release limits (L_i) for evaluating compliance with *40 CFR 191 § 13* are provided in Table 3.3-10.

Table 3.3-10. Cumulative Release Limits (L_i) to the Accessible Environment 10,000 Yr after Disposal for Evaluating Compliance with Containment Requirements (40 CFR 191, Appendix B, Table 1)

Radionuclide	Release limit (L_i) per 1 x 10^6 Ci α-emitting TRU nuclide with $t_{1/2}$ > 20 yr* (Ci)	1991 PA Release Limits $f_m L_i$ (Ci)
Americium (Am) -241 or -243	100	1187
Carbon (C) -14	100	1187
Cesium (Cs) -135 or -137	1000	11870
Iodine (I) -129	100	1187
Neptunium (Np) -237	100	1187
Plutonium (Pu) -238, -239, -240, or -242	100	1187
Radium (Ra) -226	100	1187
Strontium (Sr) -90	1000	11870
Technetium (Tc) -99	10000	118700
Thorium (Th) -230 or -232	10	118.7
Tin (Sn) -126	1000	11870
Uranium (U) -233, -234, -235, -236, or -238	100	1187
Any other α-emitting radionuclide with $t_{1/2}$ > 20 yr	100	1187
Any other non α-emitting radionuclide with $t_{1/2}$ > 20 yr	1000	11870

* Other units of waste described in 40 CFR 191, Appendix A

Waste Unit Factor

The waste unit factor (f_w) is the inventory in curies of transuranic (TRU) α-emitting radionuclides in the waste with half-lives greater than 20 yr divided by 10^6 Ci, where TRU is defined as radionuclides with atomic weights *greater* than uranium (92). Consequently, as currently defined in *40 CFR 191*, all TRU radioactivity in the waste cannot be included when calculating the waste unit factor. For the WIPP, 1.187 x 10^7 Ci of the radioactivity design total of 1.814 x 10^7 Ci comes from TRU α-emitting radionuclides with half-lives greater than 20 yr (see Tables 3.3-5 and 3.3-8).* Regardless of the waste unit, the WIPP has assumed that all nuclides listed in Tables 3.3-5 and 3.3-8 are regulated and must be included in the release calculations. Therefore, the release limits (L_i) used by the WIPP are reduced somewhat (i.e., more restrictive).

EPA Sums for Each nS Scenario Set

See discussion in Chapter 1, Section 1.4.1.

* For the remanded regulation, the following change has been suggested: Include all radionuclides in the inventory but use the activity (curie content) of the first daughter with a half-life greater than 20 yr for radionuclides with half-lives of less than 20 yr.

3.3.5 Solubility

The solubility of specific radionuclides was estimated by a panel of experts (outside Sandia) in the fields of actinide and brine chemistry (Trauth et al., 1991). Supporting calculations with EQ3/6 were performed using a standard brine that simulates the brine in the Salado Formation as the solvent (Lappin et al., 1989, Table 3-4). These efforts resulted in the estimation of the oxidation state(s) in which the radionuclides would exist in the environment of the WIPP disposal area, and corresponding solid species that would exist with that particular oxidation state.

Figure 3.3-8 depicts the estimated distributions of solubility for americium, curium, lead, neptunium, plutonium, radium, thorium, and uranium.

The points on the probability distributions that were elicited during the expert panel session are found in Figure 3.3-8 and Table 3.3-11.

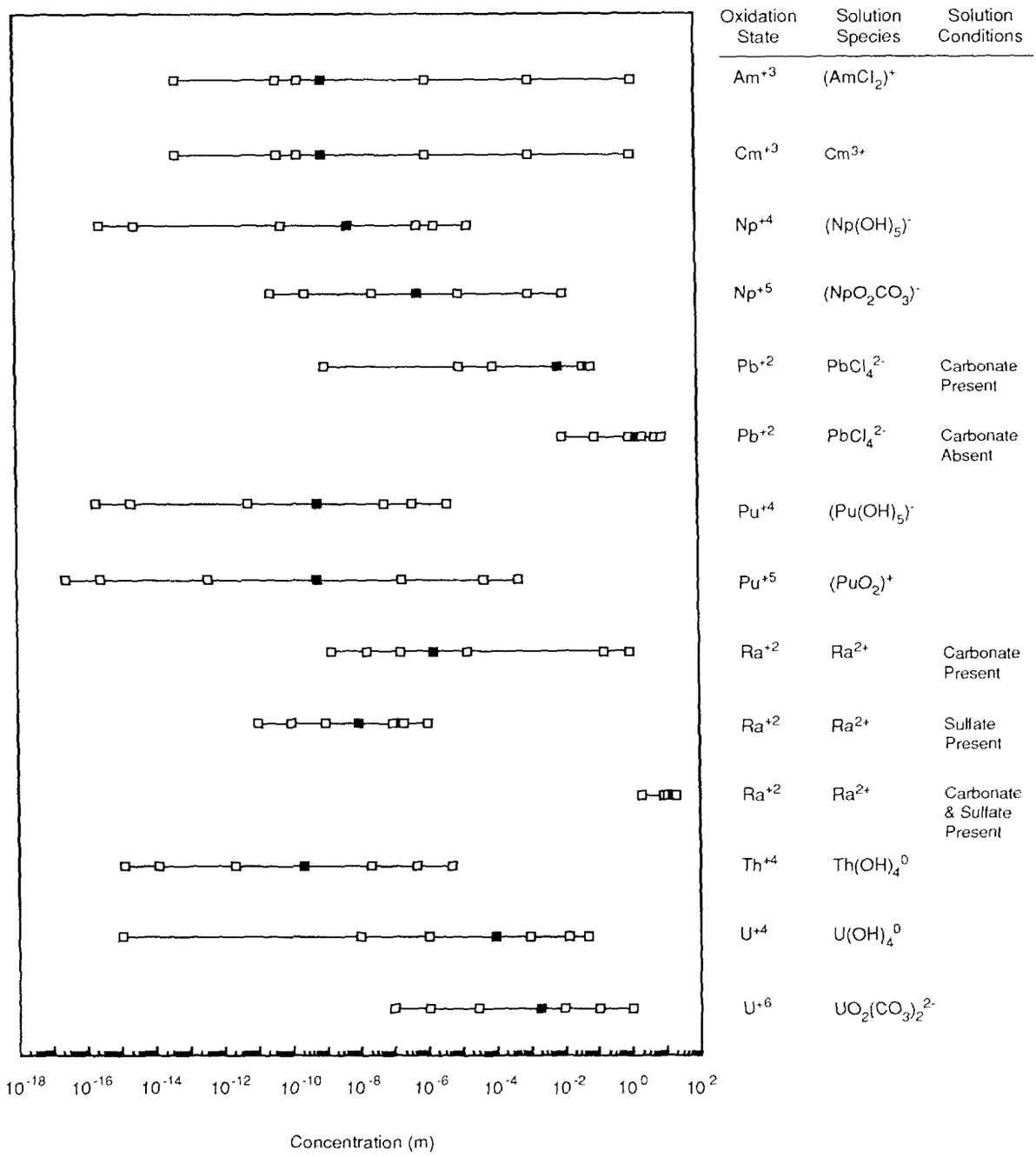

The blocks represent, from left to right, the 0.00, 0.10, 0.25, 0.50, 0.75, 0.90 and 1.00 fractiles

TRI-6342-1410-0

Figure 3.3-8. Subjective Distribution (cdf) of Solubility for Americium, Curium, Lead, Neptunium, Plutonium, Radium, Thorium, and Uranium (after Trauth et al., 1991).

Table 3.3-11. Estimated Solubilities of Radionuclides (from Trauth et al., 1991, Table 1)

Element	Solution Species	Solid Species Maximum and Minimum	Condition	Cumulative Probabilities of Concentrations (M) 0.0	0.10	0.25	0.50	0.75	0.90	1.00
Am^{3+}	$(AmCl_2)^+$	$Am(OH)_3$ $AmOHCO_3$		5.0×10^{-14}	5.0×10^{-11}	2.0×10^{-10}	1.0×10^{-9}	1.2×10^{-6}	1.4×10^{-3}	1.4
Cm^{3+}	Cm^{III}	$Cm(OH)_3$ CmO_2		5.0×10^{-14}	5.0×10^{-11}	2.0×10^{-10}	1.0×10^{-9}	1.2×10^{-6}	1.4×10^{-3}	1.4
Np^{5+}	$(NpO_2CO_3)^-$	$NpO_2(OH)$ (amorphous) $NaNpO_2CO_3 \cdot 3.5H_2O$		3.0×10^{-11}	3.0×10^{-10}	3.0×10^{-8}	6.0×10^{-7}	1.0×10^{-5}	1.2×10^{-3}	1.2×10^{-2}
Np^{6+}	$(Np(OH)_5)^-$	$Np(OH)_4$ NpO_2		3.0×10^{-16}	3.0×10^{-15}	6.0×10^{-11}	6.0×10^{-9}	6.0×10^{-7}	2.0×10^{-6}	2.0×10^{-5}
Pb^{2+}	$PbCl_4^{2-}$	$PbCO_3$	Carbonate Present	1.0×10^{-9}	1.0×10^{-5}	1.0×10^{-4}	8.0×10^{-3}	4.4×10^{-2}	6.2×10^{-2}	8.0×10^{-2}
		$PbCl_2$	Carbonate Absent	0.01	0.10	1.0	1.64	2.5	6.0	10.0
Pu^{4+}	$(Pu(OH)_5)^-$	$Pu(OH)_4$ PuO_2		2.0×10^{-16}	2.0×10^{-15}	6.0×10^{-12}	6.0×10^{-10}	6.0×10^{-8}	4.0×10^{-7}	4.0×10^{-6}
Pu^{5+}	$(PuO_2)^+$	$Pu(OH)_4$ PuO_2		2.5×10^{-17}	2.5×10^{-16}	4.0×10^{-13}	6.0×10^{-10}	2.0×10^{-7}	5.5×10^{-5}	5.5×10^{-4}
Ra^{2+}	Ra^{2+}	$RaSO_4$ and $(Ra/Ca)SO_4$	Sulfate Present	1.0×10^{-11}	1.0×10^{-10}	1.0×10^{-9}	1.0×10^{-8}	1.0×10^{-7}	2.0×10^{-7}	1.0×10^{-6}
		$RaCO_3$ and $(Ra/Ca)CO_3$	Carbonate Present	1.6×10^{-9}	1.6×10^{-8}	1.6×10^{-7}	1.6×10^{-6}	1.6×10^{-5}	1.6×10^{-1}	1.0
		$RaCl_2 \cdot 2H_2O$	Carbonate and Sulfate Absent	2.0	4.0	8.6	11.0	14.5	17.2	18.0
Th^{4+}	$Th(OH)_4^0$	$Th(OH)_4$ ThO_2		5.5×10^{-16}	5.5×10^{-15}	1.0×10^{-12}	1.0×10^{-10}	1.0×10^{-8}	2.2×10^{-7}	2.2×10^{-6}
U^{4+}	$U(OH)_4^0$	UO_2 (amorphous) U_3O_8		1.0×10^{-15}	1.0×10^{-8}	1.0×10^{-6}	4.0×10^{-3}	1.0×10^{-3}	1.4×10^{-2}	5.0×10^{-2}
U^{6+}	$UO_2(CO_3)_2^{2-}$	$UO_3 \cdot 2H_2O$ UO_2		1.0×10^{-7}	1.0×10^{-6}	3.0×10^{-5}	2.0×10^{-3}	1.0×10^{-2}	0.1	1.0

General Rationale for Constructing Cumulative Distributions

The assessment of each distribution began by establishing the upper and lower solubility regimes. The first regime was based on the solid species with the highest solubility, and thus, the highest concentration of the actinide, and the second regime was based on the solid species with the lowest solubility, and thus, the lowest concentration. The regime depends upon the chemical properties within the repository, which are uncertain. The conditions considered included the pH and ionic strength of the brine, and the presence of carbonate and sulfate. The factor(s) controlling each regime differed for each actinide.

Each of these probability distributions represents the uncertainty in estimating a fixed, but unknown, quantity. In this case, the quantity is the concentration of a particular radionuclide given a particular condition. Thus, uncertainty cannot be assigned to the concentration for a particular fractile. The uncertainty inherent in these distributions includes that due to uncertainty in the pH of the solvent in contact with the waste. When the impact of variation in pH was included, the ranges of the distributions increased. Likewise, the distributions encompass the differences of opinion of the experts. These differences also resulted in larger ranges for the distributions. Because the distributions were developed by the panel as a whole, the uncertainty in the judgments of the individual panel members cannot be quantified.

10th, 90th and 0th, 100th Percentiles. Typically, the calculated value of each actinide for each regime was used to establish a fractile, often either the 0.10 or 0.90 fractile, of the distribution. The absolute lower, or upper, end point of the distribution was obtained by considering the sensitivity of solubility to the underlying brine chemistry. For example, the calculated lower solubility limit for Am^{3+} (solid species $AmOHCO_3$) was 5×10^{-11} M. The absolute lower limit of the distribution was judged to be 5×10^{-14} M. This judgment was obtained through consideration and discussion of the sensitivity of solubility to pH. In a similar manner, the upper 0.90 fractile was set equal to the calculated solubility with the solid speciation $Am(OH)_3$. The calculated value was 1.4×10^{-3} M. The absolute upper limit was judged to be 1.4 M.

25th and 75th Percentiles. The interior fractiles (0.25 and 0.75) were obtained after the 0.10 and 0.90 fractiles and the endpoints were established and based on speciation. In some cases, one speciation was thought to be more likely, resulting in a skewed distribution. In other cases, both speciations were thought to be likely, or to perhaps coexist, so that the assessed distribution was more symmetric and either bimodal or flat.

50th Percentile. Where possible, concentration data from a well (J-13) at the Nevada Yucca Mountain site, with a correction made for the ionic strength difference between the J-13 water and the WIPP A brine (Lappin et al., 1989, Table 3-4), was used as the 0.50 fractile.

Radium and Lead

The assessments for radium and lead require special comment because they are the only ones based on the presence or absence of specific compounds—carbonateand sulfate. For radium, the solubility is controlled by the solid species $RaSO_4$ and $(Ra/Ca)SO_4$ if sulfate is present. In the absence of sulfate, but in the presence of carbonate, $RaCO_3$ and $(Ra/Ca)CO_3$ control the solubility. If neither sulfate nor carbonate is present, then $RaCl_2$ $2H_2O$ will be the solid species. In the case of lead, the solid speciation depends upon the presence of carbonate but not sulfate. If carbonate is present, the solid speciation is $PbCO_3$, otherwise, $PbCl_2$.

Colloids

The expert panel had considerable difficulty dealing with colloids because of a lack of experimental data and physical principles governing their formation. There was some diversity of opinion about the significance of colloids. One expert placed an upper limit on the concentration of colloids of 10% of the concentration due to solubility. Another expert suggested that for some actinides, such as plutonium, the concentration due to colloidal formation may be greater than that due to solubility. Another suggestion was that the activity coefficients embody some colloid formation and thus the assessed distributions reflect the presence of both dissolved and suspended materials. The panel did not believe they could make judgments about suspended solids concentrations at the present time. They plan to include recommendations for future experiments related specifically to colloids in a final panel report.

Correlations

Correlations between the concentrations assigned to the radionuclides were discussed briefly by the panel. The consensus was that correlations do exist, possibly between Am^{3+} and Cm^{3+}, and between Np^{4+} and Pu^{4+}. The panel will address this issue in their final panel report.

3.3.6 Eh - pH Conditions

Parameter:	**Relative areas of radionuclide oxidation state**
Median:	0.5
Range:	0
	1.0
Units:	Dimensionless (A_i/A_{total})
Distribution:	Uniform
Source(s):	See text.

Discussion:

From estimates of constituents in the waste, inventory estimates of radionuclide concentration in brine as a function of Eh and pH are theoretically possible. However, the work remains to be done. Currently, radionuclide solubility estimates include variations in pH when assigning the 0th and 100th percentiles (Section 3.3.5, Solubility). For Eh, the oxidizing or reducing potential of the solution is sampled from a uniform distribution with ranges dependent on the stability of water. For 1991 PA calculations, an index variable between 0 and 1 was used to select the relative areas of the estimated regimes of stability for the various oxidation states of neptunium (Np), plutonium (Pu), and uranium (U) (Figure 3.3-9).

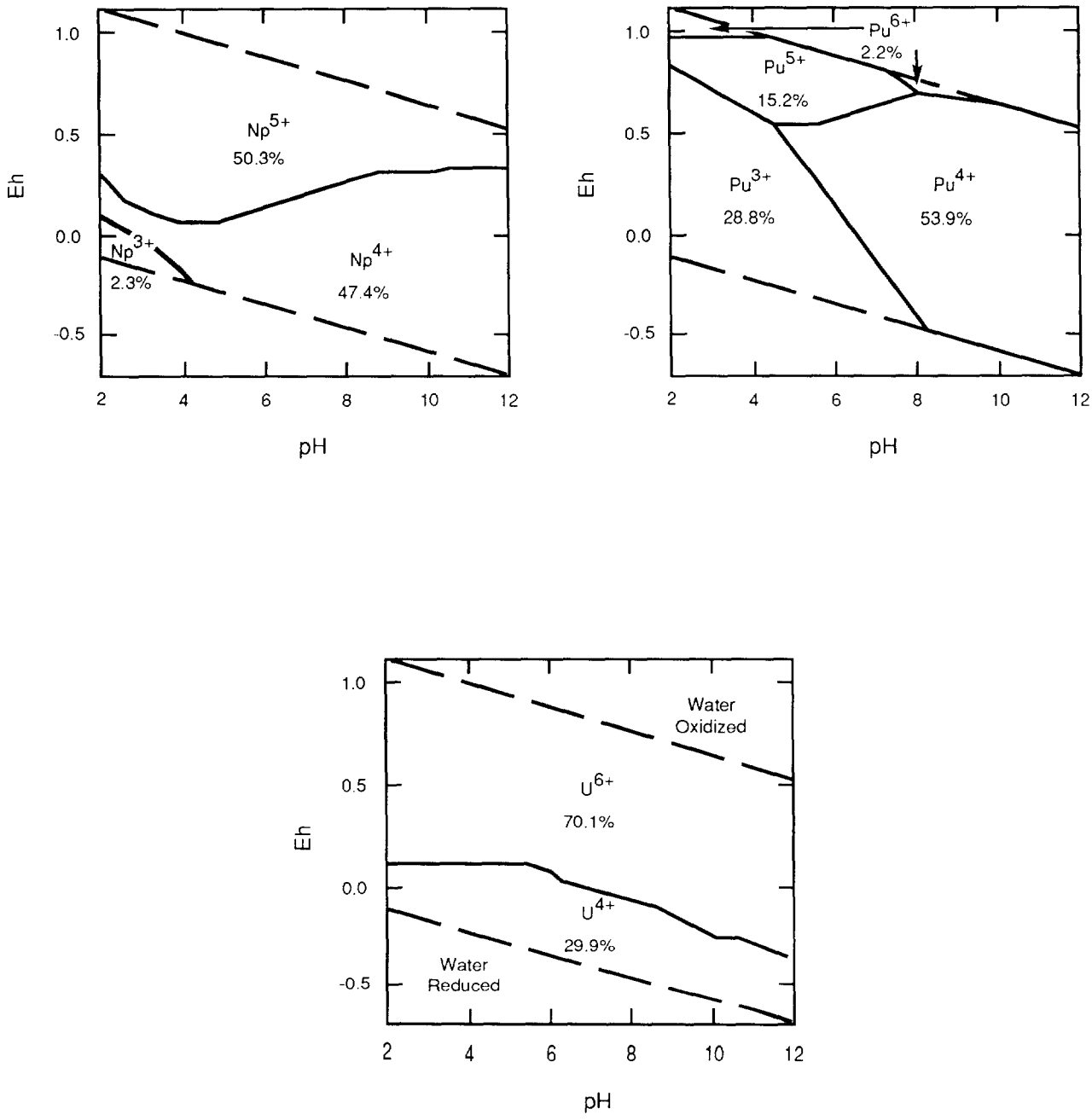

TRI--6342-1132-0

Figure 3.3-9. Estimated Regimes of Stability in the Eh-pH Space for Neptunium, Plutonium, and Uranium and Percentage of Area of Stable Water.

3.3.7 Molecular Diffusion Coefficient*

Table 3.3-12 provides estimated values of the free liquid diffusion coefficient of important actinides. Figure 3.3-10 provides the uniform distribution assumed for the average actinide.

Table 3.3-12. Estimated Molecular Diffusion Coefficient for Radionuclide Transport in Culebra Dolomite (after Lappin et al., 1989, Table E-7).

Parameter	Median	Range		Units	Distribution Type
Actinide, average	2.4×10^{-10}	4.8×10^{-11}	4.3×10^{-10}	m^2/s	Uniform
Am	1.765×10^{-10}	5.3×10^{-11}	3×10^{-10}	m^2/s	Uniform
Cm	1.765×10^{-10}	5.3×10^{-11}	3×10^{-10}	m^2/s	Uniform
Np	1.76×10^{-10}	5.2×10^{-11}	3×10^{-10}	m^2/s	Uniform
Pb	4×10^{-10}	2×10^{-10}	8×10^{-10}	m^2/s	Cumulative
Pu	1.74×10^{-10}	4.8×10^{-11}	3×10^{-10}	m^2/s	Uniform
Ra	3.75×10^{-10}	1.875×10^{-10}	7.5×10^{-10}	m^2/s	Cumulative
Th	1×10^{-10}	5×10^{-11}	1.5×10^{-10}	m^2/s	Uniform
U	2.7×10^{-10}	1.1×10^{-10}	4.3×10^{-10}	m^2/s	Uniform

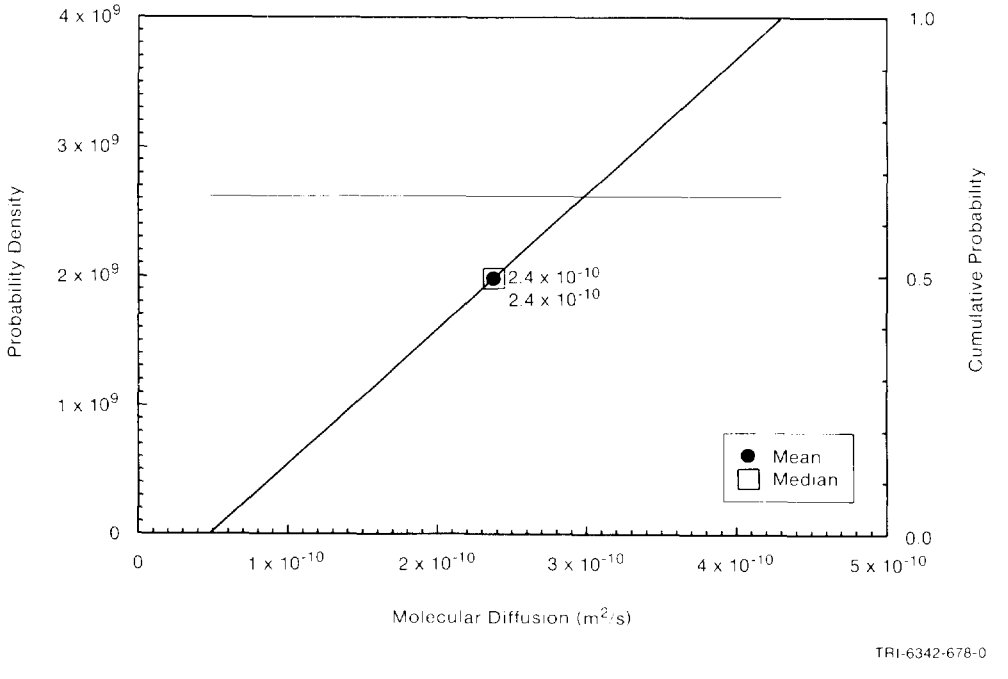

Figure 3.3-10. Uniform Distribution (pdf and cdf) for Molecular Diffusion Coefficient, D^{α}.

* This section provides data for free-liquid diffusion coefficients; the diffusion coefficient for an actual porous media is the free-liquid coefficient times the tortuosity factor for that media.

Discussion:

Table 3.3-12 provides values of the molecular diffusion estimated both from the Nernst equation at infinite dilution (upper range) (Brush, 1988; Li and Gregory, 1974) and data obtained in experiments (lower range). For cases with both experimental and Nernst equation estimates, the molecular diffusion was assumed to be uniformly distributed between the two values.

Because the experimental values were obtained from apparent diffusion coefficients in granitic ground waters and sodium bentonite, they required assumptions about retardation factors for the radionuclides, porosity, and tortuosity (Torstenfelt et al., 1982; Lappin et al., 1989, Table E-7). Therefore, considerable but unquantifiable uncertainty is associated with all the values of the actinide diffusion coefficients reported in the literature. Furthermore, there are few data to guide predictions of radionuclide diffusion coefficients in the concentrated brines. Consequently, extrapolation of the measured diffusion coefficients to the range of conditions assumed for the Salado and Culebra Dolomite brines introduces more uncertainty.

Some data suggest that diffusion coefficients for divalent cations (alkaline earth chlorides, transitions metal chlorides) decrease by a factor of 2 with increasing ionic strength over the range 0 to 6 M (Miller, 1982). This factor of 2 was used to establish ranges for Ra and Pb, for which only a single value (the upper range) is available from the Nernst expression (Li and Gregory, 1974). Specifically, the median value selected is smaller than the Nernst equation value by a factor of 2 to include some salinity effects. The lower range is smaller than the median by a factor of 2 to account for greater salinity and miscellaneous uncertainties.

Although molecular diffusion varies with each species and the concentration of ions (e.g., Na^+ from brackish water), some of the computational models used by the PA Division require a single value. For these cases, molecular diffusion is assumed to be uniformly distributed (Figure 3.3-11) with a range chosen to encompass the extremes for the actinide radionuclides, 4.8×10^{-11} to 4.3×10^{-10} m^2/s (4.5×10^{-5} to 4.0×10^{-4} ft^2/d) with a mean of 2.4×10^{-10} m^2/s (2.2×10^{-4} ft^2/d).

3.3.8 Gas Production from Corrosion

Parameter:	**Gas production rates, corrosion, inundated rate**
Median:	6.3×10^{-9}
Range:	0
	1.3×10^{-8}
Units:	mol H_2/(m^2 surface area steel • s)
Distribution:	Cumulative
Source(s):	Brush, L. H. 1991. "Current Estimates of Gas Production Rates, Gas Production Potentials, and Expected Chemical Conditions Relevant to Radionuclide Chemistry for the Long-Term WIPP Performance Assessment," Internal memo to D.R. Anderson (6342), July 8, 1991. Albuquerque, NM: Sandia National Laboratories. (Memo 3 in Appendix A of this volume)

Parameter:	**Gas production rates, corrosion, relative humid rate**
Median:	1×10^{-1}
Range:	0
	5×10^{-1}
Units:	Dimensionless
Distribution:	Cumulative
Source(s):	Brush, L. H. 1991. "Current Estimates of Gas Production Rates, Gas Production Potentials, and Expected Chemical Conditions Relevant to Radionuclide Chemistry for the Long-Term WIPP Performance Assessment," Internal memo to D.R. Anderson (6342), July 8, 1991. Albuquerque, NM: Sandia National Laboratories. (Memo 3 in Appendix A of this volume)

Parameter:	**Anoxic iron corrosion stoichiometry**
Median:	0.5
Range:	0
	1
Units:	None (mol fraction)
Distribution:	Uniform
Source(s):	Brush, L. H. and D. R. Anderson. 1989. In Lappin et al., 1989. *Systems Analysis Long-Term Radionuclide Transport and Dose Assessments, Waste Isolation Pilot Plant (WIPP), Southeastern New Mexico; March 1989.* SAND89-0462. Albuquerque, NM: Sandia National Laboratories.

Figures 3.3-11, 3.3-12, and 3.3-13 provide the assumed distributions for gas production rates from corrosion under inundated conditions; gas production rates from corrosion under humid conditions; and anoxic iron corrosion stoichiometry, respectively. These distributions were constructed using information from Brush (July 8, 1991, Memo, Appendix A).

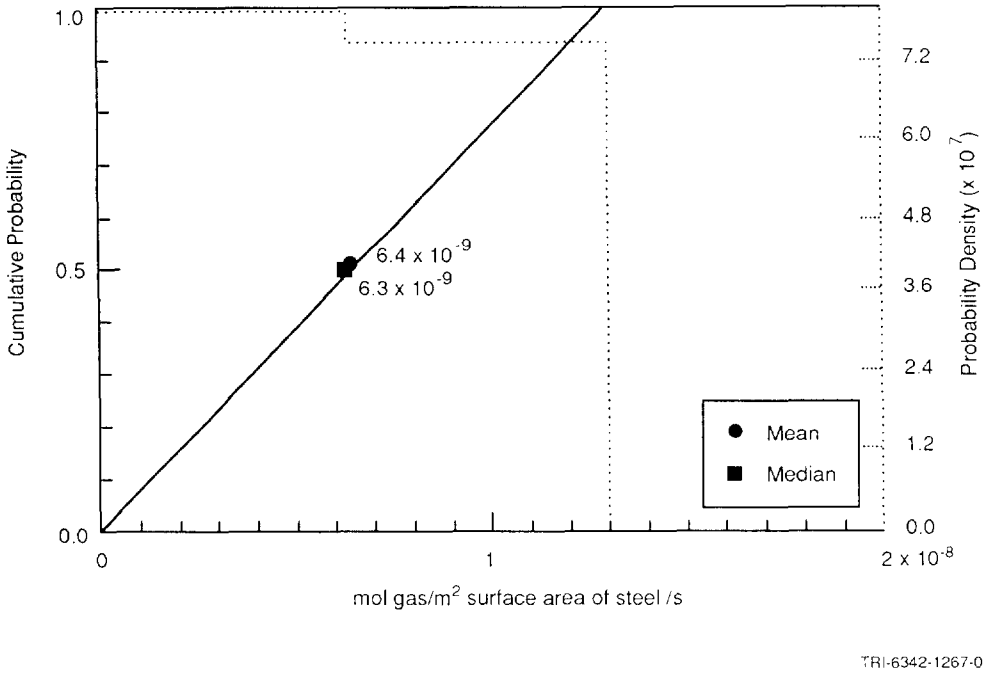

Figure 3.3-11. Assumed Distribution (pdf and cdf) for Gas Production Rates from Corrosion under Inundated Conditions.

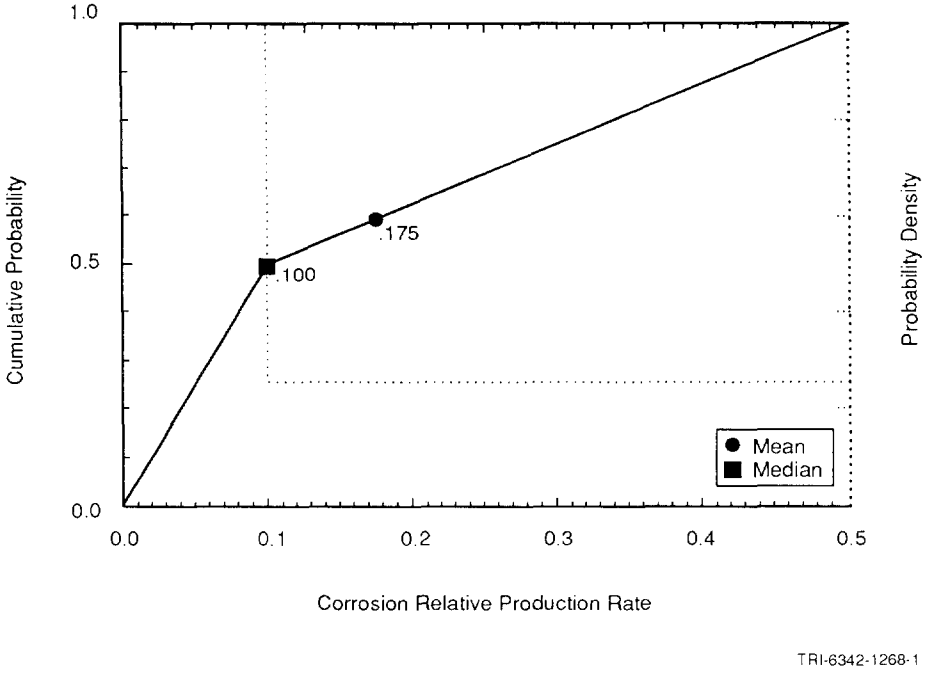

Figure 3.3-12. Assumed Distribution (pdf and cdf) for Relative Gas Production Rates from Corrosion under Humid Conditions.

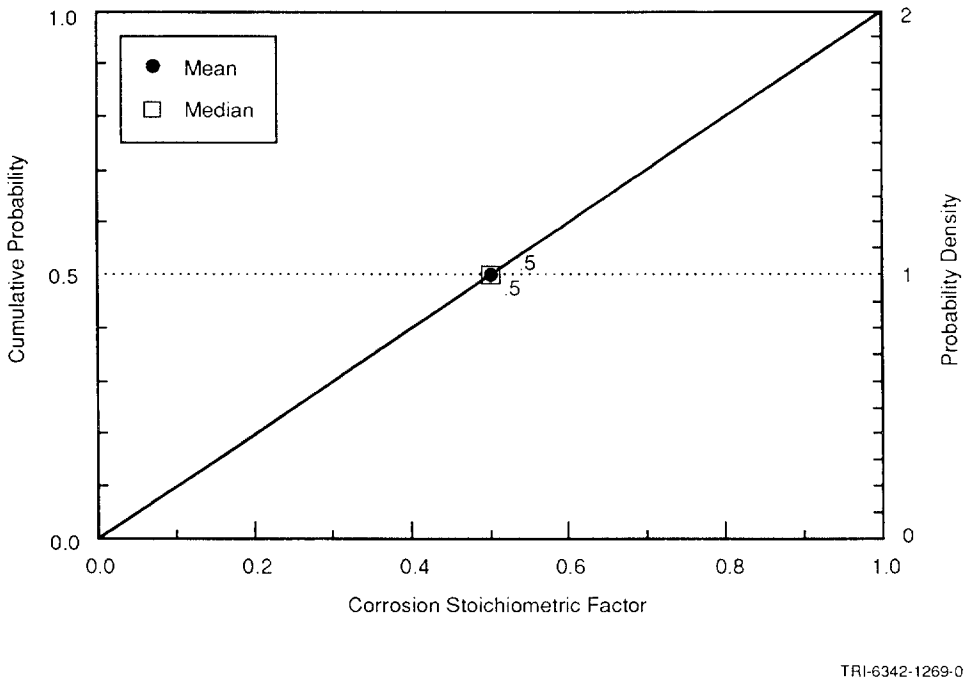

Figure 3.3-13. Assumed Distribution (pdf and cdf) for Anoxic Iron Corrosion Stoichiometric Factor, x.

Discussion:

After waste is emplaced in the WIPP repository, some gas is expected to be generated from three types of chemical reactions: (1) anoxic corrosion, (2) biodegradation, and (3) radiolysis. In theory, the rates are dependent upon several factors, such as the chemical makeup of the waste (both organic and inorganic), the types of bacteria present, interactions among the products of the reactions, characteristics of WIPP brine, pH, and Eh. Experimental data describing these dependencies are incomplete at this time. However, some rough estimates of the range of gas generation rate values under possible WIPP environmental conditions have been made using available data.

Brush (July 8, 1991, Memo [Appendix A]) estimates gas production from corrosion for inundated and humid conditions. The estimates for inundated conditions are based on 3- and 6-month experiments by R. E. Westerman of Pacific Northwest Laboratory (PNL) on ASTM A 366 and ASTM A 570 steels by WIPP Brine A when N_2 is present at low pressures (~ 0.105 MPa [150 psig]) (Brush, July 8, 1991, Memo [Appendix A]) (Figure 3.3-14). The following are estimated gas production and corrosion rates for inundated conditions: minimum, 0 mol H_2/m^2 steel/yr (0 mol H_2/drum/yr); best estimate, 0.2 mol H_2/m^2 steel/yr (1 mol/drum/yr); and maximum, 0.4 mol H_2/m^2 steel/yr (2 mol/drum/yr) with N_2 at 0.698 MPa (1000 psig) (Brush, July 8, 1991, Memo [Appendix A]).

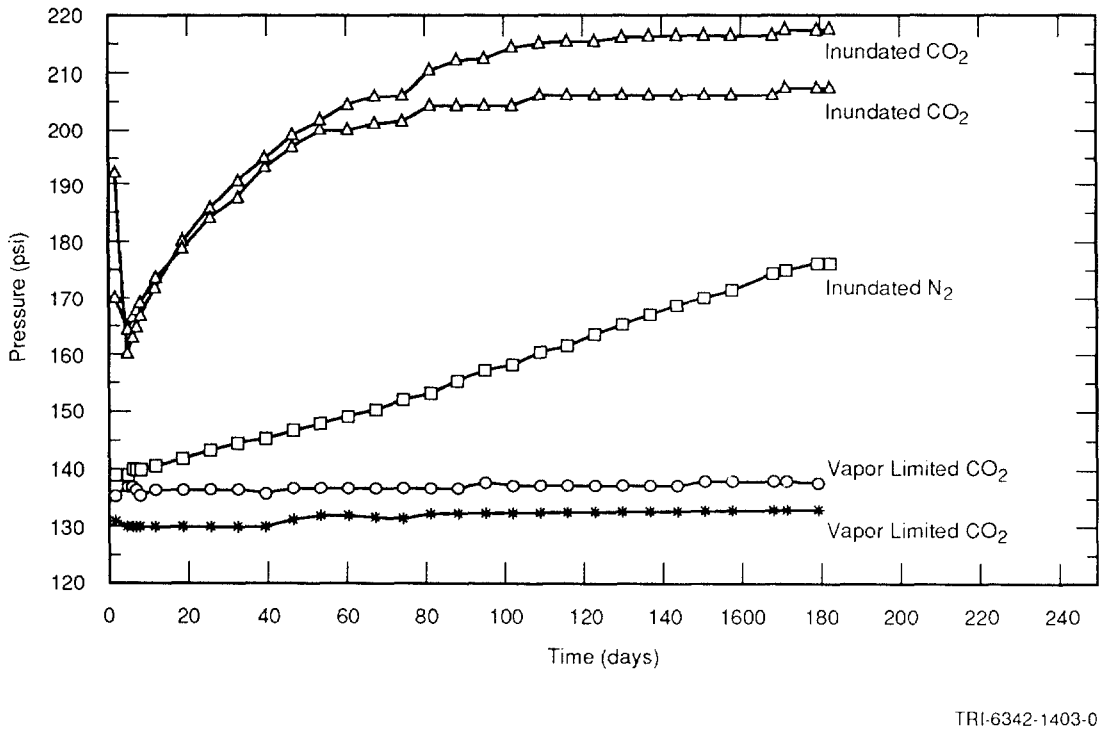

Figure 3.3-14. Pressure-Time Plots for 6-Month Anoxic Corrosion Experiments Under Brine-Inundated and Vapor-Limited ("Humid") Conditions (Davies et al., 1991).

Westerman also performed 3- and 6-month low-pressure humid experiments with either CO_2 or N_2 atmospheres (Brush, July 8, 1991, Memo [Appendix A]). No H_2 production was observed except for very limited quantities from corrosion of the bottom 10% of the specimens splashed with brine during pretest preparation of the containers. Westerman is currently quantifying H_2 production from anoxic corrosion of steels in contact with noninundated backfill materials; results are expected in late 1991. Until these results are available, the estimated rates for humid conditions are as follows: minimum, 0 mol H_2/m^2 steel/yr (0 mol H_2/drum/yr); best estimate, 0.02 mol H_2/m^2 steel/yr (0.1 mol H_2/drum/yr); and maximum, 0.2 mol H_2/m^2 steel/yr (1 mol H_2/drum/yr) with N_2 at 0.698 MPa (1000 psig) (Brush, July 8, 1991, Memo [Appendix A]). When expressed in terms of relative rates, the values are 0 to 0.5 with a median of 0.1.

Previous Simulations. Previous simulations used ficticious wells in the waste as a way to introduce reaction-generated gas. The various gas generation rates were assumed to be constant for a specified length of time after which the "wells" were turned off. However, the corrosion and biodegradation rates are dependent on brine saturation (distinguishing brine-inundated conditions from humid conditions). While it is not known if the biodegradation reactions will consume or produce water, it is believed that water will be consumed during corrosion and radiolysis.

Current Procedure. To handle the rate of reactant consumption (brine, steel, and cellulosics) and product generation (gas) in a more realistic fashion, chemical reactions, reaction mechanisms, kinetics, and stoichiometry are used in PA calculations (i.e., BRAGFLO) and replace the use of wells.

Anoxic Corrosion Stoichiometry. Brush and Anderson (Lappin et al., 1989, p. A-6) describe four possible anoxic corrosion reactions likely to occur when waste drums are exposed to WIPP brines:

$$Fe + 2H_2O = Fe(OH)_2 + H_2 \qquad (3.3\text{-}1)$$

$$3Fe + 4H_2O = Fe_3O_4 + 4H_2 \qquad (3.3\text{-}2)$$

$$Fe + H_2O = FeO + H_2 \qquad (3.3\text{-}3)$$

$$(x + y)Fe + (2(x + y) + z)H_2O + yNacl = xFe(OH)2.yFeOCl.zH_2O + yNa^+ + yOH^- + (x + 3y)H_2 \qquad (3.3\text{-}4)$$

Brush and Anderson believed that FeO would not be stable under low-temperature conditions, so reaction 3.3-3 was discounted. Sufficient data are not available to characterize reaction 3.3-4, so it, too, is ignored in current PA calculations.

The average stoichiometry of reactions 3.3-1 and 3.3-2 is

$$Fe + ((4+2x)/3)H_2O = ((4-x)/3)H_2 + (3x)Fe(OH)_2 + ((1-x)/3)Fe_3O_4 \qquad (3.3\text{-}5)$$

where x mole fraction of iron is consumed by reaction 3.3-1. The PA calculations sample the parameter x from a uniform distribution between 0 and 1.

Reaction Rate Constant. The reaction rate for corrosion under inundated conditions is sampled from the distribution shown in Figure 3.3-11, ranging from 0 to 0.4 mol H_2/m^2 steel/yr = 1.268 x 10^{-8} mol H_2/m^2 steel/s. The rate under humid conditions is sampled as a fraction of the inundated rate, the fraction ranging from 0 to 1, with the distribution shown in Figure 3.3-12. This forces the humid rate always to be less than the inundated rate as observed in preliminary tests (Figure 3.3-14).

For use in BRAGFLO, the corrosion rate (mol H_2/m^2) for both humid and inundated conditions is converted to units of mol Fe/m^3 panel/s by the following formula:

$$\mathfrak{n}_{CI} = (\mathfrak{n}'_{CI})(A_d)(n_d)/x_{CH2}/V_{pf} \qquad (3.3\text{-}6)$$

$$\mathfrak{n}_{CH} = (\mathfrak{n}'_{CH})(A_d)(n_d)/x_{CH2}/V_{pf} \qquad (3.3\text{-}7)$$

where

$\mathfrak{n}_{CH}$, $\mathfrak{n}_{CI}$ = humid and inundated corrosion reaction rate, respectively (mol Fe/m^3 panel/s)

$\mathfrak{n}'_{CH}$, $\mathfrak{n}'_{CI}$ = humid and inundated corrosion reaction rate, respectively (mol H_2/m^2 steel/s)

A_d = surface area of steel in an equivalent drum, including both the drum and its contents (Brush, July 8, 1991, Memo [Appendix A, p. A-25]) (6 m^2 steel/drum; 4.5 m^2 for drum surfaces alone)

n_d = number of equivalent drums per panel (6,804 drum/panel, Section 3.1.6)

x_{CH2} = stoichiometric coefficient in reaction 3.3-5
= (4-x)/3, where x is a sampled parameter (mol H_2/mol Fe)

V_{pf} = final enclosed volume of a panel (m^3 panel)
= $(V_{pI})(\Delta z_f/\Delta z_i)$

V_{pi} = initial enclosed volume of a panel (Table 3.1-1)
= (116.39 x 10^3 m^3 panel)

Δz_i = initial height of a panel (3.9624 m, Section 3.1.6)

Δz_f = final height of a gas-tight panel after the full potential of gas has been generated (see discussion under Waste Porosity Calculation, Section 3.4.8) (m)

Implicit in the use of average stoichiometry from Eq. 3.3-5 to determine a reaction rate is the assumption that each of the reactions (comprising the average) react at the same rate.

Model Usage. Collection of data describing the kinetic rate expressions for corrosion in the WIPP environment is continuing at this time. The available data suggest that as long as inundated conditions (liquid phase brine in contact with metal) exist, corrosion proceeds at a constant rate (e.g., in N_2 atmosphere and, at least early in the corrosion process, in a CO_2 atmosphere) (Figure 3.3-14). This suggests zero-order kinetics with respect to steel (independent of the steel concentration in the waste). Future data may suggest that the reaction rate may be a function of surface area, film resistance, gas pressure or gas composition. For the 1991 PA calculations, we assume that the rate of corrosion is independent of the parameters mentioned above as well as the concentration of steel in the waste.

Data also suggest that corrosion under humid conditions (no liquid phase brine in contact with metal) may proceed at a slower rate than that under inundated conditions. The humid rate could be dependent on the moisture content in the vapor which contacts the metal; however, in absence of data to support this, we assume that as long as brine is present the humid corrosion rate is independent of humidity. We further assume that any water consumed during corrosion under humid conditions is replenished from the brine pool as long as liquid phase brine is present.

Throughout the course of a calculation, BRAGFLO determines and uses an effective corrosion rate. Both the inundated and humid rate contribute to the effective rate. BRAGFLO calculates the effective corrosion rate from a weighted average of the inundated and humid rates. This weighting is assumed to be dependent on the portion of steel which is in contact with liquid and gas phases. BRAGFLO and numerical models in general are characterized by finite sized homogenous volumes of uniform properties called grid blocks. A typical grid block in the waste can be divided to include 4 material types: brine, gas, steel, and other (rock, backfill, other waste components, etc.) Since each block is assumed homogenous, the steel will be in contact with the brine, gas, steel, and "other." The portion of steel in contact with brine in a given grid block is assumed propotional to the volume fraction of brine in the block and similarly for the portions of steel in contact with gas, steel, and "other." These volume fractions are determined from porosity and saturation; brine volume fraction = $\phi\ s_\ell$, gas volume fraction = $\phi\ s_g$, and "other" (including steel) volume fraction = $1 - \phi$, where ϕ is the porosity (volume fraction of grid block that is void space), s_ℓ is the brine saturation (volume fraction of void space occupied by brine, and s_g is the gas saturation. The portion of steel in contact with brine is assumed to react at the inundated rate while the portion of steel in contact with gas reacts at the humid rate as long as there is some liquid phase brine present to be in equilibrium with the brine in the gas phase.

The portion of steel which is in contact with "other" does not corrode at all. The effective corrosion rate under these assumptions becomes

$$r_{Ce} = r_{CI}\ \phi\ s_\ell + r_{CH}\ \phi\ s_g + 0\ (1 - \phi) \qquad (3.3\text{-}8)$$

where

$\dot{n}_{Ce}$ = effective corrosion rate (moles of steel consumed/reservoir volume/second)

$\dot{n}_{CI}$ = inundated corrosion rate (mol/(m^3•s))

$\dot{n}_{CH}$ = humid corrosion rate (mol/(m^3•s))

Other expressions for obtaining an effective corrosion rate can be envisioned. For example, if the materials in a grid block are not uniformly distributed, all of the steel could always be in contact with either the brine phase or only the gas phase. In addition, moisture in the gas phase could condense on the metal. Nevertheless, Eq. 3.3-8 is used in BRAGFLO for the 1991 PA calculation to determine corrosion rate because (1) it is most consistent with the homogenous assumption, (2) no data are currently available to support any other relationship, and (3) it lies between the bounds set by fully inundated and humid conditions. It should be kept in mind that any uncertainty in the value of the effective rate calulated from Eq. 3.3-8 is captured by the large range of inundated and humid rate values sampled on during the calculations. It should further be pointed out that Eq. 3.3-8 implies that the corrosion rate will vary with time and position in the waste since porosity and saturation vary temporally and spatially. This is a departure from last year when corrosion rates were asumed to be constant in time and space.

The kinetic expression for inundated corrosion assuming zero-order kinetics with aspect to steel concentration in the waste is

$$k_{CI} = -\frac{\partial C_{Fe}}{\partial t} = \dot{n}_{CI} = -\dot{n}_{Fe} \qquad (3.3\text{-}9)$$

where

k_{CI} = rate constant for corrosion under inundated conditions (mole Fe/(m^3 panel•s))

$-\dot{n}_{Fe}$ = rate of steel consumption (mole Fe/(m^3 panel•s))

C_{Fe} = steel concentration (mole Fe/(m^3 panel)

A similar expression results for humid corrosion kinetics. A characteristic of zero-order kinetics is that the rate constant has the same units as the reaction rate (r_{CI}).

From Eqs. 3.3-8 and 3.3-9, the amount of iron per unit volume of panel consumed by corrosion is given by

$$(C_{Fe}^{k+1} - C_{Fe}^{k}) = (k_{CI}\ \phi\ s_{\ell} + k_{CH}\ \phi\ s_{g})\ \Delta t \qquad (3.3\text{-}10)$$

where

Δt = the time step size (s)
k = the time step level

The amount of gas produced and brine consumed by corrosion over a specified time step depends on the rate constant and stoichiometry of reaction. Assuming the stoichiometry of Eq. 3.3-5 remains valid for both humid and inundated conditions and the effective corrosion reaction rate is determined as in Eq. 3.3-8, the rate of gas production and water consumption are calculated from Eqs. 3.3-11 and 3.3-12, respectively.

$$q_{CH_2} = (k_{CI}\ \phi\ s_{\ell} + k_{CH}\ \phi\ s_{g})\ (x_{CH_2})(M_{H_2}) \qquad (3.3\text{-}11)$$

$$q_{CH_2O} = (k_{CI}\ \phi\ s_{\ell} + k_{CH}\ \phi\ s_{g})\ (x_{CH_2O})(M_{H_2O}) \qquad (3.3\text{-}12)$$

where

q_{CH_2} = rate of H_2 produced from corrosion per unit volume of panel (kg/m^3s)

q_{CH_2O} = rate of H_2O consumed by corrosion per unit volume of panel (kg/m^3s)

x_{CH_2} = corrosion stoichiometry for H_2 = (4 - x)/3 (see Eq. 3.3-5)

x_{CH_2O} = corrosion stoichiometry for H_2O = -(4 + 2x)3 (see Eq. (3.3-5)

M_{H_2} = molecular weight for H_2(kg/gmol)

M_{H_2O} = molecular weight for H_2O (kg/gmol)

Since we are concerned with brine removal rather than water, we convert the water consumption rate of Eq. 3.3-12 to that of brine using Eq. 3.3-13.

$$q_{cb} = (q_{CH_2O})/(1.0 - w_s) \qquad (3.3\text{-}13)$$

where

q_b = rate of brine consumption (kg brine/(m^3 panel • s)

w_s = weight fraction of NaCl in brine (kg NaCl/kg brine) assumed to be 25%

We do not adjust the salinity of the brine nor do we deposit salt in the pore space as water is consumed. The corrosion reaction rates, the concentration of steel, and the rates of production and consumption of the various species are computed in BRAGFLO as outlined above.

3.3.9 Gas Production from Microbiological Degradation

Parameter:	**Gas production rates, microbiologial, inundated rate**
Median:	3.2×10^{-9}
Range:	0
	1.6×10^{-8}
Units:	mol gas/kg cellulosics/s
Distribution:	Cumulative
Source(s):	Brush, L. H. 1991. "Current Estimates of Gas Production Rates, Gas Production Potentials, and Expected Chemical Conditions Relevant to Radionuclide Chemistry for the Long-Term WIPP Performance Assessment," Internal memo to D.R. Anderson (6342), July 8, 1991. Albuquerque, NM: Sandia National Laboratories. (In Appendix A of this volume)

Parameter:	**Gas production rates, microbiologial, relative humid rate**
Median:	1×10^{-1}
Range:	0
	2×10^{-1}
Units:	Dimensionless
Distribution:	Cumulative
Source(s):	Brush, L. H. 1991. "Current Estimates of Gas Production Rates, Gas Production Potentials, and Expected Chemical Conditions Relevant to Radionuclide Chemistry for the Long-Term WIPP Performance Assessment," Internal memo to D.R. Anderson (6342), July 8, 1991. Albuquerque, NM: Sandia National Laboratories. (In Appendix A of this volume)

Parameter:	**Gas generation, stoichiometry factor**
Median:	8.35×10^{-1}
Range:	0
	1.67
Units:	Dimensionless
Distribution:	Uniform
Source(s):	Brush, L. H. and D. R. Anderson. 1989. In Lappin et al., 1989. *Systems Analysis Long-Term Radionuclide Transport and Dose Assessments, Waste Isolation Pilot Plant (WIPP), Southeastern New Mexico; March 1989.* SAND89-0462. Albuquerque, NM: Sandia National Laboratories.

Figures 3.3-15 and 3.3-16 provide distributions for gas production rates from microbiological degradation under inundated and humid conditions, respectively.

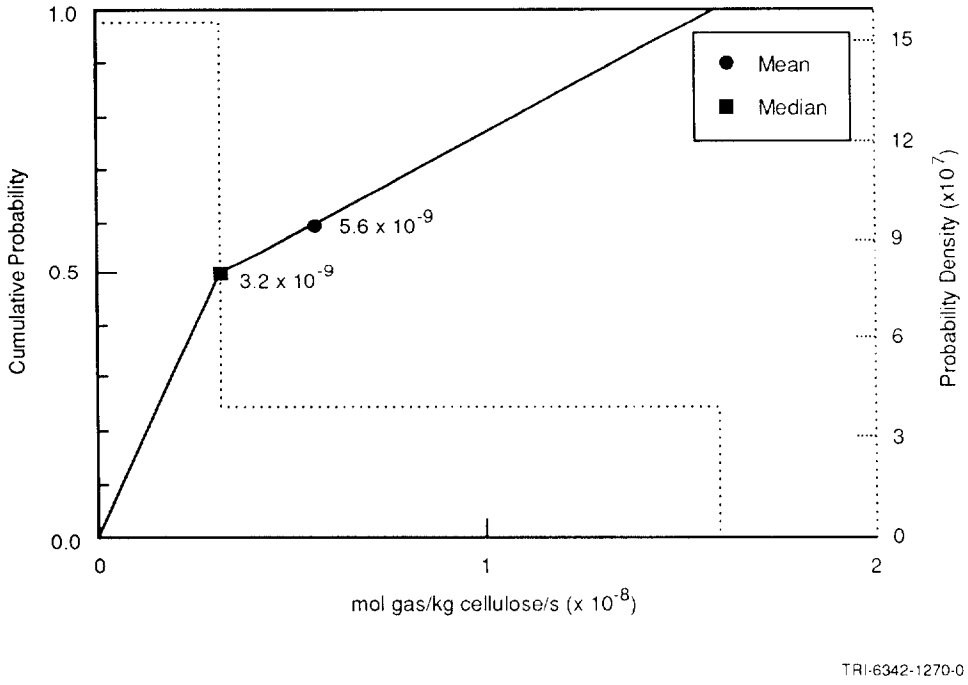

Figure 3.3-15. Estimated Distribution (pdf and cdf) for Gas Production Rates from Microbiological Degradation under Inundated Conditions.

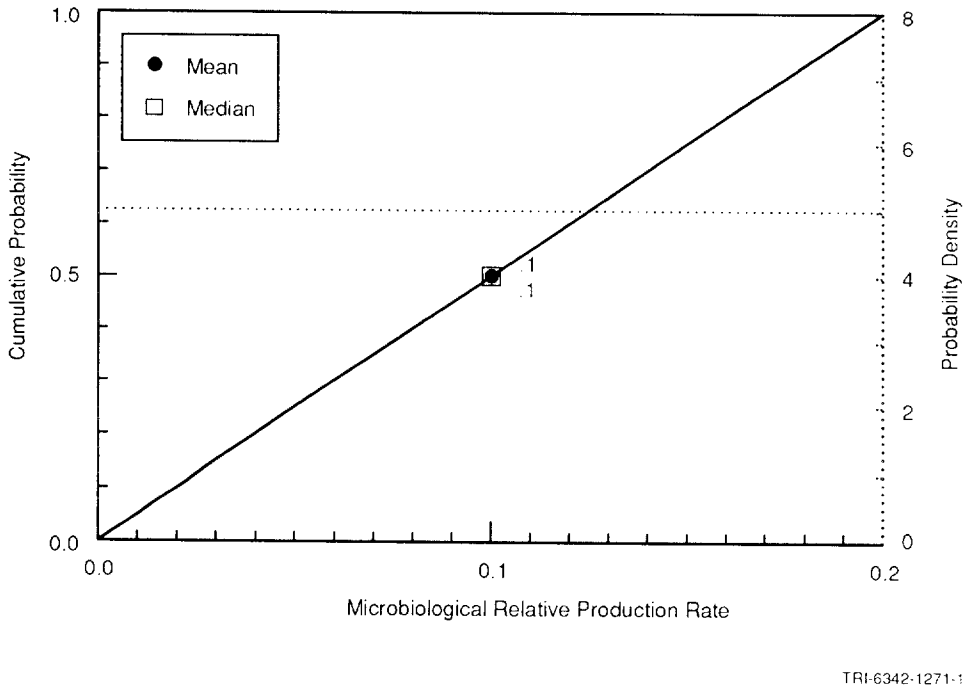

Figure 3.3-16. Estimated Distribution (pdf and cdf) for Relative Gas Production Rates from Microbiological Degradation under Humid Conditions.

Discussion:

Brush (July 8, 1991, Memo [Appendix A]) estimates activity from microbiological degradation based on a recent study at Stanford University and studies carried out during the 1970s (Barnhart et al., 1980; Caldwell, 1981; Caldwell et al., 1988; Molecke, 1979; Sandia National Laboratories, 1979). A test plan for laboratory experiments (Brush, 1990) and in-situ gas production experiments using real waste at the WIPP (Lappin et al., 1989) describe experiments currently underway. Although the Stanford tests seemed to suggest that microbial gas production may be significant under overtest conditions but not under realistic conditions, results from the earlier tests implied significant microbial gas production under both realistic and overtest conditions. However, until the Stanford tests are corroborated, the best estimate for microbial gas production has remained the same as first proposed by Brush and Anderson (in Lappin et al., 1989; Brush, 1990), 0.1 mole of various gases per kg cellulosics per year (1 mol gas/(drum•yr)). However, new minimum and maximum rates for inundated conditions are 0 and 0.5 mol/(kg•yr) (5 mol per drum per year), respectively.

For humid conditions, new minimum and best estimates for microbial gas production rates are 0 and 0.01 mol/(kg cellulosics•yr) (0.1 mol/(drum•yr)). The maximum estimate under humid conditions remains unchanged from the value estimated by Brush and Lappin (1990), 0.1 mol/(kg•yr) (1 mol/(drum•yr)). Expressed in terms of relative rates, the values are 0 to 0.2 with a median of 0.1.

Microbiologic Degradation Stoichiometry. The stoichiometry of the net biodegradation reaction is uncertain. About 20 reactions have been postulated and others may be possible, according to Brush and Anderson (Lappin et al., 1989, p. A-10). The reactions depend on such factors as what electron donors are available, the solubility of CO_2, interaction with products of corrosion, pH, and Eh. It is not known at this time what effect biodegradation has on water (brine) inventory, so it is assumed to have no net effect, neither consuming water nor producing it. Some of the postulated reactions produce gas; others consume it. At present, we know that some gas (CO_2 and some H_2, H_2S, and CH_4) may be produced and that cellulose (CH_2O) will be consumed. Using the stoichiometry recommended in Lappin et al. (1989, Supplement to Appendix A.1, p. A-30) that yields the maximum gas generation per unit of cellulose (5/3 mol gas/mol CH_2O), the biodegradation reaction may be written

$$CH_2O + \text{unknowns} + \text{microbes} = 5/3 \text{ gas} + \text{unknowns} \qquad (3.3\text{-}14)$$

However, in view of the wide variety of reactions that may occur, together with our current lack of knowledge as to precisely which reactions do occur, it is prudent to sample on the stoichiometric coefficient for gas in reaction 3.3-14. If the assumption is also made that any CO_2 that is produced will dissolve in the WIPP brine, then of the reactions presented in Lappin et al., (1989) only one reaction will consume gas, that one being

$$CH_2O + O_2 = H^+ + HCO^{3-} \qquad (3.3\text{-}15)$$

This reaction requires oxygen, which will be present initially in air and will be produced by radiolysis. Neither source of oxygen is sufficient to oxidize all of the cellulose in the inventory, and oxic corrosion will compete strongly for this oxygen, so this reaction is expected to be of minor importance. None of the other reactions consumes gas, whereas most produce gas, with the net gas production ranging from 0 to 5/3 mol gas/mol CH_2O. Therefore, the stoichiometric coefficient is sampled from a uniform distribution ranging from 0 to 5/3.

Model Usage. As with corrosion, the rate of gas generation from the biodegradation of cellulosics differs depending on whether inundated or humid conditions exist in the repository. In BRAGFLO an effective rate of biodegradation is calculated, as described in the previous corrosion rate discussion, from a weighted average of the inundated and humid rates.

There are insufficient data available at this time to quantify any biodegradation kinetics other than zero-order kinetics with respect to the concentration of cellulosic in the waste panel (rate is independent of the concentration of cellulosics). One might expect the reaction rate to depend in some way on the concentration of the reactants (organisms and cellulose) and perhaps on the concentration or partial pressure of the products as well as the gas composition, all of which vary with time. However, until such data become available, we use the zero-order assumption.

The kinetic expression for inundated biodegradation assuming zero-order kinetics with respect to the concentration of cellulosics in the waste panel is

$$k_{BI} = -\frac{\partial C_c}{\partial t} = \dot{n}_{BI} = -\dot{n}_c \qquad (3.3\text{-}16)$$

where

k_{BI} = rate constant for biodegradation under inundated conditions [mol/(m³•s)]

$-\dot{n}_c$ = consumption rate of cellulosics [mol/(m³•s)]

$\dot{n}_{BI}$ = Reaction rate for biodegradation under inundated conditions [mol/(m³•s)]

C_c = Concentration of cellulosics (mol/m³ of panel)

A similar expression results for the humid biodegradation kinetics.

The amount of cellulosics consumed and the rate of gas production follow from a development similar to that outlined in the corrosion section, Eqs. 3.3-17 and 3.3-18, respectively.

$$(C_c^{k+1} - C_c^k) = (k_{BI}\ \phi\ s_\ell + k_{BH}\ \phi\ s_g)\Delta t \qquad (3\text{-}3.17)$$

$$q_{BH_2} = (k_{BI}\ \phi\ s_\ell + k_{BH}\ \phi\ s_g)\ (s_{BH_2})(M_{wc}) \qquad (3\text{-}3.18)$$

where

q_{BH_2} = rate of H_2 produced from biodegradation per unit volume [kg/(m^3•s)]

s_{BH_2} = biodegradation stoichiometry for H_2 (moles H_2 produced/moles cellulosics consumed)

(See Section 3.3.8 for definitions of remaining variables.)

Because some potential biodegradation reactions consume water while others produce water and in absence of any experimental data, we currently assume that biodegradation does not impact brine inventory. The reaction rates, cellulosics concentration, and the rates of production and consumption of the various species are calculated in BRAGFLO as described above.

3.3.10 Radiolysis

Parameter:	**Radiolysis of brine**
Median:	1×10^{-4}
Range:	1×10^{-7}
	1×10^{-1}
Units:	mol/drum/yr
Distribution:	Constant
Source(s):	Brush, L. H. 1991. "Current Estimates of Gas Production Rates, Gas Production Potentials, and Expected Chemical Conditions Relevant to Radionuclide Chemistry for the Long-Term WIPP Performance Assessment," Internal memo to D.R. Anderson (6342), July 8, 1991. Albuquerque, NM: Sandia National Laboratories. (In Appendix A of this volume)

Early indications from experimental data that are currently being collected show that the rate of gas production from radiolysis is very small compared to that from corrosion and biodegradation. A current study is investigating gas production at low pressures by alpha radiolysis of WIPP Brine A as a function of dissolved plutonium concentration (Brush, July 8, 1991, Memo [Appendix A]). Small linear pressure increases from the solution with the highest dissolved plutonium concentration, 1×10^{-4} M, have been observed but there are not enough data to convert these rates to moles of gas per drum per year. Pressure increases were not observed with lower dissolved plutonium concentrations (1×10^{-6} and 1×10^{-8} M). Two-month runs with a dissolved plutonium concentration of 1×10^{-4} M in other WIPP brines are planned.

Until results are available from longer term studies, the radiolytic gas production rates are the same as those proposed by Brush and Lappin (1990): minimum, 1×10^{-7} mole/gases/drum/yr; best estimate, 1×10^{-4} mol/drum/yr, and maximum of 1×10^{-1} mol/drum/yr.

The PA calculations do not separately break out the radiolysis reaction, but will include its contribution to gas generation in the biodegradation reaction. Furthermore, we neglect the consumption of brine by radiolysis.

3.4 Parameters for Unmodified Waste Form Including Containers

As of 1990, the currently stored CH-TRU waste that will be disposed of in the WIPP, if authorized, is estimated to be about 60,000 m^3 (2.1 x 10^6 ft^3), which is about 34% of the design storage volume of 170,000 m^3 (6.2 x 10^6 ft^3). The stored waste consists of about 110,000 0.21-m^3 (55-gal) drums, 5,000 1.8-m^3 (64 ft^3) Standard Waste Boxes (SWBs), and 7,000 3.2-m^3 (113-ft^3) miscellaneous containers, mostly steel and fiberglass reinforced wood boxes. Drums and SWBs are the only containers that can currently be transported in a TRUPACT-II. If the waste in boxes other than SWBs were repackaged into SWBs, it was estimated that 533,000 0.21-m^3 (55-gal) drums and 33,500 1.8-m^3 (64-ft^3) SWBs could be emplaced in the WIPP repository containing 170,000 m^3 (6.2 x 10^6 ft^3) of waste, the design volume for CH-TRU waste.

The volume of RH-TRU waste is limited by the agreement between DOE and the State of New Mexico to 7,079 m^3 (0.25 x 10^6 ft^3) (U.S. DOE and NM, 1984). RH waste will likely be placed in 0.89-m^3 (31.4-ft^3) canisters in the walls of the rooms and access drifts. (Placement of canisters is discussed in Section 3.1.6.)

The parameter values for unmodified waste that is expected to be shipped (i.e., to meet the current waste acceptance criteria discussed below) are provided in Table 3.4-1. The basis for these values is provided in the tables included in this section (see Tables 3.4-3 through 3.4-14). However, the significant figures for masses that are reported in these tables should not be interpreted as known accuracy. (Indeed, the majority of waste to be emplaced in the WIPP has not been generated; hence, the amounts are uncertain.) The significant figures in the tables for masses are presented as a means to trace the work until a report detailing the assumptions and calculations pertaining to these amounts has been prepared. On the other hand, the significant figures on design volumes are important since the limits on volumes agreed upon by the DOE and the State of New Mexico (U.S. DOE and NM, 1984) were in English units and are an exact conversion.

All CH- and RH-TRU waste must meet the WIPP *Waste Acceptance Criteria* (WEC, 1989). This criteria includes requirements for the waste form. For example, the waste material shall (1) include only residual liquids in well-drained containers and limit this waste to less than 1% (volume), (2) not permit explosives or compressed gases, and (3) limit radionuclides in pyrophoric form to less than 1% by weight in each waste package. There also are limitations on the curie content in a drum, SWB, and canister based on transportation considerations (Table 3.4-2). These criteria were summarized from a draft of the *TRU Waste Acceptance Criteria for the Waste Isolation Pilot Plant*, Revision 4, WIPP-DOE-069.

Table 3.4-1. Parameter Values for Unmodified TRU Waste Categories, Containers, and Salt Backfill

Parameter	Median	Range		Units	Distribution Type	Source
CH Waste						
Molecular weight						
Cellulose	0.030			kg/mol	Constant	CH_2; Weast and Astle, 1981
Iron	0.05585			kg/mol	Constant	Fe; Weast and Astle, 1981
Density, grain (ρ_g)						
Metal/glass	3.44×10^3			kg/m^3	Constant	Butcher, 1990, Table 2
Combustibles	1.31×10^3			kg/m^3	Constant	Butcher, 1990, Table 2
Sludge	2.15×10^3			kg/m^3	Constant	Butcher, 1990, Table 2
Salt backfill	2.14×10^3			kg/m^3	Constant	See Table 2.3-1
Steel, cold-drawn	7.83×10^3			kg/m^3	Constant	Perry et al., 1969, Table 3-137
Air @ 300.15K, 1 atm	1.177			kg/m^3	Constant	Vennard and Street, 1975, p. 709
Volumes of IDB Categories						
Metal/glass fraction	3.76×10^{-1}	2.76×10^{-1}	4.76×10^{-1}	none	Normal	See Table 3.4-10
Combustibles fraction	3.84×10^{-1}	2.84×10^{-1}	4.84×10^{-1}	none	Normal	See Table 3.4-10
Salt backfill	1.712×10^5			m^3	Constant	See Figure 3.1-3
Air @ 300.15K, 1 atm	8.908×10^4			m^3	Constant	See Figure 3.1-3
Average per Drum						
Metal/glass	6.44×10^1	3.05×10^1	9.83×10^1	kg/drum	Normal	Butcher, 1989, Table 7
Combustibles	4.00×10^1	1.73×10^1	6.26×10^1	kg/drum	Normal	Butcher, 1989, Table 6
Sludge	2.25×10^2			kg/drum	Constant	See Table 3.4-10
Mass of IDB Categories						
Metal/glass	1.984×10^7					See Tables 3.4-10 and 3.4-12
Combustibles	1.348×10^7					See Tables 3.4-10 and 3.4-12
Mass of Steel Containers in IDB Categories						
Metal/glass	1.076×10^7			kg	Constant	See Table 3.4-10
Combustibles	1.178×10^7			kg	Constant	See Table 3.4-10
Sludge	3.598×10^6			kg	Constant	See Table 3.4-10
Mass of Steel Containers and Liners in IDB Categories						
Metal/glass	4.458×10^6			kg	Constant	See Table 3.4-10
Combustibles	1.214×10^7			kg	Constant	See Table 3.4-10
Sludge	1.329×10^7			kg	Constant	See Table 3.4-10
Mass of Contents						
Iron, steel, paint cans, shipping cans	1.431×10^7			kg	Constant	See Table 3.4-12
Steel in containers	2.613×10^7			kg	Constant	See Table 3.4-10
Cellulosics, + 50% gloves, Hypalon, Neoprene, rubber	7.475×10^6			kg	Constant	See Table 3.4-12
Capillary pressure (p_c) and relative permeability ($k_{\ell r}$)						
Threshold displacement pressure (p_t)	2.02×10^3	2.02×10^1	2.02×10^5	Pa	Lognormal	Davies, 1991; Davies, June 2, 1991, Memo (see Appendix A)
Residual Saturations						
Wetting phase ($S_{\ell r}$)	2.76×10^{-1}	1.38	5.52×10^{-1}	none	Cumulative	Brooks and Corey, 1964
Gas phase (S_{gr})	7×10^{-2}	3.5×10^{-2}	1.4×10^{-1}	none	Cumulative	Brooks and Corey, 1964
Brooks-Corey Exponent (η)	2.89	1.44	5.78	none	Cumulative	Brooks and Corey, 1964

Table 3.4-1. Parameter Values for Unmodified TRU Waste Categories, Containers, and Salt Backfill (Concluded)

Parameter	Median	Range		Units	Distribution Type	Source
Drilling Erosion Parameters						
Absolute roughness (ε)	2.5×10^{-2}	1×10^{-2}	4×10^{-2}	m	Uniform	Streeter and Wylie, 1975, Figure 5.32.
Shear strength (τ_{fail})	1	1×10^{-1}	1×10^{1}	Pa	Cumulative	Sargunam et al., 1973; Henderson, 1966
Partition Coefficient for clays in salt backfill						
Am	1×10^{-4}			m^3/kg	Constant	Lappin et al., 1989, Table D-5 ($K_{dclay}/1000$)
Np	1×10^{-5}			m^3/kg	Constant	Lappin et al., 1989, Table D-5 ($K_{dclay}/1000$)
Pb	1×10^{-6}			m^3/kg	Constant	Lappin et al., 1989, Table D-5 ($K_{dclay}/1000$)
Pu	1×10^{-4}			m^3/kg	Constant	Lappin et al., 1989, Table D-5 ($K_{dclay}/1000$)
Ra	1×10^{-6}			m^3/kg	Constant	Lappin et al., 1989, Table D-5 ($K_{dclay}/1000$)
Th	1×10^{-4}			m^3/kg	Constant	Lappin et al., 1989, Table D-5 ($K_{dclay}/1000$)
U	1×10^{-6}			m^3/kg	Constant	Lappin et al., 1989, Table D-5 ($K_{dclay}/1000$)
Permeability (k)						
Average	1×10^{-13}			m^2	Constant	Lappin et al., 1989, Table 4-6
Combustibles	1.7×10^{-14}	2×10^{-15}	2×10^{-13}	m^2	Cumulative	Butcher et al., 1991
Metals/glass	5×10^{-13}	4×10^{-14}	1.2×10^{-12}	m^2	Cumulative	Butcher et al., 1991
Sludge	1.2×10^{-16}	1.1×10^{-17}	1.7×10^{-16}	m^2	Cumulative	Butcher et al., 1991
Porosity (ϕ)						
Average	1.9×10^{-1}			none	Constant	See text; Butcher, 1990; Lappin et al., 1989, Table 4-6
Combustibles	1.4×10^{-2}	8.7×10^{-2}	1.8×10^{-1}	none	Data	Butcher et al., 1991
Metals/glass	4×10^{-1}	3.3×10^{-1}	4.4×10^{-1}	none	Data	Butcher et al., 1991
Sludge	1.1×10^{-1}	1×10^{-2}	2.2×10^{-1}	none	Data	Butcher et al., 1991
Saturation, initial ($S_{\ell i}$)	1.38×10^{-1}	0	2.76×10^{-1}		Uniform	See text.

Table 3.4-2. Summary of Waste Acceptance Criteria and Requirements Applicable to Performance Assessment

Description	Waste Type	WAC Criterion or Requirement
Particulates	CH	Immobilize if greater than 1% by weight below 10 microns
	RH	Immobilize if greater than 15% by weight below 200 microns
Liquids	CH & RH	Liquids that result from liquid residues remaining in well-drained containers; condensation moisture; and liquid separation from sludges or resin settling shall be less than 1% by volume of the waste container
Pyrophoric Materials	CH	Radionuclides in pyrophoric form are limited to less than 1% by weight in each waste package. No non-radionuclide pyrophorics permitted.
	RH	
Explosives and compressed gas	CH & RH	No explosives or compressed gases are permitted.
Specific Activity	CH	The specific activity shall be greater than 100 nCi/g TRU radionuclides, excluding the weight of added shielding, rigid liners, and waste containers.
	RH	The specific activity shall be greater than 100 nCi/g TRU radionuclides, excluding the weight of external shielding, rigid liners, and the waste containers. The container average maximum activity concentration shall not exceed 23 curies/liter.
Nuclear Criticality* (Pu-239 FGE)**	CH	The fissile or fissionable radionuclide content shall be less than 200 FGE for a 55-gallon drum. The fissile or fissionable radionuclide content shall be less than 325 FGE for a SWB. The fissile or fissionable radionuclide content shall be less than 325 FGE for a TRUPACT-II
	RH	The fissile or fissionable radionuclide content shall be less than 325 FGE.
Pu-239 Activity*	CH & RH	Waste packages shall not exceed 1000 Ci to Pu-239 equivalent activity.

* Transportation requirement
** Fissile gram equivalent of Pu-239

3.4.1 Composition of CH-TRU Contaminated Trash (Non-Radionuclide/ Non-RCRA Inventory)

TRU waste destined for the WIPP is generated or currently stored by ten DOE nuclear weapon facilities. Although we know that this TRU waste consists in general of laboratory and production line trash, such as glassware, metal pipes, solvents, disposal laboratory clothing, cleaning rags, and solidified sludges, the precise composition of the trash (e.g., percentages by weight and volume) is not well defined. Estimates of metals/glass combustible and sludge reported here were made based on information on volumes submitted annually to the IDB by the generator sites and therefore are from the same source as the radionuclide inventory. (A potential source in the future is the data collected specifically for the PA Division from the generators.)

Volumes of Various Categories of CH-TRU Contaminated Trash

Parameter:	**Volume fraction, combustibles**
Median:	3.84
Range:	2.84
	4.84
Units:	Dimensionless
Distribution:	Normal
Source(s):	See text and Table 3.4-10.

Parameter:	**Volume fraction, metals/glass**
Median:	3.76
Range:	2.76
	4.76
Units:	Dimensionless
Distribution:	Normal
Source(s):	See text and Table 3.4-10.

Parameter:	**Volume, backfill**
Median:	1.712×10^5
Range:	None
Units:	m^3
Distribution:	Constant
Source(s):	See Figure 3.1-3 and text.

Parameter:	**Air @ 300.15 K, 1 atm**
Median:	8.908×10^4
Range:	None
Units:	m^3
Distribution:	Constant
Source(s):	See Figure 3.1-3 and text.

Figure 3.4-1 indicates CH waste volumes by site and status.

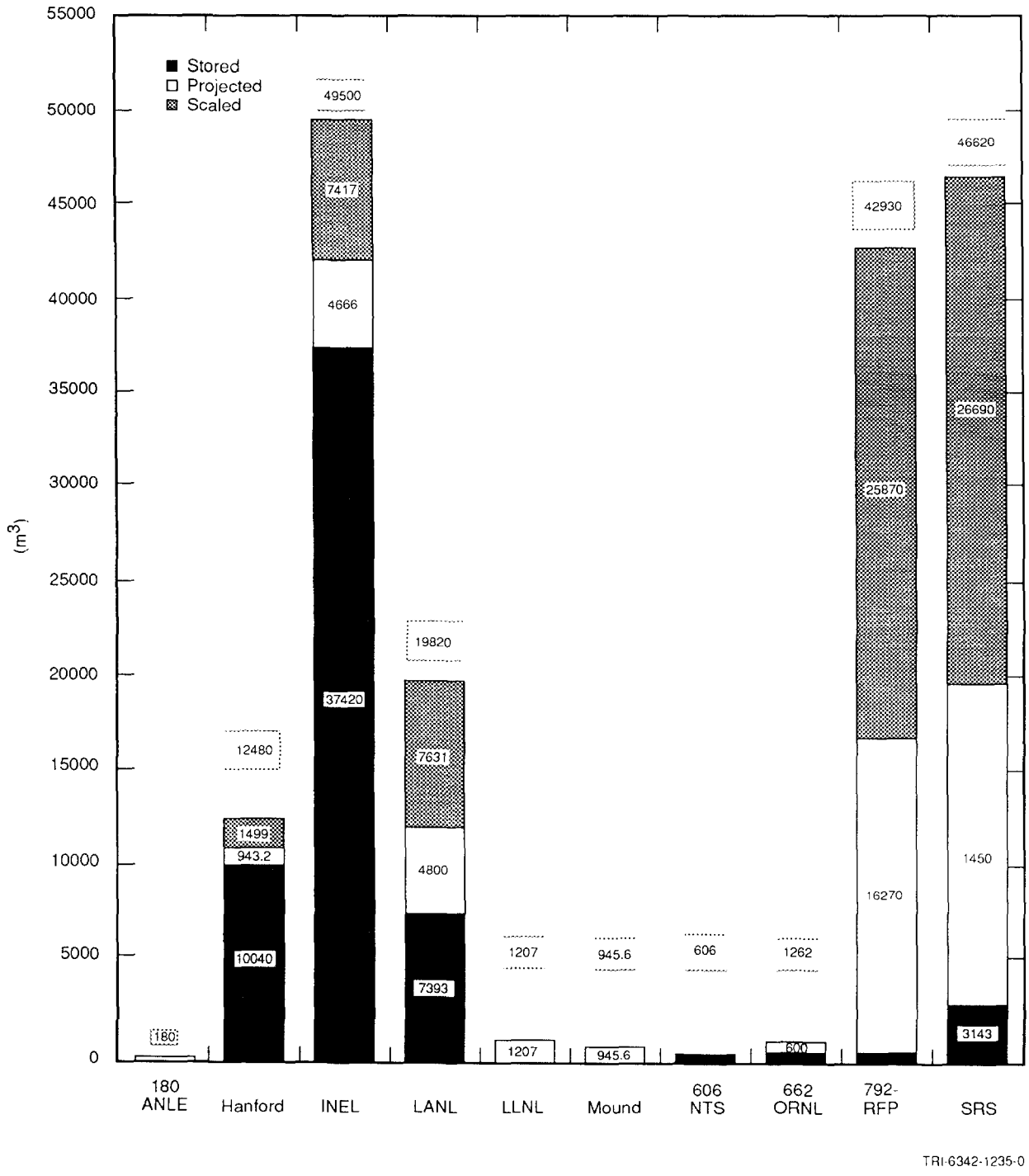

Figure 3.4-1. Estimates of CH Waste Volumes by Site and Status

Discussion:

Estimates of the masses and volumes of the constituents of TRU waste that affect gas generation, transport, and room properties are required for performance assessment. Since the majority of the waste to be emplaced in the WIPP has not been generated, the waste characterization is an estimate with a potentially large uncertainty. The estimated waste characterization is used as a base for analyses that include the uncertainty in waste characterization. The following discussion presents the method that was used to estimate the characterization of the waste. The intent was to use available information and to use a reasonable method to scale it up to a design volume, which was used in performance assessment. This method resulted in estimates of volumes and masses of waste by generator site; however, these results should not necessarily be considered as indicative of the actual masses and volumes that the sites will generate.

The total anticipated volume (stored waste and projected annual volumes) of the TRU waste calculated from information reported in the yearly IDB has been decreasing over the last four years (Table 3.4-3 and Figure 3.4-2). The most significant change from 1987 to 1990 is the percentage of concreted or cemented sludge; the estimated volume decrease was about 30%. Furthermore, the information contained in the 1990 IDB indicates that generators anticipate there will be less volume of absorbed sludges and more volume of concreted and cemented sludges in the projected waste than is contained in the stored waste.

The 1990 IDB was used as the basis for the estimate of the total volume of CH-TRU waste for the 1991 PA calculations. Table 3.4-4 lists the stored and projected (generated in the future) waste volume by generator site listed in the 1990 IDB. The IDB uses the terms "stored" and "newly generated" waste. In the discussion that follows, the term "projected" is used in place of "newly generated."

For performance assessment calculations, we assume that a design volume of 175,564 m^3 (6.2 x 10^6 ft^3) will be emplaced in the WIPP. The following discussion presents the method that was used to estimate the volumes of the waste types if the current design volume of waste was emplaced. To estimate the volume of waste by generator site to fill the WIPP, it was assumed that the five largest generators* of projected waste would provide the additional volume. The percentage of the total projected waste for each site was calculated and, based on this percentage, volumes for the five sites were calculated to provide an additional 69,105 m^3 (2.4 x 10^6 ft^3). The scaled volume for the five sites is shown in Table 3.4-4.

Details of the volumes and physical composition of CH waste as calculated from the information from the 1990 IDB (Tables 3.5, 3.7, and 3.10) are listed in Table 3.4-5.

* These five DOE defense facilities for 1990 are Hanford Reservation (HANF), Washington; Idaho National Engineering Laboratory (INEL), Idaho; Los Alamos National Laboratory (LANL), New Mexico; Rocky Flats Plant (RFP), Colorado; and Savannah River Site (SRS), South Carolina. In 1991, INEL was reclassified as a storage site rather than a generator site because a project that would generate waste was indefinitely delayed/cancelled.

For performance assessment calculations, room properties are required. To estimate the volume fraction of the sludges, combustibles, and metals and glass in CH waste, it was assumed the volume of the sludges included the absorbed liquid and sludges, concreted or cemented sludges, and dirt, gravel and asphalt categories of Table 3.4-5. The volume of filter, filter media, and "other" categories of Table 3.4-5 were distributed into the volume of sludges, combustibles, and metals and glass based on the relative volume of the initial amounts of each of these categories. Estimates for the volume fraction of stored; projected; projected plus scaled; and stored, projected, and scaled are tabulated in Table 3.4-6. The $\pm 10\%$ ranges on the volume fractions for the various categories in Table 3.4-6 were based on the historical change observed in the categories over the past 4 yr (Table 3.4-3; Figure 3.4-2).

Table 3.4-3. Estimated Composition by Volume of CH-TRU Contaminated Trash from 1987 to 1990.

	Combustibles (%)	Metal and Glass (%)	Absorbed Liquid and Sludge (%)	Concrete/ Cemented Sludge (%)	Dirt/ Gravel/ Asphalt (%)	Filters/ Filter Media (%)	Other (%)	Total Volume* (m^3)
1987	38.87	31.53	8.99	7.37	1.33	5.81	6.11	158,526
1988	39.84	34.18	7.28	8.00	2.44	4.53	3.73	136,402
1989	32.01	36.41	6.09	16.41	1.31	3.00	4.78	120,243
1990	34.24	34.31	6.28	14.43	1.30	3.67	5.77	106,459

* Design volume is 175,564 m^3.

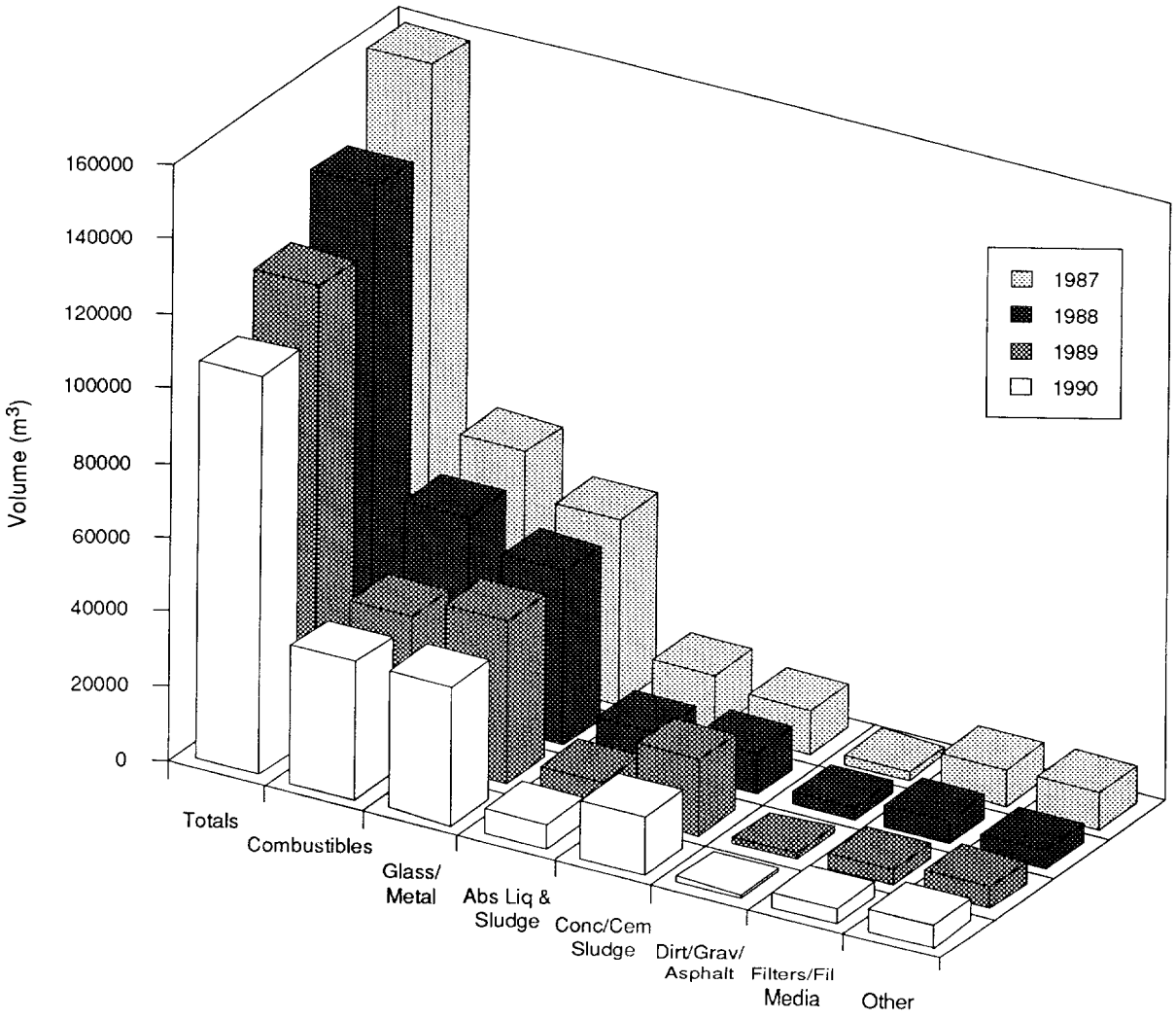

TRI-6342-1236-0

Figure 3.4-2. Changes in Volume Estimates of CH-TRU Contaminated Trash Between 1987 and 1990.

Table 3.4-4. Estimate of a Design Volume for CH-TRU Waste

Site	Stored Volume (1990 IDB) (m^3)	Projected Volume (1990 IDB) (m^3)	Total Volume (1990 IDB) (m^3)	Scaled Volume* (m^3)	Estimated Design Volume (m^3)
ANL-E	--	180	180	--	180
HANF	10,041	943	10,984	1,499	12,484
INEL	37,420	4,666	42,086	7,417	49,503
LANL	7,393	4,800	12,193	7,631	19,824
LLNL	--	1,207	1,207	--	1,207
MOUND	--	945	945	--	945
NTS	606	--	606	--	606
ORNL	662	600	1,262	--	1,262
RFP	792	16,272	17,064	25,869	42,933
SRP	3,143	16,788	19,931	26,689	46,620
Total	60,057	46,402	106,459	69,105	175,564

* Assuming that HANF, INEL, LANL, RFP, and SRP provide the difference between the current total inventory and the design volume. The difference between the total volume of 106,458 m^3 in the 1990 IDB and the design volume of 175,564 m^3 (6.2×10^6 ft^3) was ratioed between the five sites based on their estimated annual generation rates. These five sites provide 94% of the estimated total annual volume of 1,993.4 m^3 per year.

Table 3.4-5. Estimated Composition of CH-TRU Contaminated Trash in 1990 by Generator (IDB, 1990, Tables 3.5, 3.7, 3.10)

Category	ANL-E	HANF	INEL	LANL	LLNL	NTS	MOUND	ORNL	RFP	SRS	Percent	Total (m^3)	Percent of Total
STORED													
Absorbed Liquid and Sludge	--	0.0	4490.4	1626.5	--	0.0	--	0.0	122.8	0.0	10.39	--	--
Combustibles	--	4317.6	9355.0	961.1	--	312.2	--	390.3	287.5	2200.1	29.68	--	--
Concreted or Cemented Sludge	--	602.5	4864.6	2217.9	--	6.1	--	0.0	5.5	0.0	12.82	--	--
Dirt, Gravel, or Asphalt	--	301.2	0.0	0.0	--	0.0	--	6.6	5.5	0.0	0.52	--	--
Filters or Filter Media	--	0.0	1871.0	369.7	--	0.0	--	33.1	327.1	0.0	4.33	--	--
Glass/Metal/Similar Noncombustibles	--	4819.7	13097.0	2217.9	--	288.0	--	231.6	43.6	942.9	36.03	--	--
Other	--	0.0	3742.0	0.0	--	0.0	--	0.0	0.0	0.0	6.23	--	--
TOTAL	--	10041.0	37420.0	7393.1	--	606.3	--	661.6	792.0	3143.0	--	--	--
Percent of Total	--	9.43	35.15	6.94	--	0.57	--	0.62	0.74	2.95	--	--	--
PROJECTED													
Absorbed Liquid and Sludge	64.8	0.0	0.0	48.0	0.0	--	0.0	0.0	0.0	335.8	0.97	6688.2[a]	6.28[a]
Combustibles	57.6	377.3	2020.2	1944.0	881.3	--	9.5	72.0	2522.2	10744.3	40.15	36452.2	34.24
Concreted or Cemented Sludge	0.0	132.0	737.2	864.0	12.1	--	9.5	0.0	5906.7	0.0	16.51	15358.1	14.43
Dirt, Gravel, or Asphalt	0.0	113.2	0.0	0.0	0.0	--	841.6	6.0	113.9	0.0	2.32	1388.1	1.30
Filters or Filter Media	0.0	94.3	23.3	120.0	84.5	--	0.0	30.0	113.9	839.4	2.81	3906.3	3.67
Glass/Metal/Similar Noncombustibles	57.6	226.4	681.2	1824.0	181.1	--	85.1	492.0	6720.3	4616.7	32.08	36525.0	34.31
Other	0.0	0.0	1203.7	0.0	48.3	--	0.0	0.0	895.0	251.8	5.17	6140.8	5.77
TOTAL	180.0	943.2	4665.6	4800.0	1207.2	--	945.6	600.0	16272.0	16788.0		106458.6	100.00
Percent of Total	0.17	0.89	4.38	4.51	1.13	--	0.89	0.56	15.28	15.77		100.00	
PROJECTED PLUS SCALED													
Absorbed Liquid and Sludge	64.8	0.0	0.0	124.3	0.0	0.0	0.0	0.0	0.0	869.5	0.92	7298.3[b]	4.16[b]
Combustibles	57.6	977.1	5231.9	5034.5	881.3	0.0	9.5	72.0	6531.8	27825.3	40.36	64444.8	36.71
Concreted or Cemented Sludge	0.0	342.0	1909.1	2237.6	12.1	0.0	9.5	0.0	15297.1	0.0	17.15	27503.8	15.67
Dirt, Gravel, or Asphalt	0.0	293.1	0.0	0.0	0.0	0.0	841.6	6.0	295.0	0.0	1.24	1749.1	1.00
Filters or Filter Media	0.0	244.3	60.4	310.8	84.5	0.0	0.0	30.0	295.0	2173.9	2.77	5799.6	3.30
Glass/Metal/Similar Noncombustibles	57.6	586.2	1764.1	4723.7	181.1	0.0	85.1	492.0	17404.1	11956.2	32.25	58890.8	33.54
Other	0.0	0.0	3117.4	0.0	48.3	0.0	0.0	0.0	2317.7	652.2	5.31	9877.5	5.63
TOTAL	180.0	2442.7	12082.8	12430.9	1207.2	0.0	945.6	600.0	42140.7	43477.1	--	175564.0	100.00
Percent of Total	0.1	1.39	6.88	7.08	0.69	0.0	0.54	0.34	24.00	24.76	--	100.00	--

[a] Stored plus projected

[b] Stored, plus projected, plus scaled

Table 3.4-6. Calculation of Constituent Volume Distribution in CH Waste*

Category	Initial	Distributed Amount of Filter and Filter Media	Total
Stored			
Sludge**	0.2373	0.0280	0.265
Combustible	0.2968	0.0350	0.332
Glass/Metal	0.3603	0.0425	0.403
Total	0.8944	--	1.000
Projected			
Sludge**	0.1980	0.0171	0.215
Combustible	0.4015	0.0348	0.436
Glass/Metal	0.3208	0.0278	0.349
Total	0.9203	--	1.000
Stored plus Projected			
Sludge**	0.2201	0.0229	0.243
Combustible	0.3424	0.0357	0.378
Glass/Metal	0.3431	0.0358	0.379
Total	0.9056	--	1.000
Stored, Projected, plus Scaled			
Sludge**	0.2083	0.0204	0.229
Combustible	0.3671	0.0360	0.403
Glass/Metal	0.3354	0.0328	0.368
Total	0.9108	--	1.000

* The values for the initial volume percents were obtained from Table 3.4-5.
** Total of absorbed liquid and sludge, concreted and cemented sludge, and dirt, gravel, or asphalt.

Masses of Various Categories of CH-TRU Contaminated Trash

Figure 3.4-3 shows the breakdown of CH waste mass by status, IDB waste categories, and gas-producing components.

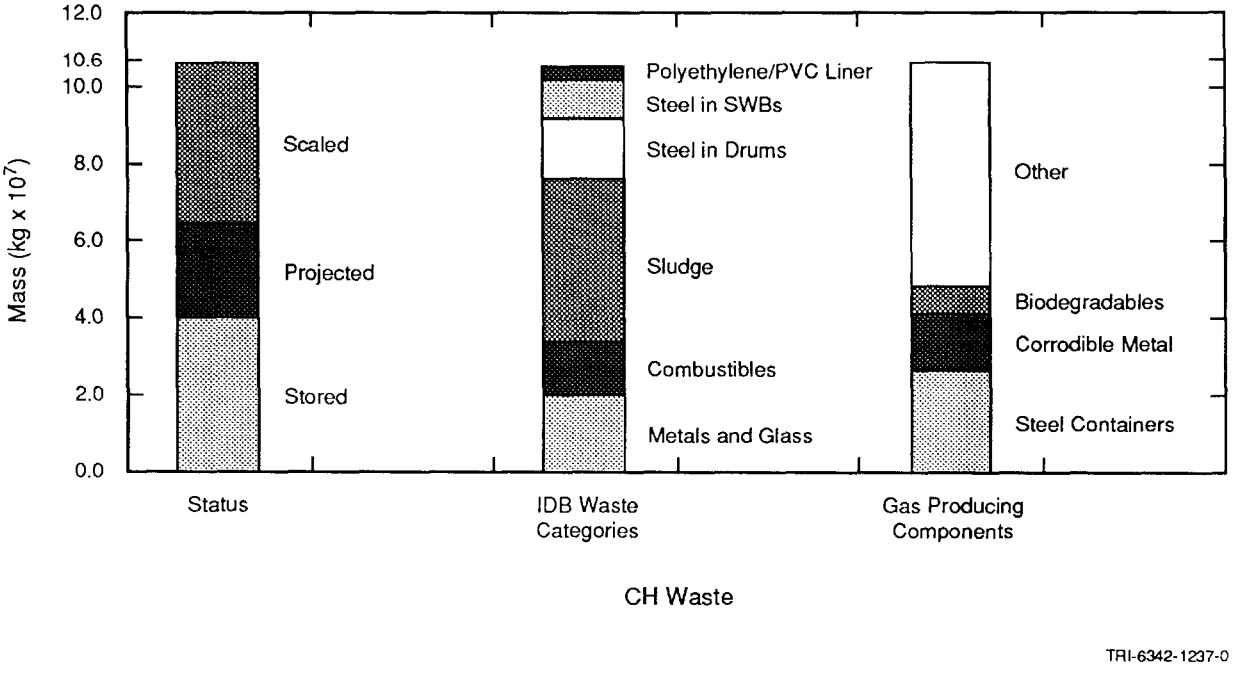

Figure 3.4-3. Breakdown of CH Waste Masses by Status, IDB Waste Categories, and Gas-Producing Components.

Discussion:

The PA calculations require an estimate of the mass of the major constituents of CH-TRU waste that affect gas generation. Because the PA analyses are based on a design volume, the mass of the waste constituents for a design volume were estimated. The generator sites provided estimates of the number, total volume, and mass of stored and projected waste to the 1990 IDB. Based on the number of containers, the masses of container steel, PVC liners, polyethylene liners, fiberglass reinforced wood, and plywood were estimated. Drez (May 9, 1989, Letter [Appendix A]) provided masses for these components.

Since detailed information was not available, it was assumed that each drum had one 4-kg polyvinyl chloride liner bag and each standard waste box (SWB) had one high-density 6.8-kg polyethylene liner. Masses for the larger boxes and bins were estimated by volume scaling to the mass of a 1.2 x 1.2 x 2.1 m (4 x 4 x 7 ft) box, which was obtained from Drez (May 9, 1989, Letter [Appendix A]). The empty mass of a drum was estimated to be 29.5 kg (65 lbm); a SWB, 310.7 kg (685 lbm). Table 3.4-7 summarizes the estimated masses.

Since currently only drums and SWBs can be transported in a TRUPACT II, excluding test bins, an estimate was made of the number of SWBs that would be required if the bins and boxes were repackaged in SWBs. The details of the masses and volumes of the waste in boxes and bins other than SWBs are summarized in Table 3.4-8. A total of 12,152 SWBs would be required to repackage the waste in the bins and boxes. Because of the mass of the SWBs, this repackaging would significantly increase the amount of steel emplaced in the WIPP. The calculations for repackaging in SWBs show (1) number of SWBs (1.9 m^3 volume), 12,150; (2) mass of SWB steel, 3.776 Gg (8.3 x 10^6 lbm); (3) mass of SWB PVC, 0.0486 Gg (1.1 x 10^5 lbm); (4) mass of waste, 5.591 Gg (1.2 x 10^7 lbm); and (5) total repackaged mass of about 9.0 Gg (2.0 x 10^7 lbm).

To obtain an estimate of the number of drums and SWBs that could be emplaced in the WIPP, the number of drums and SWBs at each generator site listed in Table 3.4-4 for stored and projected waste was calculated. Since the estimated volume for each generator from the number of containers was not consistent with the volume in Table 3.4-4, the number of containers for both stored and projected waste was adjusted to the volume of Table 3.4-4. To calculate this adjustment, the ratio of the volume of waste in each type of container in Table 3.4-7 was calculated and the number of containers increased or decreased to make the total volume consistent with the values in Table 3.4-4. The results of this estimate are summarized in Table. 3.4-9. Based on these assumptions, and assuming that the waste that cannot be currently transported is repackaged into SWBs, the inventory would contain 532,600 drums and 33,540 SWBs.

Estimates of the mass fractions were made based on the volume fractions tabulated in Table 3.4-6. Since the information that was available was the total mass of the waste and the volume fraction of sludge, combustibles, and glass/metals, other information was required to make estimates of the mass fraction. For these estimates, it was assumed that the combustible and metal and glass components had the average density listed in Butcher, 1989. An average mass of 40 kg (88.2 lbm) per drum for the combustibles and 64.5 kg (142.2 lbm) per drum for metals and glass was assumed. The mass of combustibles and metals/glass was estimated by calculating the number of drums in each category and multiplying by the average mass. The difference between the total mass of 30.18 Gg (6.6×10^7 lbm) of stored waste from Table 3.4-7 and the mass of the combustibles, metals/glass, polyethylene/PVC liners, and container steel was assumed to be the mass of the sludge, which resulted in the average mass of a sludge drum being 282.8 kg (623.6 lbm). A similar estimate was made for projected waste. The total mass of projected waste was estimated to be 17.48 Gg (3.9×10^7 lbm) as shown in Table 3.4-7. The estimated average mass of a drum of sludge of projected waste was 190.7 kg (420.5 lbm).

For the mass fraction for the design volume estimate, the mass of the sludge was estimated from the average masses of stored and projected waste. The volume of stored sludge and of projected and scaled sludge was estimated. Based on these volumes and the average masses, an average mass of 225 kg (496.1 lbm) per drum was calculated. The mass of sludge was estimated by calculating the number of drums of sludge and multiplying by the average mass. The same average mass of combustibles and metals/glass was assumed for the design volume as for the stored and projected volumes.

The calculated mass fractions for stored waste, projected waste, combined stored and projected waste, and combined stored, projected, and scaled waste are shown in Table 3.4-10. These results indicate the range of mass fractions that could be emplaced in the WIPP. As expected, the mass fraction for sludge is considerably less for projected waste than for stored waste. Note that the mass fraction for combined stored and projected waste has a somewhat higher mass fraction for sludge than was used in Lappin et al., 1989. As indicated in Table 3.4-6, the volume fraction of sludges has increased somewhat from 1987, on which earlier estimates were made, to 1990.

Table 3.4-7. Estimated Inventory of Containers in 1990

Description	Volume (m^3)	Number	Total Mass (Gg)	Total Volume (m^3)	Mass Steel (kg)	Mass PVC (kg)	Mass Polyethelene (kg)	Mass Fiberglass Reinforced Wood (kg)	Mass Plywood (kg)
Stored CH Inventory									
Drums	0.208	110120	25.060	23125	3.249	0.7488	--	--	--
SWBs	1.9	5327	5.198	10121	1.655	--	0.0213	--	--
Boxes	3.17	5925	6.819	18782	0.360	0.0296	--	1.3759	0.2899
Bins	3.4	415	0.421	1411	0.097	0.0022	--	--	--
Boxes	3.8	672	0.600	2554	0.175	0.0040	--	--	--
Boxes	3.9	35	0.036	137	0.009	0.0002	--	--	--
Boxes	5.9	23	0.047	136	0.009	0.0002	--	--	--
Boxes	6.35	11	0.025	70	0.005	0.0001	--	--	--
TOTALS			38.206	56335	5.559	0.7852	0.0213	1.3759	0.2899
Estimated mass of stored waste (Gg) 30.18									
Projected CH Inventory									
Drums	0.208	155420	18.882	32638	4.585	--	1.057	--	--
SWBs	1.9	6105	6.166	11600	1.897	0.2442	--	--	--
TOTALS			25.046	44238	6.489	0.2442	1.057	--	--
Estimated mass of projected waste (Gg) 17.48									

TOTALS	
Total Mass (Gg)	63.252
Total Volume (m^3)	0.101
Total Mass Steel (Gg)	12.04
Total Mass PVC (Gg)	0.810
Total Mass Polyethylene (Gg)	1.078
Total Mass Fiberglass Reinforced Wood (Gg)	1.376
Total Mass Plywood (Gg)	0.29
Estimated Total Mass of Waste (Gg)	47.658
Total Drums	265,540
Total SWBs	11,432
Total Bins & Boxes	7,081

Table 3.4-8. Summary of Bins and Boxes

Description	Volume (m^3)	Number	Total Mass (Gg)	Container Volume (m^3)	Mass Steel (Gg)	Mass PVC (Gg)	Mass Fiberglass Reinforced Wood (Gg)	Mass Plywood (Gg)
Boxes	3.17	5925	6.8193	18782.2	3.60	0.0296	1.3759	0.2899
Bins (1)	3.4	415	0.4210	1411.0	0.96	0.0022	--	--
Boxes (2)	3.8	672	0.6000	2553.6	1.75	0.0040	--	--
Boxes (3)	3.9	35	0.0362	136.5	0.09	0.0002	--	--
Boxes (4)	5.9	23	0.0468	135.7	0.09	0.0002	--	--
Boxes (5)	6.35	11	0.0254	69.9	0.05	0.0001	--	--
TOTALS			7.9487	23088.9	6.55	0.0364	1.3759	0.2899

Estimated metal box masses:
(1) 233.5 kg
(2) 261 kg
(3) 268 kg
(4) 405 kg
(5) 436 kg

Calculations for repackaging in SWBs:

Number of SWBs (1.9 m^3 vol)	0.012
Mass of SWB steel (Gg)	3.776
Mass of SWB PVC (Gg)	0.049
Mass of waste (Gg)	5.591
Total repackaged mass (Gg)	9.379

Table 3.4-9. Estimate of the Number of Drums and SWBs in a Design Volume

Category	Volume	Total	Adjusted Total
Stored Drums	23113	110064	121113
Stored SWBs	10121	5327	6007
Adjustment to stored* Drums	2320	11049	--
Adjustment to stored* SWBs	1425	750	--
Projected Drums	32717	155795	161294
Projected SWBs	12132	6385	6595
Adjustment to Projected* Drums	1155	5499	--
Adjustment to Projected* SWBs	399	210	--
Scaled Drums	52534	250164	250164
Scaled SWBs	16566	8719	8719
Repackaged SWBs**	23089	12152	12152
Total Drums	532571		
Total SWBs	33543		

* Adjusted to make total volume equal volume in Table 3.4-3.
** Assumed volume in Bins and Boxes were repackaged into SWBs.

Table 3.4-10. Estimated Composition of CH-TRU Contaminated Trash Including Containers in 1990

	Mass (Gg)	Volume (m^3)	Volume Fraction	Steel Containers (Gg)	SWB Steel (Gg)	Poly/ PVC (Gg)	Total Mass (Gg)	Mass Fraction
Stored Inventory								
Sludge[a]	20.106	14,928.9	0.265	2.300	--	0.217	22.623	0.570
Metals and Glass[b]	5.745	18,703.4	0.332	2.881	--	0.272	8.898	0.224
Combustibles[c]	4.324	22,703.2	0.403	3.498	--	0.330	8.152	0.205
Steel Containers	8.679							
Polyethylene/PVC liner	0.819							
Total	39.673	56,335.4		8.679	--	0.819	39.673	
Projected								
Sludge	8.618	9,511.1	0.215	1.394	--	0.227	10.239	0.409
Metals and Glass[b]	5.924	19,287.6	0.436	2.826	--	0.461	9.211	0.368
Combustibles[c]	2.941	15,439.0	0.349	2.262	--	0.369	5.572	0.223
Steel Containers	6.482							
Polyethylene/PVC liner	1.057							
Total	25.022	44,237.7		6.482	--	1.057	25.022	
Stored and Projected								
Sludge	28.717	24,444.1	0.243	3.684	--	0.462	32.863	0.508
Metals and Glass[b]	11.679	38,024.2	0.378	5.731	--	0.718	18.128	0.280
Combustibles[c]	7.262	38,124.8	0.379	5.746	--	0.720	13.728	0.212
Steel Containers	15.161							
Polyethylene/PVC liner	1.900							
Total	64.719	100,593.1		15.161	--	1.900	64.719	
Stored, Projected, and Scaled								
Sludge[d]	43.076	40,204.2	0.229	3.598	--	0.860	47.534	0.447
Metals and Glass[b]	19.844	64,607.6	0.368	5.782	4.974	1.382	31.982	0.301
Combustibles[c]	13.477	70,752.3	0.403	6.331	5.447	1.513	26.769	0.252
Steel in drums	15.711							
Steel in SWBs	10.422							
Polyethylene/ PVC liner	3.755							
Total	106.285	175,564.0		15.711	10.422	3.755	106.285	

[a] The mass of sludge is the difference between a total estimated mass of 30.18 Gg for the total waste package and the mass of the combustibles and metals and glass.

[b] The mass of metals and glass is based on an average mass of 64.5 kg per drum (Butcher, 1989).

[c] The mass of combustibles is based on an average mass of 40 kg per drum (Butcher, 1989).

[d] The mass of sludge is based on the ratio of the 14,929 m^3 of stored waste with an average mass of 282.8 kg per drum and the 25,275 m^3 of projected and scaled waste with an average mass of 190.7 kg per drum. This ratio results in an average mass of 225 kg per drum for sludge.

Estimated Curie Content of Drums and Standard Waste Boxes

Submittals from the generator sites to the 1990 IDB included estimates of the number of stored and projected waste containers in a range of total initial plutonium curie content. The current analyses were based on the design volume of waste emplaced in the WIPP. To estimate the number of drums and SWBs in the four ranges of total plutonium curie content used in the analyses, the estimates from the ranges from the generators were combined and estimates were made for total quantity of drums and SWBs for a design volume based on the quantities from Table 3.4-9. The estimated number of drums and SWBs for the stored, projected, and scaled inventory are shown in Figure 3.4-4 and listed in Table 3.4-11. Since it was assumed for the current analyses that the waste in bins and boxes would be repackaged, an estimate for the repackaged boxes was also made. The current analyses further combined the number of drums and boxes in the range of curie content. It was assumed for the removal of cuttings during drilling for human intrusion that the surface area encountered by the drill for a SWB was about 8.2 times the surface area of a drum. Therefore, the curies removed by drilling into a SWB would be about 8.2 times less than for a drum in the same range. To combine them into an equivalent number of drums, the total number of SWBs was increased by a factor of 8.22 and the curie range was decreased by a factor of ten. This results in no contribution of SWBs in the range above 100 curies and the total SWBs in the 0-to-1 and 1-to-10 range being combined in the 0-to-1 curie category for the combined drums and SWBs shown in Table 3.4-11.

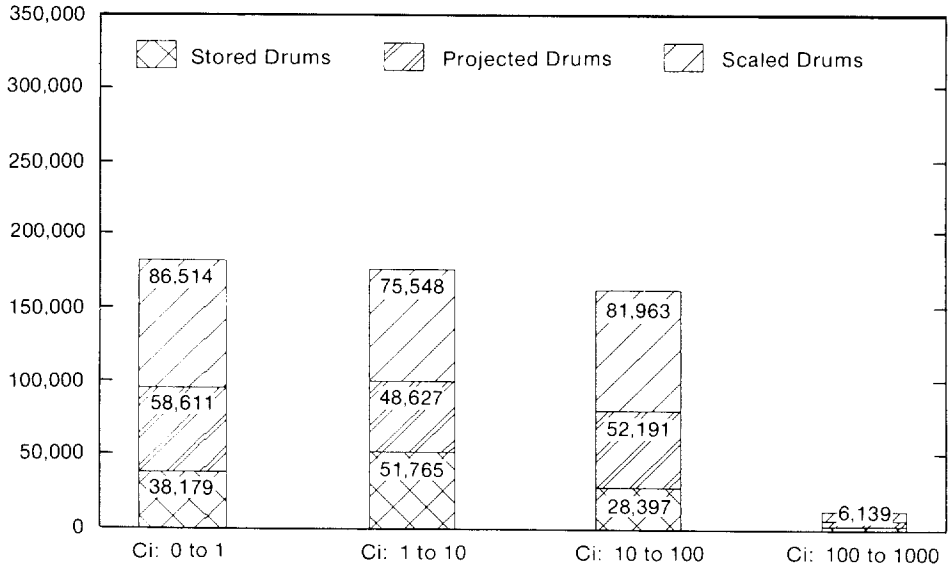

(a) Drums

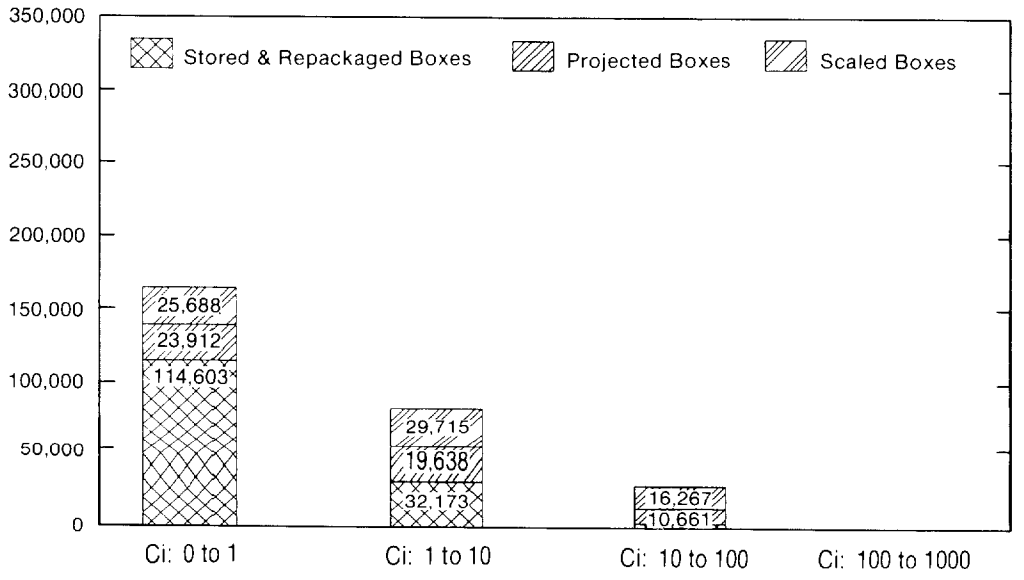

(b) SWBs

Figure 3.4-4. Estimated Number of Drums and SWBs for Stored, Projected, and Scaled Inventory in Each Activity Range.

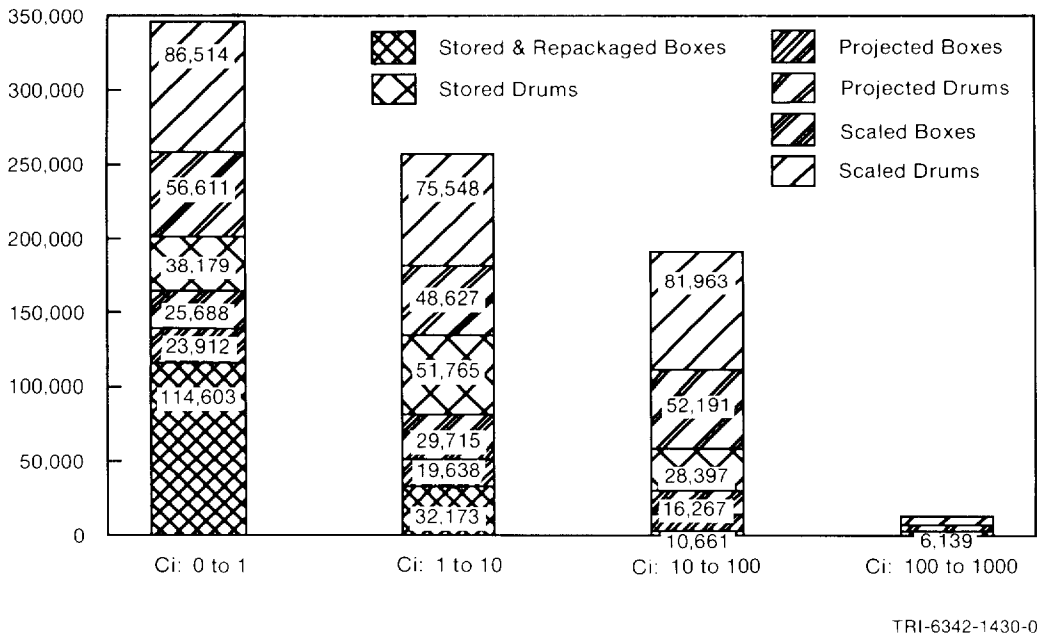

(c) Total, Drums and Boxes

Figure 3.4-4. Estimated Number of Drums and SWBs for Stored, Projected, and Scaled Inventory in Each Activity Range (Concluded).

Table 3.4-11. Estimate of Curie Content of Drums and Standard Waste Boxes in a Design Volume

	0 to 1 (Ci)	1 to 10 (Ci)	10 to 100 (Ci)	100 to 1000 (Ci)	Total (Ci)
Stored Drums					
Totals	38179	51765	28397	2772	121113
Percent	31.5	42.7	23.4	2.3	
Projected Drums					
Totals	56611	48627	52191	3865	161294
Percent	35.1	30.1	32.4	2.4	
Scaled Drums					
Totals	86514	75548	81963	6139	250164
Percent	34.6	30.2	32.8	2.5	
Total Drums					
Totals	181304	175940	162551	12776	532571
Percent	34.0	33.0	30.5	2.4	
Stored Boxes					
Totals	4070	1222	596	189	6077
Percent	67.0	20.1	9.8	3.1	
Projected Boxes					
Totals	1234	1675	2389	1297	6595
Percent	18.7	25.4	36.2	19.7	
Scaled Boxes					
Totals	775	2350	3615	1979	8719
Percent	8.9	27.0	41.5	22.7	
Repackaged (Stored) Boxes					
Totals	1608	7042	3318	184	12152
Percent	13.2	57.9	27.3	1.5	
Total Boxes					
Totals	7687	12289	9918	3649	33543
Percent	22.9	36.6	29.6	10.9	
Combination of Drums and Boxes (Equivalent Drums)					
Totals	345507	257466	192546	12776	808294
Percent	42.7	31.9	23.8	1.6	

Gas Generation Potential

Without a detailed knowledge of the mechanisms by which gas may be produced, the gas generation potentials can only be calculated based on the amount of waste received at the WIPP. Based on information in 1988 (IDB, 1988; Lappin et al., 1989, p. A-119), Sandia estimated a gas generation potential from corrosion of about 900 mole/drum equivalent and from microbial degradation of about 600 mole/drum equivalent. Because estimates of the volume of CH waste are decreasing, but the volume of RH waste is increasing, these values have changed.

An estimate of the amounts of waste that contribute to gas generation are required for PA calculations. The masses of the constituents in combustible and metals/glass were estimated in Drez (May 9, 1989, Letter [Appendix A]). The results of these estimates are shown in column 2 of Table 3.4-12. The total volume for the current PA analysis is based on the design volume of 175,564 m^3 (6.2 x 10^6 ft^3). The total volume on which the estimates in Drez (May 9, 1989, Letter [Appendix A]) were made was 95,111 m^3 (3.4 x 10^6 ft^3). Volume scaling the masses from 95,111 m^3 (3.4 x 10^6 ft^3) to a design volume of 175,564 m^3 (6.2 x 10^6 ft^3), a factor of 1.846, results in the masses listed in column 4 of Table 3.4-12. Butcher (1989) reported estimates of the percentage of various components of combustible and metals/glass. Based on these percentages and volume scaling the masses to a design volume results in the masses listed in column 6.

Another method for estimating the masses is to base the total mass of the combustibles and metals and glass on the mass estimated in Table 3.4-10 for the stored, projected, and scaled estimates. Scaling the masses of the combustibles in column 1 by the ratio of the total combustible mass of 8.593 Gg (1.9 x 10^7 lbm) to 13.467 Gg (3.0 x 10^7 lbm) from Table 3.4-10, a factor of 1.567, the estimated masses shown in columns 7 and 8 were calculated. A similar scaling was calculated for the metals and glass based on the total mass of metals and glass in Table 3.4-10 and are also tabulated in columns 7 and 8. The significant figures in Table 3.4-12 should not be interpreted as an indication of the accuracy of the estimates. These are estimates with a potentially large uncertainty and were made as a base for uncertainty analyses. The significant figures were included only for consistency with Table 3.4-10. The results listed in column 8 of Table 3.4-12 were used as the estimates of these constituents in the PA calculations because they are the same as were used in the estimates of the mass fractions for a design volume in Table 3.4-10. Figure 3.4-3 displays the breakdown of the CH waste mass including the gas-producing components. Not all of the components listed in Table 3.4-12 were included as gas-producing components. The components for microbial activity included the total cellulosics mass and one-half of the mass of surgeon's gloves, Hypalon, Neoprene, and other undefined rubber. The components for corrosion included iron, paint cans, steel, and shipping cans.

Table 3.4-12. Estimates of Masses for a CH Design Volume[a]

	Source 1[b] (kg)	Source 1 (%)	Design (kg)	Source 2[c] (%)	Source 2 (kg)	Source 2[d] (kg)	Design[d] (kg)
COMBUSTIBLES							
Cellulosics							
Paper/Kimwipes	3,890,000	45.27	7,223,730	24.0	3,829,619	3,234,390	6,100,964
Cloth	226,000	2.63	419,682	4.0	638,270	539,065	354,452
Other paper	51	0.00	95	--	--	--	80
Lumber (untreated)	73,100	0.85	135,747	--	--	--	114,648
Lumber (treated)	36,700	0.43	68,152	--	--	--	57,559
Plywood	98,400	1.15	182,729	--	--	--	154,328
Other wood (rulers)	--	0.00	0	--	--	--	0
Other wood (all types)	23,700	0.28	44,011	--	--	--	37,170
Other cellulose (phenolic binder)	1,720	0.02	3194	--	--	--	2,698
Cellulosics subtotal	4,349,671	50.62	8,077,339	28.0	4,467,888	3,773,456	6,821,898
Plastics				38.0	6,063,563	5,121,118	
Polyethylene	1,540,000	17.92	2,859,780	--	--	--	2,415,291
PVC	1,040,000	12.10	1,931,280	--	--	--	1,631,106
Surgeon's gloves (latex)	582,000	6.77	1,080,774	15.0	2,393,512	2,021,494	912,792
Leaded rubber gloves	596,000	6.94	1,106,772	2.0	319,135	269,533	934,749
(Lead-Hypalon-Neoprene)	--	0.00	0	--	--	--	0
Hypalon	114,000	1.33	211,698	--	--	--	178,794
Neoprene	129,000	1.50	239,553	--	--	--	202,320
Viton	133	0.00	247	--	--	--	209
Teflon	41,000	0.48	76,137	--	--	--	64,303
Plexiglass	18,900	0.22	35,097	--	--	--	29,642
Styrofoam	330	0.00	613	--	--	--	518
Plastic prefilters	33,600	0.39	62,395	--	--	--	52,697
Polystyrene	2,560	0.03	4,754	--	--	--	4,015
Conwed pads	2,030	0.02	3,770	--	--	--	3,184
Other plastics	75,500	0.88	140,204	--	--	--	118,412
Other rubber (kalrez)	--	0.00	0	--	--	--	0
Other rubber undefined	7,530	0.09	13,983	--	--	--	11,810
Plastics subtotal	4,182,583	48.68	7,767,057	55.0	8,776,209	7,412,145	6,559,842

[a] The estimated mass of the INEL and LANL containers (3.590 Gg) was subtracted from the 9.170 Gg of metal (Drez, May 9, 1989, Letter [Appendix A]) to obtain the estimated steel mass of 5.580 Gg.

The volume of the inventory for the estimates from Drez (1989) was based on 283,298 drums, 0.21 m^3, 5,541 4x4x7 boxes, 3.17 m^3, and 9,502 SWBs 1.9 m^3. Using this estimate results in the volume as 95,111 m^3. The ratio between the estimated volume and the design volume is 1.846.

[b] Drez. P. 1989. "Preliminary Nonradionuclide Inventory of CH-TRU waste," letter to L. Brush, May 9, 1989 (Appendix A).

[c] Butcher, B. 1989. Waste Isolation Pilot Plant Simulated Waste Compositions and Mechanical Properties. SAND89-0372. Albuquerque, NM: Sandia National Laboratories.

[d] For these estimates, the percentages were assumed to be correct and the total mass was based on combustibles having an average mass of 40 kg per drum for a total mass of 13.477 Gg; the metals and glass having an average mass of 64.5 kg per drum for a total mass of 19.844 Gg.

Table 3.4-12. Estimates of Masses for a CH Design Volume (Concluded)[a]

	Source 1[b] (kg)	Source 1 (%)	Design (kg)	Source 2[c] (%)	Source 2 (kg)	Source 2[d] (kg)	Design[d] (kg)
Other							
Blacktop	18,800	0.22	34,912	--	--	--	29,485
Other	41,700	0.49	77,437	17.0	2,712,647	2,291,027	65,401
Other subtotal	60,500	0.70	112,349	17.0	2,712,647	--	94,886
Total Combustible	8,592,754		15,956,744	--	15,956,744	13,476,627	13,476,627
METALS							
Aluminum	666,000	5.44	1,229,436	14.0	3,164,476	2,778,125	1,079,334
Beryllium	8,640	0.07	15,949	--	--	--	14,002
Cadmium	5	0.00	9	--	--	--	8
Chromium	5	0.00	9	--	--	--	8
Copper	300,000	2.45	553,800	11.0	2,486,374	2,182,812	486,187
Iron	2,620,000	21.40	4,836,520	--	--	--	4,246,029
Lead		0.00	0	7.0	1,582,238	1,389,062	0
Metallic	513,000	4.19	946,998	--	--	--	831,379
Glass (including glass mass)	1,120,000	9.15	2,067,520	--	--	--	1,815,096
Glove (including glove mass)	596,000	4.87	1,100,216	--	--	--	965,891
Lithium	1,030	0.01	1,901	--	--	--	1,669
Mercury	120	0.00	222	--	--	--	194
Paint cans	547,000	4.47	1,009,762	--	--	--	886,480
Platinum	1,500	0.01	2,769	--	--	--	2,431
Selenium	5	0.00	9	--	--	--	8
Silver	5	0.00	9	--	--	--	8
Steel	5,580,000	45.57	10,300,680	64.0	14,466,174	12,699,999	9,043,070
Shipping cans	217	0.00	401	--	--	--	352
Tantalum	125,000	0.02	230,750	4.0	904,136	793,750	202,578
Tungsten	20,000	0.16	36,920	--	--	--	32,412
Other	146,000	1.19	269,516	--	--	--	236,611
Total Metals	12,244,527	--	22,603,397	--	22,603,397	19,843,748	19,843,748

[a] The estimated mass of the INEL and LANL containers (3.590 Gg) was subtracted from the 9.170 Gg of metal (Drez, May 9, 1989, Letter [Appendix A]) to obtain the estimated steel mass of 5.580 Gg.

The volume of the inventory for the estimates from Drez (1989) was based on 283,298 drums, 0.21 m^3, 5,541 4x4x7 boxes, 3.17 m^3, and 9,502 SWBs 1.9 m^3. Using this estimate results in the volume as 95,111 m^3. The ratio between the estimated volume and the design volume is 1.846.

[b] Drez. P. 1989. "Preliminary Nonradionuclide Inventory of CH-TRU waste," letter to L. Brush, May 9, 1989 (Appendix A).

[c] Butcher, B. 1989. Waste Isolation Pilot Plant Simulated Waste Compositions and Mechanical Properties. SAND89-0372. Albuquerque, NM: Sandia National Laboratories.

[d] For these estimates, the percentages were assumed to be correct and the total mass was based on combustibles having an average mass of 40 kg per drum for a total mass of 13.477 Gg; the metals and glass having an average mass of 64.5 kg per drum for a total mass of 19.844 Gg.

Comparison with Other Estimates

The estimates that were made and discussed for the combustibles and the metals and glass for Table 3.4-10 used the average mass from Butcher (1989) for these components. The total volume for the stored and projected waste in Table 3.4-10 was 100,593 m^3 (3.6 x 10^6 ft^3). The estimates from Drez (May 9, 1989, Letter [Appendix A]) were based on a total waste volume of 95,111 m^3 (3.4 x 10^6 ft^3). A comparison of the results of the two estimates indicates some consistency. The total mass of combustibles was 8.59 Gg (1.9 x 10^7 lbm) in Drez (May 9, 1989, Letter [Appendix A]) and the estimates in Table 3.4-10 were about 7.30 Gg (1.6 x 10^7 lbm). The mass of the metals and glass in Table 3.4-10 is about 11.60 Gg (2.6 x 10^7 lbm). The estimate in Drez (1989) was a total mass of 15.80 Gg (3.5 x 10^7 lbm). This estimate included the mass of the containers for the INEL and LANL. If the estimated mass of the INEL and LANL containers in Table 3.4-7 (3.59 Gg [7.9 x 10^6 lbm] is subtracted from the total in Drez (1989), the estimated mass of the glass and metal waste is 12.21 Gg (2.7 x 10^7 lbm).

3.4.2 Composition of RH-TRU Contaminated Trash (Non-Radionuclide/ Non-RCRA Inventory)

Volumes of Various Categories of RH-TRU Contaminated Waste

Estimates of the weights and volumes of RH-TRU constituents that affect gas generation, transport, and room properties are required for performance assessment. However, the weight of RH inventory was not included in the current analyses. The total RH inventory has changed considerably in the last several years. The following discussion presents a method that was used to estimate the characterization of the RH inventory. The method resulted in estimates of the volume and weights of waste by generator site; however, these results should not be interpreted as indicative of the weights and volumes that a specific site may generate.

From the information in the IDBs, an estimate of the total volume and the percentage of selected constituent forms may be identified. Table 3.4-13 summarizes the information for the last four years and shows that the estimated total volume increase from 2,500 m^3 (8.83 x 10^4 ft^3) in 1988 to about 5,300 m^3 (1.87 x 10^5 ft^3) in 1990 (Figure 3.4-5). The reasons for the large increase are discussed in the 1990 IDB.

For the current PA calculations, it was assumed that the maximum allowed RH volume of 7,079 m^3 (0.25 x 10^6 ft^3) will be emplaced in the WIPP. The following discussion presents the method that was used to estimate the total volumes of the waste constituents if the maximum volume of RH waste was emplaced. Input to the 1990 IDB was used as the basis for these estimates. The IDB presents estimates of the stored volume and projected (newly generated) volume for each generator site. The stored and projected volumes for the five sites that have or will generate RH waste are tabulated in Table 3.4-14. To estimate the additional volume required to reach the maximum volume, it was assumed that the generators of projected waste would provide the additional volume. The percentage of projected waste for each site was calculated and, based on this percentage, volumes for the five sites were calculated to provide an additional 1,735 m^3 (6.13 x 10^4 ft^3). The scaled volumes for the five sites are shown in Table 3.4-14.

The stored and newly generated (projected) RH volume in the 1990 IDB sum to about 5,300 m^3 (8.83 x 10^4 ft^3). The containers that will be placed in an RH canister have a different volume depending on the generator site. Therefore, a canister may not contain 0.89 m^3 (31.4 ft^3) of RH waste. U.S. DOE (1991) indicates that the submittals to the 1990 IDB total 7,622 canisters. The total volume based on this number of canisters is 6,784 m^3 (2.4 x 10^5 ft^3). U.S. DOE (1991) also discusses the number of uncertainties in the projection of the RH inventory and acknowledges that the details of the RH-TRU waste canister design should be revisited for re-evaluation. Because of the uncertainty in the RH inventory and the discussion in U.S. DOE (1991) on canister design, the smaller total stored plus projected volume of waste —not the volume of the canisters —was used as a scaling factor to estimate the RH radionuclide inventory for an RH design volume.

Table 3.4-13. Estimated Composition by Volume of RH-TRU Contaminated Trash from 1987 to 1990

	Combustibles (%)	Metal and Glass (%)	Absorbed Liquid and Sludge (%)	Concrete/ Cemented Sludge (%)	Dirt/ Gravel/ Asphalt (%)	Filters/ Filter Media (%)	Other (%)	Total Volume* (m^3)
1987	45.10	19.00	30.60	2.2	0.0	0.7	2.3	2690
1988	41.20	21.80	33.00	0.0	0.0	1.4	2.5	2500
1989	41.40	17.40	33.60	0.0	0.0	7.6	0.0	2812
1990	10.50	66.50	15.70	0.1	0.0	7.1	0.3	5344

* Design volume is 7,079 m^3.

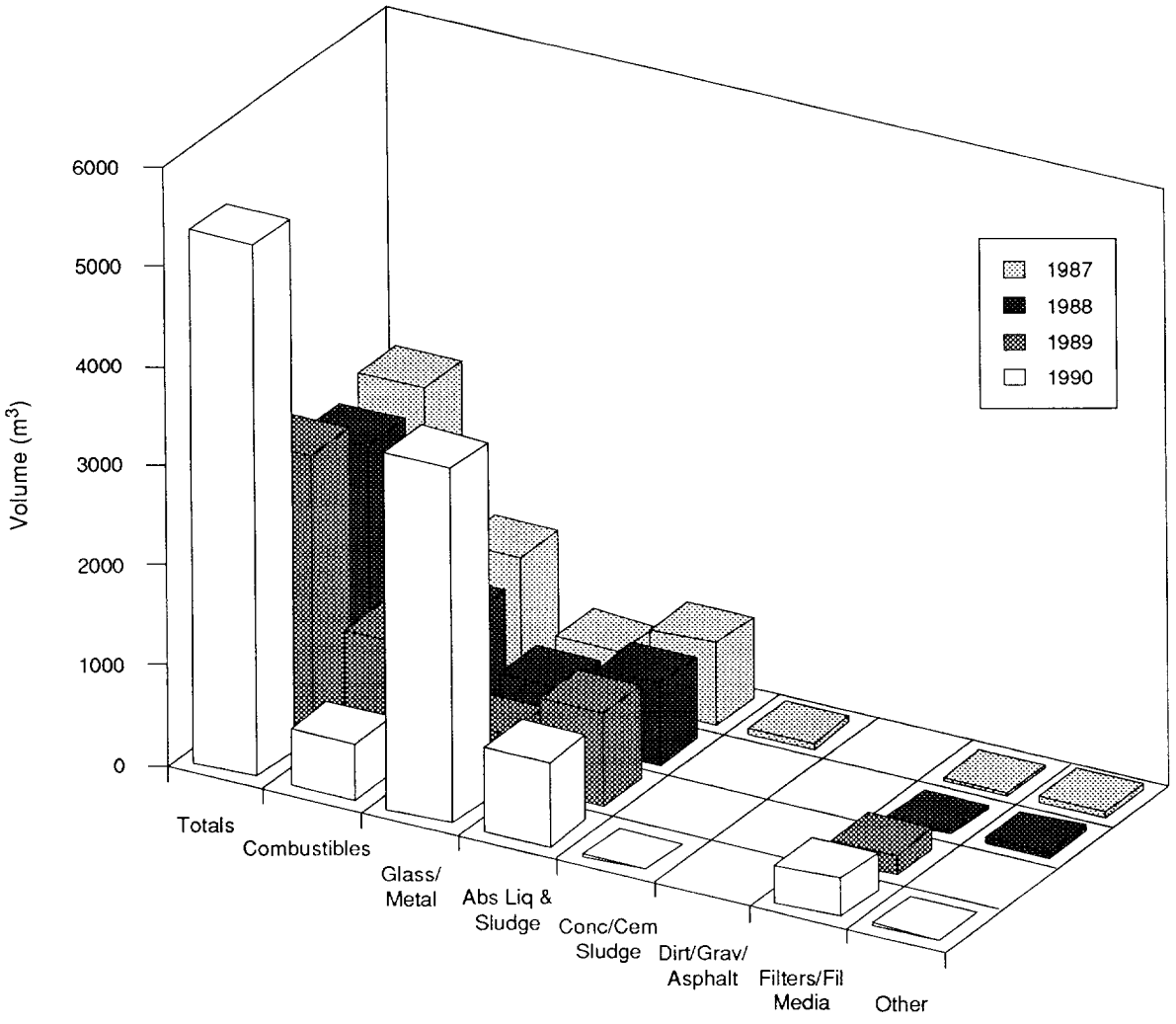

Figure 3.4-5. Changes in RH Waste Volume Estimates Between 1987 and 1990.

Table 3.4-14. Estimate of a Design Volume for RH-TRU Waste

Site	Stored Volume (1990 IDB) (m^3)	Projected Volume (1990 IDB) (m^3)	Total Volume (1990 IDB) (m^3)	Scaled Volume* (m^3)	Estimated Design Volume (m^3)
ANL-E	--	81.6	81.6	36.8	118.4
HANF	137	3535.2	3672.2	1,596.0	5,268.2
INEL	29.5	76.8	106.3	34.7	141.0
LANL	28.4	4.8	33.2	2.2	35.4
ORNL	1307	144.0	1,451.0	65.0	1,516.0
Total	1,501.9	3,842.4	5,344.3	1,734.7	7,079

* Assuming that ANL, HANF, INEL, LANL, and ORNL provide the difference between the current total inventory and the design volume. The difference between the total volume of 5,344 m^3 in the 1990 IDB and the design volume of 7,079 m^3 (0.25×10^6 ft^3) was ratioed between the five sites based on their estimated annual generation rates.

3.4.3 Inventory of Organic RCRA Contaminants

Hazardous materials are not regulated under *40 CFR 191*, but are regulated separately by the EPA and New Mexico. Some trace organic chemicals could affect the ability of radionuclides to migrate out of the repository, at least initially, until microbial activity destroyed them.

A major RCRA constituent of CH-TRU waste is lead that is present as incidental shielding, glovebox parts, and linings of gloves and aprons (U.S. DOE, 1990d). Trace quantities of mercury, barium, chromium, and nickel have also been reported in some sludges (U.S. DOE, 1990d).

Two RH-TRU waste forms contain hazardous chemical constituents. A solid waste containing mixtures of combustibles and noncombustibles was removed from a hot cell facility at Oak Ridge National Laboratory. This waste will not contain free liquids or particulates. In addition, fuel sludges and process sludges will be solidified. This waste will be a solid monolith (U.S. DOE, 1990d). Quantities of the above-mentioned RCRA constituents are being compiled for calculations necessary for the No-Migration Variance Petition but are not available at this time.

3.4.4 Capillary Pressure and Relative Permeability

Threshold Displacement Pressure, p_t

Parameter:	**Threshold displacement pressure (p_t)**
Median:	2.02×10^3
Range:	2.02×10^2
	2.02×10^5
Units:	Pa
Distribution:	Lognormal
Source(s):	Davies, P. B. 1991. *Evaluation of the Role of Threshold Pressure in Controlling Flow of Waste-Generated Gas into Bedded Salt at the Waste Isolation Pilot Plant.* SAND90-3246. Albuquerque, NM: Sandia National Laboratories.
	Davies, P. B. 1991. "Uncertainty Estimates for Threshold Pressure for 1991 Performance Assessment Calculations Involving Waste-Generated Gas." Internal memo to D. R. Anderson (6342), June 2, 1991. Albuquerque, NM: Sandia National Laboratories. (In Appendix A of this volume)

Residual Saturations

Parameter:	**Residual wetting phase (liquid) saturation ($S_{\ell r}$)**
Median:	2.76×10^{-1}
Range:	5.52×10^{-1}
	1.38
Units:	Dimensionless
Distribution:	Cumulative
Source(s):	Brooks, R. H. and A. T. Corey. 1964. "Hydraulic Properties of Porous Media," Hydrology Papers, No. 3. Fort Collins, CO: Colorado State University
	Davies, P. B. and A. M. LaVenue. 1990b. "Additional Data for Characterizing 2-Phase Flow Behavior in Waste-Generated Gas Simulations and Pilot Point Information for Final Culebra 2-D Model," Memo 11 in Appendix A of Rechard et al., 1990. *Data Used in Preliminary Performance Assessment of the Waste Isolation Pilot Plant.* SAND89-2408. Albuquerque, NM: Sandia National Laboratories

Parameter:	**Residual gas saturation (S_{gr})**
Median:	7×10^{-2}
Range:	3.5×10^{-2}
	1.4×10^{-1}
Units:	Dimensionless
Distribution:	Cumulative
Source(s):	Brooks, R. H. and A. T. Corey. 1964. "Hydraulic Properties of Porous Media," Hydrology Papers, No. 3. Fort Collins, CO: Colorado State University
	Davies, P. B. and A. M. LaVenue. 1990b. "Additional Data for Characterizing 2-Phase Flow Behavior in Waste-Generated Gas Simulations and Pilot Point Information for Final Culebra 2-D Model," Memo 11 in Appendix A of Rechard et al., 1990. *Data Used in Preliminary Performance Assessment of the Waste Isolation Pilot Plant.* SAND89-2408. Albuquerque, NM: Sandia National Laboratories.

Brooks and Corey Exponent

Parameter:	**Brooks and Corey exponent (η)**
Median:	2.89
Range:	1.44
	5.78
Units:	Dimensionless
Distribution:	Cumulative
Source(s):	Based on information in Brooks, R. H. and A. T. Corey. 1964. "Hydraulic Properties of Porous Media," Hydrology Papers, No. 3. Fort Collins, CO: Colorado State University.

Capillary Pressure and Relative Permeability

Figures 3.4-6a and 3.4-6b show the assumed values for capillary pressure and relative permeability, respectively. Figure 3.4-7 is an example of the variation in relative permeability and capillary pressure when Brooks and Corey parameters are varied.

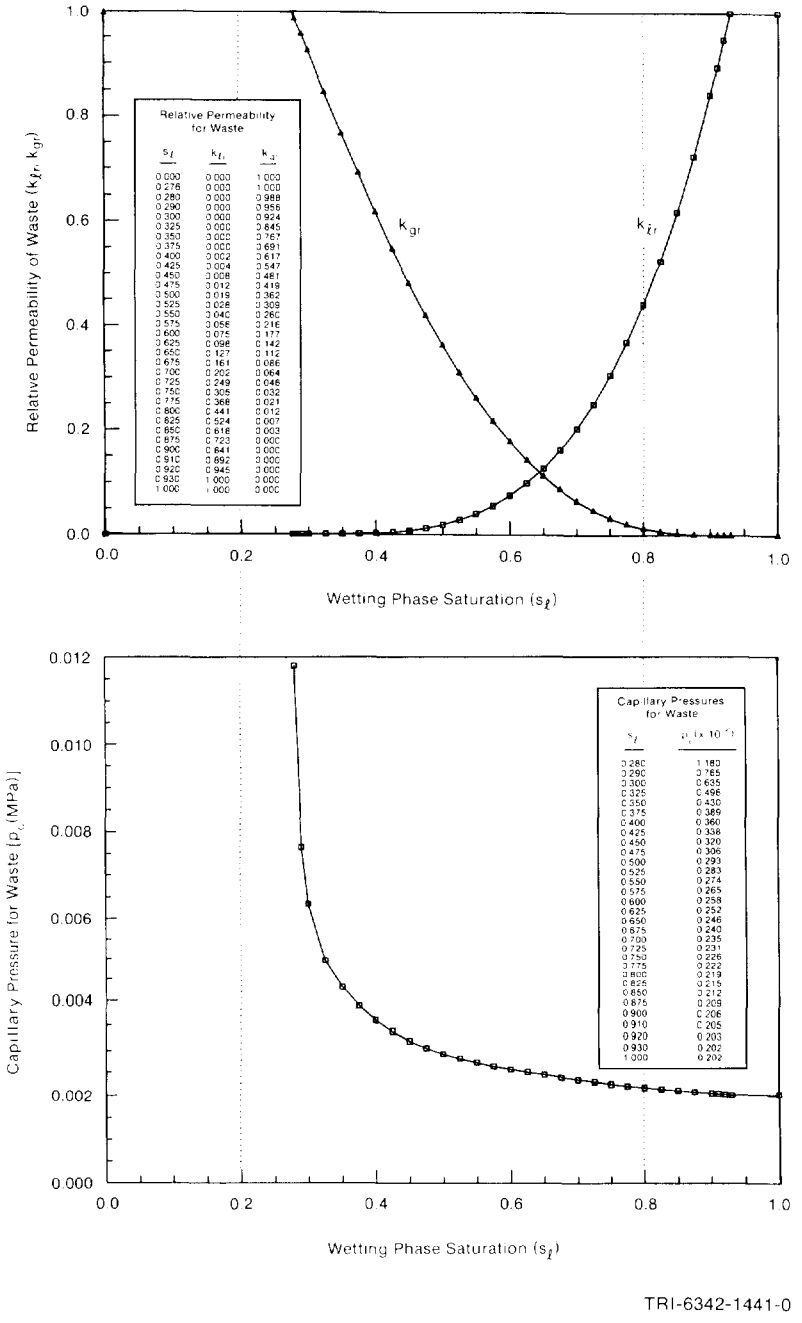

Figure 3.4-6. Estimated Capillary Pressure and Relative Permeability for Unmodified Waste.

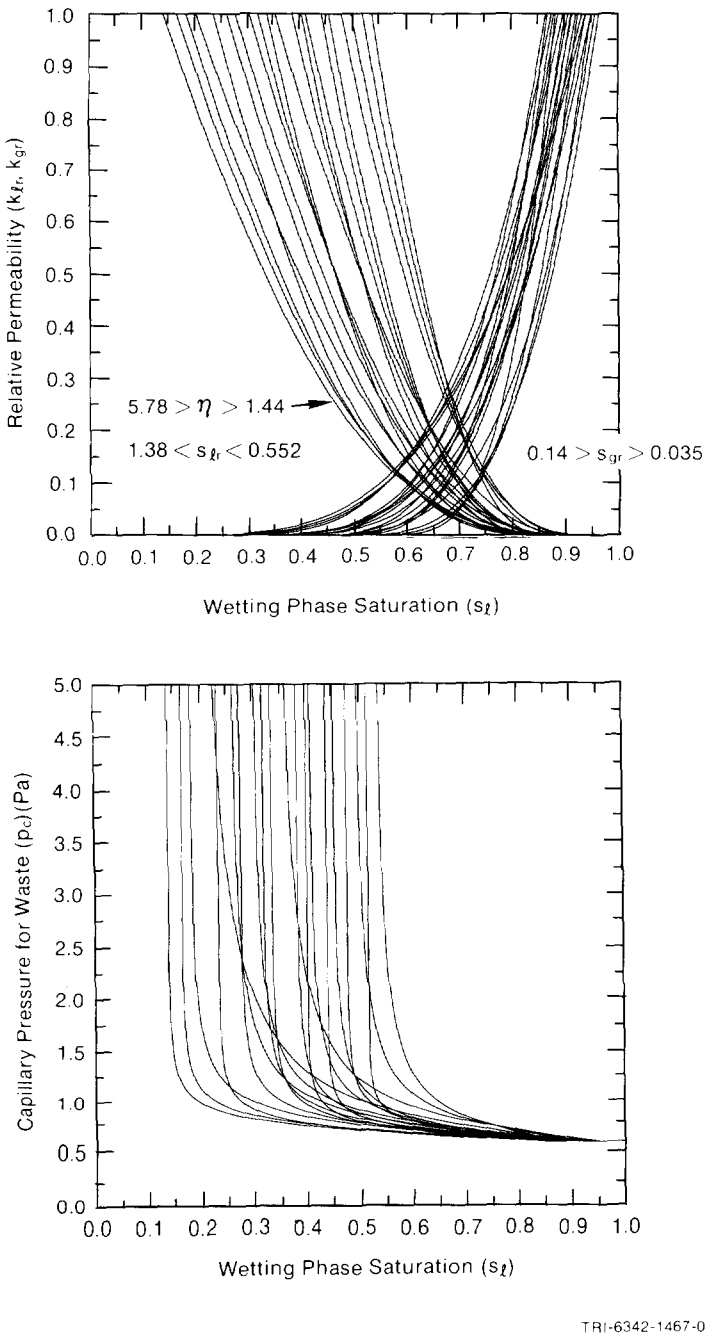

Figure 3.4-7. Example of Variation in Relative Permeability and Capillary Pressure for Unmodified Waste When Brooks and Corey Parameters Are Varied.

Discussion:

The correlations for these values were developed as discussed in the Chapter 2 section, "Hydrologic Parameters for Halite and Polyhalite within the Salado Formation." Preliminary parameter values were obtained from Brooks and Corey (1964). Their experimental data for a "poorly sorted, fragmented mixture of granulated clay, fragmented sandstone, and volcanic sand" were used as the natural analog.

An initial range was selected for the purpose of being able to run sensitivity parameter studies. The ranges shown for the parameters are quite arbitrary, corresponding to a simple doubling and halving of the median values.

Because the threshold displacement pressure (p_t) is so small, current PA calculations set the value to zero (only in the waste). This allows pressure to equilibrate faster within the waste by permitting the easy movement of phases throughout the waste and thereby reducing the computational burden of codes modeling the two-phase phenomenon.

3.4.5 Drilling Erosion Parameters

Two waste-dependent parameters influencing the amount of material that erodes from the borehole wall during drilling are shear stress generated by the drilling fluid (mud) and waste shear strength.

Absolute Roughness

Parameter:	**Absolute roughness of waste (ε)**
Median:	2.5×10^{-2}
Range:	1×10^{-2}
	4×10^{-2}
Units:	m
Distribution:	Uniform
Source(s):	Streeter, V. L., and E. B. Wylie. 1975. *Fluid Mechanics.* Sixth Edition. New York, NY: McGraw-Hill Book Co. (Figure 5.32)

Discussion:

For turbulent flow, the shear stress of the drilling fluid (mud) acting on the borehole wall is dependent upon the relative surface roughness (ε/d) at the repository level, where ε is the absolute roughness or the average depth of well irregularities, and for flow within an annulus d is the hydraulic diameter. The variable, d, is defined as the difference in borehole diameter and collar diameter. As erosion increases the borehole diameter, the relative roughness decreases if ε is fixed. The current value chosen for PA calculations exceeds that of riveted steel piping, one of the roughest pipes for which data is frequently given (Moody diagram) (Streeter and Wylie, 1975, Figure 5.32).

Figure 3.4-8 provides the distribution for waste absolute roughness.

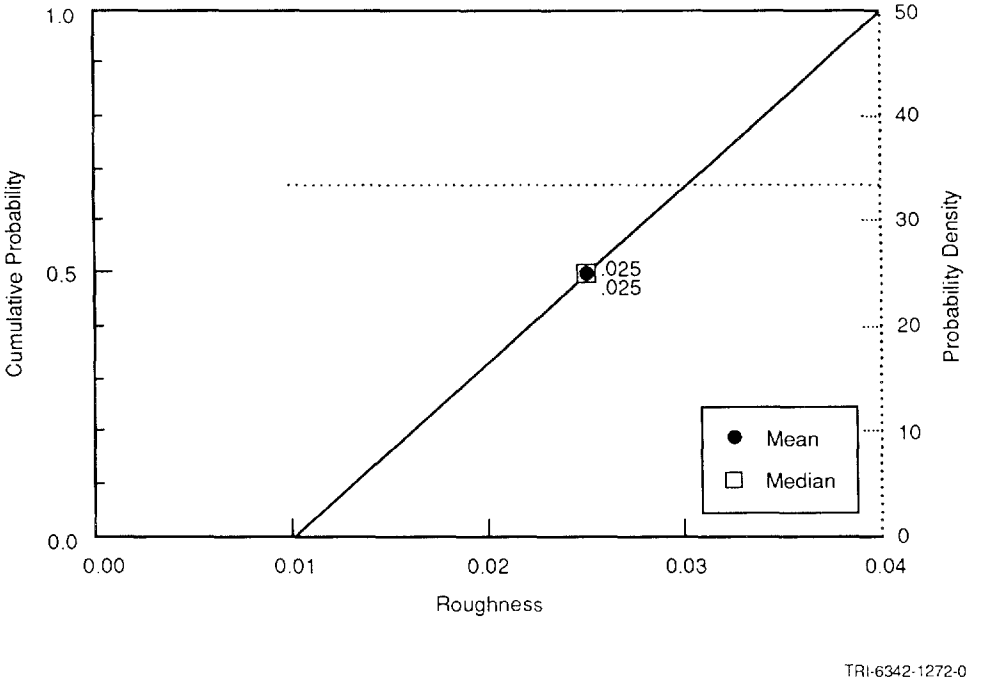

Figure 3.4-8. Estimated Distribution (pdf and cdf) for Waste Absolute Roughness.

Effective Shear Strength for Erosion

Parameter:	**Effective shear strength for erosion (τ_{fail})**
Median:	1
Range:	1×10^{-1}
	1×10^{1}
Units:	Pa
Distribution:	Cumulative
Source(s):	Sargunam, A., P. Riley, K. Arulanadum, and R. B. Krone. 1973. "Physico-Chemical Factors in Erosion of Cohesive Soils." *Journal of the Hydraulics Division, American Society of Civil Engineers* 99: 555-558.
	Henderson, F. M. 1966. *Open Channel Flow.* New York: Macmillan Publishing Co. (Figure 10-5)

Discussion:

The effective shear strength for erosion (allowable tractive force) equals the threshold* value of fluid shear stress required to sustain general erosion at the borehole wall. Parthenaides and Paaswell (1970), in discussing investigations on the erosion of seabed sediments and in channels, has noted that this effective soil shear strength is not related to the soil shear strength as normally determined from conventional soil tests. The effective shear strength for erosion is smaller by several orders of magnitude than the macroscopic soil shear strength.

Following the experimental work of Sargunam et al. (1973) on erosion of cohesive soils (see Figure 4.2-6 in Chapter 4), the PA Division assumed an effective shear strength for erosion (τ_{fail}) for the unmodified waste of 1 Pa (1.45×10^{-4} psi), a value at the low end of the range for loose (uncompacted) montmorillonite clay. The erodible shear strength of a noncohesive, fine sand (diameter near 2.5×10^{-4}) is also about 1 Pa (1.45×10^{-4} psi) (Henderson, 1966, Figure 10-5). Because the erodibility of the material at any given velocity is highly dependent on the effective diameter of the material—and for cohesive materials, its degree of compaction and plasticity index (Henderson, 1966)—the upper limit can be quite large (greater than 100 Pa). However, PA calculations assume only an order-of-magnitude range since values much greater than 10 Pa preclude erosion.

* The threshold of sediment movement (erosion) cannot be defined with absolute precision, because as the fluid shear stress gradually increases (due to velocity increase) there is no precise point at which sediment movement suddenly becomes general. Rather, at first only a few grains are dislodged every few seconds, then grain movement becomes more frequent until it affects the entire bed.

3.4.6 Partition Coefficients for Clays in Salt Backfill

Table 3.4-15 provides assumed partition coefficients for salt backfill.

Table 3.4-15. Partition Coefficients for Salt Backfill Containing Trace (0.1%) Amounts of Clay (after Lappin et al., 1989, Table D-5)

Radionuclide	Partition Coefficient* (m^3/kg)
Am	1×10^{-4}
Np	1×10^{-5}
Pb	1×10^{-6}
Pu	1×10^{-4}
Ra	1×10^{-6}
Th	1×10^{-4}
U	1×10^{-6}

* Assumed constant

Discussion:

See discussion in Section 3.2.4.

3.4.7 Permeability

Parameter:	**Permeability (k), combustibles**
Median:	1.7×10^{-14}
Range:	2×10^{-15}
	2×10^{-13}
Units:	m^2
Distribution:	Cumulative
Source(s):	Butcher, B. M., T. W. Thompson, R. G. Van Buskirk, and N. C. Patti. 1991. *Mechanical Compaction of WIPP Simulated Waste.* SAND90-1206. Albuquerque, NM: Sandia National Laboratories.

Parameter:	**Permeability (k), metals/glass**
Median:	5×10^{-13}
Range:	4×10^{-14}
	1.2×10^{-12}
Units:	m^2
Distribution:	Cumulative
Source(s):	Butcher, B. M., T. W. Thompson, R. G. Van Buskirk, and N. C. Patti. 1991. *Mechanical Compaction of WIPP Simulated Waste.* SAND90-1206. Albuquerque, NM: Sandia National Laboratories.

Parameter:	**Permeability (k), sludge**
Median:	1.2×10^{-16}
Range:	1.1×10^{-17}
	1.7×10^{-16}
Units:	m^2
Distribution:	Cumulative
Source(s):	Butcher, B. M., T. W. Thompson, R. G. Van Buskirk, and N. C. Patti. 1991. *Mechanical Compaction of WIPP Simulated Waste.* SAND90-1206. Albuquerque, NM: Sandia National Laboratories.

Discussion:

The permeability for the combustibles was estimated from a few tests on simulated waste (Butcher, 1990). After crushing a mixture of 60% by weight of pine cubes and 40% of rags for 30 days at 14 MPa, the permeability started at 2 x 10^{-13} m^2 (200 mD) and dropped to 2 x 10^{-15} m^2 (2 mD), which defined the maximum range for combustibles. (A similar test had a steady permeability of 1.3 x 10^{-14} m^2 (13 mD); two tests on a mixture of 40% plastic bottles, 40% PVC parts, and 20% gloves had permeabilities of 0 and 2.5 x 10^{-4} m^2 [0 and 25 mD].) The median permeability of 1.7 x 10^{-14} m^2 (17 mD) for combustible waste was estimated from the average of two tests on a simulated waste mixture consisting of 45% of the above plastics and 37% of the above wood mixture plus 9% 1-inch metal parts and 9% dry Portland cement.

The maximum and median values for permeability of the metals and glass component of the waste were estimated using 50% 1-inch metal parts and 50% magnetite that were crushed for one day. The latter material represented the corroded metal. One test had an initial permeability of 5.0 x 10^{-13} m^2 (500 mD) (used as the median value), but dropped to 4 x 10^{-15} m^2 (4 mD) (used as the minimum value). (A second test had a steady permeability of 1.1 x 10^{-14} m^2 [11 mD].) The maximum permeability is the value estimated for uncorroded metal waste in Lappin et al. (1989, p 4-56).

Mean Permeability of Drum. For computational ease, the PA Division assumed that the permeabilities of each component were uniformly distributed from the minimum to the maximum values given above in evaluating the permeability of an average drum. Consequently, the distribution of local permeability (i.e., the effective permeability of a collapsed drum) was the weighted sum of uniform distributions, the weights being percent by volume of each component.

Assuming that the volume fractions of the components are 40% combustibles, 40% metals/glass, and 20% sludge (values reported in Table 3.4-1 rounded to one significant digit), it is easily calculated that the expected permeability on the scale of a drum (0.27 m^3 or 9.5 ft^3) is

$$E(k) = \mu_{perm} = \int k f(\eta) d\eta = 1.7 \times 10^{-13}\ m^2 \qquad (3.4\text{-}1)$$

and the coefficient of variation $[V(k)]^{1/2}/E(k)$ is

$$([V(k)]^{1/2}/E(k)^2 = (\sigma/\mu_{perm})$$

$$= (\int m^2 f(\eta) d\eta)^{1/2}/\mu_{perm} = E(k - \mu)^2]^{1/2}/\mu_{perm} = 1.22 \qquad (3.4\text{-}2)$$

where

E(k) = expectation of k
V(k) = variance of k

The foregoing estimates establish the statistical properties of the permeability of a *single*, typical collapsed waste drum. These properties are next used to estimate the distribution of the material-property parameter: effective hydraulic conductivity of an entire, collapsed WIPP room. To estimate distribution of effective hydraulic conductivity of a room, we must make further assumptions about the way waste drums are sorted and placed into particular rooms: in the absence of any firm plans for sorting waste drums, we are forced to assume that any waste drum is equally likely to be placed in any of the (approximately) 120 rooms. Hence, there is no spatial correlation between two adjacent drums in the same room, and the "cookie cutter" autocorrelation function (see Chapter 1) is applicable with a correlation volume, a^3, of the order of the volume of a collapsed waste drum.

Model of WIPP Room. The collapsed WIPP room is modeled as a rectangular parallelopiped composed of many, small rectangular parallelopipeds (the collapsed drums) (Figure 3.4-9).

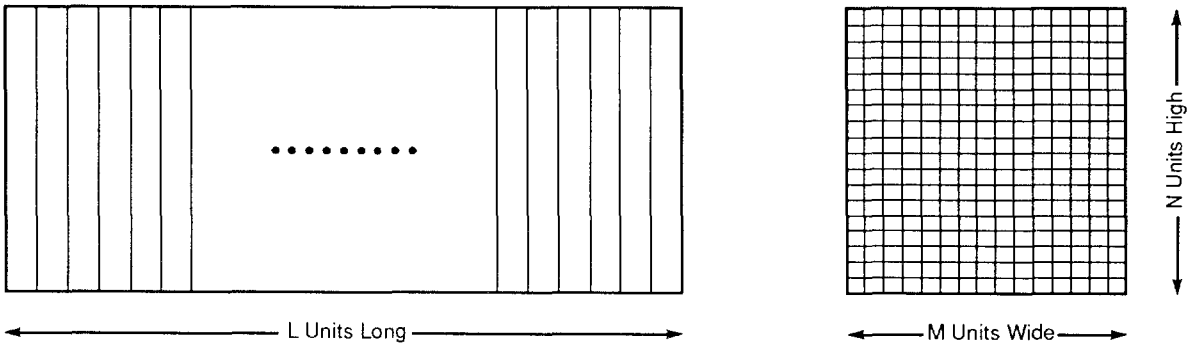

Figure 3.4-9. Model of Collapsed WIPP Room

The collapsed drums will be called "units." In Figure 3.4-8 above, LMN = 6804, or

L = number of replications of the unit down length of a room (~162, Figure 3.1-3)
M = number of replications of the unit across a room (~14, Figure 3.1-3)
N = number of replications of the unit veritically (3, Figure 3.1-3).

With each unit is associated a local porosity

$\phi_{\ell mn}$ - local porosity (assumed isotropic)

and a local hydraulic conductivity

$k_{\ell mn}$ - local hydraulic conductivity (assumed isotropic)

As previously stated, it is assumed that $\phi_{\ell mn}$ and $k_{\ell mn}$ are independent, identically distributed random variables; i.e., the $\phi_{\ell mn}$ have a density function f(c) and the $k_{\ell mn}$ have density function g(k).

Effective Permeability. The first problem is to find the distribution of k_{eff}, where

$$J = k_{eff} \frac{\Delta h}{x},$$

Δh being the applied pressure-head difference across the room in the x-direction. Now, from Freeze & Cherry (1979, p. 34, Eq. 2.32), the effective permeability, k_ℓ, of the ℓ^{th} slab follows (flow parallel to layering):

$$k_\ell = \frac{1}{MN} \sum_{m=1}^{M} \sum_{n=1}^{N} k_{\ell mn} \qquad (3.4\text{-}3)$$

Thus, viewing the slabs $\ell = 1,2,...L$ as layers and the flow being perpendicular to these layers, we have from Freeze & Cherry (1979, p. 34, Eq. 2.31)

$$k_{eff} = \frac{1}{\frac{1}{L} \sum_{\ell=1}^{L} \frac{1}{k_\ell}} \qquad (3.4\text{-}4)$$

Now if $E[k_{\ell mn}] = \mu$ and $Var\,[k_{\ell mn}] = \sigma^2$ (i.e., it is assumed that the $k_{\ell mn}$ are independent, identically distributed [iid] random variables with mean μ and variance σ^2), and if $MN >> 1$, then by the Central Limit Theorem (Ross, 1985, p. 70), the random variable K_ℓ is approximately normally distributed, i.e.,

$$Pr(k_\ell \le x) \to \Phi\left[\frac{\sqrt{MN}\,(x-\mu)}{\sigma}\right] \text{ as } MN \to \infty$$

where

$$\Phi(y) = \frac{1}{\sqrt{2\pi}} \int_{-\infty}^{y} e^{-x^2/2} dx \text{ (the standard normal distribution)}$$

In other words, k_ℓ is approximately normally distributed with mean μ and variance $\sigma_k^2 = \sigma^2/MN$.

Gauss' approximation formulae (Blom, 1989, p. 125) are next used to estimate the mean and variance of the distribution of k_{eff}, given that the mean and variance of the k_ℓ are respectively μ and σ^2/MN. Using these formulae and Eq. 3.4-4 gives, for the mean value,

$$E\left[k_{eff}\right] \sim \frac{1}{\frac{1}{L} \sum_{\ell=1}^{L} \frac{1}{\mu}} = \mu \qquad (3.4\text{-}5)$$

and for the variance,

$$\mathrm{Var}\left[k_{eff}\right] \sim \sum_{\ell=1}^{L} \mathrm{Var}[k_\ell] \cdot \left[\left(\frac{\delta k_{eff}}{\delta k_\ell}\right)_{k_\ell=\mu}\right]^2 = \sum_{\ell=1}^{L} \frac{\sigma^2}{MN} \cdot \frac{1}{L^2} = \frac{\sigma^2}{MNL} \qquad (3.4\text{-}6)$$

Magnitudes of these quantities can be estimated using the preliminary permeability estimates (Eqs. 3.4-1 and 3.4-2),

$$\mu_{perm} = 1.7 \times 10^{-13}\ m^2\ (1.25 \times 10^{-6}\ m/s)$$

$$\sigma_{perm} = 2.07 \times 10^{-13}\ m^2\ (1.52 \times 10^{-6}\ m/s),$$

and taking L = 162, M = 14, and N=3. The results are

$$E[k_{eff}] \sim \mu = 1.7 \times 10^{-13}\ m^2\ (1.25 \times 10^{-6}\ m/s)$$

and coefficient of variation of

$$\frac{E(k_{eff})}{V(k_{eff})} \sim [(MNL)^{-1/2}] \cdot (\sigma/\mu) = 1.48 \times 10^{-2}.$$

The small coefficient of variation suggests that the distribution of k_{eff} is highly concentrated about the mean value, μ. The mean varies only slightly with the permeability estimate in Lappin et al., 1989. To be consistent with this and other previous work, the PA Division used a value of 1 x 10^{-13} m^2 (100 mD).

Because the coefficient of variation is so small, the PA Division did not sample on waste permeability nor adjust its value according to the waste composition as was done for porosity. The waste permeability was so high that a large decrease (~4 orders of magnitude) would be required to have a noticeable effect on results (Rechard et al., 1989, Figure 4-2), too large a decrease to be obtained from the currently assumed variation in waste composition. (The variance of the volume fraction of waste components adds directly [not reduced by the Central Limit Theorem] to the waste unit variance.)

3.4.8 Porosity

Parameter:	**Porosity (ϕ), combustibles**
Median:	0.014
Range:	0.087
	0.18
Units:	Dimensionless
Distribution:	Data
Source(s):	Butcher, B. M., T. W. Thompson, R. G. Van Buskirk, and N. C. Patti. 1991. *Mechanical Compaction of WIPP Simulated Waste.* SAND90-1206. Albuquerque, NM: Sandia National Laboratories.

Parameter:	**Porosity (ϕ), metals/glass**
Median:	0.40
Range:	0.33
	0.44
Units:	Dimensionless
Distribution:	Data
Source(s):	Butcher, B. M., T. W. Thompson, R. G. Van Buskirk, and N. C. Patti. 1991. *Mechanical Compaction of WIPP Simulated Waste.* SAND90-1206. Albuquerque, NM: Sandia National Laboratories.

Parameter:	**Porosity (ϕ), sludge**
Median:	0.11
Range:	0.01
	0.22
Units:	Dimensionless
Distribution:	Data
Source(s):	Butcher, B. M., T. W. Thompson, R. G. Van Buskirk, and N. C. Patti. 1991. *Mechanical Compaction of WIPP Simulated Waste.* SAND90-1206. Albuquerque, NM: Sandia National Laboratories.

Discussion:

The objective of the procedure described here for calculating panel porosity is to enable Performance Assessment to determine initial and final porosities of the panel in a manner that is consistent with the estimated actual inventory of the repository and with the need to vary the composition of the waste in PA calculations. First, the initial porosity will be calculated based on the design capacity of the repository and the design waste inventory estimates discussed in Section 3.4.1. Then the final porosity of a perfectly sealed panel (no gas escapes) will be determined. Finally, the procedure will be extended to variable waste compositions.

Initial Porosity. The waste inventory is broken down into three IDB categories: metals and glass, combustibles, and sludge. In Section 3.4.1, a volume fraction of each of these categories, $f_m = 0.368$, $f_c = 0.403$, and $f_s = 0.229$, respectively, was estimated from which the volume of each category is calculated:

$$V_m = f_m V_w = 64{,}610 \text{ m}^3$$
$$V_c = f_c V_w = 70{,}750 \text{ m}^3$$
$$V_s = f_s V_w = 40{,}200 \text{ m}^3$$

where $V_w = 175{,}600$ m^3 (6.2×10^6 ft^3), the design capacity of the repository.

The mass of each category is then computed assuming a fixed average mass of waste category in each drum and the known volume of a drum, $V_d = 0.21$ m^3. The average mass of each category per drum (not including the containers), as used in Table 3.4-9, is:

$$M_{dm} = 64.5 \text{ kg/drum}$$
$$M_{dc} = 40.0 \text{ kg/drum}$$
$$M_{ds} = 225. \text{ kg/drum}$$

A fixed average mass of container is also assumed to be portioned to each category, the values obtained from Table 3.4-9 being:

$$M_{cm} = 12.40 \text{ Gg}$$
$$M_{cc} = 13.29 \text{ Gg}$$
$$M_{cs} = 4.458 \text{ Gg}$$

The total mass of each category, including containers, in the full repository is then:

$$M_m = M_{dm} V_m / V_d + M_{cm} = 31.98 \text{ Gg}$$
$$M_c = M_{dc} V_c / V_d + M_{cc} = 26.77 \text{ Gg}$$
$$M_s = M_{ds} V_s / V_d + M_{cs} = 47.53 \text{ Gg}$$

The total mass of waste, including containers, is the sum of the masses of these three categories:

$$M_w = M_m + M_c + M_s = 106.3 \text{ Gg}$$

These figures can all be found in Table 3.4-9 (under the heading "Stored, Projected, and Scaled") and in Table 3.4-1, which summarizes the data.

In addition to the waste, the repository will also contain salt backfill and an air gap between the top of the backfill and the ceiling of the repository. The masses of backfill and the initial air gap are:

$$M_b = \rho_{bb} V_b = 219.2 \text{ Gg}$$
$$M_a = \rho_a V_a = 0.1051 \text{ Gg}$$

where ρ_{bb} and ρ_a are, respectively, the bulk density of backfill and the density of air (ideal gas with molecular weight 0.02897 kg/mol at atmospheric pressure [101.3 kPa] and 300.15 K):

$$\rho_{bb} = 1280 \text{ kg/m}^3$$
$$\rho_a = 1.18 \text{ kg/m}^3$$

and the volume of salt backfill and air gap initially present when the repository is filled are (see Section 3.1.6):

$$V_b = 171{,}200 \text{ m}^3$$

$$V_a = 89{,}080 \text{ m}^3$$

The total mass of waste, backfill, and air gap initially present in the repository is:

$$M_t = M_w + M_b + M_a = 325.6 \text{ Gg}$$

The bulk density of each category (including containers) and of the waste are:

$$\rho_{bm} = M_m/V_m = 495 \text{ kg/m}^3$$
$$\rho_{bc} = M_c/V_c = 378 \text{ kg/m}^3$$
$$\rho_{bs} = M_s/V_s = 1182 \text{ kg/m}^3$$
$$\rho_{bw} = V_w = 605 \text{ kg/m}^3$$

The initial porosity of each category (including containers) and of the backfill are calculated from the above bulk densities and assumed values for the solid (grain) densities of each category (Butcher et al., 1991):

ρ_m = 3440 kg/m^3
ρ_c = 1310 kg/m^3
ρ_s = 2150 kg/m^3
ρ_b = 2140 kg/m^3

The solid densities of the three waste categories presumably include containers; this enables calculation of porosities in which a bulk density (including containers) is divided by a solid density (also including containers). The solid density of salt includes a 1% irreducible porosity that remains in compacted halite. To be fully consistent, the true grain density, 2,160 kg/m^3, should be used. This minor inconsistency will be corrected in the 1992 PA calculations. The porosities are then

$\phi_m = 1 - \rho_{bm}/\rho_m = 0.856$
$\phi_c = 1 - \rho_{bc}/\rho_c = 0.711$
$\phi_s = 1 - \rho_{bs}/\rho_s = 0.450$
$\phi_b = 1 - \rho_{bb}/\rho_b = 0.402$

Now the initial pore volumes of each category can be determined:

$V_{pm} = \phi_m V_m = 55{,}310$ m^3
$V_{pc} = \phi_c V_c = 50{,}320$ m^3
$V_{ps} = \phi_s V_s = 18{,}100$ m^3
$V_{pb} = \phi_b V_b = 68{,}820$ m^3
$V_{pa} = V_a = 89{,}080$ m^3

Summing, the net waste pore volume (including containers) is

$V_{pw} = V_{pm} + V_{pc} + V_{ps} = 123{,}700$ m^3

and the pore volume of the entire repository is initially

$V_{pt} = V_{pw} + V_{pb} + V_{pa} = 281{,}600$ m^3

The initial porosity of the repository for the design inventory is then

$\phi_t = V_{pt}/V_t = 0.646$

where V_t is the initial excavated volume of the repository, excluding seals (Table 3.1-1)

$V_t = 436{,}000$ m^3.

A number also of interest, though not needed for PA calculations, is the porosity of the waste alone, including containers, but excluding backfill and air gap:

$\phi_w = V_{pw}/V_w = 0.705$

Table 3.4-16 summarizes the calculation of initial porosity of the repository.

Table 3.4-16. Summary of Initial Porosity Calculations

	Waste Volume Fraction	Initial Volume (m^3)	Initial Mass (kg)	Bulk Density (kg/m^3)	Solid Density (kg/m^3)	Initial Porosity --	Pore Volume (m^3)	Solids Volume (m^3)
Metal + Glass	0.368	64,608	31,981,774	495	3,440	0.856	55,311	9,297
Combustibles	0.403	70,752	26,769,084	378	1,310	0.711	50,318	20,434
Sludge	0.229	40,204	47,533,716	1,182	2,150	0.450	18,095	22,109
Waste subtotal	1.000	175,564	106,284,574	605	2,050	0.705	123,724	51,840
Backfill		171,241	219,188,480	1,280	2,140	0.402	68,816	102,425
Air Gap		89,081	105,116	1	--	1.000	89,081	--
Total		436,023	325,578,170	747	2,109	0.646	281,621	154,265

Note: Figures for waste categories and subtotal include containers.

Final Porosity. The final porosity is calculated by assuming that no gas leaks from the repository and that the final gas pressure is equal to lithostatic pressure, 14.9 MPa. It is also assumed that the volume of solids in the repository is conserved. Knowing the corrodible metal content of the waste and the amount of biodegradables enables the total gas potential to be calculated. Adjusting for lithostatic pressure, this final potential gas volume, together with the air initially present (both in the air gap and in the initial pore spaces), constitutes the final pore volume of the repository.

The initial solids volume is the difference between the bulk volume and the pore volume of each category:

$$V_{sm} = V_m - V_{pm} = 9{,}297 \text{ m}^3$$

$$V_{sc} = V_c - V_{pc} = 20{,}430 \text{ m}^3$$

$$V_{ss} = V_s - V_{ps} = 22{,}110 \text{ m}^3$$

The initial solids volume in the waste is:

$$V_{sw} = V_w - V_{pw} = 51{,}840 \text{ m}^3$$

and the initial backfill solids volume is:

$$V_{sb} = V_b - V_{pb} = 102{,}400 \text{ m}^3$$

The total solids volume is the sum of waste solids volume and backfill solids volume:

$$V_{st} = V_{sw} + V_{sb} = 154{,}300 \text{ m}^3$$

Additional assumptions concerning the composition of the waste are needed. In the metals and glass category, only a portion of the total mass is corrodible and thus capable of producing gas. Of the metals listed in Table 3.4-11 (Design column), the following are considered corrodible: Iron, paint cans, steel, and shipping cans. The total mass of these materials in the Design inventory is

$$M_{Few} = 14.31 \text{ Gg}$$

and for gas potential calculations, the materials are assumed to be pure iron (Fe). The waste containers contain an even greater amount of corrodible metal. From Table 3.4-8, the container steel in the repository Design volume is

$$M_{Fec} = 26.13 \text{ Gg}$$

This mass is also assumed to be pure iron for gas potential purposes. The total iron in the repository is

$$M_{Fet} = M_{Few} + M_{Fec} = 40.44 \text{ Gg}$$

In the Combustibles category, only a portion is believed to be biodegradable. This portion includes all cellulosics and 50% of certain rubbers, including surgeon's gloves (latex), hypalon, neoprene, and other rubber undefined. The total mass of biodegradables in the Design inventory, from Table 3.4-11, is

$$M_{Bio} = 7.475 \text{ Gg}$$

Details of the gas potential from iron corrosion are discussed in Section 3.3.8. It is assumed that corrosion and biodegradation reactions produce hydrogen gas. The median stoichiometric coefficient for hydrogen using the average corrosion reaction, Eq. 3.3-4, is

$$s_{Fe} = 7/6 = 1.167 \text{ mol H2/mol Fe}$$

and the molecular weight of iron is

$$M_{Fe} = 0.055\,85 \text{ kg/mol Fe}$$

Then the gas potential from corrosion is

$$M_{H_2Fe} = M_{Fet} s_{Fe} / M_{Fe} = 844.8 \text{ Mmol } H_2$$

Details of the gas potential from biodegradation are discussed in Section 3.3.9. The median stoichiometric coefficient for hydrogen using the average biodegradation reaction, Eq. 3.3-6, is

$$s_{Bio} = 0.835 \text{ mol } H_2/\text{mol cellulose is}$$

and the molecular weight of cellulose is

$$M_{cell} = 0.030 \text{ kg/mol cellulose}$$

Then the gas potential from corrosion is

$$m_{H_2 Bio} = M_{Bio} s_{Bio} / M_{cell} = 208 \text{ Mmol } H_2$$

The total gas potential using the design inventory and median reaction parameters is

$$m_{H_2 t} = m_{H_2 Fe} + m_{H_2 Bio} = 1.053 \text{ Gmol } H_2$$

Using a molar volume for H_2 of 1.822 x 10^{-4} m^3/mol H_2 (see Section 4.1.4), the volume of this hydrogen at 14.9 MPa and 300.15 K is

$$V_{H_2} = 191{,}800 \text{ m}^3$$

In addition, the air initially present in the repository both in the air gap and in pore space is compressed from initial pressure, p_i, of 101.325 kPa to final lithostatic pressure, p_f, of 14.9 MPa, resulting in a volume (assuming ideal gas behavior) of

$$V_{af} = V_{pt} p_i / p_f = 1{,}915 \text{ m}^3$$

The total gas volume in the final repository at 14.9 MPa is

$$V_g = V_{H_2} + V_{af} = 193{,}700 \text{ m}^3$$

Then the final porosity of a gas-tight repository containing the full amount of gas that is potentially producible is

$$\phi_f = V_g/(V_g + V_{st}) = 0.557$$

Final Porosity for Variable Waste Composition. The porosity of a room or panel will vary with time as salt creep compresses the pore spaces while gas generation creates a time-dependent resistance to creep closure. These phenomena cannot yet be simulated accurately within the PA calculations, so some simplifying assumptions must be made. The first is that the porosity will not change over time, but instead will immediately attain the final porosity.

Second, it is assumed that the final porosity is the porosity of a gas-tight, perfectly sealed repository. Although this second assumption appears somewhat arbitrary, since almost any porosity between a sealed-room porosity and a completely open porosity (i.e., all gas escapes and causes no additional resistance to creep closure beyond what the solids impose) might be justified, preliminary calculations indicated that, barring any pressure release resulting from intrusions, the pressure in the repository generally reaches a value close to lithostatic, quite rapidly, and stays there for the duration of the 10,000-yr period. Furthermore, the permeabilities of the likeliest gas flow paths (the anhydrite layers and Marker Bed 139) are so low that little gas will escape over the 10,000 yr. Therefore, the repository will generally behave more like a gas-tight enclosure than like a very leaky one, so assuming it is gas-tight is reasonable.

Because the composition of the waste that will ultimately fill the repository is not known with complete certainty, it is varied in the 1991 PA calculations. Variations in the composition of the waste result in different final porosities, because the gas potential changes, depending on how much corrodible metal and biodegradable material is present. In addition to the volume fractions of metals and glass and of combustibles, two other parameters that effect the final porosity are also varied in the PA calculation: the stoichiometric coefficients x_{Fe} and x_{Bio}.

The procedure described above is used to calculate the final porosity. Three additional assumptions are required. First, the mass of containers is assumed to remain fixed; in particular, the mass of iron in the containers, M_{cm}, is assumed constant. Second, the mass fraction of metals and glass that is corrodible metal is assumed to be constant. This fraction is

$$f_{mc} = M_{Few}/(M_m - M_{cm}) = 14.31 \text{ Gg}/19.84 \text{ Gg} = 0.721$$

Third, the mass fraction of combustibles that is biodegradable is assumed to be constant. This fraction is

$$f_{cb} = M_{Bio}/(M_c - M_{cc}) = 7.475 \text{ Gg}/13.48 \text{ Gg} = 0.555$$

Then the total iron content in the repository is

$$M_{Fet} = f_{mc}M_{dm}V_m/V_d + M_{Fec}$$

and the total biodegradable mass is

$$M_{Bio} = f_{cb}M_{dc}V_c/V_d + M_{Bioc}$$

where M_{Bioc}, the mass of biodegradable container material, is currently zero. The rest of the porosity calculation is the same as described above (except that the stoichiometric coefficients vary).

Brine saturation will also affect the final porosity. This effect has not been taken into account in these calculations because the brine saturation varies greatly during the 10,000 yr, and a consistent and accurate way to incorporate this effect has not been developed.

Final room or panel height is calculated from the initial and final porosity. It is assumed that creep closure occurs only in the vertical direction, not horizontally. While not correct, this assumption has little effect on the results, except to make calculation of the final panel height much easier, since the floor area does not change.

Assuming solids volume is conserved during closure,

$$(1 - \phi_i)Ah_i = (1 - \phi_f)Ah_f$$

where A is the floor area, h_i is the initial panel height, and h_f is the final panel height. The final panel height is then

$$h_f = h_i(1 - \phi_i)/(1 - \phi_f)$$

Panel Averaging. Some PA calculations, done on a panel scale, require that certain properties be averaged over the entire panel. This is particularly true for the two-phase flow calculations, which, because of time and size constraints, must be done using two-dimensional cylindrical geometry. This necessitates using properties for a full panel that combine properties of the waste and backfill with those of the intact salt pillars that separate rooms in a panel. Properties used in the models are generally area-weighted averages of the waste properties and the pillar properties. (A notable exception is permeability; waste permeability is used as the average permeability of a panel.)

The average porosity of a panel is calculated from

$$\phi_{pav} = \frac{\phi_f A_{panx} + \phi_p A_{pil}}{A_{panx} + A_{pil}}$$

where A_{panx} is the excavated floor area of a panel (11,640 m^2, from Table 3.1-1), ϕ_p is the constant median porosity of an undisturbed halite pillar (0.01, from Table 2.3-1), and A_{pil} is the area of the pillars in a panel,

$$A_{pil} = A_{pann} - A_{panx} = 17{,}780 \text{ m}^2$$

where A_{pann} is the enclosed area of a panel (29,420 m^2, from Table 3.1-1). Note that the height of the panel does not enter into the equation. This is true because of the assumption the salt creep occurs only vertically.

The average initial brine saturation of a panel is calculated from S_{bw}, the initial brine saturation of the waste (a varied parameter), and the fixed brine saturation of undisturbed halite, S_{bpil} (1.0, i.e., fully saturated):

$$S_{bpav} = (S_{bw}\phi_f A_{panx} + S_{bpil}\phi_p A_{pil})/(\phi_f A_{panx} + \phi_p A_{pil})$$

Minimum Porosity. The minimum porosity is the porosity of the waste that is reached within about 200 yr without gas generation and sometime later (perhaps after 10,000 yr) with gas generation.

Similar to the calculations presented for permeability, the porosity of the overall waste was estimated by combining, by volume, the estimated individual porosities (on the scale of a drum) of combustibles (plastic, gloves, pine wood, and rags), metal/glass (including corroded and uncorroded steel), and sludges (liquid waste mixed with cement). Estimates for the individual components from estimates of the density at 15 MPa (148 atm) are shown above (Butcher et al., 1991).

Performance Assessment assumed that the porosities of each component were uniformly distributed between the minimum and maximum values given above. Consequently the distribution of local porosity (i.e., the porosity of a collapsed drum) was the weighted sum of uniform distributions.

The resulting mean porosity depends on the final volume fraction of the individual components, which varies in the current PA calculations. For example, we may assume that the initial volume fractions are 40% combustibles, 40% metals/glass, and 20% sludge.

Using the ranges of component porosity (Table 3.4-9), the pdf for porosity of a collapsed drum becomes

$$p(\phi)d\phi = f_c \frac{d\phi}{0.093} + f_m \frac{d\phi}{0.11} + f_s \frac{d\phi}{0.21}$$

where

f_c, f_m, f_s = volume fractions of combustibles, metals/glass, and sludges, respectively

Holding these fractions fixed, the expected value of porosity of a collapsed drum, μ_e, can be calculated:

$$\mu_e = \frac{f_c}{0.093} \int_{0.087}^{0.18} \phi d\phi + \frac{f_m}{0.11} \int_{0.33}^{0.44} \phi d\phi + \frac{f_s}{0.21} \int_{0.01}^{0.22} \phi d\phi \qquad (3.4\text{-}7)$$

$$= 0.134\, f_c + 0.385\, f_m + 0.115\, f_s$$

If the waste-component volume fractions are those given in Table 3.4-1, then

$$\mu_e = 0.134\ (.40) + 0.385(.40) + 0.115\ (.20) = 0.23$$

The variance of the porosity of a collapsed drum, σ_e^2, can also be calculated:

$$\sigma_e^2 = \frac{f_c}{0.093}\int_{0.087}^{0.18}\phi^2 d\phi + \frac{f_m}{0.11}\int_{0.33}^{0.44}\phi^2 d\phi + \frac{f_s}{0.21}\int_{0.01}^{0.22}\phi^2 d\phi - \mu_e^2$$

$$= 1.85 \times 10^{-2} f_c + 1.49 \times 10^{-1} f_m + 1.69 \times 10^{-2} f_s - \mu_e^2 \qquad (3.4\text{-}8)$$

If the waste-component volume fractions are those given in Table 3.4-1, $\sigma_e = 0.13$ and the coefficient of variation is 0.56.

Effective Minimum Porosity. The effective porosity of the collapsed WIPP room is given by (see Section 3.4.6, Permeability)

$$\phi_{eff} = \frac{1}{MN}\sum_{m=1}^{M}\sum_{n=1}^{N}\phi_{\ell mn} \qquad (3.4\text{-}9)$$

where

M = number of replications of units (waste drums) across a room (~14)
N = number of replications of units vertically (3)

Thus, if $E[\phi_{\ell mn}] = \mu_e$ and Var $[\phi_{\ell mn}] = \sigma_e^2$, the Central Limit Theorem (Ross, 1985, p. 70) guarantees that

$$P_r\left\{\phi_{eff} \le x\right\} \to \Phi\left[\frac{\sqrt{MN}\left(x - \mu_e\right)}{\sigma_e}\right] \text{ as } MN \to \infty$$

In other words, ϕ_{eff} is approximately normally distributed with mean μ_e and variance = σ_e^2/MN.

The coefficient of variation of the effective porosity is therefore

$$(MN)^{-1/2}\sigma_e/\mu_e \qquad (3.4\text{-}10)$$

where μ_e and σ_e are given respectively by Eqs. 3.4-7 and 3.4-8. Numerical exploration of Eq. 3.4-10 with M=14 and N=3, using several possible values of f_c and f_m will show that the coefficient of variation of the effective porosity is small enough (less than 10%) to justify not sampling on it. Instead, in the 1991 preliminary comparison, the PA Division sampled on the waste component volume fractions, f_c, f_m, and f_s.

Figure 3.4-10 shows predicted consolidation curves for specific waste types.

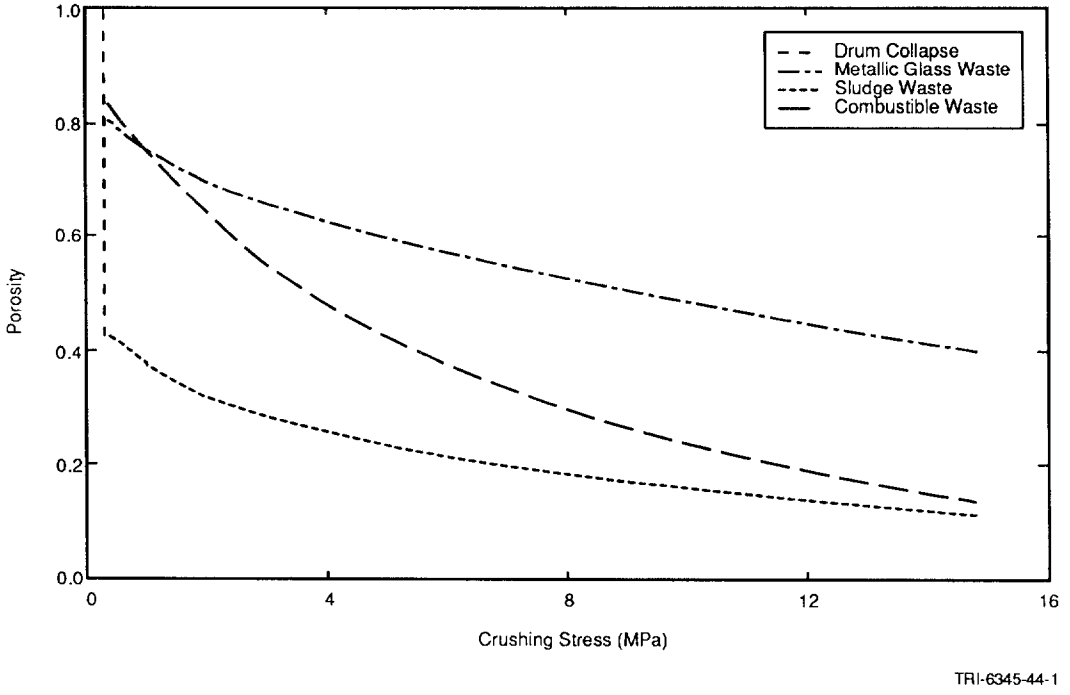

Figure 3.4-10. Predicted Consolidation Curves for Specific Waste Types, including Combustibles, Metals/Glass, and Sludge Wastes (after Butcher et al., 1991, Figure 4-1).

3.4.9 Saturation

Parameter:	**Saturation, initial ($s_{\ell i}$)**
Median:	1.38×10^{-1}
Range:	0
	2.76×10^{-1}
Units:	Dimensionless
Distribution:	Uniform
Source(s):	See text.

Discussion:

The initial fluid saturation ($s_{\ell i}$) of the waste (trash, containers, and backfill) could conceivably vary from 0 up to the residual saturation ($s_{r\ell}$) assumed for the waste provided no fluid is purposefully added. Although these endpoints are probably less likely than some intermediate point, the PA Division did not attempt to more preceisely define this distribution and thus used a uniform distribution.

3.5 Parameters for Salt-Packed Waste Form

Preliminary calculations suggest compliance with *40 CFR 191, Subpart B* can be achieved for the repository as currently designed (Volume 1 of this report; Bertram-Howery et al., 1990; Bertram-Howery and Swift, 1990). However, potential modifications to the present design of the repository and waste are being explored. In last year's PA calculations, waste modification was simulated using modified values for waste permeability, porosity, and shear strength (Table 3.5-1). These values correspond to hypothetical properties of combustible and metallic waste that has been shredded, mixed with crushed salt to reduce void space, and repackaged in new containers. All other parameters for the modified waste remained identical to those of the unmodified waste (Table 3.4-1).

Table 3.5-1. Parameter Values for Salt-Packed Waste

Parameter	Median	Range	Units	Distribution Type	Source
Drilling Erosion Parameter					
Shear strength (τ_{fail})	5		Pa	Constant	Sargunam et al., 1973
Permeability(k)	2.4×10^{-17}		m^2	Constant	See text
Porosity (ϕ)	8.5×10^{-2}		none	Constant	See text; Butcher, 1990a

3.5.1 Drilling Erosion Parameter

Effective Shear Strength for Erosion

Parameter:	**Effective shear strength for erosion (τ_{fail})**
Median:	5
Range:	None
Units:	Pa
Distribution:	Constant
Source(s):	Sargunam, A., P. Riley, K. Arulanadum, and R. B. Krone. 1973. "Physico-Chemical Factors in Erosion of Cohesive Soils." *Journal of the Hydraulics Division, American Society of Civil Engineers* 99: 555-558.

Discussion:

The PA Division assumed a shear strength for erosion (τ_{fail}) for the modified waste of 5 Pa (49 atm), a value at the upper end of the range for montmorillonite clay (Sargunam et al., 1973).

(See also Section 3.4.5.)

3.5.2 Permeability and Porosity

Permeability

Parameter:	**Permeability** (k)
Median:	2.4×10^{-17}
Range:	None
Units:	m^2
Distribution:	Constant
Source(s):	See text.

Porosity

Parameter:	**Porosity** (ϕ)
Median:	8.5×10^{-2}
Range:	None
Units:	Dimensionless
Distribution:	Constant
Source(s):	See text.
	Butcher, B. M., T. W. Thompson, R. G. Van Buskirk, and N. C. Patti. 1991. *Mechanical Compaction of WIPP Simulated Waste.* SAND90-1206. Albuquerque, NM: Sandia National Laboratories. In preparation.

Discussion:

Effective permeability and porosity of a collapsed WIPP room filled with modified waste were calculated in a manner similar to the calculations for unmodified waste (Section 3.4.6, Permeability; Section 3.4.7, Porosity); i.e., the Central Limit Theorem (Ross, 1985, p. 70) was used to show that the distributions of effective permeability and porosity are highly concentrated about the mean values of permeability and porosity that apply to a waste unit (collapsed waste drum). Hypothetical distributions of permeability and porosity for a modified waste unit are tabulated in Table 3.5-2.

Table 3.5-2. Estimated Permeability and Porosity Distributions

Permeability	Porosity	Probability
10^{-16}	0.12	1.0
10^{-19}	0.08	0.5
10^{-21}	0.06	0.0

Using information in Table 3.5-2, it is easily verified that expected permeability (μ_{perm}) and porosity (μ_{por}) on the scale of a drum (0.27 m^3 or 9.4 ft^3) are

$$\mu_{perm} = 2.4 \times 10^{-17}\ m^2 \qquad (3.5\text{-}1)$$

$$\mu_{por} = 0.085 \qquad (3.5\text{-}2)$$

and the coefficients of variation (σ/μ) are approximately 0.20.

The effective porosity of a collapsed WIPP room filled with modified waste is therefore (Section 3.4.7) approximately normally distributed with mean $\mu_{por} = 0.085$ and coefficient of variation $\sim 0.20(MN)^{-1/2} = 2.7 \times 10^{-2}$; the effective permeability is also approximately normally distributed (Section 3.4.6) with mean $\mu_{perm} = 2.4 \times 10^{-17}\ m^2$ and coefficient of variation $\sim 0.20(LMN)^{-1/2} = 2.2 \times 10^{-3}$.

Because the coefficients of variation are so small, the PA Division did not sample on either effective waste permeability or porosity.

3.5.3 Solubility

Discussion:

The solubility and leachability of the radionuclides will likely change, because the repository conditions (e.g., pH, Eh) will change. However, quantifying this change is difficult and has not yet been attempted for the PA calculations. Consequently, as with the unmodified, reference waste, the overall solubility ranges are the same as the extreme local scale (subregions within the drum) solubility; the leach rate from the contaminated material is assumed infinite.

4. PARAMETERS OF GLOBAL MATERIALS AND AGENTS ACTING ON DISPOSAL SYSTEM

This chapter contains parameters for fluid properties, climate variability, and intrusion characteristics.

4.1 Fluid Properties

The fluid parameters tabulated in Table 4.1-1 include Salado and Culebra brine, drilling mud, and hydrogen gas.

Table 4.1-1. Fluid Properties

Parameter	Median	Range		Units	Distribution Type	Source
Brine, Salado (T = 27°C [300.15 K], p = 1 atm [0.101325 MPa])						
Compressibility	2.5×10^{-10}	2.4×10^{-10}	2.6×10^{-10}	Pa^{-1}	Normal	McTigue et al., March 14, 1991, Memo (see Appendix A).
Density (ρ_f)	1.23×10^{3}	1.207×10^{3}	1.253×10^{3}	kg/m^3	Normal	McTigue et al., March 14, 1991, Memo (see Appendix A).
Viscosity (μ)	1.8×10^{-3}			Pa•s	Constant	Kaufman, 1960, p. 622
Brine, Culebra (T = 27°C [300.15 K], p = 1 atm [0.101325 MPa])						
Density (ρf)	1.09×10^{3}	9.99×10^{2}	1.154×10^{3}	kg/m^3	Spatial	Cauffman et al., 1990, Table E.1
Viscosity (μ)	1×10^{-3}			Pa•s	Constant	Haug et al.,1987, p.3-20
Brine, Castile (T = 27°C [300.15 K], p = 1 atm [0.101325 MPa])						
Compressibility	9×10^{-10}			Pa^{-1}	Constant	Popielak et al., 1983, p. H-32
Density	1.215×10^{3}			kg/m^3	Constant	Popielak et al., 1983, Table C-2
Hydrogen (T = 27°C [300.15 K])						
Density	1.1037×10^{1}	8.1803×10^{-2}	1.4442×10^{1}	kg/m^3	Table	See text (Density and Formation Volume Factor)
Viscosity (μ)	9.2×10^{-6}	8.92×10^{-6}	9.33×10^{-6}	Pa•s	Table	Vargaftik, 1975, p. 39.
Solubility in brine (χ)	3.84×10^{-4}	6.412×10^{-6}	4.901×10^{-4}	none	Table	See text (Hydrogen Solubility). Cygan, 1991.
Drilling Mud Properties (T = 22°C [295.15 K], p = 1 atm [0.101325 MPa])						
Density (ρ_f)	1.211×10^{3}	1.139×10^{3}	1.378×10^{3}	kg/m^3	Cumulative	Pace, 1990
Viscosity	9.17×10^{-3}	5×10^{-3}	3×10^{-2}	Pa•s	Cumulative	Pace, 1990
Yield stress	4	2.4	1.92×10^{1}	Pa	Cumulative	Fredrickson, 1960, p.252; Savins et al., 1966; Pace, 1990

4.1.1 Salado Brine

Salado Brine Compressibility

Parameter:	**Compressibility** @ 27°C (300.15 K)
Median:	2.5×10^{-10}
Range:	2.4×10^{-10}
	2.6×10^{-10}
Units:	Pa^{-1}
Distribution:	Normal
Source(s):	McTigue, D. F., S. J. Finley, J. H. Gieske, and K. L. Robinson. "Compressibility Measurements on WIPP Brines." Internal memorandum to Distribution, March 14, 1991. Albuquerque, NM: Sandia National Laboratories. (In Appendix A of this volume)

Discussion:

McTigue et al. (March 14, 1991, Memo [Appendix A]) measured the compressibility of Salado Formation brines over a temperature range of 20 to 40°C. They found that brine compressibility exhibits no significant dependence on temperature over this range. The compressibilities of six Salado brines ranged from 2.40×10^{-10} Pa^{-1} to 2.54×10^{-10} Pa^{-1}, with the error in each measurement estimated at 0.6%. They found a strong correlation with brine density, in that compressibility decreased with increasing density. The following linear relationship correlates well for the data for Salado brines over the small range of densities tested.

$$\beta_f = 7.662 \times 10^{-10} - 4.217 \times 10^{-13} \rho_f \qquad (4.1\text{-}1)$$

where

β_f = the compressibility (Pa^{-1}) (defined as $\frac{1}{\rho}\frac{\partial \rho_f}{\partial p}$

ρ_f = the brine density (kg/m^3).

The correlation coefficient is $r^2 = 0.91$. McTigue et al. also developed a quadratic relationship that gives β_f for densities that include pure water and lower-concentration NaCl brines as well as Salado brines:

$$\beta_f = 4.492 \times 10^{-10} - 1.138 \times 10^{-12}(\rho_f - 1000) + 1.155 \times 10^{-15}(\rho_f - 1000)^2 \qquad (4.1\text{-}2)$$

For a Salado brine density of 1230 kg/m^3 (see Salado Brine Density discussion), both Eqs. 4.1-1 and 4.1-2 give a compressibility of 2.5×10^{-10} Pa^{-1}.

Salado Brine Formation Volume Factor

The formation volume factor is the ratio of the volume at reservoir conditions to the volume at reference conditions (300.15 K [27°C], 0.101325 MPa [1 atm]). Equivalently, it is the ratio of density at reference conditions to the density at reservoir conditions. Assuming the temperature and brine compressibility do not vary, the pressure dependence of Salado brine can be obtained from the definition of compressibility:

$$\beta_f = \frac{1}{\rho_f} \frac{\partial \rho_f}{\partial p} \qquad (4.1\text{-}3)$$

Integrating

$$\int \frac{d\rho_f}{\rho_f} = \int \beta_f dp$$

gives the brine density, ρ_f, as a function of pressure, p:

$$\rho_f = \rho^o e^{\beta_f (p - p^o)} \qquad (4.1\text{-}4)$$

where

- ρ^o = brine density at reference condition (1,230 kg/m^3) (see Salado Brine Density discussion)
- p^o = reference pressure (0.101325 MPa)
- β_f = compressibility of Salado brine (2.5 x 10^{-10} Pa^{-1}) (see Salado Brine Compressibility discussion)

From the definition of formation volume factor, B_b,

$$B_b = \frac{\rho^o}{\rho_f} = e^{-\beta_f (p - p^o)}$$

Figure 4.1-1 shows the variation of Salado brine density and formation volume factor with pressure.

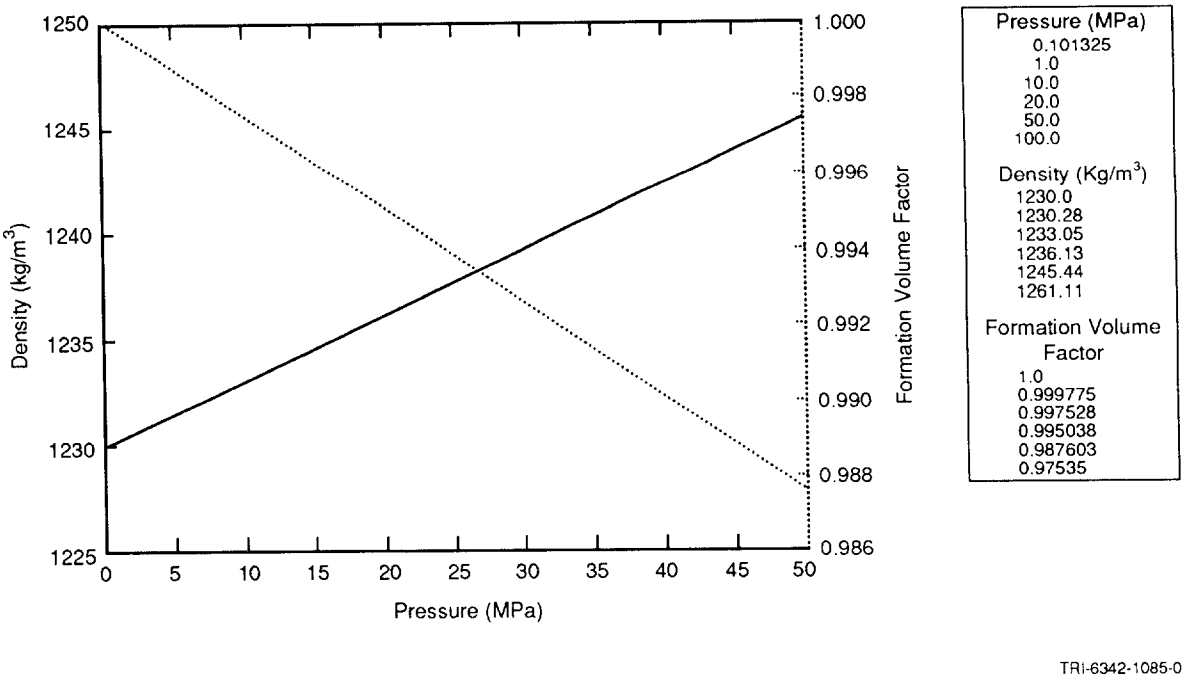

TRI-6342-1085-0

Figure 4.1-1. Variation of Salado Brine Density and Formation Volume Factor with Pressure.

Salado Brine Density

Parameter:	**Density** (ρ_f) @ 0.101325 MPa, 300.15 K
Median:	1.230×10^3
Range:	1.207×10^3
	1.253×10^3
Units:	kg/m^3
Distribution:	Normal
Source(s):	McTigue, D. F., S. J. Finley, J. H. Gieske, and K. L. Robinson. "Compressibility Measurements on WIPP Brines." Internal memorandum to Distribution, March 14, 1991. Albuquerque, NM: Sandia National Laboratories. (In Appendix A of this volume)

Discussion:

The density of brine in the Salado Formation at the repository level was reported by McTigue et al. (March 14, 1991, Memo [Appendix A]). They measured the density of six samples at 22°C and 1 atm pressure, with values ranging from 1,224 to 1,249 kg/m^3. To determine the precision of the density measurement of each individual sample, they repeated the measurement on one sample 14 times; for that sample, the average brine density was 1,249 kg/m^3 with a standard deviation of 2.6 kg/m^3 and a 95% confidence interval on the mean of 1,247 to 1,251 kg/m^3, based on Student's t distribution. The average density for the six samples was 1,232 kg/m^3 at 22°C with an overall range of 1,208 to 1,255 kg/m^3 (s = 10.1 kg/m^3). These values were corrected to the temperature of the Salado Formation at the repository level, assumed to be a uniform and constant 27°C. McTigue et al. developed the following expression to correct the densities measured at 22°C:

$$\frac{\rho_f}{\rho_{fo}} = 1 + a_1(T - 22) + a_2(T - 22)^2 + a_3(T - 22)^3 \qquad (4.1\text{-}5)$$

where

ρ_{fo} = density at 22°C
T = temperature of interest (°C)
a_1, a_2, a_3 = coefficients ($a_1 = -4.4294 \times 10^{-4}$, $a_2 = -6.3703 \times 10^{-7}$, and $a_3 = -1.3148 \times 10^{-9}$.

This expression is based on pure saturated NaCl solutions, rather than on WIPP brines; however, McTigue et al. believe the behavior of the brines will not differ significantly from pure NaCl brines. With this correction, the density of Salado brine at 27°C and 1 atm pressure is 1,230 kg/m^3 with an overall range of 1,207 to 1,253 kg/m^3 (s = 10.0 kg/m^3).

Factors Affecting Brine Density

Empirical correlations developed for petroleum reservoir brines give the dependence of brine density on salinity, gas content, temperature, and pressure (Numbere et al., 1977; Hewlett Packard, 1984). The correlation of Numbere et al. is valid over the range of conditions (temperature, pressure, and salinity) encountered in the Salado Formation, but does not agree with the measured values discussed above. At 27°C, 1 atm, and 26.5 wt% NaCl, the Numbere correlation gives a density of 1,197 kg/m^3, compared with the measured value (corrected to 27°C) of 1,230 kg/m^3.

Because the composition of Salado brines varies considerably (Krumhansl et al., 1991), simple correlations for the dependence of density on salinity (such as the Numbere and HP correlations) do not offer more accuracy or reliability than assuming that the composition does not vary from that of McTigue et al.'s samples.

The effect of dissolved gas on the density of Salado brine cannot be predicted at present. The HP correlations presumably are for natural gas, rather than H_2, N_2, and CO_2, which are relevant to the WIPP. Water (not brine) density is calculated using correlations for either gas-free or gas-saturated water. This density is then corrected for salinity. The effect of salinity on the degree of gas saturation is ignored, yet, as Cygan (1991) shows, the solute composition and concentration both have major effects on the amount of gas that dissolves in the brine, which in turn should affect the density of the brine.

The Salado Formation is assumed to have a constant and uniform temperature of 27°C, so the temperature dependence of brine density is not considered.

The effect of pressure on brine density is discussed under Salado Brine Compressibility.

Salado Brine Viscosity

Parameter:	**Viscosity (μ) @ 300 K**
Median:	1.8×10^{-3}
Range:	None
Units:	Pa•s
Distribution:	Constant
Source(s):	Kaufman, D. W. ed. 1960. *Sodium Chloride, the Production and Properties of Salt and Brine*, Monograph No. 145. Washington, DC: American Chemical Society. (p. 622)

Discussion:

Literature values for brines extrapolating to density of 1,230 kg/m^3 and a temperature of 300 K yields a viscosity of 1.8×10^{-3} Pa•s (3.76×10^{-3} lbf•ft/s) (Kauffman, 1960, p. 622).

4.1.2 Culebra Brine

Culebra Brine Density

Parameter:	**Density** (ρ_f) @ 0.101325 MPa, 300.15 K
Median:	1.09×10^3
Range:	9.99×10^2
	1.154×10^3
Units:	kg/m^3
Distribution:	Spatial
Source(s):	Cauffman, T. L., A. M. LaVenue, and J. P. McCord. 1990. *Ground-Water Flow Modeling of the Culebra Dolomite: Volume II - Data Base.* SAND89-7068/2. Albuquerque, NM: Sandia National Laboratories. (Table E.1)

Table 4.1-2 provides the brine densities at wells within the Culebra Dolomite Member. Figure 4.1-2 shows the spatial variation of brine densities.

Table 4.1-2. Average Brine Density at Wells within Culebra Dolomite Member (after Cauffman et al., 1990, Table E.1)

Well ID	Fluid Density* (kg/m^3)
DOE1	1.088×10^3
DOE2	1.041×10^3
ENGLE	1.001×10^3
H1	1.022×10^3
H2	1.006×10^3
H3	1.035×10^3
H4	1.014×10^3
H5	1.102×10^3
H6	1.038×10^3
H7B	0.999×10^3
H8B	1×10^3
H9B	1×10^3
H10B	1.047×10^3
H11	1.078×10^3
H12	1.095×10^3
H14	1.01×10^3
H15	1.154×10^3
H17	1.1×10^3
H18	1.017×10^3
P14	1.018×10^3
P15	1.015×10^3
P17	1.061×10^3
USGS1	1×10^3
USGS4	1×10^3
USGS8	1×10^3
WIPP13	1.046×10^3
WIPP19	1.059×10^3
WIPP25	1.009×10^3
WIPP26	1.009×10^3
WIPP28	1.032×10^3
WIPP30	1.018×10^3

* Average of measurements from indicated well

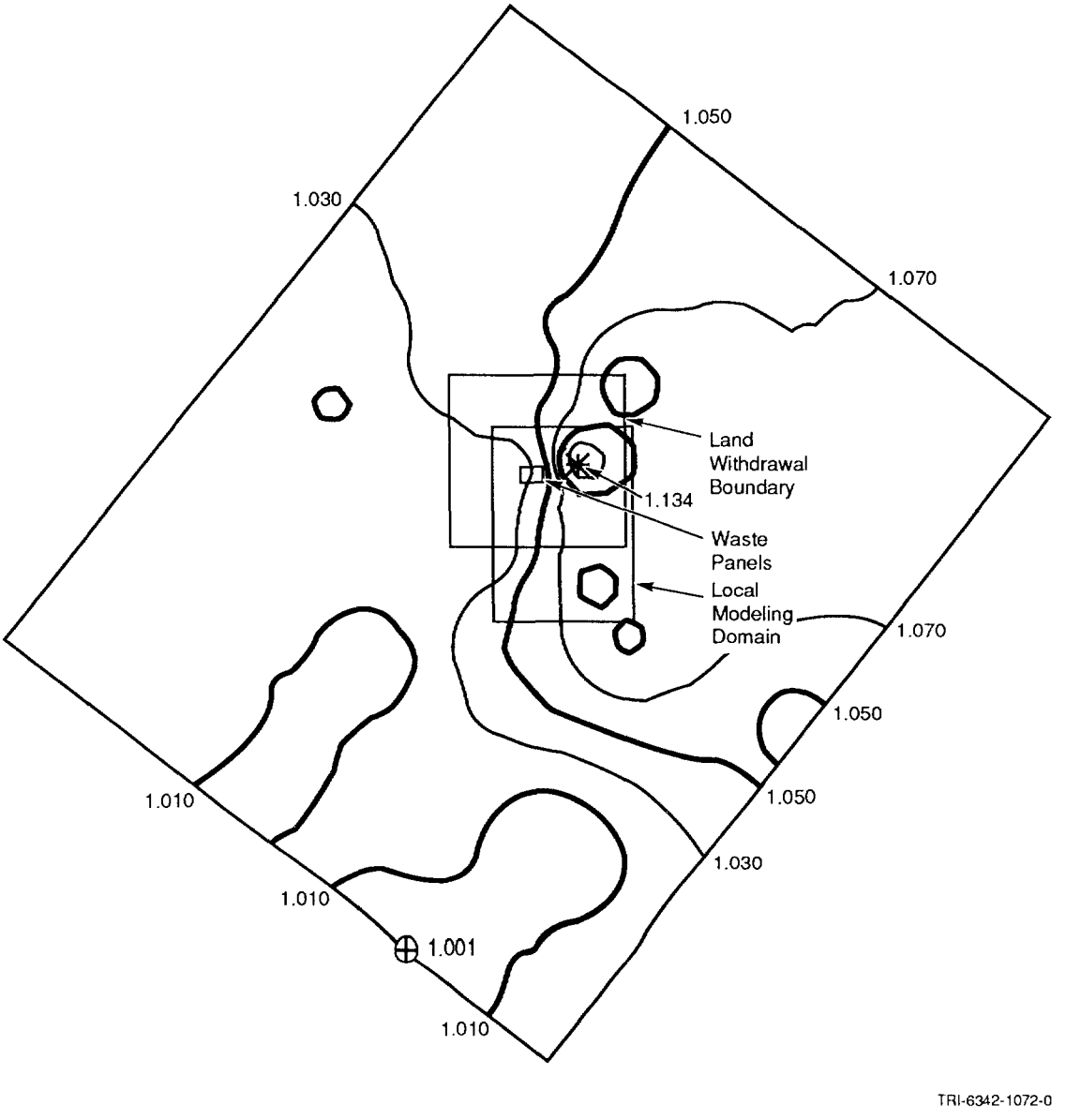

Figure 4.1-2. Variation of Brine Density within Culebra Member Estimated by 10 Nearest Neighbors Using Inverse-Distance-Squared Weighting.

Culebra Brine Viscosity

Parameter:	**Viscosity (μ)**
Median:	1 x 10^{-3}
Range:	None
Units:	Pa•s
Distribution:	Constant
Source(s):	Haug, A., V. A. Kelley, A. M. LaVenue, and J. F. Pickens. 1987. *Modeling of Groundwater Flow in the Culebra Dolomite at the Waste Isolation Pilot Plant (WIPP) Site: Interim Report.* Contractor Report SAND86-7167. Albuquerque, NM: Sandia National Laboratories. (p. 3-20)

Discussion:

Similar to other modeling studies of the Culebra Dolomite (LaVenue et al., 1990, 1988; Haug et al., 1987), PA calculations assume that the Culebra Brine viscosity is identical to pure water, 1.0 x 10^{-3} Pa•s (2.089 x 10^{-3} lbf•ft/s).

4.1.3 Castile Brine

Castile Brine Compressibility

Parameter:	**Compressibility (β_f)**
Median:	9×10^{-10}
Range:	None
Units:	Pa^{-1}
Distribution:	Constant
Source(s):	Popielak, R. S., R. L. Beauheim, S. R. Black, W. E. Coons, C. T. Ellingson, and R. L. Olsen. 1983. *Brine Reservoirs in the Castile Formation, Southeastern New Mexico, Waste Isolation Pilot Plant (WIPP) Project.* TME-3153. Carlsbad, NM: U.S. Department of Energy.

Discussion:

Popielak et al. (1983) estimated the compressibility,

$$\beta_f = \frac{1}{\rho_f} \frac{\partial \rho_f}{\partial p}$$

of Castile Formation brine to be 9×10^{-10} Pa^{-1} (6×10^{-6} psi^{-1}) for brine from well WIPP-12. Only a single value is reported with no estimate of its precision. Some indication of accuracy is obtained by comparing the value with the compressibility value cited for the nearby well ERDA-6: 3×10^{-10} Pa^{-1} (2×10^{-6} psi^{-1}) (Popielak et al., 1983). (Note, however, that Popielak et al. concluded that there was no hydraulic connection between the Castile brine reservoir encountered by WIPP-12 and ERDA-6.)

Castile Brine Formation Volume Factor

Following the discussion and assumptions under Salado Brine Formation Volume Factor, the formation volume factor, B_b, for Castile brine is given by

$$B_b = e^{-\beta_f(p - p^o)}$$

where

β_f = compressibility (9×10^{-10} Pa^{-1}) See discussion under Castile Brine Compressibility.
p = pressure (Pa)
p^o = reference pressure (0.101325 MPa)

Figure 4.1-3 shows the variation of Castile brine density and formation volume factor with pressure.

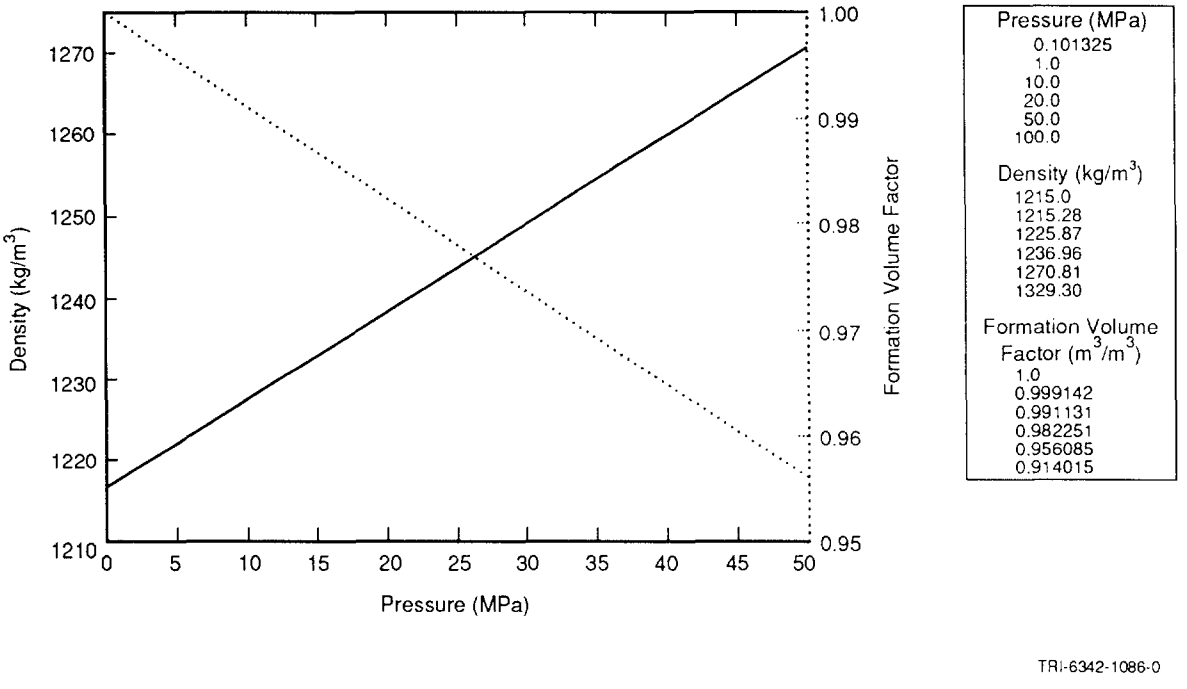

Figure 4.1-3. Variation of Castile Brine Density and Formation Volume Factor with Pressure.

Castile Brine Density

Parameter:	**Density** (ρ_f) @ 0.101325 MPa, 300.15 K
Median:	1.215×10^3
Range:	1.209×10^3
	1.221×10^3
Units:	kg/m^3
Distribution:	Constant
Source(s):	Popielak, R. S., R. L. Beauheim, S. R. Black, W. E. Coons, C. T. Ellingson, and R. L. Olsen. 1983. *Brine Reservoirs in the Castile Formation, Southeastern New Mexico, Waste Isolation Pilot Plant (WIPP) Project.* TME-3153. Carlsbad, NM: U.S. Department of Energy.

Discussion:

Popielak et al. (1983) measured the density of 59 flow samples of Castile Formation brine from well WIPP-12. The density at atmospheric pressure ranged from 1,210 to 1,220 kg/m^3. At an average temperature of 26.7°C, the average density was 1,215 kg/m^3 with a standard deviation of 2.4 kg/m^3 and a 95% confidence interval, based on Student's t distribution, of 1,214 to 1,216 kg/m^3. Using the expression discussed under Salado Brine Density, the average density corrected to 27°C is 1,215 kg/m^3 at 1 atm (0.101325 MPa) pressure. The WIPP-12 brine reservoir is the closest to the disposal region and is assumed representative of Castile brines in any reservoir under the WIPP. Other Castile brine reservoirs have minor differences, e.g., ERDA-6 brine has an average density of 1,216 kg/m^3 at 26.7°C and 1 atm pressure (Popielak et al., 1983).

4.1.4 Hydrogen Gas

Hydrogen Density and Formation Volume Factor

Parameter:	**Density**
Median:	11.037 @ 15 MPa
Range:	0.081803 @ 0.101325 MPa
	14.442 @ 20 MPa
Units:	kg/m^3
Distribution:	Table
Source(s):	See text.

Figure 4.1-4 shows the variation with pressure of density (ρ_f) and the formation volume factor for hydrogen gas (B_g). The formation volume factor, B_g, is the ratio of specific volume of a gas at reservoir conditions to specific volume of the gas at reference or standard conditions (ρ/ρ_f).

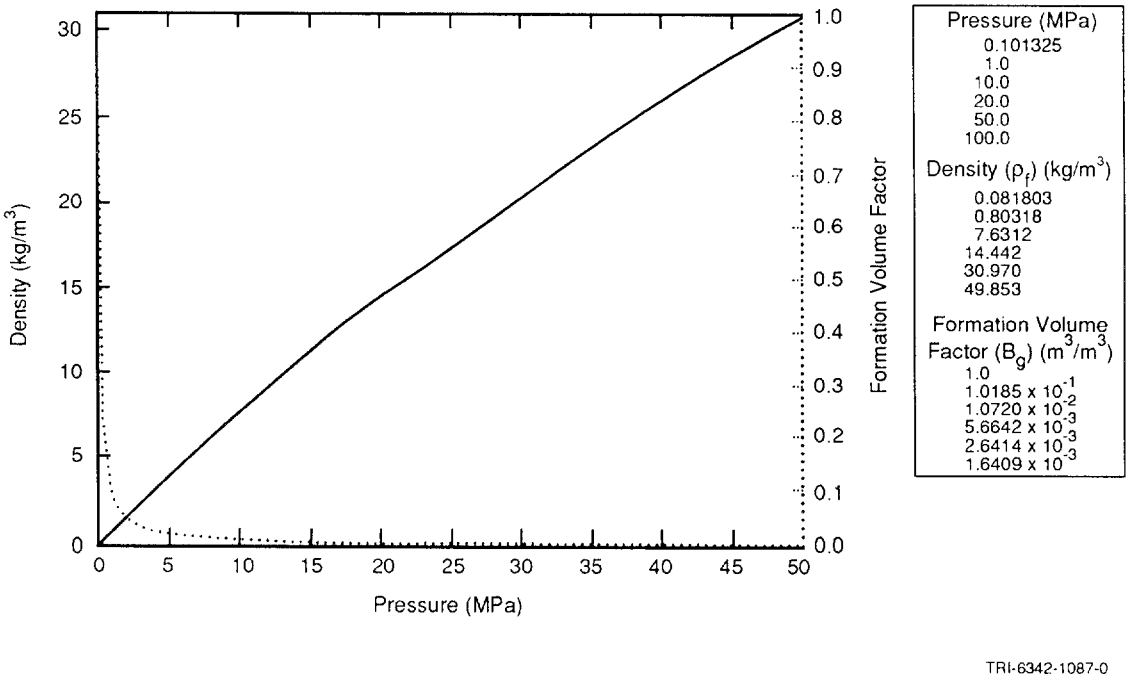

Figure 4.1-4. Formation Volume Factor for Hydrogen Gas.

Discussion:

The formation volume factor is the ratio of the volume at reservoir conditions to the volume at reference conditions (300.15 K [27°C], 0.101325 MPa [1 atm]). The molar volume of hydrogen gas is computed using the Redlich-Kwong-Soave equation of state (Walas, 1985):

$$Z = \frac{p\upsilon}{R^*T} = \frac{\upsilon}{\upsilon - b_R} - \frac{a_R \alpha_R}{R^* T(\upsilon + b_R)} \qquad (4.1\text{-}6)$$

where

a_R = $0.42747\ R^* T_{cr}^2 / p_{cr}$ ($cm^6 \cdot bar/mol^2$)

b_R = $0.08664\ R^* T_{cr} / p_{cr}$ (cm^3/mol)

p = pressure (bar)

R^* = universal gas constant = 83.1441 ($cm^3 \cdot bar/mol \cdot K$)

T = temperature (K)

υ = molar volume (cm^3/mol)

p_{cr} = critical pressure (bar)

T_{cr} = critical temperature (K)

α_R = $[1 + (0.48508 + 1.55171\ \omega_R - 0.1561\ \omega_R)(1 - T_r^{0.5} 1)]^2$ (dimensionless)

ω_R = acentric factor (dimensionless)

T_r = reduced temperature = T/T_{cr} (dimensionless)

Z = compressibility factor (dimensionless)

for hydrogen:

$$T_{cr} = \frac{43.6}{1 + \frac{21.8}{TM}} \quad (K)$$

$$p_{cr} = \frac{20.47}{1 + \frac{44.2}{TM}} \quad (bar)$$

M = molecular weight = 2.01594 g/mol

α_R = $1.202 \exp(-0.30288\ T_r)$

ω_R = 0.0

Note that temperature-dependent effective critical properties are used for hydrogen (Prausnitz, 1969). Hydrogen also requires a special expression for (α_R) (Graboski and Daubert, 1979), and an acentric factor (ω_R) of zero (Knapp et al., 1982).

Equation 4.1-6 is solved numerically for molar volume, v, at the reference condition and at reservoir conditions to provide the values used to calculate the formation volume factor (Figure 4.1-1). At the reference conditions (300.15 K, 0.101325 MPa), the density (ρ_{H_2}) of H_2 gas is 0.081803 kg/m^3 and the molar volume (v) is 0.024644 m^3/mol.

Alternative Gas Equation of State

At pressures near lithostatic, the gas in the repository deviates significantly from the behavior described by the ideal gas law, p V = n R T. The behavior is described accurately by several real gas equations. A simple yet moderately accurate gas law was developed by Iuzzolino (1983):

$$p = \frac{n R T}{V} \frac{(V + b_I V_{cr})}{(V - b_I V_{cr})} - a_i p_c (V_{cr}/V)^2 \qquad (4.1\text{-}7)$$

where

- p = pressure (Pa)
- n = number of moles
- R^* = gas constant = 8.31441 Pa•m³/mol-K
- V = volume (m³)
- T = temperature (K)
- T_c = critical temperature (K) for the gas
- p_c = critical pressure (Pa) for the gas
- V_{cr} = n R T_{cr}/p_{cr}
- a_I and b_I = constants.

The constants a and b are obtained from a least-squared-error fit to standard gas compressibility curves. The results from the original curve fit (1981) were a_I = 0.4184 and b_I = 0.078104. A recent fit (1990) using more accurate compressibility data gives a_I = 0.4377 and b_I = 0.08186. The fit is good to within about 5% at temperatures above 1.3 T_{cr} and pressures up to 40 p_{cr}. Near the critical point the errors are about 25%. Since repository gases are at temperatures above 0°C (273 K), they will be significantly above 1.3 T_{cr}, and the fit should be good to within about 5%.

The gas equation fits compressibility data with about half the mean-squared error of the standard Redlich-Kwong-Soave equation of state (EOS) (discussed earlier). The error of this gas equation is larger than that of the Redlich-Kwong-Soave EOS near the critical point and smaller at higher temperatures.

Derivation of the Gas Equation. Iuzzolino's gas equation is derived from a real-gas modification of the canonical partition function for a gas. The partition function Z for an ideal gas is

$$Z = \frac{1}{N!} \left[\left(\frac{2 \pi m_A k^* T}{h^{*2}} \right)^{3/2} V \right]^N \qquad (4.1\text{-}8)$$

where

N = number of molecules
m_A = atomic mass (kg)
k^* = Boltzmann's constant
h^* = Planck's constant.

The ideal gas equation is derived using the thermodynamic relation

$$p = k^* T \frac{\delta \ln Z}{\delta V} \qquad (4.1\text{-}9)$$

applying this relation to the partition function gives $p = N k^* T / V$. Since $N k^* = n R$, the usual form $p V = n R T$ is obtained.

Iuzzolino uses two modifications to the partition function. The volume term is multiplied by $(1 - b_I V_{cr}/V)^2$ to provide a quadratic (soft-molecule) correction for the volume taken up by the molecules. The parameter b_I is proportional to the volume of the gas at the critical point and is an excluded-volume correction. Earlier work using a two-constant quadratic correction of the form $1 - b_I V_{cr}/V + c (V_{cr}/V)^2$ indicated that a factor of the form $(1 - b_I V_{cr}/V)^2$ gave the better fit.

A second correction is applied to take into account attractive forces between molecules: the volume term is multiplied by $\exp (a_I p_{cr} V_{cr}^2/Nk^*T V)$. The form of this correction is the best result of several arbitrary trials. The real-gas partition function is

$$Z = \frac{1}{N!} \left[\left(\frac{2 \pi m_A k^* T}{(h^*)^2} \right)^{3/2} V (1 - b_I V_{cr}/V)^2 \, e^{(a_I P_{cr} V_{cr}^2 / N k^* T V)} \right]^N \qquad (4.1\text{-}10)$$

Gas Mixtures. To preserve the form of the gas equation for a mixture of gases, the critical pressure of the mixture should be

$$p_{cr} = \sum_i n_i \, p_{cr_i}$$

where

p_{cr_i} = the critical pressure of the i-th gas

n_i = the number of moles of the i-th gas.

The summation runs over each gas in the mixture.

To preserve the concept that V_{cr} is proportional to an excluded volume, for a mixture

$$V_{cr} = \sum_{I} \frac{n_i R T_{cr_i}}{p_{cr_i}} \qquad (4.1\text{-}11)$$

where

T_{cr_i} = the critical temperature of the i-th gas.

Then

$$\frac{n R T_{cr}}{p_{cr}} = \sum_{i} \frac{n_i R T_{cr_i}}{p_{cr_i}} \qquad (4.1\text{-}12)$$

implies that

$$\frac{T_{cr}}{p_{cr}} = \sum_{i} n_i \left(\frac{T_{cr_i}}{p_{cr_i}} \right) \qquad (4.1\text{-}13)$$

so that, for the mixture,

$$T_{cr} = p_{cr} \sum_{i} n_i \left(\frac{T_{cr_i}}{p_{cr_i}} \right) \qquad (4.1\text{-}14)$$

Quantum Effects. Several gases deviate significantly from the real gas compressibility curves, most notably very light gases and highly polar gases. For H_2 and He, the deviation is primarily a result of quantum effects. For NH_3 the deviation is caused by hydrogen bonding. In both cases the fit to the real gas equation can be improved by using values of p_{cr} and T_{cr} that are not the actual critical constants. For H_2, a good fit results using T_{cr} = 50 K and p_{cr} = 2.35 X 10^6 Pa.

Viscosity

Parameter:	**Viscosity (μ) @ 300.15 K**
Median:	9.20 x 10^{-6} @ 15 MPa
Range:	8.92 x 10^{-6} @ 0.101325 MPa
	9.33 x 10^{-6} @ 20 MPa
Units:	Pa•s
Distribution:	Table
Source(s):	Vargaftik, N. B. 1975. *Tables on the Thermophysical Properties of Liquids and Gases in Normal and Dissociated States.* New York: John Wiley & Sons, Inc.

Discussion:

Vargaftik (1975) tabulates numerous measurements of hydrogen viscosity covering a wide range of temperatures and pressures. At pressures of 0.100 MPa (1 bar) to 0.101325 MPa (1 atm), eight independent measurements are reported at 293 to 293.15 K (20°C), with values ranging from 8.73 x 10^{-6} to 8.86 x 10^{-6} Pa•s. Hydrogen viscosity increases with temperature; two values reported at 300 K are 8.89 x 10^{-6} and 8.91 x 10^{-6} Pa•s. Vargaftik (1975, p. 39) presents two tables with hydrogen viscosity ranging from -200°C to 1000°C and 0.1 MPa to 50 MPa. (The table value of viscosity at 20°C and 0.1 MPa is 8.80 x 10^{-6} Pa•s.) Linear interpolation within these tables between 0 and 100°C provides sufficiently precise viscosity values at the temperatures of interest; at 20°C, the viscosity is 8.79 x 10^{-6} Pa•s, which is in the middle of the range of measured values cited above. At 300 K, the temperature of the repository, the viscosity at 0.1 MPa is 8.92 x 10^{-6} Pa•s. Quadratic interpolation based on table values at pressures of 0.1, 10, and 20 MPa (interpolated linearly to 300.15 K) results in the following expression giving H_2 viscosity at 300.15 K (27°C, 80.6°F) as a function of pressure:

$$\mu = 8.920074 \times 10^{-6} + 1.020892 \times 10^{-8}\ p + 5.273692 \times 10^{-10}\ p^2 \qquad (4.1\text{-}15)$$

where

μ = viscosity (Pa•s)
p = pressure (MPa)

Figure 4.1-5 shows the variation of hydrogen viscosity with pressure.

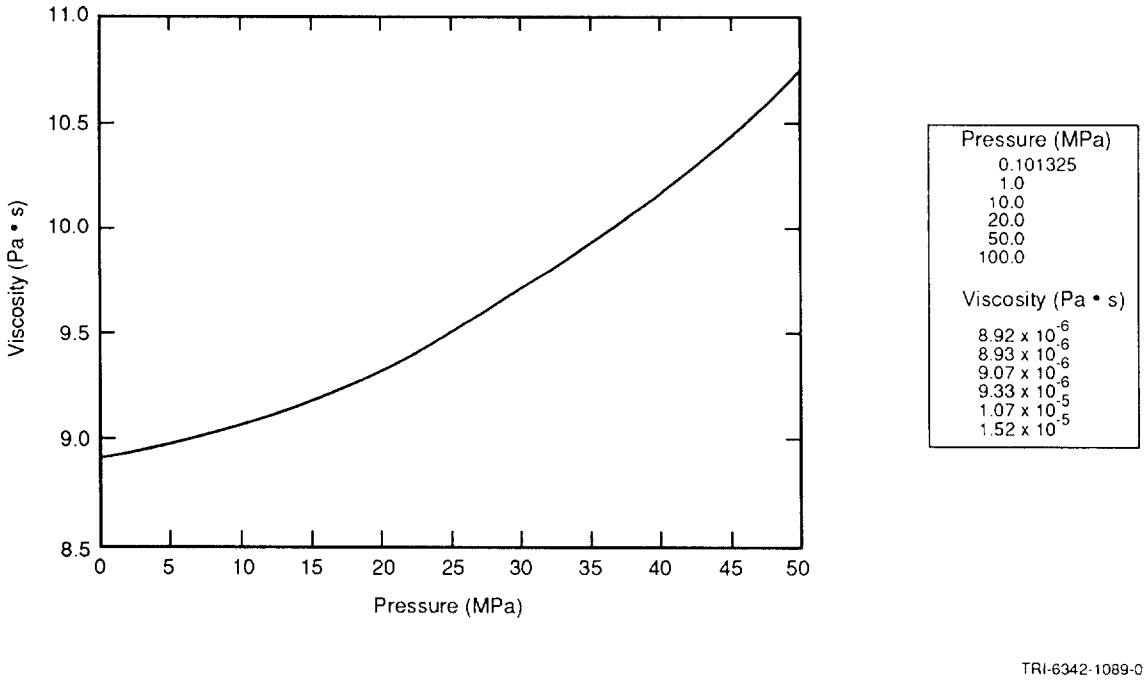

Figure 4.1-5. Variation of Hydrogen Viscosity with Pressure.

Hydrogen Solubility

Parameter:	**H_2 Solubility in brine**
Median:	3.84×10^{-4}
Range:	6.412×10^{-6}
	4.901×10^{-4}
Units:	Dimensionless
Distribution:	Table
Source(s):	Cygan, R. T. 1991. *The Solubility of Gases in NaCl Brine and a Critical Evaluation of Available Data.* SAND90-2848. Albuquerque, NM: Sandia National Laboratories.

Discussion:

Cygan (1991) estimated the solubility of H_2 in NaCl solutions at elevated pressure and developed the following correlation relating H_2 mole fraction in solution, χ_{H_2}, to pressure, p, in MPa:

$$\ln \chi_{H_2} = a_0 + a_1 \ln p \qquad (4.1\text{-}16)$$

where

a_0 = -8.8980 (pure water); -10.0789 (5 N NaCl brine at 298.15 K)
a_1 = 0.9538 (pure water); 0.8205 (5 N NaCl brine at 298.15 K)

Cygan emphasizes that this correlation is only an "educated estimate," but probably we are justified in applying it to Salado brine at 300.15 K.

Some multiphase flow models, e.g., BOAST and BRAGFLO (Rechard et al., 1989), require gas solubility expressed in terms of gas volume at reference conditions per unit volume of solution (brine), also at reference conditions. This "gas/brine ratio," $r_{g/\ell}$, is calculated from

$$r_{g/\ell} = \chi_{H_2} \frac{V^\circ_{H_2}}{V^\circ_b} \qquad (4.1\text{-}17)$$

where

V°_b = volume of a mole of brine at reference conditions ($\overline{M}/\rho^\circ$)

$V^\circ_{H_2}$ = volume of a mole of H_2 gas at reference conditions, 300.15 K and 0.101325 MPa

ρ° = density of Salado brine (1230 kg/m^3)

$\overline{M}$ = molar average molecular weight of brine.

For NaCl brine, $\overline{M}$ is calculated as follows:

$$\overline{M} = \chi_{NaCl} M_{NaCl} + \chi_{H_2O} M_{H_2O} = \chi_{NaCl}(M_{NaCl} - M_{H_2O}) + M_{H_2O} \quad (4.1\text{-}18)$$

where

χ = mole fraction of NaCl and H_2O
$\chi_{H_2O} = 1 - \chi_{NaCl}$

Molecular weights are M_{NaCl} = 58.44 g/mol and M_{H_2O} = 18.015 g/mol.

$$\chi_{NaCl} = \frac{\omega}{\omega + 1} \quad (4.1\text{-}19)$$

where

ω = molar ratio of NaCl to H_2O ($M_{H_2O}N/C_w$)
N = molarity of the solution (5 mol NaCl/ℓ)
C_w = total water concentration in the solution.

C_w is obtained by quadratic interpolation from tabulated data relating C_w to molarity for NaCl solutions (Weast and Astle, 1981, p. D-232). For N equals 5 mol NaCl/ℓ, C_w equals 893.53 g H_2O/ℓ brine, which in turn gives ω = 0.10081 mol NaCl/mol H_2O; χ_{NaCl} = 0.09158 mol NaCl/mol brine; $\overline{M}$ = 21.718 g/mol brine molecular weight; and $V_b^\circ = \overline{M}/\rho^\circ$ = 1.7657×10^{-5} m^3/mol. The molar volume of H_2 at reference conditions (see discussion under Hydrogen Density) is $V_{H_2}^\circ$ = 0.0246347 m^3/mol. Applying Eqs. 4.1-18 and 4.1-19 for 5N NaCl brine results in the following values for gas/brine ratio, $r_{g/\ell}$, at 300.15 K (Figure 4.1-6).

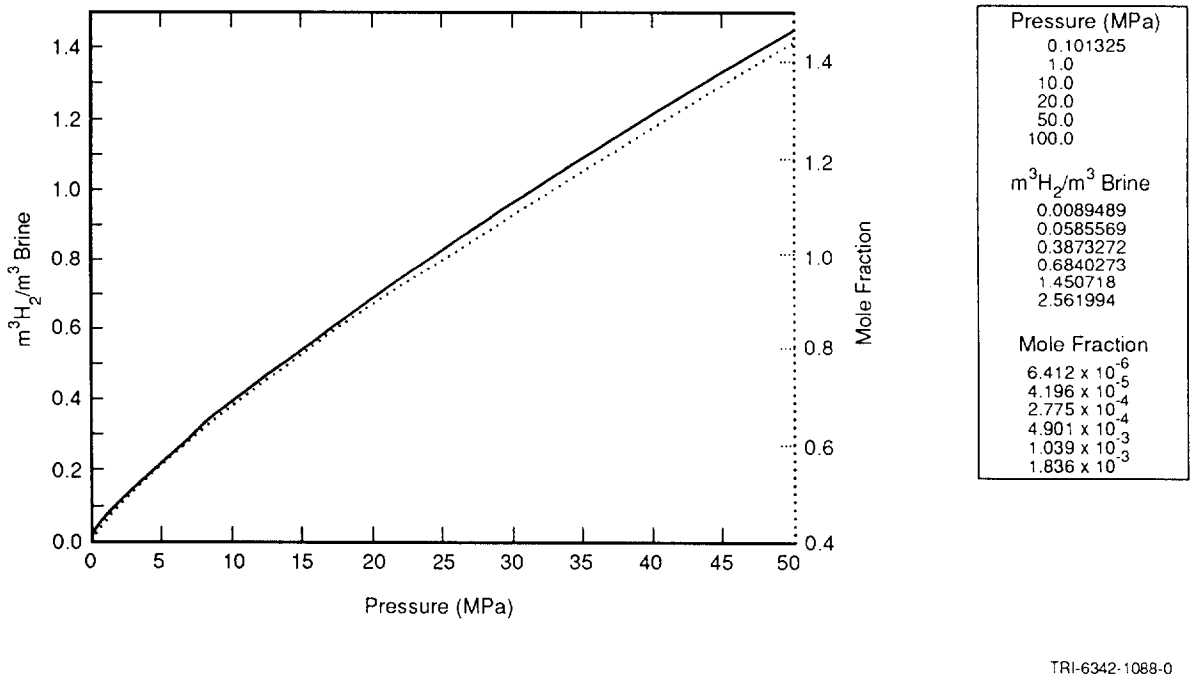

TRI-6342-1088-0

Figure 4.1-6. Variation of Hydrogen Solubility with Pressure.

4.1.5 Drilling Mud Properties

In assessing the long-term performance of the WIPP containment system, we must predict the transport of radionuclides to the accessible environment during and after a drilling procedure in which a company drills an exploratory drillhole through the underground disposal region in search of resources *(40 CFR 191, Appendix B)*. Given two assumptions -- (1) the resource is either gas or oil and (2) standard rotary drilling equipment in use today will be used in the future -- an important consideration in determining the consequence of the drilling is an estimation of the amount of material brought to the surface during the drilling procedure. The parameters for drilling mud density, viscosity, and yield point are shown below. A discussion of these parameters follows.

Density

Parameter:	**Density, mud** (ρ_f) @ 225.15 K, p = 0.101325 MPa
Median:	1.2×10^3
Range:	1.14×10^3
	1.38×10^3
Units:	kg/m^3
Distribution:	Cumulative
Source(s):	Pace, R. O. 1990. "Letter 1b: Changes to bar graphs," in Rechard et al. 1990. *Data Used in Preliminary Performance Assessment of the Waste Isolation Pilot Plant (1990)*. SAND89-2408. Albuquerque, NM: Sandia National Laboratories.

Viscosity

Parameter:	**Viscosity** (μ) @ 225.15 K, p = 0.101325 MPa
Median:	9.17×10^{-3}
Range:	5×10^{-3}
	3×10^{-2}
Units:	Pa•s
Distribution:	Cumulative
Source(s):	Pace, R. O. 1990. "Letter 1b: Changes to bar graphs," in Rechard et al. 1990. *Data Used in Preliminary Performance Assessment of the Waste Isolation Pilot Plant (1990)*. SAND89-2408. Albuquerque, NM: Sandia National Laboratories.

Yield Stress Point

Parameter:	**Yield stress point**
Median:	4
Range:	2.4
	1.92×10^1
Units:	Pa
Distribution:	Cumulative
Source(s):	Pace, R. O. 1990. "Letter 1b: Changes to bar graphs," in Rechard et al. 1990. *Data Used in Preliminary Performance Assessment of the Waste Isolation Pilot Plant (1990)*. SAND89-2408. Albuquerque, NM: Sandia National Laboratories.

Discussion:

Standard Rotary Drilling. In standard rotary drilling, a cutting bit is attached to a series of hollow drill pipe and then rotated and directed downward to cut through underlying strata. To remove the cuttings, a fluid ("mud") is pumped down the hollow drill pipe, through the bit, and up the annulus formed by the drill pipe and borehole wall. In addition to removing the cuttings, the mud cools and cleans the bit, reduces drilling friction, and helps to support the borehole. The mud also forms a thin, low-permeability filter cake on the borehole walls, thus preventing inflow of unwanted fluids from permeable formations.

Although the amount of waste removed by direct cutting is simple to calculate, calculating the amount of waste eroded from the borehole wall is more difficult. A number of factors may influence borehole erosion (e.g., eccentricity of pipe and hole, impact of solid particles in mud on the walls, physical and chemical interaction between mud and walls, and time of contact between the mud and walls [Broc, 1982]); however, industry opinion singles out fluid shear stress as the most important factor (Walker and Holman, 1971; Darley, 1969).

Three drilling mud properties (density, viscosity, and yield stress) are necessary to evaluate the fluid shear stress, which in turn is one of several parameters used to evaluate the amount of material eroded from the borehole wall by scouring from the swirling drilling fluid (e.g., CUTTINGS [Rechard et al., 1989]). (Section 4.3, Intrusion Borehole Characteristics; Chapter 3, Engineered Barriers; and Chapter 6, Probability Models, present other parameters for this anthropogenic event.)

Flow Regime. The flow regime within the annulus (laminar or turbulent) is governed by the Reynolds number, N_R. The Reynolds number is dependent upon the properties of the drilling mud (density, viscosity, and velocity) and the size of the annulus. The Reynolds number is defined as

$$N_R = \frac{\bar{\rho}\ \bar{V} d_e}{\bar{\mu}} \qquad (4.1\text{-}20)$$

where

d_e = length dimension = equivalent diameter for annulus = d_{hole}-d_{collar}

$\bar{\rho}$ = average fluid density

$\bar{V}$ = average fluid velocity

$\bar{\mu}$ = average fluid viscosity (for non-newtonian fluids, the average viscosity will depend upon the viscosity model used)

The ultimate diameter of the hole, d_{hole}, is the quantity to be evaluated, and is determined through an iterative process. The velocity is estimated from the drilling pump rates provided in Section 4.3. The fluid density and viscosity (and yield stress for non-newtonian fluids) are discussed below.

Density. The current drilling procedure for an exploratory oil or gas well in the Delaware Basin (see Figure 1.6-2) involves using a drilling fluid, which is usually a saturated brine. The brine density is maintained during the transport of cuttings by adding an emulsified oil (Pace, 1990). Consequently, the fluid density is near 1,200 kg/m^3 (75 lb/ft^3 or 10 lb/gal) with a narrow range between 1,138 and 1,377 kg/m^3 (9.5 and 11.5 lb/gal) (Figure 4.1-7).

When drilling for oil or gas, particularly in the area around the WIPP, there is the possibility of encountering a blowout. The drilling companies can respond in a relatively short time. If the drill hole intercepts a brine reservoir with sufficient pressure to cause copious amounts of brine flow to the surface, the company will add weight (usually barite) to the drilling fluid to stop the flow from the reservoir. The mud density could increase to as much as 1900 kg/m^3 (16 lb/gal). This density increase would occur long after the drill passed through the repository area, the time of greatest erosion.

Shear Stress. For both laminar and turbulent flow, the shear stress can be expressed as (Vennard and Street, 1975, p. 381):

$$\tau = \frac{f\rho V^2}{2} \qquad (4.1\text{-}21)$$

The fanning friction factor, f, is discussed below for turbulent and laminar shear stress.

Turbulent Shear Stress. In turbulent flow (Reynolds number $N_R > N_{R_{crit}}$ where $N_{R_{crit}}$ varies between 2,100 for newtonian fluids and 2,400 for some non-newtonian fluids [Vennard and Street, 1975, p. 384; Walker, 1976, p. 89]) the fanning friction factor is dependent on both N_R, and surface roughness (e.g., Moody diagram [Vennard and Street, 1975, Figure 9.5; Streeter and Wylie, 1975, Figure 5.32]), with N_R having a minor influence. Consequently, the shear stress is dependent primarily upon absolute surface roughness, ε, and kinetic energy ($\rho V^2/2$). An empirical expression for f is (Colebrook, 1938):

$$\frac{1}{\sqrt{f}} = -4 \log \left[\frac{\varepsilon/d}{3.72} + \frac{1.255}{N_R\sqrt{f}} \right] \qquad (4.1\text{-}22)$$

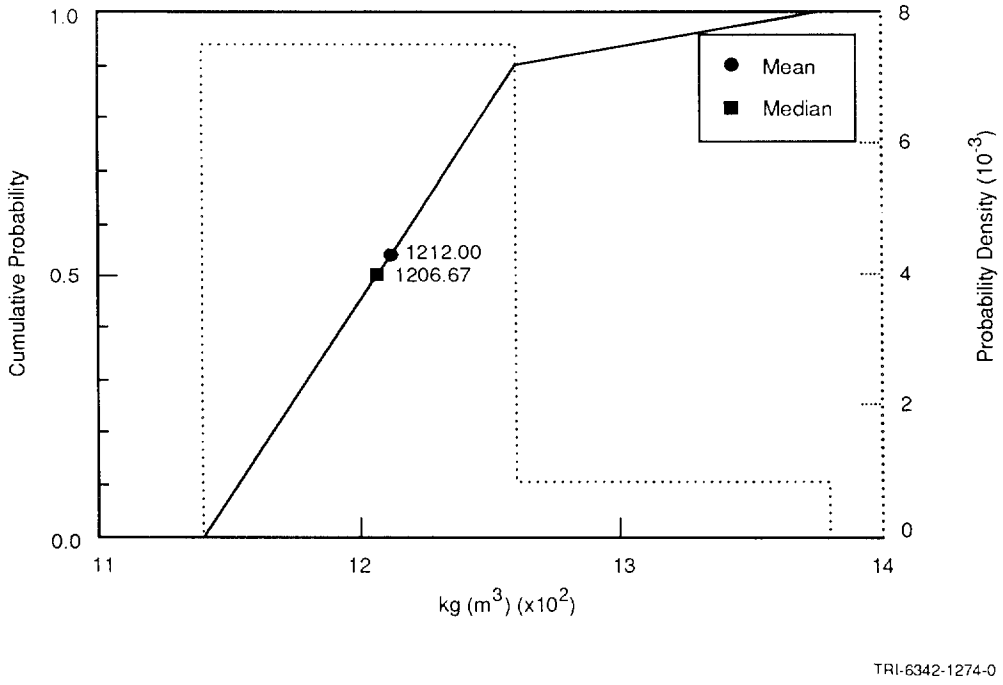

Figure 4.1-7. Distribution of Drilling Mud (Saturated Brine) Density.

where

ε = absolute roughness of material

d = hydraulic diameter = difference between borehole diameter and collar diameter

The assumed absolute roughness of waste (ε) is tabulated in the description of the waste in Chapter 3, Engineered Barriers.

Laminar Shear Stress. For laminar flow, the fanning friction factor, f, is a function of only N_R. The shear stress in laminar flow (Reynolds number N_R < 2,100 [Vennard and Street, 1975, p. 384]) depends solely on the fluid viscosity and strain rate (velocity gradient); however, for a non-newtonian fluid such as drilling mud, the viscosity varies with strain rate (Figure 4.1-8). Several functional forms are used to model this variation (Ideal Bingham Plastic, Power Law, and Oldroyd Model). The PA Division currently uses the Oldroyd model.

Ideal Bingham Plastic -- A linear (Ideal Bingham Plastic) model approximates the actual yield stress (τ_o) (Figure 4.1-8) at high strain rate

$$\tau = \tau'_o + \mu_\ell \Gamma \qquad (4.1\text{-}23)$$

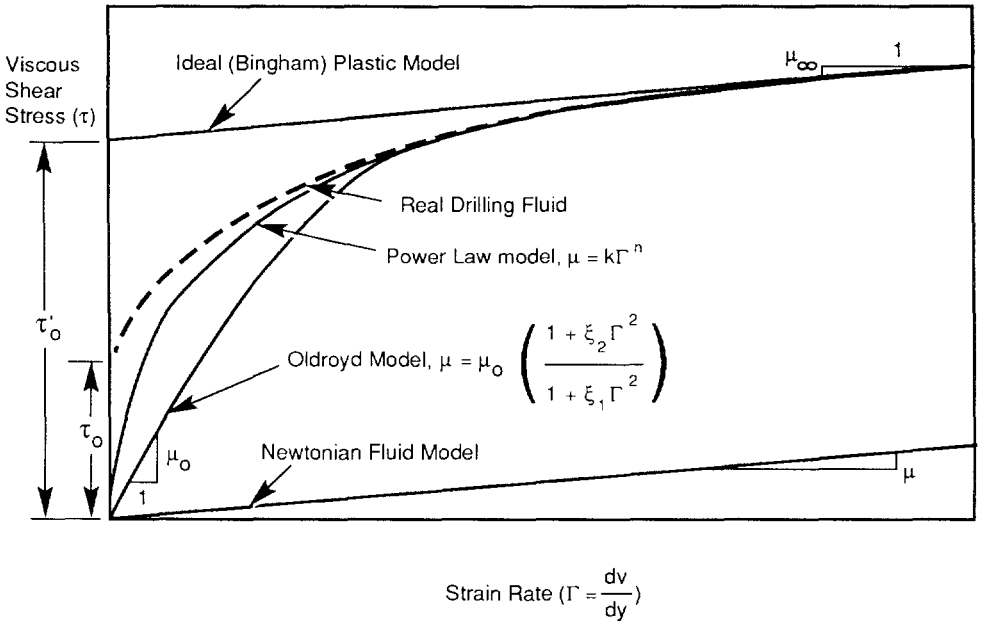

Figure 4.1-8. Various Models for Modeling Drilling Fluid Shear Stress.

where

μ_ℓ = linear viscosity (= "average" viscosity for evaluating N_R)
τ'_o = yield point (shear stress at zero strain rate)
Γ = strain rate

Oldroyd Model -- Oldroyd's (1958) shear softening model of the viscosity can also approximate the drilling fluid behavior away from the yield stress (τ_o) by the appropriate choice of parameters:

$$\tau = \mu_0 \left[\frac{1 + \zeta_2 \Gamma^2}{1 + \zeta_1 \Gamma^2} \right] \Gamma \qquad (4.1\text{-}24)$$

where

μ_∞ = $\mu_o(\zeta_2/\zeta_1)$ = limiting viscosity at infinite strain rate = μ_ℓ (= "average" viscosity for evaluating N_R)
Γ = strain rate
ζ_1, ζ_2 = Oldroyd model parameters
μ_0 = limiting viscosity at zero rate of strain

Note that for the PA calculations, ζ_1 was assumed equal to 2 ζ_2, based on viscosity measurements for an oil-based, 1.7-kg/m^3 (14-lb/gal) mud (Darley and Gray, 1988, Table 5-2). The assumption can be somewhat arbitrary since the behavior at high strain rate (away from the yield point) is of primary interest.

Using the above assumption, the parameter ζ_2 was estimated by equating the linear ideal plastic model, Eq. 4.1-23 with the Oldroyd model, Eq. 4.1-24, at a high strain rate. After simple algebraic manipulation

$$\zeta_2 = (\mu_\infty \Gamma_m - \tau_o')/2\Gamma_m^2 \tau_o' \qquad (4.1\text{-}25)$$

The high strain rate selected for the match point (Γ_m) was 1020 s^{-1}.

Linear Viscosity. For a saturated brine with the density maintained by emulsified oil and modeled as an ideal Bingham plastic, Pace (1990) estimates that μ_ℓ varies between 0.005 and 0.030 Pa•s (0.003 and 0.020 lbf•s/ft^2) with a median of 0.009 Pa•s (0.006 lbf•s/ft^2). Figure 4.1-9 shows the estimated pdf and cdf for drilling mud viscosity.

Yield Stress. For a saturated brine with the density maintained by emulsified oil and modeled as an ideal Bingham plastic, Pace (1990) estimates the yield point (τ_o') varies between 2.4 and 19 Pa (5 and 42 lb/100 ft^2) with a median of 4 Pa (9.2 lb/100 ft^2) (Figure 4.1-10).

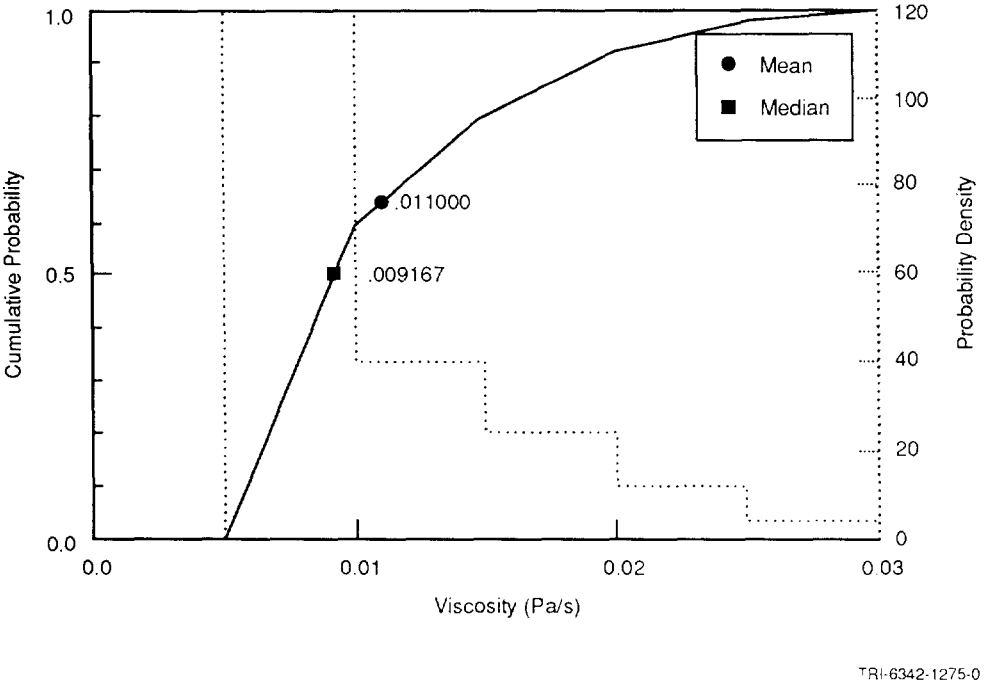

Figure 4.1-9. Estimated Distribution (pdf and cdf) for Drilling Mud Viscosity.

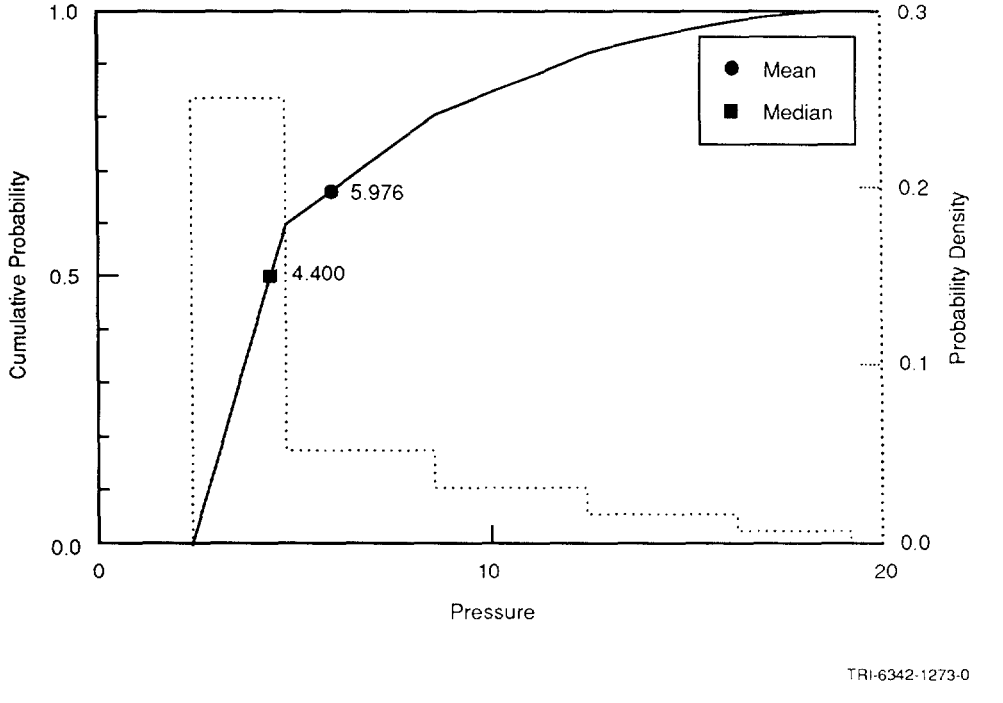

Figure 4.1-10. Estimated Distribution (pdf and cdf) for Drilling Mud Yield Stress (Ideal Plastic).

4.2 Human-Intrusion Borehole

Table 4.2-1. Characteristics of Human-Intrusion Borehole

Parameter	Median	Range		Units	Distribution Type	Source
Borehole Fill Properties						
Creep (r_o-r/r_o)		2×10^{-2}	8×10^{-1}	none	Table	Sjaardema and Krieg, 1987, Figure 4.6
Density, average (ρ_{ave})	2.3×10^{3}			kg/m^3	Constant	See text (Salado).
Density, bulk (ρ_{bulk})	2.14×10^{3}			kg/m^3	Constant	See text (Salado).
Permeability, final (k)	3.16×10^{-12}	1×10^{-14}	1×10^{-11}	m^2	Lognormal	Freeze and Cherry, Table 2.2 (silty sand)
Initial						
Plug in Castile Fm.	10^{-15}			m^2	Constant	Lappin et al., 1989, Table C-1
Plugs in Salado Fm.	10^{-18}			m^2	Constant	Lappin et al., 1989, Table C-1
Porosity (ϕ)	3.75×10^{-1}	2.5×10^{-1}	5×10^{-1}	none	Normal	Freeze and Cherry, Table 2.4 (sand)
Drilling Characteristics						
Drill bit diameter (d)						
Intrusion	3.55×10^{-1}	2.67×10^{-1}	4.44×10^{-1}	m	Uniform	See text.
Historical	2×10^{-1}	1.21×10^{-1}	4.45×10^{-1}	m	Delta	Brinster, 1990c
Drill string angular velocity ($\dot{\theta}$)	7.7	4.2	2.3×10^{1}	rad/s	Cumulative	Pace, 1990; Austin, 1983
Drilling mud flowrate (Q_f)	9.935×10^{-2}	7.45×10^{-2}	1.24×10^{-1}	$m^3/(s \cdot m)$	Uniform	Pace, 1990; Austin, 1983

4.2.1 Borehole Fill Properties

Creep

Parameter:	**Creep**
Median:	None
Range:	2×10^{-2}
	8×10^{-1}
Units:	Dimensionless
Distribution:	Table
Source(s):	Sjaardema, G. D. and R. D. Krieg. 1987. *A Constitutive Model for the Consolidation of WIPP Crushed Salt and Its Use in Analysis of Backfilled Shaft and Drift Configurations.* SAND87-1977. Albuquerque, NM: Sandia National Laboratories. (Figure 4.6)

Storage Density near Repository

Parameter:	**Density, average (ρ_{ave})**
Median:	2.3×10^3
Range:	None
Units:	kg/m^3
Distribution:	Constant
Source(s):	Krieg, R. D. 1984. *Reference Stratigraphy and Rock Properties for the Waste Isolation Pilot Plant (WIPP) Project.* SAND83-1908. Albuquerque, NM: Sandia National Laboratories. (Table 4)

Bulk Density of Halite in Salado

Parameter:	**Density, bulk (ρ_{bulk})**
Median:	2.14×10^3
Range:	None
Units:	kg/m^3
Distribution:	Constant
Source(s):	Holcomb, D. J. and M. Shields. 1987. *Hydrostatic Creep Consolidation of Crushed Salt with Added Water.* SAND87-1990. Albuquerque, NM: Sandia National Laboratories. (p. 17)

Final Permeability

Parameter:	**Permeability, final** (k)
Median:	3.16×10^{-12}
Range:	1×10^{-14}
	1×10^{-11}
Units:	m^2
Distribution:	Lognormal
Source(s):	Freeze, R. A. and J. C. Cherry. 1979. *Groundwater.* Englewood Cliffs, NJ: Prentice-Hall, Inc. (Table 2.4, silty sand)

Porosity

Parameter:	**Porosity** (ϕ)
Median:	3.75×10^{-1}
Range:	2.5×10^{-1}
	5×10^{-1}
Units:	Dimensionless
Distribution:	Normal
Source(s):	Freeze, R. A. and J. C. Cherry. 1979. *Groundwater.* Englewood Cliffs, NJ: Prentice-Hall, Inc. (Table 2.4, sand)

Discussion:

Because of the speculative nature of inadvertent human intrusion, PA calculations depend on the guidance provided by regulations on factors such as length, severity, and resulting conditions after intrusion. The EPA Standard, *40 CFR 191*, in Appendix B states

> "...the implementing agency can assume that passive institutional controls or the intruders' own exploratory procedures are adequate for the intruders to soon detect, or be warned of, the incompatibility of the area with their activities ... Furthermore, the Agency assumes that the consequences of such inadvertent drilling need not be assumed to be more severe than: ... (2) creation of a ground water flow path with a permeability typical of a borehole filled by the soil or gravel that would normally settle into an open hole over time--not the permeability of a carefully sealed borehole."

Thus while intruders "soon detect" the repository, the guidance in Appendix B suggests that the implementing agency should not take credit for any special precautions that the drilling company might pursue as the result of detection that could alter long-term borehole behavior.

Initial Conditions after Abandonment. Some PA calculations require that initial conditions be established for the time period immediately after intrusion; no regulatory guidance has been provided for these conditions. In defining initial conditions in the borehole, the PA calculations assume that future societies establish government regulations on drilling similar to those in effect today to protect natural resources. Thus, for any borehole through the repository and hypothetical brine reservoir, drillers would be required to place casing and several cement and sand plugs as follows:

Casing. The normal procedure for drilling an oil and gas well is to drill the hole to the base of the Rustler Formation (the top of salt) and set casing, called a salt string. The State Engineer Office dictates the use of this casing because the WIPP is located in a closed ground-water basin, and all hydrocarbon wells are required to protect the aquifers in the basin (e.g., Culebra Dolomite). After the hole has been drilled and the casing placed in the hole, the casing is cemented from bottom to top with an API Class C grout (intended for use in oil and gas wells from surface to a depth of 2,400 m [8,000 ft] and having a sulfate resistance).

Plug Locations. The Energy, Minerals, and Natural Resources Department, Oil Conservation Division (OCD) controls plugging when abandoning a borehole in the Delaware Basin in and around the WIPP. Exact specifications are negotiated between the drilling company and the OCD. The OCD then inspects for compliance. Because the WIPP repository is located in the potash enclave, recommended plugging procedures protect the potash horizon from foreign

fluids. Prior to 1988, specifications likely included sealing off any encountered brine reservoir in the Castile Formation with cement grout and capping the seal with a 60-m (200-ft) cement-grout plug. About 15 m (50 ft) of sand was usually emplaced above grout plugs. Weighted drilling fluid above the sand was usually emplaced to ~60 m (~200 ft) below the potash horizon, where another plug extended through the potash horizon. A second sand cap was emplaced, followed by weighted drilling mud to within ~60 m (~200 ft) of the top of the Salado Formation salt, where another plug of cement grout was emplaced, followed by sand and weighted mud. When the base of the casing was reached, the specifications either required grouting or filling with weighted mud to the surface, where a cap and abandonment marker were often placed (Lappin et al, 1989, Appendix C).

In April 1988, the OCD amended order R-111 and specified that the plug be a "solid cement plug through the salt section" (Salado Formation); the amendment was in response to conflicts between the potash and oil/gas industries (OCD, 1988, p. 10). The 1991 PA calculations assumed these latter plugging conditions.

Initial Plug Permeability. The initial plug permeabilities depend strongly on the host rock in which the plug is emplaced (e.g., clean vs. chemically altered steel casing or ahydrite vs. halite). Because most experimental studies of plug-borehole interactions extend for only hundreds of days or less, data are limited (Christensen and Petersen, 1981; Buck, 1985; Bush and Piele, 1986; Scheetz et al., 1986). Any PA calculations starting from initial conditions assume permeabilities of 10^{-15} m^2 (1 mD) for plugs in the Castile Formation and 10^{-18} m^2 (10^{-3} mD) in the Salado and Rustler Formations (Lappin et al., 1989, Table C-1).

Borehole Permeability and Porosity. Of primary concern to the PA calculations is the borehole permeability over most of the 10,000 yr. Three components of these calculations are (1) the length of time that the plug and casing remain intact, (2) the change in permeability of the deteriorating plugs with time, and (3) the ultimate deformation of the borehole.

Plug Life. Cementing companies suggest that the cement plugs should last for at least 100 yr, as would casing. PA calculations assume a life of 75 yr followed by 75 yr of degredation (Figure 4.2-2).

Degraded Plugs and Borehole Debris Permeability. PA calculations assume that the degrading concrete plugs and other debris initially present in the hole would have a permeability (Figure 4.2-3) and porosity (Figure 4.2-4) of silty sand (Freeze and Cherry, 1979), but with a bulk and average density equal to that of the Salado Formation (Table 4.2-1). The permeability and porosity were assumed to vary lognormally and normally, respectively, between the typical range for silty sand, typical of distributions of the parameters in the literature (Harr, 1987, Table 1.8.1).

Note that any drilling mud initially in the borehole or brine that drains into the borehole would have to be able to migrate through the degrading plugs before the borehole could be a viable conduit. In other words, if the fluid is trapped, the borehole is not a conduit.

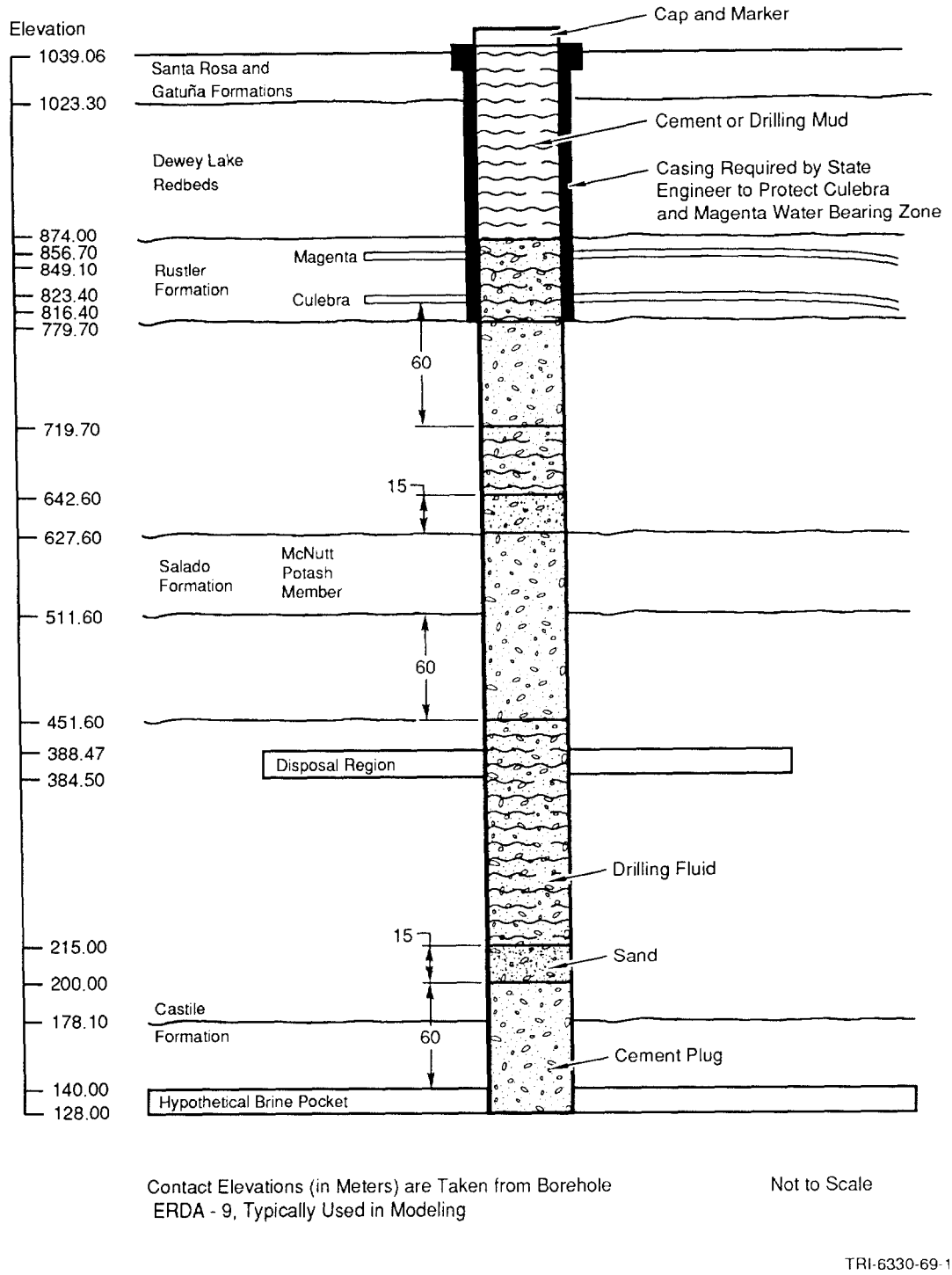

Figure 4.2-1. Required Casing and Plugs. New Mexico State Engineer requires casing through Rustler Fm. when drilling exploratory boreholes; New Mexico Energy, Mineral, and Natural Resources Department currently requires solid cement plugs in Salado Fm. to protect potash horizon when abandoning a borehole.

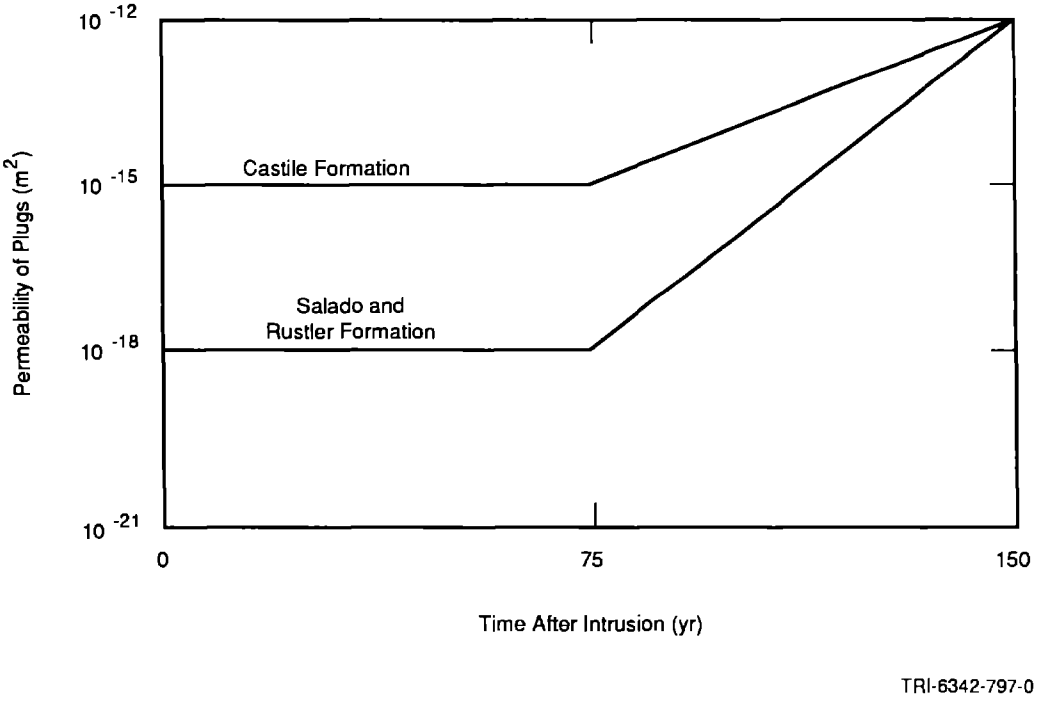

Figure 4.2-2. Increased Permeability of Cement Grout Plugs in Intrusion Borehole with Time because of Degradation.

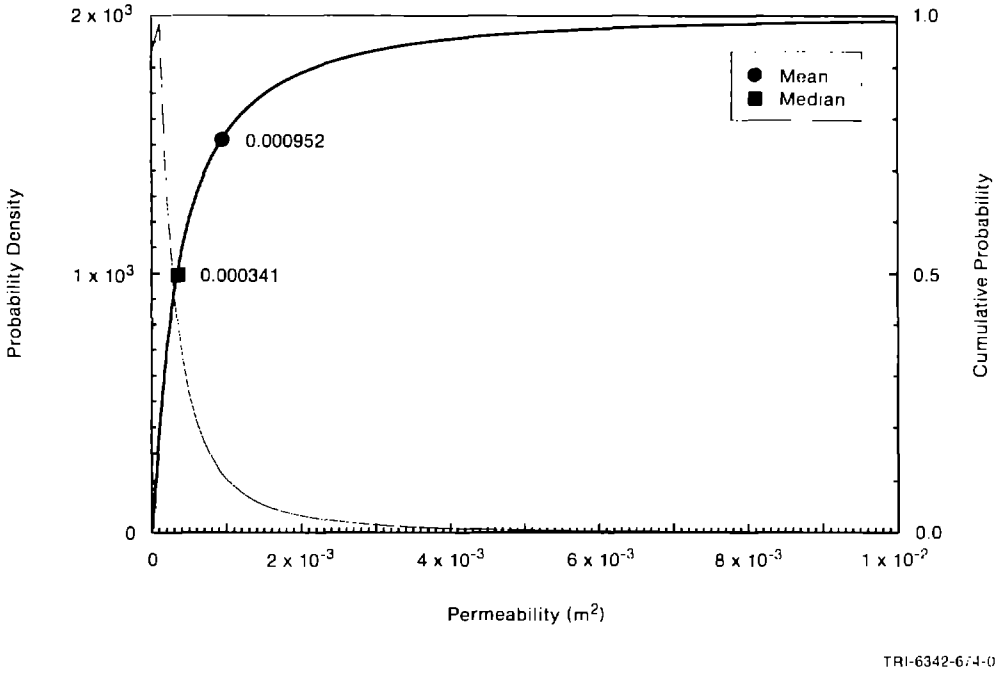

Figure 4.2-3. Lognormal Distribution (pdf and cdf) for Borehole Permeability after Degradation but before Creep Deformation.

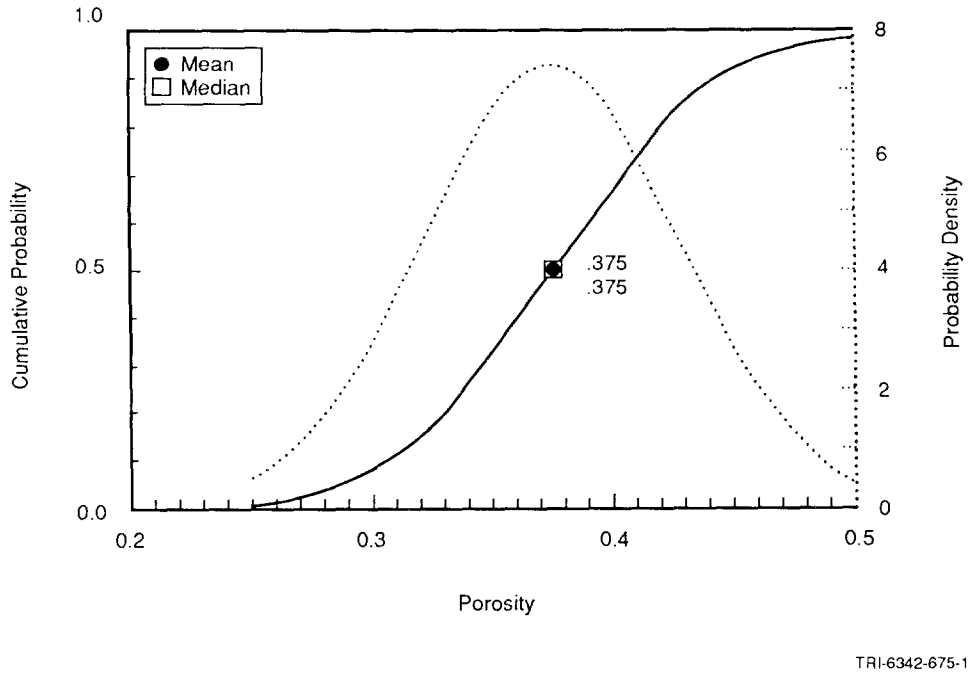

Figure 4.2-4. Normal Distribution (pdf and cdf) for Borehole Porosity after Degradation but before Creep Deformation.

Borehole Deformation. Because of the change in borehole abandonment procedures, the 1991 PA calculations did not assume any borehole deformation. This assumption contributed to a more conservative calculation.

With the previous order, salt "would normally settle into an open hole" and naturally seal the hole shut in the uncemented section of the borehole. Thus, with time, the borehole would attain very low permeabilities similar to the host salt. However, if the amended orders are followed and the borehole is filled, the use of a solid cement plug through the Salado Formation greatly decreases the likelihood that the borehole will be permanently sealed by salt creep over the long term (>100 yr).

The numerically predicted creep closure used in the 1990 PA calculations is shown in Figure 4.2-5 (Sjaardema and Krieg, 1987, Figure 4.6). Although a homogenous transient creep model may not completely predict borehole closure -- because local variations such as anhydrite layers and clay lenses play an important role in the ultimate deformation -- the homogenous model of creep will err on the conservative side, predicting much slower creep closure than actually occurs (Munson et al., 1988; 1989; 1990c). On the other hand, Figure 4.2-5 assumes no fluid is in the hole. The presence of hydrostatic pressure will greatly decrease the closure rate.

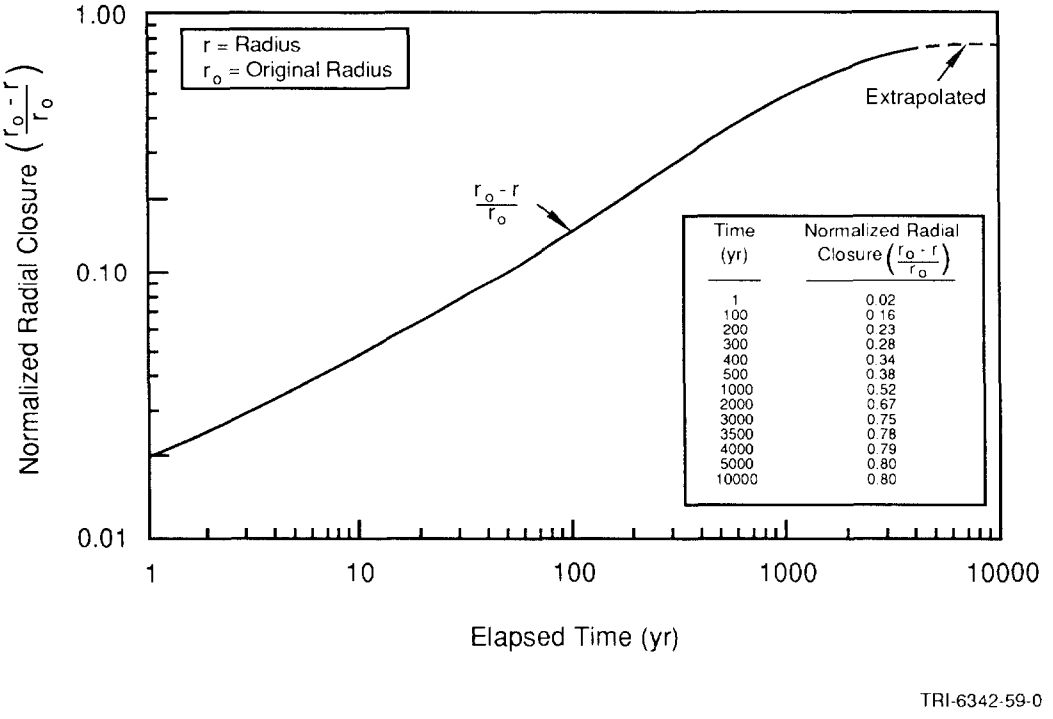

Figure 4.2-5. Normalized Closure for Shaft (Sjaardema and Krieg, 1987, Figure 4.6).

4.2.2 Drilling Characteristics

Diameter of Intrusion Drill Bit (Deep Hydrocarbon Target)

Parameter:	**Intrusion drill bit diameter** (d)
Median:	3.55×10^{-1}
Range:	2.67×10^{-1}
	4.44×10^{-1}
Units:	m
Distribution:	Uniform
Source(s):	See text.

Historical Drill Bit Diameter

Parameter:	**Historical drill bit diameters** (d)
Median:	2×10^{-1}
Range:	1.21×10^{-1}
	4.45×10^{-1}
Units:	m
Distribution:	Delta
Source(s):	Brinster, K. 1990c. "Well data from electric logs," Memo 10 in Appendix A of Rechard et al. 1990. *Data Used in Preliminary Performance Assessment of the Waste Isolation Pilot Plant (1990).* SAND89-2408. Albuquerque, NM: Sandia National Laboratories.

Figure 4.2-6 shows the uniform distribution for the diameter of the intrusion drill bit.

Figure 4.2-7 shows the distribution of drill bits used in the past.

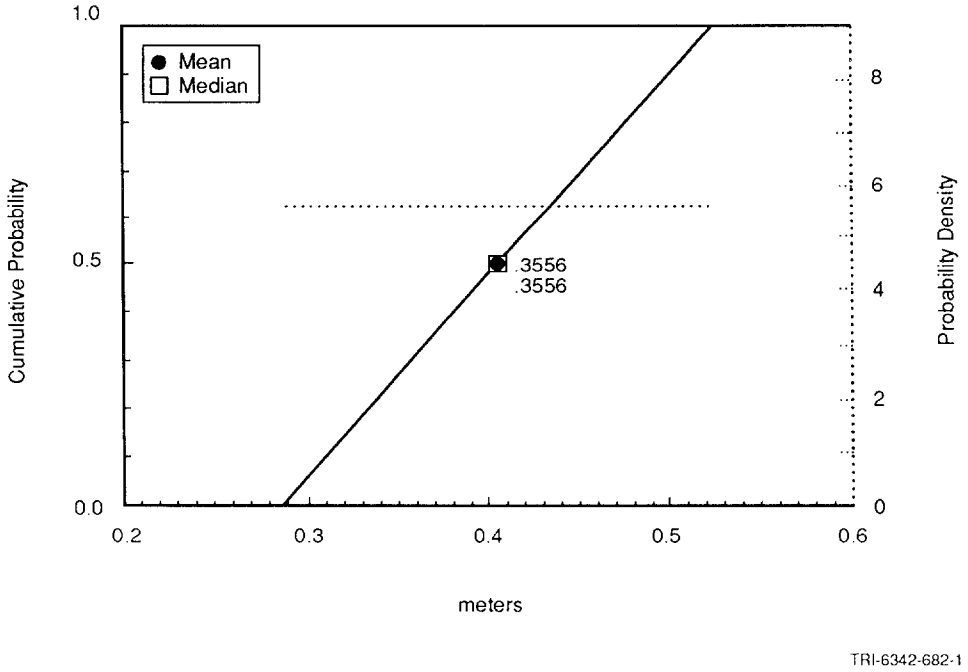

Figure 4.2-6. Estimated Probability of Drilling an Intrusion Borehole with a Specific Diameter.

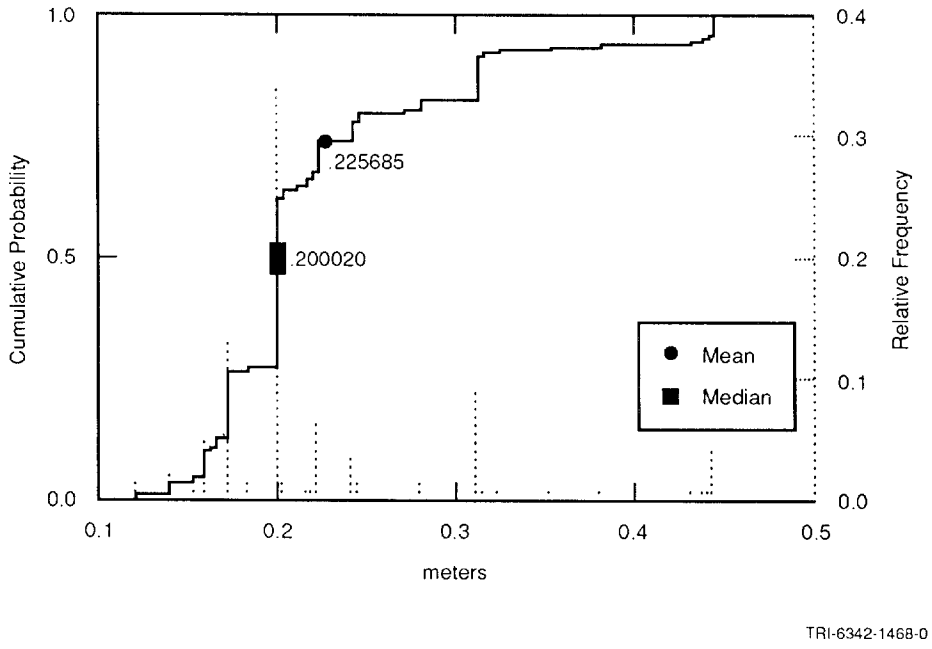

Figure 4.2-7. Distribution of Historical Drill Bit Diameter.

Discussion:

The guidance for the EPA Standard, *40 CFR 191*, (Appendix B) states that the EPA

> "...believes that the most productive consideration of inadvertent intrusion concerns those realistic possibilities that may be usefully mitigated by repository design, site selection, or use of passive controls (although passive institutional controls should not be assumed to completely rule out the possibility of intrusion). Therefore, inadvertent and intermittent intrusion by exploratory drilling for resources (other than any provided by the disposal system itself) can be the most severe intrusion scenario assumed..."

The future histories (scenarios) that must be considered are not necessarily exhaustive, but rather those that if examined might differentiate between repository sites or perhaps identify ways to improve repository design.

Consequently, the PA Division of the WIPP assumes that current standard drilling procedures for gas and oil exploration will continue into the future, and that future drillers will observe regulations similar to those currently imposed by federal and state agencies to protect resources.

Drilling for oil and gas has two main objectives: to drill the hole to the production zone as quickly and economically as safely possible, and to install casing from the reservoir to the surface for well production. The procedures used to accomplish these objectives are fairly well standardized in the drilling industry.

Currently when a company drills an exploratory oil or gas well, the operation uses a standard rotary drill rig with a mud circulation system. The differences between drilling for oil and gas depend on the depth of the well, which controls the size of casing used. Figures 4.2-6 and 4.2-7 show the distribution used in the past in the Delaware Basin for oil and gas exploration. The data are reported as a discrete distribution because bit diameters cannot vary continuously between 0.1206 m and 0.4445 m diameter (4-3/4 in. and 17-1/2 in.), but must be the diameter of a bit that was actually used (Brinster, 1990c). The median bit diameter is 0.2000 m (7-7/8 in. diameter) (Figures 4.2-6 and 4.2-7).

Currently, the normal depth for an oil well in the Delaware Basin near the WIPP site ranges from 1,200 to 1,800 m (4,000 to 6,000 ft), but gas-well depths usually exceed 3,000 m (10,000 ft). Consequently, oil wells normally have a standard 0.413-m (16 1/4-in.) drilled hole to the top of salt to accommodate 0.340-m (13 3/8-in.) steel casing, and gas wells normally have a standard 0.4445-m (17 1/2-in.) drilled hole to accommodate 0.356-m (14-in.) casing. After casing is set with grout, the company drills either a standard 0.311-m (12 1/4-in.) hole, if the target is oil, or a 0.356-m (14-in.) hole, if the target is gas (Table 4.2-2). Rather than sample from the historical diameters for evaluating the borehole as was done in the 1990 PA calculations, the 1991 PA calculations sample from a perturbation about the currently used diameter for deep gas wells (i.e., 0.356 m $\pm$ 0.0889 [14 in. $\pm$ 3.5]). This practice ensures that fairly large borehole diameters are used and thus is more conservative than the 1990 calculations.

From the bit diameter, the drilled diameter through the waste is predicted based on strength properties of the waste (e.g., shear strength) and angular velocity of the drillstring, viscosity of the drilling fluid, fluid density, and annular uphole fluid velocity (Rechard et al., 1989) (Figure 4.2-8). Shear strength and surface roughness of the waste also influence the drilled area and are discussed with waste properties.

Table 4.2-2. Specifications for Gas and Oil Exploratory Boreholes

Parameter	Value	Units
Drilled diameter		
In Rustler Formation (oil well)	0.413	m
(gas well)	0.444	m
In Salado and Castile Formations, (oil well)	0.311	m
(gas well)	0.356	m

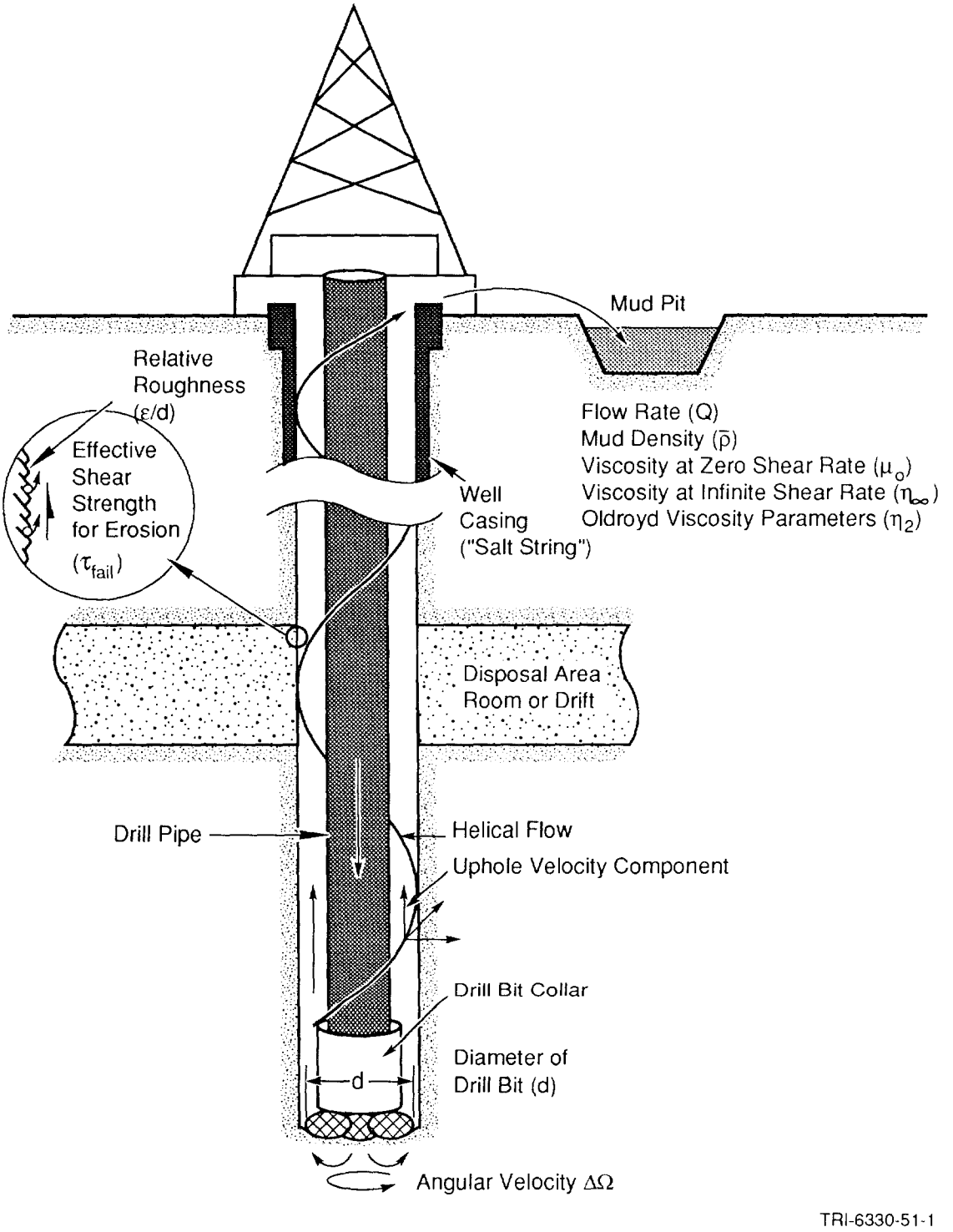

Figure 4.2-8. Definition of Parameters Describing Human Intrusion by Drilling.

Drill String Angular Velocity

Parameter:	**Drill string angular velocity ($\dot{\theta}$)**
Median:	7.7
Range:	4.2
	2.3×10^1
Units:	rad/s
Distribution:	Cumulative
Source(s):	Pace, R. O. 1990. Manager, Technology Exchange Technical Services, Baroid Drillng Fluids, Inc., 3000 N. Sam Houston Pkwy. E., Houston, TX. (Expert Opinion). Letter of 18 September 1990. Letter 1b in Appendix A of Rechard et al. 1990. *Data Used in Preliminary Performance Assessment of the Waste Isolation Pilot Plant (1990).* SAND89-2408. Albuquerque, NM: Sandia National Laboratories.
	Austin, E. H. 1983. *Drilling Engineering Handbook.* Boston, MA: International Human Resources Development Corporation.

Figure 4.2-9 shows the distribution of the drill string angular velocity.

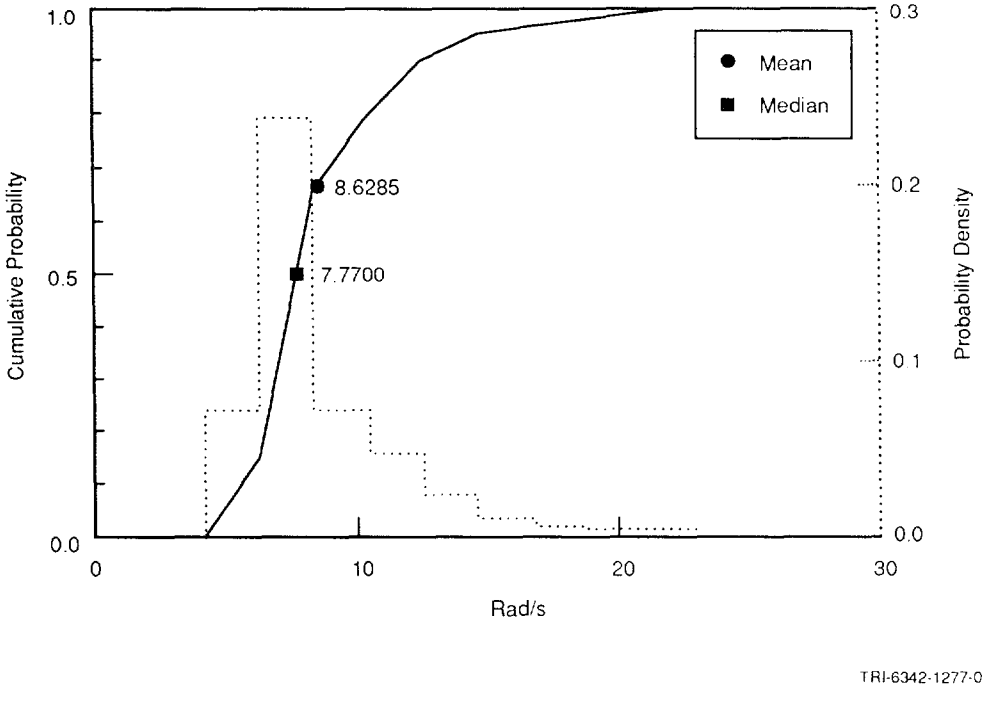

Figure 4.2-9. Distribution (pdf and cdf) of Drill String Angular Velocity.

Discussion:

For drilling through salt, the drill string angular velocity ($\dot{\theta}$) can vary between 4.18 and 23 rad/s (40 and 220 rpm) (Austin, 1983, Figure 4.5), with a median speed of about 7.75 rad/s (75 rpm) (Pace, 1990).

Mud Flowrate

Parameter:	**Drilling mud flowrate (Q_f)**
Median:	9.925×10^{-2}
Range:	7.45×10^{-2}
	1.24×10^{-1}
Units:	$m^3/(s \cdot m)$
Distribution:	Uniform
Source(s):	Austin, E. H. 1983. *Drilling Engineering Handbook.* Boston, MA: International Human Resources Development Corporation.

Discussion:

Flowrates of the drilling fluid usually vary between 7.45×10^{-2} and 1.24×10^{-1} $m^3/(s \cdot m)$ of drill diameter (30 and 50 gal/min/in.) (Austin, 1983, Table 1.15). PA calculations assumed that the annulus between the drill collar and borehole was initially about 2.5 cm (1 in.). Thus, for the minimum and maximum diameters typically used in the drilling near the WIPP, the uphole velocity varies between 0.99 and 1.73 m/s (3.2 and 5.7 ft/s).

4.3 Parameters for Castile Formation Brine Reservoir

Pressurized brine in the northern Delaware Basin has been encountered in fractured anhydrites of the Castile Formation in boreholes both north and northeast of the WIPP over the past 50 yr. In addition, Castile brines were encountered southwest of the WIPP at the Belco Well, about 6.5 km (4 mi) from the center of the WIPP. During WIPP site characterization, Castile Formation brine reservoirs were encountered in the WIPP-12 borehole, about 1.6 km (1 mi) north of the center of the WIPP, and the ERDA-6 borehole, about 8 km (5 mi) northeast of the center of the WIPP (Figure 4.3-1).

Also, a geophysical study that correlated with the known occurrence of brine at WIPP-12 indicated the presence of brine fluid within the Castile Formation under the WIPP (Earth Technology Corp., 1988). Based on borehole experience and the geophysical study, the PA calculations assume that a brine reservoir exists underneath at least a portion of the disposal region. The assumed presence of a Castile brine reservoir beneath the repository is of concern only in the event of human intrusion. (The area and thus the probability of hitting a brine reservoir and the disposal area are discussed in Chapter 5.)

Table 4.3-1 provides the parameter values for the Castile Formation Brine Reservoir.

Table 4.3-1. Parameter Values for Castile Formation Brine Reservoir

Parameter	Median	Range		Units	Distribution Type	Source
Elevation, top	1.4×10^{2}	-2.00×10^{2}	1.78×10^{2}	m	Cumulative	See text.
Density, grain (ρ_g)	2.963×10^{3}			kg/m^3	Constant	See anhydrite, Section 24.
Analytic Model						
Pressure, initial (p_i)	1.26×10^{7}	1.1×10^{7}	2.1×10^{7}	Pa	Cumulative	$\rho_f g \Delta z$, $\rho_b g \Delta z$; Lappin et al.,1989, Table 3-19; Popielak et al.,1983, p. H-52
Storativity, bulk $\hat{S}_b$	2×10^{-1}	2×10^{-2}	2×10^{1}	m^3/Pa	Loguniform	See text.
Numerical Model						
Permeability						
Intact matrix	1×10^{-19}	1×10^{-20}	1×10^{-18}	m^2	Cumulative	See Table 2.4-1.
Fractured matrix	1×10^{-13}	1×10^{-16}	1×10^{-10}	m^2	Cumulative	Freeze and Cherry, 1979; Reeves et al., 1991.
Porosity	5×10^{-3}	1×10^{-3}	1×10^{-2}	none	Cumulative	Reeves et al., 1991.
Radius, equivalent	2.32×10^{2}	3×10^{1}	8.6×10^{3}	m	Cumulative	Reeves et al., 1991.
Thickness	1.2×10^{1}	7	6.1×10^{1}	m	Constant	Reeves et al., 1991.

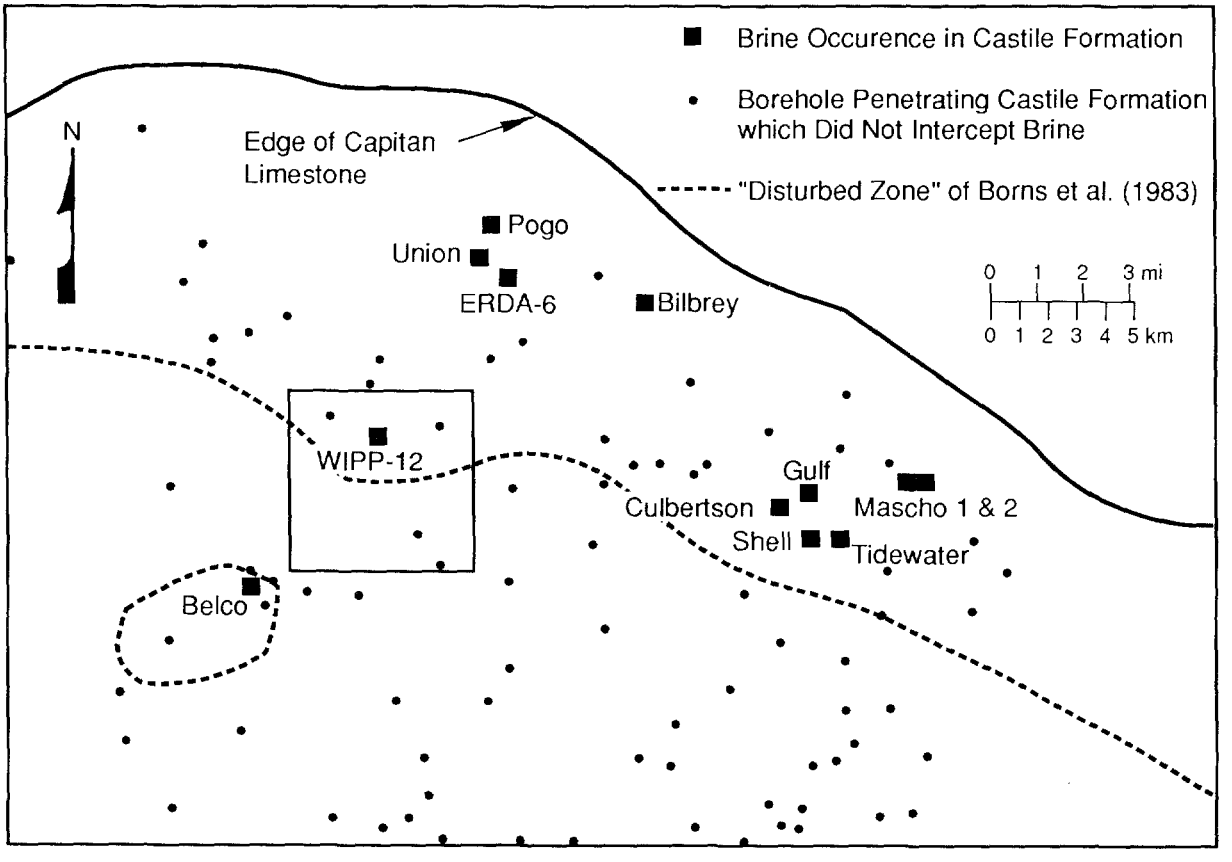

Figure 4.3-1. Deep Boreholes that Encountered Brine Reservoirs within the Castile Formation, Northern Delaware Basin (Lappin et al., 1989, Figure 3-26).

4.3.1 Analytic Brine Reservoir Model

Elevation of Top

Parameter:	**Elevation of top**
Median:	1.4×10^2
Range:	-2.0×10^2
	1.78×10^2
Units:	m
Distribution:	Cumulative
Source(s):	See Figure 2.2-1.
	Lappin, A. R., R. L. Hunter, D. P. Garber, and P. B. Davies, eds. 1989. *Systems Analysis Long-Term Radionuclide Transport, and Dose Assessments, Waste Isolation Pilot Plant (WIPP), Southeastern New Mexico; March 1989.* SAND89-0462. Albuquerque, NM: Sandia National Laboratories. (Table 3-19)

Discussion:

As discussed in Section 5.1.1, the elevation of the brine reservoir is directly tied to the areal extent. The elevation of the brine reservoir potentially varies between -200 and 178 m (-656 and 584 ft), the estimated bottom and measured top elevation, respectively, of the Castile Formation in ERDA-9. The elevation of the top of the WIPP-12 brine reservoir (140 m [457.8 ft]) was chosen as the median. For 1991 PA calculations, the hypothetical brine reservoir elevation was fixed at the median, while the areal extent was allowed to vary, independently.

Figure 4.3-2 shows the estimated distribution for elevation.

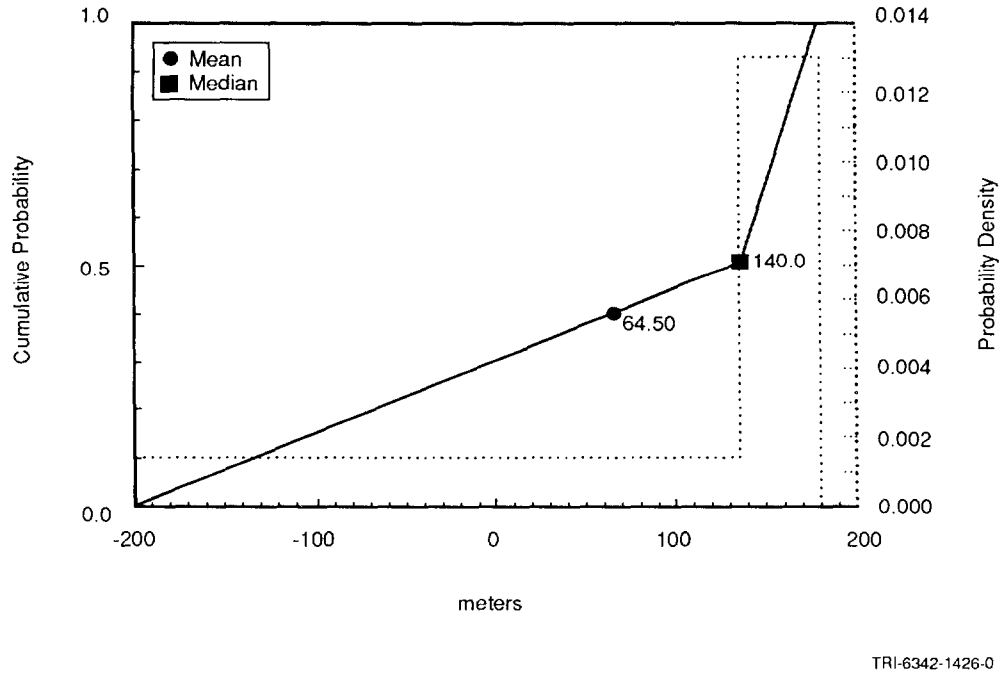

Figure 4.3-2. Estimated Distribution (pdf and cdf) for Elevation of Castile Formation Brine Reservoir.

Brine Pressure

Parameter:	**Pressure, initial** (p_i)
Median:	1.26×10^7
Range:	1.1×10^7
	2.1×10^7
Units:	Pa
Distribution:	Cumulative
Source(s):	Popielak, R. S., R. L. Beauheim, S. R. Black, W. E. Coons, C. T. Ellingson, and R. L. Olsen. 1983. *Brine Reservoirs in the Castile Fm., Waste Isolation Pilot Plant (WIPP) Project, Southeastern New Mexico.* TME-3153. Carlsbad, NM: U.S. Department of Energy.
	Lappin, A. R., R. L. Hunter, D. P. Garber, and P. B. Davies, eds. 1989. *Systems Analysis Long-Term Radionuclide Transport, and Dose Assessments, Waste Isolation Pilot Plant (WIPP), Southeastern New Mexico; March 1989.* SAND89-0462. Albuquerque, NM: Sandia National Laboratories. (Table 3-19)

Figure 4.3-3 shows the estimated distribution for initial brine reservoir pressure.

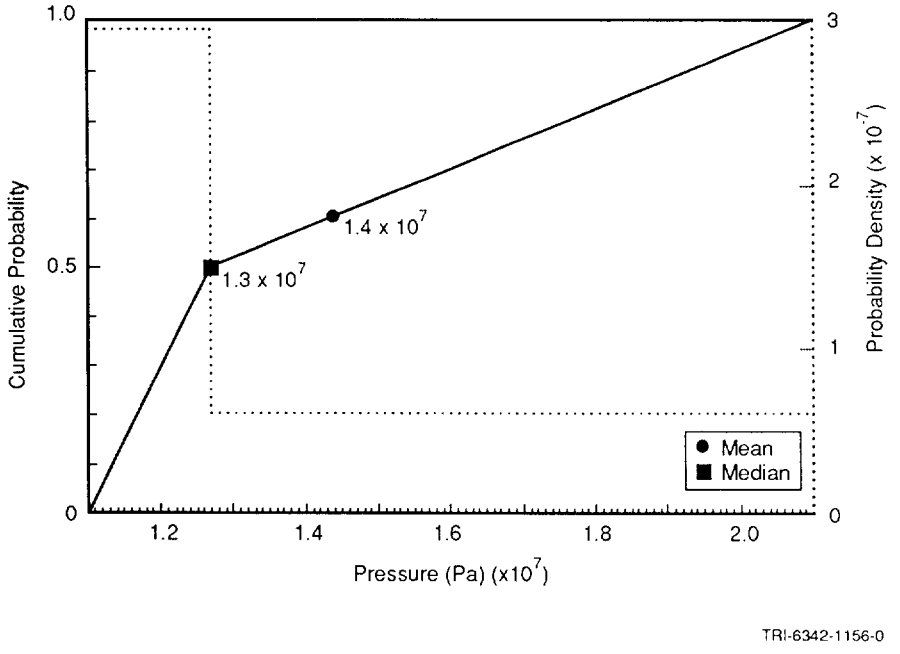

Figure 4.3-3. Estimated Distribution (pdf and cdf) for Castile Brine Reservoir Initial Pressure.

Discussion:

Median. The measured initial pressure of 12.6 MPa (125 atm) for WIPP-12 (Popielak, 1983, p. H-52) was used as the median brine reservoir initial pressure.

Range. Lappin et al. (Table 3-19, 1989, derived from Popielak et al., 1983, Table H.1) estimated the initial brine reservoir pressure from several wellhead measurements at WIPP-12 and other boreholes that encountered pressurized Castile brine. The range was between 7.0 and 17.4 MPa (69 and 172 atm). Because the range of pressures includes measurements in wells completed at various elevations, a correction for differences in elevation is required.

The origin of Castile brine reservoirs is not conclusively known. Present interpretations are that their origin is either local, by limited movement of intergranular brines from adjacent Castile halites, or regional, by the previous existence of a lateral hydraulic connection of the Castile Formation with the Capitan reef (Lappin et al., 1989). However, the initial pressure observations at other wells are only directly pertinent if (1) the reservoir fluids are from the same source (past interconnection of reservoir fluid) or (2) they had a common genesis (e.g., brine trapped along bedding planes in areas of high permeability).

For the first case (interconnection), an elevation correction assuming a hydrostatic variation with depth is most appropriate. For the second case (common genesis), an elevation correction assuming a lithostatic variation depth is most appropriate. The range using both types of elevation corrections is 10.7 to 16.8 MPa (106 to 166 atm) (Table 4.3-2). A brine density of 1,215 kg/m^3 (75.85 lb/ft^3) (Section 4.1) was assumed for the first case; an average formation density of 2,400 kg/m^3 (149.8 lb/ft^3) was assumed for the second case. Elevations (except WIPP-12 and ERDA-6) were estimated from the well location and a topographic map of the area (USGS 15 min quads, Carlsbad, NM, 1971, Nash Draw, NM, 1965).

This calculated range is similar to the maximum and minimum possible range of 11 and 21 MPa assuming hydrostatic and lithostatic pressures at the elevation of the WIPP-12 brine reservoir (140 m [457.8 ft]) (see Figure 2.2-3) and consequently this latter range was used in the PA calculations.

Table 4.3-2. Estimated Initial Pressures of Brine Reservoirs Encountered in the Region around the WIPP Corrected to the Depth at the WIPP-12 Brine Reservoir (after Popielak et al., 1983)

Well Name	Pressure with Hydrostatic Correction (MPa)	Pressure with Lithostatic Correction (MPa)	Reported Pressure at Observation (MPa)	Elevation of Observation (m)	Depth to Observation (m)	Surface Elevation* (m)
WIPP-12	12.7	12.7	12.7	140	918	1058
ERDA-6	15.5	16.8	14.1	253	826	1079
Belco	14.5	14.6	14.3	152	854	1006
Gulf	12.1	10.7	13.6	16	1097	1113
Pogo	>16.6	>15.8	>17.4	69	1013	1082
Tidewater	>14.0	>12.2	>16.0	-24	1137	1113
Union	>11.2	>12.2	>10.1	226	856	1082
H&W Danford 1	11.5	15.8	7.0	512	588	1100(?)
**Bilbrey	12.1	13.8	11.2	209	942	1151
**Culbreston	11.8	10.9	12.8	57	1071	1128
**Mascho 1	11.6	10.8	12.4	69	1013	1082
**Mascho 2	11.3	10.6	12.0	77	1005	1082
**Shell	11.8	10.4	13.4	9	1119	1128

* Elevation from well location and USGS 15 min quad topographic map, Carlsbad, NM, 1971, Nash

** According to Popielak et al. (1983, Table H.1), these wells should not be used to estimate static pressure.

Bulk Storativity

Parameter:	**Bulk storativity (S_b)**
Median:	2×10^{-1}
Range:	2×10^{-2}
	2
Units:	m^3/Pa
Distribution:	Lognormal
Source(s):	See text.
	Popielak, R. S., R. L. Beauheim, S. R. Black, W. E. Coons, C. T. Ellingson, and R. L. Olsen. 1983. *Brine Reservoirs in the Castile Formation, Southeastern New Mexico, Waste Isolation Pilot Plant (WIPP) Project.* TME-3153. Carlsbad, NM: U.S. Department of Energy.

Figure 4.3-4 shows the estimated distribution for bulk storativity.

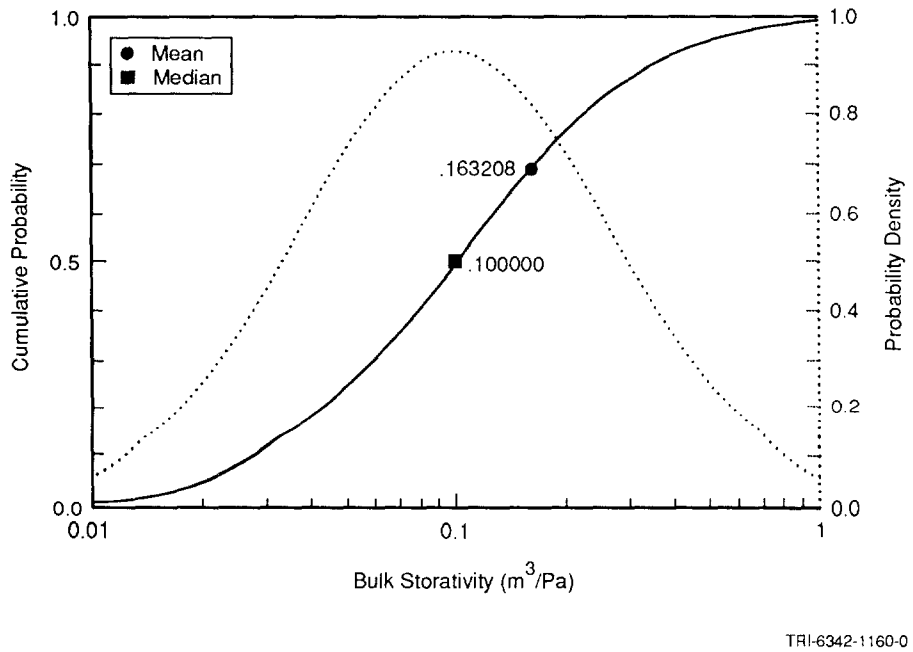

Figure 4.3-4. Estimated Distribution (pdf and cdf) for Bulk Storativity of Castile Brine Reservoir.

Discussion:

Bulk storativity (S_b) as defined herein is the total volume of fluid discharged from the reservoir per unit decrease in reservoir pressure ($\Delta V/\Delta p$). The bulk storativity can be estimated from wellhead measurements (long-term change in pressure and total discharge volume), or from the compressibility of the reservoir matrix and fluid and the total volume and porosity of the reservoir.

The pressure recovery of the WIPP-12 reservoir is characteristic of a dual-porosity medium. An initial rapid response is attributed to a highly permeable fracture set, while a more gradual component of recovery is due to repressurization of the higher permeability fracture set by intersecting lower permeability fractures. Because the human-intrusion scenarios contemplate that the Castile will be connected to the Culebra over the long term (compared to the duration of well tests), estimates of bulk storativity from long-term pressure changes are more appropriate than those made using short-term pressure changes, which may represent only the storativity of the highest permeability fractures. Estimates of bulk storativity using wellhead measurements range from 5×10^{-4} m^3/Pa (from ERDA-6 testing through October, 1982) to 2×10^{-1} m^3/Pa (from estimated total discharge volume, maximum estimated formation pressure, and apparent long-term recovery pressure at WIPP-12). Because WIPP-12 is closer to the waste disposal areathan ERDA-6, the latter number is considered more appropriate for a sub-repository reservoir.

Reservoir compressibility ($\beta_{s/\phi}$) and total volume (V_{tot}) may also be used to estimate bulk storativity:

$$S_b = \frac{\Delta V}{\Delta p} = V_{tot} \frac{1}{V_{tot}} \frac{\Delta V}{\Delta p} = V_{tot} \frac{1}{K} = V_{tot} \beta_s \qquad (4.3\text{-}1)$$

The area of the anticline associated with the WIPP-12 reservoir is approximately 1.7×10^6 m^2 (Popielak et. al., 1982 p. H-53). Popielak depicts brine occurrence in the lower 40% of the 100-m thickness of Anhydrite III-IV at WIPP-12 (Popielak et al., 1983, Figure G-2), giving a rough estimate of the reservoir total volume of 6.5×10^7 m^3. (Note that other published estimates of reservoir volume [e.g., Lappin et al., 1989, p. E-32] were made from wellhead measurements assuming some value of compressibility. These volume estimates will therefore not lead to independent estimates of S_b). Estimates of the bulk modulus $K_{bulk} = E/3(1-2\nu)$ (where E is Young's modulus and ν is Poisson's ratio) of Anhydrite III at WIPP-12 were used by Popielak et al. (1983, p. G-34) to derive a range of β_s from 3×10^{-11} Pa^{-1} to 1.4×10^{-10} Pa^{-1}. The resulting range in bulk storativity from Eq. 4.3-1 is 2×10^{-3} to 9×10^{-3} m^3/Pa. The reason this range does not include the wellhead estimate from WIPP-12 may be due to errors in the estimate of bulk volume or compressibility. For example, the apparent β_s may be larger than estimated here because of fractures in the anhydrite or trapped gas in the reservoir. However, at present there is no reason to suppose that bulk storativity is substantially higher than estimated from WIPP-12 wellhead measurements.

Based on the above considerations, the bulk storativity is assumed to lie between 2×10^{-2} and 2×10 m^3/Pa. The likelihood of the actual value falling in a given interval is described by a loguniform distribution between these limits. The median of this distribution is 0.2 m^3/Pa.

The high effective transmissivity of the Castile brine reservoir inferred from flow tests at the WIPP-12 borehole (Lappin et al., 1989; Popielak et al., 1983) implies that, in the event of its connection to the Culebra Dolomite through a sand-filled borehole, fluid flow rates from the brine reservoir will be controlled by the conductivity of the borehole fill and the area of the borehole (Rechard et al., 1990b, Figure 4-14; Reeves et al., 1991); pressure gradients within the brine reservoir will be small compared to gradients along the intrusion borehole. Observed correlation between brine occurrence and anticlines in the Castile (Lappin, 1988), and the larger differences in pressure among brine reservoirs at various locations, imply that Castile brine reservoirs have finite extent and are effectively isolated from one another over the long term. These observations suggest that in the context of discharge through an intrusion borehole(s) during the regulatory lifetime of the repository, Castile brine reservoirs would behave as finite reservoirs with effectively infinite conductivity. The reservoir state at any time could therefore be characterized by a single pressure.

Assuming constant compressibility of the brine reservoir components (fluid, matrix, and gas), the pressure in the brine reservoir will vary linearly with the volume of brine removed as follows: $dp/dV = 1/S_b$ where dp is the change in brine reservoir pressure, dV is the change in brine volume in the brine reservoir, and S_b is the bulk storage coefficient for the whole brine reservoir.

Therefore, the essential characteristics of the brine reservoir are contained in two parameters (Figure 4.3-5): the initial pressure of the brine reservoir, p_i, and bulk storativity, S_b.

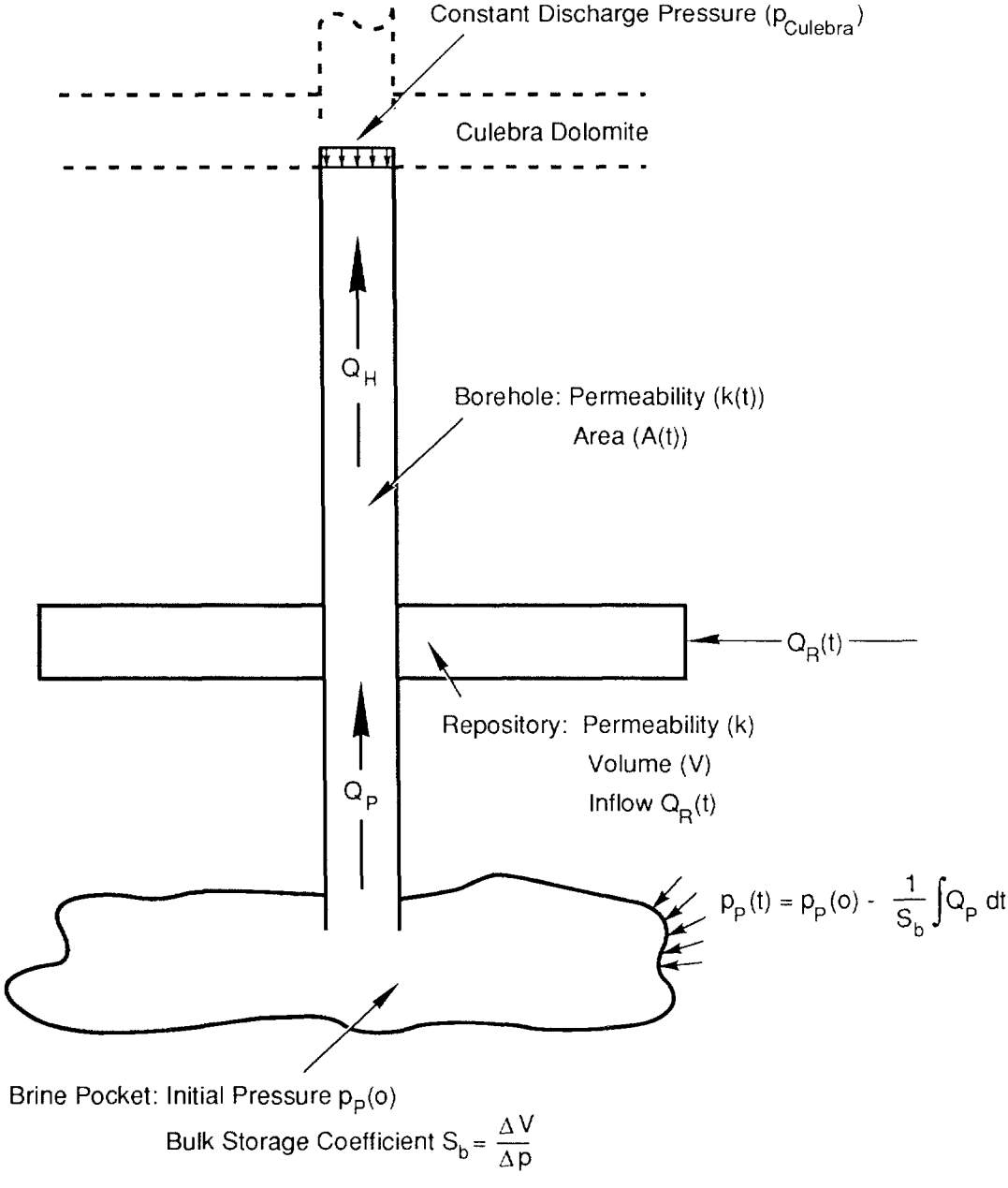

Figure 4.3-5. Conceptual Model of Castile Brine Reservoir, Repository, and Borehole Requires a Specified Initial Brine Reservoir Pressure and a Bulk Storage Coefficient (Change in Discharge Volume with Change in Brine Reservoir Pressure).

4.3.2 Numerical Brine Reservoir Model

Permeability, Intact Matrix

Parameter:	**Permeability, intact matrix**
Median:	1×10^{-19}
Range:	1×10^{-20}
	1×10^{-18}
Units:	m^2
Distribution:	Cumulative
Source(s):	See Table 2.4-1.

Permeability, Fractured Matrix

Parameter:	**Permeability, fractured matrix**
Median:	1×10^{-13}
Range:	1×10^{-16}
	1×10^{-10}
Units:	m^2
Distribution:	Cumulative
Source(s):	Freeze, R. A. and J. C. Cherry. 1979. *Groundwater.* Englewood Cliffs, NJ: Prentice-Hall, Inc. (Table 2.6)
	Reeves, M., G. Freeze, V. Kelley, J. Pickens, D. Upton, and P. Davies. 1991. *Regional Double-Porosity Solute Transport in the Culebra Dolomite under Brine-Reservoir-Breach Release Conditions: An Analysis of Parameter Sensitivity and Importance.* SAND89-7069. Albuquerque, NM: Sandia National Laboratories. (Table 2.1)

Discussion:

The mesh for the numerical model used two layers for the Castile Formation (see Figure 4.3-6). The upper layer and the lower layer beyond a radius of 2,320 m (7,586 ft) were intact Castile anhydrite matrix. The lower layer out to a radius of 2,320 m (7,586 ft) was the fractured brine reservoir. The permeability used for the reservoir was 1×10^{11} m^2. Test simulations using the median permeability of intact anhydrite, 1×10^{-19} m^2, and pressures in the brine reservoir within the range of sampled values (11 MPa to 21 MPa), showed that those pressures decayed relatively quickly by flow through the intact matrix (upper layer) and into the Salado Formation. It was apparent that, when using the reported median permeability of Castile anhydrite and assuming Darcy flow everywhere, one cannot maintain a pressurized brine reservoir in the Castile for more than a few hundred years. In order to

simulate a pressurized brine reservoir, it was necessary to isolate it completely from the Salado and from the far field by assigning a permeability of zero to the intact Castile matrix (upper Castile mesh layer and far field lower layer). When isolated in this manner, the numerical model of the Castile brine reservoir can simulate the behavior observed during well tests done by Popielak et al. (1983) with the properties described in this section and in Sections 4.3 and 4.3.2.

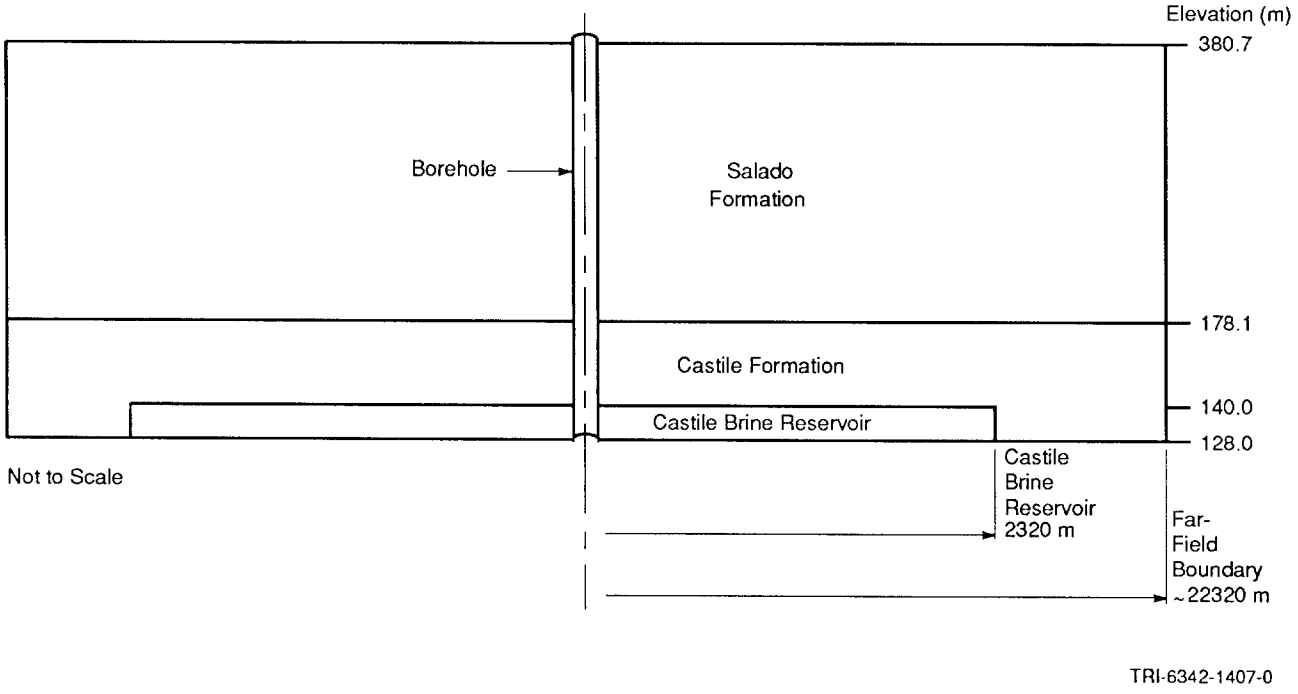

Figure 4.3-6. Numerical Model of Castile Brine Reservoir.

Porosity

Parameter:	**Porosity**
Median:	0.005
Range:	0.001
	0.01
Units:	Dimensionless
Distribution:	Cumulative
Source(s):	Reeves, M., G. Freeze, V. Kelly, J. Pickens, D. Upton, and P. Davies. 1991. *Regional Double-Porosity Solute Transport in the Culebra Dolomite under Brine-Reservoir-Breach Release Conditions: An Analysis of Parameter Sensitivity and Importance.* SAND89-7069. Albuquerque, NM: Sandia National Laboratories. (Table 2.1)

Discussion:

Bulk storativity was varied in the 1991 PA calculations. However, calculations done using the two-dimensional, two-phase porous flow model, BRAGFLO, require compressibilities of brine and rock, rather than bulk storativity to determine the storage capacity of a porous medium. A porosity, ϕ, of 0.005 was used for both the brine reservoir and the Castile Formation, and the brine compressibility, S_b, was 2.5 x 10^{-10} Pa^{-1} (Salado brine was used in the model, since brine density has to be constant in BRAGFLO; see Section 4.1.1). Brine reservoir matrix compressibility, β_s, was obtained from sampled values of bulk storativity, S_b, using the formula

$$\phi = S_b/V - \phi\beta$$

where V is the volume of the reservoir, $\pi r^2 L$. Dimensions of the reservoir (radius, r, and the thickness, L) are discussed below. The compressibility discussed here is defined by

$$\beta_s = \frac{1}{1-\phi}\frac{d\phi}{dp}$$

whereas BRAGFLO requires a compressibility, β_s', defined as

$$\beta_s' = \frac{1}{\phi}\frac{d(\phi)}{dp}$$

so one more step is needed to obtain β_s':

$$\beta_s' = \beta_s(1-\phi)/\phi$$

For the brine reservoir, the bulk storativity ranged from 0.02 to 2.0, resulting in matrix compressibility, β_s', ranging from 2.2×10^{-8} to 1.8×10^{-6} Pa^{-1}.

The value used in the two-phase flow model for the intact Castile matrix compressibility was 1.99×10^{-7} Pa^{-1}, although the zero permeability meant that this parameter was effectively unused.

Values of other material properties for the Castile Formation and the brine reservoir are discussed elsewhere in Sections 4.3 and 2.4 (Hydrologic Parameters for Anhydrite Layers within Salado Formation). Parameters used in the two-phase flow model for the intact Castile matrix include: residual brine saturation of 0.2; residual gas saturation of 0.2; Brooks-Corey relative permeability correlation exponent of 0.7; and threshold capillary pressure of 1.869 MPa. Because the permeability of the intact matrix was set to zero, none of these parameters has any effect; however, if nonzero permeabilities were used, these are the values that would be used. For the fractured brine reservoir, the following were used: residual brine and gas saturations of 0.2; Brooks-Corey exponent of 0.7; and a threshold capillary pressure of zero. Zero capillary pressure in the brine reservoir proved to be necessary for numerical stability; nonzero values caused excessively long run times, but otherwise had little effect on the results.

Radius and Thickness

Parameter:	**Radius**
Median:	2320
Range:	30
	8600
Units:	m
Distribution:	Cumulative
Source(s):	Reeves, M., G. Freeze, V. Kelly, J. Pickens, D. Upton, and P. Davies. 1991. *Regional Double-Porosity Solute Transport in the Culebra Dolomite under Brine-Reservoir-Breach Release Conditions: An Analysis of Parameter Sensitivity and Importance.* SAND89-7069. Albuquerque, NM: Sandia National Laboratories. (Table 2.1)

Parameter:	**Thickness**
Median:	12.0
Range:	7.0
	61
Units:	m
Distribution:	Constant
Source(s):	Reeves, M., G. Freeze, V. Kelly, J. Pickens, D. Upton, and P. Davies. 1991. *Regional Double-Porosity Solute Transport in the Culebra Dolomite under Brine-Reservoir-Breach Release Conditions: An Analysis of Parameter Sensitivity and Importance.* SAND89-7069. Albuquerque, NM: Sandia National Laboratories. (Table 2.1) Popielak, R. S., R. L. Beauheim, S. R. Black, W. E. Coons, C. T. Ellingson, and R. L. Olsen. 1983. *Brine Reservoirs in the Castile Formation, Southeastern New Mexico, Waste Isolation Pilot Plant (WIPP) Project.* TME-3153. Carlsbad, NM: U.S. Department of Energy. (p. H-55)

Discussion:

The size of the brine reservoir was based on several factors, including the bulk storativity (which was varied in the 1991 PA calculations), earlier estimates of the extent of the reservoir (specifically, the radius of the "outer ring" of the brine reservoir, as determined in Reeves et al. [1989]), and the size of grid blocks in the mesh. The dimensions finally used were arrived at iteratively and somewhat arbitrarily as the conceptual model and the mesh were developed and as the original data of Popielak et al. (1983) were reexamined. After establishing the grid and selecting a radius for the reservoir, the value for the thickness of the reservoir was chosen in order to accommodate the sampled range of storativities. A value of 12 m (39 ft) was selected as appropriate for use in the numerical

storativities. A value of 12 m (39 ft) was selected as appropriate for use in the numerical model for the Castile brine reservoir. As a comparison, Popielak et al. (1983) originally assumed a thickness of 61 m (199 ft), which coincided with the thickness tested during their drill stem tests, whereas Reeves et al. estimated an effective thickness of 7 to 24 m (23 to 78 ft) in their analysis of the data for Popielak et al., (1983).

4.4 Climate Variability and Culebra Member Recharge

Climate variability is a continuous process (agent) acting on and thus affecting the state of the disposal system. The primary concerns are precipitation variation and, ultimately, recharge to strata above the Salado Formation, specifically, to the Culebra Dolomite Member. The parameters for climate variability and Culebra Member recharge are shown in Table 4.4-1.

Table 4.4-1. Climate Variability and Culebra Member Recharge

Parameter	Median	Range		Units	Distribution Type	Source
Annual precipitation ($\bar{r}_p$)	3.436×10^{-1}	3.09×10^{-2}	6.563×10^{-1}	m	Normal	Hunter, 1985
Precipitation variation						
Amplitude factor (A_m)	2			none	Constant	Swift, October 10, 1991, Memo (see Appendix A).
Short-term fluctuation (Φ)	2×10^{-10}			Hz	Constant	Swift, October 10, 1991, Memo (see Appendix A).
Glacial fluctuation (Θ)	1.7×10^{-12}			Hz	Constant	Swift, October 10, 1991, Memo (see Appendix A).
Recharge amplitude factor (A_m)	8×10^{-2}	0	1.6×10^{-1}	none	Uniform	See text.

Precipitation variability is modeled as a simple combination of sine and cosine functions representing high-frequency precipitation fluctuations and low-frequency glacial (e.g., Pleistocene) fluctuations. The function is not a prediction of future precipitation but rather is a simple way to explore the influence of precipitation variation:

$$\frac{\bar{r}_f}{\bar{r}_p} = \left[\left(\frac{3A_m + 1}{4}\right) - \left(\frac{A_m - 1}{2}\right)\left(\cos\Theta t + \frac{1}{2}\cos\Phi t - \sin\frac{\Phi}{2}t\right)\right] \qquad (4.4\text{-}1)$$

4.4.1 Annual Precipitation

Parameter:	**Mean annual precipitation**
Mean median:	3.436×10^{-1}
Range:	3.09×10^{-2}
	6.563×10^{-1}
Units:	m
Distribution:	Normal
Source(s):	Hunter, R. L. 1985. *A Regional Water Balance for the Waste Isolation Pilot Plant (WIPP) Site and Surrounding Area.* SAND84-2233. Albuquerque, NM: Sandia National Laboratories. (Table 2)

Figure 4.4-1 shows the distribution for mean annual precipitation at the WIPP station. Figure 4.4-2 shows the contours for the mean annual precipitation near the WIPP.

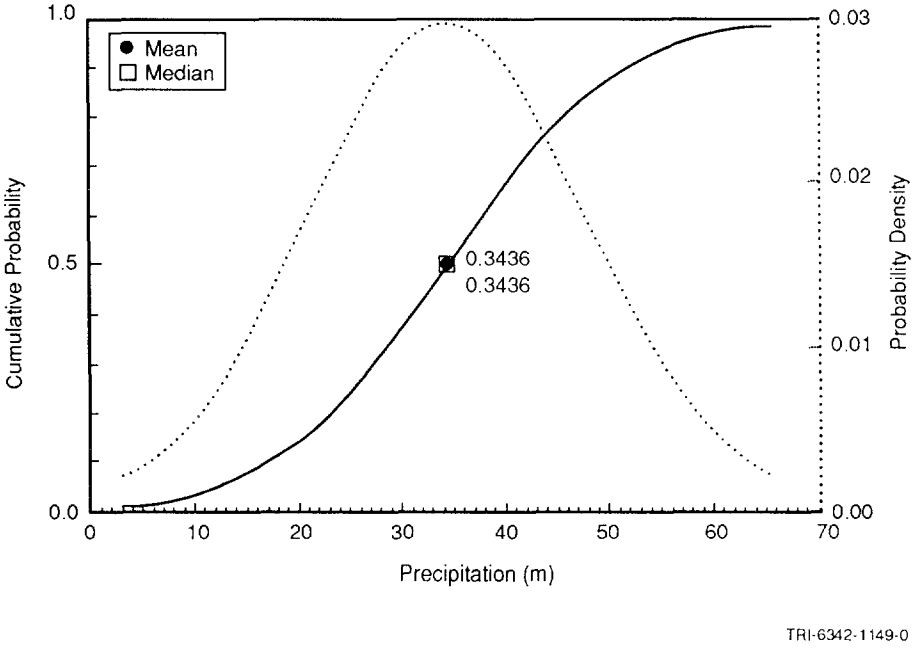

Figure 4.4-1. Normal Distribution (pdf and cdf) for Mean Annual Precipitation.

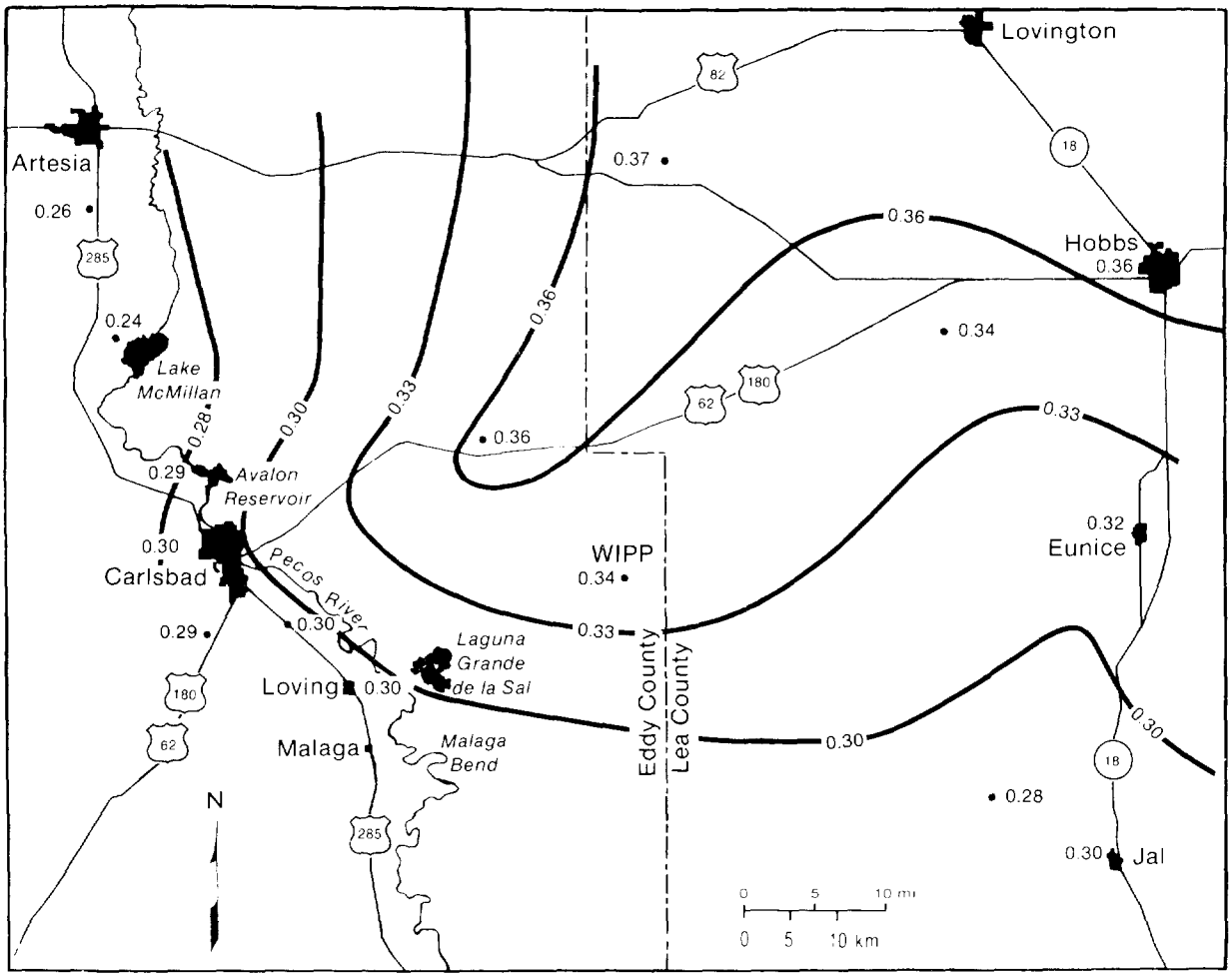

• Mean Precipitation in Meters

TRI-6342-123-1

Figure 4.4-2. Contours of Normal (Mean Annual between 1940 and 1970) Precipitation near the WIPP (after Hunter, 1985, Figure 3).

Discussion:

Southeastern New Mexico is an arid-to-semiarid fringe of the Chihuahuan Desert that receives about 0.30 m (12 in.) of annual precipitation. Three complete years of record (1977 through 1979) collected at a station located at the WIPP for the Environmental Impact Statement show that the average annual precipitation is 0.3436 m (13.53 in.), with a range of 0.0309 and 0.6563 m (1.22 and 25.84 in.), assuming a normal distribution (Figure 4.4-1) (EIS, 1980).* In general, most of the precipitation falls in the summer between May and September (Hunter, 1985, Table 2). The range of the mean from stations close to the WIPP varies between 0.28 and 0.38 m (11 and 15 in.) (Figure 4.4-2).

Precipitation at weather stations near the WIPP varies greatly from year to year. For example, Roswell's record low annual precipitation since 1878 is about 0.11 m (4.4 in.); the record annual high is about 0.84 m (33 in.) (Hunter, 1985, Figure 2). Consequently, an average precipitation for the WIPP based on three complete years of record is only a rough estimate of the long-term mean. However, this estimate is adequate for typical PA calculations.

Precipitation in the vicinity of the WIPP for years 1977 and 1979 was near normal, and 1978 was very wet. (The National Weather Service defines "normal precipitation" as the mean value for the past 30 yr, updated every 10 yr.) Hunter calculated an adjusted mean precipitation of 0.2771 m (10.91 in.) (20% difference) for the WIPP based on the mean departure during the years 1977 through 1979 of precipitation measurements from seven nearby stations (Hunter, 1985, p. 12).

---

* The WIPP began collecting precipitation data on a regular basis in 1986. This additional data will be reported in future volumes.

4.4.2 Precipitation Variation

The basic premise for assessing climatic change at the WIPP is the assumption that, because of the long-term stability of glacial cycles, future climates will remain within the range defined by the Pleistocene and Holocene. Data from deep-sea sediments indicate that fluctuations in global climate corresponding to glaciation and deglaciation of the northern hemisphere have been regular in both frequency and amplitude for at least 780,000 yr. Published results of global-warming models do not predict climatic changes of greater magnitude than those of the Pleistocene (Bertram-Howery et al., 1990).

Amplitude Factor

Parameter:	**Amplitude factor (A_m)**
Median:	2
Range:	None
Units:	Dimensionless
Distribution:	Constant
Source(s):	Swift, P. 1991. "Climate Recharge Variability Parameters for the 1991 WIPP PA Calculations, Internal memo to distribution, October 10, 1991. Albuquerque, NM: Sandia National Laboratories. (In Appendix A of this volume)

Discussion:

Field data from the American Southwest and global-climate models indicate that the wettest conditions in the past at the WIPP occurred when the North American ice sheet reached its southern limit (roughly 1,200 km [746 mi] north of the WIPP during the last glacial maximum 18,000 to 22,000 yr before present), which moved the jet stream much further south than now. The average precipitation in the Southwest increased to about twice its present value. Wet periods have occurred since the retreat of the ice sheet, but none has exceeded glacial limits.

Although the amplitude of the glacial precipitation is relatively well constrained by data (Bertram-Howery et al., 1990, p. V-37; Swift, October 10, 1991, Memo, [Appendix A]), amplitudes of the Holocene peaks are less easily determined. However, data indicate that none of the Holocene precipitation peaks exceeded glacial levels. Continuous climatic data from ice cores in Antarctica and Greenland suggest that at these locations temperature fluctuated significantly during glacial maximums (e.g., Jouzel et al., 1987). These fluctuations may reflect global climatic changes, and in the absence of high-resolution data from the American Southwest for precipitation fluctuations during glacial maximums, we have assumed that peaks comparable to those of the Holocene could have been superimposed on the glacial maximum. Therefore, there may have been relatively brief (i.e., on the order of hundreds to perhaps thousands of years) periods during the glacial maximum when precipitation at the WIPP may have averaged three times present levels.

Model of Precipitation Variation. Paleoclimatic data permit reconstruction of a precipitation curve for the WIPP for the last 30,000 yr (Figure 4.4-3). This curve shows two basic styles of climatic fluctuation: relatively low-frequency increases in precipitation that coincide with the maximum extent of the North American ice sheet; and higher-frequency precipitation increases of uncertain causes that have occurred several times in the last 10,000 yr since the retreat of the ice sheet. Variability has also occurred in the seasonality and intensity of precipitation. Most of the late Pleistocene moisture fell as winter rain. Most of the Holocene moisture falls during during a summer monsoon, in local and often intense thunderstorms.

The curve shown in Figure 4.4-3 cannot be extrapolated into the future with any confidence. The curve can be used, however, in combination with the general understanding of glacial periodicity (see Bertram-Howery et al., 1990), to make a reasonable approximation of likely future variability. The proposed function does not in any sense predict precipitation at a future time. Rather, it is a function to approximate the variability in precipitation that may occur.

Specifically, the currently proposed precipitation function is as follows:

$$\frac{\bar{r}_f}{\bar{r}_p} = \left[\left(\frac{3A_m + 1}{4}\right) - \left(\frac{A_m - 1}{2}\right)\left(\cos\Theta t + \frac{1}{2}\cos\Phi t - \sin\frac{\Phi}{2}t\right)\right] \qquad (4.4\text{-}1)$$

where

r_f = future mean annual precipitation
r_p = present mean annual precipitation
A_m = amplitude scaling factor (i.e., past precipitation maximum was A_m times the present)
Θ = frequency parameter for Holocene-type climatic fluctuations (Hz)
Φ = frequency parameter for Pleistocene glaciations (Hz)
t = time (s)

The preferred values for Θ and Φ have been chosen from examination of the past precipitation curve (Figure 4.4-3) and the glacial record. If $\Phi = 2 \times 10^{-10}$ Hz, wet maximums will occur every 2,000 yr, approximately with the same frequency shown on Figure 4.4-3. Note that we are presently near a dry minimum, and the last wet maximum occurred roughly 1000 yr ago. If $\Theta = 1.7 \times 10^{-12}$ Hz, the next full glacial maximum will occur in 60,000 yr, approximately the time predicted by simple models of the astronomical control of glacial periodicity (e.g., Imbrie and Imbrie, 1980). Figure 4.4-4 shows a plot of the climate function for these values.

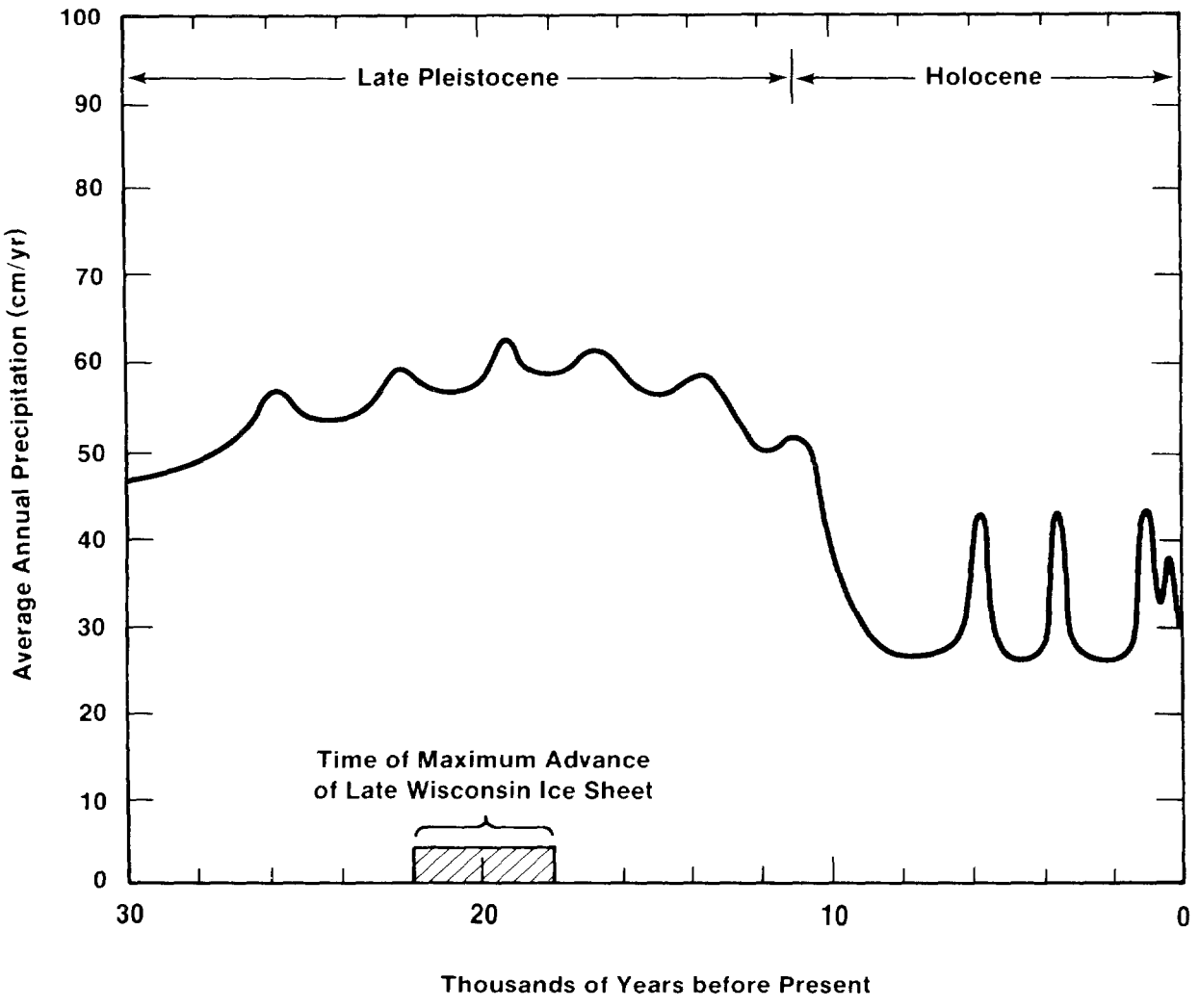

Figure 4.4-3. Estimated Mean Annual Precipitation at the WIPP during the Late Pleistocene and Holocene (after Bertram-Howery et al., 1990, Figure V-18).

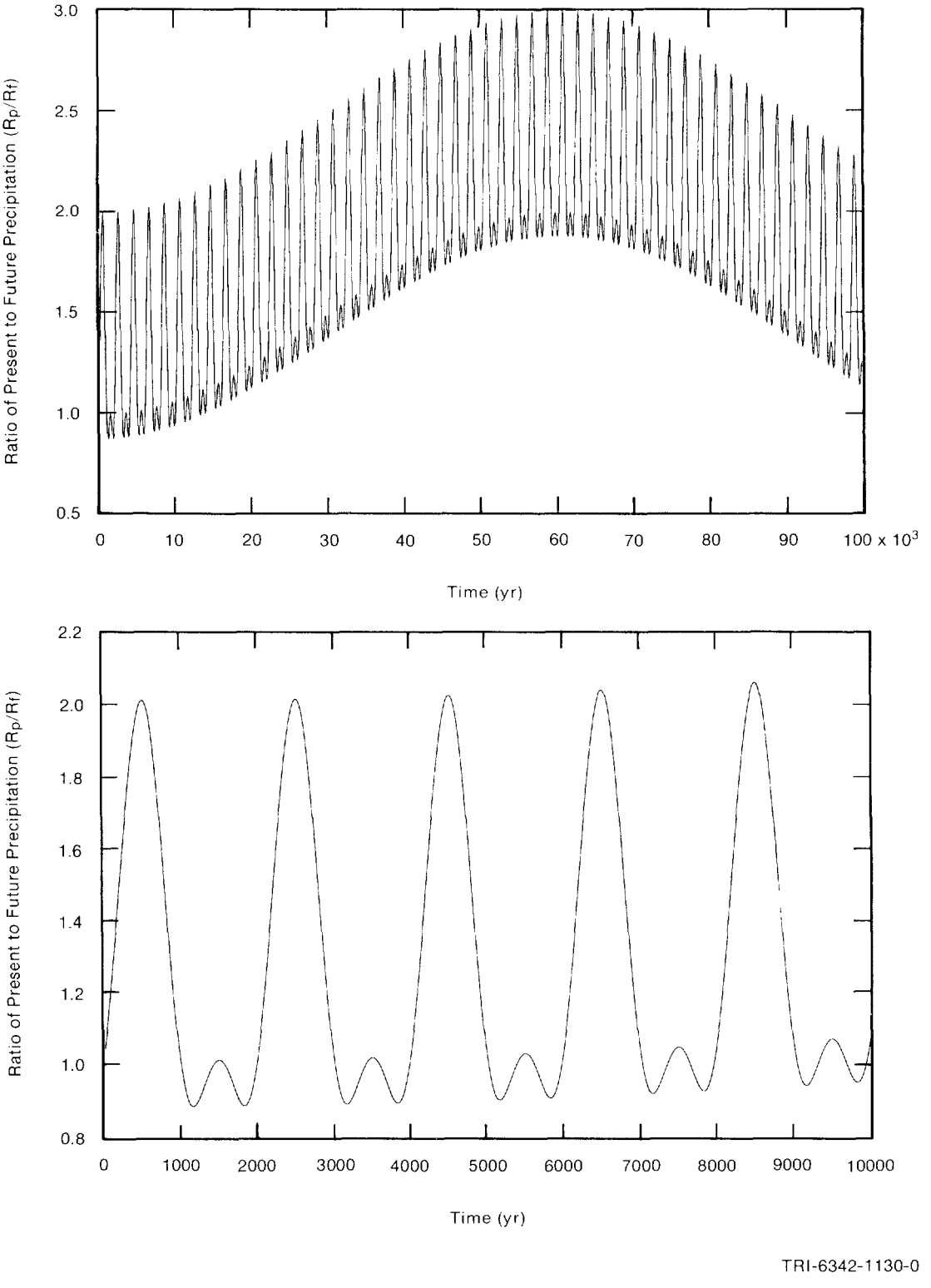

Figure 4.4-4. Precipitation Fluctuations Assumed at the WIPP for Next 10,000 Yr.

Short-Term Fluctuation

Parameter:	**Short-term precipitation fluctuation frequency (Φ)**
Median:	2×10^{-10}
Range:	None
Units:	Hz
Distribution:	Constant
Source(s):	Swift, P. 1991. "Climate and Recharge Variability Parameters for the 1991 WIPP PA Calculations," Internal memo to distribution, October 10, 1991. Albuquerque, NM: Sandia National Laboratories. (In Appendix A of this volume)

Discussion:

The approximate frequency of wet maximum is every 2,000 yr, or a value of Φ of about 0.2 nHz ($2\pi/(1000 \text{ yr} \bullet 3.155 \bullet 10^7 \text{ s/yr})$. Note that we are presently near a dry minimum; the last wet maximum occurred roughly 1,000 yr ago.

Holocene climates have been predominantly dry, with wet peaks much briefer than dry minimums (Figure 4.4-3). The Φ terms in the model equation (4.4-1) give an oscillation in which the future climate is wetter than the present one-half of the time. This value appears to be somewhat greater than the actual ratio, and, assuming that wet conditions are more likely to result in releases from the WIPP, these terms provide a conservative approximation of Holocene variability. The functions and values used give an "average" precipitation roughly 1.3 times present precipitation, with peaks of just over 2 times present precipitation.

Glacial Fluctuation

Parameter:	**Glacial fluctuation (Θ)**
Median:	1.7×10^{-12}
Range:	None
Units:	Hz
Distribution:	Constant
Source(s):	Swift, P. 1991. "Climate and Recharge Variability Parameters for the 1991 WIPP PA Calculations," Internal memo to distribution, October 10, 1991. Albuquerque, NM: Sandia National Laboratories. (In Appendix A of this volume)

Discussion:

The approximate time predicted by simple models assuming astronomical control of glacial periodicity suggest the next glacial maximum may occur in about 60,000 yr or a value of Θ of about 1.7 pHz (π/60,000 yr) (Imbrie and Imbrie, 1980). A value of Θ of 10 pHz (π/10,000 yr) gives a wet maximum in 10,000 yr, and results in extreme precipitation values 3 times those of the present. This is not a realistic value for Θ -- ice sheets grow relatively slowly, and it would be difficult to achieve full continential glaciation within 10,000 yr.

4.4.3 Boundary Recharge Variation

Parameter:	**Recharge amplitude factor (A_m)**
Median:	0.08
Range:	0
	0.16
Units:	Dimensionless
Distribution:	Uniform
Source(s):	See text.

Figure 4.4-5 shows the distribution for the recharge amplitude factor.

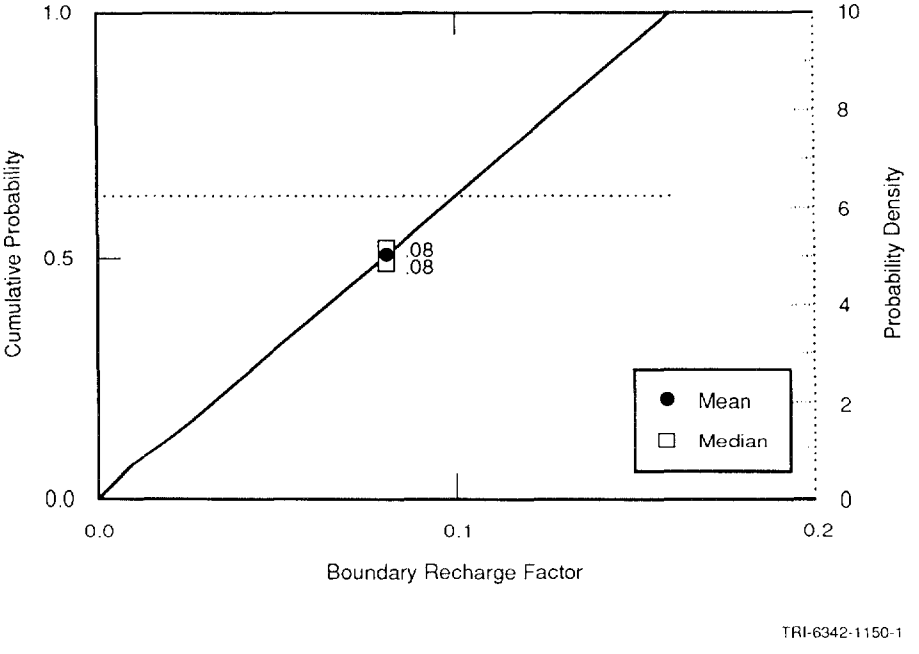

Figure 4.4-5. Uniform Distribution (pdf and cdf) for Recharge Boundary Amplitude Factor for Culebra Dolomite Member.

Discussion:

At present, the location and areal extent of the surface recharge area for the Culebra and the present amount of infiltration are not known. Hydraulic head and isotopic data indicate that very little, if any, moisture reaches the Culebra directly from the ground surface above the WIPP (Lambert and Harvey, 1987; Lambert and Carter, 1987; Lappin et al., 1989; Beauheim, 1987c). Researchers believe that regional recharge occurs several tens of kilometers to the north of the WIPP, where the Culebra is near the ground surface (Mercer, 1983; Brinster, 1991). Whether water from this hypothesized recharge area could reach the current model domain area is not known (Swift, October 10, 1991, Memo [Appendix A]).

Available literature on the relationship between precipitation and recharge is limited to examinations of recharge to a water table by direct infiltration. There is no particular reason to assume a 1-to-1 correlation between increases in precipitation and increases in model recharge. Environmental tracer research (e.g., Allison, 1988) suggests that long-term increases in precipitation in deserts may result in significantly larger increases in infiltration, particularly if the increases in precipitation coincide with lower temperatures and decreased evapotranspiration. As an extreme example, Stone (1984) estimated a 28-fold increase in infiltration for one location at the Salt Lake coal field in western New Mexico during the late Pleistocene wet maximum. Bredenkamp (1988a,b) compared head-levels in wells and sinkholes with short-term (decade-scale) precipitation fluctuations in the Transvaal, and suggested that for any specific system there may be a minimum precipitation level below which recharge does not occur. Above this uncertain level, recharge to the water table may be a linear function of precipitation.

Both the range and the distribution for the recharge factor are preliminary and should be adjusted as new data or interpretations warrant.

Recharge Model. Because of the unknown factors regarding recharge, a very simple model of recharge to the Culebra is used. The model consists of evaluating the head by scaling the relative change in precipitation with a recharge factor. The head is then applied at the hypothesized recharge area.

The current model is

$$\frac{h_f}{h_p} = \frac{3A_m + 1}{4} - \frac{A_m - 1}{2}\left(\cos \Theta t + \frac{1}{2}\cos \Phi t - \sin \frac{1}{2}\Phi t\right) \qquad (4.4\text{-}2)$$

Recharge Amplitude Factor. The recharge amplitude factor represents uncertainty in numerous parameters, including (a) the location and extent of the surface recharge area, (b) groundwater flow between the surface recharge area and the boundary of the model domain, and (c) the relationship between precipitation and infiltration in the surface recharge area, which in turn is dependent on factors such as vegetation, temperature, local topography, and soil characteristics.

To cover variability in model recharge, the PA Division incorporates recharge uncertainty in the 1991 calculations by sampling a uniformly distributed amplitude parameter (A_m) over a range that permits the range to vary from present hydraulic heads to heads equal to the land surface. Justification for the range is as follows:

Lower bound, r = 1. This value corresponds to present hydraulic head conditions. Circumstances can be imagined in which increases in precipitation result in a decrease in infiltration (e.g., development of plant cover on previously barren land, or changes in topography resulting in runoff from a previously closed drainage), but none appears likely for the WIPP area. It is more likely that an increase in the cool-season component of precipitation will result in higher infiltration.

Upper bound, r = 0.16. This value sets hydraulic heads equal to the land surface. This value is consistent with fossil evidence that springs existed in the region near the northwest corner of the regional grid (Bachman, 1981; Brinster, 1991, p. IV-7).

5. PARAMETERS FOR SCENARIO PROBABILITY MODELS

This chapter presents data used in those probability models that estimate elementary probabilities of events and processes that appear in future WIPP histories, specifically, those histories in which the WIPP is penetrated by exploratory boreholes. Elementary probabilities furnished by these models are used to calculate probabilities $P(S_j)$ of computational scenarios S_j. The mathematical approach to scenario-based performance assessment is discussed in Volume 1, Chapter 3, and Volume 2, Chapters 2 and 3, of this report; Tierney (1991); Helton et al. (1991); and Section 1.4 of this volume.

Because innumerable scenarios exist, an infinite number of groupings of scenarios exist. As in 1990, the analyzed scenarios for 1991 were grouped into four summary scenarios (see Volume 1): one base-case scenario (without human intrusion) and three human-intrusion scenarios (i.e., E1, E2, and E1E2). To more carefully explore the cause and effect relationship from hypothetical events and processes (as opposed to those that will occur but for which we do not know the precise parameter values), the three human-intrusion summary scenarios have been further refined (discretized) into computational scenarios. While this partitioning of summary scenario space is new and, consequently, the details of the probability model, are dramatically different in 1991, the parameters ($\mathbf{x}$) of the probability model $P(S_j(\mathbf{x}))$ are the same as in 1990 and the same Poisson probability model was used to evaluate the time and number of potential intrusions. The parameters are discussed in the following sections.

5.1 Area of Brine Reservoirs

5.1.1 Area of Castile Brine Reservoir below WIPP Disposal Area

Parameter:	**Areal extent of brine reservoir**
Median:	0.40
Range:	0.25
	0.552
Units:	Dimensionless (%)
Distribution:	Cumulative
Source(s):	See text.

Figure 5.1-1 shows the distribution of the areal extent.

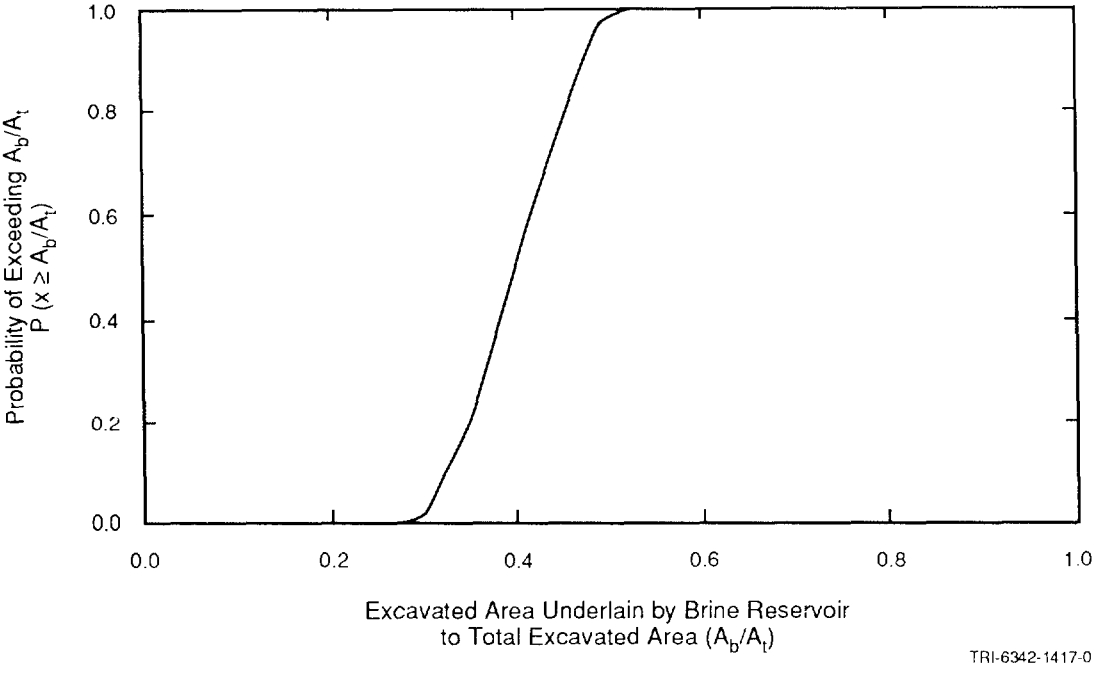

Figure 5.1-1. Distribution of Fraction of WIPP Disposal Area Overlapped by Brine Reservoir. Simulated construction uses inclusive definition of brine reservoir and block model (see text).

Discussion:

A geophysical survey, using transient electromagnetic methods, was made in 1987 to determine the presence or absence of brines within the Castile Formation under the WIPP disposal area (Earth Technology Corp., 1988). Briefly, the electromagnetic method associates high electric conductivity with fluid. (The stated precision was to within ±75 m.) The entire Bell Canyon Formation directly beneath the Castile Formation is a good conductor. However, in several places underneath the WIPP disposal area, the elevation to the first major conducting media detected lay above the top of the Bell Canyon Formation (~-200 ± 30 m [-654 ± 100 ft] in the ERDA-9 well) but below the bottom of the Salado Formation (178 m [582 ft] in ERDA-9) (see Figure 2.2-1 and Section 2.2).

The probability of hitting a brine reservoir can be evaluated for the waste disposal area as a whole or for subunits such as the panels. The current human-intrusion probability model (Volume 2, Chapters 1 and 2) uses the former data (the probability of hitting a brine reservoir over the entire waste panel) and assumes that this same probability applies to each panel. However, an examination of this assumption required the probability for each panel as well (Volume 2, Chapters 1 and 2). The following discussion emphasizes the probability over the entire disposal area, but provides data on a per panel basis as well.

Two methods were considered for determining the area of the brine reservoir. The first involved using the interpolated conductor elevations and the Anhydrite III of the Castile Formation and the Bell Canyon Formation elevations without considering uncertainty in the data. Although not used, it is discussed first because of its simplicity. The second method considers uncertainty in the data through geostatistics.

Area Estimate Assuming No Uncertainty in Data. Contours of the depth or elevation to the first major conductor are plotted in Figures 5.1-2 and 5.1-3. The data in Figure 5.1-2 was the interpretation originally reported (Earth Technology Corporation, 1988). However, Figure 5.1-3 is an equally valid interpretation of the data; it is somewhat more conservative and was computer generated from the same data.

Minimum Area (Anhydrite III Level). The brine reservoirs are usually found in fracture zones of anticlimal structures in the uppermost anhydrite layer in the Castile (Lappin, 1988) (e.g., Anhydrite III as in WIPP-12 or when Anhydrite III is absent such as Anhydrite II in ERDA-6).

In ERDA-9, the elevation to the bottom of Anhydrite III in the Castile Formation is estimated at 105 m (250 ft). Consequently, there is a possibity that no brine is present beneath the disposal area (Figure 5.1-1).

Maximum Area (Bell Canyon Level). Pressurized brine reservoirs cannot be entirely discounted until the Bell Canyon Formation is reached at about -200 m (-660 ft) (Figure 2.2-1), implying that conductors higher than about -200 m (-660 ft) could indicate brine within the Castile Formation. PA calculations use the -200 m (-660 ft) contour for defining the maximum area of any brine reservoirs under the WIPP disposal area (Figure 5.1-2), resulting in a maximum area at 45% (Table 5.1-1).

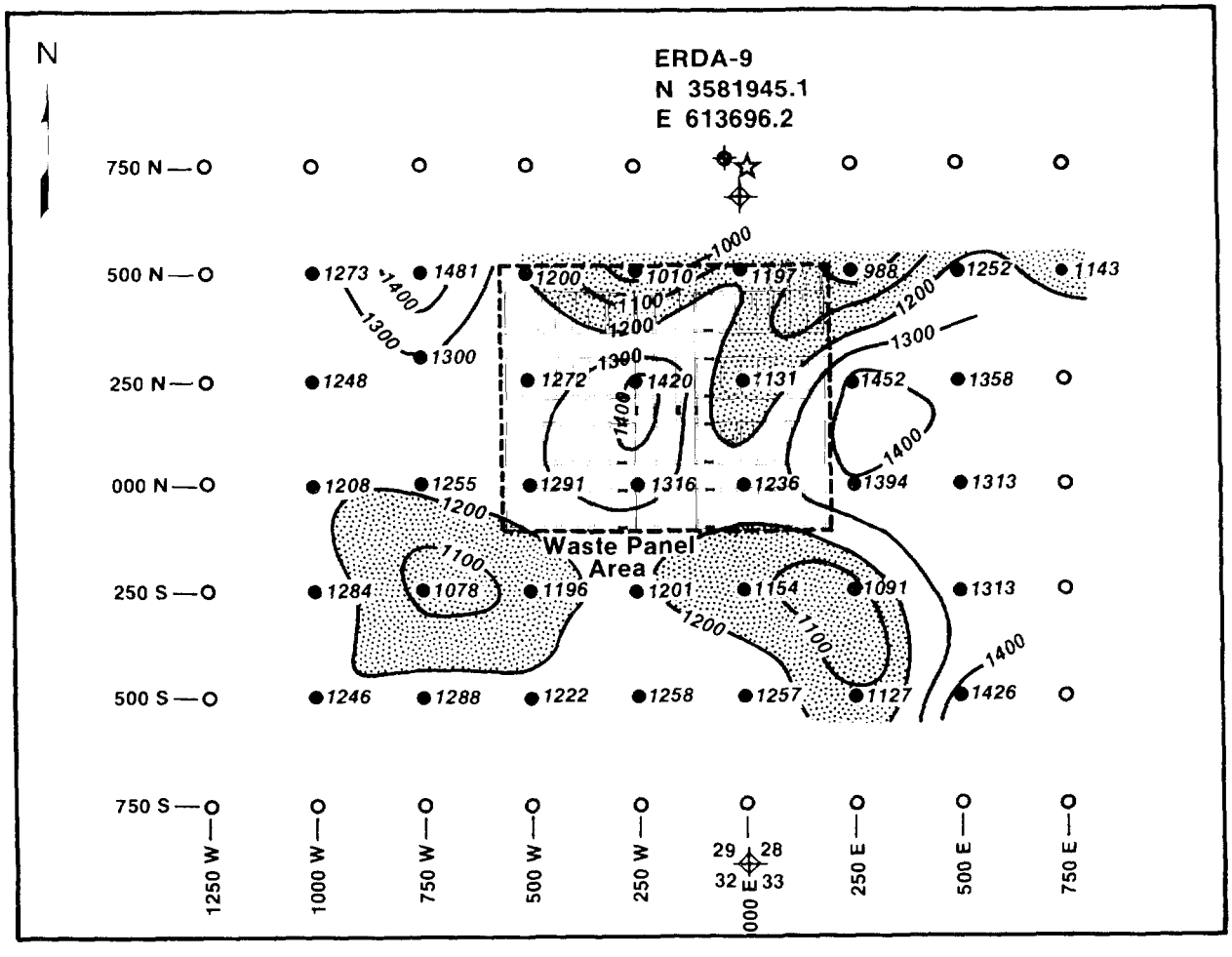

TRI-6342-256-2

Figure 5.1-2. Frequently Reported Contour Map of Depth of First Major Conductor below WIPP Disposal Area. (Map drawn by hand.) (after Earth Technology Corp., 1988).

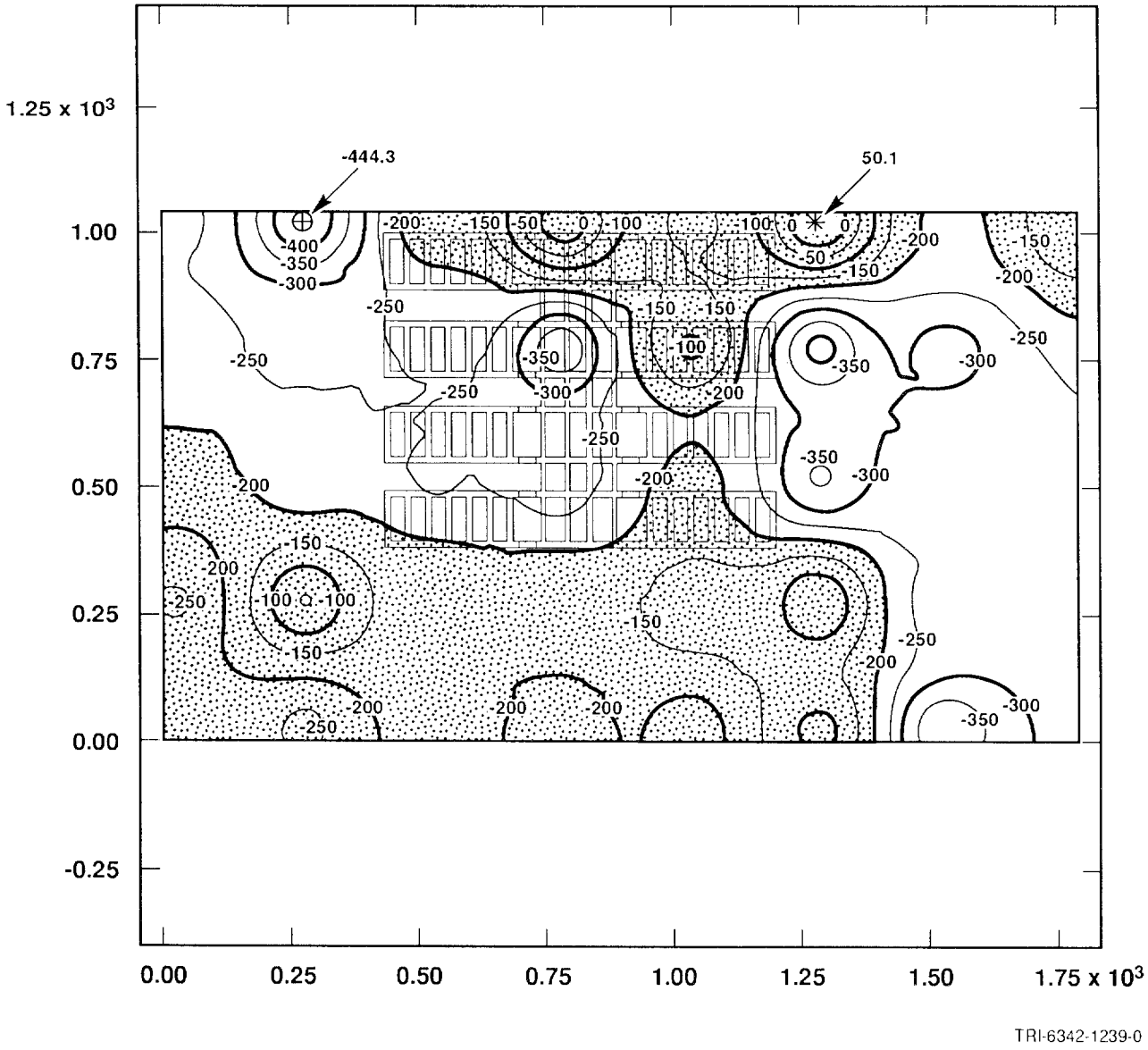

Figure 5.1-3. Conservative Contour Map of Elevation of First Major Conductor below WIPP Disposal Area.

Table 5.1-1. Cumulative Percentages of the Disposal Region Underlain by a Brine Reservoir, Assuming Various Maximum Depths

	Cumulative Percent (%) at Indicated Maximum Depths										Area
Depth (m)	0	-50	-100	-150	-180	-200	-250	-300	-350	-400	(m^2)
Panel 1			5.37	61.95	97.80	100.00	100.00	100.00	100.00	100.00	11,530.0
Panel 2			4.00	44.57	69.33	73.08	87.47	100.00	100.00	100.00	11,530.0
Panel 3						18.23	85.73	100.00	100.00	100.00	11,530.0
Panel 4					35.85	75.57	96.17	100.00	100.00	100.00	11,530.0
Panel 5						19.76	94.80	100.00	100.00	100.00	11,530.0
Panel 6							26.57	100.00	100.00	100.00	11,530.0
Panel 7							67.45	100.00	100.00	100.00	11,530.0
Panel 8			0.79	9.01	34.64	52.86	100.00	100.00	100.00	100.00	11,530.0
Southern						3.24	45.01	100.00	100.00	100.00	8,413.0
Northern	3.97	12.49	21.67	27.49	34.86	45.29	54.79	69.25	94.52	100.00	8,701.0
Cumulative Percent	0.316	0.994	2.796	14.367	27.828	39.648	77.219	97.553	99.564	100.000	
Cumulative Area (m^2)	345.3	1,086.8	3,057.6	15,711.1	30,431.4	43,357.1	84,442.3	106,678.2	108,877.4	109,354.0	

Combined Distribution. Without knowing the likelihood that either endpoint is more valid, a discrete distribution with points at 0 and 45% of equal probability is suggested.

Area Estimate Incorporating Uncertainty in the Data. Described above is a method of estimating the fractional area of the waste-panel region underlain by a Castile brine reservoir using contours of the conductor elevation. This method assumes that elevation contours drawn from the observed data correctly represent the variation of conductor depth between observation locations. The following discussion describes an alternative method that does not rely on reported depth contours, and the resulting area fraction distribution.

Conductor elevation measurements are available at 36 points (Figure 5.1-3). These data were used to estimate conductor elevation at all points within the waste panel region. Any estimate of the conductor depth at an unmeasured location had an uncertainty associated with it. The objective of this procedure is to incorporate relevant uncertainties in the estimate of area fraction.

Spatial Variability and Interpolation. Uncertainty in interpolated elevations is a consequence of spatial variability of the observed data. Quantifying spatial variability helps in estimating the error of an interpolated value. If two observations are made close together, it is reasonable to expect that similar values will be obtained (autocorrelation function, Chapter 1). As the distance between observations increases, the similarity of observed values decreases. This behavior of spatially varying fields is often represented as a variogram (Figure 5.1-4). The variogram shows the average squared difference in observed values between observations separated by a given distance vs. the distance between observations. For a given separation distance h, the average is taken over all pairs of observations that are separated by distance h.

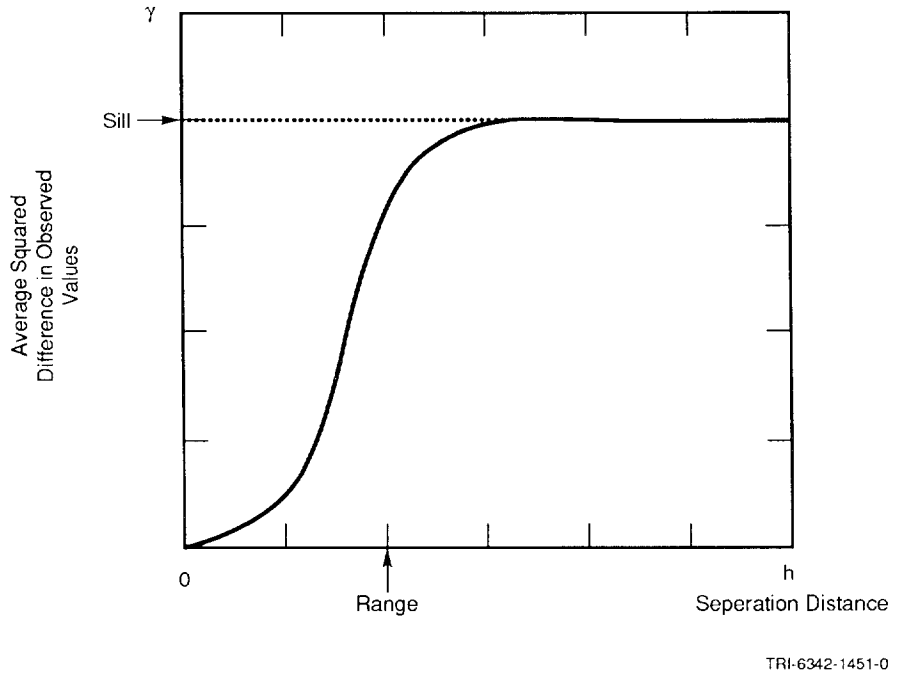

Figure 5.1-4. Example Variogram Illustrating Typical Behavior of γ with h.

The variogram in Figure 5.1.4 is a generic example illustrating two common features seen in real data. Close to the origin (i.e., small separation distances), values are similar, so that the average squared difference is small. As the distance between observations increases, observed values tend to become uncorrelated, resulting in an increase in average squared difference in observed values. The distance at which observations tend to become uncorrelated is referred to as the range of the variogram. As separation distance increases beyond the range, the average squared difference tends to a limiting value, called the sill.

Not all fields exhibit clearly defined range and sill. Systematic trends in the data, for example, can produce variograms that continually increase with separation distance. In addition, the spatial variability of the data may be different along different directions, so that a variogram constructed from separations along one direction may be different from a variogram constructed along another direction.

Information contained in the variogram is useful in interpolating from observed values for two reasons:

(1) The range of the variogram identifies the maximum distance over which observations tend to be correlated. This information is important for selecting the data points near the interpolation location having values that may be related to the actual value at the interpolation location.

(2) The average squared difference between data values, along with the distances between the interpolation location and the locations of the selected observations, may be used to estimate the potential variability of the real value from the interpolated value.

Analysis of TDEM Data. Figure 5.1-2 shows conductor elevations interpreted from the TDEM survey at 36 locations near and within the waste panel region. Figure 5.1-5 shows a cumulative distribution of observed elevations, along with the average elevation and sample standard deviation. Scatter plots of conductor elevation vs. X (E-W) location and Y (N-S) location are shown in Figure 5.1-6. There is no suggestion of a significant simple trend in elevation along either direction.

A variogram of elevations was constructed in the E-W, N-S, NE-SW, and NW-SE directions. The regular arrangement of observation points facilitates this calculation: the variogram value for a separation of 250 m in the E-W direction, for example, is simply the average of the squared difference of elevation values at points adjacent to each other in the E-W direction. Similar averages can be made for multiples of the observation grid spacing (250 m) in the E-W and N-S directions. Points in the NE-SW and NW-SE directions area separated by multiples of ~353 m. In calculating the elevation variogram, the observation at (750W, 290N) was assumed to have been made at (750W, 250N). This displacement has no important effect on the resulting variogram.

Figure 5.1-7 shows the variogram of the elevation data along the directions mentioned. The separation distances considered were 250 m and 500 m in the E-W and N-S directions, and 353 m in the diagonal directions. Larger separations have too few pairs to provide a reliable estimate of mean squared difference. The horizontal line, which shows the average squared difference over all pairs of points regardless of separation, is an estimate of the variogram sill.

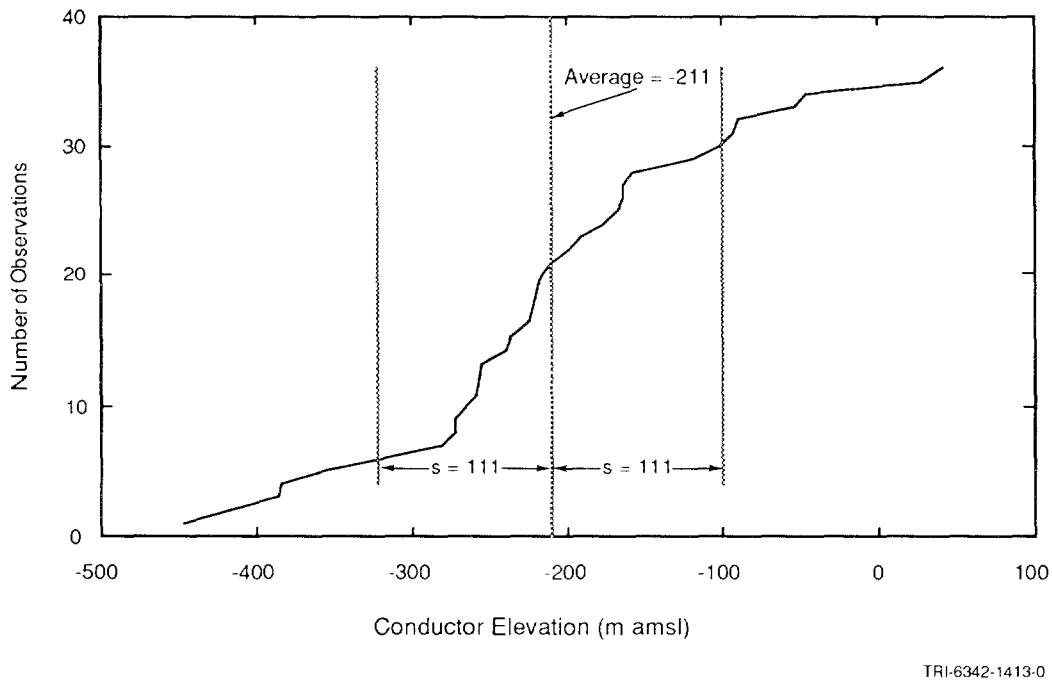

Figure 5.1-5. Population Distribution and Statistics for Conductor Elevations.

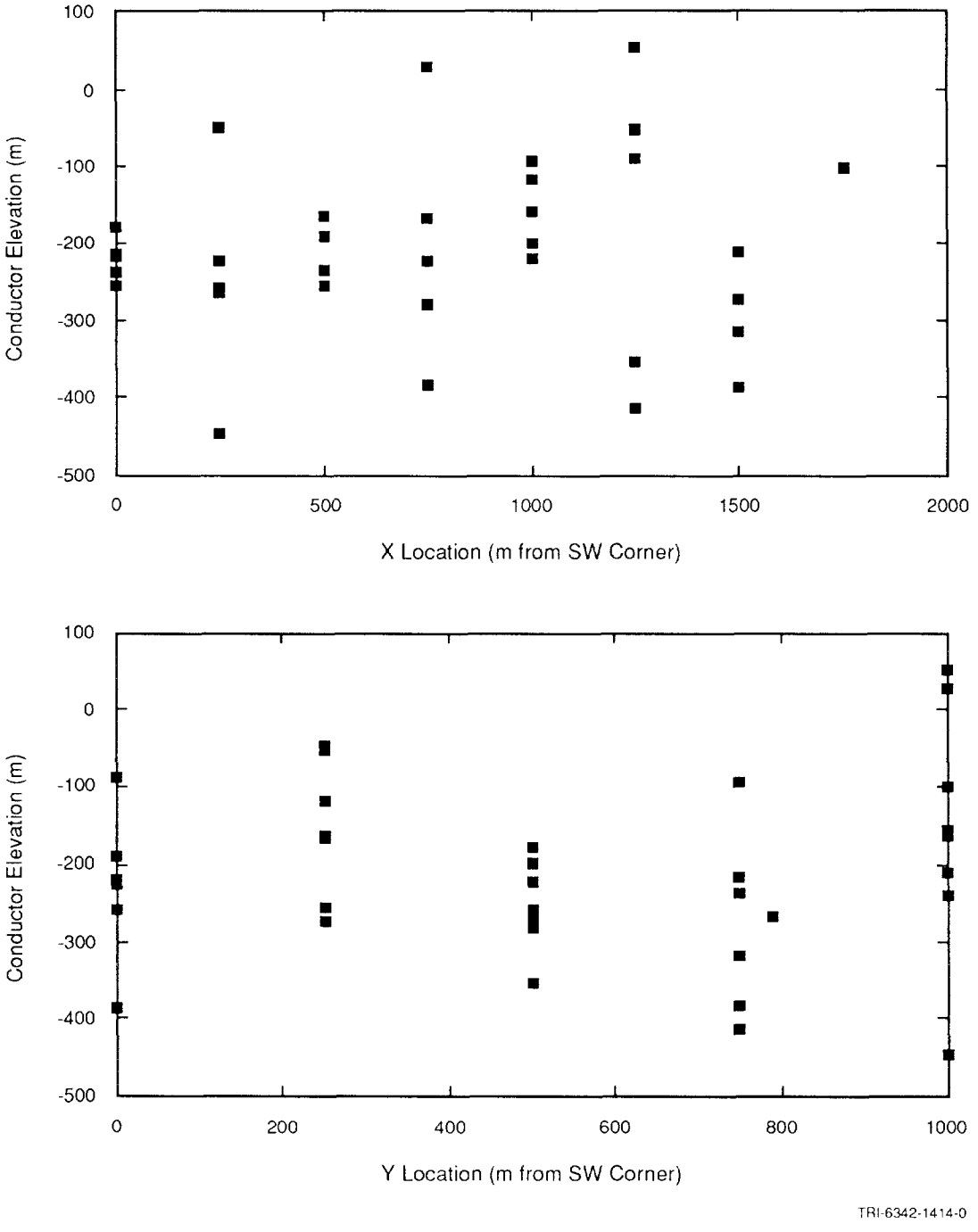

Figure 5.1-6. Scatter Plots of Conductor Elevation vs. X and Y Location.

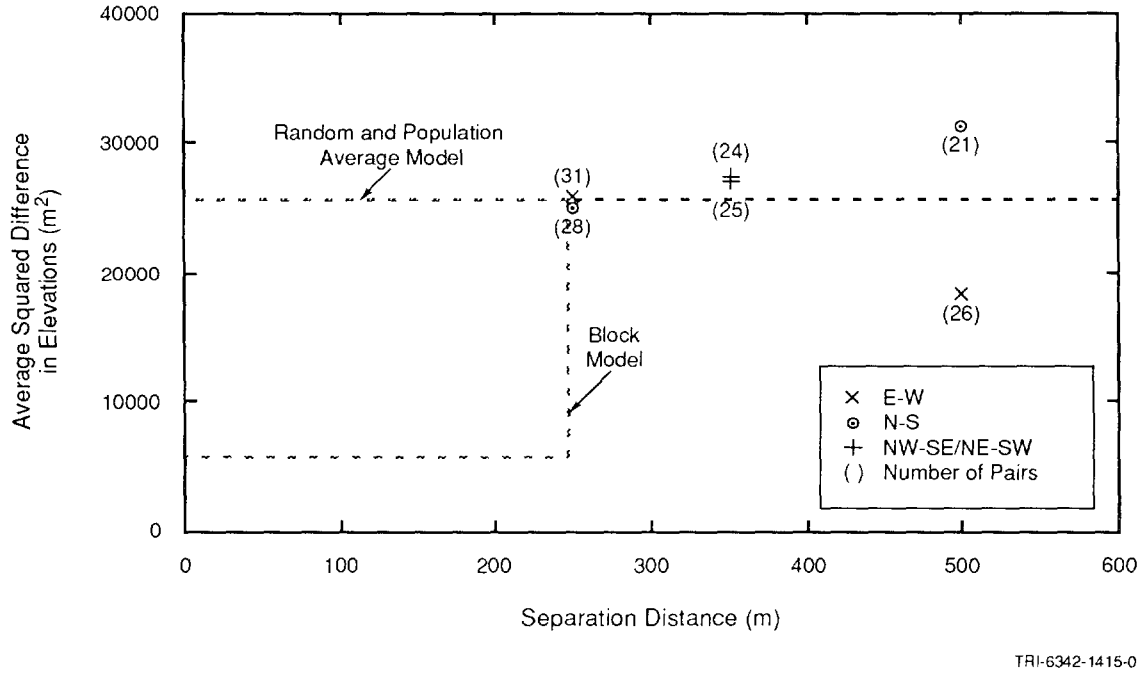

Figure 5.1-7. Empirical Variogram of Conductor Elevations.

The striking feature of the variogram is the lack of evidence for a range of correlation of observations. The average squared difference for adjacent measurements and the expected squared difference for randomly selected measurements (i.e., the sill) are indistinguishable. In other words, there is no evidence for spatial correlation of elevation over distances as small as 250 m. (In a separate analysis, the program AKRIP was used to estimate a generalized covariance for the elevation data. The identified model contained only a "nugget" term, i.e., the generalized covariance was not found to depend on separation distance.)

Estimation of Conductor Elevation. The variogram suggests that, in attempting to estimate conductor elevation at non-measured locations, observations made 250 m from the interpolation location contain no more information about the real value at the interpolation location than more distant observations. For all points within the waste panel region, at least one observation less than 250 m away will be available. The variogram analysis does not indicate whether observations less than 250 m distant can be expected to provide information about elevation at the interpolation point. In particular, the assumption of linear variation of elevation between data points made in constructing contours of conductor elevation has no support (i.e., Figures 5.1-2 and 5.1-3).

Two bounding alternatives, corresponding to different assumptions about the behavior of the variogram between 0 and 250 m have been considered (see Figure 5.1-7):

(1) "Random elevation" assumption: Conductor elevation correlation length is very small <<250 m. The variogram is equal to the sill value between 0 and 250 m.

(2) "Block elevation" assumption: The observation grid spacing is just outside the actual correlation length. Below 250 m, observations become highly correlated, with an expected squared difference equal to twice the measurement error variance ("cookie cutter" autocorrelation).

These assumptions lead to two different methods of estimating conductor elevation. Both assumptions have been carried through in estimating brine reservoir area fraction.

In the random elevation assumption, nearby data points contribute no special information about the real value at the interpolation point in virtue of their proximity. The best estimate for elevation at any point is simply the average elevation over all observations. The variance of the error of this estimate is the population variance.

In the block elevation assumption, elevation is highly correlated over distances smaller than the measurement interval. The estimate of elevation at an interpolation point is simply the observed value at the nearest observation point. The variance of the error of this estimate is the variance of the error of the observation (75 m^2).

If the interpolated value is thought of as a weighted linear combination of observed values (as in inverse distance interpolation or in kriging), the random and block assumptions lead to the extremes of uniform weighting of all observations and exclusive weighting of the nearest observation.

Estimation of Area Fraction. The area fraction is defined as the area of the waste panel excavation overlying a brine reservoir divided by the total excavation area. A point is considered to overlie a brine reservoir if there is an electrically conductive zone in a hydrologically conductive layer of the Castile Formation. Although Castile brine reservoirs encountered during drilling appear to be always associated with the uppermost Castile anhydrite (Anhydrite III at the WIPP site), there is the possibility that brine reservoirs may occur in lower Castile Anhydrites. For the purpose of estimating area fraction using the existing data, two formulations are possible:

(1) A point overlies a brine reservoir if the sub-Salado conductor elevation is greater than the elevation of the base of Anhydrite III, or
(2) A point overlies a brine reservoir if the sub-Salado conductor elevation is greater than the elevation of the base of the Castile.

For any point in the waste panel region, none of the elevations used to identify a brine reservoir by either formulation are known with certainty. In addition, there is uncertainty in which of the above formulations is appropriate. The area fraction estimate should incorporate these uncertainties.

Description of Method. Uncertainties associated with estimation of the area fraction were addressed through Monte Carlo simulations as follows:

- 200 samples from two uncorrelated uniformly distributed random variables were taken as possible values for the base elevations of the Castile and Anhydrite III. These distributions ranged from -230 m to -170 m for the base of the Castile, and from 70 m to 140 m for the base of Anhydrite III. The estimates of base elevation were uniformly distributed over the given range and were not correlated. The base elevation for the Castile and for Anhydrite III were assumed to be constant over the waste panel area.

- Along with these elevations, one of the two formulations for identifying a brine reservoir were selected at random.

- For each set of sampled base elevations and brine reservoir definition, 2000 realizations of conductor elevation were created on a uniform mesh. The relative area overlying the brine reservoir was then calculated using the sampled realizations and the selected definition of a brine reservoir.

- The relative number of simulations having a given area fraction was then used to construct an area fraction distribution. The derived area fraction distribution reflects uncertainty in conductor elevation, lithology, and the existence of brine reservoirs in lower Castile anhydrites.

The above process was applied twice, using the "random" and "block" assumptions for spatial correlation of conductor elevation in the generation of conductor realizations. In either case, conductor elevations at each mesh cell were assumed to be normally distributed around the estimated value.

Maximum Area (Bell Canyon Level). Based on the geostatistical analysis and data uncertainty described above, the use of the more conservative block model, and the assumption that a brine reservoir cannot be discounted until the Bell Canyon is reached, there is a chance that the brine reservoir has an area between 25 and 55% of the excavated area with a median of 40%. This contrasts with the best estimate of 45% from the contour method. The distribution is bell-shaped (Figure 5.1-1).

Minimum Area (Anhydrite III Level). Based on the geostatistical analysis and data uncertainty described above, the probability of the brine reservoir residing in the uppermost anhydrite layer is very small.

50% Combination. Figure 5.1.8 shows the derived cumulative distribution of area fraction using both the "random" and "block" assumptions and assuming that 50% of the time Anhydrite III is the maximum depth and 50% of the time the Bell Canyon is the maximum depth. Both distributions show a distinct bi-modality assuming very small values of area fraction correspond to the requirement that the brine reservoir be in Anhydrite III, while larger area fractions correspond to the requirement that the brine reservoir must be in the Castile Formation. The relative weighting of the two formulations for the brine reservoir controls the elevation of the plateau in the cumulative distribution, and is clearly more important than the model of spatial variability of conductor elevation (random or block).

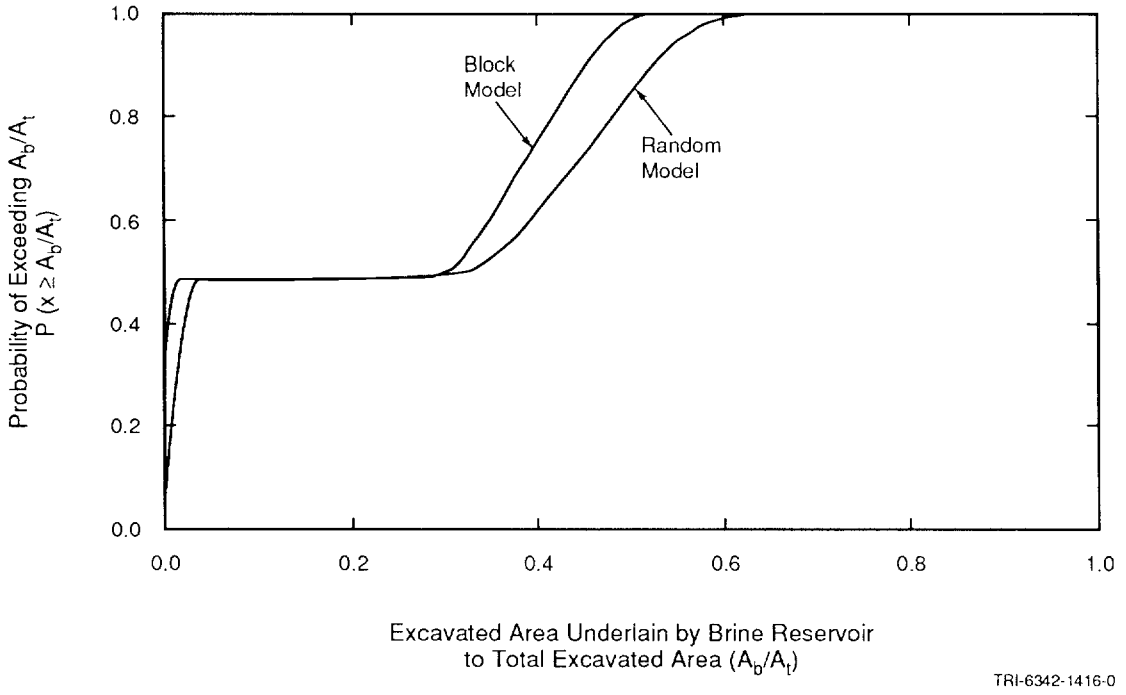

Figure 5.1-8. Cumulative Distribution of Area Fraction using the "Random" and "Block" Assumptions.

In the 1991 PA calculations, we used the maximum area distribution of 25 to 55% because the results are more conservative. We could not readily establish the likelihood that the elevation of Anhydrite III in the Castile Formation could be used as a cutoff for indicating whether a brine reservoir existed under the disposal area without further examination of the occurrence of brine reservoirs in the region.

Lack of Spatial Correlation of Conductor Elevations. The variogram analysis suggests that conductor elevations are not correlated over a distance of 250 m. Aside from ramifications for interpolation, this result appears to place limits on the areal extent of brine reservoirs beneath WIPP. This conclusion is not entirely justified. Figure 5.1-9 shows a hypothetical arrangement of measurement points, and an underlying structure dominated by narrow features at an angle to the measurement array. Although the features are continuous over the region, observations of particular features are randomly distributed through the measurement array. In order for the underlying correlation structure of the oblong features to be revealed in this hypothetical case, the measurement array must be able to resolve the minimum characteristic dimension of the features. Note that it may still be possible for the original sampling to provide a good estimate of the relative area of each feature type.

Although the above illustration is hypothetical, geologic considerations argue that brine reservoir location may be controlled by fracturing along Castile anticlines. In this situation, it is not unreasonable to expect brine reservoirs to be defined by long, narrow fracture zones along the anticline axis. Lack of correlation at a scale of 250 m would then place an upper limit on the minimum dimension of these fracture zones, but would not constraint maximum area extent.

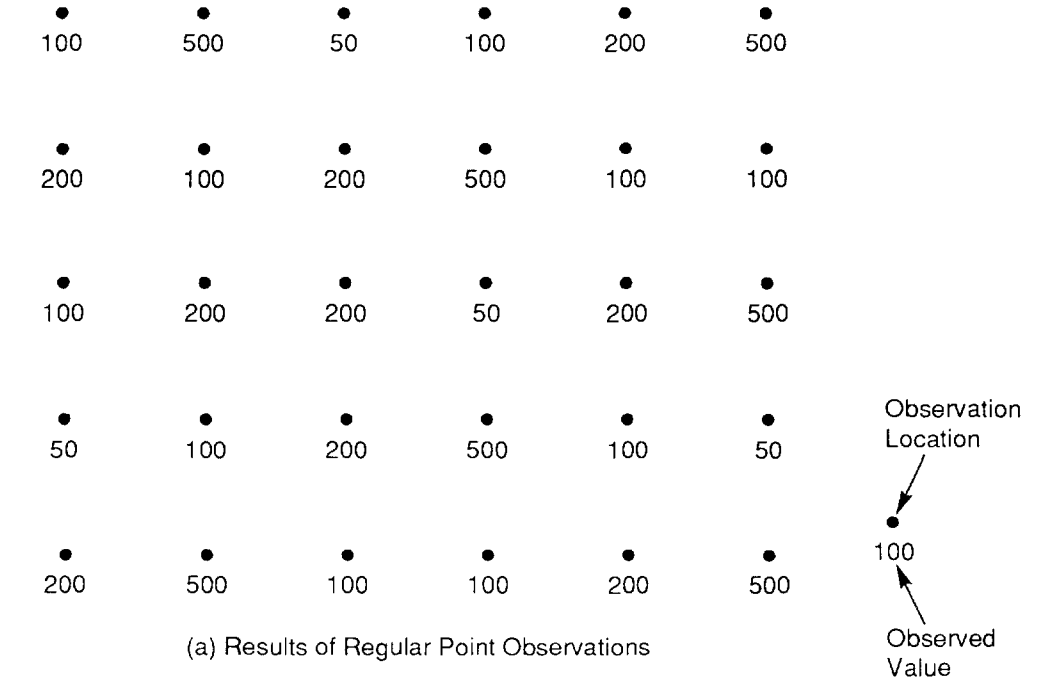

(a) Results of Regular Point Observations

(b) Underlying Structure

TRI-6342-1419-0

Figure 5.1-9. Illustration of Hypothetical Variability of Regular Sampling of Extensive Narrow Features.

5.1.2 Location of Intrusion

In 1991, the location of the borehole was fixed at the center of the disposal region (see Figure 3.1-2) to reduce the computational burden in the transport calculations until the influence of the variable transmissivity fields on fluid flow could be determined. (The most conservative position was not known a priori.) Next year's PA calculations will either use a variable position of the borehole or select a conservative location.

5.2 Human-Intrusion Probability (Drilling) Models

5.2.1 Drilling Rate Function

Parameter:	**Drilling rate function** $\Lambda(t)$
Median:	5.2×10^{-12}
Range:	$0 <$
	1.04×10^{-11}
Units:	s^{-1}
Distribution:	Uniform
Source(s):	Tierney, M. S. 1991. *Combining Scenarios in a Calculation of the Overall Probability Distribution of Cumulative Releases of Radioactivity from the Waste Isolation Pilot Plant, Southeastern New Mexico.* SAND90-0838. Albuquerque, NM: Sandia National Laboratories. (Appendix C)

Figure 5.2-1 shows the distribution for the constant failure rate function for exploratory drilling.

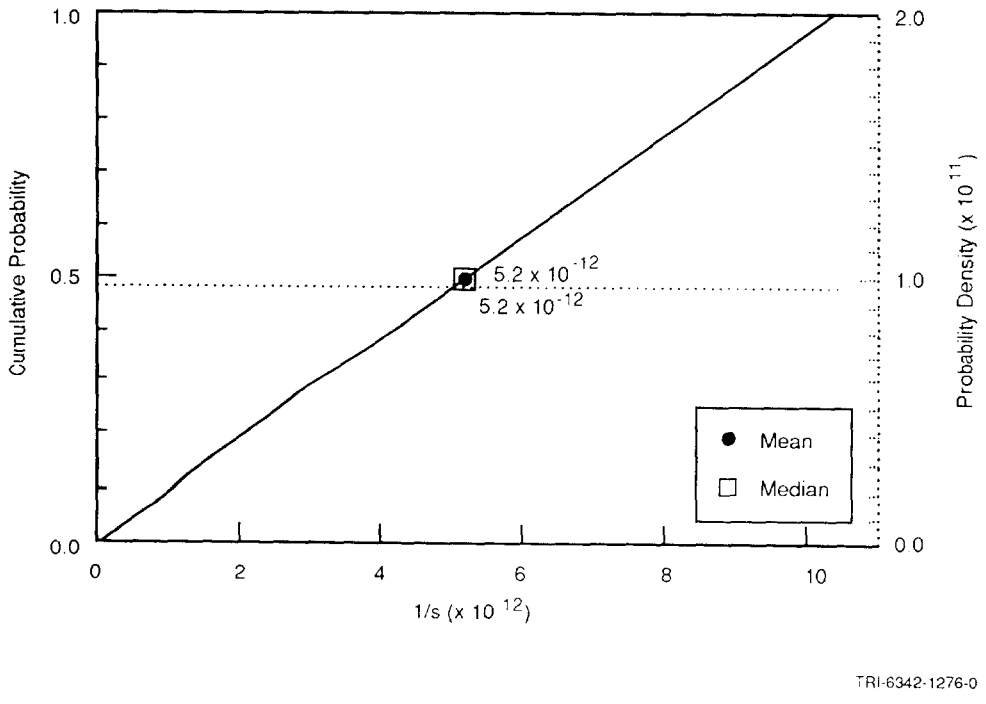

Figure 5.2-1. Estimated Distribution (pdf and cdf) of Constant Failure Rate.

Discussion:

The model for determining the probabilities of human intrusions (drilling) is based upon a general failure rate function ($\Lambda(t)$):

$$\Lambda(t) = \begin{cases} 0 & 0 < t < t_0 \\ -d/dt\ \ell n[1-F(t)], & t_0 < t \end{cases} \qquad (5.2\text{-}1)$$

where

t = time elapsed since disposal system placed in operation
t_0 = time when active government control ceases (100 yr [40 CFR 191])
$F(t)$ = cumulative distribution for first time of disturbing event.

40 CFR 191, Appendix B, places an upper bound on $\Lambda(t)$:

> ... the Agency assumes that the likelihood of such inadvertent and intermittent drilling need not be taken to be greater than 30 boreholes per square kilometer per 10,000 years for geologic repositories in proximity to sedimentary rock formations...

or

$$\lambda = \frac{30 \text{ boreholes}}{10^6 m^2\ 10^4 yr} \cdot \text{area of excavated disposal region} \qquad (5.2\text{-}2)$$

Hence for the WIPP, $\lambda = 3.28 \times 10^{-4}$ yr^{-1} assuming an excavated disposal region of about 1.09×10^5 m^2 (1.1×10^6 ft^2). The mean time of the first intrusion is $1/\lambda$ or about 3,000 yr. The number of intrusions is sampled from an associated Poisson distribution.

Similarly, *40 CFR 191*, Appendix B, places a lower bound on $\Lambda(t)$:

> ... passive institutional controls should not be assumed to completely rule out the possibility of intrusion ...

The actual variation of the drilling (failure) rate function with time is unknown but can be conservatively approximated by a piecewise linear function (Tierney, 1991, Appendix C) (Curve A, Figure 5.2-2). Currently, PA calculations assume $\Lambda(t)$ is a constant ($\Lambda(t) = \lambda$) for each simulation and uniformly distributed between certain maximum and minimum values.* The failure rate, $\Lambda(t)$, is used in estimating, for example, probabilities for multiple intrusions or evaluating the time of the first intrusion.

---

* Though conservative, the constant failure rate is unrealistic because the effects of markers (required by 40 CFR 191 to warn of the presence of the repository) are ignored.

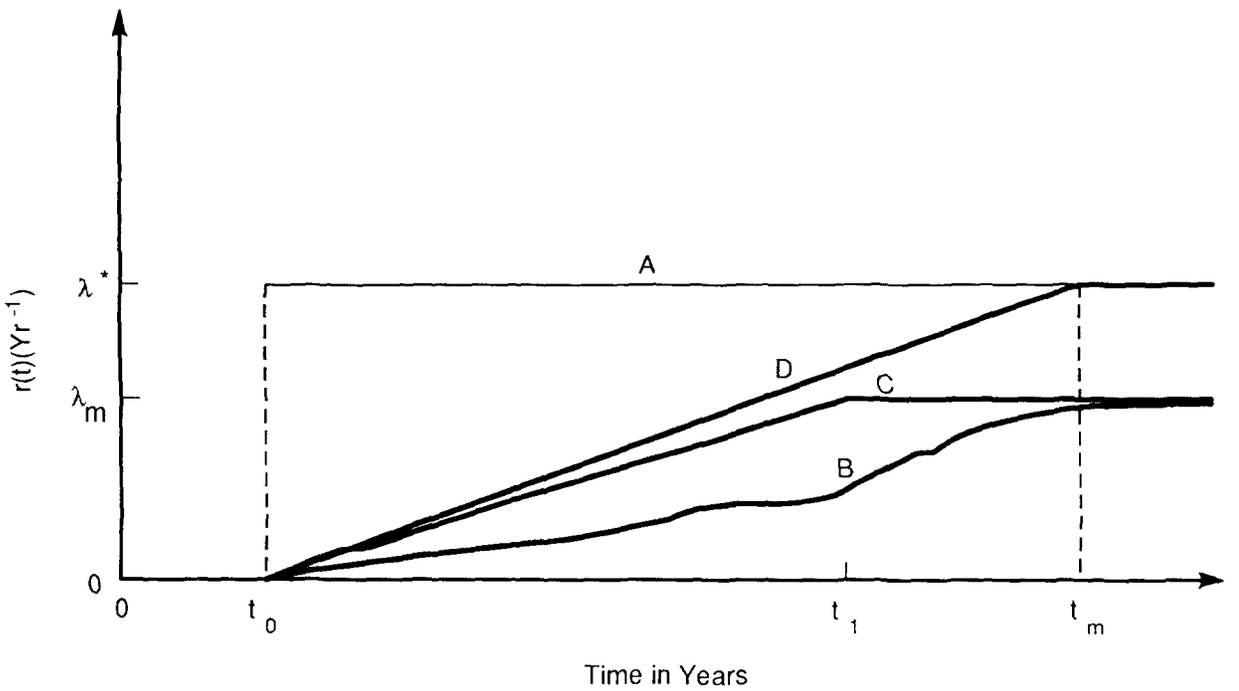

TRI-6342-606-0

Figure 5.2-2. Alternative Forms of a Failure Rate for Exploratory Drilling (after Tierney, 1991, Appendix C).

Assuming that the times of attempted drilling are independent of each other and that the failure rate $\Lambda(t)$ is a constant λ, the probability that drilling will occur exactly n times in the time interval t is given by the Poisson distribution (Ross, 1985, Chapter 7):

$$P\{N=n\} = \frac{(\lambda t)^n}{n!} \exp(-\lambda t), \quad n=0,1,2,\ldots \qquad (5.2\text{-}3)$$

where

t = time
$1/\lambda + t_0$ = average time one must wait until first drilling occurs
N = number of intrusions (a random variable).

Because the PA Division grouped the occurrence of human intrusion into separate scenarios, PA calculations used the conditional probability. The conditional probability that drilling will occur more than once ($N > 0$) is

$$P\{N=n \mid N>0\} = P\{N=n\}/P\{N>0\} \qquad (5.2\text{-}4)$$

where

$$P\{N>0\} = 1 - P\{N=0\} = 1 - \exp(-\lambda t)$$

Hence,

$$P\{N=n \mid N>0\} = \left(\frac{(\lambda t)^n}{n!} \exp(-\lambda t)\right)/[1-\exp(-\lambda t)] \qquad (5.2\text{-}5)$$

The discrete probability of intrusion, $P\{N=n \mid N>0\}$, is given in Table 5.2-1 and Figure 5.2-2 for between 1 and 13 intrusions for $\Lambda(t) - \lambda_{max} = 3.28 \times 10^{-4}$ yr^{-1}.

Table 5.2-1. Probability of Multiple Hits into Disposal Region of Repository

Median	Range		Value	Probability	Units	Source
3	1	13	1	1.2810×10^{-1}	none	Tierney, 1991, Appendix C
			2	2.1020×10^{-1}		
			3	2.2990×10^{-1}		
			4	1.8860×10^{-1}		
			5	1.2380×10^{-1}		
			6	6.77×10^{-2}		
			7	3.17×10^{-2}		
			8	1.30×10^{-2}		
			9	4.70×10^{-3}		
			10	1.60×10^{-3}		
			11	5.00×10^{-4}		
			12	1.00×10^{-4}		
			13	1.00×10^{-4}		

5.2.2 Time of First Intrusion for Scenarios

Parameter:	**Time of first intrusion**
Median:	7×10^{10}
Range:	3.156×10^{9}
	3.156×10^{11}
Units:	s
Distribution:	Exponential
Source(s):	Tierney, M. S. 1991. *Combining Scenarios in a Calculation of the Overall Probability Distribution of Cumulative Releases of Radioactivity from the Waste Isolation Pilot Plant, Southeastern New Mexico.* SAND90-0838. Albuquerque, NM: Sandia National Laboratories. (Appendix C)

Figure 5.2-3 shows the distribution for time of intrusion.

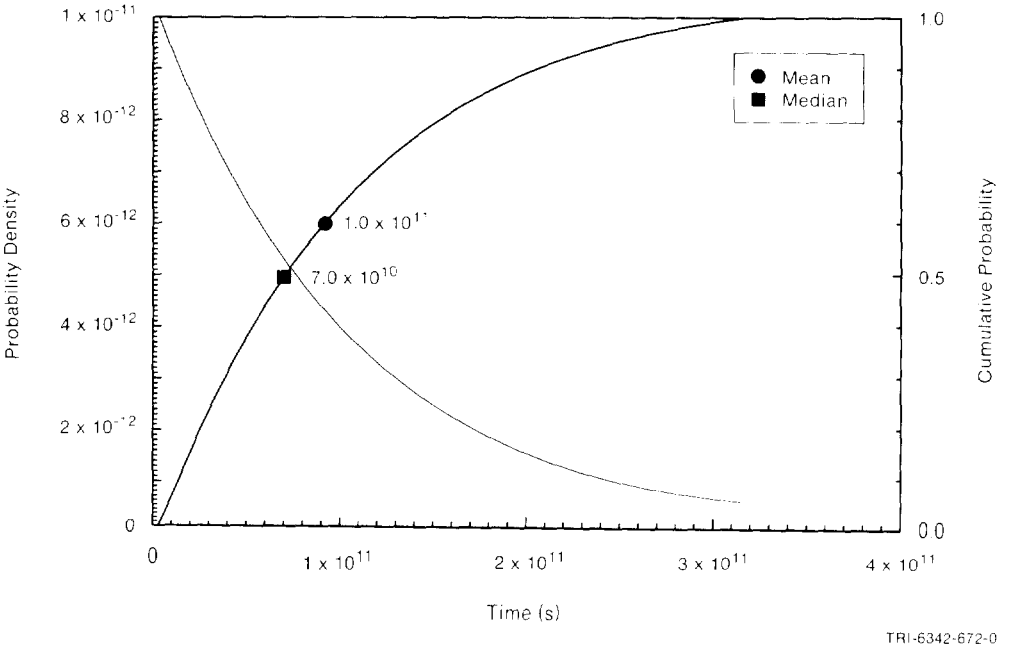

Figure 5.2-3. Estimated Distribution (pdf and cdf) for Time of Intrusion for E1, E2, and E1E2 Scenarios.

Discussion:

The time of first intrusion is evaluated from failure rate function $\Lambda(t)$ (Eq. 5.2-1). Integrating Eq. 5.2-1 to evaluate F(t) yields

$$F(t) = 1 - \exp\left[-\int_{t_o}^{t} \Lambda(\tau)\, d\tau\right] \qquad (5.2\text{-}6)$$

Since PA calculations assume $\Lambda(t)$ is a constant (λ) for each simulation, F(t) is a cumulative exponential distribution

$$F(t) = \begin{cases} 0 & \text{if } 0 < t < t_0 \\ 1 - \exp(-\lambda t), & \text{if } t \geq t_0 \end{cases} \qquad (5.2\text{-}7)$$

$$= \Pr\{\text{time of hit} < t\}$$

where

$1/\lambda + t_0$ = the average time one must wait either until the first drilling occurs that intersects the disposal region or between intrusions.

Thus, for a Poisson process, the waiting time between successive intrusions has an exponential distribution.

Because the PA Division grouped the occurrence of human intrusion into separate scenarios, PA calculations used the conditional probability. The conditional probability on the time when drilling will occur given that drilling occurs at least once before $t > t_1$, where t_1 is the regulatory period of 10,000 yr is (Miller and Freund, 1977, p. 34)

$$P\{\text{time of hit} < t \mid \text{time of hit} < t_1\}$$
$$= P\{\text{time of hit} < t\}/P\{\text{time of hit} < t_1\} \qquad (5.2\text{-}8)$$

where

$P\{\text{time of hit}$ $1 - \exp[-\lambda(t_1 - t_0)]$

Hence,

$$P\{\text{time of hit} < t \mid \text{time of hit} < t_1\}$$
$$= \{1 - \exp[-\lambda(t - t_0)]\}/\{1 - \exp[-\lambda(t_1 - t_0)]\} \qquad (5.2\text{-}9)$$

5.2.3 Times of Multiple Intrusions

Parameter:	**Time of intrusion**
Median:	1.5936×10^{11}
Range:	3.156×10^{9}
	3.156×10^{11}
Units:	s
Distribution:	Uniform
Source(s):	Tierney, M. S. 1991. *Combining Scenarios in a Calculation of the Overall Probability Distribution of Cumulative Releases of Radioactivity from the Waste Isolation Pilot Plant, Southeastern New Mexico.* SAND90-0838. Albuquerque, NM: Sandia National Laboratories. (Appendix C)

Figure 5.2-4 shows the distribution for time of intrusion used in 1990.

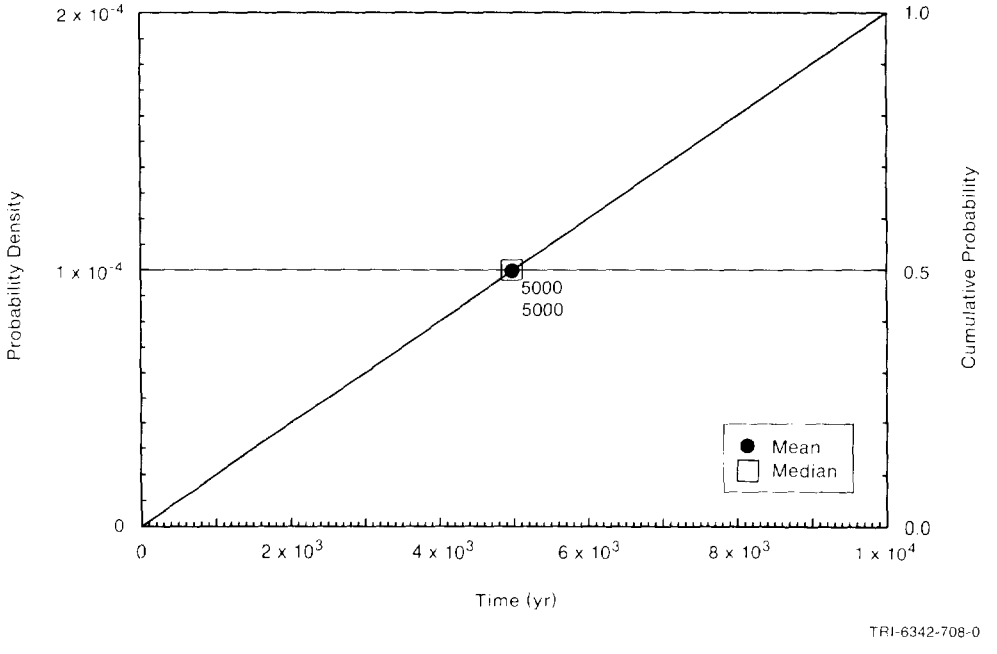

Figure 5.2-4. Estimated Distribution (pdf and cdf) for Time of Intrusion for Multiple Hits Used in 1990.

Discussion:

In 1990, the times of the N intrusions were evaluated from a uniform distribution between 100 and 10,000 yr* (Figure 5.2-4). The N random samples from the uniform distribution were then ordered from the smallest to the largest. Identical times for intrusions were permitted. Because the waiting times between successive intrusions have exponential distributions for a Poisson process, the mean time of intrusion (or mean time between intrusions) was $1/\lambda + t_0$ or about 3,000 yr.

In 1991, the time of intrusion is used to define computational scenarios. To simplify the discretization, the time of intrusion was divided into five equal intervals of 2,000 yr and the intrusion or multiple intrusions in each interval set at the midpoint (e.g., 1,000 yr).

---

* For compliance calculations, 100 yr is the time period after which active government control of the WIPP must be assumed to stop (40 CFR 191); 10,000 yr is the end of the regulatory period.

6. SUMMARY OF PARAMETERS SAMPLED IN 1991

Tables 6.0-1, 6.0-2, and 6.0-3 summarize the parameters that were sampled for the 1991 PA calculations for the geologic barriers, engineered barriers, and agents acting on the disposal system and probability models for scenarios, respectively. Figure 6.0-1 shows the rank correlation for halite and anhydrite permeability (Table 6.0-1).

Table 6.0-1. Distributions of Sample Parameters in December 1991 WIPP Performance Assessment for Geologic Barriers

Parameter	Median	Range		Units	Distribution Type	Source
Halite within Salado Formation						
Permeability (k)	5.7×10^{-21}	8.6×10^{-22}	5.4×10^{-20}	m^2	Data	Beauheim, June 14, 1991, Memo (see Appendix A)
Pore pressure (p)	1.28×10^{7}	9.3×10^{6}	1.39×10^{7}	Pa	Data	See anhydrite.
Anhydrite Layers within Salado Formation						
Pore pressure (p)	1.28×10^{7}	9.3×10^{6}	1.39×10^{7}	Pa	Data	Beauheim, June 14, 1991, Memo; Howarth, June 12, 1991, Memo (see Appendix A)
*Permeability (k)						
Undisturbed	7.8×10^{-20}	6.8×10^{-20}	9.5×10^{-19}	m^2	Data	Beauheim, June 14, 1991, Memo (see Appendix A)
Porosity (ϕ)						
Undisturbed	1×10^{-2}	1×10^{-3}	3×10^{-2}	none	Cumulative	See text.
Threshold displacement pressure (p_t)	3×10^{5}	3×10^{3}	3×10^{7}	Pa	Lognormal	Davies, 1991; Davies, June 2, 1991, Memo (see Appendix A)
Castile Formation Brine Reservoir						
Initial pressure (p)	1.26×10^{7}	1.1×10^{7}	2.1×10^{7}	Pa	Cumulative	Popielak et al., 1983, p. H-52; Lappin et al., 1989, Table 3-19
Storativity, bulk (S_b)	2×10^{-1}	2×10^{-2}	2	m^3	Lognormal	See text.
Culebra Dolomite Member						
Dispersivity, longitudinal (α_L)	1×10^{2}	5×10^{1}	3×10^{2}	m	Cumulative	Lappin et al., 1990, Table E-6
Fracture spacing (2B)	4×10^{-1}	6×10^{-2}	8	m	Cumulative	Beauheim et al., June 10, 1991, Memo (see Appendix A)
Porosity						
Fracture (ϕ_f)	1×10^{-3}	1×10^{-4}	1×10^{-2}	none	Lognormal	Lappin et al., 1989, Table 1-2, Table E-6
Matrix (ϕ_m)	1.39×10^{-1}	9.6×10^{-2}	2.08×10^{-1}	none	Spatial	Kelley and Saulnier, 1990, Table 4.4; Lappin et al., 1989 Table E-8

* Permeability of the halite and anhydrite were rank correlated with an r = 0.80 (Figure 6.0-1).

Table 6.0-1. Distributions of Sample Parameters in December 1991 WIPP Performance Assessment for Geologic Barriers (Continued)

Parameter	Median		Range	Units	Distribution Type	Source
Partition Coefficients						
Fracture						
Am	9.26×10^{1}	0.0	1×10^{3}	m^3/kg	Cumulative	See text.
Np	1	0.0	1×10^{3}	m^3/kg	Cumulative	See text.
Pu	2.02×10^{2}	0.0	1×10^{3}	m^3/kg	Cumulative	See text.
Th	1×10^{-1}	0.0	1×10^{1}	m^3/kg	Cumulative	See text.
U	7.5×10^{-3}	0.0	1	m^3/kg	Cumulative	See text.
Matrix						
Am	1.86×10^{-1}	0.0	1×10^{2}	m^3/kg	Cumulative	See text.
Np	4.8×10^{-2}	0.0	1×10^{2}	m^3/kg	Cumulative	See text.
Pu	2.61×10^{-1}	0.0	1×10^{2}	m^3/kg	Cumulative	See text.
Th	1×10^{-2}	0.0	1	m^3/kg	Cumulative	See text.
U	2.58×10^{-2}	0.0	1	m^3/kg	Cumulative	See text.
Transmissivity field	3.5×10^{1}	0	60	none	Uniform	See text.

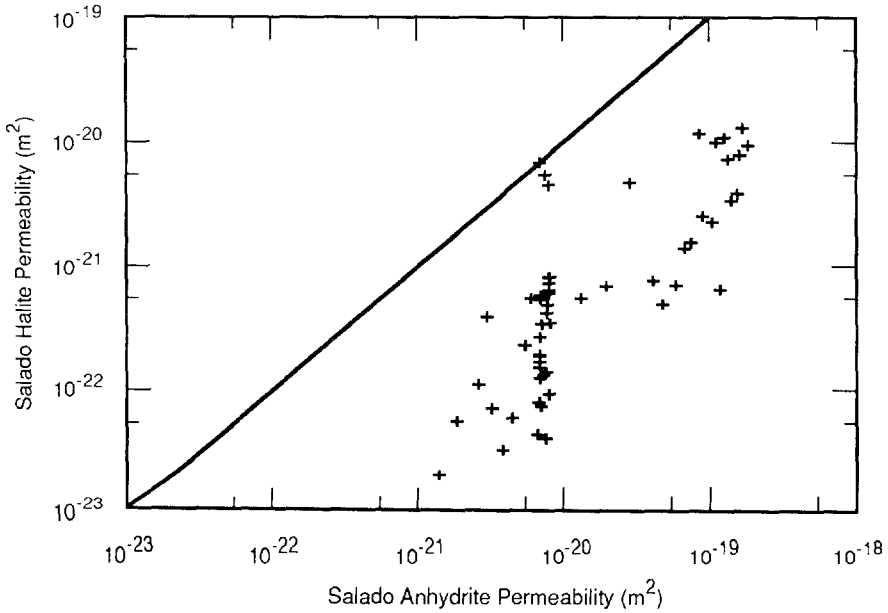

Figure 6.0-1. General Relationship Maintained between Halite and Anhydrite Permeabilities of Salado Formation Using a Rank Correlation Coefficient (r) of 0.80.

Table 6.0-2. Distributions of Sample Parameters in December 1991 WIPP Performance Assessment for Engineered Barriers

Parameter	Median	Range		Units	Distribution Type	Source
Unmodified Waste Form						
Gas Generation						
Corrosion						
Inundated rate	6.3×10^{-9}	0	1.3×10^{-8}	$mol/m^2/s$*	Cumulative	Brush, July 8, 1991, Memo (see Appendix A)
Relative humid rate	1×10^{-1}	0	5×10^{-1}	none	Cumulative	Brush, July 8, 1991, Memo (see Appendix A)
Stoichiometry	5×10^{-1}	0	1	none	Uniform	Brush and Anderson in Lappin et al., 1989, p. A-6
Microbiological						
Inundated rate	3.2×10^{-9}	0	1.6×10^{-8}	mol/kg/s**	Cumulative	Brush, July 8, 1991, Memo (see Appendix A)
Relative humid rate	1×10^{-1}	0	2×10^{-1}	none	Uniform	Brush, July 8, 1991, Memo (see Appendix A)
Stoichiometry	8.35×10^{-1}	0	1.67	none	Uniform	Brush and Anderson in Lappin et al., 1989, p. A-10.
Dissolved Concentrations (Solubility)***						
Am^{3+}	1×10^{-9}	5×10^{-14}	1.4	Molar	Cumulative	Trauth et al., 1991
Np^{4+}	6×10^{-9}	3×10^{-16}	2×10^{-5}	Molar	Cumulative	Trauth et al., 1991
Np^{5+}	6×10^{-7}	3×10^{-11}	1.2×10^{-2}	Molar	Cumulative	Trauth et al., 1991
Pu^{4+}	6×10^{-10}	2.0×10^{-16}	4×10^{-6}	Molar	Cumulative	Trauth et al., 1991
Pu^{5+}	6×10^{-10}	2.5×10^{-17}	5.5×10^{-4}	Molar	Cumulative	Trauth et al., 1991
Th^{4+}	1×10^{-10}	5.5×10^{-16}	2.2×10^{-6}	Molar	Cumulative	Trauth et al., 1991
U^{4+}	1×10^{-4}	1×10^{-15}	5×10^{-2}	Molar	Cumulative	Trauth et al., 1991
U^{6+}	2×10^{-3}	1×10^{-7}	1	Molar	Cumulative	Trauth et al., 1991
Volume Fractions of IDB Categories						
Metal/Glass	3.76×10^{-1}	2.76×10^{-1}	4.76×10^{-1}	none	Normal	See text, Table 3.4-9
Combustibles	3.84×10^{-1}	2.84×10^{-1}	4.84×10^{-1}	none	Normal	See text, Table 3.4-9
Initial waste saturation	1.38×10^{-1}	0	2.76×10^{-1}		Uniform	See text.
Eh-pH Conditions	0.5	0	1.0	none	Uniform	See text.

* $mole/m^2$ surface area steel/s

** mole/kg cellulosics/s

*** For the following elements —Np, Pu, and Th —only one species was used in each sample. The species were rank correlated at r = 0.99.

Table 6.0-3. Distributions of Sample Parameters in December 1991 WIPP Performance Assessment for Agents Acting on Disposal System and Probability Models for Scenarios

Parameter	Median	Range		Units	Distribution Type	Source
Agents Acting on Disposal System						
Intrusion Borehole Flow Parameters						
Diameter	3.55×10^{-1}	2.67×10^{-1}	4.44×10^{-1}	m	Uniform	See text.
Permeability (k)	3.16×10^{-12}	1×10^{-14}	1×10^{-11}	m^2	Lognormal	Freeze and Cherry, Table 2.2 (clean sand)
Climate parameter						
Recharge amplitude factor	8×10^{-2}	0	1.6×10^{-1}	none	Uniform	See text.
Probability Model for Scenarios						
Area of pressurized brine reservoir	4.0×10^{-1}	2.5×10^{-1}	5.52×10^{-1}	none	Cumulative	See text.
Rate constant in Poisson drilling model, $\Lambda(t)$	5.2×10^{-12}	0 <	1.04×10^{-11}	s^{-1}	Uniform	40 CFR 191.

Selection Procedure for Parameters Sampled in 1991

A parameter was chosen for sampling in the 1991 PA calculations if it fulfilled one of two criteria: (1) the parameter proved to be sensitive in the 1990 sensitivity analyses (Helton et al., 1991); or (2) the parameter was an imprecisely known quantity in a consequence model first formally used in the present (1991) series of calculations. Examples of parameters that fulfilled Criterion 1 are Culebra partition coefficients and dissolved concentrations (solubilities including Eh-pH conditions). Examples of parameters that fulfilled Criterion 2 are the parameters of dual-porosity transport in the Culebra (dispersivity, fracture spacing, matrix and fracture porosities); material properties of the anhydrite layers within the Salado Formation (pore pressure, permeability, porosity); gas generation rates in unmodified waste forms; volume fractions of unmodified waste forms; and constants in probability model for human intrusion scenarios (area of pressurized brine reservoir, rate constant in Poisson model of exploratory drilling). Some imprecisely known parameters must be sampled in any PA exercise that uses the results of certain models; examples of this kind of parameter are the transmissivity field, intrusion-borehole flow parameters (permeability, porosity), and the recharge factor for climatic change (Swift, October 10, 1991, Memo [Appendix A]).

Consequence Models for WIPP Disposal System (42 + 3 Variables)

Geologic Barriers (22 Variables)

Halite within Salado Formation Near Repository (1 variable)
- **Permeability** (1)
- Sampled in 1990 But Omitted in 1991
  - *Compressibility* — not very important in 1990

Anhydrite Layers within Salado Formation (4 variables)
- **Brine Pressure at Repository Level** (1)
- **Permeability, Intact** (1)
- **Porosity, Intact** (1)
- **Threshold pressure** (1)

Castile Formation Brine Reservoir (2 variables)
- **Bulk Storativity (S_b)** (1)
- **Initial Pressure** (1)

Culebra Dolomite Member (13 variables)
- **Dispersivity** (1)
- **Matrix Porosity** (1)
- **Fracture Porosity** (1) (no quantitative correlation with T)
- **Fracture Spacing** (1) (no quantitative correlation with T)
- **Retardation, Matrix and Fracture** (10=5x2)
- **Transmissivity Field** (1) (0 - 60, uniform distribution)
- Sampled in 1990 But Omitted in 1991
  - *Tortuosity* — not much spatial change in transport model domain

Engineered Barriers (15 + 3 Variables)

Unmodified Waste Form
- **Gas Generation Rates for Corrosion and Degradation in Humid and Saturated Conditions** (4)
- **Corrosion stoichiometry** (1)
- **Microbial stoichiometry** (1)
- **Dissolved Concentrations (Solubility)** (5 + 3) — 3 correlated at r = 0.99 for modeling convenience
- **Volumes of Metal and Combustibles** (2)
- **Initial Waste Saturation** (1)
- **Eh-pH Conditions** (1)
- Sampled in 1990 But Omitted in 1991
  - *Molecular Diffusion* -- Species dependent in 1991

Agents Acting on Disposal System (3 Variables)

- **Recharge** (1) (includes leakage from subsidence)
- **Intrusion Borehole Permeability and Drill Bit Diameter** (2) (based on deep gas reservoir target in 1991)

Probability Model for Scenarios (2 Variables)

Area of Pressurized Brine Reservoir (1)
Rate Constant in Poisson Drilling Model (1)
Sampled in 1990 but Omitted in 1991
Number of Hits -- Defining variable for computational scenario
Room Number -- Area of brine reservoir determines probability of hitting brine reservoir in 1991; location for transport is fixed at the center of the Disposal Region
Time of Intrusion -- Defining variable for computational scenario

REFERENCES

Allison, G. B. 1988. "A Review of Some of the Physical, Chemical, and Isotopic Techniques Available for Estimating Groundwater Recharge," in I. Simmers (ed.), *Estimation of Natural Groundwater Recharge.* NATO ASI series, series C, vol. 222. Dordrecht, Holland: D. Reidel. pp. 49-72.

Anderson, D. R., M. G. Marietta, and M. S. Tierney. 1990. "Request for Assistance in Assigning Probability Distribution to the Parameters Being Used for the Preliminary Performance Assessment of the WIPP relating to EPA 40 CFR 191," Memo 2 in Appendix A of Rechard et al. 1990. *Data Used in Preliminary Performance Assessment of the Waste Isolation Pilot Plant (1990).* SAND89-2408. Albuquerque, NM: Sandia National Laboratories.

Anderson, D. R., K. M. Trauth, and S. C. Hora. 1991. "The Use of Expert Elicitation to Quantify Uncertainty in Incomplete Sorption Data Bases for Waste Isolation Pilot Plant Performance Assessment." SAND91-7099C. Presented at the *Organization for Economic Cooperation and Development, Nuclear Energy Agency Sorption Workshop '91, Interlaken, Switzerland, October 16, 1991.*

Arguello, J. G. 1988. *WIPP Panel Entryway Seal-Numerical Simulation of Seal Composite Interaction for Preliminary Seal Design Evaluation.* SAND87-2804. Albuquerque, NM: Sandia National Laboratories.

Austin, E. H. 1983. *Drilling Engineering Handbook.* Boston, MA: International Human Resources Development Corporation.

Avis, J. D., and G. J. Saulnier, Jr. 1990. *Analysis of the Fluid-Pressure Responses of the Rustler Formation at H-16 to the Construction of the Air-Intake Shaft at the Waste Isolation Pilot Plant (WIPP) Site.* SAND89-7067. Albuquerque, NM: Sandia National Laboratories.

Bachman, G. O. 1981. *Geology of Nash Draw, Eddy County, New Mexico.* U.S. Geological Survey Open-File Report 81-31. Albuquerque, NM: U. S. Geological Survey.

Barnhart, B. J., E. W. Campbell, E. Martinez, D. E. Caldwell, and R. Hallett. 1980. *Potential Microbial Impact on Transuranic Wastes Under Conditions Expected in the Waste Isolation Pilot Plant (WIPP), Annual Report, October 1, 1978-September 30, 1979.* LA-8297-PR. Los Alamos, NM: Los Alamos National Laboratories.

Bayley, S. G., M. D. Siegel, M. Moore, and S. Faith. 1990. *Sandia Sorption Data Management System Version 2 (SSDMS11).* SAND89-0371. Albuquerque, NM: Sandia National Laboratories.

Bear, J. 1972. *Dynamics of Fluids in Porous Media.* New York: American Elsevier Publishing Company, Inc.

Bear, J., and A. Verruijt. 1987. *Modeling Groundwater Flow and Pollution.* Boston, MA: D. Reidel Publishing Company, p. 126.

Beauheim, R. L. 1987a. *Analysis of Pumping Tests of the Culebra Dolomite Conducted at the H-3 Hydropad at the Waste Isolation Pilot Plant (WIPP) Site.* SAND86-2311. Albuquerque, NM: Sandia National Laboratories.

Beauheim, R. L. 1987b. *Interpretation of the WIPP-13 Multipad Pumping Test of the Culebra Dolomite at the Waste Isolation Pilot Plant (WIPP) Site.* SAND87-2456. Albuquerque, NM: Sandia National Laboratories.

Beauheim, R. L. 1987c. *Interpretations of Single-Well Hydraulic Tests Conducted at and Near the Waste Isolation Pilot Plant (WIPP) Site, 1983-1987.* SAND87-0039. Albuquerque, NM: Sandia National Laboratories.

Beauheim, R. L. 1989. *Interpretation of H-11b4 Hydraulic Tests and the H-11 Multipad Pumping Test of the Culebra Dolomite at the Waste Isolation Pilot Plant (WIPP) Site.* SAND89-0536. Albuquerque, NM: Sandia National Laboratories.

Beauheim, R. L. 1990. "Review of Parameter Values to be Used in Performance Assessment," Memo 3c in Appendix A of Rechard et al. 1990. *Data Used in Preliminary Performance Assessment of the Waste Isolation Pilot Plant (1990).* SAND89-2408. Albuquerque, NM: Sandia National Laboratories.

Beauheim, R. L., G. J. Saulnier, and J. D. Avis. 1990. *Interpretation of Brine-Permeability Tests of the Salado Formation at the Waste Isolation Pilot Plant Site: First Interim Report.* SAND90-0083. Albuquerque, NM: Sandia National Laboratories.

Beauheim, R. L., G. J. Saulnier, and J. D. Avis. 1991. *Interpretation of Brine-Permeability Tests of the Salado Formation at the Waste Isolation Pilot Plant: First Interim Report.* SAND90-0083. Albuquerque, NM: Sandia National Laboratories.

Bechtel, Inc. 1985. *Quarterly Geotechnical Field Data Report, December 1985.* WIPP-DOE-211. Prepared for the U.S. Department of Energy. San Francisco, CA: Bechtel National, Inc.

Bechtel, Inc. 1986. *WIPP Design Validation Final Report.* DOE/WIPP-86-010. Prepared for U.S. Department of Energy. San Francisco, CA: Bechtel National, Inc.

Bertram-Howery, S. G., M. G. Marietta, D. R. Anderson, K. F. Brinster, L. S. Gomez, R. V. Guzowski, and R. P. Rechard. 1988. *Draft Forecast of the Final Report for the Comparison to 40 CFR Part 191, Subpart B for the Waste Isolation Pilot Plant.* SAND88-1452. Albuquerque, NM: Sandia National Laboratories.

Bertram-Howery, S. G., M. G. Marietta, R. P. Rechard, P. N. Swift, D. R. Anderson, B. Baker, J. Bean, W. Beyeler, K. F. Brinster, R. V. Guzowski, J. Helton, R. D. McCurley, D. K. Rudeen, J. Scheiber, and P. Vaughn. 1990. *Preliminary Comparison with 40 CFR Part 191, Subpart B for the Waste Isolation Pilot Plant, December 1990.* SAND90-2347. Albuquerque, NM: Sandia National Laboratories.

Bertram-Howery, S. G., and R. L. Hunter. 1989. *Preliminary Plan for Disposal-System Characterization and Long-Term Performance Evaluation of the Waste Isolation Pilot Plant.* SAND89-0178. Albuquerque, NM: Sandia National Laboratories.

Bertram-Howery, S. G., and P. Swift. 1990. *Status Report: Potential for Long-Term Isolation by the Waste Isolation Pilot Plant Disposal System, 1990.* SAND90-0616. Albuquerque, NM: Sandia National Laboratories.

Biot, M. A. 1991. "General Theory of Three-Dimensional Consolidation." *Journal of Applied Physics* vol. 12, February 1941, pp. 155-164.

Black, S. R., R. S. Newton, and D. K. Shukla, eds. 1983. "Brine Content of the Facility Interval Strata" in *Results of the Site Validation Experiments*, Vol. II, Supporting Document 10. Carlsbad, NM: U.S. Department of Energy.

Blom, G. 1989. *Probability and Statistics: Theory and Applications*. New York: Springer-Verlag.

Borns, D. J. 1985. *Marker Bed 139: A Study of Drillcore From a Systematic Array*. SAND85-0023. Albuquerque, NM: Sandia National Laboratories.

Bredenkamp, D. B. 1988a. "Quantitative Estimation of Ground-Water Recharge in Dolomite," in I. Simmers (ed.), *Estimation of Natural Groundwater Recharge*. NATO ASI series, series C, Vol. 222. Dordrecht, Holland: D. Reidel. pp. 449-460.

Bredenkamp, D. B. 1988b. "Quantitative Estimation of Ground-Water Recharge in the Pretoria-Rietondale Area," in I. Simmers (ed.), *Estimation of Natural Groundwater Recharge*. NATO ASI series, series C, vol. 222. Dordrecht, Holland: D. Reidel. pp. 461-476.

Brinster, K. F. 1990a. "Transmissivity Zones in Culebra Dolomite Member of Rustler Formation," Memo 8 in Appendix A of Rechard et al. 1990. *Data Used in Preliminary Performance Assessment of the Waste Isolation Pilot Plant (1990)*. SAND90-2408. Albuquerque, NM: Sandia National Laboratories.

Brinster, K. F. 1990b. "Transmissivities and Pilot Points for the Culebra Dolomite Member," Memo 9 in Appendix A of Rechard et al. 1990. *Data Used in Preliminary Performance Assessment of the Waste Isolation Pilot Plant (1990)*. SAND90-2408. Albuquerque, NM: Sandia National Laboratories.

Brinster, K. F. 1990c. "Well Data from Electric Logs," Memo 10 in Appendix A of Rechard et al. 1990. *Data Used in Preliminary Performance Assessment of the Waste Isolation Pilot Plant (1990)*. SAND89-2408. Albuquerque, NM: Sandia National Laboratories.

Brinster, K. F. 1991. *Preliminary Geohydrologic Conceptual Model of the Los Medaños Region Near the Waste Isolation Pilot Plant for the Purpose of Performance Assessment*. SAND89-7147. Albuquerque, NM: Sandia National Laboratories.

Broc, R., ed. 1982. *Drilling Mud and Cement Slurry Rheology Manual*. Houston, TX: Gulf Publishing Company.

Brooks, R. H., and A. T. Corey. 1964. "Hydraulic Properties of Porous Media," Hydrology Papers, No. 3. Fort Collins, CO: Colorado State University.

Brush, L. H. 1988. *Feasibility of Disposal of High-Level Radioactive Wastes into the Seabed: Review of Laboratory Investigations of Radionuclide Migration Through Deep-Sea Sediments*. SAND87-2438. Albuquerque, NM: Sandia National Laboratories.

Brush, L. H. 1990. *Test Plan for Laboratory and Modeling Studies of Repository and Radionuclide Chemistry for the Waste Isolation Pilot Plant*. SAND90-0266. Albuquerque, NM: Sandia National Laboratories.

Brush, L. H., and D. R. Anderson. 1989. "Appendix E: Estimates of Radionuclide Concentrations in Brines" in Marietta et al. 1989. *Performance Assessment Methodology Demonstration: Methodology Development for Purposes of Evaluating Compliance with EPA 40 CFR Part 191, Subpart B. for the Waste Isolation Pilot Plant*. SAND89-2027. Albuquerque, NM: Sandia National Laboratories.

Brush, L. H., and A. R. Lappin. 1990. "Additional Estimates of Gas Production Rates and Radionuclide Solubility for Use in Models of WIPP Disposal Rooms," Memo 4 in Appendix A of Rechard et al. 1990. *Data Used in Preliminary Performance Assessment of the Waste Isolation Pilot Plant (1990).* SAND89-2408. Albuquerque, NM: Sandia National Laboratories.

Buck, A. D. 1985. *Development of a Sanded Nonsalt Expansive Grout for Repository Sealing Application.* Miscellaneous Paper SL-85-6. Vicksburg, MS: Department of the Army, Waterways Experimental Station.

Buddenberg, J. W., and C. R. Wilke. 1949. *Ind. Eng. Chem.* **41**: 1345-1347.

Bush, D. D., and S. Piele. 1986. *A Full Scale Borehole Sealing Test in Salt Under Simulated Downhole Conditions: Volume 1.* BMI/ONWI-573(2). Columbus, OH: Office of Nuclear Waste Isolation, Battelle Memorial Institute.

Butcher, B. M. 1989. *Waste Isolation Pilot Plant Simulated Waste Compositions and Mechanical Properties.* SAND89-0372. Albuquerque, NM: Sandia National Laboratories.

Butcher, B. M. 1990. "Disposal Room Porosity and Permeability Values for Disposal Room Performance Assessment," Memo 5 in Appendix A of Rechard et al. 1990. *Data Used in Preliminary Performance Assessment of the Waste Isolation Pilot Plant (1990).* SAND89-2408. Albuquerque, NM: Sandia National Laboratories.

Butcher, B. M., T. W. Thompson, R. G. VanBuskirk, and N. C. Patti. 1991. *Mechanical Compaction of WIPP Simulated Waste.* SAND90-1206. Albuquerque, NM: Sandia National Laboratories.

Caldwell, D. E. 1981. *Microbial Biogeochemistry of Organic Matrix Transuranic Waste.* Unpublished Report submitted to M. A. Molecke, June 17, 1981. Albuquerque, NM: University of New Mexico.

Caldwell, D. E., R. C. Hallett, M. A. Molecke, E. Martinez, and B. J. Barnhart. 1988. *Rates of Co2 Production from the Microbial Degradation of Transuranic Wastes under Simulated Geologic Isolation Conditions.* SAND87-7170. Albuquerque, NM: Sandia National Laboratories.

Carmichael, R. S., ed. 1984. *CRC Handbook of Physical Properties of Rocks.* Vol. III. Boca Raton, FL: CRC Press, Inc.

Cauffman, T. L., A. M. LaVenue, and J. P. McCord. 1990. *Ground-Water Flow Modeling of the Culebra Dolomite: Volume II Data Base.* SAND89-7068/2. Albuquerque, NM: Sandia National Laboratories.

Chapman, N. A., and J. A. T. Smellie. 1986. "Natural Analogues to the Conditions around a Final Repository for High-Level Radioactive Waste." *Chemical Geology* vol. 55, no. 3/4.

Cheeseman, R. J. 1978. *Geology and Oil/Potash Resources of the Delaware Basin, Eddy and Lea Counties, New Mexico.* New Mexico Bureau of Mines and Mineral Resources Circular 159. Socorro, NM: New Mexico Bureau of Mines and Mineral Resources. 7-14.

Christensen, C. L., and W. W. Petersen. 1981. *The Bell Canyon Test Summary Report.* SAND80-1375. Albuquerque, NM: Sandia National Laboratories.

Clark, S. P. 1966. *Handbook of Physical Constants.* New York: The Geological Society of America, Inc.

Colebrook, C. F. 1938. "Turbulent Flow in Pipes, with Particular Reference to the Transition Region Between the Smooth and Rough Pipe Laws," *J. Inst. Civ. Eng. Long.* **11**: 133-156.

Conover, W. J. 1980. *Practical Nonparametric Statistics.* 2nd ed. New York: John Wiley and Sons.

Cranwell, R. M., and J. C. Helton. 1981. "Uncertainty Analysis for Geologic Disposal of Radioactive Waste," in D. C. Kocher, ed., *Proceedings of the Symposium on Uncertainties Associated with the Regulation of the Geologic Disposal of High-Level Radioactive Waste, Gatlinburg, TN, March 9-13, 1981.*

Cranwell, R. M., R. V. Guzowski, J. E. Campbell, and N. R. Ortiz. 1990. *Risk Methodology for Geologic Disposal of Radioactive Waste: Scenario Selection Procedure.* SAND80-1429, NUREG/CR-1667. Albuquerque, NM: Sandia National Laboratories.

Cygan, R. T. 1991. *The Solubility of Gases in NaCl Brine and a Critical Evaluation of Available Data.* SAND90-2848. Albuquerque, NM: Sandia National Laboratories.

Darley, H. C. H. 1969. "A Laboratory Investigation of Borehole Stability." *Journal of Petroleum Technology*, July, 883-392.

Darley, H. C. H., and G. R. Gray. 1988. *Composition and Properties of Drilling and Completion Fluids.* Houston, TX: Gulf Publishing Company.

Davies, P. B. 1989. *Variable-Density Ground-water Flow and Palehydrology in the Waste Isolation Pilot Plant (WIPP) Region, Southeastern New Mexico.* Open File Report 88-490. Albuquerque, NM: U.S. Geological Survey, Dept. of the Interior.

Davies, P. B. 1991. *Evaluation of the Role of Threshold Pressure in Controlling Flow of Waste-Generated Gas into Bedded Salt at the Waste Isolation Pilot Plant.* SAND90-3246. Albuquerque, NM: Sandia National Laboratories.

Davies, P. B., and A. M. LaVenue. 1990a. "Comments on Model Implementation and Data for Use in August Performance Assessment Calculations," Memo 3b in Appendix A of Rechard et al. 1990. *Data Used in Preliminary Performance Assessment of the Waste Isolation Pilot Plant (1990).* SAND89-2408. Albuquerque, NM: Sandia National Laboratories.

Davies, P. B., and A. M. LaVenue. 1990b. "Additional Data for Characterizing 2-Phase Flow Behavior in Waste-Generated Gas Simulations and Pilot Point Information for Final Culebra 2-D Model," Memo 11 in Appendix A of Rechard et al. 1990. *Data Used in Preliminary Performance Assessment of the Waste Isolation Pilot Plant.* SAND89-2408. Albuquerque, NM: Sandia National Laboratories.

Davies, P. B., L. H. Brush, and F. T. Mendenhall. 1991. "Assessing the Impact of Waste-Generated Gas from the Degradation of Transuranic Waste at the Waste Isolation Pilot Plant (WIPP): An Overview of Strongly Coupled Chemical, Hydrologic, and Structural Processes." *Proceedings of NEA Workshop on Gas Generation and Release from Radioactive Waste Repositories, Aix-en-Provence, France, September 23, 1991.* Organisation for Economic Co-operation and Development (OECD).

Dosch, R. G. 1979. "Radionuclide Migration Studies Associated with the WIPP Site in Southern New Mexico" in G. J. McCarthy, ed., *Scientific Basis for Nuclear Waste Management.* New York: Plenum Publishing Company 1: 395-398.

Dullien, F. A. L. 1979. *Porous Media Fluid Transport and Pore Structure.* New York: Academic Press.

Earth Technology Corporation. 1988. *Final Report for Time Domain Electromagnetic (TDEM) Surveys at the WIPP Site.* SAND87-7144. Albuquerque, NM: Sandia National Laboratories.

Fanchi, J. R., J. E. Kennedy, and D. L. Dauben. 1987. *BOASTII: A Three-Dimensional Three-Phase Black Oil Applied Simulation Tool.* DOE/BC-88/2/SP. U.S. Department of Energy.

Frederickson, A. G. 1960. "Helical Flow of an Annular Mass of Visco-Elastic Fluid." *Chemical Engineering Science* vol. II: 252-259.

Freeze, R. A. and J. C. Cherry. 1979. *Groundwater.* Englewood Cliffs, NJ: Prentice-Hall, Inc.

Gorham, E. 1990. "Data for Use in August Performance Assessment Calculations," Memo 3 in Appendix A of Rechard et al. 1990. *Data Used in Preliminary Performance Assessment of the Waste Isolation Pilot Plant (1990).* SAND89-2408. Albuquerque, NM: Sandia National Laboratories.

Gonzales, M. M. 1989. *Compilation and Comparison of Test - Hole Location Surveys in the Vicinity of the Waste Isolation Pilot Plant Site.* SAND88-1065. Albuquerque, NM: Sandia National Laboratories.

Graboski, M. S., and T. E. Daubert. 1979. "A Modified Soave Equation of State for Phase Equilibrium Calculations. 3. Systems Containing Hydrogen," in *Ind. Eng. Chem. Process Des. Dev.* vol. 18, no. 2: 300-306.

Guzowski, R. V. 1990. *Preliminary Identification of Scenarios that May Affect the Release and Transport of Radionuclides from the Waste Isolation Pilot Plant, Southeastern New Mexico.* SAND89-7149. Albuquerque, NM: Sandia National Laboratories.

Guzowski, R. V. 1991. *Applicability of Probability Techniques to Determining the Probability of Occurrence of Potentially Disruptive Intrusive Events at the Waste Isolation Pilot Plant.* SAND90-7100. Albuquerque, NM: Sandia National Laboratories.

Harms, J. C., and C. R. Williamson. 1988. "Deep-water Density Current Deposits of Delaware Mountain Group (Permian), Delaware Basin, Texas and New Mexico." *American Association of Petroleum Geologists Bulletin* vol. 72, no. 3: 299-317.

Harr, M. E. 1987. *Reliability Based Design in Civil Engineering.* New York: McGraw Hill Book Co.

Haug, A., V. A. Kelley, A. M. LaVenue, and J. F. Pickens. 1987. *Modeling of Groundwater Flow in the Culebra Dolomite at the Waste Isolation Pilot Plant (WIPP) Site: Interim Report.* Contractor Report SAND86-7167. Albuquerque, NM: Sandia National Laboratories.

Helton, J. C., J. M. Griesmeyer, F. E. Haskin, R. L. Iman, C. N. Amos, and W. B. Murfin. 1988. "Integration of the NUREG-1150 Analyses: Calculation of Risk and Propagation of Uncertainties." *Proceedings of the Fifteenth Water Reactor Safety Research Information Meeting, Washington, D.C.* U.S. Nuclear Regulatory Commission. 151-176.

Helton. J. C., J. W. Garner, R. D. McCurley, and D. K. Rudeen. 1991. *Sensitivity Analysis Techniques and Results for Performance Assessment at the Waste Isolation Pilot Plant.* Contractor Report SAND90-7103. Albuquerque, NM: Sandia National Laboratories.

Henderson, F. M. 1966. *Open Channel Flow.* New York: Macmillan Publishing Co.

Hills, J. M. 1984. "Sedimentation, Tectonism, and Hydrocarbon Generation in Delaware Basin, West Texas and Southeastern New Mexico." *American Association of Petroleum Geologist Bulletin* **68**: 250-267.

Hiss, W. L. 1975. *Stratigraphy and Ground-Water Hydrology of the Capitan Aquifer, Southeastern New Mexico and West Texas.* Ph.D. Dissertation. Hydrology Dept, University of Colorado, Boulder.

Holcomb, D. J., and M. Shields. 1987. *Hydrostatic Creep Consolidation of Crushed Salt with Added Water.* SAND87-1990. Albuquerque, NM: Sandia National Laboratories.

Holt, R. M., and D. W. Powers. 1988. *Facies Variability and Post-Depositional Alteration Within the Rustler Formation in the Vicinity of the Waste Isolation Pilot Plant, Southeastern New Mexico.* DOE-WIPP 88-004. Carlsbad, NM: U.S. Department of Energy.

Holt, R. M., and D. W. Powers. 1990. *Geologic Mapping of the Air Intake Shaft at the Waste Isolation Pilot Plant.* DOE-WIPP 90-051. Carlsbad, NM: U.S. Department of Energy.

Hora, S. C., and R. L. Iman. 1989. "Expert Opinion in Risk Analysis: The NUREG-1150 Methodology." *Nuclear Science and Engineering* **102**: 323-331.

Hora, S. C., D. von Winterfeldt, and K. M. Trauth. 1991. *Expert Judgment on Inadvertent Human Intrusion into the Waste Isolation Pilot Plant.* SAND90-3063. Albuquerque, NM: Sandia National Laboratories.

HP (Hewlett-Packard). 1984. *Petroleum Fluids PAC for HP-41C.* Corvallis, OR: Hewlett-Packard.

HSWA. 1984. *Hazardous and Solid Waste Amendments of 1984.* Pub. L. No. 98-616.

Hunter, R. L. 1985. *A Regional Water Balance for the Waste Isolation Pilot Plant (WIPP) Site and Surrounding Area.* SAND84-2233. Albuquerque, NM: Sandia National Laboratories.

Hunter, R. L. 1989. *Events and Processes for Constructing Scenarios for the Release of Transuranic Waste from the Waste Isolation Pilot Plant, Southeastern New Mexico.* SAND89-2546. Albuquerque, NM: Sandia National Laboratories.

Hunter, R. L., and C. J. Mann, eds. 1989. *Techniques for Determining Probabilities of Events and Processes Affecting the Performance of Geologic Repositories: Literature Review.* Vol. 1. SAND86-0196, NUREG/CR-3964. Albuquerque, NM: Sandia National Laboratories.

Huyakorn, P. S., H. O. White, Jr., and S. Panday. 1989. STAFF2D. Herndon, VA: Hydrogeologic, Inc.

IAEA (International Atomic Energy Agency). 1989. *Evaluating the Reliability of Predictions Made Using Environmental Transfer Models.* Safety Series Report No. 100. Vienna: International Atomic Energy Agency.

Ibrahim, M. A., M. R. Tek, and D. L. Katz. 1970. *Threshold Pressure in Gas Storage.* Arlington, VA: American Gas Association, Inc.

ICRP, Pub 38. 1983. Radionuclide Transformations Energy and Intensity of Emissions, ICRP Publication 38, *Annals of the International Commission on Radiological Protection (ICRP),* Vols. 11-13.

IDB (Integrated Data Base). 1987. *1987 Integrated Data Base: Spent Fuel and Radioactive Waste Inventories, Projection and Characteristics, DOE/RW-0006 Revision 3.* Oak Ridge, TN: Oak Ridge National Laboratory for U.S. Department of Energy.

IDB (Integrated Data Base). 1988. *1988 Integrated Data Base: Spent Fuel and Radioactive Waste Inventories, Projection and Characteristics, DOE/RW-0006 Revision 4.* Oak Ridge, TN: Oak Ridge National Laboratory for U.S. Department of Energy.

IDB (Integrated Data Base). 1990. *1990 Integrated Data Base: Spent Fuel and Radioactive Waste Inventories, Projection and Characteristics, DOE/RW-0006 Revision 6.* Oak Ridge, TN: Oak Ridge National Laboratory for U.S. Department of Energy.

Iman, R. L., and W. J. Conover. 1980. "Small Sample Sensitivity Analysis Techniques for Computer Models, with and Application to Risk Assessment." *Communications in Statistics A9:* 1749-1842. Rejoinder to comments, pp. 1863-74.

Iman, R. L., and J. C. Helton. 1985. *A Comparison of Uncertainty and Sensitivity Analysis Techniques for Computer Models.* SAND84-1461, NUREG/CR-3904. Albuquerque, NM: Sandia National Laboratories.

Imbrie, J., and J. Z. Imbrie. 1980. "Modeling the Climatic Response to Orbital Variations," *Science* **207**: 943-953.

Iuzzolino, H. J. 1983. *Equation of State Development from Shock Tube Calculations.* AFWL TR 82-57. Kirtland AFB, NM: Air Force Weapons Laboratory.

Johnson, N. L., and S. Kotz, 1970a. *Continuous Univariate Distributions-1.* New York: John Wiley & Sons.

Johnson, N. L., and S. Kotz, 1970b. *Continuous Univariate Distributions-2.* New York: John Wiley & Sons.

Jouzel, J., C. Lorius, J. R. Petit, C. Genton, N. I. Barkow, V. M. Kotlyakov, and V. M. Petrov. 1987. "Vostok Ice Core; A Continuous Isotope Temperature Record Over the Last Climatic Cycle (160,000 Years)." *Nature* **329**: 403-408.

Kaplan, S., and B. J. Garrick. 1981. "On the Quantitative Definition of Risk," *Risk Analysis* **1**: 11-27.

Kaufman, D. W., ed. 1960. *Sodium Chloride, the Production and Properties of Salt and Brine*, Monograph No. 145. Washington, DC: American Chemical Society.

Kelley, V. A., and J. F. Pickens. 1986. *Interpretation of the Convergent-Flow Tracer Tests Conducted in the Culebra Dolomite at the H-3 and H-4 Hydropads at the Waste Isolation Pilot Plant (WIPP) Site*. SAND86-7161. Albuquerque, NM: Sandia National Laboratories.

Kelley, V. A., and G. J. Saulnier, Jr. 1990. *Core Analysis for Selected Samples from the Culebra Dolomite at the Waste Isolation Pilot Plant Site*. SAND90-7011. Albuquerque, NM: Sandia National Laboratories.

Kipp, K. L. 1987. *HST3D: A Computer Code for Simulation of Heat and Solute Transport in Three-Dimensional Groundwater Flow Systems*. WRIR 86-4095. Denver, CO: U.S. Geological Survey.

Knapp, H., R. Doring, L. Oellrich, U. Plocker, and J. M. Prausnitz. 1982. "Vapor-Liquid Equilibria for Mixtures of Low Boiling Substances" in *Chemistry Data Series*, Vol. 6. DECHEMA

Krauskopf, K. B. 1986. "Thorium and Rare-Earth Metals as Analogs for Actinide Elements" in *Chemical Geology* **55**: 323-336.

Krieg, R. D. 1984. *Reference Stratigraphy and Rock Properties for the Waste Isolation Pilot Plant (WIPP) Project*. SAND83-1908. Albuquerque, NM: Sandia National Laboratories.

Krumhansl, J. L., K. M. Kimball, and C. L. Stein. 1991. *Intergranular Fluid Compositions from the Waste Isolation Pilot Plant (WIPP), Southeastern New Mexico*. SAND90-0584. Albuquerque, NM: Sandia National Laboratories.

Lallemand-Barres, J. and P. Peaudecerf. 1978. Recherche des Relations Entre les Valeurs Mesurèesde la Dispersivitè Macroscropique d'un Milieu Aquifère, Ses Autres Charactèristiques et ales Conditions de Mesure. Eude Bibliograaphique. *Rech. Bull. Bur. Geol. Min.* Sèr. 2, Sec. III, 4-1978. 277-284.

Lambert, S. J., and J. A. Carter. 1987. *Uranium-Isotope Systematics in Groundwaters of the Rustler Formation, Northern Delaware Basin, Southeastern New Mexico*. SAND87-0388. Albuquerque, NM: Sandia National Laboratories.

Lambert, S. J., and D. M. Harvey. 1987. *Stable-Isotope Geochemistry of Groundwater in the Delaware Basin of Southeastern New Mexico*. SAND87-0138. Albuquerque, NM: Sandia National Laboratories.

Langmuir, D., and J. S. Herman. 1980. "The Mobility of Thorium in Natural Waters at Low Temperatures." *Geochimica et Cosmochimica Acta* **44**: 1753-1766.

Langmuir, D., and A. C. Riese. 1985. "The Thermodynamic Properties of Radium." *Geochimica et Cosmochimica Acta* **49**: 1593-1601.

Lappin, A. R. 1988. *Summary of Site Characterization Studies Conducted from 1983 through 1987 at Waste Isolation Pilot Plant (WIPP) Site, Southeastern New Mexico*. SAND88-0157. Albuquerque, NM: Sandia National Laboratories.

Lappin, A. R., R. L. Hunter, D. P. Garber, and P. B. Davies, eds. 1989. *Systems Analysis Long-Term Radionuclide Transport, and Dose Assessments, Waste Isolation Pilot Plant (WIPP), Southeastern New Mexico; March 1989.* SAND89-0462. Albuquerque, NM: Sandia National Laboratories.

LaVenue, A. M., A. Haug, and V. A. Kelley. 1988. *Numerical Simulation of Ground-Water Flow in the Culebra Dolomite at the Waste Isolation Pilot Plant (WIPP) Site: Second Interim Report.* SAND88-7002. Albuquerque, NM: Sandia National Laboratories.

LaVenue, A. M., T. L. Cauffman, and J. F. Pickens. 1990. *Ground-Water Flow Modeling of the Culebra Dolomite. Volume I: Model Calibration.* SAND89-7068. Albuquerque, NM: Sandia National Laboratories.

Leckie, J. O. 1989. "Simulations of Distribution Coefficients Using Surface Complexation Models," Appendix C in M.D. Siegel, ed., *Progress in Development of a Methodology for Geochemical Sensitivity Analysis for Performance Assessment: Volume 2. Speciation, Sorption, and Transport in Fractured Media*, Letter Report to the U.S. Nuclear Regulatory Commission.

Li, Y., and S. Gregory. 1974. "Diffusion of Ions in Seawater and in Deep-Sea Sediments," *Geochimica et Cosmochimica Acta.* **38**: 703-714.

Lynch, A. W., and R. G. Dosch. 1980. *Sorption Coefficients for Radionuclides on Samples from the Water-Bearing Magenta and Culebra Members of the Rustler Formation.* SAND80-1064. Albuquerque, NM: Sandia National Laboratories.

McKay, M. D., W. J. Conover, and R. J. Beckman. 1979. "A Comparison of Three Methods for Selecting Values of Input Variables in the Analysis of OUtput from a Computer Code" in *Techometrics*, vol. 21, no. 2.

Mann, C. J., and R. L. Hunter. 1988. "Probabilities of Geologic Events and Processes in Natural Hazards." *Zeitschrift fuer Geomorphologie* N.F. **67:** 39-52.

Marietta, M. G., S. G. Bertram-Howery, D. R. Anderson, K. F. Brinster, R. V. Guzowski, H. J. Iuzzolino, and R. P. Rechard. 1989. *Performance Assessment Methodology Demonstration: Methodology Development for Purposes of Evaluating Compliance with EPA 40 CFR 191, Subpart B, for the WIPP.* SAND89-2027. Albuquerque, NM: Sandia National Laboratories.

Marsily, G. de. 1986. *Quantitative Hydrogeology: Groundwater Hydrology for Engineers.* Orlando, FL: Academic Press, Inc.

Matalucci, R. V. 1987. *In Situ Testing at the Waste Isolation Pilot Plant.* SAND87-2382. Albuquerque, NM: Sandia National Laboratories.

Mercer, J. W. 1983. *Geohydrology of the Proposed Waste Isolation Pilot Plant Site, Los Medaños Area, Southeastern New Mexico.* U.S. Geological Survey Water Resources Investigation 83-4016.

Mercer, J. W., and B. R. Orr. 1979. *Interim Data Report on the Geohydrology of the Proposed Waste Isolation Pilot Plant Site, Southeastern New Mexico.* USGS Water-Resources Investigations 79-98. Albuquerque, NM: U.S. Geological Survey.

Mercer, J. W., R. L. Beauheim, R. P. Snyder, and G. M. Fairer. 1987. *Basic Data Report for Drilling and Hydrologic Testing of Drillhole DOE-2 at the Waste Isolation Pilot Plant (WIPP) Site.* SAND86-0611. Albuquerque, NM: Sandia National Laboratories.

Miller, D. G. 1982. *Estimation of Tracer Diffusion Coefficients of Ions in Aqueous Solution.* UCRL-53319. Livermore, CA: Lawrence Livermore National Laboratory.

Miller, I., and J. E. Freund. 1977. *Probabilities and Statistics for Engineers.* 2nd ed. Englewood Cliffs, NJ: Prentice-Hall.

Molecke, M. A. 1979. *Gas Generation from Transuranic Waste Degradation: Data Summary and Interpretation.* SAND79-1245. Albuquerque, NM: Sandia National Laboratories.

Munson, D. E., A. F. Fossum, and P. E. Senseny. 1989. *Advances in Resolution of Discrepancies between Predicted and Measured In Situ Room Closures.* SAND88-2948. Albuquerque, NM: Sandia National Laboratories.

Munson, D. E., J. R. Ball, and R. L. Jones. 1990a. "Data Quality Assurance Controls through the WIPP In Situ Data Acquisition, Analysis and Management System" in *Proceedings of the International High-Level Radioactive Waste Management Conference, Las Vegas, NV, April 8-12.* Sponsored by American Nuclear Society and ASCE, New York, pp. 1337-1350.

Munson, D. E., R. V. Matalucci, J. R. Ball, and R. L. Jones. 1990b. *WIDSAAM: The WIPP In Situ Data Acquisition, Analysis, and Management System.* SAND87-2258. Albuquerque, NM: Sandia National Laboratories.

Munson, D. E., K. L. DeVries, and G. D. Gallahan. 1990c. "Comparison of Calculations and In Situ Results for a Large, Heated Test Room at the Waste Isolation Pilot Plant (WIPP)." *Proceedings of 31th U.S. Symposium on Rock Mechanics, Golden, CO, June 18-20.*

NEPA. 1969. National Environmental Policy Act of 1969. Pub. L. No. 91-190, 83 Stat. 852.

Neretnieks, I., and A. Rasmussen. 1984 "An Approach to Modeling Radionuclide Migration in a Medium with Strongly Varying Velocity and Block Sizes along the Flow Path," *Water Resources Research* vol. 20, no. 12: 1823-1836.

Novak, C. F. 1991. *An Evaluation of Radionuclide Batch Sorption Data on Culebra Dolomite for Aqueous Compositions Relevant to the Human Intrusion Scenario for the Waste Isolation Pilot Plant (WIPP).* SAND91-1299. Albuquerque, NM: Sandia National Laboratories.

Nowak, E. J., and J. C. Stormont. 1987. *Scoping Model Calculations of the Reconsolidation of Crushed Salt in WIPP Shafts.* SAND87-0879. Albuquerque, NM: Sandia National Laboratories.

Nowak, E. J., and L. D. Tyler. 1989. "The Waste Isolation Pilot Plant (WIPP) Seal System Performance Program," *Proceedings of the Joint NEA/CEC Repositories, Braunschweig, FRG, May 22-25, 1989.*

Nowak, E. J., D. F. McTigue, and R. Beraun. 1988. *Brine Inflow to WIPP Disposal Rooms: Data, Modeling and Assessment.* SAND88-0112. Albuquerque, NM: Sandia National Laboratories.

Nowak, E. J., J. R. Tillerson, and T. M. Torres. 1990. *Initial Reference Seal System Design: Waste Isolation Pilot Plant (WIPP).* SAND90-0355. Albuquerque, NM: Sandia National Laboratories.

Numbere, D., W. E. Grigham, and M. B. Standing. 1977. *Correlations for Physical Properties of Petroleum Reservoir Brines.* Palo Alto, CA: Petroleum Research Institute, Stanford University.

OCD. 1988. *State of New Mexico, Energy, Minerals, and Natural Resources Department, Oil Conservation Commission of Oil Conservation Division*, Order No. R-111-P, April 21, 1988.

Oldroyd, J. G. 1958. *Proceedings of the Royal Society (London)* **A245**: 278.

Pace, R. O. 1990. Manager, Technology Exchange Technical Services, Baroid Drilling Fluids, Inc., 3000 N. Sam Houston Pkwy. E., Houston, Texas. (Expert Opinion). Letter 1b in Appendix A of Rechard et al. 1990. *Data Used in Preliminary Performance Assessment of the Waste Isolation Pilot Plant (1990).* SAND89-2408. Albuquerque, NM: Sandia National Laboratories.

Paine, R. T. 1977. *Chemistry Related to the WIPP Site, Draft Final Report*, Sandia Contract GTK/07-1488. Albuquerque, NM: Chemistry Department, University of New Mexico.

Palmer, A. R. 1983. *The Decade of North American Geology, 1983 Geologic Time Scale.* Geological Society of North America.

Parry, G. W. 1988. "On the Meaning of Probability in Probabilistic Safety Assessment." *Reliability Engineering and System Safety* **23**: 309-314.

Parthenaides, E., and R. E. Paaswell. 1970. "Erodibility of Channels with Cohesive Boundary," *Proceedings of the American Society of Civil Engineers, Journal of the Hydraulics Division*, **99**: 555-558.

Paté-Cornell, M. E. 1986. "Probability and Uncertainty in Nuclear Safety Decisions." *Nuclear Engineering and Design* **93**: 319-327.

Perry, R. H., C. H. Chilton, and S. D. Kirkpatrick. 1969. *Chemical Engineer's Handbook.* New York: McGraw-Hill Book Company.

Peterson, A. C. 1990. "Preliminary Contact Handled (CH) and Remote Handled (RH) Radionuclide Inventories," Memo 7 in Appendix A of Rechard et al. 1990. *Data Used in Preliminary Performance Assessment of the Waste Isolation Plant (1990).* SAND89-2408. Albuquerque, NM: Sandia National Laboratories.

Pickens, J. F., and G. E. Grisak. 1981. "Modeling of Scale-Dependent Dispersion in Hydrolgeologic Systems." *Water Resources Research* vol. 17, no. 6: 1701-11.

Popielak, R. S., R. L. Beauheim, S. R. Black, W. E. Coons, C. T. Ellingson, and R. L. Olsen. 1983. *Brine Reservoirs in the Castile Formation, Southeastern New Mexico, Waste Isolation Pilot Plant (WIPP) Project.* TME-3153. Carlsbad, NM: U.S. Department of Energy.

Powers, D. W., S. J. Lambert, S. E. Shaffer, L. R. Hill, and W. D. Weart, ed. 1978. *Geological Characterization Report, Waste Isolation Pilot Plant (WIPP) Site, Southeastern New Mexico.* SAND78-1596, vols. 1 and 2. Albuquerque, NM: Sandia National Laboratories.

Prausnitz, J. M. 1969. *Molecular Thermodynamics of Fluid-Phase Equilibria.* Englewood Cliffs, NJ: Prentice-Hall, Inc.

Public Law 96-164. 1979. *Department of Energy National Security and Military Applications of Nuclear Energy Authorization Act of 1980.*

RCRA. 1976. *Resource, Conservation, and Recovery Act of 1976.* Pub. L. No. 94-580, 90 Stat. 2795.

Rechard, R. P. 1989. *Review and Discussion of Code Linkage and Data Flow in Nuclear Waste Compliance Assessments.* SAND87-2833. Albuquerque, NM: Sandia National Laboratories.

Rechard, R. P., H. J. Iuzzolino, J. S. Rath, R. D. McCurley, and D. K. Rudeen. 1989. *User's Manual for CAMCON: Compliance Assessment Methodology Controller.* SAND88-1496. Albuquerque, NM: Sandia National Laboratories.

Rechard, R. P., H. J. Iuzzolino, and J. Sandha. 1990a. *Data Used in Preliminary Performance Assessment at the Waste Isolation Pilot Plant (1990).* SAND89-2408. Albuquerque, NM: Sandia National Laboratories.

Rechard, R. P., W. Beyeler, R. D. McCurley, D. K. Rudeen, J. E. Bean, and J. D. Schreiber. 1990b. *Parameter Sensitivity Studies of Selected Components of the Waste Isolation Pilot Plant Repository/Shaft System.* SAND89-2030. Albuquerque, NM: Sandia National Laboratories.

Reeves, M., G. Freeze, V. Kelly, J. Pickens, D. Upton, and P. Davies. 1991. *Regional Double-Porosity Solute Transport in the Culebra Dolomite under Brine-Reservoir-Breach Release Conditions: An Analysis of Parameter Sensitivity and Importance.* SAND89-7069. Albuquerque, NM: Sandia National Laboratories.

Rice, J. R., and M. P. Cleary. "Stress Diffusion Solutions for Fluid-Saturated Elastic Porous Media with Compressible Constituents." *Review of Geophysics and Space Physics* vol. 14, no. 2 (May 1976): 227-241.

Richey, S. F., J. G. Wells, K. T. Stephens. 1985. *Geohydrology of the Delaware Basin and Vicinity, Texas and New Mexico.* U.S. Geological Survey Water Resources Investigations Report 84-4077. Washington, DC: U.S. Geological Survey.

Riese, A. C. 1982. "Adsorption of Radium and Thorium onto Quartz and Kaolinite: A Comparison of Solution/Surface Equilibria Models," Ph.D. Thesis. Colorado School of Mines, Golden, CO.

Rose, W., and W. A. Bruce. 1949. "Evaluation of Capillary Character in Petroleum Reservoir Rock." *Transactions of the American Institute of Mining and Metallurgical Engineers* **186:** 127-142.

Ross, S. M. 1985. *Introduction to Probability Models.* 3rd ed. New York: Academic Press, Inc.

Ross, B. 1989. "Scenarios for Repository Safety Analysis." *Engineering Geology* **26:** 285-299.

Sargunam, A., P. Riley, K. Arulanadum, and R. B. Krone. 1973. "Physico-Chemical Factors in Erosion of Cohesive Soils." *Journal of the Hydraulics Division, American Society of Civil Engineers* **99**: 555-558.

Saulnier, G. J., Jr. 1987. *Analysis of Pumping Tests of the Culebra Dolomite Conducted at the H-11 Hydropad at the Waste Isolation Pilot Plant (WIPP) Site.* SAND87-7124. Albuquerque, NM: Sandia National Laboratories.

Savins, J. G., and G. C. Wallick. 1966. "Viscosity Profiles, Discharge Rates, Pressures, and Torques for a Rheologically Complex Fluid in Helical Flow." *A.I.Ch.E. Journal* vol. 12, no. 2 (March 1966).

Scheetz, B. E., P. H. Licastro, and D. M. Roy. 1986. *A Full Scale Borehole Sealing Test in Anhydrite Under Simulated Downhole Conditions*, vols. 1 and 2. BMI/ONWI-573(2). Columbus, OH: Office of Nuclear Waste Isolation, Battelle Memorial Institute.

Shakoor, A., and H. R. Hume. 1981. *Physical Properties Data for Rock Salt: Chapter 3, Mechanical Properties, NBS Monograph 167.* Washington, DC: National Bureau of Standards: 103-203.

Siegel, M. D. 1990. "Representation of Radionuclide Retardation in the Culebra Dolomite in Performance Assessment Calculations," Memo 3a in Appendix A of Rechard et al. 1990. *Data Used in Preliminary Performance Assessment of the Waste Isolation Pilot Plant (1990).* SAND89-2408. Albuquerque, NM: Sandia National Laboratories.

Sjaardema, G. D., and R. D. Krieg. 1987. *A Constitutive Model for the Consolidation of WIPP Crushed Salt and Its Use in Analysis of Backfilled Shaft and Drift Configurations.* SAND87-1977. Albuquerque, NM: Sandia National Laboratories.

Skokan, C., J. Starrett, and H. T. Andersen. 1988. *Final Report: Feasibility Study of Seismic Tomography to Monitor Underground Pillar Integrity at the WIPP Site.* SAND88-7096. Albuquerque, NM: Sandia National Laboratories.

SNL (Sandia National Laboratories). 1979. *Summary of Research and Development Activities in Support of Waste Acceptance Criteria for the WIPP.* SAND79-1305. Albuquerque, NM: Sandia National Laboratories.

SNL (Sandia National Laboratories) and U.S. Geological Survey. 1982a. *Basic Data Report for Drillhole WIPP 11 (Waste Isolation Pilot Plant - WIPP).* SAND79-0272. Albuquerque, NM: Sandia National Laboratories.

SNL (Sandia National Laboratories) and U.S. Geological Survey. 1982b. *Basic Data Report for Drillhole ERDA 9 (Waste Isolation Pilot Plant - WIPP).* SAND79-0270. Albuquerque, NM: Sandia National Laboratories.

SNL (Sandia National Laboratories) and D'Appolonia Consulting Engineers. 1983. *Basic Data Report for Drillhole WIPP 12 (Waste Isolation Pilot Plant - WIPP).* SAND82-2336. Albuquerque, NM: Sandia National Laboratories.

Stone, W. J. 1984. *Recharge in the Salt Lake Coal Field Based on Chloride in the Unsaturated Zone.* Open File Report 214. Socorro, NM: New Mexico Bureau of Mines and Mineral Resources.

Streeter, V. L., and E. B. Wylie. 1975. *Fluid Mechanics.* 6th ed. New York: McGraw-Hill Book Co.

Sutherland, H. J., and S. Cave. 1978. *Gas Permeability of SENM Rock Salt.* SAND78-2287. Albuquerque, NM: Sandia National Laboratories.

Swanson, J. L., 1986. *Organic Complexant-Enhanced Mobility of Toxic Elements in Low-Level Wastes: Final Report.* NUREG/CR-4660, PNL-4965-10. Richland, WA: Pacific Northwest Laboratory.

Thomas, L. K., D. L. Katz, and M. R. Tek. 1968. "Threshold Pressure Phenomena in Porous Media." *Society of Petroleum Engineers Journal* vol. 8, no. 2: 174-184.

Tien, P. L., F. B. Nimick, A. B. Muller, P. A. Davis, R. V. Guzowski, L. E. Duda, and R. L. Hunter. 1983. *Repository Site Data and Information in Bedded Salt: Palo Duro Basin, Texas.* SAND82-2223, NUREG/CR-3129. Albuquerque, NM: Sandia National Laboratories.

Tierney, M. S. 1990a. *Constructing Probability Distributions of Uncertain Variables in the Models of the Performance of the Waste Isolation Pilot Plant (WIPP).* SAND90-2510. Albuquerque, NM: Sandia National Laboratories.

Tierney, M. S. 1990b. "Values of Room Porosity and Hydraulic Conductivity," Memo 6 in Appendix A of Rechard et al. 1990. *Data Used in Preliminary Performance Assessment of the Waste Isolation Pilot Plant (1990).* SAND89-2408. Albuquerque, NM: Sandia National Laboratories.

Tierney, M. S. 1991. *Combining Scenarios in a Calculation of the Overall Probability Distribution of Cumulative Releases of Radioactivity from the Waste Isolation Pilot Plant, Southeastern New Mexico.* SAND90-0838. Albuquerque, NM: Sandia National Laboratories.

Tomovic, R. 1963. *Sensitivity Analysis of Dynamic Systems.* New York: McGraw Hill.

Torstenfelt, B., H. Kipatsi, K. Anderson, B. Allard, and U. Olofsson. 1982. "Transport of Actinides Through a Bentonite Backfill" in W. Lutze, ed., *Scientific Basis for Radioactive Waste Management V.* New York: Elsevier Science Publishing Co.

Trauth, K. M., S. C. Hora, and R. P. Rechard. 1991. "Expert Judgment as Input to Waste Isolation Pilot Plant Performance-Assessment Calculations: Probability Distributions of Significant System Parameters" in *Proceedings of the First International Mixed Waste Symposium, Baltimore, MD, August 26-29, 1991.*

Tyler, L. D., R. V. Matalucci, M. A. Molecke, D. E. Munson, E. J. Nowak, and J. C. Stormont. 1988. *Summary Report for the WIPP Technology Development Program for Isolation of Radioactive Waste.* SAND88-0844. Albuquerque, NM: Sandia National Laboratories.

U.S. DOE (Department of Energy). 1982a. *Basic Data Report for Borehole DOE-1, Waste Isolation Pilot Plant (WIPP) Project, Southeastern New Mexico.* TME 3159. Albuquerque, NM: Sandia National Laboratories.

U.S. DOE (Department of Energy). 1982b. *Basic Data Report for Borehole WIPP-12 Deepening, Waste Isolation Pilot Plant (WIPP) Project, Southeastern, New Mexico.* TME 3148. Albuquerque, NM: Sandia National Laboratories.

U.S. DOE (Department of Energy). 1983a. Drawing number 35-R-004-01D Rev. A. San Francisco, CA: Bechtel National, Inc.

U.S. DOE (Department of Energy). 1983b. Drawing number 31-R-013-01D Rev. A. San Francisco, CA: Bechtel National, Inc.

U.S. DOE (Department of Energy). 1987a. *Radioactive Source Term for Use at the Waste Isolation Pilot Plant.* DOE/WIPP88-005. In preparation.

U.S. DOE (Department of Energy). 1987b. Drawing number 33-R-012-34A Rev. 5. San Francisco, CA: Bechtel National, Inc.

U.S. DOE (Department of Energy). 1989a. *Waste Isolation Pilot Plant Compliance Strategy for 40 CFR Part 191.* WIPP-DOE-86-013. Carlsbad, NM: U.S. Department of Energy.

U.S. DOE (Department of Energy). 1989b. *Addendum to No-Migration Variance Petition for WIPP.* DOE/WIPP 89-003. Carlsbad, NM: U.S. Department of Energy.

U.S. DOE (Department of Energy). 1990a. *WIPP Test Phase Plan: Performance Assessment.* DOE/WIPP 89-011, Rev. O. Carlsbad, NM: U.S. Department of Energy.

U.S. DOE (Department of Energy). 1990b. *Final Supplemental Environmental Impact Statement, Waste Isolation Pilot Plant.* DOE/EIS-0026-FS. Washington, DC: U.S. Department of Energy, Office of Environmental Restoration and Waste Management.

U.S. DOE (Department of Energy). 1990c. *Geologic Mapping of the Air Intake Shaft at the Waste Isolation Pilot Plant.* DOE-WIPP-90-051. Albuquerque, NM: IT Corporation.

U.S. DOE (Department of Energy). 1990d. *Final WIPP Safety Analysis Report, Waste Isolation Pilot Plant.* Carlsbad, NM: U.S. Department of Energy.

U.S. DOE (Department of Energy). 1991. *Recommended Strategy for the Remote-Handled Transuranic Waste Program.* DOE/WIPP 90-058, Revision 1. Carlsbad, NM: Waste Isolation Pilot Plant.

U.S. DOE (Department of Energy) and State of New Mexico. 1984. U.S. Department of Energy and State of New Mexico, 1981, First Modification to the July 1, 1981 "Agreement for Consultation and Cooperation" on WIPP by the State of New Mexico and U.S. Department of Energy, November 30, 1984.

U.S. NRC (Nuclear Regulatory Commission). 1990. *Severe Accident Risks: An Assessment of Five U.S. Nuclear Power Plants.* Summary Report of NUREG 1150. Washington, D.C.: U.S. Nuclear Regulatory Commission.

Vargaftik, N. B. 1975. *Tables on the Thermophysical Properties of Liquids and Gases in Normal and Dissociated States.* New York: John Wiley & Sons, Inc.

Vennard, J. K., and R. L. Street. 1975. *Elementary Fluid Mechanics*, 5th ed. New York: John Wiley & Sons.

Vesely, W. E., and D. M. Rasmuson. 1984. "Uncertainties in Nuclear Probabilistic Risk Analyses." *Risk Analysis* **4**: 313-322.

Voss, C. I. 1984. *SUTRA (Saturated-Unsaturated TRAnsport): A Finite-Element Simulation Model for Saturated-Unsaturated Fluid Density Dependent Groundwater Flow and Energy Transport or Chemically Reactive Single Species Solute Transport.* Reston, VA: U.S. Geological Survey National Center.

Walas, S. M. 1985. *Phase Equilibrium in Chemical Engineering.* Boston, MA: Butterworth Publishers. 52-54.

Walker, R. E., and W. E. Holman. 1971. "Computer Program Predicting Drilling-Fluid Performance." *Oil and Gas Journal* (March 29, 1971): 80-90.

Ward, J. S., and N. R. Morrow. 1985. "Capillary Pressures and Gas Permeabilities of Low-Permeability Sandstone." SPE/DOE 13882. Paper presented at the *SPE/DOE 1985 Low Permeability Gas Reservoirs, Denver, CO, May 19-22, 1985.*

Ward, R. G., C. G. St. C. Kendall, and P. M. Harris. 1986. "Upper Permian (Guadalupian) Facies and Their Association with Hydrocarbons - Permian Basin, West Texas and New Mexico." *American Association of Petroleum Geologists Bulletin* **70**: 239-262.

Wawersik, W. R., and C. M. Stone. 1985. *Application of Hydraulic Fracturing to Determine Virgin In Situ Stress Around Waste Isolation Pilot Plant--In Situ Measurements.* SAND85-1776. Albuquerque, NM: Sandia National Laboratories.

Weast, R. C., and M. J. Astle, eds. 1981. *Handbook of Chemistry and Physics.* 62nd ed. Cleveland, OH: CRC Press.

WEC (Westinghouse Electric Corporation). 1985a. *TRU Waste Acceptance Criteria for the Waste Isolation Pilot Plant,* Revision 2. WIPP-DOE-069-Rev. 2. Carlsbad, NM: Westinghouse Electric Corporation.

WEC (Westinghouse Electric Corporation). 1989. *TRU Waste Acceptance Criteria for the Waste Isolation Pilot Plant,* Revision 3. WIPP-DOE-069-Rev. 2. Prepared for U.S. Department of Energy. Carlsbad, NM: Westinghouse Electric Corporation.

WEC (Westinghouse Electric Corporation). 1990. *Waste Isolation Pilot Plant No-Migration Variance Petition.* DOE/WIPP 89-003. Prepared for U.S. Department of Energy. Carlsbad, NM: Westinghouse Electric Corporation.

Williamson, C. R. 1978. *Depositional Processes, Diagenesis and Reservoir Properties of Permian Deep-Sea Sandstone, Bell Canyon Formation,* Ph.D. Dissertation. University of Texas, Austin, TX.

WIPP Act. 1980. *Department of Energy National Security and Military Applications of Nuclear Energy Authorization Act of 1980, Title II - General Provisions: Waste Isolation Pilot Plant, Delaware Basin, NM.* Pub. L. No. 96-164, 93 Stat. 1259. (Clarify 79 or 80).

Wyllie, M. R. J., and W. D. Rose. 1950. "Some Theoretical Considerations Related to the Quantitative Evaluation of the Physical Characteristics of Reservoir Rock from Electric Log Data." *Transactions of the American Institute of Mining and Metallurgical Engineers* **189:** 105-118.

Yaglom, A. M. 1962. *An Introduction to the Theory of Stationary Random Functions.* Englewood Cliffs, NJ: Prentice-Hall, Inc.

40 CFR 191. Environmental Radiation Protection Standards for Management and Disposal of Spent Nuclear Fuel, High-Level, and Transuranic Radioactive Wastes. U.S. Environmental Protection Agency (EPA), Title 40 Code of Federal Regulations Part 191 (*40 CFR 191*).

APPENDIX A:
MEMORANDA REGARDING REFERENCE DATA

Referenced Memoranda

Related Memoranda

APPENDIX A:
MEMORANDA REGARDING REFERENCE DATA

Referenced Memoranda

The memoranda referenced are as follows:

Beauheim et al., June 10, 1991

Date: 6/10/91
To: D. R. Anderson (6342)
From: R. L. Beauheim (6344), T. F. Corbet (6344), P. B. Davies (6344), J. F. Pickens (INTERA)
Subject: Recommendations for the 1991 Performance Assessment Calculations on Parameter Uncertainty and Model Implementation for Culebra Transport Under Undisturbed and Brine-Reservoir-Breach Conditions

Beauheim, June 14, 1991

Date: 6/14/91
To: Rob Rechard (6342)
From: Rick Beauheim (6344)
Subject: Review of Salado Parameter Values to be Used in 1991 Performance Assessment Calculations

Brush, July 8, 1991

Date: 7/8/91
To: D. R. Anderson (6342)
From: L. H. Brush (6345)
Subject: Current Estimates of Gas Production Rates, Gas Production Potentials, and Expected Chemical Conditions Relevant to Radionuclide Chemistry for the Long-Term WIPP Performance Assessment

Davies, June 2, 1991

Date: 6/2/91
To: D. R. Anderson (6342)
From: P. B. Davies (6344)
Subject: Uncertainty Estimates for Threshold Pressure for 1991 Performance Assessment Calculations Involving Waste-Generated Gas

Drez, May 9, 1989

Date: 5/9/89
To: L. Brush (6334)
From: Paul Drez (International Technology Corporation)
Subject: Preliminary Nonradionuclide Inventory of CH-TRU Waste

Finley and McTigue, June 17, 1991

Date: 6/17/91
To: Elaine Gorham, 6344
From: S. J. Finley, 6344, and
D. F. McTigue, 1511
Subject: Parameter Estimates from the Small-Scale Brine Inflow Experiments

Howarth, June 12, 1991

Date: 6/12/91
To: Elaine Gorham (6344)
From: Susan Howarth (6344)
Subject: Pore Pressure Distributions for 1991 Performance Assessment Calculations

Howarth, June 13, 1991

Date: 6/13/91
To: Elaine Gorham (6344)
From: Susan Howarth (6344)
Subject: Permeability Distributions for 1991 Performance Assessment Calculations

McTigue et al., March 14, 1991

Date: 3/14/91
To: Distribution
From: D. F. McTigue, 1511; S. J. Finley, 6344, J. H. Gieske, 7552; K. L. Robinson, 6345
Subject: Compressibility Measurements on WIPP Brines

Novak, September 4, 1991

Date: 9/4/91
To: K. M. Trauth, 6342
From: Craig F. Novak, 6344
Subject: Rationale for K_d Values Provided During Elicitation of the Retardation Expert Panel, May 1991

Swift, October 10, 1991

Date: 10/10/91
To: R. P. Rechard
From: Peter Swift, 6342/Tech Reps
Subject: Climate and recharge variability parameters for the 1991 WIPP PA calculations

Related Memoranda

Gorham, July 2, 1991

Date: 7/2/91
To: Rob Rechard (6342)
From: Elaine Gorham (6344)
Subject: Aggregated Frequency Distributions for Permeability, Pore Pressure and Diffusivity in the Salado Formation

Anderson, October 25, 1991

Date: 10/25/91
To: File
From: D. R. (Rip) Anderson (6342)
Subject: Modifications to Reference Data for 1991 Performance Assessment

Mendenhall and Butcher, June 1, 1991

Date: 6/1/91
To: R. P. Rechard (6342)
From: F. T. Mendenhall (6345) and B. M. Butcher
Subject: Disposal room porosity and permeability values for use in the 1991 room performance assessment calculations

Siegel, July 14, 1989

Date: 7/14/89
To: P. Davies (6331) and A. R. Lappin (6331)
From: M. D. Siegel
Subject: Supplementary Information Concerning Radionuclide Retardation

Siegel, June 25, 1991

Date: 6/25/91
To: K. Trauth (6342)
From: M. D. Siegel
Subject: K_d Values for Ra and Pb

Beauheim et al., June 10, 1991

Date: 6/10/91
To: D. R. Anderson (6342)
From: R. L. Beauheim (6344), T. F. Corbet (6344), P. B. Davies (6344), J. F. Pickens (INTERA)
Subject: Recommendations for the 1991 Performance Assessment Calculations on Parameter Uncertainty and Model Implementation for Culebra Transport Under Undisturbed and Brine-Reservoir-Breach Conditions

Sandia National Laboratories

Albuquerque, New Mexico 87185

Date: June 10,1991

To: D.R. Anderson (6342)

From: R.L. Beauheim (6344)
T.F. Corbet (6344)
P.B. Davies (6344)
J. F. Pickens (INTERA)

Subject: Recommendations for the 1991 Performance Assessment Calculations on Parameter Uncertainty and Model Implementation for Culebra Transport Under Undisturbed and Brine-Reservoir-Breach Conditions

This memo provides input for modeling radionuclide transport for the 1991 Performance Assessment calculations. Recommendations are divided into two segments, one on double porosity-transport parameters and one on model implementation for brine-reservoir-breach scenarios.

Double-Porosity Transport

Several of the parameters used for double-porosity transport calculations are specific to a given transport code. We recommend that at some time, the code being used for performance assessment calculations be analyzed and benchmarked with the double-porosity transport code used to interpret tracer tests (SWIFT II, Reeves et al., 1986). Also, we note that the effect of many of the double-porosity parameters can be concisely characterized using dimensionless parameter groups (Reeves et al., 1991). We recommend that in future years, consideration be given to parameter sampling structured around dimensionless groups. This may save significant computational effort and eliminate inconsistencies associated with sampling correlated parameters.

The following comments on transport parameters follow the format in the data document for the 1990 PA calculations (Rechard et al., 1990).

Bulk Density

The values reported from laboratory analyses of Culebra core in Kelley and Saulnier, 1990 and in Lappin et al., 1989 are grain densities, not bulk densities. Correct range in text and table to 2.76×10^3 to 2.86×10^3 kg/m^3. Also correct arithmetic mean to

2.82×10^3 kg/m^3 and median to 2.83×10^3 kg/m^3. Change table source reference to Kelley and Saulnier, 1990, Tables 4.1, 4.2 and 4.3.

Dispersivity

No new information.

Fracture Spacing

The most recent results of tracer test interpretations for the H-3, H-6, and H-11 hydropads to obtain best-fit double-porosity parameters (fracture spacing and fracture porosity) are summarized in Table 1 (Cauffman, et al., in prep.). It is our opinion that there are too few data to construct a meaningful distribution for fracture spacing. Therefore, we recommend that the low end of the range be represented by the smallest fracture spacing interpreted from field experiments (0.06 meters) and be assigned to the 5th percentile. For the median value, we recommend the use of the average value from the limited number of available tests, 0.4 meters. For the upper end of the range, we recommend the continued use of the total Culebra thickness, 8 meters, and that this value be assigned to the 95th percentile.

Fracture Porosity

Fracture porosity is derived from the same analysis of tracer tests that produces fracture spacing (Table 1). Therefore, it is our opinion that there are too few data to construct a meaningful distribution for fracture porosity. Therefore, we recommend that the average value, 0.001, be used for the median of the distribution. Given the absence of additional data, the range should continue to be taken as one order of magnitude above and below this average value.

Matrix Porosity

The most comprehensive and up to date information on Culebra matrix porosity is Kelley and Saulnier, 1990. Table 2 is a list of porosity measurements on 79 core samples from 15 locations. The mean value is 0.15 and the median value is 0.14. The range is from 0.03 to 0.30. Note error in value reported in Table II-6 of SAND89-2408 where median value is reported as 15.2. This should be 0.152.

Storage Coefficient

No change from previous year. Correct reference in last sentence to LaVenue et al.,

1990, Table 2.5.

Thickness

Note error in Table II-6, where Culebra thickness is reported as 77 meters.

Tortuosity

The most comprehensive and up to date information on Culebra tortuosity is Kelley and Saulnier, 1990. Table 3 is a list of tortuosity measurement on 15 core samples from 11 locations. The mean value is 0.14 and the median value is 0.12. The range is from 0.03 to 0.3. Note that tortuosity is strongly related to fracture spacing. Dimensional analysis of Reeves et al. (1991) shows that the half-fracture spacing squared interpreted from a tracer test is inversely proportional to the assumed tortuosity. Therefore, we recommend that these parameters not be sampled independently.

Modeling of Brine-Reservoir Breach Scenarios

We have reviewed the draft text on proposed brine reservoir modeling and have the following comments:

> The discussion of the justification for the simplified representation of brine-reservoir response to a borehole should cite the analysis of Reeves et al. (1991) that develops and tests the technical basis for this assumption. Also the limitations of the simplified approach should be stated. For example, while this approach is valid for time scales of less than 10,000 years, for longer time periods, there is increased sensitivity to intact Castile properties (transmissivity and storage).
>
> The rationale for estimating a range of initial pressures is unnecessarily complex and may not be defensible. As an alternative approach, we suggest the following. The data show that pressures in the brine pockets are all greater than or equal to hydrostatic. No upper limit is indicated by the data, however lithostatic pressure is a defensible limit. Therefore, we suggest using the range from hydrostatic to lithostatic, calculated for the depth of the brine pocket at WIPP 12. This range is approximately 11 to 22 MPa (which compares with 10.4 to >16.6 MPa for the original approach).
>
> One general comment is that for technical accuracy, this discussion should cite original sources rather that second or third generation material.

cc: W.D. Weart (6340)
M.G. Marietta (6342)
R.P. Rechard (6342)
E.D. Gorham (6344)

Path	Interpreted Parameters (1)		Assumed Parameters (2)		
	Fracture Porosity	Fracture Spacing	Matrix Porosity	Tortuosity	Dispersivity
H-3 Test					
H-3b1 to H-3b3	1.2E-3	1.2 m	0.20	0.15	1.5 m
H-3b2 to H-3b3	1.2E-3	0.23 m	0.20	0.15	1.5 m
H-6 Test #1					
H-6b to H-6c	1.5E-3	0.41 m	0.16	0.15	1.5 m
H-6a to H-6c	1.5E-3	0.056 m	0.16	0.15	1.5 m
H-6 Test #2					
H-6b to H-6c	1.5E-3	0.44 m	0.16	0.15	1.5 m
H-11 Test					
H-11b3 to H-11b1	5.0E-4	0.32 m	0.16	0.11	1.5 m
H-11b2 to H-11b1	5.0E-4	0.11 m	0.16	0.11	1.5 m
H-11b4 to H-11b1	5.0E-4	0.28 m	0.16	0.11	1.5 m

Footnotes: (1) Parameters derived from interpretations that assume that variations in Culebra hydrologic response during tracer tests are due to a heterogeneous distribution of isotropic transmissivities (Cauffman, et al., in prep.).

(2) Matrix porosity and tortuosity values are devrived from core tests at each specific hydropad. Dispersivity is assumed to be approximately 5 percent of a typical transport path length.

Table 1. Summary of best-fit double-porosity model-input parameters from Cauffman et al. (in prep).

Borehole Number	Sample Number	Porosity
H-2a	H-2a-1	0.116
	H-2a-2	0.131 *
H-2b	1-1	0.141
	2-1/3-1	0.154 **
	1-2	0.118
	2-2/3-2	0.103 **
H-2b1	H2b1-1	0.082
	H2b1-1F	0.105
	H2b1-2	0.142 *
	H2b1-3	0.153
H-3b2	1-3	0.188
	1-4	0.168
H-3b3	2-3/3-3	0.180 **
	2-4/3-4V	0.202 **
	1-6/3-6V	0.244
	2-5/3-5	0.205 **
H-4b	1-9	0.297
	2-6/3-6V	0.208 **
H-5b	H-5b-1a	0.128 *
	H-5b-1b	0.155
	H-5b-2	0.228
	H-5b-2F	0.248
	H-5b-3	0.133
H-6b	2-7	0.108
	2-8	0.116
	1-7	0.107
	1-8/3-8V	0.255
H-7b1	H-7b1-1	0.177
	H-7b1-1F	0.149
	H-7b1-2a	0.206 *
	H-7b1-2b	0.278

Table 2. Porosity measured on 79 Culebra core samples representing 15 locations (Saulnier and Kelley, 1990, Table 4.4).

Borehole Number	Sample Number	Porosity
H-7b2	H-7b2-1	0.159 *
	H-7b2-2	0.118
H-7c	H-7c-1a	0.130 *
	H-7c-1b	0.165
	H-7c-1f	0.138
H-10b	H-10b-1	0.089 *
	H-10b-2	0.115
	H-10b-2f	0.066
	H-1-b-3	0.112
H-11	H-11-1	0.155
	H-11-2	0.105 *
	H-11-2f	0.104
	H-11b3-1	0.303
	H-11b3-1f	0.223
	H-11b3-2	0.099
	H-11b3-2f	0.123
	H-11b3-3	0.130
	H-11b3-4	0.152 *
	H-11b3-4f	0.224
WIPP-12	W-12-1a	0.028
	W-12-1b	0.114 *
	W-12-2	0.126 *
	W-12-2f	0.135
	W-12-3	0.134
WIPP-13	W-13-1	0.143
	W-13-2	0.219
	W-13-2f	0.260
	W-13-3a	0.179 *
	W-13-3b	0.097

Table 2 (continued). Porosity measured on 79 Culebra core samples representing 15 locations (Saulnier and Kelley, 1990, Table 4.4).

Borehole Number	Sample Number	Porosity
WIPP-25	W-25-1	0.115
WIPP-26	W-26-1	0.124
	W-26-1F	0.112
	W-26-2	0.126
	W-26-3	0.127 *
WIPP-28	W-28-1a	0.142
	W-28-1b	0.130 *
	W-28-2	0.187
	W-28-3	0.170
	W-28-3F	0.179
WIPP-30	W-30-1	0.128
	W-30-2	0.150
	W-30-3a	0.176
	W-30-3b	0.149 *
	W-30-3F	0.149
	W-30-4	0.239 *
AEC-8	AEC-8-1	0.079
	AEC-8-1F	0.122
	AEC-8-2	0.109

Number of samples = 79
Average porosity = 0.153
Standard deviation = 0.053
Range = 0.028 - 0.303

* Represents an average value from porosity determinations from Terra Tek Laboratories and K & A Laboratories.

** Represents an average of porosity values determined using sample bulk volume estimated from pressured sample dimensions and from fluid displacement.

Table 2 (continued). Porosity measured on 79 Culebra core samples representing 15 locations (Saulnier and Kelley, 1990, Table 4.4).

Sample Number	Helium Porosity	Formation Factor	Tortuosity *
AEC-B-1F	0.122	90.09	0.091
H-2b1-1F	0.105	326.77	0.029
H-5b-2F	0.248	12.2	0.331
H-7b1-1F	0.149	73.49	0.091
H-7C-1F	0.138	79.61	0.091
H-10b-2F	0.066	406.78	0.037
H-11-2F	0.104	94.82	0.101
H-11b3-1F	0.223	36.35	0.123
H-11b3-2F	0.123	101.93	0.080
H-11b3-4F	0.224	32.74	0.136
W-12-2F	0.135	47.3	0.157
W-13-2F	0.26	13.26	0.290
W-26-1F	0.112	68.77	0.130
W-28-3F	0.179	26.3	0.212
W-30-3F	0.149	31.49	0.213

* Tortuosity calculated from Equation (9) using formation factor determined from electrical-resistivity measurements.

Table 3. Tortuosity estimated from values of formation factor and porosity for 15 Culebra core samples representing 11 locations (Saulnier and Kelley, 1990, Table 4.6).

REFERENCES

Cauffman, T.L., V.A. Kelley, J.F. Pickens, and D.T. Upton. (in preparation). *Integration of Interpretation Results of Tracers Tests Performed in the Culebra Dolomite at the Waste Isolation Pilot Plant Site.* SAND91-7076. Albuquerque, New Mexico: Sandia National Laboratories.

Kelley, V.A., and G.J. Saulnier. 1990. *Core Analysis for Selected Samples from the Culebra Dolomite at the Waste Isolation Pilot Plant Site.* SAND90-7011. Albuquerque, New Mexico: Sandia National Laboratories.

Lappin, A.R., R.L. Hunter, D.P. Garber, and P.B. Davies (editors). 1989. *Systems Analysis, Long-Term Radionuclide Transport, and Dose Assessments, Waste Isolation Pilot Plant (WIPP), Southeastern New Mexico; March, 1989.* SAND89-0462. Albuquerque, New Mexico: Sandia National Laboratories.

Rechard, R.P., H. Iuzzolino, and J.S. Sandha. 1990. *Data Used in Preliminary Performance Assessment of the Waste Isolation Pilot Plant (1990).* SAND89-2408. Albuquerque, New Mexico: Sandia National Laboratories.

Reeves, M., D.S. Ward, N.D. Johns, and R.M. Cranwell. 1986. *Theory and Implementation for SWIFT II, the Sandia Waste-Isolation Flow and Transport Model, Release 4.84.* NUREG/CR-3328 and SAND83-1159. Albuquerque, New Mexico: Sandia National Laboratories.

Reeves M., G.A. Freeze, V.A. Kelley, J.F. Pickens, D.T. Upton, and P.B. Davies. 1991. *Regional Double-Porosity Solute Transport in the Culebra Dolomite Under brine-Reservoir-Breach Release Conditions: An Analysis of Parameter Sensitivity and Importance.* SAND89-7069. Albuquerque, New Mexico: Sandia National Laboratories.

Beauheim, June 14, 1991

Date: 6/14/91
To: Rob Rechard (6342)
From: Rick Beauheim (6344)
Subject: Review of Salado Parameter Values to be Used in 1991 Performance Assessment Calculations

Sandia National Laboratories

Albuquerque, New Mexico 87185

Date: June 14, 1991

To: Rob Rechard, 6342

From: Rick Beauheim, 6344

Subject: Review of Salado Parameter Values to be Used in 1991 Performance Assessment Calculations

From the Salado permeability testing program, we produce three types of data used in PA calculations: permeabilities, pore pressures, and specific storage/compressibility values. Presented below are the latest data in each of these three categories. At this time, I do not have a good feel for how to assign probabilities across the uncertainty ranges. I generally feel that the middle or base-case values are more probable than the extremes, particularly in the case of pore pressure.

Permeability

Permeability data can be divided on the basis of rock type (halite vs. anhydrite) and on the basis of whether they represent conditions in the far field or in the DRZ. All permeabilities presented below are considered to have an uncertainty of ± one-half order of magnitude.

Halite Data:

Test	Permeability (m^2)	Uncertainty Range (m^2)	Comments	Reference
C2H01-A	2.7E-18	8.6E-19 to 8.6E-18	DRZ	SAND90-0083
C2H01-B	5.3E-21	1.7E-21 to 1.7E-20	far field?	SAND90-0083
C2H01-B-GZ	1.9E-21	6.0E-22 to 6.0E-21	far field?	SAND90-0083
L4P51-A	6.1E-21	1.9E-21 to 1.9E-20	far field?	SAND90-0083
S0P01	8.3E-21	2.6E-21 to 2.6E-20	far field?	SAND90-0083
S1P71-A	5.4E-20	1.7E-20 to 1.7E-19	far field?	SAND90-0083
S1P72-A-GZ	8.6E-22	2.7E-22 to 2.7E-21	far field?	preliminary

Anhydrite Data:

Test	Permeability (m^2)	Uncertainty Range (m^2)	Comments	Reference
C2H01-C	9.5E-19	3.0E-19 to 3.0E-18	far field?	SAND90-0083
C2H02	7.8E-20	2.5E-20 to 2.5E-19	far field	SAND90-0083
S0P01-GZ	<5.7E-18	<1.8E-18 to <1.8E-17	DRZ	SAND90-0083
SCP01-A	8.2E-20	2.6E-20 to 2.6E-19	far field	preliminary
L4P51-B	6.8E-20	2.2E-20 to 2.2E-19	far field	preliminary
S1P71-B	6.8E-20	2.2E-20 to 2.2E-19	far field	preliminary

Pore Pressure

To date, most of our pore-pressure data appear to reflect some degree of depressurization around the repository. Only two tests provided estimates of pore pressure that I think might be representative of far-field conditions. Both of these tests were of Marker Bed 139. From C2H02, we estimated a pressure of 9.3 MPa (SAND90-0083), and from SCP01-A we estimated a pressure of 12.55 MPa (preliminary). Our estimated uncertainty is $\pm$ 0.5 MPa.

Specific Storage/Compressibility

For our test interpretations, we typically input a value of specific storage based on laboratory measurements of rock properties. We use the range of laboratory measurements to define a range of uncertainty in specific storage, and this uncertainty is one of the factors leading to our uncertainty in permeability. When we have performed only pressure-pulse tests, we have no way of telling where within the expected range for specific storage a particular test actually falls. For those tests, we simply use our base-case values of specific storage. More recently, we have been combining constant-pressure flow tests with the pulse tests. This combination allows us to identify the particular values of specific storage that best fit our data. We do not as yet have many of these combined interpretations, however, and those that we do have are still preliminary. Significantly, all of our preliminary values fall within the range established from laboratory measurements. For this year's PA calculations, therefore, I think you are safe using the laboratory range. Next year we may be able to refine the range somewhat.

For halite, we use a specific storage range from 2.8E-8 to 1.4E-6 m^{-1}, with a base-case value of 9.5E-8 m^{-1}. For anhydrite, we use a specific storage range from 9.7E-8 to 1.0E-6 m^{-1}, with a base-case value of 1.4E-7 m^{-1}.

To get from specific storage to compressibility, you can rearrange the following equation:

$$S_s = \rho_f g(\alpha + \phi\beta)$$

where: ρ_f = fluid density
g = acceleration of gravity
α = formation compressibility
ϕ = formation porosity
β = fluid compressibility

To define our ranges for specific storage, we used the following ranges of parameter values:

ρ_f: 1200 to 1250 kg/m^3, base-case value of 1220 kg/m^3
ϕ: 0.001 to 0.03, base-case value of 0.01
β: 2.9E-10 to 3.3E-10 Pa^{-1}, base-case value of 3.1E-10 Pa^{-1}

You can use these values to get to a range for formation compressibility. The reason I can't just give you the range is that we use a more complicated expression for specific storage than the one I presented above. I expect,

however, that your model does use the expression presented above, and therefore you need to go through this calculation exercise to get at the right values for your model. All of this specific-storage information can be referenced to SAND90-0083.

I hope you find this information useful. Please contact me if you have any questions.

cc: W.D. Weart, 6340
E.D. Gorham, 6344
S.M. Howarth, 6344
S.J. Finley, 6344
D.R. Anderson, 6342

Brush, July 8, 1991

Date: 7/8/91
To: D. R. Anderson (6342)
From: L. H. Brush (6345)
Subject: Current Estimates of Gas Production Rates, Gas Production Potentials, and Expected Chemical Conditions Relevant to Radionuclide Chemistry for the Long-Term WIPP Performance Assessment

Sandia National Laboratories

Albuquerque, New Mexico 87185

date July 8, 1991

to D. R. Anderson, 6342

L. H. Brush

from L. H. Brush, 6345

subject Current Estimates of Gas Production Rates, Gas Production Potentials, and Expected Chemical Conditions Relevant to Radionuclide Chemistry for the Long-Term WIPP Performance Assessment

This memorandum justifies the estimates of gas production rates, gas production potentials, and expected chemical conditions relevant to radionuclide chemistry in WIPP disposal rooms for design-basis transuranic (TRU) waste provided to R. P. Rechard last month (Table 1). Many of these estimates are new; some are based on recently obtained data from laboratory studies of anoxic corrosion.

I will provide similar estimates for the Engineered Alternatives Task Force's (in prep.) Alternatives 2 and 6 by August 1, 1991.

ANOXIC CORROSION

R. E. Westerman (1990, 1991a) of Pacific Northwest Laboratory (PNL) has observed significant H_2 production from anoxic corrosion of two heats each of ASTM A 366 and ASTM A 570 steels by WIPP Brine A under inundated conditions when N_2 is present at low pressures (about 150 psig) in the headspace above the brine. The low-C, cold-rolled steel alloy ASTM A 366 simulates the drums to be emplaced in the repository; the medium-C, hot-rolled steel alloy ASTM A 570 simulates the boxes. The H_2 production rate was essentially constant during 3- and 6-month experiments; the average value for all four heats obtained from the 6-month experiments is 0.21 moles per m^2 of steel per year. Based on my estimate of 6 m^2 of steels per equivalent drum of waste, which includes steels used to fabricate waste containers (drums and boxes) and steels contained in the waste, this is equivalent to 1.26 mole of H_2 per drum per year. Westerman also reported an average corrosion rate of 1.72 μm of steel per year for the 6-month runs. The H_2 production rates of 0.2 moles per m^2 per year or 1 mole per drum per year and the corrosion rate of 2 μm per year are my best estimates for inundated conditions, rounded to one significant figure (Table 1).

Strictly speaking, the H_2 production rates and the corrosion rate are not equivalent. Although he obtained both rates from each

experiment, Westerman used independent techniques to obtain them (pressure measurements and posttest analysis of the headspace gases for the H_2 production rate and gravimetric, or weight-loss, analysis for the corrosion rate). These techniques agreed well, but not exactly, when applied to the 6-month experiments, but not as well for the 3-month experiments. (The best estimates described above are from the 6-month runs.) The discrepancies between these techniques probably result from uncertainties as to the identity and composition of the corrosion product or products formed during these experiments. (Characterization of the corrosion product is necessary to write the chemical reactions used to convert corrosion rates to H_2 production rates.) We are still attempting to characterize the corrosion product from these runs.

Although the H_2 production rate has been constant for 6 months when N_2 is present at low-pressures, the results of high-pressure experiments at PNL imply that the build-up of H_2 pressure would eventually reduce this rate significantly (Westerman, 1991b). After 6 months, the corrosion rate of two heats of ASTM A 366 steel under inundated conditions with H_2 at a pressure of 1,000 psig was 0.356 μm per year, 21.8% of the rate of 1.63 μm per year observed for the same two heats of ASTM A 366 steel under low-pressure, inundated conditions with N_2. Multiplying 1.72 μm per year, the average rate for all four heats, by 0.218 gives 0.375 μm per year, my estimate of the average corrosion rate for all four heats of steel at 1,000 psig H_2. However, at an N_2 pressure of 1,000 psig the corrosion rate of two heats of ASTM A 366 steel was 2.96 μm per year, 81.6% higher than the low-pressure, inundated rate of 1.63 μm per year observed for the same two heats of ASTM A 366 steel. The product of 1.72 μm per year and 1.82 is 3.13 μm per year, my estimated average corrosion rate for all four heats of steel at 1,000 psig N_2. Westerman did not report H_2 production rates for the high-pressure experiments. Furthermore, we have still not identified the corrosion product or products yet. However, the corrosion product appears to be the same phase that formed in the 6-month, low pressure experiments. It is thus possible to estimate an H_2 production rate by multiplying the 6-month, low-pressure rates of 0.21 moles per m^2 or 1.26 moles per drum of waste by 0.218 (1,000 psig H_2) and 1.82 (1,000 psig N_2) to obtain 0.046 moles per m^2 per year or 0.275 moles per drum per year (1,000 psig H_2) and 0.38 moles per m^2 per year or 2.29 moles per drum per year (1,000 psig N_2). At present, we do not have corrosion rates for any pressures other than 150 and 1,000 psig. Westerman will, however, report 12-month data for 500 psig H_2 and 1,000 psig H_2 in November or December 1991. The adjusted, measured corrosion rate of 3 μm per year and the estimated H_2 production rate of 0.4 mole per m^2 per year or 2 moles per drum per year with N_2 at 1,000 psig are my maximum estimates for inundated conditions, rounded to one significant figure (Table 1).

Under low-pressure, inundated conditions with CO_2, H_2 production occurred for about 3 months, then virtually stopped after 3 or 4 months due to formation of a passivating layer of $FeCO_3$, or siderite

(Westerman, 1991a). This suggests that, if microbially produced CO_2 were present, passivation of steel surfaces by $FeCO_3$ could stop H_2 production before the generation of significant quantities of this gas. However, we do not know the partial pressure of CO_2 required to form $FeCO_3$. Furthermore, crushing of drums and boxes during room closure could disrupt the layer of $FeCO_3$ and lead to some additional H_2 production. Nevertheless, the passivation observed after 3 or 4 months is the basis for my minimum estimates of 0 moles of H_2 per m^2 per year or 0 moles of H_2 per drum per year and 0 μm of steel per year for inundated conditions (Table 1).

Because we have still not identified the corrosion product or products, we cannot calculate the number moles of H_2O consumed per mole of Fe consumed or the number moles of H_2O consumed per mole of H_2 produced from anoxic corrosion of steels. However, the corrosion reaction that produces $Fe(OH)_2$ (amakinite) a possible corrosion product identified by Brush and Anderson (1988) and Brush (1990), would consume 2 moles of H_2O per mole of Fe consumed, or consume 2 moles of H_2O per mole of H_2 produced. The corrosion reaction that produces Fe_3O_4 (magnetite), another possible corrosion product, would consume 1.33 mole of H_2O per mole of Fe consumed, or consume 1 mole of H_2O per mole of H_2 produced. These values are probably typical of other corrosion reactions.

In 3- and 6-month, low-pressure, humid experiments with either CO_2 or N_2, Westerman (1990, 1991a) observed no H_2 production except for very limited quantities from corrosion of the bottom 10% of the specimens splashed with brine during pretest preparation of the containers. These results and modeling studies conducted by Davies (personal communication) suggested to me that anoxic corrosion could be self-limiting; small quantities of brine in the repository could produce H_2, increase the pressure, prevent additional brine inflow or even cause brine outflow, and thus prevent additional H_2 production. However, the thin film of brine introduced by capillary rise or condensation followed by dissolution of salts from the backfill, or H_2O absorbed by crushed salt or bentonite in the backfill, which will be in contact with drums and boxes, could cause additional anoxic corrosion of steels and H_2 production after brine is driven away from corroding steels.

Westerman (1991c) has just started a study to quantify H_2 production from anoxic corrosion of steels in contact with noninundated backfill materials and will report preliminary results by the end of September 1991. Until then, I propose the following arbitrarily estimated rates for humid conditions: minimum estimates of 0 moles of H_2 per m^2 of steel per year or 0 moles per drum of waste per year and 0 μm of steel per year; best estimates of 0.02 moles of H_2 per m^2 per year or 0.1 moles of H_2 per drum per year and 0.2 μm per year; and maximum estimates of 0.2 moles of H_2 per m_2 per year or 1 moles of H_2 per drum per year and 2 μm per year (Table 1).

Finally, I propose that the estimated gas production potential from

anoxic corrosion remain at 900 moles per drum of waste. This value, estimated by Brush and Anderson (1989), Lappin et al. (1989), and Brush (1990), is 60% of the total gas production potential.

MICROBIAL ACTIVITY

D. Grbic-Galic and her colleagues at Stanford University observed significant microbial gas production by halophilic microorganisms in brine collected from G Seep in the WIPP underground workings with glucose, a relatively biodegradable substrate, but did not report significant gas production with cellulose, a much less biodegradable substrate. Furthermore, brine from G Seep inhibited significant gas production by nonhalophilic microorganisms, although a few experiments did show some evidence for possible microbial activity. These results seem to suggest that microbial gas production may be significant under overtest conditions (relatively biodegradable substrates, amendment of brine with nutrients, etc.), but not under realistic conditions. However, I believe that, for the reasons described below, the results obtained by Grbic-Galic and her colleagues do not rule out significant microbial gas production.

First, N. Black of Stanford University, R. H. Vreeland of West Chester University, and I compared the recent study at Stanford University and studies carried out during the 1970s (Barnhart et al., 1980; Caldwell, 1981; Caldwell et al., 1988; Molecke, 1979; Sandia National Laboratories, 1979). We concluded, as others have before us (Molecke, 1979; Brush and Anderson, 1989; Lappin et al., 1989), that the earlier results implied significant microbial gas production under both realistic and overtest conditions.

Second, Vreeland observed significant degradation of filter paper by his enrichments of halophilic and halotolerant microorganisms from the salt lakes in Nash Draw. Although he could not quantify gas production rates from these experiments, the results suggest that microorganisms could consume paper under realistic conditions in WIPP disposal rooms. Paper constitutes 70% of the 10 kg of cellulosics per equivalent drum of contact handled TRU waste to be emplaced in the repository (Brush, 1990).

Third, Black, Vreeland, and I reviewed the methods used in the earlier and recent studies in detail. We concluded that the study at Stanford University was not sensitive enough to detect gas production rates equivalent to a few tenths of a mole of gas per drum of waste per year. Davies (1990) has demonstrated that gas production rates greater than about 0.1 mole per equivalent drum of waste per year are significant from the standpoint of the long-term performance of the repository.

Because the results obtained at Stanford University do not rule out significant microbial gas production under realistic conditions, I

propose using the same best estimate for the microbial gas production rate under inundated conditions proposed by Brush and Anderson (1989), Lappin et al. (1989), and Brush (1990), 1 mole of various gases per drum per year. However, I propose new minimum and maximum rates for inundated conditions, 0 and 5 moles per drum per year, respectively. The minimum estimate is analogous to the minimum estimate for anoxic corrosion under inundated conditions. The maximum estimate is Molecke's (1979) maximum estimate for microbial activity under inundated conditions. I also propose new minimum and best estimates for microbial gas production rates under humid conditions, 0 and 0.1 moles per drum per year. These estimates, both arbitrary, are analogous to the arbitrary minimum and best estimates for anoxic corrosion under humid conditions. The maximum estimate for microbial activity under humid conditions remains unchanged from the value estimated by Brush and Lappin (1990), 1 mole per drum per year (Table 1).

To convert these estimates of microbial gas production rates to units of moles per kg of cellulosics per year, I divided each rate by 10 kg of cellulosics per drum, the estimate used by Brush (1990), to obtain the estimates given in Table 1. Strictly speaking, this is inconsistent with the fact that the rate of 1 mole per drum per year is based on experiments carried out with simulated waste that included materials other than cellulosics (Molecke, 1979). It is also inconsistent with the assumption of Molecke (1979), Brush and Anderson (1979), and Lappin et al. (1989) that microorganisms will degrade 100% of the cellulosics, 50% of the Hypalon, and 50% of the Neoprene in the waste. However, about 90% of the microbial gas production potential (below) and hence 90% of the microbial gas production rate estimated by Brush and Anderson (1989) and Lappin et al. (1989) would result from biodegradation of cellulosics and only 5% each from Hypalon and Neoprene. Furthermore, Francis will use cellulosics as the sole substrate in his study of microbial gas production, at least initially. Finally, it will be much easier to use rates normalized only to the mass of cellulosics present than rates normalized to cellulosics, Hypalon, and Neoprene in performance-assessment calculations.

I also propose that the estimated gas production potential from microbial activity stay at 600 moles per drum of waste, the value estimated by Brush and Anderson (1989), Lappin et al. (1989), and Brush (1990). This is 40% of the total gas production potential.

RADIOLYSIS

D. T. Reed of Argonne National Laboratory is carrying out a low-pressure study of gas production by α radiolysis of Brine A as a function of dissolved Pu concentration. He has observed small, linear pressure increases from the solution with the highest dissolved Pu concentration, $1 \cdot 10^{-4}$ M, but does not have enough data to convert these rates to moles of gas per drum of waste per year yet. As

expected, he has not observed pressure increases yet from the solutions with lower dissolved Pu concentrations, $1 \cdot 10^{-6}$ and $1 \cdot 10^{-8}$ M. After completion of these 3-month experiments, Reed will carry out 2-month runs with a dissolved Pu concentration of $1 \cdot 10^{-4}$ M in other WIPP brines to determine the effect of compositional variations on the radiolytic gas production rate.

As soon as he obtains longer-term data from Brine A with a dissolved Pu concentration of $1 \cdot 10^{-4}$ M, data with lower dissolved Pu concentrations in Brine A, and results from other WIPP brines with a dissolved Pu concentration of $1 \cdot 10^{-4}$ M, Reed will calculate experimentally based radiolytic gas-production rates for the radionuclide concentrations estimated by the Radionuclide Source Term Expert Panel. In addition to rates in units of moles of gas per drum of waste per year, he will provide rates in moles per cubic meter of brine for various concentrations. Until then, I propose using the radiolytic gas production rates proposed by Brush and Lappin (1990), who estimated a minimum rate of $1 \cdot 10^{-7}$ mole of various gases per drum of waste per year, a best rate of $1 \cdot 10^{-4}$ mole per drum per year, and a maximum rate of $1 \cdot 10^{-1}$ mole per drum per year (Table 1).

EXPECTED CHEMICAL CONDITIONS RELEVANT TO RADIONUCLIDE CHEMISTRY

Development of the source term for radionuclide-transport calculations will require: (1) estimates of the quantity of each nonradioactive constituent of design-basis TRU waste to be emplaced in the repository; (2) predictions of the microenvironments (Eh, pH, and the concentrations of organic and inorganic ligands) for each nonradioactive waste constituent; (3) quantification of the chemical behavior of the important radionuclides in the waste for each of these microenvironments; (4) construction of a frequency distribution of radionuclide concentrations based on the relative quantity of each nonradioactive waste constituent and the concentration associated with that constituent.

Currently, inventories of radioactive and nonradioactive waste constituents and estimates of radionuclide concentrations in brines as a function of Eh and pH are available. However, the high priority placed on the gas issue in laboratory studies of repository chemistry has precluded efforts to predict microenvironment for waste constituents. Therefore, I propose that oxidizing, acidic conditions, oxidizing, basic conditions, reducing, acidic conditions, and reducing, basic conditions be considered equally probable for interpreting Eh-pH-dependent estimates of radionuclide concentrations in WIPP brines.

REFERENCES

Barnhart, B. J., E. W. Campbell, E. Martinez, D. E. Caldwell, and R. Hallett (1980). **Potential Microbial Impact on Transuranic Wastes Under Conditions Expected in the Waste Isolation Pilot Plant (WIPP), Annual Report, October 1, 1978-September 30, 1979.** LA-8297-PR, Los Alamos Scientific Laboratory, Los Alamos, NM.

Brush, L. H. (1990). **Test Plan for Laboratory and Modeling Studies of Repository and Radionuclide Chemistry for the Waste Isolation Pilot Plant**, SAND90-0266, Sandia National Laboratories, Albuquerque, NM.

Brush, L. H., and D. R. Anderson (1989). Estimates of Gas Production Rates, Potentials, and Periods, and Dissolved Radionuclide Concentrations for the WIPP Supplemental Environmental Impact Statement, unpublished memorandum to B. M. Butcher, February 14, 1989. Sandia National Laboratories, Albuquerque, NM.

Brush, L. H., and A. R. Lappin (1990). Additional Estimates of Gas Production Rates and Radionuclide Solubilities for Use in Models of WIPP Disposal Rooms, unpublished memorandum to D. R. Anderson, August 1, 1990. Sandia National Laboratories, Albuquerque, NM.

Caldwell, D. E. (1981). Microbial Biogeochemistry of Organic Matrix Transuranic Waste, unpublished report submitted to M. A. Molecke, June 17, 1981, University of New Mexico, Albuquerque, NM.

Caldwell, D. E., R. C. Hallett, M. A. Molecke, E. Martinez, and B. J. Barnhart (1988). **Rates of CO_2 Production From the Microbial Degradation of Transuranic Wastes under Simulated Geologic Isolation Conditions**. SAND87-7170, Sandia National Laboratories, Albuquerque, NM.

Davies, P. B. (1990). Results from Recent Variable-Rate Gas Simulations that Examine the Impact of Vapor-Limited ("Humid") Gas-Generation Rates, unpublished memorandum to L. H. Brush and A. R. Lappin, December 6, 1990. Sandia National Laboratories, Albuquerque, NM.

Engineered Alternatives Task Force (in prep.). **Evaluation of the Effectiveness and Feasibility of the Waste Isolation Pilot Plant Engineered Alternatives: Final Report of the Engineered Alternatives Task Force, Vol. I and II**, DOE/WIPP 91-007, Rev. 2, US Department of Energy Waste Isolation Pilot Plant, Carlsbad, NM.

Lappin, A. R., R. L. Hunter, D. P. Garber, and P. B. Davies, Eds. (1989). **Systems Analysis, Long-Term Radionuclide Transport, and Dose Assessments, Waste Isolation Pilot Plant (WIPP), Southeastern New Mexico; March, 1989**. SAND89-0462, Sandia National Laboratories, Albuquerque, NM.

Molecke, M. A. (1979). **Gas Generation from Transuranic Waste Degradation: Data Summary and Interpretation**. SAND79-1245, Sandia National Laboratories, Albuquerque, NM.

Sandia National Laboratories (1979). **Summary of Research and Development Activities in Support of Waste Acceptance Criteria for the WIPP**. SAND79-1305, Sandia National Laboratories, Albuquerque, NM.

Westerman, R. E. (1990). Corrosion of Low-Carbon Steel in Simulated Waste Isolation Pilot Plant (WIPP) Environments, Quarterly Progress Report for the Period July 1 - September 30, 1990, unpublished report submitted to L. H. Brush, September 28, 1990. Pacific Northwest Laboratory, Richland, WA.

Westerman, R. E. (1991a). Corrosion of Low-Carbon Steel in Simulated Waste Isolation Pilot Plant (WIPP) Environments, Progress Report for the Period October 1, 1990 to March 31, 1991, unpublished report submitted to L. H. Brush, March 29, 1991. Pacific Northwest Laboratory, Richland, WA.

Westerman, R. E. (1991b). April 1991 Monthly Report, Corrosion of Low-Carbon Steel in Simulated WIPP Environments, unpublished report submitted to L. H. Brush, April 26, 1991. Pacific Northwest Laboratory, Richland, WA.

Westerman, R. E. (1991c). May 1991 Monthly Report, Corrosion of Low-Carbon Steel in Simulated WIPP Environments, unpublished report submitted to L. H. Brush, May 28, 1991. Pacific Northwest Laboratory, Richland, WA.

TABLE 1. CURRENT ESTIMATES OF GAS PRODUCTION RATES

Process	Gas Production Rate (various units)		
	Minimum	Best	Maximum
Anoxic corrosion, inundated:[1]			
moles/m^2 · year	0	0.2	0.4
moles/drum · year	0	1	2
μm/year	0	2	3
Anoxic corrosion, humid:[1]			
moles/m^2 · year	0	0.02	0.2
moles/drum · year	0	0.1	1
μm/year	0	0.2	2
Microbial activity, inundated:			
moles/drum · year	0	1	5
moles/kg cellulosics · year	0	0.1	0.5
Microbial activity, humid:			
moles/drum · year	0	0.1	1
moles/kg cellulosics · year	0	0.01	0.1
Radiolysis of brine:			
moles/drum · year	0.0000001	0.0001	0.1

1. See text for estimates of H_2O consumption by anoxic corrosion of steels.

Distribution:

V. Daub, DOE/WPO
J. Carr, DOE/WPO
D. Blackstone, DOE/WPO
W. D. Arnold, Oak Ridge National Laboratory
J. N. Butler, Harvard University
G. R. Choppin, Florida State University
A. J. Francis, Brookhaven National Laboratory
J. B. Gillow, Brookhaven National Laboratory
J. K. Lanyi, University of California at Irvine
R. E. Meyer, Oak Ridge National Laboratory
H. Nitsche, Lawrence Livermore National Laboratory
D. T. Reed, Argonne National Laboratory
R. H. Vreeland, West Chester University
R. E. Westerman, Pacific Northwest Laboratory
6340 W. D. Weart
6341 R. C. Lincoln
6341 SWCF (6): XXXRC, XXXRC/AC, XXXRC/MA, XXXRC/R, XXXRNC, XXXRNC/SOL
6342 Staff
6343 T. M. Schultheis
6344 E. D. Gorham
6344 P. B. Davies
6345 B. M. Butcher
6345 Staff
6346 J. R. Tillerson

Davies, June 2, 1991

Date: 6/2/91
To: D. R. Anderson (6342)
From: P. B. Davies (6344)
Subject: Uncertainty Estimates for Threshold Pressure for 1991 Performance Assessment Calculations Involving Waste-Generated Gas

Sandia National Laboratories

Albuquerque, New Mexico 87185

Date: June 6, 1991

To: D.R. Anderson (6342)

P.B. Davies

From: P.B. Davies (6344)

Subject: Uncertainty Estimates for Threshold Pressure for 1991 Performance Assessment Calculations Involving Waste-Generated Gas

This memorandum contains the recommended uncertainty distribution for the threshold pressure for 1991 performance assessment calculations involving waste-generated gas. Threshold pressure may play an important role in controlling which Salado lithologies are accessible as gas migration flow paths and at what gas pressures gas flow will be initiated. Threshold pressure is also a key parameter in the Brooks and Corey (1964) model used to characterize the 2-phase properties of analogue materials for preliminary gas calculations (Davies and LaVenue, 1990). Threshold pressure is strongly related to intrinsic permeability and, therefore, these parameters should not be sampled independently. The recommended approach for 1991 calculations is as follows. First sample for the intrinsic permeability for a given unit (either interbed or halite), then use the following the empirical correlation for threshold pressure from Davies (1991) to compute a median value for threshold pressure:

$$P_t\ [\text{MPa}] = 5.6 \times 10^{-7} \left(k\ [\text{m}^2] \right)^{-0.346}$$

As noted in Davies (1991), threshold pressure estimates based on this empirical correlation have uncertainty associated with the correlation itself and with factors external to the correlation. One uncertainty in the correlation is the error associated with estimating the true mean value of the threshold pressure for a given intrinsic permeability. Because of the relatively strong correlation (goodness-of-fit, R^2, is equal to 0.93), the estimation error is fairly small. A second uncertainty in the correlation is prediction error due to random variations in threshold pressure in any given rock type and to measurement error in the original data. Because measurement error in the original data was not quantified, these two sources of uncertainty cannot be evaluated independently. The interval between the bounds of this prediction error is approximately three times the estimated mean threshold pressure. One source of uncertainty that is external to the correlation is the uncertainty associated with measurements of intrinsic permeability in various lithologies of the Salado Formation. Presumably, this uncertainty will be accounted for in performance assessment calculations by sampling on permeability. Another very important source of uncertainty is the fact that while the data for the correlation span a wide range of consolidated rock types (shale, anhydrite, carbonate, and sandstone), the data do not include any actual measurements from the Salado Formation at the WIPP repository nor do the data include any actual measurements on halite.

Clearly the total uncertainty in the estimates described in the previous paragraph is quite large. Given the present lack of any WIPP-specific data, it is not possible to rigorously quantify this uncertainty. Therefore,

it is recommended that a relatively simple representation of uncertainty should be used for purposes of the 1991 performance assessment calculations. For these calculations, it is recommended that a log normal distribution be assumed, with plus/minus one order of magnitude for one standard deviation and plus/minus two orders of magnitude for two standard deviations (Figure 1). This large uncertainty should produce a wide range of hydrologic responses to waste-generated gas, which is appropriate given the present lack of WIPP-specific data.

REFERENCES

Brooks, R.H., and A.T. Corey. 1964. Hydraulic Properties of Porous Media. Colorado State University, Hydrology Paper No. 3.

Davies, P.B. 1991. Evaluation of the Role of Threshold Pressure in Controlling Flow of Waste-Generated Gas into the Bedded Salt at the Waste Isolation Pilot Plant. SAND90-3246. Albuquerque, New Mexico: Sandia National Laboratories.

Davies, P.B. and LaVenue, A.M. 1990. "Additional Data for Characterizing 2-Phase Flow Behavior in Waste-Generated Gas Simulations and Pilot Point Information for Final Culebra 2-D Model (SAND89-7068/1)." memorandum to R.P. Rechard (11-19-91). Albuquerque, New Mexico: Sandia National Laboratories.

cc: W.D. Weart (6340)
M.G. Marietta (6342)
R.P. Rechard (6342)
P. Vaughn (Applied Physics Inc.)
E.D. Gorham (6344)
S.M. Howarth (6344)
S.W. Webb (6344)

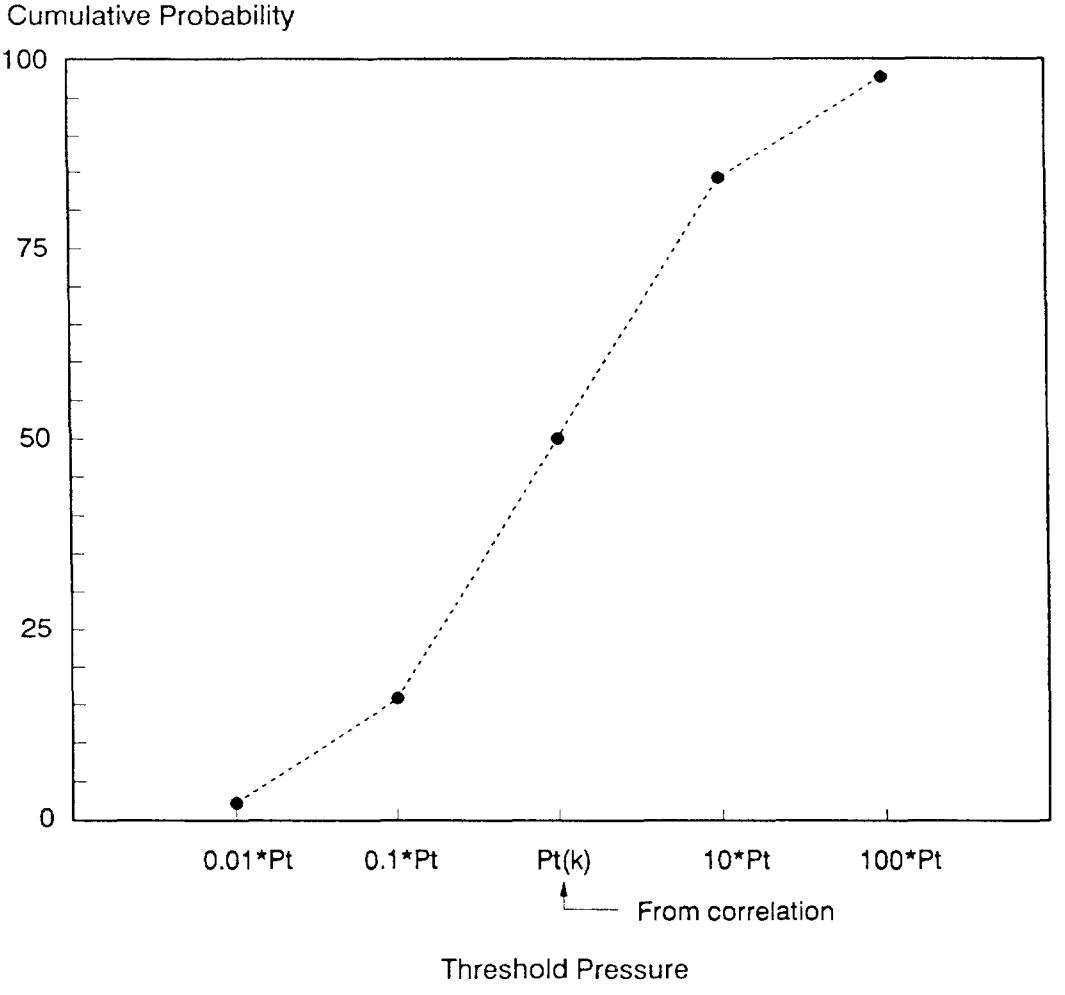

Figure 1. Uncertainty distribution for threshold pressure.

Drez, May 9, 1989

Date: 5/9/89
To: L. Brush (6334)
From: Paul Drez (International Technology Corporation)
Subject: Preliminary Nonradionuclide Inventory of CH-TRU Waste
(Note: Following the letter are Tables 3.5, 3.6, and 3.9, which were taken from the draft report, "Preliminary Nonradionuclide Inventory for CH-TRU Waste," by P. E. Drez and P. James-Lipponer, International Technology Corporation, Albuquerque, NM, May, 1989.)

INTERNATIONAL TECHNOLOGY CORPORATION

May 9, 1989

Project No. 301192.88.01

Dr. L. Brush
Sandia National Laboratories
Division 6334
P. O. Box 5800
Albuquerque, NM 87185

Preliminary Nonradionuclide Inventory of CH-TRU Waste

Dear Dr. Brush:

Attached is a preliminary report on the status of the Nonradionuclide Inventory Database and detailed tabulations of waste materials as requested in the last amendment to the IT Sandia Support contract. I am sorry for the slight delay in completing the report, but the CH-TRU generator/storage sites were late in their responses and the process of tabulating the appropriate data proved to be a difficult task. Part of the difficulty has to do with the slight variations in the way the sites report data.

Listed below is the information contained in this package:

- Report entitled: "Preliminary Nonradionuclide Inventory for CH-TRU Waste." The report includes a description of how the data was collected from the CH-TRU waste generator/storage sites, a description of the database used to compile the data, and examples of how the calculations were made including any limitations (Item 7 in Statement of Work).

- Table 3-5 in the report summarizes the total quantity of combustible materials in the waste, including cellulosics, plastics and other combustibles (Item 3 in Statement of Work).

  Although only total cellulosics were requested, data on plastics and other combustibles were also tabulated, anticipating their eventual need to support the Performance Assessment program.

- Table 3-5 in the report estimates the quantity of various types of cellulosic materials in the total cellulosic inventory (Item 4 in Statement of Work).

  A breakdown of the various types of plastic and rubber materials has also been provided in Table 3-5. Caution is advised in the interpretation of the plastics in the tables, since two sites choose to report the weight of plastic bagging and rigid liners as part of the waste totals.

- Table 3-6 in the report estimates the total quantity of metals in the CH-TRU waste and also provides a breakdown of the various types of metals in the waste (Item 5 in Statement of Work).

  Caution is advised in the interpretation of this table, since two sites choose to report the amount of metal in the waste packaging as part of the waste contents in this table. I have no way of separating out the weight of the waste cannister from the database at this time.

  In an attempt to provide a complete inventory (including waste packaging), Table 3-8 provides a preliminary estimate of the amount of plastic and other internal packaging in addition to an estimate of the metal included in the waste. Variations in the method of packaging from site to site have been accounted for in the tabulation of the data.

- Table 3-7 in the report estimates the total quantity of nitrates and total inorganic carbon (TIC) in the waste (Items 2 and 6 in Statement of Work). Graphite or charcoal is not considered part of this summary, only inorganic carbonate.

- Table 4-2 in the report lists quantitative information on selected chelating agents that occur in the waste. All chelating agents requested in your statement of work (Item 1) have been included plus any additional chelating agents that have been reported by the sites.

- Printouts for each generator/storage site that represent complete data dumps of the Nonradionuclide Inventory Database (Item 7 of Statement of Work).

- Floppy disks containing all the dBASE files for the database. An explanation of the files is provided in Appendix 2.0 of the report (Item 7 of Statement of Work).

I am very pleased to transmit this preliminary report on the Nonradionuclide Inventory Database to you. This database is important step towards an understanding of the composition and quantities of CH-TRU waste to be emplaced in WIPP. This is a "living" database that should be updated periodically as more precise information is provided by the CH-TRU waste generator/storage sites.

Do not hesitate to contact me at 262-8800 if you need any clarification of the data contained in this packet of information. Pamela James (262-8800) can provide any information about the structure and output of the database.

Sincerely,

Paul E. Drez

Paul E. Drez
Senior Technical Associate

Enclosures

cc: M. Devarakonda, IT-Albuquerque (report only)
P. James, IT-Albuquerque (report only)
J. Myers, IT-Albuquerque (report only)

Do not hesitate to contact me at 262-8800 if you need any clarification of the data contained in this packet of information. Pamela James (262-8800) can provide any information about the structure and output of the database.

Sincerely,

Paul E. Drez

Paul E. Drez
Senior Technical Associate

Enclosures

cc: M. Devarakonda, IT-Albuquerque (report only)
P. James, IT-Albuquerque (report only)
J. Myers, IT-Albuquerque (report only)

Table 3-5. Total Quantity of CH-TRU Combustible Waste to be Shipped to WIPP

Waste Material	Weight (Kilograms)
COMBUSTIBLES	
-Cellulosics	
-Paper/Kimwipes	3,890,000*
-Cloth	226,000
-Other Paper	51
-Lumber (untreated)	73,100
-Lumber (treated)	36,700
-Plywood	98,400
-Other Wood (rulers)	<1
-Other Wood (all types)	23,700
-Other Cellulose (with phenolic binder)	1,720
-Cellulosics Subtotal	4,350,000

* All numbers, including totals, rounded off to a maximum of three significant number.

Table 3-5. Total Quantity of CH-TRU Combustible Waste to be Shipped to WIPP (Continued)

Waste Material	Weight (Kilograms)
COMBUSTIBLES	
-Plastics	
-Polyethylene	1,540,000*
-Polyvinyl Chloride	1,040,000
-Surgeon's Gloves (latex)	582,000
-Leaded Rubber Gloves (Lead-Hypalon-Neoprene)	596,000
-Hypalon	114,000
-Neoprene	129,000
-Viton	133
-Teflon	41,000
-Plexiglas (including Lucite)	18,900
-Styrofoam	330
-Plastic Prefilters (polypropylene?)	33,600
-Polystyrene	2,560
-Conwed Pads (plastic fibers)	2,030
-Other Plastic	75,500
-Other Rubber (Kalrez)	<1
-Other Rubber (undefined)	7,530
-Plastics Subtotal	4,180,000

* All numbers, including totals, rounded off to a maximum of three significant number.

Table 3-5. Total Quantity of CH-TRU Combustible Waste to be Shipped to WIPP (Continued)

Waste Material	Weight (Kilograms)
COMBUSTIBLES	
-Other	
-Blacktop	18,800*
-Other	41,700
-Other Subtotal	60,500
-Cellulosics Subtotal	4,350,000
-Plastics Subtotal	4,180,000
-Other Subtotal	60,500
COMBUSTIBLES TOTAL IN CH-TRU WASTE	8,590,000

* All numbers, including totals, rounded off to a maximum of three significant number.

Table 3-6. Total Quantity of CH-TRU Metal Waste to be Shipped To WIPP

Waste Material	Weight (Kilograms)
Metals	
-Aluminum	666,000*
-Beryllium	8,640
-Cadmium	5
-Chromium	5
-Copper	300,000
-Iron	2,620,000
-Lead	
- Metallic	513,000
- Glass (includes weight of glass)	1,120,000#
- Gloves (includes weight of gloves)	596,000#
-Lithium (batteries)	1,030
-Mercury	120
-Paint Cans	547,000
-Platinum	1,500
-Selenium	5
-Silver	5

* All numbers, including totals, rounded off to a maximum of three significant number.

The reported weights for lead include the weight of the matrix, therefore, the values are conservative (too high).

Table 3-6. Total Quantity of CH-TRU Metal Waste to be Shipped To WIPP (Continued)

Waste Material	Weight (Kilograms)
Metals	
-Steel (including stainless, crushed drums inner drums, carbon steel, etc.)	9,170,000*#
-Shipping Cans	217
-Tantalum	125,000
-Tungsten	20,000
-Other	146,000
Total Metals	15,800,000

* All numbers, including totals, rounded off to a maximum of three significant number.

The weight of steel quoted in the table includes the weight of the waste containers (drums and boxes) for INEL and LANL.

Table 3-9. Average Weights Used for Calculation of Container and Packaging Materials

Type of Packaging Material	Weight (Kilograms)
Drums -	
Weight of 17C drum	29.5*
Weight of 90-mil high-density polyethylene liner	6.8
Weight of Polyvinyl Chloride drum liner bag	0.7
Weight of Polyethylene drum liner bag	0.7
Weight of Fiberboard liner for 55 gallon drum	2.0
4x4x7 Boxes -	
Weight of 4x4x7 metal box	217.7
Weight of Plywood liner for 4x4x7 metal box	175.5
Weight of PVC liner bag for 4x4x7 box	5.0
Weight of fiberboard liner for 4x4x7 box	11.8
Weight of wooden 4x4x7 box	208.7
Weight of fiberglass reinforced wooden box	322.0
Standard Waste Boxes -	
Weight of Standard Waste Box	310.7#
Weight of PVC liner bag	4.0

* All weights are based on containers and packaging materials used at the Rocky Flats Plant, except for the weight of the Standard Waste Box.

Trupact-II Safety Analysis Report, Appendix 1.3.4, Revision 0, 1989.

Finley and McTigue, June 17, 1991

Date: 6/17/91
To: Elaine Gorham, 6344
From: S. J. Finley, 6344, and D. F. McTigue, 1511
Subject: Parameter Estimates from the Small-Scale Brine Inflow Experiments

Sandia National Laboratories

Albuquerque, New Mexico 87185

date: June 17, 1991

to: Elaine Gorham, 6344

from: S. J. Finley, 6344 and D. F. McTigue, 1511

subject: Parameter Estimates from The Small-Scale Brine Inflow Experiments

Data from the small-scale brine inflow experiments has been analyzed using the one-dimensional, radial, Darcy flow model. Brine inflow data from 10 boreholes in halite and 3 boreholes testing Marker Bed 139 has been used to estimate permeability and hydraulic diffusivity. The diffusivity is determined from the time scale of the decay of the flux (inflow rate/unit area), and the product of the pore pressure and permeability is determined from the magnitude of the flux.

All of the results of the two parameter fit to the flux data are given in Table 1. Permeability values reported are estimated by assuming a uniform pore pressure of 10 MPa, 5 MPa, and 1 Mpa. (Susan Howarth and Rick Beauheim have both made measurements of pore pressure in the WIPP underground and should be consulted about the pore pressure assumptions.) Uncertainty in all parameter estimates is reported as plus or minus one standard deviation. This uncertainty is a measure of how good the fit is assuming a random error of the order of the expected measurement error is included in the data set. Any uncertainty in the model itself or the pore pressure assumed are not included in the uncertainty measure reported.

All of the boreholes included in this set of experiments are drilled from an underground excavation. Boreholes vary from 3 m to 6 m in length. For all halite tests, brine inflow was averaged over the entire length of the borehole. For the boreholes testing Marker Bed 139, the brine inflow was averaged over the thickness of Marker Bed 139 (3-feet).

Attachment

Copy to:
W. D. Weart, 6340
D. R. Anderson, 6342
R. P. Rechard, 6342
R. L. Beauheim, 6344
S. M. Howarth, 6344

Table 1: Parameter Estimates from Borehole Experiments

Borehole #	Rock Type	Permeability @Po = 10 MPa (m^2)	Permeability @Po = 5 MPa (m^2)	Permeability @Po = 1 MPa (m^2)	Diffusivity (m^2/sec)
DBT10	Halite	2.9E-22±.18E-22	5.8E-22±.36E-22	2.9E-21±.18E-21	4.7E-11 ±.78E-11
DBT11	Halite	1.1E-21±.09E-21	2.3E-21±.18E-21	1.1E-20±.09E-20	3.5E-9 ±.63E-9
DBT12	Halite	6.4E-22±.72E-22	1.3E-21±.14E-21	6.4E-21±.72E-21	1.0E-8 ±.65E-8
DBT13	Halite	1.7E-22±.26E-22	3.4E-22±.52E-22	1.7E-21± .26E-21	5.9E-11 ± 2.3E-11
DBT14A	Halite	7.8E-22±2.4E-22	1.6E-21±.48E-21	7.8E-21±2.4E-21	2.8E-8 ±4.6E-8*
DBT14B	Halite	2.2E-20±.28E-21	4.5E-21±.56E-21	2.2E-21±.28E-21	4.3E-8 ±3.3E-8
DBT15A	Halite	3.2E-22±.55E-22	6.4E-22±1.1E-22	3.2E-21±.55E-21	1.8E-10 ±.86E-10
DBT15B	Halite	1.8E-22±.59E-22	3.6E-22±1.1E-22	1.8E-21±.59E-21	1.3E-10 ±1.2E-10
L4B01	Halite	.67E-22±.43E-22	1.3E-22±.86E-22	.67E-21±.43E-21	5.8E-11 ±9.1E-11*
DBT31A	Halite	9.0E-22±2.4E-22	1.8E-21±.48E-21	9.0E-21±2.4E-21	1.27E-10±1.22E-11
QPB01 *1	Anhydrite	4.8E-21±.3E-21	9.6E-21±.06E-21	4.8E-20±.3E-20	1.1E-8 ±.34E-8
QPB02 *1	Anhydrite	8.2E-20±.03E-20	1.6E-19±.006E-19	8.2E-19±.03E-19	1.2E-9 ±.014E-9
QPB03 *1	Anhydrite	4.8E-21±1.5E-21	9.6E-21±3E-21	4.8E-20±1.5E-20	6.4E-7 ±18.8E-7*

* The lower limit of these uncertainty bounds should be assumed to be zero.

*1 For all of these borehole tests, the length of the productive unit was assumed to be equal to the average thickness of Marker Bed 139 (3-feet).

Howarth, June 12, 1991

Date: 6/12/91
To: Elaine Gorham (6344)
From: Susan Howarth (6344)
Subject: Pore Pressure Distributions for 1991 Performance Assessment Calculations

Sandia National Laboratories

Albuquerque, New Mexico 87185

DATE: June 12, 1991

TO: Elaine Gorham, 6344

FROM: Susan Howarth, 6344

SUBJECT: Pore Pressure Distributions for 1991 Performance Assessment Calculations

Attached are the Relative Frequency and Cumulative Frequency distributions for pore pressure as determined from the pre-excavation borehole tests at Room Q. There are three sets of graphs: 1) all data, 2) halite only tests, and 3) anhydrite only tests. On each frequency distribution graph, the vertical bars are centered above a pore pressure value which represents the midpoint of the pressure range. For example, the bar above the 9.5 value represents the data in the 9.0 to 9.9 range.

In determining pore pressure from a shut in (pressure build up) pressure test, pressure is extrapolated to the pore pressure using the Horner method. For each Room Q borehole, a range of pore pressure values is given: the low number is the highest pre-excavation pressure recorded for the test zone and the high number is the Horner extrapolated value. All data within the range is weighed equally. A list of the boreholes and pressure ranges is found below in Table 1.

During the pre-excavation time period, each Room Q borehole test region was located 75 feet from an existing excavation. Because these pressure tests are located farther from an excavation than any similar tests, they are thought to be most representative of far-field conditions. However, these data should be combined with data from the Small-Scale Brine Inflow Program and the Permeability Testing Program for use in Performance Assessment calculations.

TABLE 1.
Room Q Pre-excavation Pore Pressure Ranges

Borehole	Pore Pressure (MPa)
QPP01	9.3-13.9
QPP02	1.1-1.1
QPP03	11.5-12.8
QPP04	7.0-10.3
QPP05	Indeterminate
QPP11	Indeterminate
QPP12	5.8-8.6
QPP13	10.5-12.8
QPP14	Indeterminate
QPP15	Indeterminate
QPP21	Indeterminate
QPP22	8.5-9.1
QPP23	7.1-9.4
QPP24	8.7-9.4
QPP25	7.2-9.4

Copy to:

W. D. Weart, 6340 (w/o attachments)
D. R. Anderson, 6342
R. P. Rechard, 6342
R. L. Beauheim, 6344
S. J. Finley, 6344

ROOM Q

PORE PRESSURE (ALL DATA)

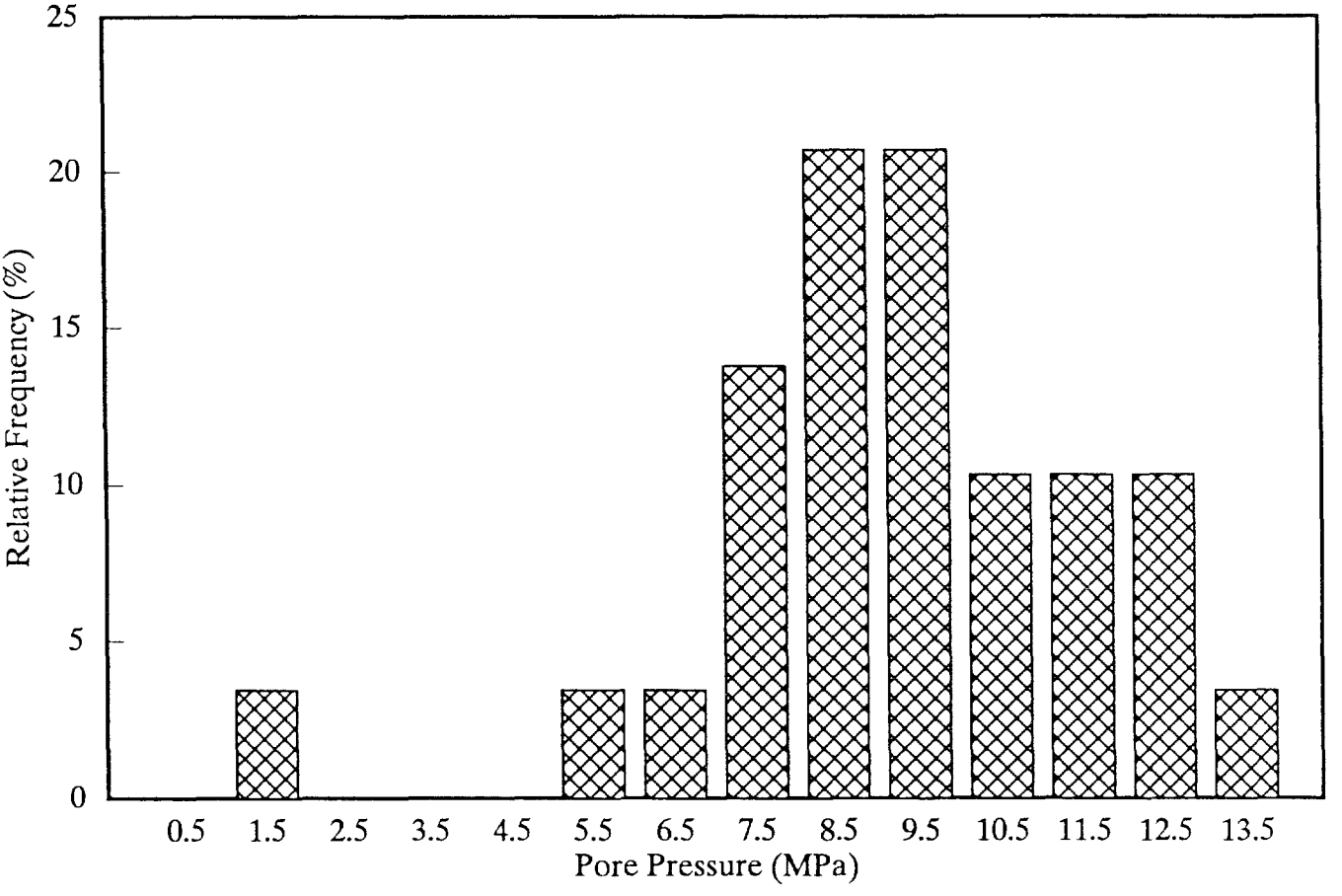

ROOM Q

PORE PRESSURE (ALL DATA)

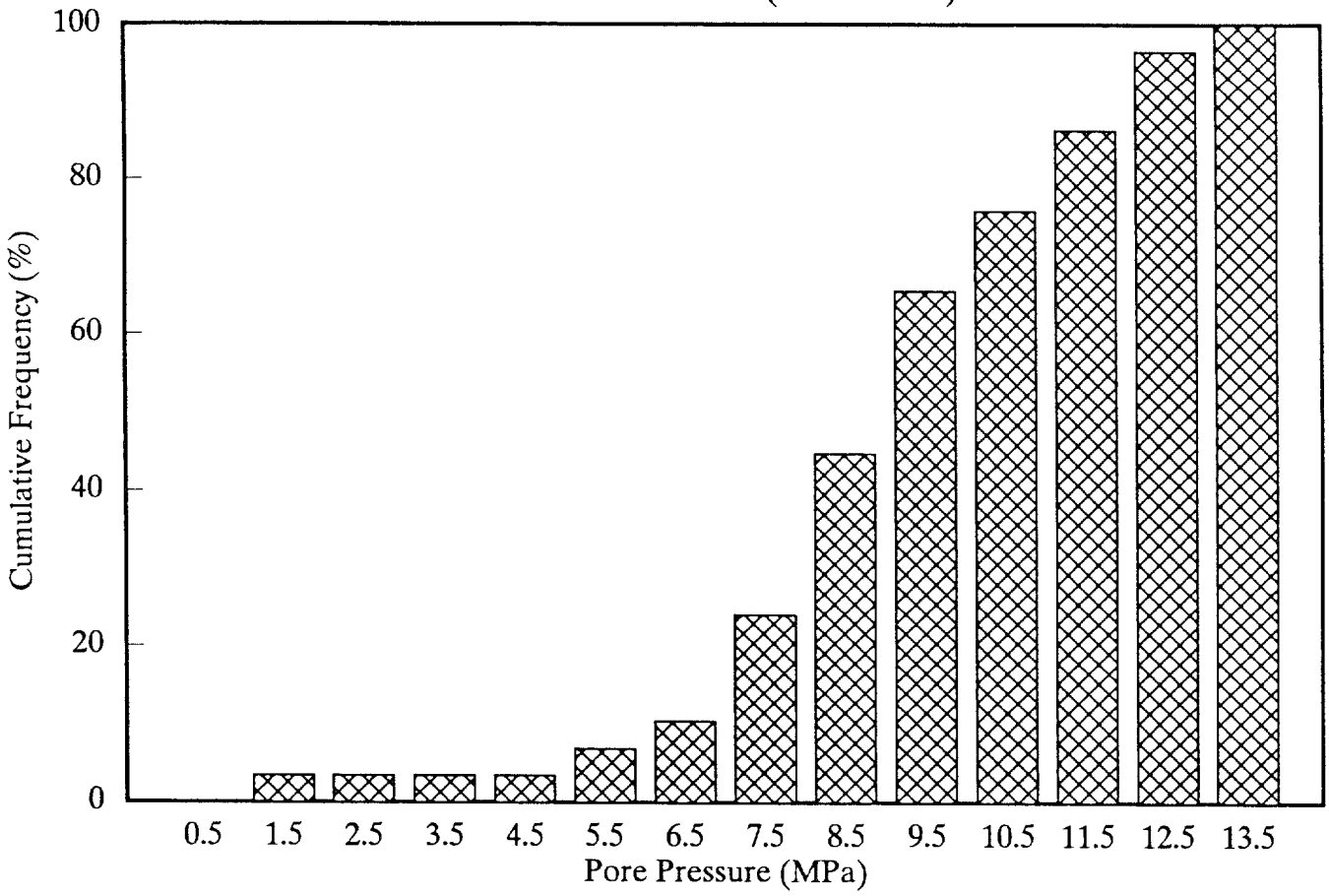

ROOM Q

PORE PRESSURE (HALITE)

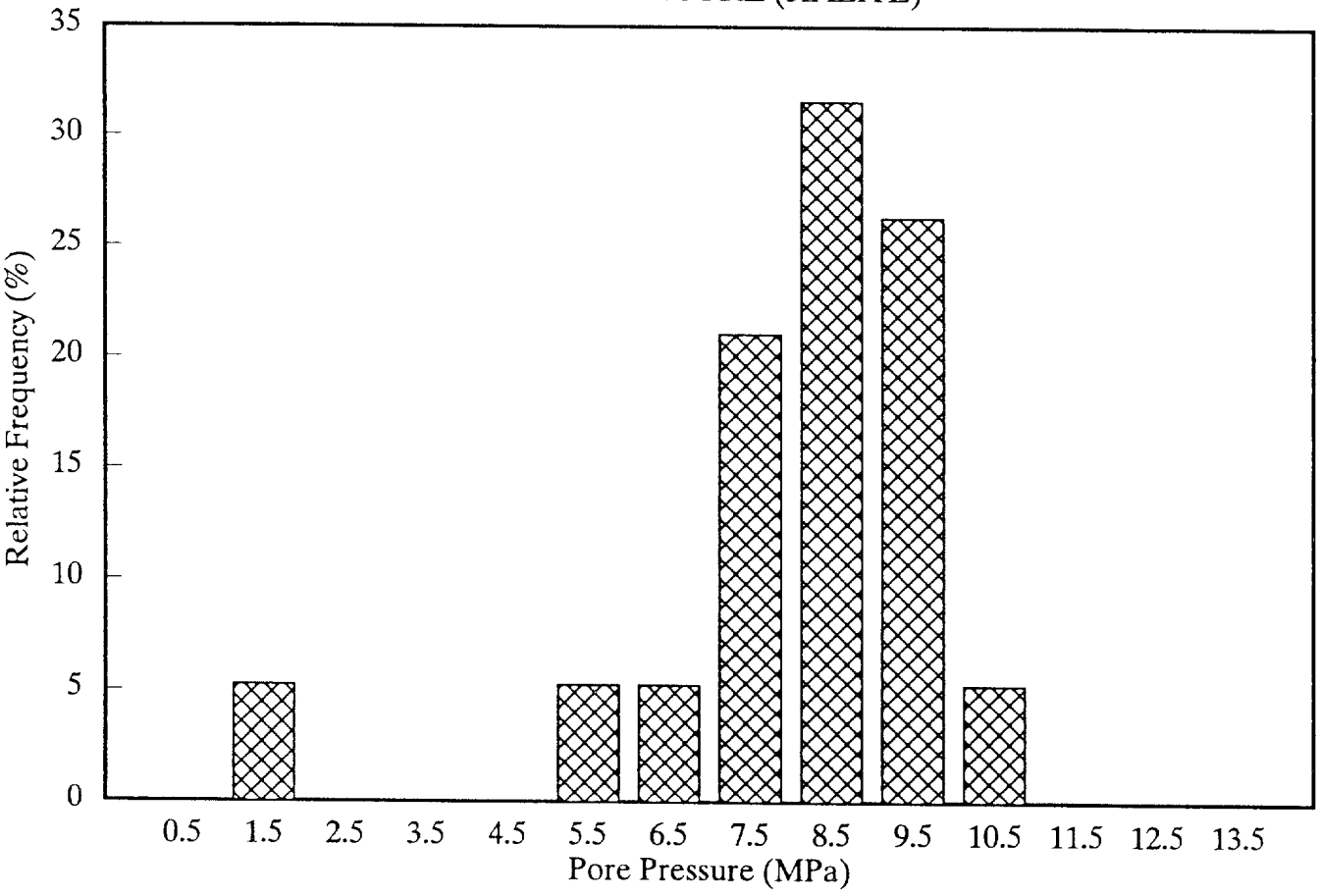

ROOM Q

PORE PRESSURE (HALITE)

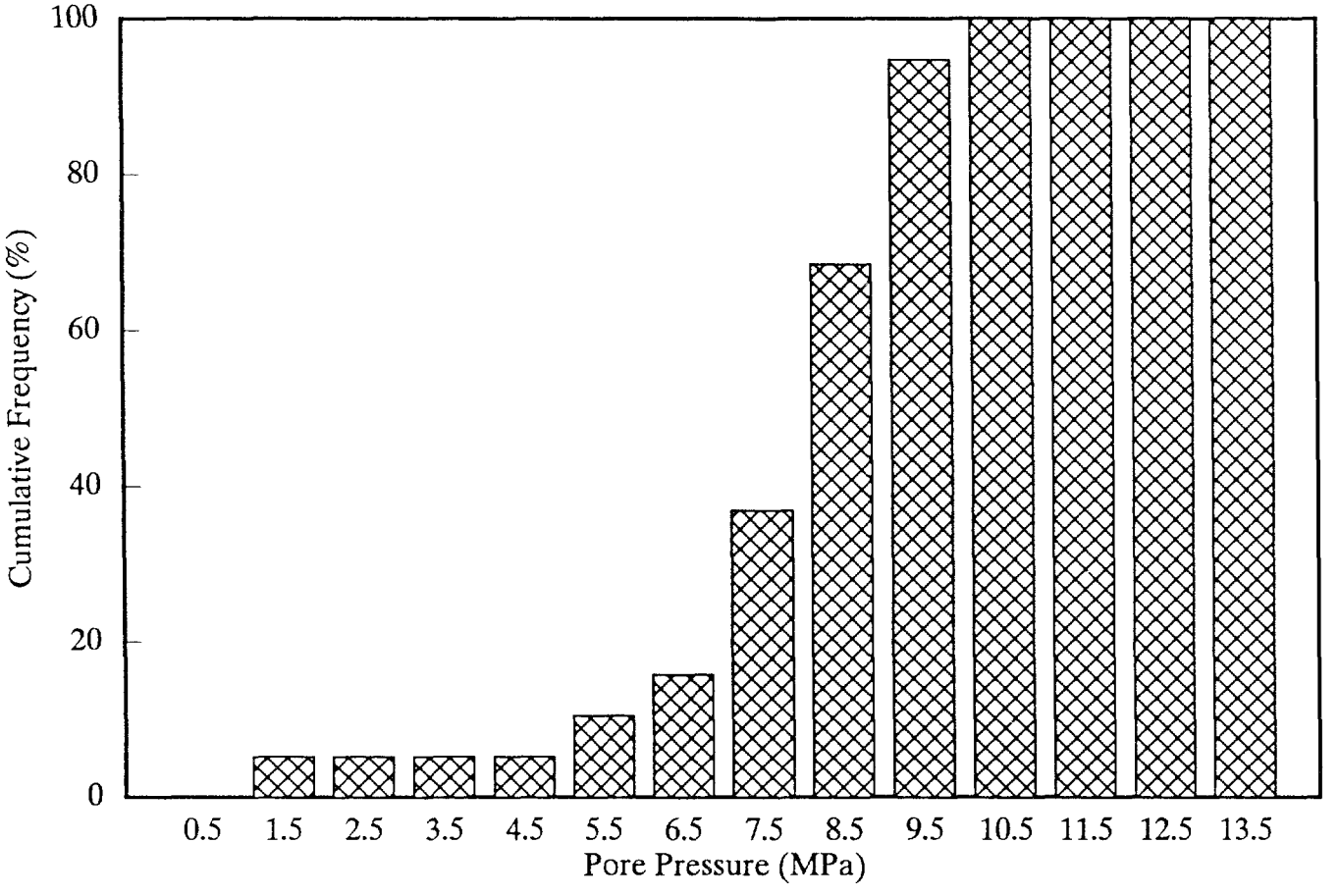

ROOM Q

PORE PRESSURE (ANHYDRITE)

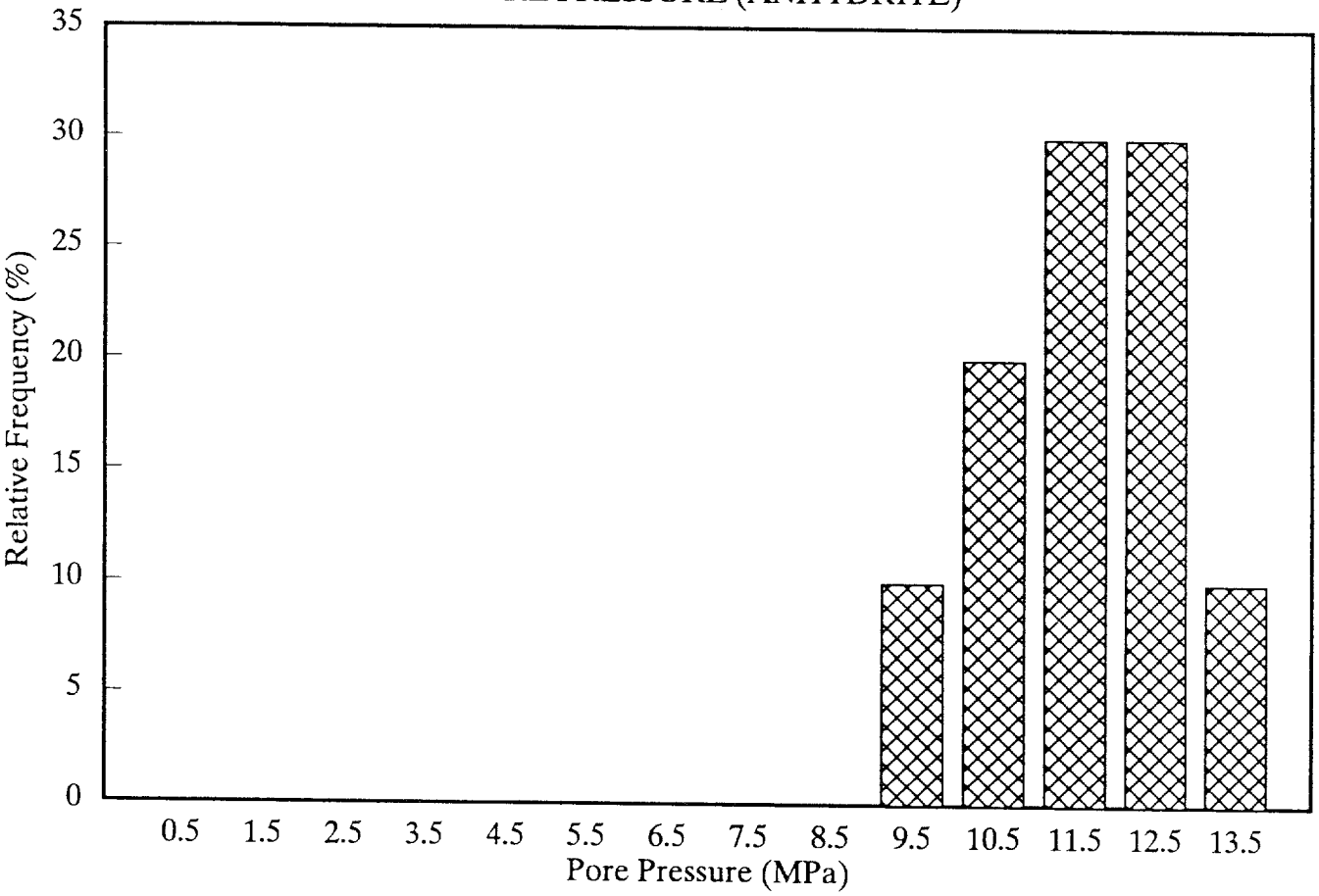

ROOM Q

PORE PRESSURE (ANHYDRITE)

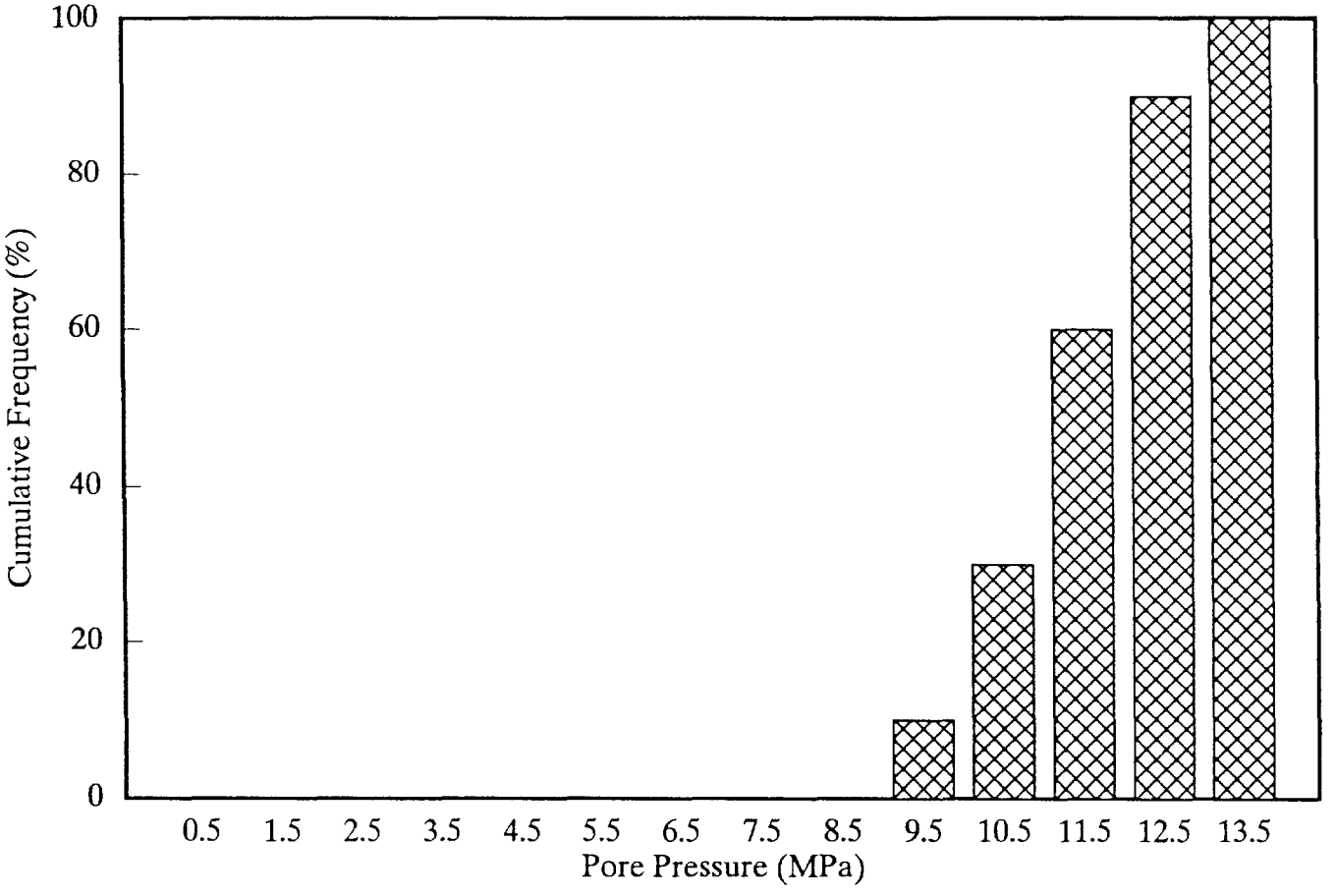

Howarth, June 13, 1991

Date: 6/13/91
To: Elaine Gorham (6344)
From: Susan Howarth (6344)
Subject: Permeability Distributions for 1991 Performance Assessment Calculations

Sandia National Laboratories

Albuquerque, New Mexico 87185

DATE: June 13, 1991

TO: Elaine Gorham, 6344

FROM: Susan Howarth, 6344

SUBJECT: Permeability Distributions for 1991 Performance Assessment Calculations

Attached are the Relative Frequency and Cumulative Frequency distributions for permeability as determined from the pre-excavation borehole tests at Room Q. There are three sets of graphs: 1) all tests, 2) halite only tests, and 3) anhydrite only tests. On each frequency distribution graph, the vertical bars are centered above a number which represents data within that order of magnitude. For example, the bar above the -23 value represents permeabilities within the LOG($1*10^{-23}$) to LOG($9.9*10^{-23}$) m^2 range.

Permeabilities were calculated using a 1-D radial Darcy-flow model with the following assumptions: 1) no damage zone, 2) constant capacitance (stiff-matrix), and 3) test zone fluid compressibility equals brine compressibility. Permeabilities calculated using these assumptions for the Room Q pre-excavation borehole tests are found in Table 1.

Division 6344 is in the process of standardizing permeability test interpretation. The current Standard Model has two important assumptions that differ from those used in the permeabilities shown in Table 1 which could significantly change the inferred permeabilities. The Standard Model assumes that the material is poroelastic (not stiff-matrix) and uses measured values for test zone fluid compressibility (not brine compressibility). Re-analysis of the Room Q pre-excavation data using the current Standard Model is not complete but it is expected that permeability values may increase by 1 to 2 orders of magnitude when re-analyzed.

In order to account for this expected[1] change, uncertainty tails were added to the Table 1 permeability values in the following manner. Because using the measured test zone fluid compressibility instead of the brine compressibility will result in larger (1 to 2 orders of magnitude) permeabilities, a 2 order of magnitude increase uncertainty tail was added. Then, because using a stiff-matrix results in a higher permeability (by 0.5 to 1 orders of magnitude) than would be calculated using the poroelastic model a 1 order of magnitude decrease uncertainty tail was added. For example, for the QPP01 data, Table 1 lists the permeability as $1.5*10^{-21}$ m^2. When uncertainty tails are added, the QPP01 permeability range becomes $1.5*10^{-22}$ to $1.5*10^{-19}$ m^2.

Confidence intervals were subsequently assigned to the permeabilities for each borehole. A 10% confidence was assigned to lowest permeability order of magnitude, 20% was assigned to the next larger order of magnitude, 50% to the next higher order of magnitude and 20% was assigned to the highest order of magnitude. Again using QPP01 as an example, a 10% confidence was assigned to permeabilities in the 1 to $9.9*10^{-22}$ m^2 range, 20% was assigned to permeabilities in the 1 to $9.9*10^{-21}$ m^2 range, 50% was assigned to permeabilities in the 1 to $9.9*10^{-20}$ m^2 range, and 20% was assigned to permeabilities in the 1 to $9.9*10^{-19}$ m^2 range.

[1] R. L. Beauheim, Personal Communication, June 12, 1991.

Frequency distributions were calculated by assigning points equal to the confidence percentage for each permeability range for each borehole test. The points assigned to each range were then summed.

During the pre-excavation time period, each Room Q borehole test region was located 75 feet from an existing excavation. Because these pressure tests are located farther from an excavation than any similar tests, they are thought to be most representative of far-field conditions. However, these data should be combined with data from the Small-Scale Brine Inflow Program and the Permeability Testing Program for use in Performance Assessment calculations.

TABLE 1.
Room Q Pre-excavation Permeability

Borehole	Permeability (m^2)
QPP01	$1.5*10^{-21}$
QPP02	TLTM
QPP03	$2.4*10^{-22}$
QPP04	$5.0*10^{-23}$
QPP05	TLTM
QPP11	TLTM
QPP12	$2.0*10^{-23}$
QPP13	$3.0*10^{-22}$
QPP14	TLTM
QPP15	TLTM
QPP21	TLTM
QPP22	$1.0*10^{-22}$
QPP23	$1.0*10^{-21}$
QPP24	$1.0*10^{-21}$
QPP25	$1.0*10^{-22}$

Copy to:

W. D. Weart, 6340 (w/o attachments)
D. R. Anderson, 6342
R. P. Rechard, 6342
R. L. Beauheim, 6344
S. J. Finley, 6344

ROOM Q

Permeability (All Data)

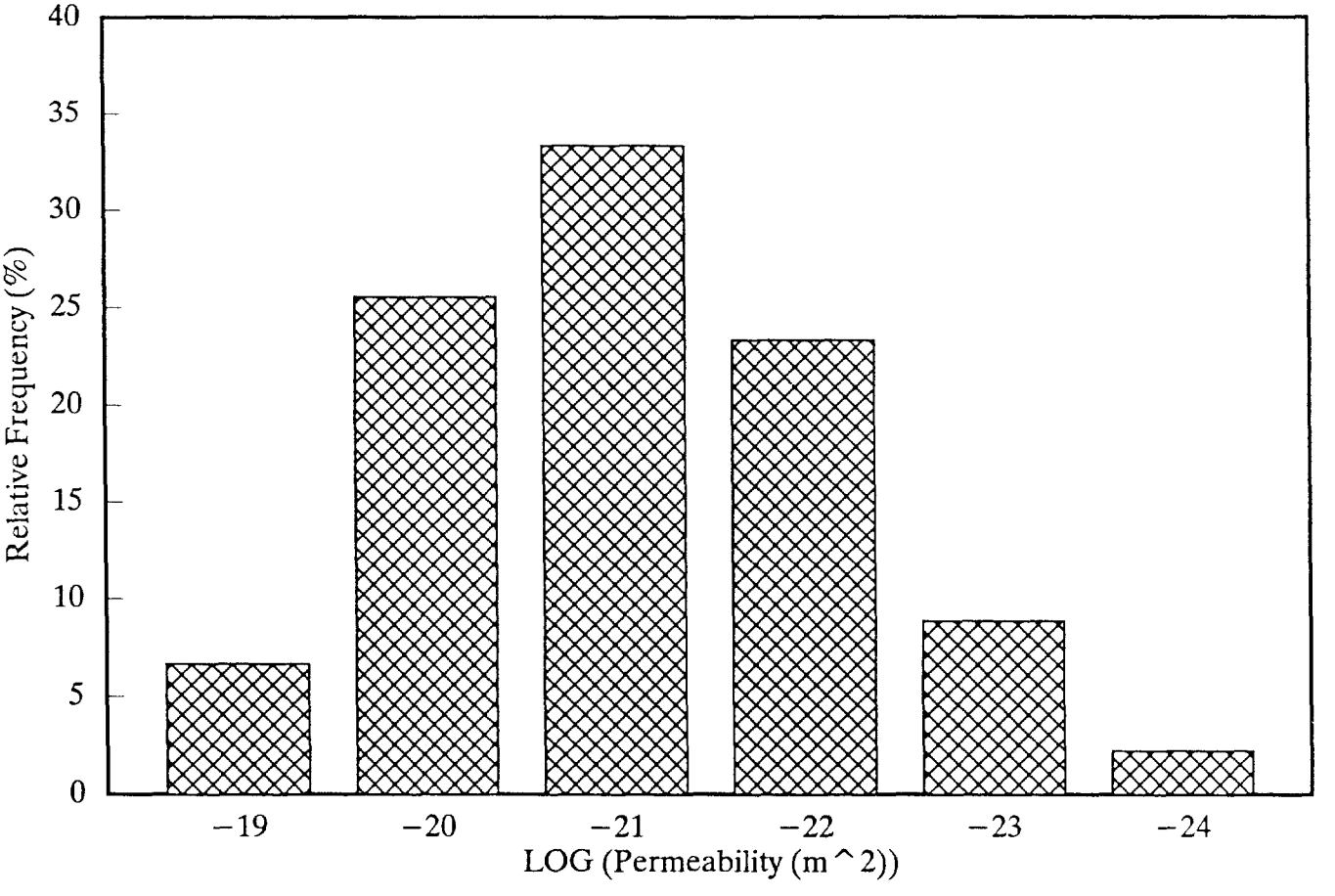

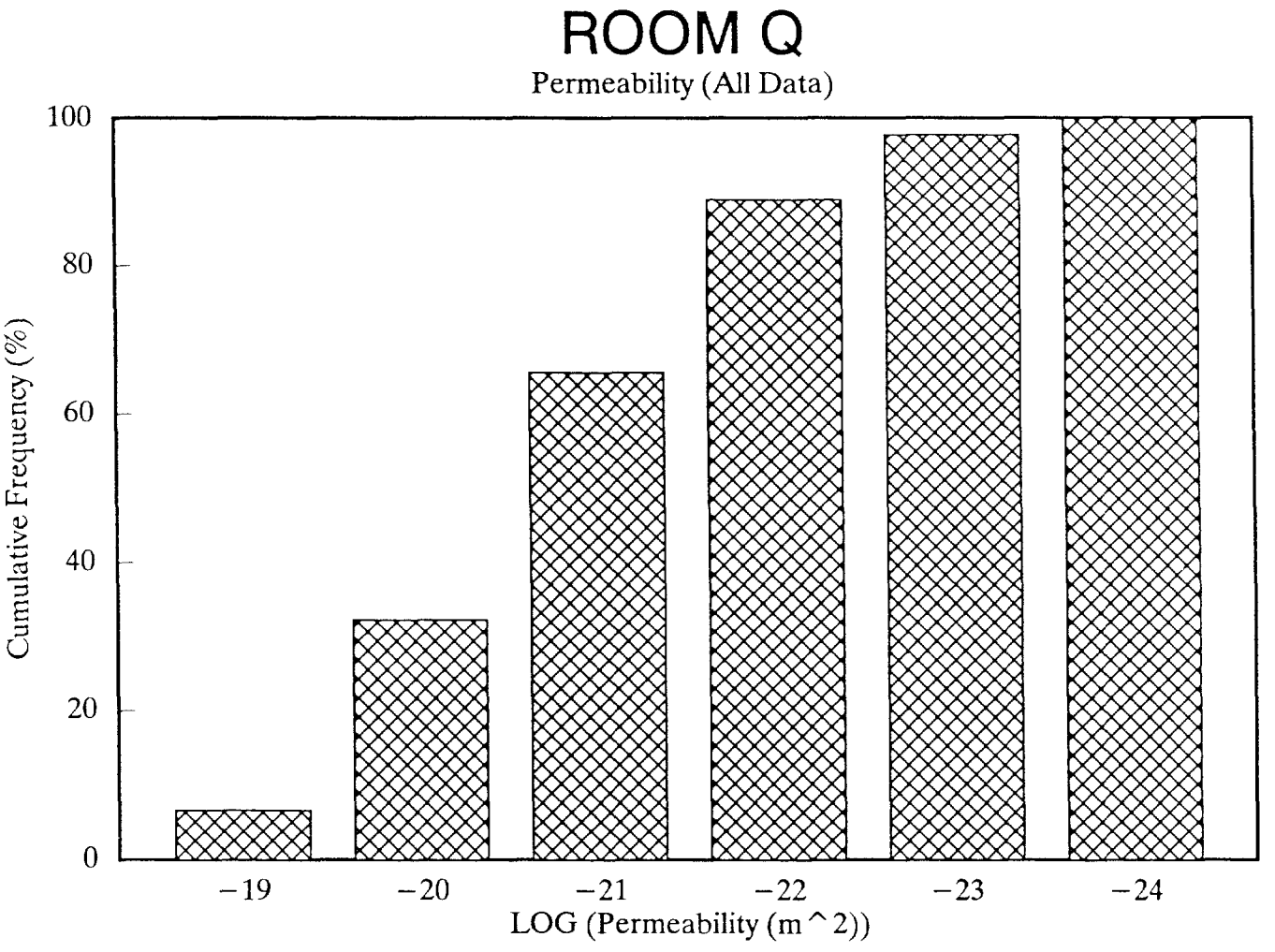
ROOM Q
Permeability (All Data)
100
80
60
40
20
0
Cumulative Frequency (%)
−19
−20
−21
−22
−23
−24
LOG (Permeability (m ^ 2))

ROOM Q

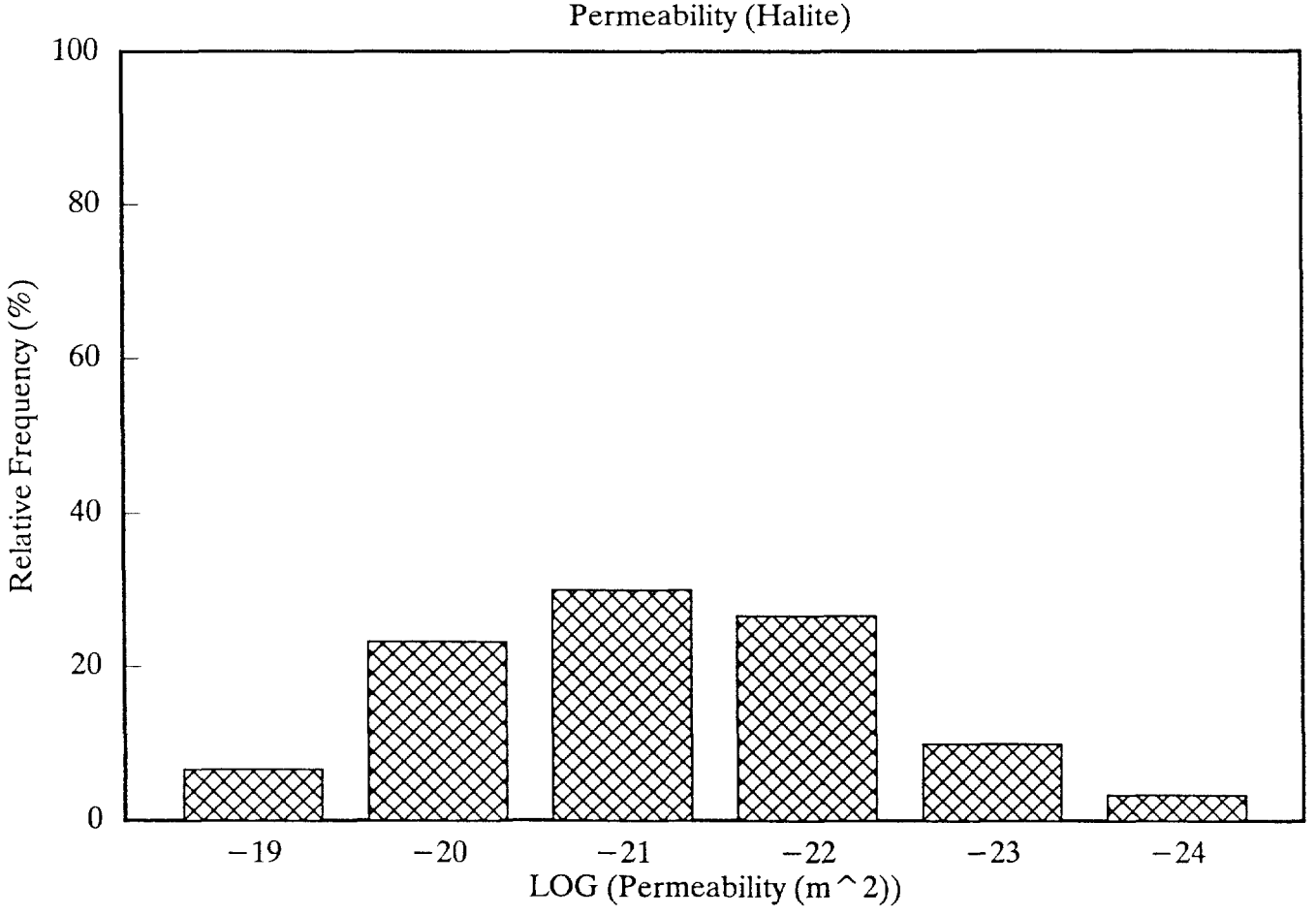
Permeability (Halite)
100
80
60
40
20
0
Relative Frequency (%)
−19
−20
−21
−22
−23
−24
LOG (Permeability (m ^ 2))

ROOM Q

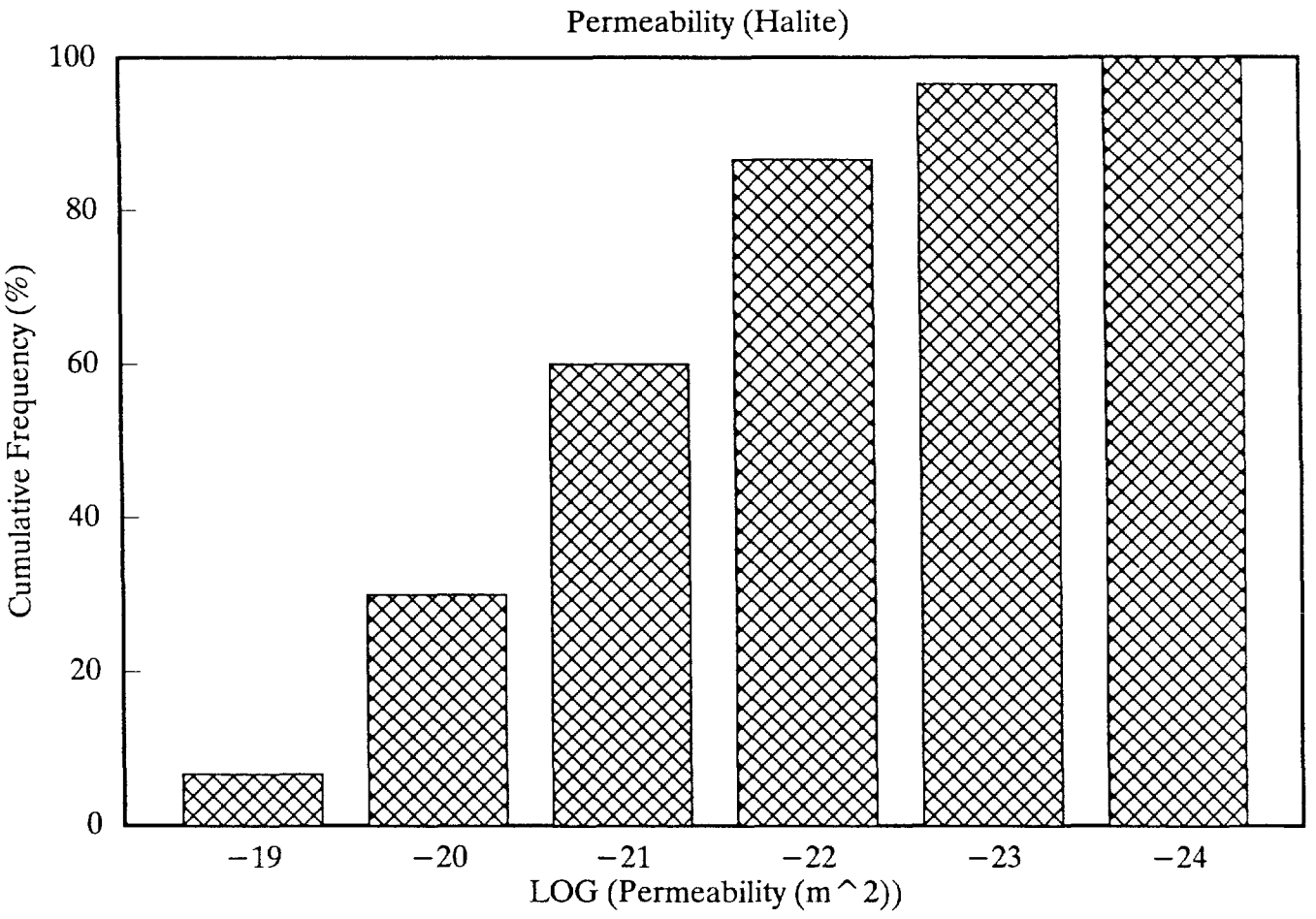
Permeability (Halite)
100
80
60
40
20
0
Cumulative Frequency (%)
−19
−20
−21
−22
−23
−24
LOG (Permeability (m ^ 2))

ROOM Q

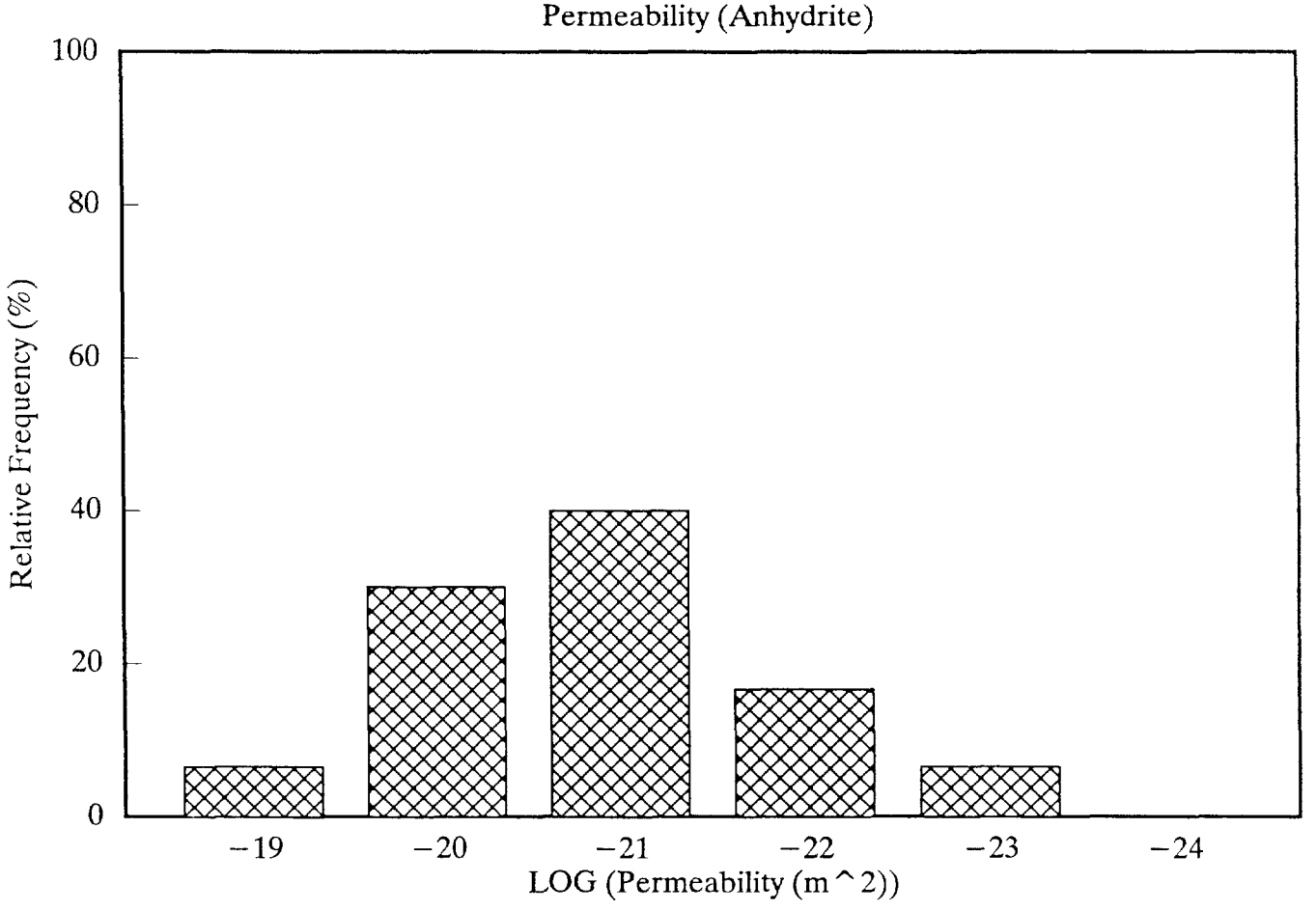
Permeability (Anhydrite)
100
80
60
40
20
0
Relative Frequency (%)
−19
−20
−21
−22
−23
−24
LOG (Permeability (m ^ 2))

ROOM Q

Permeability (Anhydrite)

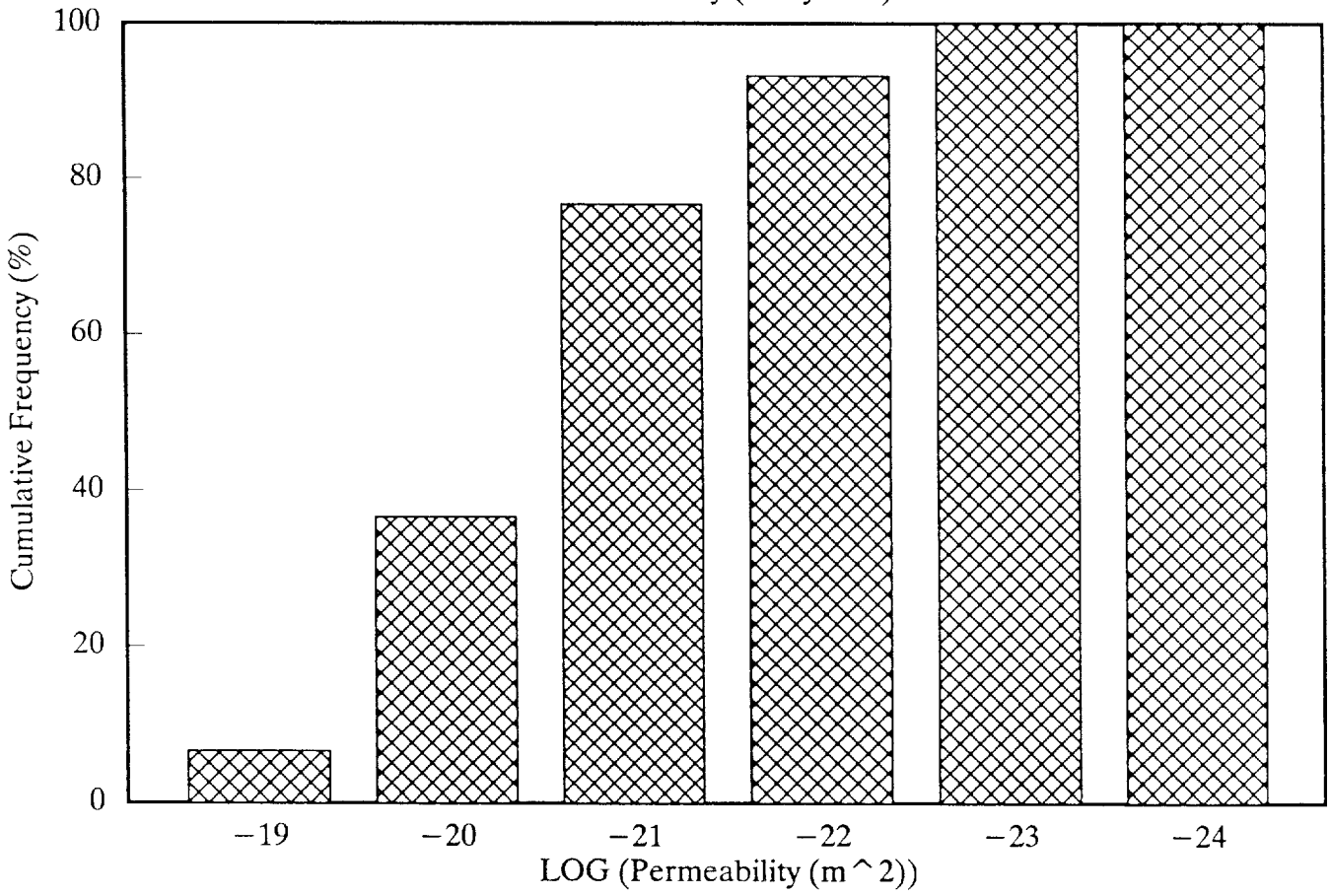

McTigue et al., March 14, 1991

Date: 3/14/91
To: Distribution
From: D. F. McTigue, 1511; S. J. Finley, 6344, J. H. Gieske, 7552; K. L. Robinson, 6345
Subject: Compressibility Measurements on WIPP Brines

Sandia National Laboratories
Albuquerque, New Mexico 87185

date: March 14, 1991

to: Distribution

D.F. McTigue S.J. Finley J.H. Gieske Karen Robinson

from: D. F. McTigue, 1511; S. J. Finley, 6344; J. H. Gieske, 7552; K. L. Robinson, 6345

subject: Compressibility Measurements on WIPP Brines

Preview Summary

The compressibility of WIPP brines has been measured using an acoustic method. For six samples collected from Room D and the Room Q access drift, measured compressibilities fall in the range $(2.40\text{–}2.54)\times10^{-10}$ Pa^{-1} at temperatures from 20 to 40 °C. The measurement error is estimated to be less than 1%.

Introduction

Most models for transient flow in porous media take into account the compressibility of the pore fluid. Compressibility allows for "storage" of fluid mass, *i.e.*, changes of fluid mass per unit volume of the medium in response to changes of fluid pressure. In a saturated medium in which the porous skeleton and the solid pore walls can be approximated as rigid, fluid compressibility is the only source of storage (or "capacitance"). In a deformable medium, there are contributions to the storage from compression of the fluid, compression of the pores, and compression of the solid comprising the pore walls. Virtually every model currently used to represent brine flow in WIPP salt requires a numerical value for the brine compressibility. To our knowledge, no direct compressibility measurements have been made previously on WIPP brines.

The purpose of this memo is to report recent measurements of the compressibility of Salado Formation brines collected from the WIPP underground. The method used exploits the simple relationship between compressibility and the sound speed in a liquid, and thus allows the use of highly developed ultrasonics technology. The direct measurement of compressibility in a static test, although very simple conceptually, is relatively difficult in practice. The compressibility of brine is of the order of 10^{-10} Pa^{-1}, indicating that one would need to resolve a volume change of the order of one part in 10^4 in order to obtain a compressibility measurement through an applied pressure change of 1 MPa (10 bars).

Definitions

As noted above, models for flow in porous media often take into account compressibilities of the fluid, the solid mineral constituent, and the porous skeleton. Thus, we adopt a subscript f here to emphasize that the present considerations address only the fluid phase.

The coefficient of compressibility, β_f, is defined by:

$$\beta_f = \frac{1}{\rho_f}\frac{\partial \rho_f}{\partial p} \quad , \tag{1}$$

where ρ_f is density and p is pressure. The compressibility is also simply the inverse of the bulk modulus, K_f:

$$\beta_f = \frac{1}{K_f} \quad . \tag{2}$$

The longitudinal wave speed, v_L, in an elastic body is given by

$$v_L = \sqrt{\frac{1}{\rho}\left(K + \frac{4}{3}G\right)} \quad , \tag{3}$$

where K and G are the bulk and shear moduli, respectively. In a fluid, in which $G = 0$, and we identify $K \equiv K_f$ and $\rho \equiv \rho_f$, (3) can be reduced and rearranged to give

$$K_f = \rho_f v_L^2 \quad . \tag{4}$$

Thus, the bulk modulus of a fluid is determined by measurements of its density and longitudinal wave speed.

Sample Selection

Six samples of Salado brine collected at the WIPP site were used for these measurements. The samples were selected from the brine sample inventory for the small-scale brine-inflow experiments. During the course of these experiments, brine flowing into boreholes in the underground is periodically pumped out of the boreholes, weighed, and saved in plastic sample bottles. The sample bottles are currently stored in metal cabinets in a building on the surface at the WIPP site.

The six samples used are listed in Table 1. After pumping, all brine samples are labeled with the borehole number and the date the sample was pumped out of the borehole. For example, the brine sample designated DBT31 12-7-88 was pumped out of borehole DBT31 on December 7, 1988. All of the DBT boreholes are vertical boreholes collared in the floor of Room D, which is situated in the northeastern corner of the WIPP underground experimental area. All of the QPB boreholes are vertical boreholes collared in the floor of the Q access drift, halfway between Room Q and the Air Intake Shaft. Brine samples 3 and 4 in Table 1, labeled QPB05A and QPB05C, respectively, were pumped from the same borehole on December 10, 1990. The letter designators A and C indicate that multiple sample bottles were filled when borehole QPB05 was pumped.

The particular samples chosen were from the subset of samples that are greater than 100 milliliters in volume, as this was assumed to be the minimum volume required for the sound speed measurements. Within this subset of larger-volume samples, those selected are believed to be representative of the Salado brine collected. Three of the samples are from Room D. These boreholes are collecting brine from the waste facility horizon, which includes Map Unit 6 and extends down through the top of Map Unit 0. The boreholes in Room D were drilled in the fall of 1987, and the brine collecting in those boreholes has been pumped out periodically since the drilling date. The Room D brine samples selected were considered to be representative of the time interval over which the brine has been collected. The other three samples are from the Q access drift, where the boreholes have been collecting brine from the lower section of Map Unit 0 and Marker Bed 139. These boreholes were drilled in the spring of 1989. All of the Q access drift samples were collected in December, 1990.

Density Measurements

The procedure used to measure the density of the brine samples is a standard laboratory procedure for measuring the density of liquids. An empty 50 ml beaker and watch glass were weighed and then filled with an aliquot of brine from the sample bottle. The aliquot was either 10 or 5 ml in volume, and was extracted from the sample bottle with a class A volumetric pipet. The beaker and watch glass with the brine sample were weighed again, and the weight of the empty beaker and watch glass was subtracted to obtain a weight for the brine itself. The weight of the brine was divided by the aliquot volume to obtain a density in grams per milliliter. These measured densities were converted to units of kg/m^3 and are listed in Table 1.

The ambient temperature of the laboratory where all density measurements were made was 22 °C. The temperature of the air in the boreholes in Room D fluctuates between 28 °C and 32 °C. Temperatures have not been measured in the QPB boreholes, but are assumed to be in the same range as in the Room D boreholes.

In order to determine the standard deviation associated with any one density measurement, the above-mentioned procedure was repeated 14 times on sample 1 (DBT31 12-7-88). The average brine density calculated was 1.249 g/ml, with a standard deviation of 0.0026 g/ml. The 95% confidence interval based on the Student's t distribution is 1.247 g/ml to 1.251 g/ml.

Table 1. Measured density; 22 °C.

Sample No.	Sample Loc. & Date	Density (kg/m^3)
1	DBT31 12-7-88	1.249×10^3
2	QPB02A 12-7-90	1.225×10^3
3	QPB05A 12-7-90	1.229×10^3
4	QPB05C 12-10-90	1.226×10^3
5	DBT32 1-18-90	1.240×10^3
6	DBT11 10-7-87	1.224×10^3

Sound Speed Measurements

The sound speed measurements reported here were obtained by the "pulse-echo-delay" method. An acoustic reflector in the shape of a "stair step" is placed in a vessel containing the brine sample (Figure 1). An acoustic transducer is positioned an arbitrary distance away from the step. The transducer is pulsed with a given waveform, and the reflections from the first and second step surfaces are recorded. The difference in travel time for the acoustic pulse can be determined very accurately from a digitized waveform of the two pulse echoes. The wave speed is related to the height of the step, L, and the time delay between echoes, T, by

$$v_L = \frac{2L}{T}. \tag{5}$$

The measurements reported here were made with a Lucite reflector with step height $L = 0.955$ cm. A 25 MHz transducer 0.635 cm in diameter was used, and the data were recorded with a LeCroy TR8828B 200 MHz transient recorder. The acoustic pulse was measured to have a frequency of 16 MHz. The pulse-echo time delay procedure was carried out on a 386 PC using a QuickBasic program. Temperatures were varied by placing the vessel in a heated water bath, and the temperature at the time of the subsequent test was recorded with a mercury thermometer with 0.1 °C graduations.

Temperature Corrections for Density

The fluid densities, ρ_f, used to compute the bulk moduli reported here are based on temperature corrections applied to a reference state.

For the pure water, densities are tabulated at discrete temperatures in [1, Table F-10]. In the temperature range from 15 to 45 °C, these data are very well represented by a four-term Taylor series expansion about a reference temperature of 30 °C:

$$\rho_f = \rho_{f0}[1 + d_1(\theta - 30) + d_2(\theta - 30)^2 + d_3(\theta - 30)^3], \quad (6)$$

where $\rho_{f0} = 0.99567$ is the density at the reference temperature of 30 °C, θ is the temperature of interest, and the coefficients take the values $d_1 = -3.0332 \times 10^{-4}$, $d_2 = -4.3866 \times 10^{-6}$, and $d_3 = 2.6828 \times 10^{-8}$. The fit was performed with the parameter-estimation code ESTIM [2]. The densities used to compute the compressibilities of distilled water shown in Table 4 were calculated from equation (6) using these parameters.

For the brines, it was assumed that each sample was saturated with respect to its dissolved species at the 22 °C laboratory temperature at which the initial density determinations were done. The thermal expansion of NaCl brines was discussed in a recent memo [3]. Based on data reported by Kaufmann [4, Table 46, p. 612], it is estimated that a saturated NaCl brine at 22 °C contains about 26.5 weight % salt. Extrapolation of the coefficients reported in [3], which were determined for brines at lower concentrations, yields the following expression for the density of brine saturated with respect to NaCl at 22 °C:

$$\frac{\rho_f}{\rho_{f0}} = 1 + d_1(\theta - 22) + d_2(\theta - 22)^2 + d_3(\theta - 22)^3, \quad (7)$$

where ρ_{f0} is the density at the reference temperature of 22 °C, and the coefficients take the values $d_1 = -4.4294 \times 10^{-4}$, $d_2 = -6.3703 \times 10^{-7}$, and $d_3 = -1.3148 \times 10^{-9}$. This expression was used to correct the reference densities measured at 22 °C (Table 1) for calculations of the compressibility at different temperatures (Tables 2, 3, 5, 6). We emphasize that the thermal expansion correction for brine is based on pure NaCl solutions rather than on WIPP brines. However, the behavior of WIPP brines is not expected to differ significantly. In any case, the density corrections are at most less than 1%.

Results

Results of the bulk modulus and compressibility determinations are shown in Tables 2–6. Tables 2 and 3 show data for all six brine samples at 20 °C and 25 °C, respectively. Table 4 shows results for distilled water at temperatures from 20 to 40 °C. The data from Table 4 are plotted as a function of temperature in Figure 2 along with reference compressibility data from the *CRC Handbook* [1, Table F-15] for comparison. The data from both the present study and the *CRC Handbook* appear to define a trend of decreasing compressibility with increasing temperature. Both data sets exhibit roughly the same degree of scatter about the general trend, suggesting that the data from the present study are of an accuracy comparable to that of the reference data. Quantitative error estimates for this study are discussed in the following section.

Tables 5 and 6 show results for two brines at temperatures from 20 to 40 °C. The brines show no significant variation in compressibility over this temperature range. This is

in contrast to pure water (Table 4; Figure 2), which shows a distinct decrease in β_f with increasing θ. Thus, the presence of a high concentration of dissolved salt serves to moderate the temperature sensitivity of the compressibility.

Figure 4 shows all compressibility measurements made on WIPP brines, regardless of temperature, plotted against density (Tables 2, 3, 5, 6). There is a strong correlation, indicating decreasing compressibility with increasing density. A linear regression on the data shown in Figure 4 yields

$$\beta_f = 7.662 \times 10^{-10} - 4.217 \times 10^{-13} \rho_f, \tag{8}$$

with a correlation coefficient of $r^2 = 0.91$. (Here, β_f has dimension Pa^{-1} and ρ_f dimension $\mathrm{kg/m}^3$.) This may provide a reasonable estimate for β_f for WIPP brines based solely on a density determination.

Table 2. Acoustic velocity; 20 °C.

Sample No.	Velocity, v_L m/s, $\times 10^{-3}$	Density, ρ_f $\mathrm{kg/m}^3$, $\times 10^{-3}$	Bulk Modulus, K_f Pa, $\times 10^{-9}$	Compressibility, β_f Pa^{-1}, $\times 10^{10}$
1	1.825	1.250	4.163	2.402
2	1.803	1.226	3.984	2.510
3	1.806	1.230	4.013	2.492
4	1.805	1.227	3.998	2.501
5	1.811	1.241	4.071	2.456
6	1.808	1.225	4.003	2.498

Table 3. Acoustic velocity; 25 °C.

Sample No.	Velocity, v_L m/s, $\times 10^{-3}$	Density, ρ_f kg/m^3, $\times 10^{-3}$	Bulk Modulus, K_f Pa, $\times 10^{-9}$	Compressibility, β_f Pa^{-1}, $\times 10^{10}$
1	1.828	1.247	4.166	2.400
2	1.807	1.223	3.993	2.504
3	1.818	1.227	4.056	2.466
4	1.814	1.224	4.027	2.483
5	1.813	1.238	4.070	2.457
6	1.811	1.224	4.009	2.494
pure water	1.493	0.997	2.223	4.498

Table 4. Acoustic velocity; distilled water.

Temperature °C	Velocity, v_L m/s, $\times 10^{-3}$	Density, ρ_f kg/m^3, $\times 10^{-3}$	Bulk Modulus, K_f Pa, $\times 10^{-9}$	Compressibility, β_f Pa^{-1}, $\times 10^{10}$
19.9	1.478	0.9983	2.181	4.586
21.0	1.483	0.9980	2.195	4.556
24.8	1.493	0.9971	2.223	4.499
30.7	1.494	0.9955	2.222	4.501
40.0	1.516	0.9922	2.280	4.385

Table 5. Acoustic velocity; sample #1, DBT31.

Temperature °C	Velocity, v_L m/s, $\times 10^{-3}$	Density, ρ_f kg/m^3, $\times 10^{-3}$	Bulk Modulus, K_f Pa, $\times 10^{-9}$	Compressibility, β_f Pa^{-1}, $\times 10^{10}$
20.0	1.825	1.250	4.163	2.402
24.9	1.828	1.247	4.167	2.400
29.7	1.827	1.245	4.156	2.406
35.1	1.830	1.242	4.159	2.404
39.6	1.820	1.239	4.104	2.437

Table 6. Acoustic velocity; sample #2, QPB02A.

Temperature °C	Velocity, v_L m/s, $\times 10^{-3}$	Density, ρ_f kg/m^3, $\times 10^{-3}$	Bulk Modulus, K_f Pa, $\times 10^{-9}$	Compressibility, β_f Pa^{-1}, $\times 10^{10}$
20.0	1.803	1.226	3.985	2.509
25.5	1.807	1.224	3.997	2.502
29.6	1.808	1.222	3.994	2.503
35.0	1.797	1.219	3.936	2.540
37.6	1.798	1.217	3.934	2.542

Propagation of Error

Estimates of the error in the compressibilities reported here were made in the following manner. The error estimate, $\lambda(x)$, for the measurement of each quantity x is given in Table 7.

In terms of measured quantities, the sound speed is given by equation (5). The error estimate for the sound speed, $\lambda(v_L)$, is then given by [5]:

$$\lambda^2(v_L) = \left(\frac{\partial v_L}{\partial L}\right)^2 \lambda^2(L) + \left(\frac{\partial v_L}{\partial T}\right)^2 \lambda^2(T), \tag{9}$$

or,

$$\lambda^2(v_L) = v_L^2 \left[\frac{\lambda^2(L)}{L^2} + \frac{\lambda^2(T)}{T^2}\right]. \tag{10}$$

For typical values of the measured quantities and the error estimates given in Table 7, equation (10) gives an estimated error for the reported wave speeds of about ±5 m/s (Table 8).

Table 7. Error estimates for measurements.

		$\lambda(x)$	
Quantity (x)	Symbol	Error Est. (As Reported)	Error Est. (SI Units)
Fluid density	ρ_f	±0.003 g/ml	±3.0 kg/m^3
Step Height	L	±0.001"	$\pm 2.5 \times 10^{-5}$ m
Time Delay	T	±0.01 μs	$\pm 1.0 \times 10^{-8}$ s
Temperature	θ	±0.1 °C	±0.1 K

In a similar fashion, the error estimates for the bulk modulus and compressibility can be shown to be:

$$\frac{\lambda^2(K_f)}{K_f^2} = \frac{\lambda^2(\beta_f)}{\beta_f^2} = \frac{\lambda^2(\rho_f)}{\rho_f^2} + \frac{4\lambda^2(L)}{L^2} + \frac{4\lambda^2(T)}{T^2}. \tag{11}$$

Evaluation of (11) using typical values of the measured quantities and the error estimates from Table 7 yields an error of about 0.6% for the bulk modulus and compressibility, or about ±0.025 GPa and $\pm 1.5 \times 10^{-12}$ Pa^{-1}, respectively (Table 8).

Table 8. Error estimates for calculated quantities.

Quantity (x)	Symbol	Error Est. $\lambda(x)$
Sound Speed	v_L	± 5.0 m/s
Bulk Modulus	K_f	$\pm 2.5 \times 10^7$ Pa
Compressibility	β_f	$\pm 1.5 \times 10^{-12}$ Pa^{-1}

Consistency with Independent Data

In addition to the test against tabulated properties for pure water discussed above, a check for consistency of the present measurements with independent values from the literature can be made for brines. The data presented here indicate a strong correlation of compressibility with fluid density (Figure 4). In fact, compressibility is reduced by nearly 50% by the addition of salt up to full saturation. The *CRC Handbook* [1, Table F-15] reports reference compressibilities for pure water, and Kaufmann [4, Table 40, p. 609] reports compressibilities determined acoustically for NaCl brines of varying concentrations. These data are shown in Figure 5 along with the present results for measurements at 25 °C, plotted against density. The conversion of weight-percent NaCl to density applied to the Kaufmann data was obtained from Kaufmann [4 Table 44, p. 611]. All the available data fall on a very smooth trend; a second-order polynomial fits this trend very well:

$$\beta_f = 4.492 \times 10^{-10} - 1.138 \times 10^{-12}(\rho_f - 1000.) + 1.155 \times 10^{-15}(\rho_f - 1000.)^2, \quad (12)$$

where ρ_f is in units of kg/m^3, and β_f is in units of Pa^{-1}.

Summary

The principal results outlined in this memo are:

- The compressibilities of six Salado brines from Room D and the Room Q access drift fall in the range (2.40–2.54)$\times 10^{-10}$ Pa^{-1}.
- The measurements were carried out over a temperature range of 20 to 40 °C; brine compressibility exhibits no significant dependence on temperature over this range.
- Compressibility exhibits a strong correlation with brine density, with β_f decreasing with increasing ρ_f; a linear relationship (eq. 8) correlates the data for WIPP brines well over the small range of densities tested.

- The results from this study are consistent with published results for NaCl brines at lower concentration; a smooth trend of decreasing β_f with increasing density (concentration) encompasses pure water, published data for lower-concentration NaCl brines, and the WIPP brines considered here (Figure 5). A quadratic relationship (eq. 12) describes this trend very well.

- The acoustic method was validated by measurements made on distilled water. Results compare very well with reference data.

- Error in the compressibility measurements is estimated to be approximately 0.6%.

Note that a number of previous calculations of flow in WIPP salt [*e.g.*, 6–8] used values for brine compressibility of 5.0×10^{-10} Pa^{-1} (bulk modulus 2.0×10^{9} Pa). This high value for β_f (low K_f) was based on an estimate for pure water (one-place accuracy for K_f). The results shown here indicate that the presence of a high concentration of salt reduces the compressibility by nearly a factor of two.

References

1. Weast, R. C., ed., *CRC Handbook of Chemistry and Physics*, CRC Press, Boca Raton, 1985.

2. Hills, R. G., ESTIM: A parameter estimation computer program, **SAND87–7063**, *Sandia National Laboratories Technical Report*, August 1987.

3. McTigue, D. F., "Thermal expansion coefficient for brine," memo to Distribution, January 22, 1991.

4. Kaufmann, D. W., Physical properties of sodium chloride in crystal, liquid, gas, and aqueous solution states, in *Sodium Chloride: The Production and Properties of Salt and Brine*, D. W. Kaufmann, ed., American Chemical Society, Washington, D. C. 587–626, 1960.

5. Shoemaker, D. F., Garland, C. W., and Steinfeld, J. I., "Propagation of errors," *Experiments in Physical Chemistry*, McGraw-Hill, New York, 1974, 51–55.

6. Nowak, E. J., and McTigue, D. F., "Interim results of brine transport studies in the Waste Isolation Pilot Plant (WIPP), *Sandia National Laboratories Technical Report*, **SAND87–0880**, May 1987.

7. McTigue, D. F., and Nowak, E. J., "Brine transport in the bedded salt of the Waste Isolation Pilot Plant (WIPP): Field Measurements and a Darcy Flow Model," *Scientific Basis for Nuclear Waste Management XI*, M. J. Apted and R. E. Westerman, eds., Materials Research Society, Pittsburgh, 209–218, 1987.

8. Nowak, E. J., McTigue, D. F., and Beraun, R., "Brine inflow to WIPP disposal rooms: data, modeling, and assessment," *Sandia National Laboratories Technical Report*, **SAND88–0112**, September 1988.

DFM:1511:dfm

Key Words: **radioactive waste, Waste Isolation Pilot Plant (WIPP), material properties, brine, compressibility**

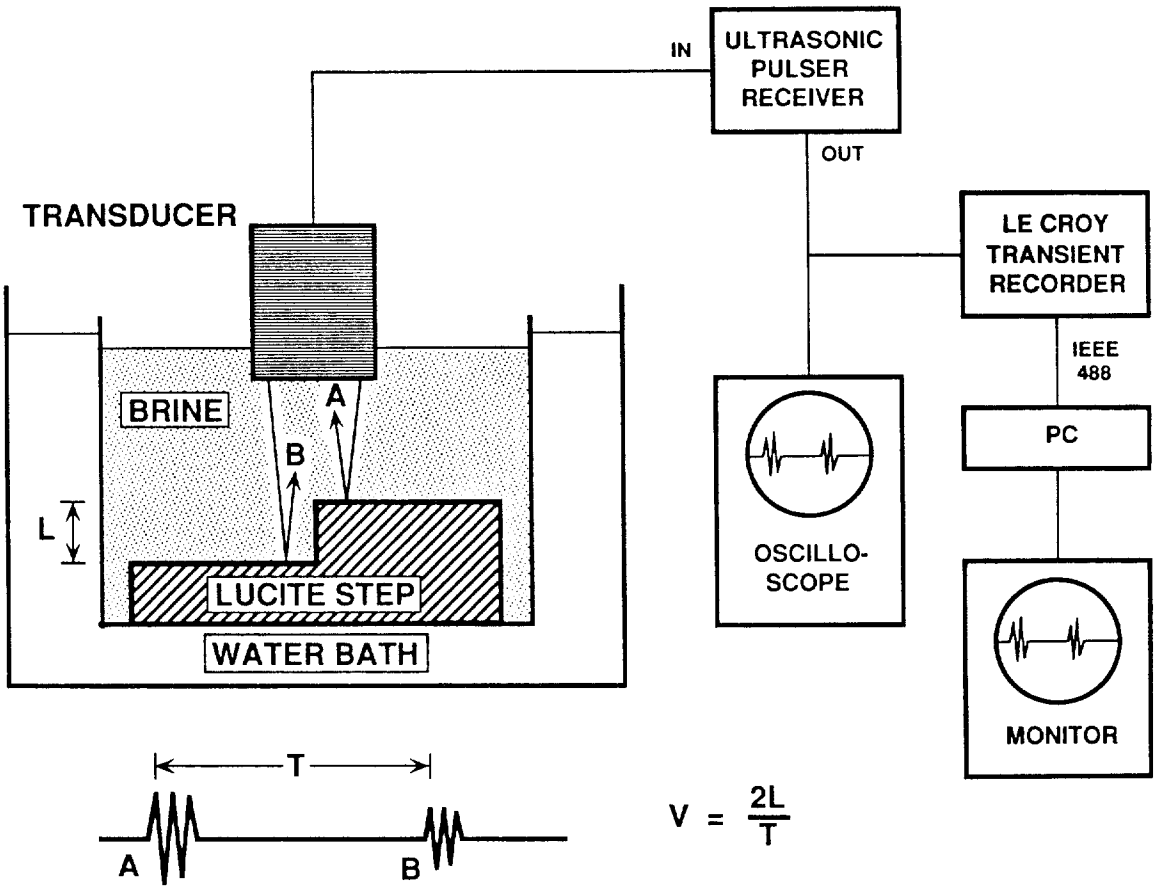

Figure 1. Schematic of the pulse-echo delay time technique for measuring acoustic velocity in a liquid.

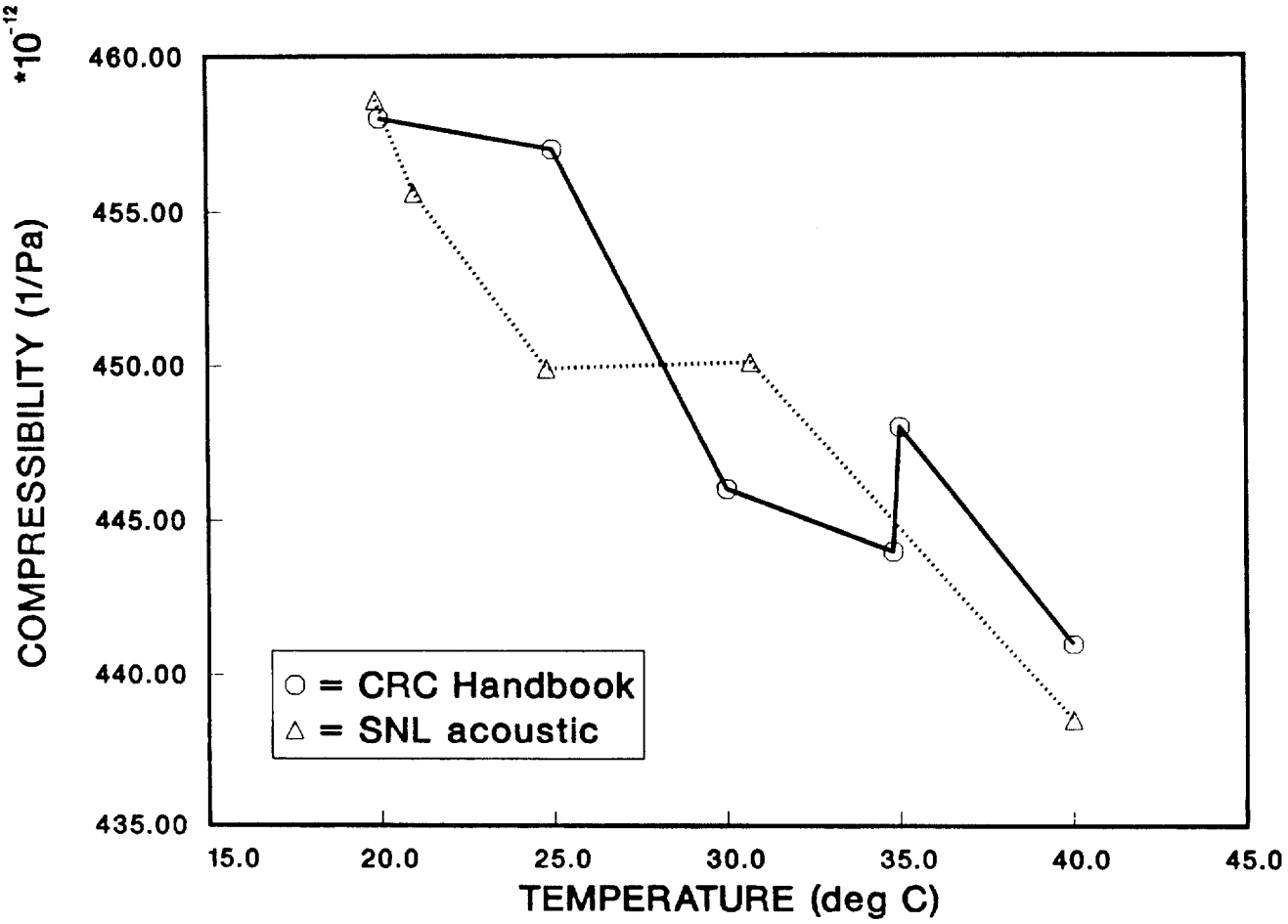

Figure 2. Comparison of compressibilities determined in this study with tabulated values [1] for distilled water.

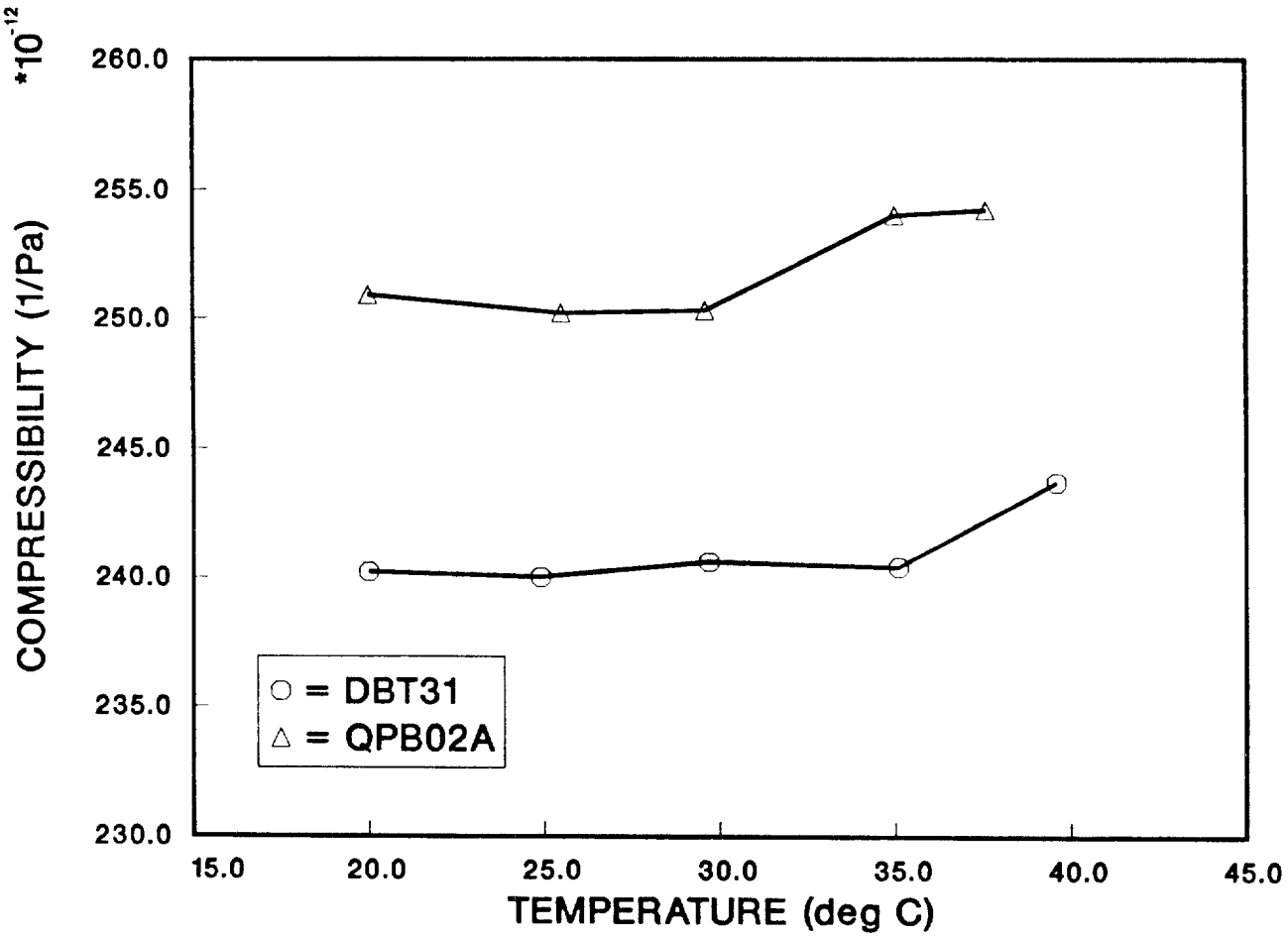

Figure 3. Compressibility of WIPP brines plotted against temperature.

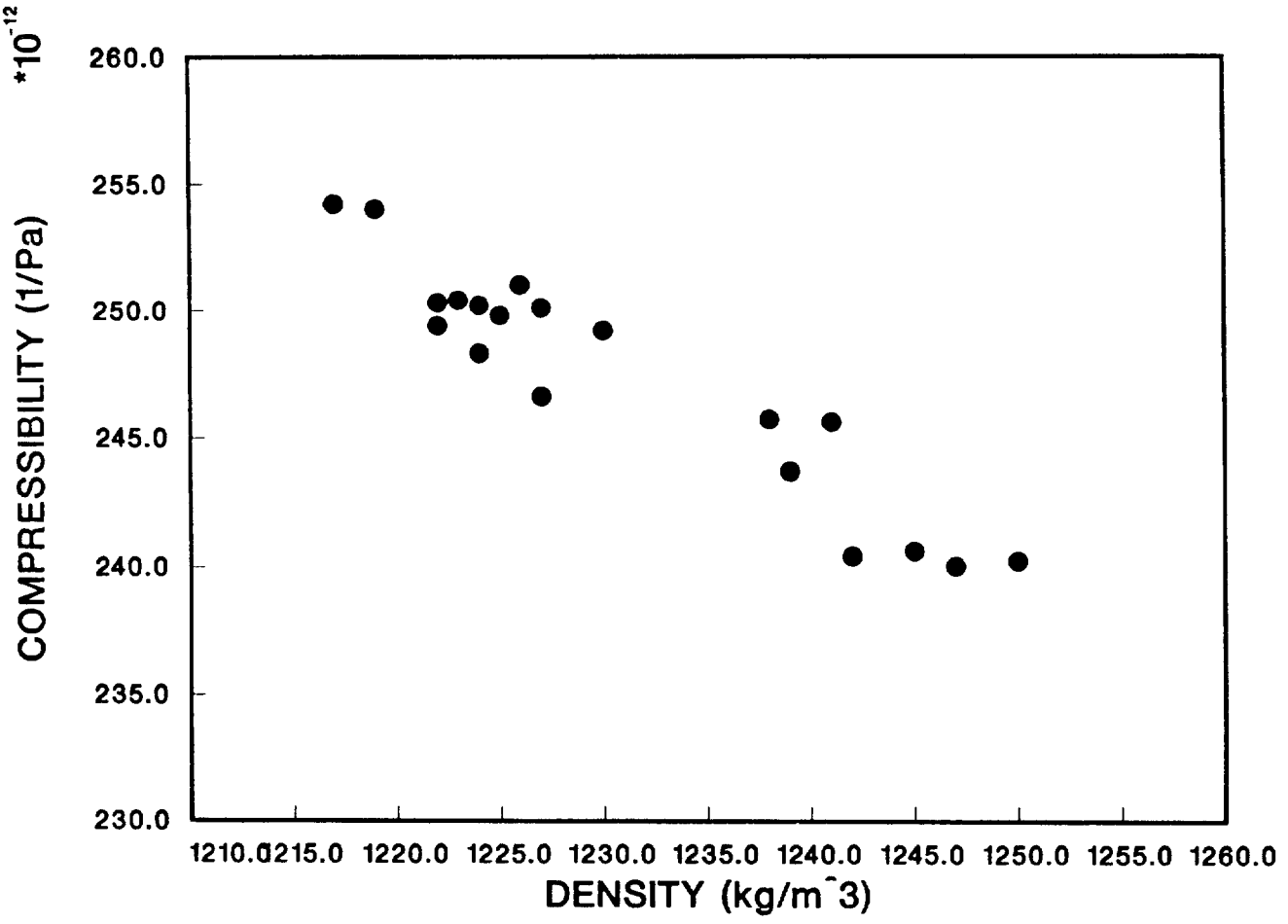

Figure 4. Compressibilities of WIPP brines plotted against fluid density.

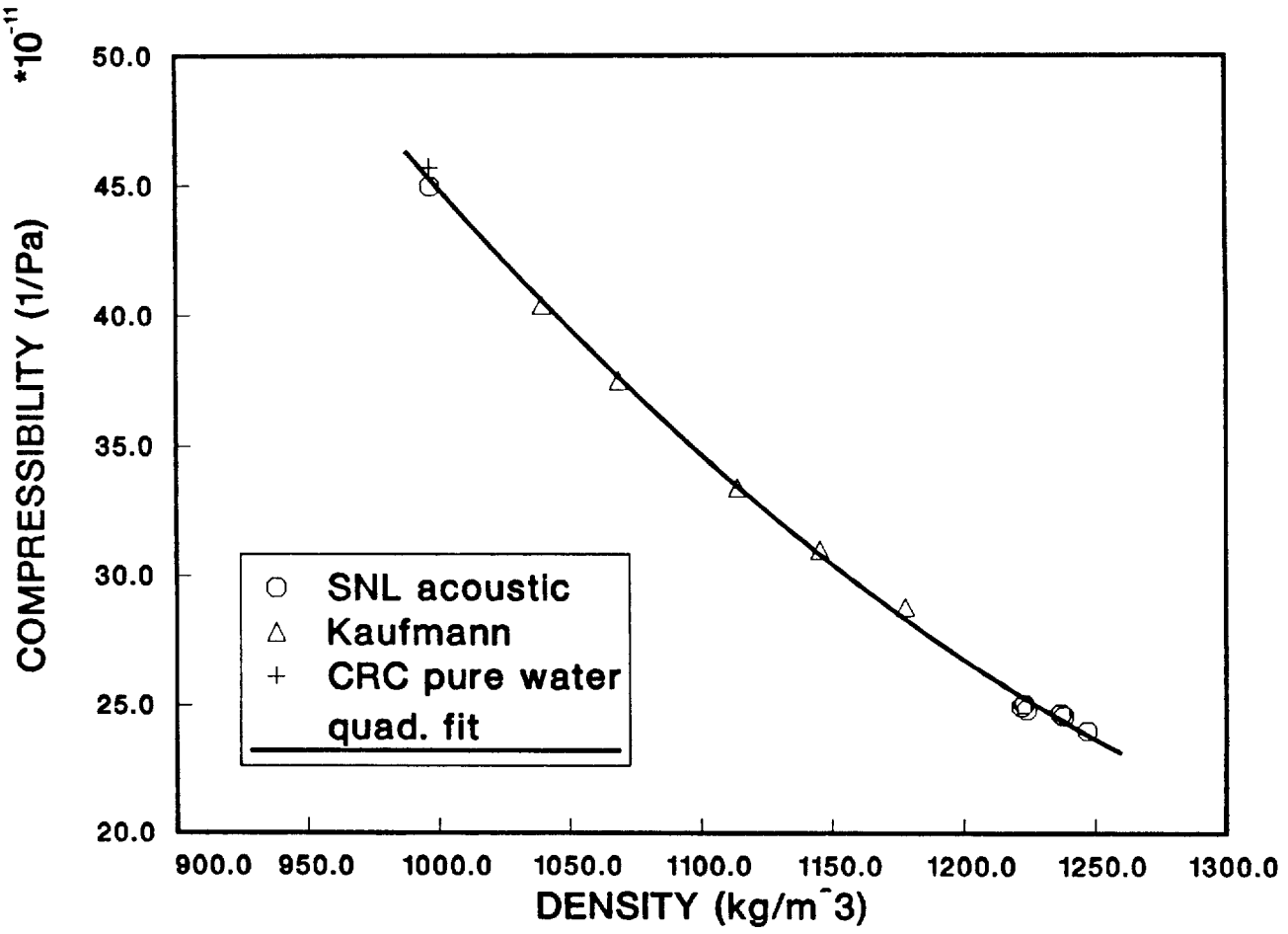

Figure 5. Compressibilities of WIPP brines and pure water determined in this study and literature values [1, 4] at 25 °C, plotted against density. Solid line shows a quadratic fit (eq. 12) to the 13 points shown. WIPP brine compressibilities appear to be on a consistent trend with the literature values.

Copy to:
1510 J. C. Cummings
1511 D. K. Gartling
1511 D. F. McTigue (day file)
1512 A. C. Ratzel
1513 Acting Supervisor
1514 H. S. Morgan
1514 J. G. Arguello, Jr.
1514 C. M. Stone
1514 J. R. Weatherby
1540 J. R. Asay
1550 C. W. Peterson, Jr.
6232 W. R. Wawersik
6257 J. L. Todd, Jr.
6340 W. D. Weart
6340 A. R. Lappin
6340 S. Y. Pickering
6341 R. C. Lincoln
6341 R. D. Klett
6342 D. R. Anderson
6342 R. P. Rechard
6344 E. D. Gorham
6344 R. L. Beauheim
6344 P. B. Davies
6344 S. J. Finley
6344 S. Howarth
6344 S. W. Webb
6345 B. M. Butcher
6345 F. T. Mendenhall
6345 K. L. Robinson
6346 J. R. Tillerson
6346 E. J. Nowak
6346 J. C. Stormont
7551 B. D. Hansche
7552 W. W. Shurtleff
7552 J. H. Gieske

Novak, September 4, 1991

Date: 9/4/91
To: K. M. Trauth, 6342
From: Craig F. Novak, 6344
Subject: Rationale for K_d Values Provided During Elicitation of the Retardation Expert Panel, May 1991
(Note: Includes addendum with correction for typographical error in Table 2.)

Sandia National Laboratories

Albuquerque, New Mexico 87185

date: 4 September 1991

to: K.M. Trauth, 6342

from: Craig F. Novak, 6344

subject: Rationale for K_d Values Provided During Elicitation of the Retardation Expert Panel, May 1991

In May 1991, I was asked to participate on a panel for estimating values of radionuclide retardation in the Culebra Dolomite Member of the Rustler Formation. Estimates were to be made using the K_d model for retardation, and according to an "expert judgement" methodology (Tierney, 1991). This memorandum summarizes my preparation for this task, and the thought processes used in responding to this request. The cumulative probability functions (CDFs) for K_d values resulting from this elicitation are given in Tables 1 and 2.

I performed a detailed examination of available research reports describing experimental measurement of K_d's using substrates and water compositions pertinent to transport in the WIPP system. This study is documented in Novak (1991). Novak showed that data are not available for all elements of interest, almost no data exist for clay substrates in the Culebra, and existing data may not be applicable to current human intrusion scenarios. Novak (1991) also questions the utility of the K_d model for estimating retardation in the Culebra. Despite these limitations, I endeavored to provide K_d values for use in the 1991 performance assessment calculations.

Estimates of K_d's were requested for two scenarios differing only in water composition. Within each scenario, K_d estimates were needed for radionuclide sorption on the matrix (i.e. dolomitic Culebra substrates) and in the fractures (i.e. on clay materials lining fractures). Scenario One assumed that water reaching the Culebra would not change the composition of Culebra water significantly, except for the presence of radionuclides. Scenario Two assumed that water reaching the Culebra would not be diluted, and thus a concentrated brine contaminated with radionuclides would flow

through the Culebra. These scenarios were chosen as bounding cases for hydrologic and chemical behavior in the Culebra under breach scenarios. Scenarios One and Two reflect the uncertainty involved with mixing in the Culebra and the observation that measured K_d values depend on water composition.

The eight elements for which K_d estimates were requested were plutonium (Pu), americium (Am), curium (Cm), uranium (U), neptunium (Np), thorium (Th), radium (Ra), and lead (Pb). I chose to group Am with Cm, U with Np, and Ra with Pb, and to provide a single CDF for each group. This choice was made because of the limited amount of data and because of analogies between the chemical behavior of the grouped elements (Lappin et al., 1989).

Among the existing data, I feel that the water composition called "Culebra H2O" is the most representative for Scenario One, while Brine A is the most representative for Scenario Two. Thus, for Scenario One, data in "Culebra H2O" were used to estimate K_d values where the data were available. Similarly for Scenario Two and data in Brine A. In the absence of these data, values were provided based on subjective "expert judgement" and interpretation of other data. The same CDFs were given for both scenarios for Th, and for Ra and Pb, because of the lack of data.

The lower bounds for K_d's in all CDFs are 0 ml/g because it is possible that any of the elements could be transported with the fluid velocity. The upper bounds in Tables 1 and 2 represent my opinions on the maximum values for K_d's that could be observed for these elements under the human intrusion scenarios. K_d values for cumulative probabilities of 0.25, 0.5, etc., represent best estimates resulting from my assimilation of data and literature on this topic.

There is a paucity of data for sorption of radionuclides on clays for solutions with water compositions pertinent to WIPP breach scenarios. However, clays are known to have large adsorption capacities, and therefore should exhibit high K_d values for radionuclides. For these reasons, CDFs for the fractures were estimated to be a factor of ten larger than for the matrix.

The values provided through the elicitation process are subjective estimates only. The human intrusion scenarios contain large uncertainties with respect to water compositions and mixing in the Culebra. Few experimental measurements of K_d's have been performed. In addition, the K_d model may have limited applicability to the WIPP Culebra system. These factors could render the CDFs given for K_d's inadequate to represent the actual values for K_d's that would occur under human intrusion scenarios.

The CDFs for K_d's are not a substitute for actual data, and should not be interpreted as such. Additional study is needed to quantify the potential for radionuclide retardation in the Culebra Dolomite Member of the Rustler Formation.

References

Lappin, A.R., and R.L. Hunter, eds. 1989. *Systems Analysis, Long-Term Radionuclide Transport, and Dose Assessments, Waste Isolation Pilot Plant (WIPP), Southeastern New Mexico; March 1989.* SAND89-0462. Albuquerque, New Mexico: Sandia National Laboratories.

Novak, C.F. 1991. *An Evaluation of Radionuclide Batch Sorption Data on Culebra Dolomite for Aqueous Compositions Relevant to the Human Intrusion Scenario for the Waste Isolation Pilot Plant (WIPP).* SAND91-1299. Albuquerque, New Mexico: Sandia National Laboratories.

Tierney, M.S. 1991. *Issue Statement for Elicitation of Expert Judgement Concerning Magnitudes of Culebra Distribution Coefficients for Use in the 1991 WIPP Performance Assessment.* 8 May 1991. Albuquerque, New Mexico: Sandia National Laboratories.

CFN:6344

Distribution:

6340 W.D. Weart
6342 D.R. Anderson
6344 E.D. Gorham
6344 C.F. Novak
DOE/WPO B. Becker

Table 1. Estimates of Matrix K_d Values from Expert Elicitation

Cumulative Probability	Scenario One, Pu Matrix K_d, ml/g	Scenario Two, Pu Matrix K_d, ml/g
0	0	0
0.1	5	0.55
0.25	80	10
0.5	300	50
0.75	1000	150
1	100000	100000

Cumulative Probability	Scenario One, Am and Cm Matrix K_d, ml/g	Scenario Two, Am and Cm Matrix K_d, ml/g
0	0	0
0.25	90	10
0.5	150	40
0.75	400	100
0.9	1000	
0.99		1000
1	100000	100000

Cumulative Probability	Scenario One, U and Np Matrix K_d, ml/g	Scenario Two, U and Np Matrix K_d, ml/g
0	0	0
0.2	0.25	1
0.5	0.75	3.3
0.8	1.5	8
1	100	100

Cumulative Probability	Scenarios One and Two, Th Matrix K_d, ml/g
0	0
0.25	5
0.5	10
0.75	100
1	1000

Cumulative Probability	Scenarios One and Two, Ra and Pb Matrix K_d, ml/g
0	0
0.25	1
0.5	10
0.75	100
0.99	1000
1	10000

Table 2. Estimates of Fracture K_d Values from Expert Elicitation

Cumulative Probability	Scenario One, Pu Fracture K_d, ml/g	Scenario Two, Pu Fracture K_d, ml/g
0	0	0
0.1	50	5.5
0.25	800	100
0.5	3000	500
0.75	10000	1500
1	1000000	1000000

Cumulative Probability	Scenario One, Am and Cm Fracture K_d, ml/g	Scenario Two, Am and Cm Fracture K_d, ml/g
0	0	0
0.25	900	100
0.5	1500	400
0.75	4000	1000
0.9	10000	
0.99		10000
1	1000000	1000000

Cumulative Probability	Scenario One, U and Np Fracture K_d, ml/g	Scenario Two, U and Np Fracture K_d, ml/g
0	0	0
0.2	2.5	10
0.5	7.5	33
0.8	15	80
1	1000	1000

Cumulative Probability	Scenarios One and Two, Th Fracture K_d, ml/g
0	0
0.25	50
0.5	100
0.75	1000
1	10000

Cumulative Probability	Scenarios One and Two, Ra and Pb Fracture K_d, ml/g
0	0
0.25	1
0.5	10
0.75	100
0.99	1000
1	10000

Sandia National Laboratories

Albuquerque, New Mexico 87185

date: 9 September 1991

to: K.M. Trauth, 6342

from: Craig F. Novak, 6344

subject: Typographical Error in Memo of 4 September 1991

My memorandum of 4 September contained a typographical error in Table 2, the fracture Kd values for Ra and Pb for Scenarios One and Two. As the test states, the fracture Kd's were estimated to be a factor of ten larger than the matrix Kd's. Thus, the Ra and Pb section of Table 2 should read

Cumulative Probability	Scenarios One and Two, Ra and Pb Fracture K_d, ml/g
0	0
0.25	10
0.5	100
0.75	1000
0.99	10000
1	100000

CFN:6344

Distribution:

6340 W.D. Weart
6342 D.R. Anderson
6344 E.D. Gorham
6344 C.F. Novak
DOE/WPO B. Becker

Swift, October 10, 1991

Date: 10/10/91
To: R. P. Rechard
From: Peter Swift, 6342/Tech Reps
Subject: Climate and recharge variability parameters for the 1991 WIPP PA calculations

TECH REPS, INC.
5000 Marble Avenue NE
Albuquerque, New Mexico 87110
505 266 5678
fax 505 260 1163

October 10, 1991

to: R. P. Rechard
Sandia National Laboratories Division 6342

from: P. N. Swift
6342/Tech Reps

subject: Climate and recharge variability parameters for the 1991 WIPP PA calculations

Summary of Recommendations for the 1991 PA Calculations

The uncertain input parameter of interest here is recharge to the regional domain of the Culebra Dolomite groundwater-flow model.

I recommend separating recharge into two component functions: variability in mean annual precipitation and variability in the amount of precipitation that reaches our Culebra model domain as recharge. For the 1991 *Preliminary Comparison*, I recommend sampling on the recharge parameter only, and using a fixed function for climatic variability. Specific functions are as follows.

Recommended function for future mean annual precipitation (P_f) as a function of time (t, measured in units of 10^4 years):

$$P_f(\text{cm/yr}) = 52.5 - 15(\cos\beta t - \sin 0.5\alpha t + 0.5\cos\alpha t)] ,$$

with $\alpha = 20\pi$, $\beta = \pi/6$.

Recommended function for future model recharge (R_f) as a function of nominal present model recharge (R_p), assuming that model recharge can be expressed as boundary flux into the regional model domain:

$$R_f = R_p \times [1 + (2r - 1)(\frac{P_f - 30}{30})] ,$$

if $P_f \geq P_p$, or

$R_f = R_p$ if $P_f < P_p$;

with P_f calculated according to the previous equation, in cm/yr, and r sampled on a uniform distribution from 1 to 10.

Introduction

Ideally, it could be possible to describe variability in recharge within a single conceptual model for flow in the Culebra using a single parameter—future recharge as a function of present recharge. I recommend, however, separating recharge into two component functions: variability in mean annual precipitation and variability in the amount of precipitation that reaches our Culebra model domain as recharge. This distinction allows examining model sensitivity to climatic change independently of the uncertainty in the physical recharge process. The distinction is meaningful because we can assess climatic variability relatively confidently, whereas uncertainty about the recharge process is high. Sampling on separate parameters will permit us to perform sensitivity analyses (to be reported by Swift et al. [in prep.], separately from the 1991 *Preliminary Comparison*) on both climate variability and the assumed recharge function.

This memo defines climate and recharge functions and the associated parameters to be sampled. The memo does not address conceptual model uncertainty about the location or amount of present recharge to the model domain, or about the location of future recharge. These model uncertainties will be addressed in 1992 or later, as results become available from the geostatistics project addressing uncertainty in the Culebra flow model. The assumption is made here that future model recharge will be expressed as a function of nominal present flux into a calibrated steady-state flow model.

For the 1991 PA calculations, there appears to be little need to sample on a distribution of climate parameter values. As explained below, we can select "best estimate" values for climate variability for the full-system simulations, and wait for the separate sensitivity analysis report to examine the impact of the assumptions. This does not mean that the 1991 calculations will not include climate variability. Climate variability will be incorporated, and the results will reflect the knowledge that some future climates will be wetter than that of the present. The function and values I am recommending will give us an "average" future precipitation roughly 1.3 times present, with peaks of just over 2 times present.

I do recommend sampling on the recharge function parameter. As defined here, this parameter is a simple multiplier that is applied to the nominal increase in precipitation, yielding the change in model recharge. The multiplier represents uncertainty in numerous parameters, including (i) the location and extent of the surface recharge area, (ii) groundwater flow between the surface recharge area and the boundary of the model domain, and (iii) the relationship between precipitation and infiltration in the surface recharge area, which in turn is dependent on factors such as vegetation, temperature, local topography, and soil characteristics. There is no particular reason to assume a 1-to-1 correlation between increases in precipitation and increases in model recharge, and limited evidence for water-table conditions in semi-arid climates suggests that increases in precipitation may result in substantially larger increases in infiltration. I recommend that we incorporate recharge uncertainty in the 1991 calculations by sampling a uniformly distributed recharge parameter (defined below) over a range that permits the relationship between mean annual precipitation and model recharge to vary between 1-to-1 and 10-to-1. This

would mean that with precipitation at a maximum of 2x present, model recharge could range from 2x to 20x present. Both the range and the distribution are preliminary, and should be adjusted as new data or interpretations warrant.

Description of Climate Variability

The basic premise for assessing climatic change at the WIPP is the assumption that, because of the long-term stability of glacial cycles, future climates will remain within the range defined by Pleistocene variation. Present understanding does not suggest that short-term (century-scale) anthropogenic changes in the Earth's greenhouse effect will invalidate this premise: published results of global-warming models do not predict climatic changes of greater magnitude than those of the Pleistocene (Swift, in prep.; Bertram-Howery et al., 1990).

Paleoclimatic data permit reconstruction of a precipitation curve for the WIPP for the last 30,000 years (Figure 1). This curve shows two basic styles of climatic fluctuation: relatively low-frequency increases in precipitation that coincide with the maximum extent of the North American ice sheet; and higher-frequency precipitation increases of uncertain causes that have occurred both during the glacial maximum and in the 10,000 years since the retreat of the ice sheet. Variability has also occurred in the seasonality and intensity of precipitation. Most of the late Pleistocene moisture fell as winter rain. Most of the Holocene precipitation falls during during a summer monsoon, in local and often intense thunderstorms. This variability probably has affected recharge: no WIPP-specific data are available, but, in general, higher temperatures increase evapotranspiration and decrease infiltration. The resulting variability in recharge is included in the recharge function described below, however, and I have made no effort to distinguish between winter and summer precipitation in the climate function.

The amplitude of the low-frequency glacial precipitation peak is relatively well-constrained by data from multiple sources. Amplitudes of the higher-frequency are less easily determined, but data indicate that none of the Holocene precipitation peaks exceeded average glacial levels. I recommend that we assume that high-frequency peaks with amplitudes comparable to those of the Holocene could have been superimposed on the glacial maximum. Therefore, there may have been relatively brief (i.e., on the order of hundreds to perhaps thousands of years) periods during the glacial maximum when precipitation at the WIPP may have averaged three times present levels.

The curve shown in Figure 1 cannot be extrapolated into the future with any confidence. The curve can be used, however, in combination with the general understanding of glacial periodicity (see Swift, in prep.) to make a reasonable approximation of likely future variability. The function I propose is not in any sense a predictive function for future precipitation. Rather, it is an admittedly simplistic function that can be readily adjusted to approximate the variability that may occur.

Specifically, my proposed precipitation function is as follows:

$$P_f = P_p \times \left[\left(\frac{3A + 1}{4} \right) - \left(\frac{A - 1}{2} \right) \left(\cos\beta t - \sin\frac{\alpha}{2} t + \frac{1}{2}\cos\alpha t \right) \right] ,$$

where

P_f = future mean annual precipitation
P_p = present mean annual precipitation
A = amplitude scaling factor (i.e., past precipitation maximum was A times the present)
α = frequency parameter for Holocene-type climatic fluctuations
β = frequency parameter for Pleistocene glaciations
t = time (after present, in 10^4 years).

The equation can be simplified considerably by using available data. The three-year precipitation record from the site is too brief to be useful for determining a long-term mean, but examination of regional data suggests an approximate value of 30 cm/yr (estimated from data presented by Hunter, 1985). Past precipitation maximums were approximately twice present (Swift, in prep.), and the amplitude scaling factor, A, can therefore be set at 2. The equation then becomes:

$$P_f(\text{cm/yr}) = 52.5 - 15(\cos\beta t - \sin 0.5\alpha + 0.5\cos\alpha t)].$$

My preferred values for α and β have been chosen from examination of the past precipitation curve (Figure 1) and the glacial record. If $\alpha = 20\pi$, wet maximums will occur every 2000 years, approximately with the same frequency shown on Figure 1. Note that we are presently near a dry minimum, and the last wet maximum occurred roughly 1000 years ago. If $\beta = \pi/6$, the next full glacial maximum will occur in 60,000 years, approximately the time predicted by simple models of the astronomical control of glacial periodicity (e.g., Imbrie and Imbrie, 1980). Figure 2 shows a plot of the climate function for these values.

Figure 3 shows how varying β can affect the curve. Choosing $\beta = \pi$ gives a wet maximum in 10,000 years, and results in extreme precipitation values 3 times those of the present. This is not a realistic value for β—ice sheets grow relatively slowly, and it would be difficult to achieve full continental glaciation within 10,000 years. I do not recommend sampling on variations in β for the 1991 calculations, but I do plan to consider the case in the separate sensitivity analyses.

Figure 4 shows the effect of varying α, in this case to yield wet peaks every 4000 years. Changes in α vary the frequency of the shorter-term fluctuations, but they do not change the ratio between wet and dry climates, and the average precipitation over 10,000 years remains the same.

Examination of Figure 1 shows that Holocene climates have been predominantly dry, with wet peaks much briefer than dry minimums. The α terms in the above equation give an oscillation in which the future climate is wetter than the present one-half of the time. I believe this value to be somewhat greater than the actual ratio, and, assuming that wet conditions are more

likely to result in releases from the WIPP, these terms provide a conservative approximation of Holocene variability. Furthermore, the choice of a single amplitude scaling factor for both Holocene and glacial peaks results in α peaks that are probably higher than all Holocene peaks and certainly higher than most.

Minor fluctuations during the dry minimums shown in Figures 2 through 4 are an artifact of the three-term function, and are not intended to represent any particular climatic variability. The minimum values of the "overshoots" do, however, correspond reasonably well to the minimum values shown in Figure 1 for the middle Holocene. Paleoclimatic data indicate that minimum Holocene precipitation may have been approximately 90% of present values (Swift, in prep.).

Glacial cycles have not been symmetric. Precipitation increases during glacial advances have been gradual, whereas decreases at the end of glaciation have been abrupt, giving a sawtooth characteristic to the curve. The assumption of a cosine function for glacial cycles may therefore not be conservative for WIPP performance assessment: precipitation during glacial advances may be underestimated. The significance of this possible underestimation will be examined in the separate sensitivity analyses by using larger β values, and accelerating the next glacial peak (Swift et al., in prep.).

Description of Recharge Variability

We know little about recharge to the Culebra. Hydraulic head and isotopic data (e.g., Holt et al., in prep.; Lambert and Harvey, 1987; Lambert and Carter, 1987, Lappin et al., 1989) indicate that very little if any moisture reaches the Culebra directly from the ground surface within the model domain. Regionally, it is believed that recharge occurs several tens of kilometers to the north, where the Culebra is near the ground surface (Mercer, 1983; Brinster, 1991). It is unknown if water from this recharge area presently reaches the model domain. Nominal recharge to the two-dimensional Culebra model has, in the past, been a prescribed boundary condition estimated from head and density data from WIPP-area wells (LaVenue et al., 1990).

Available literature on the relationship between precipitation and recharge is limited to examinations of recharge to a water table by direct infiltration. Environmental tracer research (e.g., Allison, 1988) suggests that long-term increases in precipitation in deserts may result in significantly larger increases in infiltration, particularly if the increases in precipitation coincide with lower temperatures and decreased evapotranspiration. As an extreme example, Stone (1984) estimated a 28-fold increase in infiltration for one location at the Salt Lake coal field in western New Mexico during the late Pleistocene wet maximum. Bredenkamp (1988a,b) compared head levels in wells and and sinkholes with short-term (decade-scale) precipitation fluctuations in the Transvaal, and suggested that for any specific system there may be a minimum precipitation level below which recharge does not occur. Above this uncertain level recharge to the water table may be a linear function of precipitation.

Data of this sort could perhaps be applied quantitatively to the WIPP if we (i) knew the location and extent of the surface recharge area for the Culebra, (ii) knew how much, if any, infiltration occurs there at present, and (iii) could include the recharge area in the model domain. We do not know the first two, and it is not feasible to attempt the third. Even if we could map the recharge area, uncertainty would remain about the extent of the larger area in which significant inflow to the Culebra occurs as leakage from overlying units. Even if we could quantify recharge from the surface and inflow from overlying units, extending the model domain to include the necessary area does not appear realistic.

Therefore, I recommend assigning a wide range to model recharge. The specific function I suggest is:

$$R_f = R_p \times \left[1 + \left(\frac{Ar - 1}{A - 1}\right)\left(\frac{P_f - P_p}{P_p}\right)\right] ,$$

if $P_f \geq P_p$, or

$R_f = R_p$ if $P_f < P_p$;

with terms defined to be:

R_f = future nominal flux into the modeled Culebra
R_p = present nominal flux into the modeled Culebra
r = recharge scaling parameter
P_f = future mean annual precipitation, as calculated from the above climate variability equation
P_p = present mean annual precipitation
A = precipitation amplitude scaling factor as in the climate variability function above (i.e., past precipitation maximum was A times the present).

Using values of 2 for A and 30 cm/yr for P_p, the recharge function simplifies to:

$$R_f = R_p \times \left[1 + (2r - 1)\left(\frac{P_f - 30}{30}\right)\right] ,$$

if $P_f \geq P_p$, or

$R_f = R_p$ if $P_f < P_p$.

This function applies the recharge scaling factor only to that portion of future precipitation that represents an increase over present precipitation. Thus, to achieve a 10-fold increase in recharge from a doubling of precipitation (i.e., $A = 2$, $P_f = 2P_p$), it would be necessary to use an r value of 5. Regardless of the selected r value, if precipitation remains constant, recharge also remains constant. The function does not allow for a time lag between changes in precipitation and model recharge. This is unrealistic, but of little consequence unless the lag is long relative to

the 10,000-year period of interest, in which case the assumption of instantaneous model recharge response is conservative.

The decision to hold recharge at the present level when calculated precipitation falls below present avoids "negative" recharge for large values of r. Flux across the model domain boundary may in fact have been less in the past, during times when precipitation was slightly less than present, but variation was probably slight, and it is unrealistic to assume that the same function applies for lower levels of precipitation.

I recommend sampling a uniform distribution of r values from 1 to 10 to cover variability in model recharge. Justification for the range and distribution are as follows:

Lower bound, r = 1. This value yields a 1-to-1 correspondence between precipitation and model recharge, which I believe to be a conservatively high lower bound. A less than 1-to-1 correspondence (r values less than 1) could occur if the transmissivity field between the surface recharge area and the model domain is such that precipitation fluctuations reach the model domain with strongly muted amplitudes. An improved understanding of regional hydrology may indicate that it is appropriate to include these lower values in future calculations. Circumstances can also be imagined in which increases in precipitation result in a decrease in infiltration (e.g., development of plant cover on previously barren land, or changes in topography resulting in runoff from a previously closed drainage), but none appear plausible for the WIPP area. It is more likely that an increase in the cool-season component of precipitation will result in higher infiltration and r values greater than 1.

Upper bound, r = 10. This value yields a 20-fold increase in model recharge with a doubling of mean annual precipitation and a shift from a monsoonal climate to a climate dominated by winter storms. This value is arbitrary, but is generally representative of the infiltration data reported by Stone (1984). It is less than his maximum value recorded at a single point, reflecting my belief that it is improbable that local-scale variability in infiltration will have a significant effect on confined groundwater flow tens of kilometers down-gradient. It is greater than the mean value for his study area of a 12.5-fold increase in infiltration during the late Pleistocene. My decision to use surface infiltration for an upper bound is based on the observation that the area of surface recharge is apparently relatively small compared to the area in which the Culebra is confined, and there is no reason to assume a preferential flow path from the recharge area to the model domain.

Distribution. I suggest a uniform distribution in the absence of data indicating otherwise. Choosing any distribution other than uniform would imply a greater understanding of the recharge process than we presently have.

Both the range and distribution of the recharge parameter are preliminary, and may be adjusted for future calculations if new data or interpretations warrant.

References Cited

Allen, B. D. 1991. "Effect of Climatic Change on Estancia Valley, New Mexico: Sedimentation and Landscape Evolution in a Closed-Drainage Basin," in B. Julian and J. Zidek, eds., *Field Guide to Geologic Excursions in New Mexico and Adjacent Areas of Texas and Colorado*. New Mexico Bureau of Mines and Mineral Resources Bulletin 137. Socorro, New Mexico. pp. 166-171.

Allison, G. B. 1988. "A Review of Some of the Physical, Chemical, and Isotopic Techniques Available for Estimating Groundwater Recharge," in I. Simmers (ed.), *Estimation of Natural Groundwater Recharge*. NATO ASI series, series C, vol. 222. Dordrecht, Holland: D. Reidel. pp. 49-72.

Bertram-Howery, S. G., M. G. Marietta, R. P. Rechard, P. N. Swift, D. R. Anderson, B. L. Baker, J. E. Bean, Jr., W. Beyeler, K. Brinster, R. V. Guzowski, J. C. Helton, R. D. McCurley, D. K. Rudeen, J. D. Schreiber, and P. Vaughn. 1990. *Preliminary Comparison with 40 CFR Part 191, Subpart B for the Waste Isolation Pilot Plant, December 1990*. SAND90-2347. Albuquerque, NM: Sandia National Laboratories.

Bredenkamp, D. B. 1988a. "Quantitative Estimation of Ground-Water Recharge in Dolomite," in I. Simmers (ed.), *Estimation of Natural Groundwater Recharge*. NATO ASI series, series C, vol. 222. Dordrecht, Holland: D. Reidel. pp. 449-460.

Bredenkamp, D. B. 1988b. "Quantitative Estimation of Ground-Water Recharge in the Pretoria-Rietondale Area," in I. Simmers (ed.), *Estimation of Natural Groundwater Recharge*. NATO ASI series, series C, vol. 222. Dordrecht, Holland: D. Reidel. pp. 461-476.

Brinster, K. F. 1991. *Preliminary Geohydrologic Conceptual Model of the Los Medaños Region Near the Waste Isolation Pilot Plant for the Purpose of Performance Assessment*. SAND89-7147. Albuquerque, NM: Sandia National Laboratories.

Holt, R. M., D. W. Powers, R. L. Beauheim, and M. E. Crawley. in prep. *Conceptual Hydrogeologic Model of the Rustler Formation in the Vicinity of the Waste Isolation Pilot Plant Site, Southeastern New Mexico*. SAND89-0862. Albuquerque, NM: Sandia National Laboratories.

Hunter, R. L. 1985. *A Regional Water Balance for the Waste Isolation Pilot Plant (WIPP) Site and Surrounding Area*. SAND84-2233. Albuquerque, NM: Sandia National Laboratories.

Imbrie, J., and J. Z. Imbrie. 1980. "Modeling the Climatic Response to Orbital Variations." *Science* 207: 943-953.

Lambert, S. J., and J. A. Carter. 1987. *Uranium-Isotope Systematics in Groundwaters of the Rustler Formation, Northern Delaware Basin, Southeastern New Mexico. I: Principles and Methods*. SAND87-0388. Albuquerque, NM: Sandia National Laboratories.

Lambert, S. J., and D. M. Harvey. 1987. *Stable-Isotope Geochemistry of Groundwaters in the Delaware Basin of Southeastern New Mexico*. SAND87-0138. Albuquerque, NM: Sandia National Laboratories.

Lappin, A. R., R. L. Hunter, D. P. Garber and P. B. Davies, eds. 1989. *Systems Analysis, Long-Term Radionuclide Transport, and Dose Assessments, Waste Isolation Pilot Plant (WIPP), Southeastern New Mexico; March 1989*. SAND89-0462. Albuquerque, NM: Sandia National Laboratories.

LaVenue, A. M., T. L. Cauffman, and J. F. Pickens. 1990. *Ground-Water Flow Modeling of the Culebra Dolomite. Volume I: Model Calibration*. SAND89-7068. Albuquerque, NM: Sandia National Laboratories.

Mercer, J. W. 1983. *Geohydrology of the Proposed Waste Isolation Pilot Plant Site, Los Medaños Area, Southeastern New Mexico*. Albuquerque, NM: United States Geological Survey Water Resources Investigation 83-4016.

Phillips, F. M., A. R. Campbell, C. Kruger, P. S. Johnson, R. Roberts, and E. Keyes. in prep. *A Reconstruction of the Response to Climate Change of the Water Balance in Western United States Lake Basins*. New Mexico Water Resources Research Institute Report. Socorro, New Mexico.

Pierce, H. G. 1987. "The Gastropods, with Notes on Other Invertebrates," in E. Johnson (ed.) *Lubbock Lake: Late Quaternary Studies on the Southern High Plains*. College Station, TX: Texas A&M University Press. pp. 41-48.

Swift, P. N. in prep. *Long-Term Climate Variability at the Waste Isolation Pilot Plant*. SAND91-7055J. Albuquerque, NM: Sandia National Laboratories.

Swift, P. N., B. L. Baker, K. F. Brinster, M. G. Marietta, and P. J. Roache. in prep. *Parameter and Boundary Conditions Sensitivity Studies Related to Climate Variability and Scenario Screening for the Waste Isolation Pilot Plant*. SAND89-2029. Albuquerque, NM: Sandia National Laboratories.

Stone, W. J. 1984. *Recharge in the Salt Lake Coal Field Based on Chloride in the Unsaturated Zone*. Open File Report 214. Socorro, NM: New Mexico Bureau of Mines and Mineral Resources.

Van Devender, T. R., R. S. Thompson, and J. L. Betancourt. 1987. "Vegetation History of the Deserts of Southwestern North America; the Nature and Timing of the Late Wisconsin–Holocene Transition," in W. F. Ruddiman and H. E. Wright, Jr. (eds.), *North America and Adjacent Oceans During the Last Deglaciation*. The Geology of North America Volume K-3. Boulder, CO: Geological Society of America. pp. 323-352.

Waters, M. R. 1988. "Late Quaternary Lacustrine History and Paleoclimatic Significance of Pluvial Lake Cochise, Southeastern Arizona," *Quaternary Research* 32: 1-11.

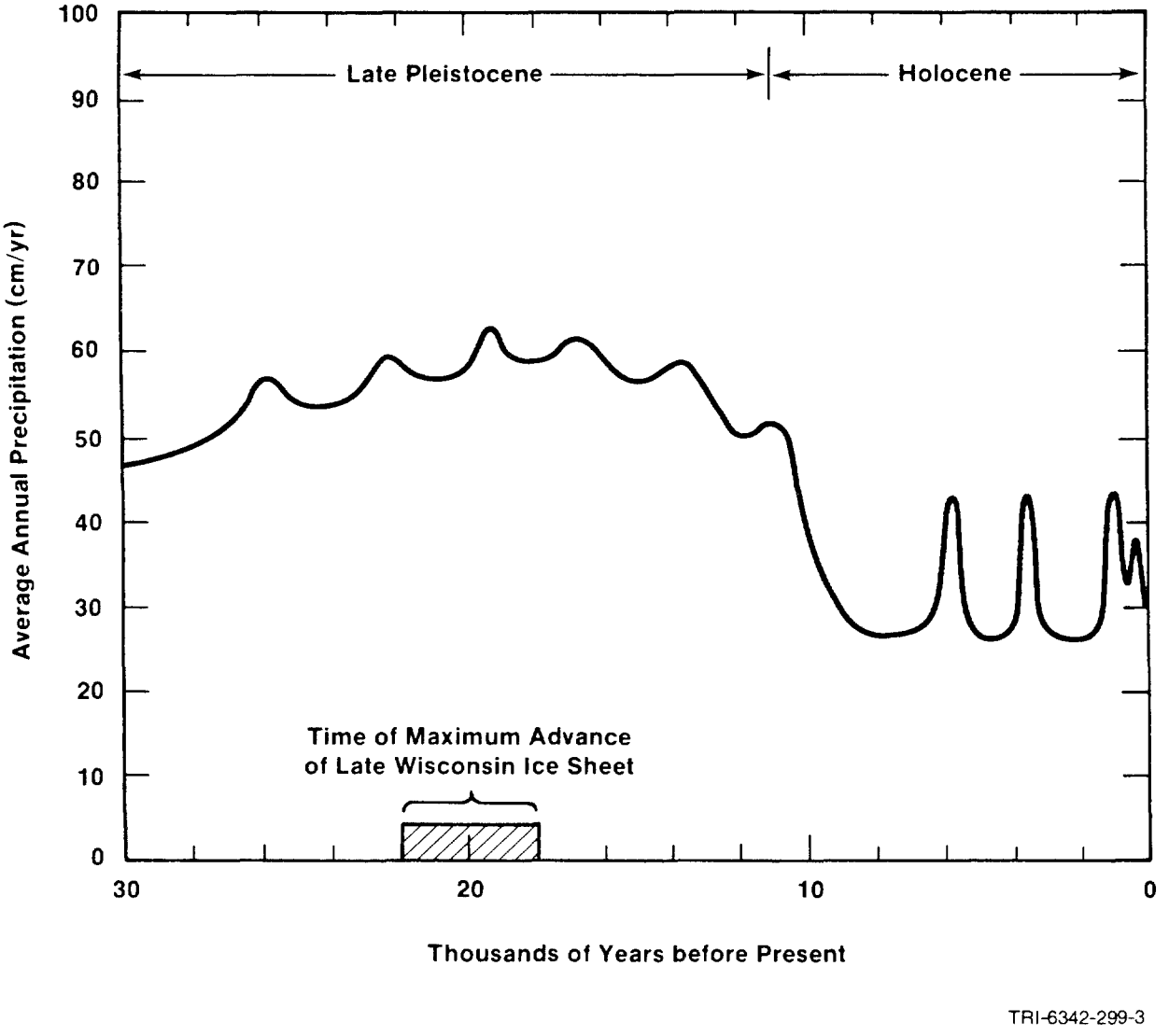

Figure 1. Estimated mean annual precipitation at the WIPP during the late Pleistocene and Holocene (Swift, in prep.). Data from Van Devender et al. (1987), Pierce (1987), Waters (1989), Phillips et al. (in prep.), Allen (1991), and other sources cited by Swift (in prep.).

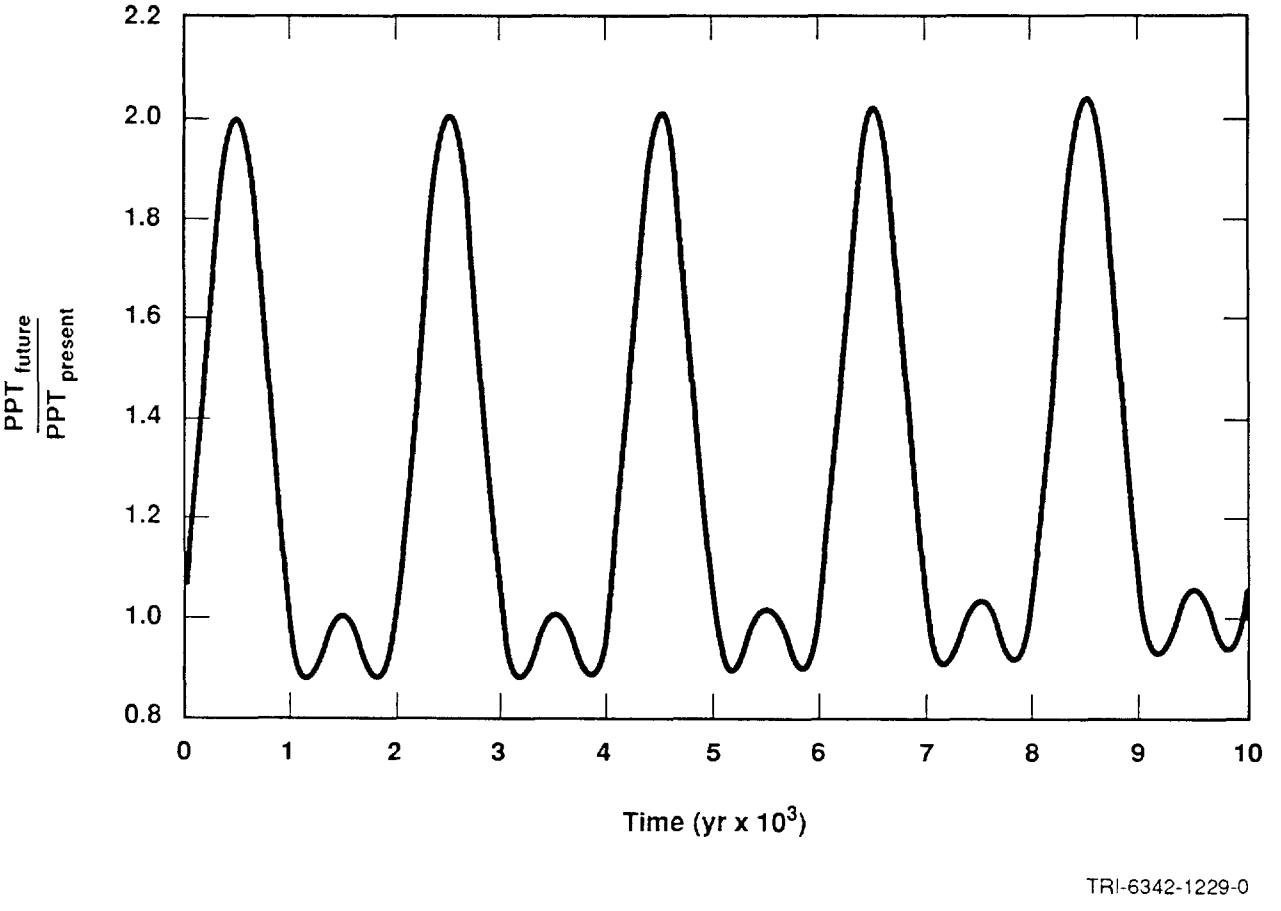

Figure 2. Ratio between future and present mean annual precipitation at the WIPP, calculated using the climate function suggested in the text and the suggested constants that yield a full glacial maximum in 60,000 years and interglacial peaks every 2000 years.

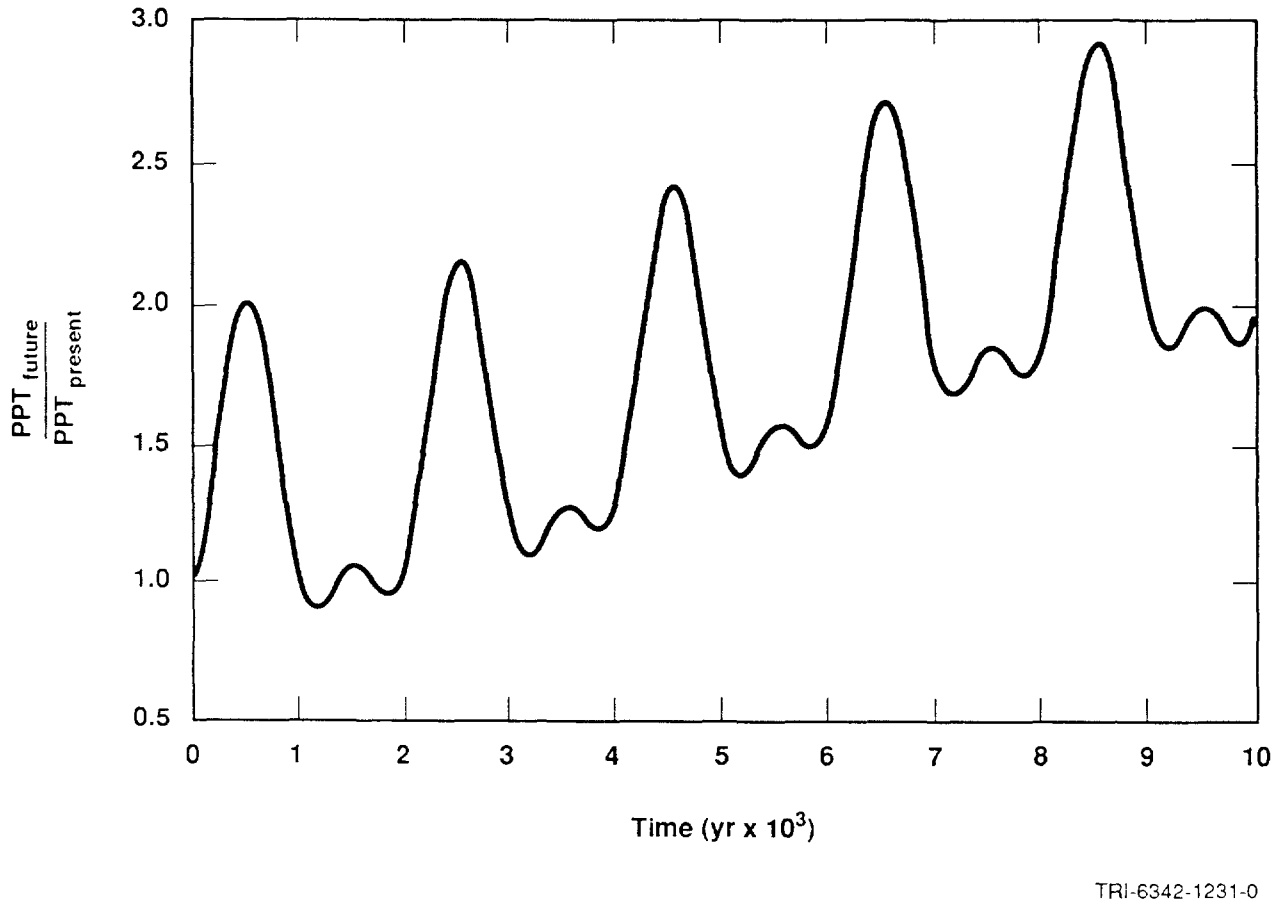

Figure 3. Ratio between future and present mean annual precipitation at the WIPP, calculated using the climate function suggested in the text and constants that yield a full glacial maximum in 10,000 years and interglacial peaks every 2000 years.

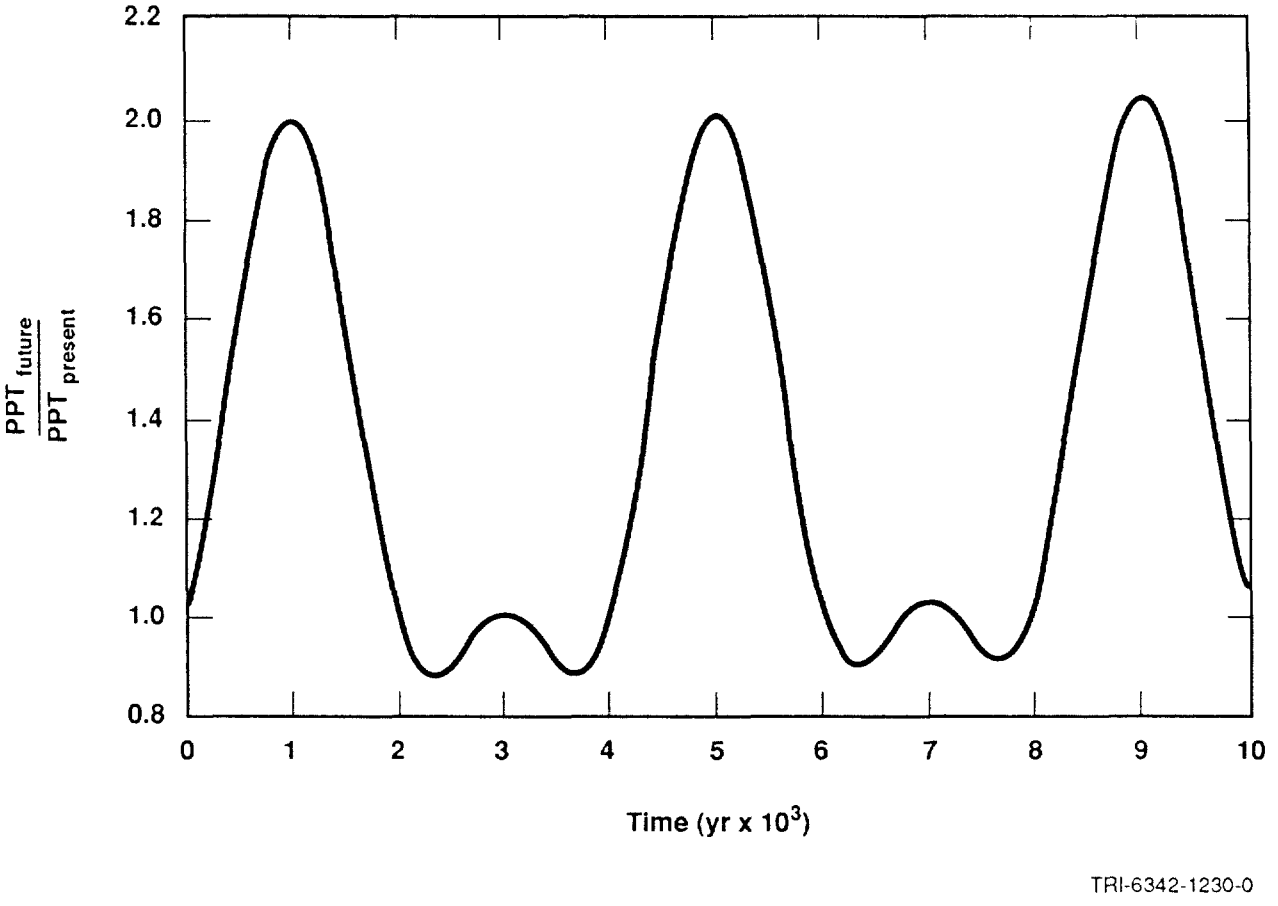

Figure 4. Ratio between future and present mean annual precipitation at the WIPP, calculated using the climate function suggested in the text and constants that yield a full glacial maximum in 60,000 years and interglacial peaks every 4000 years.

Gorham, July 2, 1991

Date: 7/2/91
To: Rob Rechard (6342)
From: Elaine Gorham (6344)
Subject: Aggregated Frequency Distributions for Permeability, Pore Pressure and Diffusivity in the Salado Formation

Sandia National Laboratories

Albuquerque, New Mexico 87185

date: July 2, 1991

to: Rob Rechard, 6342

Elaine Gorham

from: Elaine Gorham, 6344

subject: Aggregated Frequency Distributions for Permeability, Pore Pressure and Diffusivity in the Salado Formation

Attached are the frequency distributions we recommend that you use in the December 91 calculations for values of the brine permeability, pore pressure and specific storage for the Salado formation. Separate frequency distributions have been derived for halite and anhydrite layers. As we have discussed in previous meetings, the data base cannot currently support a model that clearly differentiates a disturbed rock zone from the far field. Therefore we have included data that we believe may be representative of a DRZ in formulating our property distributions for the far field.

Data and suggested frequency distributions from various experiments supported by 6344 that have been included in formulation of the recommended distributions have been transmitted to you in the following memos:

1. "Pore Pressure Distributions for 1991 Performance Assessment Calculations", S. Howarth to E. Gorham, June 12, 1991.

2. "Permeability Distributions for 1991 Performance Assessment Calculations", S. Howarth to E. Gorham, June 13, 1991.

3. "Review of Salado Parameter Values to be Used in 1991 Performance Assessment Calculations", R. Beauheim to R. Rechard, June 14, 1991.

4. "Parameter Estimates from the Small Scale Brine Inflow Experiments", S. Finley and D. McTigue, June 17, 1991.

This memo combines the information in the memos listed above in a consistent manner with the attached table of pore pressure information from the Permeability Testing Program to produce aggregated distributions for the relevant parameters. I will provide you with a publishable description of the aggregation process by your August deadline.

Permeability values inferred from the Permeability Testing Program and from the Room Q tests depend upon the assumed specific storage. At this time we have not succeeded in quantifying the correlation between these two parameters and

therefore recommend that you sample from the permeability and specific storage distributions independently.

The formation compressibility α can be obtained from the values of specific storage using the formula:

$$\alpha = S_S/\rho/g - \phi\beta,$$

where g is the gravitational acceleration, ρ the fluid density, ϕ the formation porosity and β the fluid compressibility. I recommend using average values recommended by Beauheim in Reference 3 above for the parameters in this conversion formula, since I have included considerable parameter uncertainty in the frequency distribution for the specific storage. Thus, I recommend using the expression

$$\alpha = S_S * 8.5 \times 10^{-5}/\text{Pa} - 3.1 \times 10^{-12}/\text{Pa}$$

to obtain formation compressibility from specific storage. Further, for values of specific storage smaller than 3.6×10^{-8}, α may become negative. I recommend allowing it to become negative for values of specific storage larger then 3.4×10^{-8} at which value the total compressibility will equal the lowest recommended value of fluid compressibility (2.9×10^{-10}/Pa). For values of specific storage less than 3.4×10^{-8}, which comprise less than five percent of the frequency distributions, I recommend using a formation compressibility of zero and a value of fluid compressibility of 2.9×10^{-10}/Pa.

If you have any questions please contact me.

Copies:

1511 D. McTigue
6340 W. D. Weart
6342 D. R. Anderson
6344 R. Beauheim
6344 S. Finley
6344 S. Howarth

AGGREGATED FREQUENCY DISTRIBUTIONS FOR PERMEABILITY IN THE SALADO FORMATION:

-LOG(Permeability(m^2))	HALITE Cumulative Frequency	ANHYDRITE Cumulative Frequency
16.50		0.0
17.00	0.0	0.018481
17.50	0.018481	0.036963
18.00	0.036963	0.073959
18.50	0.065434	0.126273
19.00	0.093906	0.247036
19.50	0.154012	0.476356
20.00	0.269430	0.636369
20.50	0.416616	0.819516
21.00	0.645037	0.922176
21.50	0.826056	0.948816
22.00	0.939442	0.975456
22.50	0.964834	0.987111
23.00	0.985230	0.998766
23.50	0.991890	0.998766
24.00	0.998550	0.998766

AGGREGATED FREQUENCY DISTRIBUTIONS FOR FORMATION PRESSURE IN THE SALADO FORMATION:

Pressure (MPa)	HALITE Cumulative Frequency	ANHYDRITE Cumulative Frequency
0.0	0.000	0.0
1.0	.1250	0.15
2.0	.1500	0.20
3.0	.2750	0.20
4.0	.3375	0.20
5.0	.4625	0.30
6.0	.5500	0.35
7.0	.5750	0.35
8.0	.6800	0.35
9.0	.8400	0.40
10.0	.9750	0.50
11.0	1.000	0.60
12.0	1.000	0.75
13.0	1.000	0.95
14.0	1.000	1.00

AGGREGATED FREQUENCY DISTRIBUTIONS FOR SPECIFIC STORAGE IN THE SALADO FORMATION:

-LOG(Specific Storage(/m))	HALITE Cumulative Frequency	ANHYDRITE Cumulative Frequency
0.0		
2.3	0.050	0.027
2.4	0.053	0.042
2.9	0.070	0.11
3.0	0.075	0.12
3.1	0.084	0.15
3.3	0.10	0.20
4.0	0.17	0.21
4.4	0.24	0.25
4.5	0.26	0.26
4.7	0.28	0.27
4.8	0.29	0.28
5.1	0.33	0.30
5.2	0.34	0.31
5.4	0.36	0.34
5.8	0.40	0.40
5.9	0.40	0.41
5.9	0.41	0.41
6.0	0.44	0.41
6.4	0.54	0.53
6.8	0.66	0.67
7.0	0.70	0.92
7.1	0.77	0.93
7.5	0.98	0.95
7.7	0.99	0.96
8.0	0.99	0.97
8.5	1.0	1.0

FORMATION PORE PRESSURES FROM PERMEABILITY TESTING PROGRAM

TEST	INTERVAL (m)	PRESSURE (MPa)	LITHOLOGY
C2H01-A	2.09-2.92	0.50	halite
C2H01-A-GZ	0.50-1.64	0.00	halite
C2H01-B	4.50-5.58	3.15	halite
C2H01-B-GZ	2.92-4.02	4.12	halite
C2H01-C	6.80-7.76	8.05	MB139
C2H02	9.47-10.86	9.30	MB139
L4P51-A	3.33-4.75	2.75	halite
L4P51-A-GZ	1.50-2.36	0.28	MB139
S0P01	3.74-5.17	4.45	halite
S0P01-GZ	1.80-2.76	0.52	MB139
S1P71-A	3.12-4.56	2.95	halite
S1P71-A-GZ	1.40-2.25	0.00	MB139
S1P71-B	9.48-9.80	4.88	anhydrite "c"
S1P72	4.40-6.00	1.24	MB139
S1P72-GZ	2.15-3.18	5.15	halite
SCP01	10.50-14.78	12.55	MB139
L4P51-B	9.62-9.72	5.10	anhydrite "c"
S1P73-B	10.86-11.03	4.50	MB138

Anderson, October 25, 1991

Date: 10/25/91
To: File
From: D. R. (Rip) Anderson (6342)
Subject: Modifications to Reference Data for 1991 Performance Assessment

Sandia National Laboratories

Albuquerque, New Mexico 87185

date: 25-OCT-91

to: File

D. R. Anderson

from: D. R. (Rip) Anderson, 6342

subject: Modifications to Reference Data for 1991 Performance Assessment

Memoranda regarding reference data were provided to performance assessment from principal investigators for use in the 1991 preliminary comparison. Data were requested early in the performance assessment year (March) because consequence modeling depends on early definition of conceptual models, division of summary scenarios into computational scenarios, and robustness of different flow and transport codes. Once the conceptual and computational model(s) and the ranges and distributions of imprecisely known input parameters are defined, the annual performance assessment calculations can be designed and tested.

Concerns related to calculational design include distinguishing conceptual models so CCDF comparisons, ceteris paribus, can be made; ability to perform the calculations (i.e., acknowledging code limitations); and the need to design consequence modeling so sensitivity analysis results are interpretable. Consideration of these concerns sometimes requires modification of data ranges and distributions. For example, comparison of two different conceptual models is best performed by comparing summary CCDFs derived from two independent analyses using the same sample. Therefore, submitted data may be divided between two different conceptual models, e.g., dual- and single-porosity (fracture) transport in the Culebra.

The flow and transport codes have fundamental limitations in their ability to compute realistic results over wide parameter ranges especially when there are orders of magnitude variations in material properties between adjacent zones. Data must be made available in a timely way so that codes can be tested before Monte Carlo simulations have to start. Because last-minute adjustments cannot always be made, new data or new interpretations of old data that are delivered late may not be included until the next year's calculations.

For interim performance assessments like the 1991 preliminary comparison, sensitivity analyses must be as realistic and interpretable as possible because the comparison forms the basis for providing guidance to DOE on the experimental program. The performance assessment calculations must be designed so that different

conceptual models and different sources of uncertainty (e.g., stochastic vs. subjective, various imprecisely known parameters, etc.) can be clearly distinguished. Most important, data must be consistent with model scales, e.g., measurements may be on a m^3 scale, but the model needs information on a computational cell volume of 10^3 m^3. Therefore, realistic distribution functions on the right model scales are required for providing meaningful sensitivity results on which to base our guidance to DOE. Too much or too little emphasis on distribution tails (e.g., arbitrarily wide ranges on uncertainty) can skew results. In such cases for a parameter or submodel, more than one distribution can be tested and results compared and documented in the sensitivity analysis report. The CCDFs reported in the preliminary comparison, however, must rely on realistic conceptual models and parameter CDFs.

The following discussion lists changes in parameter distributions from recommendations in submitted memoranda for the 1991 Preliminary Comparison.

1. **Pore Pressure Distribution** (ref. E. Gorham to R. Rechard, Memo, July 2, 1991)

The distribution as provided in Gorham, Memo, June 2, 1991, includes data taken from Salado halite and anhydrite. The 10 measurements included in the data and described in Howarth, Memo, June 12, 1991, are from 7 experiments in halite and three in anhydrite. For each experiment, two pressure values are reported: (1) a "shut-in" value obtained during a pressure build-up test and (2) a Horner extrapolation of this value. The Horner extrapolation provides an estimate of a steady-state pore pressure by extrapolation to infinite time.

For the 1991 PA calculations, we are using only the Horner extrapolated pressure values for the anhydrite material (reported in Howarth, Memo, June 12, 1991) and the two anhydrite values (recommended in Beauheim, Memo, June 14, 1991) for our "far-field" pore pressure distribution at the MB139 elevation. Because doing so results in using only five experimental data, the distribution is constructed using the PA standard procedure for sparse data. This procedure involves determining the mean of the data and then extending the range to $\pm 2.33\sigma$ about the mean. Since the maximum pressure of the resulting range exceeds lithostatic pressure, we limit the maximum to lithostatic. The following supports the changes made to the pore pressure distributions of Gorham, Memo, July 2, 1991.

Reason 1: One difficulty with the Gorham distribution is that both the shut-in and Horner values of each test were weighted equally and used in the construction of the distribution. This "doubling up" of data is not consistent with PA's understanding of capturing data uncertainty with probability distributions. PA methodology requires that the data points to be used in the construction of the parameter cdfs be from independent experiments.

Reason 2: The model requires steady-state or long time estimates of pore pressure that exist in the host rock prior to excavation. The early time data or shut-in values obtained during the experiments are not consistent with the model's application and should be excluded from the distribution. The transient nature of pressure response to the excavation is calculated by the model.

Reason 3: The pressure the model expects is one which is representative of the pressure at repository elevation at a horizontal distance far removed from the repository. Far removed as defined in the model is a location where neither pressure nor saturation is affected by changes occurring in the repository. The key words are "far removed." During the course of the calculations, the model BRAGFLO determines the changing pressure and saturation profiles as a function of time and position. Results from BRAGFLO indicate that a depressurized zone surrounding the waste is created at early times. This depressurized zone is created in response to the low pressure initially in the excavation. This zone is not to be confused with the DRZ (disturbed rock zone) which, if it exists, is due to mechanical stress in the surrounding rock. The size of this depressurized zone varies with time and material properties, but it can extend tens of meters into the Salado. For example, in vector 6 of this year's input, sampling the simulated pressure field 25 m from the repository into the Salado at a time 8 yr after the excavation results in a value of 5.5 MPa, while the far-field pressure remains at 8.5 MPa. Using the value of 5.5 MPa as representative of the "far-field" value, in this case, would underestimate the potential for brine inflow into the panel from the "far field" and would be 35% low. The distance from the repository where the experiments were conducted is 23 m.

Reason 4: The data are not consistent with the models' intended use. The model uses this pressure as the initial pressure at a particular elevation in the reservoir. The key word is "initial." As mentioned above, BRAGFLO calculates the magnitude and extent of the depressurized zone as a function of time. The initial time is assumed to be the time of excavation so that there is no depressurization due to the presence of the excavation. The data, of course, are taken some time after excavation.

Reason 5: The data are not consistent with our (PA) current conceptual model assumption that the Salado and other materials are homogeneous and consist of a network of interconnected pore space. Many of the data fall below their hydrostatic pressure values at the location of measurement. Assume for the moment that the low pressures (as low as 1.1 MPa) that were measured were not influenced by the presence of the excavation and that no leakage through the equipment or unseen fractures occurred. This suggests an alternative conceptual model for the Salado: one in which isolated pockets are separated by impermeable material or by material of nonconnected porosity. While our numerical models can handle this type of conceptual model, (1) some mechanism should be postulated for the formation of low-pressure

pockets in the deformable halite, (2) additional data probably should be collected to support this alternate conceptual model, and (3) these pockets should be quantified with respect to properties as well as location and spatial extent. As discussed above, when alternative conceptual models are well supported in the documented technical basis, the PA approach for including conceptual model uncertainty is to perform independent Monte Carlo simulations, compare CCDFs, ceteris paribus, then make a judgment on whether more than one conceptual model needs to be included in later CCDF construction.

2. Permeability

Two distributions are provided: one for the halite, which has a range of 1.0E-24 to 1.0E-17 and one for the anhydrite, which has a range of 1.0E-24 to 3.2E-17. For this year's calculations, PA will use instead a range of 2.0E-22 to 1.4E-19 for intact halite and 8.5E-21 to 1.8E-18 for intact anhydrite. The PA ranges are based on the data of Beauheim, Memo, June 14, 1991. In determining the PA distributions, the two values (one for each material) that are believed to be in the DRZ, are excluded. The support of PA distributions are $\pm 2.33\sigma$ about the mean of the remaining data. The following arguments support the position for not using the distributions of Gorham, July 2, 1991.

Reason 1: The support of the permeability distributions reported in Gorham, Memo, July 2, 1991, are artificially broad for reasons outlined in Howarth, Memo, June 13, 1991. In essence, the data of Howarth, June 13, 1991, were calculated using properties of a "test zone fluid" and not brine. In addition, the values are based on the assumption of a rigid matrix as opposed to the "poroelastic" assumption currently used in the standard model for determining permeability from test data by Division 6344. Both of these factors can significantly affect the calculated permeabilities and at the very least raise questions as to their appropriateness for PA calculations. In Howarth, June 13, 1991, it is estimated that the assumptions used in determining these permeabilities may be in error by 1/2 to 2 orders of magnitude.

Reason 2: The distributions as provided are not consistent with the current conceptual model. Conceptually, the anhydrite layers are thought to be the major flow paths between the "far-field" and the repository while the halite is believed to be the more impermeable material. Sampling on Gorham, July 2, 1991 distributions resulted in the halite being more permeable than the anhydrite in nearly 25% of the vectors. Again, if different conceptual models are postulated, independent and internally consistent analyses should be performed by PA and appropriate uncertainty included later. PA can do this if the more permeable halite and tighter anhydrite is a viable alternative conceptual model.

Reason 3: While the existence of a DRZ is apparently the subject of some debate, there is still some evidence that may support the existence of a DRZ. PA models are capable of differentiating a DRZ

from intact material. Beauheim, Memo, June 14, 1991 clearly states that the high permeability measurements for halite and anhydrite are representative of a DRZ. The existence or not of the DRZ could also be analyzed as conceptual model uncertainty. PA believes that this approach is preferred over identifying near-excavation permeability measurements with estimates of far-field permeabilities.

3. Specific Storage

Specific storage of the halite and anhydrite is not sampled during this year's PA calculations. The value of specific storage selected for the calculations is the upper end of the range in specific storage values suggested in Beauheim, Memo, June 14, 1991, for the halite and anhydrite materials. The upper end value of the Gorham, July 2, 1991 range was not selected because the formation compressibility used by PA models and calculated from the specific storage would become negative for some combinations of porosity and fluid compressibility. A negative formation compressibility is contrary to our conceptual model of the matrix response to pore pressure changes in the halite and anhydrite. Current PA understanding is that matrix porosity increases with increasing pore pressure. Negative rock compressibility reverses this behavior.

Mendenhall and Butcher, June 1, 1991

Date: 6/1/91
To: R. P. Rechard (6342)
From: F. T. Mendenhall (6345) and B. M. Butcher
Subject: Disposal room porosity and permeability values for use in the 1991 room performance assessment calculations

date: June 1, 1991

to: R.P. Rechard

F. T. Mendenhall B. M. Butcher

from: F.T. Mendenhall, 6345 and B.M. Butcher

subject: Disposal room porosity and permeability values for use in the 1991 room performance assessment calculations

The following information has been prepared as input for material property value distribution for the 1991 performance assessment. The approach used for determining the properties for this years calculation differs significantly from last years information because of the of gas in both the disposal room model and the use of two phase fluid flow in modeling the room in the performance assessment calculations. **All values in this memorandum refer to the values <u>for a single disposal room.</u>**

In the case where it is assumed no gas is generated (total gas potential of less than 1.4×10^6 moles is assumed to be the same as no gas generation), the recommended distributions of permeability and porosity are the same as recommended last year.[1] For the cases where the expected gas generated is more than 1.4×10^6 moles, the recommended porosity (50% probability) can be defined from:

(Eq 1)

$$\phi_{(Prob=50\%)} = \frac{1}{1 + \frac{P \cdot V_s}{N_{Total} \cdot R \cdot T}}$$

Where

ϕ=*porosity*
P=14.8×10^6 *Pa* — lithostatic
V_s=1330 M^3
R=8.23 $\frac{M^3\text{-}Pa}{g\text{-}mole\text{-}K}$
T=300*K*
N_{Total}=*Total Moles Gas*

N_{Total} is the total potential number of moles of gas contained in a disposal room. This is determined by the amount and type of waste in a room as sampled in your performance assessment model. Note that the porosity is a long term equilibrium value based on the ideal gas law and assumes that the final pressure in a room will be the lithostatic pressure of the overburden. The ideal gas law is expected to be accurate at lithostatic pressure (14.8 MPa). If your

code allows a significant amount of gas to leak out of the disposal room, we recommend that you compute the amount of moles of gas in the room at a point in time three times after all gas generation has stopped, e.g. if the total gas generation stops at 700 years, determine the number of moles in the room at 2100 years and used that value, N_{3*tend}, instead of the total potential amount of gas in the room. This should allow some influence of gas migration and leakage to be accounted for in your simulations. Again if N_{Total} or if N_{3*tend} are less than $1.4x10^6$ moles the porosity and permeability ranges revert to those given last year.

Having defined the porosity for the 50% probability level, the 10% probability level remains at 0.15 as it was last year. The lowest the porosity ever expected would be the porosity of the host halite. We see no reason to change the median value of 0.01 or range of the porosity,(.001 - .03), of the host halite from those defined last year in Table II-2 of the Data Used in Preliminary Performance Assessment of the Waste Isolation Pilot Plant (1990), SAND89-2408 by Rob P. Rechard, et.al..

Porosity at the 90% probability level would be the value determined in Equation 1 by exchanging N_{Total} with $2xN_{Total}$ (or $2xN_{3*tend}$ if that was the value used). The value of twice the base line value was selected because for corrosion the most aggressive reaction in the list of potential reactions in the DSEIS report will generate two moles of hydrogen for each mole of iron and iron corrosion has the maximum gas production potential in the waste inventory.

The large range on gas generation potentials and, hence, the porosity is expected to narrow as better information regarding gas generation becomes available from laboratory and bin scale tests.

Similarly, the permeability recommendations remain unchanged from last year in the case where no gas generation, (less than $1.4x10^6$ moles of gas), is expected. Also, as you are sampling on phi if the average room porosity is less than 0.15 , then again you should use the permeability values as determined last year.

However, when significant gas occurs and in the sampling process the room porosity exceed 0.15, the recommended permeability should be determined by averaging the expected components of materials in the room. Since the composite flow is likely to be dominated by the flow of the most permeable member, a harmonic averaging process seems most appropriate. For example, let K_b, K_c, K_m, and K_s represent the permeabilities of the backfill, combustible waste, metallic waste, and sludges respectively. Furthermore, define the following values of R as

$$V_b K_b = R1$$
$$V_c K_c = R2$$
$$V_m K_m = R3$$
$$V_s K_s = R4$$

with V_b, V_c, V_m, and V_s representing the per cent volume of the backfill, combustible waste, metallic waste, and sludges respectively. Then the expected room average permeability would be defined as

$$R_{ave} = \frac{1}{\frac{1}{R1} + \frac{1}{R2} + \frac{1}{R3} + \frac{1}{R4}}$$

$$K_{ave} = \frac{R_{ave}}{Total\ Initial\ Volume}$$

The values of the individual components of permeability should be determined from the average room porosity in the following fashion.

$$K_i = (K_0) \sqrt[3]{\frac{\phi}{\phi_0}}\ Meters^2$$

Where the values of K_0 and phi_0 are given in Table 1 for the various room components. Also note, that as you are sampling on room porosity, phi, you will automatically be sampling on the room permeability.

Component	K_0 m^2	ϕ_0
Backfill	10^{-21}	0.05
Combustibles	1.7×10^{-14}	0.136
Metallic	5×10^{-13}	0.4
Sludges	1.2×10^{-16}	.113

Table 1

Caveat

This averaging scheme for the permeability is based on the assumption of a significant amount of metallic waste, nominally 30-40%, uniformly distributed throughout the disposal room. That being the case we would expect the permeability of the metallic waste to dominate the flow though the room. If these conditions are not true, that is if the metallic waste is less than 10% of room volume or if the waste is localized in one section of the room, the average technique suggested here is not appropriate and another scheme will have to be developed.

1.B.M. Butcher and A.R. Lappin, July 24, 1990, "Disposal room porosity and permeability values for disposal room performance assessment," Memorandum of Record to M.G. Marietta.

Siegel, July 14, 1989

Date: 7/14/89
To: P. Davies (6331) and A. R. Lappin (6331)
From: M. D. Siegel
Subject: Supplementary Information Concerning Radionuclide Retardation

Date: July 14, 1989

To: P. Davies, 6331
A. R. Lappin, 6331

From: M. D. Siegel

Subject: Supplementary Information Concerning Radionuclide Retardation

The purpose of this memo is to provide supplementary information supporting the choice of distribution coefficients (K_d's) for lead and diffusion coefficients for actinides for transport calculations in the FSEIS.

DISTRIBUTION COEFFICIENTS FOR LEAD

A preliminary literature review in support of the Draft Supplemental Environmental Impact Statement (DSEIS) failed to locate lead sorption data for conditions relevant to the WIPP site. The distribution coefficients (K_d's) for lead used in the transport calculations described in Lappin et al (1989) were based on the assumption that the chemical behavior of lead was similar to that of radium. Available data suggest that radium will sorb onto clays which are similar to those identified within the matrix and lining fractures in the Culebra Dolomite. The same data indicate that the degree of sorption is dependent upon the solution composition. For example, high concentrations of competing cations such as calcium will inhibit the uptake of radium onto model clays such as kaolinite.

Based on the above information, values of 100, 10 and 5 ml/gm were chosen to represent the sorption of radium and lead onto clays in the Culebra. These K_d values correspond to sorption in dilute to moderately saline Culebra groundwaters (Case I), more saline groundwaters (Case IIA) and solutions with high contents of salts and organic ligands (Cases IIB, IIC, IID) respectively. Retardation factors for the bulk matrix were calculated using the above K_d values and a utilization factor of 0.01 to account for the occurrence of the clay as a trace constituent in the dolomite matrix.

Recently, a more extensive literature review has revealed studies of lead sorption that provide some support for the above K_d values. Hem (1976) developed an ion exchange model for the uptake of lead by a simple aluminosilicate (halloysite) in river and lake waters. The model has been partially validated by comparison to experimental data in dilute (ionic strength < 0.02 M) solutions. The model predicts that in systems of moderate concentrations of the substrate (cation exchange capacity = 10^{-3} to 10^{-5} equivalents/liter solution), 60 -100% of aqueous lead will be removed from solution by ion exchange at pH 7. At pH 9, 80% of the aqueous lead will be removed when the CEC is 10^{-3} equivalents/liter but that at low concentrations of the substrate (CEC = 10^{-5} equivalents/liter) little lead is adsorbed.

Hem's model cannot be used to quantitatively assess the effect of changes in solution composition upon the K_d. The model predicts that in systems with appreciable sodium and/or chloride concentrations (> 0.1 M), very little lead adsorbs and the K_d would be close to zero. However, the model only considers sorption of Pb^{+2} and does not include the $PbCO_3$ complex which may be adsorbed much more strongly. (Bilinsky and Stumm, 1973). In addition, it is important to note that the predictions about lead sorption at the higher ionic strengths are made for conditions that fall outside the ranges of experimental conditions used to formulate the ion exchange model. In other words, they were in no way validated against experimental data. It is also important to note that even at low ionic strengths, under conditions wherein Pb-Na exchange was predicted to dominate the lead uptake, the ion exchange model underpredicted the extent of sorption by factors of 30 to 200%.

A number of other studies indicate that lead is strongly sorbed by simple oxides such as amorphous iron oxyhydroxide (am-$Fe(OH)_3$), goethite, alumina (δ-Al_2O_3) and silica (α- SiO_2) (Davis and Leckie, 1978; Leckie et al., 1980; Hayes and Leckie; 1986). Hayes and Leckie (1986) formulated a surface complexation model (SCM) to describe the sorption of lead by goethite. The model was validated over a wide range of ionic strengths (0.01 to

1.0 M $NaNO_3$) and lead concentrations (2 to 30 mM). The experimental data show that lead is quantitatively removed from solution by sorption onto goethite in the pH range 6 - 7. These data cannot be applied directly to the WIPP, however, because no data were obtained at pH greater that 7.0, or in the presence of chloride or carbonate.

The data of Hayes and Leckie (1986) show that the extent of lead sorption is not affected appreciably by changes in ionic strength over the range 0.01 to 1.0 M $NaNO_3$. The authors show that this type of behavior is consistent with the formation of an inner sphere surface complex by lead during sorption. This kind of complex does not compete with the outer sphere complexes formed by sodium. The surface complexation model of Hayes and Leckie probably more accurately predicts lead sorption at the WIPP than does the ion exchange model of Hem (1976). This is because the former was formulated from data taken over a wider range of solution conditions. In fact, the model of Hayes and Leckie suggests that the uptake of lead by surface hydrolysis sites is not adequately represented by an ion exchange model because the two "exchanging" cations (Pb-Na) do not occupy or compete for the same type of sorption site.

If the properties of the surface hydrolysis sites on goethite are similar to those of clays, then the sorption of lead onto goethite provides a useful analog for sorption onto clays. If we assume that the Culebra has a grain density of 2.5 gm/cc, a porosity of 10%, and a clay content of 1% by weight, then a K_d of 100 ml/gm for pure clay (DSEIS Case I) corresponds to sorption of 75% of available lead onto the bulk matrix.[1] This

---

1. The relationship between K_d and percent adsorbed is:

$$\% \text{ adsorbed} = 100\% \times K_d/(Y+K_d)$$

(Footnote continues on next page)

may be a reasonable estimate for lead sorption in the Culebra groundwaters in Hydrochemical Facies Zones B and C (Siegel et al., 1989). The data presented above suggest that the extent of lead sorption will be lower in saline waters in the presence of complexing ligands. For such waters (Case II), the K_d's of 5 to 10 ml/gm for pure clay (corresponding to 13% to 23 % sorption onto the bulk matrix) may be reasonable, however this estimate is highly uncertain.

The above discussion demonstrates the large uncertainties associated with the choice of any single K_d value to represent sorption of lead at the WIPP. The data do not suggest that the K_d will be zero in the Culebra. There is theoretical and experimental evidence to suggest that some sorption of lead will occur in dilute, near-neutral groundwaters and that less lead will be sorbed in saline, organic-rich waters. However, the available data should not be considered adequate to predict the K_d values for use in the final performance assessment.

(Footnote continued from previous page)

where Y = solution to substrate ratio of the system in ml/gm.

Y = 33 ml/gm for batch experiments of Hayes and Leckie (1986).

For a porous matrix:

$$Y = \frac{\phi}{(1-\phi)\rho_s \Psi}$$

Y = 0.17 ml/gm clay for Culebra assuming matrix porosity (ϕ) of 10%, density (ρ_s) of 2.5 gm/cc, and 1% by weight clay in the bulk matrix (Ψ) is accessible to the ground water.

Siegel, June 25, 1991

Date: 6/25/91
To: K. Trauth (6342)
From: M. D. Siegel
Subject: K_d Values for Ra and Pb

Date: June 25, 1991

To: K. Trauth, 6342

From: M. D. Siegel, 6315

Subject: K_d values for Ra and Pb

Suggested Distribution for Case II (Saline Waters)

Percentile	K_d for Ra and Pb (matrix)	K_d for Ra and Pb (fracture)
100	0.3	30
75	0.23	23
50	0.15	15
25	0.07	7
0	0	0

Justification for Chosen Values:

I have assumed that Pb and Ra sorption will be controlled by the amount of clay in the matrix (1%) and fracture-filling clay (100%) (note the fractures are assumed to be 50% filled by clays in the calculation of the retardation factor.). The matrix K_d's are obtained from the clay K_d's by multiplying by a utilization factor of 0.01 as discussed in SAND89-0462. I suggested using the same values for Ra and Pb based a suggestions of Tien et al (1983) as discussed in that report. The maximum values are based on Tien et al (1983) as cited in Table 3-15 of SAND89-0462. Radium sorption has been studied by Riese (1983) and indicated that sorption will be very low in saline waters. (see SAND89-0462 for discussion and references). Attached is a memo that I wrote for P. Davies for the FSEIS discussing sorption data for lead. (I can provide the cited references if you need them.) The memo indicates that although one can wave one's arms and talk about chemical behaviour in general terms, attempts to provide meaningful probability distributions for K_d's of lead and radium are hampered by the paucity of experimental data in relevant chemical systems.

cc. (w/o encl.)

6315 F. B. Nimick
6344 E. D. Gorham

APPENDIX B:
WELL LOCATION DATA
AND
ELEVATIONS OF STRATIGRAPHIC LAYERS NEAR WIPP

Table B.1. Location of Wells used by WIPP (Universal Transverse Mercator [UTM], State Plan Coordinates [stpln], and Survey Sections [township, range and section])

	Well ID	x-UTM	y-UTM	x-STPLN	y-STPLN	Township	Range	Section	Source
2	AEC7	621117	3589387	691810	523142	21	32	31	Mercer, 1983, Table 1
3	AEC8	617522	3586435	679945	513555	22	31	11	Mercer, 1983, Table 1
4	B25	611695	3580609	660759	494504	22	31	20	Mercer, 1983, Table 1
5	CABIN1	613191	3578049	665559	486111	23	31	5	Gonzales, 1989, Tables 3-6 and 3-7
6	DH207	613634	3581973	667074	498589	0	0	0	Krieg, 1984, Table I
7	DH211	613637	3581784	667082	497966	0	0	0	Krieg, 1984, Table I
8	DH215	613634	3581588	667072	497326	0	0	0	Krieg, 1984, Table I
9	DH219	613636	3581448	667081	496864	0	0	0	Krieg, 1984, Table I
10	DH223	613634	3581247	667073	496207	0	0	0	Krieg, 1984, Table I
11	DH227	613632	3581071	667066	495630	0	0	0	Krieg, 1984, Table I
12	DH77	613476	3582573	666554	500556	0	0	0	Krieg, 1984, Table I
13	DO201	613581	3582062	666900	498880	0	0	0	Krieg, 1984, Table I
14	DO203	613630	3582376	667059	499910	0	0	0	Krieg, 1984, Table I
15	DO205	613587	3582616	667066	500696	0	0	0	Krieg, 1984, Table I
16	DO45	613632	3582263	667066	499540	0	0	0	Krieg, 1984, Table I
17	DO52	613586	3582231	666915	499432	0	0	0	Krieg, 1984, Table I
18	DO56	613587	3582375	666919	499907	0	0	0	Krieg, 1984, Table I
19	DO63	613587	3582524	666919	500396	0	0	0	Krieg, 1984, Table I
20	DO67	613516	3582572	666687	500551	0	0	0	Krieg, 1984, Table I
21	DO88	613435	3582572	666421	500551	0	0	0	Krieg, 1984, Table I
22	DO91	613395	3582575	666288	500561	0	0	0	Krieg, 1984, Table I
23	DOE1	615203	3580333	672206	493563	22	31	28	Gonzales, 1989, Tables 3-6 and 3-7
24	DOE2	613683	3585294	667317	509876	22	31	8	Gonzales, 1989, Tables 3-6 and 3-7
25	ENGLE	614953	3567454	671122	451297	24	31	4	Gonzales, 1989, Tables 3-6 and 3-7
26	ERDA10	606684	3570523	644057	461534	23	30	34	Mercer, 1983, Table 1
27	ERDA6	618226	3589011	682292	521975	21	31	35	Mercer, 1983, Table 1
28	ERDA9	613697	3581958	667297	498929	22	31	20	Mercer, 1983, Table 1
29	FFG_002	627231	3608400	712258	585415	20	33	3	Richey, 1989, Table 2
30	FFG_004	622022	3605526	695095	576082	20	33	7	Richey, 1989, Table 2
31	FFG_005	627356	3605486	712599	575853	20	33	10	Richey, 1989, Table 2
32	FFG_006	627658	3605587	713589	576183	20	33	11	Richey, 1989, Table 2
33	FFG_007	627758	3604682	713919	573213	20	33	14	Richey, 1989, Table 2
34	FFG_009	627959	3604782	714579	573543	20	33	14	Richey, 1989, Table 2
35	FFG_011	627658	3605184	713589	574863	20	33	14	Richey, 1989, Table 2
36	FFG_012	627255	3605184	712269	574863	20	33	15	Richey, 1989, Table 2
37	FFG_013	625249	3605163	705684	574827	20	33	16	Richey, 1989, Table 2
38	FFG_014	621225	3604704	692478	573420	20	33	18	Richey, 1989, Table 2
39	FFG_016	627303	3602758	712361	566901	20	33	22	Richey, 1989, Table 2

Table B.1. Location of Wells used by WIPP (Universal Transverse Mercator [UTM], State Plan Coordinates [stpln], and Survey Sections [township, range and section])

	Well ID	x-UTM	y-UTM	x-STPLN	y-STPLN	Township	Range	Section	Source
1	FFG_017	628494	3603697	716300	569948	20	33	23	Richey, 1989, Table 2
2	FFG_018	630636	3602305	723296	565346	20	33	24	Richey, 1989, Table 2
3	FFG_019	627720	3600778	713695	560402	20	33	26	Richey, 1989, Table 2
4	FFG_020	621672	3601468	693880	562799	20	33	30	Richey, 1989, Table 2
5	FFG_023	633058	3599616	731178	556481	20	33	33	Richey, 1989, Table 2
6	FFG_024	635469	3599257	739089	555233	20	33	34	Richey, 1989, Table 2
7	FFG_025	628538	3600381	716379	559068	20	33	35	Richey, 1989, Table 2
8	FFG_026	628122	3600375	715015	559082	20	33	35	Richey, 1989, Table 2
9	FFG_027	627820	3600074	714025	558092	20	33	35	Richey, 1989, Table 2
10	FFG_039	616468	3606754	676902	580244	20	32	10	Richey, 1989, Table 2
11	FFG_040	620041	3603892	688561	570786	20	32	13	Richey, 1989, Table 2
12	FFG_041	616805	3604246	677942	572014	20	32	15	Richey, 1989, Table 2
13	FFG_042	615263	3604535	672914	572994	20	32	16	Richey, 1989, Table 2
14	FFG_043	614824	3602618	671406	566704	20	32	21	Richey, 1989, Table 2
15	FFG_044	618435	3602658	683256	566770	20	32	23	Richey, 1989, Table 2
16	FFG_105	609126	3590258	652461	526265	21	30	25	Richey, 1989, Table 2
17	FFG_106	607630	3591218	647587	529450	21	30	26	Richey, 1989, Table 2
18	FFG_107	607832	3590109	648217	525810	21	30	26	Richey, 1989, Table 2
19	FFG_108	610586	3589854	657254	524908	21	31	31	Richey, 1989, Table 2
20	FFG_109	612822	3589796	664589	524686	21	31	32	Richey, 1989, Table 2
21	FFG_110	613636	3588341	667229	519875	21	31	32	Richey, 1989, Table 2
22	FFG_111	616209	3589857	675705	524786	21	31	34	Richey, 1989, Table 2
23	FFG_112	615312	3588335	672729	519825	21	31	34	Richey, 1989, Table 2
24	FFG_113	615319	3589869	672784	524858	21	31	34	Richey, 1989, Table 2
25	FFG_114	609458	3586996	653485	515558	22	30	1	Richey, 1989, Table 2
26	FFG_115	608243	3586900	649498	515244	22	30	2	Richey, 1989, Table 2
27	FFG_116	606902	3588008	645132	519179	22	30	3	Richey, 1989, Table 2
28	FFG_117	607132	3587086	645854	515889	22	30	3	Richey, 1989, Table 2
29	FFG_119	604055	3585149	635724	509600	22	30	9	Richey, 1989, Table 2
30	FFG_120	604750	3586261	638038	513251	22	30	9	Richey, 1989, Table 2
31	FFG_121	604134	3585930	636016	512165	22	30	9	Richey, 1989, Table 2
32	FFG_122	604165	3585505	636083	510770	22	30	9	Richey, 1989, Table 2
33	FFG_123	606439	3586110	643580	512686	22	30	10	Richey, 1989, Table 2
34	FFG_124	608252	3586096	649528	512608	22	30	11	Richey, 1989, Table 2
35	FFG_125	607631	3585457	647458	510544	22	30	11	Richey, 1989, Table 2
36	FFG_126	609341	3584606	653068	507720	22	30	13	Richey, 1989, Table 2
37	FFG_127	608226	3583523	649376	504163	22	30	14	Richey, 1989, Table 2
38	FFG_128	605614	3581894	640772	498885	22	30	21	Richey, 1989, Table 2

Table B.1. Location of Wells used by WIPP (Universal Transverse Mercator [UTM], State Plan Coordinates [stpln], and Survey Sections [township, range and section])

	Well ID	x-UTM	y-UTM	x-STPLN	y-STPLN	Township	Range	Section	Source
1	FFG_129	604814	3583050	638181	502679	22	30	21	Richey, 1989, Table 2
2	FFG_130	604412	3582244	636828	500068	22	30	21	Richey, 1989, Table 2
3	FFG_132	606479	3581068	643582	496139	22	30	27	Richey, 1989, Table 2
4	FFG_133	606462	3580266	643522	493544	22	30	27	Richey, 1989, Table 2
5	FFG_134	605663	3580407	640899	494006	22	30	27	Richey, 1989, Table 2
6	FFG_135	607211	3580978	645983	495845	22	30	27	Richey, 1989, Table 2
7	FFG_136	609279	3579410	652734	490667	22	30	36	Richey, 1989, Table 2
8	FFG_137	609955	3578869	654952	488858	22	30	36	Richey, 1989, Table 2
9	FFG_138	610827	3587071	657978	515773	22	31	6	Richey, 1989, Table 2
10	FFG_139	610665	3587722	657478	517912	22	31	6	Richey, 1989, Table 2
11	FFG_140	613648	3585123	667200	509316	22	31	8	Richey, 1989, Table 2
12	FFG_141	612120	3585114	662187	509317	22	31	8	Richey, 1989, Table 2
13	FFG_142	615288	3586667	672617	514350	22	31	9	Richey, 1989, Table 2
14	FFG_143	616006	3579286	674808	490129	22	31	34	Richey, 1989, Table 2
15	FFG_144	599879	3577828	621856	485641	23	29	1	Richey, 1989, Table 2
16	FFG_145	599320	3577132	620020	483389	23	29	1	Richey, 1989, Table 2
17	FFG_146	600363	3578186	623476	486818	23	29	1	Richey, 1989, Table 2
18	FFG_147	595499	3578188	607513	486922	23	29	4	Richey, 1989, Table 2
19	FFG_148	600569	3576193	624120	480278	23	29	12	Richey, 1989, Table 2
20	FFG_149	600707	3574718	624539	475434	23	29	13	Richey, 1989, Table 2
21	FFG_155	596597	3570664	610951	462232	23	29	27	Richey, 1989, Table 2
22	FFG_156	595692	3570883	607981	462952	23	29	28	Richey, 1989, Table 2
23	FFG_157	599212	3569453	619500	458190	23	29	35	Richey, 1989, Table 2
24	FFG_158	600510	3569436	623761	458104	23	29	36	Richey, 1989, Table 2
25	FFG_159	609539	3578101	653588	486370	23	30	1	Richey, 1989, Table 2
26	FFG_160	610084	3577670	655343	484923	23	30	1	Richey, 1989, Table 2
27	FFG_161	607676	3577068	647439	483015	23	30	2	Richey, 1989, Table 2
28	FFG_162	607342	3578605	646376	488059	23	30	2	Richey, 1989, Table 2
29	FFG_163	608127	3577850	648955	485549	23	30	2	Richey, 1989, Table 2
30	FFG_164	602541	3574598	630556	475010	23	30	17	Richey, 1989, Table 2
31	FFG_165	601827	3573070	628182	469995	23	30	19	Richey, 1989, Table 2
32	FFG_166	609182	3573205	652317	470305	23	30	24	Richey, 1989, Table 2
33	FFG_167	609012	3570846	651726	462566	23	30	26	Richey, 1989, Table 2
34	FFG_168	604202	3570581	635911	461795	23	30	28	Richey, 1989, Table 2
35	FFG_169	604034	3572065	635389	466662	23	30	29	Richey, 1989, Table 2
36	FFG_170	601537	3572060	627194	466716	23	30	30	Richey, 1989, Table 2
37	FFG_171	601959	3569718	628551	458995	23	30	31	Richey, 1989, Table 2
38	FFG_172	603366	3570098	633169	460209	23	30	32	Richey, 1989, Table 2

Table B.1. Location of Wells used by WIPP (Universal Transverse Mercator [UTM], State Plan Coordinates [stpln], and Survey Sections [township, range and section])

	Well ID	x-UTM	y-UTM	x-STPLN	y-STPLN	Township	Range	Section	Source
1	FFG_173	609960	3569937	654805	459582	23	30	36	Richey, 1989, Table 2
2	FFG_177	591351	3563822	593606	439877	24	29	19	Richey, 1989, Table 2
3	FFG_179	593084	3561340	599224	431698	24	29	29	Richey, 1989, Table 2
4	FFG_180	607488	3567427	646628	451374	24	30	2	Richey, 1989, Table 2
5	FFG_181	604028	3568585	635304	455245	24	30	5	Richey, 1989, Table 2
6	FFG_182	601542	3568281	627146	454314	24	30	6	Richey, 1989, Table 2
7	FFG_183	605177	3566738	639041	449147	24	30	9	Richey, 1989, Table 2
8	FFG_184	607564	3565857	646845	446225	24	30	11	Richey, 1989, Table 2
9	FFG_185	605866	3565683	641274	445686	24	30	15	Richey, 1989, Table 2
10	FFG_186	605016	3565698	638484	445736	24	30	16	Richey, 1989, Table 2
11	FFG_188	602948	3564040	631660	440361	24	30	20	Richey, 1989, Table 2
12	FFG_189	608405	3563679	649573	439043	24	30	23	Richey, 1989, Table 2
13	FFG_190	607685	3562746	647176	436015	24	30	23	Richey, 1989, Table 2
14	FFG_191	609337	3561151	652564	430748	24	30	25	Richey, 1989, Table 2
15	FFG_192	607401	3562442	646246	435019	24	30	27	Richey, 1989, Table 2
16	FFG_194	617718	3568422	680232	454446	24	31	2	Richey, 1989, Table 2
17	FFG_195	616941	3567615	677649	451793	24	31	3	Richey, 1989, Table 2
18	FFG_196	615316	3568812	672350	455759	24	31	4	Richey, 1989, Table 2
19	FFG_197	614612	3568483	670036	454709	24	31	4	Richey, 1989, Table 2
20	FFG_198	613807	3568888	667396	456038	24	31	5	Richey, 1989, Table 2
21	FFG_199	611628	3568640	660244	455257	24	31	6	Richey, 1989, Table 2
22	FFG_200	611273	3568414	659080	454549	24	31	6	Richey, 1989, Table 2
23	FFG_201	612154	3565951	661905	446431	24	31	7	Richey, 1989, Table 2
24	FFG_202	618692	3566653	683393	448607	24	31	11	Richey, 1989, Table 2
25	FFG_203	618143	3567223	681591	450478	24	31	11	Richey, 1989, Table 2
26	FFG_204	619790	3564834	686932	442604	24	31	13	Richey, 1989, Table 2
27	FFG_205	613734	3565566	667090	445140	24	31	17	Richey, 1989, Table 2
28	FFG_206	612171	3564340	661929	441145	24	31	18	Richey, 1989, Table 2
29	FFG_207	613776	3563957	667198	439860	24	31	20	Richey, 1989, Table 2
30	FFG_208	612992	3562725	664590	435847	24	31	20	Richey, 1989, Table 2
31	FFG_209	615380	3563980	672461	439901	24	31	21	Richey, 1989, Table 2
32	FFG_210	614199	3562745	668548	435879	24	31	21	Richey, 1989, Table 2
33	FFG_212	619811	3562825	686967	436012	24	31	24	Richey, 1989, Table 2
34	FFG_213	614915	3560252	670865	427664	24	31	33	Richey, 1989, Table 2
35	FFG_214	617438	3559994	679114	426785	24	31	35	Richey, 1989, Table 2
36	FFG_215	610576	3559150	656597	424152	25	30	1	Richey, 1989, Table 2
37	FFG_216	604853	3558664	637816	422688	25	30	4	Richey, 1989, Table 2
38	FFG_217	617694	3559360	679954	424705	25	31	2	Richey, 1989, Table 2

Table B.1. Location of Wells used by WIPP (Universal Transverse Mercator [UTM], State Plan Coordinates [stpln], and Survey Sections [township, range and section])

	Well ID	x-UTM	y-UTM	x-STPLN	y-STPLN	Township	Range	Section	Source
1	FFG_218	618235	3558795	681730	422820	25	31	2	Richey, 1989, Table 2
2	FFG_219	616649	3557179	676493	417552	25	31	10	Richey, 1989, Table 2
3	FFG_220	619057	3557584	684393	418848	25	31	12	Richey, 1989, Table 2
4	FFG_221	616028	3555913	674422	413427	25	31	15	Richey, 1989, Table 2
5	FFG_222	614248	3552703	668515	402929	25	31	28	Richey, 1989, Table 2
6	FFG_224	629257	3598870	718704	554099	21	32	1	Richey, 1989, Table 2
7	FFG_225	629076	3597979	718112	551174	21	32	1	Richey, 1989, Table 2
8	FFG_226	628708	3596750	716853	547172	21	32	1	Richey, 1989, Table 2
9	FFG_228	626669	3597926	710210	551066	21	32	2	Richey, 1989, Table 2
10	FFG_229	625894	3596724	707620	547120	21	32	3	Richey, 1989, Table 2
11	FFG_230	625486	3597502	706279	549709	21	32	3	Richey, 1989, Table 2
12	FFG_231	624249	3598303	702273	552336	21	32	4	Richey, 1989, Table 2
13	FFG_232	623880	3597479	701011	549665	21	32	4	Richey, 1989, Table 2
14	FFG_233	623730	3598370	700570	552588	21	32	4	Richey, 1989, Table 2
15	FFG_234	622268	3597867	695720	550968	21	32	5	Richey, 1989, Table 2
16	FFG_235	623075	3597479	698371	549665	21	32	5	Richey, 1989, Table 2
17	FFG_236	620626	3597834	690380	550899	21	32	6	Richey, 1989, Table 2
18	FFG_237	624279	3595893	702319	544429	21	32	9	Richey, 1989, Table 2
19	FFG_238	625894	3595919	707620	544480	21	32	10	Richey, 1989, Table 2
20	FFG_239	627919	3595147	714233	541912	21	32	11	Richey, 1989, Table 2
21	FFG_240	627501	3595945	712893	544532	21	32	11	Richey, 1989, Table 2
22	FFG_241	628322	3595549	715553	543232	21	32	12	Richey, 1989, Table 2
23	FFG_242	623510	3593053	699730	535143	21	32	21	Richey, 1989, Table 2
24	FFG_243	627958	3591122	714296	528704	21	32	26	Richey, 1989, Table 2
25	FFG_244	627169	3589486	711671	523370	21	32	35	Richey, 1989, Table 2
26	FFG_245	634293	3596014	735183	544627	21	33	9	Richey, 1989, Table 2
27	FFG_246	636300	3596435	741767	545977	21	33	11	Richey, 1989, Table 2
28	FFG_247	638785	3593673	749855	536845	21	33	13	Richey, 1989, Table 2
29	FFG_248	638754	3594075	749755	538165	21	33	13	Richey, 1989, Table 2
30	FFG_249	635538	3594033	739201	538094	21	33	15	Richey, 1989, Table 2
31	FFG_250	630707	3593573	723350	536681	21	33	18	Richey, 1989, Table 2
32	FFG_251	639185	3592056	751137	531538	21	33	24	Richey, 1989, Table 2
33	FFG_252	631978	3589148	727420	522161	21	33	32	Richey, 1989, Table 2
34	FFG_253	634373	3589591	735313	523550	21	33	33	Richey, 1989, Table 2
35	FFG_254	634776	3589591	736633	523550	21	33	34	Richey, 1989, Table 2
36	FFG_255	636385	3590012	741913	524900	21	33	35	Richey, 1989, Table 2
37	FFG_264	624541	3575777	702753	478415	23	32	9	Richey, 1989, Table 2
38	FFG_265	626158	3575003	708059	475842	23	32	15	Richey, 1989, Table 2

Table B.1. Location of Wells used by WIPP (Universal Transverse Mercator [UTM], State Plan Coordinates [stpln], and Survey Sections [township, range and section])

	Well ID	x-UTM	y-UTM	x-STPLN	y-STPLN	Township	Range	Section	Source
1	FFG_266	629827	3572644	720033	468035	23	32	24	Richey, 1989, Table 2
2	FFG_267	632644	3570662	729244	461468	23	33	32	Richey, 1989, Table 2
3	FFG_268	636682	3569503	742460	457597	23	33	35	Richey, 1989, Table 2
4	FFG_272	621266	3580141	692103	492804	22	32	31	Richey, 1989, Table 2
5	FFG_273	621714	3576972	693509	482402	23	32	7	Richey, 1989, Table 2
6	FFG_274	627262	3583857	711844	504897	22	32	14	Richey, 1989, Table 2
7	FFG_275	626055	3584259	707884	506217	22	32	15	Richey, 1989, Table 2
8	FFG_276	622836	3584196	697320	506076	22	32	17	Richey, 1989, Table 2
9	FFG_277	621627	3583775	693354	504725	22	32	18	Richey, 1989, Table 2
10	FFG_278	621646	3582157	693382	499416	22	32	19	Richey, 1989, Table 2
11	FFG_279	622836	3582989	697320	502116	22	32	20	Richey, 1989, Table 2
12	FFG_280	625245	3583022	705224	502190	22	32	22	Richey, 1989, Table 2
13	FFG_281	628878	3581872	717114	498350	22	32	25	Richey, 1989, Table 2
14	FFG_283	638822	3588438	749880	519668	22	33	1	Richey, 1989, Table 2
15	FFG_284	633260	3587655	731596	517227	22	33	4	Richey, 1989, Table 2
16	FFG_285	632916	3587152	730466	515577	22	33	5	Richey, 1989, Table 2
17	FFG_286	630045	3585511	721010	510259	22	33	7	Richey, 1989, Table 2
18	FFG_287	630815	3585934	723537	511615	22	33	7	Richey, 1989, Table 2
19	FFG_288	633218	3586749	731456	514257	22	33	9	Richey, 1989, Table 2
20	FFG_289	635668	3584383	739429	506427	22	33	15	Richey, 1989, Table 2
21	FFG_290	631649	3583118	726240	502376	22	33	20	Richey, 1989, Table 2
22	FFG_291	631716	3579091	726360	489157	22	33	32	Richey, 1989, Table 2
23	FFG_292	634513	3580338	735574	493186	22	33	33	Richey, 1989, Table 2
24	FFG_293	635741	3579152	739570	489260	22	33	34	Richey, 1989, Table 2
25	FFG_313	621557	3587797	693224	517925	22	32	6	Richey, 1989, Table 2
26	FFG_314	629670	3583902	719747	504978	22	32	13	Richey, 1989, Table 2
27	FFG_315	626522	3578214	709318	486382	23	32	3	Richey, 1989, Table 2
28	FFG_316	627739	3576635	713279	481164	23	32	11	Richey, 1989, Table 2
29	FFG_317	621734	3574920	693542	475670	23	32	18	Richey, 1989, Table 2
30	FFG_318	622977	3572533	697554	467800	23	32	20	Richey, 1989, Table 2
31	FFG_319	624161	3573735	701471	471749	23	32	21	Richey, 1989, Table 2
32	FFG_320	629107	3572102	717668	466290	23	32	25	Richey, 1989, Table 2
33	FFG_321	628524	3571093	715723	462981	23	32	25	Richey, 1989, Table 2
34	FFG_322	628222	3570892	714733	462321	23	32	26	Richey, 1989, Table 2
35	FFG_323	627420	3570965	712100	462590	23	32	26	Richey, 1989, Table 2
36	FFG_324	624184	3572130	701514	466480	23	32	28	Richey, 1989, Table 2
37	FFG_325	620546	3569268	689509	457154	23	32	31	Richey, 1989, Table 2
38	FFG_326	625008	3570140	704185	459917	23	32	33	Richey, 1989, Table 2

Table B.1. Location of Wells used by WIPP (Universal Transverse Mercator [UTM], State Plan Coordinates [stpln], and Survey Sections [township, range and section])

	Well ID	x-UTM	y-UTM	x-STPLN	y-STPLN	Township	Range	Section	Source
1	FFG_327	626737	3569761	709825	458640	23	32	34	Richey, 1989, Table 2
2	FFG_328	627719	3570289	713083	460341	23	32	35	Richey, 1989, Table 2
3	FFG_329	628625	3570188	716053	460011	23	32	36	Richey, 1989, Table 2
4	FFG_330	629464	3569834	718778	458813	23	32	36	Richey, 1989, Table 2
5	FFG_331	634557	3577522	735655	483942	23	33	4	Richey, 1989, Table 2
6	FFG_332	631443	3577384	725434	483557	23	33	6	Richey, 1989, Table 2
7	FFG_333	630183	3575856	721264	478574	23	33	7	Richey, 1989, Table 2
8	FFG_334	631791	3574262	726509	473313	23	33	17	Richey, 1989, Table 2
9	FFG_335	630204	3574250	721301	473303	23	33	18	Richey, 1989, Table 2
10	FFG_336	630611	3573046	722603	469355	23	33	19	Richey, 1989, Table 2
11	FFG_337	633022	3572674	730519	468066	23	33	20	Richey, 1989, Table 2
12	FFG_338	631435	3570650	725277	461460	23	33	31	Richey, 1989, Table 2
13	FFG_339	637863	3570326	746370	460265	23	33	35	Richey, 1989, Table 2
14	FFG_340	639497	3569942	751700	458973	23	33	36	Richey, 1989, Table 2
15	FFG_361	591407	3608036	594694	584951	20	29	1	Richey, 1989, Table 2
16	FFG_362	588581	3607624	585423	583663	20	29	3	Richey, 1989, Table 2
17	FFG_363	586158	3608022	577470	585038	20	29	4	Richey, 1989, Table 2
18	FFG_364	583878	3605062	569923	575355	20	29	7	Richey, 1989, Table 2
19	FFG_366	588498	3606300	585115	579318	20	29	10	Richey, 1989, Table 2
20	FFG_367	589516	3605699	588421	577345	20	29	11	Richey, 1989, Table 2
21	FFG_370	591027	3604798	593382	574358	20	29	13	Richey, 1989, Table 2
22	FFG_371	591334	3604826	594392	574416	20	29	13	Richey, 1989, Table 2
23	FFG_372	589730	3604102	589095	572070	20	29	14	Richey, 1989, Table 2
24	FFG_373	586192	3604773	577514	574376	20	29	16	Richey, 1989, Table 2
25	FFG_374	585392	3603561	574858	570394	20	29	17	Richey, 1989, Table 2
26	FFG_376	590555	3601690	591768	564155	20	29	25	Richey, 1989, Table 2
27	FFG_381	599172	3599246	619978	555961	20	29	36	Richey, 1989, Table 2
28	FFG_383	601077	3606916	626395	581073	20	30	1	Richey, 1989, Table 2
29	FFG_384	594213	3607648	603902	583643	20	30	5	Richey, 1989, Table 2
30	FFG_385	597883	3602444	615814	566466	20	30	22	Richey, 1989, Table 2
31	FFG_387	595912	3600331	609313	559598	20	30	28	Richey, 1989, Table 2
32	FFG_388	595864	3601219	609189	562513	20	30	28	Richey, 1989, Table 2
33	FFG_389	593453	3599602	601245	557239	20	30	31	Richey, 1989, Table 2
34	FFG_390	595208	3600029	607003	558608	20	30	32	Richey, 1989, Table 2
35	FFG_391	595208	3599627	607003	557288	20	30	32	Richey, 1989, Table 2
36	FFG_392	596612	3599732	611609	557599	20	30	33	Richey, 1989, Table 2
37	FFG_393	606297	3606985	643526	581199	20	31	4	Richey, 1989, Table 2
38	FFG_394	603077	3606946	632959	581140	20	31	6	Richey, 1989, Table 2

Table B.1. Location of Wells used by WIPP (Universal Transverse Mercator [UTM], State Plan Coordinates [stpln], and Survey Sections [township, range and section])

	Well ID	x-UTM	y-UTM	x-STPLN	y-STPLN	Township	Range	Section	Source
1	FFG_395	603098	3605631	632997	576823	20	31	7	Richey, 1989, Table 2
2	FFG_396	603243	3600398	633370	559652	20	31	30	Richey, 1989, Table 2
3	FFG_398	588017	3597286	583323	549759	21	28	2	Richey, 1989, Table 2
4	FFG_399	587111	3597387	580353	550089	21	28	3	Richey, 1989, Table 2
5	FFG_402	590847	3595289	592582	543138	21	28	12	Richey, 1989, Table 2
6	FFG_403	586424	3593240	578030	536512	21	28	15	Richey, 1989, Table 2
7	FFG_404	583988	3592021	570006	532548	21	28	20	Richey, 1989, Table 2
8	FFG_407	583988	3590814	570006	528588	21	28	29	Richey, 1989, Table 2
9	FFG_408	582473	3590320	565002	526999	21	28	30	Richey, 1989, Table 2
10	FFG_411	584828	3588367	572695	520558	21	28	33	Richey, 1989, Table 2
11	FFG_413	588470	3589234	584681	523337	21	28	35	Richey, 1989, Table 2
12	FFG_418	596362	3598010	610756	551972	21	29	3	Richey, 1989, Table 2
13	FFG_419	594776	3597648	605505	550814	21	29	4	Richey, 1989, Table 2
14	FFG_420	594662	3598348	605178	553113	21	29	4	Richey, 1989, Table 2
15	FFG_421	593556	3598412	601548	553321	21	29	5	Richey, 1989, Table 2
16	FFG_422	593958	3598000	602868	551971	21	29	5	Richey, 1989, Table 2
17	FFG_426	592398	3591591	597601	530971	21	29	19	Richey, 1989, Table 2
18	FFG_432	607401	3588903	646769	521852	21	30	35	Richey, 1989, Table 2
19	FFG_433	588569	3588121	584969	519682	22	28	2	Richey, 1989, Table 2
20	FFG_438	618629	3586910	683580	515081	22	31	1	Richey, 1989, Table 2
21	FFG_445	590526	3580760	591228	495462	22	28	25	Richey, 1989, Table 2
22	FFG_453	618415	3578487	682715	487442	23	31	2	Richey, 1989, Table 2
23	FFG_455	618558	3575680	683119	478229	23	31	11	Richey, 1989, Table 2
24	FFG_456	617677	3574462	680195	474264	23	31	14	Richey, 1989, Table 2
25	FFG_457	614456	3574425	669624	474210	23	31	16	Richey, 1989, Table 2
26	FFG_458	615274	3572430	672278	467629	23	31	21	Richey, 1989, Table 2
27	FFG_459	619295	3571652	685468	465012	23	31	25	Richey, 1989, Table 2
28	FFG_462	615699	3571221	673637	463662	23	31	27	Richey, 1989, Table 2
29	FFG_463	612475	3570378	663055	460962	23	31	32	Richey, 1989, Table 2
30	FFG_464	614894	3570416	670997	461022	23	31	33	Richey, 1989, Table 2
31	FFG_465	614090	3569999	668355	459685	23	31	33	Richey, 1989, Table 2
32	FFG_474	628677	3568183	716158	453428	24	32	1	Richey, 1989, Table 2
33	FFG_475	628244	3568580	714774	454733	24	32	2	Richey, 1989, Table 2
34	FFG_476	621409	3568885	692341	455866	24	32	6	Richey, 1989, Table 2
35	FFG_477	626275	3566554	708244	448117	24	32	10	Richey, 1989, Table 2
36	FFG_478	627890	3566569	713543	448132	24	32	11	Richey, 1989, Table 2
37	FFG_479	627468	3566954	712193	449429	24	32	11	Richey, 1989, Table 2
38	FFG_480	628677	3566976	716158	449468	24	32	12	Richey, 1989, Table 2

Table B.1. Location of Wells used by WIPP (Universal Transverse Mercator [UTM], State Plan Coordinates [stpln], and Survey Sections [township, range and section])

	Well ID	x-UTM	y-UTM	x-STPLN	y-STPLN	Township	Range	Section	Source
1	FFG_481	629921	3564597	720180	441628	24	32	13	Richey, 1989, Table 2
2	FFG_482	627482	3565749	712204	445477	24	32	14	Richey, 1989, Table 2
3	FFG_483	625893	3564517	706958	441463	24	32	15	Richey, 1989, Table 2
4	FFG_484	626601	3563741	709281	438885	24	32	22	Richey, 1989, Table 2
5	FFG_485	626323	3563337	708336	437561	24	32	22	Richey, 1989, Table 2
6	FFG_486	627104	3563741	710931	438885	24	32	23	Richey, 1989, Table 2
7	FFG_487	627003	3563842	710601	439215	24	32	23	Richey, 1989, Table 2
8	FFG_488	628618	3564276	715902	440608	24	32	24	Richey, 1989, Table 2
9	FFG_489	629141	3562161	717583	433668	24	32	25	Richey, 1989, Table 2
10	FFG_490	622290	3562046	695099	433421	24	32	29	Richey, 1989, Table 2
11	FFG_491	621485	3562046	692459	433421	24	32	30	Richey, 1989, Table 2
12	FFG_492	625107	3559688	704284	425618	24	32	33	Richey, 1989, Table 2
13	FFG_493	625912	3560090	706924	426938	24	32	34	Richey, 1989, Table 2
14	FFG_494	625912	3559688	706924	425618	24	32	34	Richey, 1989, Table 2
15	FFG_495	627126	3559716	710904	425675	24	32	35	Richey, 1989, Table 2
16	FFG_496	639095	3568735	750380	455013	24	33	1	Richey, 1989, Table 2
17	FFG_497	631494	3566228	725373	446949	24	33	7	Richey, 1989, Table 2
18	FFG_498	631883	3567428	726679	450888	24	33	8	Richey, 1989, Table 2
19	FFG_499	639536	3565513	751762	444438	24	33	13	Richey, 1989, Table 2
20	FFG_500	632702	3565844	729335	445656	24	33	17	Richey, 1989, Table 2
21	FFG_501	632345	3563004	728097	436369	24	33	20	Richey, 1989, Table 2
22	FFG_502	635140	3563849	737302	439075	24	33	22	Richey, 1989, Table 2
23	FFG_503	635586	3561835	738701	432466	24	33	27	Richey, 1989, Table 2
24	FFG_504	632771	3561413	729465	431115	24	33	29	Richey, 1989, Table 2
25	FFG_505	630239	3562683	721189	435349	24	33	30	Richey, 1989, Table 2
26	FFG_506	631576	3560189	725511	427131	24	33	31	Richey, 1989, Table 2
27	FFG_507	639607	3561088	751898	429920	24	33	36	Richey, 1989, Table 2
28	FFG_548	601155	3608819	626682	587316	19	30	36	Richey, 1989, Table 2
29	FFG_552	596378	3554488	609903	409146	25	29	15	Richey, 1989, Table 2
30	FFG_562	614317	3546624	668609	382978	26	31	9	Richey, 1989, Table 2
31	FFG_563	618774	3547092	683237	384417	26	31	11	Richey, 1989, Table 2
32	FFG_568	619132	3541724	684313	366799	26	31	25	Richey, 1989, Table 2
33	FFG_569	619132	3542127	684313	368119	26	31	25	Richey, 1989, Table 2
34	FFG_584	606879	3557091	644432	417458	25	30	10	Richey, 1989, Table 2
35	FFG_585	609769	3557118	653916	417516	25	30	12	Richey, 1989, Table 2
36	FFG_600	608992	3550622	651237	396198	25	30	35	Richey, 1989, Table 2
37	FFG_601	607790	3549783	647256	393477	25	30	35	Richey, 1989, Table 2
38	FFG_602	618235	3558795	681730	422820	25	31	2	Richey, 1989, Table 2

Table B.1. Location of Wells used by WIPP (Universal Transverse Mercator [UTM], State Plan Coordinates [stpln], and Survey Sections [township, range and section])

	Well ID	x-UTM	y-UTM	x-STPLN	y-STPLN	Township	Range	Section	Source
1	FFG_606	618324	3551156	681858	397752	25	31	35	Richey, 1989, Table 2
2	FFG_618	599392	3546376	619633	382460	26	29	11	Richey, 1989, Table 2
3	FFG_638	607809	3548155	647284	388134	26	30	2	Richey, 1989, Table 2
4	FFG_639	606187	3548136	641961	388102	26	30	3	Richey, 1989, Table 2
5	FFG_640	604548	3549331	636618	392062	26	30	4	Richey, 1989, Table 2
6	FFG_643	610657	3546572	656602	382873	26	30	12	Richey, 1989, Table 2
7	FFG_644	605816	3544896	640681	377470	26	30	16	Richey, 1989, Table 2
8	FFG_648	609863	3544129	653961	374890	26	30	24	Richey, 1989, Table 2
9	FFG_685	592502	3586828	597845	515341	22	29	6	Richey, 1989, Table 2
10	FFG_689	626339	3558413	708291	421399	25	32	3	Richey, 1989, Table 2
11	FFG_690	625251	3556776	704687	416062	25	32	9	Richey, 1989, Table 2
12	FFG_691	626238	3557256	707961	417604	25	32	10	Richey, 1989, Table 2
13	FFG_692	627982	3556520	713651	415154	25	32	11	Richey, 1989, Table 2
14	FFG_693	627068	3555594	710652	412151	25	32	14	Richey, 1989, Table 2
15	FFG_694	625965	3554867	706999	409798	25	32	15	Richey, 1989, Table 2
16	FFG_695	625955	3556071	706997	413752	25	32	15	Richey, 1989, Table 2
17	FFG_696	625955	3556134	706997	413957	25	32	15	Richey, 1989, Table 2
18	FFG_697	624748	3555669	703037	412432	25	32	16	Richey, 1989, Table 2
19	FFG_698	620989	3555992	690703	413589	25	32	18	Richey, 1989, Table 2
20	FFG_699	623679	3553534	699465	405455	25	32	20	Richey, 1989, Table 2
21	FFG_700	623679	3553131	699465	404135	25	32	20	Richey, 1989, Table 2
22	FFG_701	625090	3553358	704095	404846	25	32	21	Richey, 1989, Table 2
23	FFG_702	625492	3553761	705415	406166	25	32	22	Richey, 1989, Table 2
24	FFG_703	628006	3554508	713698	408555	25	32	23	Richey, 1989, Table 2
25	FFG_704	625492	3552956	705415	403526	25	32	27	Richey, 1989, Table 2
26	FFG_705	624099	3552123	700810	400825	25	32	28	Richey, 1989, Table 2
27	FFG_706	624300	3552123	701470	400825	25	32	28	Richey, 1989, Table 2
28	FFG_707	623679	3552427	699465	401825	25	32	29	Richey, 1989, Table 2
29	FFG_708	623679	3552930	699465	403475	25	32	29	Richey, 1989, Table 2
30	FFG_709	620746	3550770	689804	396452	25	32	31	Richey, 1989, Table 2
31	FFG_710	622771	3550799	696450	396515	25	32	32	Richey, 1989, Table 2
32	FFG_711	624012	3550012	700490	393900	25	32	33	Richey, 1989, Table 2
33	FFG_712	625263	3550440	704596	395271	25	32	33	Richey, 1989, Table 2
34	FFG_713	624830	3550038	703176	393951	25	32	33	Richey, 1989, Table 2
35	FFG_714	625626	3551242	705819	397905	25	32	34	Richey, 1989, Table 2
36	FFG_715	626840	3551268	709807	397957	25	32	34	Richey, 1989, Table 2
37	FFG_716	638420	3559464	747968	424622	25	33	1	Richey, 1989, Table 2
38	FFG_717	633193	3559403	730818	424522	25	33	5	Richey, 1989, Table 2

Table B.1. Location of Wells used by WIPP (Universal Transverse Mercator [UTM], State Plan Coordinates [stpln], and Survey Sections [township, range and section])

	Well ID	x-UTM	y-UTM	x-STPLN	y-STPLN	Township	Range	Section	Source
1	FFG_718	633234	3556994	730887	416614	25	33	8	Richey, 1989, Table 2
2	FFG_719	636829	3557836	742712	419312	25	33	11	Richey, 1989, Table 2
3	FFG_720	639698	3555152	752066	410438	25	33	13	Richey, 1989, Table 2
4	FFG_721	636045	3555837	740111	412751	25	33	15	Richey, 1989, Table 2
5	FFG_723	630458	3553740	721708	406002	25	33	19	Richey, 1989, Table 2
6	FFG_724	632860	3554578	729624	408686	25	33	20	Richey, 1989, Table 2
7	FFG_725	634859	3554589	736187	408691	25	33	21	Richey, 1989, Table 2
8	FFG_726	636908	3553407	742876	404776	25	33	23	Richey, 1989, Table 2
9	FFG_727	638515	3553426	748148	404806	25	33	24	Richey, 1989, Table 2
10	FFG_728	639741	3551836	752140	399555	25	33	25	Richey, 1989, Table 2
11	FFG_729	636519	3551797	741568	399493	25	33	27	Richey, 1989, Table 2
12	FFG_730	634908	3551777	736280	399460	25	33	28	Richey, 1989, Table 2
13	FFG_731	634882	3552983	736227	403421	25	33	28	Richey, 1989, Table 2
14	FFG_732	632068	3552542	726993	402039	25	33	29	Richey, 1989, Table 2
15	FFG_733	630508	3550122	721809	394129	25	33	31	Richey, 1989, Table 2
16	FFG_734	633325	3550558	731054	395493	25	33	32	Richey, 1989, Table 2
17	FFG_735	638531	3551412	748168	398200	25	33	36	Richey, 1989, Table 2
18	H1	613420	3581687	666391	498039	22	31	29	Mercer, 1983, Table 1
19	H10A	622949	3572457	697463	467561	23	32	20	Gonzales, 1989, Tables 3-6 and 3-7
20	H10B	622975	3572473	697549	467613	23	32	20	Gonzales, 1989, Tables 3-6 and 3-7
21	H10C	622976	3572449	697552	467525	23	32	20	Mercer, 1983, Table 1
22	H11B1	615346	3579130	672647	489617	22	31	33	Gonzales, 1989, Tables 3-6 and 3-7
23	H11B2	615348	3579107	672653	489542	22	31	33	Gonzales, 1989, Tables 3-6 and 3-7
24	H11B3	615367	3579127	672716	489608	22	31	33	Gonzales, 1989, Tables 3-6 and 3-7
25	H11B4	615301	3579131	672501	489620	22	31	33	Gonzales, 1989, Tables 3-6 and 3-7
26	H12	617023	3575452	678079	477535	23	31	15	Gonzales, 1989, Tables 3-6 and 3-7
27	H14	612341	3580354	662815	493697	22	31	29	Gonzales, 1989, Tables 3-6 and 3-7
28	H15	615315	3581859	672606	498572	22	31	28	Gonzales, 1989, Tables 3-6 and 3-7
29	H16	613369	3582212	666231	499726	22	31	20	Gonzales, 1989, Tables 3-6 and 3-7
30	H17	615718	3577513	673837	484304	23	31	3	Gonzales, 1989, Tables 3-6 and 3-7
31	H18	612264	3583166	662621	502926	22	31	20	Gonzales, 1989, Tables 3-6 and 3-7
32	H2A	612663	3581641	663897	497912	22	31	29	Gonzales, 1989, Tables 3-6 and 3-7
33	H2B1	612651	3581651	663860	497943	22	31	29	Gonzales, 1989, Tables 3-6 and 3-7
34	H2B2	612661	3581649	663890	497938	22	31	29	Gonzales, 1989, Tables 3-6 and 3-7
35	H2C	612663	3581662	663904	497992	22	31	29	Mercer, 1983, Table 1
36	H3	613735	3580895	667389	495440	22	31	29	Mercer, 1983, Table 1
37	H3B1	613729	3580895	667377	497440	22	31	29	Gonzales, 1989, Tables 3-6 and 3-7
38	H3B2	613701	3580906	667283	495476	22	31	29	Gonzales, 1989, Tables 3-6 and 3-7

Table B.1. Location of Wells used by WIPP (Universal Transverse Mercator [UTM], State Plan Coordinates [stpln], and Survey Sections [township, range and section])

	Well ID	x-UTM	y-UTM	x-STPLN	y-STPLN	Township	Range	Section	Source
1	H3B3	613705	3580876	667298	495376	22	31	29	Gonzales, 1989, Tables 3-6 and 3-7
2	H3D	613721	3580890	667350	495421	22	31	29	Gonzales, 1989, Tables 3-6 and 3-7
3	H4A	612407	3578469	662993	486962	23	31	5	Gonzales, 1989, Tables 3-6 and 3-7
4	H4B	612380	3578483	662906	487554	23	31	5	Gonzales, 1989, Tables 3-6 and 3-7
5	H4C	612404	3578497	662988	487603	23	31	5	Mercer, 1983, Table 1
6	H5A	616888	3584776	677828	508111	22	31	15	Gonzales, 1989, Tables 3-6 and 3-7
7	H5B	616872	3584801	677777	508194	22	31	15	Gonzales, 1989, Tables 3-6 and 3-7
8	H5C	616900	3584802	677873	508198	22	31	15	Mercer, 1983, Table 1
9	H6A	610580	3584982	657132	508881	22	31	18	Gonzales, 1989, Tables 3-6 and 3-7
10	H6B	610594	3585008	657180	508969	22	31	18	Gonzales, 1989, Tables 3-6 and 3-7
11	H6C	610609	3585027	657231	509066	22	31	18	Mercer, 1983, Table 1
12	H7A	608102	3574670	648790	475132	23	30	14	Gonzales, 1989, Tables 3-6 and 3-7
13	H7B1	608124	3574648	648862	475061	23	30	14	Gonzales, 1989, Tables 3-6 and 3-7
14	H7B2	608111	3574612	648837	474965	23	30	14	Gonzales, 1989, Tables 3-6 and 3-7
15	H7C	608086	3574632	648751	475020	23	30	14	Mercer, 1983, Table 1
16	H8A	608658	3563566	650392	438678	24	30	23	Gonzales, 1989, Tables 3-6 and 3-7
17	H8B	608683	3563556	650473	438646	24	30	23	Gonzales, 1989, Tables 3-6 and 3-7
18	H8C	608656	3563541	650397	438590	24	30	23	Mercer, 1983, Table 1
19	H9A	613958	3568260	667879	453977	24	31	4	Gonzales, 1989, Tables 3-6 and 3-7
20	H9B	613989	3568261	667979	453978	24	31	4	Gonzales, 1989, Tables 3-6 and 3-7
21	H9C	613965	3568233	667914	453889	24	31	4	Mercer, 1983, Table 1
22	MB139_1	613585	3582210	666913	499365	0	0	0	Krieg, 1984, Table I
23	MB139_2	613633	3582061	667069	498876	0	0	0	Krieg, 1984, Table I
24	MB139_3	613635	3582155	667076	499185	0	0	0	Krieg, 1984, Table I
25	MB139_4	613582	3582156	666902	499187	0	0	0	Krieg, 1984, Table I
26	P1	612339	3580339	662807	493649	22	31	29	Mercer, 1983, Table 1
27	P10	617074	3581193	678380	496355	22	31	26	Mercer, 1983, Table 1
28	P11	617016	3583462	678222	503799	22	31	23	Mercer, 1983, Table 1
29	P12	610454	3583452	656688	503899	22	30	24	Mercer, 1983, Table 1
30	P13	610539	3585079	657003	509237	22	31	18	Mercer, 1983, Table 1
31	P14	609083	3581974	652158	499079	22	30	24	Mercer, 1983, Table 1
32	P15	610624	3578793	657148	488609	22	31	31	Mercer, 1983, Table 1
33	P16	612704	3577312	663938	483715	23	31	5	Mercer, 1983, Table 1
34	P17	613929	3577459	667959	484166	23	31	4	Mercer, 1983, Table 1
35	P18	618367	3580352	682589	493561	22	31	26	Mercer, 1983, Table 1
36	P19	617687	3582410	680392	500348	22	31	23	Mercer, 1983, Table 1
37	P2	615315	3581850	672609	498541	22	31	28	Mercer, 1983, Table 1
38	P20	618541	3583770	683226	504775	22	31	14	Mercer, 1983, Table 1

Table B.1. Location of Wells used by WIPP (Universal Transverse Mercator [UTM], State Plan Coordinates [stpln], and Survey Sections [township, range and section])

	Well ID	x-UTM	y-UTM	x-STPLN	y-STPLN	Township	Range	Section	Source
1	P21	616901	3584847	677877	508345	22	31	15	Mercer, 1983, Table 1
2	P3	612799	3581888	664349	498733	22	31	20	Mercer, 1983, Table 1
3	P4	614936	3580324	671330	493533	22	31	28	Mercer, 1983, Table 1
4	P5	613686	3583535	667292	504105	22	31	17	Mercer, 1983, Table 1
5	P6	610591	3581133	657104	496288	22	31	30	Mercer, 1983, Table 1
6	P7	612305	3578476	662663	487535	23	31	5	Mercer, 1983, Table 1
7	P8	613827	3578467	667656	487472	23	31	4	Mercer, 1983, Table 1
8	P9	615365	3579125	672704	489600	22	31	33	Mercer, 1983, Table 1
9	SaltShft	613587	3582186	666919	499286	0	0	0	Krieg, 1984, Table I
10	USGS1	606462	3569459	643297	458066	23	30	34	Gonzales, 1989, Tables 3-6 and 3-7
11	USGS4	605841	3569887	641277	459483	23	30	34	Gonzales, 1989, Tables 3-6 and 3-7
12	USGS8	605879	3569888	641402	459483	23	30	34	Gonzales, 1989, Tables 3-6 and 3-7
13	WIPP11	613819	3586474	667796	513749	22	31	9	Mercer, 1983, Table 1
14	WIPP12	613709	3583524	667368	504067	22	31	17	Mercer, 1983, Table 1
15	WIPP13	612652	3584241	663901	506454	22	31	17	Mercer, 1983, Table 1
16	WIPP15	590057	3574585	589590	475231	23	35	18	Mercer, 1983, Table 1
17	WIPP16	602380	3597026	630458	548607	21	30	5	Mercer, 1983, Table 1
18	WIPP18	613731	3583179	667441	502935	22	31	20	Mercer, 1983, Table 1
19	WIPP19	613747	3582787	667461	501649	22	31	20	Mercer, 1983, Table 1
20	WIPP21	613747	3582349	667462	500213	22	31	20	Mercer, 1983, Table 1
21	WIPP22	613747	3582652	667462	501206	22	31	20	Mercer, 1983, Table 1
22	WIPP25	606391	3584037	643354	505885	22	30	15	Mercer, 1983, Table 1
23	WIPP26	604006	3581161	635496	496516	22	30	29	Mercer, 1983, Table 1
24	WIPP27	604425	3593073	637102	535603	21	30	21	Mercer, 1983, Table 1
25	WIPP28	611265	3594687	659578	540736	21	31	18	Mercer, 1983, Table 1
26	WIPP29	596981	3578700	612380	488570	22	29	34	Mercer, 1983, Table 1
27	WIPP30	613718	3589700	667532	524335	21	31	33	Mercer, 1983, Table 1
28	WIPP32	595909	3579081	608858	489850	22	29	33	Mercer, 1983, Table 1
29	WIPP33	609629	3584019	653981	505789	22	30	13	Mercer, 1983, Table 1
30	WIPP34	614333	3585141	669449	509375	22	31	9	Mercer, 1983, Table 1
31	WastShft	613595	3582061	666944	498876	0	0	0	Krieg, 1984, Table I

Table B.2. Elevations of Stratigraphic Layers Near WIPP

	Layer	Well ID	Elevation	Source
2	Anhydrt1	DOE2	-199.00	Mercer et al., 1987, Table 3-2
3	Anhydrt1	DOE2	-119.10	Mercer et al., 1987, Table 3-2
4	Anhydrt1	REF	-199.00	Rechard et al.,1991, Figure 2.2-1
5	Anhydrt1	REF	-119.10	Rechard et al.,1991, Figure 2.2-1
6	Anhydrt1	WIPP11	-43.90	SNL and USGS, 1982a, Table 2
7	Anhydrt1	WIPP11	-37.80	SNL and USGS, 1982a, Table 2
8	Anhydrt1	WIPP12	-139.00	SNL and D'Appolonia Consulting, 1983, Table 2
9	Anhydrt1	WIPP12	-131.10	SNL and D'Appolonia Consulting, 1983, Table 2
10	Anhydrt2	DOE1	-71.60	U.S. DOE, Sep 1982, Table 2
11	Anhydrt2	DOE1	-38.60	U.S. DOE, Sep 1982, Table 2
12	Anhydrt2	DOE2	-116.40	Mercer et al., 1987, Table 3-2
13	Anhydrt2	REF	-116.40	Rechard et al.,1991, Figure 2.2-1
14	Anhydrt2	WIPP11	-22.20	SNL and USGS, 1982a, Table 2
15	Anhydrt2	WIPP11	14.40	SNL and USGS, 1982a, Table 2
16	Anhydrt2	WIPP12	24.50	SNL and D'Appolonia Consulting, 1983, Table 2
17	Anhydrt2	WIPP12	57.80	SNL and D'Appolonia Consulting, 1983, Table 2
18	Anhydrt3	DOE1	30.00	U.S. DOE, Sep 1982, Table 2
19	Anhydrt3	DOE1	163.60	U.S. DOE, Sep 1982, Table 2
20	Anhydrt3	DOE2	102.30	Mercer et al., 1987, Table 3-2
21	Anhydrt3	ERDA9	162.00	SNL and USGS, 1982b, Table 2
22	Anhydrt3	ERDA9	178.10	SNL and USGS, 1982b, Table 2
23	Anhydrt3	REF	162.00	Rechard et al.,1991, Figure 2.2-1
24	Anhydrt3	REF	178.10	Rechard et al.,1991, Figure 2.2-1
25	Anhydrt3	WIPP11	309.40	SNL and USGS, 1982a, Table 2
26	Anhydrt3	WIPP11	334.10	SNL and USGS, 1982a, Table 2
27	Anhydrt3	WIPP12	127.30	SNL and D'Appolonia Consulting, 1983, Table 2
28	Anhydrt3	WIPP12	227.40	SNL and D'Appolonia Consulting, 1983, Table 2
29	Anhydrta	AirShft	386.41	Holt and Powers, 1990, Figure 22
30	Anhydrta	AirShft	386.70	Holt and Powers, 1990, Figure 22
31	Anhydrta	DH207	386.86	Krieg, 1984, Table I
32	Anhydrta	DH207	388.78	Krieg, 1984, Table I
33	Anhydrta	DH211	389.81	Krieg, 1984, Table I
34	Anhydrta	DH211	391.67	Krieg, 1984, Table I
35	Anhydrta	DH215	390.11	Krieg, 1984, Table I
36	Anhydrta	DH215	391.97	Krieg, 1984, Table I
37	Anhydrta	DH219	390.39	Krieg, 1984, Table I
38	Anhydrta	DH219	390.57	Krieg, 1984, Table I
39	Anhydrta	DH223	386.88	Krieg, 1984, Table I
40	Anhydrta	DH223	387.18	Krieg, 1984, Table I
41	Anhydrta	DH227	384.02	Krieg, 1984, Table I
42	Anhydrta	DH227	384.26	Krieg, 1984, Table I
43	Anhydrta	DH77	402.79	Krieg, 1984, Table I
44	Anhydrta	DH77	402.88	Krieg, 1984, Table I
45	Anhydrta	DO201	389.23	Krieg, 1984, Table I
46	Anhydrta	DO201	389.44	Krieg, 1984, Table I
47	Anhydrta	DO203	400.02	Krieg, 1984, Table I
48	Anhydrta	DO203	400.26	Krieg, 1984, Table I
49	Anhydrta	DO205	405.17	Krieg, 1984, Table I
50	Anhydrta	DO205	405.38	Krieg, 1984, Table I
51	Anhydrta	DO45	396.69	Krieg, 1984, Table I
52	Anhydrta	DO45	396.87	Krieg, 1984, Table I
53	Anhydrta	DO52	393.92	Krieg, 1984, Table I
54	Anhydrta	DO52	394.07	Krieg, 1984, Table I
55	Anhydrta	DO56	399.74	Krieg, 1984, Table I
56	Anhydrta	DO56	399.92	Krieg, 1984, Table I
57	Anhydrta	DO63	403.61	Krieg, 1984, Table I
58	Anhydrta	DO63	403.98	Krieg, 1984, Table I
59	Anhydrta	DO67	403.58	Krieg, 1984, Table I
60	Anhydrta	DO67	403.85	Krieg, 1984, Table I
61	Anhydrta	DO88	402.36	Krieg, 1984, Table I
62	Anhydrta	DO88	402.51	Krieg, 1984, Table I
63	Anhydrta	DO91	402.07	Krieg, 1984, Table I
64	Anhydrta	DO91	402.28	Krieg, 1984, Table I
65	Anhydrta	ExhtShft	389.78	Bechtel, Inc., 1986, Appendix F
66	Anhydrta	ExhtShft	390.03	Bechtel, Inc., 1986, Appendix F
67	Anhydrta	MB139_2	388.84	Krieg, 1984, Table I
68	Anhydrta	MB139_2	389.05	Krieg, 1984, Table I
69	Anhydrta	SaltShft	392.51	Bechtel, Inc., 1986, Appendix D
70	Anhydrta	SaltShft	392.74	Bechtel, Inc., 1986, Appendix D
71	Anhydrta	SaltShft	392.53	Krieg, 1984, Table I
72	Anhydrta	SaltShft	392.76	Krieg, 1984, Table I
73	Anhydrta	WastShft	388.76	Bechtel, Inc., 1986, Appendix E
74	Anhydrta	WastShft	388.97	Bechtel, Inc., 1986, Appendix E
75	Anhydrta	WastShft	389.01	Krieg, 1984, Table I
76	Anhydrta	WastShft	389.25	Krieg, 1984, Table I
77	Anhydrtb	DH207	386.65	Krieg, 1984, Table I

Table B.2. Elevations of Stratigraphic Layers Near WIPP (Continued)

	Layer	Well ID	Elevation	Source
2	Anhydrtb	DH207	386.70	Krieg, 1984, Table I
3	Anhydrtb	DH211	389.63	Krieg, 1984, Table I
4	Anhydrtb	DH211	389.66	Krieg, 1984, Table I
5	Anhydrtb	DH215	389.96	Krieg, 1984, Table I
6	Anhydrtb	DH215	390.02	Krieg, 1984, Table I
7	Anhydrtb	DH219	388.41	Krieg, 1984, Table I
8	Anhydrtb	DH219	388.42	Krieg, 1984, Table I
9	Anhydrtb	DH223	385.05	Krieg, 1984, Table I
10	Anhydrtb	DH223	385.05	Krieg, 1984, Table I
11	Anhydrtb	DH227	382.25	Krieg, 1984, Table I
12	Anhydrtb	DH227	382.25	Krieg, 1984, Table I
13	Anhydrtb	DH77	400.75	Krieg, 1984, Table I
14	Anhydrtb	DH77	400.83	Krieg, 1984, Table I
15	Anhydrtb	DO201	387.07	Krieg, 1984, Table I
16	Anhydrtb	DO201	387.13	Krieg, 1984, Table I
17	Anhydrtb	DO203	398.13	Krieg, 1984, Table I
18	Anhydrtb	DO203	398.19	Krieg, 1984, Table I
19	Anhydrtb	DO205	403.13	Krieg, 1984, Table I
20	Anhydrtb	DO205	403.19	Krieg, 1984, Table I
21	Anhydrtb	DO45	393.92	Krieg, 1984, Table I
22	Anhydrtb	DO45	393.95	Krieg, 1984, Table I
23	Anhydrtb	DO52	391.88	Krieg, 1984, Table I
24	Anhydrtb	DO52	391.94	Krieg, 1984, Table I
25	Anhydrtb	DO56	397.64	Krieg, 1984, Table I
26	Anhydrtb	DO56	397.70	Krieg, 1984, Table I
27	Anhydrtb	DO63	401.45	Krieg, 1984, Table I
28	Anhydrtb	DO63	401.51	Krieg, 1984, Table I
29	Anhydrtb	DO67	401.45	Krieg, 1984, Table I
30	Anhydrtb	DO67	401.53	Krieg, 1984, Table I
31	Anhydrtb	DO88	400.23	Krieg, 1984, Table I
32	Anhydrtb	DO88	400.30	Krieg, 1984, Table I
33	Anhydrtb	DO91	399.91	Krieg, 1984, Table I
34	Anhydrtb	DO91	399.96	Krieg, 1984, Table I
35	Anhydrtb	ExhtShft	387.66	Bechtel, Inc., 1986, Appendix F
36	Anhydrtb	ExhtShft	387.75	Bechtel, Inc., 1986, Appendix F
37	Anhydrtb	MB139_2	386.58	Krieg, 1984, Table I
38	Anhydrtb	MB139_2	386.61	Krieg, 1984, Table I
39	Anhydrtb	SaltShft	390.58	Bechtel, Inc., 1986, Appendix D
40	Anhydrtb	SaltShft	390.66	Bechtel, Inc., 1986, Appendix D
41	Anhydrtb	SaltShft	390.37	Krieg, 1984, Table I
42	Anhydrtb	SaltShft	390.45	Krieg, 1984, Table I
43	Anhydrtb	WastShft	386.57	Bechtel, Inc., 1986, Appendix E
44	Anhydrtb	WastShft	386.70	Bechtel, Inc., 1986, Appendix E
45	Anhydrtb	WastShft	386.91	Krieg, 1984, Table I
46	Anhydrtb	WastShft	386.97	Krieg, 1984, Table I
47	Anhydrtc	DH207	369.49	Krieg, 1984, Table I
48	Anhydrtc	DH207	369.55	Krieg, 1984, Table I
49	Anhydrtc	DH211	372.71	Krieg, 1984, Table I
50	Anhydrtc	DH211	372.80	Krieg, 1984, Table I
51	Anhydrtc	DH215	373.14	Krieg, 1984, Table I
52	Anhydrtc	DH215	373.20	Krieg, 1984, Table I
53	Anhydrtc	DH219	372.13	Krieg, 1984, Table I
54	Anhydrtc	DH219	372.19	Krieg, 1984, Table I
55	Anhydrtc	DH223	369.08	Krieg, 1984, Table I
56	Anhydrtc	DH223	369.17	Krieg, 1984, Table I
57	Anhydrtc	DH227	366.16	Krieg, 1984, Table I
58	Anhydrtc	DH227	366.22	Krieg, 1984, Table I
59	Anhydrtc	DH77	384.75	Krieg, 1984, Table I
60	Anhydrtc	DH77	384.81	Krieg, 1984, Table I
61	Anhydrtc	DO201	369.91	Krieg, 1984, Table I
62	Anhydrtc	DO201	370.03	Krieg, 1984, Table I
63	Anhydrtc	DO203	381.95	Krieg, 1984, Table I
64	Anhydrtc	DO203	382.01	Krieg, 1984, Table I
65	Anhydrtc	DO205	387.37	Krieg, 1984, Table I
66	Anhydrtc	DO205	387.43	Krieg, 1984, Table I
67	Anhydrtc	DO45	377.22	Krieg, 1984, Table I
68	Anhydrtc	DO45	377.28	Krieg, 1984, Table I
69	Anhydrtc	DO52	375.18	Krieg, 1984, Table I
70	Anhydrtc	DO52	375.24	Krieg, 1984, Table I
71	Anhydrtc	DO56	381.00	Krieg, 1984, Table I
72	Anhydrtc	DO56	381.09	Krieg, 1984, Table I
73	Anhydrtc	DO63	385.66	Krieg, 1984, Table I
74	Anhydrtc	DO63	385.84	Krieg, 1984, Table I
75	Anhydrtc	DO67	385.54	Krieg, 1984, Table I
76	Anhydrtc	DO67	385.63	Krieg, 1984, Table I
77	Anhydrtc	DO88	384.01	Krieg, 1984, Table I

Table B.2. Elevations of Stratigraphic Layers Near WIPP (Continued)

	Layer	Well ID	Elevation	Source
1	Anhydrtc	DO88	384.06	Krieg, 1984, Table I
2	Anhydrtc	DO91	384.03	Krieg, 1984, Table I
3	Anhydrtc	DO91	384.12	Krieg, 1984, Table I
4	Anhydrtc	SaltShft	373.09	Krieg, 1984, Table I
5	Anhydrtc	SaltShft	373.20	Krieg, 1984, Table I
6	B_CANyon	DOE2	-276.30	Mercer et al., 1987, Table 3-2
7	B_CANyon	DOE2	-199.00	Mercer et al., 1987, Table 3-2
8	B_CANyon	REF	-276.30	Rechard et al.,1991, Figure 2.2-1
9	B_CANyon	REF	-199.00	Rechard et al.,1991, Figure 2.2-1
10	Culebra	AEC7	848.50	Mercer, 1983, Table 1
11	Culebra	AEC8	822.70	Mercer, 1983, Table 1
12	Culebra	AirShft	824.48	Holt and Powers, 1990, Figure 22
13	Culebra	B25	824.50	Mercer, 1983, Table 1
14	Culebra	DOE1	806.10	U.S. DOE, Sep 1982, Table 2
15	Culebra	DOE2	790.80	Mercer et al., 1987, Table 3-2
16	Culebra	ERDA10	882.40	Mercer, 1983, Table 1
17	Culebra	ERDA6	862.60	Mercer, 1983, Table 1
18	Culebra	ERDA9	827.50	Mercer, 1983, Table 1
19	Culebra	ERDA9	823.40	SNL and USGS, 1982b, Table 2
20	Culebra	ExhtShft	821.57	Bechtel, Inc., 1986, Appendix F
21	Culebra	FFG_002	624.80	Richey, 1989, Table 2, p.21
22	Culebra	FFG_004	666.60	Richey, 1989, Table 2, p.21
23	Culebra	FFG_005	628.50	Richey, 1989, Table 2, p.21
24	Culebra	FFG_006	616.60	Richey, 1989, Table 2, p.21
25	Culebra	FFG_007	602.00	Richey, 1989, Table 2, p.21
26	Culebra	FFG_009	604.10	Richey, 1989, Table 2, p.21
27	Culebra	FFG_011	609.90	Richey, 1989, Table 2, p.21
28	Culebra	FFG_012	613.90	Richey, 1989, Table 2, p.21
29	Culebra	FFG_013	646.20	Richey, 1989, Table 2, p.21
30	Culebra	FFG_014	667.80	Richey, 1989, Table 2, p.21
31	Culebra	FFG_016	587.90	Richey, 1989, Table 2, p.21
32	Culebra	FFG_017	594.90	Richey, 1989, Table 2, p.22
33	Culebra	FFG_018	598.60	Richey, 1989, Table 2, p.22
34	Culebra	FFG_019	588.60	Richey, 1989, Table 2, p.22
35	Culebra	FFG_020	662.00	Richey, 1989, Table 2, p.22
36	Culebra	FFG_023	596.20	Richey, 1989, Table 2, p.22
37	Culebra	FFG_024	579.10	Richey, 1989, Table 2, p.22
38	Culebra	FFG_025	598.50	Richey, 1989, Table 2, p.22
39	Culebra	FFG_026	592.50	Richey, 1989, Table 2, p.22
40	Culebra	FFG_027	585.50	Richey, 1989, Table 2, p.22
41	Culebra	FFG_028	578.60	Richey, 1989, Table 2, p.22
42	Culebra	FFG_029	563.50	Richey, 1989, Table 2, p.22
43	Culebra	FFG_030	563.00	Richey, 1989, Table 2, p.22
44	Culebra	FFG_031	554.40	Richey, 1989, Table 2, p.22
45	Culebra	FFG_032	549.40	Richey, 1989, Table 2, p.22
46	Culebra	FFG_033	549.20	Richey, 1989, Table 2, p.22
47	Culebra	FFG_034	548.60	Richey, 1989, Table 2, p.23
48	Culebra	FFG_035	533.90	Richey, 1989, Table 2, p.23
49	Culebra	FFG_036	541.40	Richey, 1989, Table 2, p.23
50	Culebra	FFG_037	534.00	Richey, 1989, Table 2, p.23
51	Culebra	FFG_038	523.60	Richey, 1989, Table 2, p.23
52	Culebra	FFG_039	731.90	Richey, 1989, Table 2, p.23
53	Culebra	FFG_040	655.40	Richey, 1989, Table 2, p.23
54	Culebra	FFG_041	733.70	Richey, 1989, Table 2, p.23
55	Culebra	FFG_042	740.60	Richey, 1989, Table 2, p.23
56	Culebra	FFG_043	735.70	Richey, 1989, Table 2, p.23
57	Culebra	FFG_044	689.10	Richey, 1989, Table 2, p.23
58	Culebra	FFG_047	561.10	Richey, 1989, Table 2, p.23
59	Culebra	FFG_048	580.30	Richey, 1989, Table 2, p.23
60	Culebra	FFG_049	567.50	Richey, 1989, Table 2, p.23
61	Culebra	FFG_050	582.50	Richey, 1989, Table 2, p.24
62	Culebra	FFG_051	573.90	Richey, 1989, Table 2, p.24
63	Culebra	FFG_052	595.20	Richey, 1989, Table 2, p.24
64	Culebra	FFG_053	563.00	Richey, 1989, Table 2, p.24
65	Culebra	FFG_054	562.70	Richey, 1989, Table 2, p.24
66	Culebra	FFG_055	565.70	Richey, 1989, Table 2, p.24
67	Culebra	FFG_056	564.50	Richey, 1989, Table 2, p.24
68	Culebra	FFG_057	564.80	Richey, 1989, Table 2, p.24
69	Culebra	FFG_058	569.30	Richey, 1989, Table 2, p.24
70	Culebra	FFG_059	569.70	Richey, 1989, Table 2, p.24
71	Culebra	FFG_060	569.30	Richey, 1989, Table 2, p.24
72	Culebra	FFG_061	570.60	Richey, 1989, Table 2, p.24
73	Culebra	FFG_062	513.90	Richey, 1989, Table 2, p.24
74	Culebra	FFG_063	470.70	Richey, 1989, Table 2, p.24
75	Culebra	FFG_064	497.50	Richey, 1989, Table 2, p.24
76	Culebra	FFG_065	471.80	Richey, 1989, Table 2, p.24

Table B.2. Elevations of Stratigraphic Layers Near WIPP (Continued)

	Layer	Well ID	Elevation	Source
1	Culebra	FFG_066	434.30	Richey, 1989, Table 2, p.24
2	Culebra	FFG_067	470.00	Richey, 1989, Table 2, p.25
3	Culebra	FFG_068	430.10	Richey, 1989, Table 2, p.25
4	Culebra	FFG_069	447.50	Richey, 1989, Table 2, p.25
5	Culebra	FFG_070	484.60	Richey, 1989, Table 2, p.25
6	Culebra	FFG_071	755.00	Richey, 1989, Table 2, p.25
7	Culebra	FFG_072	681.20	Richey, 1989, Table 2, p.25
8	Culebra	FFG_073	659.30	Richey, 1989, Table 2, p.25
9	Culebra	FFG_074	666.40	Richey, 1989, Table 2, p.25
10	Culebra	FFG_075	717.90	Richey, 1989, Table 2, p.25
11	Culebra	FFG_076	777.60	Richey, 1989, Table 2, p.25
12	Culebra	FFG_078	814.70	Richey, 1989, Table 2, p.25
13	Culebra	FFG_079	787.00	Richey, 1989, Table 2, p.25
14	Culebra	FFG_080	765.60	Richey, 1989, Table 2, p.25
15	Culebra	FFG_081	683.10	Richey, 1989, Table 2, p.26
16	Culebra	FFG_082	711.10	Richey, 1989, Table 2, p.26
17	Culebra	FFG_083	638.10	Richey, 1989, Table 2, p.26
18	Culebra	FFG_084	661.40	Richey, 1989, Table 2, p.26
19	Culebra	FFG_085	655.40	Richey, 1989, Table 2, p.26
20	Culebra	FFG_086	665.00	Richey, 1989, Table 2, p.26
21	Culebra	FFG_087	636.70	Richey, 1989, Table 2, p.26
22	Culebra	FFG_088	626.10	Richey, 1989, Table 2, p.26
23	Culebra	FFG_089	613.90	Richey, 1989, Table 2, p.26
24	Culebra	FFG_091	652.30	Richey, 1989, Table 2, p.26
25	Culebra	FFG_092	670.90	Richey, 1989, Table 2, p.26
26	Culebra	FFG_093	673.60	Richey, 1989, Table 2, p.26
27	Culebra	FFG_094	674.20	Richey, 1989, Table 2, p.26
28	Culebra	FFG_095	651.60	Richey, 1989, Table 2, p.26
29	Culebra	FFG_096	635.50	Richey, 1989, Table 2, p.26
30	Culebra	FFG_097	614.80	Richey, 1989, Table 2, p.27
31	Culebra	FFG_098	587.90	Richey, 1989, Table 2, p.27
32	Culebra	FFG_099	582.50	Richey, 1989, Table 2, p.27
33	Culebra	FFG_100	564.80	Richey, 1989, Table 2, p.27
34	Culebra	FFG_101	533.70	Richey, 1989, Table 2, p.27
35	Culebra	FFG_102	549.00	Richey, 1989, Table 2, p.27
36	Culebra	FFG_103	609.30	Richey, 1989, Table 2, p.27
37	Culebra	FFG_104	508.10	Richey, 1989, Table 2, p.27
38	Culebra	FFG_105	867.50	Richey, 1989, Table 2, p.27
39	Culebra	FFG_106	902.60	Richey, 1989, Table 2, p.27
40	Culebra	FFG_107	887.90	Richey, 1989, Table 2, p.27
41	Culebra	FFG_108	878.70	Richey, 1989, Table 2, p.27
42	Culebra	FFG_109	862.30	Richey, 1989, Table 2, p.27
43	Culebra	FFG_110	832.10	Richey, 1989, Table 2, p.27
44	Culebra	FFG_111	836.60	Richey, 1989, Table 2, p.27
45	Culebra	FFG_112	824.50	Richey, 1989, Table 2, p.28
46	Culebra	FFG_113	838.50	Richey, 1989, Table 2, p.28
47	Culebra	FFG_114	870.50	Richey, 1989, Table 2, p.28
48	Culebra	FFG_115	857.40	Richey, 1989, Table 2, p.28
49	Culebra	FFG_116	871.40	Richey, 1989, Table 2, p.28
50	Culebra	FFG_117	868.70	Richey, 1989, Table 2, p.28
51	Culebra	FFG_119	870.90	Richey, 1989, Table 2, p.28
52	Culebra	FFG_120	874.20	Richey, 1989, Table 2, p.28
53	Culebra	FFG_121	882.40	Richey, 1989, Table 2, p.28
54	Culebra	FFG_122	876.30	Richey, 1989, Table 2, p.28
55	Culebra	FFG_123	867.10	Richey, 1989, Table 2, p.28
56	Culebra	FFG_124	837.90	Richey, 1989, Table 2, p.28
57	Culebra	FFG_125	851.20	Richey, 1989, Table 2, p.28
58	Culebra	FFG_126	852.70	Richey, 1989, Table 2, p.28
59	Culebra	FFG_127	860.70	Richey, 1989, Table 2, p.28
60	Culebra	FFG_128	887.00	Richey, 1989, Table 2, p.28
61	Culebra	FFG_129	858.30	Richey, 1989, Table 2, p.28
62	Culebra	FFG_130	897.60	Richey, 1989, Table 2, p.28
63	Culebra	FFG_132	898.60	Richey, 1989, Table 2, p.29
64	Culebra	FFG_133	901.60	Richey, 1989, Table 2, p.29
65	Culebra	FFG_134	904.40	Richey, 1989, Table 2, p.29
66	Culebra	FFG_135	880.90	Richey, 1989, Table 2, p.29
67	Culebra	FFG_136	882.50	Richey, 1989, Table 2, p.29
68	Culebra	FFG_137	892.80	Richey, 1989, Table 2, p.29
69	Culebra	FFG_138	844.10	Richey, 1989, Table 2, p.29
70	Culebra	FFG_139	855.60	Richey, 1989, Table 2, p.29
71	Culebra	FFG_140	792.70	Richey, 1989, Table 2, p.29
72	Culebra	FFG_141	820.10	Richey, 1989, Table 2, p.29
73	Culebra	FFG_142	795.90	Richey, 1989, Table 2, p.29
74	Culebra	FFG_143	804.00	Richey, 1989, Table 2, p.29
75	Culebra	FFG_144	894.30	Richey, 1989, Table 2, p.29
76	Culebra	FFG_145	893.10	Richey, 1989, Table 2, p.29

Table B.2. Elevations of Stratigraphic Layers Near WIPP (Continued)

	Layer	Well ID	Elevation	Source
1	Culebra	FFG_146	906.80	Richey, 1989, Table 2, p.29
2	Culebra	FFG_147	882.70	Richey, 1989, Table 2, p.29
3	Culebra	FFG_148	900.10	Richey, 1989, Table 2, p.29
4	Culebra	FFG_149	910.70	Richey, 1989, Table 2, p.30
5	Culebra	FFG_155	901.30	Richey, 1989, Table 2, p.30
6	Culebra	FFG_156	906.50	Richey, 1989, Table 2, p.30
7	Culebra	FFG_157	904.10	Richey, 1989, Table 2, p.30
8	Culebra	FFG_158	928.10	Richey, 1989, Table 2, p.30
9	Culebra	FFG_159	898.60	Richey, 1989, Table 2, p.30
10	Culebra	FFG_160	895.20	Richey, 1989, Table 2, p.30
11	Culebra	FFG_161	901.00	Richey, 1989, Table 2, p.30
12	Culebra	FFG_162	891.90	Richey, 1989, Table 2, p.30
13	Culebra	FFG_163	897.40	Richey, 1989, Table 2, p.30
14	Culebra	FFG_164	937.60	Richey, 1989, Table 2, p.30
15	Culebra	FFG_165	912.80	Richey, 1989, Table 2, p.30
16	Culebra	FFG_166	900.00	Richey, 1989, Table 2, p.31
17	Culebra	FFG_167	887.00	Richey, 1989, Table 2, p.31
18	Culebra	FFG_168	906.50	Richey, 1989, Table 2, p.31
19	Culebra	FFG_169	919.20	Richey, 1989, Table 2, p.31
20	Culebra	FFG_170	903.70	Richey, 1989, Table 2, p.31
21	Culebra	FFG_171	922.10	Richey, 1989, Table 2, p.31
22	Culebra	FFG_172	915.30	Richey, 1989, Table 2, p.31
23	Culebra	FFG_173	876.90	Richey, 1989, Table 2, p.31
24	Culebra	FFG_177	889.10	Richey, 1989, Table 2, p.31
25	Culebra	FFG_178	718.10	Richey, 1989, Table 2, p.31
26	Culebra	FFG_179	886.60	Richey, 1989, Table 2, p.31
27	Culebra	FFG_180	883.00	Richey, 1989, Table 2, p.31
28	Culebra	FFG_181	930.50	Richey, 1989, Table 2, p.32
29	Culebra	FFG_182	812.60	Richey, 1989, Table 2, p.32
30	Culebra	FFG_183	904.40	Richey, 1989, Table 2, p.32
31	Culebra	FFG_184	891.20	Richey, 1989, Table 2, p.32
32	Culebra	FFG_185	899.50	Richey, 1989, Table 2, p.32
33	Culebra	FFG_186	827.90	Richey, 1989, Table 2, p.32
34	Culebra	FFG_188	845.80	Richey, 1989, Table 2, p.32
35	Culebra	FFG_189	867.80	Richey, 1989, Table 2, p.32
36	Culebra	FFG_190	843.60	Richey, 1989, Table 2, p.32
37	Culebra	FFG_191	845.50	Richey, 1989, Table 2, p.32
38	Culebra	FFG_192	774.50	Richey, 1989, Table 2, p.32
39	Culebra	FFG_194	788.50	Richey, 1989, Table 2, p.33
40	Culebra	FFG_195	803.50	Richey, 1989, Table 2, p.33
41	Culebra	FFG_196	837.00	Richey, 1989, Table 2, p.33
42	Culebra	FFG_197	841.00	Richey, 1989, Table 2, p.33
43	Culebra	FFG_198	840.90	Richey, 1989, Table 2, p.33
44	Culebra	FFG_199	827.00	Richey, 1989, Table 2, p.33
45	Culebra	FFG_200	838.20	Richey, 1989, Table 2, p.33
46	Culebra	FFG_201	838.20	Richey, 1989, Table 2, p.33
47	Culebra	FFG_202	773.80	Richey, 1989, Table 2, p.33
48	Culebra	FFG_203	776.00	Richey, 1989, Table 2, p.33
49	Culebra	FFG_204	813.50	Richey, 1989, Table 2, p.33
50	Culebra	FFG_205	825.10	Richey, 1989, Table 2, p.33
51	Culebra	FFG_206	837.00	Richey, 1989, Table 2, p.33
52	Culebra	FFG_207	833.60	Richey, 1989, Table 2, p.33
53	Culebra	FFG_208	843.10	Richey, 1989, Table 2, p.34
54	Culebra	FFG_209	838.20	Richey, 1989, Table 2, p.34
55	Culebra	FFG_210	827.50	Richey, 1989, Table 2, p.34
56	Culebra	FFG_212	817.50	Richey, 1989, Table 2, p.34
57	Culebra	FFG_213	837.90	Richey, 1989, Table 2, p.34
58	Culebra	FFG_214	818.40	Richey, 1989, Table 2, p.34
59	Culebra	FFG_215	793.10	Richey, 1989, Table 2, p.34
60	Culebra	FFG_216	688.80	Richey, 1989, Table 2, p.34
61	Culebra	FFG_217	814.80	Richey, 1989, Table 2, p.34
62	Culebra	FFG_218	803.50	Richey, 1989, Table 2, p.34
63	Culebra	FFG_219	848.80	Richey, 1989, Table 2, p.34
64	Culebra	FFG_220	798.60	Richey, 1989, Table 2, p.34
65	Culebra	FFG_221	756.50	Richey, 1989, Table 2, p.34
66	Culebra	FFG_222	713.30	Richey, 1989, Table 2, p.34
67	Culebra	FFG_224	597.80	Richey, 1989, Table 2, p.35
68	Culebra	FFG_225	603.50	Richey, 1989, Table 2, p.35
69	Culebra	FFG_226	601.80	Richey, 1989, Table 2, p.35
70	Culebra	FFG_228	588.30	Richey, 1989, Table 2, p.35
71	Culebra	FFG_229	614.70	Richey, 1989, Table 2, p.35
72	Culebra	FFG_230	601.10	Richey, 1989, Table 2, p.35
73	Culebra	FFG_231	619.90	Richey, 1989, Table 2, p.35
74	Culebra	FFG_232	631.50	Richey, 1989, Table 2, p.35
75	Culebra	FFG_233	624.00	Richey, 1989, Table 2, p.35
76	Culebra	FFG_234	660.20	Richey, 1989, Table 2, p.35

Table B.2. Elevations of Stratigraphic Layers Near WIPP (Continued)

	Layer	Well ID	Elevation	Source		Layer	Well ID	Elevation	Source
1	Culebra	FFG_235	635.50	Richey, 1989, Table 2, p.35	39	Culebra	FFG_273	753.20	Richey, 1989, Table 2, p.38
2	Culebra	FFG_236	682.70	Richey, 1989, Table 2, p.35	40	Culebra	FFG_274	793.10	Richey, 1989, Table 2, p.38
3	Culebra	FFG_237	646.20	Richey, 1989, Table 2, p.35	41	Culebra	FFG_275	800.70	Richey, 1989, Table 2, p.38
4	Culebra	FFG_238	628.50	Richey, 1989, Table 2, p.36	42	Culebra	FFG_276	802.80	Richey, 1989, Table 2, p.38
5	Culebra	FFG_239	620.50	Richey, 1989, Table 2, p.36	43	Culebra	FFG_277	795.50	Richey, 1989, Table 2, p.38
6	Culebra	FFG_240	609.90	Richey, 1989, Table 2, p.36	44	Culebra	FFG_278	776.60	Richey, 1989, Table 2, p.38
7	Culebra	FFG_241	605.10	Richey, 1989, Table 2, p.36	45	Culebra	FFG_279	776.90	Richey, 1989, Table 2, p.38
8	Culebra	FFG_242	732.20	Richey, 1989, Table 2, p.36	46	Culebra	FFG_280	788.80	Richey, 1989, Table 2, p.38
9	Culebra	FFG_243	668.40	Richey, 1989, Table 2, p.36	47	Culebra	FFG_281	762.60	Richey, 1989, Table 2, p.38
10	Culebra	FFG_244	721.30	Richey, 1989, Table 2, p.36	48	Culebra	FFG_283	496.20	Richey, 1989, Table 2, p.39
11	Culebra	FFG_245	510.80	Richey, 1989, Table 2, p.36	49	Culebra	FFG_284	648.00	Richey, 1989, Table 2, p.39
12	Culebra	FFG_246	516.00	Richey, 1989, Table 2, p.36	50	Culebra	FFG_285	669.60	Richey, 1989, Table 2, p.39
13	Culebra	FFG_247	501.30	Richey, 1989, Table 2, p.36	51	Culebra	FFG_286	773.80	Richey, 1989, Table 2, p.39
14	Culebra	FFG_248	506.60	Richey, 1989, Table 2, p.36	52	Culebra	FFG_287	738.20	Richey, 1989, Table 2, p.39
15	Culebra	FFG_249	505.30	Richey, 1989, Table 2, p.36	53	Culebra	FFG_288	668.70	Richey, 1989, Table 2, p.39
16	Culebra	FFG_250	587.50	Richey, 1989, Table 2, p.36	54	Culebra	FFG_289	680.60	Richey, 1989, Table 2, p.39
17	Culebra	FFG_251	477.30	Richey, 1989, Table 2, p.36	55	Culebra	FFG_290	770.90	Richey, 1989, Table 2, p.39
18	Culebra	FFG_252	619.60	Richey, 1989, Table 2, p.36	56	Culebra	FFG_291	668.70	Richey, 1989, Table 2, p.39
19	Culebra	FFG_253	566.70	Richey, 1989, Table 2, p.36	57	Culebra	FFG_292	724.80	Richey, 1989, Table 2, p.39
20	Culebra	FFG_254	562.00	Richey, 1989, Table 2, p.36	58	Culebra	FFG_293	718.10	Richey, 1989, Table 2, p.39
21	Culebra	FFG_255	514.50	Richey, 1989, Table 2, p.37	59	Culebra	FFG_294	504.50	Richey, 1989, Table 2, p.39
22	Culebra	FFG_256	477.90	Richey, 1989, Table 2, p.37	60	Culebra	FFG_295	489.50	Richey, 1989, Table 2, p.39
23	Culebra	FFG_257	523.30	Richey, 1989, Table 2, p.37	61	Culebra	FFG_297	469.10	Richey, 1989, Table 2, p.39
24	Culebra	FFG_258	546.20	Richey, 1989, Table 2, p.37	62	Culebra	FFG_298	528.10	Richey, 1989, Table 2, p.40
25	Culebra	FFG_259	503.20	Richey, 1989, Table 2, p.37	63	Culebra	FFG_299	497.80	Richey, 1989, Table 2, p.40
26	Culebra	FFG_260	556.30	Richey, 1989, Table 2, p.37	64	Culebra	FFG_300	480.60	Richey, 1989, Table 2, p.40
27	Culebra	FFG_261	542.20	Richey, 1989, Table 2, p.37	65	Culebra	FFG_301	435.90	Richey, 1989, Table 2, p.40
28	Culebra	FFG_262	485.60	Richey, 1989, Table 2, p.37	66	Culebra	FFG_302	443.50	Richey, 1989, Table 2, p.40
29	Culebra	FFG_263	456.50	Richey, 1989, Table 2, p.37	67	Culebra	FFG_303	449.00	Richey, 1989, Table 2, p.40
30	Culebra	FFG_264	703.80	Richey, 1989, Table 2, p.37	68	Culebra	FFG_304	445.90	Richey, 1989, Table 2, p.40
31	Culebra	FFG_265	686.10	Richey, 1989, Table 2, p.37	69	Culebra	FFG_305	443.20	Richey, 1989, Table 2, p.40
32	Culebra	FFG_266	665.40	Richey, 1989, Table 2, p.37	70	Culebra	FFG_306	413.00	Richey, 1989, Table 2, p.40
33	Culebra	FFG_267	641.30	Richey, 1989, Table 2, p.37	71	Culebra	FFG_307	432.20	Richey, 1989, Table 2, p.40
34	Culebra	FFG_268	613.60	Richey, 1989, Table 2, p.37	72	Culebra	FFG_308	376.10	Richey, 1989, Table 2, p.40
35	Culebra	FFG_269	627.70	Richey, 1989, Table 2, p.38	73	Culebra	FFG_309	434.60	Richey, 1989, Table 2, p.40
36	Culebra	FFG_270	730.30	Richey, 1989, Table 2, p.38	74	Culebra	FFG_310	475.20	Richey, 1989, Table 2, p.40
37	Culebra	FFG_271	773.90	Richey, 1989, Table 2, p.38	75	Culebra	FFG_311	428.60	Richey, 1989, Table 2, p.40
38	Culebra	FFG_272	751.80	Richey, 1989, Table 2, p.38	76	Culebra	FFG_312	429.80	Richey, 1989, Table 2, p.40

Table B.2. Elevations of Stratigraphic Layers Near WIPP (Continued)

	Layer	Well ID	Elevation	Source		Layer	Well ID	Elevation	Source
1	Culebra	FFG_313	870.30	Richey, 1989, Table 2, p.41	39	Culebra	FFG_354	762.00	Richey, 1989, Table 2, p.43
2	Culebra	FFG_314	788.90	Richey, 1989, Table 2, p.41	40	Culebra	FFG_361	955.20	Richey, 1989, Table 2, p.44
3	Culebra	FFG_315	701.50	Richey, 1989, Table 2, p.41	41	Culebra	FFG_362	919.30	Richey, 1989, Table 2, p.44
4	Culebra	FFG_316	678.40	Richey, 1989, Table 2, p.41	42	Culebra	FFG_363	947.00	Richey, 1989, Table 2, p.44
5	Culebra	FFG_317	732.40	Richey, 1989, Table 2, p.41	43	Culebra	FFG_364	918.30	Richey, 1989, Table 2, p.44
6	Culebra	FFG_318	710.20	Richey, 1989, Table 2, p.41	44	Culebra	FFG_366	911.60	Richey, 1989, Table 2, p.44
7	Culebra	FFG_319	704.60	Richey, 1989, Table 2, p.41	45	Culebra	FFG_367	931.70	Richey, 1989, Table 2, p.44
8	Culebra	FFG_320	669.40	Richey, 1989, Table 2, p.41	46	Culebra	FFG_370	968.70	Richey, 1989, Table 2, p.44
9	Culebra	FFG_321	668.40	Richey, 1989, Table 2, p.41	47	Culebra	FFG_371	965.70	Richey, 1989, Table 2, p.44
10	Culebra	FFG_322	669.80	Richey, 1989, Table 2, p.41	48	Culebra	FFG_372	949.10	Richey, 1989, Table 2, p.45
11	Culebra	FFG_323	675.20	Richey, 1989, Table 2, p.41	49	Culebra	FFG_373	909.00	Richey, 1989, Table 2, p.45
12	Culebra	FFG_324	699.50	Richey, 1989, Table 2, p.41	50	Culebra	FFG_374	908.30	Richey, 1989, Table 2, p.45
13	Culebra	FFG_325	762.30	Richey, 1989, Table 2, p.41	51	Culebra	FFG_376	947.60	Richey, 1989, Table 2, p.45
14	Culebra	FFG_326	706.50	Richey, 1989, Table 2, p.41	52	Culebra	FFG_381	914.70	Richey, 1989, Table 2, p.45
15	Culebra	FFG_327	689.80	Richey, 1989, Table 2, p.42	53	Culebra	FFG_383	908.30	Richey, 1989, Table 2, p.45
16	Culebra	FFG_328	673.80	Richey, 1989, Table 2, p.42	54	Culebra	FFG_384	921.10	Richey, 1989, Table 2, p.45
17	Culebra	FFG_329	669.00	Richey, 1989, Table 2, p.42	55	Culebra	FFG_385	915.90	Richey, 1989, Table 2, p.45
18	Culebra	FFG_330	669.50	Richey, 1989, Table 2, p.42	56	Culebra	FFG_387	911.10	Richey, 1989, Table 2, p.45
19	Culebra	FFG_331	652.90	Richey, 1989, Table 2, p.42	57	Culebra	FFG_388	900.70	Richey, 1989, Table 2, p.46
20	Culebra	FFG_332	639.50	Richey, 1989, Table 2, p.42	58	Culebra	FFG_389	924.80	Richey, 1989, Table 2, p.46
21	Culebra	FFG_333	650.60	Richey, 1989, Table 2, p.42	59	Culebra	FFG_390	919.60	Richey, 1989, Table 2, p.46
22	Culebra	FFG_334	644.90	Richey, 1989, Table 2, p.42	60	Culebra	FFG_391	919.20	Richey, 1989, Table 2, p.46
23	Culebra	FFG_335	663.30	Richey, 1989, Table 2, p.42	61	Culebra	FFG_392	910.50	Richey, 1989, Table 2, p.46
24	Culebra	FFG_336	658.10	Richey, 1989, Table 2, p.42	62	Culebra	FFG_393	785.60	Richey, 1989, Table 2, p.46
25	Culebra	FFG_337	641.90	Richey, 1989, Table 2, p.42	63	Culebra	FFG_394	882.40	Richey, 1989, Table 2, p.46
26	Culebra	FFG_338	646.90	Richey, 1989, Table 2, p.42	64	Culebra	FFG_395	874.50	Richey, 1989, Table 2, p.46
27	Culebra	FFG_339	611.70	Richey, 1989, Table 2, p.42	65	Culebra	FFG_396	853.80	Richey, 1989, Table 2, p.46
28	Culebra	FFG_340	617.80	Richey, 1989, Table 2, p.42	66	Culebra	FFG_398	771.70	Richey, 1989, Table 2, p.46
29	Culebra	FFG_342	682.70	Richey, 1989, Table 2, p.43	67	Culebra	FFG_399	785.20	Richey, 1989, Table 2, p.46
30	Culebra	FFG_344	659.10	Richey, 1989, Table 2, p.43	68	Culebra	FFG_401	839.70	Richey, 1989, Table 2, p.46
31	Culebra	FFG_345	678.60	Richey, 1989, Table 2, p.43	69	Culebra	FFG_402	947.10	Richey, 1989, Table 2, p.46
32	Culebra	FFG_347	699.50	Richey, 1989, Table 2, p.43	70	Culebra	FFG_403	914.60	Richey, 1989, Table 2, p.47
33	Culebra	FFG_348	738.50	Richey, 1989, Table 2, p.43	71	Culebra	FFG_404	873.30	Richey, 1989, Table 2, p.47
34	Culebra	FFG_349	714.50	Richey, 1989, Table 2, p.43	72	Culebra	FFG_407	908.00	Richey, 1989, Table 2, p.47
35	Culebra	FFG_350	745.20	Richey, 1989, Table 2, p.43	73	Culebra	FFG_408	907.10	Richey, 1989, Table 2, p.47
36	Culebra	FFG_351	629.40	Richey, 1989, Table 2, p.43	74	Culebra	FFG_409	943.10	Richey, 1989, Table 2, p.47
37	Culebra	FFG_352	629.40	Richey, 1989, Table 2, p.43	75	Culebra	FFG_411	887.30	Richey, 1989, Table 2, p.47
38	Culebra	FFG_353	651.10	Richey, 1989, Table 2, p.43	76	Culebra	FFG_413	915.10	Richey, 1989, Table 2, p.47

Table B.2. Elevations of Stratigraphic Layers Near WIPP (Continued)

	Layer	Well ID	Elevation	Source
1	Culebra	FFG_418	930.30	Richey, 1989, Table 2, p.48
2	Culebra	FFG_419	942.80	Richey, 1989, Table 2, p.48
3	Culebra	FFG_420	936.90	Richey, 1989, Table 2, p.48
4	Culebra	FFG_421	923.30	Richey, 1989, Table 2, p.48
5	Culebra	FFG_422	923.20	Richey, 1989, Table 2, p.48
6	Culebra	FFG_426	926.90	Richey, 1989, Table 2, p.48
7	Culebra	FFG_432	884.50	Richey, 1989, Table 2, p.48
8	Culebra	FFG_433	897.60	Richey, 1989, Table 2, p.48
9	Culebra	FFG_438	835.60	Richey, 1989, Table 2, p.49
10	Culebra	FFG_445	920.20	Richey, 1989, Table 2, p.49
11	Culebra	FFG_453	782.30	Richey, 1989, Table 2, p.50
12	Culebra	FFG_455	770.20	Richey, 1989, Table 2, p.50
13	Culebra	FFG_456	776.60	Richey, 1989, Table 2, p.50
14	Culebra	FFG_457	831.20	Richey, 1989, Table 2, p.50
15	Culebra	FFG_458	833.30	Richey, 1989, Table 2, p.50
16	Culebra	FFG_459	761.40	Richey, 1989, Table 2, p.50
17	Culebra	FFG_462	828.60	Richey, 1989, Table 2, p.50
18	Culebra	FFG_463	854.40	Richey, 1989, Table 2, p.51
19	Culebra	FFG_464	843.40	Richey, 1989, Table 2, p.51
20	Culebra	FFG_465	844.90	Richey, 1989, Table 2, p.51
21	Culebra	FFG_467	430.90	Richey, 1989, Table 2, p.51
22	Culebra	FFG_468	377.70	Richey, 1989, Table 2, p.51
23	Culebra	FFG_470	408.10	Richey, 1989, Table 2, p.51
24	Culebra	FFG_471	426.10	Richey, 1989, Table 2, p.51
25	Culebra	FFG_472	501.70	Richey, 1989, Table 2, p.51
26	Culebra	FFG_473	390.40	Richey, 1989, Table 2, p.51
27	Culebra	FFG_474	677.50	Richey, 1989, Table 2, p.51
28	Culebra	FFG_475	686.30	Richey, 1989, Table 2, p.51
29	Culebra	FFG_476	760.20	Richey, 1989, Table 2, p.51
30	Culebra	FFG_477	726.70	Richey, 1989, Table 2, p.51
31	Culebra	FFG_478	702.60	Richey, 1989, Table 2, p.52
32	Culebra	FFG_479	706.80	Richey, 1989, Table 2, p.52
33	Culebra	FFG_480	688.00	Richey, 1989, Table 2, p.52
34	Culebra	FFG_481	681.60	Richey, 1989, Table 2, p.52
35	Culebra	FFG_482	711.70	Richey, 1989, Table 2, p.52
36	Culebra	FFG_483	741.20	Richey, 1989, Table 2, p.52
37	Culebra	FFG_484	725.90	Richey, 1989, Table 2, p.52
38	Culebra	FFG_485	730.30	Richey, 1989, Table 2, p.52
39	Culebra	FFG_486	716.00	Richey, 1989, Table 2, p.52
40	Culebra	FFG_487	715.40	Richey, 1989, Table 2, p.52
41	Culebra	FFG_488	698.30	Richey, 1989, Table 2, p.52
42	Culebra	FFG_489	717.30	Richey, 1989, Table 2, p.52
43	Culebra	FFG_490	806.80	Richey, 1989, Table 2, p.52
44	Culebra	FFG_491	799.80	Richey, 1989, Table 2, p.52
45	Culebra	FFG_492	765.60	Richey, 1989, Table 2, p.52
46	Culebra	FFG_493	752.40	Richey, 1989, Table 2, p.53
47	Culebra	FFG_494	754.00	Richey, 1989, Table 2, p.53
48	Culebra	FFG_495	749.80	Richey, 1989, Table 2, p.53
49	Culebra	FFG_496	616.00	Richey, 1989, Table 2, p.53
50	Culebra	FFG_497	649.90	Richey, 1989, Table 2, p.53
51	Culebra	FFG_498	645.60	Richey, 1989, Table 2, p.53
52	Culebra	FFG_499	612.40	Richey, 1989, Table 2, p.53
53	Culebra	FFG_500	643.40	Richey, 1989, Table 2, p.53
54	Culebra	FFG_501	673.00	Richey, 1989, Table 2, p.53
55	Culebra	FFG_502	638.20	Richey, 1989, Table 2, p.53
56	Culebra	FFG_503	624.00	Richey, 1989, Table 2, p.53
57	Culebra	FFG_504	674.30	Richey, 1989, Table 2, p.53
58	Culebra	FFG_505	702.30	Richey, 1989, Table 2, p.53
59	Culebra	FFG_506	700.10	Richey, 1989, Table 2, p.53
60	Culebra	FFG_507	607.00	Richey, 1989, Table 2, p.53
61	Culebra	FFG_508	688.90	Richey, 1989, Table 2, p.53
62	Culebra	FFG_509	668.10	Richey, 1989, Table 2, p.54
63	Culebra	FFG_510	670.10	Richey, 1989, Table 2, p.54
64	Culebra	FFG_511	629.10	Richey, 1989, Table 2, p.54
65	Culebra	FFG_512	643.70	Richey, 1989, Table 2, p.54
66	Culebra	FFG_513	667.00	Richey, 1989, Table 2, p.54
67	Culebra	FFG_514	645.90	Richey, 1989, Table 2, p.54
68	Culebra	FFG_515	617.20	Richey, 1989, Table 2, p.54
69	Culebra	FFG_516	612.60	Richey, 1989, Table 2, p.54
70	Culebra	FFG_517	755.30	Richey, 1989, Table 2, p.54
71	Culebra	FFG_518	742.20	Richey, 1989, Table 2, p.54
72	Culebra	FFG_519	704.10	Richey, 1989, Table 2, p.54
73	Culebra	FFG_520	590.90	Richey, 1989, Table 2, p.54
74	Culebra	FFG_521	633.10	Richey, 1989, Table 2, p.54
75	Culebra	FFG_522	434.20	Richey, 1989, Table 2, p.54
76	Culebra	FFG_523	449.30	Richey, 1989, Table 2, p.54

Table B.2. Elevations of Stratigraphic Layers Near WIPP (Continued)

	Layer	Well ID	Elevation	Source
1	Culebra	FFG_524	616.00	Richey, 1989, Table 2, p.55
2	Culebra	FFG_525	443.90	Richey, 1989, Table 2, p.55
3	Culebra	FFG_526	950.70	Richey, 1989, Table 2, p.55
4	Culebra	FFG_527	894.20	Richey, 1989, Table 2, p.55
5	Culebra	FFG_528	896.10	Richey, 1989, Table 2, p.55
6	Culebra	FFG_530	965.90	Richey, 1989, Table 2, p.55
7	Culebra	FFG_531	894.90	Richey, 1989, Table 2, p.55
8	Culebra	FFG_532	879.70	Richey, 1989, Table 2, p.55
9	Culebra	FFG_534	892.80	Richey, 1989, Table 2, p.55
10	Culebra	FFG_535	882.10	Richey, 1989, Table 2, p.55
11	Culebra	FFG_536	892.50	Richey, 1989, Table 2, p.55
12	Culebra	FFG_537	879.90	Richey, 1989, Table 2, p.55
13	Culebra	FFG_543	932.20	Richey, 1989, Table 2, p.56
14	Culebra	FFG_548	883.30	Richey, 1989, Table 2, p.56
15	Culebra	FFG_552	732.70	Richey, 1989, Table 2, p.56
16	Culebra	FFG_562	621.80	Richey, 1989, Table 2, p.57
17	Culebra	FFG_563	537.40	Richey, 1989, Table 2, p.57
18	Culebra	FFG_568	631.90	Richey, 1989, Table 2, p.57
19	Culebra	FFG_569	632.80	Richey, 1989, Table 2, p.57
20	Culebra	FFG_584	742.70	Richey, 1989, Table 2, p.58
21	Culebra	FFG_585	686.70	Richey, 1989, Table 2, p.58
22	Culebra	FFG_600	700.10	Richey, 1989, Table 2, p.58
23	Culebra	FFG_601	580.00	Richey, 1989, Table 2, p.58
24	Culebra	FFG_602	803.50	Richey, 1989, Table 2, p.58
25	Culebra	FFG_606	673.70	Richey, 1989, Table 2, p.58
26	Culebra	FFG_607	681.30	Richey, 1989, Table 2, p.59
27	Culebra	FFG_608	663.20	Richey, 1989, Table 2, p.59
28	Culebra	FFG_609	656.50	Richey, 1989, Table 2, p.59
29	Culebra	FFG_610	649.20	Richey, 1989, Table 2, p.59
30	Culebra	FFG_611	644.00	Richey, 1989, Table 2, p.59
31	Culebra	FFG_612	679.10	Richey, 1989, Table 2, p.59
32	Culebra	FFG_613	677.90	Richey, 1989, Table 2, p.59
33	Culebra	FFG_618	686.70	Richey, 1989, Table 2, p.59
34	Culebra	FFG_638	536.80	Richey, 1989, Table 2, p.60
35	Culebra	FFG_639	508.10	Richey, 1989, Table 2, p.60
36	Culebra	FFG_640	597.80	Richey, 1989, Table 2, p.60
37	Culebra	FFG_643	642.30	Richey, 1989, Table 2, p.60
38	Culebra	FFG_644	677.20	Richey, 1989, Table 2, p.60
39	Culebra	FFG_648	513.30	Richey, 1989, Table 2, p.60
40	Culebra	FFG_652	822.90	Richey, 1989, Table 2, p.60
41	Culebra	FFG_653	822.70	Richey, 1989, Table 2, p.61
42	Culebra	FFG_654	845.80	Richey, 1989, Table 2, p.61
43	Culebra	FFG_655	847.30	Richey, 1989, Table 2, p.61
44	Culebra	FFG_656	845.20	Richey, 1989, Table 2, p.61
45	Culebra	FFG_657	862.90	Richey, 1989, Table 2, p.61
46	Culebra	FFG_658	849.40	Richey, 1989, Table 2, p.61
47	Culebra	FFG_659	856.80	Richey, 1989, Table 2, p.61
48	Culebra	FFG_660	873.40	Richey, 1989, Table 2, p.61
49	Culebra	FFG_662	843.40	Richey, 1989, Table 2, p.61
50	Culebra	FFG_664	836.40	Richey, 1989, Table 2, p.61
51	Culebra	FFG_666	890.00	Richey, 1989, Table 2, p.62
52	Culebra	FFG_667	875.70	Richey, 1989, Table 2, p.62
53	Culebra	FFG_668	926.10	Richey, 1989, Table 2, p.62
54	Culebra	FFG_669	912.90	Richey, 1989, Table 2, p.62
55	Culebra	FFG_670	897.30	Richey, 1989, Table 2, p.62
56	Culebra	FFG_671	900.00	Richey, 1989, Table 2, p.62
57	Culebra	FFG_672	897.10	Richey, 1989, Table 2, p.62
58	Culebra	FFG_673	894.20	Richey, 1989, Table 2, p.62
59	Culebra	FFG_674	893.40	Richey, 1989, Table 2, p.62
60	Culebra	FFG_675	851.50	Richey, 1989, Table 2, p.62
61	Culebra	FFG_676	862.30	Richey, 1989, Table 2, p.62
62	Culebra	FFG_677	889.70	Richey, 1989, Table 2, p.62
63	Culebra	FFG_679	891.20	Richey, 1989, Table 2, p.62
64	Culebra	FFG_685	918.10	Richey, 1989, Table 2, p.63
65	Culebra	FFG_689	764.50	Richey, 1989, Table 2, p.63
66	Culebra	FFG_690	768.70	Richey, 1989, Table 2, p.63
67	Culebra	FFG_691	760.80	Richey, 1989, Table 2, p.63
68	Culebra	FFG_692	749.90	Richey, 1989, Table 2, p.63
69	Culebra	FFG_693	760.40	Richey, 1989, Table 2, p.63
70	Culebra	FFG_694	750.40	Richey, 1989, Table 2, p.63
71	Culebra	FFG_695	756.50	Richey, 1989, Table 2, p.63
72	Culebra	FFG_696	758.30	Richey, 1989, Table 2, p.63
73	Culebra	FFG_697	760.20	Richey, 1989, Table 2, p.64
74	Culebra	FFG_698	802.00	Richey, 1989, Table 2, p.64
75	Culebra	FFG_699	755.60	Richey, 1989, Table 2, p.64
76	Culebra	FFG_700	749.30	Richey, 1989, Table 2, p.64

Table B.2. Elevations of Stratigraphic Layers Near WIPP (Continued)

	Layer	Well ID	Elevation	Source		Layer	Well ID	Elevation	Source
1	Culebra	FFG_701	749.60	Richey, 1989, Table 2, p.64	39	Culebra	FFG_740	662.60	Richey, 1989, Table 2, p.66
2	Culebra	FFG_702	755.60	Richey, 1989, Table 2, p.64	40	Culebra	FFG_741	658.70	Richey, 1989, Table 2, p.66
3	Culebra	FFG_703	761.70	Richey, 1989, Table 2, p.64	41	Culebra	FFG_742	700.70	Richey, 1989, Table 2, p.67
4	Culebra	FFG_704	745.60	Richey, 1989, Table 2, p.64	42	Culebra	FFG_743	686.10	Richey, 1989, Table 2, p.67
5	Culebra	FFG_705	679.70	Richey, 1989, Table 2, p.64	43	Culebra	FFG_744	677.20	Richey, 1989, Table 2, p.67
6	Culebra	FFG_706	702.30	Richey, 1989, Table 2, p.64	44	Culebra	FFG_745	657.70	Richey, 1989, Table 2, p.67
7	Culebra	FFG_707	686.80	Richey, 1989, Table 2, p.64	45	Culebra	FFG_746	645.50	Richey, 1989, Table 2, p.67
8	Culebra	FFG_708	736.70	Richey, 1989, Table 2, p.64	46	Culebra	H1	829.70	Mercer, 1983, Table 1
9	Culebra	FFG_709	632.80	Richey, 1989, Table 2, p.64	47	Culebra	H10C	709.30	Mercer, 1983, Table 1
10	Culebra	FFG_710	631.60	Richey, 1989, Table 2, p.64	48	Culebra	H2C	839.70	Mercer, 1983, Table 1
11	Culebra	FFG_711	634.60	Richey, 1989, Table 2, p.65	49	Culebra	H3	828.50	Mercer, 1983, Table 1
12	Culebra	FFG_712	678.30	Richey, 1989, Table 2, p.65	50	Culebra	H4C	866.80	Mercer, 1983, Table 1
13	Culebra	FFG_713	620.70	Richey, 1989, Table 2, p.65	51	Culebra	H5C	794.90	Mercer, 1983, Table 1
14	Culebra	FFG_714	731.50	Richey, 1989, Table 2, p.65	52	Culebra	H6C	836.40	Mercer, 1983, Table 1
15	Culebra	FFG_715	741.80	Richey, 1989, Table 2, p.65	53	Culebra	H7C	891.90	Mercer, 1983, Table 1
16	Culebra	FFG_716	604.90	Richey, 1989, Table 2, p.65	54	Culebra	H8C	867.20	Mercer, 1983, Table 1
17	Culebra	FFG_717	672.20	Richey, 1989, Table 2, p.65	55	Culebra	H9C	840.90	Mercer, 1983, Table 1
18	Culebra	FFG_718	664.70	Richey, 1989, Table 2, p.65	56	Culebra	P1	855.60	Mercer, 1983, Table 1
19	Culebra	FFG_719	626.00	Richey, 1989, Table 2, p.65	57	Culebra	P10	785.70	Mercer, 1983, Table 1
20	Culebra	FFG_720	625.80	Richey, 1989, Table 2, p.65	58	Culebra	P11	790.00	Mercer, 1983, Table 1
21	Culebra	FFG_721	646.20	Richey, 1989, Table 2, p.65	59	Culebra	P12	835.50	Mercer, 1983, Table 1
22	Culebra	FFG_723	762.80	Richey, 1989, Table 2, p.65	60	Culebra	P13	835.50	Mercer, 1983, Table 1
23	Culebra	FFG_724	686.50	Richey, 1989, Table 2, p.65	61	Culebra	P14	849.40	Mercer, 1983, Table 1
24	Culebra	FFG_725	652.90	Richey, 1989, Table 2, p.65	62	Culebra	P15	883.00	Mercer, 1983, Table 1
25	Culebra	FFG_726	648.60	Richey, 1989, Table 2, p.65	63	Culebra	P16	858.90	Mercer, 1983, Table 1
26	Culebra	FFG_727	639.20	Richey, 1989, Table 2, p.66	64	Culebra	P17	846.70	Mercer, 1983, Table 1
27	Culebra	FFG_728	646.70	Richey, 1989, Table 2, p.66	65	Culebra	P18	782.70	Mercer, 1983, Table 1
28	Culebra	FFG_729	648.90	Richey, 1989, Table 2, p.66	66	Culebra	P19	785.80	Mercer, 1983, Table 1
29	Culebra	FFG_730	673.60	Richey, 1989, Table 2, p.66	67	Culebra	P2	799.20	Mercer, 1983, Table 1
30	Culebra	FFG_731	670.40	Richey, 1989, Table 2, p.66	68	Culebra	P20	792.50	Mercer, 1983, Table 1
31	Culebra	FFG_732	686.40	Richey, 1989, Table 2, p.66	69	Culebra	P21	795.50	Mercer, 1983, Table 1
32	Culebra	FFG_733	749.80	Richey, 1989, Table 2, p.66	70	Culebra	P3	835.40	Mercer, 1983, Table 1
33	Culebra	FFG_734	707.40	Richey, 1989, Table 2, p.66	71	Culebra	P4	813.50	Mercer, 1983, Table 1
34	Culebra	FFG_735	638.90	Richey, 1989, Table 2, p.66	72	Culebra	P5	812.90	Mercer, 1983, Table 1
35	Culebra	FFG_736	676.40	Richey, 1989, Table 2, p.66	73	Culebra	P6	858.60	Mercer, 1983, Table 1
36	Culebra	FFG_737	620.30	Richey, 1989, Table 2, p.66	74	Culebra	P7	864.40	Mercer, 1983, Table 1
37	Culebra	FFG_738	662.00	Richey, 1989, Table 2, p.66	75	Culebra	P8	846.10	Mercer, 1983, Table 1
38	Culebra	FFG_739	694.80	Richey, 1989, Table 2, p.66	76	Culebra	P9	816.30	Mercer, 1983, Table 1

Table B.2. Elevations of Stratigraphic Layers Near WIPP (Continued)

	Layer	Well ID	Elevation	Source
1	Culebra	REF	823.40	Rechard et al.,1991, Figure 2.2-1
2	Culebra	SaltShft	822.81	Bechtel, Inc., 1986, Appendix D
3	Culebra	WIPP11	786.90	Mercer, 1983, Table 1
4	Culebra	WIPP11	787.00	SNL and USGS, 1982a, Table 2
5	Culebra	WIPP12	811.30	SNL and D'Appolonia Consulting, 1983, Table 2
6	Culebra	WIPP12	811.40	Mercer, 1983, Table 1
7	Culebra	WIPP13	824.10	Mercer, 1983, Table 1
8	Culebra	WIPP16	679.70	Mercer, 1983, Table 1
9	Culebra	WIPP18	813.80	Mercer, 1983, Table 1
10	Culebra	WIPP19	816.00	Mercer, 1983, Table 1
11	Culebra	WIPP21	819.30	Mercer, 1983, Table 1
12	Culebra	WIPP22	818.00	Mercer, 1983, Table 1
13	Culebra	WIPP25	843.10	Mercer, 1983, Table 1
14	Culebra	WIPP26	904.00	Mercer, 1983, Table 1
15	Culebra	WIPP27	879.30	Mercer, 1983, Table 1
16	Culebra	WIPP28	892.20	Mercer, 1983, Table 1
17	Culebra	WIPP29	903.70	Mercer, 1983, Table 1
18	Culebra	WIPP30	852.60	Mercer, 1983, Table 1
19	Culebra	WIPP32	902.80	Mercer, 1983, Table 1
20	Culebra	WIPP33	845.30	Mercer, 1983, Table 1
21	Culebra	WIPP34	792.20	Mercer, 1983, Table 1
22	Culebra	WastShft	823.64	Bechtel, Inc., 1986, Appendix E
23	DeweyLk	AirShft	1022.02	Holt and Powers, 1990, Figure 22
24	DeweyLk	DOE1	1018.10	U.S. DOE, Sep 1982, Table 2
25	DeweyLk	DOE2	1001.30	Mercer et al., 1987, Table 3-2
26	DeweyLk	ERDA9	1023.30	SNL and USGS, 1982b, Table 2
27	DeweyLk	ExhtShft	1022.73	Bechtel, Inc., 1986, Appendix F
28	DeweyLk	REF	1023.30	Rechard et al.,1991, Figure 2.2-1
29	DeweyLk	SaltShft	1025.35	Bechtel, Inc., 1986, Appendix D
30	DeweyLk	WIPP11	995.20	SNL and USGS, 1982a, Table 2
31	DeweyLk	WIPP12	1010.90	SNL and D'Appolonia Consulting, 1983, Table 2
32	DeweyLk	WastShft	1009.97	Bechtel, Inc., 1986, Appendix E
33	Halite1	DOE1	-170.40	U.S. DOE, Sep 1982, Table 2
34	Halite1	DOE1	-71.60	U.S. DOE, Sep 1982, Table 2
35	Halite1	DOE2	-119.10	Mercer et al., 1987, Table 3-2
36	Halite1	DOE2	-116.40	Mercer et al., 1987, Table 3-2
37	Halite1	REF	-119.10	Rechard et al.,1991, Figure 2.2-1
38	Halite1	REF	-116.40	Rechard et al.,1991, Figure 2.2-1
39	Halite1	WIPP11	-37.80	SNL and USGS, 1982a, Table 2
40	Halite1	WIPP11	-22.20	SNL and USGS, 1982a, Table 2
41	Halite1	WIPP12	-131.10	SNL and D'Appolonia Consulting, 1983, Table 2
42	Halite1	WIPP12	24.50	SNL and D'Appolonia Consulting, 1983, Table 2
43	Halite2	DOE1	-38.60	U.S. DOE, Sep 1982, Table 2
44	Halite2	DOE1	30.00	U.S. DOE, Sep 1982, Table 2
45	Halite2	WIPP11	14.40	SNL and USGS, 1982a, Table 2
46	Halite2	WIPP11	309.40	SNL and USGS, 1982a, Table 2
47	Halite2	WIPP12	57.80	SNL and D'Appolonia Consulting, 1983, Table 2
48	Halite2	WIPP12	127.30	SNL and D'Appolonia Consulting, 1983, Table 2
49	L_Member	DOE1	163.60	U.S. DOE, Sep 1982, Table 2
50	L_Member	DOE2	102.30	Mercer et al., 1987, Table 3-2
51	L_Member	ERDA9	178.10	SNL and USGS, 1982b, Table 2
52	L_Member	REF	178.10	Rechard et al.,1991, Figure 2.2-1
53	L_Member	WIPP11	334.10	SNL and USGS, 1982a, Table 2
54	L_Member	WIPP12	227.40	SNL and D'Appolonia Consulting, 1983, Table 2
55	M49er	AEC7	911.90	Mercer, 1983, Table 1
56	M49er	AEC8	875.40	Mercer, 1983, Table 1
57	M49er	AirShft	877.42	Holt and Powers, 1990, Figure 22
58	M49er	B25	876.60	Mercer, 1983, Table 1
59	M49er	DOE1	855.20	U.S. DOE, Sep 1982, Table 2
60	M49er	DOE2	847.10	Mercer et al., 1987, Table 3-2
61	M49er	ERDA6	915.60	Mercer, 1983, Table 1
62	M49er	ERDA9	878.10	Mercer, 1983, Table 1
63	M49er	ERDA9	874.00	SNL and USGS, 1982b, Table 2
64	M49er	ExhtShft	872.52	Bechtel, Inc., 1986, Appendix F
65	M49er	FFG_002	686.10	Richey, 1989, Table 2, p.21
66	M49er	FFG_004	739.10	Richey, 1989, Table 2, p.21
67	M49er	FFG_005	693.80	Richey, 1989, Table 2, p.21
68	M49er	FFG_006	688.90	Richey, 1989, Table 2, p.21
69	M49er	FFG_007	678.20	Richey, 1989, Table 2, p.21
70	M49er	FFG_009	678.10	Richey, 1989, Table 2, p.21
71	M49er	FFG_011	684.60	Richey, 1989, Table 2, p.21
72	M49er	FFG_012	687.00	Richey, 1989, Table 2, p.21
73	M49er	FFG_013	696.80	Richey, 1989, Table 2, p.21
74	M49er	FFG_014	741.90	Richey, 1989, Table 2, p.21
75	M49er	FFG_016	666.90	Richey, 1989, Table 2, p.21
76	M49er	FFG_017	669.60	Richey, 1989, Table 2, p.22

Table B.2. Elevations of Stratigraphic Layers Near WIPP (Continued)

	Layer	Well ID	Elevation	Source		Layer	Well ID	Elevation	Source
1	M49er	FFG_018	672.40	Richey, 1989, Table 2, p.22	39	M49er	FFG_060	645.50	Richey, 1989, Table 2, p.24
2	M49er	FFG_019	666.30	Richey, 1989, Table 2, p.22	40	M49er	FFG_061	645.90	Richey, 1989, Table 2, p.24
3	M49er	FFG_020	740.70	Richey, 1989, Table 2, p.22	41	M49er	FFG_062	574.30	Richey, 1989, Table 2, p.24
4	M49er	FFG_023	678.50	Richey, 1989, Table 2, p.22	42	M49er	FFG_063	534.70	Richey, 1989, Table 2, p.24
5	M49er	FFG_024	662.00	Richey, 1989, Table 2, p.22	43	M49er	FFG_064	559.70	Richey, 1989, Table 2, p.24
6	M49er	FFG_025	674.10	Richey, 1989, Table 2, p.22	44	M49er	FFG_065	542.90	Richey, 1989, Table 2, p.24
7	M49er	FFG_026	670.80	Richey, 1989, Table 2, p.22	45	M49er	FFG_066	496.80	Richey, 1989, Table 2, p.24
8	M49er	FFG_027	664.20	Richey, 1989, Table 2, p.22	46	M49er	FFG_067	537.10	Richey, 1989, Table 2, p.25
9	M49er	FFG_028	629.80	Richey, 1989, Table 2, p.22	47	M49er	FFG_068	496.50	Richey, 1989, Table 2, p.25
10	M49er	FFG_029	616.00	Richey, 1989, Table 2, p.22	48	M49er	FFG_069	524.30	Richey, 1989, Table 2, p.25
11	M49er	FFG_030	616.60	Richey, 1989, Table 2, p.22	49	M49er	FFG_070	553.80	Richey, 1989, Table 2, p.25
12	M49er	FFG_031	609.60	Richey, 1989, Table 2, p.22	50	M49er	FFG_071	811.10	Richey, 1989, Table 2, p.25
13	M49er	FFG_032	611.90	Richey, 1989, Table 2, p.22	51	M49er	FFG_072	739.70	Richey, 1989, Table 2, p.25
14	M49er	FFG_033	607.20	Richey, 1989, Table 2, p.22	52	M49er	FFG_073	717.80	Richey, 1989, Table 2, p.25
15	M49er	FFG_034	601.30	Richey, 1989, Table 2, p.23	53	M49er	FFG_074	723.70	Richey, 1989, Table 2, p.25
16	M49er	FFG_035	590.30	Richey, 1989, Table 2, p.23	54	M49er	FFG_075	773.30	Richey, 1989, Table 2, p.25
17	M49er	FFG_036	602.60	Richey, 1989, Table 2, p.23	55	M49er	FFG_076	836.40	Richey, 1989, Table 2, p.25
18	M49er	FFG_037	592.90	Richey, 1989, Table 2, p.23	56	M49er	FFG_078	874.40	Richey, 1989, Table 2, p.25
19	M49er	FFG_038	579.40	Richey, 1989, Table 2, p.23	57	M49er	FFG_079	848.00	Richey, 1989, Table 2, p.25
20	M49er	FFG_039	798.60	Richey, 1989, Table 2, p.23	58	M49er	FFG_080	827.50	Richey, 1989, Table 2, p.25
21	M49er	FFG_040	740.70	Richey, 1989, Table 2, p.23	59	M49er	FFG_081	746.80	Richey, 1989, Table 2, p.26
22	M49er	FFG_041	801.00	Richey, 1989, Table 2, p.23	60	M49er	FFG_082	779.10	Richey, 1989, Table 2, p.26
23	M49er	FFG_042	805.50	Richey, 1989, Table 2, p.23	61	M49er	FFG_083	693.00	Richey, 1989, Table 2, p.26
24	M49er	FFG_043	810.00	Richey, 1989, Table 2, p.23	62	M49er	FFG_084	721.10	Richey, 1989, Table 2, p.26
25	M49er	FFG_044	762.30	Richey, 1989, Table 2, p.23	63	M49er	FFG_085	714.20	Richey, 1989, Table 2, p.26
26	M49er	FFG_047	633.40	Richey, 1989, Table 2, p.23	64	M49er	FFG_086	722.60	Richey, 1989, Table 2, p.26
27	M49er	FFG_048	653.20	Richey, 1989, Table 2, p.23	65	M49er	FFG_087	698.00	Richey, 1989, Table 2, p.26
28	M49er	FFG_049	641.90	Richey, 1989, Table 2, p.23	66	M49er	FFG_088	694.40	Richey, 1989, Table 2, p.26
29	M49er	FFG_050	648.00	Richey, 1989, Table 2, p.24	67	M49er	FFG_089	675.80	Richey, 1989, Table 2, p.26
30	M49er	FFG_051	648.90	Richey, 1989, Table 2, p.24	68	M49er	FFG_091	720.00	Richey, 1989, Table 2, p.26
31	M49er	FFG_052	651.60	Richey, 1989, Table 2, p.24	69	M49er	FFG_092	734.90	Richey, 1989, Table 2, p.26
32	M49er	FFG_053	642.80	Richey, 1989, Table 2, p.24	70	M49er	FFG_093	737.30	Richey, 1989, Table 2, p.26
33	M49er	FFG_054	641.90	Richey, 1989, Table 2, p.24	71	M49er	FFG_094	740.60	Richey, 1989, Table 2, p.26
34	M49er	FFG_055	641.60	Richey, 1989, Table 2, p.24	72	M49er	FFG_095	706.50	Richey, 1989, Table 2, p.26
35	M49er	FFG_056	644.30	Richey, 1989, Table 2, p.24	73	M49er	FFG_096	689.50	Richey, 1989, Table 2, p.26
36	M49er	FFG_057	645.60	Richey, 1989, Table 2, p.24	74	M49er	FFG_097	671.20	Richey, 1989, Table 2, p.27
37	M49er	FFG_058	641.00	Richey, 1989, Table 2, p.24	75	M49er	FFG_098	645.50	Richey, 1989, Table 2, p.27
38	M49er	FFG_059	643.40	Richey, 1989, Table 2, p.24	76	M49er	FFG_099	641.60	Richey, 1989, Table 2, p.27

Table B.2. Elevations of Stratigraphic Layers Near WIPP (Continued)

	Layer	Well ID	Elevation	Source		Layer	Well ID	Elevation	Source
1	M49er	FFG_100	624.90	Richey, 1989, Table 2, p.27	39	M49er	FFG_141	873.10	Richey, 1989, Table 2, p.29
2	M49er	FFG_101	593.10	Richey, 1989, Table 2, p.27	40	M49er	FFG_142	849.30	Richey, 1989, Table 2, p.29
3	M49er	FFG_102	613.90	Richey, 1989, Table 2, p.27	41	M49er	FFG_143	855.80	Richey, 1989, Table 2, p.29
4	M49er	FFG_103	674.60	Richey, 1989, Table 2, p.27	42	M49er	FFG_159	956.20	Richey, 1989, Table 2, p.30
5	M49er	FFG_104	572.50	Richey, 1989, Table 2, p.27	43	M49er	FFG_160	950.10	Richey, 1989, Table 2, p.30
6	M49er	FFG_105	926.90	Richey, 1989, Table 2, p.27	44	M49er	FFG_161	957.40	Richey, 1989, Table 2, p.30
7	M49er	FFG_106	954.70	Richey, 1989, Table 2, p.27	45	M49er	FFG_162	955.90	Richey, 1989, Table 2, p.30
8	M49er	FFG_107	945.20	Richey, 1989, Table 2, p.27	46	M49er	FFG_163	955.30	Richey, 1989, Table 2, p.30
9	M49er	FFG_108	933.60	Richey, 1989, Table 2, p.27	47	M49er	FFG_166	954.30	Richey, 1989, Table 2, p.31
10	M49er	FFG_109	917.20	Richey, 1989, Table 2, p.27	48	M49er	FFG_167	936.70	Richey, 1989, Table 2, p.31
11	M49er	FFG_110	887.00	Richey, 1989, Table 2, p.27	49	M49er	FFG_168	967.50	Richey, 1989, Table 2, p.31
12	M49er	FFG_111	896.70	Richey, 1989, Table 2, p.27	50	M49er	FFG_169	980.20	Richey, 1989, Table 2, p.31
13	M49er	FFG_112	879.30	Richey, 1989, Table 2, p.28	51	M49er	FFG_170	933.60	Richey, 1989, Table 2, p.31
14	M49er	FFG_113	893.40	Richey, 1989, Table 2, p.28	52	M49er	FFG_173	934.80	Richey, 1989, Table 2, p.31
15	M49er	FFG_114	924.20	Richey, 1989, Table 2, p.28	53	M49er	FFG_180	943.90	Richey, 1989, Table 2, p.31
16	M49er	FFG_115	913.80	Richey, 1989, Table 2, p.28	54	M49er	FFG_182	856.50	Richey, 1989, Table 2, p.32
17	M49er	FFG_116	929.30	Richey, 1989, Table 2, p.28	55	M49er	FFG_189	922.70	Richey, 1989, Table 2, p.32
18	M49er	FFG_117	935.70	Richey, 1989, Table 2, p.28	56	M49er	FFG_190	901.60	Richey, 1989, Table 2, p.32
19	M49er	FFG_120	944.30	Richey, 1989, Table 2, p.28	57	M49er	FFG_191	901.30	Richey, 1989, Table 2, p.32
20	M49er	FFG_121	946.40	Richey, 1989, Table 2, p.28	58	M49er	FFG_192	834.50	Richey, 1989, Table 2, p.32
21	M49er	FFG_122	944.90	Richey, 1989, Table 2, p.28	59	M49er	FFG_194	839.70	Richey, 1989, Table 2, p.33
22	M49er	FFG_123	928.10	Richey, 1989, Table 2, p.28	60	M49er	FFG_195	855.30	Richey, 1989, Table 2, p.33
23	M49er	FFG_124	900.40	Richey, 1989, Table 2, p.28	61	M49er	FFG_196	897.60	Richey, 1989, Table 2, p.33
24	M49er	FFG_125	912.20	Richey, 1989, Table 2, p.28	62	M49er	FFG_197	899.50	Richey, 1989, Table 2, p.33
25	M49er	FFG_126	904.50	Richey, 1989, Table 2, p.28	63	M49er	FFG_198	898.20	Richey, 1989, Table 2, p.33
26	M49er	FFG_127	909.50	Richey, 1989, Table 2, p.28	64	M49er	FFG_199	888.80	Richey, 1989, Table 2, p.33
27	M49er	FFG_128	948.00	Richey, 1989, Table 2, p.28	65	M49er	FFG_200	902.50	Richey, 1989, Table 2, p.33
28	M49er	FFG_129	923.80	Richey, 1989, Table 2, p.28	66	M49er	FFG_201	894.60	Richey, 1989, Table 2, p.33
29	M49er	FFG_130	954.00	Richey, 1989, Table 2, p.28	67	M49er	FFG_202	834.20	Richey, 1989, Table 2, p.33
30	M49er	FFG_132	956.50	Richey, 1989, Table 2, p.29	68	M49er	FFG_203	841.30	Richey, 1989, Table 2, p.33
31	M49er	FFG_133	959.50	Richey, 1989, Table 2, p.29	69	M49er	FFG_204	864.80	Richey, 1989, Table 2, p.33
32	M49er	FFG_134	963.80	Richey, 1989, Table 2, p.29	70	M49er	FFG_205	880.60	Richey, 1989, Table 2, p.33
33	M49er	FFG_135	937.30	Richey, 1989, Table 2, p.29	71	M49er	FFG_206	895.80	Richey, 1989, Table 2, p.33
34	M49er	FFG_136	934.30	Richey, 1989, Table 2, p.29	72	M49er	FFG_207	892.20	Richey, 1989, Table 2, p.33
35	M49er	FFG_137	946.80	Richey, 1989, Table 2, p.29	73	M49er	FFG_208	902.80	Richey, 1989, Table 2, p.34
36	M49er	FFG_138	897.40	Richey, 1989, Table 2, p.29	74	M49er	FFG_210	885.80	Richey, 1989, Table 2, p.34
37	M49er	FFG_139	907.70	Richey, 1989, Table 2, p.29	75	M49er	FFG_212	870.50	Richey, 1989, Table 2, p.34
38	M49er	FFG_140	849.10	Richey, 1989, Table 2, p.29	76	M49er	FFG_213	903.50	Richey, 1989, Table 2, p.34

Table B.2. Elevations of Stratigraphic Layers Near WIPP (Continued)

	Layer	Well ID	Elevation	Source		Layer	Well ID	Elevation	Source
1	M49er	FFG_214	877.80	Richey, 1989, Table 2, p.34	39	M49er	FFG_254	651.00	Richey, 1989, Table 2, p.36
2	M49er	FFG_215	852.50	Richey, 1989, Table 2, p.34	40	M49er	FFG_255	609.90	Richey, 1989, Table 2, p.37
3	M49er	FFG_216	737.00	Richey, 1989, Table 2, p.34	41	M49er	FFG_256	557.80	Richey, 1989, Table 2, p.37
4	M49er	FFG_217	873.60	Richey, 1989, Table 2, p.34	42	M49er	FFG_257	600.40	Richey, 1989, Table 2, p.37
5	M49er	FFG_218	863.50	Richey, 1989, Table 2, p.34	43	M49er	FFG_258	615.00	Richey, 1989, Table 2, p.37
6	M49er	FFG_219	910.40	Richey, 1989, Table 2, p.34	44	M49er	FFG_259	584.90	Richey, 1989, Table 2, p.37
7	M49er	FFG_220	859.90	Richey, 1989, Table 2, p.34	45	M49er	FFG_260	621.80	Richey, 1989, Table 2, p.37
8	M49er	FFG_221	814.40	Richey, 1989, Table 2, p.34	46	M49er	FFG_261	610.20	Richey, 1989, Table 2, p.37
9	M49er	FFG_222	770.60	Richey, 1989, Table 2, p.34	47	M49er	FFG_263	553.40	Richey, 1989, Table 2, p.37
10	M49er	FFG_224	677.00	Richey, 1989, Table 2, p.35	48	M49er	FFG_264	777.60	Richey, 1989, Table 2, p.37
11	M49er	FFG_225	683.70	Richey, 1989, Table 2, p.35	49	M49er	FFG_265	775.40	Richey, 1989, Table 2, p.37
12	M49er	FFG_226	683.20	Richey, 1989, Table 2, p.35	50	M49er	FFG_266	758.90	Richey, 1989, Table 2, p.37
13	M49er	FFG_228	673.70	Richey, 1989, Table 2, p.35	51	M49er	FFG_267	736.40	Richey, 1989, Table 2, p.37
14	M49er	FFG_229	701.60	Richey, 1989, Table 2, p.35	52	M49er	FFG_268	716.00	Richey, 1989, Table 2, p.37
15	M49er	FFG_230	688.60	Richey, 1989, Table 2, p.35	53	M49er	FFG_269	729.20	Richey, 1989, Table 2, p.38
16	M49er	FFG_231	704.00	Richey, 1989, Table 2, p.35	54	M49er	FFG_270	791.80	Richey, 1989, Table 2, p.38
17	M49er	FFG_232	717.80	Richey, 1989, Table 2, p.35	55	M49er	FFG_271	833.90	Richey, 1989, Table 2, p.38
18	M49er	FFG_233	709.30	Richey, 1989, Table 2, p.35	56	M49er	FFG_272	846.60	Richey, 1989, Table 2, p.38
19	M49er	FFG_234	745.80	Richey, 1989, Table 2, p.35	57	M49er	FFG_273	816.90	Richey, 1989, Table 2, p.38
20	M49er	FFG_235	722.40	Richey, 1989, Table 2, p.35	58	M49er	FFG_274	851.00	Richey, 1989, Table 2, p.38
21	M49er	FFG_236	768.40	Richey, 1989, Table 2, p.35	59	M49er	FFG_275	858.60	Richey, 1989, Table 2, p.38
22	M49er	FFG_237	735.30	Richey, 1989, Table 2, p.35	60	M49er	FFG_276	861.60	Richey, 1989, Table 2, p.38
23	M49er	FFG_238	716.60	Richey, 1989, Table 2, p.36	61	M49er	FFG_277	853.50	Richey, 1989, Table 2, p.38
24	M49er	FFG_239	703.10	Richey, 1989, Table 2, p.36	62	M49er	FFG_278	868.40	Richey, 1989, Table 2, p.38
25	M49er	FFG_240	695.20	Richey, 1989, Table 2, p.36	63	M49er	FFG_279	860.10	Richey, 1989, Table 2, p.38
26	M49er	FFG_241	688.90	Richey, 1989, Table 2, p.36	64	M49er	FFG_280	858.60	Richey, 1989, Table 2, p.38
27	M49er	FFG_242	799.80	Richey, 1989, Table 2, p.36	65	M49er	FFG_281	835.80	Richey, 1989, Table 2, p.38
28	M49er	FFG_243	763.80	Richey, 1989, Table 2, p.36	66	M49er	FFG_283	584.60	Richey, 1989, Table 2, p.39
29	M49er	FFG_244	798.40	Richey, 1989, Table 2, p.36	67	M49er	FFG_284	730.30	Richey, 1989, Table 2, p.39
30	M49er	FFG_245	597.10	Richey, 1989, Table 2, p.36	68	M49er	FFG_285	760.20	Richey, 1989, Table 2, p.39
31	M49er	FFG_246	601.70	Richey, 1989, Table 2, p.36	69	M49er	FFG_286	837.50	Richey, 1989, Table 2, p.39
32	M49er	FFG_247	589.10	Richey, 1989, Table 2, p.36	70	M49er	FFG_287	812.00	Richey, 1989, Table 2, p.39
33	M49er	FFG_248	594.70	Richey, 1989, Table 2, p.36	71	M49er	FFG_288	765.70	Richey, 1989, Table 2, p.39
34	M49er	FFG_249	593.70	Richey, 1989, Table 2, p.36	72	M49er	FFG_289	736.30	Richey, 1989, Table 2, p.39
35	M49er	FFG_250	674.10	Richey, 1989, Table 2, p.36	73	M49er	FFG_290	825.70	Richey, 1989, Table 2, p.39
36	M49er	FFG_251	568.70	Richey, 1989, Table 2, p.36	74	M49er	FFG_291	766.20	Richey, 1989, Table 2, p.39
37	M49er	FFG_252	708.60	Richey, 1989, Table 2, p.36	75	M49er	FFG_292	774.20	Richey, 1989, Table 2, p.39
38	M49er	FFG_253	660.50	Richey, 1989, Table 2, p.36	76	M49er	FFG_293	766.00	Richey, 1989, Table 2, p.39

Table B.2. Elevations of Stratigraphic Layers Near WIPP (Continued)

	Layer	Well ID	Elevation	Source		Layer	Well ID	Elevation	Source
1	M49er	FFG_294	595.30	Richey, 1989, Table 2, p.39	39	M49er	FFG_333	746.30	Richey, 1989, Table 2, p.42
2	M49er	FFG_295	582.80	Richey, 1989, Table 2, p.39	40	M49er	FFG_334	743.10	Richey, 1989, Table 2, p.42
3	M49er	FFG_297	567.50	Richey, 1989, Table 2, p.39	41	M49er	FFG_335	757.10	Richey, 1989, Table 2, p.42
4	M49er	FFG_298	569.20	Richey, 1989, Table 2, p.40	42	M49er	FFG_336	754.40	Richey, 1989, Table 2, p.42
5	M49er	FFG_299	594.40	Richey, 1989, Table 2, p.40	43	M49er	FFG_337	738.50	Richey, 1989, Table 2, p.42
6	M49er	FFG_300	543.70	Richey, 1989, Table 2, p.40	44	M49er	FFG_338	744.80	Richey, 1989, Table 2, p.42
7	M49er	FFG_301	514.80	Richey, 1989, Table 2, p.40	45	M49er	FFG_339	711.10	Richey, 1989, Table 2, p.42
8	M49er	FFG_302	542.50	Richey, 1989, Table 2, p.40	46	M49er	FFG_340	721.40	Richey, 1989, Table 2, p.42
9	M49er	FFG_303	535.90	Richey, 1989, Table 2, p.40	47	M49er	FFG_342	747.60	Richey, 1989, Table 2, p.43
10	M49er	FFG_304	540.40	Richey, 1989, Table 2, p.40	48	M49er	FFG_344	713.40	Richey, 1989, Table 2, p.43
11	M49er	FFG_305	534.60	Richey, 1989, Table 2, p.40	49	M49er	FFG_345	775.50	Richey, 1989, Table 2, p.43
12	M49er	FFG_306	492.20	Richey, 1989, Table 2, p.40	50	M49er	FFG_347	766.00	Richey, 1989, Table 2, p.43
13	M49er	FFG_307	517.90	Richey, 1989, Table 2, p.40	51	M49er	FFG_348	790.90	Richey, 1989, Table 2, p.43
14	M49er	FFG_308	491.30	Richey, 1989, Table 2, p.40	52	M49er	FFG_349	764.20	Richey, 1989, Table 2, p.43
15	M49er	FFG_309	535.20	Richey, 1989, Table 2, p.40	53	M49er	FFG_350	808.90	Richey, 1989, Table 2, p.43
16	M49er	FFG_310	564.20	Richey, 1989, Table 2, p.40	54	M49er	FFG_351	732.20	Richey, 1989, Table 2, p.43
17	M49er	FFG_311	498.70	Richey, 1989, Table 2, p.40	55	M49er	FFG_352	731.50	Richey, 1989, Table 2, p.43
18	M49er	FFG_312	537.40	Richey, 1989, Table 2, p.40	56	M49er	FFG_353	751.70	Richey, 1989, Table 2, p.43
19	M49er	FFG_313	934.30	Richey, 1989, Table 2, p.41	57	M49er	FFG_354	817.80	Richey, 1989, Table 2, p.43
20	M49er	FFG_314	862.30	Richey, 1989, Table 2, p.41	58	M49er	FFG_361	1011.00	Richey, 1989, Table 2, p.44
21	M49er	FFG_315	782.90	Richey, 1989, Table 2, p.41	59	M49er	FFG_366	960.40	Richey, 1989, Table 2, p.44
22	M49er	FFG_316	771.40	Richey, 1989, Table 2, p.41	60	M49er	FFG_367	975.90	Richey, 1989, Table 2, p.44
23	M49er	FFG_317	792.20	Richey, 1989, Table 2, p.41	61	M49er	FFG_371	1012.90	Richey, 1989, Table 2, p.44
24	M49er	FFG_318	758.00	Richey, 1989, Table 2, p.41	62	M49er	FFG_374	946.40	Richey, 1989, Table 2, p.45
25	M49er	FFG_319	769.30	Richey, 1989, Table 2, p.41	63	M49er	FFG_383	955.30	Richey, 1989, Table 2, p.45
26	M49er	FFG_320	762.30	Richey, 1989, Table 2, p.41	64	M49er	FFG_384	976.00	Richey, 1989, Table 2, p.45
27	M49er	FFG_321	760.50	Richey, 1989, Table 2, p.41	65	M49er	FFG_387	966.60	Richey, 1989, Table 2, p.45
28	M49er	FFG_322	755.10	Richey, 1989, Table 2, p.41	66	M49er	FFG_388	959.20	Richey, 1989, Table 2, p.46
29	M49er	FFG_323	751.10	Richey, 1989, Table 2, p.41	67	M49er	FFG_390	974.40	Richey, 1989, Table 2, p.46
30	M49er	FFG_324	761.70	Richey, 1989, Table 2, p.41	68	M49er	FFG_391	973.50	Richey, 1989, Table 2, p.46
31	M49er	FFG_325	819.60	Richey, 1989, Table 2, p.41	69	M49er	FFG_392	967.80	Richey, 1989, Table 2, p.46
32	M49er	FFG_326	754.40	Richey, 1989, Table 2, p.41	70	M49er	FFG_393	835.60	Richey, 1989, Table 2, p.46
33	M49er	FFG_327	748.30	Richey, 1989, Table 2, p.42	71	M49er	FFG_394	925.90	Richey, 1989, Table 2, p.46
34	M49er	FFG_328	757.00	Richey, 1989, Table 2, p.42	72	M49er	FFG_395	918.40	Richey, 1989, Table 2, p.46
35	M49er	FFG_329	755.60	Richey, 1989, Table 2, p.42	73	M49er	FFG_396	901.60	Richey, 1989, Table 2, p.46
36	M49er	FFG_330	754.90	Richey, 1989, Table 2, p.42	74	M49er	FFG_398	825.70	Richey, 1989, Table 2, p.46
37	M49er	FFG_331	753.50	Richey, 1989, Table 2, p.42	75	M49er	FFG_402	1002.50	Richey, 1989, Table 2, p.46
38	M49er	FFG_332	744.00	Richey, 1989, Table 2, p.42	76	M49er	FFG_403	963.00	Richey, 1989, Table 2, p.47

Table B.2. Elevations of Stratigraphic Layers Near WIPP (Continued)

	Layer	Well ID	Elevation	Source
1	M49er	FFG_404	925.70	Richey, 1989, Table 2, p.47
2	M49er	FFG_407	958.30	Richey, 1989, Table 2, p.47
3	M49er	FFG_419	997.00	Richey, 1989, Table 2, p.48
4	M49er	FFG_420	992.70	Richey, 1989, Table 2, p.48
5	M49er	FFG_421	983.60	Richey, 1989, Table 2, p.48
6	M49er	FFG_422	976.60	Richey, 1989, Table 2, p.48
7	M49er	FFG_432	931.80	Richey, 1989, Table 2, p.48
8	M49er	FFG_438	892.60	Richey, 1989, Table 2, p.49
9	M49er	FFG_455	837.60	Richey, 1989, Table 2, p.50
10	M49er	FFG_456	829.00	Richey, 1989, Table 2, p.50
11	M49er	FFG_457	885.10	Richey, 1989, Table 2, p.50
12	M49er	FFG_458	888.20	Richey, 1989, Table 2, p.50
13	M49er	FFG_459	816.60	Richey, 1989, Table 2, p.50
14	M49er	FFG_462	884.10	Richey, 1989, Table 2, p.50
15	M49er	FFG_463	913.50	Richey, 1989, Table 2, p.51
16	M49er	FFG_464	900.40	Richey, 1989, Table 2, p.51
17	M49er	FFG_465	902.80	Richey, 1989, Table 2, p.51
18	M49er	FFG_467	506.20	Richey, 1989, Table 2, p.51
19	M49er	FFG_468	493.50	Richey, 1989, Table 2, p.51
20	M49er	FFG_470	509.60	Richey, 1989, Table 2, p.51
21	M49er	FFG_471	525.80	Richey, 1989, Table 2, p.51
22	M49er	FFG_472	564.20	Richey, 1989, Table 2, p.51
23	M49er	FFG_473	491.60	Richey, 1989, Table 2, p.51
24	M49er	FFG_474	750.70	Richey, 1989, Table 2, p.51
25	M49er	FFG_475	749.70	Richey, 1989, Table 2, p.51
26	M49er	FFG_476	821.80	Richey, 1989, Table 2, p.51
27	M49er	FFG_477	774.50	Richey, 1989, Table 2, p.51
28	M49er	FFG_478	755.60	Richey, 1989, Table 2, p.52
29	M49er	FFG_479	752.50	Richey, 1989, Table 2, p.52
30	M49er	FFG_480	754.40	Richey, 1989, Table 2, p.52
31	M49er	FFG_481	731.80	Richey, 1989, Table 2, p.52
32	M49er	FFG_482	761.40	Richey, 1989, Table 2, p.52
33	M49er	FFG_483	785.10	Richey, 1989, Table 2, p.52
34	M49er	FFG_484	772.20	Richey, 1989, Table 2, p.52
35	M49er	FFG_485	779.40	Richey, 1989, Table 2, p.52
36	M49er	FFG_486	766.30	Richey, 1989, Table 2, p.52
37	M49er	FFG_487	763.90	Richey, 1989, Table 2, p.52
38	M49er	FFG_488	748.00	Richey, 1989, Table 2, p.52
39	M49er	FFG_489	764.60	Richey, 1989, Table 2, p.52
40	M49er	FFG_490	855.60	Richey, 1989, Table 2, p.52
41	M49er	FFG_491	855.90	Richey, 1989, Table 2, p.52
42	M49er	FFG_492	817.50	Richey, 1989, Table 2, p.52
43	M49er	FFG_493	803.60	Richey, 1989, Table 2, p.53
44	M49er	FFG_494	811.30	Richey, 1989, Table 2, p.53
45	M49er	FFG_495	799.40	Richey, 1989, Table 2, p.53
46	M49er	FFG_496	715.40	Richey, 1989, Table 2, p.53
47	M49er	FFG_497	721.50	Richey, 1989, Table 2, p.53
48	M49er	FFG_498	737.00	Richey, 1989, Table 2, p.53
49	M49er	FFG_499	715.40	Richey, 1989, Table 2, p.53
50	M49er	FFG_500	726.00	Richey, 1989, Table 2, p.53
51	M49er	FFG_501	731.50	Richey, 1989, Table 2, p.53
52	M49er	FFG_502	724.80	Richey, 1989, Table 2, p.53
53	M49er	FFG_503	705.40	Richey, 1989, Table 2, p.53
54	M49er	FFG_504	723.60	Richey, 1989, Table 2, p.53
55	M49er	FFG_505	754.70	Richey, 1989, Table 2, p.53
56	M49er	FFG_506	749.20	Richey, 1989, Table 2, p.53
57	M49er	FFG_507	712.80	Richey, 1989, Table 2, p.53
58	M49er	FFG_508	763.30	Richey, 1989, Table 2, p.53
59	M49er	FFG_509	767.80	Richey, 1989, Table 2, p.54
60	M49er	FFG_510	767.30	Richey, 1989, Table 2, p.54
61	M49er	FFG_511	728.20	Richey, 1989, Table 2, p.54
62	M49er	FFG_512	748.30	Richey, 1989, Table 2, p.54
63	M49er	FFG_513	763.00	Richey, 1989, Table 2, p.54
64	M49er	FFG_514	754.70	Richey, 1989, Table 2, p.54
65	M49er	FFG_515	722.60	Richey, 1989, Table 2, p.54
66	M49er	FFG_516	715.90	Richey, 1989, Table 2, p.54
67	M49er	FFG_517	809.30	Richey, 1989, Table 2, p.54
68	M49er	FFG_518	797.90	Richey, 1989, Table 2, p.54
69	M49er	FFG_519	765.70	Richey, 1989, Table 2, p.54
70	M49er	FFG_520	653.00	Richey, 1989, Table 2, p.54
71	M49er	FFG_521	673.30	Richey, 1989, Table 2, p.54
72	M49er	FFG_522	531.70	Richey, 1989, Table 2, p.54
73	M49er	FFG_523	541.30	Richey, 1989, Table 2, p.54
74	M49er	FFG_524	693.10	Richey, 1989, Table 2, p.55
75	M49er	FFG_525	543.30	Richey, 1989, Table 2, p.55
76	M49er	FFG_527	958.90	Richey, 1989, Table 2, p.55

Table B.2. Elevations of Stratigraphic Layers Near WIPP (Continued)

	Layer	Well ID	Elevation	Source		Layer	Well ID	Elevation	Source
1	M49er	FFG_528	951.60	Richey, 1989, Table 2, p.55	39	M49er	FFG_672	943.70	Richey, 1989, Table 2, p.62
2	M49er	FFG_535	939.70	Richey, 1989, Table 2, p.55	40	M49er	FFG_674	937.00	Richey, 1989, Table 2, p.62
3	M49er	FFG_548	930.60	Richey, 1989, Table 2, p.56	41	M49er	FFG_675	896.00	Richey, 1989, Table 2, p.62
4	M49er	FFG_562	670.60	Richey, 1989, Table 2, p.57	42	M49er	FFG_676	905.00	Richey, 1989, Table 2, p.62
5	M49er	FFG_563	582.50	Richey, 1989, Table 2, p.57	43	M49er	FFG_677	932.40	Richey, 1989, Table 2, p.62
6	M49er	FFG_569	689.20	Richey, 1989, Table 2, p.57	44	M49er	FFG_679	934.80	Richey, 1989, Table 2, p.62
7	M49er	FFG_584	773.20	Richey, 1989, Table 2, p.58	45	M49er	FFG_689	817.20	Richey, 1989, Table 2, p.63
8	M49er	FFG_600	729.10	Richey, 1989, Table 2, p.58	46	M49er	FFG_690	824.80	Richey, 1989, Table 2, p.63
9	M49er	FFG_601	645.60	Richey, 1989, Table 2, p.58	47	M49er	FFG_691	816.30	Richey, 1989, Table 2, p.63
10	M49er	FFG_606	723.00	Richey, 1989, Table 2, p.58	48	M49er	FFG_692	806.20	Richey, 1989, Table 2, p.63
11	M49er	FFG_607	743.10	Richey, 1989, Table 2, p.59	49	M49er	FFG_693	817.70	Richey, 1989, Table 2, p.63
12	M49er	FFG_608	754.60	Richey, 1989, Table 2, p.59	50	M49er	FFG_694	810.10	Richey, 1989, Table 2, p.63
13	M49er	FFG_609	758.30	Richey, 1989, Table 2, p.59	51	M49er	FFG_695	814.10	Richey, 1989, Table 2, p.63
14	M49er	FFG_610	746.70	Richey, 1989, Table 2, p.59	52	M49er	FFG_696	815.90	Richey, 1989, Table 2, p.63
15	M49er	FFG_611	731.80	Richey, 1989, Table 2, p.59	53	M49er	FFG_697	818.10	Richey, 1989, Table 2, p.64
16	M49er	FFG_612	733.40	Richey, 1989, Table 2, p.59	54	M49er	FFG_698	861.40	Richey, 1989, Table 2, p.64
17	M49er	FFG_613	728.50	Richey, 1989, Table 2, p.59	55	M49er	FFG_699	811.10	Richey, 1989, Table 2, p.64
18	M49er	FFG_620	759.80	Richey, 1989, Table 2, p.59	56	M49er	FFG_700	801.40	Richey, 1989, Table 2, p.64
19	M49er	FFG_638	591.70	Richey, 1989, Table 2, p.60	57	M49er	FFG_701	810.60	Richey, 1989, Table 2, p.64
20	M49er	FFG_639	566.30	Richey, 1989, Table 2, p.60	58	M49er	FFG_702	811.70	Richey, 1989, Table 2, p.64
21	M49er	FFG_640	649.10	Richey, 1989, Table 2, p.60	59	M49er	FFG_703	817.20	Richey, 1989, Table 2, p.64
22	M49er	FFG_643	688.90	Richey, 1989, Table 2, p.60	60	M49er	FFG_704	806.20	Richey, 1989, Table 2, p.64
23	M49er	FFG_644	723.50	Richey, 1989, Table 2, p.60	61	M49er	FFG_705	735.50	Richey, 1989, Table 2, p.64
24	M49er	FFG_648	558.40	Richey, 1989, Table 2, p.60	62	M49er	FFG_706	755.00	Richey, 1989, Table 2, p.64
25	M49er	FFG_652	878.70	Richey, 1989, Table 2, p.60	63	M49er	FFG_707	741.00	Richey, 1989, Table 2, p.64
26	M49er	FFG_653	880.00	Richey, 1989, Table 2, p.61	64	M49er	FFG_708	791.60	Richey, 1989, Table 2, p.64
27	M49er	FFG_654	899.50	Richey, 1989, Table 2, p.61	65	M49er	FFG_709	681.50	Richey, 1989, Table 2, p.64
28	M49er	FFG_655	897.30	Richey, 1989, Table 2, p.61	66	M49er	FFG_710	682.50	Richey, 1989, Table 2, p.64
29	M49er	FFG_656	894.30	Richey, 1989, Table 2, p.61	67	M49er	FFG_711	694.40	Richey, 1989, Table 2, p.65
30	M49er	FFG_657	906.20	Richey, 1989, Table 2, p.61	68	M49er	FFG_712	735.60	Richey, 1989, Table 2, p.65
31	M49er	FFG_658	898.20	Richey, 1989, Table 2, p.61	69	M49er	FFG_713	672.50	Richey, 1989, Table 2, p.65
32	M49er	FFG_659	901.90	Richey, 1989, Table 2, p.61	70	M49er	FFG_714	790.30	Richey, 1989, Table 2, p.65
33	M49er	FFG_660	919.20	Richey, 1989, Table 2, p.61	71	M49er	FFG_715	799.70	Richey, 1989, Table 2, p.65
34	M49er	FFG_662	894.60	Richey, 1989, Table 2, p.61	72	M49er	FFG_716	697.90	Richey, 1989, Table 2, p.65
35	M49er	FFG_664	888.20	Richey, 1989, Table 2, p.61	73	M49er	FFG_717	722.50	Richey, 1989, Table 2, p.65
36	M49er	FFG_666	938.10	Richey, 1989, Table 2, p.62	74	M49er	FFG_718	723.50	Richey, 1989, Table 2, p.65
37	M49er	FFG_667	923.30	Richey, 1989, Table 2, p.62	75	M49er	FFG_719	696.70	Richey, 1989, Table 2, p.65
38	M49er	FFG_670	946.10	Richey, 1989, Table 2, p.62	76	M49er	FFG_720	699.60	Richey, 1989, Table 2, p.65

Table B.2. Elevations of Stratigraphic Layers Near WIPP (Continued)

	Layer	Well ID	Elevation	Source
1	M49er	FFG_721	698.00	Richey, 1989, Table 2, p.65
2	M49er	FFG_723	808.20	Richey, 1989, Table 2, p.65
3	M49er	FFG_724	738.90	Richey, 1989, Table 2, p.65
4	M49er	FFG_725	712.30	Richey, 1989, Table 2, p.65
5	M49er	FFG_726	698.90	Richey, 1989, Table 2, p.65
6	M49er	FFG_727	702.90	Richey, 1989, Table 2, p.66
7	M49er	FFG_728	696.40	Richey, 1989, Table 2, p.66
8	M49er	FFG_729	706.60	Richey, 1989, Table 2, p.66
9	M49er	FFG_730	724.80	Richey, 1989, Table 2, p.66
10	M49er	FFG_731	720.70	Richey, 1989, Table 2, p.66
11	M49er	FFG_732	739.50	Richey, 1989, Table 2, p.66
12	M49er	FFG_733	806.50	Richey, 1989, Table 2, p.66
13	M49er	FFG_734	758.60	Richey, 1989, Table 2, p.66
14	M49er	FFG_735	704.10	Richey, 1989, Table 2, p.66
15	M49er	FFG_736	758.70	Richey, 1989, Table 2, p.66
16	M49er	FFG_737	702.60	Richey, 1989, Table 2, p.66
17	M49er	FFG_738	713.80	Richey, 1989, Table 2, p.66
18	M49er	FFG_739	753.90	Richey, 1989, Table 2, p.66
19	M49er	FFG_740	754.70	Richey, 1989, Table 2, p.66
20	M49er	FFG_741	721.20	Richey, 1989, Table 2, p.66
21	M49er	FFG_742	774.50	Richey, 1989, Table 2, p.67
22	M49er	FFG_743	757.20	Richey, 1989, Table 2, p.67
23	M49er	FFG_744	739.70	Richey, 1989, Table 2, p.67
24	M49er	FFG_745	730.30	Richey, 1989, Table 2, p.67
25	M49er	FFG_746	719.80	Richey, 1989, Table 2, p.67
26	M49er	H1	882.70	Mercer, 1983, Table 1
27	M49er	H10C	756.80	Mercer, 1983, Table 1
28	M49er	H2C	890.30	Mercer, 1983, Table 1
29	M49er	H3	880.30	Mercer, 1983, Table 1
30	M49er	H4C	920.20	Mercer, 1983, Table 1
31	M49er	H5C	845.80	Mercer, 1983, Table 1
32	M49er	H6C	890.40	Mercer, 1983, Table 1
33	M49er	H7C	937.60	Mercer, 1983, Table 1
34	M49er	H8C	924.80	Mercer, 1983, Table 1
35	M49er	H9C	899.40	Mercer, 1983, Table 1
36	M49er	P1	910.50	Mercer, 1983, Table 1
37	M49er	P10	860.40	Mercer, 1983, Table 1
38	M49er	P11	840.90	Mercer, 1983, Table 1
39	M49er	P12	887.90	Mercer, 1983, Table 1
40	M49er	P13	889.50	Mercer, 1983, Table 1
41	M49er	P14	906.10	Mercer, 1983, Table 1
42	M49er	P15	938.50	Mercer, 1983, Table 1
43	M49er	P16	915.00	Mercer, 1983, Table 1
44	M49er	P17	900.40	Mercer, 1983, Table 1
45	M49er	P18	868.40	Mercer, 1983, Table 1
46	M49er	P19	849.50	Mercer, 1983, Table 1
47	M49er	P2	850.10	Mercer, 1983, Table 1
48	M49er	P20	845.30	Mercer, 1983, Table 1
49	M49er	P21	845.80	Mercer, 1983, Table 1
50	M49er	P3	888.50	Mercer, 1983, Table 1
51	M49er	P4	864.10	Mercer, 1983, Table 1
52	M49er	P5	868.10	Mercer, 1983, Table 1
53	M49er	P6	913.50	Mercer, 1983, Table 1
54	M49er	P7	920.50	Mercer, 1983, Table 1
55	M49er	P8	898.50	Mercer, 1983, Table 1
56	M49er	P9	868.70	Mercer, 1983, Table 1
57	M49er	REF	874.00	Rechard et al.,1991, Figure 2.2-1
58	M49er	SaltShft	875.54	Bechtel, Inc., 1986, Appendix D
59	M49er	WIPP11	842.10	Mercer, 1983, Table 1
60	M49er	WIPP11	842.20	SNL and USGS, 1982a, Table 2
61	M49er	WIPP12	866.80	SNL and D'Appolonia Consulting, 1983, Table 2
62	M49er	WIPP12	866.90	Mercer, 1983, Table 1
63	M49er	WIPP13	880.20	Mercer, 1983, Table 1
64	M49er	WIPP16	681.20	Mercer, 1983, Table 1
65	M49er	WIPP18	866.60	Mercer, 1983, Table 1
66	M49er	WIPP19	866.90	Mercer, 1983, Table 1
67	M49er	WIPP21	870.80	Mercer, 1983, Table 1
68	M49er	WIPP22	869.50	Mercer, 1983, Table 1
69	M49er	WIPP25	908.60	Mercer, 1983, Table 1
70	M49er	WIPP26	957.70	Mercer, 1983, Table 1
71	M49er	WIPP27	921.70	Mercer, 1983, Table 1
72	M49er	WIPP28	954.70	Mercer, 1983, Table 1
73	M49er	WIPP30	908.00	Mercer, 1983, Table 1
74	M49er	WIPP32	921.40	Mercer, 1983, Table 1
75	M49er	WIPP33	891.60	Mercer, 1983, Table 1
76	M49er	WIPP34	846.10	Mercer, 1983, Table 1

Table B.2. Elevations of Stratigraphic Layers Near WIPP (Continued)

	Layer	Well ID	Elevation	Source
1	M49er	WastShft	875.18	Bechtel, Inc., 1986, Appendix E
2	MB126	AirShft	509.31	Holt and Powers, 1990, Figure 22
3	MB126	AirShft	509.64	Holt and Powers, 1990, Figure 22
4	MB126	DOE1	485.50	U.S. DOE, Sep 1982, Table 2
5	MB126	DOE2	484.90	Mercer et al., 1987, Table 3-2
6	MB126	DOE2	485.40	Mercer et al., 1987, Table 3-2
7	MB126	ERDA9	511.60	SNL and USGS, 1982b, Table 2
8	MB126	ExhtShft	512.54	Bechtel, Inc., 1986, Appendix F
9	MB126	ExhtShft	512.72	Bechtel, Inc., 1986, Appendix F
10	MB126	REF	511.60	Rechard et al.,1991, Figure 2.2-1
11	MB126	SaltShft	514.21	Bechtel, Inc., 1986, Appendix D
12	MB126	SaltShft	514.47	Bechtel, Inc., 1986, Appendix D
13	MB126	WIPP11	513.00	SNL and USGS, 1982a, Table 2
14	MB126	WIPP12	513.80	SNL and D'Appolonia Consulting, 1983, Table 2
15	MB126	WastShft	512.40	Bechtel, Inc., 1986, Appendix E
16	MB126	WastShft	512.75	Bechtel, Inc., 1986, Appendix E
17	MB136	AirShft	412.87	Holt and Powers, 1990, Figure 22
18	MB136	AirShft	417.16	Holt and Powers, 1990, Figure 22
19	MB136	ExhtShft	415.52	Bechtel, Inc., 1986, Appendix F
20	MB136	ExhtShft	418.86	Bechtel, Inc., 1986, Appendix F
21	MB136	SaltShft	418.84	Bechtel, Inc., 1986, Appendix D
22	MB136	SaltShft	421.37	Bechtel, Inc., 1986, Appendix D
23	MB136	WastShft	415.27	Bechtel, Inc., 1986, Appendix E
24	MB136	WastShft	419.66	Bechtel, Inc., 1986, Appendix E
25	MB138	AirShft	393.81	Holt and Powers, 1990, Figure 22
26	MB138	AirShft	393.98	Holt and Powers, 1990, Figure 22
27	MB138	DH207	395.92	Krieg, 1984, Table I
28	MB138	DH207	396.16	Krieg, 1984, Table I
29	MB138	DH211	398.83	Krieg, 1984, Table I
30	MB138	DH211	398.98	Krieg, 1984, Table I
31	MB138	DH215	399.23	Krieg, 1984, Table I
32	MB138	DH215	399.41	Krieg, 1984, Table I
33	MB138	DH219	397.58	Krieg, 1984, Table I
34	MB138	DH219	397.82	Krieg, 1984, Table I
35	MB138	DH223	394.10	Krieg, 1984, Table I
36	MB138	DH223	394.31	Krieg, 1984, Table I
37	MB138	DH227	391.03	Krieg, 1984, Table I
38	MB138	DH227	391.18	Krieg, 1984, Table I
39	MB138	DH77	409.65	Krieg, 1984, Table I
40	MB138	DH77	409.95	Krieg, 1984, Table I
41	MB138	DO201	396.40	Krieg, 1984, Table I
42	MB138	DO201	396.58	Krieg, 1984, Table I
43	MB138	DO203	406.94	Krieg, 1984, Table I
44	MB138	DO203	407.15	Krieg, 1984, Table I
45	MB138	DO205	412.06	Krieg, 1984, Table I
46	MB138	DO205	412.30	Krieg, 1984, Table I
47	MB138	DO45	403.83	Krieg, 1984, Table I
48	MB138	DO45	404.01	Krieg, 1984, Table I
49	MB138	DO52	401.39	Krieg, 1984, Table I
50	MB138	DO52	401.51	Krieg, 1984, Table I
51	MB138	DO56	406.69	Krieg, 1984, Table I
52	MB138	DO56	406.84	Krieg, 1984, Table I
53	MB138	DO63	410.47	Krieg, 1984, Table I
54	MB138	DO63	410.68	Krieg, 1984, Table I
55	MB138	DO67	410.38	Krieg, 1984, Table I
56	MB138	DO67	410.50	Krieg, 1984, Table I
57	MB138	DO88	409.07	Krieg, 1984, Table I
58	MB138	DO88	409.33	Krieg, 1984, Table I
59	MB138	DO91	408.81	Krieg, 1984, Table I
60	MB138	DO91	409.02	Krieg, 1984, Table I
61	MB138	DOE1	368.60	U.S. DOE, Sep 1982, Table 2
62	MB138	DOE2	370.40	Mercer et al., 1987, Table 3-2
63	MB138	ERDA9	396.00	SNL and USGS, 1982b, Table 2
64	MB138	ERDA9	396.40	SNL and USGS, 1982b, Table 2
65	MB138	ExhtShft	396.86	Bechtel, Inc., 1986, Appendix F
66	MB138	ExhtShft	397.03	Bechtel, Inc., 1986, Appendix F
67	MB138	MB139_2	396.15	Krieg, 1984, Table I
68	MB138	MB139_2	396.30	Krieg, 1984, Table I
69	MB138	REF	396.00	Rechard et al.,1991, Figure 2.2-1
70	MB138	REF	396.40	Rechard et al.,1991, Figure 2.2-1
71	MB138	SaltShft	399.79	Bechtel, Inc., 1986, Appendix D
72	MB138	SaltShft	399.80	Bechtel, Inc., 1986, Appendix D
73	MB138	SaltShft	399.76	Krieg, 1984, Table I
74	MB138	SaltShft	399.91	Krieg, 1984, Table I
75	MB138	WIPP11	430.40	SNL and USGS, 1982a, Table 2
76	MB138	WIPP12	411.00	SNL and D'Appolonia Consulting, 1983, Table 2

Table B.2. Elevations of Stratigraphic Layers Near WIPP (Continued)

	Layer	Well ID	Elevation	Source
1	MB138	WastShft	395.89	Bechtel, Inc., 1986, Appendix E
2	MB138	WastShft	396.07	Bechtel, Inc., 1986, Appendix E
3	MB138	WastShft	396.31	Krieg, 1984, Table I
4	MB138	WastShft	396.49	Krieg, 1984, Table I
5	MB139	DH207	377.63	Krieg, 1984, Table I
6	MB139	DH207	378.70	Krieg, 1984, Table I
7	MB139	DH211	380.73	Krieg, 1984, Table I
8	MB139	DH211	381.31	Krieg, 1984, Table I
9	MB139	DH215	381.03	Krieg, 1984, Table I
10	MB139	DH215	382.04	Krieg, 1984, Table I
11	MB139	DH219	379.91	Krieg, 1984, Table I
12	MB139	DH219	380.58	Krieg, 1984, Table I
13	MB139	DH223	376.70	Krieg, 1984, Table I
14	MB139	DH223	377.64	Krieg, 1984, Table I
15	MB139	DH227	373.78	Krieg, 1984, Table I
16	MB139	DH227	374.42	Krieg, 1984, Table I
17	MB139	DH77	392.37	Krieg, 1984, Table I
18	MB139	DH77	393.35	Krieg, 1984, Table I
19	MB139	DO201	378.26	Krieg, 1984, Table I
20	MB139	DO201	379.11	Krieg, 1984, Table I
21	MB139	DO203	389.84	Krieg, 1984, Table I
22	MB139	DO203	390.63	Krieg, 1984, Table I
23	MB139	DO205	394.29	Krieg, 1984, Table I
24	MB139	DO205	394.69	Krieg, 1984, Table I
25	MB139	DO45	385.11	Krieg, 1984, Table I
26	MB139	DO45	386.36	Krieg, 1984, Table I
27	MB139	DO52	383.44	Krieg, 1984, Table I
28	MB139	DO52	384.57	Krieg, 1984, Table I
29	MB139	DO56	388.89	Krieg, 1984, Table I
30	MB139	DO56	389.53	Krieg, 1984, Table I
31	MB139	DO63	392.79	Krieg, 1984, Table I
32	MB139	DO63	393.46	Krieg, 1984, Table I
33	MB139	DO67	393.19	Krieg, 1984, Table I
34	MB139	DO67	394.13	Krieg, 1984, Table I
35	MB139	DO88	392.06	Krieg, 1984, Table I
36	MB139	DO88	392.99	Krieg, 1984, Table I
37	MB139	DO91	391.62	Krieg, 1984, Table I
38	MB139	DO91	392.66	Krieg, 1984, Table I
39	MB139	DOE1	350.40	U.S. DOE, Sep 1982, Table 2
40	MB139	DOE2	339.00	Mercer et al., 1987, Table 3-2
41	MB139	DOE2	340.00	Mercer et al., 1987, Table 3-2
42	MB139	ERDA9	378.10	SNL and USGS, 1982b, Table 2
43	MB139	ERDA9	379.00	SNL and USGS, 1982b, Table 2
44	MB139	MB139_2	377.44	Krieg, 1984, Table I
45	MB139	MB139_2	378.42	Krieg, 1984, Table I
46	MB139	REF	378.10	Rechard et al.,1991, Figure 2.2-1
47	MB139	REF	379.00	Rechard et al.,1991, Figure 2.2-1
48	MB139	SaltShft	381.64	Bechtel, Inc., 1986, Appendix D
49	MB139	SaltShft	382.44	Bechtel, Inc., 1986, Appendix D
50	MB139	SaltShft	381.38	Krieg, 1984, Table I
51	MB139	SaltShft	382.29	Krieg, 1984, Table I
52	MB139	WIPP11	419.10	SNL and USGS, 1982a, Table 2
53	MB139	WIPP12	395.90	SNL and D'Appolonia Consulting, 1983, Table 2
54	MB139	WastShft	377.14	Bechtel, Inc., 1986, Appendix E
55	MB139	WastShft	378.22	Bechtel, Inc., 1986, Appendix E
56	MB139	WastShft	378.04	Krieg, 1984, Table I
57	MB139	WastShft	379.10	Krieg, 1984, Table I
58	Magenta	AEC7	890.30	Mercer, 1983, Table 1
59	Magenta	AEC8	858.70	Mercer, 1983, Table 1
60	Magenta	AirShft	858.82	Holt and Powers, 1990, Figure 22
61	Magenta	B25	858.40	Mercer, 1983, Table 1
62	Magenta	DOE1	838.60	U.S. DOE, Sep 1982, Table 2
63	Magenta	DOE2	829.00	Mercer et al., 1987, Table 3-2
64	Magenta	ERDA10	915.90	Mercer, 1983, Table 1
65	Magenta	ERDA6	897.60	Mercer, 1983, Table 1
66	Magenta	ERDA9	860.40	Mercer, 1983, Table 1
67	Magenta	ERDA9	856.70	SNL and USGS, 1982b, Table 2
68	Magenta	ExhtShft	855.39	Bechtel, Inc., 1986, Appendix F
69	Magenta	FFG_002	667.50	Richey, 1989, Table 2, p.21
70	Magenta	FFG_004	717.80	Richey, 1989, Table 2, p.21
71	Magenta	FFG_005	674.90	Richey, 1989, Table 2, p.21
72	Magenta	FFG_006	670.00	Richey, 1989, Table 2, p.21
73	Magenta	FFG_007	655.90	Richey, 1989, Table 2, p.21
74	Magenta	FFG_009	657.40	Richey, 1989, Table 2, p.21
75	Magenta	FFG_011	664.20	Richey, 1989, Table 2, p.21
76	Magenta	FFG_012	667.80	Richey, 1989, Table 2, p.21

Table B.2. Elevations of Stratigraphic Layers Near WIPP (Continued)

	Layer	Well ID	Elevation	Source
1	Magenta	FFG_013	674.80	Richey, 1989, Table 2, p.21
2	Magenta	FFG_014	721.10	Richey, 1989, Table 2, p.21
3	Magenta	FFG_016	644.90	Richey, 1989, Table 2, p.21
4	Magenta	FFG_017	648.30	Richey, 1989, Table 2, p.22
5	Magenta	FFG_018	652.30	Richey, 1989, Table 2, p.22
6	Magenta	FFG_019	644.70	Richey, 1989, Table 2, p.22
7	Magenta	FFG_020	718.40	Richey, 1989, Table 2, p.22
8	Magenta	FFG_023	654.10	Richey, 1989, Table 2, p.22
9	Magenta	FFG_024	638.80	Richey, 1989, Table 2, p.22
10	Magenta	FFG_025	652.20	Richey, 1989, Table 2, p.22
11	Magenta	FFG_026	649.50	Richey, 1989, Table 2, p.22
12	Magenta	FFG_027	643.10	Richey, 1989, Table 2, p.22
13	Magenta	FFG_028	612.70	Richey, 1989, Table 2, p.22
14	Magenta	FFG_029	599.20	Richey, 1989, Table 2, p.22
15	Magenta	FFG_030	598.30	Richey, 1989, Table 2, p.22
16	Magenta	FFG_031	590.10	Richey, 1989, Table 2, p.22
17	Magenta	FFG_032	592.10	Richey, 1989, Table 2, p.22
18	Magenta	FFG_033	588.30	Richey, 1989, Table 2, p.22
19	Magenta	FFG_034	582.40	Richey, 1989, Table 2, p.23
20	Magenta	FFG_035	572.60	Richey, 1989, Table 2, p.23
21	Magenta	FFG_036	582.20	Richey, 1989, Table 2, p.23
22	Magenta	FFG_037	571.80	Richey, 1989, Table 2, p.23
23	Magenta	FFG_038	559.60	Richey, 1989, Table 2, p.23
24	Magenta	FFG_039	778.80	Richey, 1989, Table 2, p.23
25	Magenta	FFG_040	720.90	Richey, 1989, Table 2, p.23
26	Magenta	FFG_041	780.60	Richey, 1989, Table 2, p.23
27	Magenta	FFG_042	785.40	Richey, 1989, Table 2, p.23
28	Magenta	FFG_043	788.10	Richey, 1989, Table 2, p.23
29	Magenta	FFG_044	741.00	Richey, 1989, Table 2, p.23
30	Magenta	FFG_047	613.90	Richey, 1989, Table 2, p.23
31	Magenta	FFG_048	630.90	Richey, 1989, Table 2, p.23
32	Magenta	FFG_049	620.90	Richey, 1989, Table 2, p.23
33	Magenta	FFG_050	627.60	Richey, 1989, Table 2, p.24
34	Magenta	FFG_051	627.30	Richey, 1989, Table 2, p.24
35	Magenta	FFG_052	630.30	Richey, 1989, Table 2, p.24
36	Magenta	FFG_053	623.30	Richey, 1989, Table 2, p.24
37	Magenta	FFG_054	620.60	Richey, 1989, Table 2, p.24
38	Magenta	FFG_055	621.10	Richey, 1989, Table 2, p.24
39	Magenta	FFG_056	621.80	Richey, 1989, Table 2, p.24
40	Magenta	FFG_057	625.20	Richey, 1989, Table 2, p.24
41	Magenta	FFG_058	623.60	Richey, 1989, Table 2, p.24
42	Magenta	FFG_059	623.60	Richey, 1989, Table 2, p.24
43	Magenta	FFG_060	627.30	Richey, 1989, Table 2, p.24
44	Magenta	FFG_061	626.00	Richey, 1989, Table 2, p.24
45	Magenta	FFG_062	553.20	Richey, 1989, Table 2, p.24
46	Magenta	FFG_063	513.70	Richey, 1989, Table 2, p.24
47	Magenta	FFG_064	538.60	Richey, 1989, Table 2, p.24
48	Magenta	FFG_065	520.60	Richey, 1989, Table 2, p.24
49	Magenta	FFG_066	473.90	Richey, 1989, Table 2, p.24
50	Magenta	FFG_067	516.40	Richey, 1989, Table 2, p.25
51	Magenta	FFG_068	481.90	Richey, 1989, Table 2, p.25
52	Magenta	FFG_069	502.40	Richey, 1989, Table 2, p.25
53	Magenta	FFG_070	532.20	Richey, 1989, Table 2, p.25
54	Magenta	FFG_071	790.70	Richey, 1989, Table 2, p.25
55	Magenta	FFG_072	721.10	Richey, 1989, Table 2, p.25
56	Magenta	FFG_073	699.50	Richey, 1989, Table 2, p.25
57	Magenta	FFG_074	703.30	Richey, 1989, Table 2, p.25
58	Magenta	FFG_075	756.00	Richey, 1989, Table 2, p.25
59	Magenta	FFG_076	818.10	Richey, 1989, Table 2, p.25
60	Magenta	FFG_078	855.20	Richey, 1989, Table 2, p.25
61	Magenta	FFG_079	829.70	Richey, 1989, Table 2, p.25
62	Magenta	FFG_080	808.30	Richey, 1989, Table 2, p.25
63	Magenta	FFG_081	727.90	Richey, 1989, Table 2, p.26
64	Magenta	FFG_082	759.30	Richey, 1989, Table 2, p.26
65	Magenta	FFG_083	674.70	Richey, 1989, Table 2, p.26
66	Magenta	FFG_084	702.20	Richey, 1989, Table 2, p.26
67	Magenta	FFG_085	695.60	Richey, 1989, Table 2, p.26
68	Magenta	FFG_086	705.60	Richey, 1989, Table 2, p.26
69	Magenta	FFG_087	680.00	Richey, 1989, Table 2, p.26
70	Magenta	FFG_088	674.60	Richey, 1989, Table 2, p.26
71	Magenta	FFG_089	656.00	Richey, 1989, Table 2, p.26
72	Magenta	FFG_091	700.40	Richey, 1989, Table 2, p.26
73	Magenta	FFG_092	716.60	Richey, 1989, Table 2, p.26
74	Magenta	FFG_093	718.10	Richey, 1989, Table 2, p.26
75	Magenta	FFG_094	720.20	Richey, 1989, Table 2, p.26
76	Magenta	FFG_095	688.80	Richey, 1989, Table 2, p.26

Table B.2. Elevations of Stratigraphic Layers Near WIPP (Continued)

	Layer	Well ID	Elevation	Source
1	Magenta	FFG_096	671.20	Richey, 1989, Table 2, p.26
2	Magenta	FFG_097	651.70	Richey, 1989, Table 2, p.27
3	Magenta	FFG_098	625.40	Richey, 1989, Table 2, p.27
4	Magenta	FFG_099	620.90	Richey, 1989, Table 2, p.27
5	Magenta	FFG_100	603.90	Richey, 1989, Table 2, p.27
6	Magenta	FFG_101	574.90	Richey, 1989, Table 2, p.27
7	Magenta	FFG_102	593.50	Richey, 1989, Table 2, p.27
8	Magenta	FFG_103	655.40	Richey, 1989, Table 2, p.27
9	Magenta	FFG_104	551.10	Richey, 1989, Table 2, p.27
10	Magenta	FFG_105	909.60	Richey, 1989, Table 2, p.27
11	Magenta	FFG_106	939.70	Richey, 1989, Table 2, p.27
12	Magenta	FFG_107	923.00	Richey, 1989, Table 2, p.27
13	Magenta	FFG_108	918.40	Richey, 1989, Table 2, p.27
14	Magenta	FFG_109	898.90	Richey, 1989, Table 2, p.27
15	Magenta	FFG_110	865.70	Richey, 1989, Table 2, p.27
16	Magenta	FFG_111	871.70	Richey, 1989, Table 2, p.27
17	Magenta	FFG_112	861.00	Richey, 1989, Table 2, p.28
18	Magenta	FFG_113	875.10	Richey, 1989, Table 2, p.28
19	Magenta	FFG_114	905.60	Richey, 1989, Table 2, p.28
20	Magenta	FFG_115	895.50	Richey, 1989, Table 2, p.28
21	Magenta	FFG_116	911.00	Richey, 1989, Table 2, p.28
22	Magenta	FFG_117	911.30	Richey, 1989, Table 2, p.28
23	Magenta	FFG_120	923.00	Richey, 1989, Table 2, p.28
24	Magenta	FFG_121	928.10	Richey, 1989, Table 2, p.28
25	Magenta	FFG_122	926.60	Richey, 1989, Table 2, p.28
26	Magenta	FFG_123	900.60	Richey, 1989, Table 2, p.28
27	Magenta	FFG_124	865.30	Richey, 1989, Table 2, p.28
28	Magenta	FFG_125	890.90	Richey, 1989, Table 2, p.28
29	Magenta	FFG_126	886.20	Richey, 1989, Table 2, p.28
30	Magenta	FFG_127	891.20	Richey, 1989, Table 2, p.28
31	Magenta	FFG_128	926.60	Richey, 1989, Table 2, p.28
32	Magenta	FFG_129	899.40	Richey, 1989, Table 2, p.28
33	Magenta	FFG_130	929.60	Richey, 1989, Table 2, p.28
34	Magenta	FFG_132	935.10	Richey, 1989, Table 2, p.29
35	Magenta	FFG_133	938.10	Richey, 1989, Table 2, p.29
36	Magenta	FFG_134	944.00	Richey, 1989, Table 2, p.29
37	Magenta	FFG_135	917.50	Richey, 1989, Table 2, p.29
38	Magenta	FFG_136	919.10	Richey, 1989, Table 2, p.29
39	Magenta	FFG_137	927.90	Richey, 1989, Table 2, p.29
40	Magenta	FFG_138	880.60	Richey, 1989, Table 2, p.29
41	Magenta	FFG_139	889.70	Richey, 1989, Table 2, p.29
42	Magenta	FFG_140	829.20	Richey, 1989, Table 2, p.29
43	Magenta	FFG_141	854.20	Richey, 1989, Table 2, p.29
44	Magenta	FFG_142	829.40	Richey, 1989, Table 2, p.29
45	Magenta	FFG_143	839.30	Richey, 1989, Table 2, p.29
46	Magenta	FFG_147	897.90	Richey, 1989, Table 2, p.29
47	Magenta	FFG_155	914.10	Richey, 1989, Table 2, p.30
48	Magenta	FFG_157	915.30	Richey, 1989, Table 2, p.30
49	Magenta	FFG_158	937.20	Richey, 1989, Table 2, p.30
50	Magenta	FFG_159	936.70	Richey, 1989, Table 2, p.30
51	Magenta	FFG_160	929.70	Richey, 1989, Table 2, p.30
52	Magenta	FFG_161	936.10	Richey, 1989, Table 2, p.30
53	Magenta	FFG_162	933.30	Richey, 1989, Table 2, p.30
54	Magenta	FFG_163	933.90	Richey, 1989, Table 2, p.30
55	Magenta	FFG_166	936.00	Richey, 1989, Table 2, p.31
56	Magenta	FFG_167	922.10	Richey, 1989, Table 2, p.31
57	Magenta	FFG_168	944.60	Richey, 1989, Table 2, p.31
58	Magenta	FFG_169	957.30	Richey, 1989, Table 2, p.31
59	Magenta	FFG_170	922.90	Richey, 1989, Table 2, p.31
60	Magenta	FFG_171	931.50	Richey, 1989, Table 2, p.31
61	Magenta	FFG_172	937.20	Richey, 1989, Table 2, p.31
62	Magenta	FFG_173	914.10	Richey, 1989, Table 2, p.31
63	Magenta	FFG_180	920.50	Richey, 1989, Table 2, p.31
64	Magenta	FFG_181	951.30	Richey, 1989, Table 2, p.32
65	Magenta	FFG_182	847.60	Richey, 1989, Table 2, p.32
66	Magenta	FFG_184	927.80	Richey, 1989, Table 2, p.32
67	Magenta	FFG_185	934.50	Richey, 1989, Table 2, p.32
68	Magenta	FFG_186	863.80	Richey, 1989, Table 2, p.32
69	Magenta	FFG_188	874.10	Richey, 1989, Table 2, p.32
70	Magenta	FFG_189	902.20	Richey, 1989, Table 2, p.32
71	Magenta	FFG_190	882.40	Richey, 1989, Table 2, p.32
72	Magenta	FFG_191	878.10	Richey, 1989, Table 2, p.32
73	Magenta	FFG_192	815.30	Richey, 1989, Table 2, p.32
74	Magenta	FFG_194	822.10	Richey, 1989, Table 2, p.33
75	Magenta	FFG_195	834.00	Richey, 1989, Table 2, p.33
76	Magenta	FFG_196	876.90	Richey, 1989, Table 2, p.33

Table B.2. Elevations of Stratigraphic Layers Near WIPP (Continued)

	Layer	Well ID	Elevation	Source
1	Magenta	FFG_197	878.10	Richey, 1989, Table 2, p.33
2	Magenta	FFG_198	877.50	Richey, 1989, Table 2, p.33
3	Magenta	FFG_199	867.50	Richey, 1989, Table 2, p.33
4	Magenta	FFG_200	880.90	Richey, 1989, Table 2, p.33
5	Magenta	FFG_201	873.20	Richey, 1989, Table 2, p.33
6	Magenta	FFG_202	816.50	Richey, 1989, Table 2, p.33
7	Magenta	FFG_203	823.00	Richey, 1989, Table 2, p.33
8	Magenta	FFG_204	846.50	Richey, 1989, Table 2, p.33
9	Magenta	FFG_205	860.50	Richey, 1989, Table 2, p.33
10	Magenta	FFG_206	874.50	Richey, 1989, Table 2, p.33
11	Magenta	FFG_207	872.30	Richey, 1989, Table 2, p.33
12	Magenta	FFG_208	882.10	Richey, 1989, Table 2, p.34
13	Magenta	FFG_209	873.20	Richey, 1989, Table 2, p.34
14	Magenta	FFG_210	865.90	Richey, 1989, Table 2, p.34
15	Magenta	FFG_212	852.80	Richey, 1989, Table 2, p.34
16	Magenta	FFG_213	874.50	Richey, 1989, Table 2, p.34
17	Magenta	FFG_214	854.90	Richey, 1989, Table 2, p.34
18	Magenta	FFG_215	831.20	Richey, 1989, Table 2, p.34
19	Magenta	FFG_216	716.80	Richey, 1989, Table 2, p.34
20	Magenta	FFG_217	851.40	Richey, 1989, Table 2, p.34
21	Magenta	FFG_218	844.00	Richey, 1989, Table 2, p.34
22	Magenta	FFG_219	889.70	Richey, 1989, Table 2, p.34
23	Magenta	FFG_220	836.70	Richey, 1989, Table 2, p.34
24	Magenta	FFG_221	796.20	Richey, 1989, Table 2, p.34
25	Magenta	FFG_222	749.80	Richey, 1989, Table 2, p.34
26	Magenta	FFG_224	655.70	Richey, 1989, Table 2, p.35
27	Magenta	FFG_225	662.40	Richey, 1989, Table 2, p.35
28	Magenta	FFG_226	661.00	Richey, 1989, Table 2, p.35
29	Magenta	FFG_228	651.70	Richey, 1989, Table 2, p.35
30	Magenta	FFG_229	679.40	Richey, 1989, Table 2, p.35
31	Magenta	FFG_230	665.10	Richey, 1989, Table 2, p.35
32	Magenta	FFG_231	681.80	Richey, 1989, Table 2, p.35
33	Magenta	FFG_232	695.60	Richey, 1989, Table 2, p.35
34	Magenta	FFG_233	685.80	Richey, 1989, Table 2, p.35
35	Magenta	FFG_234	722.70	Richey, 1989, Table 2, p.35
36	Magenta	FFG_235	698.60	Richey, 1989, Table 2, p.35
37	Magenta	FFG_236	746.40	Richey, 1989, Table 2, p.35
38	Magenta	FFG_237	712.10	Richey, 1989, Table 2, p.35
39	Magenta	FFG_238	691.00	Richey, 1989, Table 2, p.36
40	Magenta	FFG_239	679.10	Richey, 1989, Table 2, p.36
41	Magenta	FFG_240	671.20	Richey, 1989, Table 2, p.36
42	Magenta	FFG_241	666.30	Richey, 1989, Table 2, p.36
43	Magenta	FFG_242	783.10	Richey, 1989, Table 2, p.36
44	Magenta	FFG_243	743.10	Richey, 1989, Table 2, p.36
45	Magenta	FFG_244	780.80	Richey, 1989, Table 2, p.36
46	Magenta	FFG_245	573.00	Richey, 1989, Table 2, p.36
47	Magenta	FFG_246	578.50	Richey, 1989, Table 2, p.36
48	Magenta	FFG_247	563.80	Richey, 1989, Table 2, p.36
49	Magenta	FFG_248	571.20	Richey, 1989, Table 2, p.36
50	Magenta	FFG_249	569.70	Richey, 1989, Table 2, p.36
51	Magenta	FFG_250	651.50	Richey, 1989, Table 2, p.36
52	Magenta	FFG_251	544.90	Richey, 1989, Table 2, p.36
53	Magenta	FFG_252	683.90	Richey, 1989, Table 2, p.36
54	Magenta	FFG_253	639.20	Richey, 1989, Table 2, p.36
55	Magenta	FFG_254	630.00	Richey, 1989, Table 2, p.36
56	Magenta	FFG_255	587.70	Richey, 1989, Table 2, p.37
57	Magenta	FFG_256	535.20	Richey, 1989, Table 2, p.37
58	Magenta	FFG_257	579.40	Richey, 1989, Table 2, p.37
59	Magenta	FFG_258	594.90	Richey, 1989, Table 2, p.37
60	Magenta	FFG_259	561.10	Richey, 1989, Table 2, p.37
61	Magenta	FFG_260	603.80	Richey, 1989, Table 2, p.37
62	Magenta	FFG_261	592.80	Richey, 1989, Table 2, p.37
63	Magenta	FFG_263	526.60	Richey, 1989, Table 2, p.37
64	Magenta	FFG_264	760.50	Richey, 1989, Table 2, p.37
65	Magenta	FFG_265	755.90	Richey, 1989, Table 2, p.37
66	Magenta	FFG_266	736.70	Richey, 1989, Table 2, p.37
67	Magenta	FFG_267	713.50	Richey, 1989, Table 2, p.37
68	Magenta	FFG_268	690.70	Richey, 1989, Table 2, p.37
69	Magenta	FFG_269	702.40	Richey, 1989, Table 2, p.38
70	Magenta	FFG_270	774.50	Richey, 1989, Table 2, p.38
71	Magenta	FFG_271	815.00	Richey, 1989, Table 2, p.38
72	Magenta	FFG_272	822.50	Richey, 1989, Table 2, p.38
73	Magenta	FFG_273	797.40	Richey, 1989, Table 2, p.38
74	Magenta	FFG_274	834.20	Richey, 1989, Table 2, p.38
75	Magenta	FFG_275	840.30	Richey, 1989, Table 2, p.38
76	Magenta	FFG_276	845.20	Richey, 1989, Table 2, p.38

Table B.2. Elevations of Stratigraphic Layers Near WIPP (Continued)

	Layer	Well ID	Elevation	Source
2	Magenta	FFG_277	836.70	Richey, 1989, Table 2, p.38
3	Magenta	FFG_278	845.80	Richey, 1989, Table 2, p.38
4	Magenta	FFG_279	840.90	Richey, 1989, Table 2, p.38
5	Magenta	FFG_280	837.30	Richey, 1989, Table 2, p.38
6	Magenta	FFG_281	814.20	Richey, 1989, Table 2, p.38
7	Magenta	FFG_283	563.90	Richey, 1989, Table 2, p.39
8	Magenta	FFG_284	712.00	Richey, 1989, Table 2, p.39
9	Magenta	FFG_285	741.30	Richey, 1989, Table 2, p.39
10	Magenta	FFG_286	820.20	Richey, 1989, Table 2, p.39
11	Magenta	FFG_287	793.10	Richey, 1989, Table 2, p.39
12	Magenta	FFG_288	744.90	Richey, 1989, Table 2, p.39
13	Magenta	FFG_289	719.90	Richey, 1989, Table 2, p.39
14	Magenta	FFG_290	806.50	Richey, 1989, Table 2, p.39
15	Magenta	FFG_291	742.50	Richey, 1989, Table 2, p.39
16	Magenta	FFG_292	758.40	Richey, 1989, Table 2, p.39
17	Magenta	FFG_293	750.70	Richey, 1989, Table 2, p.39
18	Magenta	FFG_294	572.80	Richey, 1989, Table 2, p.39
19	Magenta	FFG_295	560.20	Richey, 1989, Table 2, p.39
20	Magenta	FFG_297	539.20	Richey, 1989, Table 2, p.39
21	Magenta	FFG_298	552.40	Richey, 1989, Table 2, p.40
22	Magenta	FFG_299	569.10	Richey, 1989, Table 2, p.40
23	Magenta	FFG_300	520.60	Richey, 1989, Table 2, p.40
24	Magenta	FFG_301	491.10	Richey, 1989, Table 2, p.40
25	Magenta	FFG_302	518.50	Richey, 1989, Table 2, p.40
26	Magenta	FFG_303	511.20	Richey, 1989, Table 2, p.40
27	Magenta	FFG_304	517.50	Richey, 1989, Table 2, p.40
28	Magenta	FFG_305	509.30	Richey, 1989, Table 2, p.40
29	Magenta	FFG_306	469.30	Richey, 1989, Table 2, p.40
30	Magenta	FFG_307	493.50	Richey, 1989, Table 2, p.40
31	Magenta	FFG_308	465.70	Richey, 1989, Table 2, p.40
32	Magenta	FFG_309	508.10	Richey, 1989, Table 2, p.40
33	Magenta	FFG_310	539.20	Richey, 1989, Table 2, p.40
34	Magenta	FFG_311	486.50	Richey, 1989, Table 2, p.40
35	Magenta	FFG_312	510.60	Richey, 1989, Table 2, p.40
36	Magenta	FFG_313	915.10	Richey, 1989, Table 2, p.41
37	Magenta	FFG_314	843.10	Richey, 1989, Table 2, p.41
38	Magenta	FFG_315	764.30	Richey, 1989, Table 2, p.41
39	Magenta	FFG_316	747.90	Richey, 1989, Table 2, p.41
40	Magenta	FFG_317	777.00	Richey, 1989, Table 2, p.41
41	Magenta	FFG_318	742.20	Richey, 1989, Table 2, p.41
42	Magenta	FFG_319	751.60	Richey, 1989, Table 2, p.41
43	Magenta	FFG_320	741.30	Richey, 1989, Table 2, p.41
44	Magenta	FFG_321	737.90	Richey, 1989, Table 2, p.41
45	Magenta	FFG_322	733.20	Richey, 1989, Table 2, p.41
46	Magenta	FFG_323	729.50	Richey, 1989, Table 2, p.41
47	Magenta	FFG_324	745.30	Richey, 1989, Table 2, p.41
48	Magenta	FFG_325	800.40	Richey, 1989, Table 2, p.41
49	Magenta	FFG_326	736.10	Richey, 1989, Table 2, p.41
50	Magenta	FFG_327	729.10	Richey, 1989, Table 2, p.42
51	Magenta	FFG_328	734.50	Richey, 1989, Table 2, p.42
52	Magenta	FFG_329	733.90	Richey, 1989, Table 2, p.42
53	Magenta	FFG_330	733.20	Richey, 1989, Table 2, p.42
54	Magenta	FFG_331	728.50	Richey, 1989, Table 2, p.42
55	Magenta	FFG_332	719.30	Richey, 1989, Table 2, p.42
56	Magenta	FFG_333	722.80	Richey, 1989, Table 2, p.42
57	Magenta	FFG_334	718.10	Richey, 1989, Table 2, p.42
58	Magenta	FFG_335	733.70	Richey, 1989, Table 2, p.42
59	Magenta	FFG_336	730.60	Richey, 1989, Table 2, p.42
60	Magenta	FFG_337	713.80	Richey, 1989, Table 2, p.42
61	Magenta	FFG_338	720.70	Richey, 1989, Table 2, p.42
62	Magenta	FFG_339	684.80	Richey, 1989, Table 2, p.42
63	Magenta	FFG_340	694.00	Richey, 1989, Table 2, p.42
64	Magenta	FFG_342	726.90	Richey, 1989, Table 2, p.43
65	Magenta	FFG_344	692.70	Richey, 1989, Table 2, p.43
66	Magenta	FFG_345	752.10	Richey, 1989, Table 2, p.43
67	Magenta	FFG_347	744.70	Richey, 1989, Table 2, p.43
68	Magenta	FFG_348	773.30	Richey, 1989, Table 2, p.43
69	Magenta	FFG_349	742.20	Richey, 1989, Table 2, p.43
70	Magenta	FFG_350	789.10	Richey, 1989, Table 2, p.43
71	Magenta	FFG_351	705.60	Richey, 1989, Table 2, p.43
72	Magenta	FFG_352	705.60	Richey, 1989, Table 2, p.43
73	Magenta	FFG_353	726.70	Richey, 1989, Table 2, p.43
74	Magenta	FFG_354	800.80	Richey, 1989, Table 2, p.43
75	Magenta	FFG_361	986.90	Richey, 1989, Table 2, p.44
76	Magenta	FFG_366	940.60	Richey, 1989, Table 2, p.44
77	Magenta	FFG_367	954.60	Richey, 1989, Table 2, p.44

Table B.2. Elevations of Stratigraphic Layers Near WIPP (Continued)

	Layer	Well ID	Elevation	Source
1	Magenta	FFG_371	997.70	Richey, 1989, Table 2, p.44
2	Magenta	FFG_374	940.90	Richey, 1989, Table 2, p.45
3	Magenta	FFG_383	938.80	Richey, 1989, Table 2, p.45
4	Magenta	FFG_384	945.80	Richey, 1989, Table 2, p.45
5	Magenta	FFG_387	940.30	Richey, 1989, Table 2, p.45
6	Magenta	FFG_388	936.70	Richey, 1989, Table 2, p.46
7	Magenta	FFG_390	954.00	Richey, 1989, Table 2, p.46
8	Magenta	FFG_391	951.50	Richey, 1989, Table 2, p.46
9	Magenta	FFG_392	948.60	Richey, 1989, Table 2, p.46
10	Magenta	FFG_393	816.10	Richey, 1989, Table 2, p.46
11	Magenta	FFG_394	908.60	Richey, 1989, Table 2, p.46
12	Magenta	FFG_395	901.60	Richey, 1989, Table 2, p.46
13	Magenta	FFG_396	884.30	Richey, 1989, Table 2, p.46
14	Magenta	FFG_398	805.60	Richey, 1989, Table 2, p.46
15	Magenta	FFG_402	979.40	Richey, 1989, Table 2, p.46
16	Magenta	FFG_403	941.40	Richey, 1989, Table 2, p.47
17	Magenta	FFG_404	901.60	Richey, 1989, Table 2, p.47
18	Magenta	FFG_407	940.00	Richey, 1989, Table 2, p.47
19	Magenta	FFG_408	913.20	Richey, 1989, Table 2, p.47
20	Magenta	FFG_419	976.60	Richey, 1989, Table 2, p.48
21	Magenta	FFG_420	973.50	Richey, 1989, Table 2, p.48
22	Magenta	FFG_421	960.10	Richey, 1989, Table 2, p.48
23	Magenta	FFG_422	958.30	Richey, 1989, Table 2, p.48
24	Magenta	FFG_432	924.10	Richey, 1989, Table 2, p.48
25	Magenta	FFG_438	874.60	Richey, 1989, Table 2, p.49
26	Magenta	FFG_455	817.50	Richey, 1989, Table 2, p.50
27	Magenta	FFG_456	812.50	Richey, 1989, Table 2, p.50
28	Magenta	FFG_457	868.10	Richey, 1989, Table 2, p.50
29	Magenta	FFG_458	872.60	Richey, 1989, Table 2, p.50
30	Magenta	FFG_459	799.50	Richey, 1989, Table 2, p.50
31	Magenta	FFG_462	865.80	Richey, 1989, Table 2, p.50
32	Magenta	FFG_463	893.10	Richey, 1989, Table 2, p.51
33	Magenta	FFG_464	880.00	Richey, 1989, Table 2, p.51
34	Magenta	FFG_465	883.00	Richey, 1989, Table 2, p.51
35	Magenta	FFG_467	488.20	Richey, 1989, Table 2, p.51
36	Magenta	FFG_468	465.50	Richey, 1989, Table 2, p.51
37	Magenta	FFG_470	484.90	Richey, 1989, Table 2, p.51
38	Magenta	FFG_471	500.50	Richey, 1989, Table 2, p.51
39	Magenta	FFG_472	538.30	Richey, 1989, Table 2, p.51
40	Magenta	FFG_473	468.20	Richey, 1989, Table 2, p.51
41	Magenta	FFG_474	729.40	Richey, 1989, Table 2, p.51
42	Magenta	FFG_475	728.90	Richey, 1989, Table 2, p.51
43	Magenta	FFG_476	805.00	Richey, 1989, Table 2, p.51
44	Magenta	FFG_477	760.80	Richey, 1989, Table 2, p.51
45	Magenta	FFG_478	739.70	Richey, 1989, Table 2, p.52
46	Magenta	FFG_479	736.40	Richey, 1989, Table 2, p.52
47	Magenta	FFG_480	732.50	Richey, 1989, Table 2, p.52
48	Magenta	FFG_481	715.70	Richey, 1989, Table 2, p.52
49	Magenta	FFG_482	744.30	Richey, 1989, Table 2, p.52
50	Magenta	FFG_483	767.80	Richey, 1989, Table 2, p.52
51	Magenta	FFG_484	753.60	Richey, 1989, Table 2, p.52
52	Magenta	FFG_485	762.60	Richey, 1989, Table 2, p.52
53	Magenta	FFG_486	749.50	Richey, 1989, Table 2, p.52
54	Magenta	FFG_487	746.50	Richey, 1989, Table 2, p.52
55	Magenta	FFG_488	731.20	Richey, 1989, Table 2, p.52
56	Magenta	FFG_489	748.40	Richey, 1989, Table 2, p.52
57	Magenta	FFG_490	838.80	Richey, 1989, Table 2, p.52
58	Magenta	FFG_491	836.40	Richey, 1989, Table 2, p.52
59	Magenta	FFG_492	798.60	Richey, 1989, Table 2, p.52
60	Magenta	FFG_493	785.30	Richey, 1989, Table 2, p.53
61	Magenta	FFG_494	792.10	Richey, 1989, Table 2, p.53
62	Magenta	FFG_495	783.00	Richey, 1989, Table 2, p.53
63	Magenta	FFG_496	688.60	Richey, 1989, Table 2, p.53
64	Magenta	FFG_497	701.10	Richey, 1989, Table 2, p.53
65	Magenta	FFG_498	714.10	Richey, 1989, Table 2, p.53
66	Magenta	FFG_499	689.50	Richey, 1989, Table 2, p.53
67	Magenta	FFG_500	704.70	Richey, 1989, Table 2, p.53
68	Magenta	FFG_501	710.10	Richey, 1989, Table 2, p.53
69	Magenta	FFG_502	702.90	Richey, 1989, Table 2, p.53
70	Magenta	FFG_503	684.00	Richey, 1989, Table 2, p.53
71	Magenta	FFG_504	706.00	Richey, 1989, Table 2, p.53
72	Magenta	FFG_505	739.50	Richey, 1989, Table 2, p.53
73	Magenta	FFG_506	730.90	Richey, 1989, Table 2, p.53
74	Magenta	FFG_507	692.40	Richey, 1989, Table 2, p.53
75	Magenta	FFG_508	744.10	Richey, 1989, Table 2, p.53
76	Magenta	FFG_509	745.20	Richey, 1989, Table 2, p.54

Table B.2. Elevations of Stratigraphic Layers Near WIPP (Continued)

	Layer	Well ID	Elevation	Source
1	Magenta	FFG_510	744.80	Richey, 1989, Table 2, p.54
2	Magenta	FFG_511	702.30	Richey, 1989, Table 2, p.54
3	Magenta	FFG_512	720.80	Richey, 1989, Table 2, p.54
4	Magenta	FFG_513	740.70	Richey, 1989, Table 2, p.54
5	Magenta	FFG_514	731.20	Richey, 1989, Table 2, p.54
6	Magenta	FFG_515	697.90	Richey, 1989, Table 2, p.54
7	Magenta	FFG_516	691.30	Richey, 1989, Table 2, p.54
8	Magenta	FFG_517	788.80	Richey, 1989, Table 2, p.54
9	Magenta	FFG_518	778.10	Richey, 1989, Table 2, p.54
10	Magenta	FFG_519	743.70	Richey, 1989, Table 2, p.54
11	Magenta	FFG_520	635.40	Richey, 1989, Table 2, p.54
12	Magenta	FFG_521	655.00	Richey, 1989, Table 2, p.54
13	Magenta	FFG_522	504.30	Richey, 1989, Table 2, p.54
14	Magenta	FFG_523	516.90	Richey, 1989, Table 2, p.54
15	Magenta	FFG_524	675.10	Richey, 1989, Table 2, p.55
16	Magenta	FFG_525	513.70	Richey, 1989, Table 2, p.55
17	Magenta	FFG_527	938.70	Richey, 1989, Table 2, p.55
18	Magenta	FFG_528	934.20	Richey, 1989, Table 2, p.55
19	Magenta	FFG_532	915.60	Richey, 1989, Table 2, p.55
20	Magenta	FFG_535	919.90	Richey, 1989, Table 2, p.55
21	Magenta	FFG_548	914.10	Richey, 1989, Table 2, p.56
22	Magenta	FFG_562	652.30	Richey, 1989, Table 2, p.57
23	Magenta	FFG_563	564.80	Richey, 1989, Table 2, p.57
24	Magenta	FFG_569	670.60	Richey, 1989, Table 2, p.57
25	Magenta	FFG_584	767.70	Richey, 1989, Table 2, p.58
26	Magenta	FFG_600	727.60	Richey, 1989, Table 2, p.58
27	Magenta	FFG_601	623.00	Richey, 1989, Table 2, p.58
28	Magenta	FFG_606	703.50	Richey, 1989, Table 2, p.58
29	Magenta	FFG_607	723.30	Richey, 1989, Table 2, p.59
30	Magenta	FFG_608	731.80	Richey, 1989, Table 2, p.59
31	Magenta	FFG_609	738.80	Richey, 1989, Table 2, p.59
32	Magenta	FFG_610	722.40	Richey, 1989, Table 2, p.59
33	Magenta	FFG_611	707.40	Richey, 1989, Table 2, p.59
34	Magenta	FFG_612	715.70	Richey, 1989, Table 2, p.59
35	Magenta	FFG_613	713.50	Richey, 1989, Table 2, p.59
36	Magenta	FFG_620	738.50	Richey, 1989, Table 2, p.59
37	Magenta	FFG_638	573.10	Richey, 1989, Table 2, p.60
38	Magenta	FFG_639	543.80	Richey, 1989, Table 2, p.60
39	Magenta	FFG_640	630.80	Richey, 1989, Table 2, p.60
40	Magenta	FFG_643	669.70	Richey, 1989, Table 2, p.60
41	Magenta	FFG_644	706.40	Richey, 1989, Table 2, p.60
42	Magenta	FFG_648	541.30	Richey, 1989, Table 2, p.60
43	Magenta	FFG_652	859.80	Richey, 1989, Table 2, p.60
44	Magenta	FFG_653	859.90	Richey, 1989, Table 2, p.61
45	Magenta	FFG_654	880.00	Richey, 1989, Table 2, p.61
46	Magenta	FFG_655	878.10	Richey, 1989, Table 2, p.61
47	Magenta	FFG_656	876.90	Richey, 1989, Table 2, p.61
48	Magenta	FFG_657	889.80	Richey, 1989, Table 2, p.61
49	Magenta	FFG_658	881.80	Richey, 1989, Table 2, p.61
50	Magenta	FFG_659	886.10	Richey, 1989, Table 2, p.61
51	Magenta	FFG_660	901.50	Richey, 1989, Table 2, p.61
52	Magenta	FFG_662	876.30	Richey, 1989, Table 2, p.61
53	Magenta	FFG_664	868.40	Richey, 1989, Table 2, p.61
54	Magenta	FFG_666	920.50	Richey, 1989, Table 2, p.62
55	Magenta	FFG_667	905.60	Richey, 1989, Table 2, p.62
56	Magenta	FFG_670	926.90	Richey, 1989, Table 2, p.62
57	Magenta	FFG_672	925.70	Richey, 1989, Table 2, p.62
58	Magenta	FFG_674	921.70	Richey, 1989, Table 2, p.62
59	Magenta	FFG_675	877.70	Richey, 1989, Table 2, p.62
60	Magenta	FFG_676	891.90	Richey, 1989, Table 2, p.62
61	Magenta	FFG_677	917.80	Richey, 1989, Table 2, p.62
62	Magenta	FFG_679	917.10	Richey, 1989, Table 2, p.62
63	Magenta	FFG_689	799.50	Richey, 1989, Table 2, p.63
64	Magenta	FFG_690	805.00	Richey, 1989, Table 2, p.63
65	Magenta	FFG_691	796.20	Richey, 1989, Table 2, p.63
66	Magenta	FFG_692	786.40	Richey, 1989, Table 2, p.63
67	Magenta	FFG_693	797.00	Richey, 1989, Table 2, p.63
68	Magenta	FFG_694	789.40	Richey, 1989, Table 2, p.63
69	Magenta	FFG_695	794.90	Richey, 1989, Table 2, p.63
70	Magenta	FFG_696	797.00	Richey, 1989, Table 2, p.63
71	Magenta	FFG_697	799.20	Richey, 1989, Table 2, p.64
72	Magenta	FFG_698	841.60	Richey, 1989, Table 2, p.64
73	Magenta	FFG_699	792.80	Richey, 1989, Table 2, p.64
74	Magenta	FFG_700	782.50	Richey, 1989, Table 2, p.64
75	Magenta	FFG_701	788.60	Richey, 1989, Table 2, p.64
76	Magenta	FFG_702	792.80	Richey, 1989, Table 2, p.64

Table B.2. Elevations of Stratigraphic Layers Near WIPP (Continued)

	Layer	Well ID	Elevation	Source
1	Magenta	FFG_703	798.90	Richey, 1989, Table 2, p.64
2	Magenta	FFG_704	785.50	Richey, 1989, Table 2, p.64
3	Magenta	FFG_705	715.60	Richey, 1989, Table 2, p.64
4	Magenta	FFG_706	736.10	Richey, 1989, Table 2, p.64
5	Magenta	FFG_707	720.30	Richey, 1989, Table 2, p.64
6	Magenta	FFG_708	773.30	Richey, 1989, Table 2, p.64
7	Magenta	FFG_709	664.50	Richey, 1989, Table 2, p.64
8	Magenta	FFG_710	665.40	Richey, 1989, Table 2, p.64
9	Magenta	FFG_711	675.20	Richey, 1989, Table 2, p.65
10	Magenta	FFG_712	718.80	Richey, 1989, Table 2, p.65
11	Magenta	FFG_713	655.80	Richey, 1989, Table 2, p.65
12	Magenta	FFG_714	770.20	Richey, 1989, Table 2, p.65
13	Magenta	FFG_715	783.00	Richey, 1989, Table 2, p.65
14	Magenta	FFG_716	680.80	Richey, 1989, Table 2, p.65
15	Magenta	FFG_717	703.30	Richey, 1989, Table 2, p.65
16	Magenta	FFG_718	706.70	Richey, 1989, Table 2, p.65
17	Magenta	FFG_719	679.40	Richey, 1989, Table 2, p.65
18	Magenta	FFG_720	679.10	Richey, 1989, Table 2, p.65
19	Magenta	FFG_721	679.10	Richey, 1989, Table 2, p.65
20	Magenta	FFG_723	791.70	Richey, 1989, Table 2, p.65
21	Magenta	FFG_724	719.10	Richey, 1989, Table 2, p.65
22	Magenta	FFG_725	694.90	Richey, 1989, Table 2, p.65
23	Magenta	FFG_726	682.70	Richey, 1989, Table 2, p.65
24	Magenta	FFG_727	680.00	Richey, 1989, Table 2, p.66
25	Magenta	FFG_728	677.80	Richey, 1989, Table 2, p.66
26	Magenta	FFG_729	688.90	Richey, 1989, Table 2, p.66
27	Magenta	FFG_730	705.60	Richey, 1989, Table 2, p.66
28	Magenta	FFG_731	703.00	Richey, 1989, Table 2, p.66
29	Magenta	FFG_732	720.60	Richey, 1989, Table 2, p.66
30	Magenta	FFG_733	787.60	Richey, 1989, Table 2, p.66
31	Magenta	FFG_734	741.90	Richey, 1989, Table 2, p.66
32	Magenta	FFG_735	684.60	Richey, 1989, Table 2, p.66
33	Magenta	FFG_736	739.10	Richey, 1989, Table 2, p.66
34	Magenta	FFG_737	682.80	Richey, 1989, Table 2, p.66
35	Magenta	FFG_738	697.00	Richey, 1989, Table 2, p.66
36	Magenta	FFG_739	734.40	Richey, 1989, Table 2, p.66
37	Magenta	FFG_740	736.70	Richey, 1989, Table 2, p.66
38	Magenta	FFG_741	702.90	Richey, 1989, Table 2, p.66
39	Magenta	FFG_742	753.70	Richey, 1989, Table 2, p.67
40	Magenta	FFG_743	740.40	Richey, 1989, Table 2, p.67
41	Magenta	FFG_744	722.90	Richey, 1989, Table 2, p.67
42	Magenta	FFG_745	708.90	Richey, 1989, Table 2, p.67
43	Magenta	FFG_746	699.10	Richey, 1989, Table 2, p.67
44	Magenta	H1	864.10	Mercer, 1983, Table 1
45	Magenta	H10C	741.00	Mercer, 1983, Table 1
46	Magenta	H2C	872.60	Mercer, 1983, Table 1
47	Magenta	H3	862.90	Mercer, 1983, Table 1
48	Magenta	H4C	901.30	Mercer, 1983, Table 1
49	Magenta	H5C	828.70	Mercer, 1983, Table 1
50	Magenta	H6C	871.10	Mercer, 1983, Table 1
51	Magenta	H7C	928.40	Mercer, 1983, Table 1
52	Magenta	H8C	904.40	Mercer, 1983, Table 1
53	Magenta	H9C	878.70	Mercer, 1983, Table 1
54	Magenta	P1	890.70	Mercer, 1983, Table 1
55	Magenta	P10	838.80	Mercer, 1983, Table 1
56	Magenta	P11	824.80	Mercer, 1983, Table 1
57	Magenta	P12	870.20	Mercer, 1983, Table 1
58	Magenta	P13	870.20	Mercer, 1983, Table 1
59	Magenta	P14	886.00	Mercer, 1983, Table 1
60	Magenta	P15	919.30	Mercer, 1983, Table 1
61	Magenta	P16	896.70	Mercer, 1983, Table 1
62	Magenta	P17	883.30	Mercer, 1983, Table 1
63	Magenta	P18	845.20	Mercer, 1983, Table 1
64	Magenta	P19	832.40	Mercer, 1983, Table 1
65	Magenta	P2	832.40	Mercer, 1983, Table 1
66	Magenta	P20	827.30	Mercer, 1983, Table 1
67	Magenta	P21	829.30	Mercer, 1983, Table 1
68	Magenta	P3	869.90	Mercer, 1983, Table 1
69	Magenta	P4	847.90	Mercer, 1983, Table 1
70	Magenta	P5	848.90	Mercer, 1983, Table 1
71	Magenta	P6	895.20	Mercer, 1983, Table 1
72	Magenta	P7	901.90	Mercer, 1983, Table 1
73	Magenta	P8	880.50	Mercer, 1983, Table 1
74	Magenta	P9	851.90	Mercer, 1983, Table 1
75	Magenta	REF	856.70	Rechard et al.,1991, Figure 2.2-1
76	Magenta	SaltShft	858.77	Bechtel, Inc., 1986, Appendix D

Table B.2. Elevations of Stratigraphic Layers Near WIPP (Continued)

	Layer	Well ID	Elevation	Source		Layer	Well ID	Elevation	Source
1	Magenta	WIPP11	822.60	Mercer, 1983, Table 1	39	Salado	FFG_011	570.30	Richey, 1989, Table 2, p.21
2	Magenta	WIPP11	822.70	SNL and USGS, 1982a, Table 2	40	Salado	FFG_012	572.10	Richey, 1989, Table 2, p.21
3	Magenta	WIPP12	847.30	SNL and D'Appolonia Consulting, 1983, Table 2	41	Salado	FFG_013	582.50	Richey, 1989, Table 2, p.21
4	Magenta	WIPP12	848.00	Mercer, 1983, Table 1	42	Salado	FFG_014	623.00	Richey, 1989, Table 2, p.21
5	Magenta	WIPP13	865.90	Mercer, 1983, Table 1	43	Salado	FFG_016	545.00	Richey, 1989, Table 2, p.21
6	Magenta	WIPP16	668.70	Mercer, 1983, Table 1	44	Salado	FFG_017	555.30	Richey, 1989, Table 2, p.22
7	Magenta	WIPP18	848.60	Mercer, 1983, Table 1	45	Salado	FFG_018	558.40	Richey, 1989, Table 2, p.22
8	Magenta	WIPP19	849.20	Mercer, 1983, Table 1	46	Salado	FFG_019	548.90	Richey, 1989, Table 2, p.22
9	Magenta	WIPP21	853.10	Mercer, 1983, Table 1	47	Salado	FFG_020	622.40	Richey, 1989, Table 2, p.22
10	Magenta	WIPP22	852.20	Mercer, 1983, Table 1	48	Salado	FFG_023	553.50	Richey, 1989, Table 2, p.22
11	Magenta	WIPP25	887.30	Mercer, 1983, Table 1	49	Salado	FFG_024	539.20	Richey, 1989, Table 2, p.22
12	Magenta	WIPP26	939.40	Mercer, 1983, Table 1	50	Salado	FFG_025	560.40	Richey, 1989, Table 2, p.22
13	Magenta	WIPP27	914.70	Mercer, 1983, Table 1	51	Salado	FFG_026	552.60	Richey, 1989, Table 2, p.22
14	Magenta	WIPP28	933.30	Mercer, 1983, Table 1	52	Salado	FFG_027	545.60	Richey, 1989, Table 2, p.22
15	Magenta	WIPP30	888.50	Mercer, 1983, Table 1	53	Salado	FFG_028	549.60	Richey, 1989, Table 2, p.22
16	Magenta	WIPP32	915.60	Mercer, 1983, Table 1	54	Salado	FFG_029	537.90	Richey, 1989, Table 2, p.22
17	Magenta	WIPP33	876.00	Mercer, 1983, Table 1	55	Salado	FFG_030	532.80	Richey, 1989, Table 2, p.22
18	Magenta	WIPP34	827.60	Mercer, 1983, Table 1	56	Salado	FFG_031	522.40	Richey, 1989, Table 2, p.22
19	Magenta	WastShft	857.36	Bechtel, Inc., 1986, Appendix E	57	Salado	FFG_032	519.00	Richey, 1989, Table 2, p.22
20	RSResid	AirShft	783.13	Holt and Powers, 1990, Figure 22	58	Salado	FFG_033	518.80	Richey, 1989, Table 2, p.22
21	RSResid	ExhtShft	779.98	Bechtel, Inc., 1986, Appendix F	59	Salado	FFG_034	517.80	Richey, 1989, Table 2, p.23
22	RSResid	SaltShft	780.44	Bechtel, Inc., 1986, Appendix D	60	Salado	FFG_035	504.90	Richey, 1989, Table 2, p.23
23	RSResid	WastShft	781.82	Bechtel, Inc., 1986, Appendix E	61	Salado	FFG_036	510.30	Richey, 1989, Table 2, p.23
24	ReposFlr	AirShft	383.74	Holt and Powers, 1990, Figure 22	62	Salado	FFG_037	502.90	Richey, 1989, Table 2, p.23
25	ReposFlr	ExhtShft	381.61	Bechtel, Inc., 1986, Appendix F	63	Salado	FFG_038	491.90	Richey, 1989, Table 2, p.23
26	ReposFlr	SaltShft	380.08	Bechtel, Inc., 1986, Appendix D	64	Salado	FFG_039	694.40	Richey, 1989, Table 2, p.23
27	ReposFlr	WastShft	380.70	Bechtel, Inc., 1986, Appendix E	65	Salado	FFG_040	624.90	Richey, 1989, Table 2, p.23
28	Salado	AEC7	811.60	Mercer, 1983, Table 1	66	Salado	FFG_041	691.90	Richey, 1989, Table 2, p.23
29	Salado	AEC8	776.40	Mercer, 1983, Table 1	67	Salado	FFG_042	695.20	Richey, 1989, Table 2, p.23
30	Salado	B25	782.20	Mercer, 1983, Table 1	68	Salado	FFG_043	697.00	Richey, 1989, Table 2, p.23
31	Salado	ERDA10	836.10	Mercer, 1983, Table 1	69	Salado	FFG_044	645.60	Richey, 1989, Table 2, p.23
32	Salado	ERDA6	830.60	Mercer, 1983, Table 1	70	Salado	FFG_047	526.10	Richey, 1989, Table 2, p.23
33	Salado	ERDA9	783.60	Mercer, 1983, Table 1	71	Salado	FFG_048	527.60	Richey, 1989, Table 2, p.23
34	Salado	FFG_002	578.80	Richey, 1989, Table 2, p.21	72	Salado	FFG_049	526.70	Richey, 1989, Table 2, p.23
35	Salado	FFG_004	627.90	Richey, 1989, Table 2, p.21	73	Salado	FFG_050	537.40	Richey, 1989, Table 2, p.24
36	Salado	FFG_005	581.90	Richey, 1989, Table 2, p.21	74	Salado	FFG_051	530.90	Richey, 1989, Table 2, p.24
37	Salado	FFG_007	559.00	Richey, 1989, Table 2, p.21	75	Salado	FFG_052	565.70	Richey, 1989, Table 2, p.24
38	Salado	FFG_009	575.10	Richey, 1989, Table 2, p.21	76	Salado	FFG_053	510.50	Richey, 1989, Table 2, p.24

Table B.2. Elevations of Stratigraphic Layers Near WIPP (Continued)

	Layer	Well ID	Elevation	Source
1	Salado	FFG_054	518.80	Richey, 1989, Table 2, p.24
2	Salado	FFG_055	521.20	Richey, 1989, Table 2, p.24
3	Salado	FFG_056	520.90	Richey, 1989, Table 2, p.24
4	Salado	FFG_057	524.60	Richey, 1989, Table 2, p.24
5	Salado	FFG_058	526.70	Richey, 1989, Table 2, p.24
6	Salado	FFG_059	529.70	Richey, 1989, Table 2, p.24
7	Salado	FFG_060	532.80	Richey, 1989, Table 2, p.24
8	Salado	FFG_061	532.50	Richey, 1989, Table 2, p.24
9	Salado	FFG_062	479.20	Richey, 1989, Table 2, p.24
10	Salado	FFG_063	438.40	Richey, 1989, Table 2, p.24
11	Salado	FFG_064	461.20	Richey, 1989, Table 2, p.24
12	Salado	FFG_065	449.60	Richey, 1989, Table 2, p.24
13	Salado	FFG_066	401.70	Richey, 1989, Table 2, p.24
14	Salado	FFG_067	435.90	Richey, 1989, Table 2, p.25
15	Salado	FFG_068	396.50	Richey, 1989, Table 2, p.25
16	Salado	FFG_069	407.90	Richey, 1989, Table 2, p.25
17	Salado	FFG_070	442.00	Richey, 1989, Table 2, p.25
18	Salado	FFG_071	700.20	Richey, 1989, Table 2, p.25
19	Salado	FFG_072	645.80	Richey, 1989, Table 2, p.25
20	Salado	FFG_073	623.30	Richey, 1989, Table 2, p.25
21	Salado	FFG_074	630.70	Richey, 1989, Table 2, p.25
22	Salado	FFG_075	683.40	Richey, 1989, Table 2, p.25
23	Salado	FFG_076	741.90	Richey, 1989, Table 2, p.25
24	Salado	FFG_078	776.90	Richey, 1989, Table 2, p.25
25	Salado	FFG_079	750.40	Richey, 1989, Table 2, p.25
26	Salado	FFG_080	727.50	Richey, 1989, Table 2, p.25
27	Salado	FFG_081	644.40	Richey, 1989, Table 2, p.26
28	Salado	FFG_082	673.00	Richey, 1989, Table 2, p.26
29	Salado	FFG_083	604.60	Richey, 1989, Table 2, p.26
30	Salado	FFG_084	626.00	Richey, 1989, Table 2, p.26
31	Salado	FFG_085	620.90	Richey, 1989, Table 2, p.26
32	Salado	FFG_086	630.30	Richey, 1989, Table 2, p.26
33	Salado	FFG_087	601.30	Richey, 1989, Table 2, p.26
34	Salado	FFG_088	595.30	Richey, 1989, Table 2, p.26
35	Salado	FFG_089	576.70	Richey, 1989, Table 2, p.26
36	Salado	FFG_091	614.20	Richey, 1989, Table 2, p.26
37	Salado	FFG_092	633.70	Richey, 1989, Table 2, p.26
38	Salado	FFG_093	637.70	Richey, 1989, Table 2, p.26
39	Salado	FFG_094	637.00	Richey, 1989, Table 2, p.26
40	Salado	FFG_095	618.70	Richey, 1989, Table 2, p.26
41	Salado	FFG_096	605.00	Richey, 1989, Table 2, p.26
42	Salado	FFG_097	580.60	Richey, 1989, Table 2, p.27
43	Salado	FFG_098	555.90	Richey, 1989, Table 2, p.27
44	Salado	FFG_099	550.20	Richey, 1989, Table 2, p.27
45	Salado	FFG_100	530.40	Richey, 1989, Table 2, p.27
46	Salado	FFG_101	500.20	Richey, 1989, Table 2, p.27
47	Salado	FFG_102	512.40	Richey, 1989, Table 2, p.27
48	Salado	FFG_104	474.30	Richey, 1989, Table 2, p.27
49	Salado	FFG_105	812.90	Richey, 1989, Table 2, p.27
50	Salado	FFG_106	840.70	Richey, 1989, Table 2, p.27
51	Salado	FFG_107	836.10	Richey, 1989, Table 2, p.27
52	Salado	FFG_108	836.10	Richey, 1989, Table 2, p.27
53	Salado	FFG_109	831.80	Richey, 1989, Table 2, p.27
54	Salado	FFG_110	798.60	Richey, 1989, Table 2, p.27
55	Salado	FFG_111	806.20	Richey, 1989, Table 2, p.27
56	Salado	FFG_112	784.80	Richey, 1989, Table 2, p.28
57	Salado	FFG_113	802.20	Richey, 1989, Table 2, p.28
58	Salado	FFG_114	828.80	Richey, 1989, Table 2, p.28
59	Salado	FFG_115	803.50	Richey, 1989, Table 2, p.28
60	Salado	FFG_116	795.20	Richey, 1989, Table 2, p.28
61	Salado	FFG_117	810.80	Richey, 1989, Table 2, p.28
62	Salado	FFG_119	828.20	Richey, 1989, Table 2, p.28
63	Salado	FFG_120	819.30	Richey, 1989, Table 2, p.28
64	Salado	FFG_121	830.60	Richey, 1989, Table 2, p.28
65	Salado	FFG_122	813.80	Richey, 1989, Table 2, p.28
66	Salado	FFG_123	815.30	Richey, 1989, Table 2, p.28
67	Salado	FFG_124	785.50	Richey, 1989, Table 2, p.28
68	Salado	FFG_126	813.00	Richey, 1989, Table 2, p.28
69	Salado	FFG_127	824.10	Richey, 1989, Table 2, p.28
70	Salado	FFG_128	852.60	Richey, 1989, Table 2, p.28
71	Salado	FFG_129	815.60	Richey, 1989, Table 2, p.28
72	Salado	FFG_130	854.90	Richey, 1989, Table 2, p.28
73	Salado	FFG_132	852.80	Richey, 1989, Table 2, p.29
74	Salado	FFG_133	837.60	Richey, 1989, Table 2, p.29
75	Salado	FFG_134	861.70	Richey, 1989, Table 2, p.29
76	Salado	FFG_135	844.00	Richey, 1989, Table 2, p.29

Table B.2. Elevations of Stratigraphic Layers Near WIPP (Continued)

	Layer	Well ID	Elevation	Source
1	Salado	FFG_136	844.40	Richey, 1989, Table 2, p.29
2	Salado	FFG_137	853.20	Richey, 1989, Table 2, p.29
3	Salado	FFG_138	798.30	Richey, 1989, Table 2, p.29
4	Salado	FFG_139	810.10	Richey, 1989, Table 2, p.29
5	Salado	FFG_140	750.00	Richey, 1989, Table 2, p.29
6	Salado	FFG_141	782.90	Richey, 1989, Table 2, p.29
7	Salado	FFG_142	757.80	Richey, 1989, Table 2, p.29
8	Salado	FFG_144	825.10	Richey, 1989, Table 2, p.29
9	Salado	FFG_145	830.60	Richey, 1989, Table 2, p.29
10	Salado	FFG_146	826.00	Richey, 1989, Table 2, p.29
11	Salado	FFG_147	816.30	Richey, 1989, Table 2, p.29
12	Salado	FFG_148	832.10	Richey, 1989, Table 2, p.29
13	Salado	FFG_149	842.10	Richey, 1989, Table 2, p.30
14	Salado	FFG_152	836.70	Richey, 1989, Table 2, p.30
15	Salado	FFG_155	830.90	Richey, 1989, Table 2, p.30
16	Salado	FFG_156	837.60	Richey, 1989, Table 2, p.30
17	Salado	FFG_158	856.80	Richey, 1989, Table 2, p.30
18	Salado	FFG_159	859.60	Richey, 1989, Table 2, p.30
19	Salado	FFG_160	855.60	Richey, 1989, Table 2, p.30
20	Salado	FFG_161	856.80	Richey, 1989, Table 2, p.30
21	Salado	FFG_162	857.70	Richey, 1989, Table 2, p.30
22	Salado	FFG_163	856.20	Richey, 1989, Table 2, p.30
23	Salado	FFG_164	854.70	Richey, 1989, Table 2, p.30
24	Salado	FFG_165	838.80	Richey, 1989, Table 2, p.30
25	Salado	FFG_166	858.30	Richey, 1989, Table 2, p.31
26	Salado	FFG_167	836.70	Richey, 1989, Table 2, p.31
27	Salado	FFG_168	843.10	Richey, 1989, Table 2, p.31
28	Salado	FFG_169	861.30	Richey, 1989, Table 2, p.31
29	Salado	FFG_170	839.10	Richey, 1989, Table 2, p.31
30	Salado	FFG_171	848.00	Richey, 1989, Table 2, p.31
31	Salado	FFG_172	851.90	Richey, 1989, Table 2, p.31
32	Salado	FFG_173	831.50	Richey, 1989, Table 2, p.31
33	Salado	FFG_177	812.60	Richey, 1989, Table 2, p.31
34	Salado	FFG_178	539.20	Richey, 1989, Table 2, p.31
35	Salado	FFG_179	816.80	Richey, 1989, Table 2, p.31
36	Salado	FFG_180	825.10	Richey, 1989, Table 2, p.31
37	Salado	FFG_181	869.00	Richey, 1989, Table 2, p.32
38	Salado	FFG_182	757.10	Richey, 1989, Table 2, p.32
39	Salado	FFG_183	837.30	Richey, 1989, Table 2, p.32
40	Salado	FFG_184	851.60	Richey, 1989, Table 2, p.32
41	Salado	FFG_185	840.00	Richey, 1989, Table 2, p.32
42	Salado	FFG_186	766.30	Richey, 1989, Table 2, p.32
43	Salado	FFG_188	781.20	Richey, 1989, Table 2, p.32
44	Salado	FFG_189	805.00	Richey, 1989, Table 2, p.32
45	Salado	FFG_190	793.40	Richey, 1989, Table 2, p.32
46	Salado	FFG_191	780.00	Richey, 1989, Table 2, p.32
47	Salado	FFG_192	708.00	Richey, 1989, Table 2, p.32
48	Salado	FFG_194	738.80	Richey, 1989, Table 2, p.33
49	Salado	FFG_195	753.50	Richey, 1989, Table 2, p.33
50	Salado	FFG_196	792.50	Richey, 1989, Table 2, p.33
51	Salado	FFG_197	790.10	Richey, 1989, Table 2, p.33
52	Salado	FFG_198	783.90	Richey, 1989, Table 2, p.33
53	Salado	FFG_199	780.60	Richey, 1989, Table 2, p.33
54	Salado	FFG_200	785.20	Richey, 1989, Table 2, p.33
55	Salado	FFG_201	778.70	Richey, 1989, Table 2, p.33
56	Salado	FFG_202	723.60	Richey, 1989, Table 2, p.33
57	Salado	FFG_203	727.60	Richey, 1989, Table 2, p.33
58	Salado	FFG_204	767.20	Richey, 1989, Table 2, p.33
59	Salado	FFG_205	768.50	Richey, 1989, Table 2, p.33
60	Salado	FFG_206	779.40	Richey, 1989, Table 2, p.33
61	Salado	FFG_207	775.70	Richey, 1989, Table 2, p.33
62	Salado	FFG_208	780.30	Richey, 1989, Table 2, p.34
63	Salado	FFG_209	787.30	Richey, 1989, Table 2, p.34
64	Salado	FFG_210	766.00	Richey, 1989, Table 2, p.34
65	Salado	FFG_212	768.40	Richey, 1989, Table 2, p.34
66	Salado	FFG_213	795.30	Richey, 1989, Table 2, p.34
67	Salado	FFG_214	757.70	Richey, 1989, Table 2, p.34
68	Salado	FFG_215	734.60	Richey, 1989, Table 2, p.34
69	Salado	FFG_216	520.60	Richey, 1989, Table 2, p.34
70	Salado	FFG_217	756.30	Richey, 1989, Table 2, p.34
71	Salado	FFG_218	744.00	Richey, 1989, Table 2, p.34
72	Salado	FFG_219	783.30	Richey, 1989, Table 2, p.34
73	Salado	FFG_220	742.20	Richey, 1989, Table 2, p.34
74	Salado	FFG_221	684.90	Richey, 1989, Table 2, p.34
75	Salado	FFG_222	604.50	Richey, 1989, Table 2, p.34
76	Salado	FFG_224	558.10	Richey, 1989, Table 2, p.35

Table B.2. Elevations of Stratigraphic Layers Near WIPP (Continued)

	Layer	Well ID	Elevation	Source
1	Salado	FFG_225	566.30	Richey, 1989, Table 2, p.35
2	Salado	FFG_226	561.90	Richey, 1989, Table 2, p.35
3	Salado	FFG_228	549.30	Richey, 1989, Table 2, p.35
4	Salado	FFG_229	572.10	Richey, 1989, Table 2, p.35
5	Salado	FFG_230	558.40	Richey, 1989, Table 2, p.35
6	Salado	FFG_231	578.20	Richey, 1989, Table 2, p.35
7	Salado	FFG_232	586.10	Richey, 1989, Table 2, p.35
8	Salado	FFG_233	581.90	Richey, 1989, Table 2, p.35
9	Salado	FFG_234	616.30	Richey, 1989, Table 2, p.35
10	Salado	FFG_235	595.90	Richey, 1989, Table 2, p.35
11	Salado	FFG_236	641.90	Richey, 1989, Table 2, p.35
12	Salado	FFG_237	600.80	Richey, 1989, Table 2, p.35
13	Salado	FFG_238	584.30	Richey, 1989, Table 2, p.36
14	Salado	FFG_239	570.50	Richey, 1989, Table 2, p.36
15	Salado	FFG_240	568.80	Richey, 1989, Table 2, p.36
16	Salado	FFG_241	562.70	Richey, 1989, Table 2, p.36
17	Salado	FFG_242	681.30	Richey, 1989, Table 2, p.36
18	Salado	FFG_243	615.10	Richey, 1989, Table 2, p.36
19	Salado	FFG_244	689.30	Richey, 1989, Table 2, p.36
20	Salado	FFG_245	470.60	Richey, 1989, Table 2, p.36
21	Salado	FFG_246	473.10	Richey, 1989, Table 2, p.36
22	Salado	FFG_247	460.10	Richey, 1989, Table 2, p.36
23	Salado	FFG_248	464.50	Richey, 1989, Table 2, p.36
24	Salado	FFG_249	464.20	Richey, 1989, Table 2, p.36
25	Salado	FFG_250	545.50	Richey, 1989, Table 2, p.36
26	Salado	FFG_251	432.20	Richey, 1989, Table 2, p.36
27	Salado	FFG_252	567.50	Richey, 1989, Table 2, p.36
28	Salado	FFG_253	521.90	Richey, 1989, Table 2, p.36
29	Salado	FFG_254	517.80	Richey, 1989, Table 2, p.36
30	Salado	FFG_255	467.30	Richey, 1989, Table 2, p.37
31	Salado	FFG_256	438.90	Richey, 1989, Table 2, p.37
32	Salado	FFG_257	484.00	Richey, 1989, Table 2, p.37
33	Salado	FFG_258	497.70	Richey, 1989, Table 2, p.37
34	Salado	FFG_259	456.80	Richey, 1989, Table 2, p.37
35	Salado	FFG_260	515.10	Richey, 1989, Table 2, p.37
36	Salado	FFG_261	502.60	Richey, 1989, Table 2, p.37
37	Salado	FFG_262	440.50	Richey, 1989, Table 2, p.37
38	Salado	FFG_263	406.80	Richey, 1989, Table 2, p.37
39	Salado	FFG_264	653.50	Richey, 1989, Table 2, p.37
40	Salado	FFG_265	634.60	Richey, 1989, Table 2, p.37
41	Salado	FFG_266	609.60	Richey, 1989, Table 2, p.37
42	Salado	FFG_267	582.70	Richey, 1989, Table 2, p.37
43	Salado	FFG_268	563.30	Richey, 1989, Table 2, p.37
44	Salado	FFG_269	568.30	Richey, 1989, Table 2, p.38
45	Salado	FFG_270	689.40	Richey, 1989, Table 2, p.38
46	Salado	FFG_271	733.30	Richey, 1989, Table 2, p.38
47	Salado	FFG_272	697.20	Richey, 1989, Table 2, p.38
48	Salado	FFG_273	701.70	Richey, 1989, Table 2, p.38
49	Salado	FFG_274	747.40	Richey, 1989, Table 2, p.38
50	Salado	FFG_275	767.20	Richey, 1989, Table 2, p.38
51	Salado	FFG_276	766.20	Richey, 1989, Table 2, p.38
52	Salado	FFG_277	753.50	Richey, 1989, Table 2, p.38
53	Salado	FFG_278	722.40	Richey, 1989, Table 2, p.38
54	Salado	FFG_279	735.70	Richey, 1989, Table 2, p.38
55	Salado	FFG_280	738.20	Richey, 1989, Table 2, p.38
56	Salado	FFG_281	709.30	Richey, 1989, Table 2, p.38
57	Salado	FFG_283	450.50	Richey, 1989, Table 2, p.39
58	Salado	FFG_284	596.20	Richey, 1989, Table 2, p.39
59	Salado	FFG_285	616.00	Richey, 1989, Table 2, p.39
60	Salado	FFG_286	728.70	Richey, 1989, Table 2, p.39
61	Salado	FFG_287	693.10	Richey, 1989, Table 2, p.39
62	Salado	FFG_288	616.90	Richey, 1989, Table 2, p.39
63	Salado	FFG_289	639.10	Richey, 1989, Table 2, p.39
64	Salado	FFG_290	733.40	Richey, 1989, Table 2, p.39
65	Salado	FFG_291	615.10	Richey, 1989, Table 2, p.39
66	Salado	FFG_292	686.70	Richey, 1989, Table 2, p.39
67	Salado	FFG_293	672.40	Richey, 1989, Table 2, p.39
68	Salado	FFG_294	458.20	Richey, 1989, Table 2, p.39
69	Salado	FFG_295	438.90	Richey, 1989, Table 2, p.39
70	Salado	FFG_297	420.30	Richey, 1989, Table 2, p.39
71	Salado	FFG_298	490.00	Richey, 1989, Table 2, p.40
72	Salado	FFG_299	441.40	Richey, 1989, Table 2, p.40
73	Salado	FFG_300	416.90	Richey, 1989, Table 2, p.40
74	Salado	FFG_301	359.40	Richey, 1989, Table 2, p.40
75	Salado	FFG_302	420.30	Richey, 1989, Table 2, p.40
76	Salado	FFG_303	404.80	Richey, 1989, Table 2, p.40

Table B.2. Elevations of Stratigraphic Layers Near WIPP (Continued)

	Layer	Well ID	Elevation	Source
1	Salado	FFG_304	399.30	Richey, 1989, Table 2, p.40
2	Salado	FFG_305	399.60	Richey, 1989, Table 2, p.40
3	Salado	FFG_306	361.40	Richey, 1989, Table 2, p.40
4	Salado	FFG_307	383.80	Richey, 1989, Table 2, p.40
5	Salado	FFG_308	323.00	Richey, 1989, Table 2, p.40
6	Salado	FFG_309	388.60	Richey, 1989, Table 2, p.40
7	Salado	FFG_310	430.00	Richey, 1989, Table 2, p.40
8	Salado	FFG_311	387.40	Richey, 1989, Table 2, p.40
9	Salado	FFG_312	384.10	Richey, 1989, Table 2, p.40
10	Salado	FFG_313	832.20	Richey, 1989, Table 2, p.41
11	Salado	FFG_314	734.90	Richey, 1989, Table 2, p.41
12	Salado	FFG_315	650.90	Richey, 1989, Table 2, p.41
13	Salado	FFG_316	624.20	Richey, 1989, Table 2, p.41
14	Salado	FFG_317	693.10	Richey, 1989, Table 2, p.41
15	Salado	FFG_318	666.00	Richey, 1989, Table 2, p.41
16	Salado	FFG_319	662.00	Richey, 1989, Table 2, p.41
17	Salado	FFG_320	616.00	Richey, 1989, Table 2, p.41
18	Salado	FFG_321	612.90	Richey, 1989, Table 2, p.41
19	Salado	FFG_322	616.80	Richey, 1989, Table 2, p.41
20	Salado	FFG_323	626.80	Richey, 1989, Table 2, p.41
21	Salado	FFG_324	653.20	Richey, 1989, Table 2, p.41
22	Salado	FFG_325	713.50	Richey, 1989, Table 2, p.41
23	Salado	FFG_326	657.50	Richey, 1989, Table 2, p.41
24	Salado	FFG_327	645.30	Richey, 1989, Table 2, p.42
25	Salado	FFG_328	620.50	Richey, 1989, Table 2, p.42
26	Salado	FFG_329	613.20	Richey, 1989, Table 2, p.42
27	Salado	FFG_330	611.60	Richey, 1989, Table 2, p.42
28	Salado	FFG_331	602.60	Richey, 1989, Table 2, p.42
29	Salado	FFG_332	587.00	Richey, 1989, Table 2, p.42
30	Salado	FFG_333	598.80	Richey, 1989, Table 2, p.42
31	Salado	FFG_334	589.10	Richey, 1989, Table 2, p.42
32	Salado	FFG_335	607.80	Richey, 1989, Table 2, p.42
33	Salado	FFG_336	603.20	Richey, 1989, Table 2, p.42
34	Salado	FFG_337	584.60	Richey, 1989, Table 2, p.42
35	Salado	FFG_338	589.60	Richey, 1989, Table 2, p.42
36	Salado	FFG_339	553.80	Richey, 1989, Table 2, p.42
37	Salado	FFG_340	559.90	Richey, 1989, Table 2, p.42
38	Salado	FFG_342	651.60	Richey, 1989, Table 2, p.43
39	Salado	FFG_344	622.60	Richey, 1989, Table 2, p.43
40	Salado	FFG_345	628.60	Richey, 1989, Table 2, p.43
41	Salado	FFG_347	655.30	Richey, 1989, Table 2, p.43
42	Salado	FFG_348	686.10	Richey, 1989, Table 2, p.43
43	Salado	FFG_349	678.80	Richey, 1989, Table 2, p.43
44	Salado	FFG_350	712.30	Richey, 1989, Table 2, p.43
45	Salado	FFG_351	571.50	Richey, 1989, Table 2, p.43
46	Salado	FFG_352	573.10	Richey, 1989, Table 2, p.43
47	Salado	FFG_353	598.40	Richey, 1989, Table 2, p.43
48	Salado	FFG_354	722.40	Richey, 1989, Table 2, p.43
49	Salado	FFG_361	905.80	Richey, 1989, Table 2, p.44
50	Salado	FFG_362	841.50	Richey, 1989, Table 2, p.44
51	Salado	FFG_363	881.50	Richey, 1989, Table 2, p.44
52	Salado	FFG_366	863.80	Richey, 1989, Table 2, p.44
53	Salado	FFG_367	876.90	Richey, 1989, Table 2, p.44
54	Salado	FFG_370	919.30	Richey, 1989, Table 2, p.44
55	Salado	FFG_371	919.90	Richey, 1989, Table 2, p.44
56	Salado	FFG_374	855.00	Richey, 1989, Table 2, p.45
57	Salado	FFG_376	896.40	Richey, 1989, Table 2, p.45
58	Salado	FFG_381	875.10	Richey, 1989, Table 2, p.45
59	Salado	FFG_383	867.20	Richey, 1989, Table 2, p.45
60	Salado	FFG_385	856.50	Richey, 1989, Table 2, p.45
61	Salado	FFG_387	862.00	Richey, 1989, Table 2, p.45
62	Salado	FFG_390	863.50	Richey, 1989, Table 2, p.46
63	Salado	FFG_391	868.30	Richey, 1989, Table 2, p.46
64	Salado	FFG_392	863.20	Richey, 1989, Table 2, p.46
65	Salado	FFG_393	752.70	Richey, 1989, Table 2, p.46
66	Salado	FFG_394	846.70	Richey, 1989, Table 2, p.46
67	Salado	FFG_395	842.20	Richey, 1989, Table 2, p.46
68	Salado	FFG_396	787.30	Richey, 1989, Table 2, p.46
69	Salado	FFG_403	846.90	Richey, 1989, Table 2, p.47
70	Salado	FFG_408	827.80	Richey, 1989, Table 2, p.47
71	Salado	FFG_411	789.10	Richey, 1989, Table 2, p.47
72	Salado	FFG_413	835.20	Richey, 1989, Table 2, p.47
73	Salado	FFG_421	879.40	Richey, 1989, Table 2, p.48
74	Salado	FFG_426	856.50	Richey, 1989, Table 2, p.48
75	Salado	FFG_432	837.30	Richey, 1989, Table 2, p.48
76	Salado	FFG_433	816.80	Richey, 1989, Table 2, p.48

Table B.2. Elevations of Stratigraphic Layers Near WIPP (Continued)

	Layer	Well ID	Elevation	Source
1	Salado	FFG_438	797.50	Richey, 1989, Table 2, p.49
2	Salado	FFG_445	827.20	Richey, 1989, Table 2, p.49
3	Salado	FFG_453	726.50	Richey, 1989, Table 2, p.50
4	Salado	FFG_455	723.90	Richey, 1989, Table 2, p.50
5	Salado	FFG_456	730.90	Richey, 1989, Table 2, p.50
6	Salado	FFG_457	784.50	Richey, 1989, Table 2, p.50
7	Salado	FFG_458	785.50	Richey, 1989, Table 2, p.50
8	Salado	FFG_459	717.20	Richey, 1989, Table 2, p.50
9	Salado	FFG_462	781.30	Richey, 1989, Table 2, p.50
10	Salado	FFG_463	811.40	Richey, 1989, Table 2, p.51
11	Salado	FFG_464	787.60	Richey, 1989, Table 2, p.51
12	Salado	FFG_465	783.90	Richey, 1989, Table 2, p.51
13	Salado	FFG_467	380.30	Richey, 1989, Table 2, p.51
14	Salado	FFG_468	322.20	Richey, 1989, Table 2, p.51
15	Salado	FFG_470	360.00	Richey, 1989, Table 2, p.51
16	Salado	FFG_471	372.40	Richey, 1989, Table 2, p.51
17	Salado	FFG_472	439.30	Richey, 1989, Table 2, p.51
18	Salado	FFG_473	339.50	Richey, 1989, Table 2, p.51
19	Salado	FFG_474	634.90	Richey, 1989, Table 2, p.51
20	Salado	FFG_475	637.80	Richey, 1989, Table 2, p.51
21	Salado	FFG_476	711.40	Richey, 1989, Table 2, p.51
22	Salado	FFG_477	679.70	Richey, 1989, Table 2, p.51
23	Salado	FFG_478	655.30	Richey, 1989, Table 2, p.52
24	Salado	FFG_479	661.10	Richey, 1989, Table 2, p.52
25	Salado	FFG_480	641.60	Richey, 1989, Table 2, p.52
26	Salado	FFG_481	635.20	Richey, 1989, Table 2, p.52
27	Salado	FFG_482	665.40	Richey, 1989, Table 2, p.52
28	Salado	FFG_483	690.90	Richey, 1989, Table 2, p.52
29	Salado	FFG_484	672.20	Richey, 1989, Table 2, p.52
30	Salado	FFG_485	682.80	Richey, 1989, Table 2, p.52
31	Salado	FFG_486	668.70	Richey, 1989, Table 2, p.52
32	Salado	FFG_487	669.40	Richey, 1989, Table 2, p.52
33	Salado	FFG_488	648.90	Richey, 1989, Table 2, p.52
34	Salado	FFG_489	663.10	Richey, 1989, Table 2, p.52
35	Salado	FFG_490	765.70	Richey, 1989, Table 2, p.52
36	Salado	FFG_491	752.60	Richey, 1989, Table 2, p.52
37	Salado	FFG_492	720.50	Richey, 1989, Table 2, p.52
38	Salado	FFG_493	709.70	Richey, 1989, Table 2, p.53
39	Salado	FFG_494	713.20	Richey, 1989, Table 2, p.53
40	Salado	FFG_495	696.40	Richey, 1989, Table 2, p.53
41	Salado	FFG_496	555.40	Richey, 1989, Table 2, p.53
42	Salado	FFG_497	601.70	Richey, 1989, Table 2, p.53
43	Salado	FFG_498	589.20	Richey, 1989, Table 2, p.53
44	Salado	FFG_499	549.90	Richey, 1989, Table 2, p.53
45	Salado	FFG_500	582.80	Richey, 1989, Table 2, p.53
46	Salado	FFG_501	625.40	Richey, 1989, Table 2, p.53
47	Salado	FFG_502	567.20	Richey, 1989, Table 2, p.53
48	Salado	FFG_503	573.70	Richey, 1989, Table 2, p.53
49	Salado	FFG_504	618.80	Richey, 1989, Table 2, p.53
50	Salado	FFG_505	650.50	Richey, 1989, Table 2, p.53
51	Salado	FFG_506	649.50	Richey, 1989, Table 2, p.53
52	Salado	FFG_507	549.10	Richey, 1989, Table 2, p.53
53	Salado	FFG_508	628.80	Richey, 1989, Table 2, p.53
54	Salado	FFG_509	616.30	Richey, 1989, Table 2, p.54
55	Salado	FFG_510	615.20	Richey, 1989, Table 2, p.54
56	Salado	FFG_511	570.60	Richey, 1989, Table 2, p.54
57	Salado	FFG_512	576.70	Richey, 1989, Table 2, p.54
58	Salado	FFG_513	606.00	Richey, 1989, Table 2, p.54
59	Salado	FFG_514	577.30	Richey, 1989, Table 2, p.54
60	Salado	FFG_515	556.20	Richey, 1989, Table 2, p.54
61	Salado	FFG_516	545.90	Richey, 1989, Table 2, p.54
62	Salado	FFG_517	732.50	Richey, 1989, Table 2, p.54
63	Salado	FFG_518	720.20	Richey, 1989, Table 2, p.54
64	Salado	FFG_519	659.90	Richey, 1989, Table 2, p.54
65	Salado	FFG_520	542.70	Richey, 1989, Table 2, p.54
66	Salado	FFG_521	604.70	Richey, 1989, Table 2, p.54
67	Salado	FFG_522	382.40	Richey, 1989, Table 2, p.54
68	Salado	FFG_523	388.90	Richey, 1989, Table 2, p.54
69	Salado	FFG_524	561.70	Richey, 1989, Table 2, p.55
70	Salado	FFG_525	388.40	Richey, 1989, Table 2, p.55
71	Salado	FFG_526	911.10	Richey, 1989, Table 2, p.55
72	Salado	FFG_527	871.10	Richey, 1989, Table 2, p.55
73	Salado	FFG_528	864.10	Richey, 1989, Table 2, p.55
74	Salado	FFG_530	930.20	Richey, 1989, Table 2, p.55
75	Salado	FFG_531	855.20	Richey, 1989, Table 2, p.55
76	Salado	FFG_532	838.50	Richey, 1989, Table 2, p.55

Table B.2. Elevations of Stratigraphic Layers Near WIPP (Continued)

	Layer	Well ID	Elevation	Source
1	Salado	FFG_535	850.40	Richey, 1989, Table 2, p.55
2	Salado	FFG_536	853.50	Richey, 1989, Table 2, p.55
3	Salado	FFG_537	840.60	Richey, 1989, Table 2, p.55
4	Salado	FFG_564	557.80	Richey, 1989, Table 2, p.57
5	Salado	FFG_584	690.90	Richey, 1989, Table 2, p.58
6	Salado	FFG_585	643.40	Richey, 1989, Table 2, p.58
7	Salado	FFG_602	743.70	Richey, 1989, Table 2, p.58
8	Salado	FFG_606	603.20	Richey, 1989, Table 2, p.58
9	Salado	FFG_607	624.30	Richey, 1989, Table 2, p.59
10	Salado	FFG_608	593.70	Richey, 1989, Table 2, p.59
11	Salado	FFG_609	586.10	Richey, 1989, Table 2, p.59
12	Salado	FFG_610	588.30	Richey, 1989, Table 2, p.59
13	Salado	FFG_611	579.40	Richey, 1989, Table 2, p.59
14	Salado	FFG_612	624.90	Richey, 1989, Table 2, p.59
15	Salado	FFG_613	621.80	Richey, 1989, Table 2, p.59
16	Salado	FFG_640	519.50	Richey, 1989, Table 2, p.60
17	Salado	FFG_643	576.10	Richey, 1989, Table 2, p.60
18	Salado	FFG_652	786.40	Richey, 1989, Table 2, p.60
19	Salado	FFG_653	788.60	Richey, 1989, Table 2, p.61
20	Salado	FFG_654	812.30	Richey, 1989, Table 2, p.61
21	Salado	FFG_655	812.90	Richey, 1989, Table 2, p.61
22	Salado	FFG_656	808.90	Richey, 1989, Table 2, p.61
23	Salado	FFG_657	830.00	Richey, 1989, Table 2, p.61
24	Salado	FFG_658	816.20	Richey, 1989, Table 2, p.61
25	Salado	FFG_659	821.10	Richey, 1989, Table 2, p.61
26	Salado	FFG_660	845.10	Richey, 1989, Table 2, p.61
27	Salado	FFG_662	810.20	Richey, 1989, Table 2, p.61
28	Salado	FFG_664	794.90	Richey, 1989, Table 2, p.61
29	Salado	FFG_666	860.10	Richey, 1989, Table 2, p.62
30	Salado	FFG_667	845.80	Richey, 1989, Table 2, p.62
31	Salado	FFG_668	905.10	Richey, 1989, Table 2, p.62
32	Salado	FFG_669	890.60	Richey, 1989, Table 2, p.62
33	Salado	FFG_670	876.00	Richey, 1989, Table 2, p.62
34	Salado	FFG_671	873.50	Richey, 1989, Table 2, p.62
35	Salado	FFG_672	868.10	Richey, 1989, Table 2, p.62
36	Salado	FFG_673	870.50	Richey, 1989, Table 2, p.62
37	Salado	FFG_674	860.20	Richey, 1989, Table 2, p.62
38	Salado	FFG_675	819.20	Richey, 1989, Table 2, p.62
39	Salado	FFG_676	831.80	Richey, 1989, Table 2, p.62
40	Salado	FFG_677	857.10	Richey, 1989, Table 2, p.62
41	Salado	FFG_679	861.10	Richey, 1989, Table 2, p.62
42	Salado	FFG_685	825.70	Richey, 1989, Table 2, p.63
43	Salado	FFG_689	718.10	Richey, 1989, Table 2, p.63
44	Salado	FFG_690	718.10	Richey, 1989, Table 2, p.63
45	Salado	FFG_691	711.40	Richey, 1989, Table 2, p.63
46	Salado	FFG_693	712.60	Richey, 1989, Table 2, p.63
47	Salado	FFG_694	680.30	Richey, 1989, Table 2, p.63
48	Salado	FFG_695	702.60	Richey, 1989, Table 2, p.63
49	Salado	FFG_696	703.10	Richey, 1989, Table 2, p.63
50	Salado	FFG_697	699.90	Richey, 1989, Table 2, p.64
51	Salado	FFG_698	734.90	Richey, 1989, Table 2, p.64
52	Salado	FFG_699	691.00	Richey, 1989, Table 2, p.64
53	Salado	FFG_700	682.20	Richey, 1989, Table 2, p.64
54	Salado	FFG_701	686.50	Richey, 1989, Table 2, p.64
55	Salado	FFG_702	693.70	Richey, 1989, Table 2, p.64
56	Salado	FFG_703	716.90	Richey, 1989, Table 2, p.64
57	Salado	FFG_704	686.40	Richey, 1989, Table 2, p.64
58	Salado	FFG_705	610.80	Richey, 1989, Table 2, p.64
59	Salado	FFG_706	637.10	Richey, 1989, Table 2, p.64
60	Salado	FFG_707	616.70	Richey, 1989, Table 2, p.64
61	Salado	FFG_708	669.70	Richey, 1989, Table 2, p.64
62	Salado	FFG_710	579.20	Richey, 1989, Table 2, p.64
63	Salado	FFG_711	570.60	Richey, 1989, Table 2, p.65
64	Salado	FFG_716	553.10	Richey, 1989, Table 2, p.65
65	Salado	FFG_717	621.90	Richey, 1989, Table 2, p.65
66	Salado	FFG_718	612.80	Richey, 1989, Table 2, p.65
67	Salado	FFG_719	571.20	Richey, 1989, Table 2, p.65
68	Salado	FFG_720	570.60	Richey, 1989, Table 2, p.65
69	Salado	FFG_721	594.40	Richey, 1989, Table 2, p.65
70	Salado	FFG_723	712.50	Richey, 1989, Table 2, p.65
71	Salado	FFG_724	633.80	Richey, 1989, Table 2, p.65
72	Salado	FFG_725	610.50	Richey, 1989, Table 2, p.65
73	Salado	FFG_726	589.10	Richey, 1989, Table 2, p.65
74	Salado	FFG_727	575.50	Richey, 1989, Table 2, p.66
75	Salado	FFG_728	590.40	Richey, 1989, Table 2, p.66
76	Salado	FFG_729	595.90	Richey, 1989, Table 2, p.66

Table B.2. Elevations of Stratigraphic Layers Near WIPP (Continued)

	Layer	Well ID	Elevation	Source		Layer	Well ID	Elevation	Source
1	Salado	FFG_730	622.70	Richey, 1989, Table 2, p.66	39	Salado	P20	746.80	Mercer, 1983, Table 1
2	Salado	FFG_731	617.70	Richey, 1989, Table 2, p.66	40	Salado	P21	751.60	Mercer, 1983, Table 1
3	Salado	FFG_733	698.30	Richey, 1989, Table 2, p.66	41	Salado	P3	791.50	Mercer, 1983, Table 1
4	Salado	FFG_734	654.10	Richey, 1989, Table 2, p.66	42	Salado	P4	766.20	Mercer, 1983, Table 1
5	Salado	FFG_735	584.00	Richey, 1989, Table 2, p.66	43	Salado	P5	769.40	Mercer, 1983, Table 1
6	Salado	FFG_736	615.40	Richey, 1989, Table 2, p.66	44	Salado	P6	821.40	Mercer, 1983, Table 1
7	Salado	FFG_737	559.30	Richey, 1989, Table 2, p.66	45	Salado	P7	823.60	Mercer, 1983, Table 1
8	Salado	FFG_738	610.20	Richey, 1989, Table 2, p.66	46	Salado	P8	799.80	Mercer, 1983, Table 1
9	Salado	FFG_739	628.60	Richey, 1989, Table 2, p.66	47	Salado	P9	771.50	Mercer, 1983, Table 1
10	Salado	FFG_740	609.00	Richey, 1989, Table 2, p.66	48	Salado	WIPP11	754.30	Mercer, 1983, Table 1
11	Salado	FFG_741	602.30	Richey, 1989, Table 2, p.66	49	Salado	WIPP12	767.20	Mercer, 1983, Table 1
12	Salado	FFG_742	646.50	Richey, 1989, Table 2, p.67	50	Salado	WIPP13	780.50	Mercer, 1983, Table 1
13	Salado	FFG_743	630.70	Richey, 1989, Table 2, p.67	51	Salado	WIPP18	770.50	Mercer, 1983, Table 1
14	Salado	FFG_744	630.00	Richey, 1989, Table 2, p.67	52	Salado	WIPP19	773.90	Mercer, 1983, Table 1
15	Salado	FFG_745	598.30	Richey, 1989, Table 2, p.67	53	Salado	WIPP21	776.90	Mercer, 1983, Table 1
16	Salado	FFG_746	581.80	Richey, 1989, Table 2, p.67	54	Salado	WIPP22	775.10	Mercer, 1983, Table 1
17	Salado	H1	784.50	Mercer, 1983, Table 1	55	Salado	WIPP25	807.10	Mercer, 1983, Table 1
18	Salado	H10C	666.30	Mercer, 1983, Table 1	56	Salado	WIPP26	866.50	Mercer, 1983, Table 1
19	Salado	H2C	796.70	Mercer, 1983, Table 1	57	Salado	WIPP27	841.50	Mercer, 1983, Table 1
20	Salado	H3	783.10	Mercer, 1983, Table 1	58	Salado	WIPP28	858.40	Mercer, 1983, Table 1
21	Salado	H4C	825.40	Mercer, 1983, Table 1	59	Salado	WIPP29	863.80	Mercer, 1983, Table 1
22	Salado	H5C	751.60	Mercer, 1983, Table 1	60	Salado	WIPP30	816.60	Mercer, 1983, Table 1
23	Salado	H6C	800.70	Mercer, 1983, Table 1	61	Salado	WIPP32	870.80	Mercer, 1983, Table 1
24	Salado	H7C	877.80	Mercer, 1983, Table 1	62	Salado	WIPP33	812.60	Mercer, 1983, Table 1
25	Salado	H8C	823.00	Mercer, 1983, Table 1	63	Salado	WIPP34	749.80	Mercer, 1983, Table 1
26	Salado	H9C	797.00	Mercer, 1983, Table 1	64	Supra_R	AEC7	1113.70	Mercer, 1983, Table 1
27	Salado	P1	813.30	Mercer, 1983, Table 1	65	Supra_R	AEC8	1076.60	Mercer, 1983, Table 1
28	Salado	P10	738.50	Mercer, 1983, Table 1	66	Supra_R	B25	1039.10	Mercer, 1983, Table 1
29	Salado	P11	745.50	Mercer, 1983, Table 1	67	Supra_R	ERDA10	1027.50	Mercer, 1983, Table 1
30	Salado	P12	800.10	Mercer, 1983, Table 1	68	Supra_R	ERDA6	1079.00	Mercer, 1983, Table 1
31	Salado	P13	799.80	Mercer, 1983, Table 1	69	Supra_R	ERDA9	1042.10	Mercer, 1983, Table 1
32	Salado	P14	814.70	Mercer, 1983, Table 1	70	Supra_R	FFG_002	1090.30	Richey, 1989, Table 2, p.21
33	Salado	P15	843.70	Mercer, 1983, Table 1	71	Supra_R	FFG_004	1068.30	Richey, 1989, Table 2, p.21
34	Salado	P16	814.40	Mercer, 1983, Table 1	72	Supra_R	FFG_005	1089.70	Richey, 1989, Table 2, p.21
35	Salado	P17	798.90	Mercer, 1983, Table 1	73	Supra_R	FFG_006	1091.50	Richey, 1989, Table 2, p.21
36	Salado	P18	728.20	Mercer, 1983, Table 1	74	Supra_R	FFG_007	1093.90	Richey, 1989, Table 2, p.21
37	Salado	P19	740.00	Mercer, 1983, Table 1	75	Supra_R	FFG_009	1094.80	Richey, 1989, Table 2, p.21
38	Salado	P2	753.20	Mercer, 1983, Table 1	76	Supra_R	FFG_011	1092.70	Richey, 1989, Table 2, p.21

Table B.2. Elevations of Stratigraphic Layers Near WIPP (Continued)

	Layer	Well ID	Elevation	Source		Layer	Well ID	Elevation	Source
1	Supra_R	FFG_012	1092.10	Richey, 1989, Table 2, p.21	39	Supra_R	FFG_055	1145.10	Richey, 1989, Table 2, p.24
2	Supra_R	FFG_013	1080.20	Richey, 1989, Table 2, p.21	40	Supra_R	FFG_056	1136.60	Richey, 1989, Table 2, p.24
3	Supra_R	FFG_014	1068.60	Richey, 1989, Table 2, p.21	41	Supra_R	FFG_057	1134.80	Richey, 1989, Table 2, p.24
4	Supra_R	FFG_016	1099.70	Richey, 1989, Table 2, p.21	42	Supra_R	FFG_058	1147.70	Richey, 1989, Table 2, p.24
5	Supra_R	FFG_017	1100.90	Richey, 1989, Table 2, p.22	43	Supra_R	FFG_059	1156.10	Richey, 1989, Table 2, p.24
6	Supra_R	FFG_018	1116.50	Richey, 1989, Table 2, p.22	44	Supra_R	FFG_060	1138.40	Richey, 1989, Table 2, p.24
7	Supra_R	FFG_019	1111.00	Richey, 1989, Table 2, p.22	45	Supra_R	FFG_061	1137.50	Richey, 1989, Table 2, p.24
8	Supra_R	FFG_020	1091.50	Richey, 1989, Table 2, p.22	46	Supra_R	FFG_062	1122.60	Richey, 1989, Table 2, p.24
9	Supra_R	FFG_023	1109.80	Richey, 1989, Table 2, p.22	47	Supra_R	FFG_063	1118.10	Richey, 1989, Table 2, p.24
10	Supra_R	FFG_024	1124.60	Richey, 1989, Table 2, p.22	48	Supra_R	FFG_064	1127.20	Richey, 1989, Table 2, p.24
11	Supra_R	FFG_025	1117.60	Richey, 1989, Table 2, p.22	49	Supra_R	FFG_065	1110.70	Richey, 1989, Table 2, p.24
12	Supra_R	FFG_026	1116.00	Richey, 1989, Table 2, p.22	50	Supra_R	FFG_066	1113.70	Richey, 1989, Table 2, p.24
13	Supra_R	FFG_027	1117.40	Richey, 1989, Table 2, p.22	51	Supra_R	FFG_067	1127.50	Richey, 1989, Table 2, p.25
14	Supra_R	FFG_028	1183.90	Richey, 1989, Table 2, p.22	52	Supra_R	FFG_068	1125.00	Richey, 1989, Table 2, p.25
15	Supra_R	FFG_029	1145.40	Richey, 1989, Table 2, p.22	53	Supra_R	FFG_069	1130.20	Richey, 1989, Table 2, p.25
16	Supra_R	FFG_030	1154.30	Richey, 1989, Table 2, p.22	54	Supra_R	FFG_070	1130.80	Richey, 1989, Table 2, p.25
17	Supra_R	FFG_031	1168.30	Richey, 1989, Table 2, p.22	55	Supra_R	FFG_071	1115.30	Richey, 1989, Table 2, p.25
18	Supra_R	FFG_032	1158.50	Richey, 1989, Table 2, p.22	56	Supra_R	FFG_072	1105.20	Richey, 1989, Table 2, p.25
19	Supra_R	FFG_033	1143.60	Richey, 1989, Table 2, p.22	57	Supra_R	FFG_073	1107.40	Richey, 1989, Table 2, p.25
20	Supra_R	FFG_034	1139.30	Richey, 1989, Table 2, p.23	58	Supra_R	FFG_074	1107.00	Richey, 1989, Table 2, p.25
21	Supra_R	FFG_035	1121.10	Richey, 1989, Table 2, p.23	59	Supra_R	FFG_075	1108.30	Richey, 1989, Table 2, p.25
22	Supra_R	FFG_036	1147.60	Richey, 1989, Table 2, p.23	60	Supra_R	FFG_076	1097.30	Richey, 1989, Table 2, p.25
23	Supra_R	FFG_037	1129.30	Richey, 1989, Table 2, p.23	61	Supra_R	FFG_078	1087.20	Richey, 1989, Table 2, p.25
24	Supra_R	FFG_038	1118.30	Richey, 1989, Table 2, p.23	62	Supra_R	FFG_079	1091.20	Richey, 1989, Table 2, p.25
25	Supra_R	FFG_039	1046.10	Richey, 1989, Table 2, p.23	63	Supra_R	FFG_080	1082.30	Richey, 1989, Table 2, p.25
26	Supra_R	FFG_040	1077.20	Richey, 1989, Table 2, p.23	64	Supra_R	FFG_081	1097.00	Richey, 1989, Table 2, p.26
27	Supra_R	FFG_041	1065.30	Richey, 1989, Table 2, p.23	65	Supra_R	FFG_082	1084.80	Richey, 1989, Table 2, p.26
28	Supra_R	FFG_042	1069.50	Richey, 1989, Table 2, p.23	66	Supra_R	FFG_083	1115.60	Richey, 1989, Table 2, p.26
29	Supra_R	FFG_043	1067.10	Richey, 1989, Table 2, p.23	67	Supra_R	FFG_084	1107.60	Richey, 1989, Table 2, p.26
30	Supra_R	FFG_044	1080.50	Richey, 1989, Table 2, p.23	68	Supra_R	FFG_085	1108.90	Richey, 1989, Table 2, p.26
31	Supra_R	FFG_047	1112.80	Richey, 1989, Table 2, p.23	69	Supra_R	FFG_086	1107.30	Richey, 1989, Table 2, p.26
32	Supra_R	FFG_048	1106.10	Richey, 1989, Table 2, p.23	70	Supra_R	FFG_087	1107.30	Richey, 1989, Table 2, p.26
33	Supra_R	FFG_049	1119.20	Richey, 1989, Table 2, p.23	71	Supra_R	FFG_088	1108.90	Richey, 1989, Table 2, p.26
34	Supra_R	FFG_050	1132.50	Richey, 1989, Table 2, p.24	72	Supra_R	FFG_089	1108.60	Richey, 1989, Table 2, p.26
35	Supra_R	FFG_051	1131.10	Richey, 1989, Table 2, p.24	73	Supra_R	FFG_091	1091.20	Richey, 1989, Table 2, p.26
36	Supra_R	FFG_052	1132.00	Richey, 1989, Table 2, p.24	74	Supra_R	FFG_092	1097.60	Richey, 1989, Table 2, p.26
37	Supra_R	FFG_053	1137.50	Richey, 1989, Table 2, p.24	75	Supra_R	FFG_093	1097.90	Richey, 1989, Table 2, p.26
38	Supra_R	FFG_054	1150.20	Richey, 1989, Table 2, p.24	76	Supra_R	FFG_094	1095.10	Richey, 1989, Table 2, p.26

Table B.2. Elevations of Stratigraphic Layers Near WIPP (Continued)

	Layer	Well ID	Elevation	Source
1	Supra_R	FFG_095	1138.70	Richey, 1989, Table 2, p.26
2	Supra_R	FFG_096	1174.40	Richey, 1989, Table 2, p.26
3	Supra_R	FFG_097	1149.40	Richey, 1989, Table 2, p.27
4	Supra_R	FFG_098	1208.20	Richey, 1989, Table 2, p.27
5	Supra_R	FFG_099	1205.80	Richey, 1989, Table 2, p.27
6	Supra_R	FFG_100	1153.10	Richey, 1989, Table 2, p.27
7	Supra_R	FFG_101	1142.70	Richey, 1989, Table 2, p.27
8	Supra_R	FFG_102	1127.20	Richey, 1989, Table 2, p.27
9	Supra_R	FFG_103	1108.60	Richey, 1989, Table 2, p.27
10	Supra_R	FFG_104	1127.50	Richey, 1989, Table 2, p.27
11	Supra_R	FFG_105	995.20	Richey, 1989, Table 2, p.27
12	Supra_R	FFG_106	981.50	Richey, 1989, Table 2, p.27
13	Supra_R	FFG_107	987.60	Richey, 1989, Table 2, p.27
14	Supra_R	FFG_108	1015.90	Richey, 1989, Table 2, p.27
15	Supra_R	FFG_109	1039.10	Richey, 1989, Table 2, p.27
16	Supra_R	FFG_110	1045.50	Richey, 1989, Table 2, p.27
17	Supra_R	FFG_111	1062.20	Richey, 1989, Table 2, p.27
18	Supra_R	FFG_112	1056.10	Richey, 1989, Table 2, p.28
19	Supra_R	FFG_113	1054.90	Richey, 1989, Table 2, p.28
20	Supra_R	FFG_114	1014.70	Richey, 1989, Table 2, p.28
21	Supra_R	FFG_115	970.50	Richey, 1989, Table 2, p.28
22	Supra_R	FFG_116	972.00	Richey, 1989, Table 2, p.28
23	Supra_R	FFG_117	966.20	Richey, 1989, Table 2, p.28
24	Supra_R	FFG_119	950.10	Richey, 1989, Table 2, p.28
25	Supra_R	FFG_120	956.50	Richey, 1989, Table 2, p.28
26	Supra_R	FFG_121	958.60	Richey, 1989, Table 2, p.28
27	Supra_R	FFG_122	954.00	Richey, 1989, Table 2, p.28
28	Supra_R	FFG_123	961.60	Richey, 1989, Table 2, p.28
29	Supra_R	FFG_124	977.20	Richey, 1989, Table 2, p.28
30	Supra_R	FFG_125	976.20	Richey, 1989, Table 2, p.28
31	Supra_R	FFG_126	1014.20	Richey, 1989, Table 2, p.28
32	Supra_R	FFG_127	1019.20	Richey, 1989, Table 2, p.28
33	Supra_R	FFG_128	994.30	Richey, 1989, Table 2, p.28
34	Supra_R	FFG_129	961.90	Richey, 1989, Table 2, p.28
35	Supra_R	FFG_130	979.90	Richey, 1989, Table 2, p.28
36	Supra_R	FFG_132	1002.20	Richey, 1989, Table 2, p.29
37	Supra_R	FFG_133	993.00	Richey, 1989, Table 2, p.29
38	Supra_R	FFG_134	988.20	Richey, 1989, Table 2, p.29
39	Supra_R	FFG_135	1002.50	Richey, 1989, Table 2, p.29
40	Supra_R	FFG_136	1007.50	Richey, 1989, Table 2, p.29
41	Supra_R	FFG_137	1007.40	Richey, 1989, Table 2, p.29
42	Supra_R	FFG_138	1023.90	Richey, 1989, Table 2, p.29
43	Supra_R	FFG_139	1023.50	Richey, 1989, Table 2, p.29
44	Supra_R	FFG_140	1042.60	Richey, 1989, Table 2, p.29
45	Supra_R	FFG_141	1030.40	Richey, 1989, Table 2, p.29
46	Supra_R	FFG_142	1042.80	Richey, 1989, Table 2, p.29
47	Supra_R	FFG_143	1052.70	Richey, 1989, Table 2, p.29
48	Supra_R	FFG_144	905.00	Richey, 1989, Table 2, p.29
49	Supra_R	FFG_145	905.30	Richey, 1989, Table 2, p.29
50	Supra_R	FFG_146	912.90	Richey, 1989, Table 2, p.29
51	Supra_R	FFG_147	908.30	Richey, 1989, Table 2, p.29
52	Supra_R	FFG_148	907.70	Richey, 1989, Table 2, p.29
53	Supra_R	FFG_149	916.50	Richey, 1989, Table 2, p.30
54	Supra_R	FFG_152	905.30	Richey, 1989, Table 2, p.30
55	Supra_R	FFG_155	918.10	Richey, 1989, Table 2, p.30
56	Supra_R	FFG_156	908.30	Richey, 1989, Table 2, p.30
57	Supra_R	FFG_157	926.00	Richey, 1989, Table 2, p.30
58	Supra_R	FFG_158	941.80	Richey, 1989, Table 2, p.30
59	Supra_R	FFG_159	1001.30	Richey, 1989, Table 2, p.30
60	Supra_R	FFG_160	1002.50	Richey, 1989, Table 2, p.30
61	Supra_R	FFG_161	987.90	Richey, 1989, Table 2, p.30
62	Supra_R	FFG_162	988.80	Richey, 1989, Table 2, p.30
63	Supra_R	FFG_163	988.80	Richey, 1989, Table 2, p.30
64	Supra_R	FFG_164	955.90	Richey, 1989, Table 2, p.30
65	Supra_R	FFG_165	935.70	Richey, 1989, Table 2, p.30
66	Supra_R	FFG_166	993.00	Richey, 1989, Table 2, p.31
67	Supra_R	FFG_167	1019.60	Richey, 1989, Table 2, p.31
68	Supra_R	FFG_168	1001.00	Richey, 1989, Table 2, p.31
69	Supra_R	FFG_169	986.00	Richey, 1989, Table 2, p.31
70	Supra_R	FFG_170	934.80	Richey, 1989, Table 2, p.31
71	Supra_R	FFG_171	956.80	Richey, 1989, Table 2, p.31
72	Supra_R	FFG_172	986.00	Richey, 1989, Table 2, p.31
73	Supra_R	FFG_173	1022.60	Richey, 1989, Table 2, p.31
74	Supra_R	FFG_177	913.20	Richey, 1989, Table 2, p.31
75	Supra_R	FFG_178	888.20	Richey, 1989, Table 2, p.31
76	Supra_R	FFG_179	896.40	Richey, 1989, Table 2, p.31

Table B.2. Elevations of Stratigraphic Layers Near WIPP (Continued)

	Layer	Well ID	Elevation	Source
1	Supra_R	FFG_180	1062.20	Richey, 1989, Table 2, p.31
2	Supra_R	FFG_181	1016.50	Richey, 1989, Table 2, p.32
3	Supra_R	FFG_182	986.00	Richey, 1989, Table 2, p.32
4	Supra_R	FFG_183	1020.50	Richey, 1989, Table 2, p.32
5	Supra_R	FFG_184	1047.90	Richey, 1989, Table 2, p.32
6	Supra_R	FFG_185	1022.60	Richey, 1989, Table 2, p.32
7	Supra_R	FFG_186	1013.50	Richey, 1989, Table 2, p.32
8	Supra_R	FFG_188	979.00	Richey, 1989, Table 2, p.32
9	Supra_R	FFG_189	1046.10	Richey, 1989, Table 2, p.32
10	Supra_R	FFG_190	1037.80	Richey, 1989, Table 2, p.32
11	Supra_R	FFG_191	1041.50	Richey, 1989, Table 2, p.32
12	Supra_R	FFG_192	1031.40	Richey, 1989, Table 2, p.32
13	Supra_R	FFG_194	1075.40	Richey, 1989, Table 2, p.33
14	Supra_R	FFG_195	1059.20	Richey, 1989, Table 2, p.33
15	Supra_R	FFG_196	1042.40	Richey, 1989, Table 2, p.33
16	Supra_R	FFG_197	1034.50	Richey, 1989, Table 2, p.33
17	Supra_R	FFG_198	1031.40	Richey, 1989, Table 2, p.33
18	Supra_R	FFG_199	1038.80	Richey, 1989, Table 2, p.33
19	Supra_R	FFG_200	1040.90	Richey, 1989, Table 2, p.33
20	Supra_R	FFG_201	1074.10	Richey, 1989, Table 2, p.33
21	Supra_R	FFG_202	1075.60	Richey, 1989, Table 2, p.33
22	Supra_R	FFG_203	1071.40	Richey, 1989, Table 2, p.33
23	Supra_R	FFG_204	1096.40	Richey, 1989, Table 2, p.33
24	Supra_R	FFG_205	1082.00	Richey, 1989, Table 2, p.33
25	Supra_R	FFG_206	1067.70	Richey, 1989, Table 2, p.33
26	Supra_R	FFG_207	1072.60	Richey, 1989, Table 2, p.33
27	Supra_R	FFG_208	1060.10	Richey, 1989, Table 2, p.34
28	Supra_R	FFG_209	1074.10	Richey, 1989, Table 2, p.34
29	Supra_R	FFG_210	1066.20	Richey, 1989, Table 2, p.34
30	Supra_R	FFG_212	1078.40	Richey, 1989, Table 2, p.34
31	Supra_R	FFG_213	1051.60	Richey, 1989, Table 2, p.34
32	Supra_R	FFG_214	1061.60	Richey, 1989, Table 2, p.34
33	Supra_R	FFG_215	1041.80	Richey, 1989, Table 2, p.34
34	Supra_R	FFG_216	993.60	Richey, 1989, Table 2, p.34
35	Supra_R	FFG_217	1057.70	Richey, 1989, Table 2, p.34
36	Supra_R	FFG_218	1053.10	Richey, 1989, Table 2, p.34
37	Supra_R	FFG_219	1036.30	Richey, 1989, Table 2, p.34
38	Supra_R	FFG_220	1051.00	Richey, 1989, Table 2, p.34
39	Supra_R	FFG_221	1027.80	Richey, 1989, Table 2, p.34
40	Supra_R	FFG_222	1019.90	Richey, 1989, Table 2, p.34
41	Supra_R	FFG_224	1133.60	Richey, 1989, Table 2, p.35
42	Supra_R	FFG_225	1138.30	Richey, 1989, Table 2, p.35
43	Supra_R	FFG_226	1150.30	Richey, 1989, Table 2, p.35
44	Supra_R	FFG_228	1133.60	Richey, 1989, Table 2, p.35
45	Supra_R	FFG_229	1146.00	Richey, 1989, Table 2, p.35
46	Supra_R	FFG_230	1134.50	Richey, 1989, Table 2, p.35
47	Supra_R	FFG_231	1120.10	Richey, 1989, Table 2, p.35
48	Supra_R	FFG_232	1124.10	Richey, 1989, Table 2, p.35
49	Supra_R	FFG_233	1114.70	Richey, 1989, Table 2, p.35
50	Supra_R	FFG_234	1112.80	Richey, 1989, Table 2, p.35
51	Supra_R	FFG_235	1117.10	Richey, 1989, Table 2, p.35
52	Supra_R	FFG_236	1101.20	Richey, 1989, Table 2, p.35
53	Supra_R	FFG_237	1137.80	Richey, 1989, Table 2, p.35
54	Supra_R	FFG_238	1152.80	Richey, 1989, Table 2, p.36
55	Supra_R	FFG_239	1177.10	Richey, 1989, Table 2, p.36
56	Supra_R	FFG_240	1162.20	Richey, 1989, Table 2, p.36
57	Supra_R	FFG_241	1165.30	Richey, 1989, Table 2, p.36
58	Supra_R	FFG_242	1115.00	Richey, 1989, Table 2, p.36
59	Supra_R	FFG_243	1153.70	Richey, 1989, Table 2, p.36
60	Supra_R	FFG_244	1120.00	Richey, 1989, Table 2, p.36
61	Supra_R	FFG_245	1170.70	Richey, 1989, Table 2, p.36
62	Supra_R	FFG_246	1161.90	Richey, 1989, Table 2, p.36
63	Supra_R	FFG_247	1145.40	Richey, 1989, Table 2, p.36
64	Supra_R	FFG_248	1150.00	Richey, 1989, Table 2, p.36
65	Supra_R	FFG_249	1169.20	Richey, 1989, Table 2, p.36
66	Supra_R	FFG_250	1159.80	Richey, 1989, Table 2, p.36
67	Supra_R	FFG_251	1139.00	Richey, 1989, Table 2, p.36
68	Supra_R	FFG_252	1134.10	Richey, 1989, Table 2, p.36
69	Supra_R	FFG_253	1108.60	Richey, 1989, Table 2, p.36
70	Supra_R	FFG_254	1111.60	Richey, 1989, Table 2, p.36
71	Supra_R	FFG_255	1122.60	Richey, 1989, Table 2, p.37
72	Supra_R	FFG_256	1136.00	Richey, 1989, Table 2, p.37
73	Supra_R	FFG_257	1137.20	Richey, 1989, Table 2, p.37
74	Supra_R	FFG_258	1120.40	Richey, 1989, Table 2, p.37
75	Supra_R	FFG_259	1139.60	Richey, 1989, Table 2, p.37
76	Supra_R	FFG_260	1111.00	Richey, 1989, Table 2, p.37

Table B.2. Elevations of Stratigraphic Layers Near WIPP (Continued)

	Layer	Well ID	Elevation	Source
1	Supra_R	FFG_261	1106.10	Richey, 1989, Table 2, p.37
2	Supra_R	FFG_262	1109.50	Richey, 1989, Table 2, p.37
3	Supra_R	FFG_263	1115.60	Richey, 1989, Table 2, p.37
4	Supra_R	FFG_264	1121.10	Richey, 1989, Table 2, p.37
5	Supra_R	FFG_265	1130.80	Richey, 1989, Table 2, p.37
6	Supra_R	FFG_266	1131.40	Richey, 1989, Table 2, p.37
7	Supra_R	FFG_267	1120.40	Richey, 1989, Table 2, p.37
8	Supra_R	FFG_268	1115.90	Richey, 1989, Table 2, p.37
9	Supra_R	FFG_269	1105.80	Richey, 1989, Table 2, p.38
10	Supra_R	FFG_270	1057.00	Richey, 1989, Table 2, p.38
11	Supra_R	FFG_271	1049.40	Richey, 1989, Table 2, p.38
12	Supra_R	FFG_272	1073.50	Richey, 1989, Table 2, p.38
13	Supra_R	FFG_273	1079.20	Richey, 1989, Table 2, p.38
14	Supra_R	FFG_274	1137.20	Richey, 1989, Table 2, p.38
15	Supra_R	FFG_275	1135.70	Richey, 1989, Table 2, p.38
16	Supra_R	FFG_276	1125.90	Richey, 1989, Table 2, p.38
17	Supra_R	FFG_277	1123.20	Richey, 1989, Table 2, p.38
18	Supra_R	FFG_278	1098.20	Richey, 1989, Table 2, p.38
19	Supra_R	FFG_279	1107.90	Richey, 1989, Table 2, p.38
20	Supra_R	FFG_280	1120.30	Richey, 1989, Table 2, p.38
21	Supra_R	FFG_281	1147.30	Richey, 1989, Table 2, p.38
22	Supra_R	FFG_283	1090.90	Richey, 1989, Table 2, p.39
23	Supra_R	FFG_284	1117.10	Richey, 1989, Table 2, p.39
24	Supra_R	FFG_285	1112.50	Richey, 1989, Table 2, p.39
25	Supra_R	FFG_286	1101.50	Richey, 1989, Table 2, p.39
26	Supra_R	FFG_287	1094.60	Richey, 1989, Table 2, p.39
27	Supra_R	FFG_288	1110.40	Richey, 1989, Table 2, p.39
28	Supra_R	FFG_289	1081.90	Richey, 1989, Table 2, p.39
29	Supra_R	FFG_290	1103.40	Richey, 1989, Table 2, p.39
30	Supra_R	FFG_291	1132.00	Richey, 1989, Table 2, p.39
31	Supra_R	FFG_292	1090.60	Richey, 1989, Table 2, p.39
32	Supra_R	FFG_293	1085.10	Richey, 1989, Table 2, p.39
33	Supra_R	FFG_294	1095.50	Richey, 1989, Table 2, p.39
34	Supra_R	FFG_295	1087.50	Richey, 1989, Table 2, p.39
35	Supra_R	FFG_297	1104.90	Richey, 1989, Table 2, p.39
36	Supra_R	FFG_298	1070.00	Richey, 1989, Table 2, p.40
37	Supra_R	FFG_299	1078.40	Richey, 1989, Table 2, p.40
38	Supra_R	FFG_300	1062.20	Richey, 1989, Table 2, p.40
39	Supra_R	FFG_301	1046.40	Richey, 1989, Table 2, p.40
40	Supra_R	FFG_302	1092.70	Richey, 1989, Table 2, p.40
41	Supra_R	FFG_303	1099.30	Richey, 1989, Table 2, p.40
42	Supra_R	FFG_304	1088.10	Richey, 1989, Table 2, p.40
43	Supra_R	FFG_305	1093.90	Richey, 1989, Table 2, p.40
44	Supra_R	FFG_306	1075.90	Richey, 1989, Table 2, p.40
45	Supra_R	FFG_307	1078.70	Richey, 1989, Table 2, p.40
46	Supra_R	FFG_308	1075.90	Richey, 1989, Table 2, p.40
47	Supra_R	FFG_309	1093.60	Richey, 1989, Table 2, p.40
48	Supra_R	FFG_310	1087.50	Richey, 1989, Table 2, p.40
49	Supra_R	FFG_311	1085.40	Richey, 1989, Table 2, p.40
50	Supra_R	FFG_312	1076.90	Richey, 1989, Table 2, p.40
51	Supra_R	FFG_313	1106.10	Richey, 1989, Table 2, p.41
52	Supra_R	FFG_314	1121.10	Richey, 1989, Table 2, p.41
53	Supra_R	FFG_315	1131.10	Richey, 1989, Table 2, p.41
54	Supra_R	FFG_316	1133.20	Richey, 1989, Table 2, p.41
55	Supra_R	FFG_317	1097.60	Richey, 1989, Table 2, p.41
56	Supra_R	FFG_318	1123.50	Richey, 1989, Table 2, p.41
57	Supra_R	FFG_319	1120.70	Richey, 1989, Table 2, p.41
58	Supra_R	FFG_320	1129.60	Richey, 1989, Table 2, p.41
59	Supra_R	FFG_321	1124.70	Richey, 1989, Table 2, p.41
60	Supra_R	FFG_322	1124.70	Richey, 1989, Table 2, p.41
61	Supra_R	FFG_323	1120.40	Richey, 1989, Table 2, p.41
62	Supra_R	FFG_324	1122.00	Richey, 1989, Table 2, p.41
63	Supra_R	FFG_325	1079.90	Richey, 1989, Table 2, p.41
64	Supra_R	FFG_326	1117.70	Richey, 1989, Table 2, p.41
65	Supra_R	FFG_327	1102.20	Richey, 1989, Table 2, p.42
66	Supra_R	FFG_328	1121.40	Richey, 1989, Table 2, p.42
67	Supra_R	FFG_329	1120.40	Richey, 1989, Table 2, p.42
68	Supra_R	FFG_330	1115.60	Richey, 1989, Table 2, p.42
69	Supra_R	FFG_331	1103.70	Richey, 1989, Table 2, p.42
70	Supra_R	FFG_332	1124.70	Richey, 1989, Table 2, p.42
71	Supra_R	FFG_333	1130.50	Richey, 1989, Table 2, p.42
72	Supra_R	FFG_334	1125.90	Richey, 1989, Table 2, p.42
73	Supra_R	FFG_335	1129.60	Richey, 1989, Table 2, p.42
74	Supra_R	FFG_336	1124.10	Richey, 1989, Table 2, p.42
75	Supra_R	FFG_337	1124.40	Richey, 1989, Table 2, p.42
76	Supra_R	FFG_338	1123.50	Richey, 1989, Table 2, p.42

Table B.2. Elevations of Stratigraphic Layers Near WIPP (Continued)

	Layer	Well ID	Elevation	Source
1	Supra_R	FFG_339	1107.90	Richey, 1989, Table 2, p.42
2	Supra_R	FFG_340	1107.00	Richey, 1989, Table 2, p.42
3	Supra_R	FFG_342	1056.10	Richey, 1989, Table 2, p.43
4	Supra_R	FFG_344	1040.60	Richey, 1989, Table 2, p.43
5	Supra_R	FFG_345	1073.20	Richey, 1989, Table 2, p.43
6	Supra_R	FFG_347	1039.70	Richey, 1989, Table 2, p.43
7	Supra_R	FFG_348	1035.70	Richey, 1989, Table 2, p.43
8	Supra_R	FFG_349	1034.80	Richey, 1989, Table 2, p.43
9	Supra_R	FFG_350	1041.50	Richey, 1989, Table 2, p.43
10	Supra_R	FFG_351	1102.80	Richey, 1989, Table 2, p.43
11	Supra_R	FFG_352	1103.10	Richey, 1989, Table 2, p.43
12	Supra_R	FFG_353	1095.80	Richey, 1989, Table 2, p.43
13	Supra_R	FFG_354	1051.00	Richey, 1989, Table 2, p.43
14	Supra_R	FFG_361	1012.50	Richey, 1989, Table 2, p.44
15	Supra_R	FFG_362	1010.70	Richey, 1989, Table 2, p.44
16	Supra_R	FFG_363	1009.50	Richey, 1989, Table 2, p.44
17	Supra_R	FFG_364	993.60	Richey, 1989, Table 2, p.44
18	Supra_R	FFG_366	1010.40	Richey, 1989, Table 2, p.44
19	Supra_R	FFG_367	1006.40	Richey, 1989, Table 2, p.44
20	Supra_R	FFG_370	1012.90	Richey, 1989, Table 2, p.44
21	Supra_R	FFG_371	1012.90	Richey, 1989, Table 2, p.44
22	Supra_R	FFG_372	1006.40	Richey, 1989, Table 2, p.45
23	Supra_R	FFG_373	998.10	Richey, 1989, Table 2, p.45
24	Supra_R	FFG_374	995.20	Richey, 1989, Table 2, p.45
25	Supra_R	FFG_376	1010.40	Richey, 1989, Table 2, p.45
26	Supra_R	FFG_381	1021.40	Richey, 1989, Table 2, p.45
27	Supra_R	FFG_383	1046.10	Richey, 1989, Table 2, p.45
28	Supra_R	FFG_384	976.00	Richey, 1989, Table 2, p.45
29	Supra_R	FFG_385	990.60	Richey, 1989, Table 2, p.45
30	Supra_R	FFG_387	1019.90	Richey, 1989, Table 2, p.45
31	Supra_R	FFG_388	1019.60	Richey, 1989, Table 2, p.46
32	Supra_R	FFG_389	1008.00	Richey, 1989, Table 2, p.46
33	Supra_R	FFG_390	1022.60	Richey, 1989, Table 2, p.46
34	Supra_R	FFG_391	1025.30	Richey, 1989, Table 2, p.46
35	Supra_R	FFG_392	1019.60	Richey, 1989, Table 2, p.46
36	Supra_R	FFG_393	1061.60	Richey, 1989, Table 2, p.46
37	Supra_R	FFG_394	1050.30	Richey, 1989, Table 2, p.46
38	Supra_R	FFG_395	1059.20	Richey, 1989, Table 2, p.46
39	Supra_R	FFG_396	1090.00	Richey, 1989, Table 2, p.46
40	Supra_R	FFG_398	1011.60	Richey, 1989, Table 2, p.46
41	Supra_R	FFG_399	1001.60	Richey, 1989, Table 2, p.46
42	Supra_R	FFG_401	972.30	Richey, 1989, Table 2, p.46
43	Supra_R	FFG_402	1023.10	Richey, 1989, Table 2, p.46
44	Supra_R	FFG_403	995.20	Richey, 1989, Table 2, p.47
45	Supra_R	FFG_404	976.60	Richey, 1989, Table 2, p.47
46	Supra_R	FFG_407	969.90	Richey, 1989, Table 2, p.47
47	Supra_R	FFG_408	965.00	Richey, 1989, Table 2, p.47
48	Supra_R	FFG_409	970.50	Richey, 1989, Table 2, p.47
49	Supra_R	FFG_411	957.70	Richey, 1989, Table 2, p.47
50	Supra_R	FFG_413	968.70	Richey, 1989, Table 2, p.47
51	Supra_R	FFG_418	1033.90	Richey, 1989, Table 2, p.48
52	Supra_R	FFG_419	1052.50	Richey, 1989, Table 2, p.48
53	Supra_R	FFG_420	1045.10	Richey, 1989, Table 2, p.48
54	Supra_R	FFG_421	1047.00	Richey, 1989, Table 2, p.48
55	Supra_R	FFG_422	1054.30	Richey, 1989, Table 2, p.48
56	Supra_R	FFG_426	996.10	Richey, 1989, Table 2, p.48
57	Supra_R	FFG_432	978.40	Richey, 1989, Table 2, p.48
58	Supra_R	FFG_433	968.00	Richey, 1989, Table 2, p.48
59	Supra_R	FFG_438	1082.20	Richey, 1989, Table 2, p.49
60	Supra_R	FFG_445	960.70	Richey, 1989, Table 2, p.49
61	Supra_R	FFG_453	1049.50	Richey, 1989, Table 2, p.50
62	Supra_R	FFG_455	1061.30	Richey, 1989, Table 2, p.50
63	Supra_R	FFG_456	1063.40	Richey, 1989, Table 2, p.50
64	Supra_R	FFG_457	1023.50	Richey, 1989, Table 2, p.50
65	Supra_R	FFG_458	1025.80	Richey, 1989, Table 2, p.50
66	Supra_R	FFG_459	1070.50	Richey, 1989, Table 2, p.50
67	Supra_R	FFG_462	1032.10	Richey, 1989, Table 2, p.50
68	Supra_R	FFG_463	1021.10	Richey, 1989, Table 2, p.51
69	Supra_R	FFG_464	1035.40	Richey, 1989, Table 2, p.51
70	Supra_R	FFG_465	1031.40	Richey, 1989, Table 2, p.51
71	Supra_R	FFG_467	1025.70	Richey, 1989, Table 2, p.51
72	Supra_R	FFG_468	1064.70	Richey, 1989, Table 2, p.51
73	Supra_R	FFG_470	1067.10	Richey, 1989, Table 2, p.51
74	Supra_R	FFG_471	1036.60	Richey, 1989, Table 2, p.51
75	Supra_R	FFG_472	1032.40	Richey, 1989, Table 2, p.51
76	Supra_R	FFG_473	1060.70	Richey, 1989, Table 2, p.51

Table B.2. Elevations of Stratigraphic Layers Near WIPP (Continued)

	Layer	Well ID	Elevation	Source
1	Supra_R	FFG_474	1100.60	Richey, 1989, Table 2, p.51
2	Supra_R	FFG_475	1103.70	Richey, 1989, Table 2, p.51
3	Supra_R	FFG_476	1090.10	Richey, 1989, Table 2, p.51
4	Supra_R	FFG_477	1102.80	Richey, 1989, Table 2, p.51
5	Supra_R	FFG_478	1104.80	Richey, 1989, Table 2, p.52
6	Supra_R	FFG_479	1106.40	Richey, 1989, Table 2, p.52
7	Supra_R	FFG_480	1096.10	Richey, 1989, Table 2, p.52
8	Supra_R	FFG_481	1090.90	Richey, 1989, Table 2, p.52
9	Supra_R	FFG_482	1103.40	Richey, 1989, Table 2, p.52
10	Supra_R	FFG_483	1094.20	Richey, 1989, Table 2, p.52
11	Supra_R	FFG_484	1095.60	Richey, 1989, Table 2, p.52
12	Supra_R	FFG_485	1096.50	Richey, 1989, Table 2, p.52
13	Supra_R	FFG_486	1097.60	Richey, 1989, Table 2, p.52
14	Supra_R	FFG_487	1097.00	Richey, 1989, Table 2, p.52
15	Supra_R	FFG_488	1088.60	Richey, 1989, Table 2, p.52
16	Supra_R	FFG_489	1086.60	Richey, 1989, Table 2, p.52
17	Supra_R	FFG_490	1072.60	Richey, 1989, Table 2, p.52
18	Supra_R	FFG_491	1077.50	Richey, 1989, Table 2, p.52
19	Supra_R	FFG_492	1067.40	Richey, 1989, Table 2, p.52
20	Supra_R	FFG_493	1069.20	Richey, 1989, Table 2, p.53
21	Supra_R	FFG_494	1069.50	Richey, 1989, Table 2, p.53
22	Supra_R	FFG_495	1072.30	Richey, 1989, Table 2, p.53
23	Supra_R	FFG_496	1108.30	Richey, 1989, Table 2, p.53
24	Supra_R	FFG_497	1090.60	Richey, 1989, Table 2, p.53
25	Supra_R	FFG_498	1104.90	Richey, 1989, Table 2, p.53
26	Supra_R	FFG_499	1091.50	Richey, 1989, Table 2, p.53
27	Supra_R	FFG_500	1091.50	Richey, 1989, Table 2, p.53
28	Supra_R	FFG_501	1075.60	Richey, 1989, Table 2, p.53
29	Supra_R	FFG_502	1092.40	Richey, 1989, Table 2, p.53
30	Supra_R	FFG_503	1064.10	Richey, 1989, Table 2, p.53
31	Supra_R	FFG_504	1070.50	Richey, 1989, Table 2, p.53
32	Supra_R	FFG_505	1077.80	Richey, 1989, Table 2, p.53
33	Supra_R	FFG_506	1069.80	Richey, 1989, Table 2, p.53
34	Supra_R	FFG_507	1051.90	Richey, 1989, Table 2, p.53
35	Supra_R	FFG_508	1051.90	Richey, 1989, Table 2, p.53
36	Supra_R	FFG_509	1066.50	Richey, 1989, Table 2, p.54
37	Supra_R	FFG_510	1080.50	Richey, 1989, Table 2, p.54
38	Supra_R	FFG_511	1102.80	Richey, 1989, Table 2, p.54
39	Supra_R	FFG_512	1073.50	Richey, 1989, Table 2, p.54
40	Supra_R	FFG_513	1061.00	Richey, 1989, Table 2, p.54
41	Supra_R	FFG_514	1060.10	Richey, 1989, Table 2, p.54
42	Supra_R	FFG_515	1082.30	Richey, 1989, Table 2, p.54
43	Supra_R	FFG_516	1075.00	Richey, 1989, Table 2, p.54
44	Supra_R	FFG_517	1053.10	Richey, 1989, Table 2, p.54
45	Supra_R	FFG_518	1036.30	Richey, 1989, Table 2, p.54
46	Supra_R	FFG_519	1033.90	Richey, 1989, Table 2, p.54
47	Supra_R	FFG_520	1030.80	Richey, 1989, Table 2, p.54
48	Supra_R	FFG_521	1028.70	Richey, 1989, Table 2, p.54
49	Supra_R	FFG_522	1055.20	Richey, 1989, Table 2, p.54
50	Supra_R	FFG_523	1041.80	Richey, 1989, Table 2, p.54
51	Supra_R	FFG_524	1024.10	Richey, 1989, Table 2, p.55
52	Supra_R	FFG_525	1047.00	Richey, 1989, Table 2, p.55
53	Supra_R	FFG_526	1033.90	Richey, 1989, Table 2, p.55
54	Supra_R	FFG_527	1031.70	Richey, 1989, Table 2, p.55
55	Supra_R	FFG_528	1023.50	Richey, 1989, Table 2, p.55
56	Supra_R	FFG_530	1016.50	Richey, 1989, Table 2, p.55
57	Supra_R	FFG_531	998.20	Richey, 1989, Table 2, p.55
58	Supra_R	FFG_532	990.30	Richey, 1989, Table 2, p.55
59	Supra_R	FFG_534	1021.10	Richey, 1989, Table 2, p.55
60	Supra_R	FFG_535	995.90	Richey, 1989, Table 2, p.55
61	Supra_R	FFG_536	996.10	Richey, 1989, Table 2, p.55
62	Supra_R	FFG_537	985.40	Richey, 1989, Table 2, p.55
63	Supra_R	FFG_543	997.90	Richey, 1989, Table 2, p.56
64	Supra_R	FFG_548	1047.30	Richey, 1989, Table 2, p.56
65	Supra_R	FFG_552	922.90	Richey, 1989, Table 2, p.56
66	Supra_R	FFG_562	981.50	Richey, 1989, Table 2, p.57
67	Supra_R	FFG_563	969.90	Richey, 1989, Table 2, p.57
68	Supra_R	FFG_564	969.30	Richey, 1989, Table 2, p.57
69	Supra_R	FFG_568	957.10	Richey, 1989, Table 2, p.57
70	Supra_R	FFG_569	952.20	Richey, 1989, Table 2, p.57
71	Supra_R	FFG_584	1006.80	Richey, 1989, Table 2, p.58
72	Supra_R	FFG_585	1025.00	Richey, 1989, Table 2, p.58
73	Supra_R	FFG_600	1003.40	Richey, 1989, Table 2, p.58
74	Supra_R	FFG_601	983.90	Richey, 1989, Table 2, p.58
75	Supra_R	FFG_602	1053.10	Richey, 1989, Table 2, p.58
76	Supra_R	FFG_606	1012.90	Richey, 1989, Table 2, p.58

Table B.2. Elevations of Stratigraphic Layers Near WIPP (Continued)

	Layer	Well ID	Elevation	Source		Layer	Well ID	Elevation	Source
1	Supra_R	FFG_607	1001.30	Richey, 1989, Table 2, p.59	39	Supra_R	FFG_677	1064.40	Richey, 1989, Table 2, p.62
2	Supra_R	FFG_608	1018.60	Richey, 1989, Table 2, p.59	40	Supra_R	FFG_679	1060.70	Richey, 1989, Table 2, p.62
3	Supra_R	FFG_609	1025.30	Richey, 1989, Table 2, p.59	41	Supra_R	FFG_685	1003.50	Richey, 1989, Table 2, p.63
4	Supra_R	FFG_610	1023.20	Richey, 1989, Table 2, p.59	42	Supra_R	FFG_689	1059.20	Richey, 1989, Table 2, p.63
5	Supra_R	FFG_611	1009.20	Richey, 1989, Table 2, p.59	43	Supra_R	FFG_690	1052.20	Richey, 1989, Table 2, p.63
6	Supra_R	FFG_612	977.10	Richey, 1989, Table 2, p.59	44	Supra_R	FFG_691	1052.50	Richey, 1989, Table 2, p.63
7	Supra_R	FFG_613	945.90	Richey, 1989, Table 2, p.59	45	Supra_R	FFG_692	1057.70	Richey, 1989, Table 2, p.63
8	Supra_R	FFG_618	897.00	Richey, 1989, Table 2, p.59	46	Supra_R	FFG_693	1050.60	Richey, 1989, Table 2, p.63
9	Supra_R	FFG_620	909.90	Richey, 1989, Table 2, p.59	47	Supra_R	FFG_694	1042.40	Richey, 1989, Table 2, p.63
10	Supra_R	FFG_621	905.90	Richey, 1989, Table 2, p.59	48	Supra_R	FFG_695	1048.50	Richey, 1989, Table 2, p.63
11	Supra_R	FFG_638	975.40	Richey, 1989, Table 2, p.60	49	Supra_R	FFG_696	1050.60	Richey, 1989, Table 2, p.63
12	Supra_R	FFG_639	961.50	Richey, 1989, Table 2, p.60	50	Supra_R	FFG_697	1045.80	Richey, 1989, Table 2, p.64
13	Supra_R	FFG_640	966.20	Richey, 1989, Table 2, p.60	51	Supra_R	FFG_698	1039.70	Richey, 1989, Table 2, p.64
14	Supra_R	FFG_643	975.40	Richey, 1989, Table 2, p.60	52	Supra_R	FFG_699	1029.60	Richey, 1989, Table 2, p.64
15	Supra_R	FFG_644	936.70	Richey, 1989, Table 2, p.60	53	Supra_R	FFG_700	1027.10	Richey, 1989, Table 2, p.64
16	Supra_R	FFG_648	960.70	Richey, 1989, Table 2, p.60	54	Supra_R	FFG_701	1032.10	Richey, 1989, Table 2, p.64
17	Supra_R	FFG_652	1106.40	Richey, 1989, Table 2, p.60	55	Supra_R	FFG_702	1036.60	Richey, 1989, Table 2, p.64
18	Supra_R	FFG_653	1096.10	Richey, 1989, Table 2, p.61	56	Supra_R	FFG_703	1047.00	Richey, 1989, Table 2, p.64
19	Supra_R	FFG_654	1098.50	Richey, 1989, Table 2, p.61	57	Supra_R	FFG_704	1032.70	Richey, 1989, Table 2, p.64
20	Supra_R	FFG_655	1093.00	Richey, 1989, Table 2, p.61	58	Supra_R	FFG_705	1023.80	Richey, 1989, Table 2, p.64
21	Supra_R	FFG_656	1091.80	Richey, 1989, Table 2, p.61	59	Supra_R	FFG_706	1025.70	Richey, 1989, Table 2, p.64
22	Supra_R	FFG_657	1083.30	Richey, 1989, Table 2, p.61	60	Supra_R	FFG_707	1019.30	Richey, 1989, Table 2, p.64
23	Supra_R	FFG_658	1088.10	Richey, 1989, Table 2, p.61	61	Supra_R	FFG_708	1026.60	Richey, 1989, Table 2, p.64
24	Supra_R	FFG_659	1072.60	Richey, 1989, Table 2, p.61	62	Supra_R	FFG_709	1008.60	Richey, 1989, Table 2, p.64
25	Supra_R	FFG_660	1071.10	Richey, 1989, Table 2, p.61	63	Supra_R	FFG_710	1007.40	Richey, 1989, Table 2, p.64
26	Supra_R	FFG_662	1085.70	Richey, 1989, Table 2, p.61	64	Supra_R	FFG_711	1012.90	Richey, 1989, Table 2, p.65
27	Supra_R	FFG_664	1084.50	Richey, 1989, Table 2, p.61	65	Supra_R	FFG_712	1018.00	Richey, 1989, Table 2, p.65
28	Supra_R	FFG_666	1063.10	Richey, 1989, Table 2, p.62	66	Supra_R	FFG_713	1011.30	Richey, 1989, Table 2, p.65
29	Supra_R	FFG_667	1059.20	Richey, 1989, Table 2, p.62	67	Supra_R	FFG_714	1024.10	Richey, 1989, Table 2, p.65
30	Supra_R	FFG_668	1043.30	Richey, 1989, Table 2, p.62	68	Supra_R	FFG_715	1025.30	Richey, 1989, Table 2, p.65
31	Supra_R	FFG_669	1036.30	Richey, 1989, Table 2, p.62	69	Supra_R	FFG_716	1060.60	Richey, 1989, Table 2, p.65
32	Supra_R	FFG_670	1049.10	Richey, 1989, Table 2, p.62	70	Supra_R	FFG_717	1056.10	Richey, 1989, Table 2, p.65
33	Supra_R	FFG_671	1044.90	Richey, 1989, Table 2, p.62	71	Supra_R	FFG_718	1044.90	Richey, 1989, Table 2, p.65
34	Supra_R	FFG_672	1058.00	Richey, 1989, Table 2, p.62	72	Supra_R	FFG_719	1040.40	Richey, 1989, Table 2, p.65
35	Supra_R	FFG_673	1037.20	Richey, 1989, Table 2, p.62	73	Supra_R	FFG_720	1019.90	Richey, 1989, Table 2, p.65
36	Supra_R	FFG_674	1064.70	Richey, 1989, Table 2, p.62	74	Supra_R	FFG_721	1026.90	Richey, 1989, Table 2, p.65
37	Supra_R	FFG_675	1078.40	Richey, 1989, Table 2, p.62	75	Supra_R	FFG_723	1054.30	Richey, 1989, Table 2, p.65
38	Supra_R	FFG_676	1084.50	Richey, 1989, Table 2, p.62	76	Supra_R	FFG_724	1044.20	Richey, 1989, Table 2, p.65

Table B.2. Elevations of Stratigraphic Layers Near WIPP (Continued)

	Layer	Well ID	Elevation	Source
1	Supra_R	FFG_725	1029.60	Richey, 1989, Table 2, p.65
2	Supra_R	FFG_726	1018.60	Richey, 1989, Table 2, p.65
3	Supra_R	FFG_727	1020.80	Richey, 1989, Table 2, p.66
4	Supra_R	FFG_728	1012.20	Richey, 1989, Table 2, p.66
5	Supra_R	FFG_729	1014.40	Richey, 1989, Table 2, p.66
6	Supra_R	FFG_730	1018.90	Richey, 1989, Table 2, p.66
7	Supra_R	FFG_731	1022.30	Richey, 1989, Table 2, p.66
8	Supra_R	FFG_732	1040.30	Richey, 1989, Table 2, p.66
9	Supra_R	FFG_733	1028.40	Richey, 1989, Table 2, p.66
10	Supra_R	FFG_734	1029.00	Richey, 1989, Table 2, p.66
11	Supra_R	FFG_735	1016.50	Richey, 1989, Table 2, p.66
12	Supra_R	FFG_736	1025.60	Richey, 1989, Table 2, p.66
13	Supra_R	FFG_737	1040.50	Richey, 1989, Table 2, p.66
14	Supra_R	FFG_738	1018.30	Richey, 1989, Table 2, p.66
15	Supra_R	FFG_739	1015.10	Richey, 1989, Table 2, p.66
16	Supra_R	FFG_740	1015.60	Richey, 1989, Table 2, p.66
17	Supra_R	FFG_741	1014.70	Richey, 1989, Table 2, p.66
18	Supra_R	FFG_742	1023.80	Richey, 1989, Table 2, p.67
19	Supra_R	FFG_743	1013.20	Richey, 1989, Table 2, p.67
20	Supra_R	FFG_744	1012.50	Richey, 1989, Table 2, p.67
21	Supra_R	FFG_745	1006.40	Richey, 1989, Table 2, p.67
22	Supra_R	FFG_746	1007.50	Richey, 1989, Table 2, p.67
23	Supra_R	H1	1035.70	Mercer, 1983, Table 1
24	Supra_R	H10C	1123.80	Mercer, 1983, Table 1
25	Supra_R	H2C	1029.60	Mercer, 1983, Table 1
26	Supra_R	H3	1033.30	Mercer, 1983, Table 1
27	Supra_R	H4C	1016.20	Mercer, 1983, Table 1
28	Supra_R	H5C	1068.90	Mercer, 1983, Table 1
29	Supra_R	H6C	1020.50	Mercer, 1983, Table 1
30	Supra_R	H7C	964.10	Mercer, 1983, Table 1
31	Supra_R	H8C	1046.40	Mercer, 1983, Table 1
32	Supra_R	H9C	1038.10	Mercer, 1983, Table 1
33	Supra_R	P1	1019.60	Mercer, 1983, Table 1
34	Supra_R	P10	1069.50	Mercer, 1983, Table 1
35	Supra_R	P11	1068.00	Mercer, 1983, Table 1
36	Supra_R	P12	1028.40	Mercer, 1983, Table 1
37	Supra_R	P13	1019.60	Mercer, 1983, Table 1
38	Supra_R	P14	1024.10	Mercer, 1983, Table 1
39	Supra_R	P15	1008.90	Mercer, 1983, Table 1
40	Supra_R	P16	1011.30	Mercer, 1983, Table 1
41	Supra_R	P17	1016.80	Mercer, 1983, Table 1
42	Supra_R	P18	1059.80	Mercer, 1983, Table 1
43	Supra_R	P19	1080.50	Mercer, 1983, Table 1
44	Supra_R	P2	1060.40	Mercer, 1983, Table 1
45	Supra_R	P20	1083.00	Mercer, 1983, Table 1
46	Supra_R	P21	1069.50	Mercer, 1983, Table 1
47	Supra_R	P3	1031.10	Mercer, 1983, Table 1
48	Supra_R	P4	1049.70	Mercer, 1983, Table 1
49	Supra_R	P5	1058.00	Mercer, 1983, Table 1
50	Supra_R	P6	1022.30	Mercer, 1983, Table 1
51	Supra_R	P7	1015.60	Mercer, 1983, Table 1
52	Supra_R	P8	1017.70	Mercer, 1983, Table 1
53	Supra_R	P9	1040.00	Mercer, 1983, Table 1
54	Supra_R	WIPP11	1044.20	Mercer, 1983, Table 1
55	Supra_R	WIPP12	1058.30	Mercer, 1983, Table 1
56	Supra_R	WIPP13	1037.80	Mercer, 1983, Table 1
57	Supra_R	WIPP15	996.40	Mercer, 1983, Table 1
58	Supra_R	WIPP16	1031.10	Mercer, 1983, Table 1
59	Supra_R	WIPP18	1053.40	Mercer, 1983, Table 1
60	Supra_R	WIPP19	1046.40	Mercer, 1983, Table 1
61	Supra_R	WIPP21	1041.50	Mercer, 1983, Table 1
62	Supra_R	WIPP22	1044.20	Mercer, 1983, Table 1
63	Supra_R	WIPP25	979.30	Mercer, 1983, Table 1
64	Supra_R	WIPP26	960.70	Mercer, 1983, Table 1
65	Supra_R	WIPP27	968.30	Mercer, 1983, Table 1
66	Supra_R	WIPP28	1020.20	Mercer, 1983, Table 1
67	Supra_R	WIPP29	907.40	Mercer, 1983, Table 1
68	Supra_R	WIPP30	1044.90	Mercer, 1983, Table 1
69	Supra_R	WIPP32	921.40	Mercer, 1983, Table 1
70	Supra_R	WIPP33	1012.90	Mercer, 1983, Table 1
71	Supra_R	WIPP34	1046.40	Mercer, 1983, Table 1
72	Tamarisk	AEC7	882.40	Mercer, 1983, Table 1
73	Tamarisk	AEC8	851.70	Mercer, 1983, Table 1
74	Tamarisk	AirShft	850.99	Holt and Powers, 1990, Figure 22
75	Tamarisk	B25	851.00	Mercer, 1983, Table 1
76	Tamarisk	ERDA10	910.20	Mercer, 1983, Table 1

Table B.2. Elevations of Stratigraphic Layers Near WIPP (Continued)

	Layer	Well ID	Elevation	Source		Layer	Well ID	Elevation	Source
1	Tamarisk	ERDA6	889.70	Mercer, 1983, Table 1	39	Tamarisk	FFG_043	782.00	Richey, 1989, Table 2, p.23
2	Tamarisk	ERDA9	853.10	Mercer, 1983, Table 1	40	Tamarisk	FFG_044	733.60	Richey, 1989, Table 2, p.23
3	Tamarisk	ExhtShft	847.97	Bechtel, Inc., 1986, Appendix F	41	Tamarisk	FFG_047	607.50	Richey, 1989, Table 2, p.23
4	Tamarisk	FFG_002	660.50	Richey, 1989, Table 2, p.21	42	Tamarisk	FFG_048	623.30	Richey, 1989, Table 2, p.23
5	Tamarisk	FFG_004	710.80	Richey, 1989, Table 2, p.21	43	Tamarisk	FFG_049	614.80	Richey, 1989, Table 2, p.23
6	Tamarisk	FFG_005	667.90	Richey, 1989, Table 2, p.21	44	Tamarisk	FFG_050	621.50	Richey, 1989, Table 2, p.24
7	Tamarisk	FFG_006	661.40	Richey, 1989, Table 2, p.21	45	Tamarisk	FFG_051	622.10	Richey, 1989, Table 2, p.24
8	Tamarisk	FFG_007	649.80	Richey, 1989, Table 2, p.21	46	Tamarisk	FFG_052	624.20	Richey, 1989, Table 2, p.24
9	Tamarisk	FFG_009	650.10	Richey, 1989, Table 2, p.21	47	Tamarisk	FFG_053	615.40	Richey, 1989, Table 2, p.24
10	Tamarisk	FFG_011	657.10	Richey, 1989, Table 2, p.21	48	Tamarisk	FFG_054	613.30	Richey, 1989, Table 2, p.24
11	Tamarisk	FFG_012	659.60	Richey, 1989, Table 2, p.21	49	Tamarisk	FFG_055	612.60	Richey, 1989, Table 2, p.24
12	Tamarisk	FFG_013	667.80	Richey, 1989, Table 2, p.21	50	Tamarisk	FFG_056	615.40	Richey, 1989, Table 2, p.24
13	Tamarisk	FFG_014	713.50	Richey, 1989, Table 2, p.21	51	Tamarisk	FFG_057	617.60	Richey, 1989, Table 2, p.24
14	Tamarisk	FFG_016	637.60	Richey, 1989, Table 2, p.21	52	Tamarisk	FFG_058	615.10	Richey, 1989, Table 2, p.24
15	Tamarisk	FFG_017	640.70	Richey, 1989, Table 2, p.22	53	Tamarisk	FFG_059	617.50	Richey, 1989, Table 2, p.24
16	Tamarisk	FFG_018	645.90	Richey, 1989, Table 2, p.22	54	Tamarisk	FFG_060	618.10	Richey, 1989, Table 2, p.24
17	Tamarisk	FFG_019	637.60	Richey, 1989, Table 2, p.22	55	Tamarisk	FFG_061	619.90	Richey, 1989, Table 2, p.24
18	Tamarisk	FFG_020	712.30	Richey, 1989, Table 2, p.22	56	Tamarisk	FFG_062	547.10	Richey, 1989, Table 2, p.24
19	Tamarisk	FFG_023	647.40	Richey, 1989, Table 2, p.22	57	Tamarisk	FFG_063	508.50	Richey, 1989, Table 2, p.24
20	Tamarisk	FFG_024	632.10	Richey, 1989, Table 2, p.22	58	Tamarisk	FFG_064	531.90	Richey, 1989, Table 2, p.24
21	Tamarisk	FFG_025	646.10	Richey, 1989, Table 2, p.22	59	Tamarisk	FFG_065	515.40	Richey, 1989, Table 2, p.24
22	Tamarisk	FFG_026	643.40	Richey, 1989, Table 2, p.22	60	Tamarisk	FFG_066	469.40	Richey, 1989, Table 2, p.24
23	Tamarisk	FFG_027	636.40	Richey, 1989, Table 2, p.22	61	Tamarisk	FFG_067	511.20	Richey, 1989, Table 2, p.25
24	Tamarisk	FFG_028	607.50	Richey, 1989, Table 2, p.22	62	Tamarisk	FFG_068	475.80	Richey, 1989, Table 2, p.25
25	Tamarisk	FFG_029	594.00	Richey, 1989, Table 2, p.22	63	Tamarisk	FFG_069	496.30	Richey, 1989, Table 2, p.25
26	Tamarisk	FFG_030	592.90	Richey, 1989, Table 2, p.22	64	Tamarisk	FFG_070	526.10	Richey, 1989, Table 2, p.25
27	Tamarisk	FFG_031	584.00	Richey, 1989, Table 2, p.22	65	Tamarisk	FFG_071	784.30	Richey, 1989, Table 2, p.25
28	Tamarisk	FFG_032	586.00	Richey, 1989, Table 2, p.22	66	Tamarisk	FFG_072	715.00	Richey, 1989, Table 2, p.25
29	Tamarisk	FFG_033	582.80	Richey, 1989, Table 2, p.22	67	Tamarisk	FFG_073	690.60	Richey, 1989, Table 2, p.25
30	Tamarisk	FFG_034	577.90	Richey, 1989, Table 2, p.23	68	Tamarisk	FFG_074	698.40	Richey, 1989, Table 2, p.25
31	Tamarisk	FFG_035	566.50	Richey, 1989, Table 2, p.23	69	Tamarisk	FFG_075	749.20	Richey, 1989, Table 2, p.25
32	Tamarisk	FFG_036	576.70	Richey, 1989, Table 2, p.23	70	Tamarisk	FFG_076	810.50	Richey, 1989, Table 2, p.25
33	Tamarisk	FFG_037	566.90	Richey, 1989, Table 2, p.23	71	Tamarisk	FFG_078	847.00	Richey, 1989, Table 2, p.25
34	Tamarisk	FFG_038	554.10	Richey, 1989, Table 2, p.23	72	Tamarisk	FFG_079	823.60	Richey, 1989, Table 2, p.25
35	Tamarisk	FFG_039	772.10	Richey, 1989, Table 2, p.23	73	Tamarisk	FFG_080	800.40	Richey, 1989, Table 2, p.25
36	Tamarisk	FFG_040	713.60	Richey, 1989, Table 2, p.23	74	Tamarisk	FFG_081	720.90	Richey, 1989, Table 2, p.26
37	Tamarisk	FFG_041	773.60	Richey, 1989, Table 2, p.23	75	Tamarisk	FFG_082	753.20	Richey, 1989, Table 2, p.26
38	Tamarisk	FFG_042	777.80	Richey, 1989, Table 2, p.23	76	Tamarisk	FFG_083	668.60	Richey, 1989, Table 2, p.26

Table B.2. Elevations of Stratigraphic Layers Near WIPP (Continued)

	Layer	Well ID	Elevation	Source
2	Tamarisk	FFG_084	694.60	Richey, 1989, Table 2, p.26
3	Tamarisk	FFG_085	687.40	Richey, 1989, Table 2, p.26
4	Tamarisk	FFG_086	697.30	Richey, 1989, Table 2, p.26
5	Tamarisk	FFG_087	671.40	Richey, 1989, Table 2, p.26
6	Tamarisk	FFG_088	667.20	Richey, 1989, Table 2, p.26
7	Tamarisk	FFG_089	649.60	Richey, 1989, Table 2, p.26
8	Tamarisk	FFG_091	692.80	Richey, 1989, Table 2, p.26
9	Tamarisk	FFG_092	706.50	Richey, 1989, Table 2, p.26
10	Tamarisk	FFG_093	710.20	Richey, 1989, Table 2, p.26
11	Tamarisk	FFG_094	713.20	Richey, 1989, Table 2, p.26
12	Tamarisk	FFG_095	681.50	Richey, 1989, Table 2, p.26
13	Tamarisk	FFG_096	665.10	Richey, 1989, Table 2, p.26
14	Tamarisk	FFG_097	645.00	Richey, 1989, Table 2, p.27
15	Tamarisk	FFG_098	619.90	Richey, 1989, Table 2, p.27
16	Tamarisk	FFG_099	615.40	Richey, 1989, Table 2, p.27
17	Tamarisk	FFG_100	598.10	Richey, 1989, Table 2, p.27
18	Tamarisk	FFG_101	569.40	Richey, 1989, Table 2, p.27
19	Tamarisk	FFG_102	587.40	Richey, 1989, Table 2, p.27
20	Tamarisk	FFG_103	652.00	Richey, 1989, Table 2, p.27
21	Tamarisk	FFG_104	545.00	Richey, 1989, Table 2, p.27
22	Tamarisk	FFG_105	901.30	Richey, 1989, Table 2, p.27
23	Tamarisk	FFG_106	931.80	Richey, 1989, Table 2, p.27
24	Tamarisk	FFG_107	916.90	Richey, 1989, Table 2, p.27
25	Tamarisk	FFG_108	912.30	Richey, 1989, Table 2, p.27
26	Tamarisk	FFG_109	892.80	Richey, 1989, Table 2, p.27
27	Tamarisk	FFG_110	859.60	Richey, 1989, Table 2, p.27
28	Tamarisk	FFG_111	867.10	Richey, 1989, Table 2, p.27
29	Tamarisk	FFG_112	854.90	Richey, 1989, Table 2, p.28
30	Tamarisk	FFG_113	869.00	Richey, 1989, Table 2, p.28
31	Tamarisk	FFG_114	898.30	Richey, 1989, Table 2, p.28
32	Tamarisk	FFG_115	889.40	Richey, 1989, Table 2, p.28
33	Tamarisk	FFG_116	904.90	Richey, 1989, Table 2, p.28
34	Tamarisk	FFG_117	902.20	Richey, 1989, Table 2, p.28
35	Tamarisk	FFG_119	937.90	Richey, 1989, Table 2, p.28
36	Tamarisk	FFG_120	913.80	Richey, 1989, Table 2, p.28
37	Tamarisk	FFG_121	922.00	Richey, 1989, Table 2, p.28
38	Tamarisk	FFG_122	920.50	Richey, 1989, Table 2, p.28
39	Tamarisk	FFG_123	894.50	Richey, 1989, Table 2, p.28
40	Tamarisk	FFG_124	857.70	Richey, 1989, Table 2, p.28
41	Tamarisk	FFG_125	883.20	Richey, 1989, Table 2, p.28
42	Tamarisk	FFG_126	880.10	Richey, 1989, Table 2, p.28
43	Tamarisk	FFG_127	885.10	Richey, 1989, Table 2, p.28
44	Tamarisk	FFG_128	917.50	Richey, 1989, Table 2, p.28
45	Tamarisk	FFG_129	893.30	Richey, 1989, Table 2, p.28
46	Tamarisk	FFG_130	920.50	Richey, 1989, Table 2, p.28
47	Tamarisk	FFG_132	929.00	Richey, 1989, Table 2, p.29
48	Tamarisk	FFG_133	932.00	Richey, 1989, Table 2, p.29
49	Tamarisk	FFG_134	935.50	Richey, 1989, Table 2, p.29
50	Tamarisk	FFG_135	910.80	Richey, 1989, Table 2, p.29
51	Tamarisk	FFG_136	911.50	Richey, 1989, Table 2, p.29
52	Tamarisk	FFG_137	919.30	Richey, 1989, Table 2, p.29
53	Tamarisk	FFG_138	874.50	Richey, 1989, Table 2, p.29
54	Tamarisk	FFG_139	882.40	Richey, 1989, Table 2, p.29
55	Tamarisk	FFG_140	823.10	Richey, 1989, Table 2, p.29
56	Tamarisk	FFG_141	845.70	Richey, 1989, Table 2, p.29
57	Tamarisk	FFG_142	821.80	Richey, 1989, Table 2, p.29
58	Tamarisk	FFG_143	831.70	Richey, 1989, Table 2, p.29
59	Tamarisk	FFG_144	903.50	Richey, 1989, Table 2, p.29
60	Tamarisk	FFG_145	905.30	Richey, 1989, Table 2, p.29
61	Tamarisk	FFG_146	912.90	Richey, 1989, Table 2, p.29
62	Tamarisk	FFG_147	893.70	Richey, 1989, Table 2, p.29
63	Tamarisk	FFG_148	907.70	Richey, 1989, Table 2, p.29
64	Tamarisk	FFG_149	912.20	Richey, 1989, Table 2, p.30
65	Tamarisk	FFG_155	905.60	Richey, 1989, Table 2, p.30
66	Tamarisk	FFG_157	907.10	Richey, 1989, Table 2, p.30
67	Tamarisk	FFG_158	931.10	Richey, 1989, Table 2, p.30
68	Tamarisk	FFG_159	928.80	Richey, 1989, Table 2, p.30
69	Tamarisk	FFG_160	924.20	Richey, 1989, Table 2, p.30
70	Tamarisk	FFG_161	930.00	Richey, 1989, Table 2, p.30
71	Tamarisk	FFG_162	925.40	Richey, 1989, Table 2, p.30
72	Tamarisk	FFG_163	927.80	Richey, 1989, Table 2, p.30
73	Tamarisk	FFG_164	955.90	Richey, 1989, Table 2, p.30
74	Tamarisk	FFG_165	935.70	Richey, 1989, Table 2, p.30
75	Tamarisk	FFG_166	928.40	Richey, 1989, Table 2, p.31
76	Tamarisk	FFG_167	914.40	Richey, 1989, Table 2, p.31
77	Tamarisk	FFG_168	933.90	Richey, 1989, Table 2, p.31

Table B.2. Elevations of Stratigraphic Layers Near WIPP (Continued)

	Layer	Well ID	Elevation	Source
1	Tamarisk	FFG_169	949.10	Richey, 1989, Table 2, p.31
2	Tamarisk	FFG_170	916.80	Richey, 1989, Table 2, p.31
3	Tamarisk	FFG_171	924.20	Richey, 1989, Table 2, p.31
4	Tamarisk	FFG_172	933.00	Richey, 1989, Table 2, p.31
5	Tamarisk	FFG_173	906.50	Richey, 1989, Table 2, p.31
6	Tamarisk	FFG_180	915.00	Richey, 1989, Table 2, p.31
7	Tamarisk	FFG_181	946.70	Richey, 1989, Table 2, p.32
8	Tamarisk	FFG_182	842.40	Richey, 1989, Table 2, p.32
9	Tamarisk	FFG_183	939.10	Richey, 1989, Table 2, p.32
10	Tamarisk	FFG_184	924.80	Richey, 1989, Table 2, p.32
11	Tamarisk	FFG_185	929.90	Richey, 1989, Table 2, p.32
12	Tamarisk	FFG_186	857.70	Richey, 1989, Table 2, p.32
13	Tamarisk	FFG_188	869.00	Richey, 1989, Table 2, p.32
14	Tamarisk	FFG_189	894.30	Richey, 1989, Table 2, p.32
15	Tamarisk	FFG_190	874.70	Richey, 1989, Table 2, p.32
16	Tamarisk	FFG_191	870.50	Richey, 1989, Table 2, p.32
17	Tamarisk	FFG_192	806.50	Richey, 1989, Table 2, p.32
18	Tamarisk	FFG_194	815.60	Richey, 1989, Table 2, p.33
19	Tamarisk	FFG_195	828.80	Richey, 1989, Table 2, p.33
20	Tamarisk	FFG_196	869.90	Richey, 1989, Table 2, p.33
21	Tamarisk	FFG_197	870.80	Richey, 1989, Table 2, p.33
22	Tamarisk	FFG_198	871.40	Richey, 1989, Table 2, p.33
23	Tamarisk	FFG_199	859.90	Richey, 1989, Table 2, p.33
24	Tamarisk	FFG_200	873.00	Richey, 1989, Table 2, p.33
25	Tamarisk	FFG_201	865.60	Richey, 1989, Table 2, p.33
26	Tamarisk	FFG_202	808.30	Richey, 1989, Table 2, p.33
27	Tamarisk	FFG_203	815.70	Richey, 1989, Table 2, p.33
28	Tamarisk	FFG_204	837.90	Richey, 1989, Table 2, p.33
29	Tamarisk	FFG_205	853.20	Richey, 1989, Table 2, p.33
30	Tamarisk	FFG_206	867.40	Richey, 1989, Table 2, p.33
31	Tamarisk	FFG_207	865.00	Richey, 1989, Table 2, p.33
32	Tamarisk	FFG_208	874.20	Richey, 1989, Table 2, p.34
33	Tamarisk	FFG_209	866.20	Richey, 1989, Table 2, p.34
34	Tamarisk	FFG_210	858.90	Richey, 1989, Table 2, p.34
35	Tamarisk	FFG_212	845.20	Richey, 1989, Table 2, p.34
36	Tamarisk	FFG_213	868.40	Richey, 1989, Table 2, p.34
37	Tamarisk	FFG_214	848.20	Richey, 1989, Table 2, p.34
38	Tamarisk	FFG_215	823.60	Richey, 1989, Table 2, p.34
39	Tamarisk	FFG_216	710.40	Richey, 1989, Table 2, p.34
40	Tamarisk	FFG_217	843.70	Richey, 1989, Table 2, p.34
41	Tamarisk	FFG_218	835.80	Richey, 1989, Table 2, p.34
42	Tamarisk	FFG_219	879.90	Richey, 1989, Table 2, p.34
43	Tamarisk	FFG_220	832.20	Richey, 1989, Table 2, p.34
44	Tamarisk	FFG_221	787.00	Richey, 1989, Table 2, p.34
45	Tamarisk	FFG_222	741.60	Richey, 1989, Table 2, p.34
46	Tamarisk	FFG_224	648.10	Richey, 1989, Table 2, p.35
47	Tamarisk	FFG_225	656.30	Richey, 1989, Table 2, p.35
48	Tamarisk	FFG_226	654.00	Richey, 1989, Table 2, p.35
49	Tamarisk	FFG_228	643.20	Richey, 1989, Table 2, p.35
50	Tamarisk	FFG_229	672.00	Richey, 1989, Table 2, p.35
51	Tamarisk	FFG_230	658.10	Richey, 1989, Table 2, p.35
52	Tamarisk	FFG_231	674.20	Richey, 1989, Table 2, p.35
53	Tamarisk	FFG_232	688.20	Richey, 1989, Table 2, p.35
54	Tamarisk	FFG_233	678.80	Richey, 1989, Table 2, p.35
55	Tamarisk	FFG_234	715.00	Richey, 1989, Table 2, p.35
56	Tamarisk	FFG_235	691.30	Richey, 1989, Table 2, p.35
57	Tamarisk	FFG_236	738.50	Richey, 1989, Table 2, p.35
58	Tamarisk	FFG_237	704.80	Richey, 1989, Table 2, p.35
59	Tamarisk	FFG_238	685.50	Richey, 1989, Table 2, p.36
60	Tamarisk	FFG_239	673.30	Richey, 1989, Table 2, p.36
61	Tamarisk	FFG_240	664.50	Richey, 1989, Table 2, p.36
62	Tamarisk	FFG_241	659.00	Richey, 1989, Table 2, p.36
63	Tamarisk	FFG_242	776.70	Richey, 1989, Table 2, p.36
64	Tamarisk	FFG_243	735.50	Richey, 1989, Table 2, p.36
65	Tamarisk	FFG_244	773.10	Richey, 1989, Table 2, p.36
66	Tamarisk	FFG_245	566.90	Richey, 1989, Table 2, p.36
67	Tamarisk	FFG_246	573.00	Richey, 1989, Table 2, p.36
68	Tamarisk	FFG_247	558.00	Richey, 1989, Table 2, p.36
69	Tamarisk	FFG_248	566.00	Richey, 1989, Table 2, p.36
70	Tamarisk	FFG_249	564.20	Richey, 1989, Table 2, p.36
71	Tamarisk	FFG_250	644.50	Richey, 1989, Table 2, p.36
72	Tamarisk	FFG_251	538.50	Richey, 1989, Table 2, p.36
73	Tamarisk	FFG_252	677.80	Richey, 1989, Table 2, p.36
74	Tamarisk	FFG_253	632.50	Richey, 1989, Table 2, p.36
75	Tamarisk	FFG_254	623.90	Richey, 1989, Table 2, p.36
76	Tamarisk	FFG_255	580.10	Richey, 1989, Table 2, p.37

Table B.2. Elevations of Stratigraphic Layers Near WIPP (Continued)

	Layer	Well ID	Elevation	Source
1	Tamarisk	FFG_256	529.80	Richey, 1989, Table 2, p.37
2	Tamarisk	FFG_257	573.60	Richey, 1989, Table 2, p.37
3	Tamarisk	FFG_258	587.60	Richey, 1989, Table 2, p.37
4	Tamarisk	FFG_259	553.50	Richey, 1989, Table 2, p.37
5	Tamarisk	FFG_260	597.40	Richey, 1989, Table 2, p.37
6	Tamarisk	FFG_261	586.40	Richey, 1989, Table 2, p.37
7	Tamarisk	FFG_262	1109.50	Richey, 1989, Table 2, p.37
8	Tamarisk	FFG_263	521.10	Richey, 1989, Table 2, p.37
9	Tamarisk	FFG_264	753.20	Richey, 1989, Table 2, p.37
10	Tamarisk	FFG_265	749.80	Richey, 1989, Table 2, p.37
11	Tamarisk	FFG_266	730.90	Richey, 1989, Table 2, p.37
12	Tamarisk	FFG_267	708.30	Richey, 1989, Table 2, p.37
13	Tamarisk	FFG_268	684.60	Richey, 1989, Table 2, p.37
14	Tamarisk	FFG_269	696.90	Richey, 1989, Table 2, p.38
15	Tamarisk	FFG_270	769.30	Richey, 1989, Table 2, p.38
16	Tamarisk	FFG_271	808.90	Richey, 1989, Table 2, p.38
17	Tamarisk	FFG_272	816.40	Richey, 1989, Table 2, p.38
18	Tamarisk	FFG_273	790.10	Richey, 1989, Table 2, p.38
19	Tamarisk	FFG_274	827.20	Richey, 1989, Table 2, p.38
20	Tamarisk	FFG_275	834.30	Richey, 1989, Table 2, p.38
21	Tamarisk	FFG_276	837.60	Richey, 1989, Table 2, p.38
22	Tamarisk	FFG_277	829.10	Richey, 1989, Table 2, p.38
23	Tamarisk	FFG_278	838.50	Richey, 1989, Table 2, p.38
24	Tamarisk	FFG_279	833.30	Richey, 1989, Table 2, p.38
25	Tamarisk	FFG_280	830.90	Richey, 1989, Table 2, p.38
26	Tamarisk	FFG_281	807.40	Richey, 1989, Table 2, p.38
27	Tamarisk	FFG_283	558.10	Richey, 1989, Table 2, p.39
28	Tamarisk	FFG_284	705.90	Richey, 1989, Table 2, p.39
29	Tamarisk	FFG_285	734.90	Richey, 1989, Table 2, p.39
30	Tamarisk	FFG_286	814.10	Richey, 1989, Table 2, p.39
31	Tamarisk	FFG_287	786.10	Richey, 1989, Table 2, p.39
32	Tamarisk	FFG_288	738.80	Richey, 1989, Table 2, p.39
33	Tamarisk	FFG_289	713.80	Richey, 1989, Table 2, p.39
34	Tamarisk	FFG_290	799.50	Richey, 1989, Table 2, p.39
35	Tamarisk	FFG_291	736.70	Richey, 1989, Table 2, p.39
36	Tamarisk	FFG_292	752.30	Richey, 1989, Table 2, p.39
37	Tamarisk	FFG_293	744.60	Richey, 1989, Table 2, p.39
38	Tamarisk	FFG_294	567.00	Richey, 1989, Table 2, p.39
39	Tamarisk	FFG_295	554.70	Richey, 1989, Table 2, p.39
40	Tamarisk	FFG_297	532.50	Richey, 1989, Table 2, p.39
41	Tamarisk	FFG_298	546.70	Richey, 1989, Table 2, p.40
42	Tamarisk	FFG_299	564.20	Richey, 1989, Table 2, p.40
43	Tamarisk	FFG_300	515.40	Richey, 1989, Table 2, p.40
44	Tamarisk	FFG_301	485.60	Richey, 1989, Table 2, p.40
45	Tamarisk	FFG_302	514.20	Richey, 1989, Table 2, p.40
46	Tamarisk	FFG_303	505.10	Richey, 1989, Table 2, p.40
47	Tamarisk	FFG_304	512.90	Richey, 1989, Table 2, p.40
48	Tamarisk	FFG_305	503.20	Richey, 1989, Table 2, p.40
49	Tamarisk	FFG_306	465.10	Richey, 1989, Table 2, p.40
50	Tamarisk	FFG_307	488.00	Richey, 1989, Table 2, p.40
51	Tamarisk	FFG_308	460.50	Richey, 1989, Table 2, p.40
52	Tamarisk	FFG_309	503.20	Richey, 1989, Table 2, p.40
53	Tamarisk	FFG_310	534.60	Richey, 1989, Table 2, p.40
54	Tamarisk	FFG_311	481.00	Richey, 1989, Table 2, p.40
55	Tamarisk	FFG_312	504.50	Richey, 1989, Table 2, p.40
56	Tamarisk	FFG_313	908.10	Richey, 1989, Table 2, p.41
57	Tamarisk	FFG_314	836.10	Richey, 1989, Table 2, p.41
58	Tamarisk	FFG_315	758.50	Richey, 1989, Table 2, p.41
59	Tamarisk	FFG_316	742.10	Richey, 1989, Table 2, p.41
60	Tamarisk	FFG_317	772.70	Richey, 1989, Table 2, p.41
61	Tamarisk	FFG_318	734.60	Richey, 1989, Table 2, p.41
62	Tamarisk	FFG_319	745.80	Richey, 1989, Table 2, p.41
63	Tamarisk	FFG_320	735.50	Richey, 1989, Table 2, p.41
64	Tamarisk	FFG_321	732.10	Richey, 1989, Table 2, p.41
65	Tamarisk	FFG_322	727.40	Richey, 1989, Table 2, p.41
66	Tamarisk	FFG_323	723.40	Richey, 1989, Table 2, p.41
67	Tamarisk	FFG_324	738.00	Richey, 1989, Table 2, p.41
68	Tamarisk	FFG_325	793.40	Richey, 1989, Table 2, p.41
69	Tamarisk	FFG_326	729.10	Richey, 1989, Table 2, p.41
70	Tamarisk	FFG_327	723.60	Richey, 1989, Table 2, p.42
71	Tamarisk	FFG_328	728.70	Richey, 1989, Table 2, p.42
72	Tamarisk	FFG_329	728.40	Richey, 1989, Table 2, p.42
73	Tamarisk	FFG_330	728.00	Richey, 1989, Table 2, p.42
74	Tamarisk	FFG_331	722.70	Richey, 1989, Table 2, p.42
75	Tamarisk	FFG_332	713.80	Richey, 1989, Table 2, p.42
76	Tamarisk	FFG_333	717.30	Richey, 1989, Table 2, p.42

Table B.2. Elevations of Stratigraphic Layers Near WIPP (Continued)

	Layer	Well ID	Elevation	Source
1	Tamarisk	FFG_334	712.60	Richey, 1989, Table 2, p.42
2	Tamarisk	FFG_335	724.80	Richey, 1989, Table 2, p.42
3	Tamarisk	FFG_336	725.10	Richey, 1989, Table 2, p.42
4	Tamarisk	FFG_337	708.00	Richey, 1989, Table 2, p.42
5	Tamarisk	FFG_338	715.20	Richey, 1989, Table 2, p.42
6	Tamarisk	FFG_339	680.30	Richey, 1989, Table 2, p.42
7	Tamarisk	FFG_340	688.80	Richey, 1989, Table 2, p.42
8	Tamarisk	FFG_342	720.20	Richey, 1989, Table 2, p.43
9	Tamarisk	FFG_344	685.10	Richey, 1989, Table 2, p.43
10	Tamarisk	FFG_345	746.60	Richey, 1989, Table 2, p.43
11	Tamarisk	FFG_347	736.70	Richey, 1989, Table 2, p.43
12	Tamarisk	FFG_348	768.10	Richey, 1989, Table 2, p.43
13	Tamarisk	FFG_349	738.00	Richey, 1989, Table 2, p.43
14	Tamarisk	FFG_350	783.00	Richey, 1989, Table 2, p.43
15	Tamarisk	FFG_351	701.10	Richey, 1989, Table 2, p.43
16	Tamarisk	FFG_352	699.50	Richey, 1989, Table 2, p.43
17	Tamarisk	FFG_353	721.20	Richey, 1989, Table 2, p.43
18	Tamarisk	FFG_354	795.30	Richey, 1989, Table 2, p.43
19	Tamarisk	FFG_361	982.60	Richey, 1989, Table 2, p.44
20	Tamarisk	FFG_362	956.40	Richey, 1989, Table 2, p.44
21	Tamarisk	FFG_363	972.90	Richey, 1989, Table 2, p.44
22	Tamarisk	FFG_364	942.70	Richey, 1989, Table 2, p.44
23	Tamarisk	FFG_366	933.90	Richey, 1989, Table 2, p.44
24	Tamarisk	FFG_367	948.50	Richey, 1989, Table 2, p.44
25	Tamarisk	FFG_370	1012.90	Richey, 1989, Table 2, p.44
26	Tamarisk	FFG_371	994.60	Richey, 1989, Table 2, p.44
27	Tamarisk	FFG_372	1006.40	Richey, 1989, Table 2, p.45
28	Tamarisk	FFG_373	945.00	Richey, 1989, Table 2, p.45
29	Tamarisk	FFG_374	929.70	Richey, 1989, Table 2, p.45
30	Tamarisk	FFG_376	984.80	Richey, 1989, Table 2, p.45
31	Tamarisk	FFG_381	1021.40	Richey, 1989, Table 2, p.45
32	Tamarisk	FFG_383	931.20	Richey, 1989, Table 2, p.45
33	Tamarisk	FFG_384	937.90	Richey, 1989, Table 2, p.45
34	Tamarisk	FFG_385	922.00	Richey, 1989, Table 2, p.45
35	Tamarisk	FFG_387	934.60	Richey, 1989, Table 2, p.45
36	Tamarisk	FFG_388	929.40	Richey, 1989, Table 2, p.46
37	Tamarisk	FFG_389	976.60	Richey, 1989, Table 2, p.46
38	Tamarisk	FFG_390	945.50	Richey, 1989, Table 2, p.46
39	Tamarisk	FFG_391	944.50	Richey, 1989, Table 2, p.46
40	Tamarisk	FFG_392	941.90	Richey, 1989, Table 2, p.46
41	Tamarisk	FFG_393	810.60	Richey, 1989, Table 2, p.46
42	Tamarisk	FFG_394	903.10	Richey, 1989, Table 2, p.46
43	Tamarisk	FFG_395	895.80	Richey, 1989, Table 2, p.46
44	Tamarisk	FFG_396	877.20	Richey, 1989, Table 2, p.46
45	Tamarisk	FFG_398	798.50	Richey, 1989, Table 2, p.46
46	Tamarisk	FFG_399	838.50	Richey, 1989, Table 2, p.46
47	Tamarisk	FFG_401	874.80	Richey, 1989, Table 2, p.46
48	Tamarisk	FFG_402	972.00	Richey, 1989, Table 2, p.46
49	Tamarisk	FFG_403	935.30	Richey, 1989, Table 2, p.47
50	Tamarisk	FFG_404	897.40	Richey, 1989, Table 2, p.47
51	Tamarisk	FFG_407	932.40	Richey, 1989, Table 2, p.47
52	Tamarisk	FFG_408	908.60	Richey, 1989, Table 2, p.47
53	Tamarisk	FFG_409	970.50	Richey, 1989, Table 2, p.47
54	Tamarisk	FFG_418	983.30	Richey, 1989, Table 2, p.48
55	Tamarisk	FFG_419	969.00	Richey, 1989, Table 2, p.48
56	Tamarisk	FFG_420	964.30	Richey, 1989, Table 2, p.48
57	Tamarisk	FFG_421	955.00	Richey, 1989, Table 2, p.48
58	Tamarisk	FFG_422	946.10	Richey, 1989, Table 2, p.48
59	Tamarisk	FFG_426	962.00	Richey, 1989, Table 2, p.48
60	Tamarisk	FFG_432	918.00	Richey, 1989, Table 2, p.48
61	Tamarisk	FFG_433	920.50	Richey, 1989, Table 2, p.48
62	Tamarisk	FFG_438	866.70	Richey, 1989, Table 2, p.49
63	Tamarisk	FFG_453	862.20	Richey, 1989, Table 2, p.50
64	Tamarisk	FFG_455	810.40	Richey, 1989, Table 2, p.50
65	Tamarisk	FFG_456	805.20	Richey, 1989, Table 2, p.50
66	Tamarisk	FFG_457	861.30	Richey, 1989, Table 2, p.50
67	Tamarisk	FFG_458	862.30	Richey, 1989, Table 2, p.50
68	Tamarisk	FFG_459	791.90	Richey, 1989, Table 2, p.50
69	Tamarisk	FFG_462	857.50	Richey, 1989, Table 2, p.50
70	Tamarisk	FFG_463	886.40	Richey, 1989, Table 2, p.51
71	Tamarisk	FFG_464	872.30	Richey, 1989, Table 2, p.51
72	Tamarisk	FFG_465	875.30	Richey, 1989, Table 2, p.51
73	Tamarisk	FFG_467	483.30	Richey, 1989, Table 2, p.51
74	Tamarisk	FFG_468	460.00	Richey, 1989, Table 2, p.51
75	Tamarisk	FFG_470	480.10	Richey, 1989, Table 2, p.51
76	Tamarisk	FFG_471	495.00	Richey, 1989, Table 2, p.51

Table B.2. Elevations of Stratigraphic Layers Near WIPP (Continued)

	Layer	Well ID	Elevation	Source
1	Tamarisk	FFG_472	532.80	Richey, 1989, Table 2, p.51
2	Tamarisk	FFG_473	463.60	Richey, 1989, Table 2, p.51
3	Tamarisk	FFG_474	723.30	Richey, 1989, Table 2, p.51
4	Tamarisk	FFG_475	723.80	Richey, 1989, Table 2, p.51
5	Tamarisk	FFG_476	797.40	Richey, 1989, Table 2, p.51
6	Tamarisk	FFG_477	751.70	Richey, 1989, Table 2, p.51
7	Tamarisk	FFG_478	733.60	Richey, 1989, Table 2, p.52
8	Tamarisk	FFG_479	730.00	Richey, 1989, Table 2, p.52
9	Tamarisk	FFG_480	726.40	Richey, 1989, Table 2, p.52
10	Tamarisk	FFG_481	709.00	Richey, 1989, Table 2, p.52
11	Tamarisk	FFG_482	738.60	Richey, 1989, Table 2, p.52
12	Tamarisk	FFG_483	761.40	Richey, 1989, Table 2, p.52
13	Tamarisk	FFG_484	748.10	Richey, 1989, Table 2, p.52
14	Tamarisk	FFG_485	756.80	Richey, 1989, Table 2, p.52
15	Tamarisk	FFG_486	743.40	Richey, 1989, Table 2, p.52
16	Tamarisk	FFG_487	740.40	Richey, 1989, Table 2, p.52
17	Tamarisk	FFG_488	726.60	Richey, 1989, Table 2, p.52
18	Tamarisk	FFG_489	742.30	Richey, 1989, Table 2, p.52
19	Tamarisk	FFG_490	832.70	Richey, 1989, Table 2, p.52
20	Tamarisk	FFG_491	830.30	Richey, 1989, Table 2, p.52
21	Tamarisk	FFG_492	792.50	Richey, 1989, Table 2, p.52
22	Tamarisk	FFG_493	779.80	Richey, 1989, Table 2, p.53
23	Tamarisk	FFG_494	786.00	Richey, 1989, Table 2, p.53
24	Tamarisk	FFG_495	777.20	Richey, 1989, Table 2, p.53
25	Tamarisk	FFG_496	684.30	Richey, 1989, Table 2, p.53
26	Tamarisk	FFG_497	695.60	Richey, 1989, Table 2, p.53
27	Tamarisk	FFG_498	708.40	Richey, 1989, Table 2, p.53
28	Tamarisk	FFG_499	684.60	Richey, 1989, Table 2, p.53
29	Tamarisk	FFG_500	698.60	Richey, 1989, Table 2, p.53
30	Tamarisk	FFG_501	704.00	Richey, 1989, Table 2, p.53
31	Tamarisk	FFG_502	697.40	Richey, 1989, Table 2, p.53
32	Tamarisk	FFG_503	679.40	Richey, 1989, Table 2, p.53
33	Tamarisk	FFG_504	699.90	Richey, 1989, Table 2, p.53
34	Tamarisk	FFG_505	734.30	Richey, 1989, Table 2, p.53
35	Tamarisk	FFG_506	725.40	Richey, 1989, Table 2, p.53
36	Tamarisk	FFG_507	688.40	Richey, 1989, Table 2, p.53
37	Tamarisk	FFG_508	738.60	Richey, 1989, Table 2, p.53
38	Tamarisk	FFG_509	739.10	Richey, 1989, Table 2, p.54
39	Tamarisk	FFG_510	738.70	Richey, 1989, Table 2, p.54
40	Tamarisk	FFG_511	696.50	Richey, 1989, Table 2, p.54
41	Tamarisk	FFG_512	714.80	Richey, 1989, Table 2, p.54
42	Tamarisk	FFG_513	734.90	Richey, 1989, Table 2, p.54
43	Tamarisk	FFG_514	726.00	Richey, 1989, Table 2, p.54
44	Tamarisk	FFG_515	692.80	Richey, 1989, Table 2, p.54
45	Tamarisk	FFG_516	685.50	Richey, 1989, Table 2, p.54
46	Tamarisk	FFG_517	783.70	Richey, 1989, Table 2, p.54
47	Tamarisk	FFG_518	772.00	Richey, 1989, Table 2, p.54
48	Tamarisk	FFG_519	740.10	Richey, 1989, Table 2, p.54
49	Tamarisk	FFG_520	631.70	Richey, 1989, Table 2, p.54
50	Tamarisk	FFG_521	650.40	Richey, 1989, Table 2, p.54
51	Tamarisk	FFG_522	499.70	Richey, 1989, Table 2, p.54
52	Tamarisk	FFG_523	509.30	Richey, 1989, Table 2, p.54
53	Tamarisk	FFG_524	670.80	Richey, 1989, Table 2, p.55
54	Tamarisk	FFG_525	508.50	Richey, 1989, Table 2, p.55
55	Tamarisk	FFG_526	973.50	Richey, 1989, Table 2, p.55
56	Tamarisk	FFG_527	933.60	Richey, 1989, Table 2, p.55
57	Tamarisk	FFG_528	926.00	Richey, 1989, Table 2, p.55
58	Tamarisk	FFG_530	1000.30	Richey, 1989, Table 2, p.55
59	Tamarisk	FFG_531	919.30	Richey, 1989, Table 2, p.55
60	Tamarisk	FFG_532	907.10	Richey, 1989, Table 2, p.55
61	Tamarisk	FFG_534	946.40	Richey, 1989, Table 2, p.55
62	Tamarisk	FFG_535	912.80	Richey, 1989, Table 2, p.55
63	Tamarisk	FFG_536	928.40	Richey, 1989, Table 2, p.55
64	Tamarisk	FFG_537	904.60	Richey, 1989, Table 2, p.55
65	Tamarisk	FFG_543	970.90	Richey, 1989, Table 2, p.56
66	Tamarisk	FFG_548	907.70	Richey, 1989, Table 2, p.56
67	Tamarisk	FFG_562	645.30	Richey, 1989, Table 2, p.57
68	Tamarisk	FFG_563	557.50	Richey, 1989, Table 2, p.57
69	Tamarisk	FFG_568	634.60	Richey, 1989, Table 2, p.57
70	Tamarisk	FFG_569	663.20	Richey, 1989, Table 2, p.57
71	Tamarisk	FFG_584	764.30	Richey, 1989, Table 2, p.58
72	Tamarisk	FFG_585	730.90	Richey, 1989, Table 2, p.58
73	Tamarisk	FFG_600	722.10	Richey, 1989, Table 2, p.58
74	Tamarisk	FFG_601	615.70	Richey, 1989, Table 2, p.58
75	Tamarisk	FFG_602	1053.10	Richey, 1989, Table 2, p.58
76	Tamarisk	FFG_606	695.90	Richey, 1989, Table 2, p.58

Table B.2. Elevations of Stratigraphic Layers Near WIPP (Continued)

	Layer	Well ID	Elevation	Source
1	Tamarisk	FFG_607	718.40	Richey, 1989, Table 2, p.59
2	Tamarisk	FFG_608	726.60	Richey, 1989, Table 2, p.59
3	Tamarisk	FFG_609	732.70	Richey, 1989, Table 2, p.59
4	Tamarisk	FFG_610	713.20	Richey, 1989, Table 2, p.59
5	Tamarisk	FFG_611	703.20	Richey, 1989, Table 2, p.59
6	Tamarisk	FFG_612	712.70	Richey, 1989, Table 2, p.59
7	Tamarisk	FFG_613	705.90	Richey, 1989, Table 2, p.59
8	Tamarisk	FFG_618	701.90	Richey, 1989, Table 2, p.59
9	Tamarisk	FFG_638	567.30	Richey, 1989, Table 2, p.60
10	Tamarisk	FFG_639	537.40	Richey, 1989, Table 2, p.60
11	Tamarisk	FFG_640	623.10	Richey, 1989, Table 2, p.60
12	Tamarisk	FFG_643	662.40	Richey, 1989, Table 2, p.60
13	Tamarisk	FFG_644	701.20	Richey, 1989, Table 2, p.60
14	Tamarisk	FFG_648	536.10	Richey, 1989, Table 2, p.60
15	Tamarisk	FFG_652	853.70	Richey, 1989, Table 2, p.60
16	Tamarisk	FFG_653	854.10	Richey, 1989, Table 2, p.61
17	Tamarisk	FFG_654	874.80	Richey, 1989, Table 2, p.61
18	Tamarisk	FFG_655	873.20	Richey, 1989, Table 2, p.61
19	Tamarisk	FFG_656	870.80	Richey, 1989, Table 2, p.61
20	Tamarisk	FFG_657	883.70	Richey, 1989, Table 2, p.61
21	Tamarisk	FFG_658	874.40	Richey, 1989, Table 2, p.61
22	Tamarisk	FFG_659	879.70	Richey, 1989, Table 2, p.61
23	Tamarisk	FFG_660	896.90	Richey, 1989, Table 2, p.61
24	Tamarisk	FFG_662	870.80	Richey, 1989, Table 2, p.61
25	Tamarisk	FFG_664	862.00	Richey, 1989, Table 2, p.61
26	Tamarisk	FFG_666	914.40	Richey, 1989, Table 2, p.62
27	Tamarisk	FFG_667	899.50	Richey, 1989, Table 2, p.62
28	Tamarisk	FFG_668	947.70	Richey, 1989, Table 2, p.62
29	Tamarisk	FFG_669	934.20	Richey, 1989, Table 2, p.62
30	Tamarisk	FFG_670	919.30	Richey, 1989, Table 2, p.62
31	Tamarisk	FFG_671	917.70	Richey, 1989, Table 2, p.62
32	Tamarisk	FFG_672	919.90	Richey, 1989, Table 2, p.62
33	Tamarisk	FFG_673	914.70	Richey, 1989, Table 2, p.62
34	Tamarisk	FFG_674	915.00	Richey, 1989, Table 2, p.62
35	Tamarisk	FFG_675	871.60	Richey, 1989, Table 2, p.62
36	Tamarisk	FFG_676	884.20	Richey, 1989, Table 2, p.62
37	Tamarisk	FFG_677	910.50	Richey, 1989, Table 2, p.62
38	Tamarisk	FFG_679	910.40	Richey, 1989, Table 2, p.62
39	Tamarisk	FFG_689	793.70	Richey, 1989, Table 2, p.63
40	Tamarisk	FFG_690	798.90	Richey, 1989, Table 2, p.63
41	Tamarisk	FFG_691	790.40	Richey, 1989, Table 2, p.63
42	Tamarisk	FFG_692	780.30	Richey, 1989, Table 2, p.63
43	Tamarisk	FFG_693	790.90	Richey, 1989, Table 2, p.63
44	Tamarisk	FFG_694	783.30	Richey, 1989, Table 2, p.63
45	Tamarisk	FFG_695	788.80	Richey, 1989, Table 2, p.63
46	Tamarisk	FFG_696	790.60	Richey, 1989, Table 2, p.63
47	Tamarisk	FFG_697	793.70	Richey, 1989, Table 2, p.64
48	Tamarisk	FFG_698	835.50	Richey, 1989, Table 2, p.64
49	Tamarisk	FFG_699	786.70	Richey, 1989, Table 2, p.64
50	Tamarisk	FFG_700	777.00	Richey, 1989, Table 2, p.64
51	Tamarisk	FFG_701	781.90	Richey, 1989, Table 2, p.64
52	Tamarisk	FFG_702	786.70	Richey, 1989, Table 2, p.64
53	Tamarisk	FFG_703	791.60	Richey, 1989, Table 2, p.64
54	Tamarisk	FFG_704	779.40	Richey, 1989, Table 2, p.64
55	Tamarisk	FFG_705	709.60	Richey, 1989, Table 2, p.64
56	Tamarisk	FFG_706	730.70	Richey, 1989, Table 2, p.64
57	Tamarisk	FFG_707	714.20	Richey, 1989, Table 2, p.64
58	Tamarisk	FFG_708	767.20	Richey, 1989, Table 2, p.64
59	Tamarisk	FFG_709	658.70	Richey, 1989, Table 2, p.64
60	Tamarisk	FFG_710	659.30	Richey, 1989, Table 2, p.64
61	Tamarisk	FFG_711	668.20	Richey, 1989, Table 2, p.65
62	Tamarisk	FFG_712	710.90	Richey, 1989, Table 2, p.65
63	Tamarisk	FFG_713	648.10	Richey, 1989, Table 2, p.65
64	Tamarisk	FFG_714	761.90	Richey, 1989, Table 2, p.65
65	Tamarisk	FFG_715	774.80	Richey, 1989, Table 2, p.65
66	Tamarisk	FFG_716	676.60	Richey, 1989, Table 2, p.65
67	Tamarisk	FFG_717	698.10	Richey, 1989, Table 2, p.65
68	Tamarisk	FFG_718	700.90	Richey, 1989, Table 2, p.65
69	Tamarisk	FFG_719	674.20	Richey, 1989, Table 2, p.65
70	Tamarisk	FFG_720	671.50	Richey, 1989, Table 2, p.65
71	Tamarisk	FFG_721	673.60	Richey, 1989, Table 2, p.65
72	Tamarisk	FFG_723	785.30	Richey, 1989, Table 2, p.65
73	Tamarisk	FFG_724	713.60	Richey, 1989, Table 2, p.65
74	Tamarisk	FFG_725	689.70	Richey, 1989, Table 2, p.65
75	Tamarisk	FFG_726	677.50	Richey, 1989, Table 2, p.65
76	Tamarisk	FFG_727	674.90	Richey, 1989, Table 2, p.66

Table B.2. Elevations of Stratigraphic Layers Near WIPP (Continued)

	Layer	Well ID	Elevation	Source
1	Tamarisk	FFG_728	673.30	Richey, 1989, Table 2, p.66
2	Tamarisk	FFG_729	683.70	Richey, 1989, Table 2, p.66
3	Tamarisk	FFG_730	701.30	Richey, 1989, Table 2, p.66
4	Tamarisk	FFG_731	697.80	Richey, 1989, Table 2, p.66
5	Tamarisk	FFG_732	713.20	Richey, 1989, Table 2, p.66
6	Tamarisk	FFG_733	781.20	Richey, 1989, Table 2, p.66
7	Tamarisk	FFG_734	737.00	Richey, 1989, Table 2, p.66
8	Tamarisk	FFG_735	679.10	Richey, 1989, Table 2, p.66
9	Tamarisk	FFG_736	732.40	Richey, 1989, Table 2, p.66
10	Tamarisk	FFG_737	678.80	Richey, 1989, Table 2, p.66
11	Tamarisk	FFG_738	692.50	Richey, 1989, Table 2, p.66
12	Tamarisk	FFG_739	729.80	Richey, 1989, Table 2, p.66
13	Tamarisk	FFG_740	730.60	Richey, 1989, Table 2, p.66
14	Tamarisk	FFG_741	697.70	Richey, 1989, Table 2, p.66
15	Tamarisk	FFG_742	748.60	Richey, 1989, Table 2, p.67
16	Tamarisk	FFG_743	735.20	Richey, 1989, Table 2, p.67
17	Tamarisk	FFG_744	717.80	Richey, 1989, Table 2, p.67
18	Tamarisk	FFG_745	705.90	Richey, 1989, Table 2, p.67
19	Tamarisk	FFG_746	693.00	Richey, 1989, Table 2, p.67
20	Tamarisk	H1	856.20	Mercer, 1983, Table 1
21	Tamarisk	H10C	733.70	Mercer, 1983, Table 1
22	Tamarisk	H2C	864.10	Mercer, 1983, Table 1
23	Tamarisk	H3	855.30	Mercer, 1983, Table 1
24	Tamarisk	H4C	893.40	Mercer, 1983, Table 1
25	Tamarisk	H5C	821.40	Mercer, 1983, Table 1
26	Tamarisk	H6C	863.80	Mercer, 1983, Table 1
27	Tamarisk	H7C	921.40	Mercer, 1983, Table 1
28	Tamarisk	H8C	897.70	Mercer, 1983, Table 1
29	Tamarisk	H9C	869.20	Mercer, 1983, Table 1
30	Tamarisk	P1	883.00	Mercer, 1983, Table 1
31	Tamarisk	P10	831.50	Mercer, 1983, Table 1
32	Tamarisk	P11	817.10	Mercer, 1983, Table 1
33	Tamarisk	P12	862.90	Mercer, 1983, Table 1
34	Tamarisk	P13	862.90	Mercer, 1983, Table 1
35	Tamarisk	P14	878.70	Mercer, 1983, Table 1
36	Tamarisk	P15	911.10	Mercer, 1983, Table 1
37	Tamarisk	P16	889.10	Mercer, 1983, Table 1
38	Tamarisk	P17	875.70	Mercer, 1983, Table 1
39	Tamarisk	P18	837.30	Mercer, 1983, Table 1
40	Tamarisk	P19	824.80	Mercer, 1983, Table 1
41	Tamarisk	P2	824.80	Mercer, 1983, Table 1
42	Tamarisk	P20	819.00	Mercer, 1983, Table 1
43	Tamarisk	P21	822.00	Mercer, 1983, Table 1
44	Tamarisk	P3	862.50	Mercer, 1983, Table 1
45	Tamarisk	P4	840.60	Mercer, 1983, Table 1
46	Tamarisk	P5	841.30	Mercer, 1983, Table 1
47	Tamarisk	P6	887.30	Mercer, 1983, Table 1
48	Tamarisk	P7	894.30	Mercer, 1983, Table 1
49	Tamarisk	P8	873.20	Mercer, 1983, Table 1
50	Tamarisk	P9	843.70	Mercer, 1983, Table 1
51	Tamarisk	SaltShft	848.11	Bechtel, Inc., 1986, Appendix D
52	Tamarisk	WIPP11	815.60	Mercer, 1983, Table 1
53	Tamarisk	WIPP12	840.40	Mercer, 1983, Table 1
54	Tamarisk	WIPP13	860.10	Mercer, 1983, Table 1
55	Tamarisk	WIPP18	841.30	Mercer, 1983, Table 1
56	Tamarisk	WIPP19	841.60	Mercer, 1983, Table 1
57	Tamarisk	WIPP21	846.10	Mercer, 1983, Table 1
58	Tamarisk	WIPP22	844.90	Mercer, 1983, Table 1
59	Tamarisk	WIPP25	879.30	Mercer, 1983, Table 1
60	Tamarisk	WIPP26	930.50	Mercer, 1983, Table 1
61	Tamarisk	WIPP27	909.20	Mercer, 1983, Table 1
62	Tamarisk	WIPP28	925.70	Mercer, 1983, Table 1
63	Tamarisk	WIPP29	907.40	Mercer, 1983, Table 1
64	Tamarisk	WIPP30	881.20	Mercer, 1983, Table 1
65	Tamarisk	WIPP32	910.40	Mercer, 1983, Table 1
66	Tamarisk	WIPP33	870.30	Mercer, 1983, Table 1
67	Tamarisk	WIPP34	820.50	Mercer, 1983, Table 1
68	Tamarisk	WastShft	849.83	Bechtel, Inc., 1986, Appendix E
69	Tamerisk	DOE1	831.60	TME 3159, Sep 1982, Table 2
70	Tamerisk	DOE2	821.70	Mercer et al., 1987, Table 3-2
71	Tamerisk	ERDA9	849.10	SNL and USGS, 1982b, Table 2
72	Tamerisk	REF	849.10	Rechard et al.,1991, Figure 2.2-1
73	Tamerisk	WIPP11	815.70	SNL and USGS, 1982a, Table 2
74	Tamerisk	WIPP12	840.10	D'Appolonia Consulting, 1983, Table 2
75	U_Member	AirShft	782.57	IT Corporation, 1990, Figure 22
76	U_Member	DOE1	761.00	TME 3159, Sep 1982, Table 2

Table B.2. Elevations of Stratigraphic Layers Near WIPP (Continued)

	Layer	Well ID	Elevation	Source
1	U_Member	DOE2	749.00	Mercer et al., 1987, Table 3-2
2	U_Member	ERDA9	779.70	SNL and USGS, 1982b, Table 2
3	U_Member	ExhtShft	779.82	Bechtel, Inc., 1986, Appendix F
4	U_Member	REF	779.70	Rechard et al.,1991, Figure 2.2-1
5	U_Member	SaltShft	779.83	Bechtel, Inc., 1986, Appendix D
6	U_Member	WIPP11	754.40	SNL and USGS, 1982a, Table 2
7	U_Member	WIPP12	767.40	D'Appolonia Consulting, 1983, Table 2
8	U_Member	WastShft	781.32	Bechtel, Inc., 1986, Appendix E
9	Unnamed	AEC7	840.60	Mercer, 1983, Table 1
10	Unnamed	AEC8	814.80	Mercer, 1983, Table 1
11	Unnamed	AirShft	817.19	IT Corporation, 1990, Figure 22
12	Unnamed	B25	817.20	Mercer, 1983, Table 1
13	Unnamed	DOE1	799.40	TME 3159, Sep 1982, Table 2
14	Unnamed	DOE2	784.10	Mercer et al., 1987, Table 3-2
15	Unnamed	ERDA10	873.90	Mercer, 1983, Table 1
16	Unnamed	ERDA6	855.00	Mercer, 1983, Table 1
17	Unnamed	ERDA9	820.50	Mercer, 1983, Table 1
18	Unnamed	ERDA9	816.40	SNL and USGS, 1982b, Table 2
19	Unnamed	ExhtShft	814.75	Bechtel, Inc., 1986, Appendix F
20	Unnamed	FFG_002	618.10	Richey, 1989, Table 2, p.21
21	Unnamed	FFG_004	659.90	Richey, 1989, Table 2, p.21
22	Unnamed	FFG_005	622.10	Richey, 1989, Table 2, p.21
23	Unnamed	FFG_006	608.10	Richey, 1989, Table 2, p.21
24	Unnamed	FFG_007	593.70	Richey, 1989, Table 2, p.21
25	Unnamed	FFG_009	596.50	Richey, 1989, Table 2, p.21
26	Unnamed	FFG_011	603.50	Richey, 1989, Table 2, p.21
27	Unnamed	FFG_012	606.20	Richey, 1989, Table 2, p.21
28	Unnamed	FFG_013	634.30	Richey, 1989, Table 2, p.21
29	Unnamed	FFG_014	658.90	Richey, 1989, Table 2, p.21
30	Unnamed	FFG_016	579.40	Richey, 1989, Table 2, p.21
31	Unnamed	FFG_017	587.30	Richey, 1989, Table 2, p.22
32	Unnamed	FFG_018	590.70	Richey, 1989, Table 2, p.22
33	Unnamed	FFG_019	580.30	Richey, 1989, Table 2, p.22
34	Unnamed	FFG_020	655.30	Richey, 1989, Table 2, p.22
35	Unnamed	FFG_023	587.70	Richey, 1989, Table 2, p.22
36	Unnamed	FFG_024	571.80	Richey, 1989, Table 2, p.22
37	Unnamed	FFG_025	591.80	Richey, 1989, Table 2, p.22
38	Unnamed	FFG_026	585.50	Richey, 1989, Table 2, p.22
39	Unnamed	FFG_027	578.50	Richey, 1989, Table 2, p.22
40	Unnamed	FFG_028	572.50	Richey, 1989, Table 2, p.22
41	Unnamed	FFG_029	558.10	Richey, 1989, Table 2, p.22
42	Unnamed	FFG_030	557.20	Richey, 1989, Table 2, p.22
43	Unnamed	FFG_031	547.40	Richey, 1989, Table 2, p.22
44	Unnamed	FFG_032	546.10	Richey, 1989, Table 2, p.22
45	Unnamed	FFG_033	542.20	Richey, 1989, Table 2, p.22
46	Unnamed	FFG_034	542.50	Richey, 1989, Table 2, p.23
47	Unnamed	FFG_035	530.90	Richey, 1989, Table 2, p.23
48	Unnamed	FFG_036	535.60	Richey, 1989, Table 2, p.23
49	Unnamed	FFG_037	528.80	Richey, 1989, Table 2, p.23
50	Unnamed	FFG_038	517.50	Richey, 1989, Table 2, p.23
51	Unnamed	FFG_039	725.50	Richey, 1989, Table 2, p.23
52	Unnamed	FFG_040	645.30	Richey, 1989, Table 2, p.23
53	Unnamed	FFG_041	726.40	Richey, 1989, Table 2, p.23
54	Unnamed	FFG_042	730.00	Richey, 1989, Table 2, p.23
55	Unnamed	FFG_043	728.70	Richey, 1989, Table 2, p.23
56	Unnamed	FFG_044	680.90	Richey, 1989, Table 2, p.23
57	Unnamed	FFG_047	556.00	Richey, 1989, Table 2, p.23
58	Unnamed	FFG_048	573.30	Richey, 1989, Table 2, p.23
59	Unnamed	FFG_049	559.60	Richey, 1989, Table 2, p.23
60	Unnamed	FFG_050	574.90	Richey, 1989, Table 2, p.24
61	Unnamed	FFG_051	566.30	Richey, 1989, Table 2, p.24
62	Unnamed	FFG_052	589.80	Richey, 1989, Table 2, p.24
63	Unnamed	FFG_053	555.60	Richey, 1989, Table 2, p.24
64	Unnamed	FFG_054	556.60	Richey, 1989, Table 2, p.24
65	Unnamed	FFG_055	557.80	Richey, 1989, Table 2, p.24
66	Unnamed	FFG_056	556.90	Richey, 1989, Table 2, p.24
67	Unnamed	FFG_057	558.10	Richey, 1989, Table 2, p.24
68	Unnamed	FFG_058	560.80	Richey, 1989, Table 2, p.24
69	Unnamed	FFG_059	564.80	Richey, 1989, Table 2, p.24
70	Unnamed	FFG_060	563.20	Richey, 1989, Table 2, p.24
71	Unnamed	FFG_061	565.10	Richey, 1989, Table 2, p.24
72	Unnamed	FFG_062	507.20	Richey, 1989, Table 2, p.24
73	Unnamed	FFG_063	465.80	Richey, 1989, Table 2, p.24
74	Unnamed	FFG_064	488.90	Richey, 1989, Table 2, p.24
75	Unnamed	FFG_065	464.50	Richey, 1989, Table 2, p.24
76	Unnamed	FFG_066	429.10	Richey, 1989, Table 2, p.24

Table B.2. Elevations of Stratigraphic Layers Near WIPP (Continued)

	Layer	Well ID	Elevation	Source
1	Unnamed	FFG_067	464.00	Richey, 1989, Table 2, p.25
2	Unnamed	FFG_068	424.00	Richey, 1989, Table 2, p.25
3	Unnamed	FFG_069	441.40	Richey, 1989, Table 2, p.25
4	Unnamed	FFG_070	479.10	Richey, 1989, Table 2, p.25
5	Unnamed	FFG_071	748.30	Richey, 1989, Table 2, p.25
6	Unnamed	FFG_072	674.20	Richey, 1989, Table 2, p.25
7	Unnamed	FFG_073	652.20	Richey, 1989, Table 2, p.25
8	Unnamed	FFG_074	660.30	Richey, 1989, Table 2, p.25
9	Unnamed	FFG_075	712.10	Richey, 1989, Table 2, p.25
10	Unnamed	FFG_076	771.50	Richey, 1989, Table 2, p.25
11	Unnamed	FFG_078	807.70	Richey, 1989, Table 2, p.25
12	Unnamed	FFG_079	780.90	Richey, 1989, Table 2, p.25
13	Unnamed	FFG_080	758.30	Richey, 1989, Table 2, p.25
14	Unnamed	FFG_081	674.90	Richey, 1989, Table 2, p.26
15	Unnamed	FFG_082	705.30	Richey, 1989, Table 2, p.26
16	Unnamed	FFG_083	632.00	Richey, 1989, Table 2, p.26
17	Unnamed	FFG_084	654.70	Richey, 1989, Table 2, p.26
18	Unnamed	FFG_085	649.00	Richey, 1989, Table 2, p.26
19	Unnamed	FFG_086	657.40	Richey, 1989, Table 2, p.26
20	Unnamed	FFG_087	630.00	Richey, 1989, Table 2, p.26
21	Unnamed	FFG_088	622.70	Richey, 1989, Table 2, p.26
22	Unnamed	FFG_089	606.60	Richey, 1989, Table 2, p.26
23	Unnamed	FFG_091	643.80	Richey, 1989, Table 2, p.26
24	Unnamed	FFG_092	662.30	Richey, 1989, Table 2, p.26
25	Unnamed	FFG_093	668.10	Richey, 1989, Table 2, p.26
26	Unnamed	FFG_094	666.60	Richey, 1989, Table 2, p.26
27	Unnamed	FFG_095	645.20	Richey, 1989, Table 2, p.26
28	Unnamed	FFG_096	629.40	Richey, 1989, Table 2, p.26
29	Unnamed	FFG_097	608.40	Richey, 1989, Table 2, p.27
30	Unnamed	FFG_098	581.80	Richey, 1989, Table 2, p.27
31	Unnamed	FFG_099	574.60	Richey, 1989, Table 2, p.27
32	Unnamed	FFG_100	558.70	Richey, 1989, Table 2, p.27
33	Unnamed	FFG_101	527.30	Richey, 1989, Table 2, p.27
34	Unnamed	FFG_102	542.90	Richey, 1989, Table 2, p.27
35	Unnamed	FFG_103	601.70	Richey, 1989, Table 2, p.27
36	Unnamed	FFG_104	502.10	Richey, 1989, Table 2, p.27
37	Unnamed	FFG_105	861.40	Richey, 1989, Table 2, p.27
38	Unnamed	FFG_106	894.60	Richey, 1989, Table 2, p.27
39	Unnamed	FFG_107	878.80	Richey, 1989, Table 2, p.27
40	Unnamed	FFG_108	869.60	Richey, 1989, Table 2, p.27
41	Unnamed	FFG_109	856.20	Richey, 1989, Table 2, p.27
42	Unnamed	FFG_110	824.50	Richey, 1989, Table 2, p.27
43	Unnamed	FFG_111	830.60	Richey, 1989, Table 2, p.27
44	Unnamed	FFG_112	816.80	Richey, 1989, Table 2, p.28
45	Unnamed	FFG_113	830.90	Richey, 1989, Table 2, p.28
46	Unnamed	FFG_114	863.20	Richey, 1989, Table 2, p.28
47	Unnamed	FFG_115	848.30	Richey, 1989, Table 2, p.28
48	Unnamed	FFG_116	865.30	Richey, 1989, Table 2, p.28
49	Unnamed	FFG_117	856.50	Richey, 1989, Table 2, p.28
50	Unnamed	FFG_119	864.80	Richey, 1989, Table 2, p.28
51	Unnamed	FFG_120	865.10	Richey, 1989, Table 2, p.28
52	Unnamed	FFG_121	873.30	Richey, 1989, Table 2, p.28
53	Unnamed	FFG_122	868.70	Richey, 1989, Table 2, p.28
54	Unnamed	FFG_123	861.00	Richey, 1989, Table 2, p.28
55	Unnamed	FFG_124	830.90	Richey, 1989, Table 2, p.28
56	Unnamed	FFG_125	842.10	Richey, 1989, Table 2, p.28
57	Unnamed	FFG_126	846.60	Richey, 1989, Table 2, p.28
58	Unnamed	FFG_127	851.60	Richey, 1989, Table 2, p.28
59	Unnamed	FFG_128	877.60	Richey, 1989, Table 2, p.28
60	Unnamed	FFG_129	852.20	Richey, 1989, Table 2, p.28
61	Unnamed	FFG_130	888.50	Richey, 1989, Table 2, p.28
62	Unnamed	FFG_132	890.90	Richey, 1989, Table 2, p.29
63	Unnamed	FFG_133	895.50	Richey, 1989, Table 2, p.29
64	Unnamed	FFG_134	896.80	Richey, 1989, Table 2, p.29
65	Unnamed	FFG_135	875.10	Richey, 1989, Table 2, p.29
66	Unnamed	FFG_136	876.40	Richey, 1989, Table 2, p.29
67	Unnamed	FFG_137	884.60	Richey, 1989, Table 2, p.29
68	Unnamed	FFG_138	834.90	Richey, 1989, Table 2, p.29
69	Unnamed	FFG_139	847.90	Richey, 1989, Table 2, p.29
70	Unnamed	FFG_140	785.00	Richey, 1989, Table 2, p.29
71	Unnamed	FFG_141	812.50	Richey, 1989, Table 2, p.29
72	Unnamed	FFG_142	788.30	Richey, 1989, Table 2, p.29
73	Unnamed	FFG_143	797.30	Richey, 1989, Table 2, p.29
74	Unnamed	FFG_144	883.70	Richey, 1989, Table 2, p.29
75	Unnamed	FFG_145	887.00	Richey, 1989, Table 2, p.29
76	Unnamed	FFG_146	897.70	Richey, 1989, Table 2, p.29

Table B.2. Elevations of Stratigraphic Layers Near WIPP (Continued)

	Layer	Well ID	Elevation	Source
1	Unnamed	FFG_147	875.40	Richey, 1989, Table 2, p.29
2	Unnamed	FFG_148	894.90	Richey, 1989, Table 2, p.29
3	Unnamed	FFG_149	903.10	Richey, 1989, Table 2, p.30
4	Unnamed	FFG_152	893.10	Richey, 1989, Table 2, p.30
5	Unnamed	FFG_155	894.00	Richey, 1989, Table 2, p.30
6	Unnamed	FFG_156	895.50	Richey, 1989, Table 2, p.30
7	Unnamed	FFG_157	898.60	Richey, 1989, Table 2, p.30
8	Unnamed	FFG_158	918.00	Richey, 1989, Table 2, p.30
9	Unnamed	FFG_159	891.60	Richey, 1989, Table 2, p.30
10	Unnamed	FFG_160	886.10	Richey, 1989, Table 2, p.30
11	Unnamed	FFG_161	894.90	Richey, 1989, Table 2, p.30
12	Unnamed	FFG_162	884.60	Richey, 1989, Table 2, p.30
13	Unnamed	FFG_163	888.20	Richey, 1989, Table 2, p.30
14	Unnamed	FFG_164	928.50	Richey, 1989, Table 2, p.30
15	Unnamed	FFG_165	902.20	Richey, 1989, Table 2, p.30
16	Unnamed	FFG_166	891.80	Richey, 1989, Table 2, p.31
17	Unnamed	FFG_167	877.90	Richey, 1989, Table 2, p.31
18	Unnamed	FFG_168	898.90	Richey, 1989, Table 2, p.31
19	Unnamed	FFG_169	909.20	Richey, 1989, Table 2, p.31
20	Unnamed	FFG_170	893.00	Richey, 1989, Table 2, p.31
21	Unnamed	FFG_171	909.30	Richey, 1989, Table 2, p.31
22	Unnamed	FFG_172	906.10	Richey, 1989, Table 2, p.31
23	Unnamed	FFG_173	867.80	Richey, 1989, Table 2, p.31
24	Unnamed	FFG_177	880.00	Richey, 1989, Table 2, p.31
25	Unnamed	FFG_178	711.40	Richey, 1989, Table 2, p.31
26	Unnamed	FFG_179	875.10	Richey, 1989, Table 2, p.31
27	Unnamed	FFG_180	874.70	Richey, 1989, Table 2, p.31
28	Unnamed	FFG_181	922.90	Richey, 1989, Table 2, p.32
29	Unnamed	FFG_182	804.30	Richey, 1989, Table 2, p.32
30	Unnamed	FFG_183	893.40	Richey, 1989, Table 2, p.32
31	Unnamed	FFG_184	883.60	Richey, 1989, Table 2, p.32
32	Unnamed	FFG_185	891.80	Richey, 1989, Table 2, p.32
33	Unnamed	FFG_186	819.30	Richey, 1989, Table 2, p.32
34	Unnamed	FFG_188	837.60	Richey, 1989, Table 2, p.32
35	Unnamed	FFG_189	859.60	Richey, 1989, Table 2, p.32
36	Unnamed	FFG_190	835.10	Richey, 1989, Table 2, p.32
37	Unnamed	FFG_191	839.40	Richey, 1989, Table 2, p.32
38	Unnamed	FFG_192	764.40	Richey, 1989, Table 2, p.32
39	Unnamed	FFG_194	780.60	Richey, 1989, Table 2, p.33
40	Unnamed	FFG_195	792.80	Richey, 1989, Table 2, p.33
41	Unnamed	FFG_196	827.50	Richey, 1989, Table 2, p.33
42	Unnamed	FFG_197	831.20	Richey, 1989, Table 2, p.33
43	Unnamed	FFG_198	831.80	Richey, 1989, Table 2, p.33
44	Unnamed	FFG_199	818.70	Richey, 1989, Table 2, p.33
45	Unnamed	FFG_200	828.10	Richey, 1989, Table 2, p.33
46	Unnamed	FFG_201	830.00	Richey, 1989, Table 2, p.33
47	Unnamed	FFG_202	763.20	Richey, 1989, Table 2, p.33
48	Unnamed	FFG_203	767.50	Richey, 1989, Table 2, p.33
49	Unnamed	FFG_204	805.30	Richey, 1989, Table 2, p.33
50	Unnamed	FFG_205	816.60	Richey, 1989, Table 2, p.33
51	Unnamed	FFG_206	828.10	Richey, 1989, Table 2, p.33
52	Unnamed	FFG_207	826.00	Richey, 1989, Table 2, p.33
53	Unnamed	FFG_208	834.50	Richey, 1989, Table 2, p.34
54	Unnamed	FFG_209	829.70	Richey, 1989, Table 2, p.34
55	Unnamed	FFG_210	818.70	Richey, 1989, Table 2, p.34
56	Unnamed	FFG_212	809.00	Richey, 1989, Table 2, p.34
57	Unnamed	FFG_213	828.80	Richey, 1989, Table 2, p.34
58	Unnamed	FFG_214	808.60	Richey, 1989, Table 2, p.34
59	Unnamed	FFG_215	784.90	Richey, 1989, Table 2, p.34
60	Unnamed	FFG_216	682.70	Richey, 1989, Table 2, p.34
61	Unnamed	FFG_217	805.60	Richey, 1989, Table 2, p.34
62	Unnamed	FFG_218	794.30	Richey, 1989, Table 2, p.34
63	Unnamed	FFG_219	840.30	Richey, 1989, Table 2, p.34
64	Unnamed	FFG_220	789.50	Richey, 1989, Table 2, p.34
65	Unnamed	FFG_221	744.30	Richey, 1989, Table 2, p.34
66	Unnamed	FFG_222	705.00	Richey, 1989, Table 2, p.34
67	Unnamed	FFG_224	590.10	Richey, 1989, Table 2, p.35
68	Unnamed	FFG_225	598.00	Richey, 1989, Table 2, p.35
69	Unnamed	FFG_226	594.80	Richey, 1989, Table 2, p.35
70	Unnamed	FFG_228	580.70	Richey, 1989, Table 2, p.35
71	Unnamed	FFG_229	607.10	Richey, 1989, Table 2, p.35
72	Unnamed	FFG_230	595.00	Richey, 1989, Table 2, p.35
73	Unnamed	FFG_231	613.80	Richey, 1989, Table 2, p.35
74	Unnamed	FFG_232	625.80	Richey, 1989, Table 2, p.35
75	Unnamed	FFG_233	617.90	Richey, 1989, Table 2, p.35
76	Unnamed	FFG_234	653.50	Richey, 1989, Table 2, p.35

Table B.2. Elevations of Stratigraphic Layers Near WIPP (Continued)

	Layer	Well ID	Elevation	Source
1	Unnamed	FFG_235	628.50	Richey, 1989, Table 2, p.35
2	Unnamed	FFG_236	677.20	Richey, 1989, Table 2, p.35
3	Unnamed	FFG_237	634.40	Richey, 1989, Table 2, p.35
4	Unnamed	FFG_238	621.50	Richey, 1989, Table 2, p.36
5	Unnamed	FFG_239	613.50	Richey, 1989, Table 2, p.36
6	Unnamed	FFG_240	602.60	Richey, 1989, Table 2, p.36
7	Unnamed	FFG_241	598.10	Richey, 1989, Table 2, p.36
8	Unnamed	FFG_242	724.20	Richey, 1989, Table 2, p.36
9	Unnamed	FFG_243	659.30	Richey, 1989, Table 2, p.36
10	Unnamed	FFG_244	715.20	Richey, 1989, Table 2, p.36
11	Unnamed	FFG_245	503.50	Richey, 1989, Table 2, p.36
12	Unnamed	FFG_246	508.10	Richey, 1989, Table 2, p.36
13	Unnamed	FFG_247	493.70	Richey, 1989, Table 2, p.36
14	Unnamed	FFG_248	498.30	Richey, 1989, Table 2, p.36
15	Unnamed	FFG_249	498.30	Richey, 1989, Table 2, p.36
16	Unnamed	FFG_250	580.50	Richey, 1989, Table 2, p.36
17	Unnamed	FFG_251	470.00	Richey, 1989, Table 2, p.36
18	Unnamed	FFG_252	612.60	Richey, 1989, Table 2, p.36
19	Unnamed	FFG_253	561.50	Richey, 1989, Table 2, p.36
20	Unnamed	FFG_254	554.70	Richey, 1989, Table 2, p.36
21	Unnamed	FFG_255	506.30	Richey, 1989, Table 2, p.37
22	Unnamed	FFG_256	470.90	Richey, 1989, Table 2, p.37
23	Unnamed	FFG_257	517.20	Richey, 1989, Table 2, p.37
24	Unnamed	FFG_258	536.40	Richey, 1989, Table 2, p.37
25	Unnamed	FFG_259	494.90	Richey, 1989, Table 2, p.37
26	Unnamed	FFG_260	548.90	Richey, 1989, Table 2, p.37
27	Unnamed	FFG_261	537.30	Richey, 1989, Table 2, p.37
28	Unnamed	FFG_262	477.00	Richey, 1989, Table 2, p.37
29	Unnamed	FFG_263	448.50	Richey, 1989, Table 2, p.37
30	Unnamed	FFG_264	696.20	Richey, 1989, Table 2, p.37
31	Unnamed	FFG_265	677.30	Richey, 1989, Table 2, p.37
32	Unnamed	FFG_266	656.80	Richey, 1989, Table 2, p.37
33	Unnamed	FFG_267	632.70	Richey, 1989, Table 2, p.37
34	Unnamed	FFG_268	606.30	Richey, 1989, Table 2, p.37
35	Unnamed	FFG_269	617.60	Richey, 1989, Table 2, p.38
36	Unnamed	FFG_270	721.10	Richey, 1989, Table 2, p.38
37	Unnamed	FFG_271	767.80	Richey, 1989, Table 2, p.38
38	Unnamed	FFG_272	743.90	Richey, 1989, Table 2, p.38
39	Unnamed	FFG_273	745.30	Richey, 1989, Table 2, p.38
40	Unnamed	FFG_274	785.80	Richey, 1989, Table 2, p.38
41	Unnamed	FFG_275	794.60	Richey, 1989, Table 2, p.38
42	Unnamed	FFG_276	795.80	Richey, 1989, Table 2, p.38
43	Unnamed	FFG_277	789.10	Richey, 1989, Table 2, p.38
44	Unnamed	FFG_278	765.40	Richey, 1989, Table 2, p.38
45	Unnamed	FFG_279	767.70	Richey, 1989, Table 2, p.38
46	Unnamed	FFG_280	780.00	Richey, 1989, Table 2, p.38
47	Unnamed	FFG_281	754.40	Richey, 1989, Table 2, p.38
48	Unnamed	FFG_283	489.20	Richey, 1989, Table 2, p.39
49	Unnamed	FFG_284	641.30	Richey, 1989, Table 2, p.39
50	Unnamed	FFG_285	660.50	Richey, 1989, Table 2, p.39
51	Unnamed	FFG_286	766.20	Richey, 1989, Table 2, p.39
52	Unnamed	FFG_287	733.30	Richey, 1989, Table 2, p.39
53	Unnamed	FFG_288	662.60	Richey, 1989, Table 2, p.39
54	Unnamed	FFG_289	673.90	Richey, 1989, Table 2, p.39
55	Unnamed	FFG_290	760.80	Richey, 1989, Table 2, p.39
56	Unnamed	FFG_291	660.80	Richey, 1989, Table 2, p.39
57	Unnamed	FFG_292	717.80	Richey, 1989, Table 2, p.39
58	Unnamed	FFG_293	710.50	Richey, 1989, Table 2, p.39
59	Unnamed	FFG_294	497.50	Richey, 1989, Table 2, p.39
60	Unnamed	FFG_295	480.00	Richey, 1989, Table 2, p.39
61	Unnamed	FFG_297	455.40	Richey, 1989, Table 2, p.39
62	Unnamed	FFG_298	520.40	Richey, 1989, Table 2, p.40
63	Unnamed	FFG_299	489.80	Richey, 1989, Table 2, p.40
64	Unnamed	FFG_300	473.00	Richey, 1989, Table 2, p.40
65	Unnamed	FFG_301	430.40	Richey, 1989, Table 2, p.40
66	Unnamed	FFG_302	436.80	Richey, 1989, Table 2, p.40
67	Unnamed	FFG_303	442.00	Richey, 1989, Table 2, p.40
68	Unnamed	FFG_304	438.90	Richey, 1989, Table 2, p.40
69	Unnamed	FFG_305	434.60	Richey, 1989, Table 2, p.40
70	Unnamed	FFG_306	405.30	Richey, 1989, Table 2, p.40
71	Unnamed	FFG_307	424.30	Richey, 1989, Table 2, p.40
72	Unnamed	FFG_308	367.80	Richey, 1989, Table 2, p.40
73	Unnamed	FFG_309	427.90	Richey, 1989, Table 2, p.40
74	Unnamed	FFG_310	469.10	Richey, 1989, Table 2, p.40
75	Unnamed	FFG_311	420.30	Richey, 1989, Table 2, p.40
76	Unnamed	FFG_312	424.00	Richey, 1989, Table 2, p.40

Table B.2. Elevations of Stratigraphic Layers Near WIPP (Continued)

	Layer	Well ID	Elevation	Source
1	Unnamed	FFG_313	862.00	Richey, 1989, Table 2, p.41
2	Unnamed	FFG_314	781.60	Richey, 1989, Table 2, p.41
3	Unnamed	FFG_315	694.20	Richey, 1989, Table 2, p.41
4	Unnamed	FFG_316	670.20	Richey, 1989, Table 2, p.41
5	Unnamed	FFG_317	725.10	Richey, 1989, Table 2, p.41
6	Unnamed	FFG_318	702.60	Richey, 1989, Table 2, p.41
7	Unnamed	FFG_319	696.40	Richey, 1989, Table 2, p.41
8	Unnamed	FFG_320	662.00	Richey, 1989, Table 2, p.41
9	Unnamed	FFG_321	661.70	Richey, 1989, Table 2, p.41
10	Unnamed	FFG_322	662.20	Richey, 1989, Table 2, p.41
11	Unnamed	FFG_323	667.90	Richey, 1989, Table 2, p.41
12	Unnamed	FFG_324	692.20	Richey, 1989, Table 2, p.41
13	Unnamed	FFG_325	753.20	Richey, 1989, Table 2, p.41
14	Unnamed	FFG_326	698.00	Richey, 1989, Table 2, p.41
15	Unnamed	FFG_327	681.90	Richey, 1989, Table 2, p.42
16	Unnamed	FFG_328	664.70	Richey, 1989, Table 2, p.42
17	Unnamed	FFG_329	661.40	Richey, 1989, Table 2, p.42
18	Unnamed	FFG_330	661.00	Richey, 1989, Table 2, p.42
19	Unnamed	FFG_331	646.80	Richey, 1989, Table 2, p.42
20	Unnamed	FFG_332	632.80	Richey, 1989, Table 2, p.42
21	Unnamed	FFG_333	643.00	Richey, 1989, Table 2, p.42
22	Unnamed	FFG_334	637.00	Richey, 1989, Table 2, p.42
23	Unnamed	FFG_335	655.00	Richey, 1989, Table 2, p.42
24	Unnamed	FFG_336	650.40	Richey, 1989, Table 2, p.42
25	Unnamed	FFG_337	634.30	Richey, 1989, Table 2, p.42
26	Unnamed	FFG_338	639.00	Richey, 1989, Table 2, p.42
27	Unnamed	FFG_339	604.10	Richey, 1989, Table 2, p.42
28	Unnamed	FFG_340	609.30	Richey, 1989, Table 2, p.42
29	Unnamed	FFG_342	676.30	Richey, 1989, Table 2, p.43
30	Unnamed	FFG_344	650.90	Richey, 1989, Table 2, p.43
31	Unnamed	FFG_345	671.30	Richey, 1989, Table 2, p.43
32	Unnamed	FFG_347	692.80	Richey, 1989, Table 2, p.43
33	Unnamed	FFG_348	733.00	Richey, 1989, Table 2, p.43
34	Unnamed	FFG_349	709.30	Richey, 1989, Table 2, p.43
35	Unnamed	FFG_350	739.70	Richey, 1989, Table 2, p.43
36	Unnamed	FFG_351	621.20	Richey, 1989, Table 2, p.43
37	Unnamed	FFG_352	621.80	Richey, 1989, Table 2, p.43
38	Unnamed	FFG_353	644.10	Richey, 1989, Table 2, p.43
39	Unnamed	FFG_354	756.00	Richey, 1989, Table 2, p.43
40	Unnamed	FFG_361	948.50	Richey, 1989, Table 2, p.44
41	Unnamed	FFG_362	911.00	Richey, 1989, Table 2, p.44
42	Unnamed	FFG_363	937.90	Richey, 1989, Table 2, p.44
43	Unnamed	FFG_364	909.80	Richey, 1989, Table 2, p.44
44	Unnamed	FFG_366	904.00	Richey, 1989, Table 2, p.44
45	Unnamed	FFG_367	922.60	Richey, 1989, Table 2, p.44
46	Unnamed	FFG_370	962.60	Richey, 1989, Table 2, p.44
47	Unnamed	FFG_371	958.60	Richey, 1989, Table 2, p.44
48	Unnamed	FFG_372	941.50	Richey, 1989, Table 2, p.45
49	Unnamed	FFG_373	902.00	Richey, 1989, Table 2, p.45
50	Unnamed	FFG_374	902.20	Richey, 1989, Table 2, p.45
51	Unnamed	FFG_376	939.70	Richey, 1989, Table 2, p.45
52	Unnamed	FFG_381	908.60	Richey, 1989, Table 2, p.45
53	Unnamed	FFG_383	902.20	Richey, 1989, Table 2, p.45
54	Unnamed	FFG_384	912.30	Richey, 1989, Table 2, p.45
55	Unnamed	FFG_385	906.80	Richey, 1989, Table 2, p.45
56	Unnamed	FFG_387	901.60	Richey, 1989, Table 2, p.45
57	Unnamed	FFG_388	893.70	Richey, 1989, Table 2, p.46
58	Unnamed	FFG_389	917.50	Richey, 1989, Table 2, p.46
59	Unnamed	FFG_390	913.50	Richey, 1989, Table 2, p.46
60	Unnamed	FFG_391	913.10	Richey, 1989, Table 2, p.46
61	Unnamed	FFG_392	904.40	Richey, 1989, Table 2, p.46
62	Unnamed	FFG_393	781.00	Richey, 1989, Table 2, p.46
63	Unnamed	FFG_394	877.20	Richey, 1989, Table 2, p.46
64	Unnamed	FFG_395	867.50	Richey, 1989, Table 2, p.46
65	Unnamed	FFG_396	847.10	Richey, 1989, Table 2, p.46
66	Unnamed	FFG_398	767.20	Richey, 1989, Table 2, p.46
67	Unnamed	FFG_399	780.60	Richey, 1989, Table 2, p.46
68	Unnamed	FFG_401	833.60	Richey, 1989, Table 2, p.46
69	Unnamed	FFG_402	936.70	Richey, 1989, Table 2, p.46
70	Unnamed	FFG_403	903.30	Richey, 1989, Table 2, p.47
71	Unnamed	FFG_404	867.20	Richey, 1989, Table 2, p.47
72	Unnamed	FFG_407	898.90	Richey, 1989, Table 2, p.47
73	Unnamed	FFG_408	901.00	Richey, 1989, Table 2, p.47
74	Unnamed	FFG_409	932.40	Richey, 1989, Table 2, p.47
75	Unnamed	FFG_411	873.90	Richey, 1989, Table 2, p.47
76	Unnamed	FFG_413	906.20	Richey, 1989, Table 2, p.47

Table B.2. Elevations of Stratigraphic Layers Near WIPP (Continued)

	Layer	Well ID	Elevation	Source
1	Unnamed	FFG_418	923.00	Richey, 1989, Table 2, p.48
2	Unnamed	FFG_419	936.70	Richey, 1989, Table 2, p.48
3	Unnamed	FFG_420	927.80	Richey, 1989, Table 2, p.48
4	Unnamed	FFG_421	913.80	Richey, 1989, Table 2, p.48
5	Unnamed	FFG_422	915.60	Richey, 1989, Table 2, p.48
6	Unnamed	FFG_426	919.30	Richey, 1989, Table 2, p.48
7	Unnamed	FFG_432	876.90	Richey, 1989, Table 2, p.48
8	Unnamed	FFG_433	892.40	Richey, 1989, Table 2, p.48
9	Unnamed	FFG_438	829.80	Richey, 1989, Table 2, p.49
10	Unnamed	FFG_445	911.60	Richey, 1989, Table 2, p.49
11	Unnamed	FFG_453	772.90	Richey, 1989, Table 2, p.50
12	Unnamed	FFG_455	761.40	Richey, 1989, Table 2, p.50
13	Unnamed	FFG_456	769.90	Richey, 1989, Table 2, p.50
14	Unnamed	FFG_457	822.60	Richey, 1989, Table 2, p.50
15	Unnamed	FFG_458	825.10	Richey, 1989, Table 2, p.50
16	Unnamed	FFG_459	752.30	Richey, 1989, Table 2, p.50
17	Unnamed	FFG_462	820.70	Richey, 1989, Table 2, p.50
18	Unnamed	FFG_463	843.70	Richey, 1989, Table 2, p.51
19	Unnamed	FFG_464	833.60	Richey, 1989, Table 2, p.51
20	Unnamed	FFG_465	835.10	Richey, 1989, Table 2, p.51
21	Unnamed	FFG_467	423.00	Richey, 1989, Table 2, p.51
22	Unnamed	FFG_468	373.10	Richey, 1989, Table 2, p.51
23	Unnamed	FFG_470	402.60	Richey, 1989, Table 2, p.51
24	Unnamed	FFG_471	420.60	Richey, 1989, Table 2, p.51
25	Unnamed	FFG_472	495.60	Richey, 1989, Table 2, p.51
26	Unnamed	FFG_473	383.70	Richey, 1989, Table 2, p.51
27	Unnamed	FFG_474	671.70	Richey, 1989, Table 2, p.51
28	Unnamed	FFG_475	677.70	Richey, 1989, Table 2, p.51
29	Unnamed	FFG_476	751.70	Richey, 1989, Table 2, p.51
30	Unnamed	FFG_477	718.80	Richey, 1989, Table 2, p.51
31	Unnamed	FFG_478	694.00	Richey, 1989, Table 2, p.52
32	Unnamed	FFG_479	698.90	Richey, 1989, Table 2, p.52
33	Unnamed	FFG_480	681.30	Richey, 1989, Table 2, p.52
34	Unnamed	FFG_481	674.50	Richey, 1989, Table 2, p.52
35	Unnamed	FFG_482	703.80	Richey, 1989, Table 2, p.52
36	Unnamed	FFG_483	732.70	Richey, 1989, Table 2, p.52
37	Unnamed	FFG_484	720.70	Richey, 1989, Table 2, p.52
38	Unnamed	FFG_485	723.00	Richey, 1989, Table 2, p.52
39	Unnamed	FFG_486	708.40	Richey, 1989, Table 2, p.52
40	Unnamed	FFG_487	706.90	Richey, 1989, Table 2, p.52
41	Unnamed	FFG_488	692.50	Richey, 1989, Table 2, p.52
42	Unnamed	FFG_489	708.80	Richey, 1989, Table 2, p.52
43	Unnamed	FFG_490	801.30	Richey, 1989, Table 2, p.52
44	Unnamed	FFG_491	793.10	Richey, 1989, Table 2, p.52
45	Unnamed	FFG_492	757.10	Richey, 1989, Table 2, p.52
46	Unnamed	FFG_493	743.20	Richey, 1989, Table 2, p.53
47	Unnamed	FFG_494	747.00	Richey, 1989, Table 2, p.53
48	Unnamed	FFG_495	743.10	Richey, 1989, Table 2, p.53
49	Unnamed	FFG_496	604.20	Richey, 1989, Table 2, p.53
50	Unnamed	FFG_497	642.20	Richey, 1989, Table 2, p.53
51	Unnamed	FFG_498	637.60	Richey, 1989, Table 2, p.53
52	Unnamed	FFG_499	603.20	Richey, 1989, Table 2, p.53
53	Unnamed	FFG_500	635.20	Richey, 1989, Table 2, p.53
54	Unnamed	FFG_501	665.60	Richey, 1989, Table 2, p.53
55	Unnamed	FFG_502	630.90	Richey, 1989, Table 2, p.53
56	Unnamed	FFG_503	616.30	Richey, 1989, Table 2, p.53
57	Unnamed	FFG_504	667.60	Richey, 1989, Table 2, p.53
58	Unnamed	FFG_505	696.20	Richey, 1989, Table 2, p.53
59	Unnamed	FFG_506	690.60	Richey, 1989, Table 2, p.53
60	Unnamed	FFG_507	599.40	Richey, 1989, Table 2, p.53
61	Unnamed	FFG_508	680.70	Richey, 1989, Table 2, p.53
62	Unnamed	FFG_509	662.30	Richey, 1989, Table 2, p.54
63	Unnamed	FFG_510	658.80	Richey, 1989, Table 2, p.54
64	Unnamed	FFG_511	619.40	Richey, 1989, Table 2, p.54
65	Unnamed	FFG_512	634.60	Richey, 1989, Table 2, p.54
66	Unnamed	FFG_513	659.30	Richey, 1989, Table 2, p.54
67	Unnamed	FFG_514	637.00	Richey, 1989, Table 2, p.54
68	Unnamed	FFG_515	610.80	Richey, 1989, Table 2, p.54
69	Unnamed	FFG_516	601.60	Richey, 1989, Table 2, p.54
70	Unnamed	FFG_517	750.70	Richey, 1989, Table 2, p.54
71	Unnamed	FFG_518	735.80	Richey, 1989, Table 2, p.54
72	Unnamed	FFG_519	696.50	Richey, 1989, Table 2, p.54
73	Unnamed	FFG_520	585.40	Richey, 1989, Table 2, p.54
74	Unnamed	FFG_521	628.20	Richey, 1989, Table 2, p.54
75	Unnamed	FFG_522	427.50	Richey, 1989, Table 2, p.54
76	Unnamed	FFG_523	443.20	Richey, 1989, Table 2, p.54

Table B.2. Elevations of Stratigraphic Layers Near WIPP (Continued)

	Layer	Well ID	Elevation	Source
1	Unnamed	FFG_524	607.40	Richey, 1989, Table 2, p.55
2	Unnamed	FFG_525	436.60	Richey, 1989, Table 2, p.55
3	Unnamed	FFG_526	943.10	Richey, 1989, Table 2, p.55
4	Unnamed	FFG_527	888.10	Richey, 1989, Table 2, p.55
5	Unnamed	FFG_528	891.50	Richey, 1989, Table 2, p.55
6	Unnamed	FFG_530	957.70	Richey, 1989, Table 2, p.55
7	Unnamed	FFG_531	888.80	Richey, 1989, Table 2, p.55
8	Unnamed	FFG_532	873.00	Richey, 1989, Table 2, p.55
9	Unnamed	FFG_534	883.30	Richey, 1989, Table 2, p.55
10	Unnamed	FFG_535	875.70	Richey, 1989, Table 2, p.55
11	Unnamed	FFG_536	884.50	Richey, 1989, Table 2, p.55
12	Unnamed	FFG_537	872.60	Richey, 1989, Table 2, p.55
13	Unnamed	FFG_543	926.70	Richey, 1989, Table 2, p.56
14	Unnamed	FFG_548	877.20	Richey, 1989, Table 2, p.56
15	Unnamed	FFG_552	722.00	Richey, 1989, Table 2, p.56
16	Unnamed	FFG_562	614.50	Richey, 1989, Table 2, p.57
17	Unnamed	FFG_563	528.20	Richey, 1989, Table 2, p.57
18	Unnamed	FFG_564	663.00	Richey, 1989, Table 2, p.57
19	Unnamed	FFG_568	625.80	Richey, 1989, Table 2, p.57
20	Unnamed	FFG_569	624.20	Richey, 1989, Table 2, p.57
21	Unnamed	FFG_584	736.60	Richey, 1989, Table 2, p.58
22	Unnamed	FFG_585	678.40	Richey, 1989, Table 2, p.58
23	Unnamed	FFG_600	692.50	Richey, 1989, Table 2, p.58
24	Unnamed	FFG_601	572.70	Richey, 1989, Table 2, p.58
25	Unnamed	FFG_602	794.30	Richey, 1989, Table 2, p.58
26	Unnamed	FFG_606	667.60	Richey, 1989, Table 2, p.58
27	Unnamed	FFG_607	671.80	Richey, 1989, Table 2, p.59
28	Unnamed	FFG_608	654.70	Richey, 1989, Table 2, p.59
29	Unnamed	FFG_609	646.70	Richey, 1989, Table 2, p.59
30	Unnamed	FFG_610	640.10	Richey, 1989, Table 2, p.59
31	Unnamed	FFG_611	635.50	Richey, 1989, Table 2, p.59
32	Unnamed	FFG_612	669.70	Richey, 1989, Table 2, p.59
33	Unnamed	FFG_613	668.70	Richey, 1989, Table 2, p.59
34	Unnamed	FFG_618	679.10	Richey, 1989, Table 2, p.59
35	Unnamed	FFG_620	731.20	Richey, 1989, Table 2, p.59
36	Unnamed	FFG_621	695.00	Richey, 1989, Table 2, p.59
37	Unnamed	FFG_638	530.10	Richey, 1989, Table 2, p.60
38	Unnamed	FFG_639	498.40	Richey, 1989, Table 2, p.60
39	Unnamed	FFG_640	586.60	Richey, 1989, Table 2, p.60
40	Unnamed	FFG_643	637.10	Richey, 1989, Table 2, p.60
41	Unnamed	FFG_644	670.50	Richey, 1989, Table 2, p.60
42	Unnamed	FFG_648	500.50	Richey, 1989, Table 2, p.60
43	Unnamed	FFG_652	815.90	Richey, 1989, Table 2, p.60
44	Unnamed	FFG_653	815.70	Richey, 1989, Table 2, p.61
45	Unnamed	FFG_654	839.10	Richey, 1989, Table 2, p.61
46	Unnamed	FFG_655	840.30	Richey, 1989, Table 2, p.61
47	Unnamed	FFG_656	838.50	Richey, 1989, Table 2, p.61
48	Unnamed	FFG_657	856.20	Richey, 1989, Table 2, p.61
49	Unnamed	FFG_658	842.70	Richey, 1989, Table 2, p.61
50	Unnamed	FFG_659	848.60	Richey, 1989, Table 2, p.61
51	Unnamed	FFG_660	866.40	Richey, 1989, Table 2, p.61
52	Unnamed	FFG_662	837.30	Richey, 1989, Table 2, p.61
53	Unnamed	FFG_664	830.90	Richey, 1989, Table 2, p.61
54	Unnamed	FFG_666	883.90	Richey, 1989, Table 2, p.62
55	Unnamed	FFG_667	869.30	Richey, 1989, Table 2, p.62
56	Unnamed	FFG_668	919.40	Richey, 1989, Table 2, p.62
57	Unnamed	FFG_669	905.80	Richey, 1989, Table 2, p.62
58	Unnamed	FFG_670	889.10	Richey, 1989, Table 2, p.62
59	Unnamed	FFG_671	891.20	Richey, 1989, Table 2, p.62
60	Unnamed	FFG_672	889.80	Richey, 1989, Table 2, p.62
61	Unnamed	FFG_673	887.50	Richey, 1989, Table 2, p.62
62	Unnamed	FFG_674	885.50	Richey, 1989, Table 2, p.62
63	Unnamed	FFG_675	844.20	Richey, 1989, Table 2, p.62
64	Unnamed	FFG_676	854.70	Richey, 1989, Table 2, p.62
65	Unnamed	FFG_677	883.30	Richey, 1989, Table 2, p.62
66	Unnamed	FFG_679	883.90	Richey, 1989, Table 2, p.62
67	Unnamed	FFG_685	911.10	Richey, 1989, Table 2, p.63
68	Unnamed	FFG_689	756.80	Richey, 1989, Table 2, p.63
69	Unnamed	FFG_690	760.80	Richey, 1989, Table 2, p.63
70	Unnamed	FFG_691	752.90	Richey, 1989, Table 2, p.63
71	Unnamed	FFG_692	741.60	Richey, 1989, Table 2, p.63
72	Unnamed	FFG_693	753.70	Richey, 1989, Table 2, p.63
73	Unnamed	FFG_694	743.10	Richey, 1989, Table 2, p.63
74	Unnamed	FFG_695	749.20	Richey, 1989, Table 2, p.63
75	Unnamed	FFG_696	751.60	Richey, 1989, Table 2, p.63
76	Unnamed	FFG_697	754.10	Richey, 1989, Table 2, p.64

Table B.2. Elevations of Stratigraphic Layers Near WIPP (Continued)

	Layer	Well ID	Elevation	Source
1	Unnamed	FFG_698	795.30	Richey, 1989, Table 2, p.64
2	Unnamed	FFG_699	749.50	Richey, 1989, Table 2, p.64
3	Unnamed	FFG_700	744.40	Richey, 1989, Table 2, p.64
4	Unnamed	FFG_701	740.80	Richey, 1989, Table 2, p.64
5	Unnamed	FFG_702	747.00	Richey, 1989, Table 2, p.64
6	Unnamed	FFG_703	753.80	Richey, 1989, Table 2, p.64
7	Unnamed	FFG_704	737.30	Richey, 1989, Table 2, p.64
8	Unnamed	FFG_705	671.80	Richey, 1989, Table 2, p.64
9	Unnamed	FFG_706	694.40	Richey, 1989, Table 2, p.64
10	Unnamed	FFG_707	677.00	Richey, 1989, Table 2, p.64
11	Unnamed	FFG_708	728.80	Richey, 1989, Table 2, p.64
12	Unnamed	FFG_709	625.80	Richey, 1989, Table 2, p.64
13	Unnamed	FFG_710	625.20	Richey, 1989, Table 2, p.64
14	Unnamed	FFG_711	626.10	Richey, 1989, Table 2, p.65
15	Unnamed	FFG_712	669.50	Richey, 1989, Table 2, p.65
16	Unnamed	FFG_713	613.70	Richey, 1989, Table 2, p.65
17	Unnamed	FFG_714	725.10	Richey, 1989, Table 2, p.65
18	Unnamed	FFG_715	735.10	Richey, 1989, Table 2, p.65
19	Unnamed	FFG_716	597.30	Richey, 1989, Table 2, p.65
20	Unnamed	FFG_717	665.20	Richey, 1989, Table 2, p.65
21	Unnamed	FFG_718	656.10	Richey, 1989, Table 2, p.65
22	Unnamed	FFG_719	618.70	Richey, 1989, Table 2, p.65
23	Unnamed	FFG_720	614.50	Richey, 1989, Table 2, p.65
24	Unnamed	FFG_721	639.50	Richey, 1989, Table 2, p.65
25	Unnamed	FFG_723	755.10	Richey, 1989, Table 2, p.65
26	Unnamed	FFG_724	678.00	Richey, 1989, Table 2, p.65
27	Unnamed	FFG_725	646.50	Richey, 1989, Table 2, p.65
28	Unnamed	FFG_726	641.00	Richey, 1989, Table 2, p.65
29	Unnamed	FFG_727	630.70	Richey, 1989, Table 2, p.66
30	Unnamed	FFG_728	638.20	Richey, 1989, Table 2, p.66
31	Unnamed	FFG_729	641.00	Richey, 1989, Table 2, p.66
32	Unnamed	FFG_730	665.30	Richey, 1989, Table 2, p.66
33	Unnamed	FFG_731	662.80	Richey, 1989, Table 2, p.66
34	Unnamed	FFG_732	678.20	Richey, 1989, Table 2, p.66
35	Unnamed	FFG_733	741.90	Richey, 1989, Table 2, p.66
36	Unnamed	FFG_734	699.20	Richey, 1989, Table 2, p.66
37	Unnamed	FFG_735	630.30	Richey, 1989, Table 2, p.66
38	Unnamed	FFG_736	667.80	Richey, 1989, Table 2, p.66
39	Unnamed	FFG_737	611.80	Richey, 1989, Table 2, p.66
40	Unnamed	FFG_738	654.40	Richey, 1989, Table 2, p.66
41	Unnamed	FFG_739	683.80	Richey, 1989, Table 2, p.66
42	Unnamed	FFG_740	653.20	Richey, 1989, Table 2, p.66
43	Unnamed	FFG_741	651.10	Richey, 1989, Table 2, p.66
44	Unnamed	FFG_742	690.70	Richey, 1989, Table 2, p.67
45	Unnamed	FFG_743	675.20	Richey, 1989, Table 2, p.67
46	Unnamed	FFG_744	670.80	Richey, 1989, Table 2, p.67
47	Unnamed	FFG_745	650.40	Richey, 1989, Table 2, p.67
48	Unnamed	FFG_746	637.20	Richey, 1989, Table 2, p.67
49	Unnamed	H1	822.60	Mercer, 1983, Table 1
50	Unnamed	H10C	699.80	Mercer, 1983, Table 1
51	Unnamed	H2C	833.00	Mercer, 1983, Table 1
52	Unnamed	H3	821.80	Mercer, 1983, Table 1
53	Unnamed	H4C	858.90	Mercer, 1983, Table 1
54	Unnamed	H5C	787.30	Mercer, 1983, Table 1
55	Unnamed	H6C	829.40	Mercer, 1983, Table 1
56	Unnamed	H7C	880.60	Mercer, 1983, Table 1
57	Unnamed	H8C	859.30	Mercer, 1983, Table 1
58	Unnamed	H9C	831.80	Mercer, 1983, Table 1
59	Unnamed	P1	847.40	Mercer, 1983, Table 1
60	Unnamed	P10	777.80	Mercer, 1983, Table 1
61	Unnamed	P11	782.10	Mercer, 1983, Table 1
62	Unnamed	P12	828.50	Mercer, 1983, Table 1
63	Unnamed	P13	828.50	Mercer, 1983, Table 1
64	Unnamed	P14	842.70	Mercer, 1983, Table 1
65	Unnamed	P15	876.30	Mercer, 1983, Table 1
66	Unnamed	P16	851.90	Mercer, 1983, Table 1
67	Unnamed	P17	839.10	Mercer, 1983, Table 1
68	Unnamed	P18	773.90	Mercer, 1983, Table 1
69	Unnamed	P19	776.60	Mercer, 1983, Table 1
70	Unnamed	P2	791.30	Mercer, 1983, Table 1
71	Unnamed	P20	784.60	Mercer, 1983, Table 1
72	Unnamed	P21	787.90	Mercer, 1983, Table 1
73	Unnamed	P3	828.40	Mercer, 1983, Table 1
74	Unnamed	P4	805.30	Mercer, 1983, Table 1
75	Unnamed	P5	805.90	Mercer, 1983, Table 1
76	Unnamed	P6	851.60	Mercer, 1983, Table 1

Table B.2. Elevations of Stratigraphic Layers Near WIPP (Continued)

	Layer	Well ID	Elevation	Source
1	Unnamed	P7	856.50	Mercer, 1983, Table 1
2	Unnamed	P8	838.50	Mercer, 1983, Table 1
3	Unnamed	P9	809.30	Mercer, 1983, Table 1
4	Unnamed	REF	816.40	Rechard et al.,1991, Figure 2.2-1
5	Unnamed	SaltShft	813.97	Bechtel, Inc., 1986, Appendix D
6	Unnamed	WIPP11	779.90	Mercer, 1983, Table 1
7	Unnamed	WIPP11	780.00	SNL and USGS, 1982a, Table 2
8	Unnamed	WIPP12	803.90	D'Appolonia Consulting, 1983, Table 2
9	Unnamed	WIPP12	803.80	Mercer, 1983, Table 1
10	Unnamed	WIPP13	817.10	Mercer, 1983, Table 1
11	Unnamed	WIPP15	996.40	Mercer, 1983, Table 1
12	Unnamed	WIPP16	672.70	Mercer, 1983, Table 1
13	Unnamed	WIPP18	807.10	Mercer, 1983, Table 1
14	Unnamed	WIPP19	809.60	Mercer, 1983, Table 1
15	Unnamed	WIPP21	812.00	Mercer, 1983, Table 1
16	Unnamed	WIPP22	811.30	Mercer, 1983, Table 1
17	Unnamed	WIPP25	835.40	Mercer, 1983, Table 1
18	Unnamed	WIPP26	897.00	Mercer, 1983, Table 1
19	Unnamed	WIPP27	871.40	Mercer, 1983, Table 1
20	Unnamed	WIPP28	884.30	Mercer, 1983, Table 1
21	Unnamed	WIPP29	894.60	Mercer, 1983, Table 1
22	Unnamed	WIPP30	845.60	Mercer, 1983, Table 1
23	Unnamed	WIPP32	894.00	Mercer, 1983, Table 1
24	Unnamed	WIPP33	836.70	Mercer, 1983, Table 1
25	Unnamed	WIPP34	784.30	Mercer, 1983, Table 1
26	Unnamed	WastShft	817.02	Bechtel, Inc., 1986, Appendix E
27	V_Triste	AirShft	622.89	IT Corporation, 1990, Figure 22
28	V_Triste	AirShft	625.30	IT Corporation, 1990, Figure 22
29	V_Triste	DOE1	604.50	TME 3159, Sep 1982, Table 2
30	V_Triste	DOE1	605.70	TME 3159, Sep 1982, Table 2
31	V_Triste	DOE2	598.10	Mercer et al., 1987, Table 3-2
32	V_Triste	DOE2	600.30	Mercer et al., 1987, Table 3-2
33	V_Triste	ERDA9	625.70	SNL and USGS, 1982b, Table 2
34	V_Triste	ERDA9	627.60	SNL and USGS, 1982b, Table 2
35	V_Triste	ExhtShft	625.11	Bechtel, Inc., 1986, Appendix F
36	V_Triste	ExhtShft	626.66	Bechtel, Inc., 1986, Appendix F
37	V_Triste	REF	625.70	Rechard et al.,1991, Figure 2.2-1
38	V_Triste	REF	627.60	Rechard et al.,1991, Figure 2.2-1
39	V_Triste	SaltShft	627.89	Bechtel, Inc., 1986, Appendix D
40	V_Triste	SaltShft	628.33	Bechtel, Inc., 1986, Appendix D
41	V_Triste	WIPP11	611.20	SNL and USGS, 1982a, Table 2
42	V_Triste	WIPP11	612.70	SNL and USGS, 1982a, Table 2
43	V_Triste	WIPP12	620.80	D'Appolonia Consulting, 1983, Table 2
44	V_Triste	WIPP12	621.70	D'Appolonia Consulting, 1983, Table 2
45				

REFERENCES FOR APPENDIX B

Bechtel, Inc. 1986. *WIPP Design Validation Final Report.* DOE/WIPP-86-010. Prepared for U.S. Department of Energy. San Francisco, CA: Bechtel National, Inc.

Gonzales, M. 1989. *Compilation and Comparison of Test-Hole Location Surveys in the Vicinity of the Waste Isolation Pilot Plant Site.* SAND88-1065. Albuquerque, NM: Sandia National Laboratories.

Holt, R. M. and D. W. Powers. 1990. *Geologic Mapping of the Air Intake Shaft at the Waste Isolation Pilot Plant.* DOE-WIPP 90-051. Carlsbad, NM: U.S. Department of Energy.

Krieg, R. D. 1984. *Reference Stratigraphy and Rock Properties for the Waste Isolation Pilot Plant (WIPP) Project.* SAND83-1908. Albuquerque, NM: Sandia National Laboratories.

Mercer, J. W. 1983. *Geohydrology of the Proposed Waste Isolation Pilot Plant Site, Los Medaños Area, Southeastern New Mexico.* U.S. Geological Survey Water Resources Investigation 83-4016.

Mercer, J. W., R. L. Beauheim, R. P. Snyder, and G. M. Fairer. 1987. *Basic Data Report for Drilling and Hydrologic Testing of Drillhole DOE-2 at the Waste Isolation Pilot Plant (WIPP) Site.* SAND86-0611. Albuquerque, NM: Sandia National Laboratories.

Rechard, R. P., H. J. Iuzzolino, J. S. Rath, R. D. McCurley, and D. K. Rudeen. 1989. *User's Manual for CAMCON: Compliance Assessment Methodology Controller.* SAND88-1496. Albuquerque, NM: Sandia National Laboratories.

Richey, S. F. 1989. *Geologic and Hydrologic Data for the Rustler Formation near the Waste Isolation Pilot Plant, Southeastern New Mexico.* Albuquerque, NM: U.S. Geological Survey Open-File Report 89-32.

SNL (Sandia National Laboratories) and U.S. Geological Survey. 1982a. *Basic Data Report for Drillhole WIPP 11 (Waste Isolation Pilot Plant - WIPP).* SAND79-0272. Albuquerque, NM: Sandia National Laboratories.

SNL (Sandia National Laboratories) and U.S. Geological Survey. 1982b. *Basic Data Report for Drillhole ERDA 9 (Waste Isolation Pilot Plant - WIPP).* SAND79-0270. Albuquerque, NM: Sandia National Laboratories.

SNL (Sandia National Laboratories) and D'Appolonia Consulting Engineers. 1983. *Basic Data Report for Drillhole WIPP 12 (Waste Isolation Pilot Plant - WIPP).* SAND82-2336. Albuquerque, NM: Sandia National Laboratories.

U.S. DOE (Department of Energy). 1982. *Basic Data Report for Borehole DOE-1, Waste Isolation Pilot Plant (WIPP) Project, Southeastern New Mexico.* TME 3159. Albuquerque, NM: Sandia National Laboratories.

NOMENCLATURE

Mathematical Symbols

A	-	cross-sectional area (m^2)
A_m	-	amplitude scaling factor for precipitation variation
a	-	minimum range of distribution
a_R	-	factor for Redlich-Kwong-Soave equation of state
$a_0, a_1, a_2 \ldots$	-	coefficients of empirical equations
$2B$	-	characteristic fracture spacing or block length (m)
B_ℓ, B_g	-	formation volume factor (reservoir conditions/standard conditions) for liquid or gas, respectively
b	-	maximum range of distribution
b_R	-	factor for Redlich-Kwong-Soave equation of state
$2b_f$	-	fracture aperature (m)
C	-	concentration (kg/m^3)
C_w	-	total concentration of water in solution (e.g., brine)
$C_\ell(S_j)$	-	ℓth consequence model of scenario set S_j of the performance assessment methodology
$\hat{C}$	-	mass fraction (kg/kg)
C°	-	solubility (kg chemical/m^3 fluid)
c	-	capacitance ($\beta_b + \phi\beta_\ell$) (Pa^{-1})
D_m	-	molecular diffusion in porous media matrix ($D^\square \bullet \tau$) (m^2/s)
$D^\square$	-	molecular diffusion in pure fluid (m^2/s)
D_L, D_T	-	hydrodynamic dispersion $D_m + \alpha_L\overline{V}$ and $D_m + \alpha_T\overline{V}$, respectively ($m^2/s$)

D	-	hydrodynamic dispersion tensor
d	-	diameter
d_i	-	separation distance to grid point i, e.g., separation distance between interpolated point and a nearby point
d_s	-	distance traveled by solute
E	-	Young's modulus (Pa)
e	-	weighting power for inverse-distance interpolation
f	-	fanning friction factor
f_w	-	waste unit factor
f_c, f_m, f_s	-	volume fraction of combustibles, metals/glass, and sludge, respectively
f_{rchg}	-	recharge factor evaluated from precipitation fluctuation
$F(x)$	-	cumulative distribution function, integral of f(x), probability density function of parameter x
$f(x)$	-	distribution of x
g	-	acceleration due to gravity = ~9.8 m/s^2 or $9.80616 - 2.5928 \times 10^{-2} \cos 2\phi_{lat} + 6.9 \times 10^{-5} \cos^2 2\phi_{lat} - 3.086 \times 10^{-6} z_{sur} - 1.543 \times 10^{-6} \Delta z$, where ϕ_{lat} is the latitude, z_{sur} is the surface elevation in meters, and Δz is the depth in meters below the surface (Helmert's equation) (Weast and Astle, 1981, F-78) (9.792 m/s^2 at 1039.06 m [surface] and 9.791 m/s^2 at 351 m [repository level])
h	-	multiplier factor
h^*	-	Plank's constant, 6.6262×10^{-34} J • s
K	-	hydraulic conductivity (m/s)
K_d	-	distribution (or partition) coefficient (m^3/kg)
K_{bulk}	-	bulk modulus ($E/(3(1-2\nu))$) (Pa)
k^*	-	Boltzmann's constant 1.3806×10^{-23} (J/K)
k	-	permeability (m^2)

$k_{r\ell}, k_{rg}$	-	relative liquid and gas permeability, respectively
L_i	-	release limit for radionuclide i (from *40 CFR 191* Appendix A, Table 1)
M	-	molecular weight (g/mol)
M_{dc}, M_{dm}, M_{ds}	-	average mass of combustibles, metals/glass, and sludge, respectively, per drum (kg)
m_A	-	atomic mass
$\dot{m}_b, \dot{m}_c, \dot{m}_t$	-	gas generation rate, biodegradation (mol/kg cellulose/s), corrosion (mol/m^2 surface area steel/s), and total, respectively
N_R	-	Reynold's number, $\frac{\rho_f v d}{\mu}$
Np	-	Peclet number, $\overline{V}d_{50}/\tau D^{\square}$, where d_{50} is average particle diameter (length dimension)
N	-	molarity (mol/ℓ)
n	-	number of moles
n_g	-	number of grid points used for interpolation
nR	-	number of radionuclides released from repository
nS	-	number of mutually-exclusive release scenario classes
nk	-	number of sampling vectors from Monte Carlo (LHS) sampling
nV	-	number of model parameters
P(r>R)	-	probability of r > R
$P(r>R\|S_j)$	-	conditional probability of r > R given scenario set S_j occurs
$P(S_j)$	-	probability model of scenario set S_j occurring over 10,000 yr
p	-	pressure (Pa)
p_c	-	capillary pressure (Pa)
p_{cr}	-	critical pressure (Pa)

Q - flow rate

$Q_{i,k}$ - predicted cumulative release for radionuclide i for run k (Ci)

$q_{i,k}$ - predicted release at time t for radionuclide i for run k (Ci/s)

$Risk$ - risk, $Risk = \{S_j, P(S_j), R(S_j), j = 1, ..., nS\}$

R_m, R_f - retardation, matrix and fracture, respectively

$R(S_j(\mathbf{x}_k))$ - calculated, summed, EPA normalized releases for Monte Carlo vector k

$$R(S_j(\mathbf{x}_k)) = \sum_{i=1}^{n_r} \frac{Q_{i,k}}{L_i} \quad k = 1, 2, ..., nK$$

R^* - universal gas constant $\left[8.31441 \frac{Pa \bullet m^3}{mol \bullet K}\right]$

r_{rank} - correlation coefficient, actual and rank transform, respectively

r_{vec} - Monte Carlo simulation (vector) ID

$r_{g/\ell}$ - gas (nonwetting phase)/liquid (wetting phase) ratio

$\overline{r}_p$, $\overline{r}_f$ - average annual precipitation (m/s), present and future, respectively

S_j - scenario class j

S_s - specific storage (γc) (m^{-1})

S_b - bulk storativity $\left(\frac{A \bullet \Delta z \bullet S_s}{\rho g}\right)$ (m^3/Pa)

s - standard deviation, (s^2 is variance)

s_g, s_ℓ - saturation (ratio of gas or liquid volume to total void volume), gas (nonwetting phase) and liquid (wetting phase), respectively (V/V_v)

s_{gr}, $s_{\ell r}$ - residual saturation, gas (nonwetting phase) and liquid (wetting phase), respectively

T_K - transmissivity (m^2/s)

T - temperature (K)

T_{cr} - critical temperature (Pa)

T_r	- reduced temperature (T/T_{cr})
t	- time (s)
$t_{1/2}$	- radionuclide half life (s)
V	- volume (m^3)
V_{cr}	- theoretical volume of gas assuming ideal gas behavior at critical temperature and pressure of the gas
V_d, V_s, V_w	- volume of the drum, solids, and design capacity of the repository, respectively (m^3)
v	- velocity (m/s)
x,y,z	- variable or parameter
$\bar{x}$	- mean or expected value
x_{50},x_{99}	- value of x at 50% (0.50) quantile and 99% (0.99) quantile
Z	- gas compressibility factor
Δz	- thickness
α	- parameter of probability density function
α_R	- factor for Redlich-Kwong-Soave equation of state
α_L, α_T	- dispersivity, longitudinal or transverse, respectively (m)
β_s, β_b, β_ℓ	- material compressibility solid, bulk [$(1 - \phi)\beta_s$], and liquid, respectively (Pa^{-1})
Γ	- strain rate (dv/dy) (s^{-1})
γ	- unit weight (ρg)
ε	- roughness height (m)
ξ_1,ξ_2	- oldroyd viscosity parameter
Θ	- Pleistocene glaciation frequency (s^{-1})
$\dot{\theta}$	- angular velocity of drill bit (m/s)

λ	- parameter of probability density function
$\Lambda(t)$	- failure rate function for probability model of human intrusion
μ_ℓ, μ_g	- viscosity, liquid or gas, respectively (Pa • s)
ρ_s, ρ_b, ρ_f	- density, solid, bulk, and fluid, respectively (kg/m^3)
τ	- tortuosity $(\ell/\ell_{path})^2$
Φ	- Holocene precipitation fluctuation frequency (s^{-1})
ϕ_{lat}	- latitude
ϕ_m, ϕ_f	- porosity, matrix and fracture (b/[B + b]), respectively
ζ	- skin resistance from materials lining fractures, (b_s/D_s)
v	- molar volume (m^3/mol)
ν	- Poisson's ratio
ω_R	- acentric factor for Redlich-Kwong-Soave equation of state
χ	- mole fraction
η	- Brooks-Corey relative permeability model parameter exponent

Superscripts

*	- physical constants
°	- property at reference conditions
¤	- property in pure fluid
•	- parameter with respect to time (rate)
_	- mean of parameter

Subscripts

g	- gas
ℓ	- liquid

f	- fracture
m	- matrix

Acronyms

ANL-E	- Argonne National Laboratories, East
ASCII	- American Standard Code for Information Interchange
ALGEBRA	- support program for manipulating data in CAMDAT
BLOT	- a mesh and curve plot program for CAMDAT data
BOAST	- Black Oil Applied Simulation Tool; 3-D, 3-phase code for flow-through porous media
BRAGFLO	- Brine And Gas Flow; 2-D, 2-phase code for flow-through porous media
CAM	- Compliance Assessment Methodology
CAMCON	- Compliance Assessment Methodology CONtroller——controller (driver) for compliance evaluations developed for WIPP
CAMDAT	- Compliance Assessment Methodology DATa——computational data base developed for WIPP (modification of GENESIS and EXODUS)
CCDF	- Complementary Cumulative Distribution Function
CCDFPLT	- program to calculate and display complementary cumulative distribution function
CH	- Contact Handled (TRU waste)
DCL	- Digital Equipment Corporation Command Language
DOE	- U.S. Department of Energy
DRZ	- Disturbed Rock Zone
EPA	- U.S. Environmental Protection Agency
EOS	- equation of state
FD	- Finite-Difference numerical analysis
FE	- Finite-Element numerical analysis
Fm	- formation
GENMESH	- rectilinear three-dimensional finite-difference grid generator

HANF	- Hanford Reservation
HLW	- High-Level Waste
HST3D	- a program to simulate heat and solute transport in a three-dimensional groundwater flow system
INEL	- Idaho National Engineering Laboratory
LANL	- Los Alamos National Laboratory
LHS	- Latin Hypercube Sampling (efficient, stratified Monte Carlo sampling)
LLNL	- Lawrence Livermore National Laboratory
MATSET	- a program to insert user-selected parameter or material values into the computational data base
MOUND	- Mound Laboratory
NEFTRAN	- NEtwork Flow and TRANsport code
NRC	- U.S. Nuclear Regulatory Commission
NTS	- Nevada Test Site
ORNL	- Oak Ridge National Laboratory
PCCSRC	- program for calculating partial correlation coefficients (PCC) and standardized regression coefficients (SRC)
PREBOAST	- preprocessor (translator) for input to BOAST
PREBRAG	- preprocessor (translator) for input to BRAGFLO
PREHST	- preprocessor (translator) for input to HST3D
PRELHS	- preprocessor (translator) for input to LHS
PREPCC	- preprocessor (translator) for input to PCC/SRC
PRENEF	- preprocessor (translator) for input to NEFTRAN
PRESTEP	- preprocessor (translator) for input to STEPWISE
PRESUTRA	- preprocessor (translator) for input to SUTRA
PRESWFT	- preprocessor (translator) for input to SWIFT II

POSTBOAST	- postprocessor (translator) of output from BOAST to CAMDAT
POSTBRAG	- postprocessor (translator) of output from BRAGFLO to CAMDAT
POSTHST	- postprocessor (translator) of output from HST3D to CAMDAT
POSTLHS	- postprocessor (translator) of output from LHS to CAMDAT
POSTSUTRA	- postprocessor (translator) of output from SUTRA to CAMDAT
POSTSWFT	- postprocessor (translator) of output from SWIFT II to CAMDAT
QA	- Quality Assurance
RCRA	- Resource, Conservation, and Recovery Act of 1976 (Public Law 94-580) and subsequent amendments (e.g., HSWA——Hazardous and Solid Waste Amendments of 1984)
RFP	- Rocky Flats Plant
RH	- Remote Handled (TRU waste)
SNL	- Sandia National Laboratories, Albuquerque, NM
SRS	- Savannah River Site
STEPWISE	- stepwise regression program with rank regression and predicted error sum of squares criterion
SWIFTII	- Sandia Waste-Isolation, Flow and Transport code for solving transient, three-dimensional, coupled equations for fluid flow, heat transport, brine-miscible displacement, and radionuclide-miscible displacement in porous and fractured media
SUTRA	- Saturated-Unsaturated TRAnsport code
TRACKER	- a support program to estimate the pathway of a particle released in a fluid velocity field
TRU	- Transuranic
WIPP	- Waste Isolation Pilot Plant
40 CFR 191	- Code of Federal Regulations, Title 40, Part 191

CONVERSION TABLES
FOR SI AND COMMON ENGLISH UNITS

Table 1. Base and Derived SI Units

	Quantity	Name	Symbol	Expression in Terms of Other Units	Expression in Terms of SI Base Units
Base SI Units					
	length	meter	m		
	time	second	s		
	mass	kilogram	kg		
	temperature	kelvin	K		
	amount of substance	mole	mol		
	electric current	ampere	A		
SI-Derived Units					
	force	newton	N		$kg \cdot m \cdot s^{-2}$
	pressure, stress	pascal	Pa	N/m^2	$kg \cdot m^{-1} \cdot s^{-2}$
	energy, work, quantity of heat	joule	J	$N \cdot m$	$kg \cdot m^2 \cdot s^{-2}$
	power, radiant flux	watt	W	J/s	$kg \cdot m^2 \cdot s^{-3}$
	electric potential	volt	V	W/A	$kg \cdot m^2 \cdot s^{-3} \cdot A^{-1}$
	electric resistance	ohm	Ω	V/A	$kg \cdot m^2 \cdot s^{-3} \cdot A^{-2}$
	frequency	hertz	Hz		s^{-1}
	activity (of a radionuclide)	bequerel	Bq		s^{-1}
	absorbed dose	gray	Gy	J/kg	$m^2 \cdot s^{-2}$
	quantity of electricity, electric charge	coulomb	C		$A \cdot s$

Table 2. List of Prefixes

Factor	Prefix	Symbol*
10^{12}	tera	T
10^{9}	giga	G
10^{6}	mega	M
10^{3}	kilo	k
10^{2}	hecto	h
10	deka	da
10^{-1}	deci	d
10^{-2}	centi	c
10^{-3}	milli	m
10^{-6}	micro	μ
10^{-9}	nano	n
10^{-12}	pico	p
10^{-15}	femto	f
10^{-18}	atto	a

* Only the symbols T (tera), G (giga), and M (mega) are capitalized. Compound prefixes are not allowed — for example, use nm (*nano*metre) rather than mμm (*millimicro*metre).

Table 3. Length Conversions

	m	cm	Å	in.	ft	mi	nmi
meter (m)	1	*100	*$1x10^{10}$	39.37	3.281	$6.214x10^{-4}$	$5.400x10^{-4}$
centimeter (cm)	*0.01	1	*$1x10^{8}$	0.3937	$3.281x10^{-2}$	$6.214x10^{-6}$	$5.400x10^{-6}$
angstrom (Å)	*$1x10^{-10}$	*$1x10^{-8}$	1	$3.937x10^{-9}$	$3.281x10^{-10}$	$6.214x10^{-14}$	$5.400x10^{-14}$
inch (in.)	*0.0254	*2.54	*$2.54x10^{8}$	1	$8.333x10^{-2}$	$1.578x10^{-5}$	$1.371x10^{-5}$
foot (ft)	*0.3048	*30.48	*$3.048x10^{9}$	*12	1	$1.894x10^{-4}$	$1.646x10^{-4}$
mile (U.S.) (mi)	1609	$1.609x10^{5}$	$1.609x10^{13}$	*$6.336x10^{4}$	*5280	1	0.8690
nautical mile (nmi)	*1852	*$1.852x10^{5}$	*$1.852x10^{13}$	$7.291x10^{4}$	$6.076x10^{3}$	1.151	1

* Exact

Table 4. Area or Permeability

	m^2	ha	$in.^2$	ft^2	ac	mi^2	Darcy	cm^2
square meters (m^2)	1	*$1x10^{-4}$	1550	10.76	$2.471x10^{-4}$	$3.861x10^{-7}$	$1.013x10^{12}$	*$1.000x10^{4}$
hectare (ha)	*$1x10^{4}$	1	$1.550x10^{7}$	$1.076x10^{5}$	2.471	$3.861x10^{-3}$	$1.013x10^{16}$	*$1.000x10^{8}$
square inches ($in.^2$)	$6.452x10^{-4}$	$6.452x10^{-8}$	1	$6.944x10^{-3}$	$1.594x10^{-7}$	$2.491x10^{-10}$	$6.537x10^{8}$	6.452
square feet (ft^2)	$9.290x10^{-2}$	$9.290x10^{-6}$	144	1	$2.296x10^{-5}$	$3.587x10^{-8}$	$9.413x10^{10}$	929
acre (ac)	4047	0.4047	$6.273x10^{6}$	*$4.356x10^{4}$	1	$1.563x10^{-3}$	$4.100x10^{15}$	$4.047x10^{7}$
square miles (mi^2)	$2.590x10^{6}$	2590	$4.015x10^{9}$	$2.788x10^{7}$	*640	1	2.624	$2.590x10^{10}$
darcy (D)	$9.869x10^{-13}$	$9.869x10^{-17}$	$1.530x10^{-9}$	$1.062x10^{-11}$	$2.439x10^{-16}$	$3.811x10^{-19}$	1	$9.864x10^{-9}$
square centimeters (cm^2)	*$1x10^{-4}$	$1x10^{-8}$	0.1550	$1.076x10^{-3}$	$2.471x10^{-8}$	$3.861x10^{-11}$	$1.013x10^{8}$	1

*Exact

Table 5. Volume

	m^3	l	ft^3	yd^3	gal (U.S.)	bbl	drum	std bx	room	panel	disposal	ac•ft	sec•ft•day	bushel
cubic meters (m^3)	1	*1000	35.31	1.308	264.2	6.290	4.803	0.5618	$2.744x10^{-4}$	$2.169x10^{-5}$	$2.293x10^{-6}$	$8.107x10^{-4}$	$4.087x10^{-4}$	28.38
liter (l)	*$1x10^{-3}$	1	$3.531x10^{-2}$	$1.308x10^{-3}$	0.2642	$6.290x10^{-3}$	$4.803x10^{-3}$	$5.618x10^{-4}$	$2.744x10^{-7}$	$2.169x10^{-8}$	$2.293x10^{-9}$	$8.107x10^{-7}$	$4.087x10^{-7}$	$2.838x10^{-2}$
cubic feet (ft^3)	$2.832x10^{-2}$	28.32	1	$3.704x10^{-2}$	7.481	0.1781	0.1360	$1.591x10^{-2}$	$7.770x10^{-6}$	$6.143x10^{-7}$	$6.494x10^{-8}$	$2.296x10^{-5}$	$1.157x10^{-5}$	0.8036
cubic yard (yd^3)	0.7646	7646	*27	1	201.97	4.809	3.672	0.4295	$2.098x10^{-4}$	$1.659x10^{-5}$	$1.753x10^{-6}$	$6.198x10^{-4}$	$3.125x10^{-4}$	21.70
U.S. gallon (gal)	$3.785x10^{-3}$	3.785	0.1337	$4.951x10^{-3}$	1	$2.381x10^{-2}$	$1.818x10^{-2}$	$2.127x10^{-3}$	$1.039x10^{-6}$	$8.212x10^{-8}$	$8.682x10^{-9}$	$3.069x10^{-6}$	$1.547x10^{-6}$	0.1074
barrel (bbl)	0.1590	159	5.615	0.2079	*42	1	0.7636	$8.932x10^{-2}$	$4.363x10^{-5}$	$3.449x10^{-6}$	$3.646x10^{-7}$	$1.289x10^{-4}$	$6.498x10^{-5}$	4.512
drum (55-gal)	0.2082	208.2	7.352	0.2723	*55	1.310	1	0.1170	$5.713x10^{-5}$	$4.556x10^{-6}$	$4.804x10^{-7}$	$1.688x10^{-4}$	$8.510x10^{-5}$	5.908
standard-waste box (std bx)	1.9	1780	62.86	2.328	470.2	1.120	8.550	1	$4.884x10^{-4}$	$3.895x10^{-5}$	$4.107x10^{-6}$	$1.443x10^{-3}$	$7.275x10^{-4}$	50.51
room volume (room)	3644	$3.644x10^{6}$	$1.287x10^{5}$	4767	$9.627x10^{5}$	$2.292x10^{4}$	$1.750x10^{4}$	2047	1	$7.906x10^{-2}$	$8.358x10^{-3}$	2.955	1.490	$1.034x10^{5}$
panel volume (panel)	$4.610x10^{4}$	$4.610x10^{7}$	$1.628x10^{6}$	$6.029x10^{4}$	$1.218x10^{7}$	$2.899x10^{5}$	$2.214x10^{5}$	$2.590x10^{4}$	12.65	1	0.1057	37.37	18.84	$1.308x10^{6}$
disposal area (disposal)	$4.360x10^{5}$	$4.360x10^{8}$	$1.540x10^{7}$	$5.703x10^{5}$	$1.152x10^{8}$	$2.730x10^{5}$	$2.094x10^{6}$	$2.450x10^{5}$	119.6	9.459	1	353.5	178.2	$1.237x10^{7}$
acre•foot (ac•ft)	1233	$1.233x10^{6}$	*43560	1613	$3.259x10^{5}$	7758	5925	6.930	0.3385	$2.699x10^{-2}$	$2.846x10^{-3}$	1	0.5042	$3.500x10^{4}$
second•foot•day (sec•ft•day)	2447	$2.447x10^{6}$	*86400	*3200	$6.463x10^{5}$	$1.539x10^{4}$	$1.175x10^{4}$	1374	0.6713	$5.353x10^{-2}$	$5.645x10^{-3}$	1.983	1	$6.943x10^{4}$
bushel (bu)	$3.524x10^{-2}$	35.24	1.244	$4.609x10^{-2}$	9.309	0.2216	0.1693	$1.980x10^{-2}$	$9.669x10^{-6}$	$7.711x10^{-7}$	$8.131x10^{-8}$	$2.857x10^{-5}$	$1.440x10^{-5}$	1

*Exact

Table 6. Discharge (Volume/Time)

	m^3/s	m^3/yr	l	ft^3/s	ft^3/min	ft^3/day	acre•ft/day	gal/min	gal/day	bbl/day
cubic meters per second (m^3/s)	1	$3.156x10^7$	*1000	35.31	2119	$3.051x10^6$	70.05	$1.585x10^4$	$2.282x10^7$	$5.434x10^5$
cubic meters per year (m^3/yr)	$3.169x10^{-8}$	1	$3.169x10^{-5}$	$1.119x10^{-6}$	$6.714x10^{-5}$	$9.669x10^{-2}$	$2.220x10^{-6}$	$5.023x10^{-4}$	0.7233	$1.722x10^{-2}$
liters per second (l/s)	$*1x10^{-3}$	$3.156x10^4$	1	$3.531x10^{-2}$	2.119	3051	$7.005x10^{-2}$	15.85	$2.282x10^4$	543.4
cubic feet per second (ft^3/s)	$2.832x10^{-2}$	$8.936x10^5$	28.32	1	*60	$*8.640x10^4$	1.983	448.8	$6.463x10^5$	$1.539x10^4$
cubic feet per minute (ft^3/min)	$4.719x10^{-4}$	$1.489x10^4$	0.4719	$1.667x10^{-2}$	1	1440	$3.306x10^{-2}$	7.481	$1.077x10^4$	256.5
cubic feet per day (ft^3/day)	$3.277x10^{-7}$	10.34	$3.277x10^{-4}$	$1.157x10^{-5}$	$6.944x10^{-4}$	1	$2.296x10^{-5}$	$5.195x10^{-3}$	7.481	0.1781
acre•foot per day (acre• ft/day)	$1.428x10^{-2}$	$4.505x10^5$	14.28	0.5042	30.25	$4.356x10^4$	1	226.3	$3.259x10^5$	7758
gallons per minute (gal/min)	$6.309x10^{-5}$	1991	$6.309x10^{-2}$	$2.228x10^{-3}$	0.1337	19.25	$4.419x10^{-3}$	1	1440	34.29
gallons per day (gal/day)	$4.381x10^{-8}$	1.383	$4.381x10^{-5}$	$1.547x10^{-6}$	$9.283x10^{-5}$	0.1337	$3.069x10^{-6}$	$6.944x10^{-4}$	1	$2.381x10^{-2}$
barrels per day (bbl/day)	$1.840x10^{-6}$	58.07	$1.840x10^{-3}$	$6.498x10^{-5}$	$3.899x10^{-3}$	5.615	$1.289x10^{-4}$	$2.917x10^{-2}$	*42	1

*Exact

Table 7. Velocity, Hydraulic Conductivity, Precipitation

	m/s	m/yr	in./yr	cm/yr	km/yr	ft/s	ft/day	mph	knots	gal/(day•ft^2)
meters per second (m/s)	1	3.156×10^{7}	1.242×10^{9}	3.156×10^{9}	3.156×10^{4}	3.281	2.835×10^{5}	2.237	1.944	2.120×10^{6}
meters per year (m/yr)	3.169×10^{-8}	1	39.37	*100	$*1 \times 10^{-3}$	1.040×10^{-7}	8.983×10^{-3}	7.089×10^{-8}	6.160×10^{-8}	6.719×10^{-2}
inches per year (in./yr)	8.049×10^{-10}	$*2.540 \times 10^{-2}$	1	*2.540	$*2.540 \times 10^{-5}$	2.641×10^{-9}	2.282×10^{-4}	1.800×10^{-9}	1.565×10^{-9}	1.707×10^{-3}
centimeters per year (cm/yr)	3.169×10^{-10}	$*1 \times 10^{-2}$	0.3937	1	$*1 \times 10^{-5}$	1.040×10^{-9}	8.983×10^{-5}	7.089×10^{-10}	6.160×10^{-10}	6.719×10^{-4}
kilometers per year (km/yr)	3.169×10^{-5}	*1000	3.937×10^{4}	$*1 \times 10^{5}$	1	1.040×10^{-4}	8.983	7.089×10^{-5}	6.160×10^{-5}	67.19
feet per second (ft/s)	*0.3048	9.619×10^{6}	3.787×10^{8}	9.619×10^{8}	9619	1	$*8.640 \times 10^{4}$	0.6818	0.5925	6.463×10^{5}
feet per day (ft/day)	3.528×10^{-6}	111.3	4383	1.113×10^{4}	0.1113	1.157×10^{-5}	1	7.891×10^{-6}	6.857×10^{-6}	7.481
miles per hour (mph)	0.4470	1.411×10^{7}	5.554×10^{8}	1.411×10^{9}	1.411×10^{4}	1.467	1.267×10^{5}	1	0.8690	9.479×10^{5}
knots	0.5144	1.623×10^{7}	6.391×10^{8}	1.623×10^{9}	1.623×10^{4}	1.688	1.458×10^{5}	1.151	1	1.091×10^{6}
gallons per day per square foot (gal/(day•ft^2))	4.716×10^{-7}	14.88	585.9	1488	1.488×10^{-2}	1.547×10^{-6}	0.1337	$.055 \times 10^{-6}$	9.167×10^{-7}	1

*Exact

Table 8. Force

	N	kg-force	dyne	lbf
Newton (N)	1	0.1020	*$1x10^5$	0.2248
kilogram-force (kg-force)	9.807	1	$9.807x10^5$	2.205
dyne	*$1.00x10^{-5}$	$1.020x10^{-6}$	1	$2.248x10^{-6}$
pound force (lbf)	4.448	0.4536	$4.448x10^5$	1

*Exact

Table 9. Pressure and Stress

	Pa	bar	dyne/cm^2	atm	mm Hg	psi	lb/ft^2
pascal (Pa)	1	*$1x10^{-5}$	*10	$9.869x10^{-6}$	$7.501x10^{-3}$	$1.450x10^{-4}$	$2.089x10^{-2}$
bar	*$1x10^5$	1	*$1x10^6$	0.9869	750.1	14.50	2089
dyne per square centimeters (dyne/cm^2)	*0.1	*$1x10^{-6}$	1	$9.869x10^{-7}$	$7.501x10^{-4}$	$1.450x10^{-5}$	$2.089x10^{-3}$
atmosphere (atm)	$1.013x10^5$	1.013	$1.013x10^6$	1	*760	14.70	2116
millimeter of Mercury (mm Hg)	1333	$1.333x10^{-3}$	1333	$1.316x10^{-3}$	1	$1.934x10^{-2}$	2.785
pound per square inch (psi)	698.5	$6.895x10^{-2}$	$6.895x10^4$	$6.805x10^{-2}$	51.71	1	*144
pounds per square foot (lb/ft^2)	47.88	$4.788x10^{-4}$	478.8	$4.725x10^{-4}$	0.3591	$6.944x10^{-3}$	1

*Exact

Table 10. Absolute Viscosity

	Pa•s (kg/(m•s))	cP	lbm/ft/s	slug/(ft•s) lbf • ft/s^2
Pascal-second (Pa•s) (kg/(m•s))	1	*1000	0.6720	2.089x10^{-2}
centipoise (cP)	*1x10^{-3}	1	6.720x10^{-4}	2.089x10^{-5}
pound mass per foot per second (lbm/ft/s)	1.488	1488	1	3.108x10^{-2}
slug per foot per second (slug/(ft•s) or lbf • ft/s^2)	47.88	4.788x10^4	32.17	1

*Exact

Table 11. Mass

	kg	metric tonne	oz	lbm	short ton	long ton	slug
kilogram (kg)	1	*1x10^{-3}	35.27	2.205	1.102x10^{-3}	9.842x10^{-4}	6.852x10^{-2}
metric tonne (t)	*1000	1	3.527x10^4	2205	1.102	0.9842	68.52
avoirdupois ounce (oz)	2.835x10^{-2}	2.835x10^{-5}	1	*0.0625	*3.125x10^{-5}	2.790x10^{-5}	1.943x10^{-3}
pound mass (lbm)	0.4536	4.536x10^{-4}	*16	1	*5.000x10^{-4}	4.464x10^{-4}	3.108x10^{-2}
short ton	907.2	9.072	*32000	*2000	1	0.8927	62.16
long ton	1016	1.016	*35840	*2240	*1.12	1	69.62
slug	14.59	1.459x10^{-2}	514.8	32.17	1.609x10^{-2}	1.436x10^{-2}	1

*Exact

Table 12. Density

	kg/m^3	g/cm^3	lb/ft^3	lb/gal	lb/bbl
kilogram per cubic meters (kg/m^3)	1	$*1x10^{-3}$	$6.243x10^{-2}$	$8.345x10^{-3}$	2.853
grams per cubic centimeters (g/cm^3)	*1000	1	62.43	8.345	350.5
pounds per cubic feet (lb/ft^3)	16.02	$1.602x10^{-2}$	1	0.1337	5.615
pounds per gallon (lb/gal)	119.8	0.1198	7.481	1	*42
pounds per barrel (lb/bbl)	2.853	$2.853x10^{-3}$	0.1781	$2.381x10^{-2}$	1

*Exact

Table 13. Time

	s	min	h	day	yr
mean solar second (s)	1	$1.6667x10^{-2}$	$2.7779x10^{-4}$	$1.15741x10^{-5}$	$3.1689x10^{-8}$
mean solar minute (min)	*60	1	$1.6667x10^{-2}$	$6.9444x10^{-4}$	$1.9013x10^{-6}$
mean solar hour (h)	*3600	*60	1	$4.16667x10^{-2}$	$1.1408x10^{-4}$
mean solar day	$*8.640x10^{4}$	*1440	*24	1	$2.7379x10^{-3}$
tropical time year (yr)	$3.1557x10^{7}$	$5.2595x10^{5}$	8765.8	365.24	1

*Exact

Table 14. Temperature (T)

	K	°C	°R	°F
kelvin (K)	1	K-273.15	K x 9/5	(K-273.15) x 9/5 +32
Celsius (°C)	°C + 273.15	1	(°C + 273.15) x 9/5	°C x 9/5 +32
Rankine (°R)	°R x 5/9	(°R x 5/9) -273.15	1	°R -459.67
Fahrenheit (°F)	(°F + 459.67) x 5/9	(°F - 32) x 5/9	°F + 459.67	1

Table 15. Specific Activity(1)

	Bq	Ci	kg
becquerel (Bq)	1	2.703×10^{-11}	$\frac{\ln^2}{t_{1/2}} \times \frac{6.022 \times 10^{23}}{M} \times \frac{10^3 g}{kg} = \frac{4.174 \times 10^{26}}{t_{1/2} \times M}$
curie (Ci)	*3.7×10^{10}	1	$\frac{1.128 \times 10^{16}}{t_{1/2} \times M}$
kg	$2.396 \times 10^{-27} \times t_{1/2}^{(2)} \times M^{(3)}$	$8.864 \times 10^{-17} \times t_{1/2} \times M$	1

(1) Specific Activity is $\frac{ds_A}{s_A}$; where $s_A = s_{OA}\, e^{-\lambda t}$; $\frac{\lambda = \ln^2}{t_{1/2}}$

(2) $t_{1/2}$ is half life in seconds

(3) M is gram molecular weight (g/mol)

*Exact

Table 16. Miscellaneous

To convert:	to	Multiply by	Inverse
1. Angular velocity rad/s	rpm	$\frac{30}{\pi} = 9.549$	$\frac{\pi}{30} = 0.1047$
2. Radioactivity			
a. Dose equivalent Sv	rem	100	0.01
b. Absorbed dose Gy (gray) (1J/kg)	rad	100	0.01
c. Activity (1 disintegration/s) becquerel (Bq)	Ci	2.703×10^{-11}	3.7×10^{10}
d. Charge roentgen (R)	c/kg	2.58×10^{-4}	3876

Distribution

FEDERAL AGENCIES

U. S. Department of Energy (4)
Office of Environmental Restoration
and Waste Management
Attn: L. P. Duffy, EM-1
J. E. Lytle, EM-30
S. Schneider, EM-342
C. Frank, EM-50
Washington, DC 20585

U.S. Department of Energy (5)
WIPP Task Force
Attn: M. Frei, EM-34 (2)
G. H. Daly
S. Fucigna
J. Rhoderick
12800 Middlebrook Rd.
Suite 400
Germantown, MD 20874

U.S. Department of Energy (4)
Office of Environment, Safety and
Health
Attn: R. P. Berube, EH-20
C. Borgstrum, EH-25
R. Pelletier, EH-231
K. Taimi, EH-232
Washington, DC 20585

U. S. Department of Energy (4)
WIPP Project Integration Office
Attn: W. J. Arthur III
L. W. Gage
P. J. Higgins
D. A. Olona
P.O. Box 5400
Albuquerque, NM 87115-5400

U. S. Department of Energy (12)
WIPP Project Site Office (Carlsbad)
Attn: A. Hunt (4)
M. McFadden
V. Daub (4)
J. Lippis
K. Hunter
R. Becker
P.O. Box 3090
Carlsbad, NM 88221-3090

U. S. Department of Energy, (5)
Office of Civilian Radioactive Waste
Management
Attn: Deputy Director, RW-2
Associate Director, RW-10
Office of Program
Administration and
Resources Management
Associate Director, RW-20
Office of Facilities
Siting and
Development
Associate Director, RW-30
Office of Systems
Integration and
Regulations
Associate Director, RW-40
Office of External
Relations and Policy
Office of Geologic Repositories
Forrestal Building
Washington, DC 20585

U. S. Department of Energy
Attn: National Atomic Museum Library
Albuquerque Operations Office
P.O. Box 5400
Albuquerque, NM 87185

U. S. Department of Energy
Research & Waste Management Division
Attn: Director
P.O. Box E
Oak Ridge, TN 37831

U. S. Department of Energy (2)
Idaho Operations Office
Fuel Processing and Waste
Management Division
785 DOE Place
Idaho Falls, ID 83402

U.S. Department of Energy
Savannah River Operations Office
Defense Waste Processing
Facility Project Office
Attn: W. D. Pearson
P.O. Box A
Aiken, SC 29802

U.S. Department of Energy (2)
Richland Operations Office
Nuclear Fuel Cycle & Production Division
Attn: R. E. Gerton
825 Jadwin Ave.
P.O. Box 500
Richland, WA 99352

U.S. Department of Energy (3)
Nevada Operations Office
Attn: J. R. Boland
D. Livingston
P. K. Fitzsimmons
2753 S. Highland Drive
Las Vegas, NV 87183-8518

U.S. Department of Energy (2)
Technical Information Center
P.O. Box 62
Oak Ridge, TN 37831

U.S. Department of Energy (2)
Chicago Operations Office
Attn: J. C. Haugen
9800 South Cass Avenue
Argonne, IL 60439

U.S. Department of Energy
Los Alamos Area Office
528 35th Street
Los Alamos, NM 87544

U.S. Department of Energy (3)
Rocky Flats Area Office
Attn: W. C. Rask
G. Huffman
T. Lukow
P.O. Box 928
Golden, CO 80402-0928

U.S. Department of Energy
Dayton Area Office
Attn: R. Grandfield
P.O. Box 66
Miamisburg, OH 45343-0066

U.S. Department of Energy
Attn: E. Young
Room E-178
GAO/RCED/GTN
Washington, DC 20545

U.S. Bureau of Land Management
101 E. Mermod
Carlsbad, NM 88220

U.S. Bureau of Land Management
New Mexico State Office
P.O. Box 1449
Santa Fe, NM 87507

U.S. Environmental Protection Agency (2)
Office of Radiation Protection Programs (ANR-460)
Attn: Richard Guimond (2)
Washington, D.C. 20460

U.S. Nuclear Regulatory Commission
Division of Waste Management
Attn: H. Marson
Mail Stop 4-H-3
Washington, DC 20555

U.S. Nuclear Regulatory Commission (4)
Advisory Committee on Nuclear Waste
Attn: Dade Moeller
Martin J. Steindler
Paul W. Pomeroy
William J. Hinze
7920 Norfolk Avenue
Bethesda, MD 20814

Defense Nuclear Facilities Safety Board
Attn: Dermot Winters
625 Indiana Avenue NW
Suite 700
Washington, DC 20004

Nuclear Waste Technical Review Board (2)
Attn: Dr. Don A. Deere
Dr. Sidney J. S. Parry
Suite 910
1100 Wilson Blvd.
Arlington, VA 22209-2297

Katherine Yuracko
Energy and Science Division
Office of Management and Budget
725 17th Street NW
Washington, DC 20503

U.S. Geological Survey (2)
Water Resources Division
Attn: Cathy Peters
Suite 200
4501 Indian School, NE
Albuquerque, NM 87110

INSTITUTIONAL DISTRIBUTION

NEW MEXICO CONGRESSIONAL DELEGATION:

Jeff Bingaman
U.S. Senate
524 SHOB
Washington, DC 20510

Pete V. Domenici
U.S. Senate
427 SDOB
Washington, DC 20510

Bill Richardson
House of Representatives
332 CHOB
Washington, DC 20510

Steven H. Schiff
House of Representatives
1520 LHOB
Washington, DC 20510

Joe Skeen
House of Representatives
1007 LHOB
Washington, DC 20510

STATE AGENCIES

Environmental Evaluation Group (5)
Attn: Robert Neill
Suite F-2
7007 Wyoming Blvd., N.E.
Albuquerque, NM 87109

New Mexico Bureau of Mines
and Mineral Resources
Socorro, NM 87801

New Mexico Department of Energy &
Minerals
Attn: Librarian
2040 S. Pacheco
Santa Fe, NM 87505

New Mexico Radioactive Task Force (2)
(Governor's WIPP Task Force)
Attn: Anita Lockwood, Chairman
Chris Wentz, Coordinator/Policy
Analyst
2040 Pacheco
Santa Fe, NM 87505

Bob Forrest
Mayor, City of Carlsbad
P.O. Box 1569
Carlsbad, NM 88221

Chuck Bernard
Executive Director
Carlsbad Department of Development
P.O. Box 1090
Carlsbad, NM 88221

Robert M. Hawk (2)
Chairman, Hazardous and Radioactive
Materials Committee
Room 334
State Capitol
Sante Fe, NM 87503

New Mexico Environment Department
Secretary of the Environment
Attn: J. Espinosa (3)
P.O. Box 968
1190 St. Francis Drive
Santa Fe, NM 87503-0968

New Mexico Environment Department
Attn: Pat McCausland
WIPP Project Site Office
P.O. Box 3090
Carlsbad, NM 88221-3090

ADVISORY COMMITTEE ON NUCLEAR FACILITY SAFETY

John F. Ahearne
Executive Director, Sigma Xi
99 Alexander Drive
Research Triangle Park, NC 27709

James E. Martin
109 Observatory Road
Ann Arbor, MI 48109

Dr. Gerald Tape
Assoc. Universities
1717 Massachusetts Ave. NW
Suite 603
Washington, DC 20036

WIPP PANEL OF NATIONAL RESEARCH COUNCIL'S BOARD ON RADIOACTIVE WASTE MANAGEMENT

Charles Fairhurst, Chairman
Department of Civil and
Mineral Engineering
University of Minnesota
500 Pillsbury Dr. SE
Minneapolis, MN 55455-0220

John O. Blomeke
3833 Sandy Shore Drive
Lenoir City, TN 37771-9803

John D. Bredehoeft
Western Region Hydrologist
Water Resources Division
U.S. Geological Survey (M/S 439)
345 Middlefield Road
Menlo Park, CA 94025

Fred M. Ernsberger
1325 NW 10th Avenue
Gainsville, FL 32601

Rodney C. Ewing
Department of Geology
University of New Mexico
200 Yale, NE
Albuquerque, NM 87131

B. John Garrick
Pickard, Lowe & Garrick, Inc.
2260 University Drive
Newport Beach, CA 92660

Leonard F. Konikow
U.S. Geological Survey
431 National Center
Reston, VA 22092

Jeremiah O'Driscoll
505 Valley Hill Drive
Atlanta, GA 30350

Christopher Whipple
Clement International Corp.
160 Spear St.
Suite 1380
San Francisco, CA 94105-1535

National Research Council (3)
Board on Radioactive
Waste Management
RM HA456
Attn: Peter B. Myers, Staff Director (2)
Dr. Geraldine J. Grube
2101 Constitution Avenue
Washington, DC 20418

PERFORMANCE ASSESSMENT PEER REVIEW PANEL

G. Ross Heath
College of Ocean and
Fishery Sciences HN-15
583 Henderson Hall
University of Washington
Seattle, WA 98195

Thomas H. Pigford
Department of Nuclear Engineering
4159 Etcheverry Hall
University of California
Berkeley, CA 94720

Thomas A. Cotton
JK Research Associates, Inc.
4429 Butterworth Place, NW
Washington, DC 20016

Robert J. Budnitz
President, Future Resources
Associates, Inc.
2000 Center Street
Suite 418
Berkeley, CA 94704

C. John Mann
Department of Geology
245 Natural History Bldg.
1301 West Green Street
University of Illinois
Urbana, IL 61801

Frank W. Schwartz
Department of Geology and Mineralogy
The Ohio State University
Scott Hall
1090 Carmack Rd.
Columbus, OH 43210

FUTURE SOCIETIES EXPERT PANEL

Theodore S. Glickman
Resources for the Future
1616 P St., NW
Washington, DC 20036

Norman Rosenberg
Resources for the Future
1616 P St., NW
Washington, DC 20036

Max Singer
The Potomac Organization, Inc.
5400 Greystone St.
Chevy Chase, MD 20815

Maris Vinovskis
Institute for Social Research
Room 4086
University of Michigan
426 Thompson St
Ann Arbor, MI 48109-1045

Gregory Benford
University of California, Irvine
Department of Physics
Irvine, CA 92717

Craig Kirkwood
College of Business Administration
Arizona State University
Tempe, AZ 85287

Harry Otway
Health, Safety, and Envir. Div.
Mail Stop K-491
Los Alamos National Laboratory
Los Alamos, NM 87545

Martin J. Pasqualetti
Department of Geography
Arizona State University
Tempe, AZ 85287-3806

Michael Baram
Bracken and Baram
33 Mount Vernon St.
Boston, MA 02108

Wendell Bell
Department of Sociology
Yale University
1965 Yale Station
New Haven, CT 06520

Bernard L. Cohen
Department of Physics
University of Pittsburgh
Pittsburgh, PA 15260

Ted Gordon
The Futures Group
80 Glastonbury Blvd.
Glastonbury, CT 06033

Duane Chapman
5025 S. Building, Room S5119
The World Bank
1818 H Street NW
Washington, DC 20433

Victor Ferkiss
23 Sage Brush Circle
Corrales, NM 87048

Dan Reicher
Senior Attorney
Natural Resources Defense Council
1350 New York Ave. NW, #300
Washington, DC 20005

Theodore Taylor
P.O. Box 39
3383 Weatherby Rd.
West Clarksville, NY 14786

MARKERS EXPERT PANEL

Dr. Dieter Ast
Department of Materials Science
Bard Hall
Cornell University
Ithaca, NY 14853-1501

Dr. Victor Baker
Department of Geosciences
Building #77, Gould-Simpson Building
University of Arizona
Tucson, AZ 85721

Mr. Michael Brill
President
BOSTI
1479 Hertel Ave.
Buffalo, NY 14216

Dr. Frank Drake
Board of Studies in Astronomy and
Astrophysics
Lick Observatory
University of California, Santa Cruz
Santa Cruz, CA 95064

Dr. Ben Finney
University of Hawaii at Manoa
Department of Anthropology
Porteus Hall 346, 2424 Maile Way
Honolulu, HI 96822

Dr. David Givens
American Anthropological Association
1703 New Hampshire Ave., NW
Washington, D.C. 20009

Dr. Ward Goodenough
Department of Anthropology
University of Pennsylvania
325 University Museum
33rd and Spruce Streets
Philadelphia, PA 19104-6398

Dr. Maureen Kaplan
Eastern Research Group, Inc.
6 Whittemore Street
Arlington, MA 02174

Mr. Jon Lomberg
P.O. Box 207
Honaunau, HI 96726

Dr. Louis Narens
Department of Cognitive Sciences
School of Social Sciences
University of Califorrnia, Irvine
Irvine, CA 92717

Dr. Frederick Newmeyer
Department of Linguistics
GN-40
University of Washington
Seattle, WA 98195

Dr. Woodruff Sullivan
Department of Astonomy
FM-20
University of Washington
Seattle, WA 98195

Dr. Wendell Williams
Materials Science and Engineering
White Building
Case Western Reserve University
Cleveland, OH 44106

NATIONAL LABORATORIES

Argonne National Labs (2)
Attn: A. Smith
D. Tomasko
9700 South Cass, Bldg. 201
Argonne, IL 60439

Battelle Pacific Northwest Laboratories (3)
Attn: R. E. Westerman
S. Bates
H. C. Burkholder
Battelle Boulevard
Richland, WA 99352

Lawrence Livermore National Laboratory
Attn: G. Mackanic
P.O. Box 808, MS L-192
Livermore, CA 94550

Los Alamos National Laboratories
Attn: B. Erdal, CNC-11
P.O. Box 1663
Los Alamos, NM 87544

Los Alamos National Laboratories
Attn: A. Meijer
Mail Stop J514
Los Alamos, NM 87545

Los Alamos National Laboratories (3)
HSE-8
Attn: M. Enoris
L. Soholt
J. Wenzel
P.O. Box 1663
Los Alamos, NM 87544

Los Alamos National Laboratories (2)
HSE-7
Attn: A. Drypolcher
S. Kosciewiscz
P.O. Box 1663
Los Alamos, NM 87544

Oak Ridge National Labs
Martin Marietta Systems, Inc.
Attn: J. Setaro
P.O. Box 2008, Bldg. 3047
Oak Ridge, TN 37831-6019

Savannah River Laboratory (3)
Attn: N. Bibler
M. J. Plodinec
G. G. Wicks
Aiken, SC 29801

Savannah River Plant (2)
Attn: Richard G. Baxter
Building 704-S
K. W. Wierzbicki
Building 703-H
Aiken, SC 29808-0001

CORPORATIONS/MEMBERS OF THE PUBLIC

Benchmark Environmental Corp. (3)
Attn: John Hart
C. Frederickson
K. Lickliter
4501 Indian School Rd., NE
Suite 105
Albuquerque, NM 87110

Deuel and Associates, Inc.
Attn: R. W. Prindle
7208 Jefferson, NE
Albuquerque, NM 87109

Disposal Safety, Inc.
Attn: Benjamin Ross
Suite 314
1660 L Street NW
Washington, DC 20006

Ecodynamics Research Associates (2)
Attn: Pat Roache
Rebecca Blaine
P.O. Box 8172
Albuquerque, NM 87198

E G & G Idaho (3)
1955 Fremont Street
Attn: C. Atwood
C. Hertzler
T. I. Clements
Idaho Falls, ID 83415

Geomatrix
Attn: Kevin Coppersmith
100 Pine Street #1000
San Francisco, CA 94111

Golden Associates, Inc. (3)
Attn: Mark Cunnane
Richard Kossik
Ian Miller
4104 148th Avenue NE
Redmond, WA 98052

In-Situ, Inc. (2)
Attn: S. C. Way
C. McKee
209 Grand Avenue
Laramie, WY 82070

INTERA, Inc.
Attn: A. M. LaVenue
8100 Mountain Road NE
Suite 213
Albuquerque, NM 87110

INTERA, Inc.
Attn: J. F. Pickens
Suite #300
6850 Austin Center Blvd.
Austin, TX 78731

INTERA, Inc.
Attn: Wayne Stensrud
P.O. Box 2123
Carlsbad, NM 88221

INTERA, Inc.
Attn: William Nelson
101 Convention Center Drive
Suite 540
Las Vegas, NV 89109

IT Corporation (2)
Attn: P. Drez
J. Myers
Regional Office - Suite 700
5301 Central Avenue, NE
Albuquerque, NM 87108

IT Corporation
R. J. Eastmond
825 Jadwin Ave.
Richland, WA 99352

MACTEC (2)
Attn: J. A. Thies
D. K. Duncan
8418 Zuni Road SE
Suite 200
Albuquerque, NM 87108

Pacific Northwest Laboratory
Attn: Bill Kennedy
Battelle Blvd.
P.O. Box 999
Richland, WA 99352

RE/SPEC, Inc. (2)
Attn: W. Coons
Suite 300
4775 Indian School NE
Albuquerque, NM 87110

RE/SPEC, Inc.
Attn: J. L. Ratigan
P.O. Box 725
Rapid City, SD 57709

Reynolds Elect/Engr. Co., Inc.
Building 790, Warehouse Row
Attn: E. W. Kendall
P.O. Box 98521
Las Vegas, NV 89193-8521

Roy F. Weston, Inc.
CRWM Tech. Supp. Team
Attn: Clifford J. Noronha
955 L'Enfant Plaza, S.W.
North Building, Eighth Floor
Washington, DC 20024

Science Applications International Corporation
Attn: Howard R. Pratt,
Senior Vice President
10260 Campus Point Drive
San Diego, CA 92121

Science Applications International Corporation (2)
Attn: George Dymmel
Chris G. Pflum
101 Convention Center Dr.
Las Vegas, NV 89109

Science Applications International Corporation (2)
Attn: John Young
Dave Lester
18706 North Creek Parkway
Suite 110
Bothell, WA 98011

Southwest Research Institute
Center for Nuclear Waste Regulatory Analysis (2)
Attn: P. K. Nair
6220 Culebra Road
San Antonio, Texas 78228-0510

Systems, Science, and Software (2)
Attn: E. Peterson
P. Lagus
Box 1620
La Jolla, CA 92038

TASC
Attn: Steven G. Oston
55 Walkers Brook Drive
Reading, MA 01867

Tech. Reps., Inc. (5)
Attn: Janet Chapman
Terry Cameron
Debbie Marchand
John Stikar
Denise Bissell
5000 Marble NE
Suite 222
Albuquerque, NM 87110

Tolan, Beeson, & Associates
Attn: Terry L. Tolan
2320 W. 15th Avenue
Kennewick, WA 99337

TRW Environmental Safety Systems (TESS)
Attn: Ivan Saks
10306 Eaton Place
Suite 300
Fairfax, VA 22030

Westinghouse Electric Corporation (4)
Attn: Library
L. Trego
C. Cox
L. Fitch
R. F. Kehrman
P.O. Box 2078
Carlsbad, NM 88221

Westinghouse Hanford Company
Attn: Don Wood
P.O. Box 1970
Richland, WA 99352

Western Water Consultants
Attn: D. Fritz
1949 Sugarland Drive #134
Sheridan, WY 82801-5720

Western Water Consultants
Attn: P. A. Rechard
P.O. Box 4128
Laramie, WY 82071

Neville Cook
Rock Mechanics Engineering
Mine Engineering Dept.
University of California
Berkeley, CA 94720

Dennis W. Powers
Star Route Box 87
Anthony, TX 79821

Shirley Thieda
P.O. Box 2109, RR1
Bernalillo, NM 87004

Jack Urich
c/o CARD
144 Harvard SE
Albuquerque, NM 87106

UNIVERSITIES

University of California
Mechanical, Aerospace, and
Nuclear Engineering Department (2)
Attn: W. Kastenberg
D. Browne
5532 Boelter Hall
Los Angeles, CA 90024

University of Hawaii at Hilo
Attn: S. Hora
Business Administration
Hilo, HI 96720-4091

University of New Mexico
Geology Department
Attn: Library
Albuquerque, NM 87131

University of New Mexico
Research Administration
Attn: H. Schreyer
102 Scholes Hall
Albuquerque, NM 87131

University of Wyoming
Department of Civil Engineering
Attn: V. R. Hasfurther
Laramie, WY 82071

University of Wyoming
Department of Geology
Attn: J. I. Drever
Laramie, WY 82071

University of Wyoming
Department of Mathematics
Attn: R. E. Ewing
Laramie, WY 82071

LIBRARIES

Thomas Brannigan Library
Attn: Don Dresp, Head Librarian
106 W. Hadley St.
Las Cruces, NM 88001

Hobbs Public Library
Attn: Marcia Lewis, Librarian
509 N. Ship Street
Hobbs, NM 88248

New Mexico State Library
Attn: Norma McCallan
325 Don Gaspar
Santa Fe, NM 87503

New Mexico Tech
Martin Speere Memorial Library
Campus Street
Socorro, NM 87810

New Mexico Junior College
Pannell Library
Attn: Ruth Hill
Lovington Highway
Hobbs, NM 88240

Carlsbad Municipal Library
WIPP Public Reading Room
Attn: Lee Hubbard, Head Librarian
101 S. Halagueno St.
Carlsbad, NM 88220

University of New Mexico
General Library
Government Publications Department
Albuquerque, NM 87131

NEA/PSAC USER'S GROUP

Timo K. Vieno
Technical Research Centre of Finland (VTT)
Nuclear Engineering Laboratory
P.O. Box 169
SF-00181 Helsinki
FINLAND

Alexander Nies (PSAC Chairman)
Gesellschaft für Strahlen- und
Institut für Tieflagerung
Abteilung für Endlagersicherheit
Theodor-Heuss-Strasse 4
D-3300 Braunscheweig
GERMANY

Eduard Hofer
Gesellschaft für Reaktorsicherheit (GRS)
MBH
Forschungsgelände
D-8046 Garching
GERMANY

Takashi Sasahara
Environmental Assessment Laboratory
Department of Environmental Safety Research
Nuclear Safety Research Center,
Tokai Research Establishment, JAERI
Tokai-mura, Naka-gun
Ibaraki-ken
JAPAN

Alejandro Alonso
Cátedra de Tecnología Nuclear
E.T.S. de Ingenieros Industriales
José Gutiérrez Abascal, 2
E-28006 Madrid
SPAIN

Pedro Prado
CIEMAT
Instituto de Tecnología Nuclear
Avenida Complutense, 22
E-28040 Madrid
SPAIN

Miguel Angel Cuñado
ENRESA
Emilio Vargas, 7
E-28043 Madrid
SPAIN

Francisco Javier Elorza
ENRESA
Emilio Vargas, 7
E-28043 Madrid
SPAIN

Nils A. Kjellbert
Swedish Nuclear Fuel and Waste Management Company (SKB)
Box 5864
S-102 48 Stockholm
SWEDEN

Björn Cronhjort
Swedish National Board for Spent Nuclear Fuel (SKN)
Sehlsedtsgatan 9
S-115 28 Stockholm
SWEDEN

Richard A. Klos
Paul-Scherrer Institute (PSI)
CH-5232 Villingen PSI
SWITZERLAND

NAGRA (2)
Attn: Charles McCombie
Fritz Van Dorp
Parkstrasse 23
CH-5401 Baden
SWITZERLAND

Brian G. J. Thompson
Department of the Environment
Her Majesty's Inspectorate of Pollution
Room A5.33, Romney House
43 Marsham Street
London SW1P 2PY
UNITED KINGDOM

INTERA/ECL (2)
Attn: Trevor J. Sumerling
Daniel A. Galson
Chiltern House
45 Station Road
Henley-on-Thames
Oxfordshire RG9 1AT
UNITED KINGDOM

U.S. Nuclear Regulatory Commission (2)
Attn: Richard Codell
Norm Eisenberg
Mail Stop 4-H-3
Washington, D.C. 20555

Paul W. Eslinger
Battelle Pacific Northwest Laboratories (PNL)
P.O. Box 999, MS K2-32
Richland, WA 99352

Andrea Saltelli
Commission of the European Communities
Joint Resarch Centre od Ispra
I-21020 Ispra (Varese)
ITALY

Budhi Sagar
Center for Nuclear Waste Regulatory Analysis (CNWRA)
Southwest Research Institute
P.O. Drawer 28510
6220 Culebra Road
San Antonio, TX 78284

Shaheed Hossain
Division of Nuclear Fuel Cycle and Waste Management
International Atomic Energy Agency
Wagramerstrasse 5
P.O. Box 100
A-1400 Vienna
AUSTRIA

Claudio Pescatore
Division of Radiation Protection and Waste Management
38, Boulevard Suchet
F-75016 Paris
FRANCE

FOREIGN ADDRESSES

Studiecentrum Voor Kernenergie
Centre D'Energie Nucleaire
Attn: A. Bonne
SCK/CEN
Boeretang 200
B-2400 Mol
BELGIUM

Atomic Energy of Canada, Ltd. (3)
Whiteshell Research Estab.
Attn: Michael E. Stevens
Bruce W. Goodwin
Donna Wushke
Pinewa, Manitoba
ROE 1L0
CANADA

Ghislain de Marsily
Lab. Géologie Appliqué
Tour 26, 5 étage
4 Place Jussieu
F-75252 Paris Cedex 05
FRANCE

Jean-Pierre Olivier
OECD Nuclear Energy Agency (2)
38, Boulevard Suchet
F-75016 Paris
FRANCE

D. Alexandre, Deputy Director
ANDRA
31 Rue de la Federation
75015 Paris
FRANCE

Claude Sombret
Centre D'Etudes Nucleaires
De La Vallee Rhone
CEN/VALRHO
S.D.H.A. BP 171
30205 Bagnols-Sur-Ceze
FRANCE

Bundesministerium fur Forschung und Technologie
Postfach 200 706
5300 Bonn 2
GERMANY

Bundesanstalt fur Geowissenschaften und Rohstoffe
Attn: Michael Langer
Postfach 510 153
3000 Hannover 51
GERMANY

Gesellschaft fur Reaktorsicherheit (GRS) mb (2)
Attn: Bruno Baltes
Wolfgang Muller
Schwertnergasse 1
D-5000 Cologne
GERMANY

Hahn-Mietner-Institut fur Kernforschung
Attn: Werner Lutze
Glienicker Strasse 100
100 Berlin 39
GERMANY

Institut fur Tieflagerung (2)
Attn: K. Kuhn
Theodor-Heuss-Strasse 4
D-3300 Braunschweig
GERMANY

Physikalisch-Technische Bundesanstalt
Attn: Peter Brenneke
Postfach 33 45
D-3300 Braunschweig
GERMANY

Shingo Tashiro
Japan Atomic Energy Research Institute
Tokai-Mura, Ibaraki-Ken
319-11
JAPAN

Netherlands Energy Research Foundation
ECN
Attn: L. H. Vons
3 Westerduinweg
P.O. Box 1
1755 ZG Petten
THE NETHERLANDS

Johan Andersson
Statens Kärnkraftinspektion
SKI
Box 27106
S-102 52 Stockholm
SWEDEN

Fred Karlsson
Svensk Karnbransleforsorjning AB
SKB
Box 5864
S-102 48 Stockholm
SWEDEN

Nationale Genossenschaft fur die Lagerung
Radioaktiver Abfalle (NAGRA) (2)
Attn: Stratis Vomvoris
Piet Zuidema
Hardstrasse 73
CH-5430 Wettingen
SWITZERLAND

D. R. Knowles
British Nuclear Fuels, plc
Risley, Warrington, Cheshire WA3 6AS
1002607 UNITED KINGDOM

AEA Technology
Attn: J.H. Rees
D5W/29 Culham Laboratory
Abington
Oxfordshire OX14 3DB
UNITED KINGDOM

AEA Technology
Attn: W. R. Rodwell
O44/A31 Winfrith Technical Centre
Dorchester
Dorset DT2 8DH
UNITED KINGDOM

AEA Technology
Attn: J. E. Tinson
B4244 Harwell Laboratory
Didcot
Oxfordshire OX11 ORA
UNITED KINGDOM

INTERNAL

1	A. Narath
20	O. E. Jones
1510	J. C. Cummings
1511	D. K. Gartling
3151	S. M. Wayland
3200	N. R. Ortiz
6000	D. L. Hartley
6233	J. C. Eichelberger
6300	T. O. Hunter
6301	E. Bonano
6310	T. E. Blejwas, Acting
6313	L. E. Shephard
6312	F. W. Bingham
6313	L. S. Costin
6315	Supervisor
6316	R. P. Sandoval
6320	R. E. Luna, Acting
6340	W. D. Weart
6340	S. Y. Pickering
6341	J. M. Covan
6341	D. P. Garber
6341	R. C. Lincoln
6341	J. Orona*
6341	Sandia WIPP Central Files (250)
6342	D. R. Anderson
6342	B. M. Butcher
6342	D. P. Gallegos
6342	L. S. Gomez
6342	M. Gruebel
6342	R. Guzowski
6342	R. D. Klett
6342	M. G. Marietta
6342	D. Morrison
6342	A. C. Peterson
6342	R. P. Rechard
6342	P. Swift
6342	M. Tierney
6342	K. M. Trauth
6342	B. L. Baker*
6342	J. Bean*
6342	J. Berglund*
6342	W. Beyeler*
6342	T. Blaine*
6342	K. Brinster*
6342	K. Byle*
6342	L. Clements*
6342	J. Garner*
6342	A. Gilkey*
6342	H. Iuzzolino*
6342	J. Logothetis*
6342	R. McCurley*
6342	J. Rath*
6342	D. Rudeen*
6342	J. Sandha*
6342	J. Schreiber*
6342	P. Vaughn*
6343	T. M. Schultheis
6344	R. L. Beauheim
6344	P. B. Davies
6344	S. J. Finley
6344	E. Gorham
6344	C. F. Novak
6344	S. W. Webb
6345	R. Beraun
6345	L. Brush
6345	A. R. Lappin
6345	M. A. Molecke
6346	D. E. Munson
6346	E. J. Nowak
6346	J. R. Tillerson
6347	A. L. Stevens
6400	D. J. McCloskey
6413	J. C. Helton
6415	R. M. Cranwell
6415	C. Leigh
6415	R. L. Iman
6622	M.S.Y. Chu
9300	J. E. Powell
9310	J. D. Plimpton
9325	J. T. McIlmoyle
9325	R. L. Rutter
9330	J. D. Kennedy
8523-2	Central Technical Files
3141	S. A. Landenberger (5)
3145	Document Processing (8) for DOE/OSTI
3151	G. C. Claycomb (3)

*6342/Geo-Centers

☆ U.S. GOVERNMENT PRINTING OFFICE: 1991—673-122/60034